

THE JOURNAL OF
PHYSICAL CHEMISTRY

Volume 71, Number 4 March 1967

The Electronic Structure of Ionized Molecules. VI. <i>n</i> -Alkylamines	J. C. Leclerc and J. C. Lorquet	787
Anion and pH Effects on the Potentials of Zero Charge of Gold and Silver Electrodes	D. D. Bode, Jr., T. N. Andersen, and H. Eyring	792
Photochemistry of Complex Ions. IV. The Role of Quartet Excited States in the Photochemistry of Chromium(III) Complexes	Arthur W. Adamson	798
Thermodynamics of Vaporization of Thallic Oxide	Daniel Cubicciotti and F. J. Keneshea	808
Excess and Partial Volumes of Some Alcohol-Water and Glycol-Water Solutions	Koichiro Nakanishi, Nobuyuki Kato, and Masato Maruyama	814
Effect of Pressure on the Dissociation of the (LaSO ₄) ⁺ Complex Ion	Frederick H. Fisher and Douglas F. Davis	819
Bonding in Heteromolecular Ion Clusters. N ₂ O ₂ ⁺	G. S. Janik and D. C. Conway	823
The Adsorption of Carbon Dioxide on Carbon Solids. I. Graphite and Diamond at 0°	Victor R. Deitz	830
The Transition between Localized and Condensed Layers in the Adsorption of Water Vapor onto Titania	P. T. Dawson	838
Infrared Investigation of the Adsorption and Surface Reactions of the C ₁ through C ₄ Normal Alcohols on γ-Alumina	R. O. Kagel	844
Nuances of the ECE Mechanism. II. Addition of Hydrochloric Acid and Amines to Electrochemically Generated <i>o</i> -Benzoquinones	R. N. Adams, M. Dale Hawley, and Stephen W. Feldberg	851
Some New Relations Connecting Molecular Properties and Electron and X-Ray Diffraction Intensities	R. A. Bonham	856
The Radiolysis of Thiophenol and Its Mixtures with Benzene and Benzene- <i>d</i> ₆	Gulbrand Lunde and Robert R. Hentz	863
Radiolysis Yields from γ-Irradiated Liquid Methanol Containing Nitrous Oxide and the Effect of Acid	Hiroshi Seki and Masashi Imamura	870
The Thermal Pressure Coefficient and the Entropy of Melting at Constant Volume of Isotactic Polypropylene	G. C. Fortune and G. N. Malcolm	876
The Charge Effect in Sedimentation. I. Polyelectrolytes	Mitsuru Nagasawa and Yosuke Eguchi	880
The Vapor Pressure, Heat of Sublimation, and Evaporation Coefficient of Lanthanum Fluoride	Raymond W. Mar and Alan W. Searcy	888
Specific Heats of Nematic, Smectic, and Cholesteric Liquid Crystals by Differential Scanning Calorimetry	Edward M. Barrall, II, Roger S. Porter, and Julian F. Johnson	895
Activity Coefficients for the System Water- <i>α</i> -Amino- <i>n</i> -butyric Acid-Urea	E. L. Cussler, Jr.	901
Conductances of Some Uni-univalent Electrolytes in Adiponitrile at 25°	Paul G. Sears, Joseph A. Caruso, and Alexander I. Popov	905
Activity Coefficient Measurements in Aqueous Sodium Chloride-Sodium Sulfate Electrolytes Using Sodium Amalgam Electrodes	James N. Butler, Philomena T. Hsu, and John C. Synnott	910
Acetonitrile: Far-Infrared Spectra and Chemical Thermodynamic Properties. Discussion of an Entropy Discrepancy	G. A. Crowder and Bobby R. Cook	914
Relaxation Spectra of Enzymatic Reactions	Gordon G. Hammes and Paul R. Schimmel	917

Bonding and Hybridization in the Nitrogen Molecule	Paul R. Smith and James W. Richardson	924
Azaaromatic Charge-Transfer Complexes with π -Electron Acceptors: Evidence for Formation of (π, π) Complexes	David R. Kearns, Phillip Gardner, and John Carmody	931
The Ultraviolet-Visible Absorption Spectrum of Bromine between Room Temperature and 440°	A. A. Passchier, J. D. Christian, and N. W. Gregory	937
Osmotic and Activity Coefficients of <i>cis</i> - and <i>trans</i> -Nitrobis(ethylenediamine)amminecobalt(III) Salts	W. L. Masterton, T. I. Munnely, and L. H. Berka	942
The Rates of the Reactions of Active Nitrogen with Ethylene and Propylene	G. Paraskevopoulos and C. A. Winkler	947
Temperature-Dependence Studies of Proton and Deuteron Spin-Lattice Relaxation in Ammonium Chloride	D. E. Woessner and B. S. Snowden, Jr.	952
Investigation of Micelle Structure by Fluorine Magnetic Resonance. I. Sodium 10,10,10-Trifluorocaprate and Related Compounds	Norbert Muller and Ronald H. Birkhahn	957
Infrared Spectra of the Complexes $\text{AgNO}_3 \cdot \text{CH}_3\text{CN}$ and $\text{AgNO}_3 \cdot 2\text{CH}_3\text{CN}$ and Their Solutions in Acetonitrile	George J. Janz, Malcolm J. Tait, and Jurg Meier	963
Self-Association and Hydration of Ketones in Carbon Tetrachloride	T. F. Lin, S. D. Christian, and H. E. Afsprung	968
The Rate of Oxygen Exchange between the Perrhenate Ion and Water	R. Kent Murmann	974
The Radiolysis of Concentrated Neutral Sodium Perchlorate Aqueous Solutions	J. Konstantatos and D. Katakis	979
Physicochemical Properties of Hexamethylenetetramine Aqueous Solutions	G. Barone, V. Crescenzi, A. M. Liquori, and F. Quadrifoglio	984
Diffusion in Binary Solutions	David W. McCall and Dean C. Douglass	987
Nuclear Magnetic Relaxation in Polytetrafluoroethylene	D. W. McCall, D. C. Douglass, and D. R. Falcone	998
The Effect of Oxygen on the Generation of Radical Ions by Synthetic Zeolites	F. R. Dollish and W. Keith Hall	1005
Tracer Studies of Acid-Catalyzed Reactions. V. Carbon-14 Kinetic Studies of <i>n</i> -Butene Isomerization over Alumina and Silica-Alumina Catalysts	Joe W. Hightower and W. Keith Hall	1014
Radiation Chemistry of the Aqueous Nitrate System. I. γ Radiolysis of Dilute Solutions	Malcolm Daniels and Eric E. Wigg	1024
The Effect of Ionic Hydration on Equilibria and Rates in Concentrated Electrolyte Solutions. III. The <i>H</i> -Scale in Concentrated Hydroxide Solutions	G. Yagil	1034
The Effect of Ionic Hydration on Rate and Equilibrium in Concentrated Electrolyte Solutions. IV. The Effect of Neutral Electrolytes on the Indicator Acidity of an Alkaline Solution	G. Yagil	1045
The Photochemistry of Phosphorus Compounds. V. Far-Ultraviolet Absorption Spectra of Hypophosphite, Phosphite, and Hypophosphate Ions in Aqueous Solution	Hinga Benderly and M. Halmann	1053
Molecular Orbitals for General Polyatomic Molecules. I.	Louis Chopin Cusachs and Barbara Breckinridge Cusachs	1060
Spectroscopic Studies of Self-Association Due to Hydrogen Bonding	Surjit Singh and C. N. R. Rao	1074
Hydrothermal Aging of Silica-Alumina Cracking Catalysts	Arpad Elo, Jr., and Porter Clements	1078
Kinetics and Thermodynamics of the Reaction between Iodine and Fluoroform and the Heat of Formation of Trifluoromethyl Iodide	C. A. Goy, Allan Lord, and H. O. Pritchard	1086
The Radiation Chemistry of Liquid Methane	Hugh A. Gillis	1089
Proton Mobility in Solids. I. Hydrogenic Vibration Modes and Proton Delocalization in Boehmite	J. J. Fripiat, H. Bosmans, and P. G. Rouxhet	1097
Radical Reactions in Liquid Cyclohexane. II. The Mercury-Photosensitized Decomposition of Cyclohexane	W. A. Cramer	1112
Primary Processes in the Formation of Hydrogen Atoms in the Radiolysis of Water Vapor	G. R. A. Johnson and M. Simic	1118
Diffusion Coefficients for Gases in Liquids from the Rates of Solution of Small Gas Bubbles	Irvin M. Krieger, George W. Mulholland, and Charles S. Dickey	1123

NOTES

The Crystal Structure of 1,3-Dichloro-2,4,6-trinitrobenzene	James R. Holden and Charles Dickinson 1129
The Association of $MnSO_4$ in Methanol-Water Mixtures of High Methanol Content	H. Tsubota and G. Atkinson 1131
Dielectric Study of the Hydration of Acetone in 1,2-Dichloroethane	T. F. Lin, S. D. Christian, and H. E. Afsprung 1133
An Electron Spin Resonance Study of Intermediates Induced in Carbohydrates by Titanium Trichloride-Hydrogen Peroxide	Peter J. Baugh, Oscar Hinojosa, and Jett C. Arthur, Jr. 1135
Thermodynamics of Aqueous Solutions of Noble Gases. IV. Effect of Tetraalkylammonium Salts	A. Ben-Naim 1137
Reaction of Hydrogen Atoms with Allyl Alcohol at 77°K	R. H. Johnsen, A. K. E. Hagopian, and H. B. Yun 1139
Complexes of PMDA with Aromatic Hydrocarbons in Solution	Ivor Ilmet and Paul M. Rashba 1140
Nitrogen-14 Chemical Shifts in Nitro Compounds	C. F. Poranski, Jr., and W. B. Moniz 1142
Sodium Bifluoride: Decomposition Pressure by the Knudsen Effusion Method	Alan R. Miller 1144
Attractive Potentials between Fluorochemicals and Aliphatic Hydrocarbons	J. H. Dymond and J. H. Hildebrand 1145
The Effect of Electrolyte Addition on the Viscosity of Water under Pressure	R. A. Horne and D. S. Johnson 1147
Diffusional and Electrical Mobilities of Tracer Alkali Ions in Alkali Nitrates	J. A. A. Ketelaar and J. C. Th. Kwak 1149
Stepped Isotherms on Carbons	E. Greenhalgh and E. Redman 1151
Surface Tension of Binary Liquid Mixtures	Raymond L. Schmidt 1152
Solubilities of Alkylammonium Iodides in Water and Aqueous Urea	F. Franks and D. L. Clarke 1155
Heats of Adsorption of Carbon Dioxide on Doped Zinc Oxide	O. Levy and M. Steinberg 1156
Density, Viscosity, and Dielectric Constant of Tetrahydrofuran between -78 and 30°	Donald J. Metz and Althea Glines 1158

COMMUNICATIONS TO THE EDITOR

Volume Change Accompanying the Helix-Coil Transition in Poly- γ -benzyl-L-glutamate	F. E. Karasz and J. M. O'Reilly 1159
Remarks on the Structure and Properties of Some Organocobalt Compounds, $RCoX(L)_2$ and $R_2Co(L)_2$	Kei Matsuzaki and Tamio Yasukawa 1160
Comments on the Paper, "A Chemical Kinetics Computer Program for Homogeneous and Free-Radical Systems of Reactions," by R. H. Snow	George Emanuel 1161
Computer Program for Chemical Kinetics	Reiner Kollrack 1162
Reply to Comments on the Paper, "A Chemical Kinetics Computer Program for Homogeneous and Free-Radical Systems of Reactions"	Richard H. Snow 1162
On the Heat Precipitation of Poly-L-proline	L. Mandelkern and M. H. Liberman 1163
Comments on the Note, "On the Heat Precipitation of Poly-L-proline," by L. Mandelkern and M. H. Liberman	A. Ciferri and T. A. Orofino 1165
Constant-Volume Parameters of Activation for the Hydrolysis of Benzyl Chloride in Ethanol-Water Mixtures	B. T. Baliga and E. Whalley 1166
Benzene Photosensitization of 4-Pentenal	Edward K. C. Lee and Norman W. Lee 1167
Amended Kohlrausch Ratio for Transport Numbers	L. J. M. Smits and E. M. Duyvis 1168
Comments on the Paper, "Gibbs Equation for the Adsorption of Organic Ions in Presence and Absence of Neutral Salts" by D. K. Chatteraj	B. H. Bijsterbosch and H. J. van den Hul 1169

AUTHOR INDEX

- Adams, R. N., 851
 Adamson, A. W., 798
 Affsprung, H. E., 968, 1133
 Andersen, T. N., 792
 Arthur, J. C., Jr., 1135
 Atkinson, G., 1131

 Baliga, B. T., 1166
 Barone, G., 984
 Barrall, E. M., II, 895
 Baugh, P. J., 1135
 Benderly, H., 1053
 Ben-Naim, A., 1137
 Berka, L. H., 942
 Bijsterbosch, B. H., 1169
 Birkhahn, R. H., 957
 Bodé, D. D., Jr., 792
 Bonham, R. A., 856
 Bosmans, H., 1097
 Butler, J. N., 910

 Carmody, J., 931
 Caruso, J. A., 905
 Christian, J. D., 937
 Christian, S. D., 968, 1133
 Ciferri, A., 1165
 Clarke, D. L., 1155
 Clements, P., 1078
 Conway, D. C., 823
 Cook, B. R., 914
 Cramer, W. A., 1112
 Crescenzi, V., 984
 Crowder, G. A., 914
 Cubicciotti, D., 808
 Cusachs, B. B., 1060
 Cusachs, L. C., 1060

 Cussler, E. L., Jr., 901

 Daniels, M., 1024
 Davis, D. F., 819
 Dawson, P. T., 838
 Deitz, V. R., 830
 Dickey, C. S., 1123
 Dickinson, C., 1129
 Dollish, F. R., 1005
 Douglass, D. C., 987, 998
 Duyvis, E. M., 1168
 Dymond, J. H., 1145

 Eguchi, Y., 880
 Elo, A., Jr., 1078
 Emanuel, G., 1161
 Eyring, H., 792

 Falcone, D. R., 998
 Feldberg, S. W., 851
 Fisher, F. H., 819
 Fortune, G. C., 876
 Franks, F., 1155
 Fripiat, J. J., 1097

 Gardner, P., 931
 Gillis, H. A., 1089
 Glines, A., 1158
 Goy, C. A., 1086
 Greenhalgh, E., 1151
 Gregory, N. W., 937

 Hagopian, A. K. E., 1139
 Hall, W. K., 1005, 1014
 Halmann, M., 1053

 Hammes, G. G., 917
 Hawley, M. D., 851
 Hentz, R. R., 863
 Hightower, J. W., 1014
 Hildebrand, J. H., 1145
 Hinojosa, O., 1135
 Holden, J. R., 1129
 Horne, R. A., 1147
 Hsu, P. T., 910

 Ilmet, I., 1140
 Imamura, M., 870

 Janik, G. S., 823
 Janz, G. J., 963
 Johnsen, R. H., 1139
 Johnson, D. S., 1147
 Johnson, G. R. A., 1118
 Johnson, J. F., 895

 Kagel, R. O., 844
 Karasz, F. E., 1159
 Katakis, D., 979
 Kato, N., 814
 Kearns, D. R., 931
 Keneshea, F. J., 808
 Ketelaar, J. A. A., 1149
 Kollrack, R., 1162
 Konstantatos, J., 979
 Krieger, I. M., 1123
 Kwak, J. C. Th., 1149

 Leclerc, J. C., 787
 Lee, E. K. C., 1167
 Lee, N. W., 1167

 Levy, O., 1156
 Liberman, M. H., 1163
 Lin, T. F., 968, 1133
 Liquori, A. M., 984
 Lord, A., 1086
 Lorquet, J. C., 787
 Lunde, G., 863

 Malcolm, G. N., 876
 Mandelkern, L., 1163
 Mar, R. W., 888
 Maruyama, M., 814
 Masterton, W. L., 942
 Matsuzaki, K., 1160
 McCall, D. W., 987, 998
 Meier, J., 963
 Metz, D. J., 1158
 Miller, A. R., 1144
 Moniz, W. B., 1142
 Mulholland, G. W., 1123
 Muller, N., 957
 Munnely, T. I., 942
 Murmann, R. K., 974

 Nagasawa, M., 880
 Nakanishi, K., 814

 O'Reilly, J. M., 1159
 Orofino, T. A., 1165

 Paraskevopoulos, G., 947
 Passchier, A. A., 937
 Popov, A. I., 905
 Poranski, C. F., Jr., 1142

 Porter, R. S., 895
 Pritchard, H. O., 1086

 Quadrifoglio, F., 984

 Rao, C. N. R., 1074
 Rashba, P. M., 1140
 Redman, E., 1151
 Richardson, J. W., 924
 Rouxhet, P. G., 1097

 Schimmel, P. R., 917
 Schmidt, R. L., 1152
 Searcy, A. W., 888
 Sears, P. G., 905
 Seki, H., 870
 Simic, M., 1118
 Singh S., 1074
 Smith, P. R., 924
 Smits, L. J. M., 1168
 Snow, R. H., 1162
 Snowden, B. S., Jr., 952
 Steinberg, M., 1156
 Synnott, J. C., 910

 Tait, M. J., 963
 Tsubota, H., 1131

 van den Hul, H. J., 1139

 Whalley, E., 1166
 Wigg, E. E., 1024
 Winkler, C. A., 947
 Woessner, D. E., 952

 Yagil, G., 1034, 1045
 Yasukawa, T., 1160
 Yun, H. B., 1139

THE JOURNAL OF PHYSICAL CHEMISTRY

Registered in U. S. Patent Office © Copyright, 1967, by the American Chemical Society

VOLUME 71, NUMBER 4 MARCH 15, 1967

The Electronic Structure of Ionized Molecules. VI. *n*-Alkylamines

by J. C. Leclerc and J. C. Lorquet¹

Institut de Chimie de l'Université de Liège, quai Roosevelt, Liège, Belgium (Received November 8, 1966)

Contour maps of the potential energy hypersurfaces of the ethylamine ion in its ground and first excited states are presented in an effort to understand its dissociation processes.

Introduction

The dissociation of *n*-alkylamine ions has already been studied extensively.²⁻⁵ The mass spectra of these substances are very different from those of the corresponding saturated hydrocarbons. The CC bond adjacent to the CN bond is much more easily broken than any of its neighbors. No other dissociation process competes with this one, at least within 3 eV above the ionization threshold.

In a previous paper of this series,⁶ it was shown that the use of charge-density diagrams to predict dissociation mechanisms does not always give the correct answer. In the case of the amines, a rough equivalent orbital calculation was tried. The necessary diagonal matrix elements were estimated from relations suggested by Peters⁷ and the remaining ones were obtained from existing ionization potential values. One finds that in the ground state of the molecular ion most of the positive charge is supported by the lone pair and the CN bond, whereas the adjacent CC bond is almost unaffected. This failure was attributed to the fact that the electronic charge distribution may vary considerably when the point representing the system moves over the potential energy hypersurface. A method was then developed to determine which normal modes of vibration were most likely to transform into a reaction coordinate. Unfortunately, the

method is useful only in the case of symmetrical molecular ions and when electronic rearrangements are not important. Moreover, the behavior of electronically excited states was not investigated.

It was therefore decided to calculate straightforwardly the potential energy hypersurfaces of the molecular ion. This imposed the choice of a very simplified quantum mechanical method, to be described in the next paragraph, which does still yield useful results if some elementary precautions are taken and if our ambitions remain limited.

Method

The only method presently capable of handling this 19-electron problem is the extended Hückel theory. Several versions of it have been proposed.^{8,9}

(1) To whom inquiries should be addressed.

(2) (a) J. Collin, *Bull. Soc. Roy. Sci. Liège*, **21**, 446 (1952); *Bull. Soc. Chim. Belges*, **62**, 411 (1953); **63**, 500 (1954); **67**, 549 (1958); J. E. Collin and M. J. Franskin, *Bull. Soc. Roy. Sci. Liège*, to be published; (b) H. Hurzeler, M. G. Inghram, and J. D. Morrison, *J. Chem. Phys.*, **28**, 76 (1958).

(3) W. A. Chupka, *ibid.*, **30**, 191 (1959).

(4) W. A. Chupka and J. Berkowitz, *ibid.*, **32**, 1546 (1960).

(5) H. Sjögren, *Arkiv Fysik*, **29**, 565 (1965).

(6) J. C. Lorquet, *Mol. Phys.*, **10**, 489 (1966).

(7) D. Peters, *J. Chem. Soc.*, 2901, 2908 (1964).

(8) R. Hoffmann, *J. Chem. Phys.*, **39**, 1397 (1963); **40**, 2474, 2480, 2745 (1964).

We use a basis of pure atomic orbitals and neglect the overlap everywhere, as suggested by Pople and Santry. The Coulomb integrals $H_{ii} \equiv \alpha_i$ are chosen as valence-state ionization potentials^{9,10-12} ($\alpha_{2sC} = -21.4$ eV; $\alpha_{2pC} = -11.4$ eV; $\alpha_{2sN} = -26.0$ eV; $\alpha_{2pN} = -13.4$ eV; $\alpha_{1sH} = -13.6$ eV). A great number of relations between the off-diagonal elements, $H_{ij} \equiv \beta_{ij}$, and the corresponding overlap integral, S_{ij} , have been suggested. Most of them assume direct proportionality between these two quantities.^{9,13,14} Different algebraic relations have also been tried.¹⁵⁻¹⁷ The following one was found to be the most satisfactory.

$$H_{ij} = 1/2(H_{ii} + H_{jj})KS_{ij}(1 - |S_{ij}|) \quad (1)$$

In the preceding relation, K is an arbitrary parameter. Orbitals i and j belong to neighboring atoms. The advantage of this relation is that it gives potential energy surfaces with a minimum (compare with the case of diatomic molecules, e.g., H_2 , mentioned by Hoffmann (ref 8, footnote 10)). The overlap integrals were taken from the tables by Sahni and Cooley.¹⁸ The orbital exponents were chosen as 1.20 for H, 1.625 for C, and 1.95 for N.

The relationship between the extended Hückel theory and elaborate SCF calculations has been discussed by Boer, Newton, and Lipscomb.¹⁹ These authors conclude that the Hückel method is fairly well adapted to the calculation of dissociation energies. Their analysis supports the hope that the shape of the potential energy hypersurface (*i.e.*, the variation of the atomization energy with the internuclear distances) will be satisfactorily reproduced by the extended Hückel method if the necessary parameters (*i.e.*, K) are chosen for that purpose. But, conversely, the obtained wave function will yield poor results in the calculation of other quantities.

The parameters K were chosen to reproduce the energies of dissociation of the CC bond of $CH_3CH_3^+$ and of the CN bond of $CH_3NH_2^+$. In the case of CH and NH bonds, fairly extensive calculations were made on a series of small molecules, radicals, and ions. It was soon realized that different values of K had to be

given to bonds of a different nature. This agrees with the conclusions of Boer, *et al.* The values chosen were $K_{CC} = 0.37$; $K_{CN} = 0.55$; $K_{CH} = K_{NH} = 0.58$. The dissociation energies of the $C_2H_5NH_2^+$ ion obtained with these values are given in Table I.²⁰

The obtained agreement, together with the analysis of Boer, Newton, and Lipscomb, supports our hope that the main features of the potential energy hyper-surface will be reasonably well reproduced.

Molecular Geometries

The equilibrium internuclear distances depend essentially on the form of the relation between H_{ij} and S_{ij} . In the present approximation, the bond lengths are found to be the same in the neutral molecule and its molecular ion. The following values were calculated for all molecules, radicals, and ions: $R_{CH} = 1.10$ Å; $R_{NH} = 1.02$ Å; $R_{CC} = 1.22$ Å; $R_{C-N} = 1.06$ Å; $R_{C=N} = 1.01$ Å.

There is no barrier to internal rotation in the present approximation. The valence angles appear to be fairly well reproduced,²¹ the most conspicuous exception being the CH_3 radical which is predicted to have HCH angles of 110° , with an inversion barrier of 0.42 eV. The CH_3^+ ion and the excited CH_3^* radical, however, are predicted to be planar. Otherwise the method predicts inversion barriers of 0.70 eV for NH_3 , of 0.17 eV for CH_3NH_2 , and of 0.18 eV for $C_2H_5NH_2$. In the corresponding ions, the nitrogen atom is predicted to be coplanar with the atoms attached to it. The CNH_4^+ ion is found to have an ethylene-like structure. In the $C_2H_5^+$ ion, the stable configuration is predicted to be flat around the carbon of the methylene group.

Table I: Dissociation Energies

	Calcd, ev	Exptl., ^{1,20} ev
$C_2H_6^+ \rightarrow CH_3^+ + CH_3$	(1.85)	1.86 ± 0.07
$CH_3NH_2^+ \rightarrow CH_3^+ + NH_2$	(4.36)	4.35 ± 0.14
$C_2H_5NH_2^+ \rightarrow CH_2NH_2^+ + CH_3$	0.90	$0.8 - 1.0$
$C_2H_5NH_2^+ \rightarrow C_2H_5^+ + NH_2$	4.66	$\geq 4.4 \pm 0.2$
$C_2H_5NH_2^+ \rightarrow CH_3-CH=NH_2^+ + H$	3.08	3.0
$CH_3NH_2^+ \rightarrow CH_2NH_2^+ + H$	1.71	$1.63 - 1.90$

(9) J. A. Pople and D. P. Santry, *Mol. Phys.*, **7**, 269 (1964).

(10) G. Pilcher and H. A. Skinner, *J. Inorg. Nucl. Chem.*, **24**, 937 (1962).

(11) J. Hinze and H. H. Jaffé, *J. Am. Chem. Soc.*, **84**, 540 (1962); *J. Phys. Chem.*, **67**, 1501 (1963).

(12) H. O. Pritchard and H. A. Skinner, *Trans. Faraday Soc.*, **49**, 1254 (1953); *Chem. Rev.*, **55**, 745 (1955).

(13) M. Wolfsberg and L. Helmholz, *J. Chem. Phys.*, **20**, 837 (1952).

(14) L. L. Lohr and W. N. Lipscomb, *ibid.*, **38**, 1607 (1963); *J. Am. Chem. Soc.*, **85**, 240 (1963).

(15) L. C. Cusachs, *J. Chem. Phys.*, **43**, S157 (1965).

(16) M. Zerner and M. Gouterman, *Theoret. Chim. Acta*, **4**, 44 (1966).

(17) J. A. Pople, D. P. Santry, and G. A. Segal, *J. Chem. Phys.*, **43**, S129 (1965).

(18) R. C. Sahni and J. W. Cooley, "Derivation and Tabulation of Molecular Integrals," Supplement I, NASA Technical Note D-146-I.

(19) F. P. Boer, M. D. Newton, and W. N. Lipscomb, *Proc. Natl. Acad. Sci. U. S.*, **52**, 890 (1964).

(20) J. Collin and M. J. Franksin, unpublished results.

(21) J. C. Leclerc and J. C. Lorquet, *Theoret. Chim. Acta*, **6**, 91 (1966).

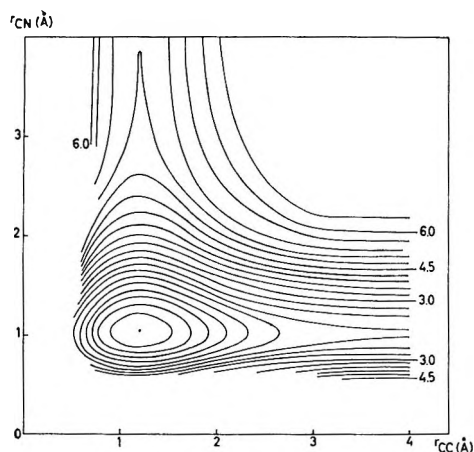


Figure 1. Contour map of the potential surface of $C_2H_5NH_2^+$ in its ground state. The contour interval is 0.3 ev.

Potential Energy Hypersurfaces of the $C_2H_5NH_2^+$ Ion

Ground State. Figure 1 represents a contour map of the potential energy surface as a function of the length of the CC and CN bonds. The contour interval is 0.3 ev. One sees immediately that the CC bond is more easily broken than the CN bond. The dissociation energies determined from this diagram are, respectively, 2.07 and 5.12 ev. These values are not directly comparable to the experimental ones, since the dissociating ion and its fragments are constrained to retain the same geometry as they had at the bottom of the surface (*i.e.*, tetrahedral angles for the carbon atoms, etc.) and are not allowed to assume their equilibrium configurations.

It is therefore necessary to correct Figure 1 and to calculate a surface representing the potential energy of the $C_2H_5NH_2^+$ ion as a function of the extension of the CC and CN bonds when the other atoms are allowed to relax to their equilibrium position during the dissociation process. We shall call it the "corrected" energy surface. It would be very tedious to vary every internuclear distance and angle for each point, and we only did this in two or three instances. We instead applied the following approximate correction method. (1) The bottom of the surface does not require any correction. (2) The points corresponding to the infinite extension of one of the bonds (*i.e.*, to dissociated fragments) were calculated in their correct configuration. (3) The energy of intermediate points was calculated with a Morse function as an interpolation function.

This process was tested in two or three instances by the more exact method of varying the geometries and found to be accurate within 0.01–0.03 ev.

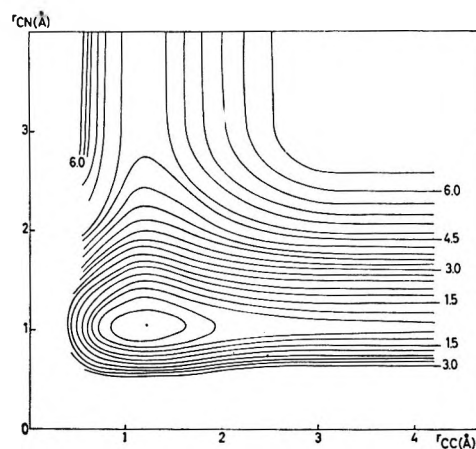


Figure 2. "Corrected" potential energy surface of $C_2H_5NH_2^+$ in its ground state. (The atoms are allowed to relax to their equilibrium positions during the dissociation process.) The contour interval is 0.3 ev.

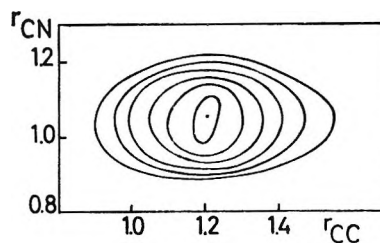


Figure 3. Bottom of the "corrected" potential energy surface of $C_2H_5NH_2^+$ in its ground state. The contour interval is 0.05 ev.

The final corrected potential surface is given in Figure 2. The corresponding dissociation energies are now 0.90 and 4.66 ev for the CC and CN bond, respectively, in good agreement with the experimental values.

The bottom of the corrected surface is reproduced on a greater scale on Figure 3. The contour interval is 0.05 ev. One sees that in the immediate neighborhood of the minimum (*i.e.*, for very small elongations) the contour lines are oriented along the CN bond, whereas for larger vibrational amplitudes they are oriented along the CC bond. In other words, the CN bond has the smallest force constant, but the CC bond dissociates first.

This stresses again the necessity of studying carefully the potential energy hypersurface in a certain range of internuclear distances and not only the point corresponding to the Franck–Condon transition in order to predict dissociation processes.

Electronically Excited States. It is well known that the Hückel method is not well adapted to the study of excited states. Errors by a factor of two or even

three may easily happen in the estimation of energy intervals. However the general behavior, which we shall presently describe, is believed to be significant.

The first excited state is calculated to be at 1.24 and 1.35 eV above the ground state for CH_3NH_2^+ and $\text{C}_2\text{H}_5\text{NH}_2^+$, respectively. According to the measurements of Al-Joboury and Turner,²² these figures should be 2.98 and 2.67 eV, respectively. From rpd measurements, Collin²³ determined a value of 2.90 eV for $\text{CH}_3\text{-NH}_2^+$. Similar experiments were not made for ethylamine, but the photoionization measurements of Hurzeler, Inghram, and Morrison^{2b} give a lower estimate of about 2 eV for this energy interval.

Immediately above this first excited state, we find a quasi-continuous set of electronic states (average spacing: 0.15 eV for CH_3NH_2^+ and 0.1 eV for $\text{C}_2\text{H}_5\text{-NH}_2^+$). This is in total disagreement with the values reported by Al-Joboury and Turner and by Collin, who both find energy intervals of the order of 1 or 2 eV above the first excited state. Our calculation may be in error by a factor of two or even three, as already said, but certainly not by a factor of ten. A calculation of the electronic levels of N_2^+ and CO^+ by the same method gave values in rough qualitative agreement with the spectroscopically reported levels. Furthermore, a more elaborate calculation would tend to increase the density of electronic states, since a Hückel calculation only deals with electronic configurations, which represent an average of several electronic states.

We therefore conclude that our results are qualitatively correct and that the values reported by Al-Joboury and Turner and by Collin and attributed by them to discrete levels are correct only for the first excited state. Beyond they correspond only to regions characterized by a high probability of transition within a continuum. This explanation is confirmed by the fact that the number of "states" detected by Al-Joboury and Turner does not increase with the complexity of the molecule. For example, they detect seven "states" for ethylamine and only four for cyclohexylamine. This is hardly understandable if we accept the current interpretation of these experiments.

We therefore restricted ourselves to the consideration of the lower envelope of the potential energy surfaces of the different excited states of the molecular ion. This corrected surface is given in Figure 4. The calculated dissociation energy of the CC bond is 0.20 eV (giving an excited CH_3 radical and the CH_2NH_2^+ ion in its ground state). The dissociation energy of the CN bond is calculated to be 4.34 eV (the fragments being an excited NH_2 radical and the C_2H_5^+ ion in its ground state).

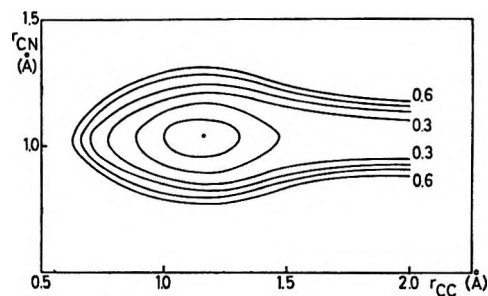


Figure 4. Envelope of the potential energy surfaces of the excited states of $\text{C}_2\text{H}_5\text{NH}_2^+$ (corrected). The contour interval is 0.1 eV.

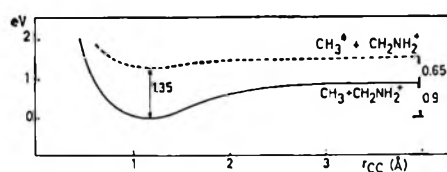


Figure 5. Cross section of the potential energy surfaces of the ground state and of the envelope of the excited states along the reaction coordinate.

Figure 5 shows a cross section of the potential energy surfaces of the ground state and of the envelope of the excited states along the reaction coordinate corresponding to the dissociation of the CC bond. The abscissas are not strictly comparable for the two curves, since they correspond to the stretching of the CC bond, together with the movement of the attached atoms towards the geometry of the final products, which is different for the two surfaces.

Radiationless Transitions

According to our calculations, stretching or bending the CC, CN, or CH bonds does not induce any crossing between the potential energy surfaces of the ground and first excited states. However it was found that the stretching, symmetrical or antisymmetrical, of the NH bonds leads to such an intersection. This happens even if the CC bond is simultaneously stretched. The crossing takes place, according to our calculations, when the NH bond reaches a value of 1.8–2.0 Å (a rather unreliable estimate, since our method is not adapted to the calculation of interatomic distances). The energy difference between the lowest point of intersection and the bottom of the potential energy surface of the ground state is of the order of 3 eV for CH_3NH_2^+ and 2.5 eV for $\text{C}_2\text{H}_5\text{NH}_2^+$ (same

(22) M. I. Al-Joboury and D. W. Turner, *J. Chem. Soc.*, 4434 (1964).

(23) J. Collin, IX Colloquium Spectroscopicum Internationale, 1961, p 596.

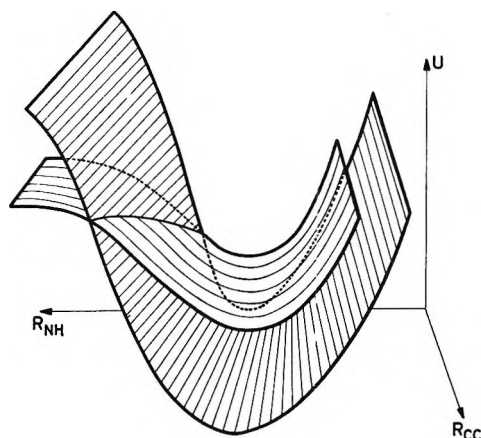


Figure 6. View of the potential energy surfaces of the ground state and of the envelope of the excited states of $C_2H_5NH_2^+$.

warning as above concerning the accuracy). These figures correspond to the antisymmetrical vibration of the NH bonds. The important point is that they are lower than the energy required for the next dissociation process (*i.e.*, loss of a hydrogen atom). Figure 6 pictures the situation.

Conclusions

The evolution of the $C_2H_5NH_2^+$ ion can be described as follows.

(a) Ions in their ground state will dissociate into a CH_3 radical and a $CH_2NH_2^+$ ion when the vibrational energy in the CC bond exceeds 0.9 eV.

(b) If the ion is created in an electronically excited

state, radiationless transitions will tend to convert this electronic energy into vibrational excitation, since the density of states is very high. Some of these states will be repulsive; others will be predissociated. The remaining ones will be converted to the first excited state. Dissociation of the CC bond in this state requires only a very low amount of energy (about 0.2 eV, according to our calculations). If a sufficient amount of vibrational energy, calculated as about 2.5 eV, affects the NH bonds, a further radiationless transition to the ground state of the ion becomes possible. The vibrational energy in excess of 0.9 eV will eventually find its way on the CC bond, and a dissociation of the latter bond will occur. The appearing fragments will carry a certain amount of kinetic energy, a lower estimate of which can be calculated as $2.5 - 0.9 = 1.6$ eV. One-third of this quantity (*i.e.*, about 0.5 eV) will affect the $CH_2NH_2^+$ ion. Preliminary measurements seem to confirm this prediction.²⁴

The previous description does not pretend to be a complete one, since other processes, such as autoionization, were not considered. Also the kinetics of these dissociations were not taken into consideration in this study.

Acknowledgment. The authors wish to thank Professor L. D'Or, Dr. J. Collin, and Dr. J. Momigny for many helpful discussions. This work has been supported by the Fonds de la Recherche Fondamentale Collective.

(24) J. Momigny, private communication.

Anion and pH Effects on the Potentials of Zero Charge of

Gold and Silver Electrodes

by D. D. Bodé, Jr., T. N. Andersen, and H. Eyring

Rate Processes Institute, University of Utah, Salt Lake City, Utah 84112 (Received June 3, 1966)

The open circuit scrape method was applied to the study of the potential of zero charge of gold and silver electrodes in aqueous solutions. With a scraper attached to a drill capable of 16,000 rpm, fresh electrode surfaces were exposed to aqueous salt solutions and transient potentials were measured. Through a study of pH and concentration effects, the conditions under which the transient peak potential (V_{pk}) is equal to the potential of zero charge (pzc) are determined. The dependence of V_{pk} on pH over certain parts of the pH range is explained by hydroxide ion adsorption or by Faradaic reactions. Over the pH range in which no rapid reactions were observed, V_{pk} was identified with the potential of zero charge. From these values, Esin and Markov profiles are given for various salts, and relative adsorbabilities for various anions are deduced.

Introduction

The open circuit scrape method has been applied to various solid metal electrodes in an attempt to ascertain the potential of zero excess charge on those metals.^{1,2} In this method, the entire surface of a solid metal electrode is scraped away rapidly and repetitively to produce zero charge conditions. If three criteria are satisfied, the potential of zero charge (pzc) is obtained as the transient peak potential (V_{pk}). (1) Adsorption must approach equilibrium before appreciable reaction occurs to change the electrode charge. (2) The experimental scraping and recording times must be sufficiently rapid to separate the adsorption and reaction processes. (3) A sufficient number of scrapes must be performed so that charge redistribution from the departing chips onto the fresh metal surface is negligible. These requirements were discussed by Perkins, *et al.*,² with respect to optimizing the experimental procedure toward these ends. Briefly, satisfaction of these criteria calls for rapid and continual scraping of an inert metal in a solution of simple ions. A tentative identification of V_{pk} with the pzc was based on (a) a constant V_{pk} independent of successively faster scraping speeds, (b) the realization of expected trends of V_{pk} with variation of ion types and concentrations, and (c) agreement of V_{pk} values with trustworthy pzc values obtained by other methods.³

In the work of the above authors,² a pH-dependent transient potential was observed for several metals with various salts. A conclusive explanation of this effect was not given, and hence the pzc could not be ascertained. In answer to the problems with pH, this work was undertaken.

In order to improve the work previously reported,² an air turbine-to-pulley operated drill was used, with a drill better fitted to the electrode geometry.⁴ The mechanical advantage and available speeds were greater than in the previous work, and continual electrode scraping was more nearly obtainable. Reactions which

(1) T. N. Andersen, R. S. Perkins, and H. Eyring, *J. Am. Chem. Soc.*, **86**, 4496 (1964).

(2) R. S. Perkins, R. C. Livingston, T. N. Andersen, and H. Eyring, *J. Phys. Chem.*, **69**, 3329 (1965).

(3) Since a wide range of pzc values are obtained by various investigators for solid electrodes, agreement with some such values is often not convincing. However, since the preparation of this manuscript, solid gallium has been scraped in this laboratory (R. S. Perkins, Ph.D. Thesis, 1967) with resulting peak potentials of -0.63 , -0.70 , and -0.73 v. nhe for 0.9 N $\text{Na}_2\text{SO}_4 + 0.1$ N H_2SO_4 , 0.9 N $\text{KCl} + 0.1$ N HCl , and 0.9 N $\text{KBr} + 0.1$ N HCl , respectively. These values are in good agreement with the potentials of the electrocapillary maximum (-0.65 , -0.73 , and -0.76 v, respectively) obtained in the same respective solutions for liquid gallium (A. Frumkin, N. Polianovskaya, N. Grigorgev, and I. Bagstskaya, *Electrochim. Acta*, **10**, 793 (1965)). Capacity studies on solid and liquid gallium (D. E. Leikis and E. C. Sevastianov, *Dokl. Akad. Nauk SSSR*, **144**, 1320 (1962)) indicate that the electrical double layer is similar for the liquid and crystalline materials.

(4) D. D. Bodé, Jr., Ph.D. Thesis, University of Utah, 1966.

interfered with the present measurement of the pzc were investigated, and it was found that the scraper could suppress the potentials arising from reaction current densities less than 0.2 ma/cm^2 . Thus this work establishes the limitations associated with criterion 2.

Experimental Section

The apparatus consisted of the drill, the reference electrode, the cell, and the recording instruments. The last three parts have been discussed by Perkins, *et al.*²

Scraping was accomplished by a Midwest handpiece which geared down an air turbine of 100,000 rpm to run a 0.090-in. centerless ground sapphire bit at 16,000 rpm as determined by measurement with a stroboscope. The mechanical advantage of the handpiece allowed cutting away of the entire surface of the 0.020-in. diameter electrode wire, exposing a new cross section, without reducing the speed below 14,500 rpm. The drill extended into the cell from the top and was connected to the main compartment by means of a nitrogen-filled inflated polyethylene bag which served as the cell lid. The electrode, which was forced through a Teflon rod, entered the cell from the bottom. The sapphire bit was ground to a sharp cutting edge, and the scraping bit more than covered the cross section of wire, easily removing the entire surface with each half revolution.

Solutions were prepared from either reagent grade or purer salts and the water was redistilled from a basic permanganate solution.

Potentials were recorded in volts *vs.* the normal hydrogen electrode (nhe) using the I.U.P.A.C. Stockholm sign convention. The reproducibility, as determined by repetitive experiments, was $\pm 15 \text{ mv}$ for gold and $\pm 20 \text{ mv}$ for silver. The greater range for silver resulted from decreasing the sensitivity of the dynograph recording instrument in order that the much larger transient differences from the steady state to the peak potential could be recorded. Junction potentials were omitted since by the use of a salt bridge they were smaller than the experimental deviations. The temperature was $23 \pm 2^\circ$. The procedure was described by Perkins, *et al.*²

Experimental Results and Discussion

Plots were made of the peak potential *vs.* pH (see Figure 1) to help clarify the relationship between V_{pk} and the potential at zero charge. We used 0.1 *N* salt solutions to which NaOH or the acid of the salt was added. The scraper was observed to outrun the decay-producing reactions (the steady-state potential was positive with respect to V_{pk}) over the entire chlo-

ride curve. This was also true for all the other solutions except in the "acidic" range where the peak potentials deviate from the horizontal. This adequacy of the scraper's speed was evident both from visual inspection of the decay rates and from experimental variation of the scraping speed. Since we outrun the interfering reactions (which are to be discussed shortly), we tentatively identify V_{pk} with the potential of zero charge for all portions of the curves of Figure 1 except for values of $\text{pH} < \sim 3$ in the case of I^- , Br^- , ClO_4^- , and SO_4^{2-} . The remainder of this work serves to justify this identification. From a consideration of the relative adsorbabilities of the various anions and the results of Figure 1, it is concluded that OH^- ions coadsorb in the alkaline region and manifest themselves in the case of solutions containing ions less adsorbable than the OH^- ion such as F^- , SO_4^{2-} , ClO_4^- , and Cl^- . This conclusion is substantiated by Figure 2, which shows V_{pk} *vs.* the activity of NaCl, HCl, and NaOH. Again, the reactions are slow compared to the scraping speed and again V_{pk} measures the pzc. It is seen that the pzc of NaOH is negative with respect to the potential for NaCl, at all concentrations. From Figures 1 and 2 we see that the V_{pk} (= pzc) values for NaCl, HCl, and LiCl are identical. In the case of mercury there is an analogous lack of dependence of the pzc on the ion size for these and other small cations.⁵ Since the assumption of negligible specific adsorption of these cations on mercury at the pzc is consistent with experimental results, we might make the same prediction for the gold electrode. The order of specific adsorption of the various anions on gold may be seen

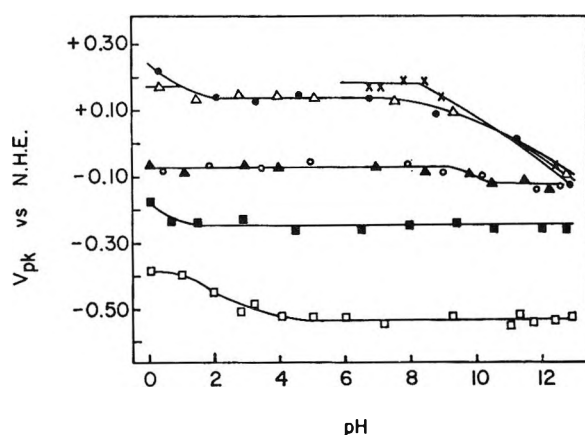


Figure 1. Peak potential *vs.* pH for 0.1 *N* solutions for the gold electrode: X, NaF; Δ , Na_2SO_4 ; \bullet , NaClO_4 ; \blacktriangle , NaCl; \circ , LiCl; \blacksquare , NaBr; \square , NaI.

(5) D. C. Grahame, E. M. Coffin, J. I. Cummings, and M. A. Poth, *J. Am. Chem. Soc.*, **74**, 1207 (1952).

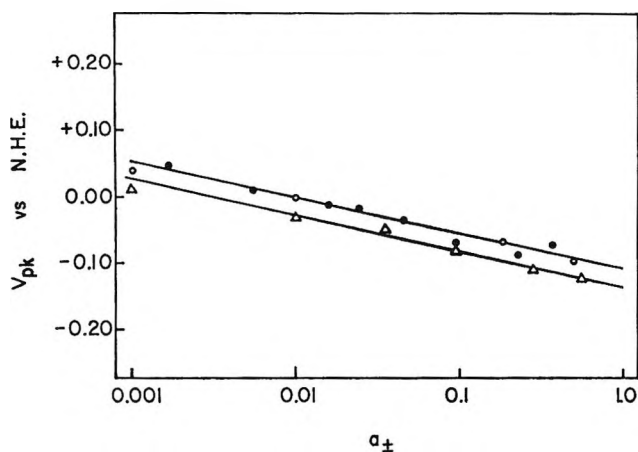


Figure 2. Peak potential vs. $\log a_{\pm}$ for the gold electrode: ●, NaCl; ○, HCl; △, NaOH.

from the relative positions and slopes of the V_{pk} (=pzc) vs. \log activity plots shown in Figure 3. The slopes of these lines are -0.050 , -0.045 , -0.040 , 0.025 , and -0.020 v for I^- , Br^- , Cl^- , $SO_4^{2-} = ClO_4^-$ and F^- , respectively. The V_{pk} values and hence potentials of zero charge have, for the 0.1 N solutions, the values -0.53 , -0.24 , -0.07 , 0.14 , 0.14 , and 0.19 , respectively.

It is interesting that for mercury the pzc of 0.1 N HCl, KCl, and KF are -0.224 , -0.225 , and -0.191 v.⁵ In these cases the specific adsorption of anions is approximately 2 $\mu\text{coulombs/cm}^2$ for Cl^- ,^{6,7} and 0.0 $\mu\text{coulombs/cm}^2$ for F^- .⁶ Since the pzc for 0.1 N KOH is -0.197 v,⁵ one would infer that OH^- ions are only slightly adsorbed. However, on the gold electrode, V_{pk} values of -0.07 , -0.07 , -0.09 , and 0.19 v are observed for 0.1 N HCl, NaCl, NaOH, and NaF, respectively (cf. Figures 1-3), indicating that OH^- ions are significantly adsorbed. It is also noted that the relative adsorbability of the ClO_4^- ion as compared to other anions is not the same on mercury and on gold. Thus, for mercury the order of adsorption according to increasing pzc and decreasing amount of adsorbed ions, is⁵⁻⁸ $I^- > Br^- > ClO_4^- > Cl^- > OH^- > SO_4^{2-} > F^-$, while for gold we conclude that $I^- > Br^- > OH^- > Cl^- > ClO_4^- = SO_4^{2-} > F^-$.

In the acid region (Figure 1), the V_{pk} , for several solutions is observed to increase with decreasing pH. This corresponds to the occurrence of a Faradaic reaction at the electrode which removes electrons and causes an anodic shift of the potential before the V_{pk} can be measured. Decay times, when the scraper was stopped, were faster, as one would expect. The hydrogen evolution reaction (h.e.r.), in NaBr and NaI solutions, having V_{pk} values hundreds of millivolts

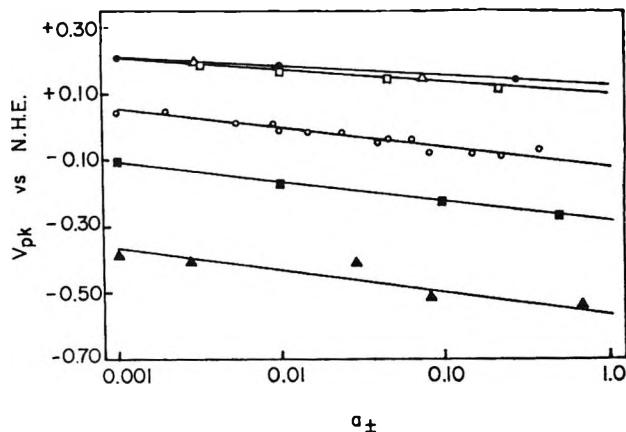


Figure 3. Peak potential vs. $\log a_{\pm}$ for the gold electrode: ●, NaF; □, Na_2SO_4 ; △, $NaClO_4$; ○, NaCl; ■, NaBr; ▲, NaI.

negative with respect to the reversible hydrogen potential, is such a fast reaction. The curve for the sulfate solution levels off at 0.18 v. This is attributed to competition for control of the potential between anion adsorption and reduction of sulfate to sulfurous acid, for which the reversible potential is 0.17 v.⁹ The anodic rise in the curve for $NaClO_4$ in the acid region corresponds to reduction of perchlorate. Finally, the fluoride salt was not studied in the acid region owing to the deleterious effect of HF on glass.

By observing Figure 4, one notes that the order of adsorbability for anions on silver must be $Br^- > Cl^- > ClO_4^-$ having V_{pk} vs. $\log a_{\pm}$ slopes of -0.050 , -0.048 , and -0.040 v, respectively. The peak potential values for 0.1 N solutions of these anions are -0.78 , -0.62 , and -0.48 v, respectively. These results are obtained from Figure 4. It was found for Ag that again the V_{pk} was independent of whether a lithium or sodium salt was employed.

The lines of Figure 4 begin to bend anodically with increasing concentration. Since all V_{pk} values are significantly negative with respect to the reversible hydrogen potential, it appears that reduction of water occurs. That a fast reaction is occurring is supported by the increase in the decay rates. The reason for the faster hydrogen evolution in more concentrated salt solutions is that the total potential difference between metal and solution is not controlling but rather $\phi_M - \phi_2$ where ϕ_M is the potential of the metal (taken

(6) D. C. Grahame and B. A. Soderberg, *J. Chem. Phys.*, **22**, 449 (1954).

(7) H. Wroblowa, Z. Kovac, and J. O'M. Bockris, *Trans. Faraday Soc.*, **61**, 1523 (1965).

(8) D. C. Grahame, *J. Am. Chem. Soc.*, **80**, 4201 (1958).

(9) A. J. deBethune and N. A. S. Loud, "Standard Aqueous Electrode Potentials and Temperature Coefficients at 25°C ," Clifford A. Hampel, Publisher, Skokie, Ill., 1964.

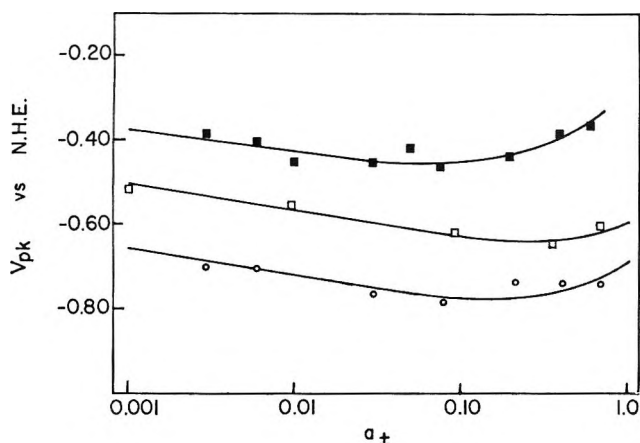


Figure 4. Peak potential vs. $\log a_{\pm}$ for the silver electrode: \blacksquare , NaClO_4 ; \square , NaCl ; \circ , NaBr .

to be constant) and where ϕ_2 is the potential of the outer Helmholtz plane. Both potentials are measured with respect to the solution^{10,11} (see eq 3). In more concentrated solutions, the potential $\phi_M - \phi_2$ increases with increased ion adsorption and so there is a faster discharge of electrons from the metal. The scraper cannot outrun this discharge of hydrogen ions or reduction of adsorbed anions and so the effect is an anodic trend away from the expected V_{pk} .

A study with HCl , NaCl , and NaOH was made (see Figure 5) to ascertain whether a dependence of V_{pk} and the pzc on the hydrogen ion activity should occur on silver. The presence of a sodium or hydronium cation made no difference in the dilute region. However, with a small increase in concentration, an anodic trend was observed for HCl . For NaCl and NaOH this was observed in the more concentrated region. The hydronium ion is being discharged in the acid case, and water in the cases of the salt and base. At the minimum of the curve (Figure 5), the scraping speed is equivalent to the rate of the h.e.r.

If the scraper is capable of preventing the effects of a given current density due to hydrogen evolution, then at the peak of the curve the speed of the scraper should be determinable from the difference between the expected potential and that actually measured. By extrapolating the lines on both sides of the minimum in 0.003 N HCl in Figure 5, it is found that there is a 10-mv difference between the observed and expected value of V_{pk} at the minimum of the curve. This means that some amount of charge, dq , must have been transferred to change the voltage by δV . Under open circuit conditions

$$i_{\text{ext}} = 0 = dq/dt + \Sigma i_{\text{cath}} - \Sigma i_{\text{anod}} \quad (1)$$

where dq/dt is the rate of change of charge on the elec-

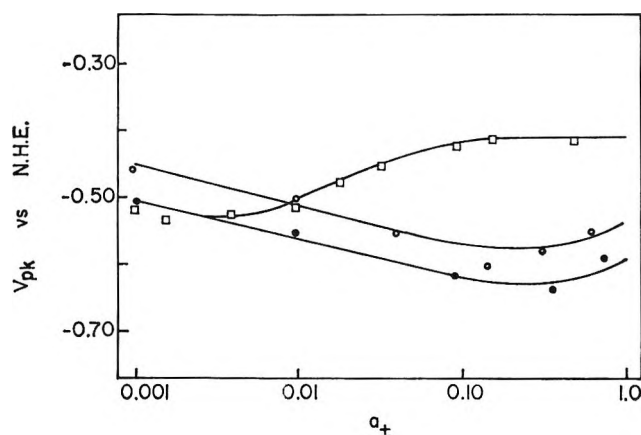


Figure 5. Peak potential vs. $\log a_{\pm}$ for the silver electrode: \square , HCl ; \circ , NaOH ; \bullet , NaCl .

trode and Σi_{cath} and Σi_{anod} are the summations of the currents produced by all cathodic and anodic reactions, respectively. For an electrode potentiostated at V_{pk} with the current i_{pk} , we have $dq/dt = 0$. Hence

$$i_{pk} = \Sigma i_{\text{cath}} - \Sigma i_{\text{anod}} \quad (2)$$

but this quantity is equal to dq/dt at V_{pk} when the electrode is on open circuit. The potential is sufficiently negative of the reversible hydrogen potential that the anodic current can be neglected; therefore, the external current should be nearly equal to the cathodic current. Hence, the time to remove the charge dq is $dt = C_{dl} \delta V / i_{pk}$, where C_{dl} is the capacitance of the double layer. This is then the time for a half-revolution of the scraper, and the inverse of dt is a measure of the rpm of the drill. It is assumed that a single coverage is reduced with each scrape. The capacitance for HCl on silver has not been reported but it must be approximately $80 \mu\text{f}/\text{cm}^2$ as it is for $1.0 N$ NaClO_4 .¹² The two solutions have nearly the same V_{pk} and should have similar double-layer structures. The calculated speed for the scraper is 14,000 rpm, in excellent agreement with the stroboscopically found value of 14,500 rpm. Hence, the scraper can outrun or prevent significant effects from currents below $0.2 \text{ ma}/\text{cm}^2$. Thus a departure from linearity appears when the V_{pk} vs. $\log a_{\pm}$ plot fails to be a true Esin and Markov (*i.e.*, a linear pzc vs. $\log a_{\pm}$) profile, and when V_{pk} fails to give the pzc.

(10) P. Delahay, "Double Layer and Electrode Kinetics," Interscience Publishers Inc., New York, N. Y., 1965.

(11) A. N. Frumkin, "Hydrogen Overvoltage and Adsorption Phenomena," in "Advances in Electrochemistry and Electrochemical Engineering," Vol. I, P. Delahay and C. W. Tobias, Ed., Interscience Publishers Inc., New York, N. Y., 1961.

(12) L. Ramaley and C. G. Enke, *J. Electrochem. Soc.*, **112**, 945 (1965).

As the h.e.r. begins to determine the V_{pk} of silver, the anodic change from the expected peak potential increases exponentially. This is discussed in detail later. In more concentrated solutions, the V_{pk} becomes independent of the acid concentration. The competition for potential control by adsorption of anions and by charge transfer from the h.e.r. results in the potential becoming independent of concentration. In the basic region, reduction of water is expected.¹³

It has been deduced that the order of adsorbability on silver for anions is $Br^- > Cl^- > OH^- > ClO_4^-$. It should be noted that there is a change in relative adsorbabilities for chloride and hydroxide in going from gold to silver. That is, for gold OH^- is more adsorbed than Cl^- , but the opposite is true for silver. Thus, there should be a marked difference in the dependence of V_{pk} on pH. Referring to Figure 6, one can observe in the neutral region that for NaCl the V_{pk} is more negative than for Na_2SO_4 and both of these are more cathodic than for 0.1 N $NaClO_4$. There is a cathodic trend in the basic region of the sulfate salt but not for the chloride since OH^- is more adsorbed than SO_4^{2-} but less than Cl^- . All have anodic trends in the acid region. Agreement is found between the concentration of HCl in Figure 4 and the pH in Figure 6 for which the h.e.r. begins to be potential-determining. In the neutral region, the V_{pk} can be identified with the pzc. Combining all of the results, the V_{pk} values for Br^- , Cl^- , OH^- , SO_4^{2-} , and ClO_4^- are, for 0.1 N solutions, -0.78 , -0.62 , -0.58 , -0.56 , and -0.48 v, respectively.

It has been pointed out that H_3O^+ reduction can cause the V_{pk} to differ from the pzc. H_3O^+ reduction is aided by anion adsorption, which increases $\phi_M - \phi_2$ in the cathodic charge-transfer equation

$$i_c = ka_{H_b} F \exp(-(\phi_M - \phi_2)\alpha F/RT) \quad (3)$$

Here the rate constant is k and α is the transfer coefficient.^{14,15} The activity of hydrogen ions in the solution is $a_{H_b^+}$ and is assumed, for simplicity of the calculation, to be the same in the preelectrode state where the potential is ϕ_2 . At the activity $a_{H_b^+}$, the reaction i_c can cause an increase in potential between scraping and measurement of approximately

$$\delta V = i_c t / C_{d1} \quad (4)$$

Here t is the time of a half-revolution of the scraper and C_{d1} is again the differential capacity of the double layer. The change in the potential then is $V = V_{pk} + \delta V$. At the increased HCl concentration of $(a_{H_b^+} + \Delta a_{H_b^+})$ the double-layer potential has decreased from $\phi_M - \phi_2$ to a new value of $\phi_M - \phi_2 + \Delta\phi$ due to increased

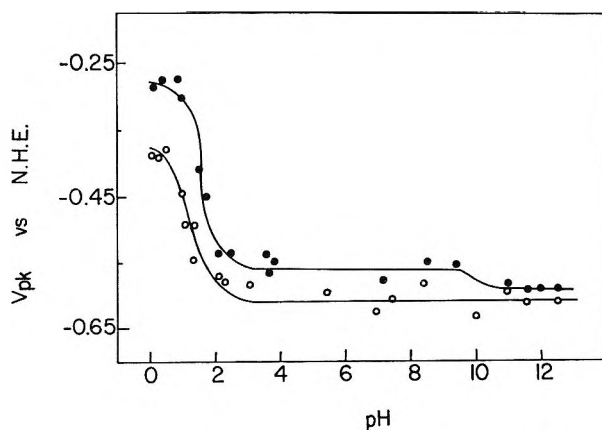


Figure 6. Peak potential vs. pH for the silver electrode: ●, Na_2SO_4 ; ○, LiCl.

anion adsorption (where $\Delta\phi$ is negative). The current now equals

$$i_c' = i_c(a_{H_b^+} + \Delta a_{H_b^+})a_{H_b^+}^{-1} \exp(-\alpha f \Delta\phi) \quad (5)$$

where $f = F/RT$. It can be shown from the work of Grahame with KI on mercury⁸ that the potential difference $\phi_M - \phi_2 = k' \ln a_{I^-}$ approximately. Accordingly, $\Delta\phi = k' \Delta \ln a_{\pm}$. The anodic shift from the pzc then becomes

$$\delta V' = [i_c t (a_{H_b^+} + \Delta a_{H_b^+}) \exp(-\alpha f k' \Delta \ln a_{\pm})] / (C_{d1} a_{H_b^+}) \quad (6)$$

Thus the interference ($\delta V'$) increases exponentially with $\ln a_{\pm}$ whereas the total potential difference is expected to decrease linearly with $\ln a_{\pm}$ as in the Esin and Markov profile. This lends support to the discussion of Figures 4 and 5 in which the deviation of V_{pk} from a linear profile was attributed to the h.e.r.

Ramaley and Enke observe that for mercury with a 1 M $NaClO_4$ solution, the pzc falls within 25 mv of the capacitance hump.¹² They obtained a capacitance hump on silver at about -0.60 v in the 1 M perchlorate solution. Their conclusion is that the double layers of Hg and Ag in these solutions are quite similar. According to their argument, the pzc of silver should lie near the capacitance hump. Several pzc values on silver have been measured, but only that of Leikis¹⁶

(13) M. A. V. Devanathan, J. O'M. Bockris, and W. J. Mehl, *J. Electroanal. Chem.*, **1**, 143 (1959).

(14) S. Glasstone, K. J. Laidler, and H. Eyring, "The Theory of Rate Processes," McGraw-Hill Book Co., Inc., New York, N. Y., 1941.

(15) B. E. Conway, "Electrode Processes," Ronald Press, New York, N. Y., 1965.

(16) D. I. Leikis, *Dokl. Akad. Nauk SSSR*, **135**, 429 (1960).

lies near the values sought. The open circuit scrape method, found by extrapolating Figure 4, gives a zero charge potential of -0.54 v for $1 M$ NaClO_4 .

The order of relative adsorbabilities of anions differs for gold and silver and the effects of Faradaic processes are more in evidence for silver. The pH effect was seen to arise both from reactions and adsorption of anions.

Conclusions

In this work the extent of interference with the measurement of the zero charge potential by Faradaic reactions has been considered. It was seen that the point where the scraping speed equaled the rate of significant h.e.r. could be used to estimate the scraping speed. This verification lends further support to the conclusion that when the linear Esin and Markov profile is obtained over a range of concentrations the effects of reactions are negligible and V_{pk} can be equated to the pzc.

Variations of the V_{pk} with pH can be attributed to both adsorption and reaction phenomena. In the absence of pH variation at constant salt concentration (the horizontal sections of Figures 1 and 6) the transient peak potential may be considered to be the potential

of zero charge for the solution without interference from the OH^- ions. In the basic region, V_{pk} represents the pzc for mixed adsorption of anions and of OH^- .

Further refinements are under way and will be reported presently. The presence of large cations has a marked effect on V_{pk} by making a more cathodic transient potential than do Na^+ or Li^+ ions. The cause of this is under study.

The pzc values reported in this work differ somewhat from those of the introductory paper.² However, the earlier values were obtained with a manual scraper or a power scraper, both of which are slower and less effective at rapidly removing the entire surface of the electrode wire than the drill used here is. Moreover, this drill is more capable of stirring the solution near the electrode and so prevents large concentration gradients at the interphase leading to improved values for the zero charge potential.

Acknowledgments. The authors wish to acknowledge the National Aeronautics and Space Administration Grant No. NaG (T-79) for financial support for this project. T. N. A. also wishes to acknowledge financial support from the U. S. Atomic Energy Commission under Contract No. AT (11-1) 1144.

Photochemistry of Complex Ions. IV. The Role of Quartet Excited States in the Photochemistry of Chromium(III) Complexes

by Arthur W. Adamson

Department of Chemistry, University of Southern California, Los Angeles, California (Received June 6, 1966)

The photochemistry of Cr(III) complexes is reviewed with particular attention to those systems which exhibit a wavelength dependence of their photolytic behavior. For such cases, at least, it appears necessary to accept that, depending on the wavelength involved, different electronic states function as intermediates differently disposed to chemical reaction. It is proposed that the lifetime of quartet excited states may be longer than that expected from an absorption band area calculation, at least in the case of certain asymmetric complexes. Excited-state distortion is suggested to be potentially important in determining the relative importance of emission, photolytic, and radiationless deactivation processes and the rate of distortional relaxation, their relative temperature dependence. Some semiempirical rules are adduced which are useful in predicting which photolytic process will dominate, where more than one is possible.

The photochemistry of Cr(III) complexes has interested several investigators, and there is perhaps more information now available on the effect of visible light on these compounds than on those of any other transition metal. Their photochemistry is particularly simple in that only substitution-type reactions are observed, *i.e.*, solvation, isomerization, and racemization. By contrast, Co(III) complexes may show a good deal of photooxidation-reduction behavior as well,¹ and similarly with Fe(III) complexes [*e.g.*, $\text{Fe}(\text{C}_2\text{O}_4)_3^{3-}$]² and those of Pt(IV).³ Only scattered examples have been reported for other transition metal compounds.

In the case of Co(III) compounds there is sufficient evidence to make it reasonably clear that the occurrence of photooxidation-reduction correlates with the presence of some charge-transfer character in the "ligand field" absorption bands.¹ These complications in nature of spectra and photochemistry appear to be absent in the case of Cr(III) complexes although, surely, they will occur if light of short enough wavelength is used. One hopes, then, that the behavior of the Cr(III) family of complexes will be relatively easy to understand, and some fairly simple analyses have been advanced.⁴⁻⁷ It is purpose of this paper to show that these are not entirely adequate and to propose some further considerations.

Absorption Spectra and Term System

A typical absorption spectrum for a Cr(III) complex of O_h symmetry is sketched in Figure 1. Such spectra characteristically show (a) two (at least) broad bands of molar extinction coefficient around 30 to 100 and (b) one or more weak features around 700 $m\mu$ which may appear as shoulders on the tail of the nearest broad band. A portion of the term system provided by ligand field theory is given in Figure 2, for the case of O_h symmetry, along with an indication of the various types of processes that may occur and a rough energy scale. These details are discussed below, but for the moment it is sufficient to note that the broad bands are thus ascribed to ${}^4A_{2g} \rightarrow {}^4T_{2g}$ and ${}^4A_{2g} \rightarrow {}^4T_{1g}$ transitions; they will be denoted as L_1 and L_2 in this paper.

It is a practical observation that such complexes as

- (1) A. W. Adamson, *Discussions Faraday Soc.*, **29**, 163 (1960).
- (2) C. A. Parker and C. G. Hatchard, *J. Phys. Chem.*, **63**, 22 (1959).
- (3) S. Penkett and A. W. Adamson, *J. Am. Chem. Soc.*, **87**, 2514 (1965).
- (4) A. W. Adamson, *J. Inorg. Nucl. Chem.*, **13**, 275 (1960).
- (5) A. W. Adamson, *Advances in Chemistry Series*, No. 49, American Chemical Society, Washington, D. C., 1965.
- (6) R. A. Plane and J. P. Hunt, *J. Am. Chem. Soc.*, **79**, 3343 (1957).
- (7) H. L. Schläfer, *J. Phys. Chem.*, **69**, 2201 (1965) (and earlier papers).

Table I: Photochemistry of Cr(III) Complexes of O_h Symmetry^a

Ligand complex	Absorption			Quantum yield, 25°		Activation energy, kcal/mole	Ref
	L ₂	L ₁	D ₁	L ₁	L ₂		
Urea	444	620	700	L ₁ 0.10 L ₂ 0.10 D ₁ 0.095		3	10
H ₂ O	408	574	669	L ₁ 0.12-0.18 L ₂ 0.06-0.18		Ca. 13	6
C ₂ O ₄ ²⁻	417	571	698	L ₁ 0.1 (15°) L ₂ 0.1 (15°)		3.1	b
NCS ⁻	421	567		L ₁ 0.27 L ₂ 0.26			10
NH ₃	354	466	655.5	L ₁ L ₂ 0.29 L ₁ 0.26 D 1.3		0	11 10 c
en	350	451	671.5	0.29 (652 mμ) L ₁ 0.47 L ₂ 0.55			10 d
CN ⁻	309	376	810	L ₁ 0.3			e

^a The values for $\text{Cr}(\text{H}_2\text{O})_6^{3+}$ reported in ref 6 are for exchange of 6 waters; they have been multiplied by 6 to be consistent with the other entries; the activation energy figure of 13 kcal/mole is somewhat uncertain because of the scatter of the data. ^b S. T. Spees and A. W. Adamson, *Inorg. Chem.*, **1**, 531 (1962); these quantum yields are for racemization, for which the breaking of a Cr-O bond is assumed to be rate controlling. ^c M. R. Edelson and R. A. Plane, *J. Phys. Chem.*, **63**, 327 (1959). ^d E. Nikolaiski, Thesis, University of Frankfurt am Main, 1962. ^e A. W. Adamson and A. Chen, unpublished results.

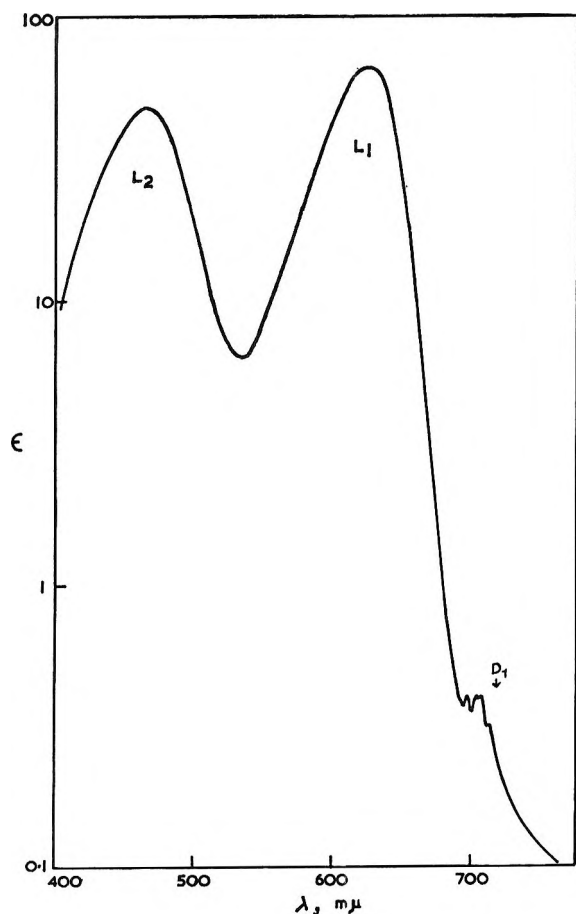


Figure 1. Schematic typical absorption spectrum for a Cr(III) complex.

$\text{Cr}(\text{CN})_6^{3-}$, $\text{Cr}(\text{H}_2\text{O})_6^{3+}$, $\text{Cr}(\text{NH}_3)_6^{3+}$, and even $\text{Cr}(\text{en})_3^{3+}$ have effective O_h symmetry. That is, only the coordinative symmetry, or that of the atoms directly bound to the central metal ion, seems to be of importance in first order. However, in the case of species of lower coordinative symmetry, additional splitting occurs.⁸

The weak, long wavelength features, generally called the doublet band, are ascribed to the transition ${}^4A_{2g} \rightarrow {}^2E_g$ (or ${}^2T_{1g}$), which is vibronic.⁹ The longest wavelength feature of the group will be designated here as D_1 .

Photochemistry of O_h Complexes

The known photochemistry of Cr(III) complexes of O_h coordinative symmetry is summarized in Table I. The only photolysis reaction observed in these aqueous systems is that of aquation (or racemization, in the case of the trisoxalato complex). Entries are in the order of decreasing wavelength of the L_1 band, which is then also that of increasing ligand field strength (or position in the spectrochemical series), and the quantum yields are seen generally to increase slightly in the same order. For a given species, the yield is nearly independent of wavelength, although detailed results for Cr-

(8) C. J. Ballhausen, "Introduction to Ligand Field Theory," McGraw-Hill Book Co., Inc., New York, N. Y., 1962.

(9) A. W. Adamson and T. M. Dunn, *J. Mol. Spectry.*, **18**, 83 (1965).

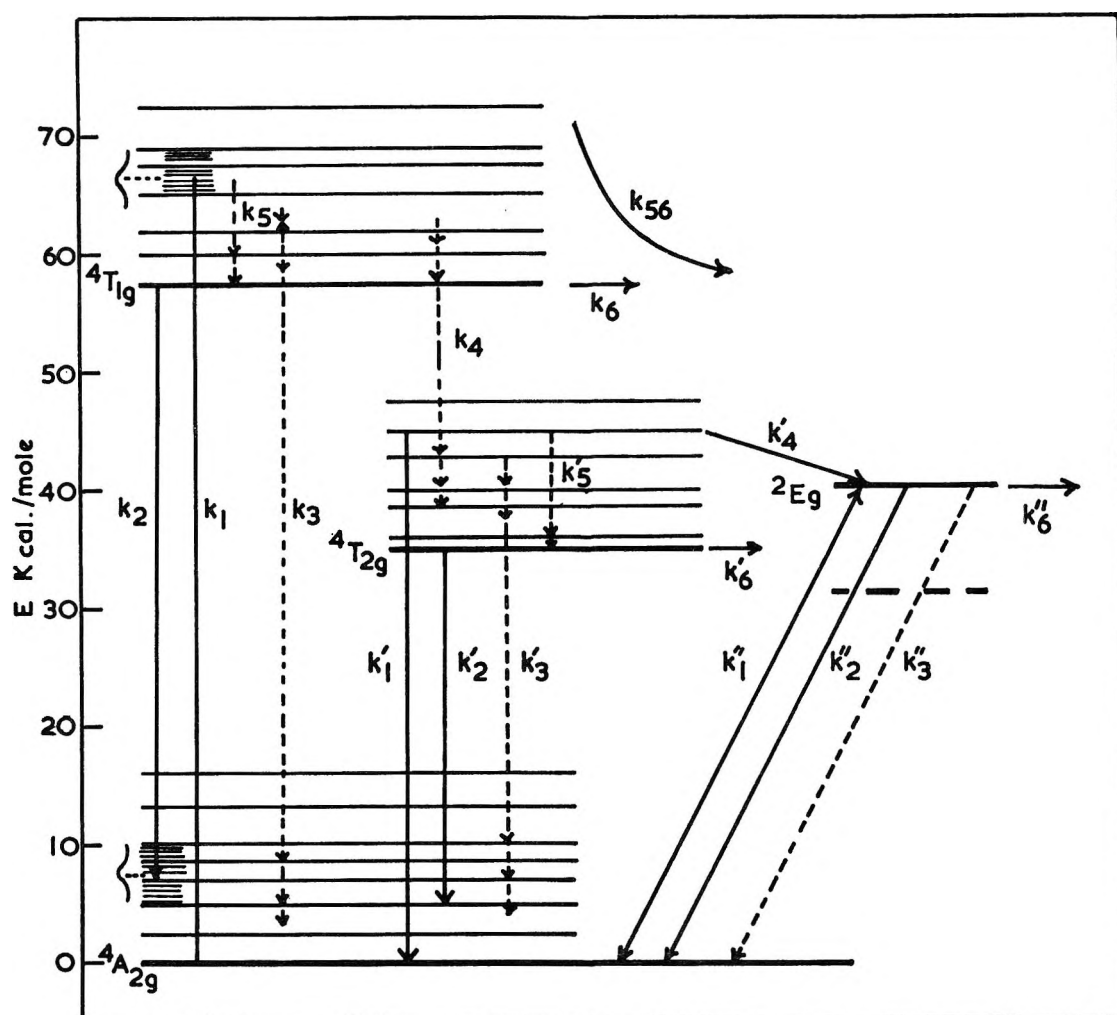


Figure 2. Energy level diagram for Cr(III) complexes. Absorption: k_1, k_1', k_1'' ; emission, k_2, k_2', k_2'' ; radiationless deactivation; k_3, k_3', k_3'' ; radiationless inter- and intralevel crossings: k_4, k_4' ; thermal equilibration: k_5, k_5' ; chemical reaction: k_6, k_6', k_6'' ; reactive deactivation: k_{56} (and k_{56}', k_{56}'' , not shown).

(urea) $_6^{3+}$ showed perhaps 10% variations from peak to trough in the region of the L bands.¹⁰

It is known that in low-temperature rigid media, fairly efficient conversion can occur from the excited quartet states to the doublet state,^{11,12} and it has been proposed that the same is true in solution at room temperature. The doublet state then undergoes chemical reaction. The mechanism explains the relative independence of quantum yield on wavelength if it is assumed that the efficiencies of the conversion processes k_4, d'_4 are high.^{6,13}

The doublet intermediate mechanism has recently been expounded very well⁷ and need not be elaborated on here. It is, however, somewhat disappointing, from the viewpoint of this hypothesis, that in no case does it appear that an actual rise in quantum yield occurs on direct excitation of the doublet excited state.

In some cases this situation could be attributed to the fact that most of the absorption is actually due to the tail of the L_1 and, but in the case of $\text{Cr}(\text{NH}_3)_6^{3+}$, for which the doublet features account for more than half of the absorption,⁹ a careful determination showed no significant effect.¹⁰

Photochemistry of Non- O_h Complexes. Empirical Rules

As summarized in Table II, Cr(III) complexes of lower than O_h coordinative symmetry exhibit a much

(10) E. Wegner and A. W. Adamson, *J. Am. Chem. Soc.*, **88**, 394 (1966).

(11) G. B. Porter and H. L. Schläfer, *Z. Physik. Chem.*, **37**, 109 (1963).

(12) K. de Armond and L. E. Forster, *Spectrochim. Acta*, **19**, 1687 (1963).

(13) H. L. Schläfer, *Z. Physik. Chem. (Frankfurt)*, **11**, 65 (1957); *Z. Elektrochem.*, **64**, 887 (1960).

Table II: Photochemistry of Cr(III) Complexes Not of O_h Symmetry

Complex Absorption max (L_2 , L_1 , D_1 in $m\mu$)	Quantum yield at 25°	Mode ^a	Activation energy, kcal/mole	Ref
Cr(NH ₃) ₆ (H ₂ O) ³⁺ (360, 484, 655)	L ₁ 0.15	NH ₃	0	b
	L ₁ L ₂ 0.17-0.20	NH ₃	0	
Cr(NH ₃) ₄ (H ₂ O) ₂ ³⁺ (368, 494, 657)	L ₁ L ₂ 0.14	NH ₃	0	b
	L ₂ 0.15	NH ₃	0	
Cr(NH ₃) ₃ (H ₂ O) ₃ ³⁺ (378, 508, 657)	L ₁ L ₂ 0.014	NH ₃	0	b
	L ₁ 0.019	NH ₃	0	
Cr(NH ₃) ₂ (H ₂ O) ₄ ³⁺ (384, 535, 660)	L ₂ 0.015	NH ₃	0	b
	L ₁ L ₂ 0.0018	NH ₃	0	
Cr(NH ₃) ₅ (NCS) ²⁺ (357, 482, ca. 650)	L ₁ 0.0017	NH ₃	0	b
	L ₂ 0.0024	NH ₃	0	
Cr(H ₂ O) ₆ (NCS) ²⁺ (410, 570, ...)	L ₁ 0.013	NCS ⁻	...	4
	L ₂ 0.018	NCS ⁻	...	
Cr(H ₂ O) ₆ (NCS) ²⁺ (410, 570, ...)	L ₁ 2.1 × 10 ⁻⁵	NCS ⁻	6	4
	L ₂ 6.0 × 10 ⁻⁵	NCS ⁻	8	
Cr(NH ₃) ₂ (NCS) ₄ ⁻ <i>trans</i> (392, 520, 746)	L ₁ 0.29	NCS ⁻ ; no NH ₃	1.3	10
	L ₂ 0.32	NCS ⁻ ; NH ₃ ?	1.3	
	D ₁ 0.29	NCS ⁻ ; no NH ₃	...	
Cr(NH ₃) ₅ Cl ²⁺ (375, 512, 632)	L ₁ 0.39	NH ₃ ; no Cl ⁻	0	c (d)
	L ₂ 0.35	NH ₃ ; no Cl ⁻	0	
Cr(en) ₂ (OH) ₂ ⁺ <i>cis</i> (377, 528, 667)	L ₁ 0.25; A/I = 2.8	en, I	1 ^e	5
	L ₂ 0.25; A/I = 1.5	en, I	4	
	D 0.26; A/I = 9.6	en, I	15	
Cr(en) ₂ (OH) ₂ ⁺ <i>trans</i> (398, 505, 685)	L ₁ 0.1; A/I = 0.3	en, I	2 ^f	5
	L ₁ 0.07; A/I = 1.3	en, I	...	
Cr(en) ₂ (OH)(H ₂ O) ²⁺ <i>cis</i> (392, 515, 681)	L ₁ 0.3	I only	...	5
	L ₂ 0.4	I only	...	
	D 0.05	I only	...	
Cr(en) ₂ (H ₂ O) ₂ ³⁺ <i>cis</i> (368, 485, 667)	L ₂ 0.3; A/I = 1	en, I	...	5
	L ₁ L ₂ 0.04	en + I	...	
Cr(en) ₂ (H ₂ O) ₂ ³⁺ <i>trans</i> (365, 445, ...)				5

^a The ligand indicated is that whose photoaquation was studied; unless specified, no other process was looked for. ^b M. R. Edelson and R. A. Plane, *Inorg. Chem.*, **2**, 231 (1964). ^c H. F. Wasgestian and H. L. Schläfer, private communication. ^d V. Carassiti and L. Moggi report that with Cr(NH₃)₅X²⁺, X = Cl, Br, both ammonia and halogen aquation occurs in proportion depending on the wavelength of light used (private communication). ^e Both ethylenediamine aquation, A, and isomerization, I, occurred. The activation energies for the partial quantum yields were, in kcal/mole: L_{1A} = -3, L_{1I} = 9, L_{2A} = 3, L_{2I} = 10, D_A = 20, D_I = 13. ^f Similarly, L_{1A} = 9 and L_{1I} = 0.

more diverse behavior than do the symmetric ones. Two types of ligand are present, either of which may aquate, and *cis-trans* isomerization may occur. It is especially important to note that the photolysis behavior may be wavelength dependent.

Thus with Cr(H₂O)₅(NCS)²⁺ a threefold change in aquation quantum yield as well as a change from 6 to 8 kcal/mole in apparent activation energy (hereafter, simply activation energy) occurred between wavelengths primarily in the L₂ and those primarily in the

L₁ band region. Also, a detailed study of the *cis*-Cr(en)₂(OH)₂⁺ system showed that both photoaquation and isomerization took place, and in proportion which varied considerably depending on whether the L₁-, L₂-, or D-band region was irradiated. Moreover, the temperature dependence of the total quantum yield was wavelength dependent, and even more so were the activation energies for the two photolysis reaction modes separately. Again, for *trans*-{Cr(en)₂(H₂O)-OH}²⁺, the quantum yield for isomerization was dis-

tinctly lower for light in the doublet band region as compared to that in the L-bands region. Finally, it has been reported that for $\text{Cr}(\text{NH}_3)_5\text{X}^{2+}$ ($\text{X} = \text{Cl}, \text{Br}$), aquation of both NH_3 and X^- can occur, and in proportion varying with the wavelength of light used.¹⁴

In view of these observations, the decrease in aquation quantum yields with increasing x in the series $\text{Cr}(\text{NH}_3)_x(\text{H}_2\text{O})_{6-x}^{2+}$ may be misleading in the sense that photoexchange of solvent was probably a competitive reaction. Quantum yields for the *sum* of both processes may well have been relatively constant. Similarly, for $\text{Cr}(\text{H}_2\text{O})_5(\text{NCS})^{2+}$, photoexchange of water should be considered. It will be useful to make the assumption that the *total* photolysis yield for a Cr(III) complex is always in the range of those for the related O_h species, at 25°.

The above observations of spectroscopicity of photolysis behavior make it clear that Cr(III) complexes are capable of being labilized differently depending on which quartet band is irradiated, and with respect to the various ligands if more than one kind is present. Leaving aside theoretical analysis for the moment, it is possible to construct empirical rules which account qualitatively for these observations. Ballhausen⁸ has pointed out a simplifying strategem for dealing with complexes of reduced symmetry. It is to regard crystal field splittings in the orthorhombic system of three mutually perpendicular axes, the effective ligand field strength of each of which is an average of those of the two ligands involved. In the case of a complex of the type CrA_4B_2 , one can then easily account qualitatively for the fact that the splitting of the L bands of the *trans* form is about twice that of the *cis*. We assume then that excitation to a quartet state labilizes the ligands on the weakest field axis, the discrimination between axes being greater in the L_1 than in the L_2 band. Further, the observation provided by the data of Table I, namely that quantum yields increase in the order of the spectrochemical series, suggests as a second rule that if the labilized axis contains two different ligands, the one higher in the series will preferentially aquate. Thus, the following three rules apply.

Rule 1. Consider the six ligands to lie in pairs at the ends of three mutually perpendicular axes. That axis having the weakest average crystal field will be the one labilized, and the total quantum yield will be about that for an O_h complex of the same average field.

Rule 2. If the labilized axis contains two different ligands, then the ligand of greater field strength preferentially aquates. This may be a type of *trans* effect.

Rule 3. The discrimination implied by rules 1 and

2 will occur to a greater extent if it is the L_1 rather than the L_2 band which is irradiated.

The application of these rules is shown in Table III. Thus the sharp drop in aquation quantum yield at $x = 3$ in the aquoamine series occurs because at this stage the preferred reaction mode shifts to water exchange. Similarly, one can account qualitatively for the differences in aquation *vs.* isomerization in the bisethylenediamine series. Also, rule 3 predicts that the partial quantum yields for disfavored reactions should rise with decreasing wavelength of irradiating light. This is the case with $\text{Cr}(\text{H}_2\text{O})_5(\text{NCS})^{2+}$ and *cis*- $\text{Cr}(\text{en})_2(\text{OH})_2^+$, but not appreciably so with $\text{Cr}(\text{NH}_3)_3(\text{H}_2\text{O})_3^{3+}$, $\text{Cr}(\text{NH}_3)_2(\text{H}_2\text{O})_4^{3+}$, and $\text{Cr}(\text{NH}_3)_5\text{NCS}^{2+}$. It may be significant that the first two systems show strongly activated behavior, but not those of the last three for which the information is available.

Quartet State Intermediates

The observation that Cr(III) complexes can show wavelength specificity in their photolytic behavior must mean that excitation to one or the other excited quartet state can lead to intermediates differently disposed to chemical reaction. A possible rationale of this observation follows.

First, nascent quartet excited states must contain some vibrational excitation, as evidenced by the fluorescent behavior of $\text{Cr}(\text{urea})_6^{3+}$.¹¹ For this complex, the L_1 band, whose maximum lies at 620 $\text{m}\mu$, gave fluorescence centering at 800 $\text{m}\mu$, so that the difference in average energy between processes k_1' and k_2' was about 11 kcal/mole (as indicated in Figure 2). For an O_h symmetry complex, excitation of an electron to an antibonding orbital should lead to some ligand repulsion and consequent increase in average bond length, plus some degree of Jahn-Teller distortion. By the Frank-Condon principle, process k_1' should then center on a high vibrational level of the ${}^4\text{T}_{2g}$ state. The nascent state should have time to undergo considerable thermal equilibration (process k_5') before emission, which would therefore in turn be to a vibrationally excited state of the ground state. If about equal vibrational excitations are involved, the radiationless process k_5' should be accompanied by transfer of about 5 kcal/mole to vibrations in the surrounding solvent medium.

Parenthetically, it should be noted that the placing of the ${}^4\text{T}_{2g}$ level below the ${}^2\text{E}_g$ one, while apparently correct for the case of $\text{Cr}(\text{urea})_6^{3+}$, may not represent the usual situation. The urea complex is virtually unique in showing fluorescence and it can be argued

(14) V. Carassiti and L. Moggi, private communication.

Table III

Complex	Low-field axis ^a	Photolysis mode	Quantum yield	
			Predicted ^b	Obsd ^c
CrA ₅ W ³⁺	A-W	A aquation	High	0.2
		O exchange	Low	...
CrA ₄ W ₂ ³⁺	A-W	A aquation	High	0.15
		O exchange	Low	...
	<i>trans</i>	W-W	A aquation O exchange	Very low High
CrA ₃ W ₃ ³⁺	A-W	A aquation	High	<i>e</i>
		O exchange	Low	<i>e</i>
	<i>trans</i>	W-W	A aquation O exchange	Very low High
CrA ₂ W ₄ ³⁺	W-W	A aquation	Very low	0.002
		O exchange	High	...
	<i>trans</i>	A-W	A aquation O exchange	High Low
CrA ₅ (NCS) ²⁺	A-NCS	A aquation	High	0.2 ^g
		NCS aquation	Low	0.02
CrW ₆ (NCS) ²⁺	W-W	O exchange	High	...
		NCS aquation	Very low	10 ⁻⁴ -10 ⁻⁶
CrA ₅ Cl ²⁺	A-Cl	A aquation	High	0.4
		Cl aquation	Low	<0.004
Cr(en) ₂ (OH) ₂ ⁺	en-OH	{ <i>en</i> aquation	High	0.2
		{ Isomerization	Mod.	0.07
		{ O exchange	Low	...
<i>trans</i>	OH-OH	{ O exchange	High	...
		{ Isomerization	Mod.	0.08
		{ <i>en</i> aquation	Very low	0.02
Cr(en) ₂ W(OH) ₂ ²⁺	en-OH	{ <i>en</i> aquation	High	0.04
		{ Isomerization	Mod.	0.03
		{ O exchange	Low	...
<i>trans</i>	O-O	{ O exchange	High	...
		{ Isomerization	Mod.	0.3
		{ <i>en</i> aquation	Very low	Nil
Cr(en) ₂ W ₂ ³⁺	en-W	{ <i>en</i> aquation	High	0.2
		{ Isomerization	Mod.	0.2
		{ O exchange	Low	...

^a A and W denote NH₃ and H₂O, respectively. ^b A mode is predicted as very low in yield if it would involve reaction of a ligand not on the low-field axis; isomerization yields are predicted on the supposition that labilization of a ligand can lead to both its aquation and to isomerization, with the former dominant. ^c Dashes indicate that no information is available on the yield for that mode. ^d The actual isomer predominantly present was not determined, but by analogy to Cr(en)₂(H₂O)₂³⁺, the *cis*-Cr(NH₃)₄(H₂O)₂³⁺ should be the preferred form. ^e No information is available as to which form of CrA₃W₃³⁺ was present; the data are consistent with its being the *trans* species. The rules proposed would in fact predict that photolysis of *cis*-CrA₄W₂³⁺ would yield predominantly the *trans* triaquo species, but with some photoisomerization. ^f Again, no information is available on isomer stability, but the data are more consistent with the form present being predominantly *cis*. ^g Preliminary value obtained here by E. Zinato and R. Lindholm (added in proof).

that this is because intersystem crossover, k_4' , would have to be activated once thermal equilibration of the ${}^4T_{2g}$ state had occurred so that the ion is effectively trapped and can undergo fluorescent emission, k_2' , without undue competition. The lack of observed fluorescence with most other Cr(III) complexes would then be explained by positioning the 2E_g level lower, as indicated by the dotted line in Figure 2, so that crossover would always be adiabatic and strongly competitive with emission.

It is equally possible, however, that the original relative level positions are representative of the general situation, and that other complexes fail to show fluorescence either because the radiationless deactivation process k_3' is more competitive than in the hexaurea case, or because there is sufficient excited-state distortion that the energy E_2' (corresponding to k_2') involves radiation far enough in the red for it to be largely absorbed by the aqueous medium and hence unobservable. Our results on temperature dependence, discussed below, suggest that Figure 2 is correct in at least one case where no fluorescence is found.

Returning to photolysis, even 5 kcal/mole of vibrational excitation in a nascent ${}^4T_{2g}$ state is apt to exceed the activation energy requirement for a substitution reaction. Schläfer⁷ estimates zero crystal field activation energy for reaction from this state. A distinct possibility, then, is that the nascent ${}^4T_{2g}$ state is very much like the activated complex of transition state theory. It contains vibrational energy in excess of that required for reaction and the reactant, water, is already present, although not in the best position for reaction. The question is then whether the excess energy E_6' of process k_5' can, as an alternative, be dissipated through chemical reaction. If the limiting rate for aquation is that for a water molecule to diffuse or rotate into a reactive configuration, the time requirement would be of the order of $\tau = x^2/2\mathfrak{D}$, where \mathfrak{D} is the self-diffusion coefficient for water and x is the distance involved, *i.e.*, about $10^{-16}/2 \times 2 \times 10^{-5}$ or about 10^{-12} sec. This is short enough that reactive deactivation could be competitive with k_3' (or k_2'); it could well be competitive with k_5' .

The situation following excitation to the ${}^4T_{1g}$ state should be similar. Again reactive deactivation, k_{56} , could be competitive with k_3 and k_5 and also with k_4 , the internal conversion rate. Schläfer⁷ considers k_4 to be exceedingly fast (10^{10} sec⁻¹), but this is by potentially dangerous analogy to singlet-singlet transitions in organic systems. Also, even for organic systems, azulene constitutes a known exception in showing fluorescence from a second excited state.¹⁵ Finally, of course, the observation of spectroscopicity

in Cr(III) photolysis virtually requires that chemical reaction can occur through the ${}^4T_{1g}$ state. For O_h symmetry complexes the ${}^4T_{1g}$ and ${}^4T_{2g}$ states differ only in electronic repulsion energy, and the various rate processes could be similar enough to explain the cases of no major wavelength dependence of quantum yields.

Lifetimes of Quartet Excited States

A point of possible difficulty arises with the reactive deactivation mechanism in the case of those systems for which the quantum yields do show appreciable activation energies. Thus, an activation energy of 10 kcal/mole implies for a unimolecular reaction of normal frequency factor a half-life of $10^{-13} \exp(E/RT)$ or about 10^{-6} sec. This is just about the fluorescence lifetime of excited quartet states as calculated from the area under an L band. In view of the absence of fluorescence, one then argues that the actual lifetimes must not be more than 10^{-8} sec, or much too short for competition by a process impeded by a 10-kcal/mole Boltzmann factor. The difficulty can be patched by assuming a sufficiently positive activation entropy, but since the problem is a quantitative one, it is desirable to examine more closely the basis for the original figure of 10^{-6} sec for a typical fluorescence lifetime.

The probability of a transition from state 1 to state 2 is given by

$$\int \epsilon d\nu = C_{12} g_{12} \nu_{12} |M_{12}|^2 \quad (1)$$

where ϵ is the (wavelength-dependent) absorption coefficient, C_{12} is a constant, g_{12} is the degeneracy factor, and ν_{12} the frequency of light absorbed, and M_{12} is the matrix element containing the electronic and nuclear wave functions. The probability for transition from state 2 to state 1, with emission, is

$$\tau^{-1} = C_{21} \nu_{21}^3 |M_{21}|^2 \quad (2)$$

The matrix elements are of the form

$$|M|^2 = \sum_v |\int \psi_{e,v} r \psi'_{e,v} d\tau_e d\tau_v|^2 \quad (3)$$

where for emission, vibrational states, v , are summed for the ground state 1, and for absorption, for the excited state, 2. In the Born-Oppenheimer approximation, the sums over vibrational states are separated out and contribute a factor of unity to the transition probability. The matrix elements $|M_{12}|^2$ and $|M_{21}|^2$ may be considered equal and eliminated from eq 1 and 2 to give

$$\tau = \frac{C_{12} g_{12} \nu_{12}}{C_{21} \nu_{21}^3 \int \epsilon d\nu} \quad (4)$$

(15) G. W. Robinson, *J. Mol. Spectry.*, **6**, 58 (1961).

If the equilibrium configurations are the same in the two states, ν_{12} can be taken as equal to ν_{21} so that eq 4 further reduces to the form given by Lewis and Kasha¹⁶

$$\tau = \frac{C}{\nu^2 \int \epsilon d\nu}; \quad \tau \cong \frac{3 \times 10^8}{\nu_{\max}^2 \int \epsilon d\nu} \quad (5)$$

Equation 5 is the one which gives the generally quoted lifetimes of *ca.* 10^{-8} sec for quartet excited states and *ca.* 10^{-3} sec for doublet excited states of Cr(III).

The factors which determine the extent to which the actual lifetime will differ from that given by eq 5 can be seen as

$$\begin{aligned} \tau' &= \left(\frac{C}{\nu_{12}^2 \int \epsilon d\nu} \right) (\nu_{12}/\nu_{21})^3 (|M_{12}|^2/|M_{21}|^2) \\ &= \tau (\nu_{12}/\nu_{21})^3 (|M_{12}|^2/|M_{21}|^2) \end{aligned} \quad (6)$$

It is the purpose of this section to show that τ' can differ significantly from τ in the case of excited quartet states of Cr(III).

First, using the case of Cr(urea)₆³⁺ as an illustration, the ratio $(\nu_{12}/\nu_{21})^3$ is about $(800/620)^3$ or about 2. For other species, it might be larger if for them ν_{21} lies further in the red.

Secondly, it was noted that the matrix elements $|M_{12}|^2$ and $|M_{21}|^2$ are taken to be equal in the conventional calculation of emission lifetimes. However, this approximation can be seriously in error if the nuclear configurations in the ground and excited states are sufficiently different, as noted by Birks and Dyson.¹⁷ Thus for diphenyloctatetraene, the ratio τ'/τ was 22. In the case of transition metal complexes, ligand field excitation generally places an electron in an antibonding d orbital and excited state distortion could well be important because of the strongly directional nature of such orbitals. Ballhausen, *et al.*,¹⁸ have suggested that Ni(CN)₄²⁻ is D_{2d} in the first excited state. In the case of Cr(III) complexes, the equilibrium configuration of a quartet excited state might, for example, be that of a pentagonal pyramid (admirably suited to undergo a rapid aquation reaction).

Furthermore, Cr(III) quartet-quartet transitions are normally forbidden; Liehr and Ballhausen¹⁹ assumed them to be partially allowed through mixing of the excited ligand field state with a higher, ungerade one by vibronic coupling. From first-order perturbation theory, the mixing coefficient may be written

$$\gamma_d(p) = - \frac{\psi_u^0(p) H'(Q_2) \psi_g^0(d)}{(E_p - E_d')} \quad (7)$$

where $H'(Q_2)$ denotes the variation of the Hamiltonian with normal coordinate Q of the excited state (2) and the 4p state was taken to be the ungerade one. For

emission, a similar coefficient is involved, but now with $H'(Q_1)$, where Q_1 is now a normal coordinate of the ground state. That is, absorption is restricted to occur from the zero vibrational state of the ground state (at any reasonable temperature) so that it is the excited state into which vibronic mixing of the 4p one occurs, with vibrations given in the coordinate system of the distorted (*e.g.*, pentagonal pyramidal) geometry. However, emission would occur from the thermally equilibrated excited state (2), and so from the zero vibrational level of that state. The vibronic mixing would now be described in terms of the vibrations of the (*e.g.*, octahedral) ground state. Thus the coefficients of the type given by (7) could be quite different for absorption and emission. In fact, the generally assumed Born-Oppenheimer approximation may not be very good in a situation of this type.

As one further example of a large value for the ratio τ'/τ , Douglas²⁰ cites the value of about 150 in the case of NO₂ (and similarly for SO₂). It would appear, then, that in the case of Cr(III) complexes, τ' might exceed τ by a factor of 10 or 100 without the effect being particularly anomalous. A factor of 100 would essentially eliminate the quantitative difficulty otherwise present in those cases, such as Cr(en)₂(OH)₂⁺, which show highly activated and spectroscopic photolysis by requiring the chemical lifetime only to be less than about 10^{-6} sec rather than less than 10^{-8} sec.

It should be noted that the above arguments about fluorescence lifetimes probably do not apply to phosphorescence. For Cr(III) doublet states, no electron promotion to antibonding orbitals is involved, and the geometry of the complex should not be subject to much distortion. Phosphorescence lifetimes are in fact about as expected.¹²

There remains the question of whether radiationless processes should be too fast to permit the reactions k_6, k_6' to occur in those cases where they are activated. First, the intersystem crossover rate, k_4' is reported to be $5 \times 10^7 \text{ sec}^{-1}$ for ruby;²¹ if it is no greater than this for aqueous complexes, then k_6' would be competitive if the activation energy were less than 10 kcal/

(16) G. N. Lewis and M. Kasha, *J. Am. Chem. Soc.*, **67**, 994 (1945); also, R. S. Mulliken, *J. Chem. Phys.*, **7**, 14 (1939).

(17) J. B. Birks and D. J. Dyson, *Proc. Roy. Soc. (London)*, **A275**, 135 (1963).

(18) C. J. Ballhausen, N. Bjerrum, R. Dingle, K. Eriks, and D. R. Hare, *Inorg. Chem.*, **4**, 514 (1965).

(19) A. D. Liehr and C. J. Ballhausen, *Phys. Rev.*, **106**, 1161 (1957); see also G. Herzberg and E. Teller, *Z. Physik. Chem.*, **B21**, 410 (1933).

(20) A. E. Douglas, *J. Chem. Phys.*, **45**, 1007 (1966).

(21) T. H. Maiman, *Phys. Rev. Letters*, **4**, 564 (1960).

mole (assuming, as before, a normal frequency factor). The difficulty in predicting the intrasystem conversion rate, k_4 , has already been noted.

Remaining are the radiationless deactivation processes k_3 and k_3' . Such processes have been viewed either in terms of a tunneling to high vibrational levels of adjacent solvent molecules,²² or as induced phonon emission.²³ While both treatments provide an explanation for the generally observed temperature dependence, neither can be regarded as quantitatively reliable. The case of azulene mentioned above suggests that radiationless deactivation of a second excited state need not always be extremely fast. In addition, either or both processes k_3' and k_3'' must be very medium sensitive. An illustration of this is provided in Figure 3. Also, the argument used by Chatterjee and Forster²⁴ to assign $(k_3' + k_4')$ as greater than 10^9 sec^{-1} is faulted by a use of eq 5 as a point of departure. Finally, it appears that most of the variation in observed doublet-state lifetime and phosphorescence yield with type of ligand is to be attributed to variation in rate of competitive radiationless processes.²⁴ There thus seems to be sufficient latitude in both theory and experiment to allow k_3 and k_3' to be sufficiently slow in specific cases not to compete unduly with activated reactive processes.

Where photolysis is activated then the reactive deactivation paths, k_{56} , k_{56}' may not be important, but activated reaction *via* k_6 , k_6' remains possible.

Temperature Dependence of the Processes

It was noted above that radiationless deactivation processes appear to be temperature dependent; qualitatively, the dependence is exponential, *i.e.*, activated. Thus k_3 , k_3' , and k_3'' can be expected to show a positive activation energy. Emission processes, except for a relatively unimportant anti-Stokes component, should be intrinsically temperature independent, and this is assumed to be the case for k_2 , k_2' , and k_2'' .

There is a possibility, however, that the thermal equilibration processes k_5 and k_5' might have a special type of temperature and medium sensitivity, related to excited-state distortion. In the case of O_h complexes such distortion may amount only to some increase in average bond length, although in principle Jahn-Teller distortion should also occur. If this last is small, however, k_5 and k_3' could be regarded as a *volume* relaxation of the nascent state, and this could occur in about the transit time of sound waves across a molecular dimension and might therefore not be very medium or temperature sensitive.

For non- O_h complexes, however, distinct changes in geometry are more likely, so that k_5 and k_5' may now

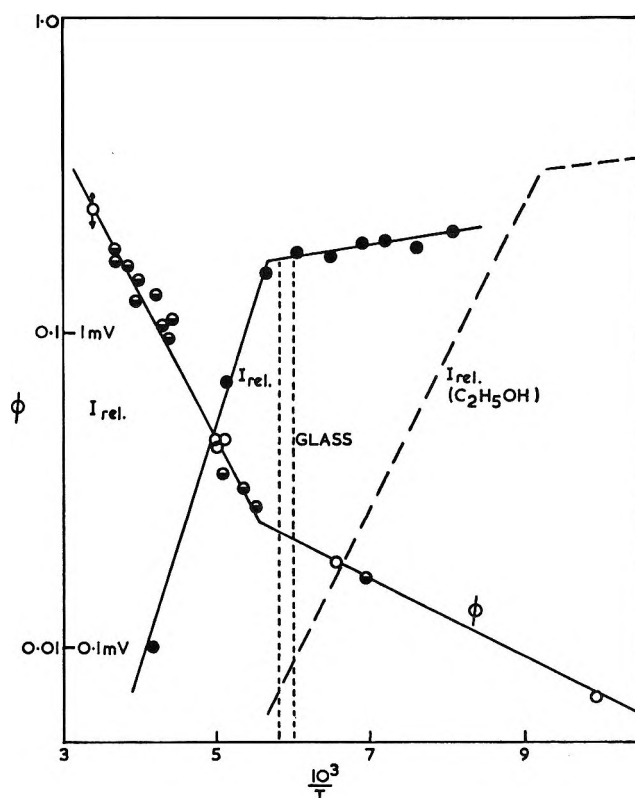


Figure 3. Temperature dependence of fluorescence and of aquation quantum yields for $\text{KCr}(\text{NH}_3)_2(\text{NCS})_4$. Solvent medium: 3 parts of H_2O , 2 parts of CH_3OH , and 2 parts of $\text{CH}_2\text{OHCH}_2\text{OH}$. O, ϕ : aquation quantum yields. Because of calibration difficulties, the two sets of data, obtained with different cells, differed by a nearly constant factor of 1.7 and the less accurate set, \bullet , have been multiplied by this number. Light of 470–670 $\text{m}\mu$ with absorbed intensity centering around 520 $\text{m}\mu$ was used. \bullet : relative phosphorescence yields (red region) stimulated by 356- $\text{m}\mu$ light. Dashed line: relative emission yields in ethanol as solvent.

involve a *distortional* relaxation from the geometry of the ground state to that of the thermally equilibrated excited state. The same would be true of O_h complexes subject to strong excited-state Jahn-Teller distortion. Complex ions of the type under consideration are heavily hydrogen bonded to solvent water; the situation in solution very likely resembles that found for the waters of hydration in crystalline $(\text{Cr}(\text{H}_2\text{O})_4\text{Cl}_2) \cdot \text{Cl} \cdot 2\text{H}_2\text{O}$, which are locked in place by hydrogen bonds to a point where coordinated and crystallization water are difficult to distinguish.²⁵

(22) G. W. Robinson, *J. Mol. Spectry.*, **6**, 58 (1961).

(23) M. Gouterman, *Chem. Rev.*, **65**, 413 (1965).

(24) K. K. Chatterjee and L. S. Forster, *Spectrochim. Acta*, **20**, 1603 (1964).

(25) I. G. Dance and H. C. Freeman, *Inorg. Chem.*, **4**, 1555 (1965).

Any appreciable rearrangement of the geometry of such a complex ion (as in the above-mentioned illustration of octahedral to pentagonal pyramidal) would very likely involve hydrogen bond breaking and making. Processes k_5 and k_5' would then be essentially diffusion controlled and their lifetimes would be of the order of the time of diffusion of water molecules from position to adjacent position. At room temperature, this time was estimated as 10^{-2} sec, but would rise to perhaps 10^{-4} sec at the glass point. In view of the arguments that excited-state distortion should hinder fluorescence, one would expect emission to be favored in media for which distortional relaxation was slow enough that fluorescence could occur from the undistorted state.

This analysis is consistent with the behavior of $\text{Cr}(\text{urea})_6^{3+}$, for which the fluorescence yield was temperature dependent above the glass point of the mixed solvent (corresponding to -1.8 kcal/mole activation energy) but much less so at lower temperatures (-0.5 kcal/mole activation energy).¹¹

Doublet *vs.* Quartet State as Photolysis Intermediate

The two mechanisms are not necessarily rivals; both may contribute in a given system. The doublet intermediate mechanism provides a particularly natural explanation of the behavior of O_h systems although in no case does it seem that the path involving reactive deactivation of excited quartet states can be ruled out. In addition, this last type of path must be important in the case of those systems showing spectroscopicity.

Indirect support for at least the ${}^4\text{T}_{2g}$ state as a chemical intermediate is now available for one complex whose photolysis is not appreciably spectroscopic and is not very activated. The data, shown in Figure 3, are for reinecke salt ($\text{KCr}(\text{NH})_2(\text{NCS})_4$) in a water-glycol-methanol mixed solvent²⁶ over the very wide temperature range of -195 to 25° . The phosphorescence yields fall on two nearly straight line sections of -3.3 and -0.18 kcal/mole activation energy, while those for aquation fall on two lines of 2.3 and 0.55 kcal/mole activation energy.

The following analysis seems possible. First, we assume that phosphorescent emission from the doublet state is intrinsically temperature independent so that the observed behavior is due to the presence of a competing radiationless process. The change in the slope of the plot of emission *vs.* $1/T$ is then to be attributed to some change in the nature of this process which occurs near the glass point. Above the glass point, then, deactivation follows an apparent activation energy of 3.3 kcal/mole and below it, one of 0.2 kcal/mole. Since the aquation quantum yield plot

shows a break at the same temperature as does that for phosphorescence, it seems reasonable to assume that the same radiationless deactivation process is affecting both yields.

Two possible situations may now be considered. First, it may be supposed that aquation occurs from the doublet state, *i.e.*, through process k_6'' , and that therefore the radiationless deactivation process is k_3'' and competes both with phosphorescent emission, k_1'' , and with aquation. The apparent activation energy of 2.3 kcal/mole for photoaquation above the glass point must then be a net of a true activation energy of 5.6 kcal/mole and the 3.3 kcal/mole for the competing deactivation. (The yields for neither the aquation nor the emission are large enough for either process to affect the other.) On this basis, then below the glass point, the apparent photoaquation activation energy should be the same 5.6 kcal/mole diminished now by only 0.2 kcal/mole, or about 5.4 kcal/mole. That is, the plot of photoaquation quantum yield *vs.* $1/T$ should *steepen* at the glass point. This is contrary to our observation.

An alternative is to suppose that the temperature-dependent radiationless deactivation process is k_5' , *i.e.*, the thermal equilibration of the ${}^4\text{T}_{2g}$ state. This would be competitive with conversion to the ${}^2\text{E}_g$ state and hence again competitive with phosphorescence. The temperature dependence of the phosphorescence yield would then still be interpreted in terms of a 3.3 -kcal/mole apparent activation energy for the radiationless process, now k_5' , above the glass point, and a 0.2 -kcal/mole value for it below the glass point. However, process k_5' is one which *leads* to, rather than competes with, aquation. The apparent photoaquation activation energy should now be the sum of the values for k_5' and k_6' , from which the value for k_6' should be -1 kcal/mole or essentially zero. Below the glass point, the apparent activation energy for photolysis should then drop to about $(0 + 0.2)$ or 0.2 kcal/mole. This is qualitatively what is observed; *i.e.*, the apparent activation energy for photolysis becomes less positive below the glass point.

Essentially, then, the behavior of the reineckate system suggests that there is a radiationless process which competes with phosphorescence but leads to photolysis. Such a situation does not appear to be explainable in terms of the doublet intermediate mechanism, but can be rationalized in terms of a reactive deactivation of the ${}^4\text{T}_{2g}$ state. Presumably,

(26) The quantum yields were obtained by R. Lindholm in this laboratory; details are to be published elsewhere, but except for the special cells, the apparatus and procedures were essentially those of ref 10. The phosphorescence yields are courtesy of Dr. L. S. Forster.

around room temperature k_5' and k_6' become large enough that the aquation quantum yield approaches a constant and fairly large value. This limiting condition could be primarily temperature determined, or it might depend mainly on the medium viscosity being low. The second possibility, especially would be consistent with k_5' being limited in rate by that of the diffusional relaxation to a distorted geometry for the thermally equilibrated ${}^4T_{2g}$ state.

The above analyses are speculative, but no more so than previously proposed ones; they at least provide a rationale for all of the observations. We hope that

the further investigations implicitly suggested will lead to more definite conclusions. For example, if the important deactivation process is k_3'' , phosphorescence lifetimes as well as yields should be temperature dependent, but only the latter should be so if deactivation is mainly *via* k_5' .

Acknowledgment. The investigations have been supported in part by Contract AT(11-1)-113 between the University of Southern California and the U. S. Atomic Energy Commission. The writer gratefully acknowledges the advice and criticism of several colleagues, particularly O. Schnepf and H. Pryce.

Thermodynamics of Vaporization of Thallous Oxide¹

by Daniel Cubicciotti and F. J. Keneshea

Stanford Research Institute, Menlo Park, California 94025 (Received June 26, 1966)

The vaporization of solid Tl_2O_3 was studied by a transpiration method under various oxygen pressures. The gaseous thallium species was found to be Tl_2O ; hence, Tl_2O_3 vaporizes by the reaction $Tl_2O_3(s) = Tl_2O(g) + O_2(g)$. At 0.01 atm of oxygen pressure the partial pressure of Tl_2O in the range 530–675° can be expressed by the equation $\log p(Tl_2O, atm) = -19.63(10^3/T) + 18.60$. The enthalpy of vaporization at 1000°K was 90 kcal/mole.

Introduction

Shchukarev, Semenov, and Rat'kovskii² made a transpiration study of the vaporization of solid Tl_2O_3 under 1 atm of oxygen. They assumed (incorrectly, as we show below) that the vapor species under 1 atm of oxygen was Tl_2O_3 and calculated their transpiration results on that basis. Their assumption was apparently based on the chemistry of the solid, for which Tl_2O is stable at low oxygen pressures, and Tl_2O_3 at high oxygen pressures.³ However, the equilibrium species in the gas often do not have the same stoichiometry as the solid⁴ (and the factors that lead to the transformation in the solid are sufficiently modified in the vapor that one should not expect the same chemical change). The same authors later⁵ made a mass spectrometer investigation of the species obtained on free

evaporation of Tl_2O_3 from a platinum ribbon. They interpreted their results to indicate that solid Tl_2O_3 evaporated as Tl_2O gas and O_2 gas; however, since their results indicated that they also had thallium in their condensed phase (*i.e.*, they observed Tl^+ with a heat of evaporation equal to that of thallium metal),

(1) This work was made possible by financial support from the Research Division of the U. S. Atomic Energy Commission under Contract No. AT(04-3)-106.

(2) S. A. Shchukarev, G. A. Semenov, and I. A. Rat'kovskii, *Russ. J. Inorg. Chem.*, **6**, 1423 (1961).

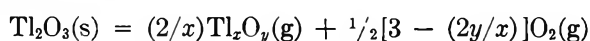
(3) See, for example, H. Remy, "Treatise on Inorganic Chemistry," Vol. I, Elsevier Publishing Co., Amsterdam, 1956, p 387.

(4) L. Brewer and G. M. Rosenblatt, *Trans. AIME*, **224**, 1268 (1962).

(5) S. A. Shchukarev, G. A. Semenov, and I. A. Rat'kovskii, *Zh. Prikl. Khim.*, **35**, 1454 (1962).

it is doubtful that their measurements corresponded to equilibrium between the gases and solid Tl_2O_3 . We felt that the nature of the gaseous species in equilibrium with Tl_2O_3 was sufficiently in doubt to warrant further investigation, so we undertook the study reported below.

The variation of the partial pressure of thallium-containing species in the equilibrium vapor would be expected to depend on the oxygen pressure through the equilibrium



in which Tl_xO_y is the unknown gaseous species. A log-log plot of the partial pressures of thallium-containing vapor species *vs.* oxygen pressure should have a slope of $-x/4[3 - (2y/x)]$. The most likely species were presumed to be Tl , Tl_2O , TlO , Tl_2O_3 , or TlO_2 . The slopes expected for these species were $-3/4$, -1 , $-1/4$, 0 , and $+1/4$, respectively. Since these slopes were sufficiently different, it seemed that an experimental determination could be made to distinguish among the possibilities and a transpiration study as a function of oxygen pressure was undertaken.

Experimental Section

Method. The method was the same as that used in our transpiration study of TlF .⁶ The cell was essentially the same as that shown in Figure 1 of ref 6 with the exceptions that it was made of CP platinum (rather than platinum-10% rhodium) and the collector did not have the extended tip but only a hole (about 0.7 mm in diameter) at the tip.

The amount of Tl_2O_3 condensed in the collector was determined by weight difference. The outside of the collector was cleaned of its film of Tl_2O_3 with concentrated HCl and by abrasion, the collector was weighed, and then the inside was cleaned with hot HCl to constant weight. The complete removal of the collected sample was difficult, and this difficulty led to some of the scatter in the final results. The difference in weights of the collector before and after the inside was cleaned was taken to be the weight of Tl_2O_3 collected because, regardless of the nature of the gaseous species, the stable solid was Tl_2O_3 under the temperatures and oxygen pressures used. In the course of the experiments it was observed that a thin, dark coating formed on the platinum. It was apparently a thallium-platinum oxide since it did not react like thallium oxide. Since the amount formed was relatively small, it was assumed that it did not interfere with the vaporization process of the Tl_2O_3 .

Materials. Tl_2O_3 was prepared by dissolving the metal (99.95+% pure, from American Smelting and

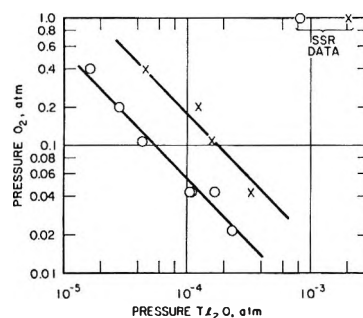


Figure 1. Variation of pressure of volatile Tl species with oxygen pressure over solid Tl_2O_3 : O, 621°; X, 649°. Two points in upper right-hand corner calculated from the equation of Shchukarev, Semenov, and Rat'kovskii for 1 atm of oxygen.

Refining Co.) in nitric acid, oxidizing with bromine water, boiling to remove excess bromine, and precipitating with ammonia. The dried oxide was analyzed for thallium by solution in sulfuric acid, reduction by SO_2 , and determination as thallos chromate. It was found to contain 88.23% Tl; theoretical for Tl_2O_3 is 89.49%. It was suspected that the product contained some bromide or oxybromide. A sample heated in an oxygen atmosphere gave rise to a yellow sublimate, which was presumed to be $TlBr$. Accordingly, the entire batch of product was heated to 450° in an oxygen atmosphere for a weekend. The 70 g of material lost about 1 g; continued heating overnight resulted in negligible weight changes. The material treated in that way was found to contain $89.61 \pm 0.07\%$ Tl and was considered to be close enough to theoretical for our purposes. After 24 transpiration experiments generally lasting about 20 hr each, the material was removed from the cell and found to contain 89.12% thallium. The change in composition was considered to be small enough to assume that the material was still Tl_2O_3 . X-Ray powder patterns were made of samples of the Tl_2O_3 before and after use. The lines observed for both samples were the same and agreed with those given in the ASTM card for Tl_2O_3 . No lines other than those of Tl_2O_3 were observed in either sample.

Mixtures of nitrogen and oxygen of 1, 2, 4, 10, 20, and 40% oxygen were used for the carrier gas. These were obtained as premixed samples from the Matheson Co. (Several experiments were made with 100% oxygen from another source with results that were almost ten times as high as expected in comparison with the other gas mixtures. This discrepancy was finally

(6) F. J. Keneshea and D. Cubicciotti, *J. Phys. Chem.*, **69**, 3910 (1965).

attributed to the fact that the 100% oxygen contained some CH_4 which was not removed by the drying traps and became H_2O and CO_2 in the furnace. The H_2O presumably enhanced the volatility of the oxide through the formation of hydroxide gaseous species. Because of this problem the results obtained with the 100% oxygen were discarded.) The gas mixtures were analyzed for O_2 content with a Beckman oxygen analyzer (Model E2), which measures the magnetic susceptibility of the gas. To ensure that the mixtures were completely homogeneous, the gas bottles containing the mixtures were partially immersed in hot water for about 1 hr. Analysis of the 4% tank before and after the hot water treatment showed no change in O_2 content, indicating that the gases as received were probably already well mixed. The O_2 contents measured for the 1, 2, 4, 10, 20, and 40% mixtures were, respectively, 1.07, 2.14, 4.33, 10.6, 19.8, and 40.0% (with an uncertainty of $\pm 1\%$ in each value). These values were used in calculating the O_2 partial pressures reported in the next section.

Results and Discussion

The variation of the partial pressure of thallium vapor species with oxygen partial pressure was determined at two temperatures, 621 and 649°. The partial pressure of the thallium-containing vapor species was calculated from the usual transpiration formula

$$p = \frac{\text{weight of Tl}_2\text{O}_3 \text{ carried}}{\text{mol wt of Tl}_2\text{O}_3} \frac{\text{pressure of carrier gas}}{\text{moles of carrier gas}}$$

In this formula p is the partial pressure of the thallium-containing vapor species under the assumptions: (a) the partial pressure of oxygen is large enough that any oxygen produced or consumed by the vaporization is negligible and (b) each molecule contains two thallium atoms, regardless of the number of oxygen atoms. (If the results showed that Tl_2O , Tl_2O_3 , or Tl_2O_4 , etc., were the species, the partial pressure calculated from the above formula would give the correct values for their pressures; however, if the molecule contained one thallium atom—*i.e.*, TlO , or Tl , or TlO_2 —its partial pressures would be given by twice the value of the formula.)

The results obtained are shown as data points in Figure 1. The slopes of the lines that best fit the data were -1 , corresponding to the species Tl_2O . In view of the scatter of the data, lines of slope $-3/4$ (corresponding to Tl as vapor species) could fit but slopes of $-1/4$, 0 , and $+1/4$ (corresponding to the other simple species TlO , Tl_2O_3 , and TlO_2) were not at all in accord with the data. The partial pressures of ele-

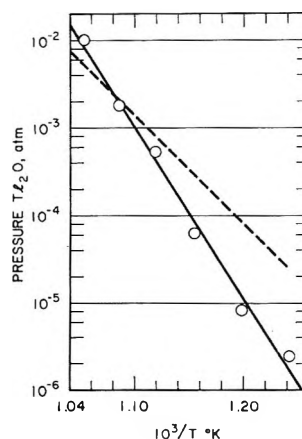
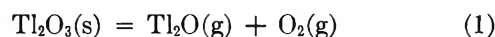


Figure 2. Partial pressure of Tl_2O over solid Tl_2O_3 at 0.01 atm of oxygen. Dashed curves are data of Shchukarev, Semenov, and Rat'kovskii for 1 atm of oxygen.

mental Tl in equilibrium with solid Tl_2O_3 at these oxygen pressures can be estimated from available thermodynamic data (see Appendix II). They are found to be about five or six orders of magnitude smaller than the pressures of gaseous thallium-containing species measured here; therefore, some species other than Tl is responsible for the vaporization under these conditions and the slope $-3/4$ should not be considered as a possibility. The only simple species that can account for the slope of the log-log plot is Tl_2O . Thus Tl_2O_3 vaporizes according to the equilibrium



The partial pressure of Tl_2O as a function of temperature at 0.01 atm of O_2 is shown in Figure 2. Below 620° the data were obtained by transpiration measurements with a gas stream containing 1.07% oxygen (with a correction to 0.01 atm). The decomposition of $\text{Tl}_2\text{O}_3(\text{s})$ to $\text{Tl}_2\text{O}(\text{s})$ must be suppressed by maintaining the oxygen partial pressure above the "decomposition" pressure. Therefore at 620° and above, transpiration measurements were made with oxygen pressures greater than 0.01 atm and the values then corrected to 0.01 on the assumption that the Tl_2O pressure was inversely proportional to the oxygen pressure. The data obtained at 621 and 649° are shown in Figure 1. The straight lines of that figure were extrapolated to 0.01 atm of O_2 to obtain the pressures of Tl_2O shown in Figure 2. At 677° the Tl_2O pressure was found to be 2.52×10^{-4} atm for 0.40 atm of O_2 pressure so that at 0.01 atm of O_2 the Tl_2O pressure was calculated to be 1.01×10^{-2} atm.

The data obtained at various temperatures, corrected to 0.01 atm of oxygen pressure, are shown in

Figure 2. A least-squares analysis resulted in the equation

$$\log p(\text{Tl}_2\text{O, atm}) = [-(19.63 \pm 0.1)(10^3/T) + 18.60] \pm 0.1$$

in which the uncertainties given are probable errors. The line drawn in Figure 2 represents the above equation. The enthalpy change for reaction 1 derived from the equation at the mid-temperature (about 900°K) is 90 kcal/mole, with a probable error of 0.5 kcal/mole.

The present data differ seriously from those of Shchukarev, *et al.*² In our opinion the material used by those authors was contaminated with bromide resulting in a bromide species that was more volatile than the oxide, so their results were dominated by the volatile impurity. The pressures calculated from their equation for the solid (under 1 atm of oxygen) are shown in Figure 1. They are about two orders of magnitude greater than expected from our data for 1 atm. The equation given by Shchukarev, *et al.*, for their results over the solid at 1 atm of O_2 pressure is represented in Figure 2 where it can be seen that the slope of their curve is quite different from ours. There is no basis for comparing the two sets of data.

A third-law evaluation of the enthalpy of vaporization of Tl_2O_3 can provide a check on the second-law value derived above. Unfortunately, the absolute entropies of the oxides have not been determined, so the third-law treatment can only be based on estimated values. For the solids at 298°K one can use Latimer's rules⁷ and estimate the absolute entropy of solid Tl_2O_3 to be 32 eu. Kubaschewski and Evans⁸ indicate that a high molecular weight triatomic gaseous molecule will have an S°_{298} of about 85 eu. At 900°K the absolute entropies of $\text{Tl}_2\text{O}_3(\text{s})$ and $\text{Tl}_2\text{O}(\text{g})$ become 69 and 100 eu, respectively, if their heat capacities are assumed⁹ to be 33.5 (*i.e.*, 5×6.7) and 14 eu. The S°_{900} for $\text{O}_2(\text{g})$ is 57.3 eu;⁹ thus $\Delta S^\circ_{900^\circ\text{K}}$ is estimated to be 78 eu for reaction 1 above.

At 900°K our data indicate $p(\text{Tl}_2\text{O}) = 6.8 \times 10^{-4}$ atm for $p(\text{O}_2) = 0.01$ atm; thus $\Delta F^\circ_{900} = 21.3$ kcal/mole. Combination of this value with the entropy estimated above gives an estimated third-law value for the enthalpy change of 92 kcal/mole. The limits of accuracy of this estimated value are about ± 10 kcal. It confirms the validity of the value obtained by the second-law treatment, but the agreement itself is fortuitous.

As the partial pressure of oxygen over solid Tl_2O_3 at a given temperature is lowered, the Tl_2O_3 will be reduced to a solid solution of Tl_2O in Tl_2O_3 and at suffi-

ciently low oxygen pressures to pure Tl_2O . An estimate of the oxygen pressure at which this occurs can be obtained by evaluating the oxygen pressures at which the partial pressure of Tl_2O over solid Tl_2O_3 becomes comparable to the vapor pressure of solid Tl_2O .

The vapor pressure of thallic oxide has been reported by Mulford¹⁰ and by Shakhtakhtinskii and Kuliev.¹¹ Both of these sets of authors used an effusion method for their measurements. Mulford's vapor pressures are about four orders of magnitude smaller than those of Shakhtakhtinskii and Kuliev (however, the heats of sublimation of the two sets of measurements are almost equal, being 29 and 30 kcal/mole, respectively). Since Mulford's results fall in with ours (see below) and since Shakhtakhtinskii and Kuliev were unsure of the composition of their solid, we have assumed Mulford's data to be the more correct.

The comparison of partial pressure of Tl_2O over solid Tl_2O_3 as a function of oxygen pressure with the vapor pressure of solid Tl_2O is made in Figure 3 at three temperatures. These temperatures were chosen in the range in which our data and Mulford's overlapped. The horizontal, full lines represent the vapor

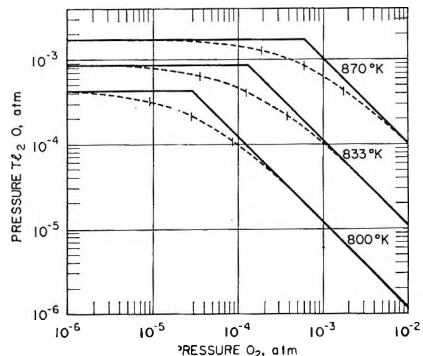


Figure 3. The variation of Tl_2O partial pressure with oxygen pressure calculated for the region of the decomposition of solid Tl_2O_3 to solid Tl_2O . Full lines assume no solid solubility; dashed lines assume Raoult's law. The three short vertical lines on each curve indicate conditions under which the solid is $1/4$, $1/2$, and $3/4$ Tl_2O_3 (from left to right, respectively).

(7) W. M. Latimer, "Oxidation Potentials," 2nd ed, Prentice-Hall, Inc., Englewood Cliffs, N. J., 1952, p 359ff.

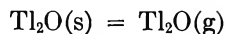
(8) O. Kubaschewski and E. L. Evans, "Metallurgical Thermochemistry," 3rd ed, Pergamon Press Inc., New York, N. Y., 1958, Chapter 3.

(9) "JANAF Thermochemical Tables," The Dow Chemical Co., Midland, Mich., Dec 31, 1965.

(10) R. N. Mulford, AEC Report No. LA-1373, 1952.

(11) M. G. Shakhtakhtinskii and A. A. Kuliev, *Dokl. Akad. Nauk SSSR*, 123, 1071 (1958).

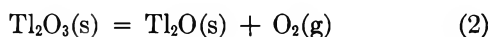
pressures of Tl_2O , which are independent of oxygen pressure insofar as the values measured by Mulford represent the equilibrium



The slanted, full lines represent the partial pressures of Tl_2O as a function of oxygen pressure according to the results given above relating to the equilibrium of eq 1.

The point at which these two curves cross, at a given temperature, gives the decomposition oxygen pressure and represents the hypothetical situation in which pure, solid Tl_2O and pure, solid Tl_2O_3 are in equilibrium with O_2 and Tl_2O gases.

Tl_2O and Tl_2O_3 seem to be miscible as solids, so the real curves will lie somewhat below the full lines of Figure 3 and will be curved. As a first approximation to the real situation it was assumed that Raoult's law would be obeyed by the solid. Thus for the equilibrium



the mass-action law with N representing mole fraction becomes

$$K = \frac{p(O_2)N(Tl_2O)}{N(Tl_2O_3)} = \frac{p(O_2)N(Tl_2O)}{1 - N(Tl_2O)}$$

and the partial pressure of Tl_2O is

$$p(Tl_2O) = p^0(Tl_2O)N(Tl_2O) = \frac{Kp^0(Tl_2O)}{p(O_2) + K}$$

in which $p^0(Tl_2O)$ is the vapor pressure of pure, solid Tl_2O . The curves corresponding to this analysis are shown dashed in Figure 3.

The equilibrium constant for eq 2 above can be evaluated from the results of Figure 3. At the crossing point of the full curves at a given temperature, the activities of Tl_2O_3 and Tl_2O are both equal to unity. Thus the equilibrium constant is simply given by the pressure of oxygen at the crossing point. These pressures were evaluated for the temperatures given in Figure 3 and the results plotted as a function of reciprocal temperature in Figure 4. The data fell on a straight line whose slope gives the enthalpy change for reaction 2 in the temperature range studied. The value obtained was 60 kcal/mole; however, because of the method of obtaining it the value is not considered to be very reliable. The same numerical value was obtained (Appendix I) from Duncan's data for the reaction in the liquid state (at 1000°K). The two values should differ by the differences in the enthalpy increments between 800 and 1000°K, which include

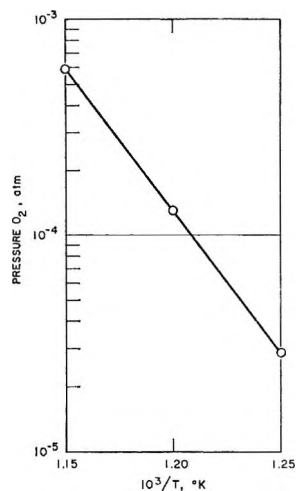


Figure 4. The pressure of O_2 over equi-activity mixtures of solid Tl_2O_3 - Tl_2O . This pressure is also equal to the equilibrium constant of reaction 2.

the heats of fusion of the two solids, and since these are not known, a more careful comparison of the two values cannot be made. A rough third-law evaluation of the enthalpy change of the reaction can be made using the entropy estimates given in Appendix I. At 800°K the estimated entropy change for reaction 2 is 43 eu; the standard free energy change, calculated from the equilibrium oxygen pressure of 2.9×10^{-5} atm, is 17 kcal/mole; so the enthalpy is 51 kcal/mole. This value may be considered to substantiate the second-law value in view of the estimations involved.

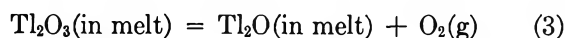
Acknowledgment. Mr. William E. Robbins performed the majority of the experimental work reported. Dr. Malcolm Barlow made the X-ray analyses. The authors are grateful to one referee of this paper who called their attention to Mulford's work.

Appendix I

Reinterpretation of the Dissociation Pressure of Tl_2O_3 . Duncan¹² has measured the partial pressures of oxygen over molten mixtures of Tl_2O_3 and Tl_2O in a series of careful experiments. His interpretation of the results was erroneous, however, since he assumed that the pressure at which Tl_2O_3 began to lose oxygen was its decomposition pressure (*i.e.*, pressure of O_2 in equilibrium with the two condensed phases, Tl_2O_3 and Tl_2O), while at the same time his results showed the two oxides were miscible.¹³ We have recalculated his results as follows. For the equilibrium

(12) A. B. F. Duncan, *J. Am. Chem. Soc.*, **51**, 2697 (1929).

(13) L. Brewer has already remarked on this problem in *Chem. Rev.*, **52**, 38 (1953).



the expression for the equilibrium constant is

$$K = \frac{\text{activity}(\text{Tl}_2\text{O in melt})}{\text{activity}(\text{Tl}_2\text{O}_3 \text{ in melt})} p(\text{O}_2)$$

For each temperature of Duncan's measurements we have calculated from his curves the partial pressure of oxygen over the melt containing equal mole fractions (0.5) of each oxide. If one assumes that the activity coefficients of the two oxides in the melt are equal, the equilibrium constant is equal simply to the partial pressure of oxygen. (We are interested in the enthalpy change for the reaction and its value, derived from the slope of a $\log K$ vs. $1/T$ plot, is subject to the less stringent assumption that the changes of the activity coefficients of the two oxides with temperature are the same.) The graph of the data is shown in Figure 5. Since the value at the lowest temperature was low in comparison with the other points, we ignored it in drawing a line through the data on the assumption that the oxide mixture may have been solid at that temperature. The slope of the line drawn through the data results in an enthalpy change at about 1000°K (the mid-temperature) of 60 kcal. This may be taken as the enthalpy change for the reaction



on the assumption that the enthalpy of mixing of the oxides is small.

There are almost no data on which to base a reliable estimate of the entropy change of the reaction; therefore an accurate third-law calculation of the enthalpy change is not possible. A rough estimate of the entropies was made as follows: Latimer's rules⁷ for the solid oxides at 298°K gives 32 eu for Tl_2O_3 and 33 for Tl_2O . The heat capacities were taken as 6.7 eu per gram-ion for the solids and 7.3 eu for the liquids.⁸ The entropy of fusion of Tl_2O_3 was assumed to be the same as Bi_2O_3 (6.2 eu) and that of Tl_2O the same as Cu_2O (8.9 eu). Together with the absolute entropy⁹ of O_2 of 58 eu the $\Delta S^\circ_{1000^\circ\text{K}}$ for reaction 4 was 45 eu. At 1000°K the partial pressure of oxygen from Duncan's data was 0.16 atm. Thus $\Delta F^\circ_{1000^\circ\text{K}}$ equals 3.6 kcal and $\Delta H^\circ_{1000^\circ\text{K}}$ was found to be 49 kcal. In view of the estimates made in arriving at this value, it can be considered to substantiate the value of 60 kcal obtained above in the second-law treatment.

There are two other reports of measurements of the "decomposition" pressure of Tl_2O_3 , that of Rassa¹⁴ and of Toropova and Pogorelyi.¹⁵ They both measured the oxygen pressures developed by solid Tl_2O_3 as it

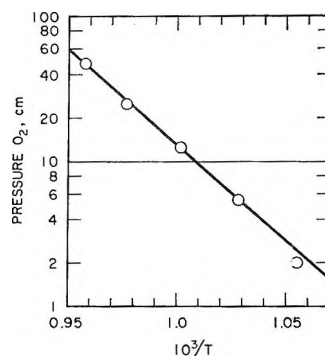
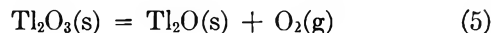


Figure 5. Partial pressure of oxygen over molten Tl_2O_3 - Tl_2O mixtures calculated from Duncan's data for equal mole fractions of Tl_2O_3 and Tl_2O .

was heated. The two sets of data are in fair agreement; however, we consider them both to be incorrect for the reasons given below.

A second-law treatment yields $\Delta H^\circ_{700^\circ\text{K}} = 6.9$ kcal from Rassa's data (he misquotes his own results, erroneously giving 69 kcal) and 5.2 kcal from Toropova and Pogorelyi. However, a third-law treatment of these data assuming the reaction to be



and using the estimates given above for the entropies gives 45 and 40 kcal, respectively, for the enthalpy changes at 700°K . These are markedly at variance with the second-law values which thus indicates that the measurements of these two sets of authors did not correspond to reaction 5.

In Rassa's work (and probably in that of Toropova and Pogorelyi also, but this reference was available to us only as an abstract) the pressure developed by a fixed amount of solid Tl_2O_3 into a fixed gas volume was measured as a function of temperature. Under these conditions the number of moles of oxygen liberated by the Tl_2O_3 and so the ratio of Tl_2O to Tl_2O_3 in the solid, increased with temperature. The change of oxygen pressure under this hypothesis (and assuming a solid solution of Tl_2O in Tl_2O_3) is the sum of its change with change of composition plus that with change of temperature at fixed composition. The enthalpy change for the reaction is related to the second term only and since the first term can be appreciable, and even dominant, it is incorrect to derive the enthalpy change from the change of oxygen pressure with temperature

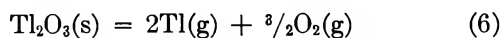
(14) M. Rassa, *Ann. Chim. (Paris)*, 8, 755 (1953).

(15) T. G. Toropova and A. D. Pogorelyi, *Tr. Sev. Kavkazsk. Gornomet. Inst.*, 17, 38 (1961). This reference was available to us only as abstracts: *Chem. Abstr.*, 61, 1293g, (1964), which reports their equation incorrectly, and *Rev. Zh. Khim.*, 1963, Abstr. No. 22B330.

(as Rassa did and Toropova and Pogorelyi probably did). Duncan was aware of this problem and measured independently the change both with composition and temperature.

Appendix II

Partial Pressure of Tl over Tl₂O₃. The partial pressure of elemental Tl in equilibrium with solid Tl₂O₃ is a function of the partial pressure of oxygen applied to the system, as well as the temperature. It can be calculated from the constant for the equilibrium



The constant was estimated from the enthalpy of reaction 5. The enthalpy of formation of Tl₂O at 298°K

is given by Roth and Meichsner,¹⁶ the enthalpy of vaporization of Tl given by Stull and Sinke,¹⁷ and the estimates given in Appendix I for the entropies and heat capacities of the oxides. At 900°K a value of 4×10^{-19} was obtained for the equilibrium constant of eq 6, so that at 0.01 atm of oxygen the partial pressure of Tl(g) is 2×10^{-8} atm, or about 10^{-6} of the pressure of gaseous thallium-containing species observed in our experiments. At 800°K the calculated pressure of Tl(g) is 2×10^{-11} atm (at 0.01 atm of O₂), about 10^{-5} of our observed pressure of thallium-containing species.

(16) W. A. Roth and A. Meichsner, *Z. Elektrochem.*, **38**, 87 (1932).

(17) D. R. Stull and G. C. Sinke, "Thermodynamic Properties of the Elements," *Advances in Chemistry Series No. 18*, American Chemical Society, Washington, D. C., 1956.

Excess and Partial Volumes of Some Alcohol-Water and Glycol-Water Solutions

by Koichiro Nakanishi, Nobuyuki Kato, and Masato Maruyama

Department of Industrial Chemistry, Shinshu University, Nagano, Japan (Received June 27, 1966)

The excess and partial volumes of binary systems of water with four glycols (1,2- and 1,3-propanediols and 1,3- and 1,4-butanediols) and with two alcohols (*t*-butyl alcohol and *t*-pentyl alcohol) have been determined by the pycnometric method. The volume contraction in the glycol-water systems is, though smaller in magnitude, similar in nature to that of the well-known ethanol-water type. The partial volumes of the solutes in the alcohol solutions have their minima at lower mole fraction (such as 0.04–0.09) than in glycol solutions. The limiting values of the partial volumes at infinite dilution are also evaluated. It was found that the presence of the methyl group in the glycol molecule is a decisive factor and is responsible for the larger volume contraction observed when 1,2-propanediol or 1,3-butanediol is dissolved in water.

Introduction

Various anomalous behavior of aqueous alcohol solutions has been reported in properties such as viscosity, partial molal volumes, ultrasonic absorption, gas solubility, etc.¹ Although a complete understanding has not yet been reached quantitatively, there is now

enough evidence that such anomalies are of structural origin. In the interpretation of many complex phenomena exhibited by various aqueous solutions, the

(1) For review, see F. Franks and D. J. G. Ives, *Quart. Rev. (London)*, **20**, 1 (1966).

"iceberg" concept of Frank and Evans² and a statistical mechanical theory proposed by Némethy and Scheraga³ based on the "flickering-cluster" model of Frank and Wen⁴ have made primary contributions.⁵

Since the problem is structural in nature, the study of the volumetric behavior of aqueous mixtures should furnish an important source of information. Although much effort has been directed to the study of monohydric alcohol-water solutions, which are also the main subject of a recent review by Franks and Ives,¹ no extensive density data have been published so far for dihydric alcohol (glycol)-water solutions.

Continuing the work of the previous report on the volumetric behavior of aqueous alcohol solutions,⁶ we have measured the density of four glycol-water solutions and two alcohol-water solutions. The glycols used were 1,2-propanediol (12PD), 1,3-propanediol (13PD), 1,3-butanediol (13BD), and 1,4-butanediol (14BD). The alcohols used were *t*-butyl alcohol (*t*-BuOH) and *t*-amyl alcohol (*t*-PeOH). In this paper, we will present new density data and discuss the general feature of the volume-of-mixing property of alcohol-water and glycol-water systems.

Experimental Section

Purification of Liquids. The samples of alcohols and glycols used in this study were prepared as follows. The best grade available from commercial sources (mostly the Guaranteed reagent) was dried over dehydrating agents such as K_2CO_3 or Na_2SO_4 and then distilled with a fractionating column (*ca.* 30 theoretical plates) at atmospheric or reduced pressure. Purity of the final samples was checked by gas chromatography on a Silicone 550 column using H_2 as the carrier gas. Only those samples which showed no trace of impurities on their chromatograms (less than 100 ppm) were used.

The water used was obtained by the repeated distillation of deionized water.

The boiling points of purified samples used for density determination are summarized in Table I.

Density Measurements. The density of pure liquids

and solutions was determined with a bicapillary-type pycnometer used in the previous study.⁶ All of the measurements were made at 25.00 or 30.00° in a water thermostat, the temperature of which was controlled to $\pm 0.005^\circ$.

Results

Densities. The density data for all the alcohols and glycols are presented in Tables II and III, respectively. The data extend over all of the composition ranges (from 0 to 1 of the alcohol fraction) except for *t*-PeOH solution, which shows partial miscibility. For the cases where the density of glycol is close to that of water, a density maximum appears, while the presence of an inflection point at a lower alcohol fraction is common to all of the solutions investigated.

Table II: Densities of *t*-Butyl Alcohol-Water Solutions and of *t*-Amyl Alcohol-Water Solutions

<i>t</i> -BuOH-H ₂ O at 25.0°		<i>t</i> -PeOH-H ₂ O at 30.0°	
w_1	d_{12}	w_1	d_{12}
0.0	0.99707	0.0	0.99568
0.01047	0.99507	0.02085	0.99265
0.02683	0.99236	0.03133	0.99120
0.05965	0.98751	0.04122	0.98998
0.07699	0.98514	0.04752	0.98925
0.09343	0.98287	0.06137	0.98743
0.12753	0.97832	0.06769	0.98666
0.14342	0.97630	0.07798	0.98526
0.16740	0.97266	0.08824	0.98375
0.18725	0.96948	0.10047	0.98209
0.21524	0.96405		
0.26791	0.95309		
0.32036	0.94117		(Phase separation)
0.38767	0.92496		
0.46265	0.90809		
0.52681	0.89310	0.80102	0.84478
0.60471	0.87494	0.84570	0.83580
0.69113	0.85492	0.87822	0.82895
0.74844	0.84149	0.90791	0.82268
0.89403	0.80673	0.94206	0.81531
0.95931	0.79133	0.97300	0.80831
1.0	0.78220	1.0	0.80179

Table I: Boiling Point of Purified Samples

Alcohol	Boiling point, °C	
	Obsd	Lit.
<i>t</i> -BuOH	81.5-82.0 (730) ^a	82.57 (760) ^a
<i>t</i> -PeOH	101.2-101.4 (730)	102.3 (760)
12PD	187.2-187.5 (730)	188.2 (760)
13PD	109-110 (12)	214.2 (760)
13BD	204.5-205.5 (730)	204 (760)
14BD	102 (5)	235 (760)

^a Pressure in mm.

Excess Volume. The excess volume of any binary solution is calculated from the density data by eq 1.

(2) H. S. Frank and M. W. Evans, *J. Chem. Phys.*, **13**, 507 (1945).

(3) G. Némethy and H. A. Scheraga, *ibid.*, **36**, 3382 (1962).

(4) H. S. Frank and W. Y. Wen, *Discussions Faraday Soc.*, **24**, 133 (1957).

(5) See also J. L. Kavanau, "Water and Solute-Water Interactions," Holden-Day Inc., San Francisco, Calif., 1964.

(6) K. Nakanishi, *Bull. Chem. Soc. Japan*, **33**, 793 (1960).

Table III: Densities of Four Glycol-Water Solutions

12PD-H ₂ O at 25.0°		13PD-H ₂ O at 25.0°		13BD-H ₂ O at 30.0°		14BD-H ₂ O at 25.0°	
w_1	d_{12}	w_1	d_{12}	w_1	d_{12}	w_1	d_{12}
0.0	0.99707	0.0	0.99707	0.0	0.99568	0.0	0.99707
0.03617	0.99939	0.03265	0.99909	0.03166	0.99639	0.06961	0.99909
0.08030	1.00265	0.04915	1.00016	0.06789	0.99747	0.08742	0.99973
0.14390	1.00781	0.12347	1.00520	0.08247	0.99805	0.13746	1.00165
0.15949	1.00906	0.15002	1.00707	0.10279	0.99885	0.17494	1.00318
0.18081	1.01098	0.18727	1.00985	0.12080	0.99973	0.19196	1.00397
0.19846	1.01249	0.21353	1.01190	0.14860	1.00073	0.28873	1.00826
0.21782	1.01416	0.23545	1.01353	0.18165	1.00232	0.31787	1.00963
0.28554	1.01995	0.26794	1.01603	0.22080	1.00402	0.38604	1.01283
0.35798	1.02558	0.28617	1.01742	0.24514	1.00502	0.51216	1.01764
0.40260	1.02895	0.32736	1.02059	0.30945	1.00788	0.56444	1.01932
0.44649	1.03156	0.35594	1.02283	0.35159	1.00956	0.62391	1.02052
0.47054	1.03324	0.39759	1.02598	0.41496	1.01178	0.75011	1.02174
0.54121	1.03661	0.44764	1.02969	0.44113	1.01279	0.80940	1.02099
0.56879	1.03755	0.54961	1.03659	0.49802	1.01406	0.85844	1.01986
0.60453	1.03881	0.63096	1.04120	0.58947	1.01504	0.89337	1.01846
0.64032	1.03954	0.69039	1.04385	0.67909	1.01459	0.91708	1.01744
0.69897	1.04018	0.72977	1.04577	0.78616	1.01207	0.93395	1.01684
0.80688	1.03983	0.81717	1.04779	0.85916	1.00852	0.94463	1.01607
0.82536	1.03946	0.88824	1.04922	0.92606	1.00414	0.95572	1.01564
0.90890	1.03706	0.96204	1.04944	0.95843	1.00162	0.96843	1.01492
1.0	1.03241	1.0	1.04889	1.0	0.99778	1.0	1.01289

$$\Delta V^E = \frac{x_1 M_1 + x_2 M_2}{d_{12}} - \left(x_1 \frac{M_1}{d_1^\circ} + x_2 \frac{M_2}{d_2^\circ} \right) \quad (1)$$

where x is the mole fraction, M is the molecular weight, d_{12} is the density of the solution in g/cc, d° is the density of pure liquid, and the subscripts 1 and 2 refer to alcohol and water, respectively.

Experimental data for ΔV^E are plotted against x_1 in Figure 1. For all of the systems investigated, ΔV^E is negative at all compositions and there is an inflection point as in the monohydric alcohol-water systems studied previously.

An attempt was made to fit ΔV^E data with an equation of the type

$$\Delta V^E = x_1 x_2 [A + B(x_1 - x_2) + C(x_1 - x_2)^2 + \dots] \quad (2)$$

where A, B, C, \dots are constants. As is evident from the $\Delta V^E/x_1 x_2$ vs. x_1 plot in Figure 2, however, ΔV^E is highly asymmetric with regard to x and it was necessary to use at least four constants in eq 2 or to determine two sets of constants by calculating ΔV^E in different ranges of x_1 . Such complex multiconstant equations are meaningless at the present stage.

Partial Volumes. The presence of an inflection point in ΔV^E is connected to the occurrence of a minimum value in the partial molal volume vs. x relationship of one component as well as to a maximum in the

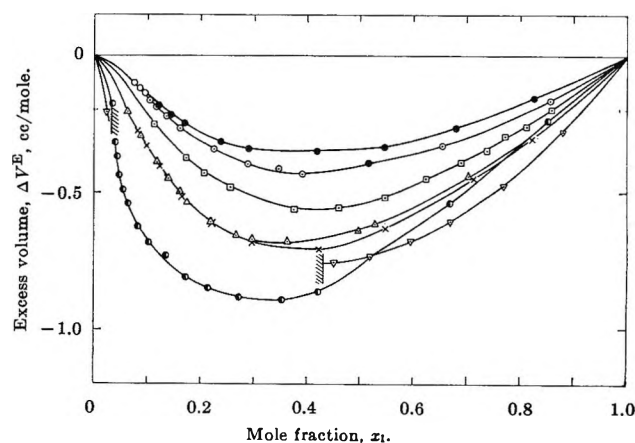


Figure 1. Excess volume of alcohol-water and glycol-water systems: ●, 12ED + H₂O at 20°; ○, 13PD + H₂O at 25°; □, 14BD + H₂O at 25°; △, 12PD + H₂O at 25°; ×, 13BD + H₂O at 30°; ▽, *t*-PeOH + H₂O at 30°; ○, *t*-BuOH + H₂O at 25°.

partial molal volume of the other. These are the consequences of a rigorous thermodynamic interrelation between ΔV^E and the corresponding partial molal volumes, v_i . Since the absolute value of ΔV^E is quite large in the present case, the partial molal volume of both components are evaluated rather precisely from density data.

The composition dependence of the computed v_1 values are shown in Figure 3, where $v_1 - v_1^\circ$ is plotted

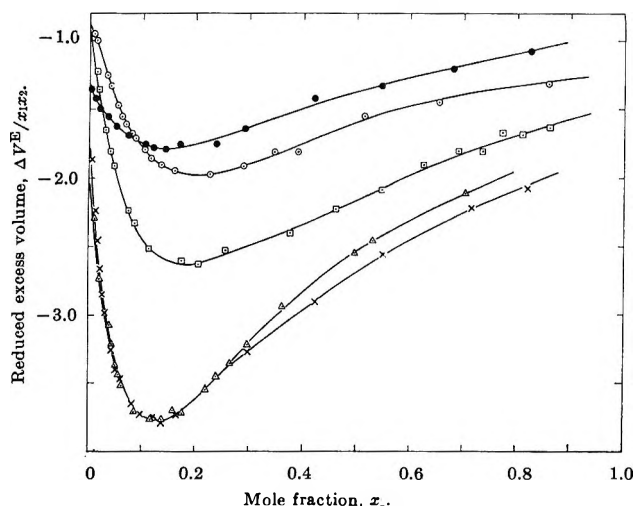


Figure 2. Reduced excess volume of glycol-water systems: ●, 12ED; ○, 13PD; □, 14BD; △, 12PD; ×, 13BD.

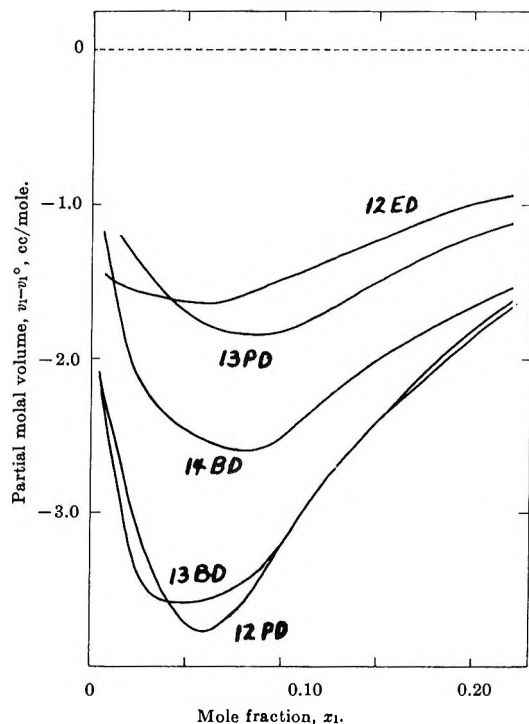


Figure 3. Partial molal volume of glycols near their minima.

against x_1 (v_1^0 is the reference molal volume of alcohols). It is obvious from the figure that the well-known ethanol-water type behavior is common to all the glycol-water systems.

Discussion

The large negative ΔV^E value observed in the liquid mixtures containing water can well be explained by the occupation of the free volume, or cavities, in the open solvent structure with another component. How-

ever, such cavity occupation simply results in a smooth v_1 vs. x_1 curve, and any theoretical approach should clarify, at least qualitatively, the nature of minimum point in a v_1 vs. x_1 curve.⁷⁻¹¹ According to Frank and Evans,² the orientation of solute molecules around the ice-like structure of water forms the so-called "ice-berg" which results in the stabilization of the water structure. Although the interpretation of the minima in v_1 is unsettled, it seems unavoidable to conclude that the minimum corresponds to the upper limit of the region where the stabilization of the water structure can take place.

Position and Depth of $(v_1)_{\min}$. As was pointed out in the previous paper,⁶ the position of the partial volume minimum shifts to lower alcohol concentration as the hydrophobic group becomes larger. This is supported by the new data on *t*-PeOH which shows the lowest value among all the alcohols studied. As was seen in the BuOH series, the effect of chain branching among isomers is of minor importance. On the other hand, in the case of glycols, the positions of minima are almost independent of the sizes and shapes of the glycols.

The volume loss of glycols is smaller than that for monohydric alcohols; roughly speaking, the average value of the percentage maximum volume contraction is ≈ 9 for the monohydric alcohols and ≈ 4 for glycols (a more detailed analysis is given in a later paragraph). Table IV summarizes the approximate values of the alcohol mole fractions at which the partial volumes of alcohols are minimal and at which there is a maximum volume contraction, $(v_1)^0 - (v_1)_{\min}$, where $(v_1)_{\min}$ is the partial molal volume of alcohol at the minimum point.

Partial Volume at Infinite Dilution. Recently, Friedman and Scheraga¹² obtained the limiting value of the partial volume, $(v_1)_{x_1 \rightarrow 0}$, for a series of monohydric alcohols at various temperatures from a very precise density measurement in dilute solution. Based on a simple theoretical treatment, they evaluated the contribution of the nonpolar group (the aliphatic portion of alcohol molecule) to the decrease in volume upon mixing with water.

(7) It is to be noted that these kinds of minima are also reported in the partial volumes of *p*-dioxane⁸ and of ethylene glycol dimethyl ether⁹ in water, but no minimum has ever been observed in acetone-water¹⁰ or in hydrogen peroxide-water solution.¹¹

(8) H. Schott, *J. Chem. Eng. Data*, **6**, 19 (1961).

(9) W. J. Wallace and A. L. Mathews, *ibid.*, **8**, 496 (1963).

(10) V. S. Griffith, *J. Chem. Soc.*, 860 (1953).

(11) A. G. Mitchell and W. F. K. Wynne-Jones, *Discussions Faraday Soc.*, **15**, 161 (1953).

(12) M. E. Friedman and H. A. Scheraga, *J. Phys. Chem.*, **69**, 3795 (1965).

Table IV: Position of $(v_1)_{\min}$ and Maximum Volume Contraction

Alcohol	Temp, °C	Min pt		$\frac{(v_1)_{\min} - (v_1^\circ)}{v_1^\circ} \times 100$	Data source
		w_1	x_1		
MeOH	15	0.17	0.105	-8.3	a
EtOH	30	0.16	0.070	-9.5	a
<i>n</i> -PrOH	30	0.14	0.045	-8.5	a
<i>i</i> -PrOH	30	0.15	0.050	-10.4	a
<i>n</i> -BuOH	20	0.06	0.015	-7.7	b
<i>i</i> -BuOH	20	No minimum		...	b
<i>sec</i> -BuOH	20	0.07	0.018	-9.0	b
<i>t</i> -BuOH	25	0.09	0.024	-10.7	
<i>t</i> -PeOH	30	0.04	0.008	-9.0	
12ED	20	0.16	0.060	-3.0	b
12PD	25	0.21	0.060	-5.2	
13PD	25	0.29	0.090	-2.5	
13BD	30	0.17	0.045	-4.4	
14BD	25	0.32	0.085	-2.9	

^a "International Critical Tables," Vol. III, McGraw-Hill Book Co., Inc., New York, N. Y., 1928, pp 115-122. ^b See ref 6.

Although our data at extremely dilute solution were less accurate, we tried to estimate $(v_1)_{x_1 \rightarrow 0}$ for all the glycols studied (including ethylene glycol (12ED) studied in the previous work),⁶ for which the concentration dependence of v_1 near infinite dilution was not too large. There are two methods of evaluating $(v_1)_{x_1 \rightarrow 0}$ from the density data. An extrapolation of either the apparent volume or $(\Delta V^E/x_1x_2)$ to $x_1 = 0$ can equally give $(v_1)_{x_1 \rightarrow 0}$.¹³ The application of $(\Delta V^E/x_1x_2)$ extrapolation which was omitted in the Friedman-Scheraga treatment appreciably compensated for the lack of data available in dilute solution and we could obtain the $(v_1)_{x_1 \rightarrow 0}$ values as shown in Table V. From the figures in Table V we can estimate $\Delta \bar{V}_R$,¹² the contribution of the nonpolar group to the volume change upon transfer of 1 mole of alcohol from the pure alcohol to an infinitely dilute aqueous solution, as

$$\begin{aligned} \Delta \bar{V}_R(-\text{CH}_2-) &= \Delta(v_1)_{x_1 \rightarrow 0}(13\text{PD}) - \\ &\quad \Delta(v_1)_{x_1 \rightarrow 0}(12\text{ED}) = -0.4 \\ &= \Delta(v_1)_{x_1 \rightarrow 0}(14\text{BD}) - \\ &\quad \Delta(v_1)_{x_1 \rightarrow 0}(13\text{PD}) = 0.0 \\ \Delta \bar{V}_R(-\text{CH}_3) &= \Delta(v_1)_{x_1 \rightarrow 0}(12\text{PD}) - \\ &\quad \Delta(v_1)_{x_1 \rightarrow 0}(12\text{ED}) = 0.7 \\ &= \Delta(v_1)_{x_1 \rightarrow 0}(13\text{BD}) - \\ &\quad \Delta(v_1)_{x_1 \rightarrow 0}(13\text{PD}) = 0.7 \end{aligned}$$

Although minor corrections due to the temperature difference and the abstraction of one hydrogen atom in the latter case are neglected, it may be concluded that $\Delta \bar{V}_R$ for the methylene group is nearly equal to zero—doubtlessly smaller than that in monohydric alcohols—and that the methyl group causes a large negative contribution which indicates its effective occupation of the open structure in water.

Table V: Estimates of Partial Volume at Infinite Dilution for Glycols

Glycol	Temp, °C	Molal volume, v_1°	From ϕ_1^a		From $(\Delta V^E/x_1x_2)$
			$(v_1)_{x_1 \rightarrow 0}$	$\Delta(v_1)_{x_1 \rightarrow 0}^b$	$\Delta(v_1)_{x_1 \rightarrow 0}^b$
12ED	20	55.762	55.4	-1.4	-1.3 ± 0.05
12PD	25	73.705	71.7	-2.0	-2.1 ± 0.1
13PD	25	72.547	71.6	-0.9	-0.9 ± 0.05
13BD	30	90.325	88.7	-1.6	-1.7 ± 0.1
14BD	25	88.977	88.2	-0.8	-0.9 ± 0.1

^a Apparent molal volume of glycol in water; $\phi_1 = M_1[d_1^\circ - (d_{12} - d_1^\circ)/d_1^\circ d_2 w_1]$. ^b Volume decrease at infinite dilution; $\Delta(v_1)_{x_1 \rightarrow 0} = (v_1)_{x_1 \rightarrow 0} - v_1^\circ$ in cc/mole.

In conclusion, the volumetric behavior of the glycols in water, which is found to be similar to that of the monohydric alcohols, can be divided into two groups. In the first group, which includes 12ED, 13PD, and 14BD, the $(v_1)_{x_1 \rightarrow 0}$ are almost the same, although their ΔV^E increases slightly with molecular size. On the other hand, 12PD and 13BD, which belong to the second group, have almost the same ΔV^E and $(v_1)_{x_1 \rightarrow 0}$. In the interpretation of these results, recent analysis by Franks and Ives¹ is suggestive; our glycol data indicate that, owing to the introduction of the second hydroxyl group into the molecule, the glycol molecules will mix "substitutionally" with water and their behavior is very much like that of methanol. However, if one of the hydroxyl groups is not located at the end of molecule, the "interstitial" contribution due to a possible cavity occupation by a methyl group will increase to result in a larger volume loss. Thus the presence of the secondary hydroxyl or methyl group is one of the decisive factors in determining the volumetric behavior of glycols in water.

(13) H. C. Van Ness, "Classical Thermodynamics of Non-Electrolyte Solutions," Pergamon Press, New York, N. Y., 1964, p 100.

Effect of Pressure on the Dissociation of the (LaSO₄)⁺ Complex Ion¹

by Frederick H. Fisher and Douglas F. Davis

University of California, San Diego, Marine Physical Laboratory of the Scripps Institution of Oceanography, San Diego, California 92162 (Received June 30, 1966)

Electrical conductance as a function of pressure up to 2000 atm has been measured on aqueous solutions of lanthanum sulfate at 25° at seven concentrations from 0.0002 to 0.0082 equiv/l. The effect of pressure on the dissociation constant of the (LaSO₄)⁺ complex ion pair was calculated using three different methods. At atmospheric pressure ΔV° ranged from -21.2 to -26.2 ml/mole and at 2000 atm ΔV° ranged from -6.8 to -11.8 ml/mole depending on the method used and concentration. Based on the atmospheric pressure value of $\bar{V}_2^\circ = -23.8$ for La₂(SO₄)₃ the partial molal volume of the (LaSO₄)⁺ ion at the lowest concentration is -0.9 to 0.2 ml/mole.

The very small partial molal volume assigned by Owen and Brinkley^{2a} to the La³⁺ ion, $\bar{V}_1^\circ = -38.3$ ml/mole relative to the H⁺ ion for which $\bar{V}_1^\circ = 0$ ml/mole, suggested to F. H. F. that there might be an even greater effect of pressure on La₂(SO₄)₃ than was observed for MgSO₄^{2b} or MnSO₄.³

Measurements of the electrical conductivity were made on aqueous solutions of La₂(SO₄)₃ at 25° in essentially the same manner as for MgSO₄. It was possible to use Pyrex connected electrodes throughout the measurements with a small correction (10⁻⁶ atm⁻¹) for the coefficient of linear compression of Pyrex.⁴

Lanthanum chloride was prepared from Lindsay lanthanum oxide in the manner of Nathan,⁵ while the lanthanum sulfate purchased from K and K Laboratories was recrystallized once, also after Nathan. Reagent grade potassium chloride and potassium sulfate were obtained from Mallinckrodt and Matheson Coleman and Bell, respectively. All solutions were within ±0.2 pH unit of the conductance water (pH 5.8).

Results

Ratios of equivalent conductivities as a function of pressure are shown in Table I. By making use of earlier data^{6,7} obtained at 1 atm, values for equivalent conductance as a function of pressure were calculated using the ratios in Table I and are shown in Table II. In Table III measurements to 2000 atm on KCl solutions obtained in the 30-ml cylindrical Teflon cell show agreement to within 0.1% with those obtained in a 12-cc spherical Pyrex cell.

Table I: Λ_p/Λ_1 for Aqueous Solutions of La₂(SO₄)₃ at 25°

P, atm	mequiv/l.						
	0.2	0.3	0.6	1.2	2.4	3.1	8.2
250	1.036	1.044	1.056	1.064	1.072	1.074	1.078
500	1.063	1.078	1.102	1.119	1.135	1.139	1.147
750	1.082	1.106	1.140	1.166	1.190	1.198	1.213
1000	1.096	1.125	1.169	1.206	1.239	1.249	1.274
1250	1.104	1.140	1.193	1.239	1.292	1.296	1.326
1500	1.107	1.149	1.209	1.263	1.314	1.330	1.372
1750	1.107	1.153	1.222	1.283	1.342	1.361	1.411
2000	1.103	1.156	1.231	1.299	1.365	1.387	1.447

If c is concentration of the solute in equivalents, then the dissociation constant for the reaction



may be expressed as follows⁸

$$K = [(c/3 - x)(c/2 - x)/x]\pi^f \quad (2)$$

(1) This paper represents results of research sponsored by the Office of Naval Research.

(2) (a) B. B. Owen and S. R. Brinkley, Jr., *Chem. Rev.*, **29**, 461 (1941); (b) F. H. Fisher, *J. Phys. Chem.*, **66**, 1607 (1962).

(3) F. H. Fisher and D. F. Davis, *ibid.*, **69**, 2595 (1965).

(4) L. H. Adams, *J. Am. Chem. Soc.*, **53**, 3780 (1931).

(5) C. C. Nathan, W. E. Wallace, and A. L. Robinson, *ibid.*, **65**, 790 (1943).

(6) F. H. Spedding and S. Jaffe, *ibid.*, **76**, 882 (1954).

(7) I. L. Jenkins and C. B. Monk, *ibid.*, **72**, 2695 (1950).

(8) At atmospheric pressure the difference between molar and molal units will be neglected.

Table II: Λ_p , Equivalent Conductance for Aqueous $\text{La}_2(\text{SO}_4)_3$ Solutions at 25°

P , atm	mequiv/l.						
	0.2	0.3	0.6	1.2	2.4	3.1	8.2
1	119.0 ^c	109.5 ^c	94.7 ^c	80.7 ^a	67.1 ^b	63.3 ^b	48.8 ^b
250	123.3	114.3	100.0	85.9	71.9	68.0	52.6
500	126.5	118.0	104.4	90.3	76.2	72.1	56.0
750	128.8	121.1	108.0	94.1	79.8	75.8	59.2
1000	130.4	123.2	110.7	97.3	83.1	79.1	62.2
1250	131.4	124.8	113.0	100.0	86.7	82.0	64.7
1500	131.7	125.8	114.5	101.9	88.2	84.2	67.0
1750	131.7	126.3	115.7	103.5	90.0	86.2	68.9
2000	131.3	126.6	116.6	104.8	91.6	87.8	70.6

^a I. L. Jenkins and C. B. Monk, *J. Am. Chem. Soc.*, **72**, 2695 (1950). ^b F. H. Spedding and S. Jaffe, *ibid.*, **76**, 882 (1954). ^c Interpolated graphically from combined data of *a* and *b*.

Table III: Comparison of KCl Conductance Ratios Λ_p/Λ_1 for Two Cells at 25.00 ± 0.02° and 10-kc Bridge Frequency

P , atm	Teflon cell ^a	Glass cell ^b
250	1.0090	1.0094
500	1.0145	1.0147
750	1.0175	1.0178
1000	1.0177	1.0180
1250	1.0167	1.0168
1500	1.0133	1.0134
1750	1.0086	1.0087
2000	1.0028	1.0025

^a Λ_p/Λ_1 average over five concentrations of KCl from 0.0005 to 0.02 *M* measured in 30-ml cylindrical Teflon cell with parallel Pyrex-spaced platinum electrodes coated with platinum black. ^b Λ_p/Λ_1 for 0.02 *M* KCl measured in 12-ml spherical Pyrex cell with parallel shiny platinum electrodes.

where x is the concentration in equivalents of the $(\text{LaSO}_4)^+$ complex ion and π^f is the activity coefficient product.

Calculations were made using the mixture rule in which the solution is regarded as a mixture⁹ of a 1-2 salt, $(\text{LaSO}_4)_2\text{SO}_4$, at equivalent concentration x and the 3-2 salt, $\text{La}_2(\text{SO}_4)_3$, at equivalent concentration $c - 3x$. The observed equivalent conductance of the solution is written then as

$$\Lambda_{\text{obs}} = (x/c)\Lambda_{12} + (c - 3x)/c\Lambda_{23} \quad (3)$$

where the Λ_{12} and Λ_{23} are calculated from theory and x is solved for by successive approximations. The activity coefficient product is⁶

$$\pi^f = [(f_{32\pm})^{5/2}/(f_{12\pm})^{3/2}] \quad (4)$$

where

$$-\log f_{ij\pm} = (A|z_i z_j| \sqrt{I}) / (1 + B\delta \sqrt{I}) \quad (5)$$

and the ionic strength $I = 2.5c - 6x$.

Calculations of x and K were made using three different methods as follows.

Method a: The Davies-Otter-Prue equation with appropriate modifications for pressure-dependent terms^{2b}

$$\Lambda = \Lambda^\circ - [(R\Lambda^\circ / \{1 + B\delta \sqrt{I/2}\}) + E] \times (\sqrt{I} / \{1 + B\delta \sqrt{I}\}) \quad (6)$$

was used to calculate the equivalent conductance. Bjerrum distances (at atmospheric pressure) of 21.4 Å for the 3-2 and 7.14 Å for the 1-2 salt were used for δ and the same pressure dependence was applied as in the MgSO_4 work.

Method b: Equation 6 was used but distances of $\delta = 5$ Å for the 3-2 and $\delta = 3.6$ Å for the 1-2 salt were used; these are the same values that Spedding and Jaffe used.

Method c: The Onsager equation⁹

$$\Lambda = \Lambda^\circ - [R\Lambda^\circ + E]\sqrt{I} \quad (7)$$

was used to calculate the equivalent conductance and the δ distances of 5 and 3.6 Å were used in the activity coefficient calculation.

The pressure-dependent forms of eq 6 and 7 were used to calculate x and K as a function of pressure in a manner similar to that described earlier,^{2b} and the results for x in molar units are shown in Table IV. The molal dissociation constant, K_m , shown in Table V was obtained by dividing the values of K in molar units by the ratio of the density of water at pressure P to that at atmospheric pressure.

From the equation^{2a}

$$(\partial \ln K_m / \partial p)_{T,m} = -(\Delta V^\circ / RT) \quad (8)$$

values of ΔV° are calculated corresponding to the three different methods and are shown in Table VI.

The pressure dependence of infinite dilution equivalent conductivity, Λ°_p , for the $\text{La}_2(\text{SO}_4)_3$ was determined from the equation

$$\Lambda^\circ_p [\text{La}_2(\text{SO}_4)_3] = \Lambda^\circ_p [\text{LaCl}_3] + \Lambda^\circ_p [\text{K}_2\text{SO}_4] - \Lambda^\circ_p [\text{KCl}] \quad (9)$$

The Λ°_p values for the La^{3+} and SO_4^{2-} ions were calculated using the KCl transference number data of Wall and Gill.¹⁰ It was assumed that their transference number data to 1000 atm could be extrapolated linearly to 2000 atm. The Jenkins and Monk⁷ value for

(9) C. W. Davies, "Ion Association," Academic Press, New York, N. Y., 1962.

(10) F. T. Wall and S. J. Gill, *J. Phys. Chem.*, **59**, 278 (1955).

Table IV: Concentration ($\times 10^3$, equiv./l.) of LaSO₄⁺ in Aqueous La₂(SO₄)₃ at 25°

P, atm	mequiv./l. of La ₂ (SO ₄) ₃						
	0.2	0.3	0.6	1.2	2.4	3.1	8.2
a)	0.015	0.031	0.088	0.22	0.54	0.72	2.3
b) 1	0.015	0.030	0.086	0.22	0.53	0.70	2.2
c)	0.015	0.030	0.085	0.21	0.52	0.69	2.2
500	0.011	0.025	0.073	0.19	0.48	0.65	2.1
	0.011	0.024	0.070	0.18	0.47	0.63	2.1
	0.011	0.023	0.069	0.18	0.46	0.61	2.0
1000	0.009	0.020	0.061	0.17	0.43	0.59	2.0
	0.008	0.019	0.058	0.16	0.41	0.56	1.9
	0.008	0.018	0.057	0.15	0.40	0.54	1.8
1500	0.007	0.016	0.052	0.15	0.40	0.54	1.9
	0.007	0.015	0.049	0.14	0.37	0.50	1.7
	0.007	0.015	0.048	0.13	0.36	0.48	1.6
2000	0.006	0.014	0.045	0.13	0.36	0.49	1.8
	0.006	0.013	0.041	0.12	0.33	0.45	1.6
	0.006	0.012	0.040	0.12	0.32	0.43	1.5

^a Data obtained using the Davies-Otter-Prue conductance equation with $\bar{\alpha}$ calculated from Bjerrum's equation, $\bar{\alpha} = |Z_1 Z_2| e^2 / 2 \epsilon K T$. ^b Data obtained using the Davies-Otter-Prue conductance equation, but with $\bar{\alpha} = 5$ Å for the 3-2 case and $\bar{\alpha} = 3.6$ Å for the 2-1 case. ^c Data obtained using the basic Onsager conductance equation.

Table V: Dissociation Constant K_m ($\times 10^4$) for Aqueous La₂(SO₄)₃ at 25°

P, atm	mequiv./l. of La ₂ (SO ₄) ₃						
	0.2	0.3	0.6	1.2	2.4	3.1	8.2
a)	2.4	2.1	2.0	2.0	2.0	2.0	1.9
b) 1	2.4	2.1	2.0	1.9	1.8	1.8	1.6
c)	2.4	2.2	2.1	2.0	1.9	1.9	1.8
500	3.6	3.2	3.1	3.1	3.0	3.1	3.1
	3.7	3.2	3.1	3.0	2.8	2.8	2.6
	3.8	3.3	3.2	3.1	3.0	3.0	2.9
1000	5.2	4.6	4.4	4.3	4.3	4.5	4.6
	5.4	4.7	4.4	4.3	4.1	4.1	3.8
	5.6	4.8	4.6	4.5	4.3	4.5	4.5
1500	6.5	5.9	5.7	5.3	5.6	5.9	6.2
	6.9	6.1	5.8	5.3	5.4	5.5	5.2
	7.1	6.4	6.0	5.3	5.8	6.0	6.3
2000	8.0	7.6	7.3	7.2	7.2	7.5	8.0
	8.6	8.0	7.6	7.2	7.0	7.2	6.9
	8.9	8.4	8.0	7.7	7.6	8.0	8.4

^a See footnote a of Table IV. ^b See footnote b of Table IV. ^c See footnote c of Table IV.

$\Lambda^\circ_{\text{LaSO}_4^+}$ of 23.2 is used rather than the value of 40.0 proposed by Spedding and Jaffe⁶ because this value yielded values of K_m which showed less concentration

Table VI: $-\Delta V^\circ$ (ml/mole) for Aqueous La₂(SO₄)₃ at 25°

P, atm	mequiv./l.						
	0.2	0.3	0.6	1.2	2.4	3.1	8.2
a)	22.9	21.6	21.2	21.5	22.7	22.6	25.3
b) 1	23.7	22.2	21.7	22.0	23.1	23.0	25.2
c)	24.0	22.4	22.0	22.4	23.6	23.6	26.2
500	18.9	18.5	18.3	18.4	19.2	19.3	21.3
	19.6	19.2	18.9	19.0	19.7	19.8	21.5
	19.9	19.5	19.2	19.4	20.3	20.4	22.6
1000	14.9	15.5	15.4	15.3	15.7	16.0	17.3
	15.6	16.2	16.1	15.9	16.3	16.6	17.8
	15.8	16.5	16.5	16.4	16.9	17.3	19.0
1500	10.8	12.5	12.6	12.2	12.2	12.6	13.4
	11.5	13.2	13.3	12.9	12.9	13.4	14.1
	11.8	13.5	13.7	13.4	13.5	14.1	15.4
2000	6.8	9.4	9.7	9.1	8.7	9.3	9.4
	7.4	10.2	10.5	9.9	9.5	10.2	10.4
	7.7	10.5	10.9	10.4	10.1	10.9	11.8

^a See footnote a of Table IV. ^b See footnote b of Table IV. ^c See footnote c of Table IV.

Table VII: Equivalent Conductivities at Infinite Dilution as a Function of Pressure

P, atm	La ₂ (SO ₄) ₃	La ³⁺	SO ₄ ²⁻	LaSO ₄ ⁻
1	149.5	69.5	80.0	23.2
250	150.4	69.8	80.6	23.3
500	150.6	69.4	81.2	23.1
750	150.6	69.2	81.4	23.1
1000	150.0	68.6	81.4	22.9
1250	149.6	68.2	81.4	22.7
1500	148.9	67.4	81.5	22.5
1750	147.5	66.3	81.2	22.1
2000	146.3	65.4	80.9	21.8

dependence. The pressure dependence of the LaSO₄⁻ ion was taken to be the same as for Λ_p° for La₂(SO₄)₃.

Results for pressure dependence of equivalent conductance at infinite dilution are shown in Table VII. The original data for La₂(SO₄)₃ solution are shown in Table VIII.

Discussion

It is seen from Table V that regardless which method is used, K_m at atmospheric pressure approaches values in the neighborhood of 2.4×10^{-4} at low concentration, in agreement with the results of Spedding and Jaffe.⁶ The Davies-Otter-Prue equation used with the Bjerrum distances appears to give K values slightly less concentration dependent than for the other methods.

Table VIII: Copy of Original Conductivity Data for Aqueous Solutions of $\text{La}_2(\text{SO}_4)_3$ at 25°; Teflon Cell with Pyrex Bar between Electrodes: Cell Constant 0.457, Measured at 0.02 *M* KCl

<i>P</i> , atm	10^3 equiv./l. of $\text{La}_2(\text{SO}_4)_3$							H_2O
	0.2046	0.3072	0.6144	1.206	2.412	3.072	8.190	
	Conductivity in μmhos							
1	53.88	76.31	131.2	217.1	361.2	433.4	880.7	2.31
250	56.73	80.81	140.3	233.9	391.6	470.8	960.0	2.70
500	59.16	84.69	148.4	248.9	419.5	505.1	1033.5	3.11
750	61.22	88.08	155.3	262.2	444.6	536.7	1103.8	3.59
1000	63.01	90.87	161.1	274.1	467.6	565.3	1171.0	4.09
1250	64.53	93.35	166.4	284.5	488.1	590.9	1229.8	4.64
1500	65.85	95.45	170.7	293.2	505.7	613.5	1284.5	5.26
1750	66.94	97.18	174.4	300.8	521.2	633.5	1332.3	5.88
2000	67.85	98.73	177.6	307.2	534.7	650.9	1376.8	6.52
1 ^a	54.11	76.42	131.4	217.1	361.3	433.8	883.8	2.59

^a Readings taken the day after the pressure run.

At atmospheric pressure there is at most only a 5% difference in the ΔV° values obtained by the three methods. At the highest pressures and highest concentration the largest difference in the ΔV° values occur.

The atmospheric pressure values of ΔV° are of the same order as observed for NH_4OH ¹¹ and organic solutions¹² and very close to the value of -23.4 ml/mole calculated by Owen and Brinkley^{2a} for water. It is not known if a possible multistate configuration^{13,14} exists similar to that of MgSO_4 or MnSO_4 or if there exists only one form of the $(\text{LaSO}_4)^+$ ion pair. There is some indication that the rare earth sulfates show large ultrasonic absorption¹⁵ but until detailed experimental results are available, it is not possible to make an interpretation incorporating acoustic data.

Based on values of partial molal volume assigned by Owen and Brinkley^{2a} to La^{3+} of -38.3 ml/mole and SO_4^{2-} of $+14.5$, the partial molal volume of the $(\text{LaSO}_4)^+$ ion pair at atmospheric pressure and at the lowest concentration varies from -0.9 to $+0.2$ ml/mole depending upon the method used to calculate theoretical values of equivalent conductance.

(11) S. D. Hamann, "Physico-Chemical Effects of Pressure," Academic Press, New York, N. Y., 1957, p 151.

(12) A. Disteche and S. Disteche, *J. Electrochem. Soc.*, **112**, 350 (1965).

(13) F. H. Fisher, *J. Phys. Chem.*, **69**, 695 (1965).

(14) G. Atkinson and S. K. Kor, *ibid.*, **69**, 128 (1965).

(15) G. Atkinson, private communication.

Bonding in Heteromolecular Ion Clusters. $N_2O_2^+$

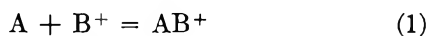
by G. S. Janik and D. C. Conway

Department of Chemistry, Texas A&M University, College Station, Texas (Received July 15, 1966)

Equilibrium constants for the reaction $N_2 + O_2^+ = N_2O_2^+$ have been determined mass spectrometrically from 177 to 249°K. It was found that $\Delta H^\circ_{200} = -5.69 \pm 0.08$ kcal/mole, $\Delta S^\circ_{200} = -18.9 \pm 0.4$ eu, and the bond energy $D_0(N_2-O_2^+) = 5.51 \pm 0.11$ kcal/mole. The $D_0(N_2-O_2^+)$ is about three times larger and the ΔS°_{200} is at least 2 eu more negative than predicted by the loose cluster model in which it is assumed that the N_2 and O_2^+ are freely rotating in the complex and isotropic interaction potentials are used. When anisotropic interaction potentials are used in which the ion-quadrupole interaction is considered, the bond energy and entropy change computed from the potential curves are in reasonable agreement with the experimental data.

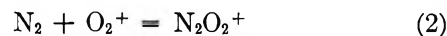
Introduction

When ions are generated in the gas phase, they may form ion-molecule complexes, the so-called ion clusters.^{2a} Equilibrium constants for reactions of the type



and bond energies $D_0(A-B^+)$ have been calculated by Eyring, *et al.*,^{2b} by approximating the interaction potential between A and B^+ as the sum of a Lennard-Jones potential between the neutral molecules and the ion-induced dipole interaction energy. In the FER^{2b} model, as in the earlier EHT³ model, the complex is taken to be loose; *i.e.*, it is assumed that the A and B^+ are freely rotating in the cluster and isotropic interaction potentials are used. However, it has been shown that homomolecular ion clusters are much more stable than predicted. Thus, $D_0(N_2-N_2^+)$ is seven times larger⁴ and $D_0(O_2-O_2^+)$ is five times larger⁵ than those obtained by the FER model. In addition, the model predicts that $[O_4^+]/[O_2^+] \approx 1$ at 10 atm pressure at 288°K, whereas this ratio was actually observed at a few torr. This has been interpreted as evidence for the importance of electron-exchange interactions in homomolecular ion clusters.⁶

This still leaves the question of the applicability of the FER model when the ligand is nonpolar and exchange interactions are a minimum; *i.e.*, when the ionization potential difference $IP(A) - IP(B) \gg D_0(A-B^+)$. To elucidate the nature of the bonding in such heteromolecular clusters, the equilibrium



has been studied.

Experimental Section

To determine the equilibrium constant for reaction 2, the ion ratio $(N_2O_2^+)/[O_2^+]$ was determined mass spectrometrically as in the O_4^+ investigation.⁵ The apparatus and experimental procedure are the same as in the previous investigation except as follows. (1) The gas was purified by passing it over 5-A Molecular Sieve and through two glass bead-packed liquid N_2 traps. Nitrogen was condensed in the first trap, so the N_2 gas could be purged by bubbling it through the liquid. (2) The gas was cooled by a 0.25-in. o.d. by 8-ft Cu coil heat exchanger and passed through a new ionization chamber (Figure 1). The heat exchanger and all but about 2 cm of the apparatus shown in Figure 1 were immersed in a 4.2-l. dewar which was filled with various organic slush baths or a Dry Ice-trichloroethylene mixture. The temperature of the bath was determined with a calibrated thermocouple. (3) The sensitivity was increased threefold by using a

- (1) Taken in part from the doctoral dissertation of G. S. Janik.
- (2) (a) S. C. Lind, "Radiation Chemistry of Gases," Reinhold Publishing Corp., New York, N. Y., 1961; (b) T. Fueno, H. Eyring, and T. Ree, *Can. J. Chem.*, **38**, 1693 (1960).
- (3) H. Eyring, J. O. Hirschfelder, and H. S. Taylor, *J. Chem. Phys.*, **4**, 479 (1936).
- (4) R. N. Varney, *ibid.*, **31**, 1314 (1959); **33**, 1709 (1960).
- (5) J. H. Yang and D. C. Conway, *ibid.*, **40**, 1729 (1964).
- (6) D. C. Conway and J. H. Yang, *ibid.*, **43**, 2900 (1965).

2.1 Ci titanium triiodide ionization source. (4) The ions effused into the mass spectrometer through six 18- μ holes in the 0.1-mil Pt foil window. (5) A time-of-flight mass spectrometer was used.

Since the spectrometer is not a commercial instrument, it will be described in more detail. After entering the spectrometer, the ions were pulsed out of the "trapping grids" (Figure 2) at a frequency of 29 kHz with the focusing pulse.⁷ The ions were gated by applying a delayed pulse to the gate grids at the end of the drift tube.⁸ The delayed trigger was obtained

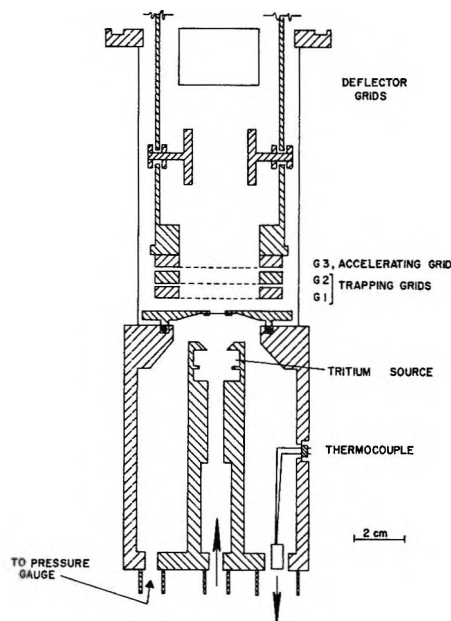


Figure 1. Ionization chamber and bottom part of the mass spectrometer.

from a Type 546 Tektronix oscilloscope and the gate pulse from a Type 214A Hewlett-Packard pulse generator. Ordinarily, a rather wide gate pulse of 58-v amplitude was used, such that any ion which received a gate pulse would pass the repeller grids and be detected by the Bendix M-306 ion multiplier, which was fitted with a Cu-Be cathode. Under these conditions the effective resolution⁹ $M/\Delta M = 27$. The ion intensity was determined by conventional pulse-counting techniques. The resolving time of the amplifier-scaler is 1 μ sec, and the drift time of the O_2^+ ion is 10 μ sec. Thus it can be seen that only one pulse is recorded if two ions of the same mass are pulsed down the drift tube at the same time. Therefore, the observed counting rate, R , was corrected by up to 3% to the true counting rate, R^* , by the relation

$$R^* = R/(1 - R\tau_t) \quad (E1)$$

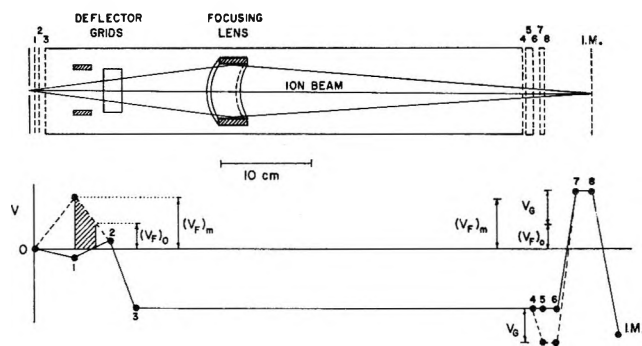


Figure 2. Schematic of the time-of-flight mass spectrometer and polarity of the grid potentials. The dashed lines indicate the potentials when either the focus pulse or the gate pulse is applied. Typical static grid potentials (V) are as follows: 1 and 2, -0.5 and $+2.1$, respectively (trapping grids); 3 and 4, -490 ; 5 and 6, -490 (gate grids); 7 and 8, $+60$ (repeller grids). To pass the repeller grids an ion must have the proper mass and be in the shaded region between G1 and G2 when G1 is pulsed.

where τ_t is the reciprocal of the (focus) pulsing frequency.

Since O_4^+ and N_4^+ are much more stable than $N_2O_2^+$ and $IP(N_2) > IP(O_2)$, reaction 2 can only be studied with $(N_2) \gg (O_2)$ where the O_2^+ is formed by charge exchange.¹⁰ Although $(N_4^+) \gg (N_2^+)$, a rough estimate of the required O_2 pressure can be calculated from the rate constant of 2×10^{-10} cc/sec obtained¹¹ for charge exchange with N_2^+ at room temperature. At the maximum flow rate (1000 cc/sec) it takes the ions $\sim 10^{-3}$ sec to reach the Pt window, so the O_2 pressure must be of the order of 10^{-4} torr. Initially (196 and 249°K) sufficient O_2 was bled into the N_2 stream to produce the O_2^+ at this flow rate, but the rest of the data were taken at a flow rate of 250 cc/sec since there was sufficient O_2 in the "pure" N_2 ¹² to form O_2^+ under these conditions. There were no major impurity peaks other than O_4^+ and/or N_4^+ .

(7) W. C. Wiley and I. H. McLaren, *Rev. Sci. Instr.*, **26**, 1150 (1955).

(8) W. E. Glenn, Jr., AECD-3337, Jan 1952.

(9) This can not be defined quantitatively because of the low intensity at the extremes of the peak. If the peaks were gaussian, this would correspond to a 1% contribution of the $M + \Delta M$ peak to the M peak intensity. The resolution could be adjusted to 100 (full width at half-height) to prove spectral purity.

(10) Simple charge exchange between N_2^+ and O_2 is more than 2000 times as probable as the reaction to produce $NO^+ + NO$ [P. Warneck and W. P. Poschenrieder, *Bull. Am. Phys. Soc.*, **11**, 505 (1966)].

(11) W. L. Fite, J. A. Rutherford, W. R. Snow, and V. A. J. van Lint, *Discussions Faraday Soc.*, **33**, 264 (1962).

(12) Matheson, prepurified grade, with the O_2 content listed as typically 8 ppm.

Results

To prove that reaction 2 is at equilibrium, the flow rate was decreased by a factor of four from the maximum at 12 torr and 249°K and a factor of two from 250 cc/sec at 12 torr and 227°K. In each case the increase in reaction time caused less than a 1% change in the equilibrium constant, K_P . This also shows that the $m/e = 60$ peak is not the complex between NO and NO^+ produced by a reaction such as



which is exothermic by $22 + D_0(\text{NO}-\text{NO}^+)$ kcal. [On the basis of the small value obtained for ΔH° , -5.69 kcal, it is apparent that the observed (equilibrium) ratio of the 60/32 peaks cannot be $[(\text{NO})_2^+]/(\text{O}_2^+)$.] Since the ion density is a function of flow rate, these experiments also show that the electric field strength in the ionization chamber was not large enough to cause an appreciable increase in the kinetic energy of the ions.⁵ The twofold reduction in flow rate at 227°K resulted in a fourfold reduction in ion intensity.

The average of the equilibrium constants determined at four N_2 pressures, p (3, 6, 9, and 12 torr), are reported in Table I. Two corrections have been applied to

Table I: Corrected Equilibrium Constants, K_P , for Reaction 2

Temp, °K	$K_P \times 10^4$ torr ⁻¹
177.3	937 ± 31 ^a
195.5	212 ± 8
227.4	32.0 ± 0.7
249.1	8.72 ± 0.25

^a Standard deviation.

these constants. (1) The uncorrected constants $(K_P)_p$ were found to decrease by up to 18% over this pressure range. Since the drift tube pressure $p_d \propto p$ and N_2O_2^+ has the larger geometrical cross section, it is possible that this is caused by the N_2O_2^+ being preferentially scattered out of the ion beam in the drift tube. The slope of each $\ln (K_P)_p$ vs. p_d curve was used to correct the constants to $(K_P)_0$ at zero pressure. (2) Mass discrimination occurs in mass transport to the window of the spectrometer and in the trapping grids. The result of an approximate analysis is

$$K_P = (K_P)_0 [(m_d + M)/(m_n + M)]^{1/2} \quad (\text{E2})$$

where M , m_n , and m_d are, respectively, the masses of the neutral gas molecule, the ion in the numerator,

and the ion in the denominator of the K_P expression (see Appendix). No correction was made for mass discrimination by the ion multiplier, although this was minimized since the ions were accelerated to 5000 v between the repeller grids and the cathode of the ion multiplier and the pulse-counting technique was used.

The usual method of evaluating the enthalpy change, ΔH° , is from a plot of $\log K$ vs. $1/T$. However, this is not a good method when ΔH° is small and there is a large contribution to the heat capacity from the internal degrees of freedom. In the present case there are not very many internal degrees of freedom, so the heat capacity change, ΔC_P° , could be estimated or even assumed to be zero to obtain ΔH° . In the latter case $\Delta H^\circ_{200} = -5.64$ kcal/mole for reaction 2. However, to obtain ΔH°_0 the vibrational frequencies of the weak modes must be estimated. In addition, it is best to treat all ion-cluster data by a general method which can be used for the large clusters which have been studied⁶ where heat capacity effects are relatively large. In this method standard free energies are evaluated at each temperature from the relation $\Delta G^\circ = -RT \ln 760K_P$. The left side of eq E3 is computed as a function of the temperature difference, ΔT , and

$$\begin{aligned} \Delta G_2^\circ - (\Delta C_P^\circ)_{\text{TR}}[\Delta T - T_2 \ln (T_2/T_1)] - \\ (\Delta H_2^\circ)_v + (\Delta E_1^\circ)_v + T_2[(\Delta S_2^\circ)_v - \\ (\Delta S_1^\circ)_v] = \Delta G_1^\circ - \Delta T \Delta S_1^\circ \quad (\text{E3}) \end{aligned}$$

ΔG_1° and the entropy change, ΔS_1° , at temperature T_1 are determined by least-squares analysis. In this equation $(\Delta C_P^\circ)_{\text{TR}}$ is the contribution to the heat capacity change in reaction 2 from the translational and rotational degrees of freedom and $(\Delta H^\circ)_v$ and $(\Delta S^\circ)_v$ are the change in enthalpy and entropy, respectively, at temperature T_i due to the weak vibrational modes. Contributions from the strong modes are assumed to cancel. On the basis of entropy considerations and theoretical calculations to be presented, the N_2O_2^+ is taken to be nonlinear with no internal rotations, so there are four weak modes. The frequencies of these modes were estimated by an iterative technique since the frequencies must be derived from ΔS_1° by statistical mechanics in order to calculate $(\Delta H^\circ)_v$ and $(\Delta S^\circ)_v$.

Since the frequency distribution of the weak modes is unknown, two vibrational models were used. In model I all frequencies were assumed to be the same; in model II the frequencies were distributed over a factor of five in a geometrical series. It can be seen from the results given in Table II that ΔS°_{200} is relatively insensitive to the uncertainties in the frequency

Table II: Entropy Data for Reaction 2 at 200°K (in cal/mole deg)

S_m^a A	Geometry	ΔS°_{200}	$(\Delta S^\circ)_{\text{tran}}$	$(\Delta S^\circ)_{\text{rot}}$	$(\Delta S^\circ)_{\text{vib}}$	Vib model	Max freq, cm ⁻¹
3.25	T ^b	-18.95 ^c	-32.08	3.12	10.01	I	110
3.25	T ^b	-18.94 ^c	-32.08	3.12	10.02	II	251
2.90	Rectang	-18.95 ^c	-32.08	3.25	9.88	I	112
2.90	Rectang	-18.93 ^c	-32.08	3.25	9.90	II	256

^a Distance between molecular centers at potential minimum. ^b O₂⁺ is at the top of the T. ^c Standard deviation = 0.39 eu.

distribution and the geometry of the cluster. This is also true of ΔH°_{200} which equals -5.69 ± 0.08 kcal/mole for the four cases considered. By correcting ΔH°_{200} to 0°K, $D_0(\text{N}_2\text{-O}_2^+)$ is found to be 5.53-4 and 5.47-8 kcal for models I and II, respectively.

Discussion

If we use the FER loose cluster model with $S_m = 3$ A and neglect the entropy associated with the weak stretching mode, the computed ΔS°_{200} is 2.3 eu more positive than the experimental value, which shows that the O₂⁺ and N₂ are not *freely* rotating in the cluster. In addition, the experimental bond energy is about three times larger than predicted by this model. The entropy disparity suggests that the FER model be modified by introducing the anisotropy in the interaction potentials. We would also like to account for the nonuniformity in the electric field near an ion by considering the interaction between the charge on the O₂⁺ and all the permanent and induced point electric multipoles on the N₂.¹³ However, because of the dearth of experimental data, the only interactions we can consider are the ion-induced dipole (VID) and the ion-quadrupole (VQ). The total potential is then

$$VT = VR + VD + VID + VQ \quad (\text{E4})$$

where VR and VD represent, respectively, the repulsive and attractive parts of the van der Waals interaction between the neutral molecules.

VD. Three models are used to account for the molecular attraction (dispersion) interaction. The first two are normalized to the experimental average potential $\langle VD \rangle = -\langle c \rangle / S^6$ at the potential minimum $\langle S_m \rangle = 3.861$ A by assuming all collision angles to be equally probable. From viscosity data the value of $\langle c \rangle$ is found to be 1180 kcal A⁶.¹⁴ To use the London formulation¹⁵ of the interaction energy (model D1), one must assume that $\bar{v}_1 = \bar{v}_2$ and $\bar{v}_1' = \bar{v}_2'$, where \bar{v}_1 and \bar{v}_2 represent the "characteristic mean (electron) oscillation frequencies" along and perpendicular to

the N₂ bond axis, respectively, etc., for O₂⁺. The equation for VD is then

$$VD = -\frac{\langle c \rangle}{6\alpha\alpha'S^6} [(\alpha_2\alpha_2' + \alpha_1\alpha_1' - \alpha_2\alpha_1' - \alpha_1\alpha_2') \times (\sin\theta \sin\theta' \cos\varphi - 2\cos\theta \cos\theta')^2 + 3(\alpha_1\alpha_2' - \alpha_2\alpha_2') \cos^2\theta + 3(\alpha_2\alpha_1' - \alpha_2\alpha_2') \times \cos^2\theta' + \alpha_2\alpha_1' + \alpha_1\alpha_2' + 4\alpha_2\alpha_2'] \quad (\text{E5})$$

where $\alpha \equiv \alpha_1/3 + 2\alpha_2/3$ and α' are angle average polarizabilities see (Figure 3). The bond polarizabilities are $\alpha_1 = 2.43$, $\alpha_2 = 1.43$, $\alpha_1' = 2.43$, and $\alpha_2' = 1.19 \times 10^{-24}$ cc.¹⁶ Model D1 is the only "dispersion" model in which the anisotropy in polarizability is considered.

In the next two models, VD is taken to be the sum of isotropic atom-atom interactions.

$$VD = -\sum_{j=1}^4 c_j r_j^{-6} = -c \sum r_j^{-6} \quad (\text{E6})$$

In model D2 c is obtained by equating $-\langle c \rangle / \langle S_m \rangle^6$ to the angle average of E6 at $\langle S_m \rangle$. The integration is straightforward. In model D3, c is calculated from the Slater-Kirkwood equation by the method outlined by Scott and Scheraga¹⁷ except that the atomic polarizabilities are taken to be one-half the (molecular) angle average polarizabilities.

VR. In all three repulsion models VR is taken to be the sum of atom-atom interactions. In model R1

$$VR = \sum_{j=1}^4 a_j e^{-b_j r_j} = a \sum e^{-b r_j} \quad (\text{E7})$$

(13) (a) A. D. Buckingham, *Discussions Faraday Soc.*, **24**, 151 (1957); (b) J. Stecki, *Advan. Chem. Phys.*, **6**, 413 (1964).

(14) J. T. Vanderslice, E. A. Mason, and W. G. Maisch, *J. Chem. Phys.*, **31**, 738 (1959). These authors use semiempirical combination rules to obtain the N₂-O₂ potential from the N₂-N₂ and O₂-O₂ potentials.

(15) F. London, *J. Phys. Chem.*, **46**, 305 (1942).

(16) K. G. Denbigh, *Trans. Faraday Soc.*, **36**, 936 (1940).

(17) R. A. Scott and H. A. Scheraga, *J. Chem. Phys.*, **42**, 2209 (1965).

Table III: Potential Minima Calculated for $N_2-O_2^+$ by Eq E4-E9 for $\varphi = 0^\circ$

VD-VR model ^a	$a \times 10^{-5}$, kcal	b , A ⁻¹	c , kcal A ⁶	S_m , ^b A	$\theta' = 90^\circ$ $\theta = 90^\circ$	90° 0°	0° 0°	0° 90°
D1-R1	2.103	4.471	...	3.25	-1.76	-4.84	-3.44	-0.69
D2-R1	2.103	4.471	238	3.25	-1.43	-5.08	-3.60	-0.74
D3-R2	2.55	4.59	355	3.15	-2.31	-6.07	-4.22	-1.26
D1-R3	0.0371	2.654	...	3.70	-0.17	-2.52	-2.01	-0.06

^a These models are discussed in the text. ^b S at the potential minimum for most stable geometry.

the angle average of VR is fitted at $\langle S_m \rangle$ and 3.2 A to the experimental average potential $\langle VR \rangle = 3.04 \times 10^6 e^{-4.403S}$ obtained from viscosity data.¹⁴ The equation relating $\langle VR \rangle$ to a and b has been given previously.¹⁴ Model R2 is the model used by Scott and Scheraga¹⁷ where D3 is used for the dispersion interaction, b is estimated by interpolating rare gas data, and a is estimated by minimizing the atom-atom potential curve at the sum of the van der Waals radii taken from Bondi.¹⁸ In model R3 the values of a and b are those obtained by Vanderslice, *et al.*,¹⁴ from the potential curves for various states of NO by use of certain quantum-mechanical relations derived by a modified "perfect pairing approximation."¹⁹

VID. It is assumed that there is a charge $q_j = +e/2$ at each O nucleus, so

$$VID = -\sum_{n=1}^2 \frac{\alpha_n}{2} \left[\sum_{j=1}^2 q_j \cos \gamma_{jn} / L_j^2 \right]^2 \quad (\text{E8})$$

VQ. The equation for VQ is^{13b}

$$VQ = \sum_{j=1}^2 q_j Q (3 \cos^2 \gamma_{j1} - 1) / 2L_j^3 \quad (\text{E9})$$

where the quadrupole moment $Q = \int (3z^2 - r^2) \rho dv / 2$ for the linear molecule. Here ρ is the charge density at r and z is the projection of r on the symmetry axis. Q is taken to be $-(1.3 \pm 0.2) \times 10^{-26}$ esu,^{13a,20} where the sign of the moment comes from theoretical calculations.²¹

Equations for r_j , L_j , and $\cos \gamma_{jn}$ were derived from the law of cosines (Figure 3) and used in evaluating VT on a digital computer. The computed potential minima are given in Table III. It can be seen that the most stable structure is predicted to be T shaped and, with the exception of the last model, the agreement with the experimental bond energy is now good. However, model D1-R3 is the poorest one for the present calculation as the R3 potential is not valid when $r_j > \sim 2.8$ A, whereas the potential curve derived from the viscosity data is reliable when $S > \sim 3.2$ A.¹⁴

Let us consider model D1-R1 with $\theta' = 90^\circ$ and $\theta = 0^\circ$ in more detail. At S_m , $VR = 1.85$, $VD = -0.99$,

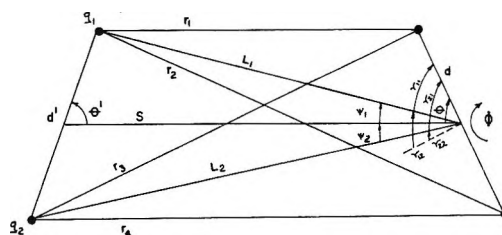


Figure 3. Geometrical relationships for the $N_2-O_2^+$ complex. Here d' and d are the internuclear separations in O_2^+ and N_2 , respectively, and φ is the angle between the Sd and Sd' planes. The electric field vector at the center of the N_2 molecule lies in the plane defined by the x (dashed line) and z (bond) axes of the molecule.

$VID = -3.31$, and $VQ = -2.39$ kcal/mole. The quadrupole moment has a strong influence on orientation; if it were zero, the rectangular geometry would have the largest computed bond energy.

As an independent check on the accuracy of the computed potential curves, they will be used to estimate $(\Delta S^\circ)_{\text{vib}}$. It is assumed that the four weak modes that contribute to $(\Delta S^\circ)_{\text{vib}}$ are completely decoupled from the strong N_2 and O_2^+ stretching modes. In addition, to simplify the computation, it is assumed that only one molecule moves in each of the B_2 modes. The weak modes are then as follows: (1) $N_2-O_2^+$ stretch (A_1), (2) N_2 out-of-plane torsion (B_1), (3) N_2 in-plane torsion (B_2), and (4) O_2^+ in-plane torsion (B_2). The computed curves for in-plane motion are shown in Figures 4 and 5. The frequencies are estimated from the shapes of the curves at S_m in the usual way,²² except for the O_2^+ torsion where the potential function $\Delta(VT) = V_0(1 + \cos 2\theta')/2$ is fitted to the potential curves with $\theta' \geq 54^\circ$. (At 200°K it is expected that

(18) A. Bondi, *J. Phys. Chem.*, **68**, 441 (1964).

(19) C. A. Coulson, "Valence," Oxford University Press, London, 1952, pp 166-184.

(20) G. Birnbaum and A. A. Maryott, *J. Chem. Phys.*, **36**, 2032 (1962).

(21) C. W. Scherr, *ibid.*, **23**, 569 (1956).

(22) G. Herzberg, "Molecular Spectra and Molecular Structure," D. Van Nostrand Co., Inc., Princeton, N. J., 1945, pp 62, 226.

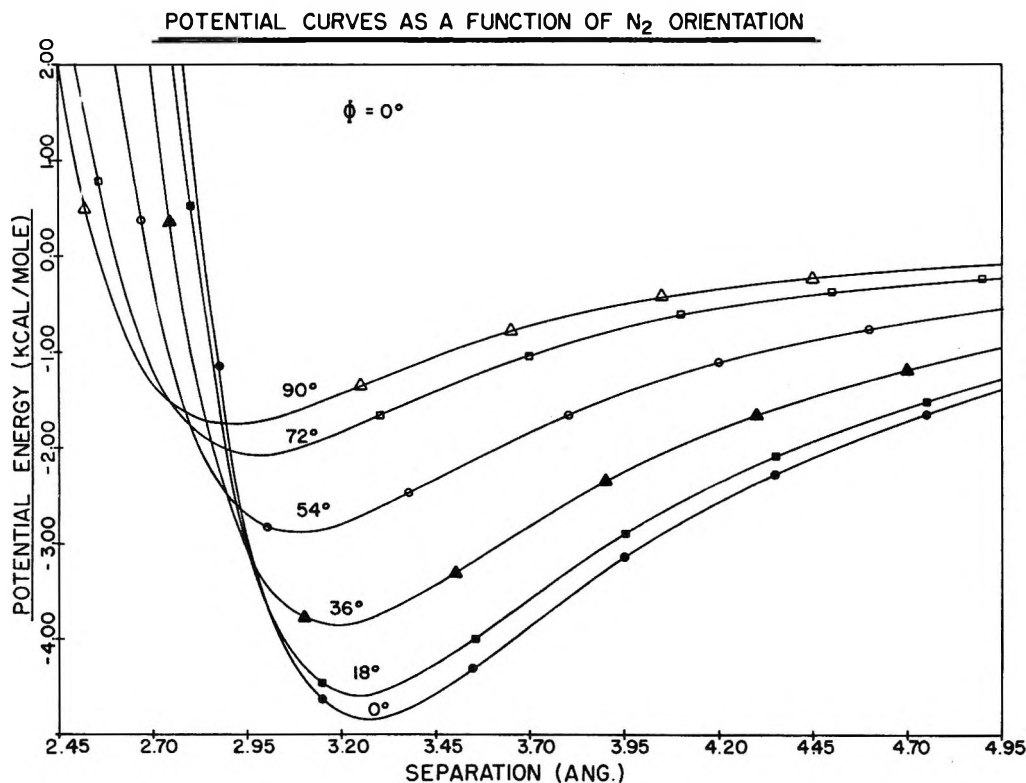


Figure 4. VT vs. S when $\theta' = 90^\circ$ and $\varphi = 0^\circ$. The angle θ between the axis of the N_2 molecule and S is indicated for each curve. The potential energy curves for $\theta' = 90^\circ$ and $\varphi = 90^\circ$ are very similar to these.

$\theta' < 54^\circ$ in only a small fraction of the oscillations.) The results are $\omega_1 = 136$, $\omega_2 = 102$, $\omega_3 = 99$, and $\omega_4 = 116$ cm^{-1} from which $(\Delta S^\circ)_{\text{vib}} = 9.85$ eu, in good agreement with the experimental result of 10.0 eu.

From ω_1 the computed value of $D_0(N_2-O_2^+)$ for model D1-R1 is 4.65 kcal, somewhat lower than the experimental result. The computed bond energy would be larger if the $VR + VD$ potential were corrected for the plus charge on the O_2^+ and if hyperpolarizability^{13a} were considered. The first correction is probably not large, as the correction for model D3-R2 is estimated to be only 0.3 kcal.²⁵ The next terms in the charge-multipole interaction equation for N_2 are the ion-hexadecapole term ($\propto L_j^{-5}$) and the term ($\propto L_j^{-6}$) for the interaction between the gradient of the field and the quadrupole moment induced by the gradient of the field.^{13a} It is possible that these two interactions are not very important at the molecular separations of interest, since the uncertainty in $VR + VD + VQ$ is as large as the difference between the experimental and computed bond energies.

Appendix

An analysis of mass transport throughout the ionization chamber is difficult because of the lack of sym-

metry and certain uncertainties, such as the rate of ionization and the electron temperature. In addition, it appears that only part of the data was taken at the ambipolar diffusion limit.²⁴ However, to determine the mass discrimination factor, the mass transport equation

$$\Gamma_{iz} = -D_i(dn_i/dz) + k_i n_i E_z + n_i v_z \quad (\text{E10})$$

need only be solved in the region close to the window. Here Γ_{iz} , E_z , and v_z are, respectively, the i th ion current per unit area, the electric field strength, and the linear velocity of the gas stream in the z direction (normal to the Pt window). The diffusion coefficient, D_i , and mobility, k_i , for each ion of density n_i are related by the equation,²⁴ $D_i/k_i = kT/e$, where k is the Boltzmann constant. It is estimated that the Σn_i varied from 1×10^6 cc^{-1} (3 torr, maximum flow) to 2×10^7 cc^{-1} (12 torr, one-fourth maximum flow). These ion densities correspond to Debye lengths,²⁴ λ_D for the positive ions of 0.08–0.02 cm. Let us confine our discussion to the region within $0.5\lambda_D$ of the window

(23) The method used is similar to that outlined in ref 5 and is not considered to be very accurate.

(24) W. P. Allis and D. J. Rose, *Phys. Rev.*, **93**, 84 (1954).

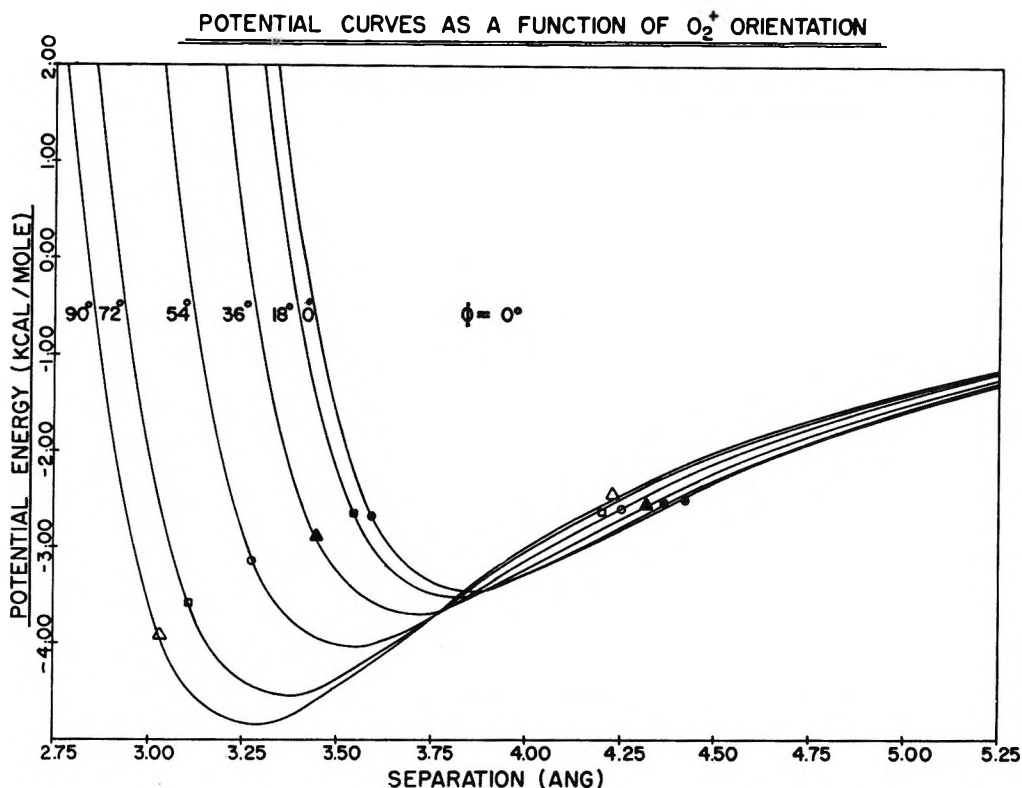


Figure 5. VT vs. S when $\theta = 0^\circ$ and $\varphi = 0^\circ$. The angle θ' between the axis of the O_2^+ ion and S is indicated for each curve.

where it is certain that $-D_i(dn_i/dz) \gg n_i v_z$. Therefore, the last term in eq E10 can be neglected and the resulting equation solved to yield

$$\frac{n_1}{n_2} = \frac{\Gamma_{1z} D_2}{\Gamma_{2z} D_1} = \frac{\Gamma_{1z} [m_1(m_2 + M)]^{1/2}}{\Gamma_{2z} [m_2(m_1 + M)]^{1/2}} \quad (\text{E11})$$

since²⁵ $D_i \propto [(m_i + M)/m_i M]^{1/2}$ where m_i and M are the masses of an ion and neutral gas molecule, respectively.

The next question is whether or not reaction 2 is at equilibrium $0.5\lambda_+$ from the window. The n_i decreases fairly rapidly between $0.5\lambda_+$ and the wall,²⁴ so the diffusion term in eq E10 can be taken to be dominant. The mean time, τ_ω , for an ion to reach the wall is then $\sim \lambda_+^2/8D_i \approx 10^{-4}$ sec.²⁶ The mean time, τ_{eq} , for reaction 2 to approach equilibrium can be estimated²⁷ from the rate constant for ion-molecule collisions^{3,28} and the estimated rate constant for dissociation of the resulting $N_2O_2^+$.²⁹ It is found that $\tau_\omega \gg \tau_{eq}$, which means that reaction 2 is at equilibrium within $0.5\lambda_+$ of the window and the equilibrium ratio $(n_1/n_2)_{eq}$ is given by eq E11.³⁰

The time that an ion spends between the trapping grids is $A\sqrt{m_i}$, where A is a constant. Therefore, the probability that an ion which enters the spectrometer will be between the trapping grids when the focus pulse is applied is $A\sqrt{m_i}/\tau_f$. Combining this result with that given above, we find that

$$(n_1/n_2)_{eq} = (I_1/I_2) [(m_2 + M)/(m_1 + M)]^{1/2} \quad (\text{E12})$$

where I_1/I_2 is the observed ion current ratio.

Acknowledgments. The authors wish to thank The Robert A. Welch Foundation for its generous support of this research and the Phillips Petroleum Co. for awarding G. S. J. a fellowship.

(25) L. B. Loeb, "Basic Processes in Gaseous Electronics," University of California Press, Berkeley, Calif., 1961, p 53.

(26) See ref 25, pp 53, 191, 200.

(27) D. C. Conway, *J. Geophys. Res.*, **69**, 3304 (1964).

(28) K. Yang and T. Ree, *J. Chem. Phys.*, **35**, 558 (1961).

(29) (a) M. Burton and J. L. Magee, *J. Phys. Chem.*, **56**, 842 (1952);

(b) R. A. Marcus and O. K. Rice, *ibid.*, **55**, 894 (1951).

(30) Given that the reaction is at equilibrium far from the window, the other limit is when there is a point close to the window where $n_i v_z \gg -D_i(dn_i/dz) + k_i n_i E_z$ and $\tau_{eq} \gg \tau_\omega$. Then $(n_1/n_2)_{eq} = \Gamma_{1z}/\Gamma_{2z}$.

The Adsorption of Carbon Dioxide on Carbon Solids. I.

Graphite and Diamond at 0°

by Victor R. Deitz

U. S. Naval Research Laboratory, Washington, D. C. 20390 (Received July 22, 1966)

The high-temperature physical adsorption of carbon dioxide ($\ll 1\%$ coverage) was measured on a number of relatively well-defined carbon solids. The results provide an experimental means to differentiate between two arrays of adsorption sites that may originate in the strong anisotropy of the graphite structure. The adsorption isotherms at 0° indicate two distinct regions of surface coverage that are separated by a wide plateau. The adsorption at very low pressures (< 0.01 torr) is compatible with high-energy adsorption on one array of carbon atoms located in the prism faces. Additional adsorption at higher pressures then takes place on sites of lesser energy in the more abundant basal planes. Similar behavior was observed for graphitized carbon black FT (2700°), mineral graphite, an annealed pyrolytic graphite, and a deashed, heat-treated (1500°) coconut charcoal. In contrast, the adsorption of carbon dioxide on purified natural diamond fragments followed a simple Langmuir isotherm compatible with the known isotropic structure of diamond. The amounts adsorbed expressed per unit area bring out similarities among the carbon solids that are characteristic of graphite. The large adsorption on the coconut charcoal appears due almost entirely to a large area that is essentially basal plane in structure. There is evidence that the pyrolytic graphite has a porosity that may be invaded more completely by carbon dioxide than by krypton.

Introduction

In view of the well-known strongly anisotropic properties of graphite,¹ the boundary surfaces of graphitic solids should present two arrays of adsorption sites. One array is located in the abundant basal planes; part of these sites originate in the discontinuity of the crystal lattice associated with the formation of a surface and another part is due to defects such as warping of the basal plane. The second array of sites is located in the prism faces of the graphite crystal, where the constituent carbon atoms are also the edges of the basal planes. If the surface energy contained in these edge atoms is not entirely self-compensated in some way by bond isomerism,² much stronger adsorption sites relative to the basal plane should be present. Different specimens of graphite could then vary in surface properties according to the proportion of basal plane and prism faces that are present.

The basic assumption here, of course, is that the anisotropic properties of the crystal extend into the bound-

ary surface. This is a likely possibility and it is suggested in this paper that the high-temperature physical adsorption (0°) of carbon dioxide may provide an experimental means to differentiate between the two sets of adsorption sites on the total boundary surface of graphitic carbons. It is necessary to combine a high temperature and low pressure (below 1 torr) in order that the surface coverage be sufficiently low to discriminate between the adsorption sites. It is also essential that the experimental conditions permit a physical adsorption process to be the dominating interaction.

That carbon dioxide is a desirable adsorbate to make such a differentiation may be seen from two considerations.

1. The first consideration is that the diameter

(1) A. R. Ubbelohde and F. A. Lewis, "Graphite and its Crystal Compounds," Oxford Press, 1960.

(2) C. A. Coulson, *Proc. Conf. Carbon, 4th, Buffalo*, 215 (1959).

attributed to this molecule is 3.53 Å as determined from spectroscopic measurements,³ 3.23 Å from the van der Waals equation of state of the gas, 3.40 Å from thermal conductivity theory, and 3.34 Å from viscosity determination. These coincide fairly closely with the separation of basal planes in crystalline graphite (3.347 Å). On the other hand, the distance of closest approach of carbon atoms in the basal plane is 1.42 Å and the potential field of the basal plane surface which contributes to the adsorption of a gas is concerned with carbon separations of 1.42 (*ortho*), 2.46 (*meta*), and 2.84 Å (*para*). Because the long axis of the carbon dioxide molecule is a good fit in the prism face (either in directions vertically or parallel to the basal plane) and a misfit in the basal plane, the distances of closest approach between the prism faces and the gas are smaller. This could result in a greater van der Waals attraction at the prism face than at the basal plane.

2. An equally important consideration in the selection of carbon dioxide is the polarizability, α . At right angles to the C-C bond in graphite α_{\perp} is very small, and parallel to the bond α_{\parallel} is 3.42×10^{-24} cm³.⁴ Moreover, the carbon dioxide molecule itself is anisotropic; at right angles to the linear molecule $\alpha_{\perp} = 1.97 \times 10^{-24}$ and along the molecule $\alpha_{\parallel} = 4.01 \times 10^{-24}$ cm³. Accordingly, the mean value of α_{ij} to be used in the summation of interactions between gas molecule and surface will show greater values for the prism faces than for the basal planes.

As a result, the van der Waals energy of attraction when summed over the required distances

$$-\sum_{i,j} \frac{C_{ij}}{r_{ij}^6}$$

will be much larger for the prism faces than for the basal planes, the polarizability factor being included in the constant C_{ij} .

The total adsorption of gas on two arrays of sites that differ greatly in energy should be reflected in the shape of the isotherm. The pressures must be of a sufficiently wide range to span the anticipated coverages. The Langmuir adsorption is

$$\theta = \frac{bp}{1 + bp}$$

where θ is the coverage, p is the pressure, and b is a constant containing the energy terms in an exponential form, and the influence of changes in b on the relative shape of the isotherms is shown in the top half of Figure 1. If two arrays of sites exist of $b = 1$ and $b = 1000$, the total isotherm should have the shape shown at the lower part of Figure 1. A similar dependency

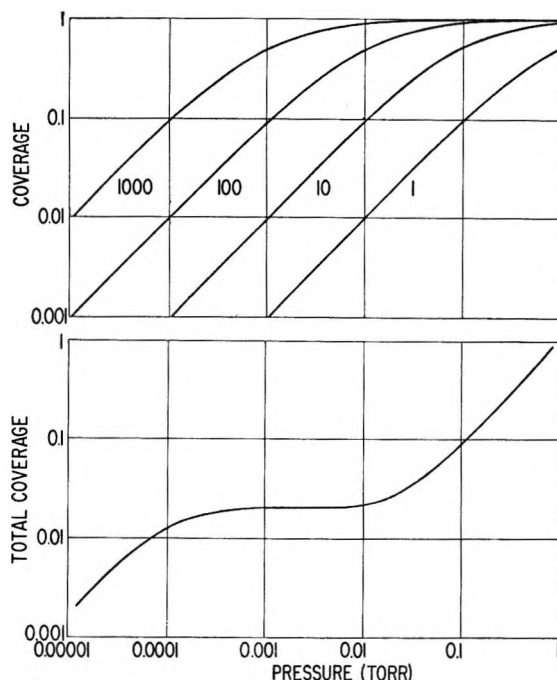


Figure 1. Top, Langmuir isotherms for different values of b (energies of adsorption); bottom, summation of two isotherms with $b = 1$ and $b = 1000$.

of adsorption on crystal planes was pointed out a number of years ago by Cremer⁵ in connection with a catalyst problem.

Experimental Procedure

The volumetric adsorption equipment included metal valves (Granville-Phillips, Bakeable, Type C) mounted securely on a slotted angle beam in a vertical position. The glass connections were constructed so as to provide the flexibility required in manipulating the metal valves with a torque wrench. The pressure measurements were made with a thermocouple gauge (RCA 1946) thermostated at $28.0 \pm 0.1^\circ$. The controlled current through the gauge (about 60 ma) was frequently checked and adjusted so that the emf reading under vacuum (below 10^{-5} torr) was 10.030 mv. The recorder used in making all readings had a range of 1 mv full scale of 100 divisions so that a difference of 1 μ v was observable. The thermocouple heating current was derived from a high-capacity storage battery (2.5 v, Eveready T-2600, National

(3) H. J. M. Bowen, *et al.*, "Table of Interatomic Distances and Configuration in Molecules and Ions," Special Publication #11, Chemical Society, London, 1958.

(4) E. R. Lippincott and J. M. Stutman, *J. Phys. Chem.*, **68**, 2926 (1964).

(5) E. Cremer, *Monatsh. Chem.*, **77**, 126 (1947); *J. Chem. Phys.*, **46**, 411 (1949).

Carbon Co) and the current was manually adjusted before each reading to the value required in high vacuum to give the reference emf. The recorder was calibrated at regular intervals against the counter emf of a standard potentiometer.

A calibration was made for each gas using two McLeod gauges with overlapping pressure ranges. The mercury vapor was trapped by a U-tube immersed in an alcohol-Dry Ice bath. The heights of the mercury levels of the McLeod gauge were read relative to a fixed mark scratched on the glass near the end of the closed capillary. A Gaertner cathetometer solidly mounted on a cement block was used and the measurements reported to 0.01 mm. The usual trials and tribulations attendant in McLeod gauge operation were encountered, but these could be minimized by frequent outgassing of the gauges. The thermocouple calibrations for carbon dioxide and krypton have shown good reproducibility over several years of operation using the above described procedures.

When adequately outgassed, the system without the sample held a vacuum below 10^{-6} torr for periods longer than those used in sample operations. The pumping system included a Consolidated Vacuum all-glass diffusion pump which when charged with Convalex-10 produced a vacuum well below 10^{-6} torr without a liquid nitrogen trap.

Materials

The five materials that were used are listed in Table I. Three were graphite specimens: FT carbon black (2700°), a purified mineral graphite, and an annealed sample of pyrolytic graphite. Also, an acid-washed sample of coconut charcoal was prepared and heated under vacuum to 1500°. The analyses of these materials for residual hydrogen are given in Table I, this constituent being the principal impurity. The surface areas are also given in Table I, that of charcoal and FT carbon having been determined with nitrogen (16.2 A² cross-sectional area) at 77.4°K and the remaining three with krypton (17.2 A² cross-sectional area) at 77.4°K. The vapor pressure of krypton was determined and agreed with that reported by Fischer and McMillan.⁶

The samples contained in quartz or Vycor tubes were attached to the Pyrex apparatus with graded seals; the weights ranged from 1 to 20 g. The outgassing was conducted at elevated temperatures (up to 900°) until the gas evolution from the hot sample decreased to about 6 nmoles/hr.

The sample of natural diamond fragments (19.5 g) was acid washed and the final washings gave no detectable sulfide or hydroxide tests. The indicated surface

Table I: Properties of the Materials Investigated

Materials	Surface area, m ² /g	H content, ^a wt %	Carbon content, ^a wt %
Coconut charcoal ^b	900	0.006	99.99
FT carbon (2700°) ^c	10	0.00	100.0
Mineral graphite ^d	0.74	0.00	100.0
Pyrolytic graphite ^e	0.029	0.00	100.0
Diamond fragments ^f	0.045	0.00	99.92

^a Kindly supplied by R. A. Paulson of the Analytical Chemistry Division, National Bureau of Standards. ^b Acid washed with HCl and HF and heated to 1500° under vacuum. ^c Kindly furnished by Dr. Walter Smith, Cabot Carbon Co. ^d Acid washed with HCl-HF and heated to 1000° in argon. ^e Kindly furnished by Dr. R. J. Diefendorf, General Electric Research Lab. ^f Kindly supplied by the National Bureau of Standards.

area (BET with krypton) actually decreased from 530 to 450 cm² as a result of this treatment.

All pressure measurements with the sample below room temperature were corrected for thermal transpiration. The modified procedure of Takaishi and Sensui⁷ was used for both krypton and carbon dioxide. Both of these gases were of spectroscopic grade supplied by the Air Reduction Co., Inc.

Experimental Results

The adsorption of carbon dioxide at 0° on graphitized FT carbon black is shown in Figure 2. At pressures above 1 torr, a linear isotherm was obtained as shown by the approach of the observed isotherm to a slope of unity. At still higher pressures linear isotherms for this graphitized carbon black have been reported at 0° between 20 and 400 torr by Deitz, Carpenter, and Arnold⁸ and between 150 and 350 torr by Myers and Prausnitz.⁹ Linear isotherms were also reported by Constabaris, Singleton, and Halsey¹⁰ for Ne, Ar, and Kr on a similar material, P-33 carbon black (2200°).

Below 1 torr the adsorbed carbon dioxide becomes increasingly less dependent on pressure for several decades. The development of a plateau in the isotherm occurs only after the sample has been outgassed at a suitably high temperature. This is illustrated by the four groups of points shown in Figure 2. All were

(6) B. B. Fischer and W. G. McMillan, *J. Phys. Chem.*, **62**, 494 (1958).

(7) T. Takaishi and Y. Sensui, *Trans. Faraday Soc.*, **59**, 2503 (1963).

(8) V. R. Deitz, F. G. Carpenter, and R. G. Arnold, *Carbon*, **1**, 245 (1964).

(9) A. L. Myers and J. M. Prausnitz, *Trans. Faraday Soc.*, **61**, 755 (1965).

(10) G. Constabaris, J. H. Singleton, and G. D. Halsey, *J. Phys. Chem.*, **63**, 1355 (1959).

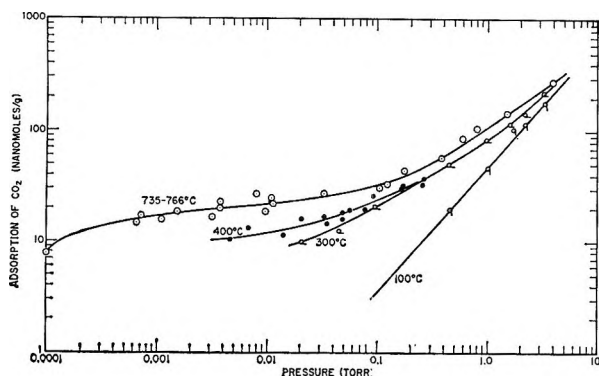


Figure 2. Adsorption isotherms of carbon dioxide at 0° on graphitized FT carbon (2700°). The exposure to carbon dioxide was at 22.5° and 1.5 torr for 3 hr. Subsequent outgassing at the temperatures indicated for 4 days before cooling at 0°.

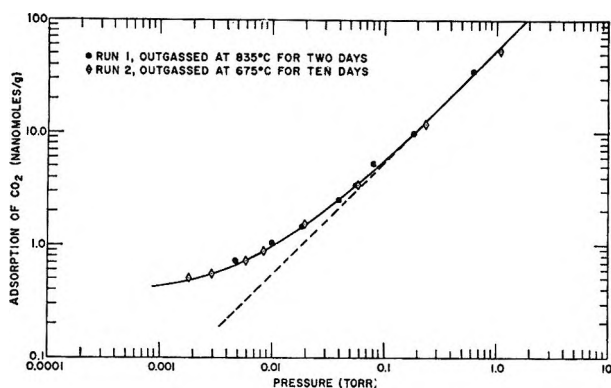


Figure 3. Adsorption of carbon dioxide at 0° on an annealed pyrolytic graphite.

determined after exposure of the sample of FT carbon to carbon dioxide at 22.5° and 1.5 torr for 3 hr. The isotherm of the lower right obtained after the sample was outgassed at nearly 100° for 4 days and then cooled to 0°. Subsequently, the outgassing was conducted at temperatures of 300, 400, and 730° and the corresponding isotherms for each case show that the approach to the plateau appears to be asymptotic.

Similar behavior is shown in Figure 3 for the adsorption of carbon dioxide at 0° on a pyrolytic graphite. The solid points were obtained after the sample of 24.25 g was outgassed at 835° for 2 days; the points in open diamonds are for an independent run after outgassing at 575° for 10 days. The results at pressures above 0.1 torr define a linear isotherm, and the results at lower pressures level off in a manner similar to those for graphitized FT carbon black in Figure 2.

The isotherm for mineralogical graphite is given in Figure 4. The outgassing of this material (8.712 g) was rather time consuming. Eventually, a gas evolu-

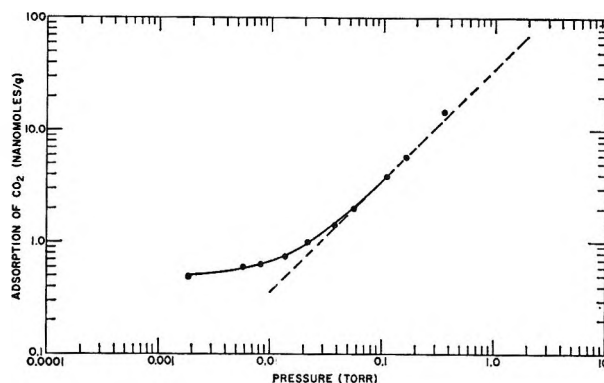


Figure 4. Adsorption of carbon dioxide at 0° on purified mineral graphite outgassed at 750°.

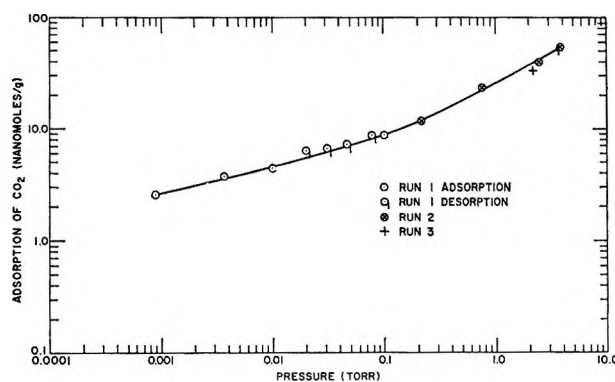


Figure 5. Adsorption of carbon dioxide at 0° on purified diamond fragments (see Figure 12 for Langmuir plots).

tion of approximately 6 nmoles/hr was reached with the sample at 750° and maintained at this level for several days.

The diamond fragments, after acid washing as mentioned above, were outgassed at 480° and the rate of gas evolution from the hot sample readily decreased to 6 nmoles/hr. Two independent sets of measurements at 0° were made 6 months apart. The isotherm shown in Figure 5 includes points obtained by both adsorption and desorption.

The adsorption of carbon dioxide on the sample of treated coconut-shell charcoal (Figure 6) exhibited a very slow approach to a steady state. Although this behavior was most pronounced for the charcoal, the graphites also behaved similarly for the points on the isotherm at pressures below the plateau region. For these samples, too, a somewhat greater time dependence was found in the approach to a steady state than in the region of higher pressures above the plateau. The pressure-time dependence for nine successive doses of carbon dioxide on the charcoal at 0° is shown in Figure 6. The adsorption of the first three doses

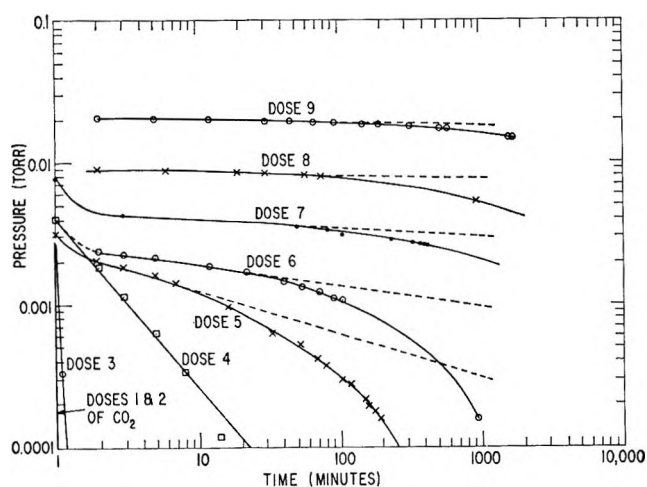


Figure 6. Time-dependent adsorption of carbon dioxide on acid-washed heat-treated (1500°) coconut-shell charcoal. The numbers denote successive doses of carbon dioxide.

took place so rapidly that the pressure change could not be followed. The succeeding doses were adsorbed more slowly and the kinetics appeared to follow various schemes. For example, the pressure changes following dose 9 were closely proportional to the square root of the time for the 28 hr during which the observations were made. This behavior is illustrated in Figure 7. On the other hand, dose 4 followed a linear dependence on time as shown in Figure 6.

The amounts adsorbed at various times were calculated, and these are plotted in Figure 8 as a function of pressure. The adsorption increased with time, but this is not evident in Figure 8 due to the large scale required on the ordinate axis to cover all of the data. There is first a very rapid adsorption which is followed by much slower adsorption, and it is the pressure change due to the latter that is recorded in Figure 6. The significance of this behavior is the main subject of another paper of this series which is concerned with diffusion-controlled aspects of the adsorption process. The weight of the charcoal sample was 8.374 g which corresponded to an area of about 7500 m². The more detailed study of the rates of adsorption between 0 and 100° will be concerned with sample weights between 1 and 50 g in order to reach both lower and higher surface coverages.

Discussion

The experimental adsorption isotherms for carbon dioxide on adequately outgassed graphite solids have a shape suggested by the simplified model given in the bottom half of Figure 1. At pressures above the plateau region, the adsorption process at 0° is dominated by adsorption on the sparsely covered and high-

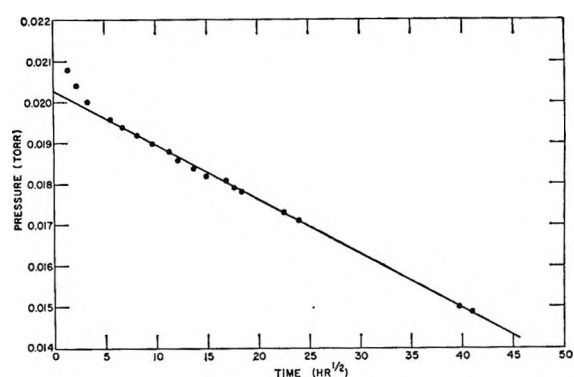


Figure 7. Pressure change of carbon dioxide during adsorption of dose 9 (see Figure 6) on charcoal and followed for 28 hr.

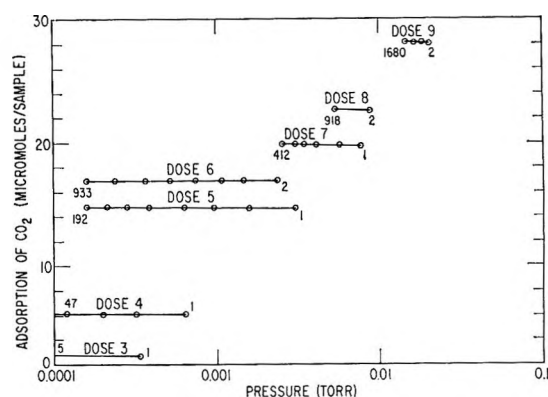


Figure 8. Adsorption of carbon dioxide on the charcoal during the designated time intervals (minutes) as a function of the corresponding pressures.

area basal plane. The numerous collisions of carbon dioxide molecules with the boundary surface rapidly populate the prism faces, since these present a greater heat of adsorption. The heats of adsorption for coverages above the plateau region are only somewhat larger than the heats of vaporization of liquid carbon dioxide. The latter¹¹ are plotted for various temperatures in Figure 9 where the rapid drop between 0° and the critical temperature may be seen. The isosteric heats of adsorption of carbon dioxide on pyrolytic and mineralogical graphites were estimated. Qualitatively, the heats at higher coverages approached a constant value as the linear isotherm region was reached. At lower coverages the heats were larger. However, the uncertainty then became large due to insufficient precision in determining the adsorption isotherms in the plateau region at different temperatures. It is readily apparent that in this region a small change in the amount adsorbed corresponds to a large pressure

(11) *Bull. Intern. Inst. Refrig.*, 22, No. 2, 55 (1941).

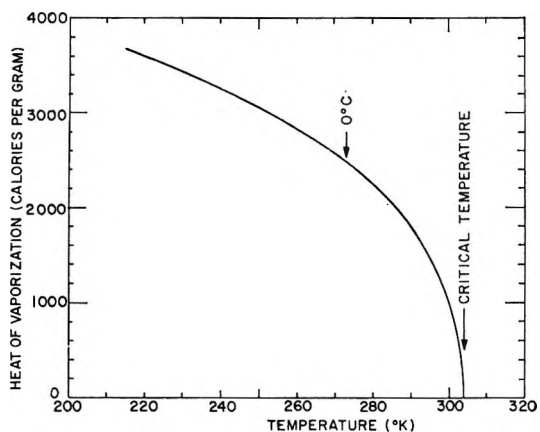


Figure 9. Heats of vaporization of carbon dioxide corresponding to the vapor pressure of the liquid.

change and, therefore, to a large change in the calculated isosteric heat. Further discussion of the heats of adsorption of carbon dioxide is postponed until data are obtained with a new apparatus now being designed with more precision at the lower pressures. The literature values for the heats of adsorption of carbon dioxide on graphite are given in Table II.

Table II: Heat of Adsorption of Carbon Dioxide

Sample	Measurement	Temp, °C	Kcal/mole	Ref
Sterling FT (2700)	Calorimetric	-79	4.8-6	12
Sterling FT (3100)			4.4-6	
Sterling FT (2700)	Isotherm at const spreading pressure	0 and 36.07	2.978 and 2.956	9
Sterling FT (2700)	Isosteric heat	0 and -5	2.52	8
Pyrolytic graphite	Isosteric heat	0 and 21	1.6	a

^a This paper.

In order to express the adsorption per unit surface, it is necessary to have the cross-sectional area (σ) of an adsorbed carbon dioxide molecule at 0°. There is considerable uncertainty in the value to be used in this investigation as well as in previous studies at -78°. Using the molar volume of the liquid¹¹ and assuming hexagonal close packing in both the liquid and the adsorbed two-dimensional layer, the calculated values of σ_{CO_2} are given by the solid line of Figure 10 which covers temperatures from -50° to the critical point.¹²⁻¹⁸ The value of $\sigma_{CO_2} = 20 \text{ \AA}^2$ corresponds to the cross-sectional area of carbon dioxide at 0°.

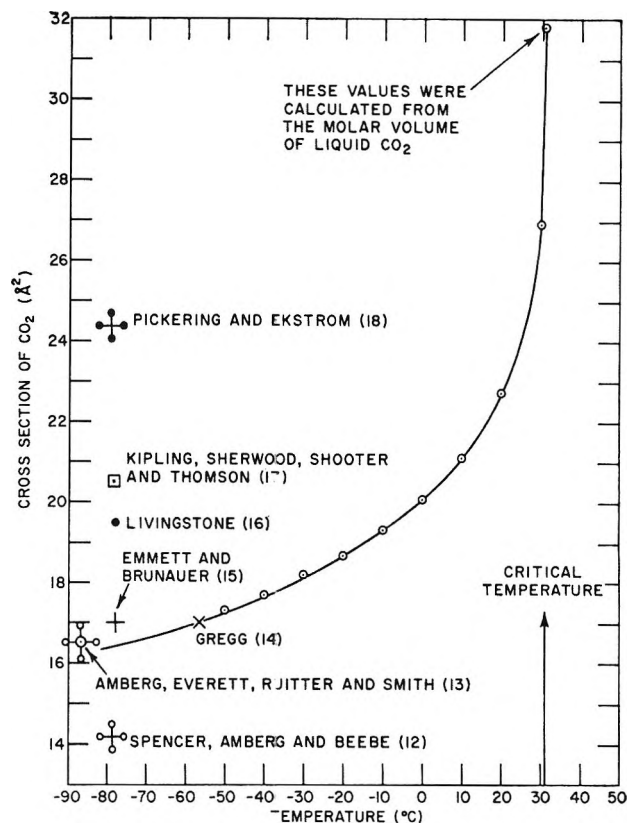


Figure 10. Values proposed for the molecular cross section of carbon dioxide in physical adsorption.

The adsorption for the five carbon solids is expressed in Figure 11 as nanomoles of carbon dioxide per square meter. The graphitized FT carbon black (B in Figure 11), the coconut charcoal (F), and the mineralogical graphite (A) approach a common plateau at the lower pressures ranging between 1 and 2 nmoles/m². A monomolecular layer of liquid-like carbon dioxide at 0° would require about 8300 nmoles/m²; thus, the plateau for these three carbon solids corresponds to a fractional coverage in the range 0.0001-0.0002. The similarity of coconut-shell charcoal (when expressed on a *per unit area* basis) to mineralogical graphite and

(12) W. B. Spencer, C. H. Amberg, and R. A. Beebe, *J. Phys. Chem.*, **62**, 719 (1958).
 (13) C. H. Amberg, D. H. Everett, L. H. Ruitter, and F. W. Smith, "Proceedings of the Second International Congress of Surface Activity," Vol. 2, Academic Press, Inc., New York, N. Y., 1957, pp 3-17.
 (14) S. J. Gregg, "The Surface Chemistry of Solids," Chapman and Hall, Ltd., London, 1961, Table 2.4.
 (15) P. H. Emmett and S. Brunauer, *J. Am. Chem. Soc.*, **59**, 1553 (1937).
 (16) H. K. Livingston, *J. Colloid Sci.*, **4**, 447 (1949).
 (17) J. J. Kipling, J. N. Sherwood, P. V. Shooter, and N. R. Thompson, *Carbon*, **1**, 321 (1964).
 (18) H. L. Pickering and H. C. Eckstrom, *J. Am. Chem. Soc.*, **74**, 4775 (1952).

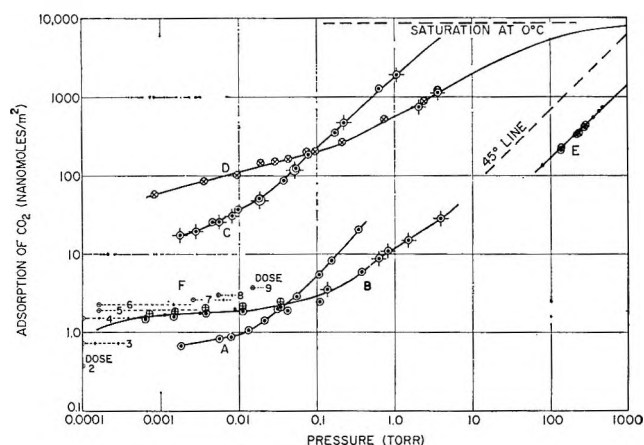


Figure 11. Adsorption of carbon dioxide per unit area on five samples: (A) mineral graphite; (B) FT carbon black; (C) pyrolytic graphite; (D) diamond fragments; (E) previous observations, (8.9) on FT; and (F) coconut-shell charcoal.

to FT graphitized black at pressures below 0.01 torr emphasizes the dependence of the adsorption on basal plane area alone. The adsorption corresponding to the plateau when expressed per gram of charcoal is 1800 nmoles/g. This corresponds to an average fractional coverage of 0.00025.

One may readily estimate the total isotherm for the FT carbon black as the sum of two Langmuir isotherms using the above values for monolayer coverage and reasonable values of the energy constants, K_1 and K_2 .

$$N_{\text{total}} = \frac{K_1 N_1 P}{1 + K_1 P} + \frac{K_2 N_2 P}{1 + K_2 P}$$

The curves numbered in Figure 12 correspond to the following constants

Curve	N_1	N_2	K_1	K_2
1	20	83,000	7×10^3	1×10^{-3}
2	20	83,000	7×10^2	1×10^{-3}
3	20	83,000	7×10^4	1×10^{-3}
4	20	83,000	7×10^3	1×10^{-2}
5	20	83,000	7×10^3	1×10^{-4}

The experimental points are in best agreement with set 1. The ratio K_1/K_2 is 6.7×10^6 , and this corresponds to $q_1 - q_2 = 8400$ cal for the difference between the heats of adsorption on the prism face and basal plane. This substantiates the choice of the CO_2 molecule to demonstrate the influence of anisotropy in physical adsorption. A calculation of the adsorption energies of the rare gases on either the basal plane or the prism planes of graphite has since been made and the results show that anisotropic adsorption should be observable for these gases.¹⁹ Preliminary measurements with krypton, however, showed that in order to do so, more precision was necessary in the pressure measurements

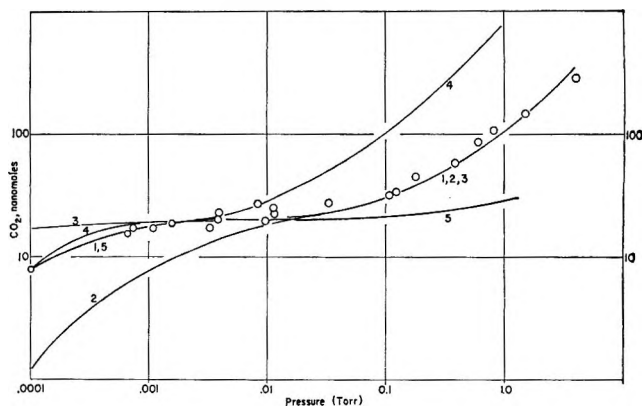


Figure 12. Calculated isotherms for the adsorption of carbon dioxide on dual energy sites.

than was available when the measurements with CO_2 were made.

The adsorption of carbon dioxide by Graphon, a carbon black of 98 m^2/g area, was reported by Healey, Yu, and Chessick.²⁰ The isotherm was linear and the adsorption at 20 torr was 0.029 ml/g at room temperature. This corresponds to 13 nmoles/ m^2 , a value somewhat less than that reported in this paper for FT carbon black. The Graphon had been degassed at 400° for 12 hr before use and the FT black received the more extreme pretreatment at 750° already reported.

It is of interest to note that water vapor is also adsorbed by Graphon with surface coverage of the same magnitude. Young, Chessick, Healey, and Zettle-moyer²¹ reported that this carbon black adsorbed water at a BET value of $V_m = 0.017$ ml. This amounted to about $1/1500$ of the value expected from the BET nitrogen area and corresponds to 8 nmoles/ m^2 .

The adsorption per unit area on diamond (D) is approximately 100-fold greater than the three solids mentioned above. The polarizability of the aliphatic C-C bond and its isotropic distribution at the boundary surface of the diamond structure qualitatively may account for the greater adsorption. Linear Langmuir plots were found as shown in Figure 13 for the adsorption of carbon dioxide on diamond at 0°. The slopes of the two sets of measurements differ somewhat, but this can be accounted for by a small variation in the heat treatments during the outgassing. It is likely that the surface of this diamond sample is fairly homogeneous between 0.005 and 0.05 coverage.

(19) E. F. Meyer and V. R. Deitz, *J. Phys. Chem.*, in press.

(20) F. H. Healey, Y. F. Yu, and J. J. Chessick, *ibid.*, 59, 399 (1955).

(21) G. J. Young, J. J. Chessick, F. H. Healey, and A. C. Zettle-moyer, *ibid.*, 58, 313 (1954).

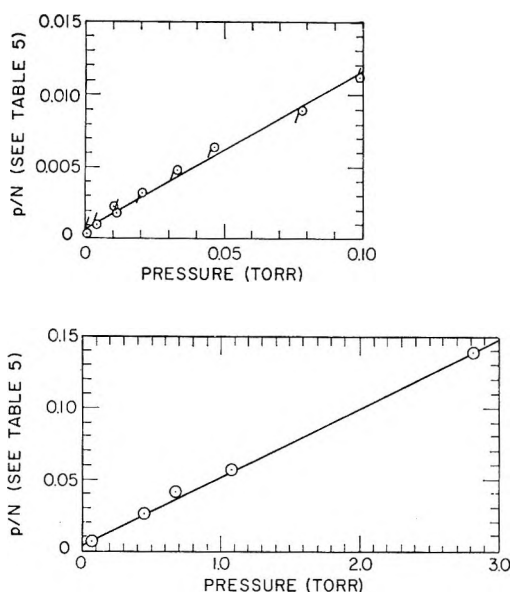


Figure 13. Langmuir plots for adsorption of carbon dioxide on diamond fragments.

The interesting behavior of the pyrolytic graphite (C) was at first surprising. Although the general shape of the isotherm is similar to that of the mineral graphite, it is displaced in the direction of greater adsorption by a factor of about 100. Unpublished results from this laboratory for the BET area (krypton) of a similar specimen of annealed pyrolytic graphite indicate that it may have appreciable porosity. In order to account for the present results it would be necessary to postulate a greater penetration of the carbon dioxide at 0° into the pyrolytic graphite than realized by adsorbed krypton at 78°K . X-Ray diffraction results have shown that the basal plane separation of the sample of mineral graphite was 3.345 Å and that of the pyrolytic graphite sample was 3.414 Å. This is a significant difference and it may correspond to the required magnitude necessary to permit entrance of a carbon dioxide molecule into a narrow internal

slit opening when the molecule is limited to a single rotation degree of freedom. Measurements are now in progress to determine whether the carbon dioxide molecule can, under favorable conditions, actually intercalate the structure of pyrolytic graphites and, if so, whether intercalation occurs to a significant extent in pyrolytic graphite in comparison to any intercalation in some mineral graphites.

Conclusion

The similar behavior of the coconut-shell charcoal, graphitized FT carbon black, and a mineral graphite when the adsorption is expressed on a per-unit-area basis may be a significant observation. The greater part of the carbon dioxide adsorption on the charcoal is thus attributed to adsorption on the basal plane structure. Moreover, the results for diamond suggest that should it be possible to combine large BET area and surface aliphatic C-C bonds (stabilized perhaps as in diamond), there would be formed a carbon adsorbent of a greatly enhanced capacity. It is suggested that Saran charcoal, the pyrolysis residue of polyvinylidene chloride, may be viewed as one such a synthesis. The most interesting properties of a number of partially pyrolyzed polymers in the adsorption of carbon dioxide at -78° have been described by Kipling, *et al.*¹⁷

The system studied in this paper is one of general occurrence, where an anisotropic adsorbate interacts with a surface of a solid having anisotropic properties. In all likelihood the anisotropy of the solid extends into the boundary surface, and the composition of the boundary will vary with those pretreatments that influence the crystallization process of the solid. This may or may not be dependent on an impurity which may also be present in the gas-solid interface. A nonuniform surface, therefore, is a natural consequence of inherent anisotropy of the adsorbent. Incidentally, the commercial solid adsorbents have pronounced anisotropy in the crystallites of which they are composed.

The Transition between Localized and Condensed Layers in the Adsorption of Water Vapor onto Titania^{1a}

by P. T. Dawson^{1b}

Department of Colloid Science, University of Cambridge, Cambridge, England (Received July 25, 1966)

Water vapor adsorption isotherms have been determined on rutile samples of differing surface area. Discontinuous isotherms were observed for samples containing small particles (50-Å diameter). The discontinuities are interpreted by a mechanism which postulates the existence of two states for the adsorbed layer, one localized and one condensed, with an energy barrier to transition between them. Water isotherms on a larger particle size sample were not discontinuous, but had two linear sections between relative pressures of about 0.05 and 0.23 and above 0.23. It is assumed that a different crystal face is dominant in the larger particles and the energy barrier is reduced so that condensation becomes continuous. Close-packed monolayer formation is thought to occur at the beginning of the second linear section which would imply that the BET theory gives erroneous monolayer volumes.

Introduction

The surface properties of the oxides titania, silica, and alumina are similar in many respects. Under atmospheric conditions they are often strongly hydrated; the surface species are not oxide ions but hydroxyl groups, and these are covered by at least a monolayer of adsorbed water molecules. The mechanism whereby surface hydroxyl groups condense to lose water at high temperatures under vacuum has been subject to much investigation, especially for silica and alumina. The present paper describes an attempt to characterize hydroxylated titania surfaces and to understand the mechanism of water vapor adsorption onto such surfaces.

Experimental Section

The rutile samples used have been described previously.² Surface areas, as determined by the BET method, were 11.5, 158.0, and 44.8 m²/g, and particle diameters, as determined by electron microscopy, were 0.01–0.3, 0.005, and 0.005–0.1 μ for rutile samples A, B, and C, respectively.

Quartz double-distilled water was boiled to remove dissolved gases. The water was confined in a glass bulb by a capillary column of mercury.

Adsorption isotherms were determined by a con-

ventional volumetric technique. Vapor pressures were measured using a wide bore (25-mm i.d.) mercury manometer in which the heights of the menisci were determined to 0.01 mm by means of a cathetometer.

Results

Water vapor adsorption isotherms at 20° were determined on samples of rutile A which had been evacuated for 50 hr at 250, 200, 150, 100, 60, and 20°, as shown in Figure 1. The choice of 10.1 Å² as the close-packed area per water molecule is subsequently justified. Experiments were carried out to determine the effect of degassing time on the adsorption capacity; this rapidly increased over the first 15 hr and subsequently increased very slowly. Thus after 150 hr the adsorption capacity had increased by only 10% of its value after 15 hr. The choice of 50 hr as the outgassing time was arbitrary. The amount of water vapor adsorbed increased markedly with increased degassing temperature, although the shape of the isotherms did not change. The adsorption of water

(1) (a) Work was performed in part at the Ames Laboratory of the U. S. Atomic Energy Commission. Contribution No. 2051. (b) Institute for Atomic Research, Iowa State University, Ames, Iowa.

(2) P. T. Dawson, G. T. Rich, and D. A. Haydon, *J. Phys. Chem.*, **68**, 3550 (1964).

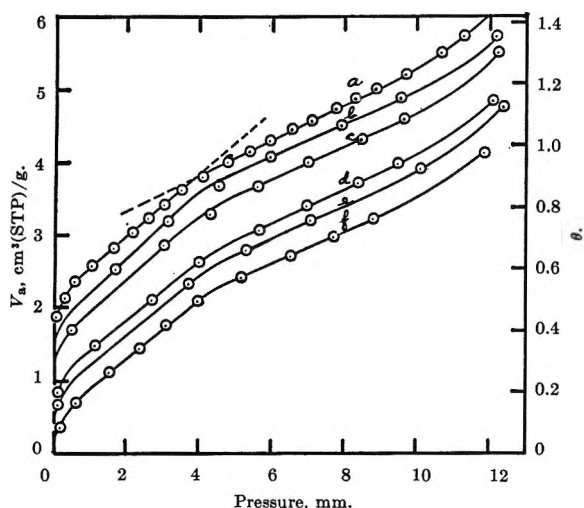


Figure 1. Water vapor adsorption isotherms at 20° for rutile A (11.5 m²/g) evacuated at: (a) 250, (b) 200, (c) 150, (d) 100, (e) 60, and (f) 20°. Coverage, θ , calculated on the basis of an area of 10.1 Å² per water molecule.

vapor onto rutile A was much slower than nitrogen adsorption, and it usually took at least 30 min to attain equilibrium.³ Equilibrium pressures were always measured at least 1 hr after dosing the sample. The isotherms did not have a simple sigmoid shape, and two linear portions could be quite clearly discerned. Isotherms for water adsorption onto rutile which have a similar anomalous shape have already been published,^{4,5} though the authors did not suggest that their isotherms were unusual. The linear portions of the present isotherms commenced at relative pressures of about 0.05 and 0.23 compared with values taken from the earlier data of approximately 0.03 and 0.25,⁴ and 0.05 and 0.20.⁵ As all these isotherms have a very similar shape, the observed shape must presumably be of significance. The particle sizes of the present sample (rutile A) and those described in both previous publications are comparable.

The adsorption of water vapor onto rutile samples B and C was even more anomalous than that for sample A, as can be seen from the isotherms in Figures 2 and 3. At coverages far below unity, stable films are formed in apparent equilibrium with quite high vapor pressures. The stability of the films can be gauged from the times which were allowed for the system to come to equilibrium. Thus, for example, consider the first point on the isotherm for rutile B representing an adsorption of 24.02 cm³ (STP)/g at an equilibrium vapor pressure of 4.60 mm. The rapid initial adsorption was followed by a slow adsorption for the next 5 hr and then no further change could be detected after 24 hr had elapsed. The next dose caused this film

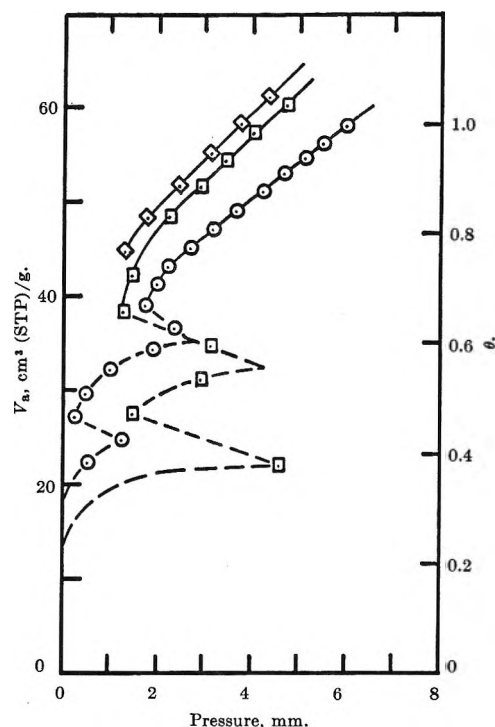


Figure 2. Water vapor adsorption isotherms at 20° for rutile B (158 m²/g) evacuated at 250°. Coverage, θ , calculated on the basis of an area of 10.1 Å² per water molecule.

to collapse, and equilibrium was attained much more rapidly at a lower vapor pressure. A second collapse occurred at a fractional coverage of about 0.6, and the adsorption became similar to that on rutile A after a coverage of approximately 0.8 had been attained. It should be noted, however, that the linear portion of this isotherm corresponds to the second linear part of the isotherm on rutile A. Although all isotherms measured had this characteristic form, the actual shape of the isotherm, in part sensitive to the choice of dosing pressure and volume, was not reproducible. The rate of adsorption varied with coverage as can be seen in Figure 4 for rutile C. As the critical coverage for collapse was approached, the adsorption became much slower.

Both water and nitrogen adsorption isotherms on rutile C showed some of the characteristics of the isotherms for both rutile A and rutile B. This was not surprising since the particle size distribution in sample

(3) The use of the term equilibrium in this case implies only that the rate of adsorption was so small as to be undetectable over any reasonable time interval and, as the subsequent discussion makes clear, all such states of the adsorbed film are not to be considered true equilibrium states.

(4) W. D. Harkins and G. Jura, *J. Am. Chem. Soc.*, **66**, 1356 (1944).

(5) C. M. Hollabaugh and J. J. Chessick, *J. Phys. Chem.*, **65**, 109 (1961).

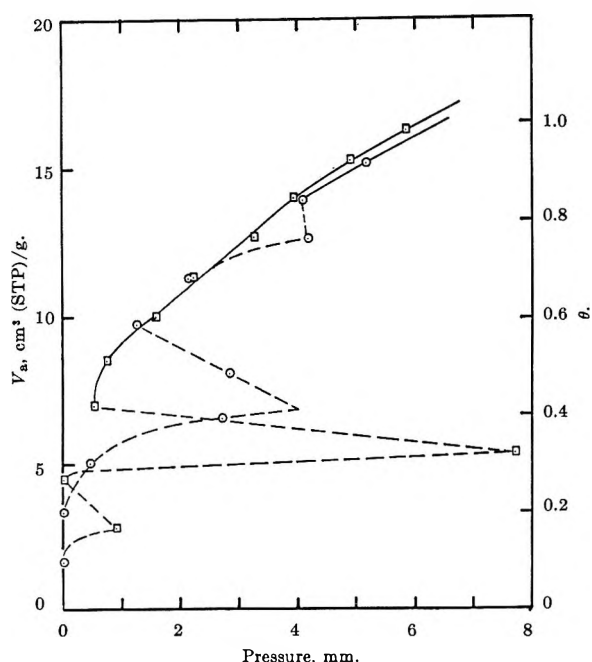


Figure 3. Water vapor adsorption isotherms at 20° for rutile C (44.8 m²/g) evacuated at 200°, □; and 250°, ○. Coverage, θ , calculated on the basis of an area of 10.1 Å² per water molecule.

C suggested that it could be likened to a mixture of samples A and B.

Discussion

Water Adsorption on Rutile A (Large Particle Size). Considerable evidence supports the contention that the surface of rutile is extremely heterogeneous,⁵⁻⁷ which affords an explanation for the results shown in Figure 1. An increase in the evacuation temperature will increase the mean kinetic energy of the adsorbed water molecules, and molecules which are more strongly bound to the surface will also evaporate. An approximate calculation based on a modified Langmuir model⁸ indicates that a variation in the heat of adsorption with coverage from 28 to 16 kcal mole⁻¹ would account for the present results. This variation compares well with 29 to 16 kcal/mole determined calorimetrically.⁵

Hollabaugh and Chessick⁵ have shown that the evacuation of a rutile sample covered with water, adsorbed after evacuating at 450°, at 26 and 90° leaves some water irreversibly adsorbed on the surface. The volume of water irreversibly adsorbed at 90° is interpreted as that which had rehydroxylated Ti-O-Ti groups formed by evacuation at 450°. However, if a fully hydroxylated surface can adsorb a close-packed monolayer of water, then including this irreversibly adsorbed water should lead to apparent monolayer coverages greater than unity rather than substantially less, *viz.*,

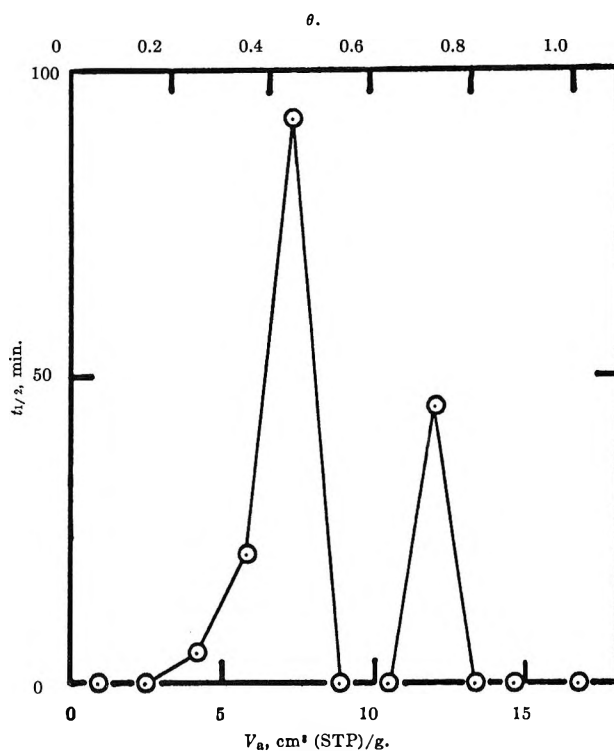


Figure 4. Variation with coverage of the half-time for the attainment of "equilibrium" in the adsorption of water vapor onto rutile C.

about two-thirds of the nitrogen value. The second "knee" of their isotherm, obtained after evacuation at 90°, corresponds to the same coverage as the equivalent point on the present isotherm obtained after evacuation at 100°. It can be seen from Figure 1 that the coverage at this point on the isotherms increases with temperature of activation until at 250° it attains a value of 0.86. Presumably it would reach unity when the evacuation temperature was sufficient to desorb the strongly adsorbed water molecules remaining on the surface at 250°, a temperature of about 300-350°. However, a further increase in activation temperature to 450° (Hollabaugh's sample) causes the apparent coverage at the second "knee" to drop to about 0.75.

Wade and Hackerman⁹ have shown that the heats of immersion of rutile in water pass through a maximum with respect to outgassing temperature in the region

(6) W. D. Harkins and G. Jura, *J. Am. Chem. Soc.*, **66**, 919 (1944).

(7) L. E. Drain and J. A. Morrison, *Trans. Faraday Soc.*, **48**, 316 (1952).

(8) J. H. DeBoer, "The Dynamical Character of Adsorption," Oxford University Press, London, 1953.

(9) W. H. Wade and N. Hackerman, *J. Phys. Chem.*, **65**, 1681 (1961).

(10) D. J. C. Yates, *ibid.*, **65**, 746 (1961).

of 300 to 350°. They suggest that heating the samples above 300° leads to a condensation of hydroxyl groups which is irreversible. This affords a possible explanation for the decrease in coverage on increasing the activation temperature from 250 to 450°; thus Ti-O-Ti groups are formed and adsorbed water molecules are very strongly localized over these groups without, however, rehydrating them. Only one water molecule is adsorbed for two Ti atoms instead of two for the hydroxylated surface.

Yates¹⁰ has studied the surfaces of rutile and anatase by infrared techniques. After evacuation at 150°, H-O-H bending modes were detected indicating residual water molecules, whereas after evacuation at 350° only residual OH groups were detected on the surface. Similar results have been reported for silica¹¹ and alumina.¹²

The present results are taken to be consistent with these spectroscopic observations and with the calorimetric measurements of Wade and Hackerman. The increased adsorption on raising the temperature of evacuation from 20 to 250° occurs because the more strongly adsorbed water molecules on the higher energy sites have been removed, and the monolayer capacity is increased.

Models for the Adsorbent and Adsorbate. In order to explain the peculiar results obtained for the adsorption of water vapor onto the higher area samples B and C and to account for the two linear sections of the isotherm for sample A, we must examine the surface structure in more detail.

In the rutile unit cell¹³ the Ti⁴⁺ and O²⁻ ions have been assigned diameters of 1.32 and 2.58 Å, respectively. The (100) and (110) planes are considered. These are two of the four most common faces for the rutile crystal, and in different crystal habits either could be the dominant face. The (110) and (100) planes are the only planes for which cleavage is distinct.¹⁴ Figure 5a depicts the (100) plane perpendicular and in the plane of the surface. The large and small open circles are O²⁻ and Ti⁴⁺ ions, respectively, and the hatched circles represent surface OH groups. Similarly, the (110) plane is shown in Figure 5b.

Adsorbed water on a rutile surface is considered to be localized since strong specific hydrogen bonding to high energy sites (OH groups) will occur. In such cases, intermediate between chemisorption and physical adsorption the choice of a monolayer coverage to which experimentally determined surface coverages can be related is not obvious. For the purpose of this discussion, surface coverages are compared to that represented by a close-packed monolayer, rather than an assumed total number of surface sites.

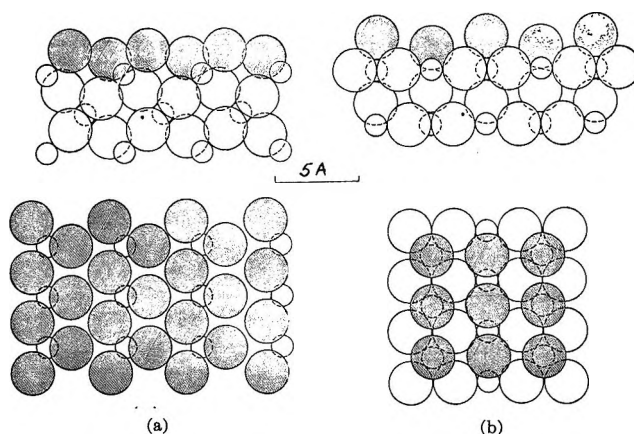


Figure 5. (a) The (100) face and (b) the (110) face of rutile in section and plan. The large and small open circles are O²⁻ and Ti⁴⁺ ions, respectively. Hatched circles represent surface OH groups.

The value usually quoted¹⁵ for the close-packed area of a water molecule, 10.8 Å², was calculated by comparing the adsorption of N₂ and H₂O on TiO₂ so the use of this value is suspect in the present discussion. Assuming the bulk liquid to have a close-packed structure and the adsorbed molecules to be hexagonally close packed, the molecular area can be calculated from the liquid density by the formula¹⁶ $A_0 = 1.091 \times (M/N_0)^{2/3}$. For water at 20°, $A_0 = 10.5$ Å²/molecule. Since liquid water has a partly hydrogen-bonded structure, it will not be close-packed and this value of A_0 must be in error. Water can be likened to an ideal mixture of two liquids, one with an ice-like structure and the other close-packed,¹⁷ and if the density of the latter can be estimated, we can circumvent this problem. Using an empirical formula of Jacobson and Heedman,¹⁸ the volume of 1 g of close-packed water at T (°K), is given by¹⁷

$$V_T = 0.7582[1.546 - 0.546(1 - T/T_c)^{1/4}]^3 \quad (1)$$

T_c is the critical temperature and taken as 647°K. The density of close-packed water at 20° is calculated

(11) B. Imelik, "The Structure and Properties of Porous Materials," D. H. Everett and F. S. Stone, Ed., Butterworth and Co. Ltd., London, 1958, p 236.

(12) J. B. Peri and R. B. Hannan, *J. Phys. Chem.*, **64**, 1526 (1960).

(13) G. Greenwood, *Phil. Mag.*, **48**, 654 (1924).

(14) J. D. Dana, "The System of Mineralogy," 7th ed, Chapman and Hall Ltd., London, 1944, p 554.

(15) H. K. Livingstone, *J. Colloid Sci.*, **4**, 447 (1949).

(16) H. K. Livingstone, *J. Am. Chem. Soc.*, **66**, 569 (1944).

(17) K. Grjotheim and J. Krogh-Moe, *Acta Chem. Scand.*, **8**, 1193 (1954).

(18) B. Jacobson and P. A. Heedman, *ibid.*, **7**, 705 (1953).

to be 1.059 g/cm^3 , which gives a value of $A_0 = 10.1 \text{ \AA}^2/\text{molecule}$.

Mechanism of Water Adsorption onto Samples B and C (Small Particle Size). Rutile sample B and C both contain small primary particles (50-Å diameter), but these are absent in rutile A. These small particles are the most likely cause of the observed differences in isotherm shape. In order to explain the anomalous isotherms, we assume that the surfaces of the large and small particles differ in structure. For rutile samples comparable in size to samples A and B, Wade and Hackerman⁹ have found large differences in their heats of immersion in water. It is expected that the surfaces of the large and especially the small primary particles will be imperfect. However, in different crystal habits either the (100) or (110) face will dominate.¹⁴ For the purposes of this discussion, we will assume that the small primary particles are in a (100) form, but crystal growth causes the (110) face to develop at the expense of the (100) and thus the (110) face is dominant in the large particles.

In the scale drawing, Figure 6, the points represent the hexagonal arrangement of the hydroxyl groups on a (100) face of rutile. These are assumed to be high-energy sites on the surface. Water molecules are represented simply as spheres of such a radius that when hexagonally close-packed they would occupy an area of 10.1 \AA^2 per molecule. Adsorption will occur rapidly until as many high energy sites are occupied as is sterically possible. This will occur when one-third of the sites are occupied and represents a fractional coverage of about 0.5, which fits the experimental data shown in Figure 2 if about 10% of the high-energy sites were occupied at the start of the experiment. Further adsorption must occur in a second layer on top of a first layer which is not condensed. The heat of adsorption in this second layer would be expected, on the one hand, to be greater than the heat of liquefaction (10.5 kcal/mole) owing to polarization by the surface, but on the other hand, less since the first layer is not close-packed. If the heat and entropy changes on adsorption and liquefaction were equal, we would need to increase the pressure to the saturation vapor pressure to obtain any further adsorption. Almost certainly the entropy change, and perhaps the heat change, will be more favorable in the adsorption process, and consequently the pressures required for further adsorption may be expected to be somewhat less than the saturation vapor pressure. Thus, referring to Figures 2 and 3, we can see that the small increase in coverage with quite large increases in vapor pressure, as the first collapse point is approached, are reasonable. This situation is not necessarily a stable one since the

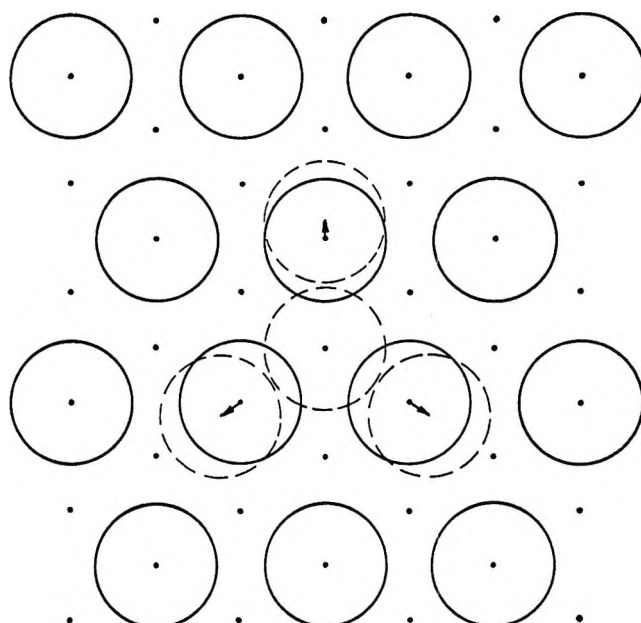


Figure 6. First-layer water adsorption on the (100) face of rutile. The points represent the positions of high energy sites (OH groups) and the full circles represent localized water molecules. Further adsorption in the first layer can only occur by displacement of localized molecules (broken circles).

molecules adsorbed in the first layer are assumed to be only localized, not immobile, and could conceivably be displaced laterally allowing further adsorption to occur in the first layer. In Figure 6, we can see that the displacement of three molecules in the first layer by one from the second is sterically possible, but it is questionable whether the process is energetically favorable. The free-energy change for the process will be

$$\Delta G = (Q_0 + 3Q_z) - (3Q_0 + Q_2) - T\Delta S \quad (2)$$

where the heats of interaction of a water molecule with the surface, located over a high-energy site, displaced a distance x from a site, and in the second layer are Q_0 , Q_z , and Q_2 , respectively. The entropy change ΔS can be interpreted as the loss of the remaining two degrees of translational freedom which the molecule will possess in the second layer. Ignoring the small entropy gain arising from the appearance of new degrees of vibrational freedom, the entropy change can be calculated¹⁹ as $-23.6 \text{ cal/deg mole}$. Choosing reasonable values⁵ for Q_0 and Q_2 of -25 and -12 kcal/mole , respectively, we find that the free-energy change would be favorable only if Q_z was less than -23 kcal/mole . Q_z is the heat of adsorption of a water molecule

(19) J. H. DeBoer and S. Kruyer, *Proc. Koninkl. Ned. Akad. Wetenschap.*, **58B**, 61 (1955).

displaced about 0.7 Å from a position where it can form a very strong hydrogen bond, presumably of definite length. It is likely that such a displacement will cause a far greater change in the heat of adsorption than the 10% required for a favorable over-all free-energy change. If the present model is a reasonable approximation the process will certainly not occur.

However, experimentally, as we have seen in Figures 2 and 3, the adsorbed film does collapse eventually, and this will occur when the number of molecules in the second layer reaches a critical value such that

$$\sum_{n=1}^N Q_{zn} + W < nQ_0 + (N - n)Q_2 - (N - n)T\Delta S \quad (3)$$

where W is the heat of condensation and ΔS is the entropy change for the process. Thus when the total number of molecules adsorbed is N , of which $(N - n)$ are in the second layer, the molecules in the second layer pass into the first layer. Then all N molecules will rearrange to give the most energetically favorable configuration; *i.e.*, $\sum_{n=1}^N Q_{zn}$ has a minimum value, and the system gains the heat of condensation, W .

This condensation will cause some of the high-energy sites to become unoccupied and the subsequent adsorption on these sites will again be rapid (Figures 2 and 4). When all the active sites are again occupied, the process outlined above will be repeated causing a second collapse of the film. Once the first layer is complete, the surface hydroxyl groups will cease to have any localizing influence on the subsequent adsorption which will consequently be quite normal. The "knee" of the isotherms on rutile B corresponds to a coverage of between 0.8 and 0.9, again suggesting that perhaps the surface is still about 10 to 20% covered with "physically" adsorbed water even after evacuating at 250° for 50 hr. Alternatively, the area per molecule in the close-packed film may be somewhat greater than 10.1 Å².

The isotherms in Figure 2 and 3 suggest that at the same water vapor pressure, two states of the adsorbed film are possible, one containing considerably more molecules than the other. Both states cannot be equilibrium states; the one containing fewer molecules must represent a higher energy or metastable state. The barrier to the formation of the lower energy state is the low free energy for adsorption in the second layer. A sufficiently large number of molecules must be adsorbed in the second layer to take advantage of any instantaneous displacement of the localized molecules from their high-energy sites in the first layer.

It is interesting to note that the adsorption of formic acid on these rutile samples² was not anomalous in this way. Consequently, in this case there can be no

free-energy barrier to the formation of a close-packed monolayer. The formic acid molecule is about twice as large as a water molecule ($A_0 = 20.5 \text{ Å}^2$) and has two hydrogen bonding centers. It can be conjectured on these grounds that the formic acid molecule will be far less sensitive to its position on the surface than a water molecule, and the energy barrier to condensation will be very much smaller.

Since the condensation effects start and end at surface coverages well below unity, it is unlikely that they can be the result of a capillary condensation mechanism. This view is further supported by the absence of similar peculiarities in the adsorption of formic acid on the same adsorbents.² Any capillary condensation behavior for formic acid and water would be expected to be comparable since the product of surface tension and molar volume for both liquids are almost equal. However, it is possible that the precursor to overcoming the energy barrier to the formation of a close-packed monolayer is a capillary condensation at high relative pressures rather than the second-layer adsorption already described.

Mechanism of the Adsorption of Water Vapor onto Rutile A. Rutile sample A did not exhibit this unusual behavior, and the adsorption process must be examined more closely in the light of the model used to interpret the water vapor adsorption on samples B and C. Following the course of the isotherm on the sample evacuated at 250°, we observe a steep initial portion corresponding to the rapid localized adsorption on the high-energy sites. This is equivalent to the readsorption of the water which cannot be desorbed at 20°, and which causes the difference between the isotherms on samples evacuated at 250 and 20°. It is not surprising that the steep portion of the isotherms ends at a coverage exactly equal to the difference between the two isotherms, $\theta = 0.45$. The maximum coverage attainable by adsorption only on high-energy sites on both the (100) and (110) faces is about 0.5.

There is no evidence of the discontinuous process which occurs on the samples containing small particles. It appears to have been replaced by the first linear portion of the isotherm. We must postulate that the process does occur, but with such small increments of adsorption in the second layer that the process appears to be continuous. Thus the energy barrier to condensation must be markedly reduced. This can be achieved firstly by increasing the free energy of adsorption in the second layer, and secondly by reducing the amount of displacement necessary for molecules to pass from the second to the first layers. If the surface hydroxyl groups on the large particles were further apart than those on the small particles, both

of these conditions would be met. The second-layer molecules could then approach the surface hydroxyl groups more closely, increasing their heat of adsorption, and the localized first-layer molecules will be further apart, reducing the displacement necessary for the condensation process. In Figure 5 we can see that the surface hydroxyl groups are indeed further apart on the (110) face than on the (100) face. Therefore, the absence of the discontinuous adsorption process on rutile A might be explained by assuming that the dominant exposed crystal plane in the larger particles is the (110) plane. Wade and Hackerman⁹ have shown that the heats of immersion of rutile and anatase in water decrease with decreasing particle size. In the (100) plane the separation of the O²⁻ ions, 2.7 Å, is very close to that of the hydrogen-bonded O atoms in

ice, 2.76 Å. Thus the lower surface energy of the (100) plane over that of the (110) plane could be attributed to the formation of hydrogen bonds between the surface hydroxyl groups only on the (100) face.

The first linear portion of the adsorption isotherm represents this continuous condensation process. Consequently, a close-packed monolayer is not formed until the second "knee" of the isotherm. The BET theory would identify the formation of a monolayer as the first "knee" in the isotherm and should be applied with caution to adsorption isotherms of water vapor onto rutile.

Acknowledgment. The author wishes to thank Dr. D. A. Haydon and Professor R. S. Hansen for many helpful discussions.

Infrared Investigation of the Adsorption and Surface Reactions of the C₁ through C₄ Normal Alcohols on γ -Alumina

by R. O. Kagel

*Chemical Physics Research Laboratory, The Dow Chemical Company, Midland, Michigan
(Received July 25, 1966)*

Infrared investigations of the adsorption of the C₁ through C₄ normal alcohols on the surface of γ -alumina in the temperature range from 25 to 500° are described. Three different surface species are observed: physically adsorbed alcohol (I), an alkoxide-like chemisorbed surface species (II), and a carboxylate-like chemisorbed surface species (III), in agreement with previous work by Greenler.² Mechanisms for these adsorption processes are proposed and supported with mass spectral data.

1. Introduction

Studies of the adsorption of both ethanol and methanol on γ -alumina have previously been reported for a restricted temperature range by Babushkin, *et al.*,¹ and more recently by Greenler² in the range from 35 to 430°. There is some significant disagreement about the interpretation of similar data in these two studies; the interpretations given here essentially support those

of Greenler. The adsorption of *n*-propyl alcohol and *n*-butyl alcohol have recently been reported by Corso³ but only at one temperature, 250°. The purpose of this study is to ascertain mechanisms for the formation

(1) A. A. Babushkin, A. V. Uvarov, and L. A. Ignat'va, *Fiz. Skornik, L'vov Univ.*, No. 3, 161 (1957).

(2) R. G. Greenler, *J. Chem. Phys.*, **37**, 2094 (1962).

(3) V. Corso, *Compt. Rend.*, **259**, 1413 (1964).

of the adsorbed species. Mechanisms have been proposed by other workers, but these mechanisms for the most part are not substantiated by experimental evidence.

2. Experimental Section

The experimental procedure follows closely the methods employed by Greenler.² The stainless steel adsorption cell described in ref 4 was used in this work. Greenler's technique² of preparing the catalyst sample by slowly spraying a water slurry of a small particle alumina, Alon-C,⁵ onto a potassium bromide support plate with an artists's air brush was employed with only a slight modification: a small amount of acetone added to the water slurry prevents the alumina particles from conglomerating on the surface. High surface area films which are quite uniform and highly infrared transmitting can be prepared by this slightly modified technique. Treatment of the catalyst film, after placing the supporting KBr plate in the adsorption cell, is the same as Greenler's.²

Alcohols were introduced into the cell at their equilibrium vapor pressures at room temperature. The γ -Al₂O₃ was heated in the presence of alcohol vapor for about 0.5 hr at the desired temperature and then allowed to cool to room temperature before scanning. Excess alcohol vapor was removed by mild evacuation ($\sim 100 \mu$). Physically adsorbed alcohol was removed by evacuation at elevated temperatures ($\sim 100^\circ$) to pressures less than 5×10^{-5} mm. These samples were then cooled to room temperature before scanning. All spectra were recorded on a Beckman IR-9 spectrometer scanning from 900 to 3800 cm⁻¹. Because of the thickness of these films, it was necessary to introduce an attenuator into the reference beam; a 2x slit program was employed to recover servo energy lost from attenuating the reference beam. The γ -Al₂O₃ absorption in the 950–1200-cm⁻¹ region was compensated in some cases by placing an untreated γ -Al₂O₃ film in the reference beam. The adsorption processes were continually monitored on a Perkin-Elmer Model 12C single beam spectrometer (NaCl optics).

3. Results and Discussion

Adsorption of these normal alcohols on γ -Al₂O₃ is temperature dependent. The temperature dependence is the same for each alcohol in this series. Near room temperature both physically adsorbed alcohol and chemisorbed alkoxide are formed. The latter is observed at all temperatures up to about 430°. In the temperature range between 150 and $\sim 430^\circ$ both chemisorbed alkoxide and chemisorbed carboxylate are formed. Only chemisorbed carboxylate exists above

$\sim 430^\circ$, and this decomposes at temperatures above $\sim 500^\circ$. All the results obtained on methanol and ethanol are essentially identical with those obtained by Greenler² and will not be discussed specifically; results on *n*-propyl alcohol and *n*-butyl alcohol are exactly analogous.

Spectra of the *n*-propyl alcohol and *n*-butyl alcohol surface species which exist at temperatures below 150° are shown in Figures 1a and 1b, respectively. Bands due to *n*-butyl alcohol vapor (spectrum A, Figure 1b), for example, disappear upon initial evacuation revealing the band system shown in spectrum B, Figure 1b. Upon prolonged evacuation at pressures $< 10^{-5}$ mm most of the absorption in 1080-cm⁻¹ region of spectrum B, Figure 1b, disappears while the remaining band system becomes more distinct as shown in spectrum C, Figure 1b. Such behavior suggests that at least one physically adsorbed species (species I) and one chemisorbed species (species II) are present. This conclusion is entirely in agreement with Greenler's² observations on methanol and ethanol.

That species I is physically adsorbed alcohol has been amply demonstrated by Greenler for methanol and ethanol. The interpretation of these data for *n*-propyl alcohol and *n*-butyl alcohol (spectra B, Figures 1a and 1b) is entirely analogous.

The spectral features of species II (spectra C, Figures 1a and 1b) are consistent with those of the corresponding alkoxides, again in agreement with Greenler.² Further support for this interpretation is given by the comparison between the *n*-butyl alcohol surface species II, spectrum C, Figure 1b, and the spectrum of tri-*n*-butoxyaluminum, Figure 2. These two spectra clearly have several features in common which are attributed to the presence of Al-O-R groups in both samples. The differences observed between the two spectra probably arise from a lower alkoxide to aluminum atom ratio in the surface species as previously proposed by Greenler² for methanol and ethanol. Moreover, since it would be necessary to rupture Al-O lattice bonds (a remote possibility under these conditions) in order for the surface aluminum atom to accommodate more than one alkoxide group, it then seems reasonable to assume one alkoxide group per active surface aluminum atom.

When the catalyst is heated above $\sim 150^\circ$ in the presence of alcohol vapor, the band systems (species III) shown in Figures 2a and 3b are observed. The intense band at 1570 cm⁻¹ and the two weaker bands

(4) R. O. Kagel and L. W. Herscher, to be published.

(5) Godfrey L. Cabot, Inc., Boston 10, Mass.

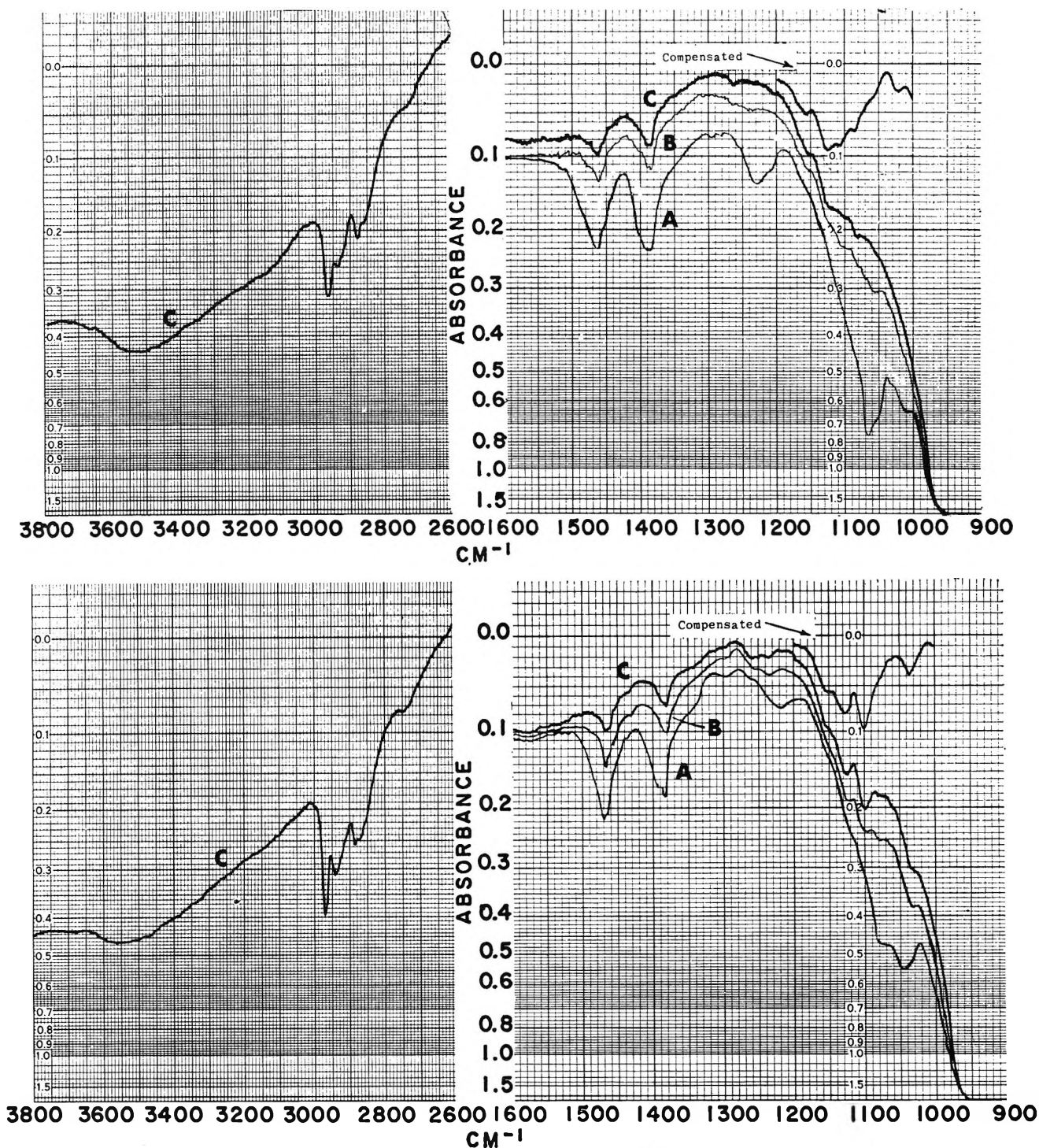


Figure 1. Spectra taken after heating the γ - Al_2O_3 sample to (a, top) 70° in *n*-propyl alcohol vapor and (b, bottom) 50° in *n*-butyl alcohol vapor. The samples were cooled to 25° before scanning. Spectrum A shows alcohol vapor over the γ - Al_2O_3 sample. Spectrum B was taken after mild evacuation ($\sim 100 \mu$). Spectrum C was taken after prolonged evacuation ($\sim 10^{-5}$ mm). Spectrum A and spectrum B are retracings of the originals.

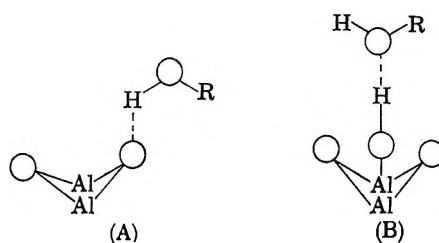
at 1475 and 1450 cm^{-1} in the spectrum of chemisorbed *n*-propyl alcohol (Figure 3a) and at 1565 and 1460 cm^{-1} in the spectrum of chemisorbed *n*-butyl

alcohol (Figure 3b) are in good agreement with those reported by Corso.³ These bands are characteristic of the antisymmetric and symmetric stretching vibra-

tions of a $-\text{COO}^-$ group. Species III is thus interpreted as a chemisorbed carboxylate, and this interpretation is entirely in agreement with those of Corso³ and Greenler (methanol and ethanol).²

The broad band at $\sim 1645\text{ cm}^{-1}$ in both Figures 3a and 3b is probably the HOH bending vibration of chemisorbed water. Neither Greenler nor Corso have reported chemisorbed water in their experiments; we attribute the presence of this water to secondary reactions as discussed below.

Many speculations have been made about surface sites on alumina. The simplest model identifies surface sites with exposed aluminum or oxide ions at



Unfortunately, the interpretation of the infrared spectrum does not allow a determination of whether structures A or B or both are present. In the following discussion it will be assumed that both structures can exist simultaneously on the surface.

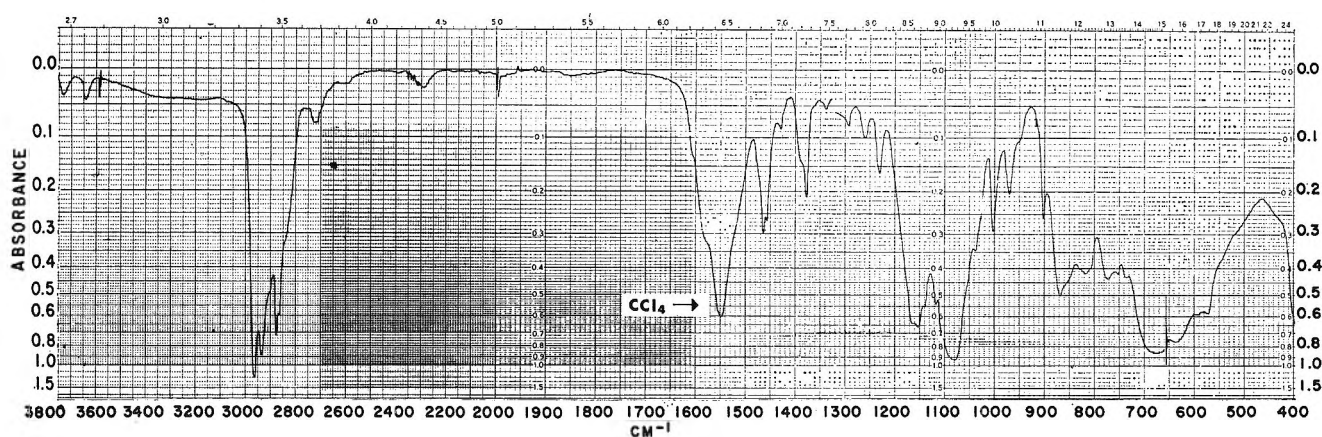


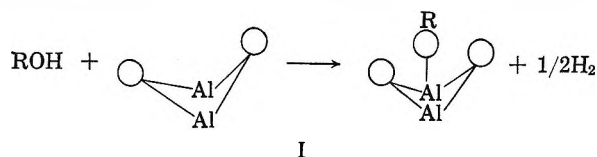
Figure 2. Spectra of $(\text{CH}_3\text{CH}_2\text{CH}_2\text{CH}_2\text{O})_3\text{Al}$ in 3.5% CCl_4 solution using a 0.2-mm KBr cell ($3800\text{--}1333\text{ cm}^{-1}$) and in 10% CS_2 solution using a 0.1-mm KBr cell ($1333\text{--}400\text{ cm}^{-1}$).

the surface and assumes the surface to be completely free of hydroxyl groups. Other models take into account cation defects or strained sites resulting from dehydration of the surface originally covered with OH groups.^{6,7}

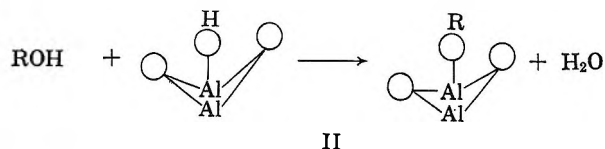
A more detailed model for the alumina surface has been given by Peri.^{8,9} This model assumes that the surface retains a random configuration of hydroxyl groups after dehydration, leaving adjoining residual oxide ions and oxide vacancies and exposed aluminum ions. This model will be adopted for the purpose of discussing mechanisms for the adsorptions reported here.

A. Physically Adsorbed Alcohol. The most reasonable mechanism for physical adsorption on the alumina surface is hydrogen bonding. Absence of any detectable OH stretching absorption above 3600 cm^{-1} (not shown in Figures 1a and 1b) suggests that the OH groups are indeed involved in hydrogen bonding. This bonding could occur at either a surface oxide ion or a surface hydroxyl group, as shown below

B. Alkoxide Surface Species. Active surface sites for this chemisorption might either be an exposed surface aluminum ion or a surface hydroxyl group. A mechanism for the adsorption at an aluminum ion is given by mechanism I. Adsorption at a hydroxyl



group is given by mechanism II. In order to de-



(6) E. B. Cornelius, T. H. Milliken, G. A. Mills, and A. G. Oblad, *J. Phys. Chem.*, **59**, 809 (1955).

(7) S. G. Hindin and S. W. Weller, *Advan. Catalysis*, **9**, 70 (1957).

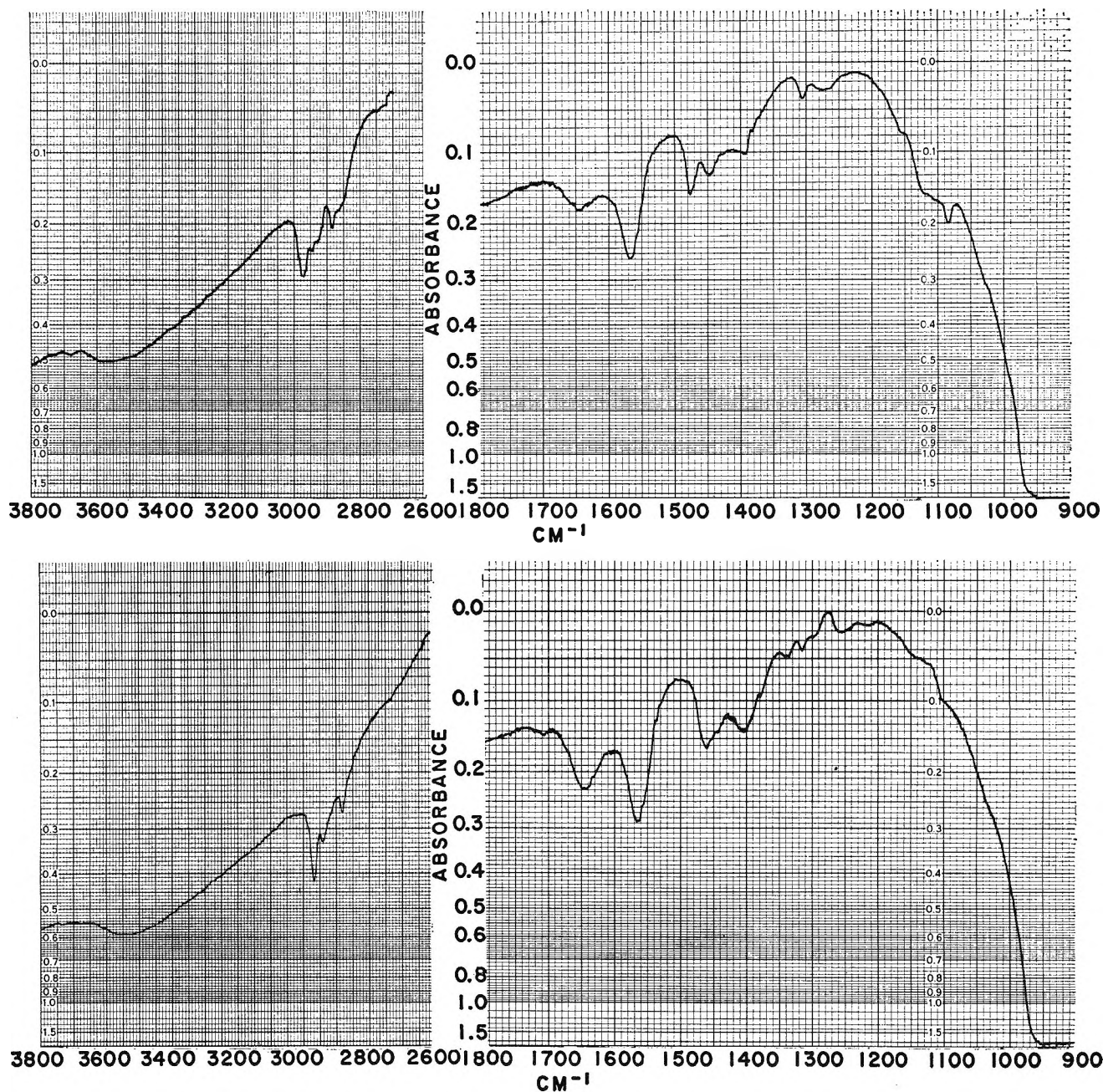


Figure 3. Spectra taken after heating the γ - Al_2O_3 sample to (a, top) 320° in *n*-propyl alcohol vapor and (b, bottom) 330° in *n*-butyl alcohol vapor. The samples were cooled to 25° and subjected to prolonged evacuation ($\sim 10^{-5}$ mm) before scanning.

termine which, if either, of the above mechanisms is correct, the gaseous contents of the cell were analyzed by means of mass spectrometry immediately after the formation of chemisorbed alkoxide. After the adsorption of ethanol-Od, neither H_2 , HD, nor D_2 was detected, thus ruling out mechanism I. Repeated experiments produced similar results.

A trap maintained at liquid nitrogen temperatures was used to isolate less volatile components in the

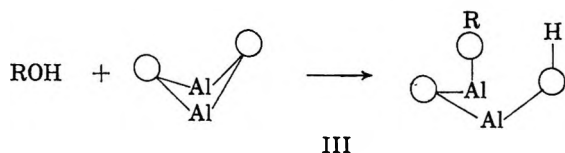
vapor. The trapped material proved to be mostly ethanol and ethanol-Od. The presence of H_2O and HDO was not firmly supported by mass spectral analysis since ethanol and ethanol-Od fragments could account for the mass peaks observed at 18 and 19. A

(8) J. B. Peri, *Actes Congr. Intern. Catalyse, 2^e, Paris, 1*, 1333 (1961).

(9) J. B. Peri, *J. Phys. Chem.*, **69**, 220 (1965).

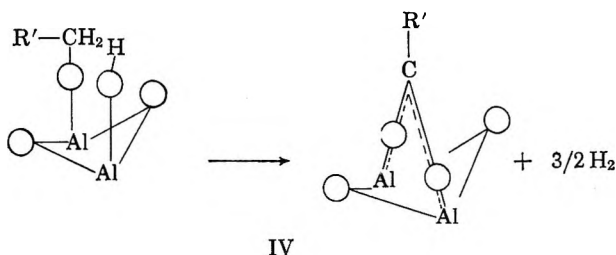
weak mass peak at 20 lends questionable support to the presence of D_2O . However, the validity of mechanism II is suspect on other grounds. First, water is not observed in the infrared spectrum of the chemisorbed alkoxide (not shown in Figures 1a and 1b). If water were present even in the adsorbed state, one should expect to observe the bending vibration at $\sim 1645\text{ cm}^{-1}$ and this band is absent. Second, it is very doubtful that both the alkoxide and water could be present simultaneously in this system; aluminum trimethoxide, for example, is extremely unstable in the presence of atmospheric water. Moreover, it has been shown experimentally that the alkoxide-like surface species does indeed readily react with water vapor giving back the alcohol.

An alternate mechanism, mechanism III, reasonably accounts for these experimental facts. Arguments in



support of mechanism III are given in section C.

C. Carboxylate Surface Species. Greenler's studies involving the adsorption of CD_3OH and CH_3OD on $\gamma\text{-Al}_2\text{O}_3$ have shown rather conclusively that the surface formate-hydrogen comes from the alcohol methyl group.² In all the systems studied here the relative carboxylate to alkoxide ratio increased as the temperature of the $\gamma\text{-Al}_2\text{O}_3$ was increased. In fact, the carboxylate was observed to form merely by heating the $\gamma\text{-Al}_2\text{O}_3$ with surface alkoxide on it to temperatures above 150° . Such behavior would suggest that the chemisorbed alkoxide is the precursor to chemisorbed carboxylate *via* mechanism IV.

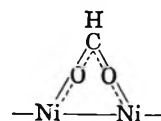


A significant test of the mechanism depends on whether or not hydrogen is evolved during the formation of carboxylate. In order to determine this, the following experiment was performed. Propoxide and propionate were simultaneously formed on the surface at 320° (Figure 3a). The system was evacuated at 150° to a pressure of 2×10^{-6} mm and cooled to room temperature. The cell was closed off to the pumps and

the sample heated to 410° . After the sample had cooled to room temperature the spectrum in Figure 4 was recorded, showing that the propoxide had disappeared and chemisorbed propionate had formed. (The small band at $\sim 1700\text{ cm}^{-1}$ may result from a small amount of free propionic acid.) The gaseous contents of the cell were analyzed by means of mass spectrometry and found to be mostly hydrogen. These observations are consistent with the mechanism proposed in IV.

Similar experiments were repeated with *n*-butyl alcohol and ethyl alcohol. In both cases the results were analogous to those obtained for *n*-propyl alcohol.

The bridged structure proposed for the surface carboxylate is in agreement with a similar structure proposed by Eischens and Pliskin¹⁰ for formic acid chemisorbed on a bare nickel surface. This covalently bridged structure is shown below. The Ni-Ni distance



is 2.492 Å compared to the Al-Al in Al_2O_3 of about 2.6 Å.

4. Conclusions

The mechanism proposed in eq IV is a mechanism only in the sense that it adequately explains the structures of the initial and final species without regard to intermediate or secondary processes. Intermediate species probably do exist on the surface, but below our level of detection. A possible explanation for the water observed in Figures 3a and 3b is that hydrogen evolved by mechanism IV undergoes a secondary reaction with surface hydroxyl groups leading to the formation of the chemisorbed water.

Our model of the alumina surface thus postulates that even when the surface is covered with alkoxide, it still retains an abundance of hydroxyl groups; this is a necessary condition for both mechanisms III and IV and these are the only mechanisms which seem to be consistent with all the experimental facts.

It has been suggested that traces of chemisorbed oxygen are responsible for the formation of surface carboxylate.³ This is not only inconsistent with experimental observations reported above, but also with those reported by Greenler.² Greenler followed the oxygen treatment with a high-temperature ($\sim 400^\circ$), hydrogen treatment in order to remove any trace amounts of chemisorbed oxygen. The results of his experiments appeared to be independent of the hy-

(10) R. P. Eischens and W. A. Pliskin, *Actes Congr. Intern. Catalyse*, 2^e, Paris, (1960).

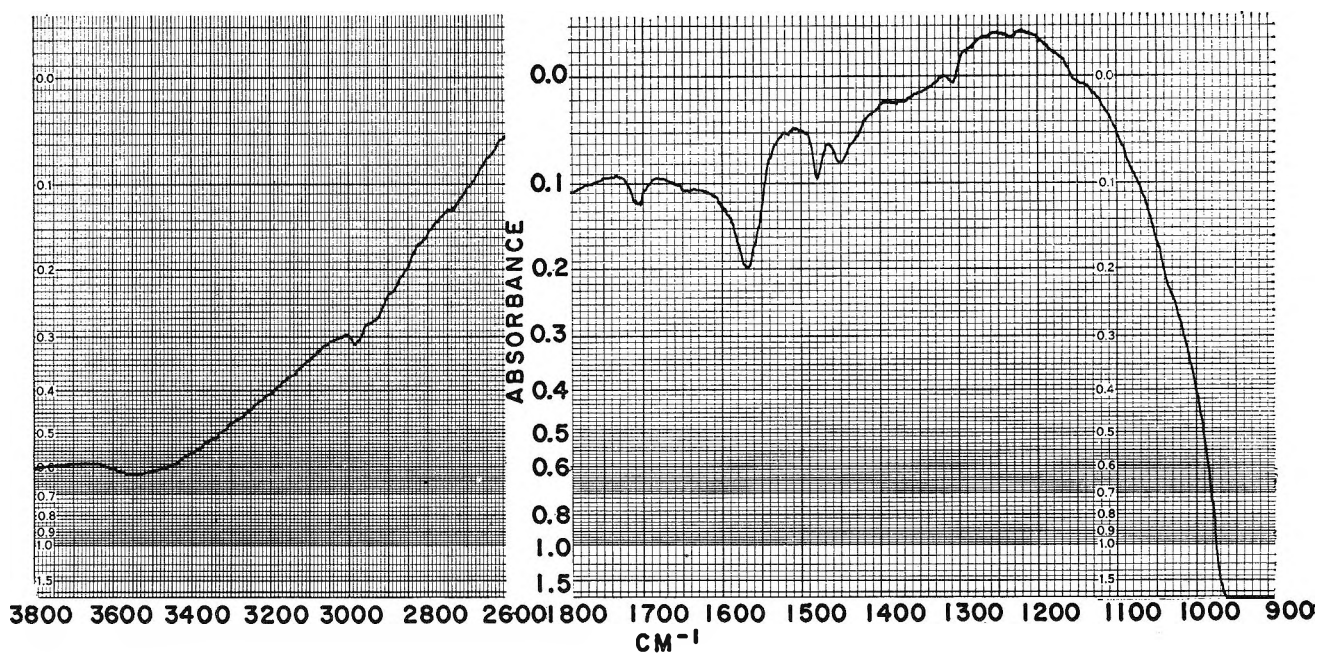


Figure 4. Spectrum taken after heating sample 3a to 410° without evacuation.

drogen treatment. Analogous experiments were conducted in this study, giving the same result. This strongly suggests that chemisorbed oxygen is not responsible for the formation of surface carboxylate.

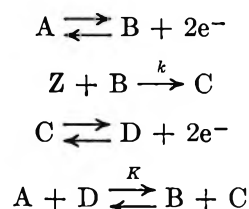
Acknowledgments. The author wishes to thank E. O. Camehl, who did the mass spectral analysis, W. J. Potts, R. A. Nyquist, and H. R. Friedli for their helpful suggestions and encouragement in this work.

Nuances of the ECE Mechanism. II. Addition of Hydrochloric Acid and Amines to Electrochemically Generated *o*-Benzoquinones

by R. N. Adams, M. Dale Hawley, and Stephen W. Feldberg¹

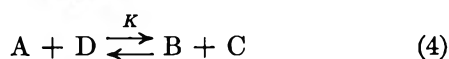
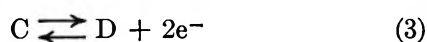
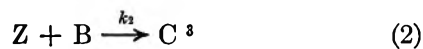
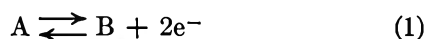
Brookhaven National Laboratory, Upton, New York (Received July 26, 1966)

The kinetics of the 1,4 addition of HCl and amines to electrochemically generated *o*-benzoquinones have been studied and are shown to proceed by a modified ECE mechanism



where A corresponds to 4-methylcatechol; B to 4-methyl-*o*-benzoquinone; Z to HCl, aniline, or *p*-aminobenzoic acid; C to the substituted 4-methylcatechol; and D to the substituted 4-methyl-*o*-benzoquinone. Chronoamperometry shows clearly that the behavior of these systems is dependent upon the equilibrium constant, *K*, as well as the rate constant for the addition reaction. The work is interpreted on the basis of previously elucidated theory.

The kinetics of the 1,4 addition of HCl and amines to electrochemically generated *o*-benzoquinones have been studied and are shown to proceed by a modified ECE mechanism²



where A corresponds to 4-methylcatechol; B to 4-methyl-*o*-benzoquinone; Z to HCl, aniline, or *p*-aminobenzoic acid; C to the substituted 4-methylcatechol; and D to the substituted 4-methyl-*o*-benzoquinone. Using the chronoamperometric technique of Alberts and Shain⁴ we show that the behavior of these systems is dependent upon the equilibrium constant, *K*, as well as the rate constant for the addition reactions. The work is interpreted on the basis of theory elucidated in part I of this work² in which the current-time-

kinetic relationships were calculated introducing the equilibrium constant for reaction 4 as an additional parameter. In addition to chronoamperometry, cyclic voltammetry and chronopotentiometry were used as diagnostic techniques.

Experimental Section

Reagents and Apparatus. All organic and inorganic chemicals were reagent grade and were used without further purification. All solutions were prepared with triply distilled water.

A carbon paste electrode, having a geometric area of

(1) Work performed under the auspices of the U. S. Atomic Energy Commission.

(2) M. D. Hawley and S. W. Feldberg, *J. Phys. Chem.*, **70**, 3459 (1966).

(3) The rate constant, *k*₂, is second order, first order in species A and first order in species Z. Throughout this work the concentration of species Z is maintained sufficiently large so that it is not polarized at the electrode. Thus we can calculate the pseudo-first-order rate constant, *k*, where *k* = *k*₂α*C*_z where *C*_z is the analytical concentration of species Z and α is the fraction of the species existing in reactive form.

(4) G. S. Alberts and I. Shain, *Anal. Chem.*, **35**, 1859 (1963).

0.238 cm², was used exclusively. Details for the construction of this electrode and the renewal of its surface have been reported previously.⁵ The reference electrode was a saturated calomel, having a potential of 0.246 v *vs.* s.h.e. All potentials are reported *vs.* sce. The combination potentiostat-galvanostat was constructed from Philbrick USA-3-M3 operational amplifiers using standard configuration.⁶ The electronic scanner was a modified version of a unit described previously.⁷ The cell was thermostated at 25° ± 0.1.

Eleven solutions were prepared for investigation by cyclic voltammetry, chronopotentiometry, and chronoamperometry. Their compositions are shown in Table I.

Cyclic Voltammetry and Chronopotentiometry. Cyclic voltammograms and chronopotentiograms were run on some of the solutions for diagnostic purposes. The results will be discussed briefly. The voltammogram of 4-methylcatechol in perchloric acid solution, 1a, Table I, was run at a scan rate 2.00 v/min from 0.00 (*vs.* sce) to 0.68 and back to 0.00 v (Figure 1). A single wave on the anodic sweep ($E_{pa} = 0.516$ v) corresponds to the oxidation of 4-methylcatechol to 4-methyl-*o*-benzoquinone and the cathodic wave ($E_{pc} = 0.375$) corresponds to the reduction of the quinone. For the anodic sweep the difference between the peak

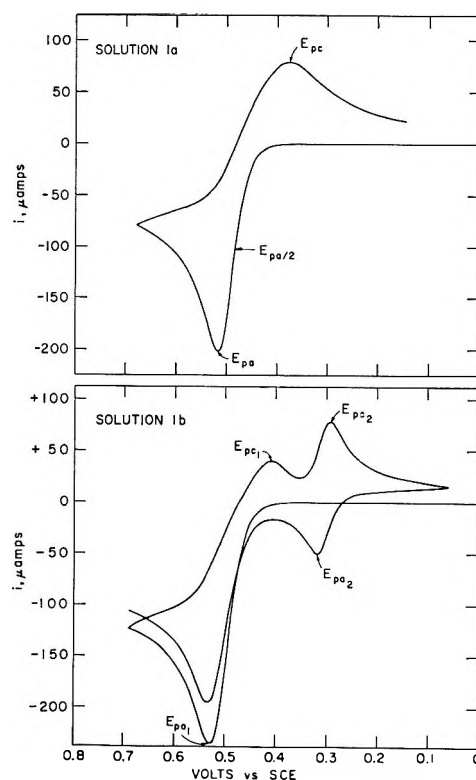


Figure 1. Cyclic voltammograms, solution 1a, Table I: 9.20×10^{-4} M 4-methylcatechol in 1.0 M perchloric acid, scan rate = 2.0 v/min; solution 1b, Table I: solution 1a + 2.22×10^{-2} M *p*-aminobenzoic acid, scan rate = 6.0 v/min.

Table I: Compositions of Solutions Investigated

Soln no.	4-Methylcatechol concn, M	Substituent (Z)	Substituent concn, M	HClO ₄ concn, M
1a	9.20×10^{-4}	<i>p</i> -Aminobenzoic acid	0	1.00
1b	9.20×10^{-4}	<i>p</i> -Aminobenzoic acid	2.22×10^{-2}	1.00
1c	1.37×10^{-3}	<i>p</i> -Aminobenzoic acid	2.69×10^{-2}	1.00
1d	1.37×10^{-3}	<i>p</i> -Aminobenzoic acid	3.40×10^{-2}	1.00
1e	2.21×10^{-3}	<i>p</i> -Aminobenzoic acid	4.07×10^{-2}	1.00
2a	6.45×10^{-4}	Aniline	0	0.29
2b	6.45×10^{-4}	Aniline	2.71×10^{-2}	0.29
2c	9.62×10^{-4}	Aniline	6.86×10^{-2}	0.29
2d	1.32×10^{-3}	Aniline	7.50×10^{-2}	0.29
3a	4.06×10^{-3}	HCl	0	3.00
3b	4.06×10^{-3}	HCl	3.00	0.00

potential (E_{pa}) and the half-peak potential ($E_{pa/2}$) is 33 mv compared to the theoretical value of 28.2 mv for a two-electron process calculated from the equations of Nicholson and Shain.⁸ This indicates that the electron-transfer process is slightly irreversible. The cyclic voltammogram of the above solution with *p*-aminobenzoic acid added (solution 1b) was run at 6.0 v/min from 0.00 to 0.69 to 0.06 to 0.69 v (Figure 1). On the first anodic sweep the oxidation of 4-methylcatechol to the corresponding *o*-quinone is observed ($E_{pa1} = 0.53$ v). Upon reversal of the linear scan at 0.69 v, two reduction waves are observed, the first wave ($E_{pc1} = 0.41$ v) corresponding to the reduction of the 4-methyl-*o*-benzoquinone and the second, more cathodic wave ($E_{pc2} = 0.2$ v) corresponding to the reduction of the substituted 4-methyl-*o*-benzoquinone. The subsequent anodic scan shows a new peak ($E_{pa2} = 0.33$ v) corresponding to the oxidation of the substi-

(5) C. Olson and R. N. Adams, *Anal. Chim. Acta*, **22**, 582 (1960).

(6) W. L. Underkofler and I. Shain, *Anal. Chem.*, **35**, 1778 (1963).

(7) J. R. Alden, J. Q. Chambers, and R. N. Adams, *J. Electroanal. Chem.*, **5**, 512 (1963).

(8) R. S. Nicholson and I. Shain, *Anal. Chem.*, **36**, 706 (1964).

tuted 4-methylcatechol. Thus, $E_{cd}^{\circ} - E_{ab}^{\circ}$ (the E° 's of the C/D and A/B couples, respectively) is about -120 mv. From the equation

$$K = \exp \left[\frac{nF}{RT} (E_{cd}^{\circ} - E_{ab}^{\circ}) \right] \quad (5)$$

one can calculate $K \approx 10^{-4}$.

Nearly identical results are obtained for the 1,4 addition of aniline (solution 2b).

The cyclic voltammogram of 4-methylcatechol in hydrochloric acid (solution 3b), however, exhibits quite different behavior. The voltammogram looks qualitatively similar to that obtained in perchloric acid, but higher peak heights indicate that the 1,4 addition of HCl and subsequent oxidation are occurring. Anodic chronopotentiograms of 4-methylcatechol in the absence of HCl and of the 1,4-addition product itself (5-chloro-4-methylcatechol) indicate that $E_{cd}^{\circ} - E_{ab}^{\circ}$ is about $+25$ mv and thus $K \approx 10$.

These observations agree qualitatively with the data presented by Fieser and Fieser⁹ showing the effect of 2-substituents on the potential of 1,4-naphthoquinone. Amines (aliphatic) have a large negative effect (>200 mv); *i.e.*, the 2-substituted 1,4-dihydroxynaphthalene is easier to oxidize than the unsubstituted 1,4-dihydroxynaphthalene. Chloride, on the other hand, has a small positive effect (about 24 mv) indicating that the substituted 1,4-dihydroxynaphthalene is more difficult to oxidize than the unsubstituted *p*-hydroxyphenol.

We will demonstrate by chronoamperometric studies that because of the difference in the equilibrium constants for the HCl and amine systems, distinctly different behavior is observed.

Chronoamperometry. The potential was stepped from 0.4 ($E_{i \leq 0}$, where $i = 0$) to 0.75 v ($E_{i > 0}$, where $A_{z=0} = C_{z=0} = 0$). The current-time curves were recorded and the resulting data for solutions 1a, 1b, 2a, 2b, 3a, and 3b are shown in Table II. Though we consider the precision of the data to be only about $\pm 1\%$, the extra significant figures in the table were carried through until the final evaluation of the rate constant.

Data Analysis. The data were analyzed using the curve-fitting technique described in part I.² The theoretical current-time-kinetic relationships for various values of the equilibrium constant, K , are shown in Figure 2. Superimposed upon these curves in order to obtain a best fit are experimental plots of n_{app}/n_1 vs. $\log t$ (see Table II) for solutions 1b (*p*-aminobenzoic acid), 2b (aniline), and 3b (HCl). The three $\log t$ axes correspond to the plot for each solution. Thus, for a given solution, one can obtain the value of \log

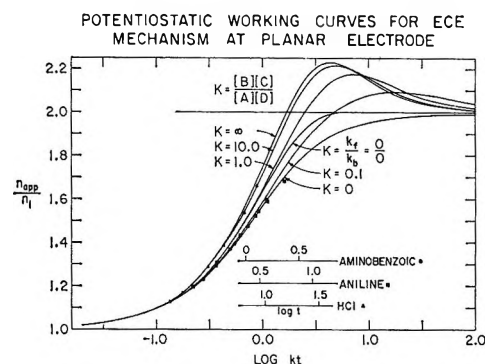


Figure 2. Best fit of 1,4-addition data to theoretical curves: ●, *p*-aminobenzoic acid, solution 1b; ■, aniline, solution 2b; ▲, HCl, solution 3b. Theoretical curves are for different values of K for equilibrium reaction 4.

t corresponding to the value of $\log kt$ for the theoretical curve. Then

$$\log k = \log kt - \log t \quad (6)$$

The pseudo-first-order rate constant, k , and the corresponding second-order rate constant, k_2 , calculated for each of the solutions are shown in Table III.

Since the 1,4-addition rate increases with pH and since nucleophilic attack by a protonated species (of aniline or *p*-aminobenzoic acid) is highly unlikely, the reactive species is probably the unprotonated form. The second-order rate constant is obtained by dividing the pseudo-first-order rate constant by the concentration of the free base present. From the data of Robinson and Biggs¹⁰ for *p*-aminobenzoic acid, the fractions of $H_3N^+C_6H_4COOH$, $H_2NC_6H_4COOH$, $H_3N^+C_6H_4COO^-$, and $H_2NC_6H_4COO^-$ in 1.0 *M* perchloric acid are estimated to be 9.97×10^{-1} , 2.94×10^{-3} , 6.14×10^{-4} , and 4.27×10^{-8} , respectively. Of the two unprotonated forms most likely to be involved in the nucleophilic attack upon the *o*-quinone nucleus, the fraction of $H_2NC_6H_4COO^-$ present is insignificant. Thus, only the fraction of $H_2NC_6H_4COOH$ was considered in the calculation of the second-order rate constant. For the 1,4 addition of aniline to the *o*-quinone one can calculate the fraction of free base in 0.29 *M* $HClO_4$ as approximately 7.3×10^{-5} . This calculation is based on the value of 4.67 for the pK reported by Vandenberg, Henrich, and Vander Berg.¹¹ The second-order rate constant for HCl is based on the analytical concen-

(9) L. F. Fieser and M. Fieser, "Organic Chemistry," 3rd ed, D. C. Heath and Co., Boston, Mass., p 712.

(10) R. A. Robinson and A. I. Biggs, *Australian J. Chem.*, 10, 128 (1957).

(11) J. M. Vandenberg, C. Henrich, and S. G. Vander Berg, *Anal. Chem.*, 26, 726 (1954).

Table II: Chronoamperometric Data

Soln	$E_{t \leq 0}^a$	$E_{t > 0}^b$	t, sec^c	$it^{1/2}/C_A^d$	$(it^{1/2})_{k=0}/C_A$	n_{app}/n_1^e
1b Z = <i>p</i> -amino- benzoic acid	0.40	0.75	0.60	88.5	73.5 (for soln 1a)	1.203
			0.75	90.8		1.234
			1.00	95.1		1.292
			1.50	102.5		1.396
			2.00	108.0		1.476
			2.50	113.0		1.544
			3.00	117.0		1.598
2b Z = aniline	0.40	0.75	2.33	98.3	75.2 (for soln 2a)	1.307
			3.11	103.3		1.373
			3.89	107.8		1.434
			5.44	115.0		1.524
			7.00	120.3		1.590
			10.10	127.9		1.679
3b Z = HCl	0.40	0.75	2.33	86.9	77.2 (for soln 3a)	1.126
			3.11	90.0		1.166
			3.89	92.8		1.202
			5.44	99.4		1.287
			7.77	107.0		1.386
			11.66	118.5		1.535
			15.54	128.5		1.664

^a $E_{t \leq 0}$ = potential where $i = 0$. ^b $E_{t > 0}$ = potential where $A_{x=0} = C_{x=0} = 0$. ^c t time after potential stepped from $E_{t \leq 0}$ to $E_{t > 0}$. ^d i = current observed after potential step. ^e $(n_{app}/n_1) = [it^{1/2}/C_A] / [(it^{1/2})_{k=0}/C_A]$.

Table III: Rate Constants Calculated for 1,4-Addition Reactions

Soln	Pseudo-first-order k_1, sec^{-1}	α^a	Second-order ^b $k_2, \text{sec}^{-1} M^{-1}$
1b	3.67×10^{-1}		5.5×10^3
1c ^c	4.6×10^{-1}		5.8×10^3
1d ^c	5.9×10^{-1}	2.94×10^{-3}	5.9×10^3
1e ^c	6.8×10^{-1}		5.8×10^3
2b	1.58×10^{-1}		7.8×10^4
2c ^c	4.1×10^{-1}	7.3×10^{-5}	8.2×10^4
2d ^c	4.5×10^{-1}		8.2×10^4
3b	5.7×10^{-2}	1.0	1.9×10^2

^a α = fraction of adding species present as free base. ^b $k_2 = k/(C_Z\alpha)$. ^c Electrode fouling.

tration of HCl (3.0 M). It is assumed of course that acid-base equilibria are extremely rapid.

One major problem was encountered: at higher concentrations of 4-methylcatechol and *p*-aminobenzoic acid or of 4-methylcatechol and aniline, electrode fouling was observed. The problem manifested itself as a decrease in observed currents with continued use of an electrode. The problem was minimized by using a fresh electrode surface for each run. Nevertheless, the value of k was still slightly time dependent (*i.e.* a plot of kt vs. t was not a straight line.)² This prob-

lem was circumvented by calculating the value of k at each time, plotting k vs. t , and extrapolating to zero time for the true value of k . The solutions reported which led to electrode fouling are footnoted in Table III. We wish to emphasize that fouling occurs only at the higher concentrations.

Discussion. From the cyclic voltammograms and chronopotentiograms it was possible to estimate $E_{cd} - E_{ab}$ and then calculate from eq 5 the equilibrium constant for reaction 4. For *p*-aminobenzoic acid and aniline additions this constant is very small ($K \approx 10^{-4}$), but for HCl addition it is approximately ten. These estimates are substantiated by the theoretical curves which give the best fit for the data plots (Figure 2 and Table II). There is no doubt that the effect of the equilibrium constant upon the current-time-kinetic relationship is significant, but there are several other factors which can contribute to the differences observed between the HCl and amine additions. In the development of the theory² we assumed that the diffusion coefficient of each of the four species (A, B, C, D) were identical. This may not be so, especially when C and D are large addition compounds, but when $K = 0$, as is essentially the case for aniline and *p*-aminobenzoic acid, species C is virtually nonexistent. Thus, the diffusion coefficient of species C and D should not affect the theoretical curve for $K = 0$. In the case of

HCl addition all of the species seem sufficiently alike, so that their diffusion coefficients are probably not too different.

In the determination of $it^{1/2}/C_{k=0}$ we observed a slight increase in this value at times greater than about 5 sec. This increase was more pronounced in 3 M HClO₄ (solution 3a) than in 1 M HClO₄. Thus we feel that it is not simply convection or spherical edge effects. It may possibly be 1,4 addition of impurities. The following correction, however, may be made, though we question its validity: $it^{1/2}/C_{k=0}$ was determined over the time range of interest. Then in the presence of reactant Z the values of $it^{1/2}/C$ were divided by the term $it^{1/2}/C_{k=0}$ obtained at the same value of t . The resulting values of n_{app}/n_1 plotted against $\log t$ gave a best fit with the $K = 1$ curve instead of the $K = 10$ curve. This result is not necessarily contradictory to the cyclic voltammetric and chronopotentiometric evidence indicating $E_{cd} - E_{ab}$ is +25 mv. It is possible that the kinetics of reaction 4 are slow. If they are sufficiently slow the n_{app}/n_1 vs. $\log t$ plot would collapse to the shape of the Alberts and Shain curve (curve $k_t/k_b = 0/0$, Figure 2). The recent work of Marcus¹² shows that the rate of a homogeneous electron-transfer cross reaction is directly related to the rate of the heterogeneous electron transfer of each of the two couples involved. In principle, it

should be possible to evaluate the heterogeneous rate constants for the A/B and C/D electron-transfer reactions and then to calculate k_t and k_b for the cross reaction, eq 4.

The cyclic voltammograms indicate a slight irreversibility in the electron-transfer process. The chronoamperometric data, however, indicate that reaction 4 is quite rapid when B and C correspond to 4-methyl-*o*-benzoquinone and the amine-substituted 4-methylcatechol, respectively. The reaction of the 4-methyl-*o*-benzoquinone with the chloro-substituted 4-methylcatechol may be slower since the ΔF° for the reaction is less.¹² As ΔF° for reaction 4 approaches zero ($K \rightarrow 1$) it also becomes more difficult to distinguish between the chronoamperometric working curves for $K = 1$, and $k_t/k_b = 0/0$ (Figure 2). At larger values of kt , of course, the $K = 1$ curve exhibits a peak. The longest times which could be used in this study (about 15 sec) were dictated by practical limitations such as convection and edge effects which can introduce significant errors. Consequently, data that might be in the peak region were not obtained. Thus, it might be questioned whether or not fast equilibrium for reaction 4 obtains in the HCl addition studies.

(12) R. A. Marcus, *J. Phys. Chem.*, **67**, 853 (1963).

Some New Relations Connecting Molecular Properties and Electron and X-Ray Diffraction Intensities¹

by R. A. Bonham

Department of Chemistry, University of Oslo, Blindern, Norway, and Department of Chemistry, Indiana University, Bloomington, Indiana (Received August 1, 1966)

New integral relations connecting certain molecular properties with scattered electron and X-ray intensities from molecules are presented. The relationships connect molecular expectation values of various powers of the electron-nuclear and electron-electron distances, electronic charge densities at nuclear positions, and the molecular electron density with potentially observable diffraction intensities. A brief review of previously derived relations connecting diffraction intensities with molecular quantities is given.

A number of elegant integral relationships connecting certain observable quantities obtained from diffraction experiments with molecular properties have been given by Tavard and co-workers² and by Silverman and Obata.³ Using the notation introduced by Tavard, Rouault, and Roux^{2b} it is possible to summarize these relations as follows.

The total and elastically scattered intensities for electrons (ED) and X-rays (XR) scattered by molecules may be written in the first Born approximation as

$$\begin{aligned} \sigma_T^{\text{ED}}(s) &= s^4 I_T^{\text{ED}}(s) / I_0^{\text{ED}} - \\ &\quad \sum_{k=1}^N (Z_k^2 + Z_k) - \sum_{n \neq m=1}^N \sum_{n=1}^N Z_n Z_m \langle j_0(sr_{nm}) \rangle_{\text{vib}} \\ &= -2 \sum_{n=1}^N Z_n \left\langle \int_0^\infty dr D_n(r) j_0(sr) \right\rangle_{\text{vib}} + \\ &\quad \left\langle \int_0^\infty dr P(r) j_0(sr) \right\rangle_{\text{vib}} \quad (1) \end{aligned}$$

$$\begin{aligned} \sigma_e^{\text{ED}}(s) &= s^4 I_e^{\text{ED}}(s) / I_0^{\text{ED}} - \\ &\quad \sum_{k=1}^N Z_k^2 - \sum_{n \neq m=1}^N \sum_{n=1}^N Z_n Z_m \langle j_0(sr_{nm}) \rangle_{\text{vib}} \\ &= -2 \sum_{n=1}^N Z_n \left\langle \int_0^\infty dr D_n(r) j_0(sr) \right\rangle_{\text{vib}} + \\ &\quad \left\langle \int_0^\infty dr E(r) j_0(sr) \right\rangle_{\text{vib}} \quad (2) \end{aligned}$$

$$\sigma_T^{\text{XR}}(s) = I_T^{\text{XR}}(s) / I_0^{\text{XR}} - \sum_{k=1}^N Z_k = \left\langle \int_0^\infty dr P(r) j_0(sr) \right\rangle_{\text{vib}} \quad (3)$$

and

$$\sigma_e^{\text{XR}}(s) = I_e^{\text{XR}}(s) / I_0^{\text{XR}} = \left\langle \int_0^\infty dr E(r) j_0(sr) \right\rangle_{\text{vib}} \quad (4)$$

where $j_0(x)$ is the zero-order spherical Bessel function $\sin x/x$, I stands for intensity, the subscripts T and e for total and elastic, Z_k is the atomic number of the k th atom in a molecule containing N atoms, and r_{nm} is an internuclear distance. The brackets $\langle \rangle_{\text{vib}}$ stand for vibrational average and the terms I_0^{ED} and I_0^{XR} are constants characteristic of the experimental method employed. In the electron diffraction case I_0^{ED} can usually be selected by matching the experimental intensity with the theoretical Coulomb intensity at a large value of the scattering variable s ($s = 4\pi \sin(\theta/2)/\lambda$). This is equivalent to selecting I_0^{ED}

(1) Contribution No. 1427 from the Chemical Laboratories of Indiana University; the author wishes to thank the John Simon Guggenheim Foundation, The Royal Norwegian Council for Scientific and Industrial Research and the National Science Foundation for their financial support.

(2) (a) C. Tavard and M. Roux, *Compt. Rend.*, **260**, 4933 (1965); (b) C. Tavard, M. Rouault, and M. Roux, *J. Chim. Phys.*, **62**, 1410 (1965).

(3) J. N. Silverman and Y. Obata, *J. Chem. Phys.*, **38**, 1254 (1963).

so that $\sigma_T^{\text{ED}}(s)$ and $\sigma_e^{\text{ED}}(s)$ go to zero at some large value of s (i.e., $s \geq 30$ for 40-kv electrons and molecules possessing only atoms in the first row of the periodic table). In eq 1-4 the electron densities are defined as

$$D_n(r) = r^2 \int d\Omega \rho(\mathbf{r} + \mathbf{r}_n) \quad (5)$$

$$P(r) = r^2 \int d\Omega \rho_c(r) \quad (6)$$

and

$$E(r) = r^2 \int d\mathbf{r}' \rho(\mathbf{r}') \int d\Omega \rho(\mathbf{r} + \mathbf{r}') \quad (7)$$

where

$$\rho(\mathbf{r}) = \sum_{i=1}^M \int d\tau_1 \dots \int d\tau_M |\Psi_e|^2 \delta(\mathbf{r} - \mathbf{r}_i) \quad (8)$$

and

$$\rho_c(\mathbf{r}) = \sum_{i \neq j=1}^M \int d\tau_1 \dots \int d\tau_M |\Psi_e|^2 \delta(\mathbf{r} - \mathbf{r}_i + \mathbf{r}_j) \quad (9)$$

where the vector \mathbf{r}_n may be taken to be an interatomic vector or a vector from the origin of an arbitrarily chosen coordinate system to the n th nucleus. In the above equations $d\tau_n$ is the volume element for integration over both spin and space variables of the n th electron in a molecule containing M electrons. The quantities in eq 8 and 9 are the diagonal components of the first- and second-order molecular density matrices where Ψ_e is the many electron molecular wave function. The notation $D_n(r)$ and $P(r)$ in eq 5 and 6 is similar to that used by Bartell and Gavin⁴ who have discussed the relations of the type presented here in the case of atomic scattering.

Tavard, Rouault, and Roux^{2b} have devised a numerical scheme for obtaining an estimate of the three-dimensional molecular electron density, $\rho(\mathbf{r})$, from the Fourier transform of the quantity

$$\begin{aligned} \Delta\sigma(s) &= \sigma_T^{\text{XR}}(s) - \sigma_T^{\text{ED}}(s) = \sigma_e^{\text{XR}}(s) - \sigma_e^{\text{ED}}(s) \\ &= 2 \sum_n Z_n \left\langle \int_0^\infty dr D_n(r) j_0(sr) \right\rangle_{\text{vib}} \end{aligned} \quad (10)$$

In addition Tavard and Roux^{2a} have pointed out the connection between various components of the molecular potential energy and the electron and X-ray scattered intensities. The most direct method for deriving these results is to utilize the Fourier transform relation^{2a,5}

$$\frac{1}{r_{12}} = \frac{1}{2\pi^2} \int \frac{d\mathbf{s}}{s^2} e^{i\mathbf{s}\cdot\mathbf{r}_{12}} \quad (11)$$

In this way the total molecular potential energy, \bar{U} , becomes

$$\begin{aligned} \bar{U} &= \left\langle \Psi_e \left| \sum_{i<j} \sum \frac{Z_i Z_j}{r_{ij}} - \sum_i \sum_\mu \frac{Z_i}{r_{i\mu}} + \sum_{\mu<\nu} \sum \frac{1}{r_{\mu\nu}} \right| \Psi_e \right\rangle \\ &= \frac{1}{4\pi^2} \int \frac{d\mathbf{s}}{s^2} \left\langle \Psi_e \left| \sum_i Z_i e^{i\mathbf{s}\cdot\mathbf{r}_i} - \sum_\mu e^{i\mathbf{s}\cdot\mathbf{r}_\mu} \right|^2 - \sum_i (Z_i^2 + Z_i) \right| \Psi_e \right\rangle \end{aligned} \quad (12)$$

where i, j refer to the nuclei and μ, ν to the electrons, or finally^{2a}

$$\bar{U} = \frac{1}{\pi} \int_0^\infty ds \left[s^4 I_T^{\text{ED}}(s) / I_0^{\text{ED}} - \sum_{i=1}^N (Z_i^2 + Z_i) \right] \quad (13)$$

Before performing the same type of analysis on the other diffraction quantities it is helpful to introduce notation for the various constituent parts of the potential energy as

$$U_{\text{nn}} = \sum_{i<j} \sum \frac{Z_i Z_j}{r_{ij}} \quad (\text{nuclear-nuclear}) \quad (14)$$

$$U_{\text{en}} = - \sum_i Z_i \int_0^\infty dr \frac{D_i(r)}{r} \quad (\text{electron-nuclear}) \quad (15)$$

$$U_{\text{ee}}^{\text{coul}} = 1/2 \int d\mathbf{r} \rho(\mathbf{r}_1) \int d\mathbf{r}_2 \rho(\mathbf{r}_2) \frac{1}{r_{12}} = 1/2 \int_0^\infty dr \frac{E(r)}{r} \quad (\text{Coulomb}) \quad (16)$$

and

$$U_{\text{ee}}^{\text{ex}} = 1/2 \int_0^\infty dr \frac{P(r)}{r} - U_{\text{ee}}^{\text{coul}} \quad (\text{exchange}) \quad (17)$$

In terms of this notation the relations between potential energies and diffract on intensities can be written as

$$\begin{aligned} \bar{U} &= U_{\text{nn}} + U_{\text{en}} + U_{\text{ee}}^{\text{coul}} + U_{\text{ee}}^{\text{ex}} = \\ &= \frac{1}{\pi} \int_0^\infty ds \left[s^4 I_T^{\text{ED}} - \sum_{i=1}^N (Z_i^2 + Z_i) \right] \end{aligned} \quad (18)$$

$$\begin{aligned} U_{\text{nn}} + U_{\text{en}} + U_{\text{ee}}^{\text{coul}} &= \\ &= \frac{1}{\pi} \int_0^\infty ds \left[s^4 I_e^{\text{ED}}(s) / I_0^{\text{ED}} - \sum_{i=1}^N Z_i^2 \right] \end{aligned} \quad (19)$$

$$U_{\text{ee}}^{\text{coul}} + U_{\text{ee}}^{\text{ex}} = \frac{1}{\pi} \int_0^\infty ds \left[I_T^{\text{XR}}(s) / I_0^{\text{XR}} - \sum_{i=1}^N Z_i \right] \quad (20)$$

and

$$U_{\text{ee}}^{\text{coul}} = \frac{1}{\pi} \int_0^\infty ds I_e^{\text{XR}}(s) / I_0^{\text{XR}} \quad (21)$$

(4) L. S. Bartell and R. M. Gavin, Jr., *J. Am. Chem. Soc.*, **86**, 3493 (1964).

(5) R. A. Bonham, J. L. Peacher, and H. L. Cox, *J. Chem. Phys.*, **40**, 3083 (1964).

where strictly speaking all potential energies are vibrationally averaged and the terminology Coulomb and exchange are adopted by analogy with Hartree-Fock usage, although here the relationships refer to the exact wave function for the system. Silverman and Obata³ have pointed out the existence of eq 21 as well as the fact that eq 15 is also closely related to the nuclear diamagnetic shielding constant which is of interest in nuclear magnetic resonance (nmr) work. The remaining relations are due to Tavad and co-workers.² Perhaps more importantly, Tavad⁶ and later Iijima⁷ have shown that by using eq 18 it is possible to derive a formula for the total molecular binding energy, E_b , with the aid of the virial theorem. The total potential energy is given by the molecular virial theorem

$$\bar{U}(\mathbf{X}_i) = 2E(\mathbf{X}_i) + \sum_i \mathbf{X}_i \cdot \nabla_i E(\mathbf{X}_i) \quad (22)$$

where the sum is over all the nuclear cartesian coordinates.⁸ This expression can be transformed successively from cartesian to mass-weighted cartesian displacement coordinates and finally to the normal coordinates, \mathbf{Q}_i , by linear transformations with the result

$$\bar{U}(\mathbf{Q}_i) = 2E(\mathbf{Q}_i) + \sum_{\alpha} \mathbf{Q}_{\alpha} \cdot \nabla_{\alpha} E(\mathbf{Q}_i) + \sum_{\beta} \mathbf{X}_{\beta}^e \cdot \nabla_{\beta} E(\mathbf{X}_i) \quad (23)$$

where the last term on the right has been left in terms of mass-weighted cartesian displacement coordinates and \mathbf{X}_i^e is the vector specifying the equilibrium position of the l th atom. The vibrational average of the term $\nabla_i E(\mathbf{X}_i)$ is zero at the equilibrium state (*i.e.*, $\langle \partial V(\mathbf{X}_i) / \partial X_{ij} \rangle_{\text{vib}}$, $i = 1, 2, 3$ are all zero). The energy in normal coordinates through quadratic terms can be written as $E(\mathbf{Q}_i) = E_{\text{eq}} + 1/2 \sum_{\alpha} k_{\alpha} \mathbf{Q}_{\alpha} \cdot \mathbf{Q}_{\alpha}$ which allows the vibrational average of eq 23 to be simplified to

$$\langle \bar{U} \rangle_{\text{vib}} = 2E_{\text{eq}} + 2 \sum_{\alpha} k_{\alpha} \langle \mathbf{Q}_{\alpha} \cdot \mathbf{Q}_{\alpha} \rangle_{\text{vib}} \quad (24)$$

where the k_{α} are force constants and E_{eq} is the equilibrium electronic energy. Since $\sum_i k_{\alpha} \langle \mathbf{Q}_{\alpha} \cdot \mathbf{Q}_{\alpha} \rangle_{\text{vib}}$ is the harmonic vibrational energy for the α th normal mode it may be replaced by the sum of the harmonic vibrational energies in terms of the normal frequencies ω_{α} , so that the total electronic energy in the equilibrium state becomes approximately

$$E_{\text{eq}} = 1/2 \langle \bar{U} \rangle_{\text{vib}} - \sum_{\alpha} \hbar \omega_{\alpha} (n_{\alpha} + 1/2) \quad (25)$$

The last term in eq 25 is simply the well-known zero-point vibrational energy correction. It is now possible to write the binding energy as

$$E_b = \frac{1}{2\pi} \int_0^{\infty} ds [s^4 I_T^{\text{ED}}(s) / I_0^{\text{ED}} - s^4 I_A^{\text{ED}}(s)] - \sum_{\alpha} \hbar \omega_{\alpha} (\langle n_{\alpha} \rangle_T + 1/2) \quad (26)$$

where $\langle n_{\alpha} \rangle_T$ is the thermal average over vibrational states and $s^4 I_A^{\text{ED}}(s)$ is the theoretical atomic background obtained by letting r_{ij} go to infinity in eq 12. It is more convenient to write eq 26 as^{6,7}

$$E_b = \frac{1}{2\pi} \int_0^{\infty} ds [s^4 I_T^{\text{ED}}(s) / I_0^{\text{ED}} - s^4 I_{\text{IAM}}^{\text{ED}}(s)] + \frac{1}{2\pi} \int_0^{\infty} ds [s^4 I_{\text{IAM}}^{\text{ED}}(s) - s^4 I_A^{\text{ED}}(s)] - \sum_i \hbar \omega_i (\langle n_i \rangle_T + 1/2) \quad (27)$$

because the integrand of the first integral converges to zero at small values of s ($s \sim 15$) for molecules containing only light atoms. $I_A^{\text{ED}}(s)$ and $I_{\text{IAM}}^{\text{ED}}(s)$ are given theoretically as⁹

$$s^4 I_A^{\text{ED}}(s) = \sum_k^N \{ [Z_k - F_k(s)]^2 + S_k(s) \}$$

$$s^4 I_{\text{IAM}}^{\text{ED}}(s) = s^4 I_A^{\text{ED}}(s) + \sum_{i \neq j}^N \sum_{i=1}^N [Z_i - F_i(s)] \times [Z_j - F_j(s)] e^{-l_{ij}^2 s^2 / 2} \sin sr_{ij} / sr_{ij} \quad (28)$$

In addition, the second integral in eq 27 reduces to

$$1/2 \int_0^{\infty} ds [s^4 I_{\text{IAM}}^{\text{ED}}(s) - s^4 I_A^{\text{ED}}(s)] = 1/4 \sum_{i \neq j}^N \sum_{i=1}^N Z_i Z_j \times \left\{ \sum_{\substack{l \\ (\lambda_i^l \neq \lambda_k^l)}} \sum_k \gamma_i^l \gamma_k^l [\lambda_i^{2l} \exp(-r_{ij} \lambda_i^{2l} + l_{ij}^2 \lambda_i^{2l} / 2) - \lambda_k^{2l} \exp(-r_{ij} \lambda_k^{2l} + l_{ij}^2 \lambda_k^{2l} / 2)] / [(\lambda_i^{2l} - \lambda_k^{2l}) r_{ij}] \right\} \quad (29)$$

where the term in brackets becomes

$$-\sum_{\substack{l \\ (\lambda_i^l = \lambda_k^l)}} \frac{\gamma_i^{2l} \exp(-r_{ij} \lambda_i^{2l} + l_{ij}^2 \lambda_i^{2l} / 2)}{r_{ij}}$$

if $\lambda_i^l = \lambda_k^l$ and where the constants γ_i^l , λ_i^l for the first 36 neutral elements have been given by Strand and Tietz¹⁰ for the Hartree-Fock atomic fields. Values for γ_i^l and λ_i^l are also available for the Thomas-Fermi-Dirac field.¹¹ The magnitude of the contribu-

(6) C. Tavad, private communication.

(7) T. Iijima, *Bull. Chem. Soc. Japan*, **39**, 843 (1966).

(8) B. J. Laurenzi and D. D. Fitts, *J. Chem. Phys.*, **43**, 317 (1965).

(9) For an explanation of the terms used in eq 8 the reader may consult the article, R. A. Bonham and L. S. Bartell, *J. Chem. Phys.*, **31**, 702 (1959).

(10) T. G. Strand and T. Tietz, *Nuovo Cimento*, **B41**, 89 (1966).

(11) R. A. Bonham and T. G. Strand, *J. Chem. Phys.*, **39**, 2200 (1963).

tion from eq 29 is small compared to the experimentally dependent term⁷ and its calculation depends only on a knowledge of the molecular structural parameters (r_{ij} , l_{ij}) and the atomic fields (γ_i^t , λ_i^t).

It should be argued at this point that serious error may arise in the use of eq 27 if Hartree-Fock (HF) atomic wave functions are used in the calculation of the quantity $I_A^{\text{ED}}(s)$ because such wave functions neglect electron correlation. In addition the interpretation may be affected by errors in the simple Born theory of scattering. Iijima¹² has shown how the correlation problem can be solved for those cases where the atomic correlation energies are known. If HF wave functions are employed, it should be noted that since the virial theorem holds, the total HF energy is given by

$$E^{\text{HF}} = \frac{1}{2} \langle \Psi^{\text{HF}} | U | \Psi^{\text{HF}} \rangle = \frac{1}{2\pi} \int_0^\infty ds [s^4 I_A^{\text{ED}}(s) / I_0^{\text{ED}} - Z^2 - Z] \quad (30)$$

where $I_A^{\text{ED}}(s)$ is calculated with HF wave functions. The exact wave function, on the other hand, can be written as $\Psi_e = \Psi^{\text{HF}} + \Lambda$, where Λ is a correction term to include correlation. The exact total energy is then given as

$$E = \frac{1}{2} \langle \Psi^{\text{HF}} | U | \Psi^{\text{HF}} \rangle + R_p \langle \Psi^{\text{HF}} | U | \Lambda \rangle + \frac{1}{2} \langle \Lambda | U | \Lambda \rangle \quad (31)$$

where the first term is the HF energy and the last two terms must be the correlation energy. From these results it follows that HF atomic quantities may be employed in eq 27 if the sum of all the atomic correlation energies in the molecule is subtracted from the final result.

Besides the foregoing relations presented by other authors it is possible to obtain additional relations by utilizing a generalization of eq 11 as well as some other transformations. For brevity vibrational averages have been omitted. For instance since r_{12}^n may be written

$$r_{12}^n = \lim_{\alpha \rightarrow 0} r_{12}^n e^{-\alpha r_{12}} = \lim_{\alpha \rightarrow 0} \left(-\frac{d}{d\alpha} \right)^{n+1} \frac{1}{2\pi^2} \int \frac{ds e^{i\mathbf{s}\mathbf{r}_{12}}}{(s^2 + \alpha^2)} \quad (32)$$

the result for $\sigma_T^{\text{ED}}(s)$ is

$$\frac{2}{\pi} \left(-\frac{d}{d\alpha} \right)^{n+1} \int_0^\infty \frac{dss^2 \sigma_T^{\text{ED}}(s)}{(s^2 + \alpha^2)} = -2 \sum_{n=1}^N Z_n \int_0^\infty dr r^n e^{-\alpha r} D_n(r) + \int_0^\infty dr r^n e^{-\alpha r} P(r) \quad (33)$$

Unfortunately the limit as $\alpha \rightarrow 0$ does not exist so that it is not possible to obtain exact relations for the moments of r to the n th power by this means. On the other hand, for sufficiently small α the approximate moment relation

$$\frac{2}{\pi} \left(-\frac{d}{d\alpha} \right)^{k+1} \int_0^\infty \frac{dss^2 \sigma_T^{\text{ED}}(s)}{(s^2 + \alpha^2)} \cong -2 \sum_{n=1}^N Z_n \int_0^\infty dr \{ r^k - \alpha r^{k+1} \dots \} D_n(r) + \int_0^\infty dr \{ r^k - \alpha r^{k+1} \dots \} P(r) \quad (34)$$

can be derived. Various difference formulas can be developed which may also prove useful. For instance if the left-hand side of eq 34 is denoted by C_k , then it is possible to write moment relations such as

$$C_k + \alpha C_{k+1} = -2 \sum_{n=1}^N Z_n \int_0^\infty dr \left\{ r^k - \frac{\alpha^2}{2} r^{k+2} \dots \right\} \times D_n(r) + \int_0^\infty dr \left\{ r^k - \frac{\alpha^2}{2} r^{k+2} \dots \right\} P(r) \quad (35)$$

and finally

$$\sum_{l=0}^L \frac{\alpha^l}{l!} C_{k+l} = -2 \sum_{n=1}^N Z_n \int_0^\infty dr \times \left\{ r^k - \frac{\alpha^{L+1}}{(L+1)!} r^{k+L} \dots \right\} D_n(r) + \int_0^\infty dr \left\{ r^k - \frac{\alpha^{L+1}}{(L+1)!} r^{k+L} \dots \right\} P(r) \quad (36)$$

Similar relations for the other diffraction intensities can be derived in an identical manner. In addition to eq 32-36 the interesting relations

$$\langle \frac{1}{2} \pi^2 \rangle \int_0^\infty dss^2 \sigma_T^{\text{ED}}(s) = -2 \sum_{n=1}^N Z_n \rho(\mathbf{r}_n) + \rho_c(0) \quad (37)$$

$$\langle \frac{1}{2} \pi^2 \rangle \int_0^\infty dss^2 \sigma_e^{\text{ED}}(s) = -2 \sum_{n=1}^N Z_n \rho(\mathbf{r}_n) + \int d\mathbf{r} [\rho(\mathbf{r})]^2 \quad (38)$$

$$\langle \frac{1}{2} \pi^2 \rangle \int_0^\infty dss^2 \sigma_T^{\text{XR}}(s) = \rho_c(0) \quad (39)$$

and

$$\langle \frac{1}{2} \pi^2 \rangle \int_0^\infty dss^2 \sigma_e^{\text{XR}}(s) = \int d\mathbf{r} [\rho(\mathbf{r})]^2 \quad (40)$$

may be obtained by integrating eq 1-4 over $d\mathbf{s}$ directly and by making use of the properties of the Dirac

(12) T. Iijima, private communication.

δ function $\left(4\pi \int_0^\infty ds s^2 j_0(sr) = 8\pi^3 \delta(\mathbf{r})\right)$. These results are related to quantities used in nmr studies.¹³ Of course the individual $\rho(\mathbf{r}_n)$ are the quantities of greatest interest in nmr work, but the sum of the $\rho(\mathbf{r}_n)$ values can serve as a check on theoretically computed values of electron densities at the nuclei and can also be used to supplement other data in order to determine $\rho(\mathbf{r})$ from diffraction quantities.

Besides the Fourier transform relation of eq 26 the Laplace transform of the intensities can be used as

$$\int_0^\infty ds s^n = \lim_{\alpha \rightarrow 0} \int_0^\infty ds s^n e^{-\alpha s} = \lim_{\alpha \rightarrow 0} \left(-\frac{d}{d\alpha}\right)^n \int_0^\infty ds e^{-\alpha s} \quad (41)$$

to obtain

$$\int_0^\infty ds s^{k+2} e^{-\alpha s} \sigma_T^{\text{ED}}(s) = -2 \left(-\frac{d}{d\alpha}\right)^{k+1} \sum_{n=1}^N Z_n \times Z_n \int_0^\infty dr \frac{D_n(r)}{(r^2 + \alpha^2)} + \left(-\frac{d}{d\alpha}\right)^{k+1} \int_0^\infty \frac{dr P(r)}{(r^2 + \alpha^2)} \quad (42)$$

Similar relations for the other diffraction intensities can be developed in the same manner. Here it appears that the case where $k = -1$ is finite in the limit as $\alpha \rightarrow 0$ although the results for higher powers of $(1/r)$ are probably singular in the limit. The result for $k = -1$ can be written as

$$\int_0^\infty ds s \sigma_T^{\text{ED}}(s) = -2 \sum_{n=1}^N Z_n \int_0^\infty \frac{dr D_n(r)}{r^2} + \int_0^\infty dr \frac{P(r)}{r^2} \quad (43)$$

As in the case of eq 33-36 it is possible to expand the exponential on the left of eq 42 with the result

$$\int_0^\infty ds \left\{ s^{k+2} - \alpha^{L+1} \frac{s^{k+L+3}}{(L+1)!} \dots \right\} \sigma_T^{\text{ED}}(s) = -2 \sum_{n=1}^N Z_n \sum_{l=1}^L C_{k+l} \frac{\alpha^l}{l!} + \sum_{l=1}^L D_{k+l} \frac{\alpha^l}{l!} \quad (44)$$

where

$$C_{k+l} = \left(-\frac{d}{d\alpha}\right)^{k+l+1} \int_0^\infty \frac{dr D_n(r)}{(r^2 + \alpha^2)} \quad (45)$$

and

$$D_{k+l} = \left(-\frac{d}{d\alpha}\right)^{k+l+1} \int_0^\infty \frac{dr P(r)}{(r^2 + \alpha^2)}$$

Additional moments may be obtained by expanding

$\sin(sr)/sr$ in eq 1-4 and by determining the expansion coefficients by least-squares analysis of the small-angle scattering data. For the total electron scattering this expansion leads to

$$\sigma_T^{\text{ED}}(s) = \left[-\left(\sum_{i=1}^N Z_i\right) \left(\sum_{i=1}^N Z_i + 1\right) - \frac{s^2}{6} \left\{ -2 \sum_{i=1}^N Z_i \int_0^\infty dr D_i(r) r^2 + \int_0^\infty dr P(r) r^2 \right\} + \frac{s^4}{120} \left\{ -2 \sum_{i=1}^N Z_i \int_0^\infty dr D_i(r) r^4 + \int_0^\infty dr P(r) r^4 \right\} \dots \right] \quad (46)$$

from which it should be possible to obtain estimates of the sums of the lower order expectation values. At this point it appears that the only useful expectation values of a power of r which is missing in the present analysis is $\langle 1/r^3 \rangle$ which is related to the nuclear paramagnetic shielding constant used in nmr work.

Finally it is of interest to investigate the possibility of obtaining information about molecular electron densities in a different fashion than the one given by Tavard, Rouault, and Roux.^{2b} To do this it is convenient to expand the three-dimensional electron density $\rho(\mathbf{r})$ and the three-dimensional electron-electron density $\rho_c(\mathbf{r})$ as

$$\rho(\mathbf{r}) = \sum_{n=0}^\infty \sum_{l=-n}^n \rho_n(r) Y_n^l(\theta, \varphi) \quad (47)$$

and

$$\rho_c(\mathbf{r}) = \sum_{n=0}^\infty \sum_{l=-n}^n \rho_n^c(r) Y_n^l(\theta, \varphi) \quad (48)$$

where the $Y_n^l(\theta, \varphi)$ are the unnormalized spherical harmonics $P_n^l(\cos \theta) \cos l\varphi$.

The modified diffraction intensities can then be written as

$$\sigma_T^{\text{ED}}(s) = \sum_{n=0}^\infty D_n(s) B_n(s) + C_0(s) \quad (49)$$

$$\sigma_e^{\text{ED}}(s) = \sum_{n=0}^\infty D_n(s) B_n(s) + \frac{1}{2\pi} \sum_{n=0}^\infty B_n^2(s) \quad (50)$$

$$\sigma_T^{\text{XR}}(s) = C_0(s) \quad (51)$$

and

$$\sigma_e^{\text{XR}}(s) = \frac{1}{2\pi} \sum_{n=0}^\infty B_n^2(s) \quad (52)$$

where

$$D_n(s) = -2 \left[Z_1 \delta_{n0} + \sum_{i=2}^N Z_i j_n(sr_{1i}) \sum_{l=-n}^n Y_n^l(\theta_{1i}, \varphi_{1i}) \right] \quad (53)$$

(13) C. J. Jameson and H. S. Gutowsky, *J. Chem. Phys.*, **40**, 1714 (1964).

$$B_n(s) = 4\pi \int_0^\infty dr r^2 \rho_n(r) j_n(sr) \quad (54)$$

and

$$C_l(s) = 4\pi \int_0^\infty dr r^2 \rho_0^c(r) j_0(sr) \quad (55)$$

A procedure can now be set up to obtain the radial coefficients $\rho_n(r)$ directly from the intensities $\sigma_T^{\text{ED}}(s)$ or $\sigma_e^{\text{ED}}(s)$. It is important to note at this point that in principle an approximate three-dimensional electron density can be determined from diffraction data for polyatomic molecules. The density is approximate because the terms $D_n(s)B_n(s)$ are coupled by the vibrational average since the density quantities are functions of the nuclear positional coordinates. However these densities can be expanded in terms of normal coordinates about the equilibrium structure as

$$\rho(\mathbf{r}, \mathbf{Q}_i) = \rho(\mathbf{r}, \mathbf{Q}_i^e) + \sum_i X_i \partial \rho(\mathbf{r}, \mathbf{Q}_i) / \partial Q_i |_{Q_i = Q_i^e} \dots \quad (56)$$

The vibrational averages can then be carried out and the previous equations can be modified to include correction terms depending on the slope and curvature of the electron density at the equilibrium nuclear positions. Even without this correction the uncertainty in the determination of the electron density should not be serious in the case of small molecules where bond distances are short and amplitudes of vibration are reasonably small.

By use of the well-known Fourier-Bessel integral the density coefficients can be determined directly from the total scattered electron-diffraction intensity as

$$\begin{aligned} \rho_n(r) = & \frac{1}{2\pi^2} \int_0^\infty ds s^2 j_n(sr) \frac{\sigma_T^{\text{ED}}(s)}{D_n(s)} - \\ & \frac{1}{2\pi^2} \sum_{k \neq n=0}^\infty \int_0^\infty ds s^2 j_n(sr) \frac{D_k(s)B_k(s)}{D_n(s)} - \\ & \frac{1}{2\pi^2} \int_0^\infty ds s^2 j_n(sr) \frac{C_0(s)}{D_n(s)} \quad (57) \end{aligned}$$

and

$$\begin{aligned} \rho_0^e(r) = & \frac{1}{2\pi^2} \int_0^\infty ds s^2 j_0(sr) \sigma_T^{\text{ED}}(s) - \\ & \sum_{n=0}^\infty \frac{1}{2\pi^2} \int_0^\infty ds s^2 j_0(sr) D_n(s) B_n(s) \quad (58) \end{aligned}$$

Of course the quantities on the far right of eq 57 and 58 both depend on the unknown densities, so these terms must be evaluated using an initial guess as to the molecular density. The results obtained for $\rho_n(r)$,

$\rho_0^c(r)$ on the left of eq 57 and 58 must then be reiterated to self-consistency. In addition, the numerous expectation values discussed previously may be utilized as constraints along with the usual conservation of probability density utilized by Tavard and co-workers,^{2b} that is

$$\int d\mathbf{r} \rho(\mathbf{r}) = 4\pi \int_0^\infty dr r^2 \rho_0(r) = \sum_{i=1}^N Z_i = M \quad (59)$$

and

$$\int d\mathbf{r} \rho_c(\mathbf{r}) = 4\pi \int_0^\infty dr r^2 \rho_0^c(r) = M(M-1) \quad (60)$$

Of course the utility of the above scheme will depend on the availability of accurate intensity data and a set of initial guesses for the $\rho_n(r)$ and $\rho_0^c(r)$ that are sufficiently close to the final result to ensure convergence of the iterative procedure.

It is difficult to judge at this early state of development of the experimental method whether or not sufficiently accurate data can be obtained. Nonetheless the foregoing points out the important fundamental difference between X-ray diffraction where three-dimensional molecular charge density information is largely lost and the electron case where in principle the information is present. It is of interest to note that preliminary work on H_2 and CH_4 has yielded binding energies which are within 15% of the thermochemical value.^{7,14} It is hoped that presently available experimental refinements coupled with a better understanding of scattering theory will yield sufficiently accurate data to make the above outlined approach feasible. As to the problem of an accurate initial guess a possible solution might be to use a density based on a superposition of spherical atom densities for the $\rho_n(r)$ terms. For the $\rho_0^c(r)$ term a first approximation might be to let $\rho_0^c(r)$ be given by $(M-1) \cdot \rho_0^0(r)$, where $\rho_0^0(r)$ is the zero-order approximation for $\rho_0(r)$. The $\rho_n(r)$ can be approximated by taking a superposition of spherical atoms in the proper molecular geometry and then expanding the resultant molecular density in spherical harmonics. For the Hartree-Fock¹¹ or Thomas-Fermi-Dirac¹² atomic densities, the general radial component $\rho_n(r)$ can be written as eq 61 where K is the number of terms in the potential field expansion, γ_i^k and λ_i^k are electron density parameters for the atomic field of the k th atom, and θ_{1k} and φ_{1k} are orientation angles of the vector \mathbf{r}_{1k} to the Z axis \mathbf{r}_{12} . Equation 57 thus provides a convenient estimate with which to start the calculation of the molecular electron density.

(14) T. Iijima, R. A. Bonham, C. Tavard, M. Roux, and M. Cornille, *Bull. Chem. Soc. Japan*, **38**, 1758 (1965).

$$\begin{aligned}
 \rho_n(r) = & \frac{Z_1}{4\pi} \sum_{i=1}^K \gamma_i^1 \lambda_i^1 \frac{e^{-\lambda_i^1 r}}{r} \delta_{n0} + \\
 & \frac{Z_2}{4\pi} \sum_{i=1}^K \gamma_i^2 \lambda_i^2 \left\{ \begin{array}{l} j_n(i\lambda_i^2 r_{12}) h_n(i\lambda_i^2 r) \\ (r_{12} < r) \\ j_n(i\lambda_i^2 r) h_n(i\lambda_i^2 r_{12}) \\ (r_{12} > r) \end{array} \right\} + \\
 & \sum_{k=3}^N \frac{Z_k}{4\pi} \sum_{i=1}^K \gamma_i^k \lambda_i^k \left\{ \begin{array}{l} j_n(i\lambda_i^k r_{1k}) h_n(i\lambda_i^k r) \\ (r_{1k} < r) \\ j_n(i\lambda_i^k r) h_n(i\lambda_i^k r_{1k}) \\ (r_{1k} > r) \end{array} \right\} \sum_{l=-n}^n Y_n^l(\theta_{1k}, \varphi_{1k})
 \end{aligned}
 \tag{61}$$

Finally, it should be emphasized that the ease in obtaining the various experimental intensity values as well as the accuracy with which they may be obtained may possibly be in the order $\sigma_T^{\text{ED}}(s) > \sigma_e^{\text{ED}}(s) > \sigma_T^{\text{XR}}(s) > \sigma_e^{\text{XR}}(s)$. Unfortunately, X-ray work of the type referred to here does not appear to be currently in vogue and it is difficult to determine what improvements might be made in X-ray techniques because of modern technological advances. At any rate it appears that because of the wealth of interesting information obtainable from such data that work in this area might fruitfully be reinstigated.

Acknowledgment. The author wishes to thank Professor Otto Bastiansen for his kind hospitality, Drs. Tavard, Iijima, and Strand for results in advance of publication, and Professor L. S. Bartell for his helpful comments and suggestions.

The Radiolysis of Thiophenol and Its Mixtures with Benzene and Benzene- d_6

by Gulbrand Lunde and Robert R. Hentz

Department of Chemistry and the Radiation Laboratory,¹ University of Notre Dame, Notre Dame, Indiana 46556
(Received August 10, 1966)

G values obtained in γ irradiation of liquid thiophenol at room temperature are as follows: H_2 , 4.2 ± 0.1 ; $(C_6H_5S)_2$, 4.6 ± 0.1 ; C_6H_6 , 1.4 ± 0.1 ; H_2S , 0.44 ± 0.03 ; and $(C_6H_5)_2S$, 0.049 ± 0.004 . Cleavages of C_6H_5S-H and C_6H_5-SH bonds are suggested as the major modes of decomposition with some contribution from a process that yields molecular hydrogen. Abstraction from the C_6H_5S-H bond to form H_2 is considered the almost exclusive fate of H in pure thiophenol. Like the large $G(H_2)$ in pure thiophenol, the $G(H_2)$ results obtained in γ irradiation of benzene-thiophenol mixtures are a novelty in the radiation chemistry of aromatic systems; these $G(H_2)$ values lie appreciably above the law-of-averages line in a conventional electron-fraction plot. Results on $C_6H_5SH-C_6D_6$ mixtures indicate a sensitization of thiophenol decomposition by energy transfer from benzene; such transfer appears essentially complete at $\sim 0.2 M$ thiophenol. The behavior of H_2 and HD yields at higher concentrations of thiophenol is determined by the competition between (1) abstraction from thiophenol by hydrogen atoms to give hydrogen and (2) addition of hydrogen atoms to the benzene ring. The data on HD yields give $k_1/k_2 = 22 \pm 1$ and a lower limit for the yield of D atoms from pure C_6D_6 of $G_D^\circ = 0.085$.

Introduction

A characteristic feature of the radiolysis of liquid aromatics is the small $G(H_2)$ obtained.² For ^{60}Co γ - and high-energy (~ 1 Mev) electron irradiation of liquid benzene, Cherniak, *et al.*,³ give $G(H_2) = 0.039 \pm 0.003$ as the most probable yield. Such a value is ~ 100 -fold smaller than values characteristic of saturated hydrocarbons.⁴ Reactivity of the benzene ring with H atoms has been recognized for some time.⁵ Patrick and Burton attempted to assess the role of such reactivity in the "protective" effect observed in radiolysis of benzene-cyclohexane mixtures⁶ by study of the radiolysis of mixtures of benzene- d_6 with propionaldehyde⁷ and with cyclohexane.⁸ However, these authors did not consider that the small $G(H_2)$ in radiolysis of liquid benzene might be a consequence of such reactivity, rather than being indicative of a small primary yield of H atoms and H_2 . Burr and co-workers⁹ have emphasized that $G(H)$ in radiolysis of liquid aromatics may be appreciable but that H atoms make little or no contribution to $G(H_2)$ owing to the efficiency with which they are scavenged by the benzene ring. Thus, Burr¹⁰ argues that 0.35% of $H + C_6H_6$ reactions are abstractive (the remainder being addi-

tive);¹¹ assuming $G(H) = 0.4$ from benzene, one-half the radical yield, Burr estimates $G(H_2) = 0.0014$ as the contribution of H atoms to the total $G(H_2) = 0.039$.

(1) The Radiation Laboratory of the University of Notre Dame is operated under contract with the U. S. Atomic Energy Commission. This is AEC Document No. COO-38-502.

(2) R. R. Hentz and M. Burton, *J. Am. Chem. Soc.*, **73**, 532 (1951); T. J. Sworski, R. R. Hentz, and M. Burton, *ibid.*, **73**, 1998 (1951); S. Gordon and M. Burton, *Discussions Faraday Soc.*, **12**, 88 (1952).

(3) E. A. Cherniak, E. Collinson, and F. S. Dainton, *Trans. Faraday Soc.*, **60**, 1408 (1964).

(4) See, *e.g.*, T. J. Hardwick, *J. Phys. Chem.*, **65**, 101 (1961).

(5) K. G. Geib and P. Harteck, *Chem. Ber.*, **66**, 1815 (1933); G. S. Forbes and J. E. Cline, *J. Am. Chem. Soc.*, **63**, 1713 (1941); H. W. Melville and J. C. Robb, *Proc. Roy. Soc. (London)*, **A202**, 181 (1950); P. E. M. Allen, H. W. Melville, and J. C. Robb, *ibid.*, **A218**, 311 (1953).

(6) J. P. Manion and M. Burton, *J. Phys. Chem.*, **56**, 560 (1952).

(7) W. N. Patrick and M. Burton, *ibid.*, **58**, 424 (1954).

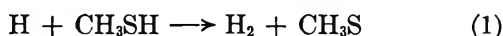
(8) M. Burton and W. N. Patrick, *ibid.*, **58**, 421 (1954).

(9) J. G. Burr, J. M. Scarborough, J. D. Strong, R. I. Akawie, and R. A. Meyer, *Nucl. Sci. Eng.*, **11**, 218 (1961); J. G. Burr, *Nucleonics*, **19**, No. 10, 49 (1961).

(10) J. G. Burr and J. M. Scarborough, *J. Phys. Chem.*, **64**, 1367 (1960).

(11) The argument is based on measurement of $G(HD)$ in radiolysis of aqueous solutions of C_6D_6 reported by P. V. Phung and M. Burton, *Radiation Res.*, **7**, 199 (1957).

Assessment of the yield of thermal H in radiolysis of liquid benzene requires an additive that can compete effectively for H atoms to give an easily measured product, preferably hydrogen. Thiophenol seems ideally suited for such a purpose. In one molecule are present both the benzene ring and the very labile S-H bond. The dissociation energy of this bond in thiophenol is obtained from the data of Mackle¹² as 76 kcal mole⁻¹. Free-radical abstraction reactions at the S-H bond of mercaptans appear to occur with negligible activation energy.^{13,14} Greig and Thynne¹⁵ have pointed out that CH₃SH and H₂S are among the most reactive molecules studied for H atom abstraction by alkyl radicals. This high reactivity is noted to be a consequence of the low activation energy (2.6–4.7 kcal mole⁻¹), which can only partly be explained by the relative weakness of the S-H bond. The strongest argument for the efficacy of mercaptans as H donors derives from the work of Inaba and Darwent,¹⁶ who found $E_1-E_2 = 0.42-0.67$ kcal mole⁻¹ for reactions 1 and 2. Such a value may be compared with $E_3-E_2 = 0.9$ kcal mole⁻¹ reported by Yang.^{17,18}



The evidence cited, particularly considering the 12 kcal mole⁻¹ smaller dissociation energy of C₆H₅S-H relative to CH₃S-H,¹² suggests that thiophenol can compete readily with benzene for H atoms *via* the analog of reaction 1.

The radiolysis of thiophenol first was studied (no such previous study appears to have been published), which provided a basis for the study of mixtures with C₆H₆ and C₆D₆. The radiolysis of thiophenol in benzene¹⁹ has been reported; however, only $G(-\text{C}_6\text{H}_5\text{-SH})$ and $G(\text{H}_2\text{S})$ were measured and conversions of thiophenol were so great as to preclude reliable mechanistic conclusions.

Experimental Section

Materials. Fisher (crystallizable) benzene was purified by three successive crystallizations with rejection of about one-fourth of the benzene at each freezing. No impurities were detectable by vapor phase chromatography (glpc).²⁰ Benzene-*d*₆ obtained from Merck Sharp and Dohme (99.5% deuterated) was used without purification. A mass spectrometric analysis of hydrogen formed from radiolysis of the C₆D₆ showed 2.3% H (all as HD).

Thiophenol (Eastman grade) was obtained from Eastman Organic Chemicals and stored over Drierite

prior to purification. Because benzene and phenyl disulfide are products of the radiolysis, it was necessary to minimize their concentration in the thiophenol. A vacuum-line distillation procedure utilizing two cold traps proved effective for reduction of benzene content. Thiophenol first was deaerated by the conventional freeze-pump-thaw technique in a bulb on the vacuum line. The bulb with thiophenol at room temperature then was opened through two traps to the vacuum system. Dry Ice in acetone was placed on the first trap and liquid nitrogen on the second. By proper adjustment of the level of Dry Ice-acetone on the first trap, it was possible to transfer 10–20% of the thiophenol through this trap into the liquid nitrogen trap. By such a procedure the benzene content was reduced to ~0.002 mole % in the thiophenol retained by the first trap. It was found that phenyl disulfide could be removed by a single distillation of thiophenol on the vacuum line from a bulb at room temperature into a trap at 77°K. Usually two such distillations were performed, and the thiophenol was stored on the vacuum line. Just prior to use, because some disulfide may form on storage, another such bulb-to-bulb distillation was carried out.

Phenyl disulfide from Eastman Organic Chemicals was recrystallized twice in 95% ethyl alcohol and washed with triply distilled water. No impurities were detectable by glpc in benzene solutions of the purified disulfide.²⁰ The following chemicals were used as additives or standards without purification: biphenyl (Matheson), biphenyl-*d*₁₀ (Merck Sharp and Dohme), and phenyl sulfide (Eastman).

Procedures. Samples (2 ml) were deaerated on the vacuum line by repeated cycles of freeze (77°K)-pump-thaw and then were sealed. Irradiations were

(12) H. Mackle, *Tetrahedron*, **19**, 1159 (1963).

(13) C. Walling and R. Rabinowitz, *J. Am. Chem. Soc.*, **81**, 1137 (1959); C. Walling, "Free Radicals in Solution," John Wiley and Sons, Inc., New York, N. Y., 1957, pp 322–326.

(14) S. G. Cohen, D. A. Laufer, and W. V. Sherman, *J. Am. Chem. Soc.*, **86**, 3060 (1964); references are given to earlier papers in the series.

(15) G. Greig and J. C. J. Thynne, *Trans. Faraday Soc.*, **62**, 379 (1966).

(16) T. Inaba and B. de B. Darwent, *J. Phys. Chem.*, **64**, 1431 (1960).

(17) K. Yang, *J. Am. Chem. Soc.*, **84**, 3795 (1962).

(18) Normal A factors (*i.e.*, comparable with those for H abstraction from hydrocarbons by alkyl radicals) are quoted in ref 15 for CH₃ + CD₃SH (or H₂S) → CH₄ + CD₃S (or HS). Consequently, the A factors for reactions 1, 2, and 3 should be comparable.

(19) W. Ando, K. Sugimoto, and S. Oae, *Bull. Chem. Soc. Japan*, **36**, 893 (1963).

(20) Analyses were performed on an F and M Model 810 gas chromatograph with a flame-ionization detector and a 0.25-in. × 4-ft column of silicone grease (10 wt % liquid phase) on 60–80 mesh Chromosorb P.

performed in the Notre Dame 10-ke ^{60}Co facility at a dose rate to the Fricke dosimeter solution, based on $G(\text{Fe}^{3+}) = 15.6$, of 1.61×10^{18} $\text{ev ml}^{-1} \text{min}^{-1}$. Dose to a particular solution was determined by correction for the electron density of the solution relative to that of the dosimeter. All irradiations were carried out at room temperature.

After irradiation, the sample was attached to the vacuum line. An automatic Toepler pump transferred hydrogen from the sample at 77°K , through two traps at 77°K , and into a gas buret. This procedure was repeated after each cycle of thaw and freeze of the sample until hydrogen removal was complete. The same procedure was used for H_2S removal except that the sample and both traps were maintained at -118° (ethyl bromide mush) during transfer to the gas buret. Measurement of H_2S in the gas buret proved erratic owing, apparently, to the presence of other substances in the H_2S fraction. Therefore, H_2S in this fraction was measured mass spectrometrically by comparison of the H_2S peak height from the sample with that obtained from a standard quantity of pure H_2S .

Products other than H_2 and H_2S were determined by glpc.²⁰ With all columns and under all conditions tried for analysis of phenyl disulfide, partial decomposition of the solvent thiophenol resulted in a broad peak that extended into the region of the phenyl disulfide peak. Therefore, after gas product removal, thiophenol was distilled from the reaction cell into a liquid nitrogen trap. Quantitative retention in the cell of both phenyl disulfide and sulfide was achieved. The residue was dissolved in benzene for determination of the sulfide and disulfide. Benzene, because of a shorter retention time than thiophenol, could be determined directly in the irradiated solutions. In mixtures of benzene and <5 vol % thiophenol, it was possible to analyze the irradiated solutions directly for all products other than H_2 and H_2S . At higher thiophenol concentrations, the preliminary separation of sulfide and disulfide was necessary. Analysis for biphenyl and dihydrobiphenyls was always performed on the irradiated solutions. Biphenyl was used as the standard for determination of dihydrobiphenyls. In the radiolysis of $\text{C}_6\text{H}_5\text{SH}-\text{C}_6\text{D}_6$ mixtures, D_2 and HD were determined by mass spectrometric analysis of the hydrogen fraction. A Consolidated 21-103A mass spectrometer was used for all gas analyses.

A test was made for exchange in $\text{C}_6\text{H}_5\text{SH}-\text{C}_6\text{D}_6$ mixtures by separation of the thiophenol after a period that was long compared with that of an experiment. No HD or D_2 was detectable in hydrogen generated from the thiophenol by reaction with sodium. The same

procedure indicated no incorporation of D into thiophenol during radiolysis.

Results

Thiophenol. The following G values (100-ev yields) were obtained in radiolysis of pure thiophenol: $G(\text{H}_2) = 4.2 \pm 0.1$, $G(\text{C}_6\text{H}_5\text{SSC}_6\text{H}_5) = 4.6 \pm 0.1$, $G(\text{C}_6\text{H}_6) = 1.4 \pm 0.1$, $G(\text{H}_2\text{S}) = 0.44 \pm 0.03$, and $G(\text{C}_6\text{H}_5\text{SC}_6\text{H}_5) = 0.049 \pm 0.004$. These values were constant for doses up to 4×10^{20} ev ml^{-1} , the maximum dose used. The material balance is fair; e.g., in the products, $G(\text{C}_6\text{H}_5) = 10.7$, $G(\text{H}) = 10.7$, and $G(\text{S}) = 9.7$. It is particularly noteworthy that there is a deficiency of S, not H. Some possible sources of such a deficiency appear in the relationships I and II. Equa-

$$2G(\text{H}_2) + G(\text{H}_2\text{S}) + G(\text{C}_6\text{H}_6) - 2G(\text{Ph}_2\text{S}_2) - G(\text{Ph}_2\text{S}) = 1.0 \quad (\text{I})$$

$$G(\text{C}_6\text{H}_6) + G(\text{Ph}_2\text{S}) - G(\text{H}_2\text{S}) = 1.0 \quad (\text{II})$$

tion I represents a deficiency of $\text{C}_6\text{H}_5\text{S}$ relative to H for cleavage at the $\text{C}_6\text{H}_5\text{S}-\text{H}$ bond, and eq II represents a deficiency of SH relative to C_6H_5 for cleavage at the $\text{C}_6\text{H}_5-\text{SH}$ bond. Extraction of H_2S from the irradiated solutions may not have been quantitative; consequently, $G(\text{H}_2\text{S})$ could represent a lower limit, which would account for part of the sulfur deficiency. However, a larger yield of H_2S would enhance the deficiency of $\text{C}_6\text{H}_5\text{S}$ relative to H, represented by eq I, and also would introduce a deficiency between $G(\text{H})$ and $G(\text{C}_6\text{H}_5)$.

Irradiation of thiophenol produces a yellow color that is considerably more intense than that produced by an equivalent dose in benzene. The same yellow color could be produced by heat or exposure to ultraviolet light. The colored product remains behind with the sulfide and disulfide when thiophenol is removed by distillation into a trap at 77°K . Takebayashi, *et al.*,²¹ have reported formation of a resinous substance in ultraviolet photolysis of thiophenol. Their resinous substance appeared to be a polymer derived from thiophenol that decomposed at $160-190^\circ$ to give thiophenol and the disulfide. Cohen²² reports formation of a thiophenol polymer in inhibition by thiophenol and the disulfide of the photoinduced pinacol reaction. A thiophenol polymer also has been reported as the product of $\text{C}_6\text{H}_5\text{S}$ addition to the benzene ring.²³ Consequently, the yellow product

(21) M. Takebayashi, T. Shingaki, and T. Mitsuyama, *Sci. Rept.*, **10**, 35 (1961).

(22) S. G. Cohen, S. Orman, and D. A. Laufer, *J. Am. Chem. Soc.*, **84**, 3905 (1962).

(23) Y. Schaafsma, A. F. Bickel, and E. C. Kooyman, *Tetrahedron*, **10**, 76 (1960).

formed in radiolysis may be a result of some C_6H_5S addition to the benzene ring, which could account for part of the S deficiency; however, such a reaction must be of minor importance relative to dimerization of C_6H_5S . Occurrence of reaction 4 in a spur or cage²⁴



could provide a perfect balance to the material accounting. Information on the nature and composition of the "polymer" would be of value.

It is important to note that radiolysis of thiophenol resembles that of saturated hydrocarbons rather than that of aromatics, both in the large $G(H_2)$ ⁴ and the large $G(-C_6H_5SH) \approx 11$,²⁵ based on $G(C_6H_5)$ in the products. We are not aware of any report of similar behavior for an aromatic liquid.

Thiophenol-Benzene Mixtures. In Figure 1, a conventional electron-fraction plot is presented of yields of the major products, phenyl disulfide and hydrogen, in radiolysis of thiophenol-benzene mixtures. A similar plot of yields of minor products is given in Figure 2. The straight lines joining end points of the curves represent yields expected for partition of deposited energy between components on the basis of their respective electron fractions. Such an assumption, of course, should not be accepted uncritically.²⁶ The G values shown in Figures 1 and 2 represent initial yields. They were constant for doses $\leq 4 \times 10^{20}$ $ev\ ml^{-1}$ at $\epsilon(C_6H_5SH) \geq 0.03$ (0.24 M). At lower concentrations of thiophenol, G values were constant for doses less than $0.5-1 \times 10^{20}$ $ev\ ml^{-1}$.

Like the value of $G(H_2)$ for pure thiophenol, the curve for $G(H_2)$ in Figure 1 is a novelty in the radiation chemistry of aromatic systems; it is the first case of which we are aware in which $G(H_2)$ of a mixture containing benzene lies appreciably above the law-of-averages line in a conventional electron-fraction plot. Such behavior could be a result of either (1) a benzene-sensitized decomposition of thiophenol or (2) the conversion of H atoms generated from radiolysis of benzene into H_2 by abstraction from thiophenol. To distinguish between these alternatives, $C_6H_5SH-C_6D_6$ mixtures were studied with the results shown in Figure 3. The conversion of D atoms into HD, although occurrent, makes a minor contribution to the enhancement of hydrogen yields; *e.g.*, $G(HD)$ represents $\sim 4\%$ of the enhanced hydrogen yield at both $\epsilon(C_6H_5SH) = 0.012$ and 0.12. Obviously, a benzene-sensitized decomposition of thiophenol is involved. The value $G(D_2) = 0.0136$ for pure C_6D_6 is in accord with that of Dyne and Jenkinson.²⁷ The effect of added biphenyl on product yields in radiolysis of $C_6H_5SH-C_6D_6$ mixtures is shown in Table I.

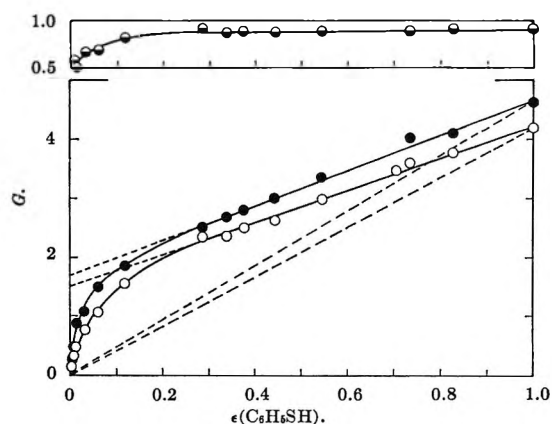


Figure 1. Yields of hydrogen and phenyl disulfide in γ irradiation of $C_6H_6-C_6H_5SH$ mixtures: \circ , $G(H_2)$; \bullet , $G(C_6H_5SSC_6H_5)$; \ominus , $G(H_2)/G(C_6H_5SSC_6H_5)$.

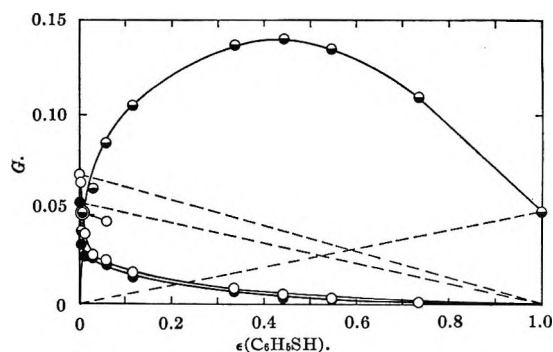


Figure 2. Yields of minor products in γ irradiation of $C_6H_6-C_6H_5SH$ mixtures: \circ , $G(C_6H_5C_6H_5)$; \bullet , $G(C_6H_5C_6H_7)$; \ominus , $G(C_6H_5SC_6H_5)$.

Table I: The Effect of Added Biphenyl on Product Yields in Radiolysis of a Solution of 1.5 M C_6H_5SH in C_6D_6 ^a

[[C_6H_5]] ₂ , M	G				
	$(C_6H_5)_2S$	$(C_6H_5)_2$	H_2	D_2	HD
0	0.111	2.25	1.83	0.0058	0.053
0.12	0.109	1.90	1.41	0.0055	0.050
0.33	0.113	1.36	1.09	0.0052	0.045
0.50	0.113	1.26	0.89	0.0052	0.044

^a $\epsilon(C_6H_5SH) = 0.175$.

(24) G. R. Seely, *J. Am. Chem. Soc.*, **84**, 4404 (1962), obtained a quantum yield of 0.13 for photodissociation of $C_6H_5SSC_6H_5$ in toluene. Such a low value was shown to be in accord with a diffusion-model calculation of the probability of escape from geminate recombination, based on a primary $\phi = 1$.

(25) Compare with $G(-c-C_6H_{12}) = 7-8$, calculated from the results of S. K. Ho and G. R. Freeman, *J. Phys. Chem.*, **68**, 2189 (1964).

(26) *Cf.*, R. R. Hentz, D. B. Peterson, S. B. Srivastava, H. F. Barzynski, and M. Burton, *ibid.*, **70**, 2362 (1966); and H. F. Barzynski, R. R. Hentz, and M. Burton, *ibid.*, **69**, 2034 (1965). Particularly, note ref 7 of the latter paper.

(27) P. J. Dyne and W. M. Jenkinson, *Can. J. Chem.*, **40**, 1746 (1962).

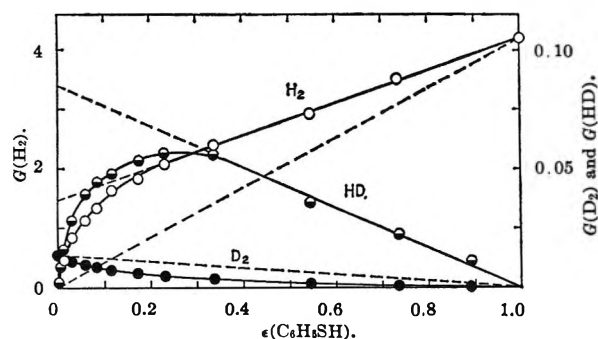
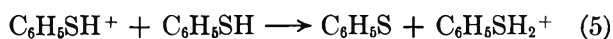


Figure 3. Hydrogen yields in γ irradiation of C_6D_6 - C_6H_6SH mixtures.

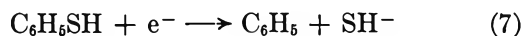
Discussion

Thiophenol. Delineation of a definitive mechanism for radiolysis of thiophenol is not possible from the results of this study with presently available supplementary information; however, such information does place certain limitations on mechanism and thereby permits some reasonable conclusions with regard to general features of the mechanism.

Exothermicity of reaction 5 requires that thiophenol have a proton affinity > 198 kcal mole $^{-1}$. Such a large



value does not seem reasonable;²⁸ therefore, appreciable product formation by neutralization of $C_6H_5SH_2^+$ is considered improbable. Reactions 6 and 7 for exothermicity require an electron affinity of

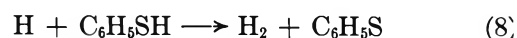


> 3.3 eV for C_6H_5S and SH ; again, such a value seems unreasonably large. Values of 1.6²⁹ and 2.6 eV³⁰ have been given for the electron affinity of SH . Consequently, it is tentatively concluded that reactions 6 and 7 do not play a role in the radiolysis of thiophenol in nonpolar solvents, although electron capture to form the anion $C_6H_5SH^-$ may.

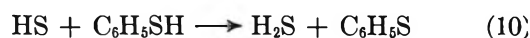
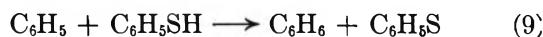
Decomposition of the lowest excited triplet state of thiophenol also would appear unlikely. Such a triplet should lie below that of benzene for which the lowest triplet energy³¹ is 84 kcal mole $^{-1}$. The weakest bond in thiophenol,¹² the C_6H_5S-H bond, has a dissociation energy of 76 kcal mole $^{-1}$ and that of C_6H_5-SH is 78 kcal mole $^{-1}$. At the very least, an unreasonably efficient conversion of triplet excitation energy into dissociation energy of a particular bond would be required. Thiophenol apparently does decompose from its lowest excited singlet state. Thus, Haines, *et al.*,³² report H_2 and H_2S in a ratio of 99:1 as the only

gas products in photolysis of liquid thiophenol. Takebayashi, *et al.*,²¹ also report decomposition of the liquid at 2537 Å and find H_2S , $(C_6H_5S)_2$, and a polymer among the products (H_2 was not sought). In exploratory experiments, we have confirmed such decomposition and find H_2 and $(C_6H_5S)_2$ as principal products (H_2S was not measured). Unfortunately, quantum yields have not been reported; careful study of thiophenol photolysis has yet to be done. Nevertheless, some cleavage of the C_6H_5S-H bond is evidently ensuant on formation of the lowest excited singlet state with subsequent abstraction from thiophenol by the H atoms produced.

We conclude that thiophenol decomposition in radiolysis of the liquid is predominantly a consequence of neutralization of the parent ion with an additional contribution from states (other than the lowest triplet) produced by excitation alone. For reasons discussed in the following section on benzene-thiophenol mixtures, cleavages of the C_6H_5S-H and C_6H_5-SH bonds are suggested as the major modes of decomposition with some contribution from a process that yields molecular hydrogen. In accordance with arguments presented in the Introduction, reaction 8 is considered



to be almost the exclusive fate of H, while C_6H_5 and HS may disappear by reaction 4 as well as reactions 9 and 10. Some small loss of C_6H_5S by addition to



the benzene ring is assumed, as discussed in the section on Results.

Thiophenol-Benzene Mixtures. The longest wavelength absorption band of thiophenol, at 2875 Å,³² corresponds to an energy of 100 kcal mole $^{-1}$; corresponding values for benzene³¹ are 2500 Å and 115 kcal mole $^{-1}$. The photoionization potentials of thiophenol and benzene are 8.33 and 9.24 eV, respectively.³⁴ Thus, sensitization of thiophenol decomposition by

(28) Compare with values given for various substances by F. W. Lampe and F. H. Field, *Tetrahedron*, **7**, 189 (1959).

(29) O. Rosenbaum and H. Neuert, *Z. Naturforsch.*, **A9**, 990 (1954).

(30) H. O. Pritchard, *Chem. Rev.*, **52**, 529 (1953).

(31) N. J. Turro, *J. Chem. Educ.*, **43**, 13 (1966).

(32) W. E. Haines, G. L. Cook, and J. S. Ball, *J. Am. Chem. Soc.* **78**, 5213 (1956).

(33) J. C. Morris, W. J. Lanum, R. V. Helm, W. E. Haines, G. L. Cook, and J. S. Ball, *J. Chem. Eng. Data*, **5**, 112 (1960).

(34) K. Watanabe, T. Nakayama, and J. Mottl, "Final Report on Ionization Potential of Molecules by a Photoionization Method," Department of Army Project No. 5B 99-01-004, 1959.

benzene is possible *via* either a charge- or excitation-transfer process. The data of Figures 1 and 3 leave little doubt that sensitization by energy transfer is occurrent. Ando, *et al.*,¹⁹ also have suggested the occurrence of an energy-transfer process in radiolysis of solutions of aromatic mercaptans (including thiophenol) and disulfides in benzene and toluene.

Constancy of the ratio $G(\text{H}_2)/G(\text{C}_6\text{H}_5\text{SSC}_6\text{H}_5)$ is observed over the range $\epsilon(\text{C}_6\text{H}_5\text{SH}) \approx 0.3\text{--}1.0$, as shown in Figure 1. Such constancy indicates that, at least for these major products, thiophenol decomposition processes and subsequent reactions of H and free radicals are essentially the same at $\epsilon(\text{C}_6\text{H}_5\text{SH}) = 0.3$ ($\sim 2.5 M$) as in the pure liquid; *i.e.*, for 25 vol % of thiophenol in benzene, the consequences of energy localization in thiophenol are essentially the same as in pure thiophenol. It follows that reaction 8 is almost the exclusive fate of H atoms for $\epsilon(\text{C}_6\text{H}_5\text{SH}) > 0.3$.

Examination of the results in terms of an electron-fraction partition of deposited energy (although necessarily subject to certain reservations) provides a rather plausible and consistent interpretation of the major observations. For example, the curve for $G(\text{HD})$ in Figure 3 suggests that some D atoms, measured as HD, are formed from C_6D_6 in a process that is essentially unaffected by the presence of thiophenol. The linear portion of the curve for $G(\text{HD})$ indicates that disappearance of D atoms *via* reaction 11 is al-



most quantitative at $\epsilon(\text{C}_6\text{H}_5\text{SH}) > 0.3$, a conclusion previously reached without reference to the electron-fraction postulate. Extrapolation of the linear portion of $G(\text{HD})$ to $\epsilon(\text{C}_6\text{H}_5\text{SH}) = 0$ gives, as a yield of D atoms in radiolysis of pure C_6D_6 , the value $G_{\text{D}}^\circ = 0.085$. Because there may be other processes yielding D from C_6D_6 that are quenched at low thiophenol concentration, such a value represents a lower limit for G_{D}° .

Assumption of a competition for D atoms between reaction 11 and reactions 12 and 13 gives eq III, where ϵ_{B} is the electron fraction of benzene, $G_{\text{D}}^\circ =$



$$G(\text{HD}) = G_{\text{D}}^\circ \epsilon_{\text{B}} k_{11} N_{\text{T}} / (k_{11} N_{\text{T}} + k_{12} N_{\text{T}} + k_{13} N_{\text{B}}) \quad (\text{III})$$

0.085 (the yield of D from pure C_6D_6 obtained by extrapolation), and N_{T} and N_{B} are mole fractions of thiophenol and benzene, respectively. For $k_{12} = k_{13}$, eq III reduces to

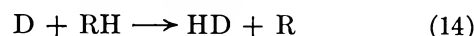
$$F \equiv G(\text{HD})/G_{\text{D}}^\circ \epsilon_{\text{B}} = k_{11} N_{\text{T}} / (k_{11} N_{\text{T}} + k_{13}) \quad (\text{IV})$$

from which is obtained

$$k_{11}/k_{13} = F/(1 - F) N_{\text{T}} \quad (\text{V})$$

Substitution of values of F and N_{T} into V , for the five concentrations in Figure 3 corresponding to $\epsilon(\text{C}_6\text{H}_5\text{SH})$ between 0.02 and 0.2, gives $k_{11}/k_{13} = 22 \pm 1$; a corresponding value of k_8/k_3 would give $\sim 96\%$ consumption of H *via* reaction 8, the analog of (11), in pure thiophenol. For $\epsilon(\text{C}_6\text{H}_5\text{SH}) \leq 0.012$ ($\sim 0.1 M$), values of k_{11}/k_{13} calculated from eq V become larger, which suggests a contribution of D atoms from certain C_6D_6 decompositions that are quenched at higher thiophenol concentrations.

The results of Burton and Patrick for the mixtures $\text{C}_2\text{H}_5\text{CHO}-\text{C}_6\text{D}_6$ ⁷ and $c\text{-C}_6\text{H}_{12}-\text{C}_6\text{D}_6$ ⁸ may be treated in a manner similar to that used for $\text{C}_6\text{H}_5\text{SH}-\text{C}_6\text{D}_6$. Reaction 14 with 13, where RH denotes $\text{C}_2\text{H}_5\text{CHO}$ or $c\text{-C}_6\text{H}_{12}$, gives eq VI. The plot of $\epsilon_{\text{B}}/G(\text{HD})$ *vs.* $N_{\text{B}}/N_{\text{T}}$



$$\epsilon_{\text{B}}/G(\text{HD}) = (1/G_{\text{D}}^\circ)(1 + k_{13} N_{\text{B}}/k_{14} N_{\text{T}}) \quad (\text{VI})$$

gives reasonably good straight lines for both $\text{C}_2\text{H}_5\text{CHO}$ and $c\text{-C}_6\text{H}_{12}$, from which are obtained $G_{\text{D}}^\circ = 0.23$ and $k_{13}/k_{14} = 1.2$ in $\text{C}_2\text{H}_5\text{CHO}-\text{C}_6\text{D}_6$ and $G_{\text{D}}^\circ = 1.7$ and $k_{13}/k_{14} = 13$ in $c\text{-C}_6\text{H}_{12}-\text{C}_6\text{D}_6$. The value of G_{D}° for $\text{C}_2\text{H}_5\text{CHO}-\text{C}_6\text{D}_6$ is not necessarily inconsistent with that for $\text{C}_6\text{H}_5\text{SH}-\text{C}_6\text{D}_6$; however, the value $G_{\text{D}}^\circ = 1.7$ for $c\text{-C}_6\text{H}_{12}-\text{C}_6\text{D}_6$ exceeds the value of $G(-\text{C}_6\text{H}_6) = 0.8$,³ as determined from polymer yields, and cannot be correct. It would appear that some sensitization of $\text{C}_6\text{D}_6 \rightarrow \text{C}_6\text{D}_5 + \text{D}$ may occur in the process of $c\text{-C}_6\text{H}_{12}$ protection⁶ or that other processes (presumably ionic) play a role in HD formation in this system. For the analogous k_{13}/k_{14} in $c\text{-C}_6\text{H}_{12}-\text{C}_6\text{H}_6$ mixtures, Burr⁹ and Hardwick⁴ obtain values of 18 and 19, respectively, by a kinetic treatment of the suppression of hydrogen yields at low C_6H_6 concentrations.

Like the $G(\text{HD})$ curve in Figure 3 and the ratio $G(\text{H}_2)/G(\text{C}_6\text{H}_5\text{SSC}_6\text{H}_5)$ in Figure 1, the curves for $G(\text{C}_6\text{H}_5\text{SSC}_6\text{H}_5)$ and $G(\text{H}_2)$ in Figures 1 and 3 become linear for $\epsilon(\text{C}_6\text{H}_5\text{SH}) > 0.3$. Such behavior indicates that not only are the secondary reactions essentially invariant at $\epsilon(\text{C}_6\text{H}_5\text{SH}) > 0.3$, but transfer of energy into thiophenol from the effective states of benzene also must be essentially complete. Extrapolation of the linear portions of $G(\text{H}_2)$ and $G(\text{C}_6\text{H}_5\text{SSC}_6\text{H}_5)$ in Figure 1 gives $G'(\text{H}_2) = 1.51$ (1.46 is obtained from Figure 3) and $G'(\text{C}_6\text{H}_5\text{SSC}_6\text{H}_5) = 1.68$ at $\epsilon(\text{C}_6\text{H}_5\text{SH}) = 0$; the ratio $G'(\text{H}_2)/G'(\text{C}_6\text{H}_5\text{SSC}_6\text{H}_5)$ is 0.90 as compared to 0.91 in pure thiophenol. The ratio of $G'(\text{H}_2) = 1.51$ to $G^\circ(\text{H}_2) = 4.21$ (for pure thiophenol) is

0.36; this value corresponds to the yield in pure benzene of excited states able to sensitize thiophenol decomposition relative to the yield in pure thiophenol of those states that decompose.

In Table II, column 3, the values of $G(\text{H}_2)$ have been calculated from eq VII, in derivation of which it has been assumed that $k_8/k_3 = k_{11}/k_{13} = 22$, that H_2 arises only *via* reaction 8, and that energy transfer is quantitative at all concentrations. $G'(\text{H}_2)$ denotes

$$G(\text{H}_2) = 22G'(\text{H}_2)/(23 + N_{\text{B}}/N_{\text{T}}) \quad (\text{VII})$$

values on the extrapolated straight line in Figure 1, whose equation is

$$G'(\text{H}_2) = 2.70\epsilon_{\text{T}} + 1.51 \quad (\text{VIII})$$

where $\epsilon_{\text{T}} = \epsilon(\text{C}_6\text{H}_5\text{SH})$. The calculated values of $G(\text{H}_2)$ in column 3 are appreciably larger than the measured values in column 2 at all values of ϵ_{T} . Consequently, some hydrogen formation by a molecular elimination process appears to be required. The data are not adequate for accurate assessment of the contribution of such a molecular elimination process. However, column 4 of Table II shows values of $G(\text{H}_2)$ calculated from eq IX, in which the assumption is

$$G(\text{H}_2) = (2/3)22G'(\text{H}_2)/(23 + N_{\text{B}}/N_{\text{T}}) + (1/3)G'(\text{H}_2) \quad (\text{IX})$$

made that one-third of $G'(\text{H}_2)$ arises from a molecular elimination process and two-thirds from H atoms *via* reaction 8. Reasonable agreement is obtained between such calculated values in column 4 and the measured values in column 2 for $\epsilon_{\text{T}} > 0.03$. Such agreement suggests, in accordance with interpretation of the $G(\text{HD})$ results, that energy transfer is essentially complete for $\epsilon_{\text{T}} \geq 0.03$ (0.24 *M*). For $\epsilon_{\text{T}} < 0.03$, decrease in energy-transfer efficiency causes measured values of $G(\text{H}_2)$ to decrease relative to calculated values.³⁵ The behavior of $G(\text{H}_2)$ and $G(\text{HD})$ at values of $\epsilon_{\text{T}} \geq 0.03$ is determined almost wholly by the competition between abstraction from thiophenol and addition to the benzene ring.

Variations in minor product yields are not susceptible to detailed interpretation. The rather sharp decrease in yields of $(\text{C}_6\text{H}_5)_2$ and $\text{C}_6\text{H}_5\text{C}_6\text{H}_7$ on addition of thio-

Table II: Comparison of Measured and Calculated Hydrogen Yields in Radiolysis of Thiophenol-Benzene Mixtures

ϵ_{T}^a	$G(\text{H}_2)^b$	$G(\text{H}_2)^c$	$G(\text{H}_2)^d$
0.0012	0.1	0.028	0.52
0.0030	0.2	0.069	0.55
0.0060	0.28	0.13	0.60
0.012	0.45	0.25	0.68
0.030	0.83	0.51	0.87
0.059	1.12	0.82	1.10
0.084	1.33	1.00	1.25
0.117	1.63	1.20	1.42

^a Electron fraction of thiophenol. ^b Measured hydrogen yield. ^c Hydrogen yield calculated from eq VII. ^d Hydrogen yield calculated from eq IX.

phenol to benzene may be attributable in part to protection of the responsible benzene states by thiophenol; however, reaction 9 is probably largely responsible for this effect. The behavior of $(\text{C}_6\text{H}_5)_2\text{S}$ yields is quite similar to that reported for yields of $(\text{C}_6\text{H}_5)_2\text{CH}_2$ in benzene-toluene mixtures and $\text{CH}_3\text{C}_6\text{H}_4\text{CH}_2\text{C}_6\text{H}_5$ in toluene.³⁶ A spur reaction, as suggested by Hoigné and Gäumann to explain their results, is proposed for $(\text{C}_6\text{H}_5)_2\text{S}$ formation. Occurrence of a maximum in $G(\text{C}_6\text{H}_5\text{SC}_6\text{H}_5)$ near the equimolar composition and failure of added biphenyl to affect the yield (*cf.* Table I) are consistent with such an interpretation. As shown in Table I, appreciable suppression of $G(\text{H}_2)$ and $G(\text{C}_6\text{H}_5\text{SSC}_6\text{H}_5)$ occurs on addition of biphenyl to 1.5 *M* $\text{C}_6\text{H}_5\text{SH}$ in C_6D_6 with relatively little effect on $G(\text{D}_2)$ or $G(\text{HD})$. Protection of thiophenol by added biphenyl is indicated. Because biphenyl has a lower ionization potential (8.27 eV)³⁴ than thiophenol and also is an effective electron scavenger,³⁷ a detailed study of the observed protective effect would be necessary for specification of a mechanism.

(35) Additional confirmation of such an interpretation was noted in $G(\text{H}_2\text{S})$. Although measurements of H_2S yields in the mixtures were too few and unreliable to justify inclusion in the Results, such yields were essentially constant for $\epsilon_{\text{T}} \geq 0.012$ (~ 0.1 *M*) and decreased below this concentration.

(36) J. Hoigné and T. Gäumann, *J. Phys. Chem.*, **65**, 2111 (1961); J. Hoigné and T. Gäumann, *Helv. Chim. Acta*, **44**, 2141 (1961).

(37) M. R. Ronayne, J. P. Guarino, and W. H. Hamill, *J. Am. Chem. Soc.*, **84**, 4230 (1962); J. P. Guarino, M. R. Ronayne, and W. H. Hamill, *Radiation Res.*, **17**, 379 (1962).

Radiolysis Yields from γ -Irradiated Liquid Methanol Containing Nitrous Oxide and the Effect of Acid

by Hiroshi Seki and Masashi Imamura

The Institute of Physical and Chemical Research, Tokyo, Japan (Received August 12, 1966)

The effect of nitrous oxide on the product yields from γ -irradiated liquid methanol in the presence and absence of sulfuric acid has been studied. Upon addition of nitrous oxide to neutral methanol, $G(\text{H}_2)$ decreases and $G(\text{N}_2)$ increases sharply in the low concentration range of nitrous oxide, whereas all other yields show little or no variation in the entire concentration range of nitrous oxide studied. Addition of sulfuric acid to nitrous oxide solutions gives rise to an increase in $G(\text{H}_2)$ and a decrease in $G(\text{N}_2)$. The result can be treated as a competition of solvated electrons for nitrous oxide and hydrogen ions, $k(e_{\text{sol}}^- + \text{H}^+)/k(e_{\text{sol}}^- + \text{N}_2\text{O}) = 3$. From these results, it can be concluded that the yield of solvated electrons produced by γ irradiation is 2.0, and a "true" $G(\text{H}_2)$ from γ -irradiated liquid methanol is 5.4. Disagreement in $G_{e_{\text{sol}}^-}$ between the present and other values reported is also discussed briefly.

Introduction

The formation of solvated electrons in γ -irradiated liquid methanol has been proposed by Baxendale and Mellows,¹ who ascribed the disagreement among the yields of hydrogen reported by many workers to a trace of electron scavenger present in liquid methanol and estimated the yield of solvated electrons to be 1.3. Since then, Dorfman and his co-workers have determined the yield of solvated electrons by pulse radiolysis technique for aliphatic alcohols including methanol, the yield for methanol being 1.1.^{2,3} The yield of solvated electrons in γ -irradiated methanol as well as ethanol has recently been determined by Hayon and Moreau by using NiCl_2 and CoSO_4 .⁴ They denoted "readily scavengable" yield of solvated electrons as 1.05 and "total scavengable" yield of electrons as 1.85 for methanol.

The present authors intended to determine the yield of solvated electrons in γ -irradiated methanol using nitrous oxide which has successfully been used by many workers for aqueous solutions to estimate the yield of hydrated electrons.⁵⁻¹⁰ Nitrous oxide has been used as an electron scavenger also for 2-propanol¹¹ and cyclohexane.¹²⁻¹⁴ Experimental results obtained preliminarily with neutral methanol at relatively low concentrations of nitrous oxide have already been re-

ported.¹⁵ In this paper more extensive results over a wide concentration range of nitrous oxide and of sulfuric acid added are reported.

Experimental Section

Methanol was purified in the fashion similar to that

- (1) J. H. Baxendale and F. W. Mellows, *J. Am. Chem. Soc.*, **83**, 4720 (1961).
- (2) I. A. Taub, D. A. Harter, M. C. Sauer, Jr., and L. M. Dorfman, *J. Chem. Phys.*, **41**, 979 (1964).
- (3) M. C. Sauer, Jr., S. Arai, and L. M. Dorfman, *ibid.*, **42**, 708 (1965).
- (4) E. Hayon and M. Moreau, *J. Phys. Chem.*, **69**, 4053 (1965).
- (5) F. S. Dainton and D. B. Peterson, *Nature*, **186**, 878 (1960); *Proc. Roy. Soc. (London)*, **A267**, 443 (1962).
- (6) G. Scholes, M. Simic, and J. J. Weiss, *Discussions Faraday Soc.*, **36**, 214 (1963).
- (7) G. Scholes and M. Simic, *J. Phys. Chem.*, **68**, 1731 (1964).
- (8) J. T. Allan and C. M. Beck, *J. Am. Chem. Soc.*, **86**, 1483 (1964).
- (9) F. S. Dainton and D. C. Walker, *Proc. Roy. Soc. (London)*, **A285**, 339 (1965).
- (10) D. Head and D. C. Walker, *Nature*, **207**, 517 (1965).
- (11) W. V. Sherman, *J. Phys. Chem.*, **70**, 667 (1966).
- (12) S. Sato, R. Yugeta, K. Shinsaka, and T. Terao, *Bull. Chem. Soc. Japan*, **39**, 156 (1966).
- (13) G. Scholes and M. Simic, *Nature*, **202**, 895 (1964).
- (14) W. V. Sherman, *J. Chem. Soc.*, 599 (1966).
- (15) H. Seki and M. Imamura, *Bull. Chem. Soc. Japan*, **38**, 1229 (1965).

described previously.¹⁶ Extra pure methanol obtained from Wako Chemicals was rectified on a 30-theoretical plate fractionation column after refluxing with sodium borohydride for about 5 hr. The middle third of the distillate was then subjected to drying with $Mg(OCH_3)_2$, prepared by dissolving 2–3 g of Mg turnings in 150 ml. Dried methanol was degassed by bulb-to-bulb distillation with repeated chill-and-thaw cycles and finally distilled into an irradiation ampoule.

Nitrous oxide (Takachiho Chemicals standard gas, >99.9%), purified further by distillation, was introduced onto methanol in an irradiation ampoule to a definite pressure, a concentration of nitrous oxide in methanol being calculated from solubility data.¹⁷ Blank experiments showed that, under the present conditions, no detectable amount of nitrous oxide was decomposed when the ampoule was sealed off.

In the preparation of acid solutions, a sulfuric acid (extra pure grade) solution of known concentration in methanol was pipetted into an irradiation ampoule before degassing.

Irradiation ampoules, made of hard glass, were cleaned with great caution by using hot acid dichromate solution, distilled water, and finally triply distilled water. The ampoule was about 15 mm in diameter and about 20 mm in length with a total capacity of about 30 ml. The amount of solution was usually about 12 ml.

Irradiations with ^{60}Co γ rays were carried out at a dose rate to methanol in the vicinity of 1.5×10^{17} ev/ml min for about 150 min. Dose rate was determined by means of Fricke dosimetry [$G(Fe(III)) = 15.6$] and corrected for electron density of methanol. All the experiments were done at room temperature.

Analytical methods employed in the present study were essentially the same as those described previously.¹⁶ Gaseous products were removed by Toepler pumping from irradiated methanolic solution at Dry Ice temperature. Nitrous oxide as well as methanol vapor included in the gaseous products was completely removed with a liquid nitrogen trap. The residual gas remaining in the Saunders–Taylor manometric microcombustion apparatus was assumed to be nitrogen. Some separate experiments by gas chromatography revealed that no oxygen was detected in the gaseous products in the presence of nitrous oxide.

Results and Discussion

Neutral Solutions. In Figure 1 are shown the yields of products—hydrogen, ethylene glycol, formaldehyde, methane, carbon monoxide, and nitrogen—as a function of nitrous oxide concentration. The upper curve illustrates the sum of $G(H_2)$ and $G(N_2)$. Similar curves

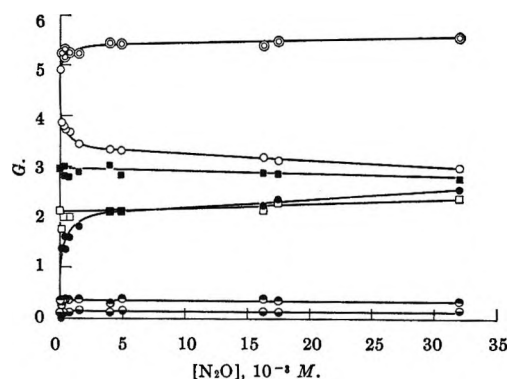


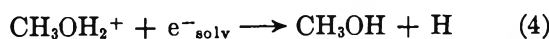
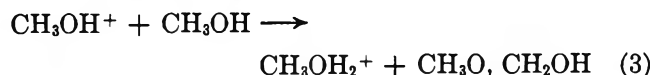
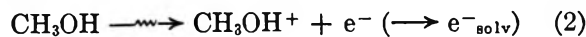
Figure 1. Product yields (G) as a function of N_2O concentration: \circ , H_2 ; \bullet , N_2 ; \blacksquare , $C_2H_6O_2$; \square , CH_2O ; \ominus , CH_4 ; \oplus , CO ; \odot , $H_2 + N_2$.

have been reported in the previous paper,¹⁵ in which $G(H_2)$ and $G(N_2)$ seemed to reach plateau values and all the other yields are unchanged; this may be because of the narrower concentration range of nitrous oxide then used. In the present study, however, all the yields except those of methane and carbon monoxide are found to show a small, steady variation with increasing concentration of nitrous oxide above $4 \times 10^{-3} M$. It should be noted that no large changes in $G(C_2H_6O_2)$ and $G(CH_2O)$ are observed at concentrations of nitrous oxide lower than $4 \times 10^{-3} M$, at which $G(H_2)$ and $G(N_2)$ change abruptly.

These results seem to indicate that nitrous oxide reacts only with a precursor of hydrogen, *i.e.*, solvated electrons, in the low concentration range of nitrous oxide. If nitrous oxide reacts with electrons which



would otherwise return to the parent ions to produce no products, a more distinct effect, especially on $G(C_2H_6O_2)$, should be expected. Here it is assumed for the γ radiolysis of pure methanol that the ionic processes which lead to the formation of hydrogen and ethylene glycol are

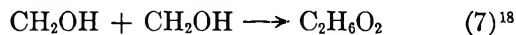


followed by



(16) M. Imamura, S. U. Choi, and N. N. Lichtin, *J. Am. Chem. Soc.*, **85**, 3565 (1963).

(17) "International Critical Tables," Vol. III, p 264, 1928.

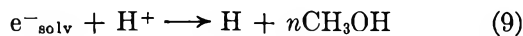


In the presence of nitrous oxide, abstraction of hydrogen atoms from methanol with O^- (produced by reaction 1) or with OH (presumably resulting from the reaction of O^- with CH_3OH_2^+) takes place to leave CH_2OH radicals in place of reaction 5. Therefore reactions of nitrous oxide with solvated electrons do not affect $G(\text{C}_2\text{H}_6\text{O}_2)$.

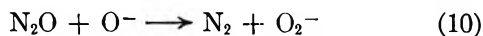
Another possible reaction of nitrous oxide that produces nitrogen is



The rate constant of reaction 8 is known to be much lower than that of reaction 1.^{19,20} Furthermore, the possibility that reaction 8 is competitive in the present case can be ruled out from the fact that, as shown in Figure 2, little or no nitrogen is produced at pH in the vicinity of 1 where almost all the solvated electrons are expected to be converted to hydrogen atoms.



It has been proposed in the gas-phase radiolysis of hydrocarbons that the reaction between nitrous oxide and O^- produced by reaction 1 may take place to double $G(\text{N}_2)$.²¹ In the present case, however, reaction 10



apparently does not take place. Although the γ -radiolysis yield of hydrogen for pure methanol, $G(\text{H}_2)$, is 4.92 in the present study, $G(\text{H}_2) + G(\text{N}_2)$ at low concentration range of nitrous oxide is about 5.4, which is in excellent agreement with the highest values of $G(\text{H}_2)$ for the γ radiolysis of methanol reported by Meshitsuka and Burton²² and Baxendale and Mellows.¹ If reaction 10 would participate in production of nitrogen, $G(\text{H}_2) + G(\text{N}_2)$ should be expected to be higher than 5.4.

Thus it may reasonably be concluded that in the low concentration range of nitrous oxide nitrogen is produced principally by reaction 1, other possible nitrogen-forming reactions being neglected.

At higher concentrations of nitrous oxide, however, reactions other than reaction 1 apparently become of increasing importance. Product yields at highest concentrations of nitrous oxide studied (not shown in Figure 1) are summarized in Table I. Inspecting Table I together with Figure 1, one can see that variations of yields with concentration of nitrous oxide are quite continuous up to $[\text{N}_2\text{O}] \approx 0.1 \text{ M}$, $G(\text{CH}_4)$ and $G(\text{CO})$ being unchanged over the entire range studied.

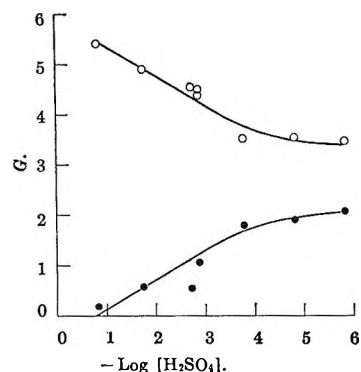


Figure 2. $G(\text{H}_2)$ and $G(\text{N}_2)$ from $(4-6) \times 10^{-3} \text{ M}$ N_2O solutions as a function of $-\log [\text{H}_2\text{SO}_4]$: \circ , H_2 ; \bullet , N_2 .

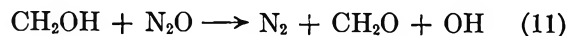
Table I: Product Yields from Neutral Methanol at High Concentrations of Nitrous Oxide^a

Product	Yield, $G(\text{molecules}/100 \text{ ev})$	
	7.9×10^{-2}	9.5×10^{-2}
H_2	2.91	2.88
N_2	3.06	3.13
$\text{H}_2 + \text{N}_2$	5.97	6.01
$\text{C}_2\text{H}_6\text{O}_2$	2.56	...
CH_2O	2.79	2.62
CH_4	0.35	0.39
CO	0.12	0.13

^a Total dose = $1.64 \times 10^{19} \text{ ev/ml}$.

Some reactions which yield more nitrogen in the high concentration range of nitrous oxide could be considered. The reaction between nitrous oxide and electrons in spurs would give rise to additional nitrogen. The simultaneous decrease in $G(\text{H}_2)$ and $G(\text{C}_2\text{H}_6\text{O}_2)$ as well as the increases in $G(\text{N}_2)$ and $G(\text{CH}_2\text{O})$ could be accounted for by assuming the oxidation of CH_2OH radicals with O^- (or OH) produced by $\text{N}_2\text{O} + \text{e}^- \rightarrow \text{N}_2 + \text{O}^-$.

Hydroxymethyl radicals, CH_2OH , might also react with nitrous oxide to produce nitrogen and formaldehyde.



This reaction, however, may give rise to a chain

(18) Formaldehyde is assumed to form principally molecularly. Experimental results which may support this assumption will be published elsewhere.

(19) F. Czapski and J. Jortner, *Nature*, **188**, 50 (1960).

(20) F. S. Dainton and S. A. Sills, *Proc. Chem. Soc. (London)*, **223** (1962).

(21) G. R. A. Johnson and J. M. Warman, *Nature*, **203**, 74 (1964).

(22) G. Meshitsuka and M. Burton, *Radiation Res.*, **8**, 285 (1958).

production of nitrogen and formaldehyde owing to OH radicals produced and can hardly account for the decrease in $G(\text{H}_2)$. The slow decrease in $G(\text{H}_2)$ accompanied by the slow increase in $G(\text{N}_2)$ at high concentrations of nitrous oxide might be explained by reaction 8. However, it seems unable to account for the variation of all the product yields satisfactorily.

Although the nature of the reaction taking place in the high concentration range of nitrous oxide is not fully understood at the present time, it is apparent that the variations of $G(\text{H}_2)$ and $G(\text{N}_2)$ in the higher concentration range of nitrous oxide are much less than those in the lower concentration range. Therefore, if the linear portions of the curves representing the variations of $G(\text{N}_2)$ and $G(\text{H}_2)$ are extended to zero nitrous oxide concentration, the intercepts should give the yield of solvated electrons which lead to the formation of the products in the absence of nitrous oxide and the total yield of H and "molecular" H_2 , respectively.

$$G^\circ(\text{N}_2) = G_{e^-_{\text{solv}}} = 2.0$$

$$G^\circ(\text{H}_2) = G_{\text{H}_2} + G_{\text{H}} = 3.4$$

Therefore

$$G^\circ(\text{N}_2) + G^\circ(\text{H}_2) = G_{e^-_{\text{solv}}} + G_{\text{H}_2} + G_{\text{H}} = 5.4$$

Disagreement in $G_{e^-_{\text{solv}}}$ with several investigations reported so far will be discussed later.

If solvated electrons are assumed to form hydrogen according to reactions 4 and 5, total hydrogen yield from γ -irradiated pure methanol should be

$$G_{e^-_{\text{solv}}} + G_{\text{H}_2} + G_{\text{H}} = 5.4$$

The lower $G(\text{H}_2)$ for the "pure" methanol used in this investigation may be due to a trace of impurity such as carbon dioxide,^{7,23,24} which can compete with nitrous oxide for solvated electrons in the low concentration range of nitrous oxide as seen from the curve of $G(\text{H}_2) + G(\text{N}_2)$ in Figure 1.

From Figure 1 and Table I, it can be seen that both $G(\text{CH}_4)$ and $G(\text{CO})$ are not affected by nitrous oxide. This fact serves to indicate that methane and carbon dioxide are formed independently of solvated electrons.

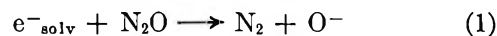
Effect of Added Acid. An increasing yield of hydrogen from acid methanol reported by Baxendale and Mellows¹ is also observed in the present study. A few examples are listed in Table II. Such an acid effect is understood as due to the reaction between hydrogen ions and electrons in spurs.^{1,25}

The effect of sulfuric acid on the radiolysis yields from methanol containing $(4-6) \times 10^{-3} M$ nitrous oxide is illustrated in Figure 2. $G(\text{H}_2)$ increases and

Table II: Product Yields from Acid Methanol in the Absence of Nitrous Oxide

Product	Yield, $G(\text{molecules}/100 \text{ ev})$			
	[H_2SO_4], M			
	2.1×10^{-3}	2.2×10^{-3}	1.8×10^{-3}	2.3×10^{-3}
H_2	5.16	4.93	5.72	5.72
$\text{C}_2\text{H}_6\text{O}_2$	3.46	3.22
CH_2O	2.06	2.04	3.10	3.28
CH_4	0.35	0.38	0.28	0.37
CO	0.10	0.18	0.13	0.10

$G(\text{N}_2)$ decreases with increasing concentration of acid. These effects are readily accounted for by assuming competition of hydrogen ions with nitrous oxide for solvated electrons. If, as discussed above, nitrogen is



produced solely by reaction 1 in the low concentration range of nitrous oxide, $G(\text{N}_2)$ from acid methanol should be expressed by

$$G(\text{N}_2) = G_{e^-_{\text{solv}}} \frac{k_1[\text{N}_2\text{O}]}{k_1[\text{N}_2\text{O}] + k_9[\text{H}^+]}$$

or

$$\frac{1}{G(\text{N}_2)} = \frac{1}{G_{e^-_{\text{solv}}}} + \frac{1}{G_{e^-_{\text{solv}}}} \frac{k_9[\text{H}^+]}{k_1[\text{N}_2\text{O}]} \quad (1)$$

A plot of $1/G(\text{N}_2)$ against $[\text{H}^+]/[\text{N}_2\text{O}]$ is illustrated in Figure 3. The data in Figure 3 are obtained at acid concentrations which are low enough as not to yield high values of $G(\text{H}_2)$ in the absence of nitrous oxide. The $[\text{H}^+]$ is calculated on the basis of only the first dissociation to H^+ and HSO_4^- in dilute methanolic solution.² A straight line in Figure 3 indicates the validity of the simple competition mentioned above. From the intercept and the slope, one can obtain

$$e^-_{\text{solv}} = 2.0$$

and

$$k_9/k_1 = 3.0$$

In addition, under the conditions that all the solvated electrons are to be scavenged with nitrous oxide,

(23) G. Scholes, M. Simic, and J. J. Weiss, *Nature*, **188**, 1019 (1960).

(24) G. E. Adams, J. H. Baxendale, and J. W. Boag, *Proc. Roy. Soc. (London)*, **A277**, 549 (1964).

(25) E. Hayon, *J. Phys. Chem.*, **68**, 1242 (1964); *Trans. Faraday Soc.*, **61**, 723 (1965).

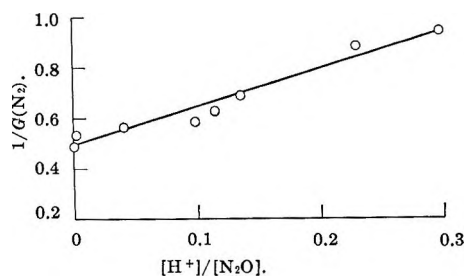


Figure 3. A plot of $1/G(\text{N}_2)$ against $[\text{H}^+]/[\text{N}_2\text{O}]$ (eq I).

the yield of hydrogen from acid solution should be expressed.

$$G(\text{H}_2) = G_{\text{H}_2} + G_{\text{H}} + G_{\text{e}^-_{\text{solv}}} \frac{k_9[\text{H}^+]}{k_1[\text{N}_2\text{O}] + k_9[\text{H}^+]}$$

Using $G_{\text{H}_2} + G_{\text{H}} = 3.4$, one can obtain

$$\frac{1}{G(\text{H}_2) - 3.4} = \frac{1}{G_{\text{e}^-_{\text{solv}}}} + \frac{1}{G_{\text{e}^-_{\text{solv}}}} \frac{k_1[\text{N}_2\text{O}]}{k_9[\text{H}^+]} \quad (\text{II})$$

$G(\text{H}_2)$ values obtained at nitrous oxide concentrations, $(0.4\text{--}1.5) \times 10^{-2} M$, and at sulfuric acid concentrations, $(1.4\text{--}1.8) \times 10^{-3} M$, are plotted in Figure 4 according to eq II. The straight line is drawn so as to make $G_{\text{e}^-_{\text{solv}}} = 2.0$, as illustrated in Figure 4. From the slope one can obtain $k_9/k_1 = 3$, which is in good agreement with that obtained from Figure 3.

Rate constants of the reactions of hydrated electrons with nitrous oxide and with hydrogen ions have been determined separately from pulse radiolysis study²⁸ to be $k(\text{e}^-_{\text{aq}} + \text{H}^+) = (2.36 \pm 0.24) \times 10^{10} M^{-1} \text{sec}^{-1}$ in the concentration range of H^+ 10–100 μM at pH 4–5 and $k(\text{e}^-_{\text{aq}} + \text{N}_2\text{O}) = (8.67 \pm 0.6) \times 10^9 M^{-1} \text{sec}^{-1}$ in the concentration range of N_2O 50–300 μM at pH 7. The ratio of $k(\text{e}^-_{\text{aq}} + \text{H}^+)$ to $k(\text{e}^-_{\text{aq}} + \text{N}_2\text{O})$ is calculated from these results to be 2.75 ± 0.48 , which is close to that obtained with solvated electrons in methanol in the present study.

Furthermore, if one uses the rate constant of solvated electrons in methanol with hydrogen ions that has been determined from pulse radiolysis study,² $k(\text{e}^-_{\text{solv}} + \text{H}^+) = (3.9 \pm 0.9) \times 10^{10} M^{-1} \text{sec}^{-1}$, the rate constant of solvated electrons with nitrous oxide, k_1 , is to be $1.3 \times 10^{10} M^{-1} \text{sec}^{-1}$, which is compared with the above-mentioned value for $k(\text{e}^-_{\text{aq}} + \text{N}_2\text{O})$.

Comparison of $G_{\text{e}^-_{\text{solv}}}$ with Other Results. In the present study, $G_{\text{e}^-_{\text{solv}}}$ in γ -irradiated methanol is concluded to be 2.0. This value is, however, substantially higher than those reported so far. Dorfman and his co-workers obtained from pulse radiolysis studies $G_{\text{e}^-_{\text{solv}}} = 1.1$.² Disagreement between the pulse radiolysis result and the present one might be explained,

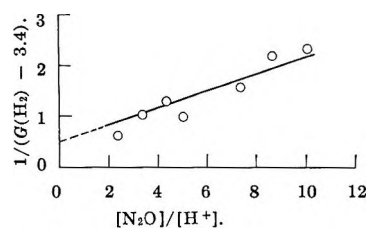


Figure 4. A plot of $1/(G(\text{H}_2) - 3.4)$ against $[\text{N}_2\text{O}]/[\text{H}^+]$ (eq II).

at least in part, as due to the large difference in dose rate, because the dose rate of pulsed electrons is higher than that of γ rays by several orders of magnitude. The yields of solvated electrons obtained with ethanol,² propanol, and 2-propanol³ by pulse radiolysis technique are also in the vicinity of $G = 1$. No studies on the dose rate effect on the yield of hydrated or solvated electrons have been reported. It is interesting to note, however, that greatly reduced yields both of solvated and of hydrated electrons have been found in the $^{10}\text{B}(n, \alpha)^7\text{Li}$ -recoil radiolysis of methanolic²⁷ and aqueous²⁸ solutions. Furthermore, very low yields of solvated electrons have been reported for the recoil radiolysis of ethanol and methyltetrahydrofuran glasses at -196° ²⁹ compared with those for γ radiolysis.³⁰ Although the dose rate effect is not essentially similar to the linear energy transfer (LET) effect,³¹ the conditions of pulse irradiation may be somewhat different from those of γ irradiation.

On the other hand, several papers have been published in which yields of solvated electron were determined by chemical kinetics for methanol, ethanol, and 2-propanol irradiated with γ rays. $G_{\text{e}^-_{\text{solv}}}$ for methanol was estimated by Baxendale and Mellows to be 1.3 from the difference between their highest $G(\text{H}_2)$, 5.4, and lowest one, 4.1.¹ According to the recent investigation of Hayon and Moreau⁴ using NiCl_2 , CoSO_4 , and LiNO_3 , the "total scavengable" yield of electron, $G(\text{e}^-)$, is 1.85 in methanol and 1.65 in ethanol. They discriminate "readily scavengable" yield, $G(\text{e}^-) = 1.05$ and 0.90 for methanol and ethanol, respectively, from "total scavengable" one. It should

(26) S. Gordon, E. J. Hart, M. S. Matheson, J. Rabani, and J. K. Thomas, *Discussions Faraday Soc.*, **36**, 193 (1963).

(27) M. Imamura and H. Seki, to be published.

(28) A. Henglein, K.-D. Asmus, G. Scholes, and M. Simic, *Z. Physik. Chem.*, **45**, 39 (1965).

(29) J. Wendenburg and A. Henglein, *Z. Naturforsch.*, **19b**, 995 (1964).

(30) J. P. Guarino, M. R. Ronayne, and W. H. Hamill, *Radiation Res.*, **17**, 379 (1962).

(31) W. G. Burns and R. Barker in "Progress in Reaction Kinetics," Vol. 3, G. Porter, Ed., Pergamon Press Ltd., London, 1965.

be noted that these values were determined from plateau values of $G(\text{H}_2)$ in the presence of salts, assuming $G(\text{H}_2)$ for pure methanol and ethanol to be 5.26 and 5.00, respectively.

The yield of solvated electrons in ethanol has also been determined by Adams and Sedgwick³² and Myron and Freeman.³³ The former authors used several solutes reactive toward precursors of hydrogen to calculate $G(\text{total electrons}) = 1.02$ on the basis of $G(\text{H}_2) = 4.85$ for pure ethanol. Myron and Freeman carefully investigated the variation of $G(\text{H}_2)$ from pure ethanol with dose. Assuming that the value of $G(\text{H}_2)$ for pure ethanol extrapolated to zero dose was 5.0, they concluded that $G_{e^-_{\text{solv}}} = 0.9$.

The yield of solvated electron in γ -irradiated 2-propanol has recently been determined by Sherman¹¹ from the effect of nitrous oxide and sulfuric acid on the radiolysis yield of hydrogen. Assuming that $G(\text{H}_2) = 4.0$ for pure 2-propanol, he concluded that $G_{e^-_{\text{solv}}} = 0.9$ from the decrease in $G(\text{H}_2)$. He also

suggested that the excess yield of nitrogen over the decrease in $G(\text{H}_2)$ is due to the reaction between nitrous oxide and other species which does not lead to hydrogen in the absence of nitrous oxide.

All these results obtained by chemical kinetics under steady irradiation are based on the difference in $G(\text{H}_2)$ between systems in the presence and in the absence of electron scavenger. It is apparent, therefore, that the estimated yields of solvated electron must more or less depend upon the $G(\text{H}_2)$ determined separately for pure alcohols. In the present study, a "true" value of $G(\text{H}_2)$ for pure methanol is taken to be 5.4, although the experimental value is 4.92. The assumed value of 5.4 is probably reasonable from the discussion given above and the coincidence of $-\Delta G(\text{H}_2)$ with $\Delta G(\text{N}_2)$ may not be adventitious.

(32) G. E. Adams and R. D. Sedgwick, *Trans. Faraday Soc.*, **60**, 865 (1964).

(33) J. J. J. Myron and G. R. Freeman, *Can. J. Chem.*, **43**, 381 (1965).

The Thermal Pressure Coefficient and the Entropy of Melting at Constant Volume of Isotactic Polypropylene

by G. C. Fortune and G. N. Malcolm

University of Otago, Dunedin, New Zealand (Received August 15, 1966)

Measurements have been made of the thermal pressure coefficient of isotactic polypropylene melt. The results have been used to calculate the entropy of melting at constant volume from the value at constant pressure. It is shown that the previously neglected dependence of the thermal pressure coefficient on the specific volume of the sample is an important factor in this calculation.

A knowledge of the energy and entropy of fusion of a polymer at constant volume is of value in the examination of the relationship between the melting behavior of the polymer and its molecular structure.¹ The energy and entropy changes on melting at constant volume are related to those at constant pressure by the equations

$$\Delta H_f = (\Delta E_f)_v + T_m \int_{V_c}^{V_1} (dP/dT)_{v,T_m} dV \quad (1)$$

and

$$\begin{aligned} \Delta S_f &= \Delta H_f/T_m \\ &= (\Delta S_f)_v + \int_{V_c}^{V_1} (dP/dT)_{v,T_m} dV \quad (2) \end{aligned}$$

V_c and V_1 are the volumes of the crystalline and amorphous phases at the melting temperature, T_m . Values of ΔH_f for isotactic polypropylene have been obtained by a variety of methods and have been reviewed recently by Kirshenbaum, *et al.*,² and by Krigbaum and Uematsu.³ The specific volumes of crystalline and amorphous forms of the polymer have been determined by Danusso, *et al.*⁴ We report here the results of some measurements of the thermal pressure coefficient, $(dP/dT)_v$, of isotactic polypropylene melt, which is the third quantity required for the calculation of $(\Delta E_f)_v$, and $(\Delta S_f)_v$ from eq 1 and 2. The symbol γ will be used to denote the thermal pressure coefficient.

Experimental Section

Apparatus. The measurements were made in the

glass cell shown in Figure 1. A known weight of polymer in the form of very small pieces was placed in the part of the cell surrounding the capillary tube while the lower end of the cell was still open. The end of the vessel was then closed by a piece of glass shaped like a thimble, which could be sealed in position without charring the polymer. The complete cell was evacuated and filled with a known weight of mercury to a predetermined level in the capillary tube. The amount of mercury in the cell was such that at temperatures just above the polymer melting point contact was made with the wire, A, sealed into the top end of the capillary tube. A second wire, B, sealed into the side of the vessel made permanent contact with the mercury. By joining these two wires to a battery and a pilot light in series, it was possible to determine when the mercury level in the capillary was just at the tip of wire A. The glass vessel was suspended inside a steel pressure bomb fitted with insulated electrical leads through the head-nut.

The steel bomb was placed inside an aluminum heating block which has been described already.⁵ Pressures were generated by the compression of water

(1) L. Mandelkern, "Crystallization of Polymers," McGraw-Hill Book Co., Inc., New York, N. Y., 1964.

(2) I. Kirshenbaum, Z. W. Wilchinsky, and B. Groten, *J. Appl. Polymer Sci.*, **8**, 2723 (1964).

(3) W. R. Krigbaum and I. Uematsu, *J. Polymer Sci., Part A*, **3**, 767 (1965).

(4) F. Danusso, G. Moraglio, W. Ghiglia, L. Motta, and G. Talamini, *Chim. Ind. (Milan)*, **41**, 74 (1959).

(5) G. N. Malcolm and G. L. D. Ritchie, *J. Phys. Chem.*, **66**, 852 (1962).

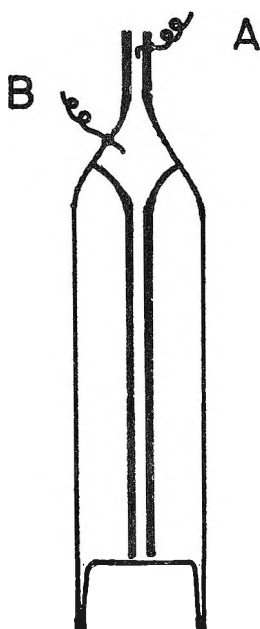


Figure 1. Cell for measuring thermal pressure coefficients of high-melting polymers.

and were measured with a gauge calibrated on a dead-weight tester.

The measurements were made with polymer samples in the liquid phase. A period of over 1 hr was allowed for equilibrium to be attained at each temperature and pressure. The plot of pressure against temperature for each amount of polymer and mercury in the cell was linear within the experimental error over the whole pressure range of 200 atm. The method of least squares was used to determine the best straight line through each set of points. The slope of each line gave a value of γ_{obs} for the contents of the cell. The thermal pressure coefficient of the polymer itself was calculated from γ_{obs} by the formula

$$\gamma_p = \gamma_{\text{obs}} \left(1 + \frac{V_{\text{Hg}}\beta_{\text{Hg}} - V_g\beta_g}{V_p\alpha_p/\gamma_p} \right) + \frac{V_g\alpha_g - V_{\text{Hg}}\alpha_{\text{Hg}}}{V_p\alpha_p/\gamma_p} \quad (3)$$

In this formula V_g , V_{Hg} , and V_p are the volumes of the glass cell, the mercury, and the polymer, and α and β are the coefficients of thermal expansion and isothermal compressibility. The volumes of the mercury and the molten polymer at each temperature and pressure were calculated from their weights and densities. The polymer densities at 1 atm of pressure as a function of temperature (and hence α_p) were obtained from the work of Dannusso, *et al.*,⁴ and of Newman.⁶ α_p for polypropylene melt at 1 atm of pressure was taken

as $7.1 \times 10^{-4} \text{ deg}^{-1}$ independent of temperature. The value of α_{Hg} at 1 atm was taken as $1.80 \times 10^{-4} \text{ deg}^{-1}$ for temperatures between 100 and 200°. For Pyrex glass at 1 atm of pressure α_g was taken as $9.9 \times 10^{-6} \text{ deg}^{-1}$ and β_g as $3.00 \times 10^{-6} \text{ atm}^{-1}$. Values of β_{Hg} at various temperatures and 1 atm of pressure were estimated by linear interpolation between the values $3.92 \times 10^{-6} \text{ atm}^{-1}$ at 0° and $4.60 \times 10^{-6} \text{ atm}^{-1}$ at 192°. The mechanical coefficients for mercury and glass are known to be effectively constant over the small pressure range of 200 atm used in this work. No direct information on the variation with pressure of α_p for polypropylene is available. But for polyethylene, Matsuoka⁷ has shown that the compressibility up to very high pressures is almost unaffected by temperature increase. Since $(d\alpha/dP)_T = -(d\beta/dT)_P$, it follows that α is almost independent of pressure at fixed temperature up to several thousand atmospheres of pressure. On the basis of this evidence for polyethylene, it was assumed that α_p for polypropylene was constant throughout the comparatively small pressure range of 200 atm.

The magnitude of the correction term depends largely on the ratio of the volumes of mercury and polymer. This ratio could not be made particularly small because the polymer had to be introduced into the vessel in the form of small pieces which could not be packed closely together. As a result the correction term was of the order of 30% of γ_{obs} and could be determined to within $\pm 3\%$ of its own value. The error in γ_{obs} itself was estimated as $\pm 1\%$ and the error in γ_p as $\pm 3\%$.

Materials. Isotactic polypropylene powder was kindly supplied by ICI, Plastics Division, Welwyn City, England. Before use it was melted under high vacuum and was held in this condition for about 4 hr. The material suffered a 6% loss in weight as a result of this treatment, but showed no further weight loss when the process was repeated. The molten polymer had the unfortunate property of strongly adhering to a glass surface so that most of the glass cells were shattered when the polymer solidified on cooling to room temperature.

Results and Discussion

Thermal Pressure Coefficients and Internal Pressures. In Table I the values of γ calculated from γ_{obs} are given as functions of the temperature for the three pressures of 1, 100, and 200 atm. The values at 1 atm of pressure have been fitted to the equation

(6) S. Newman, *J. Polymer Sci.*, **47**, 111 (1960).

(7) S. Matsuoka, *ibid.*, **42**, 511 (1960).

$$\gamma(P = 1 \text{ atm}) = 5.25 - 0.027(t - 176) + 4.16 \times 10^{-4}(t - 176)^2 \quad (4)$$

in which t is the centigrade temperature. The goodness of fit is indicated by the deviations in the third column of Table I for $P = 1$ atm. The values of γ at 1 atm are recorded to two decimal figures for the sake of comparison with the deviations, although the prob-

Table I: Thermal Pressure Coefficients of Isotactic Polypropylene Melt

$T, ^\circ\text{C}$	$\gamma(P = 1 \text{ atm}), \text{ atm deg}^{-1}$	$\gamma_{\text{eq 4}} - \gamma_{\text{exptl}}$
158.2	5.86	-0.01
163.2	5.72	0.05
163.8	5.68	0.03
170.8	5.38	-0.02
174.2	5.37	0.06
183.6	5.01	-0.06
190.3	4.98	0.03
194.6	4.87	-0.02

$T, ^\circ\text{C}$	$\gamma(P = 100 \text{ atm}), \text{ atm deg}^{-1}$	$T, ^\circ\text{C}$	$\gamma(P = 200 \text{ atm}), \text{ atm deg}^{-1}$
170.5	5.9	182.9	5.9
175.1	5.7	187.1	5.7
175.6	5.7	187.4	5.7
183.5	5.4	196.2	5.4
186.7	5.4	199.3	5.4
199.1	5.0	214.5	5.0
205.9	5.0	221.5	5.0
209.3	4.9	224.0	4.9

able error in γ amounts to one part in the first decimal figure. The curvature of the plot of γ vs. t at 1 atm is similar to that obtained for other polymers.⁸ Some of the values of γ in the table for $P = 1$ atm are for temperatures below the polymer melting point. These values were obtained from pressure-temperature measurements above the melting point, which were extrapolated down to the abscissa corresponding to 1 atm. Consequently, these values refer to the polymer in the supercooled liquid state at these temperatures.

Values of γ calculated from eq 4 have been used to calculate values of the internal pressure, P_i , from the equation

$$P_i \equiv (\partial E / \partial V)_T = T(\partial P / \partial T)_V - P \quad (5)$$

The function $P_i V^2$ where V is the specific volume of the melt has been calculated also using the specific volumes of the polymer melt given by the equation^{3,4}

$$V(P = 1 \text{ atm}) = 1.1340 + 9.28 \times 10^{-4}t \quad (6)$$

The values of $P_i V^2$ decreased slowly with increase in temperature, the change being 0.15% deg⁻¹ over the 40° range of the measurements.

Entropy of Fusion at Constant Volume. Sufficient information is now available for the calculation of the entropy of fusion of isotactic polypropylene at constant volume from eq 2. The specific volumes of the crystalline and amorphous phases at 176° and 1 atm of pressure^{3,4} are 1.133 and 1.297 cc g⁻¹. These are the limits of the integration in eq 2. From eq 4 γ at 176° and 1 atm is 5.2 atm deg⁻¹. It has usually been assumed in calculations of this kind that γ is not a function of the specific volume of the melt.¹ If this assumption is made here, the difference between the entropy of fusion at constant pressure and at constant volume is given by

$$\begin{aligned} \gamma(\Delta V_f) &= 5.2 \times 0.164 \times 0.0242 \text{ cal deg}^{-1} \text{ g}^{-1} \\ &= 0.021 \text{ cal deg}^{-1} \text{ g}^{-1} \\ &= 0.88 \text{ cal deg}^{-1} (\text{mole of repeating units})^{-1} \end{aligned}$$

It has been pointed out by Allen⁹ that the common assumption that γ is independent of the specific volume at constant temperature is very unlikely to be valid and may lead to an error in the correction term from constant pressure to constant volume as large as 50%. The present results enable this suggestion to be investigated.

Values of γ at the normal melting point (176°) at pressures of 1 and 100 atm can be read from Table I. Values at other pressures between 1 and 150 atm can be obtained from the original pressure-temperature isochores. Some of these values are recorded in Table II. The values at elevated pressures will refer to the polymer melt in a supercooled state. The specific volumes of the polymer melt at increased pressures can be calculated from the compressibility of the polymer. At 176° and 1 atm the compressibility is given by

$$\begin{aligned} \beta &\equiv \alpha / \gamma = 7.1 \times 10^{-4} / 5.25 \text{ atm}^{-1} \\ &= 1.34 \times 10^{-4} \text{ atm}^{-1} \end{aligned}$$

If the reasonable assumption is made that β remains constant over the limited pressure range of 150 atm, the values of the specific volume listed in Table II are obtained. The integration required in eq 2 can now be carried out graphically. Because of the extremely high pressures which would be required to compress the polymer melt to the volume of the crystalline phase

(8) G. Allen, G. Gee, D. Mangaraj, D. Sims, and G. J. Wilson, *Polymer*, **1**, 467 (1960).

(9) G. Allen, *J. Appl. Chem.*, **14**, 1 (1964).

at 176°, the experimental points are restricted to the neighborhood of the upper limit of the integral. The measured values of γ at 176° vary linearly with specific volume. If it is assumed for the present that γ varies linearly with specific volume right down to the specific volume of the crystalline polymer, the value of the

evident that the variation of γ with specific volume is an important factor in the calculation.

Calculations similar to these for polyethylene from the data of Lupton¹⁰ indicate that the difference between the entropy of fusion at constant pressure and at constant volume is probably nearer to 1.54 than 1.04¹¹ cal deg⁻¹ per mole of C₂H₄ units. It is of interest that the revised value of the entropy of fusion at constant volume for polyethylene would agree more closely than the old value with the result calculated by the theory of Starkweather and Boyd.¹¹

If the entropy of fusion of polypropylene at constant pressure is taken as 5.4 eu per mole of repeating units,² the corresponding entropy change at constant volume will be less than 4.5 eu (calculated assuming γ is constant) and may be as low as 4.1 eu mole⁻¹. This value can be regarded as approximate only because of the long extrapolation which is involved in its determination.

Table II: Thermal Pressure Coefficients and Specific Volumes of Polypropylene Melt as a Function of Pressure

<i>P</i> , atm	γ_{176° , atm deg ⁻¹	<i>V</i> , cc g ⁻¹
1	5.2	1.297
40	5.4	1.290
100	5.7	1.280
141	5.9	1.273

integral is 1.3 eu mole⁻¹. This is approximately 43% greater than the value calculated with the assumption that γ is constant. Although it cannot yet be claimed that the integral has been evaluated accurately, it is

(10) J. M. Lupton, 134th National Meeting of the American Chemical Society, Chicago, Ill., Sept 1958.

(11) H. W. Starkweather and R. H. Boyd, *J. Phys. Chem.*, **64**, 410 (1960).

The Charge Effect in Sedimentation. I. Polyelectrolytes

by Mitsuru Nagasawa and Yosuke Eguchi

*Department of Applied and Synthetic Chemistry, Nagoya University, Chikusa-ku, Nagoya, Japan
(Received August 16, 1966)*

Since macroions in general have higher sedimentation coefficients than counterions, a sedimentation potential is set up in solution which diminishes the sedimentation velocity of the macroion. It has been believed that the effect of sedimentation potential can be eliminated either by extrapolating the observed sedimentation coefficients to zero macroion concentration or by increasing the ionic strength to infinity. In this paper, however, it is pointed out that even the limiting sedimentation coefficient is not free from the effect of ionic atmosphere, so that it may not be considered to be the value for the corresponding un-ionized macromolecule of the same molecular size, conformation, and partial specific volume. This fact is experimentally shown from the ionic strength dependence of the Mandelkern-Flory coefficient which would be constant if there were no effect of ionic atmosphere. The change of the Mandelkern-Flory coefficient with ionic strength can be quantitatively accounted for if the macroion coil is nondraining. In practice, however, it is suggested that the effect of partial drainage should be taken into account if the molecular weight is low and the ionic strength is low.

Introduction

When charged macromolecules such as charged proteins or linear polyelectrolytes are centrifuged in aqueous solution, a difference between the sedimentation coefficient of the macroion and that of the counterions creates an electrostatic potential gradient in solution (sedimentation potential) which, in turn, affects the sedimentation velocity of the macroion. Since the sedimentation coefficient of the macroion is generally much higher than that of the counterion, the sedimentation potential tends to diminish the sedimentation velocity of the macroion. That is, the observed sedimentation coefficient is generally much lower than that of the corresponding un-ionized macromolecule of the same molecular size, conformation, and partial specific volume. This phenomenon was well studied by Pederson.¹ According to his theory, it was shown that the sedimentation coefficient of the corresponding un-ionized macromolecule may be obtained either by increasing the ionic strength with neutral salt to eliminate the sedimentation potential or by extrapolating the observed sedimentation coefficient to zero macroion concentration. Although the difference between the sedimentation coefficients of cation and anion of the added salt may also set up an

electrostatic potential gradient in solution which affects the sedimentation velocity of the macroion, the problem may be of little importance if ions having the same sedimentation velocities such as NaCl are used.

The above-mentioned procedures to eliminate the effect of sedimentation potential are commonly used in protein chemistry for the purpose of finding the molecular weight of charged macromolecules.^{2,3} However, it seems to the present authors that the procedure includes an imprecise assumption. Suppose that a macroion is in an infinitely large volume of a simple electrolyte solution; in other words, suppose that the observed sedimentation velocities of the macroions are extrapolated to zero macroion concentration at a constant concentration of added salt. The macroion must then be surrounded by an ionic atmosphere. As is well known in electrochemistry, the sedimentation velocity of the macroion must be decreased by the

(1) T. Svedberg and K. O. Pederson, "Die Ultrazentrifuge," Steinkoff, Dresden and Leipzig, 1940; K. O. Pederson, *J. Phys. Chem.*, **62**, 1282 (1958).

(2) S. Claesson and I. Moring-Claesson, "Ultracentrifugation," in "Determination of the Size and Shape of Protein Molecules," P. Alexander and R. J. Block, Ed., Pergamon Press, London, 1961.

(3) H. K. Schackman, "Ultracentrifuge in Biochemistry," Academic Press Inc., New York, N. Y., 1959.

effect of the ionic atmosphere.⁴ Except in some special cases, the effect of ionic atmosphere disappears only when the ionic strength becomes zero. In most of the studies thus far published,^{1,5-11} however, the effect of ionic atmosphere on the sedimentation velocity of the macroion has been completely neglected. Perhaps the lack of attention is to be expected since in those studies all ions, not only the macroions but also the counterions, are assumed to be distributed uniformly in the solution so that the ionic atmosphere would disappear at the limit of infinite dilution of the macromolecule. The assumption of uniform distribution of counterions in solution is obviously too simplified.¹² They must gather around the macroion, and the ionic atmosphere cannot disappear even at the limit of infinite dilution of macroion so long as the concentration of added salt (*i.e.*, ionic strength) is kept finite. Therefore, it is doubtful that the sedimentation coefficient of the corresponding un-ionized macromolecule can be obtained by extrapolating the observed sedimentation coefficient of the macroion to infinite dilution. Moreover, the effect of ionic atmosphere is expected to become even stronger as the concentration of added salt goes to infinity if the macroion is a solid sphere having a definite number of charges on the surface.

If the macroion is a linear polyelectrolyte, the sedimentation velocity is changed not only by the effect of ionic atmosphere but also by the change in conformation of polymer chain. According to Flory,¹⁵ the sedimentation coefficient S_p is related to the expansion factor α which is defined by the ratio of the radius of gyration of polymer $\langle S^2 \rangle^{1/2}$ to its value at the Θ point $\langle S_0^2 \rangle^{1/2}$, that is

$$S_p = \frac{M}{N_A} (1 - \bar{v}\rho) / \Xi \quad (1)$$

$$\Xi = \eta_0 P_0 \langle S_0^2 \rangle^{1/2} \alpha^3$$

where

$$\alpha^2 = \langle S^2 \rangle / \langle S_0^2 \rangle \quad (2)$$

\bar{v} is the partial specific volume of polymer and ρ is the density of the solution. The expansion factor α is also related to the intrinsic viscosity $[\eta]$ by the equation

$$[\eta] = \Phi_0 \frac{\langle S_0^2 \rangle^{3/2}}{M} \alpha^3 \quad (3)$$

From eq 1 and 3, the expansion factor can be canceled and the following Mandelkern-Flory coefficient is obtained.

$$\Phi_0^{1/3} P_0^{-1} = [N_A \eta_0 / (1 - \bar{v}\rho)] S_p [\eta]^{1/3} / M^{2/3} \quad (4)$$

It is well known that $\Phi_0^{1/3} P_0^{-1}$ is 2.5×10^6 for non-ionic polymer solutions independent of solvent, temperature, and molecular weight.¹⁴⁻¹⁶ In polyelectrolyte solutions, however, the coefficient cannot be constant if there is an effect of ionic atmosphere. To test whether the effect of ionic atmosphere on S_p really exists or not, it seems best to see whether $\Phi_0^{1/3} P_0^{-1}$ is independent of ionic strength and molecular weight.

Strictly speaking, the sedimentation coefficient of eq 1 and the intrinsic viscosity of eq 3 may be proportional to a lower power of α than 1 and 3, respectively. In particular, when there is a drainage through the polymer coil, which may be more or less expected because of the high expansion of polyion coils, the power of α in eq 1 and 3 may be considerably different from 1 and 3.¹⁷ However, $\Phi_0^{1/3} P_0^{-1}$ must be almost constant over a wide range of α , because the drainage effect in S_p and that in $[\eta]$ cancel each other. Even if a change in $\Phi_0^{1/3} P_0^{-1}$ occurs because of the drainage effect, $\Phi_0^{1/3} P_0^{-1}$ should increase with an increase in α , that is, with a decrease in ionic strength. The tendency is opposite to that caused by the effect of ionic atmosphere. A precise discussion on the effect of drainage on $\Phi_0^{1/3} P_0^{-1}$ was given by Kurata and Yamakawa.¹⁷

It is well known that the so-called electroviscous effect is observed in the viscosity measurement of charged particles.⁶ Here, however, it is assumed that

(4) H. S. Harned and B. B. Owen, "The Physical Chemistry of Electrolyte Solutions," Reinhold Publishing Corp., New York, N. Y., 1950.

(5) G. J. Howard and D. O. Jordan, *J. Polymer Sci.*, **12**, 209 (1954); J. Kraut, *ibid.*, **14**, 222 (1954).

(6) Z. Alexandrowicz and E. Daniel, *Biopolymers*, **1**, 447, 473 (1963).

(7) G. Sitaramaiah and D. A. I. Goring, *J. Polymer Sci.*, **58**, 1107 (1962).

(8) G. Sitaramaiah, R. F. Robertson, and D. A. I. Goring, *J. Phys. Chem.*, **66**, 1364 (1962).

(9) S. R. Erlander and F. R. Senti, *Makromol. Chem.*, **73**, 14, 31 (1964).

(10) S. R. Erlander, *ibid.*, **65**, 91 (1963).

(11) K. Iso, *Nippon Kagaku Zasshi*, **84**, 95 (1963).

(12) P. J. Mijnlief, "Effects of Charge on the Sedimentation, the Diffusion and the Sedimentation Equilibrium of Colloidal Electrolytes," in "Ultracentrifugal Analysis," J. W. Williams, Ed., Academic Press, New York, N. Y., 1963.

(13) P. J. Flory, "Principles of Polymer Chemistry," Cornell University Press, Ithaca, N. Y., 1953.

(14) L. Mandelkern and P. J. Flory, *J. Chem. Phys.*, **20**, 212 (1952).

(15) L. Mandelkern, W. R. Krigbaum, H. A. Sheraga, and P. J. Flory, *ibid.*, **20**, 1392 (1952).

(16) T. G. Fox, Jr., and L. Mandelkern, *ibid.*, **21**, 187 (1953).

(17) M. Kurata and H. Yamakawa, *ibid.*, **28**, 785 (1958); **29**, 311 (1958).

the electroviscous effect will disappear at infinite dilution of macroion and that the effect of ionic atmosphere will have little effect on the intrinsic viscosity since the rotational frictional coefficient is discussed in intrinsic viscosity. This assumption may be justified by the experimental fact that the intrinsic viscosity of globular proteins is independent of the charges on their surface¹⁸ and also by the fact that the intrinsic viscosity of linear polyions is accounted for by theories which take into account only the expansion of the polymer coil.¹⁹⁻²¹

The Sedimentation Equation for Macroions

If we define the fluxes of solutes, $(J_k)_c$, in relation to the cell as they are experimentally observed, we have the following phenomenological equation.²²

$$(J_k)_c = \sum_i (K_{ki})_v X_i \quad (5)$$

Here, it is assumed that one molecule of polyelectrolyte is dissociated into one polyion of valency $-Z_p$ and Z_p cations of valency $+1$, and also that a neutral salt of 1-1 valence type which has a common counterion with the polyelectrolyte is added to the solution. The suffixes p, +, and - denote polyanion, counterion, and by-ion, respectively. X_i is the force acting on component i per its unit mass, and the $(L_{ki})_v$'s are phenomenological coefficients. Since the solutes have charges, the forces X_k are given by the equation

$$X_k = (1 - \bar{v}_k \rho) \omega^2 r - \sum_j \left(\frac{\partial \mu_k}{\partial n_j} \right)_{T,P,n_m} \left(\frac{\partial n_j}{\partial r} \right)_{T,P} + Z_k e \left(\frac{\partial \psi}{\partial r} \right)_{T,P} \quad (6)$$

where \bar{v}_k , μ_k , Z_k , and n_j are the partial specific volume, chemical potential, valence, and concentration of component k or j , respectively. The ω is the angular velocity of ultracentrifugation, r is the distance from the center of rotation, and $\partial \psi / \partial r$ is the electrostatic potential gradient set up in the solution. The last term of eq 6 arises from the interaction between solute charges. Then, the equation for the flow of solute, $(J_k)_c$, may be expressed by

$$(J_k)_c = (S_k)_v n_k \omega^2 r - \sum_j (D_{kj})_v \left(\frac{\partial n_j}{\partial r} \right)_{T,P} + (l_k)_v n_k \left(\frac{\partial \psi}{\partial r} \right)_{T,P} \quad (7)$$

where $(S_k)_v$, $(D_{kj})_v$, and $(l_k)_v$ are defined as

$$(S_k)_v = \frac{1}{n_k} \sum_i (L_{ki})_v (1 - \bar{v}_i \rho) \quad (8)$$

$$(D_{kj})_v = \sum_i (L_{ki})_v \left(\frac{\partial \mu_i}{\partial n_j} \right)_{T,P,n_m} \quad (9)$$

$$(l_k)_v = \frac{Z_k e}{n_k} \sum_i (L_{ki})_v \quad (10)$$

and m denotes all solutes other than solute j . At a steady state, no current should flow in the cell so that we may use the following condition.

$$\sum_k (Z_k e) (J_k)_c = 0 \quad (11)$$

Therefore, we have

$$\left(\frac{\partial \psi}{\partial r} \right)_{P,T} = \frac{\sum_k \sum_j Z_k (D_{kj})_v \left(\frac{\partial n_j}{\partial r} \right)_{T,P}}{\sum_k Z_k (l_k)_v n_k} - \frac{\sum_k Z_k (S_k)_v n_k}{\sum_k Z_k (l_k)_v n_k} \omega^2 r \quad (12)$$

Insertion of eq 12 into eq 7 gives

$$(J_k)_c = (S_k)_v^a n_k \omega^2 r - \sum_j (D_{kj})_v^a \frac{\partial n_j}{\partial r} \quad (13)$$

in which $(S_k)_v^a$ and $(D_{kj})_v^a$ are defined by

$$(S_k)_v^a = (S_k)_v - (l_k)_v \frac{\sum_k Z_k (S_k)_v n_k}{\sum_k Z_k (l_k)_v n_k} \quad (14)$$

$$(D_{kj})_v^a = (D_{kj})_v - (l_k)_v \frac{\sum_k Z_k (D_{kj})_v}{\sum_k Z_k (l_k)_v n_k} \cdot n_k \quad (15)$$

If $S_+ = S_-$ as in NaCl solutions, eq 14 is simplified as

$$\frac{1}{(S_k)_v^a} = \frac{1}{(S_p)_v} [1 + k_1 n_p + k_2 n_p^2 + \dots] \quad (16)$$

and

$$k_1 = \frac{Z_p (l_p)_v}{\{(l_+)_v - (l_-)_v\} n_s} \quad (17)$$

$$k_2 = -k_1^2 \quad (18)$$

where n_p and n_s are the concentrations of polyion and added salt, respectively. Thus, $(S_p)_v$, which is called the limiting sedimentation coefficient in this paper, can be obtained as the limit of the observed sedimentation coefficient, $(S_p)_v^a$, at the infinite dilution of macromolecule.

(18) R. Townend, L. Weinberger, and S. N. Timasheff, *J. Am. Chem. Soc.*, **82**, 3175 (1960).

(19) H. Eisenberg and D. Woodside, *J. Chem. Phys.*, **36**, 1844 (1962).

(20) A. Takahashi and M. Nagasawa, *J. Am. Chem. Soc.*, **86**, 543 (1964).

(21) S. Lapanje and S. Kovac, Preprint of IUPAC Symposium on Makromolekular Chemistry, Prague, 1965.

(22) H. Fujita, "Mathematical Theory of Sedimentation Analysis," Academic Press, New York, N. Y., 1962.

As is clear from eq 8, $(S_p)_v$ includes not only $(L_{pp})_v$ but also $(L_{p+})_v$ and $(L_{p-})_v$. Therefore, $(S_p)_v$ of a linear polyion must change with the concentration of added salt in two ways: $(L_{pp})_v$ is changed due to the change in the conformation of polyion and the $(L_{p\pm})_v$ are altered by the interaction between polyion and simple ions. That is, the limiting sedimentation coefficient of a polyion must be a function of the concentration of added salt even at infinite dilution of the polyion.

The derivation of eq 16 is, in principle, based on the idea of Pederson¹ and is equivalent to Mijlieff's derivation.⁴ The discussions reported by Kraut⁵ and Alexandrowicz and Daniel⁶ are along this same line, though in their theories the charge number of macroion, Z_p , is assumed to be diminished by ion binding, and the change in radius of gyration with ionic strength is completely neglected.

Experimental Section

Samples. The sodium polystyrene sulfonate used is the same as that used in previous works.²³ The crude sample, which was kindly provided by Dr. Vanderkooi and Dr. Mock of Dow Chemical Co., was purified by precipitation from aqueous solution with isopropyl alcohol and was fractionated. Details of the fractionation procedure will be described in a separate paper.²⁴ Nine fractions were obtained, but among them (only seven) fractions having suitable molecular weights were used for measurements in this work.

The weight-average molecular weights of the samples were determined from light-scattering measurements,²⁴ but some of them were calculated from their intrinsic viscosities in 0.5 M NaCl aqueous solution at 25°C using the equation²⁴

$$[\eta] = 1.86 \times 10^{-4} M_w^{0.64} \quad (19)$$

The intrinsic viscosities and molecular weights of the samples are shown in Table I.

Table I: Molecular Weights of the Samples^a

	Sample no.						
	2	4	5	6	7	8	9
$M_w \times 10^{-4}$	234		155		100	49	39
$M_v \times 10^{-4}$	265	210	157	126	90	47	35

^a M_w was determined from light-scattering experiments and M_v was calculated from eq 19.

The distilled water used was deionized with a mixed-bed column of ion-exchange resins (Amberlite 120 and 400). The sodium chloride used was of an analytical

grade from Katayama Chemical Co. The concentrations were determined from the weights of solutes dissolved.

Sedimentation Experiments. Sedimentation experiments were performed at 59,780 rpm in a Spinco Model E analytical ultracentrifuge with a schlieren optical system. The temperature was controlled at $25.0 \pm 0.1^\circ$. All runs were carried out in standard Kel-F cells of 12 mm. Sedimentation coefficients were calculated from the traveling distance of the maximum of the schlieren peak. Measurements of distance were carried out using a microcomparator manufactured by Shimadzu Seisakusho Ltd. Because of the high concentration dependence of the sedimentation coefficient, the schlieren pattern was not a gaussian distribution curve but was like a sharp spike. However, the skewed shape of the pattern seems to have little effect on the observed sedimentation coefficient since the shape did not change at all during a run.

Viscosity and Density Measurements. The intrinsic viscosity determination was carried out with a capillary viscometer of modified Ubbelohde type, which had three bulbs for giving rate of shear corrections to the measured values. The details of the measurements are the same as already reported in a previous paper.²⁰ Density measurements of solution were carried out in a 50-ml flask at 25°C.

Results

Examples of the sedimentation coefficient *vs.* polymer concentration plots at various ionic strengths are shown in Figure 1. The molecular weights of the samples used in Figure 1 are the lowest and the highest of all those used in the present work. The graphs are straight lines if the molecular weight is low or if the ionic strength is high, but slightly curved if the molecular weight is high and the ionic strength is low. The limiting sedimentation coefficients, $(S_p)_v$, obtained by graphical extrapolation to zero polymer concentration are shown in Table II for different ionic strengths and molecular weights. The reliability of $(S_p)_v$ obtained is high for the samples of low molecular weight and at high ionic strength, but becomes low for the samples of high molecular weight at low ionic strength. The ambiguity may be $\pm 2-3\%$ (5% at the maximum). The intrinsic viscosities of the samples in the same solvents are also shown in Table II.

The limiting sedimentation coefficient of linear poly-

(23) L. Kotin and M. Nagasawa, *J. Am. Chem. Soc.*, **83**, 1026 (1961); M. Nagasawa and H. Fujita, *ibid.*, **86**, 3005 (1964).

(24) A. Takahashi, T. Kato, and M. Nagasawa, to be published.

Table II: Sedimentation Coefficients and Intrinsic Viscosities of the Samples

NaCl concn., <i>M</i>	Sample no.													
	2		4		5		6		7		8		9	
	$S_p \times 10^{13}$	$[\eta]$	$S_p \times 10^{13}$	$[\eta]$	$S_p \times 10^{13}$	$[\eta]$	$S_p \times 10^{13}$	$[\eta]$	$S_p \times 10^{13}$	$[\eta]$	$S_p \times 10^{13}$	$[\eta]$	$S_p \times 10^{13}$	$[\eta]$
0.2	16.4	3.09	14.7	2.90	12.8	2.47	12.8	2.20	11.5	1.71	8.13	1.05	7.10	0.85
0.05	13.2	5.28	12.5	5.01	11.8	4.33	10.1	3.83	9.80	3.10	7.75	1.74	6.45	1.39
0.02	10.2	7.91	10.0	7.50	10.0	6.51	9.18	5.68	8.85	4.52	6.41	2.52	5.88	1.97
0.01	8.13	10.82	8.00	10.08	8.00	9.03	7.69	7.80	7.30	6.29	5.88	3.36	5.38	2.60
0.005	6.67	20.90	6.80	16.70	6.54	14.80	6.21	12.0	5.88	9.60	5.13	5.10	4.95	3.47

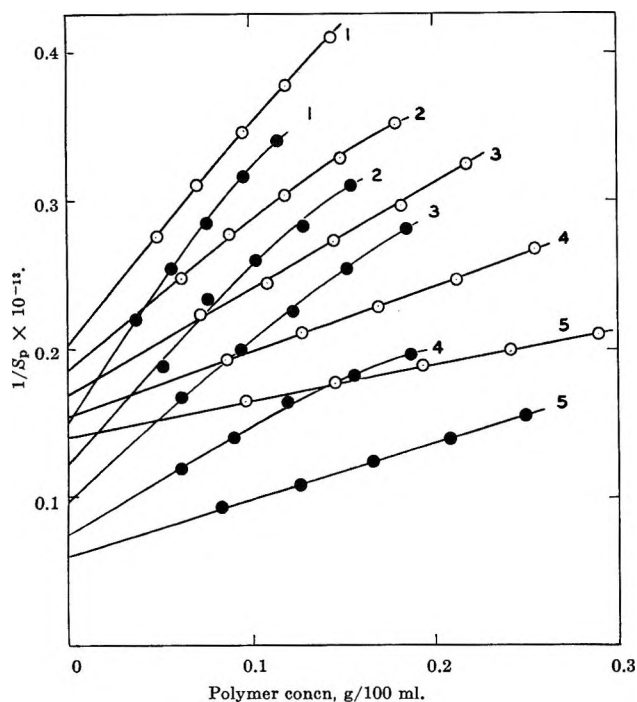


Figure 1. Examples of the sedimentation coefficient vs. polymer concentration plots. Open circles: sample no. 9; solid circles: sample no. 2. Concentration of NaCl: 1, 0.005; 2, 0.01; 3, 0.02; 4, 0.05; 5, 0.2 *M*. Speed of rotation: 59,780 rpm.

mer is, in general, related to its molecular weight by the equation

$$S_p = K_s M_w^{\nu_s} \quad (20)$$

where K_s and ν_s are constants depending on solvent and temperature. The relationship between S_p and M_w obtained in the present experiment is shown in Figure 2. It is observed that ν_s is decreased from 0.5 to zero as the ionic strength is decreased, *i.e.*, as the solvent becomes better. However, the graph deviates from a straight line if the molecular weight is very high.

According to eq 17, the slope of a $1/(S_p)_v^2$ vs. C_p plot should be proportional to the inverse molar concentration of added salt. However, the values of k_1 graphi-

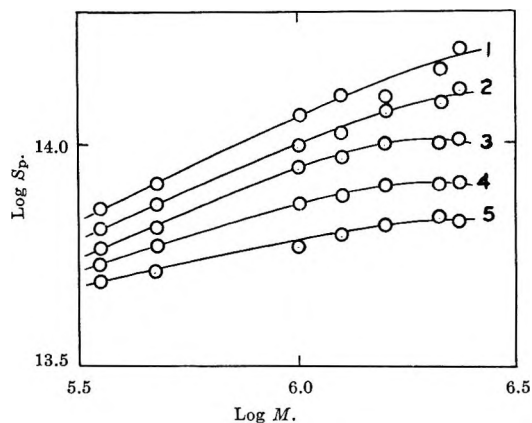


Figure 2. Relationship between sedimentation coefficient and molecular weight at various ionic strengths. Concentration of NaCl: 1, 0.2; 2, 0.05; 3, 0.02; 4, 0.01; 5, 0.005 *M*.

cally obtained from Figure 1 do not satisfy eq 17. The reason for the disagreement may be that the hydrodynamic interactions between polyion spheres are completely neglected.

Using the data in Tables I and II, the Mandelkern-Flory coefficient $\Phi_0^{1/3} P_0^{-1}$ is calculated as shown in Figure 3. The figure clearly shows that $\Phi_0^{1/3} P_0^{-1}$ is not constant but changes with ionic strength and also with molecular weight. At a constant molecular weight, the ambiguity in $\Phi_0^{1/3} P_0^{-1}$ obtained is determined by the ambiguity in S_p since $[\eta]^{1/3}$ can be determined quite accurately. Therefore, the changes in $\Phi_0^{1/3} P_0^{-1}$ with ionic strength are clearly beyond the experimental error. All experimental values in Figure 3, excluding the data at 0.2 *M* NaCl, tend to the value of 2.0×10^6 as the ionic strength is increased. The limiting value, which is supposed to be the value for the corresponding un-ionized polymer, is a little lower than the value usually accepted for nonionic polymers, 2.5×10^6 . The decrease of $\Phi_0^{1/3} P_0^{-1}$ at $C_2 = 0.2$ *M* may look unusual, but is in agreement with some former observations using sodium polyacrylate.²⁵

(25) A. Takahashi, A. Soda, and I. Kagawa, *Nippon Kagaku Zasshi*, 83, 873 (1962).

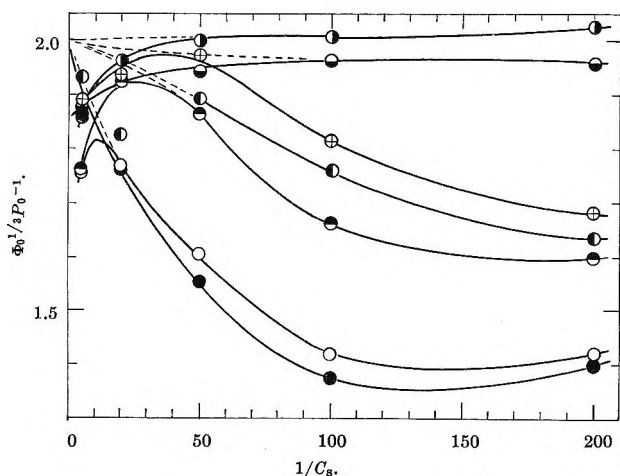


Figure 3. Ionic strength dependence of the Mandelkern-Flory coefficient. Samples: \bullet , no. 9; \ominus , no. 8; \oplus , no. 7; \odot , no. 6; \ominus , no. 5; \circ , no. 4; \bullet , no. 2. The partial specific volume of the polymer \bar{v} is 0.60, independent of ionic strength and molecular weight. The values of η_0 and ρ of the solvents are taken from G. Jones and S. M. Christian, *J. Am. Chem. Soc.*, **59**, 484 (1937).

Eisenberg and Casassa²⁶ also reported that $\Phi_0^{1/3}P_0^{-1}$ for potassium polyvinyl sulfonate in 0.5 M KCl and also for ammonium polyvinyl sulfonate in 0.5 M NH_4Cl are about 1.0×10^6 . The reason for the abnormal decrease will be discussed later.

Thus, it may be concluded that $\Phi_0^{1/3}P_0^{-1}$ for linear polyions is lower than the value for the corresponding un-ionized polymers due to the effect of the ionic atmosphere. As was explained in the Introduction, the intrinsic viscosities of linear polyions as well as those of nonionic polymers, are determined only by their radii of gyration. That is, the intrinsic viscosity of polyion satisfies the equation.¹⁹⁻²¹

$$\frac{[\eta]}{\sqrt{M}} = K + 0.51\Phi_0 B \sqrt{M} \quad (21)$$

which was presented for nonionic polymers with the idea that $[\eta]$ is determined only by radius of gyration. The constants K and B are called the short-range and long-range interaction parameters. In the present experiments, it was confirmed that $[\eta]$ of the present samples, at least qualitatively, satisfies eq 21.²⁴ If the sedimentation coefficient of polyion is also determined only by radius of gyration, it should satisfy the following equation which can be derived by the same procedure as eq 21

$$\left(\frac{\sqrt{M}}{S_p}\right)^3 = (\text{constant})_1 + (\text{constant})_2 \sqrt{M} \quad (22)$$

Equation 22 is well satisfied by the sedimentation co-

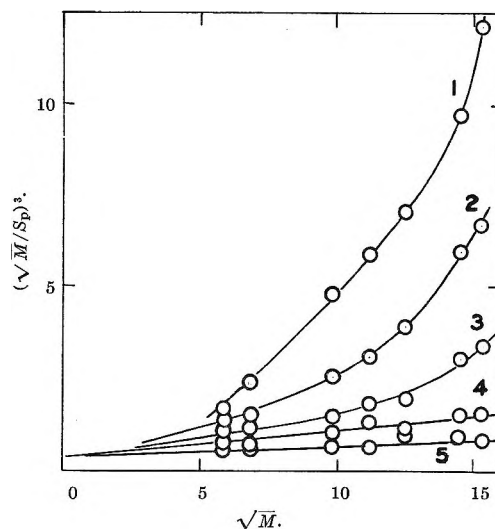


Figure 4. Relationship between $(\sqrt{M}/S_p)^3$ and \sqrt{M} at various ionic strengths. Concentrations of NaCl was the same as in Figure 1.

efficients of nonionic polymers, for example, poly(α -methylstyrene).²⁷ However, it is clear from Figure 4 that the present experimental results cannot satisfy eq 22. This fact means that the sedimentation coefficient of polyion is not a function of radius of gyration only, but may be changed by the effect of ionic atmosphere. That is, we may safely conclude that the change in $\Phi_0^{1/3}P_0^{-1}$ shown in Figure 3 is not due to the change in Φ_0 but due to the change in P_0 .

Discussion

It is assumed that the polyion coil is represented by a hydrodynamically equivalent sphere having uniform distribution of fixed charges as assumed by Hermans and Overbeek,²⁸ and also that the counterions, whose number is equal to the number of fixed charges of the polyion, are distributed outside and inside the polymer sphere, forming an ionic atmosphere. The counterions must sediment together with the polyion at the same speed. A counterion which sediments at a velocity relative to solvent, $u(r)$, gives the following force to the solvent

$$k = -6\pi\eta_0 a u(r) \quad (23)$$

where a is the effective radius of the counterion. Then, the force acting on a spherical shell at a distance r from the center of polyion sphere is

$$-4\pi r^2 (n_+ - n_-) k dr \quad (24)$$

(26) H. Eisenberg and E. F. Casassa, *J. Polymer Sci.*, **47**, 29 (1960).

(27) I. Noda, S. Saito, and M. Nagasawa, to be published.

(28) J. J. Hermans and J. T. G. Overbeek, *Rec. Trav. Chim.*, **67**, 761 (1948).

This force is in the opposite direction of sedimentation and causes the sphere of radius r to move with the velocity dv ⁶

$$dv = \frac{-4\pi r^2(n_+ - n_-)kdr}{6\pi\eta r} \quad (25)$$

Here $(n_+ - n_-)$ is given by Hermans and Overbeek's equation. That is, the electrostatic potential ψ at the position of radius r is given by

$$\psi_1 = E_D \left\{ 1 - e^{-\kappa R} (1 + \kappa R) \frac{\sinh(\kappa r)}{\kappa r} \right\} \quad (r < R) \quad (26)$$

$$\psi_2 = \frac{1}{2} E_D \left\{ (1 + \kappa R) e^{-\kappa R} - (1 - \kappa R) e^{\kappa R} \right\} \frac{e^{-\kappa r}}{\kappa r} \quad (r > R)$$

where κ is the reciprocal Debye radius defined by

$$\kappa^2 = \frac{8\pi e^2 n_s}{DkT} \quad (27)$$

and E_D is given by

$$E_D = -\frac{kT}{e} \ln \frac{1 + \sqrt{1 + x^2}}{x} \quad (28)$$

$$x = \frac{8\pi}{3} \frac{1}{Z_p} R^3 n_s$$

In the original paper of Hermans and Overbeek,²⁸ the limiting form of E_D at infinitely small values of x , *i.e.*

$$E_D^0 = \frac{3}{8\pi} \frac{kT}{e} \frac{Z_p}{R^3 n_s}$$

was used, but it was advised that eq 28 has wider applicability.^{29,30} Hence, we can calculate $(n_+ - n_-)$ by inserting eq 26 into the equation

$$n_+ - n_- = -2 \sinh(e\psi/kT) n_s \quad (29)$$

The force of all counterions acting on the polyion sphere may be divided into two parts. One is the force of ions outside the polyion sphere and the other is the force of ions inside the sphere. The velocity change of the polyion sphere due to the force of the counterions outside the sphere ΔV_2 is given by integration of eq 25 from the sphere surface to infinity

$$\Delta V_2 = \int_R^\infty dv \quad (30)$$

Outside the polyion sphere it can be safely assumed

$$u(r) = U \quad (r > R) \quad (31)$$

where U is the sedimentation velocity of polyion relative to the cell. Thus from eq 25, 30, and 31, we have

$$\Delta V_2 = 4\pi a U n_s E_D \left\{ (1 + \kappa R) e^{-\kappa R} - (1 - \kappa R) e^{\kappa R} \right\} \frac{e^{-\kappa R}}{\kappa^2} \quad (32)$$

Since $\kappa R \gg 1$ in most experiments, eq 32 becomes

$$\Delta V_2 = -\frac{DkT}{2e^2} a U (\kappa R) \ln \frac{1 + \sqrt{1 + x^2}}{x} \quad (33)$$

If the assumption of the nondraining model is applicable for polyelectrolytes, the effect of the counterions inside the sphere on the sedimentation velocity of polyion, ΔV_1 , must be negligible. Thus, the velocity change of the polyion due to the total effect of ionic atmosphere, ΔV , is

$$\Delta V = \Delta V_2$$

That is, $\Phi_0^{1/3} P_0^{-1}$ for nondraining polyion is given by

$$\Phi_0^{1/3} P_0^{-1} = (\Phi_0^{1/3} P_0^{-1})_0 \times \left[1 - 2.303 \frac{DkT}{2e^2} a (\kappa R) \log \frac{1 + \sqrt{1 + x^2}}{x} \right] \quad (34)$$

where $(\Phi_0^{1/3} P_0^{-1})_0$ is the value for the corresponding unionized polyion.

Theoretically speaking, however, the assumption of a nondraining sphere is correct only when the molecular weight is infinitely high. Although the nondraining model is applicable for nonionic polymers in almost all cases, it cannot *a priori* be assumed that the nondraining model is always applicable to polyions which have very expanded conformations.

If the polyion coil is partially draining, ΔV_1 is calculated as

$$\Delta V_1 = \int_0^R dv$$

$$dv = \frac{-4\pi r^2(n_+ - n_-)kdr}{6\pi\eta R\psi(\sigma)} \quad (35)$$

where $\psi(\sigma)$ is the well-known function of Debye-Bueche-Brinkman,³¹ *i.e.*

$$\psi(\sigma) = \frac{1 - Tgh\sigma/\sigma}{1 + (3/2)\sigma^2(1 - Tgh\sigma/\sigma)}$$

and

$$\sigma = \nu f R^2 / \eta; \quad \nu = Z_p / 4 / 3 \pi R^3$$

(29) S. Lifson, *J. Chem. Phys.*, **27**, 700 (1957).

(30) M. Nagasawa and I. Kagawa, *Bull. Chem. Soc. Japan*, **30**, 961 (1957); M. Nagasawa, *J. Am. Chem. Soc.*, **83**, 300 (1961).

At present, however, we cannot carry out the integration of eq 35.

If the polymer sphere is completely free draining so that

$$u(r) = U \quad (\text{for all } r) \quad (36)$$

eq 35 can be integrated to be

$$\Delta V_1^0 = -\frac{1}{6} \frac{DkT}{e^2} \frac{a}{Z_p a_s} U \times \ln \frac{1 + \sqrt{1 + x^2}}{x} \left[\frac{2(\kappa R)^3}{\kappa} - \frac{3(\kappa R)^2}{\kappa} \right] \quad (37)$$

where the frictional coefficient of the polymer sphere, $6\pi\eta R\psi(\sigma)$, was replaced by the value for a free-draining sphere, $Z_p 6\pi\eta a_s$ (a_s is the radius of a segment). Thus, the total effects of ionic atmosphere give

$$\begin{aligned} \Delta V^0 &= \Delta V_1^0 + \Delta V_2^0 \\ &= -\frac{DkT}{2e^2} aU \ln \frac{1 + \sqrt{1 + x^2}}{x} \times \\ &\quad \left[\frac{1}{Z_p a_s} \left\{ \frac{2}{3} \frac{(\kappa R)^3}{\kappa} - \frac{(\kappa R)^2}{\kappa} \right\} + (\kappa R) \right] \quad (38) \end{aligned}$$

At the limits of $x \gg 1$ and $\kappa R \gg 1$, which are satisfied in most experiments in this paper, we have

$$\Delta V^0 = \frac{a}{a_s} U \quad (39)$$

Therefore, if the free-draining model were applicable, ΔV^0 would be independent of ionic strength and molecular weight. This does not mean, however, that $\Phi_0^{1/3} P_0^{-1}$ for a free-draining polyion sphere would be constant, because the assumption of the cancellation of α between S_p and $[\eta]$ cannot be satisfied at high drainage. Rather, $\Phi_0^{1/3} P_0^{-1}$ must increase with decrease of ionic strength, since $(\Phi_0^{1/3} P_0^{-1})_0$ must increase with degree of drainage¹⁷ and the degree of drainage must increase with decrease of ionic strength. Perfect free drainage cannot be observed even for polyelectrolytes, but the effect of partial drainage, which can be qualitatively understood from the above discussion on the effect of the perfect free drainage, is important for understanding the behavior of a polyion shown in Figure 3. The ordinary hydrodynamic effect of partial drainage can be cancelled between S_p and $[\eta]$, but the effect of partial drainage on the force of ionic atmosphere cannot be cancelled and must have a great effect on $\Phi_0^{1/3} P_0^{-1}$.

The conclusions we can obtain from the above discussions may be summarized as follows. (1) If the molecular weight is so high that the assumption of a nondraining sphere may be satisfied, the experimental

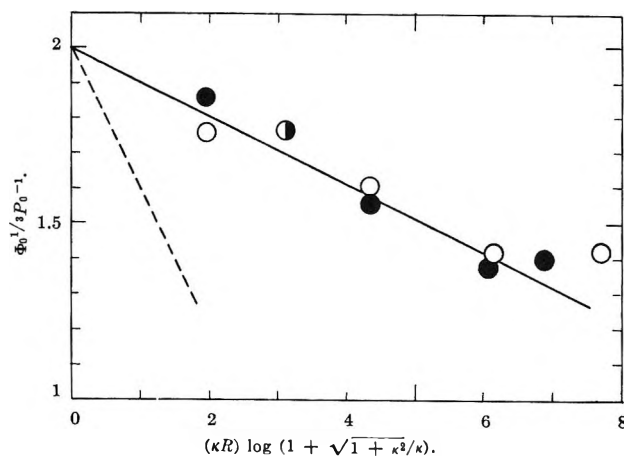


Figure 5. Plots of $\Phi_0^{1/3} P_0^{-1}$ vs. $(\kappa R) \log(1 + \sqrt{1 + x^2}/x)$. Samples: solid circles, no. 2; open circles, no. 4. The dotted line is the one calculated from eq 34 assuming $a = 2.5$ Å.

data must satisfy eq 34, which shows a linear relationship between $\Phi_0^{1/3} P_0^{-1}$ and $(\kappa R) \ln(1 + \sqrt{1 + x^2}/x)$ independently of molecular weight. In this work, samples no. 2 and 4 satisfy the linearity as seen in Figure 5. The dotted line in Figure 5 was calculated from eq 34 assuming $a = 2.5$ Å. The disagreement between the experimental slope and the calculated one is expected because the calculated values of E_D must be much higher than the actual ones.^{30,32-34} Such disagreement is often observed in the study of polyelectrolyte solutions and usually explained by assuming ion binding. (2) The data of the samples other than no. 2 and 4 do not satisfy the linear relationship between $\Phi_0^{1/3} P_0^{-1}$ and $(\kappa R) \ln(1 + \sqrt{1 + x^2}/x)$. This seems to be due to the effect of partial drainage. As the molecular weight decreases, the polyion sphere is more freely drained. Therefore, $\Phi_0^{1/3} P_0^{-1}$ must become less dependent on the ionic strength as is clear from the discussion of eq 39. This speculation might explain the experimental behavior of low molecular weight samples in Figure 3. (3) As the ionic strength decreases, the drainage must increase because of the expansion of polymer coil. Therefore, $\Phi_0^{1/3} P_0^{-1}$ may increase as the ionic strength decreases if the molecular weight is so low that the assumption of cancellation of α between S_p and $[\eta]$ is violated, though the effect of free drainage is not so predominant

(31) P. Debye and A. M. Bueche, *J. Chem. Phys.*, **16**, 573 (1948).

(32) M. Nagasawa, A. Takahashi, M. Izumi, and I. Kagawa, *J. Polymer Sci.*, **38**, 213 (1959).

(33) L. Kotin and M. Nagasawa, *J. Chem. Phys.*, **36**, 873 (1962).

(34) S. A. Rice and M. Nagasawa, "Polyelectrolyte Solutions," Academic Press, New York, N. Y., 1962.

for most of the samples used in this work. The data of the sample no. 9 in Figure 3 show the slight increase of $\Phi_0^{1/2}P_0^{-1}$ with decrease of ionic strength. This seems to be due to the draining effect. The data of Alexandrowicz and Daniel⁶ also show a slight increase of S_p (i.e., of $\Phi_0^{1/2}P_0^{-1}$) with decrease of ionic strength, though they treated the data as independent of molecular weight. It is our opinion that this arises from the low molecular weight of the sample they used.

The reason for the abnormal decrease of $\Phi_0^{1/2}P_0^{-1}$ at high ionic strength ($C_s = 0.2 M$) is not completely clear, but our speculation is that the decrease may be caused by the effect of ionic atmosphere around a

segment. As was frequently discussed, it is too unrealistic to assume that all counterions are distributed smoothly over the polymer sphere. It is more realistic to assume that the polyion skeleton surrounded by cylindrical ionic atmosphere has a coiled conformation. The effect of the ionic atmosphere around the polymer skeleton must become stronger as the ionic strength increases, so that $\Phi_0^{1/2}P_0^{-1}$ may decrease with increase of ionic strength. This effect may be more important if the polymer coil is free draining.

Acknowledgment. The authors wish to thank Drs. Mock and Vanderkooi for supplying the sample.

The Vapor Pressure, Heat of Sublimation, and Evaporation

Coefficient of Lanthanum Fluoride

by Raymond W. Mar and Alan W. Searcy

*Inorganic Materials Research Division, Lawrence Radiation Laboratory, and
Department of Mineral Technology, College of Engineering, University of California,
Berkeley, California (Received August 18, 1966)*

The vapor pressure of solid lanthanum fluoride in the temperature range 1340–1650°K has been found by the torsion-effusion method to be given by the equation, $\log P_{\text{atm}} = -(2.173 \pm 0.009)(10^4/T) + 9.608 \pm 0.065$. Estimated heat capacities were used with the measured pressures to calculate the heat of sublimation at 298.15°K to be 107 ± 4 kcal. Comparison of torsion-Langmuir measurements from the (0001) crystal faces with the effusion data yields an evaporation coefficient of 0.95 ± 0.1 in the experimental range.

I. Introduction

Accurate thermodynamic data for most of the rare earth fluorides are still not available, although Brewer¹ has estimated data for most of them. Lim and Searcy² have studied the vaporization of cerium trifluoride by the torsion-effusion method. Mass spectrometric studies have been made on the trifluorides of scandium, yttrium, and lanthanum by Kent, Zmbov, Kana'an, Besenbruch, McDonald, and Margrave.³

This paper reports a torsion-Langmuir and torsion-effusion^{4,5} investigation of lanthanum fluoride in the

(1) L. Brewer, "The Chemistry and Metallurgy of Miscellaneous Materials—Thermodynamics," L. L. Quill, Ed., McGraw-Hill Book Co., Inc., New York, N. Y., 1950.

(2) M. J. Lim and A. W. Searcy, *J. Phys. Chem.*, **70**, 1762 (1966).

(3) R. A. Kent, K. F. Zmbov, A. S. Kana'an, G. Besenbruch, J. D. McDonald, and J. L. Margrave, *J. Inorg. Nucl. Chem.*, **28**, 1419 (1966).

(4) H. Mayer, *Z. Physik.*, **67**, 249 (1931).

(5) M. Vollmer, *Z. Physik. Chem.*, 863 (1931).

Table I: Orifice Dimensions

Cell	Orifice diam., cm		Apex angle, deg	Channel length, cm		Cor factors	
	(a)	(b)		(a)	(b)	(a)	(b)
Knudsen 1	0.0990	0.0986	...	0.1499	0.1524	0.4697	0.4645
Knudsen 2	0.1594	0.1524	...	0.1633	0.1591	0.5508	0.5621
Knudsen 3	0.1866	0.1940	...	0.1628	0.1631	0.6063	0.6155
Knudsen 4	0.2633	0.2634	...	0.1506	0.1491	0.7043	0.7067
Knudsen 5	0.3452	0.3529	...	0.1613	0.1621	0.7465	0.7500
Langmuir 1	0.0999	0.0982	120	0.3144	0.3172	1.129	1.130
Langmuir 2	0.1525	0.1517	120	0.3172	0.3172	1.122	1.122
Langmuir 3	0.3056	0.3213	120	0.3172	0.3172	1.104	0.102

temperature range from 1325 to 1650°K. From the effusion measurements the heat of sublimation at 298.15°K has been calculated and from comparison of Langmuir and effusion measurements the evaporation coefficient has been determined in the experimental temperature range. Apparently, no previous study of the evaporation coefficient of a halide of a main group III element has been reported.

II. Experimental Section

A graphite cell with two eccentrically placed orifices was suspended in a furnace by a 0.005-cm diameter tungsten fiber of about 43-cm length. The torsion cell used for the Knudsen studies consisted of a cell block, two cylindrical cells, and two cell end plates, all of graphite. The cells fit snugly into holes in the side faces of the cell block. The cell end plates had orifices drilled through the centers through which vapor could escape. The torsion cell used for the Langmuir studies was modified to allow the LaF₃ crystal surfaces to be held flush against inner faces of orifice lids by graphite back-up washers. All gaseous molecules escaping from crystal surface areas other than those exposed by the orifices were vented out through a 3.5-mm hole in the top of the torsion cell block. Pressures can be calculated by means previously described from angular deflections caused by vaporization in effusion^{6,7} and Langmuir experiments.⁸ The dimensions and correction factors^{9,10} for the various orifices are given in Table I.

The cells were heated in a resistance furnace by radiation from tungsten hairpin-shaped elements. As escape of vapor caused the cell to rotate in one direction, it was manually returned to its original position by twisting the upper point of attachment of the fiber in the opposite direction. The angles of twist were recorded to the nearest five-thousandths of a degree by means of a modified goniometer.

Temperatures were read by means of an optical

pyrometer which was focused on a black body hole drilled into the bottom of the cell block. Temperature gradients in the Knudsen and Langmuir cells are believed to have been negligible because (1) cells were suspended in the central portion of an 8-cm vertical zone for which the temperature had been demonstrated to be constant to within 2° and (2) optical pyrometer measurements revealed no variation in temperature across the bottom surface of the cell.

The pyrometer was calibrated by comparison with platinum—platinum—10% rhodium thermocouple measurements. For these calibrations a graphite cell was heated in the furnace with the thermocouple placed in the cell within 0.6 cm of the black body hole.

The validity of the calibrations was checked by measuring the vapor pressure of tin. Thirty-three tin datum points yielded an average third-law heat of sublimation of 72.0 kcal/mole, which is in good agreement with the values of 71.8 and 72.2 reported by Schulz¹¹ and Hultgren.¹²

Pairs of cells which had no orifices were loaded with lanthanum fluoride and the assembly was then heated to 1600°K to demonstrate the absence of significant leakage before effusion orifices were drilled into the cell end plates.

Each new sample was heated slowly to 1650°K

(6) A. W. Searcy and R. D. Freeman, *J. Am. Chem. Soc.*, **76**, 5229 (1954).

(7) D. J. Meschi and A. W. Searcy, *J. Phys. Chem.*, **63**, 1175 (1959).

(8) Z. A. Munir and A. W. Searcy, *J. Chem. Phys.*, **42**, 4223 (1965).

(9) R. D. Freeman and A. W. Searcy, *ibid.*, **22**, 762 (1954).

(10) R. D. Freeman, "Molecular Flow and the Effusion Process in the Measurement of Vapor Pressures," Part II, ASD-TDR-63-754, Oklahoma State University, 1963.

(11) D. A. Schulz, Ph.D. Thesis, University of California, Berkeley, Calif., 1961.

(12) R. Hultgren, R. L. Orr, P. D. Anderson, and K. K. Kelly, "Selected Values of Thermochemical Properties of Metals and Alloys," John Wiley and Sons, Inc., New York, N. Y., 1963.

Table II: Temperature Effusion Pressure, Ratio of Mean Free Path to Orifice Diameter, and the Third-Law Heat of Sublimation of LaF₃

Temp, °K	Pressure, atm	Mean free path/ diameter	$\Delta H^{\circ}_{298.15}$, kcal/mole	Temp, °K	Pressure, atm	Mean free path/ diameter	$\Delta H^{\circ}_{298.15}$, kcal/mole
0.10-cm Diameter Orifice				0.19-cm Diameter Orifice			
1540	3.65×10^{-5}	2.6	102.8	1437	2.92×10^{-6}	16	103.7
1559	5.48×10^{-6}	1.8	102.9	1466	7.72×10^{-6}	6.5	103.0
1582	8.91×10^{-5}	1.1	102.6	1487	1.046×10^{-5}	9.6	103.3
1577	7.82×10^{-5}	1.2	102.7	1435	2.84×10^{-6}	16.0	103.7
1579	8.26×10^{-5}	1.2	102.6	1496	1.287×10^{-5}	3.7	103.2
1578	8.32×10^{-6}	1.2	102.6	1497	1.287×10^{-5}	3.7	103.3
1599	1.175×10^{-4}	0.84	102.7	1512	1.624×10^{-5}	3.0	103.5
1615	1.623×10^{-4}	0.62	102.6	1408	1.433×10^{-6}	32	103.8
1640	2.52×10^{-4}	0.40	102.6	1393	1.053×10^{-6}	43	103.6
1638	2.41×10^{-4}	0.42	102.6	1418	1.815×10^{-6}	25	103.8
1595	9.53×10^{-5}	1.0	103.2	1441	3.32×10^{-6}	14	103.8
1622	1.616×10^{-4}	0.62	103.0	1445	3.85×10^{-6}	12	103.5
1601	1.034×10^{-4}	0.96	103.2	1462	6.09×10^{-6}	7.7	103.6
1609	1.184×10^{-4}	0.84	103.3	1481	8.64×10^{-6}	5.5	103.4
1619	1.536×10^{-4}	0.65	103.0	1496	1.320×10^{-5}	3.6	103.2
1582	7.37×10^{-5}	1.3	103.2	1506	1.320×10^{-5}	3.7	103.8
1562	4.77×10^{-5}	2.0	103.3	1489	9.61×10^{-6}	5.0	103.7
1572	6.17×10^{-5}	1.6	103.1	1474	8.19×10^{-6}	5.8	103.2
1560	4.20×10^{-5}	2.3	103.6	1455	5.23×10^{-6}	8.9	103.2
1540	3.05×10^{-5}	3.1	103.7	1436	3.17×10^{-6}	15	103.4
1444	3.53×10^{-6}	25.0	103.1	1423	2.33×10^{-6}	21	103.4
1472	7.38×10^{-6}	12.0	103.3	1474	6.61×10^{-6}	7.2	103.8
1500	1.257×10^{-6}	7.4	103.6	1388	1.001×10^{-6}	45	103.4
1521	2.01×10^{-6}	4.7	103.5	1394	1.173×10^{-6}	38	103.4
1535	2.87×10^{-6}	3.3	103.3	1423	2.03×10^{-6}	23	103.8
1566	5.89×10^{-6}	1.6	102.9	1431	2.43×10^{-6}	19	103.8
1605	1.162×10^{-4}	0.86	103.1	1402	1.395×10^{-6}	32	103.4
1528	2.50×10^{-6}	3.8	103.2	1443	3.75×10^{-6}	13	103.4
1552	4.31×10^{-6}	2.4	103.1	1453	4.08×10^{-6}	11	103.8
1557	4.31×10^{-6}	2.2	103.3	1459	5.00×10^{-6}	9.4	103.6
1562	5.05×10^{-6}	1.9	103.2	1469	5.83×10^{-6}	8.1	103.8
1582	7.16×10^{-6}	1.4	103.2	1479	7.74×10^{-6}	6.1	103.7
1604	1.064×10^{-6}	0.93	103.3	1498	1.137×10^{-6}	4.2	103.7
1631	1.925×10^{-6}	0.52	103.0	1470	7.94×10^{-6}	6.0	103.0
0.15-cm Diameter Orifice				0.26-cm Diameter Orifice			
1523	2.18×10^{-6}	2.8	103.3	1395	9.67×10^{-7}	34	104.0
1536	2.86×10^{-6}	2.2	103.3	1373	5.97×10^{-7}	53	103.8
1556	4.16×10^{-6}	1.5	103.4	1354	3.64×10^{-7}	86	103.7
1471	7.62×10^{-6}	7.8	103.2	1349	2.94×10^{-7}	107	104.0
1499	1.288×10^{-5}	4.7	103.4	1359	4.09×10^{-7}	77	103.8
1522	2.17×10^{-5}	2.8	103.3	1379	6.90×10^{-7}	46	103.8
1523	2.17×10^{-5}	2.8	103.4	1388	9.80×10^{-7}	33	103.5
1502	1.374×10^{-5}	4.4	103.4	1391	1.170×10^{-6}	28	103.2
1490	9.81×10^{-6}	6.1	103.7	1403	1.469×10^{-6}	22	103.4
1484	9.99×10^{-6}	6.0	103.2	1414	1.836×10^{-6}	18	103.5
1456	5.66×10^{-6}	10.4	103.1	1404	1.513×10^{-6}	22	103.3
0.19-cm Diameter Orifice				0.26-cm Diameter Orifice			
1389	1.108×10^{-6}	40	103.2	1369	5.70×10^{-7}	56	103.5
1386	8.98×10^{-7}	50	103.6	1354	3.94×10^{-7}	80	103.5
1380	6.74×10^{-7}	66	103.9	1347	3.11×10^{-7}	100	103.6
1403	1.214×10^{-6}	37	103.9	1368	5.37×10^{-7}	59	103.8
1413	1.810×10^{-6}	25	103.5	1381	7.02×10^{-7}	46	103.9
				1390	1.004×10^{-6}	32	103.5
				1403	1.251×10^{-6}	26	103.7
				1377	6.09×10^{-7}	53	104.0

Table II (Continued)

Temp, °K	Pressure, atm	Mean free path/ diameter	$\Delta H^{\circ}_{298-15}$, kcal/mole
0.34-cm Diameter Orifice			
1359	4.35×10^{-7}	55	103.6
1345	2.76×10^{-7}	85	103.8
1343	2.64×10^{-7}	89	103.8
1360	4.43×10^{-7}	54	103.7
1376	6.82×10^{-7}	35	103.6

and held at that temperature for 1 hr to vaporize volatile impurities. Data were then collected by making either random temperature changes of about 40° or by making smaller successive temperature increases or decreases. The background pressure for all measurements was between 1×10^{-9} and 7×10^{-9} atm.

To ensure that the pressure data were due to the vaporization of lanthanum fluoride only, samples of the original material, of a characteristic sublimate from heating at 1600°K, and of residue were analyzed spectrographically. The analyses performed by the American Spectrographic Laboratories showed lanthanum to be the principal metallic constituent in both starting material and sublimate. The principal impurity in the starting material was 0.015% iron. The sublimate contained 0.3% silicon (presumably from the quartz walls on which the sublimate was collected) and 0.03% iron as the principal metallic impurities.

The lanthanum fluoride crystal used in the Langmuir experiments was purchased from Nuclear Elements Corp. Weller and Kucza¹³ have reported easy basal cleavage, but it proved necessary to orient the crystals by the back-reflection Laue method before 1.5-mm slices could be made along the basal plane. Final polish was accomplished with 0.3- μ alumina grit in a kerosene medium.

III. Results and Discussion

The results of 100 Knudsen vapor-pressure determinations collected in the range 1340–1650°K are presented in Table II and Figure 1. The results of 21 free surface-pressure determinations are given in Table III and Figure 1. A least-squares fit of the effusion data yielded the equation

$$\log P_{\text{atm}} = -(2.173 \pm 0.009) \frac{10^4}{T} + 9.608 \pm 0.065 \quad (1)$$

where the errors are standard deviations.

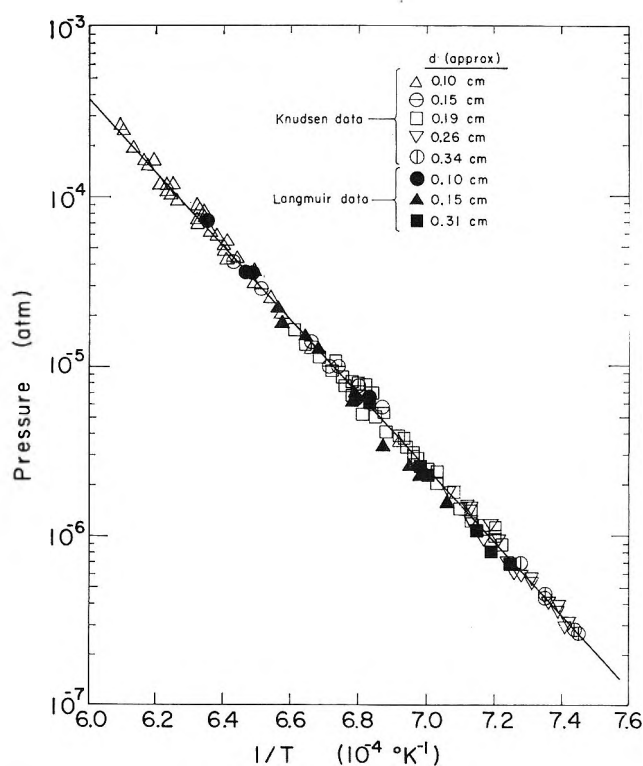


Figure 1. Vapor pressure of lanthanum fluoride.

The vapor was assumed to consist only of LaF_3 molecules. This is the molecule indicated to be the principal vapor species at 1300–1400°K by the mass spectrometric study of Kent, *et al.*³ Furthermore, thermodynamic calculations indicate that partial pressures of other species, LaF , LaF_2 , CF_4 , C_2F_4 , C_2F_6 , La , and F_2 , which might be produced by dissociation or reaction with carbon, should be negligible. The possibility that the vapor was $\text{H}_2\text{O}(\text{g})$ or lanthanum-oxygen products from a partially hydrated sample was eliminated by the 1-hr heat treatment at 1650°K. It has been shown that hydrated rare earth fluorides are completely dehydrated by such treatment.^{14,15}

Because it has been shown that too low a λ/d ratio implies the inapplicability of molecular flow equations,^{16,17} the ratio of the mean free path to the orifice diameter, λ/d , was calculated at all readings by means of a hard-sphere approximation¹⁸ with the sphere

(13) P. F. Weller and J. A. Kucza, *J. Appl. Phys.*, **35**, 1945 (1964).

(14) E. Staritsky and L. Asprey, *Anal. Chem.*, **29**, 855 (1957).

(15) L. P. Batsanova, G. N. Grigor'eva, and S. S. Batsonov, *Zh. Strukt. Khim.*, **4**, 37 (1963).

(16) D. A. Schulz and A. W. Searcy, *J. Chem. Phys.*, **38**, 772 (1963).

(17) K. O. Carlson, P. W. Gilles, and R. J. Thorn, *ibid.*, **38**, 2064 (1963).

(18) S. Dushman, "Scientific Foundations of Vacuum Technique," John Wiley and Sons, Inc., New York, N. Y., 1949.

radius taken as the sum of the experimental La-F distance¹⁹ and the fluoride ion radius. In this research, in which the lowest value of λ/d was 0.40, no indications of a significant change in flow characteristics with λ/d was observed.

Table III: Torsion-Langmuir Data for LaF₃

Orifice diam, mm	Temp, °K	Pressure, atm	Evapn coeff
1	1464	6.44×10^{-6}	1.12
	1471	6.44×10^{-6}	0.96
	1544	3.54×10^{-5}	1.07
	1542	3.56×10^{-5}	1.13
	1573	7.12×10^{-6}	1.07
2	1437	2.53×10^{-6}	0.84
	1504	1.510×10^{-6}	1.07
	1524	2.18×10^{-6}	0.98
	1520	1.751×10^{-5}	0.87
	1497	1.226×10^{-6}	1.00
	1472	6.83×10^{-6}	0.97
	1455	3.32×10^{-6}	0.71
	1432	2.25×10^{-6}	0.83
	1416	1.551×10^{-6}	0.85
	1474	6.22×10^{-6}	0.84
3	1378	6.78×10^{-7}	1.01
	1398	1.070×10^{-6}	0.70
	1428	2.24×10^{-6}	1.01
	1464	6.19×10^{-6}	1.08
	1432	2.53×10^{-6}	0.93
	1390	8.07×10^{-7}	0.85

The heat of sublimation was calculated from the effusion data by the second-law and third-law methods.²⁰ It was necessary to estimate heat capacities and free energy functions for both the solid and the gas.

The heat capacity of crystalline lanthanum fluoride was estimated to be $C_p = 19.77 + 8.48 \times 10^{-3}T - 4.90 \times 10^{-4}T^2$ cal/mole by assuming that the difference between the heat capacities of La₂O₃²¹ and 2(LaF₃) is the same as the difference between the heat capacities of Ce₂O₃²² and 2(CeF₃).²³

The La-F valence vibration in crystalline LaF₃ is reported to be 403 cm⁻¹.¹⁵ The La-F stretch frequency for gaseous LaF₃ was estimated to be 419 cm⁻¹ on the assumption that the ratio of the valence vibration frequency in the crystalline state to the stretch frequency in the gaseous state is the same as the ratio for AlF₃.²⁴ The stretching force constant for La-F bonds in the gaseous molecules is then calculated to be 1.96×10^6 dynes/cm. Lim and Searcy² have shown that for CeF₃ this means for estimating the force constant gives a result that differs by only 10% from

that calculated from an independent empirical equation formulated by Herschbach and Laurie.²⁵

Plots of the out-of-plane bend force constant $ln(k_2/l^2)$ and the in-plane bend force constant $ln(k_3/l^2)$, where l is the La-F distance, *vs.* k_1 for the constants of D_{3h} point group species show a straight line relationship. k_2/l^2 and k_3/l^2 for LaF₃ were assumed to fall on this line. These force constants were thus estimated to be 0.192×10^5 and 0.103×10^5 dynes/cm. Using the three force constants and the valence-force model,²⁶ the vibrational frequencies for LaF₃(g) were calculated to be 419, 156, 461(2), and 179(2) cm⁻¹.

The electronic contribution to the heat capacity was assumed to be the same as that of La³⁺ ion.²⁷ Brewer, *et al.*,²⁸ have shown that transition metal dihalides values so estimated are in reasonable agreement with known data. Heat capacities for the gas were calculated at 100° intervals from 300 to 1800°K and the equation, $C_p = 21.42 - 4.06 \times 10^{-4}T - 3.38 \times 10^{-5}T^2$ cal/mole, was fitted to the values.

The free energy functions for the crystalline state were calculated from the estimated heat capacity and Glassner's²⁹ estimate of $S^\circ_{298} = 27.0$ eu/mole. Glassner's entropy estimate for CeF₃ was only 0.04 eu smaller than the experimental value found by Westrum and Beale.³⁰ The probable error in the estimate of S°_{298} for LaF₃(s), 0.2 eu, could cause a 0.3-kcal/mole error in the calculated heat of sublimation. The estimated free energy functions for lanthanum fluoride between 1000 and 1800° are given in Table IV. The average

(19) P. A. Akishin and V. A. Naumor, *Chem. Abstr.*, **53**, 13, 702 (1959).

(20) G. N. Lewis, M. Randall, K. S. Pitzer, and L. Brewer, "Thermodynamics," McGraw-Hill Book Co., Inc., New York, N. Y., 1961.

(21) J. O. Blomoeke and W. T. Ziegler, *J. Am. Chem. Soc.*, **73**, 5099 (1951).

(22) F. A. Kuznetsov and T. N. Rezhukhina, *Zh. Fiz. Khim.*, **35**, 956 (1961).

(23) E. G. King and A. L. Christensen, U. S. Bureau of Mines Bulletin RI 6610, U. S. Government Printing Office, Washington, D. C., 1957.

(24) "JANAF Thermochemical Tables," Dow Chemical Co., Midland, Mich., 1963.

(25) D. R. Herschbach and V. Z. Laurie, *J. Chem. Phys.*, **35**, 458 (1961).

(26) G. Herzberg, "Molecular Spectra and Molecular Structure II, Infrared and Raman Spectra of Polyatomic Molecules," D. Van Nostrand Co., Inc., New York, N. Y., 1959.

(27) M. A. El'yashevich, "Spectra of the Rare Earths," Book II, AEC-tr-4403, 1961, The State Publishing House of Technical-Theoretical Literature, Moscow, 1953.

(28) L. Brewer, G. R. Somayajulu, and E. Brackett, *Chem. Rev.*, **63**, 111 (1963).

(29) A. Glassner, "The Thermochemical Properties of the Oxides, Fluorides, and Chlorides to 2500°K," Argonne National Laboratory, ANL-5750, 1957.

(30) E. F. Westrum, Jr., and A. F. Beale, Jr., *J. Phys. Chem.*, **65**, 353 (1961).

third-law value for the heat of sublimation over all datum points was 103.5 ± 0.4 , where the error is the standard deviation from the mean.

Table IV: Calculated Free Energy Functions for LaF_3

Temp, °K	$-(F^\circ T - H^\circ_{298})/T$ (s), cal/deg mole	$-(F^\circ T - H^\circ_{298})/T$ (g), cal/deg mole	$-(\Delta F^\circ T - \Delta H^\circ_{298})/T$ (sub), cal/deg mole
1000	38.972	87.411	48.439
1100	40.797	88.977	48.180
1200	42.355	90.073	47.718
1300	43.950	91.307	47.357
1400	45.486	92.475	46.989
1500	46.969	93.588	46.619
1600	48.400	94.650	46.250
1700	49.784	95.569	45.875
1800	51.129	96.622	45.493

The second-law data yielded $\Delta H^\circ_{298.15} = 107.5 \pm 0.4$ kcal/mole and $\Delta S^\circ_{298.15} = 53.2 \pm 0.3$ eu.

The major sources of error in calculated heats of sublimation by the third-law method were the estimations of the free energy functions. Because experimental data are unavailable for $\text{LaF}_3(\text{g})$ and for similar molecules, the possible errors are difficult to assess. If errors of 10% in the vibrational frequencies, 5% in the molecular radius, and 15% in the electronic contribution to the free energy function are assumed, an error of 1% in the gaseous free energy function is calculated to result. Assuming the solid heat capacity and S°_{298} to be in error by 1 cal/mole and 0.2 eu/mole leads to an error of 2.0% of the solid free energy function. Errors in calibrating the wire, measuring the orifice diameter, channel length, and axis arms, and reading the angles of deflection could cause an error of about 0.5% in ΔH°_{298} . The temperatures are believed to be correct to within $\pm 5^\circ$. An error of $\pm 5^\circ$ causes an error of $\pm 0.5\%$ in the heat of sublimation. The effect of all these estimated errors is an uncertainty in the third-law heat of sublimation of ± 4 kcal/mole.

The estimated errors in the molecular constants cause a 0.2-cal/mole error in the gaseous heat capacity. An assumed error of 1 cal/mole in the heat capacity for the solid causes an uncertainty of ± 0.5 kcal/mole in the second-law heat of sublimation. The assumption that the temperature scale was in error by -5° at the lower end of the experimental range and by $+5^\circ$ at the high end causes an error of -3 kcal in ΔH°_{298} . The second-law heat of sublimation is therefore estimated to be accurate to within ± 4 kcal/mole.

This error analysis leads to the same estimated uncertainty in the heats derived by the two methods.

But we cannot be certain that the errors in estimation of thermochemical data have not been seriously underestimated. Second-law calculations are insensitive to errors in estimates of these data. In these circumstances the second-law analysis should probably be given principal weight in fixing $\Delta H^\circ_{298.15}$ as 107 ± 4 kcal.

The sublimation pressures for lanthanum fluoride measured recently by Kent, *et al.*,³ lie about a factor of two below pressures reported in this paper. Kent, *et al.*, used Langmuir weight-loss measurements and mass spectrometric measurements calibrated by use of the Langmuir weight-loss data. Discrepancies of about a factor of two have also been noted between data for CaF_2 and BaF_2 collected in Margrave's laboratory^{31,32} and data of Schulz and Searcy¹⁶ and Hart and Searcy.³³ A temperature-independent error of a factor of two in pressure determinations would contribute about a 2-kcal error to a third-law heat of sublimation for lanthanum fluoride and negligible error to a second-law heat of sublimation.

The uncertainty in the determination of the evaporation coefficient was greatly reduced by collecting the equilibrium pressure data and the free surface sublimation data in the same apparatus by the same techniques so that most systematic errors in pressure determinations would be common to both sets of data and would cancel in calculations of the coefficient. It is seen on Figure 1 that the torsion-Langmuir data are in very close agreement with the effusion data. Comparison of the Langmuir pressures with the equilibrium pressures given by eq 1 shows no significant temperature dependence of the evaporation coefficient and yields a coefficient of 0.95 ± 0.12 , the error being the standard deviation from the mean. The estimated experimental error in the determination of the evaporation coefficient is ± 0.1 and is attributed primarily to a $\pm 5^\circ$ uncertainty in the surface temperature of the lanthanum fluoride crystal relative to the temperature in an effusion cell.

A microscopic examination of the evaporated Langmuir surfaces showed them to be essentially planar but irregular. The 1-mm surfaces were flat with no surface irregularities. The 1.5-mm surfaces consisted of about 40% flat areas and 60% mountain-shaped features that averaged $1.5 \times 10^4 \mu^2$ in basal area and 50μ in height. The 3-mm surfaces were planar with a fine network of surface irregularities

(31) G. D. Blue, T. C. Ehlert, J. W. Green, and J. L. Margrave, *J. Chem. Phys.*, **41**, 2245 (1964).

(32) G. D. Blue, J. W. Green, R. G. Bautista, and J. L. Margrave, *J. Phys. Chem.*, **67**, 877 (1963).

(33) P. E. Hart and A. W. Searcy, *ibid.*, in press.

estimated to be about 10μ in height. For evaporation from the (0001) plane of lanthanum fluoride, the difference between the apparent evaporation coefficient (that measured without correction for surface irregularities) and the true evaporation coefficient is probably less than 1%.

To determine if the apparent pressures from a given area of surface changed measurably as the surface receded during evaporation, data were collected with the 1-mm orifice until a recess 1 mm deep formed. No change in the pressure-temperature relationship was observed as the cavity deepened. This fact further substantiates the conclusion that the evaporation coefficient is near unity. If the coefficient were much less than unity, the Langmuir pressures would have increased noticeably with time because the deepening cavity would provide an increasingly close approximation to an effusion cell.

We conclude that the evaporation coefficient for the (0001) plane of lanthanum fluoride is unity to within a small probable error and that evaporation coeffi-

cients for other trifluorides of lanthanide and main group three elements are probably close to unity as well.

Burns³⁴ has recently reported convincing evidence that the evaporation coefficients for the various vapor species from solid Al_2O_3 , solid Ga_2O_3 , and solid In_2O_3 approach one-third as a limiting value at the melting point. He points out that Hirth and Pound³⁵ have predicted that surface diffusion would set an upper limit of $\alpha = 1/3$ for single crystals of metals, and he draws attention to the fact that several other studies in addition to his own support the hypothesis that a similar limit may apply to many inorganic solids. The present research and the recent study of barium fluoride sublimation³³ demonstrate that no such limit applies for some inorganic solids. Further study is needed to ascertain why for some inorganic solids the evaporation coefficient may be unity over a considerable temperature range and for others it does not reach unity in a realizable temperature range.

(34) R. P. Burns, *J. Chem. Phys.*, **44**, 3307 (1966).

(35) J. P. Hirth and G. M. Pound, *ibid.*, **26**, 1216 (1957).

Specific Heats of Nematic, Smectic, and Cholesteric Liquid Crystals by Differential Scanning Calorimetry¹

by Edward M. Barrall, II, Roger S. Porter, and Julian F. Johnson

Chevron Research Company, Richmond, California (Received August 19, 1966)

Differential scanning calorimetry has been applied to the study of three pure compounds exhibiting liquid crystal or mesophase behavior. The compounds were *p*-azoxyanisole, anisaldazine, and cholesteryl myristate. The first two compounds exhibit a single mesophase of the nematic type, and the last compound forms both a smectic and a cholesteric-type mesophase. The three basic types of mesophases are thus evaluated in this study of specific heats. Measurements were made in the temperature ranges for the crystalline solid, the mesophase, and the corresponding isotropic liquid. Specific heats were also measured on supercooled phases and at temperatures close to the first-order mesophase transitions. The measurements on *p*-azoxyanisole compare well with previous literature values. Specific heat measurements on cholesteryl esters have not been presented heretofore. The results on the three basic mesophase types are intercompared.

A group of organic compounds designated as "liquid crystal"² materials have the unusual property of exhibiting one or more phases or mesophases which are liquid in mobility yet solid in structure. This is accomplished by having crystal-like order in one or more directions and liquid-like disorder in the other spatial orientations. In excess of 1500 compounds are known to exhibit liquid crystal properties.³⁻⁶ The various liquid crystal phases which exist between true solid and isotropic liquid, *viz.*, mesophases, are classified as smectic, nematic, and cholesteric. Briefly, the smectic mesophase is characterized by having the molecules stratified, *i.e.*, arranged in layers with long axes approximately normal to the plane of the layers. The molecules can move in two directions (in plane) and rotate in plane. The nematic structure is somewhat less restricted. The molecules are arranged parallel to one another. Movement can occur in three directions, and rotation in one. The cholesteric mesophase is exhibited principally by the esters of cholesterol and is due to the helical stacking of the cholesterol plates. The plates in each layer of the mesophase are displaced from the next layer by a small amount due to the ester tail and the 4-hydrogen which leads to a helical stacking order. The cholesteric mesophase

is exhibited by cholestane or cholestene derivatives only when rings A and B are in the *trans* configuration.

Surprisingly few thermodynamic data are available on these basic types of mesophases. Until recently,⁷ only one heat of transition had been reported for a cholesteryl ester, by Hulett for cholesteryl benzoate,^{3a} and less than a dozen transition heats were known⁸⁻¹² for all other liquid crystal systems. Specific heat data determined by a direct method were nonexistent until

- (1) Part X of a series on order and flow of liquid crystals.
- (2) O. Lehmann, *Z. Physik. Chem.*, **5**, 427 (1890).
- (3) (a) G. H. Brown and W. G. Shaw, *Chem. Rev.*, **57**, 1049 (1957);
(b) V. A. Usol'tseva and I. G. Chistyakov, *Russ. Chem. Rev.*, **32**, 495 (1963).
- (4) R. vonBrauns, "Flüssige Kristalle und Lebewesen," Schweizerbartische Verlagsgesellschaft, Stuttgart, 1931.
- (5) D. Vorländer, *Ber.*, **41**, 2033 (1908).
- (6) W. Kast, *Angew. Chem.*, **67**, 592 (1955).
- (7) E. M. Barrall, R. S. Porter, and J. F. Johnson, "Heats of Transition of Some Cholesteryl Esters," to be published.
- (8) E. M. Barrall, R. S. Porter, and J. F. Johnson, *J. Phys. Chem.*, **68**, 2810 (1964).
- (9) H. Martin and F. H. Müller, *Kolloid-Z.*, **187**, 107 (1963).
- (10) R. Schenck, "Kristalline Flüssigkeiten und Flüssige Kristalle," Leipzig, 1905, pp 84-89.
- (11) K. Kreutzer, *Ann. Physik*, (5) **33**, 192 (1938).
- (12) K. Kreutzer and W. Kast, *Naturwissenschaften*, **25**, 233 (1937).

Arnold's study of homologous dialkoxyazobenzoates.^{13,14}

Recently, a differential scanning calorimetric (dsc) method has been developed for the rapid, direct measurement of specific heat.¹⁵ Since the method is continuously recording, it is possible to determine the specific heat of a phase over a very narrow, defined temperature range within the limits of a dynamic method. Such a method is ideal for the initial study of liquid crystals which are noted for pretransitional effects in narrow temperature intervals on each side of first-order mesophase transitions.^{2,7}

This new technique is further substantiated by a direct correlation of data with those obtained by classic calorimetry. In this study, the specific heats measured on *p*-azoxyanisole (PAA) by dsc are compared with Arnold's measurements obtained by classical calorimetry in the same temperature range.¹⁴ In addition, the specific heats of anisaldazine (AAD) and cholesteryl myristate (CM) are also developed over a wide temperature range using dsc. These measurements constitute the first determination of the specific heat of a cholesteric mesophase. The thermodynamic reversibility and identity of mesophase formation from cooled melt and from heated solid is also explored.

Classical thermodynamics, which disregards statistical considerations, treats crystals and liquids as completely independent entities. This gives no basis for either expecting or predicting pretransitional effects. However, calculation of pretransitional anomalies by the theories of cooperative fluctuations predict some temperature effects on both sides of first-order transitions. The parameter controlling the magnitude of the observed effects is the interfacial energy.¹⁶ This parameter is difficult to estimate exactly. However, it is reasonable to estimate that the interfacial energy will be small for liquid crystal transitions due to the small size of the heat of transformation. This should and does lead to large pretransitional effects as reported in the following results. Transition temperatures and heats for the three compounds studied are compiled in Table I.

Experimental Section

The origin and purification of the liquid crystal materials has been discussed in detail in previous works.^{7,8,17} Briefly, PAA and AAD were obtained from Eastman Organic Chemicals, Rochester, N. Y., and the CM was obtained in a highly purified form from Applied Science Laboratories, State College, Pa. All materials were recrystallized from ethanol three times. Carbon-hydrogen and spectrophotometric analyses indicated a purity of better than 99.9%,^{8,17} the acid

Table I: Transition Temperatures and Heats for Mesophase Systems

	Transition temp, °C ^a	Transition heat, cal/g
<i>p</i> -Azoxyanisole		
Solid-nematic	117.6	28.1 ± 0.9
Nematic-isotropic	133.9	0.68 ± 0.02
Anisaldazine		
Solid-nematic	168.9	26.5 ± 0.5
Nematic-isotropic	180.5	0.59 ± 0.02
Cholesteryl myristate		
Solid-smectic	73.6	18.7
Smectic-cholesteric	79.7	0.52
Cholesteric-isotropic	85.5	0.41

^a By differential thermal analysis.

chloride and cholesterol reactant content being used as an index of purity.

The scanning calorimeter (Perkin-Elmer Model DSC 1-B) was calibrated using a 0.03-g sapphire standard plate supplied for this purpose by the Perkin-Elmer Co. The detailed technique of calibration has been given in full by Wunderlich.¹⁸ A useful description of the experimental details is available from the Perkin-Elmer Co.¹⁹ The sapphire specific heat data used for calibration were obtained from the work of Ginnings and Furukawa.²⁰ All calculations were carried out using a computer program developed at Chevron Research Co. Measurements of programmed base line displacement were made with a precision vernier rule at 2° intervals. Specific heats were calculated at 0.5° intervals for the smectic mesophase and the isotropic liquid range. A 10°/min heating rate was used to cover the full temperature range of heat capacity measurements on all compounds. Detailed studies over narrow temperature ranges near transitions were carried out at a 5°/min heating rate. Intervals of 30–40° were taken between reference base line determinations. All samples were contained within sealed planchettes which were weighed before

(13) H. Arnold, *Z. Chem.*, **6**, 211 (1964).

(14) H. Arnold, *Z. Physik. Chem.*, **226**, 146 (1964).

(15) A. P. Gray and N. Brenner, *Polymer Preprints*, **6**, 956 (1965).

(16) R. R. Ubbelohde, "Melting and Crystal Structure," Clarendon Press, Oxford, 1965, pp 68, 243.

(17) E. M. Barrall, R. S. Porter, and J. F. Johnson, *J. Phys. Chem.*, **70**, 385 (1966).

(18) B. Wunderlich, *ibid.*, **69**, 2078 (1965).

(19) Thermal Analysis News Letter No. 3, Perkin-Elmer Co., Norwalk, Conn., 1965, p 1.

(20) D. C. Ginnings and G. T. Furukawa, *J. Am. Chem. Soc.*, **75**, 522 (1953).

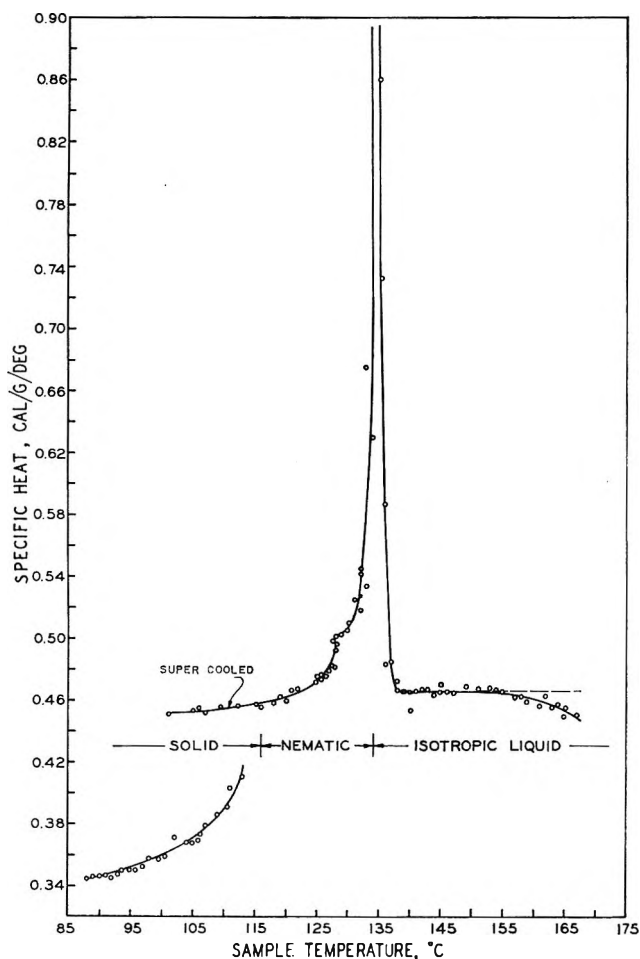


Figure 1. Specific heat of *p*-azoxyanisole from 87 to 167°.

and after each run. No weight losses were noted except in the case of PAA. Each data point shown represents an average of three points measured in each of three separate experiments. The average deviation was $\pm 3\%$. In some cases the error increased to $\pm 6\%$ near sharp transitions due to nonequilibrium conditions. Vertices of known transition peaks are not shown since these became indefinitely large, >10 cal/g deg.

Results

p-Azoxyanisole (PAA). A single, nematic liquid crystal phase is reported for PAA.^{8,9,14} The transition heat from solid to nematic phase is large, 28.8 cal/g at 117.6°. The transition from the nematic to isotropic liquid is small, 0.68 cal/g at 133.9°.^{8,9} The transition heats and temperatures were determined by dta on pure PAA. Two determinations of specific heat on this compound have been made: by Arnold¹⁴ using classical calorimetric techniques, and by Martin and Müller using differential thermal analysis (dta).⁹

Agreement between Arnold's data and Figure 1 is excellent within the stated error limits of the two methods except in the low temperature limit where values obtained here are about 3% lower than given by Arnold. (See Table II.) One earlier set of data also gave lower specific heats for this crystalline region. (See ref 10.) The data of Arnold reportedly have a high precision of $\pm 0.3\%$. The isotropic liquid phase relationship dips down above 155° due to a small vaporization of sample, noted earlier. The dashed line in Figure 1 represents extrapolated heat capacity data.

Table II: Comparison of Literature and Scanning Calorimetry Values for the Heat Capacity of *p*-Azoxyanisole

Temp, °C	Heat capacity, cal/g deg		Phase
	Lit. ¹⁴	This work	
95	0.3631	0.3520	Solid
100	0.3688	0.3595	
105	0.3762	0.3700	
110	0.3949	0.3895	
113	0.4359	0.4295	
110	0.4524	0.4549	Nematic
115	0.4596	0.4575	
118.2	0.4647	0.4600	
120	0.4682	0.4620	
125.5	0.4792	0.4740	
127	0.4853	0.4795	
128	0.4894	0.4842	
129	0.4934	0.4925	Isotropic liquid
130	0.4986	0.4970	
131	0.5058	0.5120	
137	0.4756	0.4850	
138	0.4734	0.4680	
140	0.4712	0.4650	
142	0.4701	0.4658	
144	0.4897	0.4660	
146	0.4696	0.4660	
148	0.4697	0.4662	
150	0.4698	0.4668	

The transition from solid to the nematic mesophase is characterized by a gradual upward sweep of the specific heat prior to sharp transition; that is, the curve for the solid phase approaches infinity at temperatures just above 112.5°. This type of curve has been described by Westrum and McCullough as either a type 2I or a type 3I transition.²¹ It was impossible to measure the descending portion of the specific heat curve just above the solid-nematic transition

(21) E. F. Westrum and J. P. McCullough, "Physics and Chemistry of the Organic Solid State," D. Fox, M. M. Labes, and A. Weissberger, Ed., Interscience Publishers Inc., New York, N. Y., 1963, p 40 ff.

with sufficient precision to determine if the transformation is truly isothermal at the finish. Therefore, further separations of the transition by empirical type are difficult. However, since the purity of the PAA is known to exceed 99.9%, it is difficult to assign the 2I transition type, which is supposed to be characteristic of the melting of an impure compound.²¹ Premelting molecular rotation in the solid phase seems more likely. The size and shape of nematic aggregates may also change near the transition so that there may be a minor order and entropy change in the pretransition range. This places the solid-nematic transition in the 3I category with the higher normal paraffins. Since the PAA molecules are approximately rod-shaped about a flat benzene plane, such a rotational adjustment on the basis of molecular geometry is to be expected.

Several workers have observed thermal changes in the nematic phase prior to the nematic-isotropic liquid transition.^{9,14} Martin and Müller⁹ reported a pretransition between 128 and 132° (the 132° temperature being taken as the clarification temperature of the melt). This corresponds to the possible break and gently upward sweeping portion of the specific heat curve found in this study (see Figure 1 between 128 and 134.4°). The sharp break at 128° is comparable to a simple first-order melting range transition, classified type I.²¹ The portion of the nematic specific heat between 128 and 134.4° appears to be reproducible and stable. This section of the curve was repeated on heating and cooling four times on different samples with identical results and no supercooling or superheating. The resolution of this mesophase region is not evident on dta curves of normal resolution.⁸ The only other evidence for existence other than the present work is given by Martin and Müller.⁹ Arnold¹⁴ observed a change in his values but discounted the data. Since this minor anomaly has been observed by at least three independent workers, it is apparently not a calorimetric artifact. However, specific volume, viscosity, and surface tension measurements in this range do not show a distinguishable anomaly.^{2,22,23}

An attempt was made to determine if the specific heat of the nematic mesophase formed by cooling the isotropic liquid was identical with that formed by heating the crystalline solid. The melt was cooled to 107° and heated, as previously described, to 121°. In a second experiment, the solid phase was heated into the nematic region, cooled to 107°, and heated to 121°. The results are shown in Figure 2. Within the limits of experimental error, the nematic mesophase structure of PAA formed from the solid and from the isotropic liquid are identical and readily

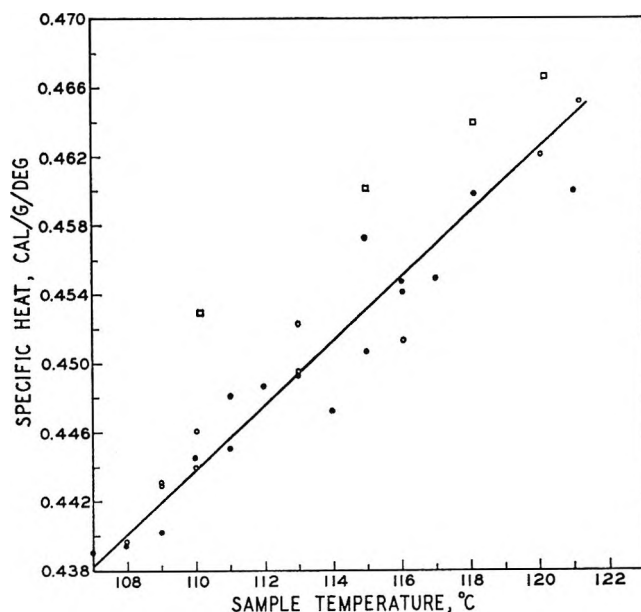


Figure 2. *p*-Azoxyanisole nematic mesophase: O, formed from the solid; ●, from the liquid; □, Arnold's data.¹⁴

reversible. Actual cooling curves were not employed because of instrumental difficulties.

Anisaldazine (AAD). The specific heat-temperature relationships of AAD (see Figure 3) are simpler than those observed for PAA. Both the solid-nematic and the nematic-isotropic liquid show premelting specific heat changes. They belong to the type 2I or 3I transitions of Westrum and McCullough.²¹ Premelting or pretransition chain rotation and adjustment are prominent features in both dta⁹ and depolarized light intensity²⁴ studies of AAD. Data in the range of the nematic-isotropic liquid transition from 187 to 200° identifies it empirically as a type 3I nonisothermal chain rotation. The shape of such specific heat curves has been compared to the Greek capital Λ and referred to as Λ -type transitions. The general findings, consistent with these results, indicate that Λ -type transitions arise when the differences are small between the structures undergoing the transition.¹⁶

No evidence was found for two nematic mesophases in AAD. The steep premelting slope of the nematic specific heat-temperature relationship could mask the kind of step observed for PAA. Specific heat measurements have not been reported heretofore on AAD. The results in combination with data on PAA

(22) W. A. Hoyer and A. W. Nolle, *J. Chem. Phys.*, **24**, 803 (1956).

(23) R. S. Porter and J. F. Johnson, *J. Appl. Phys.*, **34**, 55 (1963).

(24) E. M. Barrall and E. J. Gallegos, "Depolarized Light and Differential Thermal Analyses of Some Polyolefin Transitions," *J. Polymer Sci.*, in press.

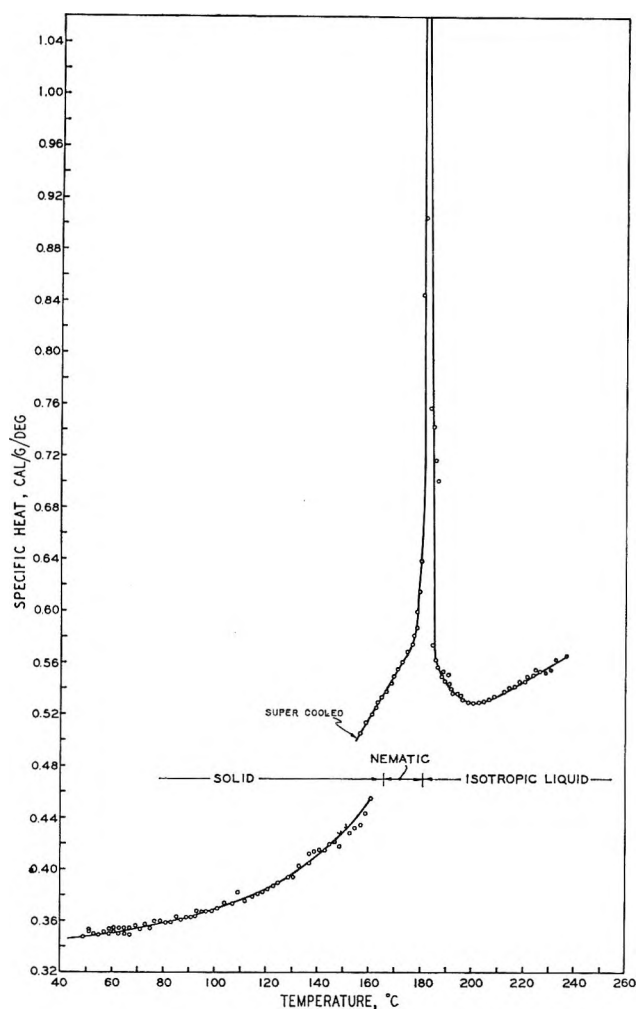


Figure 3. Specific heat of anisaldazine from 47 to 237°.

help to establish the general calorimetric characteristics of nematic mesophases.

Cholesteryl Myristate (CM). The specific heat-temperature relationship of CM, Figure 4, is noteworthy for the broad transition near ambient temperature and the steep slope of the specific heat curve prior to the solid-smectic transition. The broad transition fits the type H transition of Westrum and McCullough.²¹ The example chosen as typical by those authors was 1,2-dichloroethane at -93°. These broad transitions are easily moved on the temperature axis by rapidly cooling the sample from room temperature. The dashed line in Figure 4 shows the effect of rapidly cooling the solid phase to -60° and then heating. The solid line was obtained by slow cooling, refrigerating, and then heating.

Depolarized light studies have indicated that a large amount of structural adjustment occurs on heating prior to the solid-smectic transition.²⁵ The solid-smectic

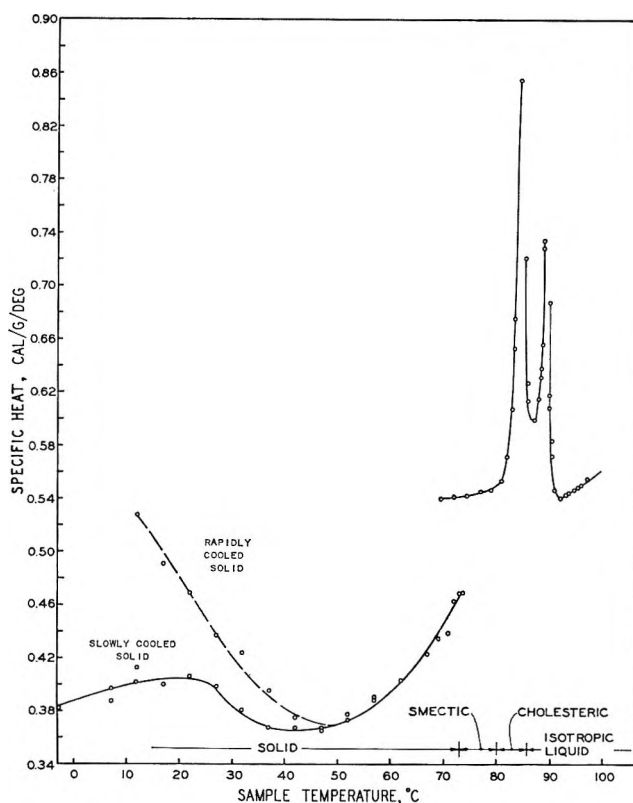


Figure 4. Specific heat of cholesteryl myristate from -3 to 97°.

transition belongs normally to type 3I. The smectic specific heat is almost identical with that of the isotropic liquid. However, it was difficult to supercool the smectic phase into the solid temperature range by more than 20°, so that only a short smectic specific heat curve could be obtained. The slope of the smectic curve is comparable to that expected for a true solid. The specific heat values are approximately the same for the smectic and solid phases for MC as for the previously discussed nematic systems. The transition from smectic to cholesteric mesophase appears to be a type 3I transition as have been the other liquid crystal transitions discussed in this work.

Figure 5 shows higher resolution data (5°/min heating rate) for the smectic to isotropic liquid interval for CM. The cholesteric mesophase has a higher apparent specific heat than either the smectic or isotropic liquid. The cholesteric mesophase is a thermally stable mesophase. However, the temperature interval of stability is extremely narrow, and its specific heat curve is continuously changing in slope. Since the smectic-

(25) E. M. Barrall, R. S. Porter, and J. F. Johnson, *Mol. Cryst.*, in press.

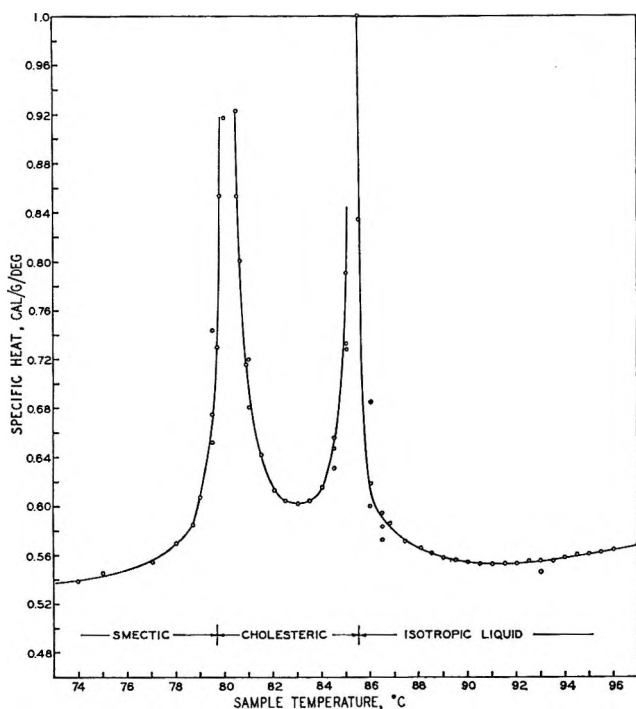


Figure 5. Specific heat of cholesteryl myristate in the liquid crystal and isotropic liquid ranges.

cholesteric and the cholesteric-isotropic transitions are completely reversible with little supercooling, a more detailed study of the cholesteric mesophase specific heat over a broader temperature range has been impossible. It is not surprising that the duration of the mesophase is so narrow, since only a few tenths of a calorie separate it from the two neighboring phases.⁷

No evidence of two cholesteric mesophases is apparent in the heat capacity data. Studies using optical microscopy, depolarized light intensity, and dta have suggested two transitions in the cholesteryl mesophase.²⁵ It is possible that the specific heat differences between two possible modifications of the cholesteryl helix may be too small to detect by the present calorimetric methods.

Discussion

The specific heat curves of nematic, smectic, and cholesteric types of liquid crystals indicate that the transitions from solid to nematic or smectic as well as interphase transitions are not simple first-order phase changes. Using the classification system set up by Westrum and McCullough,²¹ it appears that most of the transitions are either type 2I or 3I. The pre-melting phase transition of PAA reported from other studies^{9,14} has been noted as a sharp step in the present work. The significance of the type 3I or 2I transitions structurally is that the phase changes proceed through chain rotation comparable to that observed prior to the true melting of the higher *n*-paraffins.

In addition to the liquid crystal transitions, CM exhibits a movable type H transition near 0°. This transition is indicative of an intercrystal adjustment of the kind observed for 1,2-dichloroethane and certain simple metal chelates. This is probably a consequence of the platelike structure of the crystal.

Further work is in progress on the specific heat-temperature relationships of more complex cholesteryl liquid crystals.

Activity Coefficients for the System Water- α -Amino-*n*-butyric Acid-Urea

by E. L. Cussler, Jr.¹

Department of Physical and Inorganic Chemistry, University of Adelaide, Adelaide, South Australia
(Received August 19, 1966)

Isopiestic vapor pressure measurements at 25° are reported for the system water- α -amino-*n*-butyric acid-urea. The concentration varied from 0 to 2 *m* for the amino acid and from 0 to 9 *m* for urea. The results for dilute solutions are discussed in terms of a model which includes hydrophobic bonding of the amino acid, dimerization of urea, and the effect of urea on the acid dimerization. A method for obtaining a series expression for the water activity assuming an arbitrary model is summarized.

When amino acids are dissolved in water, they show a large excess free energy, indicating that they change the structure of the surrounding water.²⁻⁴ Osmotic coefficients of amino acid solutions show evidence both of these changes and of association between solute molecules.⁵⁻⁷ Both the zwitterion and the hydrocarbon residue contribute to these effects. The zwitterion is thought to increase the density of the surrounding water;² the hydrocarbon residue has a similar effect.⁸⁻¹⁰ At higher solute concentrations the hydrocarbon residues may associate, forming hydrophobic bonds, but the state of the zwitterion is substantially unchanged. Such association decreases the contact of the solute with the surrounding water. The addition of urea to solutions of this type increases the solubility of amino acids based on large hydrocarbon residues, but decreases the solubility of those based on methyl and ethyl groups.^{11,12} Urea decreases hydrophobic bonding of acids based on larger hydrocarbon residues, possibly by creating large interstitial sites in the water structure.¹³ This paper applies these ideas to isopiestic vapor pressure measurements on the system α -amino-*n*-butyric acid-urea-water. This amino acid was chosen because in binary solutions its chemical potential shows the large negative deviations from Raoult's law typical of amino acids with larger hydrocarbon residues.⁷ However, it is sufficiently soluble to allow study over a moderate range of concentrations.

Experimental Section

The α -amino-*n*-butyric acid, urea, and sodium chloride samples have been described previously.^{7,14} Portions of the samples which were recrystallized in

additional time were indistinguishable by the isopiestic method from the samples which were used in this study. The water was doubly distilled. All solutions were prepared by weight and corrected to vacuum using densities of 1.231, 1.330, and 2.165 g/cm³ and molecular weights of 103.122, 60.058, and 58.443 for α -amino-*n*-butyric acid, urea, and sodium chloride, respectively.

Vapor pressure measurements were made by the isopiestic method, for which the apparatus and general experimental procedure have been described previously.¹⁴ In most experiments, 22 dishes were equilibrated simultaneously for at least 7 days. While the reference solute was present in quadruplicate, the amino

(1) To whom all correspondence should be addressed at Department of Chemistry, Yale University, New Haven, Conn.

(2) E. J. Cohn and J. T. Edsall, "Proteins, Amino Acids, and Peptides," Reinhold Publishing Corp., New York, N. Y., 1943, p 157 ff.

(3) H. S. Frank and M. W. Evans, *J. Chem. Phys.*, **13**, 507 (1945).

(4) H. S. Frank and W.-Y. Wen, *Discussions Faraday Soc.*, **24**, 133 (1957).

(5) E. R. B. Smith and P. K. Smith, *J. Biol. Chem.*, **117**, 209 (1937); *ibid.*, **121**, 607 (1937); *ibid.*, **135**, 273 (1940).

(6) R. A. Robinson, *ibid.*, **199**, 71 (1952).

(7) H. D. Ellerton, G. Reinfelds, D. E. Mulcahy, and P. J. Dunlop, *J. Phys. Chem.*, **68**, 398 (1964).

(8) W. Kauzmann, *Advan. Protein Chem.*, **14**, 1 (1959).

(9) G. Némethy and H. A. Scheraga, *J. Chem. Phys.*, **36**, 3401 (1962).

(10) G. Némethy and H. A. Scheraga, *J. Phys. Chem.*, **66**, 1173 (1962).

(11) Y. Nozaki and C. Tanford, *J. Biol. Chem.*, **238**, 4074 (1963).

(12) G. C. Kresheck and L. Benjamin, *J. Phys. Chem.*, **68**, 2476 (1964).

(13) M. Abu-Hamdiyyah, *ibid.*, **69**, 2720 (1965).

(14) H. D. Ellerton and P. J. Dunlop, *ibid.*, **70**, 1831 (1966). Δ is found from eq 11.

Table I: Ternary Isopiestic Data at 25° for the System Water- α -Amino-*n*-butyric Acid-Urea^a

m_R	m_A	m_U	$-\Delta_{\text{exptl}}/m_A m_U$	$-\Delta_{\text{calcd}}/m_A m_U$	$\delta, \%$	m_R	m_A	m_U	$-\Delta_{\text{exptl}}/m_A m_U$	$-\Delta_{\text{calcd}}/m_A m_U$	$\delta, \%$
0.26931	0.24416	0.25625	0.0430	0.0424	0.01	2.2459	0.22890	4.8749	0.0200	0.0155	0.06
0.51996	0.14955	0.84070	0.0436	0.0400	0.04		0.50743	4.5581	0.0224	0.0201	0.08
	0.28574	0.69771	0.0426	0.0402	0.04		0.79715	4.2135	0.0220	0.0239	-0.11
	0.44266	0.53298	0.0500	0.0407	0.17		1.1399	3.8019	0.0235	0.0269	-0.19
	0.53124	0.43853	0.0422	0.0409	0.04		1.5283	3.3197	0.0250	0.0280	-0.22
	0.65789	0.30049	0.0488	0.0409	0.14		1.8616	2.8915	0.0261	0.0276	-0.13
	0.80160	0.14418	0.0489	0.0407	0.06	2.3774	0.54445	4.8908	0.0217	0.0184	0.10
0.69366	0.16459	1.1750	0.0369	0.0378	-0.01		0.85526	4.5207	0.0219	0.0226	-0.03
	0.40557	0.91808	0.0425	0.0391	0.09		1.2210	4.0727	0.0226	0.0259	-0.19
	0.88037	0.39760	0.0341	0.0394	-0.10		1.6370	3.5557	0.0249	0.0272	-0.20
	1.0920	0.16022	0.0346	0.0386	-0.04		1.9918	3.0936	0.0260	0.0264	-0.05
0.84535	0.20338	1.4518	0.0377	0.0364	0.01	2.4534	0.20532	5.5004	0.0173	0.0107	0.34
	0.50014	1.1322	0.0340	0.0380	0.10		0.48890	5.1663	0.0176	0.0162	0.07
	0.78171	0.82251	0.0377	0.0386	-0.05		1.0734	4.4744	0.0217	0.0238	-0.16
	1.0775	0.48662	0.0375	0.0379	0.00		1.8145	3.5436	0.0248	0.0266	-0.22
	1.3295	0.19506	0.0379	0.0365	0.01	2.5509	0.21550	5.7730	0.0181	0.0088	0.18
1.0532	1.0138	1.0104	0.0428	0.0369	0.20		0.51355	5.4269	0.0197	0.0147	0.25
1.0542	0.92480	1.1040	0.0330	0.0370	-0.18		0.84905	5.0411	0.0232	0.0198	0.28
	1.4490	0.48930	0.0337	0.0348	-0.03		1.4958	4.2382	0.0240	0.0254	-0.18
	1.6936	0.19440	0.0299	0.0325	-0.11		1.9029	3.7160	0.0257	0.0258	-0.01
1.0544	0.27138	1.8341	0.0308	0.0345	-0.08	2.8937	0.15373	6.9083	0.0013	-0.0010	0.27
	0.62643	1.4438	0.0334	0.0366	-0.09		0.47247	6.5288	0.0123	0.0067	0.30
	1.1969	0.79311	0.0378	0.0363	0.05		0.76803	6.1791	0.0161	0.0125	0.28
	1.4515	0.49060	0.0381	0.0348	0.14		1.2931	5.5310	0.0187	0.0199	-0.15
	1.6949	0.19455	0.0335	0.0324	0.08		1.5737	5.1799	0.0204	0.0222	-0.21
1.2415	0.26932	2.2603	0.0328	0.0321	0.03		2.3531	4.1523	0.0236	0.0226	-0.12
	0.48002	2.0234	0.0287	0.0339	-0.20	3.0134	0.16204	7.2819	-0.0062	-0.0040	-0.02
	0.73328	1.7418	0.0324	0.0352	-0.12		0.49795	6.8809	0.0102	0.0045	0.29
	0.90809	1.5391	0.0316	0.0356	-0.20		0.80940	6.5119	0.0151	0.0108	0.32
	1.1713	1.2339	0.0341	0.0354	-0.05		1.3616	5.8239	0.0179	0.0189	-0.12
	1.3896	0.97445	0.0356	0.0345	0.04		1.6562	5.4515	0.0196	0.0214	-0.21
1.4046	0.30965	2.5987	0.0322	0.0304	0.05		2.4748	4.3670	0.0234	0.0215	-0.23
	0.55250	2.3289	0.0326	0.0325	0.00	3.1867	0.32422	7.6561	-0.0017	-0.0043	0.05
	0.84104	1.9978	0.0321	0.0341	-0.10		0.56646	7.3669	0.0078	0.0019	0.22
	1.0421	1.7664	0.0342	0.0344	-0.01		0.86833	7.0108	0.0138	0.0084	0.30
	1.3394	1.4109	0.0349	0.0340	0.04		1.1756	6.6183	0.0149	0.0137	0.09
	1.5845	1.1111	0.0359	0.0326	0.14		1.4825	6.2269	0.0165	0.0176	-0.10
1.5760	0.35176	2.9651	0.0268	0.0285	-0.02		1.6788	5.9756	0.0176	0.0195	-0.18
	0.56991	2.7214	0.0289	0.0307	-0.07	3.5010	0.29765	8.7604	-0.0285	-0.0141	-0.24
	0.93103	2.3059	0.0300	0.0328	-0.17		0.73056	8.2447	0.0030	-0.0020	0.29
	1.5104	1.6085	0.0327	0.0323	0.03		1.1194	7.7646	0.0103	0.0066	0.28
	2.0324	0.94574	0.0335	0.0278	0.31		1.5156	7.2607	0.0140	0.0131	0.09
1.7228	0.27454	3.4200	0.0246	0.0254	-0.02		1.8396	6.8536	0.0169	0.0168	0.01
	0.53177	3.1308	0.0263	0.0284	-0.04		2.0862	6.5195	0.0179	0.0186	0.08
	0.82050	2.7996	0.0280	0.0307	-0.16	3.6119	0.31052	9.1392	-0.0383	-0.0172	-0.47
	1.0542	2.5225	0.0283	0.0318	-0.24		0.76166	8.5956	-0.0004	-0.0042	0.23
	1.3877	2.1213	0.0303	0.0319	-0.09		1.1665	8.0915	0.0083	0.0051	0.26
	1.6980	1.7330	0.0312	0.0307	-0.04		1.5789	7.5643	0.0127	0.0122	0.06
1.8733	0.30323	3.7773	0.0240	0.0234	0.01		1.9146	7.1329	0.0155	0.0160	-0.07
	0.90323	3.0819	0.0250	0.0266	-0.12		2.1744	6.7954	0.0175	0.0179	-0.07
	1.1591	2.7735	0.0255	0.0307	-0.37						
	1.8618	1.9002	0.0295	0.0290	0.05						
2.0796	0.21852	4.4255	0.0227	0.0185	0.08						
	0.48829	4.1160	0.0225	0.0226	0.00						
	0.78857	3.7658	0.0235	0.0261	-0.20						
	1.2790	3.1707	0.0244	0.0291	-0.31						
	2.0549	2.1883	0.0286	0.0269	0.15						

^a Dimensions: m_i = moles/10³ g of water; Δ = moles/10³ g of water.

acid-urea solutions were present in duplicate or triplicate. The solutions were assumed equilibrated if the molalities of each triplicate or quadruplicate set differed by less than 0.1% and those of each duplicate set by less than 0.05%. After some experiments had equilibrated, the solutions were diluted and allowed to reequilibrate. All calculations were made on a CDC 3200 computer.

Results

The equilibrium concentrations of the sodium chloride reference solutions and the α -amino-*n*-butyric acid-urea solutions are given in Table I. The quantities m_R , m_A , and m_U represent the molalities of sodium chloride, amino acid, and urea, respectively, while the quantity $\Delta_{\text{exptl}}/m_A m_U$ is defined by the relation

$$\Delta_{\text{exptl}} = \nu_R \phi_R m_R - \phi_A^{(B)} m_A - \phi_U^{(B)} m_U \quad (1)$$

where $\phi_i^{(B)}$ is the osmotic coefficient of a binary solution of solute molality m_i . The experimental values of $\Delta_{\text{exptl}}/m_A m_U$ are represented by the relation

$$\frac{\Delta_{\text{calcd}}}{m_A m_U} = -0.04375 + 0.00032 m_A + 0.00511 m_U + 0.00369 m_A^2 - 0.00262 m_A m_U + 0.00025 m_U^2 \quad (2)$$

with an average deviation of ± 0.0026 . Using this relation, we may calculate the percentage error, δ , in the reference molality which would account for the difference between Δ_{exptl} and Δ_{calcd} .¹⁴ This quantity and Δ_{calcd} are also given in Table I. Although the values of δ are not markedly better than the expected error, thought to be 0.3%, more elaborate polynomials did not give a significantly better representation. The activity coefficients of the solutes are given by¹⁴

$$\ln \gamma_A = \ln \gamma_A^\circ - 0.04375 m_U + 0.00032 m_A m_U + 0.00256 m_U^2 + 0.00369 m_A^2 m_U - 0.00175 m_A m_U^2 + 0.00008 m_U^3 \quad (3)$$

$$\ln \gamma_U = \ln \gamma_U^\circ - 0.04375 m_A + 0.00016 m_A^2 + 0.00511 m_A m_U + 0.00123 m_A^3 - 0.00175 m_A^2 m_U + 0.00025 m_A m_U^2 \quad (4)$$

where γ_A° and γ_U° are the activity coefficients of the appropriate binary systems.^{7,14} The water activity is easily found from the definition of the osmotic coefficient.

Discussion

*α -Amino-*n*-butyric Acid-Water System.* Before discussing the ternary results, we briefly review the binary data for the α -amino-*n*-butyric acid-water and urea-

water systems. Both the zwitterion portion² and the hydrocarbon residue⁸⁻¹⁰ interact with water, changing the structure of the surrounding water. In solutions of higher concentration, the state of the zwitterions is assumed unchanged. However, two hydrocarbon residues may form hydrophobic bonds, thus decreasing the amount of the water surrounding the molecules. This surrounding water may be called "water of hydration,"^{15,16} although it does not refer to the more usual definition involving the molecular binding of water molecules to the solute. However, since the energy levels of these water molecules have been perturbed by the amino acid, they are regarded as part of the solute molecule in solution.

To obtain an expression for the water activity, we assume that the hydrated solute exists as monomers, each of which is surrounded by h water molecules, and dimers, each of which is surrounded by $(2h - 2)$ water molecules.¹⁷ The logarithm of the water activity, $\ln a_0$, is assumed to be¹⁸

$$\ln a_0 = \ln x_0 = \ln (1 - x_{A1} - x_{A2}) \quad (5)$$

where x_0 , x_{A1} , and x_{A2} are the mole fractions of the free (*i.e.*, unhydrated) water, the acid monomer, and the acid dimer, respectively. From the condition that the sum of all the acid molecules is N_A and of all the water molecules is N_0 , we obtain

$$\frac{N_A}{N_0} [1 + (h - 1)x_{A1} + (2h - 3)x_{A2}] = x_{A1} + 2x_{A2} \quad (6)$$

We now must assume the equilibrium

$$x_{A2} x_0^2 = K_1 x_{A1}^2 \quad (7)$$

Combining eq 6 and 7, we obtain an equation for x_{A1} in terms of N_A/N_0 . Although the closed solution of this equation is difficult, a series solution is easily obtained by assuming x_{A1} is a power series in N_A/N_0 , inserting the assumed series into eq 6, and evaluating the coefficients of the assumed series by equating coefficients of like powers in N_A/N_0 . This technique, which may be used for any model, is also applied to the urea-water system and the ternary system discussed below. Combining the series for x_{A1} with eq 5 and 7, we obtain

(15) H. S. Frank and A. S. Quist, *J. Chem. Phys.*, **34**, 604 (1961).

(16) F. Franks and H. T. Smith, *J. Phys. Chem.*, **68**, 3581 (1964).

(17) The assumption that eight water molecules move in this reaction, which would be consistent with the formation of a hydrophobic bond of "maximum strength,"⁶ leads to imaginary values for h .

(18) This equation is independent of free-energy changes between monomer and dimer if these changes are independent of composition (*cf.* eq 12-16 of ref 9).

$$\ln a_0 = -N_A/N_0 - (h - 1/2 - K_1)(N_A/N_0)^2 - [(h^2 - h - 1/3) + 4K_1^2 - 4K_1h + 5K_1](N_A/N_0)^3 - [(h^3 - 3/2h^2 + h - 1/4) - 3h^2K_1 + 12hK_1^2 - 10K_1h + 20.5K_1^2 + 12K_1 - 20K_1^3](N_A/N_0)^4 - \dots \quad (8)$$

Using the first two terms of the reported series of the osmotic coefficient⁷ to give two simultaneous equations for h and K_1 , we obtain $h = 6.8$ and $K_1 = 4.9$. These values represent the reported activity data up to 1.5 m within experimental error. However, the calculated value of the $(N_A/N_0)^4$ term is twice the experimental value. Thus, until independent estimates of h and K_1 exist, this model must be regarded as a speculation.

Urea-Water System. Although the deviations from ideality of urea solutions can be explained by a variety of mechanisms, the two most common both assume the formation of urea polymers in solution and the absence of interactions between the urea molecules and the water surrounding them. The older approach^{19,20} postulates polymers of any size, with the concentrations of each governed by the equilibrium

$$x_{U(i+1)} = K_{i+1}x_{U_i}x_{U1} \quad (9)$$

where x_{U_i} is the mole fraction of an i -mer of urea. The constants K_i are assumed equal. More recently, a second approach has assumed that at least at low concentration, only dimers have formed.^{14,20} However, there has been no attempt to use the available activity data for urea-water solutions to test which of these models is better at higher concentrations. To make this test, we assume that eq 9 is valid but that all the K_i have different values. By writing equations which are exactly analogous to eq 5 and 6, we obtain a series solution for $\ln a_0$ in exactly the same manner as above

$$\ln a_0 = -N_U/N_0 + (K_1 + 1/2)(N_U/N_0)^2 - (4K_2^2 + 2K_2 - 2K_2K_3 + 1/3)(N_U/N_0)^3 + (20K_2^3 + 13.5K_2^2 - 28K_2^2K_3 + 3K_2 - 6K_2K_0 + 3K_2K_3K_4 + 1/4)(N_U/N_0)^4 - \dots \quad (10)$$

Using the least-squares series for the osmotic coefficient,²¹ we obtain an equation for K_2 from the first term, K_2 and K_3 from the second term, etc. Solving the equations, we get values of 1.9, 0, and -6 for K_2 , K_3 , and K_4 , respectively. The zero value for K_3 indicates that of the two models being considered, the approximation that urea forms just dimers is superior to the approximation of polymers. However, the (impossible) negative value for K_4 shows that to give the best fit of the experimental data, the effect of the water surrounding the urea must be included in an improved

model. Such an improved model, which would give similar equations to those written above for the amino acid, might still involve polymer formation. A positive value of K_0 would be offset by a new hydration parameter. In the remaining section, we assume urea forms only dimers.

α -Amino-n-butyric Acid-Urea-Water System. The water activity in the ternary system may be explained in terms of a model similar to that used for the binary results. Urea is assumed to replace one of the water molecules which surround the amino acid. Such a hydrated amino acid-urea group would be expected to form hydrophobic bonds less readily with another acid molecule. In dilute solution, only one urea-water substitution per amino acid molecule would occur. The urea and amino acid dimers would be present in sufficiently small quantities so that they would not take part in this substitution but would remain subject to the same equilibria as in the binary solutions (eq 7 and 9).²²

If the system conforms to this model, the mole fraction, x_{AU} , of the amino acid-urea group will be subject to the restraint

$$x_{AU}x_0 = K_0x_{A1}x_{U1} \quad (11)$$

To obtain an expression for the water activity, we use the procedure described above for binary solutions, leading to two normalization equations analogous to eq 6. However, the series assumed for x_{A1} and x_{U1} now both involve terms in (N_A/N_0) and (N_U/N_0) . Combining the resulting expression for the water activity with eq 1, we obtain

$$\frac{\Delta}{m_A m_U} = (h - 1 - K_0) \frac{M_0}{10^3} + [(h - 1)^2 + K_0^2 + 4K_1K_0 - 2K_1 - 2K_0h] \left(\frac{M_0^2}{10^6} \right) m_A + [K_0^2 - h + 2 - 2K_2h + 4K_2 + 4K_2K_0] \frac{M_0^2}{10^6} m_U \quad (12)$$

Using a value for K_0 of 8.2, we can fit the experimental data for $\Delta/m_A m_U$ within ± 0.003 over a concentration

(19) J. A. Schellman, *Compt. Rend. Trav. Lab. Carlsberg*, 29, 223 (1955).

(20) R. H. Stokes, *J. Phys. Chem.*, 69, 4012 (1965).

(21) Equation 10 of ref 14.

(22) We have considered only the effect causing Δ/m_1m_2 which is dominant at low concentrations. Models including the formation of complexes between a hydrated amino acid molecule and either a urea dimer or two urea monomers were also considered. Equations similar to eq 12 derived for these more elaborate models did not give a better quantitative description of the data.

range of 0–2 and 2.5 *m* for the amino acid and the urea, respectively. Since this is roughly the range over which the binary models fit, the model chosen to represent the ternary system seems justified.

Acknowledgments. The author is indebted to the University of Adelaide for postdoctoral support and to Dr. P. J. Dunlop for discussion during the course of this work.

Conductances of Some Uni-univalent Electrolytes in Adiponitrile at 25°

by Paul G. Sears, Joseph A. Caruso, and Alexander I. Popov

Department of Chemistry, Michigan State University, East Lansing, Michigan 48823
(Received August 23, 1966)

Conductances of five sodium and potassium salts and twelve quaternary ammonium salts in adiponitrile have been measured at 25°. The data have been analyzed by the Fuoss-Onsager conductance equation using the latest FORTRAN computer program of Kay for both nonassociated and associated electrolytes. The dissociating power of adiponitrile is reflected by fourteen of the salts showing no association and the other three having association constants of 28 or less. Limiting ionic equivalent conductances have been evaluated by the method of Coplan and Fuoss using triisooamylbutylammonium tetraphenylborate as a reference electrolyte. The dielectric constant of adiponitrile was determined to be 32.45 at 25°.

Introduction

This paper reports a part of a systematic investigation of nonaqueous solvents as reaction media especially, but not exclusively, as media for complexation reactions. In this respect adiponitrile presents an especially interesting case since it is a relatively polar solvent with high dielectric constant and an appreciable dipole moment and, at the same time, it has respectable donor properties towards Lewis acids such as transition metal ions.

However, before one can undertake the study of complexation reactions in adiponitrile, it is essential to determine the behavior of simple electrolytes in this solvent. Several previous papers have described the conductances of electrolytes in mononitriles such as acetonitrile,^{1–10} benzonitrile,^{9–12} propionitrile,¹² isobutyronitrile,⁸ and α -naphthonitrile.⁹ The study described in this article supplements the preceding investigations and, more importantly, involves the initial use of a dinitrile as an electrolytic solvent. Literature

reports indicate that adiponitrile (1,4-dicyanobutane) has a viscosity of 0.0621 poise,¹³ density of

- (1) D. F. Evans, C. Zawoyski, and R. L. Kay, *J. Phys. Chem.*, **69**, 3878 (1965).
- (2) A. C. Harkness and H. M. Daggett, Jr., *Can. J. Chem.*, **43**, 1215 (1965).
- (3) J. F. Coetzee and G. P. Cunningham, *J. Am. Chem. Soc.*, **87**, 2529 (1965).
- (4) M. A. Coplan and R. M. Fuoss, *J. Phys. Chem.*, **68**, 1181 (1964).
- (5) A. I. Popov and R. E. Humphrey, *J. Am. Chem. Soc.*, **81**, 2043 (1959).
- (6) C. M. French and D. F. Muggleton, *J. Chem. Soc.*, 2131 (1957).
- (7) P. Walden and E. J. Birr, *Z. Physik. Chem.*, **A144**, 269 (1929).
- (8) A. M. Brown and R. M. Fuoss, *J. Phys. Chem.*, **64**, 1341 (1960).
- (9) C. M. French and I. G. Roe, *Trans. Faraday Soc.*, **49**, 314 (1953).
- (10) G. J. Janz, A. E. Marcinkowsky, and I. Ahmad, *J. Electrochem. Soc.*, **112**, 104 (1965).
- (11) A. R. Martin, *J. Chem. Soc.*, 3270 (1928); 530 (1930).
- (12) P. Walden, *Z. Physik. Chem.*, **54**, 129 (1906); **55**, 683 (1906).
- (13) A. L. Woodman, W. J. Murbach, and M. H. Kaufman, *J. Phys. Chem.*, **64**, 658 (1960).

0.9579 g/l.,¹³ and a dipole moment of 3.76 D.¹⁴ It has a very broad liquid range (2–~300°) and may be purified by fractional freezing or fractional distillation. Most quaternary ammonium salts readily dissolve in adiponitrile whereas alkali metal salts generally are much less soluble even though some such as sodium perchlorate and sodium iodide form solvates.

Experimental Section

Purification and Properties of Solvent. Adiponitrile (Eastman grade) was subjected initially to successive fractional freezings until a constant freezing temperature of 2.15° was obtained. The solvent then was fractionally distilled over barium oxide through a 24-in. Vigreux column at 1 mm and 123°. The retained middle fractions had the following properties at 25°: specific conductance, $1-2 \times 10^{-8}$ ohm⁻¹ cm⁻¹; dielectric constant at 1 Mc, 32.45; viscosity, 0.0599 poise; density, 0.9585 g/ml. The procedures for the measurements of the dielectric constant, viscosity, and density have been described in detail previously.¹⁵ Comparison data for the specific conductance and dielectric constant are unavailable. However, our values for the viscosity and density of adiponitrile differ somewhat from the corresponding data of 0.0621 poise and 0.9579 g/ml in the literature.¹³ The solvent was recovered from the salt solutions for reuse by distillation.

Salts. Triisoamylbutylammonium iodide and triisoamylbutylammonium tetraphenylborate were synthesized and purified using the method of Coplan and Fuoss.¹⁶ Good agreement was found with the reported melting point of the former salt, but the melting point of the tetraphenylborate (using a Fisher-Johns apparatus with a calibrated thermometer) was found to be 264–265° instead of 274–275° reported in the literature.¹⁶ The melting point remained constant on several recrystallizations. Eastman grade tetra-butylammonium iodide, tetrahexylammonium iodide and tetrahexylammonium bromide, along with reagent grade potassium and sodium salts, were used without further purification. The other seven quaternary ammonium salts were recrystallized at least twice from appropriate systems. All salts were dried *in vacuo* at 50° to constant weight prior to their use in the preparation of stock solutions. The subsequent confirmation of additivity of ionic conductances reflected that the salts were generally pure.

Apparatus and Procedures. Resistances were measured normally at 2000 cps with a bridge assembly designed and described by Thompson and Rogers.¹⁷ An oscilloscope was used as a null-point detector. Periodic measurements were made also at 400 and 4000

cps, but no significant frequency dependency on resistance was observed. When the cell resistances were greater than 30,000 ohms, the cell was shunted in parallel with 30,000 ohms and the conductance cell resistance was computed from the measured parallel resistance.

Two flask cells, similar to those designed by Daggett, Bair, and Kraus,¹⁸ were employed. Following the recommendation and procedure of Jones and Bollinger,¹⁹ the electrodes were lightly platinized (6 coulombs/cm²). The cell constants of 0.2409 ± 0.0001 and 0.2320 ± 0.0001 cm⁻¹ were determined using dilute aqueous potassium chloride solutions and data of Lind, Zwolenik, and Fuoss.²⁰ The cell constants were checked periodically during the study; no changes were observed. Resistance measurements were made at $25.00 \pm 0.03^\circ$ by maintaining the cells in a Sargent S-84805 thermostatic bath assembly filled with light mineral oil. The temperature of the bath was established with a thermometer calibrated by the National Bureau of Standards.

The weight dilution method was used for the preparation of the solutions in the flask cells. The preparation of the stock solutions, the filling of the cells and the Friedman-LaMer weighing pipets, and the addition of stock solutions to the conductance cells were made under normal laboratory conditions since brief exposures of the nonhygroscopic solvent and solutions to the atmosphere caused no observable changes in resistances. In calculating concentrations on a volume basis, it was assumed that the densities of the very dilute solutions were equal to that of the solvent. All weights were corrected to vacuum. The conductivity of a salt was calculated by subtracting the conductivity of the solvent from that of the solution. Two independent series of measurements of the conductance of each salt were made.

Results and Discussion

The measured equivalent conductances and the corresponding concentrations in moles per liter are summarized in Table I. These data were analyzed by

(14) H. B. Thompson and S. L. Hanson, *J. Phys. Chem.*, **65**, 1005 (1961).

(15) J. W. Vaughn and P. G. Sears, *ibid.*, **62**, 183 (1958).

(16) M. A. Coplan and R. M. Fuoss, *ibid.*, **68**, 1177 (1964).

(17) H. B. Thompson and M. T. Rogers, *Rev. Sci. Instr.*, **27**, 1079 (1956).

(18) H. M. Daggett, E. J. Bair, and C. A. Kraus, *J. Am. Chem. Soc.*, **73**, 799 (1951).

(19) G. Jones and D. M. Bollinger, *ibid.*, **57**, 280 (1935).

(20) J. E. Lind, Jr., J. J. Zwolenik, and R. M. Fuoss, *ibid.*, **81**, 1557 (1959).

Table I: Conductances of Salts in Adiponitrile at 25^oa,b

10°C	Λ	10°C	Λ	10°C	Λ	10°C	Λ	10°C	Λ	10°C	Λ
—NaI—		—KI—		—KSCN—		—Pr ₄ NI—		—Bu ₄ NBr—		—Bu ₄ NI—	
2.461	12.07 ^a	1.337	12.92 ^a	2.538	15.36 ^a	2.181	11.67 ^a	2.545	10.53 ^a	2.688	10.87 ^a
10.23	11.69	9.093	12.43	5.978	15.04	5.026	11.49	4.851	10.38	5.208	10.72
16.50	11.47	15.74	12.19	12.85	14.51	9.937	11.27	9.616	10.20	9.979	10.52
24.88	11.25	24.69	11.93	23.41	13.96	16.86	11.05	16.01	9.99	16.91	10.31
37.10	11.00	37.72	11.64	38.43	13.40	26.16	10.82	24.71	9.79	25.99	10.09
2.245	12.11 ^b	4.441	12.68 ^b	57.24	12.86	39.55	10.57	37.59	9.56	39.15	9.86
4.418	11.96	9.874	12.40	2.362	15.38 ^b	2.180	11.68 ^b	2.560	10.53 ^b	2.693	10.87 ^b
8.944	11.74	17.15	12.14	5.675	15.03	4.980	11.50	4.869	10.39	5.083	10.73
14.95	11.53	27.72	11.85	12.05	14.56	9.756	11.28	9.745	10.19	10.03	10.52
23.38	11.31	41.78	11.57	22.95	14.01	16.43	11.07	16.53	9.98	16.69	10.32
35.56	11.05			36.96	13.48	25.62	10.83	25.54	9.77	25.32	10.13
				55.56	12.94	38.80	10.58	38.50	9.55	38.67	9.88
—NaClO ₄ —		—NaBPh ₄ —		—Et ₄ NBr—		—Hex ₄ NBr—		—Hex ₄ NI—		—(<i>i</i> -Am) ₄ BuNI—	
4.562	12.53 ^a	4.535	8.68 ^a	4.853	12.44 ^a	3.434	9.60 ^a	5.467	9.85 ^a	2.492	10.49 ^a
11.04	12.21	9.013	8.52	10.38	12.17	6.978	9.44	9.872	9.66	6.160	10.30
18.29	11.94	14.68	8.38	18.00	11.90	12.44	9.26	15.86	9.49	10.14	10.15
28.05	11.67	22.95	8.21	28.17	11.61	19.69	9.08	25.00	9.29	16.84	9.95
42.03	11.34	34.52	8.04	42.52	11.32	29.21	8.90	36.95	9.09	25.84	9.75
6.606	12.43 ^b	5.116	8.64 ^b	3.893	12.51 ^b	43.57	8.69	5.019	9.86 ^b	38.91	9.52
12.96	12.14	9.306	8.50	9.272	12.22	2.262	9.65 ^b	9.237	9.68	2.978	10.47 ^b
21.29	11.86	15.30	8.35	16.43	11.95	4.764	9.54	15.95	9.50	5.324	10.34
33.58	11.55	23.81	8.18	25.61	11.68	9.011	9.37	25.07	9.30	9.683	10.15
50.58	11.19	35.44	8.02	39.18	11.38	16.31	9.18	37.73	9.09	17.60	9.92
						24.50	9.02			27.01	9.71
						37.04	8.82			40.07	9.49
—Me ₃ PhNBr—		—Me ₃ PhNI—		—Pr ₄ NBr—		(i-Am) ₃ BuNBPh ₄		Me ₃ PhNO ₃ SPh			
2.778	12.38 ^a	2.382	12.83 ^a	1.921	11.33 ^a			4.061	7.149 ^a	1.816	11.44 ^a
5.716	12.15	9.796	12.39	4.817	11.14			7.542	7.025	5.125	11.12
11.37	11.78	17.16	12.08	10.63	10.87			10.81	6.929	10.00	10.84
19.35	11.40	27.08	11.77	17.53	10.67			16.88	6.789	17.20	10.51
30.56	10.99	41.17	11.44	27.51	10.42			25.91	6.634	27.10	10.17
45.55	10.59	1.993	12.88 ^b	41.37	10.18			37.77	6.480	40.88	9.79
2.401	12.43 ^b	4.846	12.65	1.932	11.34 ^b			3.410	7.185 ^b	1.535	11.49 ^b
5.202	12.19	9.693	12.37	5.301	11.11			7.262	7.041	5.259	11.13
11.65	11.76	17.19	12.08	10.26	10.90			10.622	6.940	9.481	10.88
19.29	11.40	26.40	11.78	17.67	10.67			16.84	6.797	16.85	10.54
30.79	10.98	40.54	11.46	26.94	10.44			25.56	6.644	26.62	10.20
46.66	10.56			41.24	10.19			37.38	6.490	40.48	9.82

^a Superscripts a and b designate series of determinations. ^b Ph = phenyl; Me = methyl; Et = ethyl; Pr = *n*-propyl; Bu = *n*-butyl; Hex = *n*-hexyl; *i*-Am = isoamyl.

the Fuoss-Onsager conductance equation^{21,22} which can be expressed as

$$\Lambda = \Lambda_0 - SC^{1/2} + EC \log C + JC \quad (1)$$

for unassociated electrolytes and as

$$\Lambda = \Lambda_0 - S(C\gamma)^{1/2} + EC\gamma \log C\gamma + JC\gamma - K_A C\gamma \Lambda f^2 \quad (2)$$

for associated electrolytes. In these equations all symbols have their usual meanings.²² Owing to the lack of information concerning the viscosities of solu-

tions of salts in adiponitrile, the normally small viscosity corrections associated with J were omitted. The viscosity correction in each case has no effect on Λ_0 or on the association constant and, if applied, leads only to slightly higher values for J and a° . For each salt the upper concentration limit was below the concentration at which $\kappa a = 0.2$. Calculations were made not only with unweighted values of Λ but also with

(21) R. M. Fuoss and L. Onsager, *J. Phys. Chem.*, **61**, 668 (1957).

(22) R. M. Fuoss and F. Accascina, "Electrolytic Conductance," Interscience Publishers, Inc., New York, N. Y., 1959.

Table II: Calculated Parameters of the Fuoss-Onsager Equation for Salts in Adiponitrile

Salt	Series	$\sigma\Lambda$	Λ_0	α°	K_A	S	E	J^a
NaI	a	0.004	12.52 ± 0.01	3.8 ± 0.1	0	24.81	75.9	181.6
	b	0.004	12.52 ± 0.01	4.0 ± 0.1	0	24.81	75.9	188.8
KI	a	0.004	13.26 ± 0.01	3.5 ± 0.1	0	25.45	81.4	181.1
	b	0.001	13.26 ± 0.004	3.6 ± 0.03	0	25.45	81.4	182.2
KSCN	a	0.004	15.93 ± 0.03	3.4 ± 0.5	24 ± 4	27.75	101.4	211.4
	b	0.002	15.89 ± 0.01	2.9 ± 0.2	18 ± 2	27.71	101.0	182.4
NaClO ₄	a	0.005	13.15 ± 0.01	2.9 ± 0.1	0	25.35	80.5	153.5
	b	0.005	13.16 ± 0.01	2.9 ± 0.1	0	25.36	80.7	152.4
NaBPh ₄	a	0.004	9.17 ± 0.01	5.2 ± 0.2	0	21.92	50.8	172.3
	b	0.003	9.15 ± 0.01	5.2 ± 0.1	0	21.90	50.6	173.5
Et ₄ NBr	a	0.003	13.05 ± 0.007	3.3 ± 0.1	0	25.27	79.8	168.6
	b	0.002	13.06 ± 0.004	3.3 ± 0.1	0	25.27	79.9	167.3
Me ₃ PhNBr	a	0.003	12.93 ± 0.02	4.0 ± 0.6	27 ± 4	25.16	78.9	197.0
	b	0.002	12.93 ± 0.01	4.2 ± 0.5	28 ± 3	25.16	78.9	202.7
Me ₃ PhNI	a	0.003	13.27 ± 0.01	2.7 ± 0.1	0	25.46	81.5	145.5
	b	0.004	13.26 ± 0.01	2.8 ± 0.1	0	25.44	81.3	149.8
Pr ₄ NBr	a	0.003	11.70 ± 0.01	3.9 ± 0.1	0	24.10	69.7	173.8
	b	0.003	11.71 ± 0.01	3.9 ± 0.1	0	24.11	69.7	174.3
Pr ₄ NI	a	0.003	12.08 ± 0.01	4.0 ± 0.1	0	24.42	72.5	182.4
	b	0.004	12.08 ± 0.01	3.9 ± 0.1	0	24.43	72.6	180.0
Bu ₄ NBr	a	0.004	10.94 ± 0.01	4.2 ± 0.1	0	23.44	64.0	171.9
	b	0.002	10.94 ± 0.01	4.2 ± 0.1	0	23.44	64.0	172.3
Bu ₄ NI	a	0.003	11.30 ± 0.01	4.1 ± 0.1	0	23.75	66.7	173.7
	b	0.005	11.30 ± 0.01	4.2 ± 0.1	0	23.76	66.7	177.2
Hex ₄ NBr	a	0.004	10.06 ± 0.01	4.4 ± 0.1	0	22.69	57.4	165.8
	b	0.006	10.05 ± 0.02	5.0 ± 0.2	0	22.67	57.4	181.8
Hex ₄ NI	a	0.002	10.40 ± 0.01	4.4 ± 0.1	0	22.98	60.0	169.8
	b	0.005	10.40 ± 0.01	4.5 ± 0.1	0	22.98	60.0	173.4
<i>(i</i> -Am) ₃ BuNI	a	0.005	10.91 ± 0.01	4.2 ± 0.1	0	23.42	63.8	172.6
	b	0.003	10.91 ± 0.01	4.1 ± 0.1	0	23.42	63.8	170.2
<i>(i</i> -Am) ₃ BuNBPh ₄	a	0.002	7.585 ± 0.006	4.9 ± 0.1	0	20.55	38.9	138.4
	b	0.002	7.578 ± 0.005	4.9 ± 0.1	0	20.55	38.9	138.4
Me ₃ PhNO ₃ SPh	a	0.003	11.79 ± 0.02	2.6 ± 0.5	13 ± 4	24.18	70.4	125.7
	b	0.002	11.81 ± 0.01	2.9 ± 0.4	15 ± 3	24.20	70.5	137.7

^a No viscosity correction applied.

values of Λ weighted by C . Since weighted data yielded a considerably better fit to the theoretical equations, as evidenced by much smaller values of $\sigma\Lambda$, the final results are reported on that basis.

The conductance parameters obtained from least-squares analyses²³ of the data in Table I with respect to eq 1 and 2 using a CDC-3600 computer are summarized in Table II. Included also in Table II are data for $\sigma\Lambda$, the standard deviation associated with the

individual Λ values. The detailed results given in Table II are summarized in Table III where the result of the two series of measurements on each salt have been averaged by weighting each parameter inversely by its standard deviation.

(23) Dr. R. L. Kay of the Mellon Institute, Pittsburgh, Pa., kindly provided the FORTRAN program which was used in the treatment of our data.

Table III: Averaged Conductance Parameters for Adiponitrile Solutions

Salt	Λ_0	α°	K_A
NaI	12.52	3.9	0
KI	13.26	3.6	0
KSCN	15.91	3.1	20
NaClO ₄	13.16	2.9	0
NaBPh ₄	9.16	5.2	0
Et ₄ NBr	12.06	3.3	0
Me ₃ PhNBr	12.93	4.2	28
Me ₃ PhNI	13.27	2.7	0
Pr ₄ NBr	11.71	3.9	0
Pr ₄ NI	12.08	4.0	0
Bu ₄ NBr	10.94	4.2	0
Bu ₄ NI	11.30	4.2	0
Hex ₄ NBr	10.06	4.6	0
Hex ₄ NI	10.40	4.4	0
(<i>i</i> -Am) ₃ BuNI	10.91	4.1	0
(<i>i</i> -Am) ₃ BuNBPh ₄	7.58	4.9	0
Me ₃ PhNO ₃ SPh	11.80	2.8	14

The constants α , β , E_1 , and E_2 for adiponitrile at 25° have values of 0.8620, 14.014, 7.479, and 17.806, respectively, where S and E in eq 1 and 2 are defined by

$$S = \alpha\Lambda_0 + \beta; E = E_1\Lambda_0 - E_2$$

The Λ_0 values listed in Table II consistently are 0.01–0.02 unit larger than those calculated using unweighted data and about 0.05 unit larger than the corresponding values obtained from preliminary Shedlovsky plots²⁴ of Λ'_0 vs. C . Calculation of the conductance differences at infinite dilution between corresponding bromides and iodides and between corresponding sodium and triisoamylbutylammonium salts indicates an uncertainty in Λ_0 values of 0.03 unit or about 0.3%. This apparent level of accuracy is nevertheless quite satisfactory in comparison to the results for most other nonaqueous systems and reflects the general consistency of the over-all results.

Single-ion limiting equivalent conductances were obtained on the basis of the assumption that the limiting conductance of the triisoamylbutylammonium ion, shown by Coplan and Fuoss¹⁶ to be equal to that of the tetraphenylborate ion in methanol, is the same as that of the latter in all solvents. That is

$$\lambda_{0(i-Am)_3BuN^+} = \lambda_{0(BPh_4^-)} = \frac{1}{2}\Lambda_{0(i-Am)_3BuNBPh_4} \quad (3)$$

Using data for salts with common ions, limiting equivalent conductances of 14 ions in adiponitrile have been

calculated; the results are summarized in Table IV. These data will reproduce the Λ_0 value for each of the salts within 0.01 unit. The potassium and sodium ions have limiting conductances between those of the trimethylphenylammonium and tetra-*n*-propylammonium ions; all other ionic conductances occur in the expected sequences.

Table IV: Single-Ion Limiting Equivalent Conductances in Adiponitrile Based on Triisoamylbutylammonium Tetraphenylborate as Reference Electrolyte

Ion	λ_0^+	Ion	λ_0^-
Et ₄ N ⁺	6.29	SCN ⁻	9.79
Me ₃ PhN ⁺	6.15	ClO ₄ ⁻	7.77
K ⁺	6.12	I ⁻	7.13
Na ⁺	5.38	Br ⁻	6.77
Pr ₄ N ⁺	4.94	PhSO ₃ ⁻	5.65
Bu ₄ N ⁺	4.17	BPh ₄ ⁻	3.79
(<i>i</i> -Am) ₃ BuN ⁺	3.79		
Hex ₄ N ⁺	3.28		

It is seen from the above results that adiponitrile is a good dissociating or smenocolytic²⁵ solvent, since only three of the seventeen salts studied show any ion-pair association in the concentration range of $\sim 10^{-4}$ to 5×10^{-3} *M*. The relatively high viscosity is reflected in the low values obtained for the limiting conductance (*e.g.*, Λ_0 value for Bu₄NI is 11.30 as compared with 164.6 for the same salt in acetonitrile¹ and 101.72 in methanol²⁶). It is interesting to note that the dielectric constants of acetonitrile and methanol are very close to that of adiponitrile (36.02 and 32.63 vs. 32.45 at 25°). The latter seems to have comparable and perhaps greater dissociating power, since it has been shown that tetraalkylammonium salts generally are very slightly associated both in acetonitrile¹ and in methanol.²⁶ Despite its high viscosity, therefore, adiponitrile should be a very useful solvent for the study of inorganic reactions.

Acknowledgment. The authors are very grateful to Dr. Robert L. Kay for the use of his FORTRAN program in this investigation.

(24) T. Shedlovsky, *J. Am. Chem. Soc.*, **54**, 1405 (1932).

(25) R. M. Fuoss, *J. Chem. Educ.*, **32**, 527 (1955).

(26) R. L. Kay, C. Zawoyski, and D. F. Evans, *J. Phys. Chem.*, **69**, 4209 (1965).

Activity Coefficient Measurements in Aqueous Sodium Chloride–Sodium Sulfate Electrolytes Using Sodium Amalgam Electrodes

by James N. Butler, Philomena T. Hsu, and John C. Synnott

Tyco Laboratories, Inc., Waltham, Massachusetts 02154 (Received August 29, 1966)

Measurements of the activity coefficient of NaCl in NaCl–Na₂SO₄ electrolytes have been made using the cell Na, Hg|Na⁺, Cl⁻, SO₄²⁻–|AgCl|Ag, and have been compared with literature values obtained using cation-sensitive glass electrodes. Harned's rule is shown to be obeyed for both components within experimental errors over the ionic strength range from 0 to 6 *m*.

Introduction

The activity of NaCl in a multicomponent salt solution can be obtained by measuring the emf of a sodium amalgam–silver chloride cell



where MX is a salt whose ions do not interfere with the reversibility of the two electrodes, such as Na₂SO₄. By using two identical cells, one containing only NaCl solution and the other containing the multicomponent salt solution, the activity of NaCl in the multicomponent solution can be compared directly with a solution of known activity. The amalgam composition need not be known accurately provided it is the same for both cells.

This method has been used to determine the activity coefficients of NaCl in NaCl–NaOH electrolytes,¹ but has not been applied to other multicomponent systems. Recently, Lanier² and Gieskes³ have reported activity coefficient data for NaCl in multicomponent electrolytes obtained using a cation-sensitive glass electrode. The results reported in this paper are compared with those obtained with the glass electrode, and are in general agreement.

Experimental Section

Solutions were prepared from reagent grade salts (Fisher Scientific Co.). The sodium chloride stock solutions were analyzed for chloride by the Volhard method and the sodium sulfate stock solutions were analyzed gravimetrically by precipitation as barium sulfate. Triply distilled conductivity water was used

to clean the cell and to prepare all solutions. To minimize effects due to corrosion of the sodium amalgam, the pH of the solution was adjusted to 11 or 12 with NaOH of accurately known concentration. Solutions were deoxygenated by passing hydrogen over a large platinum black electrode in the solution for several hours. The hydrogen was obtained by electrolysis of water in a cell with a silver–palladium cathode and contained less than 0.1 ppm of oxygen.

Silver–silver chloride electrodes were prepared by the thermal electrolytic process⁴ and aged for several weeks in 1 *m* NaCl before use. Because of the large mass of the electrode (0.2 g), up to 1 hr was required to reach equilibrium with the solution, but after that the potential was stable. Normally, the electrodes were equilibrated overnight with the solution to be measured. Bias potentials between different electrodes were less than 0.05 mv and changed by less than 0.005 mv over periods of several days.

Sodium amalgam was prepared by electrolysis of saturated NaOH solution at a mercury cathode and stored under a prepurified argon atmosphere. The amalgam was analyzed by treating it with standard H₂SO₄ and back-titrating with NaOH. A single reservoir fed two dropping amalgam electrodes in the

(1) H. S. Harned and M. A. Cook, *J. Am. Chem. Soc.*, **59**, 1890 (1937).

(2) R. D. Lanier, *J. Phys. Chem.*, **69**, 3992 (1965).

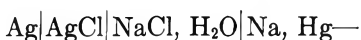
(3) J. M. T. M. Gieskes, *J. Physik. Chem. (Frankfurt)*, **50**, 78 (1966).

(4) D. J. G. Ives and G. J. Janz, "Reference Electrodes," Academic Press, New York, N. Y., 1961, Chapter 4.

test cell and reference cell. The electrodes were prepared by attaching 1-cm lengths of polarographic capillary to a 1-mm i.d. capillary stem using thin-walled Teflon tubing. In this way the capillary could easily be changed when it became plugged with solid material from the amalgam. The most precise measurements were obtained with capillaries which were kept scrupulously dry until after the amalgam was flowing. Drops with a maximum diameter of 1 mm were formed at a rate of approximately one per second. The cell was constructed so the drops from the capillary fell through a 4-mm diameter hole in the bottom of the cell, through a gas space, and into a waste compartment. Solution was prevented from flowing through this hole by a slight back pressure of hydrogen. When it was desired to drain the cell, a vacuum was applied to the waste compartment, which drew the solution through the hole in the bottom of the cell. Fresh deoxygenated solution was then added from a solution reservoir without opening the cell to the air. All measurements were conducted in a thermostat at $25.00 \pm 0.02^\circ$.

Potentials were measured with a Leeds and Northrup Model K-3 potentiometer using a Honeywell Model 104W1-G galvanometer with a sensitivity of 0.001 μ a/mm and a response time of approximately 0.2 sec for full-scale deflection (40 mm). The standard cell (Eppley Laboratory Type 100) was calibrated against a U. S. National Bureau of Standards cell and guaranteed to have the value 1.01922 ± 0.00005 v.

The potential of the combined cell



was measured during the period when the drops of both amalgam electrodes were nearly fully formed; such potentials were reproducible to ± 0.02 mv for periods of up to 1 hr under favorable conditions. Changes of solution sometimes had a negligible effect on the potential, but at other times produced changes as large as 0.5 mv. These large changes were attributed to traces of oxygen being admitted to one of the cells and whenever possible, the value taken to be correct was one which remained constant through several changes of solution as well as at least 0.5 hour of amalgam flow.

Results and Discussion

The results obtained for emf and the activity coefficients calculated from these values are given in Table I. The mean activity coefficient, γ_{12} , of NaCl in the mixed electrolyte was calculated using the equation which follows.

$$E = -\frac{RT}{F} \ln \left[\frac{(m_{\text{Na}^+})(m_{\text{Cl}^-})(\gamma_{12})^2}{(m_{\text{Na}^+}^0)(m_{\text{Cl}^-}^0)(\gamma_{10})^2} \right] \quad (1)$$

where m_{Na^+} and m_{Cl^-} are the molalities of Na⁺ and Cl⁻ in the mixed electrolyte, $m_{\text{Na}^+}^0$ and $m_{\text{Cl}^-}^0$ are the molalities in the reference solution, and γ_{10} is the mean activity coefficient of NaCl in the reference solution. E is the measured emf of the combined cells, R is the gas constant, T is the absolute temperature, and F is the Faraday constant. The electrolyte in the reference cell was in each case the solution listed as "100% ionic strength NaCl," the first entry in each part of Table I. The other electrolytes were made by mixing accurately weighed amounts of this solution with Na₂SO₄ stock solution of approximately the same ionic strength.

To minimize the possible interference from hydrogen evolution at the amalgam electrodes, the solutions were made 0.098 m in NaOH. The ionic strength listed in Table I includes a contribution from the NaOH present; but since this was a constant amount, it was not included in calculating the ionic strength fraction present as NaCl. Thus the stock solution (designated "100% NaCl") really was 0.098 m in NaOH and 0.986 m in NaCl, making a total ionic strength of 1.084, as listed.

The activity coefficients of the stock solutions were calculated using the activity coefficient values for pure NaCl solutions given by Robinson and Stokes,⁵ together with values of the Harned's rule constants for NaOH-NaCl mixtures obtained by Harned and Cook.¹ The replacement of 0.098 m NaCl by NaOH at a total ionic strength of 1.084 m changes $\log \gamma_{\text{NaCl}}$ from -0.1838 to -0.1864 . This corresponds to an emf difference of 0.35 mv, which is of the same order of magnitude as the uncertainty in the literature values for γ_{NaCl} . The effect of NaOH on the activity coefficient of NaCl in solutions containing large fractions of Na₂SO₄ may be somewhat different, but no data yet exist by which further corrections may be made.

Figure 1 compares our measurements with those made by Lanier² using a cation-sensitive glass electrode. The different value of $-\log \gamma$ at 100% NaCl reflects the presence of added NaOH as well as the range of choice for literature values.

In most mixed aqueous electrolytes, the activity coefficient of at least one of the components has been found to obey Harned's rule.^{5,6}

(5) R. A. Robinson and R. H. Stokes, "Electrolyte Solutions," Butterworth and Co. Ltd., London, 1959, Chapter 15 and Appendix 8.10.

(6) H. S. Harned and B. B. Owen, "The Physical Chemistry of Electrolytic Solutions," 3rd ed, Reinhold Publishing Corp., New York, N. Y., 1958, Chapter 14.

Table I: Mean Activity Coefficient of NaCl in NaCl-Na₂SO₄ Electrolytes at 25°

Total ionic strength ^a	Ionic strength % NaCl ^b	E, mv	-Log γ_{\pm}	-Log γ_{\pm} cor ^d
1.084	100.00	0	0.1864 ^c	0.1856
1.085	89.47	4.53	0.1938	0.1925
1.086	74.70	11.02	0.1995	0.1976
1.170	49.93	26.85	0.2144	0.2088
1.090	35.00	36.10	0.2169	0.2132
1.124	24.63	49.65	0.2242	0.2186
1.102	12.13	70.00	0.2261	0.2208
1.089	5.02	93.94	0.2272	0.2223
1.093	2.28	110.5	0.2242	0.2189
1.083	0.90	132.3	0.173	0.168
3.080	100.00	0	0.1462 ^c	0.1491
3.072	90.01	5.35	0.1605	0.1628
3.065	75.00	15.33	0.1927	0.1943
3.040	49.89	30.94	0.2133	0.2138
3.020	25.06	56.50	0.2546	0.2546
3.008	10.01	83.5	0.266	0.266

^a Containing 0.098 *m* NaOH to adjust pH. ^b Based on total of NaCl and Na₂SO₄, but excluding NaOH. ^c Activity coefficients of pure NaCl from ref 5, Appendix 8. 10, and Harned rule coefficients for NaCl-NaOH mixtures from ref 1. ^d Corrected to *I* = 1.000 for the first set and *I* = 3.000 for the second set, assuming α_{12} = 0.048, and using data for pure NaCl from ref 5.

$$\log \gamma_{12} = \log \gamma_{10} - \alpha_{12} X_2 I \quad (2)$$

where γ_{12} is the activity coefficient of component 1 (NaCl) in the mixed electrolyte of ionic strength *I*, γ_{10} is the activity coefficient of component 1 alone at ionic strength *I* (our reference solution), *X*₂ is the ionic strength fraction of component 2 (Na₂SO₄) in the mixed electrolyte, α_{12} is the Harned rule coefficient, which depends to some extent on the total ionic strength *I*, but not on the fraction of the second component *X*₂.

From Figure 1 it is apparent that the activity coefficient of NaCl in NaCl-Na₂SO₄ electrolytes obeys Harned's rule within experimental error from 100% NaCl to 5 or 10% NaCl. The positive deviations at low fractions of NaCl were also observed by Lanier² and probably reflect a systematic error resulting from the effect of SO₄²⁻ ions on the AgCl electrode, not a true thermodynamic deviation from Harned's rule. Gieskes³ did not make measurements at low fractions of NaCl.

If both components of a mixed electrolyte obey Harned's rule, then

$$\log \gamma_{21} = \log \gamma_{20} - \alpha_{21} X_1 I \quad (3)$$

is obeyed as well as eq 2, and making use of the Gibbs-

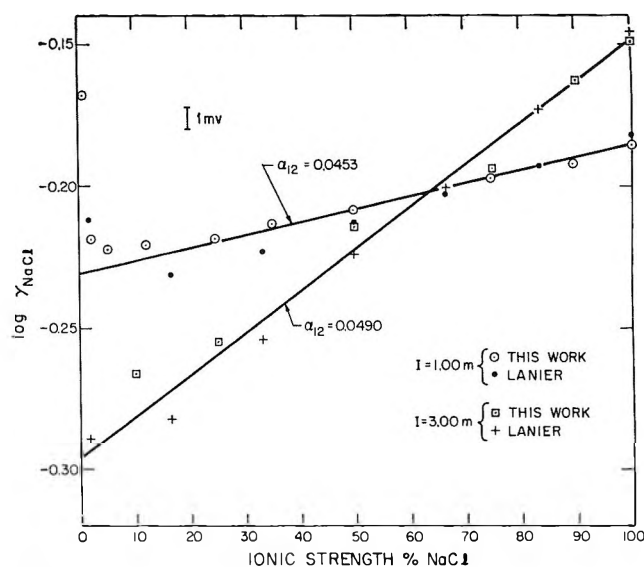


Figure 1. Dependence of activity coefficient for NaCl on composition of electrolyte at constant ionic strength and comparison with the data of Lanier.²

Duhem relation, it is possible to derive an expression relating α_{21} to α_{12} which involves only the properties of the pure component electrolytes.^{5,6} For NaCl(component 1)-Na₂SO₄(component 2) electrolyte mixtures, this takes the form

$$\alpha_{21} = 2\alpha_{12} - \frac{2}{2.303I} [2\phi_1^0 - \phi_2^0 - 1] \quad (4)$$

where ϕ_1^0 and ϕ_2^0 are the osmotic coefficients of the pure electrolytes at ionic strength *I*.

In Table II are given the values of α_{12} obtained from our data and the values of α_{21} calculated from them, together with the values of the osmotic coefficients used in the calculation. Note that the values obtained for the Harned rule coefficients are quite different from those obtained by Lanier.²

If both electrolytes obey Harned's rule, then thermodynamic cross-differentiation relations require that a further test of thermodynamic consistency be satisfied.^{5,6} The quantity

$$S' = 6\alpha_{12} + 3\alpha_{21} \quad (5)$$

should be independent of ionic strength. Lanier² found that *S'* varied with ionic strength and from this concluded that the activity coefficients of Na₂SO₄ did not necessarily obey Harned's rule. Our data also show that *S'* is different for ionic strengths of 1 and 3 *m*, but the difference is in the opposite direction to that reported by Lanier. The comparison of values α_{12} , α_{21} , and *S'* is most clearly seen in Figure 2. An estimate of the error in *S'* is most clearly seen in Figure 2.

Table II: Activity Coefficient Parameters

Parameter	$I = 1$	$I = 3$	Ref
α_{12}	0.0453	0.0490	This work
α_{12}	0.0605	0.0537	2
Log γ_{01} (exptl)	-0.231	-0.296	This work
Log γ_{01} (exptl)	-0.243	-0.307	2
Log γ_{01} (Brønsted theory)	-0.235	-0.288	2
Log γ_{20}	-0.059	-0.690	5
ϕ_1	0.9363	1.042	5
ϕ_2	0.717	0.642	5
α_{21}	-0.0431	-0.0319	This work
α_{21}	-0.0141	-0.0205	2
S'	0.142	0.198	This work
S'	0.321	0.261	2

An estimate of the error in S' resulting from all the random and systematic errors in our experimental measurements is approximately ± 0.05 , which implies that within the experimental errors, S' is independent of ionic strength. This conclusion is confirmed by the recent measurements of Gieskes³ at ionic strength 0.7, using a cation-sensitive glass electrode. His three series of measurements gave $\alpha_{12} = 0.0511$, 0.0517, and 0.0589, respectively. These values are indicated in Figure 2. Note that Gieskes' values fall between Lanier's and ours, but agree with both sets within experimental error. Note also that Lanier's data can give values of S' which are independent of ionic strength if osmotic coefficients are used which vary by less than 1% from those in Table II.

If S' is assumed to be independent of ionic strength, then the precise dependence of α_{12} and α_{21} on ionic strength can be calculated. Combining eq 4 and 5, we obtain

$$\alpha_{12} = (S' + 3B)/12 \quad (6)$$

$$\alpha_{21} = (S' - 3B)/6 \quad (7)$$

where B is defined by

$$B = \frac{2}{2.303I} [2\phi_1^0 - \phi_2^0 - 1] \quad (8)$$

Using tabulated values⁵ for the osmotic coefficients of NaCl and Na₂SO₄, B can be calculated as a function of ionic strength and a value for S' can be chosen which best fits the experimental data at all values of ionic strength. In Figure 2, the broken lines are calculated values of α_{12} and α_{21} based on the assumption $S' = 0.190$. Increasing the assumed value of S' makes both

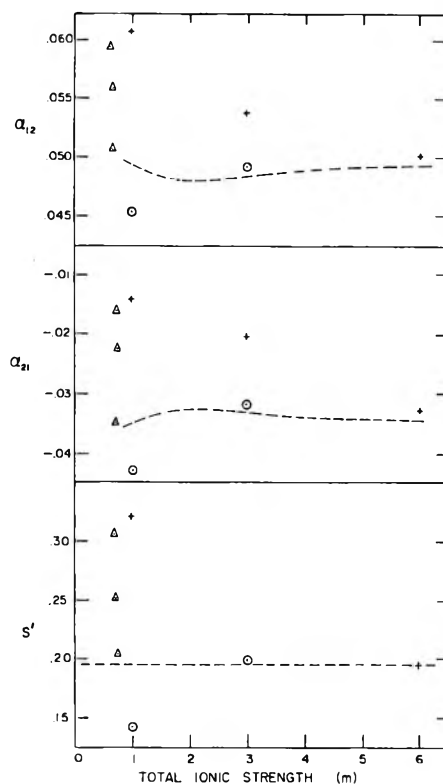


Figure 2. Variation of the Harned rule coefficients with composition. The quantity S' is required by thermodynamic consistency to be independent of ionic strength if Harned's rule is obeyed. The broken lines were calculated using tabulated values of osmotic coefficients as described in the text. Experimental values of this work (\circ), Lanier² ($+$), and Gieskes³ (Δ) are shown.

α_{12} and α_{21} more positive, but does not change the shape of the curves. Thus, if one places more weight on our measurements at 1 m ionic strength, one might choose a smaller value of S' , perhaps as low as 0.16.

The results of this investigation may be best summarized as follows: eq 2 and 3 can be used to predict the activity coefficients of NaCl and Na₂SO₄ in electrolytes containing both components using the tabulated activity coefficients of the pure components⁵ and taking the Harned rule coefficients to be $\alpha_{12} = 0.048$ and $\alpha_{21} = -0.034$. These values may be assumed to hold for any composition from pure NaCl to pure Na₂SO₄ and for any ionic strength from 0 to 6, and the calculated values will agree with experimental results within ± 0.01 in $\log \gamma$. This limit of error is only a factor of 2 or 3 larger than the experimental errors in the measurements and represents a substantial improvement over the assumption that ionic strength alone determines the activity coefficient of a given component.

Acknowledgments. This research was supported by the U. S. Department of the Interior, Office of Saline Water. The authors thank Drs. W. H. McCoy and A. B. Gancy for helpful discussions during the course

of the work and Drs. R. A. Robinson and R. D. Lanier for criticism of the manuscript. Mrs. Mary L. Meehan assisted in the design of the apparatus and in the preliminary experiments.

Acetonitrile: Far-Infrared Spectra and Chemical Thermodynamic Properties.

Discussion of an Entropy Discrepancy

by G. A. Crowder¹ and Bobby R. Cook

Department of Chemistry, West Texas State University, Canyon, Texas (Received August 31, 1966)

Liquid- and vapor-state infrared spectra in the region 75–650 cm^{-1} were obtained for acetonitrile. The entropy discrepancy at 298.15°K was shown to result partially from the use of the liquid-state frequency for the skeletal bending vibration. The remaining entropy discrepancy is discussed. A table of the chemical thermodynamic properties of acetonitrile at selected temperatures was prepared.

Introduction

The entropy of acetonitrile at 298.15°K, corrected to the ideal gas state at 1 atm, was determined by Putnam, McEachern, and Kilpatrick (PMK)^{2a} to be 58.67 ± 0.20 cal deg⁻¹ mole⁻¹. This value is 0.66 cal larger than the value of 58.01 cal deg⁻¹ mole⁻¹ calculated by Gunthard and Kovats^{2b} using the rigid rotator-harmonic oscillator model. This discrepancy suggests an error either in the vibrational assignment or molecular parameters used in the calculation or in the experimental data. The present work was undertaken to examine the discrepancy. The examination consisted of a recalculation of the statistical mechanical entropy using vapor-state wavenumbers and a revised set of molecular parameters and a critical look at the gas imperfection correction and experimental entropy of vaporization.

Experimental Section

Far-infrared spectra of acetonitrile were determined at room temperature with a Perkin-Elmer Model 301 spectrophotometer. A stainless steel cell, with path

length variable in increments of 1–6 m, was used in obtaining the vapor-state spectrum. The sample of acetonitrile was obtained from the Eastman Kodak Co. Infrared spectra in the region 650–4000 cm^{-1} did not show any impurity bands.

Results and Discussion

Far-Infrared Spectra. It has been shown that vibrations with a wavenumber lower than about 250 cm^{-1} usually have a lower wavenumber in the vapor than in the liquid state.³ Since the low-frequency vibrations contribute the most to the thermodynamic functions, vapor-state values for these vibrational frequencies are necessary in calculations of vapor-state thermodynamic properties. Gunthard and Kovats

(1) To whom all correspondence should be addressed at Department of Chemistry, West Texas State University, Canyon, Texas 79015.

(2) (a) W. E. Putnam, D. M. McEachern, Jr., and J. E. Kilpatrick, *J. Chem. Phys.*, **42**, 749 (1965); (b) H. H. Gunthard and E. Kovats, *Helv. Chim. Acta*, **35**, 1190 (1952).

(3) W. G. Fateley, I. Matsubara, and R. E. Witkowski, *Spectrochim. Acta*, **20**, 1461 (1964); G. A. Crowder and D. W. Scott, *J. Mol. Spectry.*, **16**, 122 (1965).

used the value 380 cm^{-1} for the doubly degenerate skeletal bending vibration of acetonitrile. This value was taken from the liquid-state Raman spectrum. Although no large frequency shifts have been observed for bands in this region of the spectrum, it was thought that this band might shift to a lower wavenumber in going from liquid to vapor because of the high degree of polarity of the molecule. Figure 1 shows the infrared spectrum of acetonitrile in the region $75\text{--}650\text{ cm}^{-1}$. A shift of the skeletal bend in the right direction is clearly observed, with the vapor-state wavenumber being 360 cm^{-1} . This is 20 cm^{-1} lower than the value used in the previous calculation of the entropy and use of the vapor-state value will result in an increase of $0.17\text{ cal deg}^{-1}\text{ mole}^{-1}$ in the calculated entropy. The liquid-state infrared value of the skeletal bend is 376 cm^{-1} , so the shift amounts to 16 cm^{-1} .

The skeletal bending vibration is the only fundamental vibration with a frequency in the region below 650 cm^{-1} . The acetonitrile molecule has a small moment of inertia about the molecular axis and it may be possible for rotational bands to be observed in the far-infrared region. In the vapor-state spectrum, the broad band observed at 195 cm^{-1} and the increasing absorption near 75 cm^{-1} may be superpositions of unresolved rotational bands. Jones and Sheppard⁴ have given evidence that the acetonitrile molecule has a considerable degree of rotational freedom in the liquid state. The increasing absorption below about 275 cm^{-1} in the liquid-state spectrum may be due to rotational transitions in the liquid state. The weak bands observed at 418 , $510\text{--}515$, and 575 cm^{-1} may be impurity bands, because no difference combination bands can be assigned to any of these.

Calculation of Thermodynamic Functions. The thermodynamic functions of acetonitrile were recalculated, using the vapor-state value for the skeletal bend. The calculations, based on the rigid rotator-harmonic oscillator approximation, were made with the usual formulas of statistical thermodynamics.⁵ The wavenumbers used in this calculation and their degeneracies are: $360(e)$, $922(a_1)$, $1038(e)$, $1372(a_1)$, $1443(e)$, $2262(a_1)$, $2941(a_1)$, and $3001(e)$. All these values except for the skeletal bend were taken from ref 6.

For the rotational contribution, Gunthard and Kovats used the data of Kessler, *et al.*⁷ Costain⁸ has redetermined the molecular parameters of acetonitrile and his data were used in the present calculation. The molecular structure constants used were 1.104 \AA for the C-H distance, 1.458 \AA for the C-C distance, 1.157 \AA for the C \equiv N distance, and all C-C-H and H-C-H angles were taken as tetrahedral.

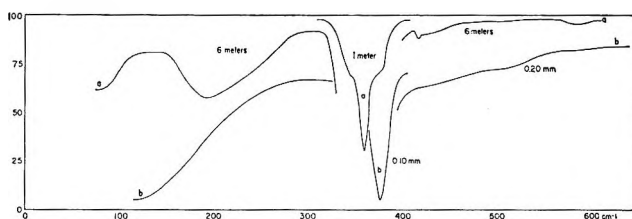


Figure 1. Far-infrared spectra of acetonitrile: a, vapor at 83 torr, pathlength indicated on figure; b, liquid, path length indicated on figure or unknown; ordinate given in per cent transmittance.

The moments of inertia were calculated to be $I_a = 5.441 \times 10^{-40}\text{ g cm}^2$, $I_b = I_c = 91.11 \times 10^{-40}\text{ g cm}^2$.

Gas Imperfection. The total entropy of acetonitrile in the ideal gas state at 298.15°K and 1 atm was calculated to be $58.20\text{ cal deg}^{-1}\text{ mole}^{-1}$. Although significantly higher than the value calculated by Gunthard and Kovats, this value is $0.47\text{ cal deg}^{-1}\text{ mole}^{-1}$ lower than the experimental value of PMK. Examination of their data shows an unusually large gas imperfection, 0.55 cal . This correction was determined from the rather inaccurate data of Lambert, *et al.*,⁹ for the second virial coefficient as a function of temperature. From a reexamination of Lambert's data, the eq $B = -250 - 7.50 \exp(2000/T)\text{ cc mole}^{-1}$ was fitted to the curve. Extrapolation to 298.15°K gives $dB/dT = 138$ and from this the gas imperfection is 0.39 cal . Use of this value gives $S^\circ_{\text{obsd}} = 58.51\text{ cal deg}^{-1}\text{ mole}^{-1}$, which is still $0.31\text{ cal deg}^{-1}\text{ mole}^{-1}$ higher than the calculated value.

Enthalpy of Vaporization. Another possibility for error lies in the experimental enthalpy of vaporization. Measurements of enthalpies of vaporization at about room temperature or higher, during which the liquid is distilled from a low-temperature calorimeter and the vapor condensed into a weighed glass sample bulb immersed in liquid air, have been known to be in error. For example, Aston, Finke, and Schumann¹⁰ used this type of measurement for cyclopentane and found the

(4) W. J. Jones and N. Sheppard, *Trans. Faraday Soc.*, **56**, 625 (1960).

(5) K. S. Pitzer, "Quantum Chemistry," Prentice-Hall, Inc., Englewood Cliffs, N. J., 1953.

(6) J. C. Evans and G. Y.-S. Lo, *Spectrochim. Acta*, **21**, 1033 (1965).

(7) M. Kessler, H. Ring, R. Trambarulo, and W. Gordy, *Phys. Rev.*, **79**, 54 (1950).

(8) C. C. Costain, *J. Chem. Phys.*, **29**, 864 (1958).

(9) J. D. Lambert, G. A. H. Roberts, J. S. Rowlinson, and V. J. Wilkinson, *Proc. Roy. Soc. (London)*, **A196**, 113 (1949).

(10) J. G. Aston, H. L. Finke, and S. C. Schumann, *J. Am. Chem. Soc.*, **65**, 341 (1943).

enthalpy of vaporization to be 6982 ± 8 cal mole⁻¹. A more accurate value is 6818 cal mole⁻¹.¹¹

PMK give vapor-pressure data for acetonitrile in the temperature range 280–300°K. They fitted an Antoine equation to the data and from the Clapeyron equation and the value of dp/dt determined from the Antoine equation they calculated $\Delta H_{\text{vap}} = 7865$ cal mole⁻¹. Quinn¹² determined the vapor pressure for the range 310–378°K and his Antoine equation reproduces the data of PMK as well as their equation. From Quinn's equation, ΔH_{vap} was calculated to be 7848 cal mole⁻¹, in good agreement with the value obtained from the vapor-pressure data of PMK. We fitted a Cox equation to the PMK data by a least-squares method and found ΔH_{vap} to be 7830 cal mole⁻¹. We also fitted a Cox equation to the combined data of PMK and Quinn. The following equation, good in the range 280–380°K, was obtained.

$$\log P(\text{atm}) = A(1 - 354.776/T) \quad (1)$$

In eq 1, A is given by

$$\log A = 0.772542 - 3.94845 \times 10^{-4}T + 4.06868 \times 10^{-7}T^2 \quad (2)$$

In eq 1 and 2, T is in °K. From eq 1 and 2, the enthalpy of vaporization was calculated to be 7848 cal mole⁻¹, in good agreement with the values given above, but lower than the experimental value of PMK, which is 7941 cal mole⁻¹. We feel that this is the experimental measurement that is most likely to be in error and prefer the calculated value of 7848 cal mole⁻¹. When this value is used, the calculated and experimental entropies at 298.15°K are in agreement.

Comparison of Experimental and Theoretical Entropies and Table of Thermodynamic Functions. Table I summarizes the experimental entropy tabulation for acetonitrile at 298.15°K. Table II gives the thermodynamic functions, calculated at selected temperatures for acetonitrile.

Table I: The Molal Entropy of Acetonitrile at 25° (cal deg⁻¹)

Liquid ^a	35.76 ± 0.15
Vaporization, 7848 ^b /298.15	26.32
Gas imperfection ^c	0.39
Compression	-4.27
Total experimental entropy	58.20 ± 0.20
Statistical mechanical entropy	58.20

^a From ref 2a. ^b From vapor-pressure data in ref 2a and 12. ^c From data in ref 9.

Table II: The Molal Thermodynamic Properties of Acetonitrile in the Ideal Gas State at 1 Atm

T , °K	$-(G^\circ - H^\circ_0)/T$, cal/deg	$(H^\circ - H^\circ_0)/T$, cal/deg	$H^\circ - H^\circ_0$, kcal	S° , cal/deg	C° , cal/deg
273.15	47.65	9.474	2.588	57.12	11.99
298.15	48.49	9.706	2.894	58.20	12.51
300	48.55	9.724	2.917	58.27	12.55
400	51.48	10.70	4.278	62.18	14.66
500	53.98	11.69	5.846	65.67	16.65
600	56.19	12.67	7.601	68.86	18.42
700	58.22	13.60	9.521	71.82	19.97
800	60.09	14.49	11.59	74.58	21.32
900	61.85	15.31	13.78	77.16	22.51
1000	63.50	16.08	16.08	79.58	23.55

Acknowledgments. This investigation was supported by Grant 660-A from the Petroleum Research Fund of the American Chemical Society, administered by Oklahoma State University, and was carried out in the Thermodynamics Laboratory of the Bartlesville Petroleum Research Center, Bureau of Mines, U. S. Department of the Interior, Bartlesville, Okla. The authors are grateful to Dr. Donald W. Scott for discussions of this work.

(11) J. P. McCullough, R. E. Pennington, J. C. Smith, I. A. Hosenlopp, and G. Waddington, *J. Am. Chem. Soc.*, **81**, 5880 (1959).

(12) G. L. Quinn, Thesis, University of Wisconsin, 1951.

Relaxation Spectra of Enzymatic Reactions¹

by Gordon G. Hammes and Paul R. Schimmel²

Department of Chemistry, Cornell University, Ithaca, New York 14850 (Received September 12, 1966)

A general and systematic approach for calculating the relaxation spectrum of some typical enzymatic mechanisms is presented. Reactions involving one or more substrates and products and mechanisms involving an arbitrary number of intermediates are considered. A schematic method is developed which permits individual relaxation times to be calculated by examination; for many cases, the entire relaxation spectrum of these mechanisms may be explicitly calculated by examination. The effect of pH and, under certain conditions, parallel pathways is incorporated into the schematic method. The practical application of these methods is illustrated and discussed.

Introduction

Chemical relaxation techniques are now being applied to reactions of biochemical interest.³⁻⁵ Relaxation techniques are particularly applicable to kinetic studies of enzymatic reactions, which are usually extremely rapid. These methods have been successfully applied to several enzymatic reactions⁶⁻¹⁰ and have given new and unique information pertaining to the mechanism of enzyme catalysis which cannot be obtained from conventional techniques.

Several theoretical treatments of the steady-state kinetics of enzymatic reactions are available.¹¹⁻¹⁶ Rate laws employed in these treatments may be extended to describe the relaxation of the system in the steady state,¹⁷ i.e., when the concentrations of all enzyme species are vanishingly small. However, relaxation experiments are most profitably conducted with concentrations of enzyme comparable to that of substrate in order that reaction intermediates can be detected.

In this paper, a general approach for calculating the relaxation spectrum of some typical enzymatic mechanisms is presented. A schematic method is developed which permits individual relaxation times to be calculated without recourse to complex mathematics. These methods are applicable to reactions involving one or more substrates and products and to mechanisms with an arbitrary number of isomeric intermediates; the effect of pH and, under certain conditions, parallel pathways is also considered. Our treatment is limited, however, to the most frequently considered mechanisms

whereby the reactions occur sequentially, that is without mechanistic "loops"; the free enzyme, of course, participates in the first and last reactions of the sequence. Although emphasis is placed on enzyme mechanisms, the results are applicable to other related reaction kinetic processes. The treatment presented here is based on the works of Castellan¹⁸ and Hammes and

(1) This work was supported by a grant from the National Institutes of Health (GM13292).

(2) National Institutes of Health Predoctoral Fellow.

(3) M. Eigen and L. de Maeyer in "Technique of Organic Chemistry," Vol. VIII, Part II, S. L. Friess, E. S. Lewis, and A. Weissberger, Ed., Interscience Publishers, Inc., New York, N. Y., 1963, p 895.

(4) M. Eigen and G. G. Hammes, *Advan. Enzymol.*, **25**, 1 (1963).

(5) G. G. Hammes, *Advan. Protein Chem.*, in press.

(6) G. G. Hammes and P. Fasella, *J. Am. Chem. Soc.*, **84**, 4644 (1962).

(7) P. Fasella and G. G. Hammes, *ibid.*, **85**, 3929 (1963).

(8) R. E. Cathou and G. G. Hammes, *ibid.*, **86**, 3240 (1964).

(9) R. E. Cathou and G. G. Hammes, *ibid.*, **87**, 4674 (1965).

(10) G. Czerlinski and J. Malkewitz, *Biochemistry*, **4**, 1127 (1965).

(11) E. L. King and C. Altman, *J. Phys. Chem.*, **60**, 1375 (1956).

(12) R. A. Alberty, *Advan. Enzymol.*, **17**, 1 (1956).

(13) L. Peller and R. A. Alberty, *J. Am. Chem. Soc.*, **81**, 5907 (1959).

(14) V. Bloomfield, L. Peller and R. A. Alberty, *ibid.*, **84**, 4367 (1962).

(15) M. Dixon and E. C. Webb, "Enzymes," Academic Press, Inc., New York, N. Y., 1964.

(16) L. Peller and R. A. Alberty, *Progr. Reaction Kinetics*, **1**, 237 (1961).

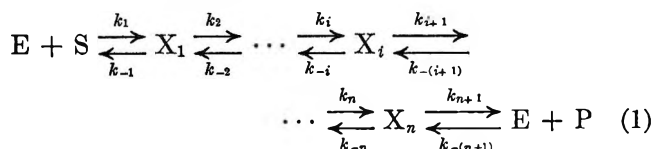
(17) G. G. Hammes and R. A. Alberty, *J. Am. Chem. Soc.*, **82**, 1564 (1960).

(18) G. W. Castellan, *Ber. Bunsenges. Physik. Chem.*, **67**, 898 (1963).

Schimmel.¹⁹ Czerlinski²⁰ and Kustin, *et al.*,²¹ have given a related but quite different discussion of the application of relaxation theory to biology.

Theoretical Treatment

The Single Substrate-Single Product Mechanism. The Michaelis-Menten mechanism for a single substrate and product with an arbitrary number of isomeric intermediates is



Here E, S, P and X_i denote enzyme, substrate, product, and the i th intermediate, respectively; the various k_i 's are the associated rate constants. The $n + 1$ relaxation times of eq 1 are the $n + 1$ eigenvalues of the secular equation^{18,19}

$$\left| \mathbf{b} - \frac{1}{\tau} \mathbf{I} \right| = 0 \quad (2)$$

where $|\mathbf{b} - (1/\tau)\mathbf{I}|$ is the determinant of the matrix $\mathbf{b} - (1/\tau)\mathbf{I}$, \mathbf{I} is the unit matrix, and the matrix \mathbf{b} has been previously defined.^{18,19} Applying the rules for computing \mathbf{b} ^{18,19} to eq 1 yields

$$\mathbf{b} = \begin{bmatrix} k'_1 + k_{-1} & -k_{-1} & 0 & \cdots & -k_1 \bar{S} \\ -k_2 & k_2 + k_{-2} & -k_{-2} & \cdots & 0 \\ 0 & -k_3 & k_3 + k_{-3} & \cdots & 0 \\ \vdots & \vdots & \vdots & \ddots & \vdots \\ -k_{-(n+1)} \bar{P} & 0 & \cdots & -k_{n+1} & k_{n+1} + k'_{-(n+1)} \end{bmatrix} \quad (3)$$

where the bars denote equilibrium concentrations and $k'_1 = k_1(\bar{E} + \bar{S})$, $k'_{-(n+1)} = k_{-(n+1)}(\bar{E} + \bar{P})$. The matrix elements $b_{1,n+1} = -k_1 \bar{S}$, and $b_{n+1,1} = -k_{-(n+1)} \bar{P}$ arise because the first and $n + 1$ st equilibria are coupled by E.

Relaxation times may be systematically calculated by the determinantal method.¹⁹ For example, if the j th reaction is assumed to be slowly equilibrated relative to all other reactions, then the relaxation time for this step is¹⁹

$$1/\tau_j = \frac{|\mathbf{b}|}{|\mathbf{b}_{jj}|} \quad (4)$$

where \mathbf{b}_{jj} is the matrix obtained by deleting the j th row and column of \mathbf{b} .¹⁹ The next longest relaxation time is then calculated in an analogous manner by substituting the matrix \mathbf{b}_{jj} for \mathbf{b} in eq 2. For example, if the l th reaction equilibrates slowly relative to all

other steps except the j th

$$1/\tau_l = \frac{|\mathbf{b}_{jj}|}{|\mathbf{b}_{jjll}|} \quad (5)$$

where \mathbf{b}_{jjll} is the matrix obtained by deleting the j th and l th rows and columns. This procedure is continued until the shortest relaxation time is obtained; this is the diagonal element associated with the fastest reaction in the original \mathbf{b} matrix. (For a 1×1 matrix, \mathbf{b}_{jj} is defined as unity.) This procedure for obtaining explicit expressions for each of the $n + 1$ relaxation times is valid as long as steps which equilibrate at comparable rates are not coupled together *via* rapid reactions. If two of the equilibria, the k th and m th, equilibrate at a comparable rate and are coupled *via* rapid reactions to the remaining equilibria, then the two relaxation times are given by the solutions of the quadratic¹⁹

$$|\mathbf{b}_{kk,mm}| \left(\frac{1}{\tau} \right)^2 - (|\mathbf{b}_{kk}| + |\mathbf{b}_{mm}|) \frac{1}{\tau} + |\mathbf{b}| = 0 \quad (6)$$

The matrix $\mathbf{b}_{kk,mm}$ may be used to calculate the remaining relaxation times by the systematic procedure outlined above. (For a 2×2 determinant, $\mathbf{b}_{kk,mm}$ is defined as unity.)

To calculate relaxation times by this procedure, an evaluation of the appropriate determinants is neces-

sary. To do this, the determinant of \mathbf{b} in eq 3 is first expanded by the cofactors of the elements in the first row

$$|\mathbf{b}| = (k'_1 + k_{-1})|\mathbf{b}_{11}| + k_{-1}|\mathbf{b}_{12}| \pm k_1 \bar{S} |\mathbf{b}_{1,n+1}| \quad (7)$$

where the plus sign is applicable to the last term if n is odd, and the minus sign if n is even. Use of previous results¹⁹ and simple matrix manipulations gives

$$\begin{aligned} |\mathbf{b}_{11}| &= P_2^{n+1} \\ |\mathbf{b}_{12}| &= -k_2 P_3^{n+1} - \prod_{i=2}^n k_{-i} k_{-(n+1)} \bar{P} \\ |\mathbf{b}_{1,n+1}| &= \pm \prod_{i=2}^{n+1} k_i \pm k_{-(n+1)} \bar{P} P_2^n \begin{cases} +, n_{\text{even}} \\ -, n_{\text{odd}} \end{cases} \end{aligned}$$

(19) G. G. Hammes and P. R. Schimmel, *J. Phys. Chem.*, **70**, 2319 (1966).

(20) G. Czerlinski, *J. Theoret. Biol.*, **7**, 435, 463 (1964).

(21) K. Kustin, D. Shear, and D. Kleitman, *ibid.*, **9**, 186 (1965).

where¹⁹

$$P_m^s = \sum_{p=m-1}^s \prod_{i=m}^p k_i \prod_{j=p+1}^s k_{-j} \quad (8)$$

and it is understood that the second-order rate constants are written as k'_1 and $k'_{-(n+1)}$ in P_m^s .

Therefore

$$|\mathbf{b}| = P_1^{n+1} - \prod_{i=2}^{n+1} k_i k_1 \bar{S} - \prod_{i=1}^n k_{-i} k_{-(n+1)} \bar{P} - k_1 k_{-(n+1)} \bar{P} \bar{S} P_2^n \quad (9)$$

where use has been made of the equality

$$(k'_1 + k_{-1}) P_2^{n+1} - k_{-1} k_2 P_3^{n+1} = P_1^{n+1}$$

It is convenient to define the *reduced product* $\prod_{i=m}^s (k_i + k_{-i})_R$ which is obtained by *deleting* from the product $\prod_{i=m}^s (k_i + k_{-i})$ all terms which contain one or more factors of the form $k_{-j} k_{j+1}$ ($j = m, \dots, s-1$) and $k_1 \bar{S} k_{-(n+1)} \bar{P}$. For the case of interest, eq 1, these are pairs of rate constants which "lead away" from the j th enzyme species, i.e., $\xleftarrow{k_{-j}} X_j \xrightarrow{k_{j+1}}$ and $\xleftarrow{k_{-(n+1)} \bar{P}} E \xrightarrow{k_1 \bar{S}}$. (E can be defined as the *zeroth* enzyme species.) In addition, the products of rate constants leading from X_j back to X_j ($j = 0, 1, \dots, n$), i.e., $k_1 \bar{S} \prod_{i=2}^{n+1} k_i$ and $\prod_{i=1}^n k_{-i} k_{-(n+1)} \bar{P}$, are also deleted. In forming $\prod (k_i + k_{-i})_R$ from $\prod (k_i + k_{-i})$, terms are always deleted and are never added. Thus, for the mechanism under consideration, the terms $k_1 \bar{S} \prod_{i=2}^{n+1} k_i$ and $\prod_{i=1}^n k_{-i} k_{-(n+1)} \bar{P}$ occur only in expanding the product $\prod_{i=1}^{n+1} (k_i + k_{-i})$ and must be eliminated in obtaining $\prod_{i=1}^{n+1} (k_i + k_{-i})_R$. These terms do not occur in the product $\prod_{i=2}^{n+1} (k_i + k_{-i})$ and hence cannot be eliminated from it in obtaining $\prod_{i=2}^{n+1} (k_i + k_{-i})_R$. Finally, it is understood that the bimolecular rate constants which may occur in the product $\prod (k_i + k_{-i})$ are modified as previously discussed. For the mechanism under consideration it is easily verified that

$$P_m^s = \prod_{i=m}^s (k_i + k_{-i})_R; \quad (P_m^s \neq P_1^{n+1})$$

For the case of $m = 1, s = n + 1$, it follows from eq 8 and the definition of the reduced product that

$$P_1^{n+1} = \prod_{i=1}^{n+1} (k_i + k_{-i})_R + k_1 \bar{S} \prod_{i=2}^n k_i + \prod_{i=1}^n k_{-i} k_{-(n+1)} \bar{P} + k_1 k_{-(n+1)} \bar{P} \bar{S} P_2^n \quad (10)$$

The terms added to the reduced product on the right side of eq 10 are among the terms deleted from $\prod_{i=1}^{n+1} (k_i + k_{-i})$ in obtaining $\prod_{i=1}^{n+1} (k_i + k_{-i})_R$; therefore, these terms are not in $\prod_{i=1}^{n+1} (k_i + k_{-i})_R$ but must be present in P_1^{n+1} (cf. eq 8). Substitution of eq 10 into eq 9 yields

$$|\mathbf{b}| = \prod_{i=1}^{n+1} (k_i + k_{-i})_R \quad (11)$$

The determinant $|\mathbf{b}_{jj}|$ may be expanded by cofactors of the first row in a similar manner. The result is

$$|\mathbf{b}_{jj}| = (k'_1 + k_{-1}) P_2^{j-1} P_{j+1}^{n+1} - k_{-1} k_2 P_3^{j-1} P_{j+1}^{n+1} - k_1 k_{-(n+1)} \bar{P} \bar{S} P_2^{j-1} P_{j+1}^n \quad (j \neq l, n+1) \quad (12)$$

$$= P_1^{j-1} P_{j+1}^{n+1} - k_1 k_{-(n+1)} \bar{P} \bar{S} P_2^{j-1} P_{j+1}^n \quad (j \neq l, n+1) \quad (12a)$$

$$= \prod_{i=1}^{n+1} (k_i + k_{-i})_R \quad i \neq j \quad (12b)$$

For the case $j = 1$ or $n + 1$, it follows from our previous results¹⁹ that

$$|\mathbf{b}_{11}| = P_2^{n+1} = \prod_{i=2}^{n+1} (k_i + k_{-i})_R \quad (13a)$$

and

$$|\mathbf{b}_{n+1, n+1}| = P_1^n = \prod_{i=1}^n (k_i + k_{-i})_R \quad (13b)$$

Therefore, it follows from eq 12 and 13 that

$$|\mathbf{b}_{jj}| = \prod_{i=1}^{n+1} (k_i + k_{-i})_R \quad (j = 1, 2, \dots, n, n+1) \quad (14)$$

In general, if the j th, l th, etc., rows and columns are deleted from $|\mathbf{b}|$, the resulting determinant is

$$|\mathbf{b}_{jj, ll, \text{etc.}}| = \prod_{i \neq j, l, \text{etc.}} (k_i + k_{-i})_R \quad (15)$$

Relaxation times are given by the ratio of determinants (cf. eq 4). Thus, the relaxation time of the l th step of eq 1 which is coupled *via* rapid reactions to several other steps in the mechanism is

$$1/\tau_l = \frac{\prod_{i \neq l} (k_i + k_{-i})_R}{\prod_{i \neq l} (k_i + k_{-i})_R} \quad (16)$$

volving binary complexes,²³ may also be treated in a similar manner. In general, any mechanism which involves a sequence of reactions where the *i*th enzyme species participates in the *i*th and *i* + 1st reaction only may be treated by the methods described above. (The zeroth species, the free enzyme, is coupled to the first and last reactions of the sequence, of course.)

Illustrations of the Method

For the mechanisms being considered, the relaxation time of the *j*th equilibrium which is coupled *via* rapid reactions to several other steps is

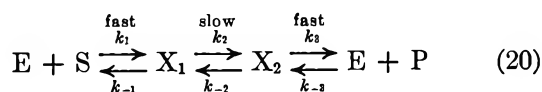
$$1/\tau_j = \frac{\prod_{i \neq j} (k_i + k_{-i})_R}{\prod_{i \neq j} (k_i + k_{-i})_R}$$

where $\prod_{i \neq j} (k_i + k_{-i})_R$ is the reduced product and the index *i* runs over all equilibria coupled *via* rapid reactions to the *j*th step including the *j*th step. The reduced product is defined and discussed in the previous section and may be written by examination. If the *j*th and *m*th equilibria equilibrate at comparable rates and are coupled to each other *via* rapid reactions, the two relaxation times are solutions of the quadratic

$$\prod_{i \neq j, m} (k_i + k_{-i})_R \left(\frac{1}{\tau}\right)^2 - \left(\prod_{i \neq j} (k_i + k_{-i})_R + \prod_{i \neq m} (k_i + k_{-i})_R \right) \left(\frac{1}{\tau}\right) + \prod_{i \neq m} (k_i + k_{-i})_R = 0$$

where $\prod_{i \neq m} (k_i + k_{-i})_R$ runs over all steps coupled *via* rapid reactions to the *j*th and *m*th reactions, including the *j*th and *m*th.

As an illustration, we consider the mechanism



The relaxation time of the slow step is

$$\frac{1}{\tau_2} = \frac{\prod_{i=1}^3 (k_i + k_{-i})_R}{\prod_{i=1}^3 (k_i + k_{-i})_R} = \frac{\{[k_1(\bar{E} + \bar{S}) + k_{-1}][k_2 + k_{-2}][k_3 + k_{-3}(\bar{E} + \bar{P})]\}_R}{\{[k_1(\bar{E} + \bar{S}) + k_{-1}][k_3 + k_{-3}(\bar{E} + \bar{P})]\}_R} \quad (21)$$

To reduce $\prod_{i=1}^3 (k_i + k_{-i})$ to $\prod_{i=1}^3 (k_i + k_{-i})_R$, we delete from $\prod_{i=1}^3 (k_i + k_{-i})$ all terms containing one or more of the factors $k_{-1}k_2$, $k_{-2}k_3$, $k_{-3}\bar{P}k_1\bar{S}$, and $k_1k_2k_3\bar{S}$, $k_{-1}k_{-2}k_{-3}\bar{P}$. The result is

$$\prod_{i=1}^3 (k_i + k_{-i})_R = (k_1k_2k_3 + k_{-1}k_{-2}k_{-3})\bar{E} + (k_1k_2k_{-3} + k_1k_{-2}k_{-3})(\bar{E}^2 + \bar{E}\bar{S} + \bar{E}\bar{P})$$

Similarly

$$\prod_{i=1}^3 (k_i + k_{-i})_R = (k_1k_3 + k_{-1}k_{-3})\bar{E} + k_1k_{-3}(\bar{E}^2 + \bar{E}\bar{S} + \bar{E}\bar{P}) + k_1k_3\bar{S} + k_{-1}k_{-3}\bar{P} + k_{-1}k_3$$

Finally, we obtain by eq 21

$$1/\tau_2 = \frac{k_2}{1 + \frac{k_1k_3\bar{S} + k_{-1}k_{-3}\bar{P} + k_{-1}k_{-3}\bar{E} + k_{-1}k_3}{k_1k_3\bar{E} + k_1k_{-3}(\bar{E}^2 + \bar{E}\bar{S} + \bar{E}\bar{P})} + \frac{k_{-2}}{1 + \frac{k_1k_3\bar{S} + k_{-1}k_{-3}\bar{P} + k_1k_3\bar{E} + k_{-1}k_3}{k_{-1}k_{-3}\bar{E} + k_1k_{-3}(\bar{E}^2 + \bar{E}\bar{S} + \bar{E}\bar{P})}}$$

The relaxation times of the fast bimolecular steps are solutions of the quadratic

$$\prod_{i=1,2,3}^3 (k_i + k_{-i})_R \left(\frac{1}{\tau}\right)^2 - \left\{ \prod_{i=1}^3 (k_i + k_{-i})_R + \prod_{i=2,3}^3 (k_i + k_{-i})_R \right\} \left(\frac{1}{\tau}\right) + \prod_{i=2}^3 (k_i + k_{-i})_R = 0$$

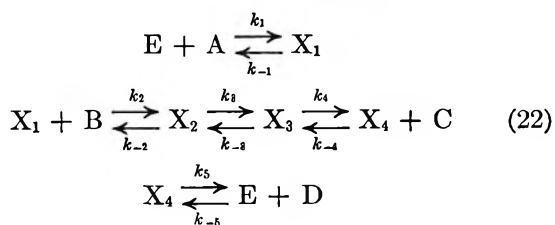
with $\prod_{i=1,2,3}^3 (k_i + k_{-i})_R \equiv 1$.

Evaluation of the products gives

$$\left(\frac{1}{\tau_{1,3}}\right)^2 - (k_1(\bar{E} + \bar{S}) + k_{-1} + k_3 + k_{-3}(\bar{E} + \bar{P})) \times \left(\frac{1}{\tau_{1,3}}\right) + (k_1k_3(\bar{E}^2 + \bar{E}\bar{S} + \bar{E}\bar{P}) + \bar{E}(k_1k_3 + k_{-1}k_{-3}) + k_1k_3\bar{S} + k_{-1}k_{-3}\bar{P} + k_{-1}k_3) = 0$$

Thus the relaxation spectrum of eq 20 has been explicitly calculated.

As a second example, consider the relaxation time for the unimolecular step in the mechanism



The expression for this relaxation time is very complex, but it is readily derived by the schematic method.

(23) H. Theorell and B. Chance, *Acta Chem. Scand.*, 5, 1127 (1951).

If this step is slow compared to the bimolecular steps, we obtain

$$\frac{1}{\tau} = \frac{\prod_{i=1}^5 (k_i + k_{-i})_R}{\prod_{\substack{i=1 \\ i \neq 3}}^5 (k_i + k_{-i})_R}$$

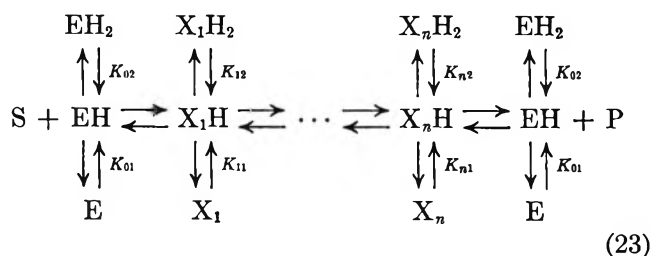
To reduce the product $\prod_{i=1}^5 (k_i + k_{-i})_R$ to $\prod_{i=1}^5 (k_i + k_{-i})_R$, all terms containing the factors $k_{-1}k_2\bar{B}$, $k_{-2}k_3$, $k_{-3}k_4$, $k_{-4}\bar{C}k_5$, $k_1\bar{A}k_{-5}\bar{D}$, and $k_1\bar{A}k_2\bar{B}k_3k_4k_5$, $k_{-1}k_{-2}k_{-3}k_{-4}\bar{C}k_{-5}\bar{D}$ are eliminated from $\prod_{i=1}^5 (k_i + k_{-i})_R$. The reduced products are

$$\begin{aligned} \prod_{i=1}^5 (k_i + k_{-i})_R &= k_1k_2k_3k_4k_5(\bar{E}\bar{B} + \bar{E}\bar{X}_1 + \bar{X}_1\bar{A}) + \\ & (k_3 + k_{-3})(k_1k_2k_{-4}k_5)\bar{X}_4(\bar{E} + \bar{A})(\bar{X}_1 + \bar{B}) + \\ & (k_3 + k_{-3})(k_1k_2k_{-4}k_{-5})(\bar{E})(\bar{X}_4 + \bar{C})(\bar{E}\bar{B} + \bar{E}\bar{X}_1 + \\ & \bar{X}_1\bar{A} + \bar{A}\bar{B} + \bar{B}\bar{D} + \bar{D}\bar{X}_1) + \\ & (k_3 + k_{-3})(k_{-1}k_2k_{-4}k_{-5})\bar{X}_1(\bar{X}_4 + \bar{C})(\bar{E} + \bar{D}) + \\ & k_1k_2k_3k_4k_{-5}[\bar{E}(\bar{E}\bar{B} + \bar{E}\bar{X}_1 + \bar{X}_1\bar{A} + \bar{A}\bar{B} + \bar{B}\bar{D} + \\ & \bar{D}\bar{X}_1)] + k_1k_{-2}k_{-3}k_{-4}k_{-5}\bar{E}(\bar{E}\bar{X}_4 + \bar{A}\bar{X}_4 + \bar{A}\bar{C} + \\ & \bar{E}\bar{C} + \bar{D}\bar{X}_4 + \bar{D}\bar{C}) + k_{-1}k_{-2}k_{-3}k_{-4}k_{-5}(\bar{E}\bar{C} + \\ & \bar{D}\bar{X}_4 + \bar{X}_1\bar{D}) + k_{-1}k_2k_3k_4k_5\bar{X}_1 + k_{-1}k_{-2}k_{-3}k_{-4}k_5\bar{X}_4 + \\ & (k_3 + k_{-3})(k_{-1}k_2k_{-4}k_5)\bar{X}_1\bar{X}_4 + \\ & k_1k_{-2}k_{-3}k_{-4}k_5(\bar{E} + \bar{A})\bar{X}_4 + k_{-1}k_2k_3k_4k_{-5}\bar{X}_1(\bar{E} + \bar{D}) \\ \prod_{\substack{i=1 \\ i \neq 3}}^5 (k_i + k_{-i})_R &= k_1k_2k_4k_5(\bar{E} + \bar{A})(\bar{X}_1 + \bar{B}) + \\ & k_{-1}k_2k_4k_5\bar{X}_1 + k_1k_{-2}k_4k_5(\bar{E} + \bar{A}) + k_{-1}k_{-2}k_4k_5 + \\ & k_1k_2k_{-4}k_5\bar{X}_4(\bar{E} + \bar{A})(\bar{X}_1 + \bar{B}) + k_{-1}k_2k_{-4}k_5\bar{X}_1\bar{X}_4 + \\ & k_1k_{-2}k_{-4}k_5(\bar{E} + \bar{A})\bar{X}_4 + k_{-1}k_{-2}k_{-4}k_5\bar{X}_4 + \\ & k_1k_2k_4k_{-5}[\bar{E}(\bar{E}\bar{X}_1 + \bar{E}\bar{B} + \bar{A}\bar{X}_1 + \bar{A}\bar{B} + \\ & \bar{D}\bar{X}_1 + \bar{D}\bar{B})] + k_{-1}k_2k_4k_{-5}\bar{X}_1(\bar{E} + \bar{D}) + \\ & k_1k_{-2}k_4k_{-5}(\bar{E}^2 + \bar{E}\bar{A} + \bar{E}\bar{D}) + \\ & k_{-1}k_{-2}k_4k_{-5}(\bar{E} + \bar{D}) + \\ & k_1k_2k_{-4}k_{-5}[\bar{E}(\bar{X}_4 + \bar{C})(\bar{E}\bar{B} + \bar{E}\bar{X}_1 + \bar{X}_1\bar{A} + \\ & \bar{A}\bar{B} + \bar{B}\bar{D} + \bar{D}\bar{X}_1)] + \\ & k_1k_{-2}k_{-4}k_{-5}\bar{E}(\bar{E}\bar{X}_4 + \bar{A}\bar{X}_4 + \bar{A}\bar{C} + \bar{E}\bar{C} + \bar{D}\bar{X}_4 + \\ & \bar{D}\bar{C}) + k_{-1}k_{-2}k_{-4}k_{-5}(\bar{X}_4 + \bar{C})(\bar{E} + \bar{D}) + \\ & k_{-1}k_2k_{-4}k_{-5}\bar{X}_1(\bar{X}_4 + \bar{C})(\bar{E} + \bar{D}) + \\ & k_{-1}k_{-2}k_{-4}k_{-5}(\bar{X}_4 + \bar{C})(\bar{E} + \bar{D}) \end{aligned}$$

The four remaining relaxation times may also be calculated by the schematic method provided that no more than two equilibria are coupled *via* rapid reactions.

The Effect of pH

Only the single substrate-single product mechanism is treated in this section, but the results are applicable to the other mechanisms discussed. The catalytic activity of many enzymes depends markedly on pH. To discuss the effect of pH, eq 1 can be modified in the usual fashion.¹³



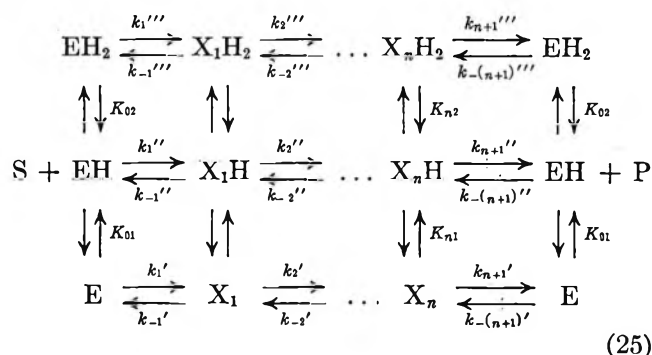
Only the monoprotonated form of the enzyme is assumed to be catalytically active. The double subscript K 's are acid dissociation constants¹³ and protons have been omitted from the mechanism for the sake of simplicity. To compute the relaxation times, two assumptions are employed: the protolytic equilibria are rapidly adjusted compared to other reactions, and the hydrogen ion concentration is buffered, that is $\Delta(\text{H}^+) \approx 0$. This condition is easily satisfied by working at sufficiently high buffer concentrations. A matrix analogous to eq 3 may be constructed and in fact the resulting matrix is identical with eq 3 except that the rate constant k_i is replaced by an apparent rate constant θ_i , where $\theta_i = k_i/\psi_{i-1}$, $\theta_{-i} = k_{-i}/\psi_i$, and

$$\psi_i = 1 + \frac{k_{i1}}{[\text{H}^+]} + \frac{[\text{H}^+]}{K_{i2}} \quad (24)$$

In addition, \bar{E} is replaced by $\bar{E}\bar{H}\psi_0$ (*i.e.*, the total free enzyme concentration).

The previously derived results are applicable if the rate constants k_i are replaced by their pH-dependent analogs θ_i . The θ_i 's vary in the familiar bell-shaped fashion.

Another scheme which may be employed to describe the effect of pH is



where S and P can react with all of the ionization states of the enzyme. This mechanism has more equilibria than relaxation times (*cf.* ref 19, where the relaxation spectrum of a similar mechanism is discussed in detail). We can calculate the relaxation times for the horizontal steps if we again assume that the vertical protolytic steps are rapidly adjusted and buffering occurs. All of the previously derived results are then applicable except that each k_i in the **b** matrix of eq 3 is replaced by an apparent rate constant θ_i where

$$\theta_i = \frac{\beta_i}{\psi_{i-1}}; \quad \theta_{-i} = \frac{\beta_{-i}}{\psi_i}$$

$$\beta_i = k_i'' + k_i''' \frac{K_{i-1,1}}{[H^+]} + k_i' \frac{[H^+]}{K_{i-1,2}}$$

$$\beta_{-i} = k_{-i}'' + k_{-i}''' \frac{K_{i1}}{[H^+]} + \frac{k_{-i}'[H^+]}{K_{i2}}$$

and \bar{E} is again replaced by $\bar{E}H\psi_0$. The apparent rate constants may or may not vary with changes in pH depending on the relative values of the pH-independent rate constants.

Discussion

The results presented here provide a systematic and straightforward method for calculating the relaxation spectrum of enzymatic reactions involving an arbitrary number of intermediates. Individual relaxation times may be calculated by examination. Although only those mechanisms frequently employed to interpret the kinetics of enzyme-catalyzed reactions are considered, the determinantal method provides a straightforward means for calculating the relaxation spectrum of any reaction mechanism. For a more general discussion of this method, the papers of Castellán¹⁸ and Hammes and Schimmel¹⁹ should be consulted.

Bonding and Hybridization in the Nitrogen Molecule¹

by Paul R. Smith and James W. Richardson

General Atomic Division of General Dynamics Corporation, Special Nuclear Effects Laboratory, San Diego, California, and the Department of Chemistry, Purdue University, Lafayette, Indiana (Received September 13, 1966)

Molecular orbital wave functions from successively improved LC-STO SCF calculations for the N₂ molecule are compared. In addition to the usual physical properties and Mulliken population analyses, the total electronic charge distribution and the density difference function $\delta\rho(R) = \rho_M(R) - \rho_A(R)$ are considered. Although improvements in the wave function lead to difficulties with the population analysis, they do give a more satisfactory picture of the bond charge density. With such "flexibilization," the electronic charge density is found to increase in the internuclear region over that of the superposed atoms; general agreement with Ruedenberg's "clustering" hypothesis is found. By changing the "valence state" of the constituent atoms, ρ_A changes also. A $2s-2p\sigma$ hybridization of about 10% minimizes the average value over all space of $|\delta\rho(R)|$.

Introduction

A knowledge of the charge distribution in a molecule is essential for understanding the chemical behavior of the molecule. The characteristics of the molecular charge distribution, particularly when compared with the charge densities of the noninteracting constituent atoms, reflect the nature of the chemical bonding mechanism and provide insight into traditional concepts, such as localized chemical bonds.

The recent progress toward better approximations in molecular wave functions has increased their complexity and created a need for methods of comparison and evaluation. For some molecules, the techniques of improving self-consistent field molecular orbital (SCF-MO) wave functions have been carefully studied and a significant increase in accuracy has been achieved by expanding the basis set. The general improvement in computed observable properties is accompanied, however, by increasing difficulties in applying other techniques of analysis which attempt to correlate molecular orbitals with useful chemical concepts, such as localized chemical bonds and hybridization. There has been some utilization of density matrices² and approximate natural spin orbitals,³ but most of the studies have used Mulliken's population analysis⁴ as their basis. Recently, Mulliken has surveyed this problem and has drawn attention to the need for careful prior judgment in specifying an extended basis set in order that apparently misleading physical

interpretations not be made from the population analysis.⁵

For a great many systems, Roux and collaborators,⁶⁻¹¹ Rosenfeld,¹² Bader and Henneker,¹³⁻¹⁵ Smith and Richardson,¹⁶ and Politzer^{17,18} have studied the

(1) (a) This work was supported primarily by the Advanced Research Projects Agency under a contract with Purdue University and partly by General Atomic; (b) presented in part at the Symposium on Molecular Structure and Spectroscopy, The Ohio State University, Columbus, Ohio, June 10-14, 1963.

(2) (a) R. McWeeny, *Proc. Roy. Soc. (London)*, **A232**, 114 (1954); (b) P.-O. Löwdin, *Phys. Rev.*, **97**, 1474, 1490 (1955); (c) R. McWeeny, *Rev. Mod. Phys.*, **32**, 335 (1960).

(3) (a) P.-O. Löwdin and H. Shull, *Phys. Rev.*, **101**, 1730 (1956); (b) H. Shull, *J. Am. Chem. Soc.*, **82**, 1287 (1960).

(4) R. S. Mulliken, *J. Chem. Phys.*, **23**, 1833 (1955).

(5) R. S. Mulliken, *ibid.*, **36**, 3428 (1962).

(6) M. Roux, S. Besnainou, and R. Daudel, *J. Chim. Phys.*, **54**, 218, 939 (1956).

(7) M. Roux, *ibid.*, **55**, 754 (1960).

(8) M. Roux, *ibid.*, **57**, 53 (1960).

(9) S. Bratoz, R. Daudel, M. Roux, and M. Allavena, *Rev. Mod. Phys.*, **32**, 412 (1960).

(10) M. Roux, M. Cornille, and G. Bessis, *J. Chim. Phys.*, **58**, 389 (1961).

(11) M. Roux, M. Cornille, and L. Burnelle, *J. Chem. Phys.*, **37**, 933 (1962).

(12) J. L. J. Rosenfeld, *Acta Chem. Scand.*, **18**, 1719 (1964).

(13) R. F. W. Bader, *J. Am. Chem. Soc.*, **86**, 5070 (1964).

(14) R. F. W. Bader and W. H. Henneker, *ibid.*, **87**, 3063 (1965).

(15) R. F. W. Bader and W. H. Henneker, *ibid.*, **88**, 280 (1966).

(16) P. R. Smith and J. W. Richardson, *J. Phys. Chem.*, **69**, 3346 (1965).

character of the function

$$\delta\rho(R) = \rho_M(R) - \rho_A(R) \quad (1)$$

where $\rho_M(R)$ is the total electronic charge density at the point R of the molecule M and $\rho_A(R)$ is the electronic charge density at the same point R which would result if the constituent atoms of the molecule M were superposed at the molecular equilibrium distance. In a careful analysis and interpretation of the nature and cause of chemical bond formation, Ruedenberg has ascribed some considerable importance to such a function.¹⁹ Ruedenberg suggests, among other things, that the real source of energy lowering during bond formation occurs when electrons pull in closer, or cluster nearer, to the nuclei.

The objectives of this study are (1) to compare the actual form of wave functions and charge densities with results of corresponding population analyses, (2) to utilize the $\delta\rho(R)$ function to detect the clustering phenomenon, and (3) to utilize the $\delta\rho(R)$ function in determining an alternative, more general definition of hybridization in a molecule.

The N_2 molecule in its ground state was selected for the present study because it has a variety of bonding interactions and because there are several sets of MO wave functions available which represent a wide range in flexibility and polarization as indicated by the choice of basis orbitals.⁵

Wave Functions for the N_2 Molecule

The wave functions considered here represent various stages of approximation to a closed-shell Hartree-Fock (HF) solution of the Schrödinger equation. Four successively improved sets of single-determinant MO wave functions were studied in detail: (1) the Scherr SCF-MO wave function,²⁰ which uses a minimal set of Slater-type orbitals (STO's) with the free-atom orbital exponents (ζ 's) fixed by Slater's rules; (2) the Best Limited (BL) SCF-MO's (or Best Minimal in Mulliken's most recent terminology²¹) of Ransil,²² in which the orbital exponents of the Scherr function are varied in order to minimize the total molecular energy and thus achieve the best over-all ζ 's; (3) the "double- ζ " SCF-MO's of Richardson,²³ in which the basis set is expanded by doubling the number of second quantum STO's included; and (4) a more nearly exact set of Hartree-Fock SCF-MO's of Cade, *et al.*,²⁴ which for most practical purposes give the most accurate wave function in the orbital approximation. The wave function used here is for $R = R_e(\text{exptl})$ not $R = R_e(\text{HF})$.

Some comparisons of theoretical and predicted ex-

perimental properties are given in Tables I, II, and III. A steady decrease is seen in the total-energy error toward the residual correlation energy of 16.1 ev. Also seen is a steady increase in a predicted "bond energy," defined here as the difference between the energies of the N_2 molecule and two N atoms, the atomic and the molecular wave functions each having the same degree of improvement. Although there is no special justification for this definition in general, it is relevant to some calculations of $\delta\rho(R)$ reported below.

Table I: Comparisons of Some Physical Properties

Wave function	ΔE^a	D_0^b	Q^c	eQq^d
Scherr	27.5	1.20	-1.90	1.49
Ransil BL ^e	25.9	2.61	-1.02	3.49
2 ζ	21.8	3.48	-1.38	4.41
Hartree-Fock ^f	16.1	5.20
Experimental	...	9.90	-1.11	4.65

^a Error in computed total energy, in ev. ^b Dissociation energy (in ev) computed as indicated in text. ^c Molecular Quadrupole moment, in au. Computed as indicated by C. Greenhow and W. V. Smith, *J. Chem. Phys.*, **19**, 1298 (1951). The necessary integrals were obtained from a molecular properties integral program written by Dr. A. C. Wahl for the IBM 704 computer at Argonne National Laboratories. ^d Quadrupole coupling constants, in Mc; calculated values assume the nuclear quadrupole moment to be 0.02×10^{-24} cm. ^e The necessary atomic data were calculated from Roothaan's Best Atomic wave functions (see ref 27). ^f Based on $R = R_0(\text{exptl}) = 2.068$ au.

A general improvement is clearly seen in total energy and in a few available experimental quantities, which depend on the molecular charge distribution.

Shapes of the Various MO's and Corresponding Population Analysis

The N_2 molecule has the ground-state electronic configuration

$$1\sigma_g^2 1\sigma_u^2 2\sigma_g^2 2\sigma_u^2 1\pi_u^4 3\sigma_g^2$$

Appropriate contour maps, as described below, were drawn for each of the occupied MO's.²⁵ The drawings

- (17) P. Politzer, *J. Phys. Chem.*, **70**, 1174 (1966).
 (18) P. Politzer and R. E. Brown, *J. Chem. Phys.*, **45**, 451 (1966).
 (19) K. Ruedenberg, *Rev. Mod. Phys.*, **34**, 326 (1962).
 (20) C. W. Scherr, *J. Chem. Phys.*, **23**, 569 (1955).
 (21) R. S. Mulliken, *Rev. Mod. Phys.*, **32**, 232 (1960).
 (22) B. J. Ransil, *ibid.*, **32**, 245 (1960).
 (23) J. W. Richardson, *J. Chem. Phys.*, **35**, 1829 (1961).
 (24) P. E. Cade, K. D. Sales, and A. C. Wahl, *ibid.*, **44**, 1973 (1966).
 (25) For a visual presentation of these MO contour maps, see ref 16 and A. C. Wahl, *Science*, **151**, 961 (1966).

Table II: Comparison of Orbital Energies and Experimental Ionization Potential (in au)

Orbital	Scherr	BL	2 ζ	HF	Exptl
1 σ_g	-15.72176	-15.80452	-15.70512	-15.68195	...
1 σ_u	-15.71965	-15.80219	-15.70192	-15.67833	...
2 σ_g	-1.45241	-1.47922	-1.49301	-1.47360	...
2 σ_u	-0.73066	-0.75409	-0.76287	-0.77796	-0.69
1 π_u	-0.57951	-0.60486	-0.61378	-0.61544	-0.62
3 σ_g	-0.54451	-0.56759	-0.62225	-0.63495	-0.57

Table III: Overlap Populations and $s-p\sigma$ Hybridization

MO	Scherr	BL	2 ζ
2 σ_g	0.85	0.83	0.78
2 σ_u	-0.37	-0.68	-2.05
3 σ_g	-0.08	0.07	0.10
1 π_u	0.88	0.91	0.95
Total	1.28	1.12	-0.22
Hybridization	26%	21%	2%

represent a cross section of the three-dimensional wave function on a plane passing through the internuclear axis. The comparisons detailed below are made chiefly between the Scherr and 2 ζ functions. The BL functions were intermediate in all cases and, except for 2 σ_g , the 2 ζ and HF-MO's are essentially the same.

Upon improvement of the basis set, the most marked change is observed in the 2 σ_g MO, which becomes considerably more concentrated in the internuclear region. Note that this is in contradiction to the moderate decrease in the overlap population for this MO, which becomes even more concentrated in the internuclear region in the HF case.

Although the use of population analyses in correlating the bonding and antibonding character of various molecular orbitals and total overlap populations has been attempted,^{4,20,26} the general validity of the population analyses remains questionable. That these analyses must be used with reservation is indeed borne out by the very negative overlap population of the 2 σ_u MO of the 2 ζ wave function, which leads to an over-all negative value for the total overlap population even though the over-all shape of the 2 σ_u is virtually unchanged by improvements in the wave functions. To emphasize this point, drawings from the Scherr and the 2 ζ approximations are superimposed in Figure 1. Despite the uniformity in Figure 1, there is a drastic change in the overlap population from the reasonable -0.37 to the disastrous -2.05. This extreme negative value causes even the total overlap population to become negative.

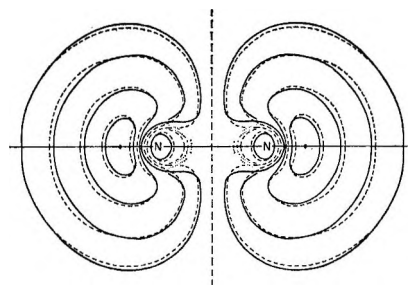


Figure 1. Superposition of the 2 σ_u MO as obtained from the Scherr wave function and the 2 ζ wave function for N₂. For clarity, the solid lines represent the 2 ζ wave function and the dashed lines represent the Scherr wave function.

The 3 σ_g MO remains essentially the same when the wave function is improved, even though the orbital energy of this most loosely bound MO is seen to fluctuate most widely. There is only a slight change in the overlap population from -0.08 to 0.10.

The 1 π_u MO has its familiar shape and retains a strong resemblance to the free atom 2 $p\pi$. As the total wave function is improved, the MO becomes slightly more diffuse, even though a moderate increase in the overlap population is observed.

In order to see how the overlap population of the 2 σ_u MO changed so much, first note that the $\varphi(2\sigma_u)$ may be written as

$$\varphi(2\sigma_u) = hy - hy^+ \quad (2)$$

where hy is the sum of all STO's centered on nucleus a and hy^+ is the mirror-image sum on nucleus b . Graphs of hy for the Scherr and 2 ζ MO's are given in Figure 2.

In the Scherr function, the magnitude of the 2 σ_u MO is decreased in the internuclear region by considerable 2 $s-2p\sigma$ hybridization; *i.e.*, the 2 s AO is strongly polarized outward. Subtraction of hy^+ from hy decreases it a small amount more and leads to the moderate negative overlap population. On the other hand, in the 2 ζ function, the 2 s is polarized only in a region nearer the nucleus (by hybridization of the

(26) S. Fraga and B. J. Ransil, *J. Chem. Phys.*, **34**, 727 (1961).

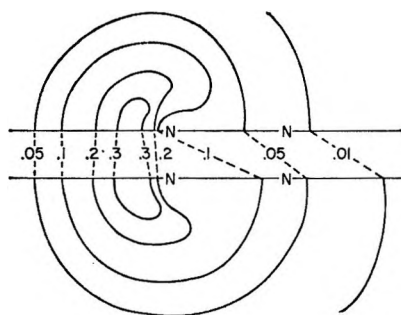


Figure 2. Comparison between h_y (Scherr) and $h_y(2\zeta)$. See text for discussion. Upper plane, Scherr approximation; lower plane, 2ζ approximation.

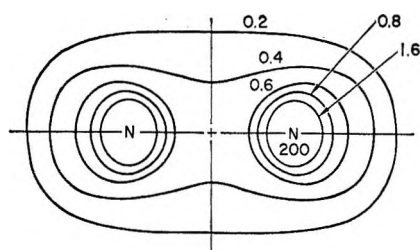


Figure 3. Total electronic charge density for the N_2 molecule in the Scherr approximation. The numbers correspond to the density in units of electron per cubic atomic unit. The value 200 represents the density at the nitrogen nucleus.

larger- ζ $2p\sigma$ STO of the double- ζ function) and instead the $2s$ becomes much more diffuse. Now the $2\sigma_u$ MO becomes small in the internuclear region only by a large cancellation of h_y by h_y^+ . There is thus found the large negative overlap population and also the greatly decreased $s-p\sigma$ hybridization noted in Table III.

In other words, expansion of the $2s$ AO at one center has partially replaced hybridization at the other center. In many respects this situation is like that found, for example, in some studies of HF and discussed by Mulliken.⁵ There, when additional hydrogen STO's but not fluorine AO's were included in the basis set, the hydrogen STO's assumed a disproportionate share of the bonding and an unreasonable charge distribution was obtained from the population analysis. In this case, a reasonable situation returns only when expansion of the basis set is judiciously balanced between H and F.

Molecular Charge Distributions

A contour drawing of the total electronic charge density in a plane passing through the nuclei is given in Figure 3. The curves from the Scherr approximation are given; those from the other functions are quite similar.

Although all the charge densities obtained from the various approximations are nearly the same, their resemblance is only superficial. The distinction between the charge densities becomes appreciable and significant when the difference function $\delta\rho(R)$ is examined. Figures 4 and 5 represent $\delta\rho(R)$ for the Scherr, BL, 2ζ , and HF wave functions. The same convention was followed here as in Table I; e.g., $\delta\rho(R)$ for the BL function is the difference between the densities from Roothaan's Best Atomic²⁷ wave function in the 4S state and Ransil's Best Limited molecular function. Although such a convention is arbitrary, it is consistent and does eliminate some artificial disparities, such as those arising near the nuclei when different orbital exponents are used for the $1s$ AO's or at large distances where even small differences in $2s$ and $2p$ ζ 's cause a large change in charge densities. If, for example, the 2ζ atomic density is subtracted from the Scherr molecular density, $\delta\rho(R)$ is greatly changed in character.

The density difference function, $\delta\rho(R)$, for the Scherr wave function was first sketched out by Roux.⁸ The most conspicuous feature is the *decrease* in electronic charge in the region between the nuclei and the *increase* in electronic charge at the ends of the molecule. There is, however, a slightly positive annular ring which was taken to support the notion of bent

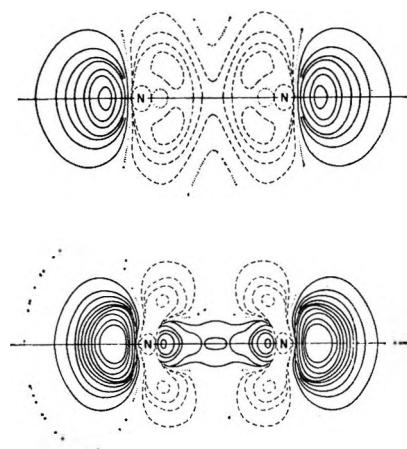


Figure 4. $\delta\rho(R)$ for the Scherr and Best Limited approximations for N_2 . The dotted lines are the zero contours, solid lines are positive contours, and dashed lines are negative contours. Contours are drawn at intervals of 0.02 electron per cubic atomic unit. Upper, $\delta\rho(R)$ Scherr approximation; lower, $\delta\rho(R)$ Best Limited approximation.

(27) C. C. J. Roothaan, Technical Report, Laboratory of Molecular Structure and Spectra, Department of Physics, The University of Chicago, Chicago, Ill., 1955, p 24.

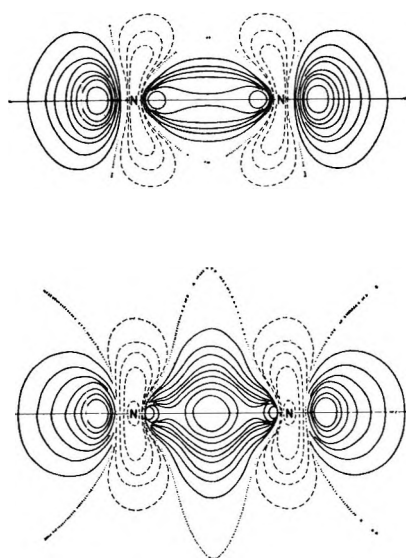


Figure 5. $\delta\rho(R)$ for the 2ζ and Hartree-Fock approximations for N_2 . Upper, $\delta\rho(R)$ 2ζ approximation; lower, $\delta\rho(R)$ Cade-Sales-Wahl approximation.

bonding, as suggested by Pauling,²⁸ among others. Over-all, the description of the bonding in N_2 in this instance seems to be in fair agreement with the usual Lewis formula for N_2 .

As the wave function is improved by allowing the orbital effective nuclear charges to vary, a more conventional picture emerges. Electronic charge moves into the central bonding region, an effect which is more pronounced in the 2ζ calculation and still more in the HF limit. There is no vestige of annular density, as was observed in the Scherr calculation.

The characteristics of $\delta\rho(R)$ are seen to depend very strongly on the quality of the approximate wave function. Indeed, serious doubt is shed upon results published for other molecules using wave functions lacking orbital exponent adjustment and/or adequate provision for atomic promotion.

Again, it is interesting to compare the extent of internuclear charge buildup with total overlap populations; as one goes up, the other goes down. In total energy, there is only a 5.7-ev difference (in some 3000 ev) between the Scherr and the 2ζ function. The D_0 corresponding to Figure 4 is 1.20 ev, compared to 3.48 for Figure 5, as contrasted with the value 5.20 ev in the HF limit.

Even though variations occur in the internuclear region when the wave function is improved, a consistent feature displayed by these various $\delta\rho(R)$ results is the significant electronic charge accumulation at the ends of the molecule. Clearly this must be related to hybridization of lone-pair electrons. This effect seems

to be primary; it apparently occurs before the internuclear charge buildup that results from adjusting the effective nuclear charges.

Approximate numerical integration of the 2ζ $\delta\rho(R)$ function gives the following increases: (1) an increase of 15% in charge density at the bond midpoint with a total increase of 0.09 electron within the internuclear region (Figure 5) bounded by the nodal contour, and (2) an increase up to 25% in charge density outside the bond along the internuclear axis, yielding a net increase of 0.16 electron at each end.

When one considers the vigorous covalent bonding that N_2 undergoes and the considerable electronic reorganization which is deemed to have taken place, these net charge dislocations seem rather small. Contrast, for example, an increase of less than 0.01 electron in the positive annular ring of the Scherr calculation and an increase of 0.03, 0.09, and 0.26 electron in the nodally bounded internuclear regions of the BL, the 2ζ , and the HF functions. Obviously, a poor choice in a basis set can lead to serious and misleading variations in the disposition of $\delta\rho(R)$. A clear demonstration of this same type of effect has been observed for various wave functions of the HF molecule.²⁹

It is certainly clear that electronic correlation effects are of considerable importance in determining bond energies. One might suggest, therefore, that the character of $\delta\rho(R)$ might be quite different if calculated from wave functions in which correlation was taken into account. Brillouin³⁰ and Möller and Plesset³¹ in their early investigations demonstrated that electron correlation induces only second-order corrections to the HF density. In a complicated system such as N_2 , little can be said about the magnitude and sign of the correlation effect in different regions of space except that the error in the charge density for a Hartree-Fock wave function is of the same order as the error in the total energy. This would seem to indicate that introduction of electron correlation into the wave function would not change the character of the $\delta\rho(R)$ function and should eliminate any possibility of the annular-ring, bent-bond configuration being restored.

One further point merits note. For all the degrees of orbital adjustment which were permitted in the wave functions, there still is found no increase of molecular charge density at the nuclei over that of the superposed atoms. This apparent contradiction of Rueden-

(28) L. Pauling, "Nature of the Chemical Bond," 3rd ed, Cornell University Press, Ithaca, N. Y., 1960, p 136.

(29) C. W. Kern and M. Karplus, *J. Chem. Phys.*, **40**, 1374 (1964).

(30) (a) L. Brillouin, *Actualités Sci. et Ind.*, No. 71 (1933); (b) L. Brillouin, *ibid.*, No. 159 (1934).

(31) C. Möller and M. S. Plesset, *Phys. Rev.*, **46**, 618 (1934).

berg's clustering hypothesis is tempered in two ways. First, Ruedenberg's postulate of clustering concerns the contraction of AO's in passing to the valence state appropriate to the molecule, but in N_2 , this valence state also involves some promotion out of the $2s$ AO into the $2p$ (and higher l) AO's and a consequent decrease in charge density at the nuclei (see below). Second, and much more important, the valence AO's, which are *second* quantum AO's, are being dealt with here. The largest magnitude effects of clustering or orbital contraction will not be at the nucleus as in H_2 , but farther outward at the maxima of the second quantum AO's.

Thus the clustering phenomenon is indeed observed and it turns out to be synonymous with charge buildup in the bond region.

Alternative Definition and Determination of the Valence State

Consideration of the $\delta\rho(R)$ function suggests that it might lend itself for use in determining valence states for atoms in a molecule. Instead of the usual criterion, one might define the valence state as that state (or combination of states) for each atom which, when all atoms are superposed, most nearly reproduces the *molecular* charge density. This definition has been discussed briefly by Ruedenberg.¹⁹

We first use this criterion here under the restriction that only *one* excited atomic state be mixed with the ground state, *i.e.*, that only atomic $2s$ - $2p\sigma$ hybridization be permitted. The complications and possible indeterminacies which arise with greater flexibility will be treated subsequently.

The difference function now to be considered is

$$\delta\rho(R;\alpha) = \rho_M(R) - \rho_A(R;\alpha) \quad (3)$$

which is exactly the same as eq 1, except that here the atoms are hybridized 100 α per cent. Specifically, this promoted state is described by

$$1s)^2 h)^2 k)^2 2\rho\pi)^1 2\rho\bar{\pi})^1$$

in which the "lone pair" hybrid

$$h = \sqrt{1 - \alpha}(2s) - \sqrt{\alpha}(2p\sigma) \quad (4)$$

and the orthogonal "bonding" hybrid

$$k = \sqrt{\alpha}(2s) + \sqrt{1 - \alpha}(2p\sigma) \quad (5)$$

Now $\delta\rho(R;\alpha)$ may be evaluated as a function of the hybridization parameter α .

The criterion selected here for optimal reproduction of the molecular charge density is to minimize the expression (eq 6).

$$I(\alpha) = \int |\delta\rho(R;\alpha)| dv \quad (6)$$

Although this criterion is arbitrary, preliminary studies indicate that minimizing

$$\int [\delta\rho(R;\alpha)]^2 dv$$

for example, yields virtually the same results. Still to be examined is the possibility of incorporating some weighting function, such as $\rho_M(R)$.

The evaluation of eq 6 was accomplished by a simple numerical integration. Specifically, the function $\delta\rho(R;\alpha)$ was evaluated at 1254 points in a quarterplane through the bond axis and multiplied at each point by the appropriate volume element and then the products were summed. To assess the accuracy of this procedure, the $\int \delta\rho(R;\alpha) dv$, which is identically zero, was numerically integrated in the same way. In all cases, a very small positive residual of no more than 0.02 electron was found.

Using the Scherr molecular function and hybridized Slater atoms, $I(\alpha)$ vs. α is given in Figure 6. The minimum occurs at approximately 11% hybridization, contrasted with a value of 26% from population analy-

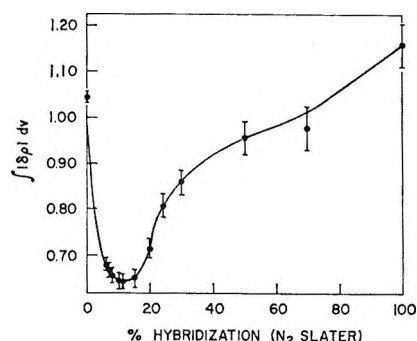


Figure 6. Variation of $\int |\delta\rho(R;\alpha)| dv$ with α , the degree of $2s$ - $2p\sigma$ hybridization, for the Scherr wave function.

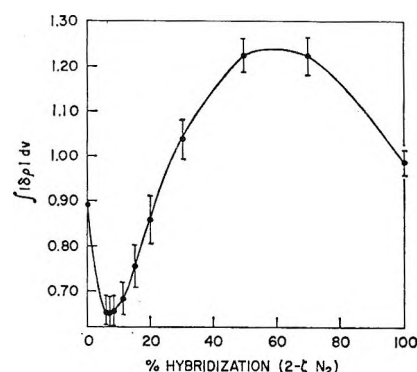


Figure 7. Variation of $\int |\delta\rho(R;\alpha)| dv$ with α , the degree of $2s$ - $2p\sigma$ hybridization, for the 2ζ wave function.

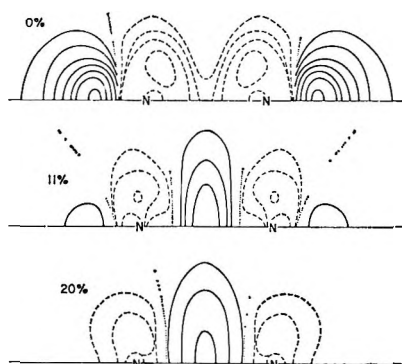


Figure 8. Variation of $\delta\rho(R;\alpha)$ with α , the degree of $2s-2p\sigma$ hybridization, for the Scherr wave function.

sis. The "error" indicated in the figure is plus or minus the value of $\int \delta\rho(R;\alpha)dv$. Results for a similar calculation using the 2ζ molecular wave function and hybridized HF atoms are presented in Figure 7; the minimum occurs at about 8% compared to 2% from the population analysis.

It is quite satisfying that these two different approximations to the wave function *now* give much more nearly equal predictions to the valence state of the atoms. On the other hand, it is disturbing that the values obtained are so much smaller than those suggested by established notions. Perhaps what are revealed from this new definition of hybridization are the contributions from attached atoms to the effective charge polarization.

In Figures 8 and 9, $\delta\rho(R;\alpha)$ for the Scherr and the 2ζ functions are drawn, each at $\alpha = 0$, $\alpha = \alpha_{\min}$, and $\alpha = 0.2$. The $\delta\rho(R;\alpha)$ curves for $\alpha = \alpha_{\min}$ correspond to those defined by Ruedenberg, *i.e.*, for the noninteracting atoms in a promoted state. Now, for the Scherr approximation, we see a very striking example of clustering. At 0% hybridization, an apparent lack of contraction is observed because no provision

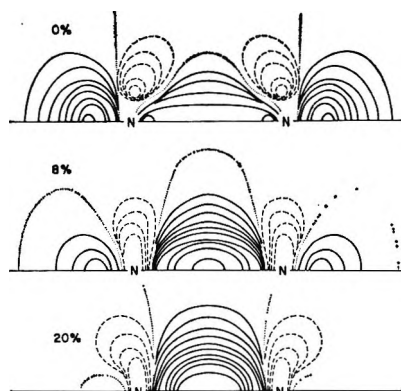


Figure 9. Variation of $\delta\rho(R;\alpha)$ with α , the degree of $2s-2p\sigma$ hybridization, for the 2ζ wave function.

was made in the wave function for adequate atomic promotion, *i.e.*, the orbital exponents were fixed. However, bonding of the *promoted* atoms produces an accumulation of charge in the internuclear region.

It is tempting to extend this procedure to refine the specification of the N atom promotion state by inclusion of perhaps atomic $3s$, $3p$, and $3d$ character. The immediate difficulty, however, is that of minimizing a function of several nonlinear parameters plus a set of constraints.

A more fundamental problem is whether a unique valence state actually exists for the atoms. Just as in the case of the $2\sigma_u$ MO discussed earlier, it is quite possible that including $3s$ character, for example, in the promotion state of one atom may displace $2p\sigma$ character from the promotion state of the other atom and *vice versa*.

Acknowledgments. The authors wish to express their thanks to Dr. A. C. Wahl for computing the necessary quadrupole moment integrals and to Drs. P. Cade, K. Sales, and A. C. Wahl for releasing their N_2 wave functions prior to publication.

Azaaromatic Charge-Transfer Complexes with π -Electron Acceptors:

Evidence for Formation of (n, π) Complexes

by David R. Kearns,¹ Phillip Gardner, and John Carmody

Department of Chemistry, University of California, Riverside, California (Received September 19, 1966)

The spectroscopic properties of complexes formed between eight azaaromatic donors and the π -electron acceptors trinitrobenzene, *p*-benzoquinone, and tetrachloro-1,4-benzoquinone have been investigated at 77°K. From a consideration of donor ionization potentials, energy of the charge-transfer bands, and substituent effects on the energy of the charge-transfer absorption bands, it is concluded that quinoline, 6-bromo-, 8-bromo-, 1,2,3,4-tetrahydro- and 2-methylquinoline, and isoquinoline function as n-electron donors, whereas acridine and 8-hydroxyquinoline function as π donors. Azine complexes with dichlorodicyano-*p*-benzoquinone appear to be ionic.

Introduction

Although there is a variety of different types of electron-donating molecules (π , n, and σ),² most of the work on charge-transfer complexes has involved the use of aromatic hydrocarbons which function only as π -electron donors. In spite of their importance in biology and elsewhere, there have been surprisingly few investigations of the properties of donor molecules containing nonbonding electrons (n electrons).³ The few studies which have been carried out with this latter group of donors have usually involved molecules such as amines, ethers, or alcohols which function only as n donors.^{4,5}

The azaaromatics are a particularly interesting class of donor molecules, because potentially they can function either as n donors or as π donors. Theory suggests that the azines should function as n donors with σ -electron acceptors because overlap between n and σ orbitals is larger than the overlap between π and σ orbitals, and this seems to be borne out by experiment.⁶⁻⁹ When π acceptors are used, however, it is not clear from overlap considerations alone whether azines should function as n or as π donors. Unfortunately, the experimental situation is not much clearer.

Although the electron-donating properties of azines have been the subject of several investigations, the results appear to be somewhat inconclusive.¹⁰⁻¹³ Miller and Wynne-Jones,^{11,12} for example, examined

the spectral properties of pyridine complexes with the π -electron acceptor trinitrobenzene (TNB) and found that these systems were chemically unstable at room temperature. Although they presented some evidence for the formation of a short-lived pyridine-TNB charge-transfer complex, even they did not consider the evidence conclusive. From an investigation of azine complexes with the π -electron acceptor tetrachlorophthalic anhydride (TCPA), Chowdhury and Basu concluded that the azines were functioning as π donors rather than as n donors.⁷ Mukherjee and

(1) Alfred P. Sloan Fellow.

(2) R. S. Mulliken, *J. Phys. Chem.*, **56**, 801 (1952).

(3) R. S. Mulliken and W. B. Person, *Ann. Rev. Phys. Chem.*, **13**, 107 (1962).

(4) M. Tamres and M. Brandon, *J. Am. Chem. Soc.*, **82**, 2134 (1960).

(5) G. Briegleb, "Elektronen-Donator-Acceptor-Komplexe," Springer Verlag, Berlin, 1961.

(6) V. G. Krishna and M. Chowdhury, *J. Phys. Chem.*, **67**, 1067 (1963).

(7) M. Chowdhury and S. Basu, *Trans. Faraday Soc.*, **56**, 335 (1959).

(8) E. K. Plyler and R. S. Mulliken, *J. Am. Chem. Soc.*, **81**, 823 (1959).

(9) C. Reid and R. S. Mulliken, *ibid.*, **76**, 3869 (1954).

(10) M. Chowdhury, *J. Phys. Chem.*, **65**, 1899 (1961).

(11) R. E. Miller and W. F. K. Wynne-Jones, *J. Chem. Soc.*, 2372 (1959).

(12) R. E. Miller and W. F. K. Wynne-Jones, *ibid.*, 4886 (1961).

(13) D. C. Mukherjee and A. K. Chandra, *Spectrochim. Acta*, **19**, 731 (1963).

Chandra,¹³ on the other hand, assigned the weak absorption bands which they observed in azine haloquinone solutions to (n, π) charge-transfer complexes.

Certainly it is possible for an azine to function as an n donor with one π acceptor and as a π donor with a different π acceptor, but there were other aspects of the above-mentioned experiments which were disturbing. In the first place, most of the authors noted that the azine-acceptor solutions were unstable at room temperature;¹¹⁻¹³ secondly, in certain of the experiments, the spectra of the complexes were obtained by a difference method; thirdly, with the haloquinone-azine complexes, the absorption bands which were assigned as charge-transfer transitions of (n, π) complexes were extremely weak ($\epsilon_{\max} < 1$).¹³

Because of the lack of definitive experimental information on the properties of azine- π -acceptor complexes, we decided to carry out a more thorough investigation of this type of charge-transfer complex. The multiple electron-donation properties of the azines and the possible importance of such complexes in biological systems provided further inducement for this study.

Experimental Section

All spectra were measured with a Cary 14 spectrometer using either a 1-cm cell or 0.2-cm "lollypop." Through the use of solvent mixtures which formed glasses at liquid nitrogen temperatures, we were able to carry out spectral measurements at 77°K. For these low-temperature measurements, the lollypop was first filled with a glassing solution of the donor and acceptor molecules. This cell was then placed in a partially silvered dewar which was filled with liquid nitrogen and mounted in the sample compartment of the Cary. Spectrograde solvents were used without further purification, except in the case of ethyl ether where it was necessary to carry out a distillation to remove peroxides formed during storage. Quinoline and other liquid quinoline derivatives were purified by low-temperature vacuum distillation of the commercial material. Acridine, 8-hydroxyquinoline, and the acceptors tetrachloro-1,4-benzoquinone and TNB were purified by recrystallization. Dichlorodicyano-*p*-benzoquinone (DDQ) and *p*-benzoquinone were used as obtained commercially.

Results and Discussion

Since previous studies by others and preliminary investigations of our own demonstrated that mixtures of azines with various acceptors were unstable at room temperature, most of our spectral measurements were carried out at 77°K to prevent chemical reactions

from occurring. This was a particularly fortuitous decision, because complex formation was found to be highly temperature dependent. Most of the complexes were stable only at the reduced temperatures.

Upon cooling to 77°K the azine-acceptor solutions usually became brightly colored, and the low-temperature absorption spectra of these solutions are presented in Figures 1-5. The donor and acceptor molecules were transparent in the spectral regions of interest for most of the complexes studied, although there was significant "tail" absorption in the case of the TNB complexes and the acridine complexes. The spectral properties of these donor-acceptor solutions are summarized in Table I along with similar data for the parent hydrocarbon complexes with the same acceptor.

Table I: Position of Charge-Transfer Band of Azine- π -Acceptor Complexes (m μ)

Donor	Acceptor					
	—TNB—		<i>p</i> -Benzo-quinone		Tetrachloro-1,4-benzo-quinone	
	Pred ^b	Obsd	Pred	Obsd	Pred	Obsd
Naphthalene (8.12 ev) ^a		370		370		480
Quinoline (8.2 ev)	355	505	350	520	450	605
Quinaldine		500		530		635
Isoquinoline		510		...		650
6-Bromoquinoline		...		510		570
8-Chloroquinoline			590
1,2,3,4-Tetrahydro-quinoline		...		565		650
8-Hydroxyquinoline (8.1 ev) ^c	370	400	370	...	480	500
Anthracene (7.38 ev)		460		457		625
Acridine (7.78 ev)		525	500

^a The π -ionization potential given in parentheses. ^b Predicted location of the π - π charge-transfer band obtained using the expression,⁸ $h\nu_{CT} = \text{I.P.} - (C_1 + C_2)/(\text{I.P.} - C_1)$, where I.P. is the gas-phase π -ionization potential of the donor and where $C_1 = 5.7$ ev, $C_2 = 0.44$ ev for tetrachloro-1,4-benzoquinone and $C_1 = 5.0$ ev, $C_2 = 0.7$ ev for trinitrobenzene. ^c Estimated.

Evidence for Reversible Formation of Charge-Transfer Complexes. Because of the known room-temperature instability of the azine-acceptor solutions, it was important first to establish that the colored species which we observed at 77°K were actually reversibly formed donor-acceptor complexes and secondly, that the complexes were actually charge-transfer complexes.

The reversibility of the complex formation was established by the following experimental observations.

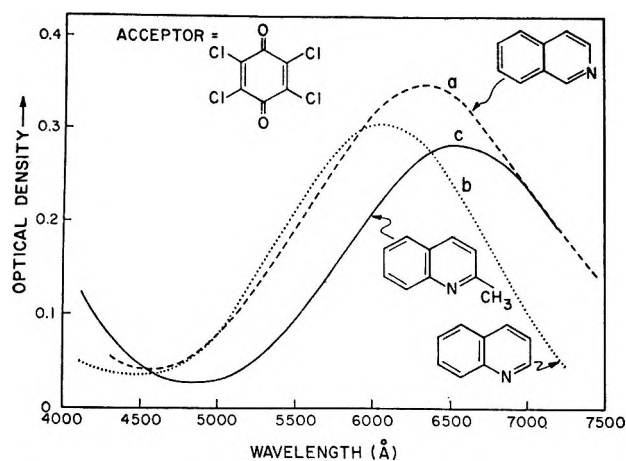


Figure 1. Absorption spectra of charge-transfer complexes with tetrachloro-1,4-benzoquinone at 77°K (0.2-cm cell): a, 0.3 *M* isoquinoline and 5×10^{-4} tetrachloro-1,4-benzoquinone in 3:1 ether-isopropyl alcohol; b, 0.3 *M* quinoline and 4.3×10^{-4} *M* tetrachloro-1,4-benzoquinone in 3:1 ether-isopropyl alcohol; c, 0.3 *M* quinaldine and 4×10^{-4} *M* tetrachloro-1,4-benzoquinone in 3:1 ether-isopropyl alcohol.

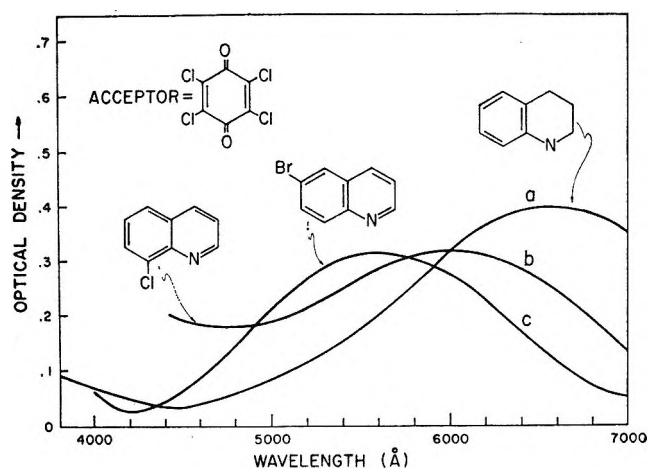


Figure 2. Absorption spectra of charge-transfer complexes with tetrachloro-1,4-benzoquinone at 77°K (0.2-cm cell): a, 1,2,3,4-tetrahydroquinoline and tetrachloro-1,4-benzoquinone in 1:1:0.4 ethanol-tetrahydrofuran-methanol; b, 0.4 *M* 8-chloroquinoline and 2×10^{-3} *M* tetrachloro-1,4-benzoquinone in 1:1:0.4 ethanol-tetrahydrofuran-methanol; c, 6-bromoquinoline and 2×10^{-3} *M* tetrachloro-1,4-benzoquinone in 1:1:0.4 ethanol-tetrahydrofuran-methanol.

When the azine-acceptor solutions were warmed from 77 to 200°K, the intensity of the visible absorption bands always decreased (factor of ~ 10), but upon re-cooling to 77°K, the solutions immediately returned to their original intensity; secondly, when the concentration of the acceptor was reduced, the intensity

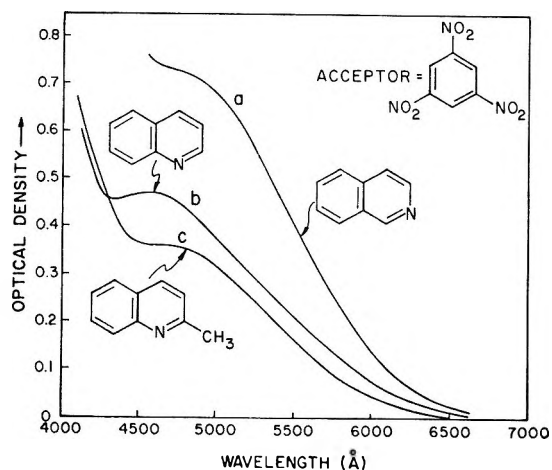


Figure 3. Absorption spectra of charge-transfer complexes with trinitrobenzene at 77°K: a, 0.3 *M* isoquinoline and 5×10^{-2} *M* TNB in 3:1 ether-isopropyl alcohol, 1-cm cell; b, 0.3 *M* quinoline and 5×10^{-2} *M* TNB in 3:1 ether-isopropyl alcohol, 0.2-cm cell; c, 0.3 *M* quinaldine and 5×10^{-2} *M* TNB in 3:1 ether-isopropyl alcohol, 0.5-cm cell.

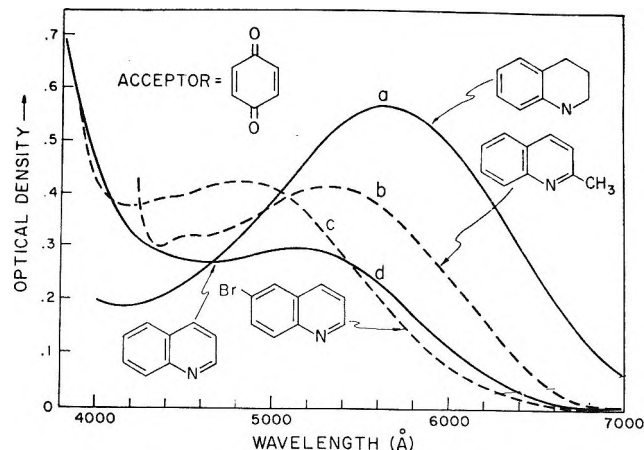


Figure 4. Absorption spectra of charge-transfer complexes with *p*-benzoquinone at 77°K: a, 1,2,3,4-tetrahydroquinoline and *p*-benzoquinone in 1:1:0.4 ethanol-tetrahydrofuran-methanol; b, quinaldine and *p*-benzoquinone in 1:1:0.4 ethanol-tetrahydrofuran-methanol; c, 6-bromoquinoline and *p*-benzoquinone in 1:1:0.4 ethanol-tetrahydrofuran-methanol; d, quinoline and *p*-benzoquinone in 1:1:0.4 ethanol-tetrahydrofuran-methanol.

of the visible absorption band decreased. Since the solutions always contained an excess of the donor molecules, there was generally no significant change in the intensity of the visible absorption band when the concentration of the donor was varied over a small range. Finally, we noted that although the solutions appeared to be indefinitely (days) stable at Dry Ice temperature, they were not stable at room temperature. This room-temperature instability was evidenced by the

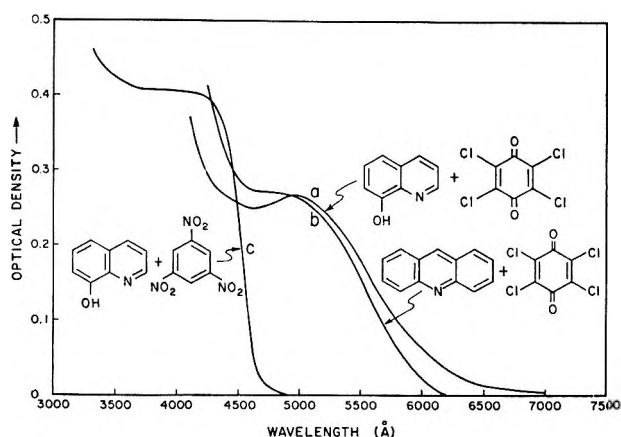


Figure 5. Absorption spectra of charge-transfer complexes (0.2-cm cell): a, 8-hydroxyquinoline and $3 \times 10^{-2} M$ tetrachloro-1,4-benzoquinone in 1:1:0.4 ethanol-tetrahydrofuran-methanol at room temperature; b, $10^{-2} M$ acridine and $2 \times 10^{-3} M$ tetrachloro-1,4-benzoquinone in 1:1 ether-isopentane; c, 8-hydroxyquinoline and TNB in 1:1:0.4 ethanol-tetrahydrofuran-methanol at room temperature.

slow appearance of new, temperature-independent absorption bands and by the disappearance of the low-temperature absorption bands which we have attributed to formation of a complex.

These various observations established that the new light-absorbing species which we observed at low temperature were formed *reversibly* as the result of an interaction between the azines and the electron acceptors and that the chemical reactions which occurred at or near room temperature were detrimental to the formation of the complexes.

Although the temperature and concentration dependence of the low-temperature absorption bands definitely indicated reversible formation of complexes, these data did not distinguish between the various types of complexes (ion-pair, charge-transfer) which might be formed. Evidence that the low-temperature azine-acceptor complexes are charge-transfer complexes is obtained from a consideration of variation of the energy of the complex absorption band with the nature of the acceptor and the donor.

If the absorption bands of the complex were due to charge-transfer transitions of ion pairs, the bands should *blue* shift, with increasing acceptor strength. From the data presented in Table I, it is evident that with a given donor, the stronger the electron acceptor, the lower the energy of the transition. This shift in the absorption is opposite that expected for a charge-transfer transition of an ion-pair complex, but as expected for the charge-transfer band of a complex between neutral molecules.⁵

The spectral data definitely rule out the possibility of ion formation in the case of the tetrachloro-1,4-benzoquinone complexes.¹⁴ The tetrachloro-1,4-benzoquinone radical anion has absorption bands at 425 and 455 $m\mu$,^{14,15} whereas the tetrachloro-1,4-benzoquinone complexes which we studied exhibited absorption bands in the region 570–650 $m\mu$, with minima in the 450- $m\mu$ region. Similar consideration applies to the *p*-benzoquinone complexes, since the benzoquinone radical anion should have a spectrum only slightly blue shifted from that of the tetrachloro-1,4-benzoquinone radical anion.¹⁴ The spectrum of the TNB radical anion has not been reported so that it is not possible to apply the same test in the case of the TNB complexes. However, since the benzoquinone complexes are not ionic, it is unlikely that the corresponding complexes with the weaker electron acceptor TNB will be ionic.¹⁶ These various considerations all indicate that the azine-donor complexes are charge-transfer complexes in the usual sense.

Nature of the Charge-Transfer Complex. The next problem was to determine whether the complexes were (n, π) or (π, π) type of charge-transfer complexes. In order to distinguish experimentally an (n, π) from a (π, π) complex, it is necessary to find some property or set of properties which are predictably different for the two types of complexes. Because of our inadequate knowledge of the properties of (n, π) complexes, most of the properties which one might like to use (heat of formation, molar extinction coefficient, solvent effects on λ_{\max}) to distinguish between (n, π) and (π, π) complexes are not useful for this purpose. With the exception of an X-ray structure determination, about the only reliable criterion which we have for distinguishing between these two types of complexes is based on the relation between the energy of the charge-transfer transitions and the π -ionization potential of the donor.^{3,5}

From previous studies of (π, π) charge-transfer complexes it has been established that there is a fairly linear relation between the π -ionization potential of the donor and the frequency of the charge-transfer band. Consequently, if the π -ionization potential of a particular donor is known, it is possible to predict with a fair degree of accuracy the energy of the charge-transfer band for a (π, π) complex of this donor with a particular π acceptor.⁵ Accordingly, we have used

(14) R. Forster and T. J. Thomas, *Trans. Faraday Soc.*, **58**, 860 (1962).

(15) I. M. Kolthoff, D. Stocesoca, and T. S. Lee, *J. Am. Chem. Soc.*, **75**, 1834 (1953).

(16) G. Briegleb, *Angew. Chem.*, **76**, 326 (1964).

data obtained from studies of (π, π) complexes of various aromatic hydrocarbon donors along with known or estimated π -ionization potentials of the azines to predict the probable energy of the charge-transfer transition for (π, π) complexes of the azines with the electron acceptors TNB, *p*-benzoquinone, and tetrachloro-1,4-benzoquinone.¹⁷⁻²⁰ The predicted charge-transfer bands are compared with the observed bands in Table I. We note from this comparison that the complexes of 8-hydroxyquinoline and acridine exhibit charge-transfer bands at about the position expected for (π, π) complexes. In marked contrast to the behavior of these two donors, the rest of the quinoline derivatives exhibit charge-transfer bands which appear about 5000 cm^{-1} ($\sim 180 \text{ m}\mu$) lower in energy than predicted for π donation. The discrepancy between the predicted and observed values is clearly much larger than any experimental error. We conclude that with the exception of acridine and 8-hydroxyquinoline, the azines which we studied function as n donors with the π acceptors.

Although we cannot predict with certainty which of the azines will form π, π complexes and which will form n, π complexes, our observations can easily be rationalized in the following way. The formation of (π, π) complexes with acridine can be understood in terms of the lower π ionization of acridine relative to most of the quinoline derivatives.

Certainly 8-hydroxyquinoline is a better π -electron donor because the OH substituent lowers the π -ionization potential.²⁰ Furthermore, it is expected to be a poorer n -electron donor than quinoline because of the possibility of intramolecular hydrogen bonding with the lone-pair electrons. It is therefore not surprising that 8-hydroxyquinoline does not function as a n -electron donor.

We have shown that 8-hydroxyquinoline is not forming an n, π complex with tetrachloro-1,4-benzoquinone, but the true nature of the complex remains to be established. Bailey, *et al.*, observed a band at $500 \text{ m}\mu$ with an impure, solid sample of the 8-hydroxyquinoline-tetrachloro-1,4-benzoquinone which they attributed to a charge-transfer complex.²¹ Although we observed a band at $500 \text{ m}\mu$ in solution of these two components, we found that the intensity of the band increased (factor of 10) upon standing for several hours. Furthermore, we were unable to observe this band at low temperatures when freshly prepared solutions were used. The clear implication is that the $500\text{-m}\mu$ band observed with 8-hydroxyquinoline-tetrachloro-1,4-benzoquinone mixtures is not due to formation of a charge-transfer complex. The TNB-8-hydroxyquinoline complex, on the other hand, appeared

to behave normally, exhibiting a charge-transfer band at about $400 \text{ m}\mu$.

In addition to those mentioned above, there are other experimental considerations which support our assignments. The different character of the (π, π) and the (n, π) complexes is also evidenced by the low stability of the (n, π) complexes as compared with the (π, π) charge-transfer complexes. Although acridine and possibly 8-hydroxyquinoline formed charge-transfer complexes with TNB and tetrachloro-1,4-benzoquinone at room temperature, the (n, π) complexes of the other quinoline derivatives could be observed only at reduced temperatures.

In most of our experiments, the concentration of the azine was considerably larger than that of the acceptor. By assuming that all of the acceptor molecules were complexed at 77°K , it was possible to obtain from the spectral data an approximate *lower limit* on the value of the extinction coefficient for the charge-transfer transition. For the tetrachloro-1,4-benzoquinone complexes which we have assigned as n, π complexes, the apparent extinction coefficients fall in the range 2500-4000. The apparent ϵ values for the TNB complexes were generally quite small ($\epsilon \simeq 100$), but this probably can be attributed to incomplete complexation of all of the TNB.

Interestingly enough, the extinction coefficient for the acridine tetrachloro-1,4-benzoquinone complex was 500, quite close to the value of 457 observed for the anthracene-tetrachloro-1,4-benzoquinone complex. This is, of course, consistent with the assignment of the acridine-tetrachloro-1,4-benzoquinone complex as a (π, π) type charge-transfer complex.

Although there has been much discussion of the intensities of charge-transfer bands,^{13,22,23} they still are not very well understood. Consequently, it is not possible at this time to use the intensity of the charge-transfer band to distinguish between different types of complexes.

On the basis of the various experimental results summarized above, we conclude that TNB, *p*-benzoquinone, and tetrachloro-1,4-benzoquinone form (n, π) charge-transfer complexes with quinoline, quinaldine, isoquinoline, 6-bromoquinoline, 8-chloroquinoline, and

(17) J. N. Murrell, *Quart Rev.* (London), **15**, 191 (1961).

(18) M. A. El-Sayed, M. Kasha, and Y. Tanaka, *J. Chem. Phys.*, **34**, 334 (1961).

(19) J. E. Parkin and K. K. Innes, *J. Mol. Spectry.*, **15**, 407 (1965).

(20) F. I. Vilesov, *Soviet Phys. Usp.*, **6**, 888 (1964).

(21) A. S. Bailey, R. P. J. Williams, and J. D. Wright, *J. Chem. Soc.*, 2579 (1956).

(22) J. N. Murrell, *J. Am. Chem. Soc.*, **81**, 5037 (1959).

(23) R. S. Mulliken, *ibid.*, **79**, 4839 (1957).

1,2,3,4-tetrahydroquinoline. Acridine, on the other hand, forms (π , π) complexes with these same acceptors and 8-hydroxyquinoline apparently reacts with tetrachloro-1,4-benzoquinone. We now want to discuss briefly some other azine-acceptor systems which did not appear to form charge-transfer complexes.

Other Azine- π -Electron Acceptor Systems

*Azine Complexes with Dichlorodicyano-*p*-benzoquinone (DDQ).* We observed that low-temperature solutions of DDQ with various azines (quinoline, isoquinoline, dipyridyl) all exhibited absorption bands with maxima at 700 $m\mu$ suggesting perhaps that the DDQ complexes are ion pairs, that free DDQ ions are produced, or perhaps that DDQ undergoes some reaction to produce a species which absorbs at 700 $m\mu$. DDQ is a much stronger electron acceptor than tetrachloro-1,4-benzoquinone or TNB²⁴ so that ion formation is certainly a possibility.

Unsuccessful Attempts to Observe Azine- π -Electron Acceptor Complexes. In contrast to the behavior of the quinoline derivatives, there were a number of azines (pyridine, pyrazine, phenanthridine, 5,6-benzoquinoline, tetramethylpyrazine, 2,3-dimethylquinoxaline, dipyridyl, β -naphthoquinoline) which did not appear to form colored charge-transfer complexes with TNB or tetrachloro-1,4-benzoquinone. We believe that several factors (not necessarily the same in each case) were probably responsible for this. In general, the donors which did not form complexes (i) were somewhat less soluble in the solvents used than the donor molecules which did form charge-transfer complexes, (ii) have pK_a values which are smaller than those which did form complexes and, (iii) often appeared to be somewhat more reactive at room temperature toward the acceptors than donor molecules which formed complexes. Other investigators have also noted similar solubility and reactivity problems.¹⁰⁻¹³

Relation to Previous Investigations of Azine- π -Electron Acceptor Complexes

As some of our conclusions differ with those presented elsewhere by others, it is perhaps worthwhile to mention these and to point out why these differences might arise.

Kinoshita measured the absorption spectra of acridine-tetrabromo-1,4-benzoquinone solutions in carbon tetrachloride and observed an absorption band at 493 $m\mu$,²⁴ but made no attempt to determine whether this was due to the formation of an (n , π) or a (π , π) complex. As noted in Table I, the acridine-tetrachloro-1,4-benzoquinone complex has an absorption band at

500 $m\mu$. Because of the similarity in the electron-accepting properties of tetrabromo-1,4-benzoquinone and tetrachloro-1,4-benzoquinone and the similarity in the position of the absorption bands for the complexes with acridine, it appears likely that the tetrabromo-1,4-benzoquinone-acridine complex is a (π , π) charge transfer.

Miller and Wynne-Jones studied the pyridine-TNB system in pyridine and observed slow formation (order of 10-20 min) of new absorption bands at 470 and 570 $m\mu$ which they attributed to the formation of pyridine-TNB ion pairs and the TNB ion.^{11,12} They also reported some evidence for a short-lived species which absorbed in the region of 3000 Å and suggested this might be due to the pyridine-TNB charge-transfer complex. In contrast to the pyridine complex, the TNB complexes of the quinoline derivatives which we studied were formed only when the solutions were cooled to 77°K; they formed immediately upon cooling and they absorbed light in the vicinity of 490-510 $m\mu$, not at 570 $m\mu$.

Mukherjee and Chandra studied the absorption spectra of various azines with the acceptors tetrachloro-1,4-benzoquinone, tetrabromo-1,4-benzoquinone, and *p*-iodanil and observed new absorption bands in the region of 470-490 $m\mu$ which they attributed to the formation of (n , π) charge-transfer complexes.¹³ There are several reasons for questioning this assignment. In the first place, the spectra were obtained by a difference method. In view of the exceedingly small extinction coefficients obtained ($\epsilon_{\max} \simeq 0.015-1.0$) the use of a difference method would appear questionable. Furthermore, it is difficult to believe that the (n , π) charge-transfer transition could be so weak, particularly in view of the fact that even contact charge-transfer complexes of O₂ with aniline, benzene, and ethanol have extinction coefficients which are greater than 100.^{25,26} It is interesting to note that extinction coefficients for singlet-triplet transitions in halogenated aromatic molecules are on the order of 0.1²⁷ and that the lowest singlet-triplet transitions of quinoline and isoquinoline occur in the same region as the weak absorption bands which Mukherjee and Chandra attributed to (n , π) charge-transfer complexes.²⁸ Finally, although they noted that the azines reacted with the

(24) M. Kinoshita, *Bull. Chem. Soc. Japan*, **35**, 1609 (1962).

(25) H. Tsubomura and R. S. Mulliken, *J. Am. Chem. Soc.*, **82**, 5966 (1960).

(26) E. C. Lim and V. L. Kowalski, *J. Chem. Phys.*, **36**, 1729 (1962).

(27) D. S. McClure, *ibid.*, **17**, 665 (1949).

(28) D. R. Kearns and A. Case, unpublished data.

quinones, they made no attempt to prove that the faint absorption bands which they observed were not due to some reaction products.

Acknowledgment. The support of the U. S. Public

Health Service (Grant No. GM-10499) is most gratefully acknowledged. The assistance of Mr. Jess Long in some of the temperature-dependence studies is also acknowledged with thanks.

The Ultraviolet-Visible Absorption Spectrum of Bromine between Room Temperature and 440°

by A. A. Passchier, J. D. Christian, and N. W. Gregory

Department of Chemistry, University of Washington, Seattle, Washington 98105 (Received September 19, 1966)

The absorption spectrum of Br₂(g) at wavelengths between 200 and 750 m μ and at temperatures between 25 and 440° has been measured. Molar absorptivities suitable for quantitative use are reported. The temperature dependence is compared with that predicted by a Sulzer and Wieland equation. A marked temperature and concentration dependence in the ultraviolet region and evidence for Br₁ are discussed.

We have found it convenient and sometimes necessary in the study of certain equilibrium systems to determine the concentration of bromine vapor from its absorption of light in the visible region of the spectrum. The bromine spectrum has been studied previously by a number of investigators.¹⁻⁸ Although results are in general qualitative agreement, no two independent studies give values of the molar absorptivity at various wavelengths with sufficient consistency for quantitative use. Only Ribaud¹ and Acton, Aickin, and Bayliss² report experimental results for the temperature dependence in the visible region. Sulzer and Wieland⁹ have developed a semi-empirical theory for the temperature dependence of a continuous absorption spectrum for diatomic molecules. They conclude that the shape of a given absorption peak is essentially determined by three characteristic parameters which may be evaluated from the observed spectrum at any one temperature. They test their equation with results for chlorine, bromine, and iodine, using the data of Acton, Aickin, and Bayliss for bromine. Recently, Seery and Britton⁷ have reported

a study of the bromine spectrum at 25° and their results differ substantially from those of Acton, Aickin, and Bayliss. Seery and Britton have used their data to find new parameters for the Sulzer-Wieland equation but did not experimentally verify the molar absorptivities which it predicts for higher temperatures.

Hence for quantitative use we have felt it essential to make an additional experimental study of the

-
- (1) G. Ribaud, *Ann. Phys.*, **12**, 107 (1909).
 - (2) A. P. Acton, R. G. Aickin, and N. S. Bayliss, *J. Chem. Phys.*, **4**, 474 (1936).
 - (3) L. T. M. Gray and D. W. G. Style, *Proc. Roy. Soc. (London)*, **A126**, 603 (1929).
 - (4) R. G. Aickin and N. S. Bayliss, *Trans. Faraday Soc.*, **34**, 1371 (1938).
 - (5) D. F. Evans, *J. Chem. Phys.*, **23**, 1426 (1955).
 - (6) G. Burns and R. G. W. Norrish, *Proc. Roy. Soc. (London)*, **A271**, 289 (1963).
 - (7) D. J. Seery and D. Britton, *J. Phys. Chem.*, **68**, 2263 (1964).
 - (8) E. A. Ogryzlo and B. C. Sanctuary, *J. Phys. Chem.*, **69**, 4423 (1965).
 - (9) P. Sulzer and K. Wieland, *Helv. Phys. Acta*, **25**, 653 (1952).

bromine spectrum as a function of temperature. Molar absorptivities have been determined from 300 to 750 $m\mu$ at various temperatures in the interval between room temperature and 440°. The results are compared with those of previous workers and the Sulzer and Wieland treatment. A large temperature and concentration dependence observed between 200 and 300 $m\mu$ has been studied in some detail and evidence for Br_4 is discussed. Ogryzlo and Sanctuary⁸ have also recently published a communication on this aspect of the spectrum.

Experimental Section

The spectra were obtained with a Beckman DU spectrophotometer equipped with a specially constructed cell compartment which could be heated uniformly to any desired temperature up to 500°. The instrument was calibrated periodically. Seven independent samples of bromine were studied. Three were taken from Baker's Analyzed reagent grade (specified as <0.15% chlorine and <0.05% iodine) and four from Mallinckrodt Analytical reagent grade (<0.30% chlorine, <0.05% iodine). Samples of bromine were admitted to a vacuum system, frozen onto P_2O_5 with liquid oxygen, and the system pumped down to 10^{-6} torr. The mixture was isolated, the bromine melted, refrozen, and pumped on again; this procedure was repeated several times to remove dissolved air. In three instances KBr was initially added to ensure the absence of significant amounts of chlorine. This precaution appeared to be unnecessary. The bromine was finally distilled from the P_2O_5 into a "finger" cooled with ice. Two different methods were used to introduce the sample into the quartz absorption cell. (1) The bromine was expanded *via* a Teflon stopcock into a bulb attached to the cell; this part of the apparatus had been carefully evacuated and flamed to remove adsorbed gases. After isolating the desired quantity, established by measuring the pressure (*via* a Pyrex diaphragm gauge) in a calibrated volume, the bromine was frozen into the cell and the connecting side arm sealed off. After measurement of the spectra at various temperatures, the cell was opened, the bromine dissolved in KI, and the quantity determined by titration with $Na_2S_2O_3$. The cell volume was determined from its weights when empty and when filled with water. (2) In the alternative procedure, the cell remained connected to a Pyrex finger outside the furnace compartment and to a Pyrex diaphragm gauge by which the bromine pressure could be measured. The external finger was immersed in a thermostated bath; the bromine pressure could be adjusted to any desired value by varying the tempera-

ture of the condensed liquid. In this way the cell, once placed in the furnace compartment, did not need to be handled and the empty cell absorbance could easily be determined by freezing out the bromine sample.

Results and Discussion

The molar absorptivity, ϵ , is defined by the relationship $\epsilon = A/bC = (1/bC) \log P_0/P$, where A is the absorbance, P_0 the incident radiant power, P the transmitted radiant power, b the length in centimeters of the absorbing medium, and C the molar concentration of the absorbing medium. Mean values of ϵ and the average deviation at various wavelengths between 300 and 750 $m\mu$ and temperatures between 25 and 440° are shown in Table I. Results at 25° are compared graphically with those of Acton, Aickin, and Bayliss² and those of Seery and Britton⁷ in Figure 1. Our values are slightly higher than those of Seery and Britton in the vicinity of the maximum and around 540 $m\mu$, but in general are in excellent agreement with their results. The curves drawn (Figure 1) represent correlations according to the equations of Sulzer and Wieland.⁹ They derive the following equations with the aid of a number of simplifying assumptions which include use of harmonic oscillator wave functions and gaussian curves of constant area for the absorption peaks

$$\begin{aligned}\epsilon_T(\omega) &= \epsilon_T^m \exp\left[-\left(\frac{\omega - \omega_0}{\Delta\omega_T}\right)^2\right] \\ \epsilon_T^m &= \epsilon_0^m \left[\tanh\left(\frac{hc\omega_v}{2kT}\right)\right]^{1/2} \\ \Delta\omega_T &= \Delta\omega_0 \left[\tanh\left(\frac{hc\omega_v}{2kT}\right)\right]^{-1/2}\end{aligned}$$

$\epsilon_T(\omega)$ represents the molar absorptivity at frequency ω and temperature $T^\circ K$; ϵ_0^m is the molar absorptivity at the maximum at 0°K, ω_0 the frequency of the maximum at 0°K, $\Delta\omega_0$ the natural half-width of the gaussian peak at 0°K, and ω_v is the vibration frequency of the molecule in its ground state. The latter is well known (323.2 cm^{-1} for Br_2);¹¹ the other parameters can be evaluated from spectral data taken at a particular temperature. The bromine spectrum in the visible range consists of two overlapping peaks; hence six parameters are needed. Once these have been determined, from results at 25°, for example, molar absorptivities at any temperature may be predicted.

(10) For details see the Ph.D. Thesis of J. D. Christian, University of Washington, 1965; University Microfilms Publ. No. 66-5850, Ann Arbor, Mich.

(11) "JANAF Thermochemical Tables," Dow Chemical Co., Midland, Mich., June 1965 Supplement.

Table I: Molar Absorptivities of Bromine

λ , m μ	25°	75°	150°	225°	300°	375°	440°
750	0.2 (0.07) ^a	0.2 (0.04)	0.2 (0.13)	0.2 (0.02)	0.2 (0.16)	0.5 (0.17)	0.1 (0.14)
725	0.1 (0.08)	0.2 (0.04)	0.1 (0.11)	0.2 (0.05)	0.3	1.0 (0.47)	0.5 (0.42)
700	0.1 (0.13)	0.1 (0.04)	0.1 (0.06)	0.4 (0.05)	0.4 (0.40)	1.1 (0.27)	1.3 (0.44)
675	0.3 (0.09)	0.3 (0.05)	0.7 (0.04)	1.1 (0.07)	1.2 (0.40)	2.2 (0.22)	2.7 (0.48)
650	0.5 (0.15)	1.0 (0.11)	1.6 (0.21)	2.2 (0.29)	3.0 (0.51)	4.3 (0.37)	5.0 (0.47)
640	0.8 (0.13)	1.4 (0.09)	2.0 (0.32)	3.0 (0.30)	3.6 (0.38)	4.9 (0.28)	6.0 (0.38)
630	1.3 (0.24)	2.1 (0.08)	2.8 (0.48)	4.4 (0.34)	5.5 (0.26)	7.0 (0.20)	8.2 (0.16)
620	2.0 (0.13)	3.0 (0.10)	3.9 (0.26)	5.7 (0.36)	6.9 (0.11)	8.9 (0.35)	10.0 (0.04)
610	2.8 (0.27)	3.9 (0.18)	5.1 (0.16)	7.2 (0.26)	8.4 (0.40)	10.4 (0.10)	11.5 (0.01)
600	4.4 (0.29)	5.7 (0.26)	7.4 (0.18)	9.8 (0.37)	11.6 (0.23)	13.5 (0.13)	15.3 (0.05)
590	6.1 (0.28)	7.6 (0.19)	9.3 (0.27)	12.1 (0.52)	14.1 (0.32)	16.0 (0.41)	18.2 (0.20)
580	9.4 (0.38)	11.5 (0.34)	14.1 (0.37)	17.0 (0.37)	19.9 (0.08)	21.6 (0.52)	24.0 (0)
570	13.5 (0.54)	15.6 (0.34)	18.7 (0.88)	21.2 (0.42)	23.7 (0.10)	25.5 (0.54)	27.6 (0.29)
560	17.6 (0.51)	19.7 (0.45)	22.6 (0.75)	25.7 (0.56)	28.6 (0.64)	30.0 (0.92)	32.6 (0.35)
550	22.7 (0.72)	24.6 (0.76)	27.7 (1.22)	30.9 (0.90)	34.3 (0.76)	35.3 (1.00)	37.8 (0.04)
540	29.6 (0.91)	31.7 (1.09)	34.9 (0.83)	38.9 (0.58)	41.8 (0.49)	43.1 (0.94)	45.2 (0.36)
530	38.4 (2.26)	40.5 (1.88)	44.8 (2.28)	48.1 (1.33)	51.2 (0.46)	51.8 (0.76)	54.4 (0.28)
520	52.3 (1.02)	54.5 (1.27)	57.3 (1.15)	59.5 (0.59)	61.5 (0.45)	62.1 (0.53)	63.3 (0.24)
514	64.5 (0.99)	65.0 (0.36)	65.3 (0.43)	66.8 (0.26)	67.8 (0.40)	67.8 (0.53)	68.9 (0.40)
510	72.2 (0.87)	71.7 (0.31)	71.3 (0.69)	71.5 (0.46)	72.3 (0.26)	71.7 (0.47)	72.5 (0.80)
500	84.2 (1.08)	82.8 (0.13)	81.8 (0.85)	81.5 (0.38)	81.5 (0.19)	80.7 (0.59)	81.1 (0.44)
490	94.9 (0.98)	93.4 (0.57)	92.0 (0.94)	91.4 (0.26)	90.9 (0.16)	89.9 (0.63)	89.5 (0.82)
480	104 (0.88)	103 (0.58)	102 (1.02)	101 (0.58)	100 (0.46)	98.5 (0.98)	98.2 (0.88)
470	111 (1.16)	110 (0.90)	110 (1.35)	109 (0.66)	108 (0.54)	108 (0.82)	106 (1.72)
460	118 (1.20)	119 (0.66)	118 (1.64)	118 (0.69)	117 (0.41)	115 (1.02)	113 (1.44)
450	129 (1.09)	128 (1.07)	128 (1.31)	126 (0.59)	125 (0.16)	122 (1.03)	120 (1.51)
440	143 (0.99)	142 (0.16)	138 (1.48)	134 (0.54)	131 (0.46)	128 (0.94)	125 (1.74)
430	158 (0.55)	153 (0.56)	147 (1.24)	141 (0.67)	137 (0.78)	132 (1.57)	128 (1.89)
428	160 (0.59)	155 (0.10)	148 (0.79)	143 (0.67)	138 (0.80)	132 (1.54)	129 (1.76)
424	165 (0.61)	159 (0.51)	150 (1.08)	144 (0.61)	139 (0.99)	134 (1.63)	129 (2.04)
420	169 (0.99)	161 (0.48)	152 (1.57)	145 (0.97)	139 (0.96)	133 (1.96)	128 (1.44)
416	170 (1.38)	162 (0.28)	152 (1.24)	144 (1.06)	138 (1.00)	132 (1.02)	127 (1.36)
412	168 (0.68)	161 (0.18)	151 (1.15)	143 (0.91)	137 (0.67)	131 (0.98)	126 (1.44)
408	165 (0.76)	158 (0.12)	148 (1.36)	140 (1.17)	134 (0.74)	129 (0.75)	123 (1.60)
404	159 (0.94)	153 (0.14)	144 (1.02)	136 (0.89)	130 (0.30)	124 (1.01)	120 (1.37)
400	151 (1.80)	145 (0.06)	138 (0.91)	130 (0.84)	125 (0.85)	120 (0.84)	116 (1.98)
395	136 (0.88)	132 (0.54)	127 (0.19)	121 (0.85)	117 (0.80)	113 (1.10)	109 (2.09)
390	118 (0.96)	117 (0.23)	113 (0.85)	110 (0.98)	108 (0.83)	105 (1.33)	102 (1.74)
385	99.7 (0.96)	100 (0.12)	100 (0.28)	98.3 (0.57)	97.1 (0.59)	94.6 (0.88)	93.6 (1.44)
380	80.8 (1.01)	82.6 (0.12)	83.2 (1.16)	84.4 (0.69)	85.3 (0.20)	83.9 (0.89)	83.2 (1.30)
370	47.3 (0.93)	50.7 (0.21)	55.0 (0.30)	57.9 (0.53)	61.1 (0.64)	62.0 (0.90)	63.3 (1.22)
360	22.8 (0.38)	26.0 (0.14)	30.3 (0.15)	34.4 (0.64)	38.5 (0.26)	40.6 (0.61)	42.0 (1.44)
350	8.8 (0.41)	11.1 (0.12)	14.0 (0.12)	17.1 (0.45)	21.0 (0.52)	23.2 (0.59)	25.2 (1.48)
340	2.9 (0.27)	3.8 (0.21)	5.1 (0.35)	7.1 (0.43)	9.7 (0.56)	11.5 (0.57)	13.0 (1.21)
330	0.7 (0.15)	1.2 (0.09)	1.3 (0.39)	2.1 (0.38)	3.7 (0.78)	4.8 (0.40)	5.8 (0.98)
320	0.2 (0.03)	0.3 (0.03)	0.5 (0.02)	0.7 (0.04)	0.8 (0.67)	2.0 (0.56)	2.0 (1.02)
310	0.1 (0.03)	0.1 (0.02)	0.2 (0.04)	0.3 (0.04)	0.3 (0.11)	0.8 (0.08)	1.6
300	0.1 (0.02)	0.1 (0.03)	0.0 (0.02)	0.1 (0.02)	0.1 (0.12)	0.4 (0.03)	1.6

^a Values in parentheses are the average deviations from the mean.

Figure 1 shows Sulzer and Wieland's original curve, fitted to the data at 20° of Acton, Aickin, and Bayliss, and the one calculated by Seery and Britton to fit their data at 25°. For the gaussian curve (1), peaking at longer wavelengths, Seery and Britton obtained:

$\epsilon_0^m = 90.1$ l. mole⁻¹ cm⁻¹, $\omega_0 = 20,452$ cm⁻¹, and $\Delta\omega_0 = 1582$ cm⁻¹; for the peak at shorter wavelengths (2): $\epsilon_0^m = 204.2$, $\omega_0 = 24,159$, and $\Delta\omega_0 = 2102$. Seery and Britton's molar absorptivities on the short-wavelength side of peak 2 agree exceptionally well

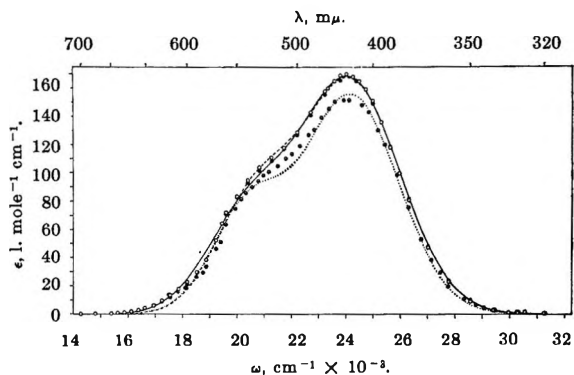


Figure 1. Comparison of various studies of the bromine spectrum at room temperature. The circles represent experimental points and the curves are the correlations given by Sulzer and Wieland's equation:⁹ ○ —, this work (25°); ● — — —, Seery and Britton (25°);⁷ ⊙ · · · ·, Sulzer and Wieland's fit to the data of Acton, Aikin, and Bayliss (20°).²

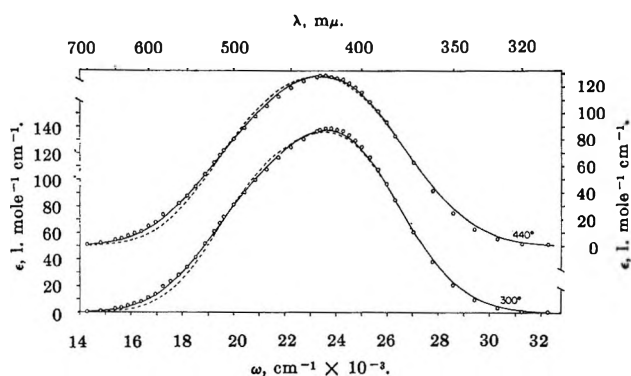


Figure 2. Bromine spectrum at 300 and 440°. The solid curves are the Sulzer–Wieland equations based on parameters determined from our data at 25°. The dashed curves are the Sulzer–Wieland equations based on Seery and Britton's parameters. Note the ordinate has been displaced to separate the data at the two different temperatures.

with our observations and we have adopted their values for the parameters for this peak. The contribution of peak 2 at longer wavelengths was calculated and subtracted from our total. A new set of parameters was then obtained for peak 1 by the method of least squares: $\epsilon_0^m = 86.6$, $\omega_0 = 20,393$, $\Delta\omega_0 = 1735$. Combination of peaks 1 and 2 gave the curve shown in Figure 1.

The Sulzer–Wieland equation gives an excellent correlation of data at the various temperatures for this wavelength interval. Figure 2 shows the result at 300 and at 440°. At 25° the Seery and Britton constants provide as good an over-all fit as our modified values and the two curves are probably within experimental error. The regions on either side of the maximum of peak 1 show the largest deviations. Our

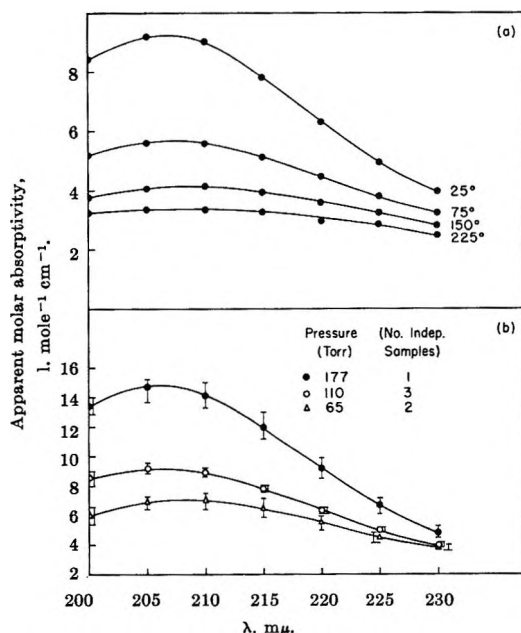


Figure 3. Absorption characteristics of bromine in the ultraviolet region: (a) temperature dependence of the apparent molar absorptivity of Br_2 for a constant-pressure (177 torr) sample; (b) pressure dependence of the apparent molar absorptivity of Br_2 at 25°. The range indicated, Φ , represents the variation encountered on comparison of results from independent samples or on checking a particular sample after a period of *ca.* 1 month. Values of the molar absorptivities in Table II are based on the average of results from the various samples.

parameters give an appreciably better fit at the higher temperatures, Figure 2. A more elaborate attempt to improve the fit did not seem justified in view of the assumptions in the model and the experimental uncertainty (*ca.* 1% in the vicinity of the maximum).

Anomalous Behavior in the Ultraviolet Region. The bromine spectrum between 200 and 300 μm shows a relatively weak absorption band at room temperature with a maximum near 205 μm . From 200 to 240 μm the apparent molar absorptivities of Br_2 , Figure 3, are strongly dependent on both pressure and temperature. We have studied more than ten independent samples in this wavelength interval at various temperatures (up to 440°) and pressures (up to 180 torr). The existence of bromine molecules larger than Br_2 has been suggested by Dobbie and Fox¹² and by Evans.⁵ Kokovin,¹³ using diaphragm-gauge *PVT* data at pressures up to 3.5 atm, attributed apparent gas imperfections to the

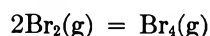
(12) J. J. Dobbie and J. J. Fox, *Proc. Roy. Soc. (London)*, **A99**, 456 (1921).

(13) G. A. Kokovin, *Zh. Neorgan. Khim.*, **10**(1), 287 (1965); *Russ. J. Inorg. Chem.*, **10**, 150 (1965).

Table II: Calculated Molar Absorptivities of Br₂ and Br₄ in the 200–230-mμ Range (l. mole⁻¹ cm⁻¹)

λ	ε ₂					ε ₄				
	25°	75°	150°	225°	Av	25°	75°	150°	225°	Av
200	1.4	1.4	1.3	2.7	1.7	1091	1342	1342	966	1185
205	2.2	2.2	1.5	2.4	2.1	1003	1183	1405	1157	1187
210	2.0	2.5	1.9	2.2	2.2	1075	1140	1240	1197	1163
215	2.0	2.5	2.0	2.3	2.2	866	920	1051	963	950
220	2.6	2.7	2.2	2.2	2.4	557	615	741	744	664
225	2.8	3.1	2.4	2.4	2.7	317	299	458	458	383
230	2.6	2.9	2.4	2.3	2.6	181	186	272	306	236

presence of Br₄ and deduced the equation $\log K_{\text{corr}} = 576 T^{-1} - 6.16$ for the postulated reaction



over the temperature interval 368–458°K. On the other hand, Lasater, *et al.*,¹⁴ fit their vapor density results (at 1 atm between 78 and 155°) using a van der Waals equation of state for Br₂. Kokovin's equation indicates that the concentration of Br₄ at total pressures, *ca.* 1 atm, is very small and its effect on PVT data would be difficult to distinguish from gas imperfections.

If one assumes that the apparent failure of Beer's law in the 200–300-mμ range of the spectrum is due to equilibrium between Br₂ and Br₄, one can write

$$A_t = A_2 + A_4 = \epsilon_2 b C_2 + \epsilon_4 b K R T C_2^2$$

where A_t , A_2 , and A_4 are the total absorbance, absorbance due to Br₂, and absorbance due to Br₄, respectively; ϵ_2 and ϵ_4 are the molar absorptivities of Br₂ and Br₄, respectively; b is the path length, K is the equilibrium constant (P_4/P_2^2) for the association reaction, and C_2 is the concentration of Br₂. C_2 can be taken as the total moles of bromine (determined by analysis) divided by the cell volume, since the fraction which appears to be in the form of Br₄ is only of the order of 1%. From a plot of A_t/bC_2 vs. C_2 for the various samples at a particular temperature and wavelength, ϵ_2 and $\epsilon_4 K$ may be obtained. If ϵ_4 is assumed not to be strongly dependent on temperature, a plot of $\log \epsilon_4 K$ vs. $1/T$ at a particular wavelength will give the standard enthalpy change for the association reaction. Such a treatment was carried out at 5-mμ intervals from 200 to 230 mμ and over the temperature interval 25–225°. At wavelengths longer than 230 mμ, instrument errors became large relative to total absorption. An average value of ΔH° of -2270 ± 250 cal/mole of Br₄ was obtained. The constant in Kokovin's equation gives -2640 cal.

If one assumes that Kokovin's equilibrium constants are valid, molar absorptivities of Br₂ and Br₄ may be evaluated. Results are shown in Table II. The ap-

parent molar absorptivities of Br₄ show rather large variations and hence, although the interpretation is generally consistent with the observations, we have not been able to establish clearly that the absorbance can be entirely attributed to Br₂ and a single polymeric species such as Br₄. Both HBr and SiBr₄, suspect as trace impurities, absorb strongly near 200 mμ. Whereas such impurities could not account for the pressure-temperature dependence of the spectrum, varying trace amounts of these substances in the different samples could cause the difficulty in reproducing results.

When the system was held at temperatures in the vicinity of 400°, a slow irreversible increase in absorbance in the 200–250-mμ range was noted. The species responsible for the increase has not been identified; its presence suggests that a slow interaction of bromine and quartz may occur at high temperatures. Even though the increase in absorbance was easily perceptible after a day at 400°, the amount of bromine in the cell, as indicated by its absorption in the visible range, did not change within the limits of error of the instrument. However, in view of the apparent interaction, conclusions relative to the possible existence of Br₄ were based on studies of samples which had not been heated above 225° and in which no such effect was observed.

Ogryzlo and Sanctuary⁸ have recently published a communication giving absorption curves for bromine in the short-wavelength region; these show the same general behavior, qualitatively at least, as we observe. They did not attempt to deduce molar absorptivities. Their plot of $\log A_4/T$ vs. $1/T$ shows significant curvature, possibly due to their method of taking into account the contribution of Br₂. They assume that all the absorption at 200° is due to Br₂ and subtract this from the total absorbance at lower temperatures to obtain that to be attributed to Br₄. Our results

(14) J. A. Lasater, S. D. Colley, and R. C. Anderson, *J. Am. Chem. Soc.*, **72**, 1845 (1950).

indicate, however, that for their sample (130 torr at 14°) the absorbances of Br₂ and Br₄ are nearly equal at 200°.

Mixtures of Bromine and Water. To test the effect of water as a possible impurity and also as a preliminary to a study of systems in which both bromine and water vapor were present, the ultraviolet-visible absorption spectrum of *ca.* equimolar mixtures of water vapor and bromine were examined. Some extraneous absorption in the short-wavelength region, suggestive of the presence of small amounts of HBr, was observed. However, the apparent contribution of this species was constant and no evidence of a systematic relationship of its contribution to the amounts of Br₂ and H₂O present could be seen. HBr may have been

introduced as a contaminant by reaction of traces of moisture with the "anhydrous" CuBr₂ used as a source of bromine. The shape of the bromine absorption curve between 300 and 750 m μ was not noticeably affected by the presence of water vapor at partial pressures of 100 torr or less. The total pressure of a similar mixture was also measured as a function of temperature in a diaphragm gauge (the total pressure reached 1 atm near 500°). Once vaporization was complete, ideal gas behavior was observed. Thus these studies gave no evidence for significant chemical interaction of bromine and water.

Acknowledgment. This work was supported by a grant from the National Science Foundation (GP 3775) which we acknowledge with thanks.

Osmotic and Activity Coefficients of *cis*- and

trans-Nitrobis(ethylenediamine)aminocobalt(III) Salts

by W. L. Masterton, T. I. Munnely, and L. H. Berka¹

Department of Chemistry, University of Connecticut, Storrs, Connecticut (Received September 20, 1966)

Osmotic and activity coefficients are reported for *cis*- and *trans*-[Co(en)₂NH₃NO₂]X₂, where X = NO₃⁻, I⁻, Br⁻, or Cl⁻. Up to 0.1 *m*, the osmotic and activity coefficients of these compounds are similar to each other but significantly lower than those of simple 2:1 salts. At higher concentrations, ϕ and γ_{\pm} are somewhat smaller for the *cis* isomers than for the *trans* isomers, implying a greater degree of ion association with the unsymmetrical *cis* cation. Values of ϕ and γ_{\pm} for both series of salts are smaller than those found previously for compounds of the type [Co(NH₃)₅A]X₂. It is suggested that this effect may result from a difference in the polarizabilities of the cations. Such an explanation is consistent with anion effects, where association appears to increase with increasing anionic size.

Introduction

Previous studies^{2,3} have established that the osmotic and activity coefficients of acidopentaaminocobalt(III) salts in aqueous solution are significantly lower than those of simple 2:1 electrolytes. These results have been interpreted in terms of ion association in solution; calculated ion-pair dissociation constants⁴

for these salts range from 0.05 to 0.08. Values of ϕ or γ_{\pm} for the various salts at concentrations above 0.1 *m*

- (1) Abstracted in part from the Ph.D. Thesis of T. I. Munnely.
- (2) W. L. Masterton and J. A. Scola, *J. Phys. Chem.*, **68**, 14 (1964).
- (3) L. H. Berka and W. L. Masterton, *ibid.*, **70**, 1641 (1966).
- (4) W. L. Masterton and L. H. Berka, *ibid.*, **70**, 1924 (1966).

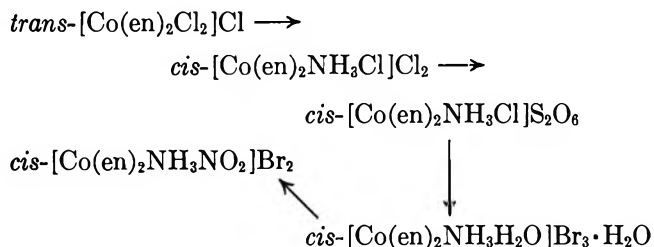
suggest that the extent of association increases with increasing anionic size (e.g., $\text{Cl}^- < \text{Br}^- < \text{I}^-$). On the other hand, replacing one acid ligand by another appears to have little effect on ϕ or γ_{\pm} , even at quite high concentrations.

To obtain more information about the effect of ligand substitution on the extent of association, we have measured the osmotic and activity coefficients of a series of nitrobis(ethylenediamine)amminecobalt(III) salts of general formula $[\text{Co}(\text{en})_2\text{NH}_3\text{NO}_2]\text{X}_2$, where $\text{X} = \text{NO}_3^-, \text{I}^-, \text{Br}^-, \text{or } \text{Cl}^-$. Salts of both the *cis* and *trans* series were studied to determine whether the polarity of the cation has any effect upon ion association in water.

Since each of the eight salts studied has an aqueous solubility of at least 0.3 *m*, osmotic coefficients could be measured over a wide range of concentrations. Although the rates of aquation of these compounds do not appear to have been measured, one can infer from literature values for comparable compounds⁵ that their water solutions should be extremely stable.

Experimental Section

Compounds. (1) *cis*- $[\text{Co}(\text{en})_2\text{NH}_3\text{NO}_2]\text{X}_2$ Series. (a) $\text{X} = \text{Br}^-$. This compound was prepared by the reaction sequence



Werner's procedure⁶ was followed with one significant deviation. In preparing the aquo bromide, a mixture of 1 equiv of HBr and 2 equiv of KBr was substituted for the 3 equiv of HBr used by Werner to bring down the product. This served to remove most of the dithionate anion as $\text{K}_2\text{S}_2\text{O}_6$. The presence of a small amount of dithionate in the next step is desirable since it serves to indicate the progress of reaction by the precipitation of *cis*- $[\text{Co}(\text{en})_2\text{NH}_3\text{NO}_2]\text{S}_2\text{O}_6$. However, if too much dithionate is present, the product is badly contaminated by this compound.

The final product was recrystallized twice from hot water using KBr; in a third recrystallization the KBr was omitted. *Anal.* Calcd: Br, 39.8; N, 20.9; C, 11.9; H, 4.8. Found: Br, 39.0; N, 21.0; C, 12.1; H, 4.6.

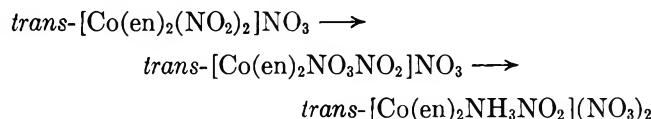
(b) $\text{X} = \text{NO}_3^-$. A solution of the bromide salt was treated with slightly less than the equivalent

amount of AgNO_3 . After filtration, the solution was passed through a column of Amberlite IRA-400 resin in the nitrate form to remove the small amount of Br^- remaining. The product was brought out of solution by freeze-drying. *Anal.* Calcd: N, 30.6; C, 13.1; H, 5.2. Found: N, 30.5; C, 13.2; H, 5.3.

(c) $\text{X} = \text{I}^-$. Addition of KI to a concentrated solution of the nitrate gave, upon cooling, a precipitate of *cis*- $[\text{Co}(\text{en})_2\text{NH}_3\text{NO}_2]\text{INO}_3$. A solution of this compound was passed through an anion-exchange column in the iodide form and the water removed by freeze-drying. *Anal.* Calcd for *cis*- $[\text{Co}(\text{en})_2\text{NH}_3\text{NO}_2]\text{I}_2 \cdot \text{H}_2\text{O}$: I, 49.4; N, 16.3; C, 9.3; H, 4.1; H_2O , 3.5. Found for sample dried at 50°: I, 49.4; N, 16.3; C, 9.7; H, 4.0; H_2O , 3.5.

(d) $\text{P} = \text{Cl}^-$. A solution of the bromide salt was shaken with AgCl . The filtered solution was passed through an anion-exchange column in the chloride form and the water removed by freeze-drying. *Anal.* Calcd for *cis*- $[\text{Co}(\text{en})_2\text{NH}_3\text{NO}_2]\text{Cl}_2 \cdot 1.5\text{H}_2\text{O}$: Cl, 20.9; N, 24.7; C, 14.1; H, 6.5; H_2O , 7.9. Found for sample dried at 50°: Cl, 20.8; N, 24.6; C, 14.2; H, 6.4; H_2O , 7.5.

(2) *trans*- $[\text{Co}(\text{en})_2\text{NH}_3\text{NO}_2]\text{X}_2$ Series. (a) $\text{X} = \text{NO}_3^-$. This compound was prepared as described by Werner⁷ following the reaction sequence



The product was recrystallized twice from hot water. *Anal.* Calcd: N, 30.6; C, 13.1; H, 5.2. Found: N, 30.8; C, 13.1; H, 5.5.

(b) $\text{X} = \text{I}^-$. A solution of the nitrate salt was precipitated with KI and the product recrystallized from hot water. *Anal.* Calcd for *trans*- $[\text{Co}(\text{en})_2\text{NH}_3\text{NO}_2]\text{I}_2 \cdot 1.5\text{H}_2\text{O}$: I, 48.5; N, 16.1; C, 9.2; H, 4.2; H_2O , 5.2. Found for sample dried at 50°: I, 48.3; N, 15.8; C, 9.4; H, 4.2; H_2O , 4.5.

(c) $\text{X} = \text{Br}^-$. A solution of the iodide salt was shaken with AgBr . The filtered solution was passed through an anion-exchange column in the bromide form and the water removed by freeze-drying. *Anal.* Calcd for *trans*- $[\text{Co}(\text{en})_2\text{NH}_3\text{NO}_2]\text{Br}_2 \cdot \text{H}_2\text{O}$: Br, 38.0; N, 20.0; C, 11.4; H, 5.0; H_2O , 4.3. Found for sample dried at 50°: Br, 38.1; N, 19.8; C, 11.6; H, 5.1; H_2O , 4.0.

(5) F. Basolo and R. G. Pearson, "Mechanisms of Inorganic Reactions," John Wiley and Sons, Inc., New York, N. Y., 1958, pp 115-122.

(6) A. Werner, *Ann. Chem. Liebigs*, **386**, 165, 166, 187, 218 (1912).

(7) A. Werner, *ibid.*, **386**, 224, 252 (1912).

(d) $X = Cl^-$. This compound was prepared in a manner entirely analogous to *cis*-[Co(en)₂NH₃NO₂]Cl₂, except that the starting material was the *trans* iodide. *Anal.* Calcd for *trans*-[Co(en)₂NH₃NO₂]Cl₂·0.5H₂O: Cl, 22.0; N, 26.1; C, 14.9; H, 6.3; H₂O, 2.8. Found for sample dried at 50°: Cl, 22.1; N, 26.0; C, 15.1; H, 6.2; H₂O, 2.6.

The configurations of the parent compounds, *cis*-[Co(en)₂NH₃NO₂]Br₂ and *trans*-[Co(en)₂NH₃NO₂](NO₃)₂, were confirmed by comparing their infrared spectra with those of similar *cis* and *trans* isomers reported by Baldwin.⁸ Consistent agreement with literature values was found in the differentiating areas. In particular, the *cis* isomer gave two absorption peaks in the region 850–900 cm⁻¹ while the *trans* isomer showed only one peak. Configurations of the other salts in the two series were tested chemically by adding K₄[Fe(CN)₆] to their saturated solutions. In agreement with Werner's observations, the *trans* salts gave precipitates while the *cis* salts did not.

Apparatus. Osmotic coefficients were determined at 37° using a Mechrolab vapor pressure osmometer.⁹ Potassium chloride solutions approximately isopiestic with those being studied were used for both the reference bead and the solvent cup. Values of ϕ were calculated from measured ΔR values as described previously.³ Measurements were taken at 0.01 *m* intervals from 0.03 to 0.10 *m*, at 0.1 *m* intervals from 0.10 to 1.0 *m*, and at approximately 0.4 *m* intervals from 1.0 *m* up to the solubility limit.

Readings were taken within an hour or less of the time the solutions were prepared. In no case was there any evidence of decomposition in solution; no solids were deposited in the syringes and the resistance readings did not change with time. With the *cis* and *trans* nitrates, the solutions were tested with K₄[Fe(CN)₆] after a particular run to ensure that isomerization had not taken place in solution.

Treatment of Data and Results

Osmotic coefficients from 0.03 to 1.0 *m* were fitted with an average deviation of 0.003 to a power series of the form

$$1 - \phi = am^{1/2} + bm + cm^{3/2} + dm^2 \quad (1)$$

Activity coefficients at 0.03 *m* were calculated with the aid of the extended Debye-Hückel equation

$$\log \gamma_{\pm} = \frac{-2A\mu^{1/2}}{1 + a^0B\mu^{1/2}}; \quad (\mu = m \times 3) \quad (2)$$

The parameter a^0 was evaluated from the smoothed osmotic coefficient at 0.03 *m*, using the derived relation, eq. 3.

$$1 - \phi = \frac{4.605A}{\mu(a^0B)^3}(x - 2 \ln x - 1/x) \quad (3)$$

where $x = 1 + a^0B\mu^{1/2}$. Values of a^0 obtained in this manner ranged from 2.2 to 2.7 Å for the compounds studied.

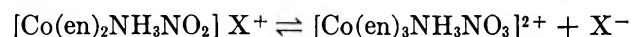
Activity coefficients at higher concentrations were obtained by integrating the relation

$$d \ln \gamma_{\pm} = d\phi + (\phi - 1)d \ln m \quad (4)$$

between the limits $m = 0.03$ and m . Between 0.03 and 1.0 *m*, the integration was performed analytically using eq. 1. Above 1.0 *m*, integration was carried out graphically, using experimentally determined osmotic coefficients.

The error in the osmotic and activity coefficients given in Tables I and II is estimated to be $\pm 1\%$ for ϕ and $\pm 3\%$ for γ_{\pm} in the concentration range 0.03–0.10 *m* and $\pm 0.5\%$ for ϕ and $\pm 3\%$ for γ_{\pm} above 0.10 *m*.

Ion-pair dissociation constants for the process



were calculated as described in ref. 3 from the osmotic coefficients at 0.10 *m*.

Discussion

Up to 0.1 *m*, the osmotic and activity coefficients of the eight salts are quite close to one another. Those for the chlorides are slightly higher than for the other salts; for example, ϕ of *cis*-[Co(en)₂NH₃NO₂]Cl₂ at 0.10 *m* is about 2% higher than the average for the other *cis* salts. The ion-pair dissociation constants listed in Table III show this same trend, with the chlorides having the highest values.

The osmotic and activity coefficients of these compounds, like those of other 2:1 complex-ion electrolytes reported earlier,^{2,3} are considerably lower than those of simple salts of the same valence type (e.g., CaCl₂). This difference is obvious at concentrations as low as 0.10 *m*, where the average value of ϕ for the compounds listed in Tables I and II is 0.75 as compared to an average of about 0.87 for simple, unassociated 2:1 electrolytes.¹⁰ This effect is even more striking at high concentrations. At 1.0 *m*, where the osmotic coefficients of 2:1 electrolytes are commonly greater than unity, ϕ for these complex-ion electrolytes ranges from 0.47 to 0.59.

It appears that the low values of ϕ , γ_{\pm} , and a^0

(8) M. E. Baldwin, *J. Chem. Soc.*, 4369 (1960).

(9) D. E. Burge, *J. Phys. Chem.*, **67**, 2590 (1963).

(10) R. A. Robinson and R. H. Stokes, "Electrolyte Solutions," Butterworth and Co. Ltd., London, 1959, pp 486–488.

Table I: Smoothed Osmotic and Activity Coefficients of *cis*-[Co(en)₂NH₃NO₂]₂X₂

<i>m</i>	NO ₃ ⁻		I ⁻		Br ⁻		Cl ⁻	
	φ	γ±	φ	γ±	φ	γ±	φ	γ±
0.03	0.827	0.560	0.827	0.560	0.821	0.553	0.831	0.565
0.04	0.808	0.521	0.809	0.522	0.802	0.514	0.814	0.528
0.05	0.792	0.491	0.795	0.492	0.786	0.483	0.801	0.499
0.06	0.779	0.466	0.783	0.468	0.773	0.458	0.790	0.476
0.08	0.758	0.427	0.762	0.430	0.752	0.418	0.773	0.439
0.10	0.740	0.396	0.745	0.400	0.734	0.389	0.759	0.411
0.20	0.681	0.306	0.679	0.307	0.674	0.298	0.715	0.328
0.30	0.640	0.256	0.625	0.253	0.630	0.248	0.683	0.281
0.40	0.605	0.222	0.579	0.215	0.594	0.214	0.655	0.249
0.50	0.574	0.196	0.542	0.188	0.562	0.189	0.630	0.224
0.60	0.547	0.176	0.516	0.168	0.534	0.169	0.607	0.204
0.80					0.493	0.141	0.572	0.175
1.0					0.467	0.123	0.555	0.157
1.2							0.544	0.140
1.6							0.524	0.123
2.0							0.507	0.108
2.4							0.500	0.098
2.8							0.499	0.091

Table II: Smoothed Osmotic and Activity Coefficients of *trans*-[Co(en)₂NH₃NO₂]₂X₂

<i>m</i>	NO ₃ ⁻		I ⁻		Br ⁻		Cl ⁻	
	φ	γ±	φ	γ±	φ	γ±	φ	γ±
0.03	0.827	0.560	0.833	0.568	0.824	0.557	0.832	0.566
0.04	0.808	0.521	0.818	0.532	0.806	0.519	0.816	0.529
0.05	0.792	0.490	0.805	0.504	0.792	0.490	0.803	0.500
0.06	0.779	0.466	0.794	0.480	0.780	0.465	0.792	0.477
0.08	0.757	0.426	0.775	0.443	0.761	0.427	0.776	0.441
0.10	0.740	0.396	0.758	0.413	0.746	0.398	0.763	0.414
0.20	0.680	0.305	0.687	0.318	0.693	0.311	0.722	0.333
0.30	0.639	0.255	0.638	0.264	0.654	0.262	0.694	0.287
0.40	0.605	0.221			0.620	0.228	0.669	0.256
0.50	0.576	0.196			0.590	0.203	0.647	0.232
0.60	0.550	0.176			0.563	0.183	0.628	0.213
0.80	0.509	0.147			0.526	0.154	0.603	0.186
1.0					0.504	0.137	0.591	0.169
1.2					0.482	0.122	0.581	0.154
1.6					0.444	0.101	0.563	0.134
2.0					0.425	0.087	0.561	0.120
2.4					0.418	0.078	0.560	0.110

Table III: Dissociation Constants for [Co(en)₂NH₃NO₂]₂X⁺

	NO ₃ ⁻	I ⁻	Br ⁻	Cl ⁻
<i>cis</i>	0.050	0.054	0.044	0.071
<i>trans</i>	0.050	0.070	0.055	0.075

found with these compounds can be attributed primarily to association between oppositely charged ions in solution. The ion-pair dissociation constants are comparable to those of the relatively few simple 2:1 elec-

trolytes known to be ion paired, such as Ba(NO₃)₂ (*K* = 0.12) and Pb(NO₃)₂ (*K* = 0.066).¹¹ At high concentrations, one might expect another factor, that of cationic hydration, to make the osmotic and activity coefficients of simple electrolytes higher than those of complex-ion electrolytes. However, even at 1.0 *m*, assuming a difference of six in hydration number between Ca²⁺ and a complex cation such as *cis*-[Co-

(11) C. W. Davies, "Ion Association," Butterworth Inc., Washington, D. C., 1962, pp 170, 171.

Table IV: Effect on ϕ of Substituting Ethylenediamine for Ammonia

	0.10	0.20	0.50	1.0	2.0
ϕ [Co(NH ₃) ₅ A]Cl ₂ ^a	0.763	0.731	0.682	0.670	0.672
ϕ <i>trans</i> -[Co(en) ₂ NH ₃ NO ₂]Cl ₂	0.763	0.722	0.647	0.591	0.561
ϕ <i>cis</i> -[Co(en) ₂ NH ₃ NO ₂]Cl ₂	0.759	0.715	0.630	0.555	0.507
ϕ [Co(NH ₃) ₅ A]Br ₂ ^a	0.761	0.721	0.660	0.618	
ϕ <i>trans</i> -[Co(en) ₂ NH ₃ NO ₂]Br ₂	0.746	0.693	0.590	0.504	
ϕ <i>cis</i> -[Co(en) ₂ NH ₃ NO ₂]Br ₂	0.734	0.674	0.562	0.467	

^a Average for three compounds in which A is an organic acid ligand.

(en)₂NH₃NO₂]²⁺, one can calculate¹² that the hydration effect alone should raise the osmotic coefficient by only about 12%. The observed value of ϕ for CaCl₂ at 1.0 *m*, 1.046, is nearly twice that of *cis*-[Co(en)₂NH₃NO₂]Cl₂, indicating that even at high concentrations ion association is the major factor responsible for the abnormally low osmotic and activity coefficients of the latter compound.

Above 0.1 *m*, differences among the compounds listed in Tables I and II become apparent. In particular, the osmotic coefficients of the chlorides become significantly greater than those of the other salts. Compare, for example, the ϕ values for the *cis* salts at 0.60 *m* (Cl⁻ = 0.607, NO₃⁻ = 0.547, Br⁻ = 0.534, I⁻ = 0.516). At high concentrations, the general order of the osmotic coefficients of the halides is Cl⁻ > Br⁻ > I⁻, implying an increase in association with increasing anionic size.

The osmotic and activity coefficients of the *cis* salts are somewhat lower than those of the *trans* salts. At low concentrations, the differences between isomers are very small, of the order of the experimental error in the measurements. At 0.10 *m*, for example, the average value of ϕ for the *cis* salts (0.744) is only about 1% less than that of the *trans* salts (0.751). As the concentration increases, these differences become more significant, amounting to about 5% at 0.60 *m* and 7% at 1.0 *m*. Curiously enough, the *cis* and *trans* nitrates, contrary to this trend, have virtually identical osmotic coefficients up to the highest concentration at which a comparison is possible (0.60 *m*).

The generally lower osmotic and activity coefficients of the *cis* halides as compared to the *trans* halides can presumably be attributed to a greater degree of ion association with the less symmetrical *cis* cation. The *trans* cation, which one would expect to be less polar, should show less tendency to associate with anions. This interpretation is consistent with the observations of Pearson, Henry, and Basolo,¹³ who deduced from a

study of the ultraviolet spectra of *cis*- and *trans*-[Co(en)₂Cl₂]Cl in methanol solution that the *cis* isomer was strongly ion paired while the *trans* isomer showed no evidence of association.

It is interesting to compare the data reported here to those³ for salts in which the complex cation has the general formula [Co(NH₃)₅A]²⁺. Here again, differences in ϕ or γ_{\pm} become pronounced only at relatively high concentrations.¹⁴ In general, the substitution of two ethylenediamine molecules for four ammonia molecules leads to lower osmotic and activity coefficients (Table IV).

The trend evident from the data in Table IV is perhaps most simply explained in terms of the role of dispersion forces in this type of ion association. One would expect the substitution of ethylenediamine for ammonia to yield a larger, more polarizable cation. If dispersion forces are of major importance in the stability of the ion pair, this would lead to more extensive association and hence to lower osmotic and activity coefficients. Such an explanation is, of course, consistent with the observation that the extent of association of a given cation with different halide ions increases Cl⁻ < Br⁻ < I⁻, the order of increasing polarizability of the anions.

Acknowledgment. We thank Howard Sepowitz for checking calculations and the Institute of Water Resources of the University of Connecticut and the National Science Foundation for grants in support of this research.

(12) R. H. Stokes and R. A. Robinson, *J. Am. Chem. Soc.*, **70**, 1870 (1948).

(13) R. G. Pearson, P. M. Henry, and F. Basolo, *ibid.*, **79**, 5382 (1957).

(14) This unfortunately limits the validity of the most obvious comparison, that between [Co(en)₂NH₃NO₂]Cl₂ and [Co(NH₃)₅NO₂]Cl₂, since data for the latter compound are available only up to 0.10 *m*, its solubility limit. At that concentration, the osmotic coefficient of [Co(NH₃)₅NO₂]Cl₂ is 0.771, about 1% higher than that of *trans*-[Co(en)₂NH₃NO₂]Cl₂ and 1.5% higher than that of *cis*-[Co(en)₂NH₃NO₂]Cl₂.

The Rates of the Reactions of Active Nitrogen with Ethylene and Propylene

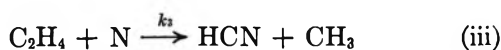
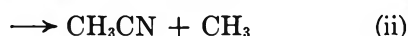
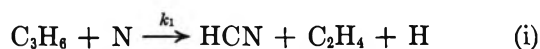
by G. Paraskevopoulos¹ and C. A. Winkler

*Physical Chemistry Laboratory, Department of Chemistry, McGill University,
Montreal, Quebec, Canada (Received September 20, 1966)*

Second-order rate constants for the initial attack of N atoms on ethylene and propylene have been determined over a range of temperatures, olefin flow rates, and reaction times. The rate constants may be expressed by $k_{\text{C}_2\text{H}_4} = 1.6 \times 10^{10} \exp(-700/RT)$ cc mole⁻¹ sec⁻¹ and $k_{\text{C}_3\text{H}_6} = 1.5 \times 10^{11} \exp(-1650/RT)$ cc mole⁻¹ sec⁻¹. The ratios of the rate constants for the initial attack of N atoms on propylene and ethylene were obtained from a treatment of the propylene reaction as a sequence of two competitive, consecutive reactions in which ethylene, as a primary product, is subsequently attacked by N atoms. They agreed with values obtained independently for the two reactions.

Introduction

Two studies of the reaction of active nitrogen with propylene have been reported. In the first study,^{2a} HCN and C₂H₄ were found to be the main products, together with small amounts of C₂H₆, C₃H₈, traces of C₂H₂, and a C₄ fraction. A subsequent study,^{2b} with both ordinary and labeled (¹⁴C) propylene, indicated that CH₃CN was also a product, second only to HCN in abundance. Direct attack of ground-state (⁴S) nitrogen atoms on C₃H₆ was assumed to occur to form HCN, C₂H₄, and CH₃CN with subsequent attack of N atoms on C₂H₄ and CH₃CN to form mainly HCN. The main features of the reaction may be represented by



No kinetic studies of the propylene reaction that might enable a test of the above mechanism have yet been reported. For the above mechanism, the ratio k_3/k_1 may be estimated from the concentrations of C₃H₆ and C₂H₄ during the reaction. The value so obtained should then be comparable with that given by independent measurements of k_1 and k_3 . The present paper presents data that enable such a comparison

to be made for a range of initial concentrations, reaction times, and temperatures.

Experimental Section

Active nitrogen was generated by a condensed discharge in nitrogen gas. The apparatus was essentially similar to that used in a previous investigation.³ A reaction vessel of Pyrex glass, 25 mm id and 60 cm long, formed part of a fast-flow system. The hydrocarbon reactants were introduced into the reaction tube through a fixed spherical jet, 10 cm below the inlet from the discharge tube. The reaction time was controlled by stopping the reaction at different distances along the reaction tube, using a cobalt target described previously³ to destroy N atoms. For conditions of complete reaction, the cobalt target was removed and the reaction was allowed to proceed to completion. The materials used were the best available grades and were purified as described previously.³

Experiments were made at a pressure of 1.95 mm. The molecular nitrogen flow rate was 164×10^{-6} mole sec⁻¹. The initial concentration of N atoms was based on the gas-phase titration with NO.⁴ Recent

(1) Holder of a Union Carbide Ltd. fellowship, 1963-1964.

(2) (a) G. S. Trick and C. A. Winkler, *Can. J. Chem.*, **30**, 915 (1952);
(b) Y. Shinozaki, R. Shaw, and N. L. Lichtin, *J. Am. Chem. Soc.*, **86**, 341 (1964).

(3) E. M. Levy and C. A. Winkler, *Can. J. Chem.*, **40**, 686 (1962).

(4) G. B. Kistiakowsky and G. G. Volpi, *J. Chem. Phys.*, **27**, 1141 (1957).

evidence^{5,6} has indicated that this method rather than the maximum HCN production from ethylene⁷ gives a valid estimate of the N atom flow rate. For the experimental conditions of this work, the N atom flow rate was $(5.80 \pm 0.30) \times 10^{-6}$ mole sec^{-1} and the ratio of the estimates given by the two methods was $\text{NO}:\text{HCN} = 1.8 \pm 0.1$.

The condensable products were trapped at liquid air temperatures and in most experiments were analyzed by mass spectrometry. In a few experiments, only HCN was determined by titration with AgNO_3 .

Flow rates were converted to concentrations in the customary manner. The reaction time was calculated from the linear velocity of the gas and the distance between the point of injection of the reactant and the plane of termination of the reaction. The effect of temperature was considered in both these calculations.

Results and Discussion

Complete Reaction. The amount of C_3H_6 reacted and the yields of all the condensable products at 44 ± 5 , 321 ± 5 , and $416 \pm 5^\circ$ are plotted as functions of the propylene flow rate in Figures 1 and 2. The main products were HCN and C_2H_4 , with smaller amounts of C_3H_8 , CH_3CN , C_2N_2 , and C_2H_6 . Trace amounts of C_2H_2 were found in some of the experiments. A small peak at mass 53 might be ascribed to traces of cyanoethylene.⁸ Average carbon balances were 98%.

The limiting ("plateau") yields of HCN and C_2H_4 and the amount of C_3H_6 reacted were independent of temperature and C_3H_6 flow rate. Determination of HCN only by titration with AgNO_3 (Figure 1) agreed well with the mass spectrometric results. Within experimental error, the plateau yields of HCN were found to be the same for the reactions of C_3H_6 and C_2H_4 for essentially identical experimental conditions.

Methyl cyanide was not found as a product in the first study of the reaction.^{2a} Later, Shinozaki, *et al.*,^{2b} found by gas chromatography that it was the second most abundant product after HCN, while the present experiments, with relatively good carbon balances (98%), indicate the relative amounts of the various products to be in the order HCN , C_2H_4 , C_3H_8 , CH_3CN , and about equal amounts of C_2N_2 and C_2H_6 .

The stoichiometry of the reaction, *i.e.*, the number of nitrogen atoms found in the products per molecule of C_3H_6 reacted, has been found to change from 1.8–2 at low C_3H_6 flow rates to about 1.1–1.3 at high C_3H_6 flow rates. This change might be expected for competitive consecutive reactions, as the relative proportions of nitrogen atoms and the parent hydrocarbon are altered.

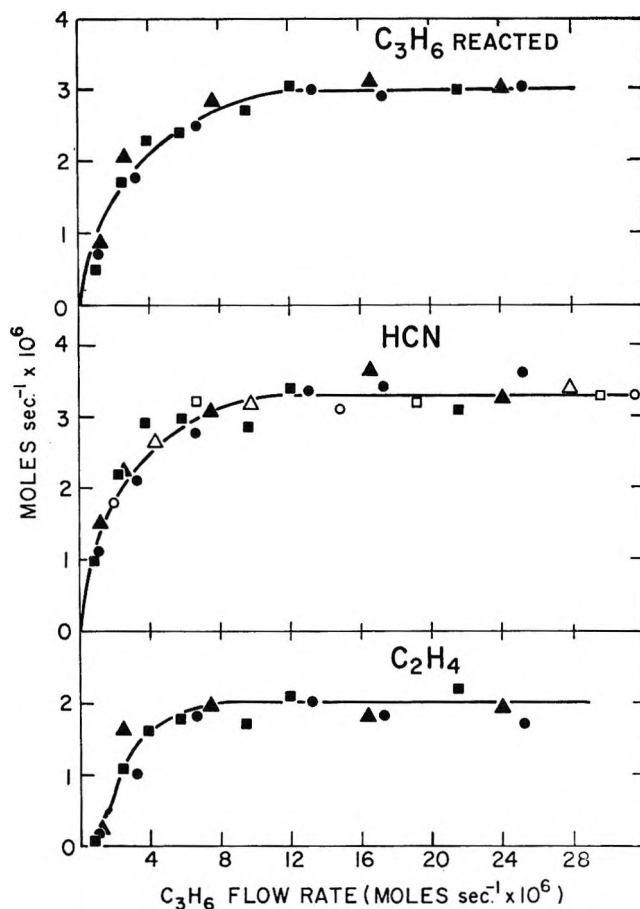
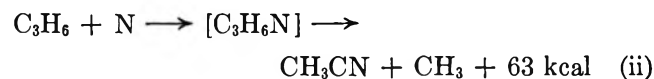


Figure 1. C_3H_6 reacted, and HCN and C_2H_4 yields plotted as functions of C_3H_6 flow rate: ●, $44 \pm 5^\circ$; ▲, $321 \pm 5^\circ$; ■, $416 \pm 5^\circ$; ○, △, □, HCN determined by titration with AgNO_3 .

The yields of C_3H_8 and C_2H_6 paralleled the amounts of C_3H_6 and C_2H_4 recovered, from which it would appear that the saturated products were formed by reaction of H atoms with the corresponding olefins. On the other hand CH_3CN appears to be a primary product, since measurable amounts of it were recovered in the region of incomplete N atom consumption, where CH_3 radicals would probably react rapidly with N atoms rather than combine with CN radicals to form CH_3CN . It seems possible that CH_3CN might be formed by the energetically favorable reaction



in competition with reaction i.

(5) A. A. Westenberg and N. de Haas, *J. Chem. Phys.*, **40**, 3087 (1964).

(6) L. Elias, *ibid.*, **42**, 4311 (1965).

(7) A. N. Wright, R. L. Nelson, and C. A. Winkler, *Can. J. Chem.*, **40**, 1082 (1962).

(8) J. T. Herron, J. L. Franklin, and P. Bradt, *ibid.*, **37**, 579 (1959).

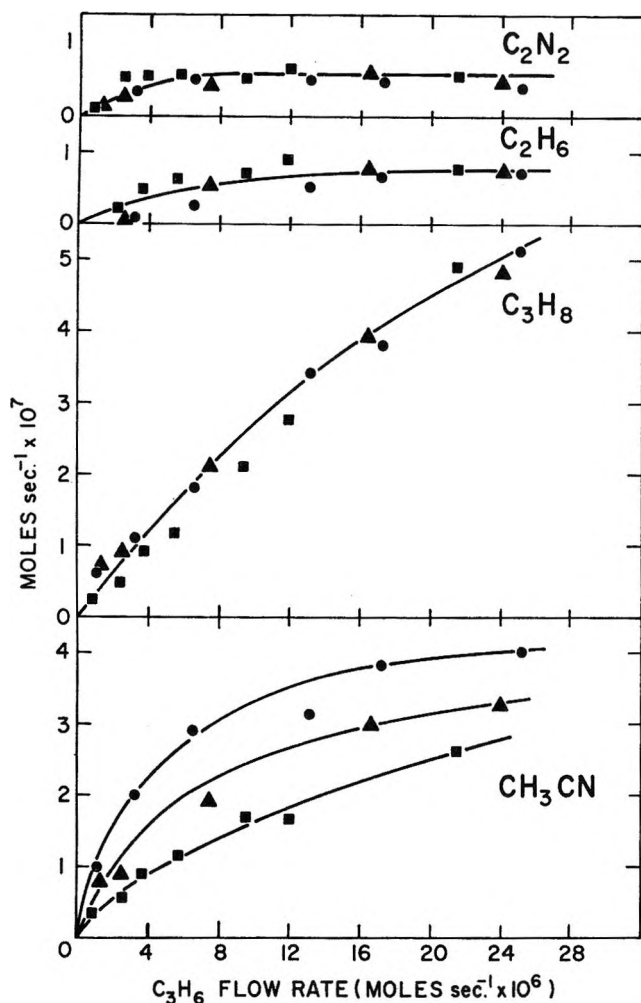


Figure 2. CH_3CN , C_3H_8 , C_2H_6 , and C_2N_2 yields plotted as functions of C_3H_6 flow rate: \bullet , $44 \pm 5^\circ$; \blacktriangle , $321 \pm 5^\circ$; \blacksquare , $416 \pm 5^\circ$.

The CH_3CN formed reacts further with active nitrogen (reaction v). It has been shown^{9,10} that the maximum (plateau value) for the amount of CH_3CN reacted increased with temperature. This would explain the decrease of CH_3CN yields with increasing temperature (Figure 2).

Rate Constant Measurements. For the calculation of rate constants, it was assumed that losses of N atoms by homogeneous and wall recombinations were negligible relative to their consumption in the fast reaction with C_2H_4 or C_3H_6 .

On the assumption that the rate-controlling step is the relatively slow, spin-forbidden N atom attack on the olefin (reactions i and iii), the rate constant for the disappearance of the olefin was calculated from the integrated second-order rate equation

$$k = \frac{1}{t} \frac{2.303}{(a - nb)} \log \frac{b(a - nx)}{a(b - x)} \quad (1)$$

where x = concentration of olefin consumed, a = initial concentration of N atoms, b = initial concentration of olefin, n = $[\text{N in products}]/x$ (stoichiometry of the reaction), and t = reaction time.

Equation 1 is valid at low olefin flow rates where by-product formation is negligible and at reaction times smaller than the time required for the reaction to attain completion. These were the conditions imposed for the experiments.

Rate Constant, k_3 , for the Reaction of C_2H_4 . Rate constants for the reaction of active nitrogen with C_2H_4 , k_3 , have been determined previously by a variety of techniques. The rate-controlling step has been assumed to be the attack of ground-state N atoms on C_2H_4 (reaction iii) to produce HCN.^{3,11-15} A value $n = 2$ was taken for one investigation³ and $n = 1.5$ for another.¹³ In the present study, the stoichiometry was established analytically and values of k_3 were determined under the same experimental conditions as those for the subsequent measurements of k_1 for the C_3H_6 region.

To determine the value of n applicable to the C_2H_4 reaction, the condensable products were analyzed mass spectrometrically for experiments at 476 and 701°K, with two reaction times (in the range 0.6×10^{-2} to 2.5×10^{-2} sec) at each temperature and two flow rates (in the range 1–4 $\mu\text{moles sec}^{-1}$) of C_2H_4 at each reaction time. Hydrogen cyanide accounted for about 90% of all the products and for over 95% of the nitrogen-containing products. Very small quantities of C_2N_2 , CH_3CN , C_3 hydrocarbons, traces of C_2H_2 , and possibly traces of NH_3 were also present. Carbon balances were about 98%. From these experiments, an average value for the stoichiometry, n , was found to be 1.53 ± 0.07 moles of HCN/mole of C_2H_4 reacted. This value was then used to calculate rate constants at two more temperatures, 318 and 574°K, from experiments in which only HCN was determined, by titration with AgNO_3 . The C_2H_4 consumed was taken to be $x = \text{HCN}/n$. These analyses were made for four reaction times (in the range 0.5×10^{-2} to 3.8×10^{-2} sec) at each temperature, with three flow rates (in the range 0.6–2.7 $\mu\text{moles sec}^{-1}$) of C_2H_4 at each reac-

(9) W. Forst and C. A. Winkler, *J. Phys. Chem.*, **60**, 1424 (1956).

(10) E. D. Böhme, Ph.D. Thesis, McGill University, Montreal, 1963.

(11) J. H. Greenblatt and C. A. Winkler, *Can. J. Res.*, **B27**, 732 (1949).

(12) E. R. V. Milton and H. B. Dunford, *J. Chem. Phys.*, **34**, 51 (1961).

(13) A. N. Wright and C. A. Winkler, *Can. J. Chem.*, **40**, 5 (1962).

(14) L. I. Avramenko and V. M. Krasnen'kov, *Izv. Akad. Nauk SSSR, Otd. Khim. Nauk*, 600 (1964).

(15) J. T. Herron, *J. Phys. Chem.*, **69**, 2736 (1965).

tion time. Values of k_3 , averaged for all flow rates and reaction times at each temperature, are summarized in Table I.

Table I: The Reaction of Active Nitrogen with Ethylene. Second-Order Rate Constants Averaged for All Reaction Times and Flow Rates at Each Temperature

Temp, °K	k_3 , cm ³ mole ⁻¹ sec ⁻¹ × 10 ⁻¹⁰	Std dev
318	0.54	0.13
476	0.80	0.16
574	0.88	0.12
701	0.96	0.20

The data give an activation energy, E_3 , and a pre-exponential factor, A_3 , of 700 cal mole⁻¹ and 1.6×10^{10} cm³ mole⁻¹ sec⁻¹, respectively. Accordingly

$$k_3 = 1.6 \times 10^{10} \exp(-700/RT)$$

A steric factor, P_3 , of 7×10^{-5} was estimated from the data.

The values of k_3 agree as well as might be expected with those obtained previously by similar experimental techniques,^{3,13,14} when it is recognized that in the previous work N atom concentrations were estimated by the maximum yield of HCN from C₂H₄. They are somewhat lower than the upper limit for k_3 at 320°K (0.7×10^{10} cm³ mole⁻¹ sec⁻¹) suggested by Herron¹⁵ from a mass spectrometric study of the reaction and are about one order of magnitude lower than the values obtained by a diffusion flame technique.^{11,12} The value of 700 cal mole⁻¹ obtained for the activation energy lies between the two other values reported, *i.e.*, 400 cal mole⁻¹³ and 1500 cal mole⁻¹.^{14,15a}

Rate Constant, k_1 , for the Reaction of C₃H₆. All the condensable products from the C₃H₆ reaction were analyzed mass spectrometrically for experiments at four temperatures (338, 447, 602, and 697°K) for three reaction times (in the range 0.8×10^{-2} to 3.7×10^{-2} sec) at each temperature, with two or three flow rates (in the range 0.7–2.9 μmoles sec⁻¹) of C₃H₆ at each reaction time. For the experimental conditions used, some of the products were formed in only minor amounts compared with their yields for complete reaction, *e.g.*, little C₃H₈ and C₂N₂ and no C₂H₆ or C₂H₂. Average carbon balances were 98% and HCN accounted for 78–92% of the nitrogen-containing products.

Some typical data for the second-order rate constant, k_1 , for different reaction times, based on disappearance of C₃H₆ and N atoms (inferred from the stoichiometry) are shown in Table II. Values of k_1

averaged for all reaction times and flow rates at each temperature are summarized in Table III.

Table II: The Reaction of Active Nitrogen with Propylene. Typical Second-Order Rate Constants, k_1 , at 338°K

Time, sec × 10 ²	C ₃ H ₆ , moles cm ⁻³ × 10 ¹⁰	x , moles cm ⁻³ × 10 ¹⁰	k_1 , cm ³ mole ⁻¹ sec ⁻¹ × 10 ⁻¹⁰
3.71	4.39	3.07	1.1
	13.8	9.00	1.1
2.39	5.44	3.24	1.3
	15.4	9.66	1.6
1.59	4.62	2.31	1.4
	6.92	3.73	1.6
	13.8	7.25	1.6

Table III: The Reaction of Active Nitrogen with Propylene. Second-Order Rate Constants, Averaged for All Reaction Times and Flow Rates at Each Temperature

Temp, °K	k_1 , ^a cm ³ mole ⁻¹ sec ⁻¹ × 10 ⁻¹⁰	Std dev
338	1.4	0.3
477	2.6	0.5
602	3.9	0.7
697	4.9	0.5

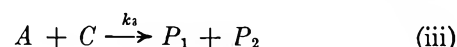
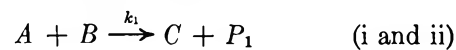
^a NOTE ADDED IN PROOF. Cf. the recent value of $(1.9 \pm 0.6) \times 10^{10}$ cc mole⁻¹ sec⁻¹ at 340°K, reported by J. T. Herron, *J. Phys. Chem.*, **70**, 2803 (1966).

An activation energy, E_1 , of 1650 cal mole⁻¹ and a preexponential factor, A_1 , of 1.5×10^{11} cm³ mole⁻¹ sec⁻¹ were evaluated from the data. Hence

$$k_1 = 1.5 \times 10^{11} \exp(-1650/RT)$$

The corresponding steric factor, P_1 , was estimated to be 6×10^{-4} .

Ratio k_3/k_1 . The mechanism for the C₃H₆ reaction, outlined previously, may be written



where A = concentration of N atoms, B = concentration of C₃H₆, C = concentration of (C₂H₄ + CH₃CN), P_1 and P_2 = concentrations of HCN and other products. Reactions i and ii may be combined and C

(15a) NOTE ADDED IN PROOF. Cf. also the more recent values reported by K. D. Foster, P. Kebarle, and H. B. Dunford, *Can. J. Chem.*, **44**, 2691 (1966); J. T. Herron, *J. Phys. Chem.*, **70**, 2803 (1966).

taken to represent the combined concentrations of C_2H_4 and CH_3CN , since both react with N atoms to yield mainly HCN.⁹ The measured amounts of CH_3CN accounted for roughly 5–24% of the total amount of C_2H_4 and CH_3CN , depending on the temperature.

The kinetic system written above consists of two competitive and consecutive irreversible second-order reactions. Following the treatment given by McMillan¹⁶ for such systems, the ratio k_3/k_1 may be obtained from a knowledge of any two concentrations at a single time of the components A , B , and C . Choice of B and C has the advantage that the resulting values of k_3/k_1 will be independent of the N atom concentration.

The rates of change of B and C are

$$dB/dt = -k_1AB \quad (2)$$

$$dC/dt = k_1AB - k_3AC \quad (3)$$

Dividing eq 3 by eq 2, substituting $k_3/k_1 = K$, $b = B/B_0$, and $c = C/B_0$, where B_0 = initial concentration of C_3H_6

$$dc/dt = -1 + Kc/b \quad (4)$$

With the variables taken to be b and $y = c/b$, eq 4 may be integrated and the original values restored, with boundary conditions, initial (1, 0) and final (b , c) to obtain

$$K \ln b = \ln [b + (1 - K)c]$$

or

$$b^K = b + (1 - K)c \quad (5)$$

For any measured pair of experimental parameters (b , c) the value of K satisfying eq 5 may be found by numerical inspection or by direct determination of the intersection of the left- and right-hand sides of eq 5, considered as functions of K . In the present work K was calculated from eq 5 with a computer.

Values of $K = k_3/k_1$ that satisfied eq 5 at each reac-

tion time were averaged over all reaction times at each temperature to obtain the data summarized in column 2 of Table IV. They are based on C_3H_6 and C_2H_4 present at each reaction time. In column 3 of the table are ratios of k_3/k_1 , calculated from the experimental values of k_3 and k_1 in Tables I and III, respectively. It will be recalled that both k_1 and k_3 are based on the consumption of N atoms and hydrocarbon at each reaction time. From the satisfactory agreement between the two sets of values of k_3/k_1 , it seems reasonable to conclude that the suggested mechanism is consistent with the experimental data.

Table IV: Comparative Values of the Ratio k_3/k_1

Temp, °K	k_3/k_1 (eq 5)	k_3/k_1 (eq 1)
338	0.46	0.40
477	0.32	0.29
602	0.21	0.23
697	0.20	0.19

The C_3H_6 reaction was found to be two to five times faster than the C_2H_4 reaction, depending on the temperature. Unfortunately, the activation energies and frequency factors estimated for the two reactions are subject to large uncertainties. As the reactant concentration was changed, the intensity of the reaction flame was observed to change along the reactor. The temperatures recorded by two fixed thermocouples in the reaction zone may therefore differ considerably from the true reaction temperatures. As a consequence, the calculated activation energies might be in error by as much perhaps as a factor of about 2 and have little significance other than to indicate that they are small for both reactions.

(16) W. G. McMillan, *J. Am. Chem. Soc.*, **79**, 4838 (1957).

Temperature-Dependence Studies of Proton and Deuteron

Spin-Lattice Relaxation in Ammonium Chloride

by D. E. Woessner and B. S. Snowden, Jr.

Mobil Oil Corporation, Field Research Laboratory, Dallas, Texas 75221 (Received September 20, 1966)

The λ transition in ammonium chloride at 242.8°K has been detected by proton spin-lattice relaxation temperature-dependence measurements. The temperature trend of the nuclear correlation time (τ_c) is in qualitative agreement with the volume temperature dependence. However, considering the effect of volume change on electrostatic forces, it is evident that a simple change in electrostatic potential cannot account for the quantitative temperature dependence of τ_c . Better quantitative agreement is obtained when the change of the temperature dependence of τ_c is compared with that of the shear elastic constant, c_{44} . There appears to be an indirect relation between the temperature dependence of τ_c and the degree of order in the crystal lattice in the region of the λ transition.

Introduction

Detection of the λ thermal transition in the ammonia halides by nuclear magnetic resonance (nmr) spin-lattice relaxation has been previously reported¹⁻³ as being unsuccessful. In the present work the transition was clearly observed for solid NH_4Cl at 242.8°K. This has been reported⁴ to be an order-disorder transition.

The NH_4^+ ions in the CsCl-type lattice are oriented in the unit cell so that the hydrogen atoms point toward the nearest neighbor chloride ion. This gives two possible tetrahedron orientations. If the orientations of the ammonium tetrahedrons in the unit cells are identical, the lattice is in its ordered state. When the orientations of the ammonium tetrahedrons are randomly distributed among the two possible orientations, the lattice is in the completely disordered state.

Experimental Results

All measurements were made with the standard nuclear resonance pulse apparatus previously described.⁵ The only significant modification to this experimental apparatus is the use of a fast response probe.⁶ The T_1 values were obtained in the temperature range from 140 to 373°K by the nmr pulse technique utilizing repeated 180-90° pulse sequences. The deuteron T_1 values were measured at a resonance frequency of 9.5 MHz and those for protons at resonance

frequencies of 9.5 and 25 MHz. The ND_4Cl was prepared by successive exchanges of NH_4Cl with D_2O . The samples were dried overnight by vacuum pumping and then sealed in Pyrex vials.

The T_1 temperature dependences are shown in Figures 1 and 2. Note that in each instance there is a T_1 shift of a factor of approximately 2.0 at the λ -point transition (249.4°K for ND_4Cl ⁴ and 242.8°K for NH_4Cl ⁷). The T_1 minima are presented in Table I.

Table I: T_1 Minima For ND_4Cl and NH_4Cl

Nucleus	Resonance frequency, MHz	Min T_1 value, msec	Temp of T_1 min, °K	Calcd T_1 min values, msec
Deuteron	9.5	0.455	192	0.435
Proton	9.5	1.86	191	1.77
Proton	25.0	5.05	200	4.67

- (1) E. M. Purcell, *Physica*, **17**, 282 (1951).
- (2) A. H. Cooke and L. E. Drain, *Proc. Phys. Soc. (London)*, **A65**, 894 (1952).
- (3) J. E. Anderson and W. P. Slichter, *J. Chem. Phys.*, **44**, 1797 (1966).
- (4) H. A. Levy and S. W. Peterson, *J. Am. Chem. Soc.*, **75**, 1536 (1953).
- (5) J. C. Buchta, H. S. Gutowsky, and D. E. Woessner, *Rev. Sci. Instr.*, **29**, 55 (1958).
- (6) R. A. McKay and D. E. Woessner, *J. Sci. Instr.*, **43**, 838 (1966).
- (7) F. Simon, *Ann. Physik*, **68**, 241 (1922).

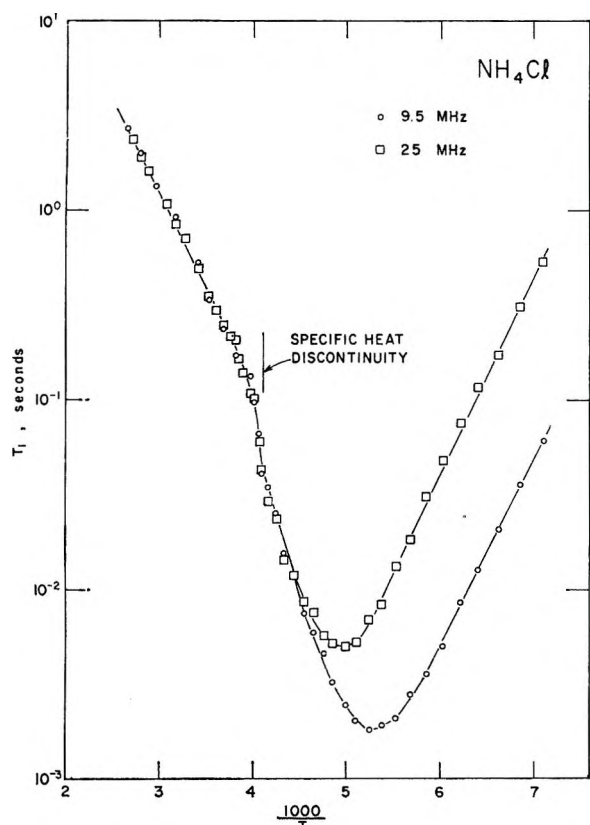


Figure 1. The temperature dependence of the proton T_1 for NH_4Cl at 9.5 and 25 MHz.

The T_1 values are analyzed by use of the widely known expressions⁸ for protons and deuterons.

$$\frac{1}{T_1} = \frac{2}{3}\omega_p^2 \left[\frac{\tau_c}{1 + \omega_0^2\tau_c^2} + 4 \frac{\tau_c}{1 + 4\omega_0^2\tau_c^2} \right] \quad (1)$$

for the protons and

$$\frac{1}{T_1} = \frac{3}{10}\pi^2 \left(1 + \frac{\eta^2}{3} \right) \left(\frac{e^2qQ}{h} \right)^2 \times \left[\frac{\tau_c}{1 + \omega_0^2\tau_c^2} + 4 \frac{\tau_c}{1 + 4\omega_0^2\tau_c^2} \right] \quad (2)$$

for the deuterons, where ω_p^2 is the second moment of the proton resonance expressed in angular units, $(e^2qQ)/h$ is the quadrupole coupling constant, η is the asymmetry parameter of the quadrupole interaction, ω_0 is the angular resonance frequency, and τ_c is the correlation time of the ammonium tetrahedron reorientation.

Each T_1 passes through a minimum value when $\omega_0\tau_c = 0.6158$. Using the 78°K value,⁹ $\omega_p^2 = 3.54 \times 10^{10}$ radians²/sec², the computed proton minimum T_1 value is 4.67 msec at 25 MHz and 1.77 msec at 9.5 MHz. For the deuteron T_1 , the 119°K values¹⁰ $(e^2qQ)/h =$

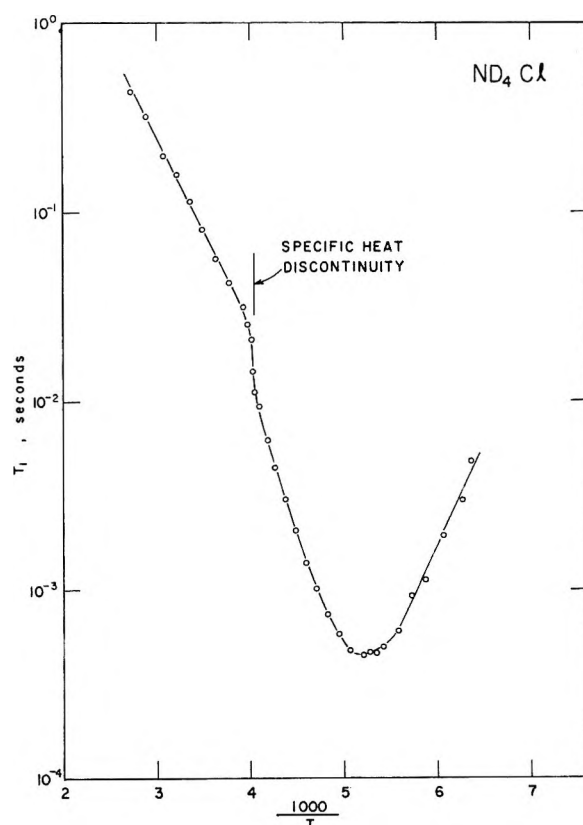


Figure 2. The temperature dependence of the deuteron T_1 for ND_4Cl at 9.5 MHz.

180.2 kHz and $\eta = 0.00 \pm 0.01$ lead to 0.435 msec for the T_1 minimum value.

The correlation time values are deduced by use of the equations and the data as follows. The T_1 ratios give the simple relation

$$(T_1)_{\min}/T_1 = 0.702 \left[\frac{\omega_0\tau_c}{1 + \omega_0^2\tau_c^2} + 4 \frac{\omega_0\tau_c}{1 + 4\omega_0^2\tau_c^2} \right] \quad (3)$$

The experimental $(T_1)_{\min}$ and T_1 values are then used to evaluate τ_c as a function of temperature. The resultant values are presented in Figure 3. Straight lines are drawn through the τ_c values calculated from the 9.5-MHz proton data. A large change in slope of the curve is noted at the apparent λ point, *i.e.*, the temperature at which the λ transition occurs.

Using the 9.5-MHz measurements, it is possible to determine the ratio of the τ_c values of the deuterons to

(8) A. Abragam, "The Principles of Nuclear Magnetism," Oxford University Press, London, 1961, Chapter 8.

(9) H. S. Gutowsky, G. E. Pake, and R. Bersohn, *J. Chem. Phys.*, **22**, 643 (1954).

(10) M. Linzer and R. A. Forman, *Bull. Am. Phys. Soc.*, **11**, 33 (1966).

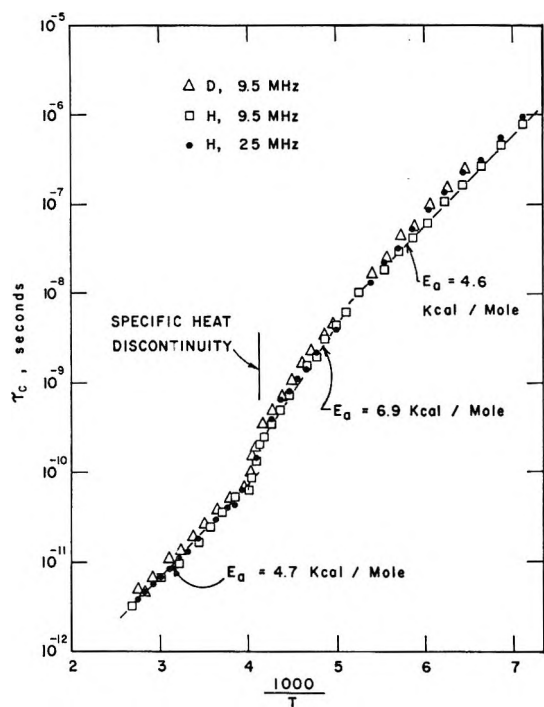


Figure 3. The temperature dependence of the correlation time for ammonium ion reorientation calculated from the proton and deuteron T_1 values.

those of the protons. Above the λ point and in the transition region, this ratio is approximately 1.22 and below the transition temperature this ratio is 1.36. Below the transition region there is a small discrepancy between the proton τ_c values calculated at 9.5 and 25.0 MHz, which causes an uncertainty to the absolute value of this ratio. However, even in this region, the τ_c values for the deuterons are consistently higher than those for the protons. This is expected since the moment of inertia of the ND_4^+ ion is higher than that of the NH_4^+ ion.^{11,12}

For purely descriptive purposes, the temperature dependence of τ_c may be expressed in terms of the following Arrhenius equation

$$\tau_c = \tau_c^\circ \exp(E_a/RT) \quad (4)$$

Application of this equation gives an E_a which increases from 4.7 above the λ point to 6.9 kcal/mole in the transition region¹³ below the λ point. However, below 195°K, the E_a value is 4.7 kcal/mole. The τ_c° values are 6×10^{-16} and 1.7×10^{-16} sec above and below the λ transition, respectively.

These results for ammonium chloride are consistent with those obtained from similar measurements on several other ammonium salts.¹⁴ An increase of E_a with a decrease in temperature through the λ transition

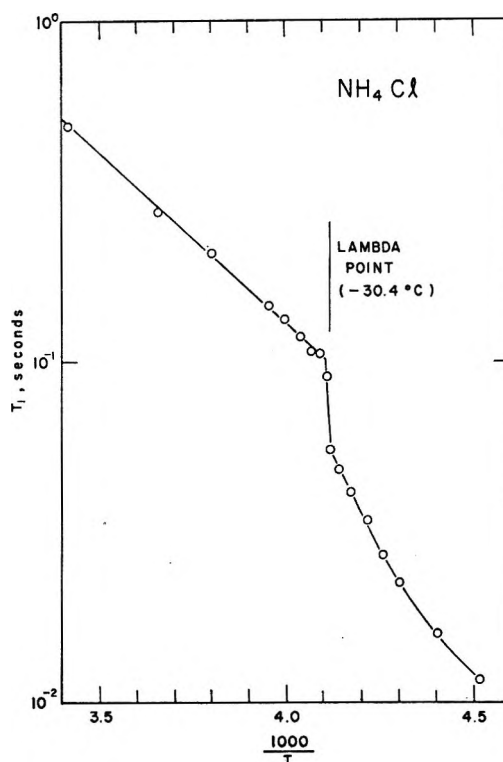


Figure 4. The proton T_1 values near the λ point measured at 25 MHz with the use of a probe designed to minimize temperature variations over the sample.

has been observed for $(\text{NH}_4)_2\text{SO}_4$, $(\text{NH}_4)_2\text{BeF}_4$, and NH_4HSO_4 . The ammonium chloride τ_c° values are close to those found for $(\text{NH}_4)_2\text{SO}_4$.

Discussion

Theoretically, the transition at the λ point should result in a discontinuity of the temperature dependence of τ_c . However, owing to a small temperature gradient in the sample, the discontinuity may be less apparent. The data in Figures 1 and 2 show this effect. Figure 4 shows T_1 values measured in the temperature range near the λ point at 25 MHz. These values were obtained with a special probe arrangement¹⁵ which was designed to minimize any possible temperature gradient. The transition is markedly sharper than shown in Figure 1. A sufficiently large temperature gradient could obscure detection of the transition by spin-lattice relaxation measurements.

(11) E. L. Wagner and D. F. Hornig, *J. Chem. Phys.*, **18**, 296 (1950).

(12) J. S. Waugh and E. I. Fedin, *Soviet Phys. Solid State*, **4**, 1633 (1963).

(13) The temperature range from approximately 195°K to the λ point will be designated as the transition region.

(14) S. R. Miller, R. Blinc, M. Brennan, and J. S. Waugh, *Phys. Rev.*, **126**, 528 (1962).

(15) D. E. Woessner and B. S. Snowden, Jr., in press.

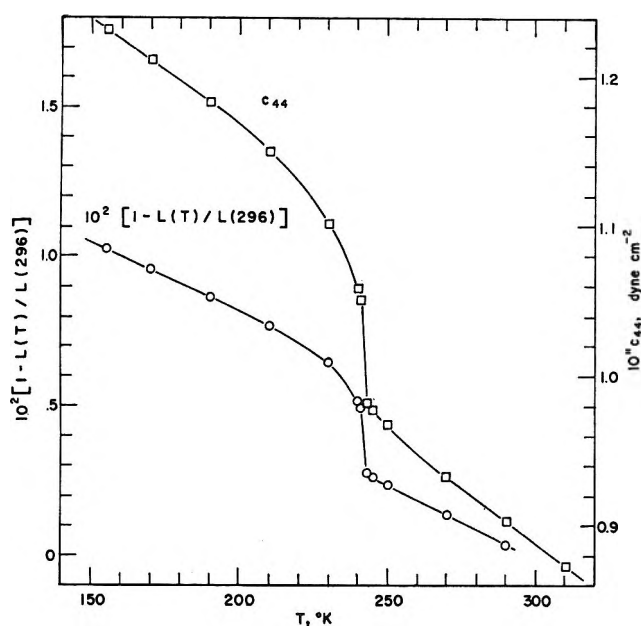


Figure 5. The temperature dependence of the relative linear dimension $[1 - L(T)/L(296)]$ and of the shear elastic constant, c_{44} , for a single crystal of ammonium chloride. The data are taken from Table I of ref 18.

The λ transition manifests itself through other crystal properties. This is illustrated in Figure 5. The crystal volume exhibits temperature trends which are in the same direction as those for τ_c (see Figure 3). It is possible that these quantities are related through the electrostatic interactions in the crystal lattice. However, a specific relationship which connects the temperature, volume, and correlation time by the electrostatic interactions is not known. Also, there may be other lattice parameters which are more closely related to τ_c .

Making the assumption that the temperature dependence follows an Arrhenius equation, it is possible to calculate the effect of the change in volume on electrostatic forces of the crystal lattice. Assuming that the lattice expands uniformly, the results of an electrostatic calculation⁹ indicate that the potential energy barrier to rotation of the ammonium ion is inversely proportional to the fifth power of the linear dimension of the unit cell. By use of thermal expansion data,¹⁶ one finds that the potential barrier should be only 3.0% greater at 224°K than it is at 273.2°K. There is an increase in E_a of 47% below the λ point as compared to the value above the λ point. This indicates that the simple electrostatic picture cannot explain the magnitude of the changes of the temperature dependence of τ_c .

The ammonium ions undergo torsional oscillations¹¹

at frequencies of 390 and 280 cm^{-1} for NH_4Cl and ND_4Cl , respectively. Occasionally, a torsional oscillation causes a complete reorientation of the ammonium ion to another equivalent position.⁹ Usually¹² it is assumed that there is a certain probability that a given oscillation results in such a reorientation. This probability is given by the equation

$$\tau_c = \frac{1}{\omega_t} e^{V_0/RT} \quad (5)$$

where ω_t is the torsional oscillation frequency in units of radians per second and V_0 is the classical barrier to the reorientation. For this equation, the ratio of the deuteron to proton correlation times is approximately the square root of 2, because the moment of inertia of the ND_4^+ ion is twice that of the NH_4^+ ion. This relationship is obeyed by the torsional frequencies obtained from infrared spectroscopy.¹¹ It is obeyed approximately by our observed ratio of deuteron to proton correlation times obtained from the 9.5-MHz data. However, the values of correlation times deduced from relaxation times are dependent on the details of the reorientation process. These details are not the same for NH_4Cl and ND_4Cl . The proton relaxation depends on reorientation of the proton-proton internuclear vector, whereas the deuteron relaxation depends on the nitrogen-deuteron internuclear vector. For this reason we did not attempt a more detailed analysis of the ratio of the correlation times.

Below the transition region the temperature dependence of τ_c for NH_4Cl obeys the simple relation: $\tau_c = 4.4 \times 10^{-14} e^{4.7 \times 10^3/RT}$. Since the reciprocal of the torsional frequency observed¹¹ for the molecule is 1.36×10^{-14} (radian/sec)⁻¹ the τ_c values obey eq 5 below the transition region. In the transition region τ_c decreases with increasing temperature faster than this equation predicts. This phenomenon can be attributed to a decrease in the preexponential factor in eq 4 and a simultaneous increase in E_a . However, previous electrostatic arguments suggest that the change in the classical potential energy barrier (*i.e.*, V_0) is too small to account for the change in τ_c . Therefore, the change in τ_c temperature dependence in the transition region must be greatly influenced by a temperature-dependent preexponential factor in eq 4.

A similar deviation from electrostatic theory in the transition region is reported for the shear elastic modulus, c_{44} .^{17,18} The relaxation times for long-range order-

(16) A. W. Lawson, *Phys. Rev.*, **57**, 417 (1940).

(17) C. W. Garland and C. F. Yarnell, *J. Chem. Phys.*, **44**, 3678 (1966).

(18) C. W. Garland and R. Renard, *ibid.*, **44**, 1130 (1966).

ing near the λ point have been deduced from ultrasonic attenuation measurements¹⁷ and found to be the same order of magnitude as the nuclear correlation times. This indicates a relationship between the ease of ammonium ion reorientation and the elastic properties of the crystals.

The temperature dependence¹⁸ of the shear elastic modulus, c_{44} (see Figure 5), shows a close correspondence between c_{44} and the temperature dependence of τ_c . This may reflect the variation of the volume with temperature because the value of c_{44} varies almost linearly with volume. Elastic constant data far from the transition region can be interpreted in terms of a crystal which is completely ordered or disordered. The temperature dependences of c_{44} in the completely ordered and completely disordered temperature regions are essentially the same. It has been suggested¹⁹ that these comparable temperature dependences should exist only if the coupling between the ammonium tetrahedron and the lattice is weak. The lattice energy of the ammonium ions depends only slightly on the anisotropic coupling between neighboring ammonium ions. This coupling is short range and mainly determined by octopole–octopole interactions.²⁰ As the temperature decreases through the λ point, the c_{44} data exhibit an increased variation with temperature. This behavior is in qualitative agreement with the theory which predicts the effects of ordering for a compressible Ising model lattice.

The change of c_{44} in passing through the λ point is about 7%. This is much greater than the change in electrostatic potential barrier and appears to be consistent with twofold change of τ_c . If eq 4 applies at the λ point and τ_c° is constant, the change in E_a required to this change in τ_c is 0.335 kcal/mole. This is 7.1% of the $E_a = 4.7$ kcal/mole which describes τ_c

above the λ point. This latter value of E_a agrees with the electrostatic energy barrier.⁹

Conclusions

The above results together with several other factors suggest that in the transition region the temperature dependence of τ_c is strongly influenced by the degree of order. First, the E_a values above and below the transition region are consistent with the electrostatic energy barrier. This suggests weak coupling between the ammonium ions in these temperature regions. The sizable difference between these E_a values and the E_a value in the transition region indicates an effect of the changing degree of order. Second, there is the twofold change of τ_c at the λ point.

We have also shown that the relative changes of the temperature dependence of τ_c do not follow a simple electrostatic approach. The connection between τ_c and the degree of order is apparently indirect in the transition region. It is possible that the elastic constants are related to the τ_c values.

Possibly similar studies on ammonium bromide will provide insight into this relationship. At the λ point the ammonium bromide changes lattice type²¹ and the volume change is opposite²² to that in ammonium chloride. This study is now in progress.

Acknowledgments. The authors wish to thank J. E. Fagan and P. H. Haagen for performing the spin-relaxation measurements and A. C. Hall, W. L. Medlin, and J. R. Zimmerman for their many helpful comments in the preparation of this paper. We also wish to thank the Mobil Oil Corp. for permission to publish this work.

(19) C. W. Garland and R. Renard, *J. Chem. Phys.*, **44**, 1120 (1966).

(20) C. W. Garland and J. S. Jones, *ibid.*, **41**, 1165 (1964).

(21) J. A. A. Ketelaar, *Nature*, **134**, 250 (1934).

(22) F. Simon and R. Bergmann, *Z. Physik. Chem.*, **B8**, 255 (1930).

Investigation of Micelle Structure by Fluorine Magnetic Resonance. I.

Sodium 10,10,10-Trifluorocaprato and Related Compounds¹

by Norbert Muller and Ronald H. Birkhahn

Department of Chemistry, Purdue University, Lafayette, Indiana 47907 (Received September 26, 1966)

Soaps of the type $\text{CF}_3(\text{CH}_2)_n\text{COONa}$ have been prepared with $n = 8, 10,$ and 11 . In aqueous solution each soap produces a single, concentration-dependent fluorine magnetic resonance signal. The data readily yield values of the critical micelle concentrations and of the chemical shifts of both the monomeric soap ions and the micellar material. As judged by the cmc values these soaps are essentially similar in their behavior to the ordinary alkyl carboxylates. Comparison of the micelle shifts with shifts observed for the soaps and for $\text{CF}_3(\text{CH}_2)_8\text{CF}_3$ in various solvents shows that the medium surrounding the CF_3 group when it is in the micelle has characteristics about midway between those of water and of hydrocarbon. This suggests that there is considerable penetration of water into the interior of the micelles, a conclusion also supported by determinations of the fluorine chemical shift of solubilized benzotrifluoride. The micelle shift is virtually unaffected by changes in the size of the micelles brought about either by changing the chain length of the soap or by adding simple electrolytes.

Introduction

Formation of micelles in soap or detergent solutions is attributed to hydrophobic interactions and the study of such solutions offers an approach to the determination of energy and entropy changes involved in the formation of a hydrophobic "bond."² Unambiguous interpretation of such data requires considerably more detailed knowledge of the constitution of micellar material than is presently available.³ For example, the analysis of Poland and Scheraga² involves a parameter $\theta(s)_{\text{H}_2\text{O}}$, which represents the fraction of the surface of the hydrocarbon tail of a soap molecule which is actually removed from contact with the aqueous medium as a result of micelle formation. No method is given for evaluating this parameter empirically or studying its dependence on the length of the hydrocarbon chain, the aggregation number of the micelles, or other relevant variables. This research was designed to explore the utility of the nuclear magnetic resonance (nmr) technique as a means of answering these and related questions.

In seeking to investigate hydrophobic interactions by nmr a cardinal requirement is that the material to be studied must contain one or more nuclear species

with a chemical shift that changes appreciably when the molecule is transferred from an aqueous to a non-aqueous environment. Small solvent dependences of this sort occur in hydrogen nmr spectra, particularly for molecules with aromatic groups, and a few nmr studies of micelle formation have been published recently which take advantage of this effect.⁴⁻⁷ However, it has been known for several years that the chemical shifts of fluorine nmr signals are much more drastically affected by changes in molecular environment than proton chemical shifts.⁸ This prompted us to under-

(1) Preliminary results of this work were presented at the 151st National Meeting of the American Chemical Society, Pittsburgh, Pa., March 1966.

(2) D. C. Poland and H. A. Scheraga, *J. Phys. Chem.*, **69**, 2431 (1965).

(3) D. B. Wetlaufer, S. K. Malik, L. Stoller, and R. L. Coffin, *J. Am. Chem. Soc.*, **86**, 508 (1964).

(4) J. C. Eriksson, *Acta Chem. Scand.*, **17**, 1478 (1963).

(5) T. Nakagawa and K. Tori, *Kolloid-Z.*, **194**, 143 (1964).

(6) H. Inoue and T. Nakagawa, *J. Phys. Chem.*, **70**, 1108 (1966).

(7) J. Clifford and B. A. Pethica, *Trans. Faraday Soc.*, **60**, 1493 (1964), have reported small concentration-dependent changes in the position of the water nmr signal in some detergent solutions.

(8) D. F. Evans, *Proc. Chem. Soc.*, 115 (1958).

Table I: Analytical Data and Physical Properties for $\text{CF}_3(\text{CH}_2)_n\text{COOH}$ and $\text{CF}_3(\text{CH}_2)_n\text{CF}_3$

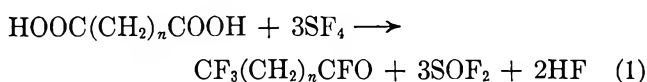
Compound	Mp, °C	Bp, °C	Mol wt		% C		% F		% H	
			Mass spectr	Calcd	Found	Calcd	Found	Calcd	Found	Calcd
$\text{CF}_3(\text{CH}_2)_8\text{COOH}$	39	...	226	226	53.3	53.1	25.4	25.2	7.62	7.5
$\text{CF}_3(\text{CH}_2)_{10}\text{COOH}$	49	...	254	254	56.4	56.7	22.5	22.5	8.24	8.3
$\text{CF}_3(\text{CH}_2)_{11}\text{COOH}$	42	...	268	268	57.5	58.2	20.3	21.3	8.65	8.6
$\text{CF}_3(\text{CH}_2)_7\text{CF}_3$...	28 ^a
$\text{CF}_3(\text{CH}_2)_9\text{CF}_3$...	34 ^a
$\text{CF}_3(\text{CH}_2)_{10}\text{CF}_3$...	58 ^a

^a At 2 mm.

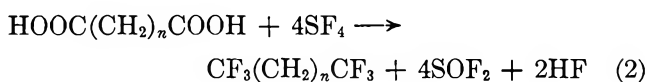
take a program of research consisting of fluorine nmr measurements on a variety of especially prepared synthetic soaps and detergents labeled with fluorine atoms at one or more known positions. The first such compounds which we have obtained are carboxylates of the type $\text{CF}_3(\text{CH}_2)_n\text{COONa}$. We show in this paper that the fluorine nmr signals from these materials in aqueous solution depend markedly on concentration and hydrocarbon chain length and that such data can furnish valuable information about micelle stability and constitution.

Experimental Procedures and Results

Materials. *n*-Alkane dicarboxylic acids were allowed to react with sulfur tetrafluoride in stainless-steel vessels at elevated temperatures and pressures.^{9,10} The major products isolated after distillation of the reaction mixtures were the trifluoroalkanoic acid fluorides and the hexafluoroalkanes formed by the reactions



and



respectively. The acid fluoride fractions were hydrolyzed with aqueous base. Acidification of the resulting solutions precipitated the trifluorocarboxylic acids which were filtered out, dried, and purified by sublimation. Analytical data and physical constants for the products with $n = 8, 10,$ and 11 are given in Table I.

Sodium salts of $\text{CF}_3(\text{CH}_2)_n\text{COOH}$ with $n = 8$ and 10 were made by neutralizing solutions of the acids in ethanol with ethanolic NaOH. The precipitated salts were recrystallized from additional ethanol and used to prepare the ethanolic solutions used in the chemical-shift measurements. However, the aqueous

soap solutions were not made from the solid salts. Instead, weighed amounts of the acids were dissolved in appropriate quantities of standard aqueous NaOH (or in some cases KOH) solutions and the resulting 0.5 *M* stock solutions were then diluted with either pure water or electrolyte solutions to produce samples with varying soap concentration, pH, and ionic strength. All water used in preparing solutions was distilled water from the laboratory supply which had been boiled to remove dissolved carbon dioxide. A few solutions were made with commercially obtained D_2O , which was not further purified before use.

Nmr determinations were made with a Varian V-4311 spectrometer equipped with a VK-3529 high-sensitivity kit and operated at 56.445 MHz. The temperature could not be accurately controlled when the high-sensitivity probe insert was used and it varied between about 30 and 36°. The chemical shifts are somewhat temperature dependent and this appeared to be the major factor causing a slight lack of reproducibility (± 0.05 ppm at worst) in data obtained on different days. A detailed investigation of the effect of changing temperature upon these systems will form the subject of a subsequent publication.

Each solution yielded a single fluorine resonance from the CF_3 groups, split into a triplet by spin-spin coupling with the protons of the adjacent methylene group, with $J_{\text{HF}} = 11$ Hz. Chemical shifts were measured, using audio side bands, with respect to the signal of benzotrifluoride enclosed in capillaries inserted into the thin-walled precision nmr tubes. Each value represents an average of ten scans over the spectrum, with mean deviations better than ± 0.01 ppm. Bulk susceptibility corrections were not applied because approximate calculations showed that they would not materially affect the results.

(9) W. R. Hasek, W. C. Smith, and V. A. Engelhardt, *J. Am. Chem. Soc.*, **82**, 543 (1960).

(10) R. H. Birkhahn, Ph.D. Thesis, Purdue University, in preparation.

Table II: Fluorine Chemical Shifts (ppm from External Benzotrifluoride) for Aqueous Soap Solutions as a Function of Concentration

Concn., <i>M</i>	CF ₃ (CH ₂) ₈ Na in H ₂ O	CF ₃ (CH ₂) ₈ COOK in H ₂ O	CF ₃ (CH ₂) ₁₀ COONa in H ₂ O	CF ₃ (CH ₂) ₁₁ COONa in H ₂ O	CF ₃ (CH ₂) ₈ COONa in D ₂ O
0.50	2.23	2.25	2.50	...	2.30
0.45	2.22	2.21	2.48	...	2.23
0.40	2.15	2.16	2.49	...	2.18
0.35	2.11	2.06	2.46	...	2.12
0.30	1.94	1.94	2.43	...	2.05
0.275	1.87	2.01
0.25	1.80	1.81	2.38	2.55	1.97
0.225	1.75	1.76	2.34	2.54	1.91
0.20	1.63	1.65	2.31	2.53	1.79
0.175	1.51	1.53	2.28	2.51	1.72
0.15	1.43	1.42	2.20	2.48	1.65
0.125	1.39	1.38	2.11	2.44	1.60
0.10	1.40	1.35	1.99	2.38	1.59
0.075	1.39	1.37	1.81	2.27	1.59
0.050	1.39	1.37	1.47	2.07	1.59
0.025	1.41	1.36	1.36	1.48	1.60
0.010	1.35	1.40	...

The nmr data are presented in Tables II-VI. Table II contains chemical shifts as a function of concentration for CF₃(CH₂)₈COONa, CF₃(CH₂)₈COOK, CF₃(CH₂)₁₀COONa, and CF₃(CH₂)₁₁COONa, all in H₂O, and for CF₃(CH₂)₈COONa in D₂O. Table III contains chemical shifts for hexafluorodecane and for the tri-

Table III: Fluorine Chemical Shifts (ppm from External Benzotrifluoride) for Fluorinated Acids, Soaps, and Hexafluoroalkanes as 0.2 *M* Solutions in Ethanol

Compound	Shift
CF ₃ (CH ₂) ₈ CF ₃	3.75
CF ₃ (CH ₂) ₈ COOH	3.69
CF ₃ (CH ₂) ₈ COONa	3.66
CF ₃ (CH ₂) ₁₀ COOH	3.68
CF ₃ (CH ₂) ₁₀ COONa	3.67

Table IV: Fluorine Chemical Shift (ppm from External Benzotrifluoride) for 0.2 *M* CF₃(CH₂)₈CF₃ in Organic Solvents

Solvent	Shift
Perfluorooctane	6.13
<i>n</i> -Hexane	3.93
Neat CF ₃ (CH ₂) ₈ CF ₃	3.84
Cyclohexane	3.76
Absolute ethanol	3.75
Acetone	3.52
Benzene	2.75
Carbon tetrachloride	2.53
Pyridine	2.40

Table V: Fluorine Chemical Shift (ppm from External Benzotrifluoride) for Benzotrifluoride Solubilized in 0.5 *M* Soap Solutions

Soap	Benzotrifluoride concn., <i>M</i>	δ ^a
CH ₃ (CH ₂) ₈ COOK	0.05	-1.29
CH ₃ (CH ₂) ₈ COONa	0.063	-1.19
CH ₃ (CH ₂) ₁₀ COONa	0.070	-1.00
CH ₃ (CH ₂) ₁₀ COONa	0.035	-1.10
CH ₃ (CH ₂) ₁₀ COONa	0.014	-1.16
CF ₃ (CH ₂) ₈ COONa	Satd	-0.99
CF ₃ (CH ₂) ₁₀ COONa	Satd	-0.67
CF ₃ (CH ₂) ₁₁ COONa	Satd	-0.78

^a The negative sign denotes a shift to lower applied field.

fluoroalkanoic acids and soaps with *n* = 8 and 10, as 0.2 *M* solutions in absolute ethanol. Table IV gives the shifts for the hexafluorodecane in a variety of organic solvents including a sample of perfluorooctane obtained from the 3M Co. Table V contains the results of chemical-shift determinations for benzotrifluoride solubilized in 0.5 *M* solutions of the fluorinated soaps or ordinary hydrocarbon soaps of comparable chain length. The data in Table VI show the effect of added NaCl or NaOH on the fluorine shifts of CF₃(CH₂)₈COONa solutions.

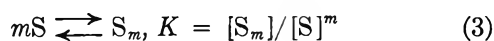
Discussion

Variation of Chemical Shift with Soap Concentration.
A highly idealized, commonly used model for the

Table VI: Effect of Added Electrolyte on the Fluorine Shift of Aqueous $\text{CF}_3(\text{CH}_2)_8\text{COONa}$

Soap concn, M	Electrolyte	Chemical shift, ppm	Shift without added electrolyte, ppm
0.4	0.4 M NaOH	2.31	2.15
0.175	0.325 M NaOH	1.89	1.51
0.150	0.350 M NaOH	1.79	1.43
0.125	0.375 M NaOH	1.72	1.39
0.100	0.400 M NaOH	1.57	1.40
0.075	0.425 M NaOH	1.39	1.39
0.050	0.450 M NaOH	1.28	1.39
0.25	0.25 M NaOH	2.04	1.80
0.25	0.25 M NaCl	2.13	1.80
0.25	0.5 M NaOH	2.17	1.80
0.25	0.5 M NaCl	2.21	1.80
0.25	1.0 M NaOH	2.38	1.80
0.25	1.0 M NaCl	2.37	1.80

process of micelle formation¹¹ is based on the equilibrium



where S represents the detergent ion and m the aggregation number, which is assumed to be large compared with unity and to have the same value for all micelles in a given solution. Conclusions based on this model cannot be strictly correct since it is known¹¹ that a large number of counterions are associated with the micelles, but it serves as a useful first approximation. The critical micelle concentration (cmc) is defined as the value of $[S]$ in a solution in which just half of the total detergent is present in the monomeric form, *i.e.*, in which $[S] = m[S_m]$. Then $K = (\text{cmc}/m)/(\text{cmc})^m$, or

$$\text{cmc} = (mK)^{-1/(m-1)} \quad (4)$$

It is readily verified that whenever the over-all detergent concentration, S_0 , is less than cmc the concentration of micelles will be negligible, while for $S_0 > \text{cmc}$ $[S]$ remains essentially equal to cmc so that the micelle concentration becomes $[S_m] = (S_0 - \text{cmc})/m$.

Since only one fluorine signal is found in the nmr spectra of the soap solutions, it is natural to attempt to correlate the data using this model with the additional assumption that the reactions of (3) occur rapidly enough to cause complete coalescence of the signals from the monomeric and the micellar species. Denoting their chemical shifts, respectively, by $\delta(S)$ and $\delta(S_m)$, one then expects that the exchange-averaged shift, δ , will be equal to $\delta(S)$ when $S_0 < \text{cmc}$ and when $S_0 > \text{cmc}$.

$$\delta = \delta(S_m) + (\text{cmc}/S_0)[\delta(S) - \delta(S_m)] \quad (5)$$

A plot of δ against $1/S_0$ should then consist of two straight-line segments intersecting at $1/S_0 = 1/\text{cmc}$. Extrapolation to the intercept at $1/S_0 = 0$ should yield the value of $\delta(S_m)$, while $\delta(S)$ is obtained directly from the measurements for $S_0 < \text{cmc}$.

The results of plotting some of the chemical shifts from Table II in this way are shown in Figure 1 and they conform quite closely to the above scheme. The deviations in the region near $1/S_0 = 1/\text{cmc}$ are the expected consequence of the fact that eq 5 becomes accurate in this region only in the limit as m tends to infinity and the actual value of m is perhaps of the order of 50. The derived cmc values, given in Table VII, decrease with increasing chain length in somewhat the same way as reported values for ordinary sodium alkanoates and for any given n the cmc of $\text{CF}_3(\text{CH}_2)_n\text{COONa}$ is roughly twice that of $\text{CH}_3(\text{CH}_2)_n\text{COONa}$. This is in contrast to the very low cmc values reported¹² for sodium perfluoroalkanoates of comparable chain length. The monomer shift is 1.38 ± 0.03 ppm and the micelle shift, 2.66 ± 0.03 ppm. Both are essentially independent of the number of carbon atoms in the lipophylic chain.

Table VII: Critical Micelle Concentrations Evaluated from the Data in Table II

Material	Cmc, M
$\text{CF}_3(\text{CH}_2)_8\text{COONa}$ in H_2O	0.167
$\text{CF}_3(\text{CH}_2)_8\text{COOK}$ in H_2O	0.164
$\text{CF}_3(\text{CH}_2)_8\text{COONa}$ in D_2O	0.160
$\text{CF}_2(\text{CH}_2)_{10}\text{COONa}$ in H_2O	0.051
$\text{CF}_3(\text{CH}_2)_{11}\text{COONa}$ in H_2O	0.024

Significance of the Micelle Shift. The implication of the value found for $\delta(S_m)$ emerges when one contrasts it with an estimated shift for the soap molecule in a hydrocarbon environment. Direct determination of such a value is ruled out by solubility considerations. However, the hexafluoroalkanes are readily soluble in a variety of organic solvents and it is to be expected that in any given medium $\text{CF}_3(\text{CH}_2)_n\text{COONa}$ and $\text{CF}_3(\text{CH}_2)_n\text{CF}_3$ will have very nearly the same fluorine chemical shift. One solvent in which this assumption could be checked was absolute ethanol and indeed the shifts fall within a range of 0.1 ppm (see Table III).

(11) P. Becher, "Emulsions: Theory and Practice," 2nd ed, Reinhold Publishing Corp., New York, N. Y., 1965, p 39.

(12) H. B. Klevens and M. Raison, *J. Chim. Phys.*, 51, 1 (1954).

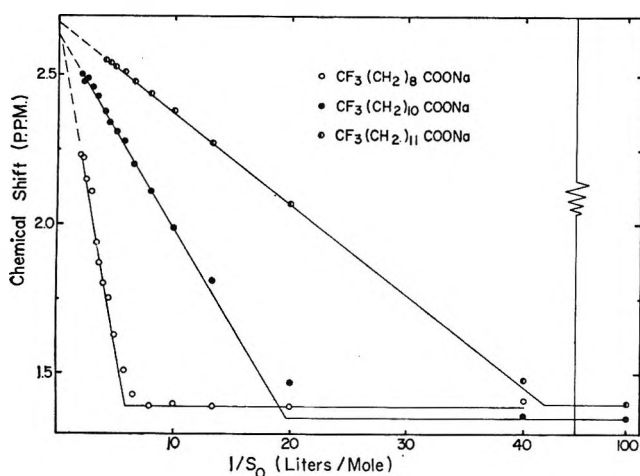


Figure 1. Fluorine chemical shifts for $\text{CF}_3(\text{CH}_2)_n\text{COONa}$ from Table II plotted against the reciprocal concentration.

Table IV shows that hexafluorodecane as a pure liquid, or dissolved in hexane or cyclohexane, yields shifts within 0.2 ppm of the value obtained in ethanol. (The completely fluorinated solvent shifts the peak markedly upfield, while carbon tetrachloride and several unsaturated solvents displace it to lower fields.) It seems safe to conclude that the soap molecules in a medium consisting of either hydrocarbon chains or hexafluoroalkane chains would produce fluorine signals at 3.8 ± 0.15 ppm. The same value is to be anticipated for a terminal CF_3 group on the interior of an idealized micelle, assuming that water is rigorously excluded from this region.

The actual micelle shift is approximately midway between the monomer shift in water and the value just derived, suggesting that in fact the CF_3 group "inside" the micelle remains exposed to water to quite a significant extent. Numerically, it is convenient to describe the environment of CF_3 by the empirical parameter

$$Z = [\delta(S_m) - \delta(S)] / [3.8 - \delta(S)] \quad (6)$$

which measures the "degree of hydrocarbon-like character" and thus is somewhat analogous to the parameter $\theta(s)_{\text{H}\Phi}$ mentioned in the introduction. It is remarkable that all three of the soaps used in this study yield $Z = 0.53 \pm 0.03$.

At least two factors must be considered in attempting to rationalize the value of Z . First, in packing the flexible $\text{CF}_3(\text{CH}_2)_n\text{COO}^-$ ions into the micelle, it is inevitable that a certain number of CF_3 groups will find themselves in contact with water because they are at or near the micellar surface. If this were the dominant factor, one would expect Z to increase with increasing chain length because of the concomitant in-

crease in micellar volume and the associated lowering of the surface:volume ratio. The second possibility is that CF_3 groups remain partially exposed to water even when they are well removed from the micellar surface because of penetration of water into the interior of the micelles. The idea that micelles are indeed hydrated is not new,¹³ although it is usually assumed that the water of hydration forms a fairly well-defined layer on the surface of the micelle.

Solubilized Benzotrifluoride. To obtain further information about the micellar interior, the investigation was broadened to include benzotrifluoride solubilized in several soap solutions. Benzotrifluoride is so sparingly soluble in water that it must be presumed that virtually all of this material which dissolved in a soap solution is intimately associated with the micelles. Moreover, the solubilized oil should tend to avoid the surface region of the micelle in order to minimize contact with the aqueous medium.

Some results are given in Table V. The shifts are somewhat dependent on the concentrations of benzotrifluoride and soap and the data so far available do not suffice for an extrapolation to infinite dilution of benzotrifluoride. The interpretation again requires a knowledge of the shift of the material in hydrocarbon solvents and in water. Shifts for benzotrifluoride in several organic solvents have been reported.⁸ Like hexafluorodecane, the shift for benzotrifluoride is nearly the same in dilute solutions in ethanol or hexane as it is for the neat liquid and it seems permissible to adopt $\delta = 0$ as a value in a "typical" nonaqueous environment. The shift in water was obtained by the following indirect method. Solutions containing 0.4% by weight of benzotrifluoride in water-ethanol mixtures were examined and it was found that the fluorine shifts conform fairly closely to the empirical equation^{10,14}

$$\delta(\text{C}_6\text{H}_5\text{CF}_3) = -2.51 + 3.48v - 1.10v^2 \quad (7)$$

where v is the volume fraction of ethanol, which varied between 0.3 and 0.95. The desired shift in water, obtained by extrapolating to $v = 0$, is -2.5 ppm. It is difficult to judge the accuracy of this procedure, but it is encouraging that the measured shifts for $\text{CF}_3(\text{CH}_2)_8\text{COONa}$ monomers in alcohol and in water differ

(13) W. L. Courchene, *J. Phys. Chem.*, **68**, 1870 (1964), and references given there.

(14) We had expected that instead of eq 7 we would find a linear dependence of δ on v . The observed nonlinearity perhaps shows that the composition of solvent in the immediate neighborhood of a benzotrifluoride molecule, which determines δ , differs from the bulk composition. This suggests that fluorine nmr may be used to demonstrate that, when a water-insoluble organic species is dissolved in such a mixed solvent, water tends to be excluded from the nearest neighbor sphere.

by 2.3 ppm, while this method yields a difference of 2.4 ppm for benzotrifluoride in the two solvents.

The medium bathing a solubilized benzotrifluoride molecule can now be characterized by a Z parameter similar to that defined by eq 6, *i.e.*

$$Z(\text{C}_6\text{H}_5\text{CF}_3) = [\delta(\text{C}_6\text{H}_5\text{CF}_3) + 2.5]/2.5 \quad (8)$$

The data in Table V then yield Z values of about 0.5 when the soap is sodium or potassium caprate, 0.5–0.6 in sodium laurate, and 0.6–0.7 in the fluorinated soaps. It would be premature to attach much significance to the differences between these values, but it is striking that again the environment within the micelle appears to be substantially different from an ideal nonaqueous medium.

The resonance signal from the CF_3 groups of the fluorinated soap moves upfield slightly (up to 0.25 ppm) when the benzotrifluoride is added. The direction of this shift is consistent with the supposition that the solubilize displaces some water from the micelle interior, or that it lowers the cmc. The fact that this effect is small is not surprising, since a considerable excess of soap is present.

Effect of Added Electrolytes. Numerous authors have reported that addition of simple electrolytes lowers the cmc values of ionic detergents and increases the average size of the micelles.¹⁵ It therefore seemed desirable to find out whether this would produce a marked effect on the micelle shift. Results of some measurements with added NaOH or NaCl appear in Table VI.

From a plot of some of these data it appears that in the presence of 0.4 M added NaOH the cmc of $\text{CF}_3(\text{CH}_2)_8\text{COONa}$ is between 0.07 and 0.08 M and the monomer shift is about 1.24 ppm. When the concentrations of soap and of the excess NaOH are each 0.4 M , the observed shift is 2.31 ppm and with eq 5 these values yield $\delta(S_m)$ in the range 2.54–2.58 ppm. The accuracy of this result is open to question,¹⁶ but it is so nearly equal to the value obtained without added electrolyte as to suggest that the environment of the CF_3

groups within the micelles is very nearly independent of the aggregation number. The failure of $\delta(S_m)$ to change with variations in chain length (see above) supports the same conclusion.

Replacing NaOH by NaCl as the added electrolyte produced no significant change in the data, showing that hydrolysis of the soap produces no major effect on these results.

Miscellaneous Experiments. As expected, data (Table II) obtained with the potassium salt of $\text{CF}_3(\text{CH}_2)_8\text{COOH}$ essentially duplicate those found with the sodium salt.

Replacement of H_2O by D_2O as the solvent for $\text{CF}_3(\text{CH}_2)_8\text{COONa}$ gave data (Table II) which yielded $\delta(S) = 1.60$, $\delta(S_m) = 2.63$ ppm, and $\text{cmc} = 0.160 M$. The change in cmc is comparable with the experimental error, but is in the same direction as a similar small change recently reported for the cmc values of sodium decyl and lauryl sulfates.¹⁷ The change in $\delta(S)$ is unexpectedly large and, with eq 6, yields a Z value in these solutions of 0.47. The apparent reduction in Z , while small, illustrates again that a factor which tends to promote aggregation, as evidenced by the lowering of the cmc, will not, as might have been anticipated, cause an increase in Z .

Acknowledgment. The authors wish to thank the Purdue Research Foundation for providing financial support for this work through a David Ross grant.

(15) M. J. Schick, *J. Phys. Chem.*, **68**, 3585 (1964).

(16) It is usually stated¹⁶ that the cmc depends on the *total* counterion concentration rather than, as tacitly assumed here, the *excess* counterion concentration. This rule entails difficulties when it is applied to the solutions made without added electrolyte. Although the concentration of free counterions depends on the extent of counterion adsorption on the micelles, which is not known, it seems certain that the counterion concentration will continue to rise as S_0 increases beyond the cmc. As a result, the cmc itself should vary with S_0 , so that at high soap concentrations one should observe what might be called a self-salt effect, which would spoil the linear relation between δ and $1/S_0$ predicted by eq 5 and actually found experimentally (Figure 1). Further experiments have been planned in the hope of clearing up this anomaly.

(17) P. Mukerjee, P. Kapayan, and H. G. Meyer, *ibid.*, **70**, 783 (1966).

Infrared Spectra of the Complexes $\text{AgNO}_3 \cdot \text{CH}_3\text{CN}$ and $\text{AgNO}_3 \cdot 2\text{CH}_3\text{CN}$ and Their Solutions in Acetonitrile

by George J. Janz, Malcolm J. Tait, and Jurg Meier

Department of Chemistry, Rensselaer Polytechnic Institute, Troy, New York (Received September 30, 1966)

The complexes $\text{AgNO}_3 \cdot \text{CH}_3\text{CN}$ and $\text{AgNO}_3 \cdot 2\text{CH}_3\text{CN}$ have been isolated from silver nitrate solutions in acetonitrile. Their infrared spectra are reported and compared with that of solid silver nitrate and its solutions in acetonitrile of concentration up to 9.6 moles l^{-1} . The results in solution can be understood in terms of the formation constants of the complexed or solvated ions $\text{Ag}(\text{NCCH}_3)_2^+$ and $\text{Ag}(\text{NCCH}_3)^+$. Evidence is also presented that in solutions of concentration less than 3 moles l^{-1} there is an equilibrium between free and paired ions. The spectrum of the cation-anion pair suggests that the ions are in contact in CH_3CN solutions and not solvent separated as in aqueous AgNO_3 solutions.

Introduction

Little is known about the behavior of electrolytes in concentrated solutions. Attempts to extend the dilute solution model have met with only moderate success.^{1,2} A thorough investigation of a suitable system by a number of experimental methods seems essential. Such an investigation is in progress in these laboratories.

The solubility of silver nitrate in acetonitrile is about 9.6 moles l^{-1} at room temperature corresponding to a mole fraction of silver nitrate of 0.43. Diffusion data are available³ for this system up to 5 moles l^{-1} . Viscosity and conductance measurements⁴ detect ion pairs at 0.1 moles l^{-1} and increasing concentrations of triple ions from 1 to 6 moles l^{-1} . Infrared and Raman spectra⁵ can be said to confirm that ion pairs are present from 0.2 to 9 moles l^{-1} and in addition they established the existence of the solvated ion $\text{Ag}(\text{NCCH}_3)_2^+$ in these solutions. In the present work it has proved possible to isolate from solution the complex $\text{AgNO}_3 \cdot 2\text{CH}_3\text{CN}$ and also one other of composition $\text{AgNO}_3 \cdot \text{CH}_3\text{CN}$. The purpose of this work has been to use the infrared spectra of these solid complexes as fingerprints in order to gain a better understanding of the cation-solvent interactions in solution. It has also proved possible to make a more detailed investigation of the ion-pair equilibrium in solutions of concentration less than 3 moles l^{-1} . Comparison with the spectra of fused silver

nitrate and its aqueous solutions suggests that in acetonitrile the paired ions are in contact.

Experimental Section

The purification of AgNO_3 and CH_3CN has been described previously.⁵ Deuterated acetonitrile, CD_3CN (98%), was used as received from Merck Sharp and Dohme. Solutions of silver nitrate in acetonitrile were prepared and stored under N_2 .

Crystals of $\text{AgNO}_3 \cdot 2\text{CH}_3\text{CN}$ were prepared by cooling a solution of silver nitrate in acetonitrile of mole ratio 1:3 to -10° . It was found necessary first to seed the solution or to initiate the crystallization by cooling rapidly to -70° for a short time. The crystals were found to melt at a temperature somewhat less than that of the room, so that it was necessary during their isolation to operate at a temperature of about 0° . The bulk of the mother liquor was removed and the crystals were washed twice with double their volume of anhydrous cold ether. The crystals were cooled to

(1) C. A. Kraus, *J. Phys. Chem.*, **58**, 673 (1954).

(2) R. A. Robinson and R. H. Stokes, "Electrolyte Solutions," Butterworth and Co. Ltd., London, 1959.

(3) G. J. Janz, G. R. Lakshminarayanan, and M. P. Klotz, *J. Phys. Chem.*, **70**, 2562 (1966).

(4) G. J. Janz, A. E. Marcinkowsky, and I. Ahmad, *J. Electrochem. Soc.*, **112**, 104 (1965).

(5) C. B. Baddiel, M. J. Tait, and G. J. Janz, *J. Phys. Chem.*, **69**, 3634 (1965).

-70° to prevent evaporation of the acetonitrile component and the last traces of ether were removed in a stream of dry nitrogen. The crystals were dried to constant weight.

Crystals of $\text{AgNO}_3 \cdot \text{CH}_3\text{CN}$ and $\text{AgNO}_3 \cdot \text{CD}_3\text{CN}$ were isolated from their saturated solutions which were found to crystallize almost completely at 0° . They did not melt at room temperature. They were filtered off in a drybox, washed with ether, and dried to constant weight as described above.

The composition of the crystals was determined by analysis both for silver and for acetonitrile. Both methods agreed to within 1%. Silver analysis was effected by precipitation of silver chloride in water and the acetonitrile content was gained from the weight loss after pumping under vacuum for 8 hr at room temperature. Acetonitrile evaporates readily from the complexes. Crystals of both complexes, $\text{AgNO}_3 \cdot \text{CH}_3\text{CN}$ and $\text{AgNO}_3 \cdot 2\text{CH}_3\text{CN}$, are unstable at atmospheric pressure: a weight loss of about 0.01%/min is observed in an open system. They were therefore stored under N_2 in a closed bottle at -10° .

The melting points of the crystals were determined by differential thermal analysis. The melting point of the 1:2 complex was 8.5° and that of the 1:1 complex was 43° . However, whereas the melting point of $\text{AgNO}_3 \cdot 2\text{CH}_3\text{CN}$ crystals was reproducible several times with the same sample, this is not the case for $\text{AgNO}_3 \cdot \text{CH}_3\text{CN}$ crystals because of loss of acetonitrile on melting. Some interesting results were obtained from the data measurements on a silver nitrate solution in acetonitrile of composition 1:2. On cooling slowly, the solution crystallized at about -30° . These crystals had a well-defined melting point of 8.5° so that in fact the 1:2 complex could be prepared from its "molten state."

For the infrared studies a Perkin-Elmer 221 double-beam grating spectrometer was used. The instrument was calibrated from the spectra of liquid and solid CH_3CN ^{6,7} and CD_3CN .^{7,8} In previous work⁵ it had been found that AgCl windows are the most suitable to contain the solutions in the infrared cells. Cells were used which prevented any contact between the solutions and metal surfaces. For the more dilute solution studies, the cells employed⁹ could be sealed very effectively to prevent evaporation of solvent.

It was observed that solid AgNO_3 reacted even on simple mixing with KBr . KBr pellets were therefore not used for any of the solid spectra. Melts were prepared with Nujol and hexachlorobutadiene. Tests showed that neither of these materials dissolved the acetonitrile out of the complexes.

Because of its low melting point, the infrared spec-

tra of 1:2 complex had to be measured at temperatures less than 8.5° . The sample cell was mounted on a copper rod penetrating the base of a dewar-like vessel. The latter served as a cooling well which could be filled with liquid N_2 . This assembly was finally placed inside a glass vessel and this outer jacket could be evacuated or filled with argon in order to prevent condensation of atmospheric moisture on the cold windows of the cell. The complete assembly has been described elsewhere in detail.¹⁰ The temperature of the sample closely approached liquid N_2 temperature (77°K). The spectrum of the 1:2 solid measured as a Nujol mull was found to be identical with that of a 1:2 solution cooled slowly to liquid N_2 temperature. The latter technique, being the easier of the two, was therefore the one more often employed to determine spectral details of the 1:2 complex.

Results

The nitrate bands observed in the infrared spectra of silver nitrate and the solid complexes are recorded in Table I. For all three solids the spectral region from 1200 to 1500 cm^{-1} was the most difficult to investigate. For the complexes, crystals of $\text{AgNO}_3 \cdot \text{CD}_3\text{CN}$ and $\text{AgNO}_3 \cdot 2\text{CD}_3\text{CN}$ had to be used because CH_3CN absorbs strongly at 1376 and 1443 cm^{-1} . Absorption by the nitrate is so intense that a reliable spectrum could not be obtained from a film of pure 1:2 complex. In all cases, hexachlorobutadiene mulls were therefore used since hexachlorobutadiene itself contributes only a number of weak bands to this region of the spectrum.

Except for the AgNO_3 absorption and the 1200–1400- cm^{-1} absorption by the 1:1 complex, the nitrate bands reported for the 1200–1500- cm^{-1} region could be seen superimposed on the hexachlorobutadiene contour. For AgNO_3 it was necessary to subtract the contribution of the hexachlorobutadiene from the observed contour. The resulting nitrate band was very similar to that shown by Vratny¹¹ if the shoulder at ~ 1400 cm^{-1} , which may be due to an inadequate compensation for Nujol absorption in his spectrum, is neglected. The maximum absorption is at 1370 cm^{-1} and a shoulder is quite evident at 1250 cm^{-1} . These frequencies are recorded in Table I, but because one band is almost sub-

(6) P. Venkateswarlu, *J. Chem. Phys.*, **19**, 293 (1951).

(7) D. E. Milligan and M. E. Jacox, *J. Mol. Spectry.*, **8**, 126 (1962).

(8) J. C. Evans and H. J. Bernstein, *Can. J. Chem.*, **33**, 1746 (1955).

(9) "Throwaway Infrared Liquid Cells," Limit Research Corp., Darien, Conn.

(10) K. J. Eisentraut, Ph.D. Thesis, Rensselaer Polytechnic Institute, 1964.

(11) F. Vratny, *Appl. Spectry.*, **13**, 59 (1959).

Table I: Infrared Frequencies (cm^{-1}) of the Nitrate Ion for Crystals of AgNO_3 , $\text{Ag}(\text{CH}_3\text{CN})\text{NO}_3$, and $\text{Ag}(\text{CH}_3\text{CN})_2\text{NO}_3$

	$\nu_4(\text{A}_1)$	$\nu_2(\text{B}_2)$	$\nu_6(\text{B}_1)$	$\nu_3(\text{A}_1)$	$\nu_1(\text{A}_1)$	$\nu_5(\text{B}_2)$	$2\nu_6$
AgNO_3		724	801		1250? ^a	1370? ^a	
$\text{AgNO}_3 \cdot \text{CH}_3\text{CN}$	708	718	809	~ 1015 sh			
$\text{AgNO}_3 \cdot \text{CD}_3\text{CN}$	710	720	809	~ 1010 sh	1200 \longleftrightarrow 1400		1460 w
$\text{AgNO}_3 \cdot 2\text{CH}_3\text{CN}$		721	816	1023 sh			
$\text{AgNO}_3 \cdot 2\text{CD}_3\text{CN}$		721	815	1014	1214 w, 1224 w	1369	1444 w

^a The “?” indicates that the broad band in the 1200–1400 cm^{-1} region is not clearly resolved and that the above values are estimates.

merged in the other, they cannot represent the true ν_{max} . A similar calculation for the 1:1 complex revealed absorption in the 1200–1400- cm^{-1} region. This band may consist of unresolved components.

Comparison of the spectra of the complexes with that of pure acetonitrile shows that the major changes occur in the CN and CC stretching frequencies. These are recorded in Table II. Figure 1 illustrates the concentration dependence of the CN stretching frequencies in concentrated acetonitrile solutions.

Table II: CN and CC Stretching Frequencies (cm^{-1}) of the Complexes

	Temp	ν_{CN}	ν_{CC}
CD_3CN	20°C	2263	833
$\text{AgNO}_3 \cdot \text{CD}_3\text{CN}$	20°C	2274	
CH_3CN	20°C	2254	917
$\text{AgNO}_3 \cdot \text{CH}_3\text{CN}$	20°C	2264	924
$\text{AgNO}_2 \cdot \text{CH}_3\text{CN}$	77°K	2261	
CH_3CN	77°K	2252	917
$\text{AgNO}_3 \cdot 2\text{CH}_3\text{CN}$	77°K	2269	929
$\text{AgNO}_3 \cdot 2\text{CD}_3\text{CN}$	77°K	2278	
CD_3CN	77°K	2260	832

In the previous study⁵ it had been found that the asymmetric stretching vibration of the nitrate ion was no longer degenerate in solutions of silver nitrate in acetonitrile. In solutions of concentration from 3 to 9 moles l^{-1} , absorption maxima were found at 1300 and 1425 cm^{-1} . However it appeared that at ~ 0.2 mole l^{-1} the low-frequency band shifted to 1350 cm^{-1} . This concentration dependence has now been more thoroughly investigated and the results are shown in Figure 2.

Discussion

Solid Spectra—Vibrational Assignments. It can be seen from Table I that four frequencies are observed in the infrared spectrum of silver nitrate. If the point group of the nitrate ion is D_{3h} , only three

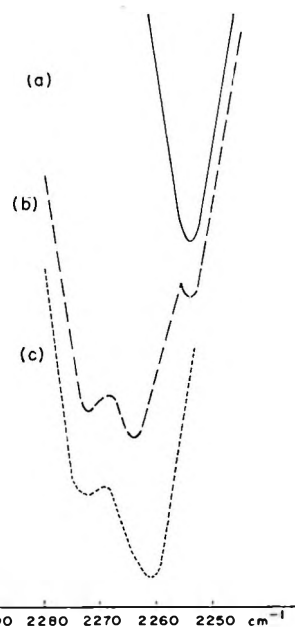


Figure 1. The concentration dependence of the CN stretching frequencies for $\text{AgNO}_3\text{-CH}_3\text{CN}$ solutions. The mole fractions of AgNO_3 are (a) 0.00, (b) 0.33, and (c) 0.43.

infrared frequencies (ν_2, A_2'' ; ν_3, E' ; ν_4, E') should be observed. It is apparent the symmetry of the nitrate ion is lower than D_{3h} in silver nitrate since one of the doubly degenerate modes (ν_3, E') has split into two bands, 1250 and 1370 cm^{-1} , respectively. Similarly in the spectra of the 1:1 and 1:2 complexes of silver nitrate with acetonitrile, there is evidence that the symmetry of the nitrate ion is lower than D_{3h} . The symmetrical stretching vibration at ~ 1016 cm^{-1} is infrared active in both complexes, a definite splitting of a degenerate mode is detected in the 700- cm^{-1} region for the 1:1 solid, and, as in the spectrum of silver nitrate, the absorption band of the 1:2 solid at ~ 1300 cm^{-1} is split. The symmetry of the nitrate-cation pair in all three of the solids in Table I may therefore be either C_{2v} or C_s . For each of these point groups all six fundamental vibrations should be infrared active. The classification of the fundamental vibrations of the

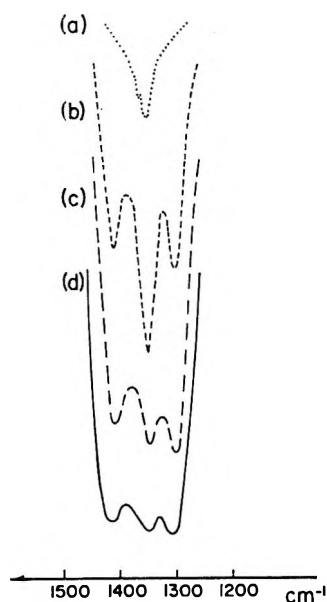


Figure 2. The concentration dependence of the NO_3 bands between 1250 and 1450 cm^{-1} for $\text{AgNO}_3\text{-CD}_3\text{CN}$ solutions. The concentrations of AgNO_3 are (a) 0.02, (b) 0.2, (c) 1.3, and (d) 2.7 moles l^{-1} .

C_{2v} point group is given in Table I according to the assignments developed by Topping¹² from a study of metal-unidentate nitrate complexes.

This anion-cation pair model is unquestionably an oversimplification. It has been shown¹³ to be preferable to interpret the spectra of solid alkali metal nitrates in terms of their crystal structure. This approach has been used successfully for fused silver nitrate¹⁴ to support the hypothesis that local order prevails in the melt. However in the absence of crystallographic data for the silver nitrate complexes with acetonitrile, no detailed treatment can be attempted.

It is interesting that for silver nitrate no bands were recorded at ~ 1450 or ~ 1015 cm^{-1} which could be identified with the $2\nu_3$ or ν_2 vibrations. However Katzin¹⁵ has reported an infrared band at 1471 cm^{-1} for this salt. The presence of the 1015- cm^{-1} absorption in only the spectra of the silver nitrate complexes with acetonitrile is analogous to the infrared results¹⁶ for $\text{Co}(\text{NO}_3)_2$ and $\text{Co}(\text{NO}_3)_2 \cdot 2\text{H}_2\text{O}$ where only the dihydrate absorbs at this frequency.

In the spectra of the complexes, the number of fundamental frequencies observed for the acetonitrile component was the same as in the spectrum of pure acetonitrile. CH_3CN must therefore retain the point group C_{3v} symmetry in the complexed state. X-Ray analysis¹⁷ of $\text{CH}_3\text{CN} \cdot \text{BF}_3$ has shown that the CNB angle is 180° . The donor-acceptor bond in this¹⁸ and other¹⁹ acetonitrile complexes is thought to be formed by the lone

pair of electrons in an sp orbital on the nitrogen atom. Consequently it would be expected that the complex ion $[\text{AgNCCH}_3]^+$ also has a linear Ag-N-C-C skeletal structure. However the NAgN angle in the 1:2 complex ion $[\text{CH}_3\text{CNAgNCCH}_3]^+$ need not be 180° to preserve the C_{3v} symmetry of the acetonitrile molecules.

From Table II it can be seen that the CN and CC bands of acetonitrile are shifted to higher frequencies in the complexes. Thus $\Delta\nu_{\text{CN}} = 18$ cm^{-1} and $\Delta\nu_{\text{CC}} = 12$ cm^{-1} for the 1:2 complex, whereas in the 1:1 complex $\Delta\nu_{\text{CN}} = 11$ cm^{-1} and $\Delta\nu_{\text{CC}} = 7$ cm^{-1} . The fact that the CN frequency increases in acetonitrile complexes has been shown²⁰ by normal coordinate analysis to be a result of the increase in the force constant of the CN bond and can be explained¹⁸ by a change in hybridization of the nitrogen orbital contributing to the σ bond of the CN group. In the 1:1 complex the CN frequency is lower than in the 1:2. With SnCl_4 , the same order of CN frequencies is observed¹⁹ with propionitrile complexes but the order is reversed in the acetonitrile complexes. It was found²⁰ in the normal coordinate analysis treatment of acetonitrile complexes that the lower the CN frequency, the weaker is the donor-acceptor bond. The weaker Ag-N bond in the $[\text{AgNCCH}_3]^+$ ion may be due to the more extensive interaction in the anion-cation pair of the 1:1 solid. Some evidence of this is recorded in Table I where the nitrate band in the 700- cm^{-1} region of the spectrum, which, for a NO_3^- ion of D_{3h} symmetry arises from a degenerate vibration, is split for the 1:1 solid but not for the 1:2.

Solution Spectra—Vibrational Assignments. The spectra of concentrated solutions in the region of the CN absorption is given in Figure 1. For the solution of mole fraction 0.33, three bands are observed at 2254, 2265, and 2271 cm^{-1} . The first two of these frequencies correspond exactly to those of the CN bands of pure acetonitrile and $\text{AgNO}_3 \cdot \text{CH}_3\text{CN}$ solid at room temperature and the third frequency is 2 cm^{-1} higher than that

(12) G. Topping, *Spectrochim. Acta*, **21**, 1743 (1965).

(13) (a) K. Buijs and C. J. H. Schutte, *ibid.*, **18**, 307 (1962); (b) C. J. H. Schutte, *Z. Physik. Chem. (Frankfurt)*, **39**, 241 (1963).

(14) J. P. Devlin, K. Williamson, and G. Austin, *J. Chem. Phys.*, in press.

(15) L. I. Katzin, *J. Inorg. Nucl. Chem.*, **24**, 245 (1962).

(16) J. R. Ferraro and A. Walker, *J. Chem. Phys.*, **42**, 1278 (1965).

(17) J. L. Hoard, T. B. Owen, A. Buzzell, and O. N. Salmon, *Acta Cryst.*, **3**, 130 (1950).

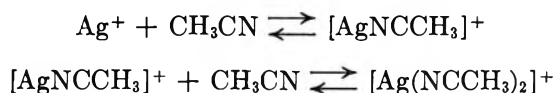
(18) V. N. Filimonov and D. S. Bystrov, *Opt. Spectry.*, **12**, 31 (1962).

(19) V. H. A. Brune and W. Zeil, *Z. Naturforsch.*, **16a**, 1251 (1961).

(20) K. F. Purcell and R. S. Drago, *J. Am. Chem. Soc.*, **88**, 919 (1966).

of $\text{AgNO}_3 \cdot 2\text{CH}_3\text{CN}$ solid at liquid nitrogen temperature (see Table II). Freezing acetonitrile to liquid nitrogen temperature decreases the CN absorption by 2 cm^{-1} . One can therefore with confidence interpret the origin of the bands observed in solution of mole fraction 0.33 as the CN vibrations of the species CH_3CN , $[\text{AgNCCH}_3]^+$, and $[\text{Ag}(\text{NCCH}_3)_2]^+$.

The relative intensity of these bands is concentration dependent. It can be seen from Figure 1 that at a mole fraction of silver nitrate of 0.43 there is no "free" solvent absorption band. In very dilute solutions, mole fraction less than 0.05 (*i.e.*, $c < 1 \text{ mole l.}^{-1}$), the species $[\text{AgNCCD}_3]^+$ is no longer detectable; neither is the concentration of the $[\text{Ag}(\text{NCCD}_3)_2]^+$ ion sufficient for observation at mole fractions less than 10^{-4} (*i.e.*, $c < 2 \times 10^{-3} \text{ mole l.}^{-1}$), in which solutions only the "free" solvent can be detected. These results are explicable in terms of the equilibria



If a solution of mole fraction 0.33 in which all three species are detectable at room temperature is cooled, then the concentration of "free" acetonitrile decreases. Both equilibria must therefore be shifted to the right. To obtain the spectrum of the solid $\text{AgNO}_3 \cdot 2\text{CH}_3\text{CN}$ complex it was therefore necessary to cool this solution slowly to liquid nitrogen temperature.

Some very accurate measurements of the proton magnetic resonance spectra of silver nitrate solutions in acetonitrile have recently been published.²¹ They are in adequate agreement with our previous work.²² From their results, Schneider and Strehlow calculate solvation numbers of 4 for the Ag^+ ion and 2 for the NO_3^- ion. In view of our infrared results it would seem possible to rationalize the concentration dependence of the chemical shift in terms of the formation constants of $[\text{AgNCCH}_3]^+$ and $[\text{Ag}(\text{NCCH}_3)_2]^+$.

For the unperturbed nitrate ion with D_{3h} point group symmetry, the asymmetric stretching vibration (ν_3 , E') occurs at 1384 cm^{-1} . This degeneracy is lost²³ in aqueous $\text{Ca}(\text{NO}_3)_2$ where the cation-anion pair has C_{2v} symmetry. Two bands are found at 1355 and 1435 cm^{-1} . For silver nitrate solutions in acetonitrile of concentration between 3 and $0.2 \text{ moles l.}^{-1}$ there are three absorption bands in this region of the spectrum. The concentration dependence of these bands is shown in Figure 2. The relative intensity of the high- and low-frequency bands decreases as the concentration falls until at $0.02 \text{ mole l.}^{-1}$ only the central band is detectable. We therefore assign the bands at 1306 and 1411 cm^{-1} to cation-anion pairs of symmetry C_{2v}

point group and the central band at 1353 cm^{-1} to NO_3^- ions (D_{3h}) in equilibrium with ion pairs.

The structure of these ion pairs is of interest. In solutions of very high concentration,⁵ 3–9 moles l.^{-1} , only the ion-pair absorptions at 1300 ± 10 and $1425 \pm 3 \text{ cm}^{-1}$ are observed. In the infrared²⁴ and Raman spectra^{25,26} of fused silver nitrate, bands are detected at 1310, 1395 and 1280, 1410 cm^{-1} , respectively. An interpretation of the fused-salt spectrum of molten silver nitrate based on normal coordinate vibrational analysis has been advanced^{25,26} in which this observed splitting correlates with a contact ion-pair model. In aqueous AgNO_3 solutions the frequencies of the equivalent Raman lines (at 1340 and 1420 cm^{-1} in a saturated solution,²⁷ $\sim 8 \text{ moles l.}^{-1}$) show marked concentration dependence,²⁸ this has been attributed to the existence of solvent-separated ion pairs. Irish and Walrafen²³ present further evidence that ion pairs (in $\text{Ca}(\text{NO}_3)_2$ solutions) giving rise to the concentration-dependent Raman frequencies at 1358 and 1450 cm^{-1} are solvent-separated ion pairs. In molten AgNO_3 , a contact ion-pair model appears adequate for a theoretical analysis of the observed spectral properties. It is of interest to note that the anion-cation pair frequencies in acetonitrile solutions, at ~ 1300 and $\sim 1415 \text{ cm}^{-1}$, correspond closely to values for AgNO_3 in the molten state. A further observation is that the above ion-pair frequencies remain almost invariant over the entire concentration range studied (0.2 – 9 moles l.^{-1} , Figure 2); this is in marked contrast to the spectra of aqueous AgNO_3 solutions. The spectrum of the cation-anion pair thus suggests that the ions are in contact in CH_3CN solutions and not solvent separated as in aqueous AgNO_3 solutions. This feature may be a significant factor to be considered in any complete analysis of the physicochemical properties of such nonaqueous electrolytes.

Acknowledgments. We thank Professor Dr. H. Strehlow (Göttingen) for a copy of the Ph.D. Thesis of H. Schneider and Drs. J. P. Delvin (Oklahoma State University), G. E. Walrafen (Bell Telephone Laboratories), and D. E. Irish (University of Waterloo) for

(21) H. Schneider and H. Strehlow, *Z. Physik. Chem.* (Frankfurt), **49**, 44 (1966).

(22) Erroneous magnetic susceptibility corrections were applied to our results in ref 5.

(23) D. E. Irish and G. E. Walrafen, *J. Chem. Phys.*, in press.

(24) J. K. Wilmshurst and S. Senderoff, *ibid.*, **35**, 1078 (1961).

(25) S. C. Wait and A. T. Ward, *ibid.*, **44**, 448 (1966).

(26) S. C. Wait, A. T. Ward, and G. J. Janz, *ibid.*, **45**, 133 (1966).

(27) R. E. Hester and R. A. Plane, *J. Am. Chem. Soc.*, **3**, 769 (1964).

(28) H. Lee and J. K. Wilmshurst, *Australian J. Chem.*, **17**, 943 (1964).

providing prepublication copies of their articles.^{14,23} This work was made possible in large part by financial

support from the U. S. Atomic Energy Commission, Division of Chemistry, Washington, D. C.

Self-Association and Hydration of Ketones in Carbon Tetrachloride¹

by T. F. Lin, S. D. Christian, and H. E. Affsprung

Department of Chemistry, University of Oklahoma, Norman, Oklahoma (Received October 5, 1966)

The self-association and hydration of acetone, 2,3-butanedione, and acetylacetone in carbon tetrachloride solution has been investigated by partition, solubility, and isopiestic techniques. The results indicate that the complex species ketone monomer monohydrate, ketone dimer, and ketone dimer monohydrate are needed to obtain a satisfactory explanation of all the data. A study of acetone in hexadecane was made to substantiate the observation of dimerization of ketones in nonpolar solution. The dimers are assumed to be formed by dipole-dipole interactions. The basic strengths of the ketones were found to be in the order acetone > acetylacetone > 2,3-butanedione. Equilibrium constants are reported at 15 and 25° and Henry's law constants for acetone are given through the range 20–60°.

Introduction

There are few published reports of the relative basicities of ketones involved in hydrogen-bonding reactions.^{2,3} Recently⁴ we reported the results of an investigation of the hydration of acetone in 1,2-dichloroethane using partition, solubility, nmr, and dielectric constant techniques.⁵ We concluded that the acetone monomer monohydrate is the major associated species in the ternary system acetone–1,2-dichloroethane–water at concentrations of acetone less than 0.55 mole/l. It was determined that the basic strength of the acetone carbonyl group is comparable to that of oxygen in the hydroxyl group of water and aliphatic alcohols. We have now completed a similar study of three additional ternary systems of the type ketone–water–CCl₄. The ketones employed were acetone, 2,3-butanedione, and acetylacetone. Since the nmr and dielectric constant techniques are limited by the low solubility of water in CCl₄, only the partition and water solubility techniques were used in the present investigation.

Experimental Section and Results

Acetone, 2,3-butanedione, acetylacetone, and CCl₄ were purified by fractional distillation; the middle portion of distillate was collected. Hexadecane was purified by vacuum distillation. The partition, solubility, and isopiestic techniques used are similar to methods described previously.^{6,7} Concentrations of ketones in the CCl₄ and aqueous phases were deter-

(1) Abstracted in part from the Ph.D. Dissertation of T. F. Lin, University of Oklahoma, Norman, Okla., 1966.

(2) J. M. Wisdom, R. J. Philippe, and M. E. Hobbs, *J. Am. Chem. Soc.*, **79**, 1383 (1957).

(3) H. Fritzsche and H. Dunken, *Acta Chim. Acad. Sci. Hung.*, **40**, 37 (1964).

(4) T. F. Lin, S. D. Christian, and H. E. Affsprung, *J. Phys. Chem.*, **69**, 2980 (1965).

(5) T. F. Lin, S. D. Christian, and H. E. Affsprung, submitted.

(6) S. D. Christian, H. E. Affsprung, and J. R. Johnson, *J. Chem. Soc.*, 1896 (1963).

(7) S. D. Christian, H. E. Affsprung, J. R. Johnson, and J. D. Worley, *J. Chem. Educ.*, **40**, 419 (1962).

mined spectrophotometrically using a Beckman DU spectrophotometer. The measurements of absorbances were made at the wavelength of maximum absorption of the ketone carbonyl groups; organic samples were diluted with CCl_4 where necessary to yield absorbances less than 1.0. In the case of acetylacetone, owing to the large absorptivity (about $1600 \text{ l. mole}^{-1} \text{ cm}^{-1}$), the concentrations of the ketone were determined by extracting the compound into a large volume of water to give concentrations in the 10^{-4} to 10^{-3} M range. Concentrations of water in the CCl_4 phase were determined by Karl Fisher titration with the Beckman KF-3 aquameter. Ordinary Karl Fisher reagent was used for water titration of samples containing ketones other than acetone. In the case of acetone, the fading of end point of the water titration was avoided by using a modified Karl Fisher reagent.⁴ The vapor pressure techniques for the investigation of the acetone-hexadecane system are similar to the methods previously reported from this laboratory.⁸

Partition and solubility data are reported for the three systems (1) acetone-water- CCl_4 , (2) 2,3-butanedione-water- CCl_4 , and (3) acetylacetone-water- CCl_4 . Figure 1 shows partition data for the system acetone-water- CCl_4 plotted as the concentrations of acetone in water, $f_A^{\text{H}_2\text{O}}$, against the concentration of acetone in CCl_4 , $f_A^{\text{CCl}_4}$. Figure 2 shows water solubility data for the same system plotted as the formal concentration of water in CCl_4 , $f_W^{\text{CCl}_4}$. For the other ketone-water- CCl_4 systems, the partition and solubility curves

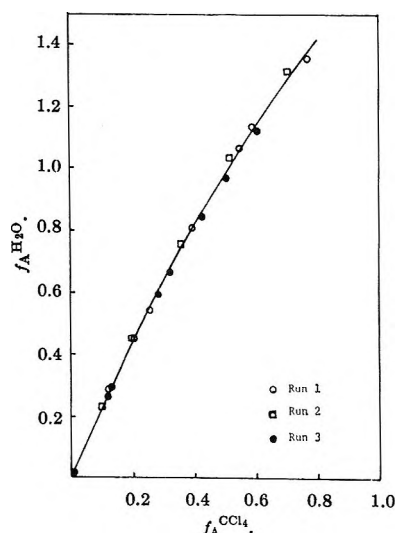


Figure 1. Partition data for the system acetone-water- CCl_4 at 25° .

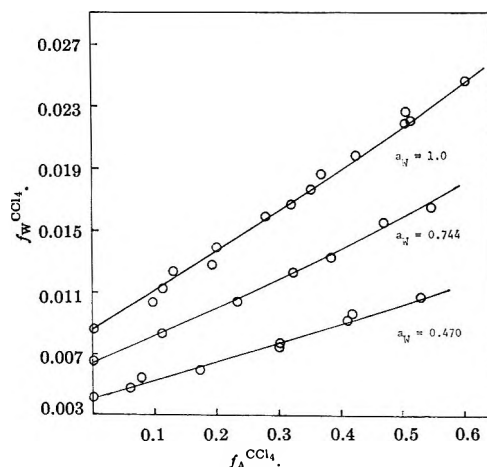


Figure 2. Solubility of water in CCl_4 in the presence of acetone at various water activities at 25° .

Table I: Partition Data of the System 2,3-Butanedione-Water-Carbon Tetrachloride at 25°

	$f_A^{\text{H}_2\text{O}}$, M	$f_A^{\text{CCl}_4}$, M	$f_A^{\text{CCl}_4}$ (calcd), M
Run 1	0.660	0.600	0.600
	0.601	0.522	0.515
	0.555	0.482	0.460
	0.541	0.441	0.443
	0.483	0.380	0.383
	0.372	0.298	0.278
	0.353	0.268	0.264
	0.321	0.244	0.236
	0.186	0.133	0.126
	0.092	0.063	0.058
Run 2	0.595	0.520	0.507
	0.532	0.455	0.432
	0.489	0.391	0.390
	0.380	0.292	0.287
	0.372	0.281	0.278
	0.325	0.248	0.240
	0.188	0.134	0.130
	0.100	0.064	0.065

are similar to those for the acetone-water- CCl_4 system; *i.e.*, the partition curves, $f_A^{\text{H}_2\text{O}}$ vs. $f_A^{\text{CCl}_4}$, are concave downward, whereas the water solubility curves, $f_W^{\text{CCl}_4}$ vs. $f_A^{\text{CCl}_4}$, are concave upward for each water activity. Partition and water solubility data for the other two systems are given in Tables I-VI. The nonlinearity of partition as well as solubility curves indicates that associated species of greater complexity are present in these systems than in the system acetone-water-1,2-dichloroethane, for which partition and solubility curves appear to be linear. From the partition and solubility data, it is possible to determine what types of complex species are present. Since the systems

(8) A. A. Taha, Ph.D. Dissertation, University of Oklahoma, Norman, Okla., 1965.

Table II: Solubility of Water in CCl_4 in the Presence of 2,3-Butanedione at Various Water Activities at 25°

	$f_A^{\text{CCl}_4}$, <i>M</i>	$f_W^{\text{CCl}_4}$, <i>M</i>	$f_W^{\text{CCl}_4}$ (calcd), <i>M</i>
$a_w = 1.00$	0.660	0.0167	0.0171
	0.520	0.0154	0.0151
	0.501	0.0152	0.0148
	0.455	0.0146	0.0141
	0.391	0.0137	0.0133
	0.358	0.0128	0.0129
	0.292	0.0125	0.0121
	0.281	0.0117	0.0120
	0.226	0.0109	0.0113
	0.134	0.0102	0.0102
	0.073	0.0095	0.0095
	0.064	0.0096	0.0094
	0.000	0.0088	0.0088
	$a_w = 0.842$	0.718	0.0146
0.584		0.0130	0.0130
0.417		0.0112	0.0113
0.279		0.0099	0.0100
0.104		0.0083	0.0084
0.000		0.0075	0.0074
$a_w = 0.687$	0.755	0.0129	0.0124
	0.594	0.0112	0.0109
	0.432	0.0099	0.0095
	0.252	0.0081	0.0080
	0.094	0.0069	0.0068
	0.000	0.0062	0.0061

Table III: Partition Data of the System 2,3-Butanedione-Water-Carbon Tetrachloride at 15°

$f_A^{\text{H}_2\text{O}}$, <i>M</i>	$f_A^{\text{CCl}_4}$, <i>M</i>	$f_A^{\text{CCl}_4}$ (calcd), <i>M</i>
0.770	0.535	0.515
0.760	0.513	0.505
0.687	0.437	0.438
0.629	0.400	0.414
0.628	0.391	0.414
0.550	0.331	0.327
0.525	0.313	0.310
0.476	0.274	0.274
0.421	0.236	0.235
0.364	0.198	0.198
0.364	0.199	0.198
0.199	0.103	0.100
0.196	0.103	0.098
0.063	0.030	0.030

studied are relatively dilute solutions, highly polarized or associated species are unlikely to be present in significant concentration and can be neglected. Accordingly, assuming no species larger than trimers to be present, the formal concentrations of ketone and of water, f_A and f_W , can be separately expressed as

$$f_A = C_A + 2K_{20}C_A^2 + 3K_{30}C_A^3 + K_{11}C_AC_W + 2K_{21}C_A^2C_W + K_{12}C_AC_W^2 \quad (1)$$

$$f_W = C_W + 2K_{02}C_W^2 + 3K_{03}C_W^3 + K_{11}C_AC_W + K_{21}C_A^2C_W + 2K_{12}C_AC_W^2 \quad (2)$$

where C_A is the concentration of the acetone monomer, C_W is the concentration of water monomer, and K_{ij} is the equilibrium constant for the formation of complex species consisting of i acetone molecules and j water molecules. Inasmuch as the water monomer is the primary form of water in pure CCl_4 ⁹ and since, in the solutions investigated, ketones do not appear to exist as species larger than dimers, we can set K_{30} and K_{02}

Table IV: Solubility of Water in CCl_4 in the Presence of 2,3-Butanedione at Various Water Activities at 15°

	$f_A^{\text{CCl}_4}$, <i>M</i>	$f_W^{\text{CCl}_4}$, <i>M</i>	$f_W^{\text{CCl}_4}$ (calcd), <i>M</i>	
$a_w = 1.00$	0.437	0.0111	0.0111	
	0.400	0.0101	0.0106	
	0.391	0.0105	0.0104	
	0.331	0.0099	0.0096	
	0.313	0.0096	0.0094	
	0.236	0.0083	0.0084	
	0.198	0.0082	0.0080	
	0.103	0.0070	0.0069	
	0.030	0.0068	0.0066	
	0.000	0.0059	0.0059	
	$a_w = 0.645$	0.526	0.0083	0.0080
		0.405	0.0067	0.0068
		0.221	0.0051	0.0053
0.125		0.0044	0.0046	
0.010		0.0042	0.0044	
0.000		0.0038	0.0038	

Table V: Partition Data of the System Acetylacetone-Water-Carbon tetrachloride at 25°

$f_A^{\text{H}_2\text{O}}$, <i>M</i>	$f_A^{\text{CCl}_4}$, <i>M</i>	$f_A^{\text{CCl}_4}$ (calcd), <i>M</i>
0.303	1.302	1.251
0.279	1.091	1.132
0.250	0.971	0.990
0.212	0.828	0.814
0.183	0.676	0.687
0.155	0.571	0.569
0.129	0.466	0.462
0.097	0.350	0.338
0.069	0.224	0.235
0.028	0.093	0.091

(9) J. R. Johnson, Ph.D. Dissertation, University of Oklahoma, Norman, Okla., 1966.

Table VI: Water Solubility in CCl_4 in the Presence of Acetylacetone at Various Water Activities at 25°

	$f_A^{\text{CCl}_4}$, M	$f_W^{\text{CCl}_4}$, M	$f_W^{\text{CCl}_4}$ (calcd), M	
$a_W = 1.00$	1.110	0.0284	0.0283	
	0.971	0.0264	0.0259	
	0.971	0.0256	0.0259	
	0.775	0.0211	0.0220	
	0.695	0.0201	0.0203	
	0.570	0.0184	0.0179	
	0.445	0.0163	0.0158	
	0.320	0.0135	0.0136	
	0.190	0.0119	0.0115	
	0.060	0.0099	0.0096	
	0.000	0.0090	0.0088	
	$a_W = 0.470$	1.110	0.0130	0.0135
0.925		0.0109	0.0116	
0.745		0.0095	0.0099	
0.563		0.0083	0.0083	
0.372		0.0068	0.0071	
0.242		0.0054	0.0057	
0.107		0.0049	0.0048	
0.000		0.0042	0.0041	
$a_W = 0.0744$		1.120	0.0224	0.0215
		0.955	0.0193	0.0189
	0.760	0.0161	0.0160	
	0.580	0.0132	0.0134	
	0.381	0.0107	0.0108	
	0.245	0.0087	0.0091	
	0.107	0.0079	0.0076	
	0.000	0.0066	0.0065	

equal to zero. In addition, in view of the very low concentration of water monomers in CCl_4 , the ketone dihydrate is assumed not to be present in measurable concentration. Therefore, eq 1 and 2 reduce to

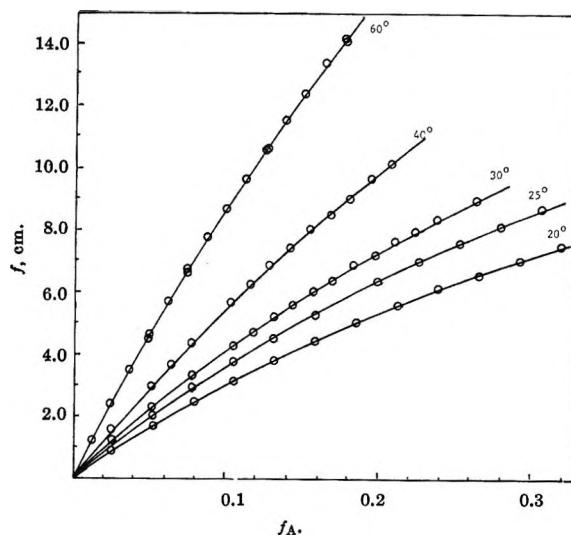
$$f_A = C_A + 2K_{20}C_A^2 + K_{11}C_A C_W + 2K_{21}C_A^2 C_W \quad (3)$$

$$\Delta f_W = f_W - C_W = K_{11}C_A C_W + K_{21}C_A^2 C_W \quad (4)$$

$$C_A = K_D C_A^W \quad (5)$$

where C_A^W is the concentration of ketone in the water phase and K_D is the distribution ratio. It is impossible to reduce further the number of species because the $K_{21}C_A^2 C_W$ term in eq 4 is needed to account for the positive curvature of the water solubility curves and the $2K_{20}C_A^2$ term in eq 3 is also needed, since if K_{20} were zero, relations 3, 4, and 5 would require that $(f_A - 2\Delta f_W)/C_A^W$ is not constant for any of the three ketone systems. Thus to fit the data for all three systems, it is necessary to assume the presence of three complex species—the ketone dimer, ketone monomer monohydrate, and ketone dimer monohydrate.

Using eq 3, 4, and 5, all the partition and solubility


Figure 3. Solubility of acetone in hexadecane at various acetone fugacities.

data were treated by a nonlinear least-squares analysis to obtain the best values of the four parameters, K_D , K_{11} , K_{20} , K_{21} , and their standard deviations. Partition data were first treated by using the observed eq 3 to minimize the square sum of the residuals of f_A by a two-parameter optimum-seeking method;¹⁰ thus the four parameters were reduced to two parameters. Then the best values of the remaining two parameters were obtained by treating the water solubility data, using the observed eq 4 to minimize the square sum of the squares of the residuals of Δf_W . Sillén's theorem^{10,11} of least-squares analysis was utilized in calculating the standard deviations for the four parameters. A digital computer method was used to obtain the maximum value of each of the four parameters on the standard deviation contour in four-dimensional hyperspace. Table VII lists the derived values of K_D , K_{11} , K_{20} , K_{21} , and their standard deviations. The solid lines in Figures 1 and 2 have been calculated using the derived values of the four parameters. Calculated values of f_A for the partition systems and changes in f_W for the water solubility experiments are included in Tables I–VI.

For the systems ketone–water– CCl_4 , we have shown that the presence of ketone dimers must be assumed in the interpretation of the partition and water solubility data. In order to support this conclusion, it was decided to investigate the dependence of acetone activity on its concentration in an inert solvent, hexadecane.

(10) L. G. Sillén, *Acta Chem. Scand.*, **16**, 159 (1962).

(11) L. G. Sillén, *ibid.*, **18**, 1085 (1964).

Table VII: Equilibrium Constants of the System Ketone-Water-Carbon Tetrachloride

Substance	K_D	K_{11} , mole ⁻¹ l.	K_{21} , mole ⁻² l. ²	K_{20} , mole ⁻¹ l.
Acetone at 25°	0.388 ± 0.004	2.45 ± 0.13	3.89 ± 0.31	0.39 ± 0.03
2,3-Butanedione at 25°	0.604 ± 0.006	1.17 ± 0.11	2.41 ± 0.26	0.57 ± 0.04
2,3-Butanedione at 15°	0.430 ± 0.005	1.24 ± 0.13	6.12 ± 0.40	0.78 ± 0.05
Acetylacetone at 25°	3.143 ± 0.005	1.48 ± 0.10	1.33 ± 0.20	0.146 ± 0.005

Hexadecane was used primarily because its vapor pressure is less than 0.1 mm, so that no complication arises from the presence of hexadecane in the vapor phase. The results of the vapor pressure measurements are shown in Figure 3, in which the fugacities of acetone are plotted against the formal concentration of acetone in hexadecane. The fugacities were calculated from the vapor pressure of acetone by the equation $f = P \exp(BP/RT) = P(1 + BP/RT)$. The second virial coefficients, B , were obtained from the reported values by Lambert and Robert.¹² It was observed that the vapor pressure data can be adequately treated by using the equation

$$f_A = K_h f + 2K_2 K_h^2 f^2 + 3K_3 K_h^3 f^3$$

assuming no solute species larger than trimers are present in significant concentrations. Least-squares values of K_h (the reciprocal of the Henry's law constant for the monomer) and the two association constants, K_2 and K_3 , are given in Table VIII.

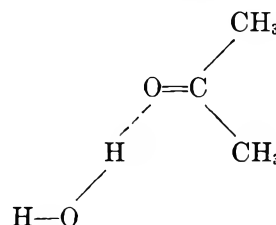
Table VIII: The Equilibrium Henry's Law Constants of the System Acetone-Hexadecane

$f_A = K_h f + 2K_2 K_h^2 f^2 + 3K_3 K_h^3 f^3$	20°	25°	30°	40°	60°
	$K_h \times 10^3$, ml ⁻¹ mm ⁻¹	2.74	2.34	2.09	1.60
K_2 , mole ⁻¹ l.	0.94	0.84	0.79	0.66	0.52
K_3 , mole ⁻² l. ²	1.32	1.32	0.97	0.82	0.64

Discussion

The partition and solubility data for the acetone-water-1,2-dichloroethane system reported previously were adequately interpreted by assuming that the only important complex species is the acetone monomer monohydrate. For the present systems, in addition to the ketone monomer monohydrate, we have assumed the presence of two additional complex species, *i.e.*, ketone dimer and ketone dimer monohydrate, in order to obtain a satisfactory explanation of all the data. The relative inertness of CCl₄ compared to

1,2-dichloroethane leads to an increase in the number of complex species and also increases the magnitude of the equilibrium constant K_{11} for the formation of the acetone monomer monohydrate (K_{11} is 0.85 l. mole⁻¹ in 1,2-dichloroethane and 2.45 l. mole⁻¹ in CCl₄). A plausible geometric structure of the 1:1 species in 1,2-dichloroethane, consistent with the dielectric constant data, was proposed previously⁵ to be



In the CCl₄ systems, the ketone monomer monohydrates probably have similar structures.

The basic strengths of the ketones which were used in this investigation are in the order acetone > acetylacetone > 2,3-butanedione. 2,3-Butanedione, which has two carbonyl groups, might be expected to be more basic than acetone, but results of the water solubility study clearly indicate that it is less basic. Apparently conjugation leads to a considerable decrease in the basicity of the adjacent carbonyl groups. Since acetylacetone molecules exist approximately 95% in the enol form in CCl₄, the determined basic strength of acetylacetone is primarily that of its intramolecularly hydrogen-bonded form.

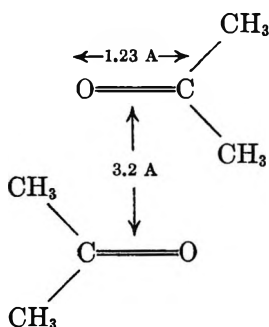
By kinetic arguments, the equilibrium constant of the ketone monomer monohydrate should be approximately related to the equilibrium constants of the ketone dimer monohydrate by the expression $K_{21} = K_{11}^2/4$.¹³ However, the values given in Table II indicate that K_{21} is somewhat greater than $K_{11}^2/4$ for the three systems. A reasonable explanation for the large values of K_{21} is that the acetone dimer monohydrate is not only stabilized by the specific interaction of the

(12) J. D. Lambert, G. A. H. Roberts, J. S. Rowlinson, and V. J. Wilkinson, *Proc. Roy. Soc. (London)*, **A196**, 113 (1949).

(13) S. D. Christian, H. E. Affsprung, and C. Ling, *J. Chem. Soc.*, 2378 (1965).

carbonyl groups with the water protons to form a water-bridged complex, but also by an additional weak dipole-dipole interaction between the two ketone molecules. Inductive effects cannot be used to explain the increased stability of the 2:1 species, since induction should lead to a decrease in the acidity of the non-bonded proton of the water molecule in the monomer monohydrate as compared to the acidity of a proton in a free water molecule.¹⁴

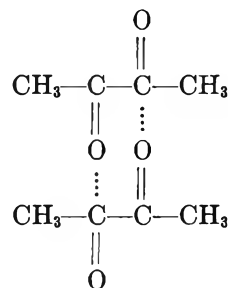
Acetone dimers were found to be present in CCl_4 and hexadecane. The change of enthalpy for the formation of acetone dimers in hexadecane was found to be -2.8 kcal/mole, which is less than that of ordinary hydrogen bonding. It is interesting to calculate the interaction energy of an antiparallel dipole pair of the type



From the known dipole moment of acetone (2.8 D.) and the carbonyl bond length (1.23 Å), the net charge on either end of the carbonyl group was calculated to be 2.28×10^{-10} statcoulomb. The minimum distance between two parallel carbonyl groups is assumed to be 3.2 Å, which is the sum of van der Waals' radii of carbon and oxygen. Using these values, the total electric energy calculated by adding all the point-charge interaction energy is -3 kcal/mole, which is close to the experimental values, $\Delta U = -2.8$ kcal/mole. The actual geometric structure is probably not a rigid antiparallel arrangement of two dipoles and undoubtedly many variations from the antiparallel align-

ment are possible. The less rigid structure of a "random dipole pair," noted by Saum,¹⁵ should result in a less negative entropy change than that found for hydrogen-bonded complexes having similar energy changes. This is illustrated by the entropy change for formation of the acetone dimer in hexadecane, which is $\Delta S = -9.7$ eu, in comparison with -12.0 eu for the formation of the acetone monomer monohydrate in CCl_4 .

The large value of K_2 for 2,3-butanedione probably reflects a double interaction of two local dipoles. The dimer may exist as



This explanation is supported by a large enthalpy change (-5.4 kcal/mole) for the formation of the 2,3-butanedione dimer, a value nearly twice that of the acetone dimer. The acetylacetone dimer is relatively less stable than the dimers of acetone and 2,3-butanedione; this can be rationalized by noting that 95% of the acetylacetone molecules are in the enol form, which would not be expected to be so capable of intermolecular self-association as the keto form.

Acknowledgment. This research was supported by the U. S. Department of the Interior, Office of Saline Water.

(14) H. S. Frank and W. Y. Wen, *Discussions Faraday Soc.*, **24**, 133 (1957); H. S. Frank, *Proc. Roy. Soc. (London)*, **A247**, 481 (1958); H. S. Frank, *Natl. Acad. Sci. Natl. Res. Council Publ.*, **42**, 141 (1963).

(15) A. M. Saum, *J. Polymer Sci.*, **42**, 57 (1960).

The Rate of Oxygen Exchange between the Perrhenate Ion and Water

by R. Kent Murmann

Chemistry Department, University of Missouri, Columbia, Missouri (Received October 5, 1966)

The rate law for the exchange of oxygen between perrhenate ion and water in the liquid phase is $R = k_0[\text{ReO}_4^-][\text{H}_2\text{O}] + k_1[\text{ReO}_4^-][\text{H}_2\text{O}][\text{H}^+]^2 + k_2[\text{ReO}_4^-][\text{H}_2\text{O}][\text{OH}^-]$. The order with respect to water in each rate term is assumed. The experimental order with respect to $[\text{H}^+]$ was found to be 1.92 ± 0.05 in the $[\text{H}^+]$ range of 4×10^{-5} to 6×10^{-3} M and with respect to $[\text{OH}^-]$, 0.990 ± 0.016 in the $[\text{OH}^-]$ range of 8×10^{-5} to 6×10^{-2} M . At $\mu(\text{LiCl}) = 0.10$ and 25° , $k_0 = 1.4 \pm 0.1 \times 10^{-3}$ l. mole⁻¹ sec⁻¹, $k_1 = 3.36 \pm 0.15 \times 10$ l.³ mole⁻³ sec⁻¹, and $k_2 = 1.555 \pm 0.023 \times 10^{-4}$ l.² mole⁻² sec⁻¹. The Arrhenius activation energy, E^* (kcal/mole), for each term was found to be 15.44 ± 1.4 , 4.16 ± 0.15 , and 11.15 ± 0.47 , respectively. The rates are slightly affected by changes in μ and replacement of Na^+ for Li^+ or NO_3^- for Cl^- has only a moderate effect.

In order to carry out oxygen-transfer experiments in the oxidation of $[\text{Re}(\text{en})_2\text{O}_2]^+$ and similar-type ions to ReO_4^- , it was necessary to know precisely the rates of oxygen exchange between ReO_4^- and H_2O solvent and its H^+ and OH^- dependence. A previous study¹ had evaluated the rate in the acidic and neutral region but was of limited precision owing to the method used to convert ReO_4^- to a volatile oxygen-containing gas suitable for mass spectrometric analysis. Also the order with respect to H^+ was determined by measuring R as a function of a glass-electrode-measured pH. There was some reason to doubt the validity of the measured pH over an extended range and as will be described in this paper, using the added $[\text{H}^+]$ gives a different rate law with considerably higher precision. This paper reports attempts to evaluate the rate law and its temperature coefficient for the ReO_4^- , H_2O isotopic exchange.

Experimental Section

Preparation of Materials. NaReO_4 enriched in O^{18} was prepared from a concentrated (1 g of Re/ml) solution of HReO_4 (S. W. Shattuck Co.) by mixing with an equal volume of $8 \times \text{O}^{18}$ -enriched water, redistilled from KMnO_4 . After equilibration for 2 hr, which was known from previous work to cause complete exchange, reagent grade $\text{Na}_2\text{CO}_3(\text{s})$ was slowly added in slight excess. Then a small excess of HReO_4 was added until it was just acidic after boiling. The solution was filtered and concentrated to half its

initial volume under vacuum at room temperature and AR acetone (50 ml/g of Re) added. It was filtered to remove a trace of insoluble material and AR ethyl ether added (200 ml/g of Re). After 2 hr at 0° the white precipitate was collected, washed with anhydrous ether, and dried at 70° under vacuum for 2 days. Yield was 80–90% of theory. Analysis² for Re gave 68.2% (calculated for NaReO_4 , 68.16). The analysis only shows the compound to be essentially pure; it would not indicate the presence of catalytically important impurities. In order to clarify this point, NaReO_4 was prepared through recrystallized AgReO_4 ¹⁸ by reaction with the stoichiometric amount of AR NaCl. After removal of the AgCl , the solution was evaporated until crystallization occurred and the product was removed and dried under vacuum. The two preparations of NaReO_4 showed identical ($\pm 1\%$) rates of oxygen exchange in both the acidic and basic regions.

LiCl , NaCl , and LiNO_3 stock solutions were prepared from AR solids and the filtered solutions analyzed for content by standard methods.

The $\text{CsCl-H}_2\text{O}$ precipitating solution was made by adding ca. 25 g of AR CsCl to 50 ml of filtered solution. All of the other chemicals were of reagent grade. Two types of solvent water were used: doubly distilled once from KMnO_4 and distilled and passed over double-bed ion-exchange resin. Since no difference was ob-

(1) R. Kent Murmann, *J. Inorg. Nucl. Chem.*, **18**, 226 (1961).

(2) J. Guyon and R. K. Murmann, *Anal. Chem.*, **36**, 1058 (1964).

served, the latter solvent was used for the majority of the work.

Isotopic Measurement. A standard normal water sample was equilibrated with a small amount of CO_2 for several weeks at 25° . The CO_2 isotopic composition was measured $[46/(44 + 45)]$ and from the known $\text{CO}_2\text{-H}_2\text{O}$ O^{18} isotopic equilibrium constant³ the isotopic composition of the water was calculated. This was arbitrarily set at $2.00 \times 10^{-3} [(\text{H}_2\text{O}^{18})/(\text{H}_2\text{O}^{16})]$. All samples were normalized to this value.

The isotopic composition of NaReO_4 was determined by a modified Anbar⁴ method. The NaReO_4 was heated to 525° in a sealed tube with 1:1 $\text{HgCl}_2\text{-Hg}(\text{CN})_2$ for 3 hr and $(\text{CN})_2$ and CO_2 were collected. The $(\text{CN})_2$ was removed by the method of Shakhaskiri and Gordon⁵ and the CO_2 collected for isotopic measurement. The isotopic composition of NaReO_4 was also determined after solution in cold, neutral water and precipitation as CsReO_4 . The solid CsReO_4 was treated as above and gave values for the O^{18} content identical with that from NaReO_4 ($\pm 0.2\%$). This showed that neither solution in pure water nor the Cs^+ precipitation induced exchange.

ReO_4^- - H_2O Exchange. To volumetric flasks were added the required amounts of stock solutions of LiCl , HCl , NaOH , etc., and the volume was brought to 25.00 ml with water at the required temperature. After equilibration in a constant-temperature bath ($\pm 0.05^\circ$) a weighed quantity (usually ≈ 0.2 g of $\text{NaReO}_4 \pm 0.01$ mg) was quickly added. Solution occurred within 10 sec after which the solution was transferred to a constant-temperature-controlled vessel having a valved outlet at the bottom. At timed intervals 2.0-ml samples were released to a test tube containing 500 μl of CsCl stock solution at 0° . Precipitation was complete within 30 sec. After *ca.* 5 min at 0° , the CsReO_4 was removed on a filter, washed three times with dry AR acetone, and quickly dried over $\text{Mg}(\text{ClO}_4)_2$. It was then converted to CO_2 for isotopic analysis as described for NaReO_4 . Tests showed that no induced exchange occurred during precipitation nor during the time (5–20 min) of $\text{CsReO}_4(\text{s})\text{-H}_2\text{O}$ contact at 0° . In the highly acidic and basic regions where the rates were extremely rapid, the solution was quenched and precipitated by a mixture of NaOH and CsCl (in acid range) or HCl and CsCl (in basic range). The correct amounts of acid or base were used to give a nearly neutral resulting solution.

In the initial experiments the exchange law, $\ln(1 - F) = kt$, was followed where F is the fraction of exchange completed. Graphs of $\ln(1 - F)$ vs. t were linear over 98% of the reaction and the slope as determined by a linear least-squares treatment on a

7040 computer had an average standard deviation of 0.2%. Duplicate runs, however, gave slopes differing by $\pm 0.6\%$ in both the acidic and basic region. All rates reported consist of six to eight individual points. The over-all rate of reaction, R , was calculated using the expression

$$R = \text{slope} \left[\frac{4[\text{ReO}_4^-][\text{H}_2\text{O}]}{4[\text{ReO}_4^-] + [\text{H}_2\text{O}]} \right] \text{mole l.}^{-1} \text{sec}^{-1}$$

and k^* is defined as

$$k^* = \frac{R}{[\text{ReO}_4^-][\text{H}_2\text{O}]} \text{l. mole}^{-1} \text{sec}^{-1}$$

In the acidic region a graph of $-\log R$ vs. $-\log [\text{H}^+]$ was linear with an approximate slope of 2. A linear least-squares treatment of all R values in the acidic range gave for the slope, which is the order with respect to H^+ , a value of 1.924 ± 0.046 .⁶

In the basic region a graph of $-\log R$ vs. $-\log [\text{OH}^-]$ was also linear with an approximate slope of 1. A linear least-squares treatment of all R values in the basic range gave for the slope, which is the order with respect to $[\text{OH}^-]$, a value of 0.990 ± 0.016 .

In the neutral region ($\text{pH} \sim 6$) no appreciable contribution from the acid or base paths is present and thus this represents the uncatalyzed path.

The experimental orders with respect to H^+ and OH^- are very near integers and the deviations noted are thought to arise from ionic atmosphere changes and/or nonrandom measurement errors. Thus the experimental rate constants were based on the integral values of 2 and 1 for the H^+ and OH^- orders, respectively, according to the expression

$$R = k_0[\text{ReO}_4^-][\text{H}_2\text{O}] + k_1[\text{ReO}_4^-][\text{H}_2\text{O}][\text{H}^+]^2 + k_2[\text{ReO}_4^-][\text{H}_2\text{O}][\text{OH}^-]$$

Using all values obtained, $k_0 = 1.4 \pm 0.1 \times 10^{-8}$ l. mole⁻¹ sec⁻¹, $k_1 = 3.36 \pm 0.15 \times 10^3$ l.³ mole⁻³ sec⁻¹, and $k_2 = 1.555 \pm 0.023 \times 10^{-4}$ l.² mole⁻² sec⁻¹. These values are at $\mu = 0.10$ with LiCl and at 25.0° .⁷

Results and Discussion

Figure 1 shows the behavior of k^* as a function of acid and base concentration. As can be seen graphi-

(3) D. Samuel in "Oxygenases," O. Hayaishi, Ed., Academic Press Inc., New York, N. Y., 1962, p 67.

(4) M. Anbar and S. Guttman, *Intern. J. Appl. Radiation Isotopes*, **4**, 233 (1959).

(5) B. Z. Shakhaskiri and G. Gordon, *Talanta*, **13**, 142 (1966).

(6) All \pm values listed refer to two standard deviations, the 95% confidence level.

(7) Inclusion of H_2O in each rate term, although reasonable, is by choice and has not been demonstrated.

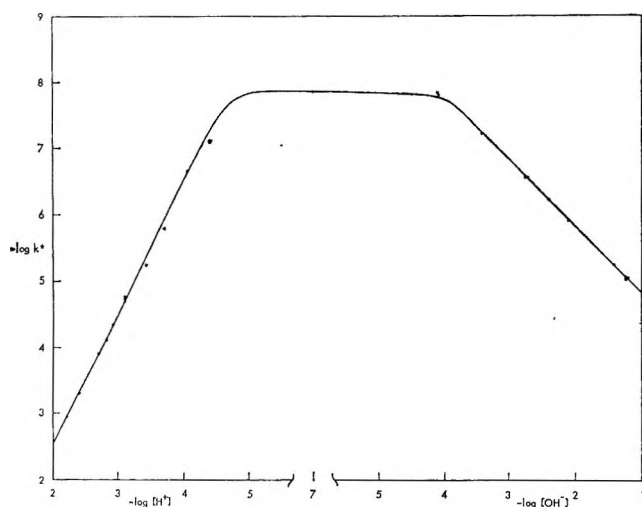


Figure 1. Rate constant for ReO_4^- – H_2O exchange at 25° and $\mu = 0.1$.

cally or more precisely from calculations using the rate expression, no appreciable contribution to k^* in the neutral region comes from the acid or base paths. These results are to be compared to the previous study (at 0°) using pH measurement as a measure of acidity.

Table I lists the changes in $-\log k^*$ as a function of $[\text{ReO}_4^-]$. The essential constancy in acidic and in

Table I: Apparent Rate Constants of Exchange of ReO_4^- with H_2O ($\mu(\text{LiCl}) = 0.10$; $T = 25.0^\circ$; $k^* = R/[\text{ReO}_4^-][\text{H}_2\text{O}]$ l. mole $^{-1}$ sec $^{-1}$)

Acidic Region, $[\text{H}^+] = 8.0 \times 10^{-4} M$	
$10^2[\text{ReO}_4^-], M$	$-\log k^*$
1.500	4.741
3.015	4.723
6.000	4.731
Basic Region, $[\text{OH}^-] = 6.0 \times 10^{-2} M$	
$10^2[\text{ReO}_4^-], M$	$-\log k^*$
1.486	5.014
3.022	5.030
4.018	5.031

Figure 1 shows the effect of changing acidity on the over-all rate, R , and Table II lists the rate data from which the individual rate constants were evaluated. In the neutral region there is an increase in rate in the presence of light but this was not observed in either acidic or basic media.

Table II: ReO_4^- – H_2O Oxygen Exchange Rates ($k^* = R/[\text{ReO}_4^-][\text{H}_2\text{O}]$ l. mole $^{-1}$ sec $^{-1}$; $T = 25.0^\circ$; $\mu(\text{LiCl}) = 0.100$)

Acidic Region			
$-\log [\text{H}^+](\text{added})$	$10^2[\text{ReO}_4^-], M$	Slope, min $^{-1}$	$-\log k^*$
4.3979	2.998	6.810×10^{-6}	7.092
4.0969	2.992	1.857×10^{-4}	6.653
3.6990	2.997	1.296×10^{-3}	5.808
3.3979	3.041	4.780×10^{-3}	5.242
3.0969	3.015	1.581×10^{-2}	4.723
2.9208	3.009	3.801×10^{-2}	4.342
3.0969	1.486	1.516×10^{-2}	4.741
3.0969	4.018	1.556×10^{-2}	4.731
2.7959	3.004	7.526×10^{-2}	4.045
2.6990	2.991	1.070×10^{-1}	3.892
2.3979	3.012	4.351×10^{-1}	3.303
2.2185	3.009	9.570×10^{-1}	2.941
Neutral Region			
pH	$10^2[\text{ReO}_4^-], M$	Slope, min $^{-1}$	$-\log k^*$
6.55 ^a	3.008	1.192×10^{-6}	7.845
6.15 ^a	2.993	1.157×10^{-6}	7.858
6.93 ^b	3.005	1.783×10^{-6}	7.670
6.59 ^b	3.002	1.772×10^{-6}	7.673
Basic Region			
$-\log [\text{OH}^-](\text{added})$	$10^2[\text{ReO}_4^-], M$	Slope, min $^{-1}$	$-\log k^*$
4.0969	3.008	1.192×10^{-6}	7.845
4.0969	3.003	1.101×10^{-6}	7.880
3.3979	3.013	4.937×10^{-6}	7.228
2.6990	2.985	2.361×10^{-4}	6.549
2.3979	2.995	5.132×10^{-4}	6.221
2.0969	3.006	1.016×10^{-3}	5.915
1.3979	3.005	4.928×10^{-3}	5.229
1.2219	1.486	8.080×10^{-3}	5.014
1.2219	4.018	7.773×10^{-3}	5.031
1.2219	3.022	7.795×10^{-3}	5.030

^a Dark. ^b Room light.

basic media suggests the inclusion of ReO_4^- in the rate expression to the first power. The slight changes seen are due to the changes in ionic environment since some substitution of Na^+ for Li^+ occurs when $[\text{NaReO}_4]$ increases. Similar experiments in the neutral region were not attempted because of the small but important changes in acidity which would occur owing to the unbuffered media.

Table III shows the effect of ionic strength changes in acidic media. The rate constant decreases with increasing salt concentration. One is tempted to suggest from this that the rate-controlling step involves association between unlike charged ions, *i.e.*, H^+ and ReO_4^- . However, the activity of HCl will decrease at higher μ which may also account for this

effect. When Cl^- and NO_3^- or Li^+ and Na^+ are compared, no important rate changes occur. It should be noted, however, that in all solutions using Li salts as the supporting electrolyte some Na^+ is present ($3 \times 10^{-2} M$) from NaReO_4 and in using LiNO_3 some Cl^- is present ($8 \times 10^{-4} M$) from the acid. These quantities are too small to modify the conclusions reached.

Table III: Salt Effects ($T = 25.0^\circ$; $[\text{ReO}_4^-] = 3.00 \pm 0.02 \times 10^{-2} M$; $[\text{H}^+] = 8.0 \times 10^{-4} M$; $k^* = R/[\text{ReO}_4^-][\text{H}_2\text{O}]$ l. mole $^{-1}$ sec $^{-1}$)

Salt	μ	$-\text{Log } k^*$
LiCl	0.0426	4.694
LiCl	0.100	4.723
LiCl	0.169	4.762
NaCl	0.100	4.805
LiNO_3	0.100	4.799

Table IV lists the temperature variation of k^* . In the ranges chosen, the reaction is carried almost completely by either the k_0 , k_1 , or k_2 term. The Arrhenius parameters are

	E^*	Log A
k_0	15.44 ± 0.50	3.47
k_1	4.16 ± 0.15	4.58
k_2	11.15 ± 0.47	4.37

The estimated errors represent one standard deviation as calculated by a weighted linear least-squares treatment.

Table IV: Temperature Dependence ($[\text{ReO}_4^-] = 3.00 \pm 0.02 \times 10^{-2} M$; $\mu(\text{LiCl}) = 0.100$; $k^* = R/[\text{ReO}_4^-][\text{H}_2\text{O}]$ l. mole $^{-1}$ sec $^{-1}$)

Temp, $^\circ\text{C}$	$-\text{Log } k^*$
Neutral Region	
25	7.862
50	6.931
75	5.958
Acidic Region, $[\text{H}^+] = 1.20 \times 10^{-3} M$	
0	4.599
25	4.342
35	4.228
50	4.082
Basic Region, $[\text{OH}^-] = 6.00 \times 10^{-2} M$	
0	5.730
25	5.030
50	4.346

A comparison to previous results¹ can be made at $[\text{H}^+] = 10^{-3} M$ and 0° . When the previous results are converted to k_1 using a second-order hydrogen ion term and interpolating to $[\text{H}^+] = 10^{-3} M$, the value of k_1 is a factor of approximately 2 larger than that observed here. This is not unreasonable in view of the discrepancy between pH as measured by the glass-calomel electrode system and the $[\text{H}^+]$ added as is discussed below. In the neutral region at 0° there is a greater difference in results. The values quoted here are considerably smaller. There are probably two reasons for this: (a) it was not recognized in the early work that the reaction was accelerated by light and the studies were carried out in laboratory light, and (b) evidently in the neutral region the reaction is catalyzed by trace impurities. This is suggested by this work in which the reproducibility is considerably less in the neutral region than on either side of it. For this reason the value of k_0 must be considered to be an upper limit even though samples of NaReO_4 prepared in this work by different methods gave essentially identical results.

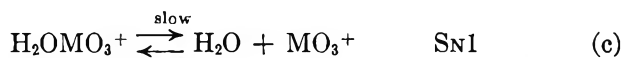
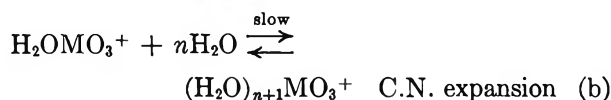
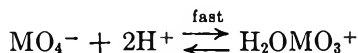
Our earlier paper¹ suggested a two-term rate law (since the basic region was not studied)

$$R/[\text{ReO}_4^-][\text{H}_2\text{O}] = k_0 + k_1[\text{H}^+]^2$$

Our present results show conclusively that the order with respect to $[\text{H}^+]$ is two. The difference in conclusions comes about primarily from the two methods of measuring $[\text{H}^+]$, glass-calomel pH, and amount of acid added. The latter method is more precise and accurate outside of the neutral region. The pH by a glass-calomel electrode system was taken on each of the solutions studied here. A graph of $-\log k^*$ vs. measured pH had no completely straight portions. In the basic region the order with respect to OH^- appeared to be between 0.8 and 1.2 while in the acidic region the slope gradually changed from about 2 to less than 1 going toward less acidic solutions. To check if the measured pH was linear with $-\log [\text{H}^+]$ added, a titration was carried out in the presence and absence of NaReO_4 , LiCl being present. The presence of NaReO_4 had little effect on the curve obtained, but over a wide acidity range the pH as measured by our system showed nonlinear behavior when compared with $-\log [\text{H}^+ \text{ added}]$. Further there was considerably more scatter when R was graphed against pH than when against $-\log [\text{H}^+ \text{ added}]$. This coupled with the added inaccuracies caused by measuring the pH at 0° led to an incorrect order with respect to H^+ in the previous work.

Many oxyanions such as SO_4^{2-} , NO_3^- , MnO_4^- , ClO_3^- , BrO_3^- , NO_2^- , and now ReO_4^- show a second-

order rate dependence on H^+ . In certain cases a zero-order rate term has also been established and it is surprising that with most of the above ions no first-order path in H^+ can be demonstrated. It is generally agreed that a preassociation of the oxyanion with $2H^+$ occurs before the rate-determining step and there are several lines of evidence suggesting this. Three mechanisms are consistent with the rate law for this path.



Reactions a and b are nearly identical, differing only in whether the expanded coordination number (C.N.) has a finite stability or exists only in the transition state. The question with respect to whether the H^+ 's both reside on a single oxygen or are on two oxygens is unanswered. Mechanism a is most reasonable for NO_3^- and BrO_3^- since Cl^- catalysis has been observed, Cl^- apparently being effective in displacing H_2O from $H_2ONO_2^+$. With ReO_4^- and other tetrahedral ions, however, there does not appear to be a Cl^- path. SN2 displacement by an incoming group would be more difficult with a tetrahedral ion than with a planar one such as NO_3^- . Thus for ReO_4^- reactions b or c seem more probable. A comparison of the rate constants of MnO_4^- and ReO_4^- is of some help in differentiating between these possibilities. In the measurable region MnO_4^- behaves according to the same rate law as ReO_4^- .⁸

Values of k_0 and k_1 , when written in the same form used here are as follows for MnO_4^- at 30° and $\mu = 0.28$

$$k_0 = 4.5 \times 10^{-7} \quad E^* = 13.1$$

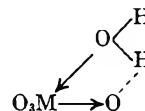
$$k_1 = 3.0 \times 10^{-3} \quad E^* = 11.9$$

and for ReO_4^- at 25° and $\mu = 0.10$

$$k_0 = 1.4 \times 10^{-8} \quad E^* = 15.5$$

$$k_1 = 3.4 \times 10 \quad E^* = 4.2$$

Considering first the noncatalyzed path (k_0), both the rate constants and E^* reflect the tighter Re-O bond compared to that of manganese. This path may be described as a solvent-assisted oxygen dissociation which may be pictured in this fashion



with bond breaking being more important than bond making.

For the H^+ -catalyzed path, ReO_4^- is 10^4 times faster and has a much lower activation energy. In view of the variation of k_0 with the two ions, this behavior would not be expected for path c. Since path a seems unlikely owing to the lack of Cl^- catalysis, path b is suggested. This is in agreement with the known tendency of the larger ion to expand its coordination number. The difference in acidity of HMO_4 or $H_2MO_4^+$ does not appear to modify this conclusion. Thus, these results suggest that acid exchange occurs by an expansion of the Re coordination number.

Little can be said about the mechanism of the base-catalyzed exchange. There is evidence of increased coordination number in strongly basic media where a yellow species is formed whose formula is given as $[ReO_4(OH)_2]^{-3.9}$. Whether the exchange is caused by a displacement by OH^- or by the formation of a species of higher coordination number cannot be discerned at present.

Acknowledgment. The support of the National Science Foundation is gratefully acknowledged.

(8) H. O. McDonald, to be published.

(9) R. D. Peacock, "The Chemistry of Technetium and Rhenium," Elsevier Publishing Co., New York, N. Y., 1966, p 38.

The Radiolysis of Concentrated Neutral Sodium Perchlorate Aqueous Solutions

by J. Konstantatos and D. Katakis

Nuclear Research Center Democritos, Aghia Paraskevi Attikis, Athens, Greece (Received November 7, 1966)

The products of decomposition of ClO_4^- in the γ radiolysis of neutral concentrated aqueous solutions of NaClO_4 are mainly ClO_3^- , ClO_2^- , and possibly some Cl^- . A small amount of ClO_2 was also detected, which decreases further by a postirradiation reaction. The ClO_3^- and ClO_2^- yields were found to be proportional to the NaClO_4 molar concentration up to 8 M. Bromide ion decreases the chlorate and increases the chlorite yields. The formation of H_2O_2 in air-saturated solutions is also influenced by the NaClO_4 concentration, the (H_2O_2) vs. dose curves resembling, however, those obtained in pure neutral water.

Introduction

The so-called direct action of radiation on the perchlorate ion in acid solutions has been studied by a number of investigators¹⁻³ and some of the general features of the mechanism were revealed. In the present paper, these studies are extended to neutral solutions of ClO_4^- . The advantage of the perchlorate system in studying the direct effect of radiation over other systems such as formic acid,⁴ sulfuric acid,⁵ hydrogen peroxide,⁶ nitrate,⁷ etc., is that it seems to be unreactive toward the water free radicals¹ at least in the bulk of the solution and free of confusing chain reactions. In addition, high concentrations can be attained throughout the pH range, and the form of the anion species present (ClO_4^-) remains unchanged, which is not the case in most of the other compounds studied.

In the present work attention is paid to the effect of varying concentrations of Br^- which is used as a scavenger. The reactions of Br^- with the radiolysis products of water in dilute solutions are well known⁸⁻¹⁰ and may be used to draw conclusions about the processes in the radiolysis of water containing large amounts of perchlorate ion.

Experimental Section

Dosimetry and Solutions. The irradiations were made with a Co^{60} source. The rate of energy absorption, ca. 4×10^{19} ev/l. min, was determined with the Fricke dosimeter and corrected on the basis of the electron density of each concentrated NaClO_4 solution.

All reagents were of analytical grade. The NaClO_4 solutions were prepared from the appropriate HClO_4

solutions by neutralization with sodium hydroxide. Solutions prepared from recrystallized analytical grade NaClO_4 were found to contain an impurity which reacted with Fe^{2+} . Such an impurity was not found in solutions prepared by neutralization of HClO_4 .

Analytical Methods. Chloride was determined by potentiometric titration with AgNO_3 using a silver electrode and a calomel electrode with a chloride-free bridge. The determination was done in the absence of Fe^{2+} and Fe^{3+} which interfere with the analysis. The iodide method,¹¹ with ammonium molybdate as a catalyst, sodium hydrogen phthalate as buffer, and NaI instead of KI to avoid precipitation of KClO_4 , could not be used unmodified for the analysis of H_2O_2 at pH 4.5-4.8 in irradiated concentrated NaClO_4 solutions. A product is formed during the radiolysis of such solutions, reacting slowly at this pH with the iodide reagent (Figure 1), whereas H_2O_2 reacts instantly (Figures 1 and 2). At pH 7 the reaction of this product with the iodide reagent becomes negligible, whereas

- (1) D. Katakis and A. O. Allen, *J. Phys. Chem.*, **68**, 3107 (1964).
- (2) M. Cottin, *J. Chim. Phys.*, **53**, 903 (1956).
- (3) B. Milling, G. Stein, and J. Weiss, *Nature*, **170**, 710 (1952).
- (4) D. Smithies and E. J. Hart, *J. Am. Chem. Soc.*, **82**, 4775 (1960).
- (5) J. W. Boyle, *Radiation Res.*, **17**, 427 (1962).
- (6) D. J. Currie and F. S. Dainton, *Trans. Faraday Soc.*, **61**, 1156 (1965); A. R. Anderson and E. J. Hart, *J. Phys. Chem.*, **65**, 804 (1961).
- (7) H. A. Mahlman, *J. Chem. Phys.*, **35**, 936 (1961); **32**, 601 (1960).
- (8) T. J. Sworski, *J. Am. Chem. Soc.*, **76**, 4687 (1954).
- (9) A. O. Allen and R. A. Holroyd, *ibid.*, **77**, 5852 (1955).
- (10) A. Rafi and H. C. Sutton, *Trans. Faraday Soc.*, **61**, 877 (1965).
- (11) C. J. Hochanadel, *J. Phys. Chem.*, **56**, 587 (1952).

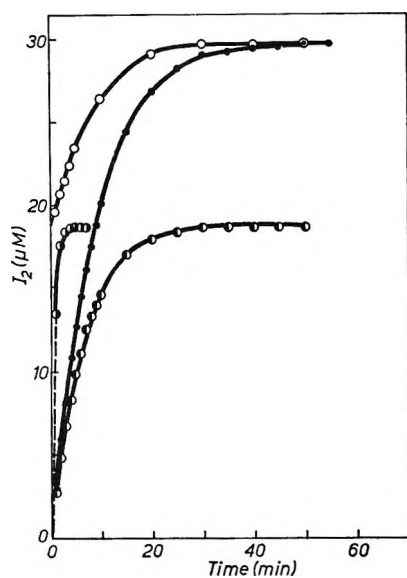


Figure 1. Iodide analysis of a 2.5 M NaClO₄, 10 mM NaBr air-saturated, pH 5.5 solution, irradiated at a dose of ca. 5×10^{21} ev/l.; ○ and ●, pH 4.8 with and without catalyst, respectively; ○ and ●, pH 7 with and without catalyst, respectively.

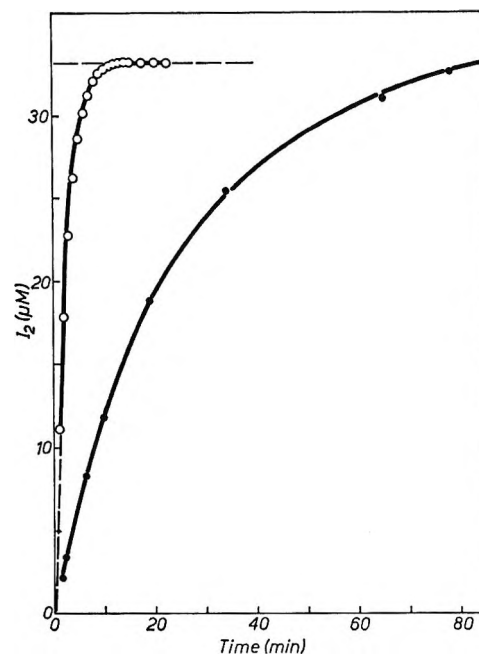


Figure 2. Iodide analysis of H₂O₂: ○, 33 μM H₂O₂ solution at pH 7, with catalyst added; - - -, the value obtained instantly at pH 4.8; ●, 1.2 mM H₂O₂ solution at pH 1.5 without catalyst.

the reaction with H₂O₂ (Figure 2) in the presence of the ammonium molybdate catalyst also slows down, but much less, tending to completion within ca. 10 min. In the absence of the catalyst the reaction of H₂O₂ becomes slower even at pH 4.8 or 1.5.

The values at pH 4.8 in the presence of catalyst (Figure 1) were found to be ca. 10% lower when the analysis was performed 24 hr after the end of irradiation.

The product of decomposition of the perchlorate ion, which has the behavior described above, is identified as the chlorite ion. Chlorate is excluded because, under the condition of the analysis, it does not react with the iodide reagent. Cl₂ and ClO₂ are also excluded as major products, since the results are practically not affected when the irradiated solutions are degassed before the analysis. ClO₂ in particular has a high extinction coefficient, 1300, at 350 mμ.¹² The absorption of the irradiated solutions at this wavelength corresponded, immediately after irradiation, to no more than 1–2 μM ClO₂. Three hours after irradiation even this small absorption disappears. Finally ClO⁻ is also excluded because the irradiated solutions did not give any reaction with iodide (without catalyst) at pH 9 where hypochlorite has been reported¹³ to react. The presence of H₂O₂ in most of the samples is an additional reason for ruling out ClO⁻, which reacts fast with it.¹⁴ BrO⁻ and BrO₂⁻ are also ruled out because they are too reactive to persist in

the irradiated solution and BrO₃⁻ because it is not expected to react with iodide in neutral solution. Only trace amounts of bromine were found in the radiolysis of up to 10 mM aqueous bromide solutions saturated with air.¹⁰

On the basis of these observations the analysis was done as follows.

(a) Chlorite was determined at pH 1.5 where it reacts fast with iodide. At this pH, without catalyst, the reaction of H₂O₂ with I⁻ is slow (Figure 2), amounting to a small correction in the determination of chlorite. The extinction coefficient of iodine at 350 mμ under these conditions is about 2% higher than with the usual iodide reagent.

(b) Determination of the sum of ClO₂⁻ and H₂O₂ is done at pH 4.5 with the iodide reagent containing catalyst. The reaction is complete within 45 min. Peroxide is calculated by subtracting the ClO₂⁻ determined as described in (a). Oxidation of I⁻ by air was taken into account in the blank, both for pH 1.5 and 4.8.

(c) The sum of ClO₃⁻, ClO₂⁻, and H₂O₂ is measured by heating with a Fe²⁺ solution 1 mM in Fe²⁺, 1 M in

(12) W. Buser and H. Hanish, *Helv. Chim. Acta*, **35**, 2547 (1952).

(13) L. A. Prince, *Anal. Chem.*, **36**, 613 (1964).

(14) R. E. Connick, *J. Am. Chem. Soc.*, **69**, 1509 (1947); B. Makower and W. C. Bray, *ibid.*, **55**, 4765 (1933).

HClO₄, containing Cd²⁺ as a catalyst, and spectrophotometric determination of the Fe³⁺ formed, at 240 mμ. From this sum, by subtraction, one calculates chlorate. The presence of excess Fe²⁺ eliminates the possibility of interference by the reactions between the possible intermediate chlorine compounds HClO₂, HClO, and ClO₂⁻¹⁶ and the reaction¹⁴



which are reported to be fast. Besides, except for the reaction of HClO with H₂O₂, the other reactions are not expected to alter the stoichiometry of the over-all oxidation of the ferrous ion.

Results

The only oxygen compounds of chlorine found in appreciable quantities in the radiation-induced decomposition of ClO₄⁻ in neutral concentrated aqueous solutions are ClO₃⁻ and ClO₂⁻. Chloride was found to be formed in small amounts. In a solution 6 M in NaClO₄, with no Br⁻ added, G(Cl⁻) was less than 0.2. The corresponding chloride yield in acid solutions is at least 2–3 times larger. From the absorption at 350 mμ, ClO₂ seems to be present in a low (1–2 μM) steady-state concentration and probably plays an important role during irradiation. Its disappearance after irradiation and perhaps partly during the irradiation also may be due to reaction with H₂O₂. This post-irradiation effect is too small in magnitude to affect appreciably the analysis of the other products. Larger amounts of ClO₂ were found in 8 M NaClO₄ solutions.^{2,16} In acid solutions we found no evidence for the formation of either ClO₂⁻ or ClO₂.

The yields of ClO₃⁻ and ClO₂⁻ at 2 and 6 M NaClO₄ and varying concentrations of bromide are summarized in Table I. The ClO₃⁻ concentration is linear with dose up to 10²² ev/l. in all ClO₄⁻ concentrations studied. The ClO₂⁻ lines usually had an intercept suggesting high initial G values. After this initial period the yields of ClO₂⁻ seemed to be linear with dose, although the low concentrations do not permit a definite statement to be made.

The ClO₃⁻ lines had no intercept. Air and oxygen do not seem to have an effect on the yields of ClO₃⁻, ClO₂⁻, and Cl⁻ larger than experimental error. No decomposition of chlorate was detected in an irradiated air-saturated neutral 0.1 mM KClO₃ solution, in agreement with the observations of Bugaenko.¹⁷ Addition to this solution of 1 mM NaBr did not induce any decomposition of KClO₃ under irradiation.

Bromide ion affects both the chlorate and chlorite formed in neutral concentrated NaClO₄ solutions. With increasing Br⁻ concentration there is a decrease

Table I: Chlorate and Chlorite Yields in Concentrated NaClO₄ Solutions at Various Concentrations of Bromide (pH 5.8–6.0)^a

(NaClO ₄), M	(Br ⁻), mM	G(ClO ₃ ⁻)	G(ClO ₂ ⁻)
2	50	0.41	0.05 ± 0.02
2	10	0.41	0.05 ± 0.02
2	1	0.43	0.05 ± 0.02
2	0.3	0.48	0.05 ± 0.02
2	0.01	0.52	0.05 ± 0.02
2	0	0.58	0.05 ± 0.02
6	10	1.18	0.26
6	1	1.24	0.22
6	0	1.60	0.16

^a No change in pH was recorded after irradiation.

of G(ClO₃⁻), both in aerated and deaerated solutions. The corresponding increase in G(ClO₂⁻) is more clearly illustrated in the results at 6 M NaClO₄; at 2 M NaClO₄ the G values of ClO₂⁻ are too low to permit accurate comparisons. The decrease in G(ClO₃⁻) is somewhat larger than the increase in G(ClO₂⁻). The G(ClO₂⁻) over G(ClO₃⁻) ratio seems to be higher at the higher NaClO₄ concentrations. It is interesting to note that in acid solutions Cl⁻ and Br⁻ were found to protect rather than to decrease the observed chlorate yields.

In deaerated solutions hydrogen peroxide is formed in small nonreproducible amounts, as in the case of pure water¹⁸ and of scavenger-free HClO₄ solutions.¹ The hydrogen peroxide at various concentrations of NaClO₄ and Br⁻ as a function of dose in aerated solutions is given in Figure 3. Contrary to ClO₃⁻, the peroxide concentration is not linear with dose. The amount of the peroxide formed is generally higher at lower bromide concentrations. Increase in the NaClO₄ concentration causes also a decrease in the peroxide formed. The H₂O₂ concentration vs. dose curves at a given bromide concentration bend over faster in the presence of NaClO₄ than in pure water, this being more pronounced at the high NaClO₄ concentrations. At 6 M NaClO₄ and 10 mM NaBr, peroxide is already suppressed to negligible amounts. However, this suppression does not seem to be extended to the initial yields. At 6 M NaClO₄ the initial yield appears much

(15) R. C. Thompson and G. Gordon, *Inorg. Chem.*, **5**, 557, 562 (1966).

(16) L. T. Bugaenko, *Bull. Univ. Moscow, Chem. Ser.*, No. 3, 21 (1961).

(17) L. T. Bugaenko, *Russ. J. Phys. Chem.*, **38**, 2899 (1964).

(18) H. Fricke, E. J. Hart, and H. P. Smith, *J. Chem. Phys.*, **6**, 229 (1938).

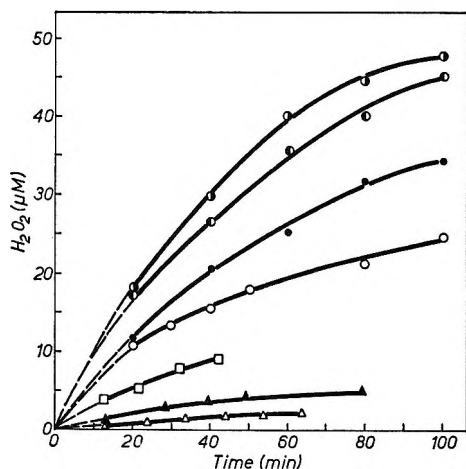


Figure 3. Hydrogen peroxide formation in air-saturated NaClO_4 solutions at pH 5.8–6.0. Dose rate 4×10^{19} ev/l. min; solutions 2 M in NaClO_4 : O, 10 mM; ●, 1 mM; ○, 0.01 mM; and ○, 0 mM NaBr added; □, 4 M NaClO_4 , NaBr 10 mM; △, 6 M NaClO_4 , 10 mM NaBr; ▲, 6 M NaClO_4 , 1 mM NaBr.

smaller than at 2 M NaClO_4 , but this may be partly due to the fast bending of the curves. The initial H_2O_2 production in 2 M NaClO_4 solutions is faster than that reported^{8,9} for water. Allen and Holroyd⁹ have shown that impurities in water cause high initial peroxide yields by removing OH radicals from the system. The possibility that such impurities are introduced in our solutions with the sodium perchlorate cannot be disregarded, although this is probably not the only reason for the high initial yields.

The peroxide concentration *vs.* dose curve obtained with an air-saturated neutral solution containing 1 mM KClO_3 and 1 mM NaBr was essentially identical with the one obtained without KClO_3 . This observation is consistent with the absence of a radiation-induced decomposition of KClO_3 in neutral solutions.

Figure 4 gives $G(\text{ClO}_3^-)$ and the final $G(\text{ClO}_2^-)$ as a function of the NaClO_4 concentration in solutions containing 10 mM NaBr. Up to the concentration studied (8 M NaClO_4) the plot is linear. Deviation from linearity in acid solutions was observed at concentrations as low as 3 M in HClO_4 . The values for $G(\text{ClO}_3^-)$ in scavenger-free solutions reported here generally agree with the values of Cottin,² although they are considerably lower than those of the Russian investigators.

An air-saturated 2 M NaClO_4 solution, carefully freed from carbonate and at pH 7.5, gave within experimental error the same ClO_3^- and ClO_2^- yields as those reported in Table I. Carbonate, therefore,

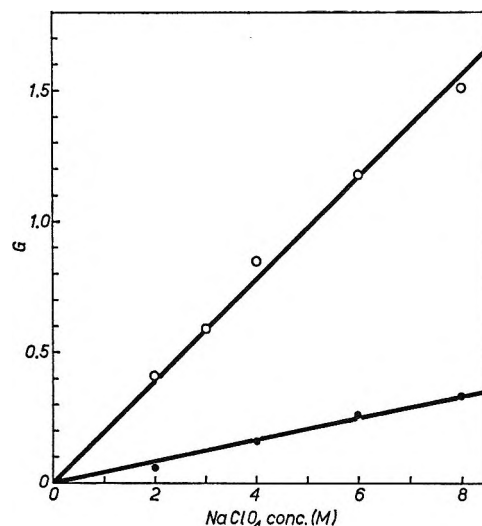


Figure 4. Chlorate and chlorite yields in NaClO_4 solutions 10 mM NaBr: O, ClO_3^- ; ●, ClO_2^- .

or the small difference of pH have no influence on these yields.

Discussion

The proportionality of $G(\text{ClO}_3^-)$ and of the final $G(\text{ClO}_2^-)$ to the NaClO_4 concentration suggests direct effect.^{1–3} Furthermore, the fact that ClO_3^- has rates of formation independent of dose indicates that the ClO_3^- yields do not depend on competition with H_2O_2 for the free radicals in the bulk of the solution. The involvement of ClO_2^- in competition kinetics cannot be excluded because of the intercept in the concentration *vs.* dose lines observed, although this intercept may be due to impurities, as in the case of H_2O_2 . The lack of reproducibility in the values of the intercept favors this interpretation. A small contribution to the chlorate due to reactions of ClO_2^- could hardly be detected. The formation and the reactions that ClO_3^- undergo have ended when this compound or its precursor diffuses out of the spur. Additional evidence that ClO_3^- does not react in the bulk of the solution is provided by the observation that in neutral solutions ClO_3^- is unaffected by radiation, both in the presence and absence of bromide.

Three different values were reported¹⁹ for the rate constant of the hydrated electron with ClO_3^- , covering a range of two orders of magnitude. The reason for this discrepancy is not known, but even the highest value, 3.5×10^8 l. mole⁻¹ sec⁻¹²⁰ is about $1/50$ as large as the corresponding rate constants of H_2O_2 and O_2

(19) M. Anbar and P. Neta, Report of Israel Atomic Energy Commission, IA-1079, 1966.

(20) J. H. Baxendale, *et al.*, *Nature*, **201**, 468 (1964).

which are present in our system in concentrations comparable to or even higher than (ClO_3^-) . With the lowest value, $4 \times 10^6 \text{ l. mole}^{-1} \text{ sec}^{-1}$,²¹ the reaction of e_{aq}^- with ClO_3^- is even more unfavorable. Moreover, the lack of an effect by KClO_3 in neutral solutions on the peroxide yield seems also to indicate negligible scavenging by this compound of OH radicals.

One of the arguments that can be advanced is that the reactions which the products of decomposition of ClO_4^- or ClO_4^- itself possibly undergo do not affect the qualitative features of the phenomenological kinetics of the $\text{H}_2\text{O}_2\text{-O}_2$ system, at least after a short initial period. Both in aerated and deaerated solutions the H_2O_2 formation has the same general characteristics as in neutral water. The effect of Br^- in particular in decreasing the H_2O_2 formed at a given dose, the nonlinearity of the H_2O_2 vs. dose plots, and the low, irreproducible H_2O_2 yields in deaerated solutions are all phenomena familiar from the radiolysis of dilute neutral water solutions. No attempt is made in this paper to make a complete analysis of the $\text{H}_2\text{O}_2\text{-O}_2$ system. It is only pointed out that the peroxide yields obtained (Figure 3) are consistent with the results obtained in concentrated perchloric acid solutions.¹ There it was found that not only the molecular hydrogen but also the hydrogen atom yield decrease with increasing ClO_4^- concentration, which led to the conclusion that ionization of ClO_4^- to ClO_4 and e_{aq}^- is relatively unimportant. More specifically, the decrease at higher NaClO_4 concentrations of the peroxide formed at a given dose can be considered as a consequence of a corresponding decrease in the difference, expressed in equivalents, between the G values of the reducing species (*e.g.*, H, e_{aq}^- , H_2O_2) and those of the oxidizing species (*e.g.*, OH, oxygen atoms) and to reactions of H_2O_2 with the radiolysis products of ClO_4^- (*e.g.*, with ClO_2).

Reactions of HO_2 or further stepwise free-radical reduction of the radiolysis products of ClO_4^- are unlikely since such processes are expected to depend on whether oxygen is present or not in the system, contrary to our observations.

The observed decrease in $G(\text{ClO}_3^-)$ and increase in final $G(\text{ClO}_2^-)$ when Br^- is added to the concentrated NaClO_4 solutions may be due to one or more of the following reasons.

(a) Bromide facilitates the reformation of ClO_4^- from ClO_3^- or from precursors of ClO_3^- , or somehow inhibits the formation of ClO_3^- from ClO_4^- .

(b) It causes further reduction of ClO_3^- or its precursors.

(c) It inhibits the oxidation of lower oxidation states of chlorine to ClO_3^- .

The results of Table I and in particular at 2 M NaClO_4 show that the chlorate yield does not change when bromide concentration is increased beyond a certain limit (*ca.* 10 mM). This indicates that any process for the effect of bromide must be considered as taking place in the bulk of the solution rather than in the spur. Generally, of course, one expects Br^- to react with OH but the present experiments do not provide a means to distinguish between the resulting bromine atoms and the OH radicals in the spurs. The results, however, obtained with helium ions¹ showed that free radicals in the spur induce the decomposition of the excited perchlorate ion or inhibit the reformation of ClO_4^- . It was also suggested, based on the linearity of the G values of the decomposition products with the ClO_4^- concentration, that at least at moderate concentrations the reformation of ClO_4^- or dissipation of its excitation energy involves one species from perchlorate and one or none from H_2O rather than two species from perchlorate.

Part of the difference in the ClO_3^- yield in the presence of Br^- appears as ClO_2^- . The rest may be attributed to an over-all decrease in $G(-\text{ClO}_4^-)$ or a further reduction, eventually to Cl^- . The fact that KClO_3 in neutral solutions does not decompose under irradiation and that KClO_3 does not affect the H_2O_2 yield indicates that if process (b) operates, it refers to the effect of Br^- on the precursors of ClO_3^- rather than on ClO_3^- itself.

On the basis of the above arguments the reactions



must be postulated as taking place in the bulk of the solution. The effect of Br^- on the perchlorate decomposition products in neutral solutions can be attributed mainly to suppression of reaction 1. The low concentration of ClO_2 suggests that reaction 1 is fast, in agreement with Bugaenko.¹⁷ From the results of Table I and Figure 3 one can estimate that the rate constant for reaction 1 is of the same order of magnitude as that for the reaction of OH with Br^- .

Acknowledgment. This work was performed under the auspices of the Greek Atomic Energy Commission. The authors are grateful to Dr. A. O. Allen who, during his stay at the N.R.C. Democritos as an expert from the International Atomic Energy Agency, made valuable suggestions and constructive criticism of this work.

(21) J. K. Thomas, S. Gordon, and E. J. Hart, *J. Phys. Chem.*, **68**, 1524 (1964).

Physicochemical Properties of Hexamethylenetetramine Aqueous Solutions

by G. Barone, V. Crescenzi, A. M. Liquori, and F. Quadrifoglio

Centro Nazionale di Chimica delle Macromolecole (CNR) Sezione III, Istituto Chimico, Università di Napoli, Naples, Italy (Received November 8, 1966)

Some experimental results concerning physicochemical properties of the hexamethylenetetramine (HMT)-water system are discussed. These results indicate that HMT behaves as a typical water structure reinforcing agent. As an interesting aspect of this property, the influence exerted by HMT on hydrophobic interactions in simple systems is illustrated.

Hexamethylenetetramine (HMT) solubility in water decreases with increasing temperature.¹ This property, which is shared by some other tertiary amines, is explicable in terms of increasing association with water at low temperatures. Furthermore, by decreasing the temperature of a saturated HMT aqueous solution toward 0° an HMT hexahydrate is easily obtained. For this hydrate, X-ray data have revealed a novel type of clathrate structure in which each HMT molecule is located in a cage within a clathrating framework of hydrogen-bonded water molecules.²

HMT also forms a large series of complexes with different inorganic salts, linking a high number of water molecules, the crystal structure of some of which has been recently determined in detail.^{3,4} All of these findings clearly suggest that HMT should exert a marked influence on water structural organization also at room temperature. HMT might thus also influence the occurrence of certain phenomena in aqueous systems in which hydrophobic interactions are of critical importance.

The interesting possibility has prompted an investigation, which is being carried out in this laboratory, on some physicochemical properties of HMT aqueous solutions. Properties studied include, besides density, viscosity and near-infrared spectra of HMT-water systems, their solubilizing power toward some hydrocarbons, and the effect on micellization of colloidal electrolytes.

We wish to report here some preliminary results of this investigation. For comparison purposes, data regarding analogous properties of urea and methylurea are also reported.

In Figure 1, the relative density and the relative

viscosity at 25° of HMT aqueous solutions are plotted as functions of HMT molality. In the same plot, similar data for urea and methylurea are also reported. All HMT, urea, and methylurea (carefully purified samples) solutions were prepared shortly before use at room temperature to avoid hydrolysis of the compounds. The apparent potentiometric pH of the more concentrated solutions of HMT is below 9.

The density and particularly the viscosity of HMT-water solutions suggest that HMT would exert an influence on solvent organization. An indication of this is also obtained by considering the near-infrared spectra of water in 2.5 *M* HMT solution reported in Figure 2 together with those of water in 8 *M* methylurea and urea solutions. With reference also to the spectra reported by Buijs and Choppin,⁵ HMT appears to exhibit a unique structure-forming power.

In Figure 3, data are reported on the solubility at 25° of *n*-pentane in HMT, urea, and methylurea aqueous solutions, respectively, determined by means of a gas chromatographic procedure.⁶ S_r is the increment in *n*-pentane solubility in the aqueous solutions relative to the solubility in water at 25°. Higher solubility of *n*-pentane is thus seen to occur in the HMT solutions. A few data on the solubility at 25° of pyrene and 3,4-benzpyrene in HMT, urea, and methylurea solutions

(1) J. F. Walker, "Formaldehyde," 3rd ed, Reinhold Publishing Corp., New York, N. Y., 1964, p 524.

(2) T. C. W. Mak, *J. Chem. Phys.*, **43**, 2799 (1965).

(3) P. DeSantis, A. L. Kovacs, A. M. Liquori, and L. Mazzarella, *J. Am. Chem. Soc.*, **87**, 4965 (1965); L. Mazzarella, A. L. Kovacs, P. DeSantis, and A. M. Liquori, *Acta Cryst.*, in press.

(4) A. L. Kovacs and L. Mazzarella, *Ric. Sci.*, in press.

(5) K. Buijs and G. R. Choppin, *J. Chem. Phys.*, **39**, 3025 (1963).

(6) G. Barone, V. Crescenzi, B. Pispisa, and F. Quadrifoglio, to be published.

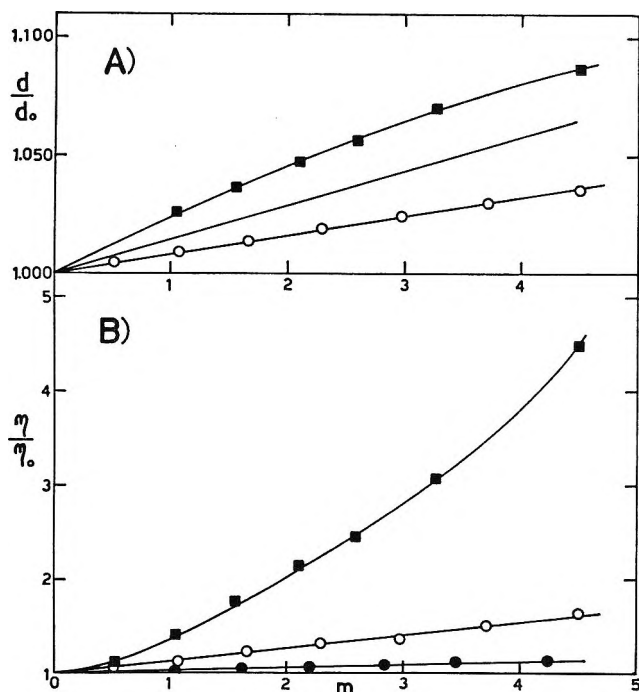


Figure 1. (A) Relative density at 25° of urea (O, methylurea and ■, hexamethylenetetramine aqueous solutions) as a function of molality. The line for urea has been drawn using the data reported by F. T. Gucker, Jr., F. W. Gage, and C. E. Moser, *J. Am. Chem. Soc.*, **60**, 2582 (1938). (B) Relative viscosity at 25° of ●, urea, O, methylurea, and ■, hexamethylenetetramine aqueous solutions as a function of molality, m .

obtained by means of experimental procedures fully illustrated elsewhere⁷ are reported in Table I.⁸

Table I

Hydrocarbon	Solubility at 25°, in moles/l.			
	H ₂ O	8 M urea	2.9 M HMT	8 M methylurea
Pyrene	7.7×10^{-7a}	6.6×10^{-6}	4.4×10^{-5}	1.4×10^{-4}
3,4-Benzopyrene	1.9×10^{-8b}	1.8×10^{-7}	2.8×10^{-6}	1.3×10^{-5}

^a See ref 8. ^b See ref 7.

Concentrations of solubilizing agent were chosen in order to obtain figures for the solubility of the two polycyclic hydrocarbons studied, of the maximum attainable accuracy in each case.

Studies carried out by different authors⁹⁻¹¹ have shown that urea increases the critical micelle concentration (cmc) of typical colloidal electrolytes, such as sodium lauryl sulfate (NaLS). Our results indicate

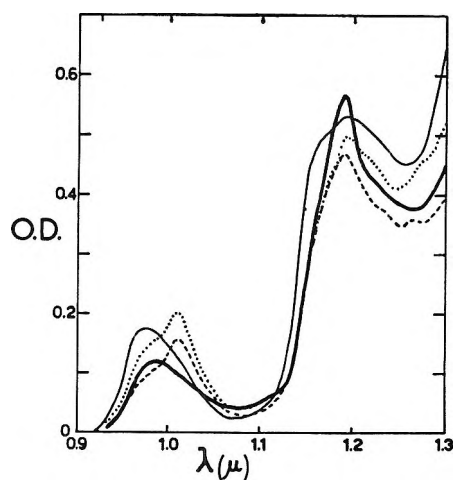


Figure 2. Near-infrared spectra at 25° of: —, water, and of water in: - - -, 8 M methylurea; ····, 8 M urea; and — · —, 2.5 M hexamethylenetetramine. Optical path = 1.000 cm.

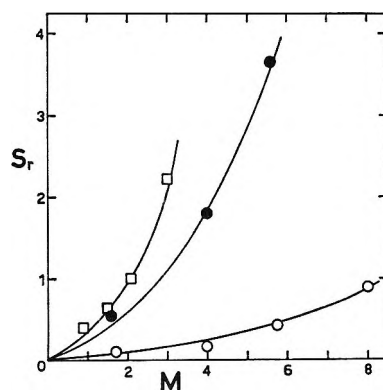


Figure 3. Relative increment in solubility, S_r , at 25° of n -pentane in: O, urea, ●, methylurea, and □, hexamethylenetetramine aqueous solutions (with respect to n -pentane solubility in water at 25°)⁸ as a function of the concentration, M , of the latter three compounds.

that methylurea, and more so HMT, are capable of exerting a similar action, to a higher degree. This is illustrated in Figure 4, in which the specific conductivity of NaLS in H₂O, 2 M methylurea, 1 M and 2 M HMT, respectively, is plotted against NaLS concentration. Critical micelle concentration is revealed in

(7) G. Barone, V. Crescenzi, A. M. Liquori, and F. Quadrifoglio, *J. Phys. Chem.*, in press.

(8) H. B. Klevens, *J. Phys. Chem.*, **54**, 283 (1950); W. W. Davis, M. E. Krahl, and G. H. A. Clowes, *J. Am. Chem. Soc.*, **64**, 108 (1942).

(9) P. Mukerjee and A. Ray, *J. Phys. Chem.*, **67**, 190 (1963).

(10) W. Bruning and A. Holtzer, *J. Am. Chem. Soc.*, **83**, 4865 (1961).

(11) M. J. Schick, *J. Phys. Chem.*, **68**, 3585 (1964).

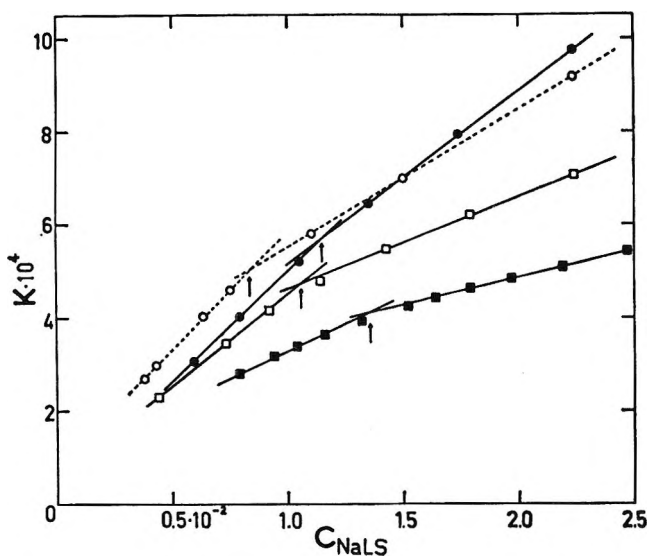


Figure 4. Specific conductivity of sodium lauryl sulfate (NaLS) in: \circ , water; \bullet , 2 *M* methylurea; \square , 1 *M* hexamethylenetetramine; and \blacksquare , 2 *M* hexamethylenetetramine at 25°. Concentration of colloidal electrolyte is given as equivalents per liter of solution.

the plots of Figure 4 by the breaks in the dependence of specific conductivity upon colloidal electrolyte con-

centration. Details on the experimental procedure and other results will be soon reported and discussed elsewhere.¹²

It is relevant to point out here that the cmc for NaLS in 2 *M* methylurea is shifted to $1.15 \times 10^{-2} N$, while in 2 *M* HMT it is $1.35 \times 10^{-2} N$ as compared to the cmc value in water, $0.81 \times 10^{-2} N$. Similar but less marked effects have been found by Schick¹¹ in his investigation on the influence of urea on the cmc of NaLS, by means of surface tension measurements.

The set of data reported here appears to afford, in our opinion, evidence that HMT behavior in aqueous solution has many points of similarity with those typical of strong water-structure perturbing agents. These observations deserve further detailed investigations: work is being carried out along these lines in our laboratory. The study of the possible influence of HMT on the stability of biological macromolecules secondary structures in water appears a logical extension of the present research.

(12) HMT is a very weak base, and its limited ionization should not affect appreciably, by itself, the cmc of NaLS. See H. Tada, *J. Am. Chem. Soc.*, **82**, 255 (1960).

Diffusion in Binary Solutions¹

by David W. McCall and Dean C. Douglass

Bell Telephone Laboratories Inc., Murray Hill, New Jersey (Received August 1, 1966)

Experimental self-diffusion results are reported for the binary systems benzene-cyclohexane, acetone-chloroform, acetone-benzene, and acetone-water. Data were recorded as a function of concentration at 25° using the nmr spin-echo method. The data are discussed in connection with mutual diffusion results, previously published, with particular emphasis on the equations $D = (\partial \ln a_1 / \partial \ln x_1)(x_1 D_2 + x_2 D_1)$ (Hartley-Crank and Darken) and $D = D_1(\partial \ln a_1 / \partial \ln c_1)$ (Bearman and Eyring). These equations are qualitatively but not quantitatively descriptive of the experimental data. A theoretical analysis is presented in which the mutual and self-diffusion coefficients are expressed in terms of integrals of molecular velocity correlation functions. This analysis approaches a molecular view of the three diffusion coefficients and gives some insight into the nature of the Hartley-Crank relationship.

I. Introduction

In this paper we discuss diffusion in binary liquid solutions of nonelectrolytes. Two groups of experiments can be distinguished—self-diffusion and mutual diffusion. Self-diffusion is a measure of the mobility of the molecules. It occurs in chemically uniform systems and it is made experimentally accessible by isotopic labeling or application of a magnetic field gradient in nmr spin-echo studies. In binary solutions there are two self-diffusion coefficients, one for each component. If $\langle r_i^2 \rangle$ is the mean-square displacement of a molecule of component i in time τ , the self-diffusion coefficient of component i is given by

$$D_i = \langle r_i^2 \rangle / 6\tau \quad (1)$$

Mutual diffusion studies, on the other hand, are concerned with the rate at which concentration gradients approach their equilibrium values (zero in miscible systems). In general, one can show that a single diffusion coefficient is sufficient in binary systems to describe this rate and we call this the mutual diffusion coefficient, D . Intuitively we expect D to be closely related to D_1 and D_2 and, in fact, for thermodynamically ideal solutions, it has been claimed that^{2a}

$$D_{12} \equiv x_1 D_2 + x_2 D_1 = D \quad (2)$$

where the x values are mole fractions. Equation 2 is derived from the requirement that the pressure within

the system must remain uniform. That is, if one component diffuses much more rapidly than the other, there must be a compensating bulk flow to keep the molecules from piling up at one end of the container.

Thermodynamic considerations must enter the discussion of mutual diffusion because the driving force for mutual diffusion is the gradient of the chemical potential rather than the concentration gradient. It follows^{2b} that the mutual diffusion coefficient is proportional to $(\partial \ln a_i / \partial \ln c_i)_{T,p}$, where a_i and c_i are the activity and concentration of component i . An equation that incorporates the mixture rule of eq 2 and the thermodynamic factor is

$$D = Q(x_1 D_2 + x_2 D_1) \quad (3)$$

$$Q = [1 + (\partial \ln \gamma_1 / \partial \ln x_1)_{T,p}] \quad (4)$$

where γ_1 is the mole fraction activity coefficient. This equation can be regarded as a form of the Hartley-Crank relation.³ Bearman^{2b} has given an illuminating discussion of the basis for this and other relations between D and D_1 and D_2 .

(1) Some of the data reported herein were previously published in a preliminary note (D. W. McCall and E. W. Anderson, *J. Phys. Chem.*, **70**, 601 (1966)). The preliminary data were not corrected for the isotope effect and the present paper supersedes the earlier note.

(2) (a) J. E. Mayer and M. G. Mayer, "Statistical Mechanics," John Wiley and Sons, New York, N. Y., 1940, p 30; (b) R. J. Bearman, *J. Phys. Chem.*, **65**, 1961 (1961).

(3) G. S. Hartley and J. Crank, *Trans. Faraday Soc.*, **45**, 801 (1949).

Equation 3 and other relations between mutual and self-diffusion parameters have often been discussed but rarely tested directly. Adequate data on activity and self-diffusion are unavailable for most systems. In the present study we have determined the self-diffusion coefficients for four binary systems at 25°. Thermodynamic data exist for all four of the solutions studied. The systems are: benzene-cyclohexane, acetone-benzene, acetone-chloroform, and acetone-water. Mutual diffusion coefficients have been reported for the acetone solutions by Anderson, Hall, and Babb⁴ and Rodwin, Harpst, and Lyons⁵ have studied mutual diffusion in the benzene-cyclohexane solutions. Self-diffusion results relevant to the latter system have been reported by Collins and Watts⁶ and Birkett and Lyons.⁷ A tracer study by Mills⁸ has appeared more recently in which self-diffusion⁹ coefficients for both components of the benzene-cyclohexane system were measured. The agreement between Mills' tracer data and the nmr data reported herein is gratifying. Albright and Mills⁹ prefer the term *intradiffusion* to self-diffusion in the discussion of results for solutions. We use the term self-diffusion in discussing results determined by the nmr method whether the medium contains more than one kind of molecule or not.

II. Experimental Section

The proton magnetic resonance spin-echo method has been used in this study.^{10,11} All data were obtained at $25 \pm 1^\circ$. The absolute accuracy of the method has been estimated as somewhat better than 5% for liquids with strong resonance signals. In solutions dilute in protons, the accuracy is not as good. For example, in our spectrometer the 0.18 mole fraction of CHCl_3 in $(\text{CD}_3)_2\text{CO}$ solution had a signal-to-noise ratio of about 5 and the results are probably accurate to within 10%.

The deuterated compounds were obtained from Merck Sharp and Dohme of Canada except for the d_{12} cyclohexane which was purchased from Volk Radiochemical Co. Isotopic purity was stated to be greater than 99% in each case. The solutions were examined by means of high-resolution nmr and it was found that no hydrogen-deuterium exchange occurred and that the resonance from the undesired compound was always negligible.

The method involves the use of solutions for which one component is completely deuterated so that the other component can be studied separately. This procedure introduces some error, however, owing to the isotope effect on the self-diffusion rate. That is, deuteration of one component increases the viscosity and decreases the diffusion rate of the other component.

To correct for this effect, we have made self-diffusion measurements on the undeuterated solutions. The peak echo voltage is given by¹¹

$$V(\tau, G) = \sum_{i=1}^2 V_i(\tau, 0) \exp[-2(\gamma G)^2 \tau^3 D_i / 3] \quad (5)$$

where G is the magnetic field gradient and τ is the echo time. $V_i(\tau, 0)$ is the decay function for the i th component in a homogeneous field, $G = 0$. For the substances investigated in this study, $V_i(\tau, 0) = V_i(0, 0)$ for all τ of interest. $V_i(0, 0)/V(0, 0) \equiv p_i$ is the fraction of protons in component i . $p_i = x_i z_i$ where z_i is the number of protons for each i molecule. In the two-component systems studied here

$$V(\tau, G)/V(0, 0) = p_1 \exp(-KD_1\tau^3) + p_2 \exp(-KD_2\tau^3) \quad (6)$$

A trial and error procedure has been adopted. $V(\tau, G)/V(0, 0)$ is measured as a function of τ . The right-hand side of eq 6 is calculated for a given τ using D_1 and D_2 obtained from the deuterated solutions at the same concentration. D_1 and D_2 are then increased a few per cent and the right-hand side is recalculated. This is continued until the calculated and observed $V(\tau, G)/V(0, 0)$ agree. Then a new τ is picked and further adjustments are made, if necessary. The corrections have not exceeded 10%.

We would not claim that these isotope-effect corrections are very accurate, but the magnitudes seem to be reasonable. In analyzing our data, we have applied the same correction to both components at a given concentration. Even though this may not appear to be entirely logical, the result is consistent with the data.

III. Results

The data for the benzene-cyclohexane system are plotted in Figure 1 for comparison with the data of Mills.⁸ The agreement is excellent by our standards of accuracy. Figure 2 shows our data in comparison with the mutual diffusion results of Rodwin, Harpst, and Lyons.⁵ The proper limiting behavior is observed.

(4) D. K. Anderson, J. R. Hall, and A. L. Babb, *J. Phys. Chem.*, **62**, 404 (1958).

(5) L. Rodwin, J. A. Harpst, and P. A. Lyons, *ibid.*, **69**, 2783 (1965).

(6) D. A. Collins and H. Watts, *Australian J. Chem.*, **17**, 516 (1964).

(7) J. D. Birkett and P. A. Lyons, *J. Phys. Chem.*, **69**, 2782 (1965).

(8) R. Mills, *ibid.*, **69**, 3116 (1965).

(9) J. G. Albright and R. Mills, *ibid.*, **69**, 3120 (1965).

(10) H. Y. Carr and E. M. Purcell, *Phys. Rev.*, **94**, 630 (1954).

(11) D. C. Douglass and D. W. McCall, *J. Phys. Chem.*, **62**, 1102 (1958).

$$\lim_{x_c \rightarrow 0} D = D_c$$

$$x_c \rightarrow 0$$

and

$$\lim_{x_b \rightarrow 0} D = D_b \quad (7)^{12}$$

$$x_b \rightarrow 0$$

The isotope corrections amounted to about 4% in the middle concentration range.

Self-diffusion results for the acetone solutions are compared with mutual diffusion results of Anderson, Hall, and Babb⁴ in Figures 3-5. In each case the limiting behavior, eq 7, is satisfactory. The isotope correction was negligible for the acetone-benzene system. In the acetone-chloroform solutions the isotope cor-

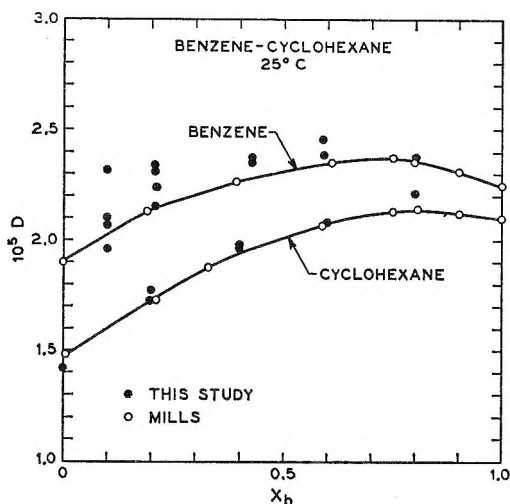


Figure 1. Comparison of nmr self-diffusion results with the tracer data of Mills³ for the system benzene-cyclohexane at 25°.

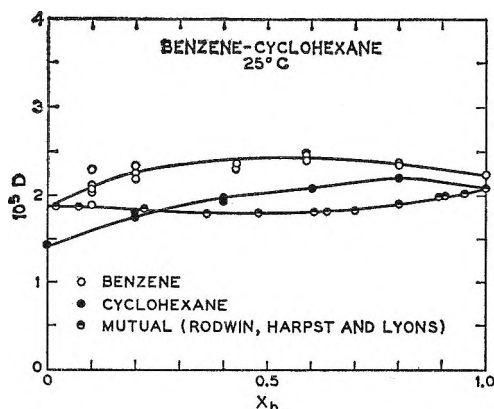


Figure 2. Concentration dependence of mutual⁶ and self-diffusion coefficients (cm²/sec) for the system benzene-cyclohexane at 25°.

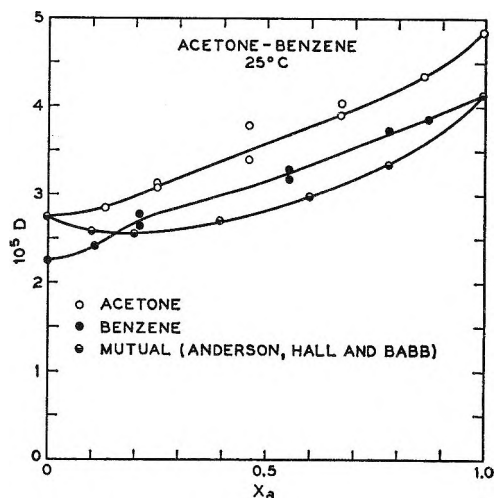


Figure 3. Concentration dependence of mutual⁴ and self-diffusion coefficients (cm²/sec) for the system acetone-benzene at 25°.

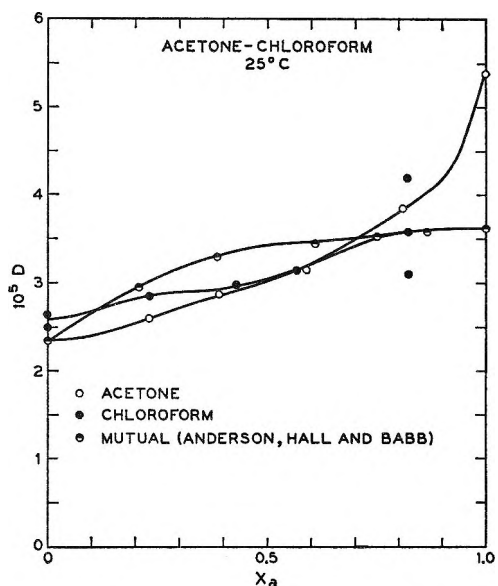


Figure 4. Concentration dependence of mutual⁴ and self-diffusion coefficients (cm²/sec) for the system acetone-chloroform at 25°.

rection was not appreciable at high acetone concentrations (≥ 0.8) and peaked at about 10% near $x_a = 0.2$. In the acetone-water system the isotope correction was 9% in the middle concentration range falling to 3% at $x_a = 0.3$.

IV. Discussion

As noted in the Introduction, a form of the Hartley-

(12) We use the subscripts b, c, a, and w to identify the components benzene, cyclohexane, acetone, and water.

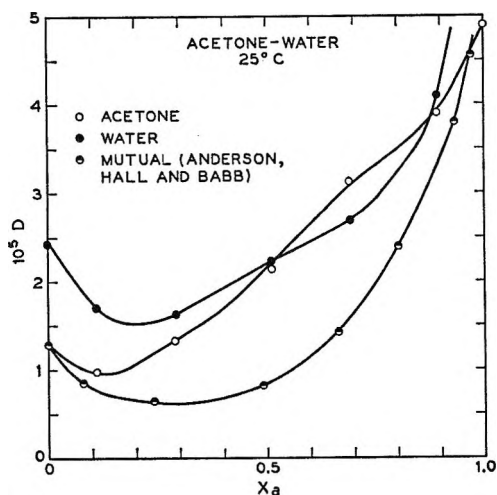


Figure 5. Concentration dependence of mutual⁴ and self-diffusion coefficients (cm^2/sec) for the system acetone-water at 25° .

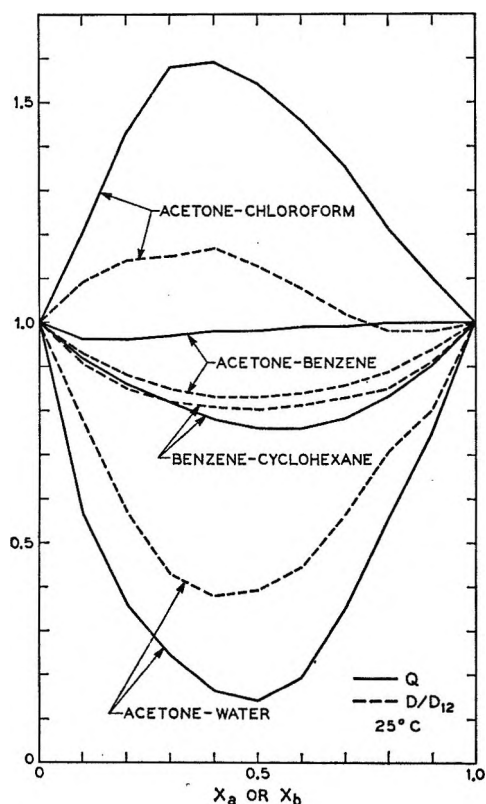


Figure 6. Comparison of the thermodynamic factor $Q = (\partial \ln a_1 / \partial \ln x_1)_{T,p}$, with the diffusion ratio $D/(x_1 D_2 + x_2 D_1)$ at 25° .

Crank relation, eq 3, would indicate that D/D_{12} should equal $Q = (\partial \ln x_1 \gamma_1 / \partial \ln x_1)_{T,p}$. An empirical comparison of these quantities is given in Tables I, II, III, and IV and Figure 6. The thermodynamic factor

Table I

x_b	Benzene-cyclohexane 25°					Q
	$10^5 D_b$	$10^5 D_c$	$10^5 D_{bc}$	$10^5 D$	D/D_{bc}	
0.0	1.88	1.42	1.88	1.88	1.00	1.00
0.1	2.11	1.58	2.05	1.87	0.91	0.92
0.2	2.26	1.76	2.17	1.84	0.85	0.86
0.3	2.34	1.87	2.20	1.80	0.82	0.82
0.4	2.41	1.97	2.23	1.80	0.81	0.78
0.5	2.44	2.03	2.24	1.80	0.80	0.76
0.6	2.44	2.09	2.24	1.81	0.81	0.76
0.7	2.42	2.15	2.24	1.85	0.83	0.78
0.8	2.38	2.21	2.24	1.91	0.85	0.83
0.9	2.31	2.14	2.16	1.97	0.91	0.90
1.0	2.25	2.09	2.09	2.09	1.00	1.00

Table II

x_a	Acetone-benzene 25°					Q
	$10^5 D_a$	$10^5 D_b$	$10^5 D_{ab}$	$10^5 D$	D/D_{ab}	
0.0	2.75	2.28	2.75	2.75	1.00	1.00
0.1	2.81	2.38	2.77	2.58	0.93	0.96
0.2	2.97	2.67	2.90	2.56	0.88	0.96
0.3	3.19	2.86	3.09	2.61	0.85	0.97
0.4	3.39	3.01	3.24	2.70	0.83	0.98
0.5	3.59	3.16	3.38	2.81	0.83	0.98
0.6	3.79	3.35	3.52	2.97	0.84	0.99
0.7	3.99	3.54	3.68	3.16	0.86	0.99
0.8	4.18	3.74	3.83	3.42	0.89	1.00
0.9	4.46	3.93	3.98	3.72	0.94	1.00
1.0	4.86	4.12	4.12	4.12	1.00	1.00

was computed from published data.¹³⁻¹⁶ Room-temperature activity data were available only for the acetone-chloroform system.

It is obvious that D/D_{12} and Q are qualitatively similar. Deviations from unity are in the same direction in each case. The acetone-water system exhibits the largest deviation in both quantities. The concentration at which Q and D/D_{12} deviate most from unity seems to be the same: $x_a = 0.45$ for acetone-water; $x_a = 0.40$ for acetone-chloroform; and $x_b = 0.55$ for benzene-cyclohexane. For acetone-benzene the deviation of Q from unity probably lies within experimental error. Quantitative agreement, within the estimated 5% accuracy range, is observed only for the benzene-cyclohexane solutions.

(13) (a) G. Scatchard, S. E. Wood, and J. M. Mochel, *J. Phys. Chem.*, **43**, 119 (1939); (b) W. Reinders and C. H. de Minjer, *Rec. Trav. Chim.*, **59**, 369 (1940).

(14) H. Rock and W. Schroder, *Z. Physik. Chem. (Frankfurt)*, **11**, 41 (1957).

(15) D. F. Othmer and R. F. Benenati, *Ind. Eng. Chem.*, **37**, 299 (1945).

(16) R. York and R. C. Holmes, *ibid.*, **34**, 345 (1942).

Table III

x_a	Acetone-chloroform 25°					Q
	$10^5 D_a$	$10^5 D_o$	$10^5 D_{ao}$	$10^5 D$	D/D_{ao}	
0.0	2.35	2.58	2.35	2.35	1.00	1.00
0.1	2.41	2.67	2.45	2.67	1.09	1.20
0.2	2.54	2.83	2.60	2.97	1.14	1.43
0.3	2.72	2.89	2.77	3.18	1.15	1.58
0.4	2.86	2.91	2.88	3.37	1.17	1.59
0.5	3.02	3.05	3.04	3.44	1.13	1.54
0.6	3.23	3.21	3.22	3.47	1.08	1.46
0.7	3.49	3.42	3.44	3.52	1.02	1.36
0.8	3.80	3.60	3.64	3.56	0.98	1.21
0.9	4.20	3.62	3.68	3.60	0.98	1.10
1.0	4.90	3.62	3.62	3.62	1.00	1.00

Table IV

x_a	Acetone-water 25°				D/D_{aw}	Q
	$10^5 D_a$	$10^5 D_w$	$10^5 D_{aw}$	$10^5 D$		
0.0	1.28	2.45	1.28	1.28	1.00	1.00
0.1	0.97	1.74	1.05	0.82	0.78	0.57
0.2	1.08	1.51	1.16	0.66	0.57	0.36
0.3	1.36	1.64	1.45	0.62	0.43	0.24
0.4	1.70	1.91	1.78	0.67	0.38	0.16
0.5	2.14	2.20	2.17	0.85	0.39	0.14
0.6	2.65	2.44	2.52	1.12	0.44	0.19
0.7	3.13	2.74	2.86	1.60	0.56	0.35
0.8	3.50	3.23	3.27	2.32	0.71	0.56
0.9	3.99	4.24	4.22	3.39	0.80	0.76
1.0	4.94	~5.5	~5.5	~5.5	1.00	1.00

Bearman^{2b} has proposed that rate-process theory¹⁷ will yield a relation between D and D_1 or D_2 . The relation he suggests is

$$D = D_1 (\partial \ln f_1 c_1 / \partial \ln c_1)_{T,p} \equiv Q_1 D_1 \quad (8)$$

where f is the activity coefficient appropriate to the molar concentration, c . Note that this thermodynamic factor is not the same as the mole fraction thermodynamic factor, eq 4 *i.e.*, $Q_1 \neq Q$. Further, $Q_1 \neq Q_2$. The factors are related by

$$Q_1 = Q (\partial \ln x_1 / \partial \ln c_1)_{T,p} \quad (9)$$

Solution densities were taken from the "International Critical Tables."¹⁸

We have evaluated Q_1 and Q_2 for the solutions studied. These results and the comparisons relevant to eq 8 are shown in Table V. Figures 7-10 exhibit the results graphically. The solid lines are the computed mutual diffusion coefficients and the circles are literature data points.^{4,5} Keep in mind that no adjustments have been made; the solid lines are taken from self-diffusion and thermodynamic data by means

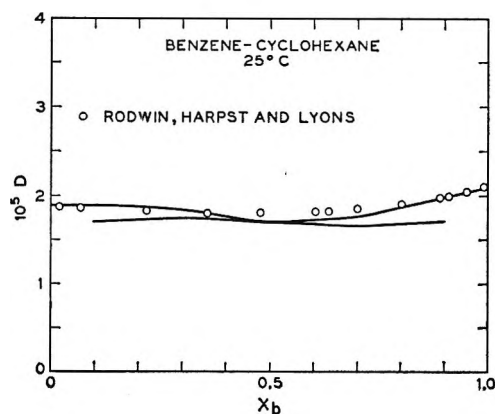


Figure 7. Comparison of mutual diffusion data⁶ with predictions based on eq 8 for the system benzene-cyclohexane at 25°. The solid curves are calculated results, eq 8.

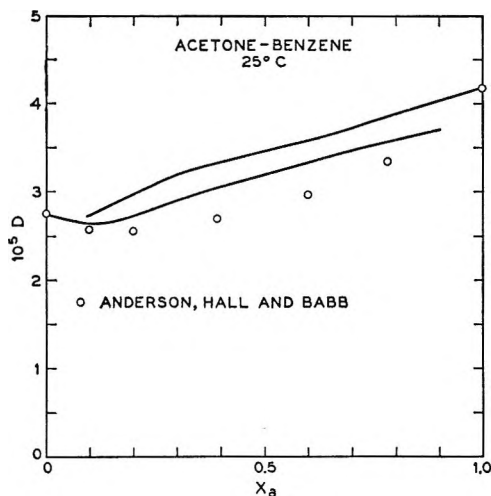


Figure 8. Comparison of mutual diffusion data⁴ with predictions based on eq 8 for the system acetone-benzene at 25°. The solid curves are calculated results, eq 3.

of eq 8. It is seen that eq 8, like eq 3, gives a quantitative description of the data only for the system benzene-cyclohexane. The present data do not provide a basis for choosing between eq 3 and 8.

In making these comparisons it is necessary to do considerable analysis on the thermodynamic data. We have carried this through in a primitive way and we have no doubt that superior analyses are possible. A thermodynamic identity

$$Q_1 \bar{V}_2 = Q_2 \bar{V}_1 \quad (10)$$

(17) S. Glasstone, K. J. Laidler, and H. Eyring, "Theory of Rate Processes," McGraw-Hill Book Co., Inc., New York, N. Y., 1941.

(18) "International Critical Tables," McGraw-Hill Book Co., Inc., New York, N. Y., 1928.

Table V

Benzene-cyclohexane					Acetone-benzene					Acetone-chloroform					Acetone-water				
x_b	Q	Q_b	$10^5 Q_b D_b$	$10^5 D$	x_a	Q	Q_a	$10^5 Q_a D_a$	$10^5 D$	x_a	Q	Q_a	$10^5 Q_a D_a$	$10^5 D$	x_a	Q	Q_a	$10^5 Q_a D_a$	$10^5 D$
0.1	0.92	0.91	1.91	1.87	0.1	0.96	0.94	2.64	2.58	0.1	1.20	1.21	2.91	2.67	0.1	0.57	0.73	0.71	0.82
0.3	0.82	0.78	1.83	1.80	0.3	0.97	0.92	2.94	2.61	0.3	1.58	1.61	4.39	3.18	0.3	0.24	0.48	0.65	0.62
0.5	0.76	0.69	1.69	1.80	0.5	0.98	0.89	3.20	2.81	0.5	1.54	1.63	4.92	3.44	0.5	0.14	0.38	0.81	0.85
0.7	0.78	0.68	1.64	1.79	0.7	0.99	0.87	3.47	3.16	0.7	1.36	1.44	5.03	3.52	0.7	0.35	1.21	3.79	1.60
0.9	0.90	0.74	1.71	1.98	0.9	1.00	0.83	3.71	3.72	0.9	1.10	1.22	5.13	3.60	0.9	0.76	3.48	13.9	3.39

x_c	Q	Q_c	$10^5 Q_c D_c$	$10^5 D$	x_b	Q	Q_b	$10^5 Q_b D_b$	$10^5 D$	x_c	Q	Q_c	$10^5 Q_c D_c$	$10^5 D$	x_w	Q	Q_w	$10^5 Q_w D_w$	$10^5 D$
0.1	0.90	0.92	1.98	1.98	0.1	1.00	1.02	4.02	3.72	0.1	1.10	1.09	3.95	3.60	0.1	0.76	0.70	3.0	3.4
0.3	0.78	0.82	1.76	1.79	0.3	0.99	1.05	3.71	3.16	0.3	1.36	1.32	4.52	3.52	0.3	0.35	0.27	0.74	1.60
0.5	0.76	0.84	1.71	1.80	0.5	0.98	1.09	3.45	2.81	0.5	1.54	1.46	4.45	3.44	0.5	0.14	0.09	0.20	0.85
0.7	0.82	0.94	1.76	1.80	0.7	0.97	1.12	3.20	2.61	0.7	1.58	1.52	4.40	3.18	0.7	0.24	0.11	0.18	0.62
0.9	0.92	1.07	1.69	1.87	0.9	0.96	1.15	2.73	2.58	0.9	1.20	1.07	2.85	2.67	0.9	0.57	0.19	0.33	0.82

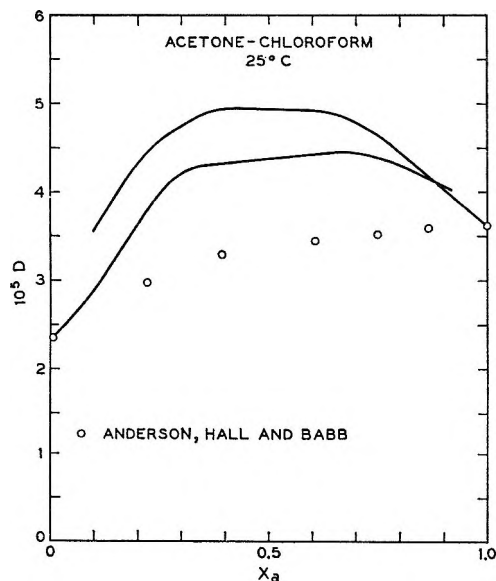


Figure 9. Comparison of mutual diffusion data⁴ with predictions based on eq 8 for the system acetone-chloroform at 25°. The solid curves are calculated results, eq 8.

where the \bar{V}_i values are partial molar volumes provides a consistency check on the Q_i factors. We have computed the values \bar{V}_i ¹⁸ and find that eq 10 is obeyed adequately, Table VI. This check does not bear on the accuracy of Q , however, as Q cancels in the ratio Q_1/Q_2 , by eq 9.

By eq 8

$$D = D_1 Q_1 = D_2 Q_2 \quad (11)$$

and, using eq 12

$$D_1/D_2 = Q_2/Q_1 = \bar{V}_2/\bar{V}_1 \quad (12)$$

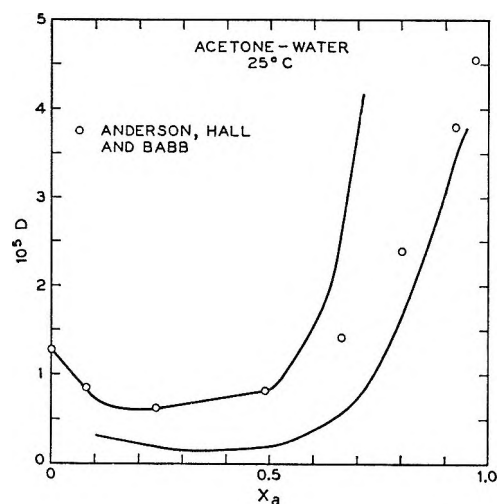


Figure 10. Comparison of mutual diffusion data⁴ with predictions based on eq 8 for the system acetone-water at 25°. The solid curves are calculated results, eq 8.

Thus we have included the ratio D_1/D_2 in Table VI. Equation 12 holds fairly well for benzene-cyclohexane and acetone-benzene solutions, holds roughly for acetone-chloroform solutions, and is not obeyed for acetone-water solutions. Bearman¹⁹ and Mills²⁰ have discussed this equation previously. We should keep in mind that eq 8 does not follow from eq 12 even though the reverse does follow.

A rather different point of view can be stated as follows. Acetone-chloroform solutions exhibit negative deviations from Raoult's law and the thermo-

(19) R. J. Bearman, *J. Chem. Phys.*, **32**, 1308 (1960).

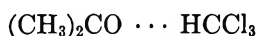
(20) R. Mills, *J. Phys. Chem.*, **67**, 600 (1963).

Table VI

—Benzene-cyclohexane—				—Acetone-benzene—			
x_b	D_b/D_c	\bar{V}_c/\bar{V}_b	Q_c/Q_b	x_a	D_a/D_b	\bar{V}_b/\bar{V}_a	Q_b/Q_a
0.1	1.32	1.21	1.26	0.1	1.16	1.22	1.22
0.3	1.28	1.22	1.21	0.3	1.12	1.22	1.22
0.5	1.20	1.22	1.22	0.5	1.13	1.22	1.22
0.7	1.13	1.23	1.21	0.7	1.12	1.22	1.21
0.9	1.08	1.23	1.18	0.9	1.15	1.22	1.23

—Acetone-chloroform—				—Acetone-water—			
x_a	D_a/D_c	\bar{V}_c/\bar{V}_a	Q_c/Q_a	x_a	D_a/D_w	\bar{V}_w/\bar{V}_a	Q_w/Q_a
0.1	0.91	1.11	1.12	0.1	0.62	0.27	0.26
0.3	0.94	1.11	1.07	0.3	0.81	0.24	0.23
0.5	1.00	1.11	1.12	0.5	0.99	0.23	0.24
0.7	1.03	1.11	1.10	0.7	1.09	0.22	0.22
0.9	1.25	1.11	1.13	0.9	~1.0	~0.16	0.20

dynamic behavior has been discussed extensively²¹ in connection with various models for deviations from ideality. Although there are several ways of expressing the ideas, they all involve association or compound formation of the type

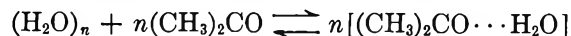


This ties in directly with the empirical fact that $D_a = D_c$ at $x_a = 0.5$. In the context of the diffusion experiments the distinction between association and compound formation is not important; *i.e.*, the rate of exchange can be quite large by chemical standards and still be small compared with the diffusion jump rate. At concentrations other than equimolar, the interpretation of the measured self-diffusion coefficients is complicated owing to the introduction of an associated entity. D_a will be some sort of a weighted average of the self-diffusion coefficients of the free acetone (present in solution) and the complex. Similarly, D_c will be an average. Each of these coefficients will be concentration dependent. The interpretation of the mutual diffusion coefficient could be complicated as well.

Stokes has recently²² published a paper dealing with the effects of dimerization equilibria on diffusion. He discusses the problem of the relation between dimer and monomer mobilities in terms of a modified Stokes-Einstein hydrodynamic theory.²³

Acetone-water solutions exhibit large positive deviations from Raoult's law that are usually attributed to association of one of the components.²¹ Of course, water is a strongly associated liquid and the thermodynamic behavior is of the expected form. Experimentally we observe that $D_a = D_w$ at $x_a = 0.5$ and this is somewhat more surprising than the similar result for the acetone-chloroform system. A successful model

must provide for breaking down the water structure and the formation of a water-acetone complex



This is not an unreasonable suggestion, but we do not wish to imply that the data lead directly to such a model. It is possible that the equality of the self-diffusion coefficients is merely a coincidence. In any case, interpretations are complicated owing to our ignorance of the diffusion coefficients for the various components of the model.

V. Theory

To clarify the relationship between mutual and self-diffusion experiments, it is useful to make a comparison in the language of irreversible thermodynamics.²⁴ The approach is to write down linear relations between particle fluxes, j_i , and chemical potential gradients, $\nabla\mu_i$. The diffusion coefficients are then derived in terms of the linear (Onsager) coefficients, Ω_{ij} . For a binary solution

$$-j_1 = \Omega_{11}\nabla\mu_1 + \Omega_{12}\nabla\mu_2 \equiv VD_1'\nabla n_1 \quad (13)$$

where n_1 is the concentration, *i.e.*, number per cm^3 . At constant temperature and pressure the Gibbs-Duhem relation

$$n_1\nabla\mu_1 + n_2\nabla\mu_2 = 0 \quad (14)$$

places a constraint on the variables so that we find

$$D_1' = [\Omega_{11} - (n_1/n_2)\Omega_{12}](\partial\mu_1/\partial n_1)(1/V) \quad (15)$$

and

$$D_2' = [-(n_2/n_1)\Omega_{21} + \Omega_{22}](\partial\mu_2/\partial n_2)(1/V) \quad (16)$$

for the diffusion coefficients of components 1 and 2, respectively.

For a mass-fixed reference frame in mechanical equilibrium it can be shown that

$$m_1^2\Omega_{11} = -m_1m_2\Omega_{12} = -m_1m_2\Omega_{21} = m_2^2\Omega_{22} \quad (17)$$

Thus

$$D_1' = (\Omega_{11}m/n_2m_2V)(\partial\mu_1/\partial n_1) \quad (18)$$

where

$$m \equiv n_1m_1 + n_2m_2 \quad (19)$$

The m_i values are molecular masses.

(21) J. H. Hildebrand and R. L. Scott, "The Solubility of Nonelectrolytes," 3rd ed, Reinhold Publishing Corp., New York, N. Y., 1950, Chapter 11.

(22) R. H. Stokes, *J. Phys. Chem.*, **69**, 4012 (1965).

(23) F. Perrin, *J. Phys. Radium*, **7**, 1 (1936).

(24) D. D. Fitts, "Nonequilibrium Thermodynamics," McGraw-Hill Book Co., Inc., New York, N. Y., 1962.

In general, D_1' and D_2' are not equal in this frame of reference. However, using the thermodynamic identity

$$n_1 \bar{v}_2 (\partial \mu_1 / \partial n_1) = n_2 \bar{v}_1 (\partial \mu_2 / \partial n_2) \quad (20)$$

it follows that

$$(D_1' / D_2') = (m_2 \bar{v}_1 / m_1 \bar{v}_2) \quad (21)$$

Following Fitts, we define a mutual-diffusion coefficient

$$D \equiv (m \bar{v}_2 / m_2) D_1' = (m \bar{v}_1 / m_1) D_2' \quad (22)$$

which is the same for the two components. This corresponds to the experimental mutual-diffusion coefficient commonly encountered. For self-diffusion, $D = D_1' = D_2'$.

As in the case of single-component systems, the diffusion coefficients may be expressed in terms of velocity correlation functions *via* the results of Kirkwood and others.²⁵⁻²⁷ According to these results the linear coefficients may be expressed as

$$\Omega_{ij} = (1/3kT) \int_0^{\tau} \langle J_i(s) J_j(0) \rangle ds \quad (23)$$

where the pointed brackets indicate an average over an equilibrium ensemble.

$$J_i(s) = \sum_{k=1}^{n_i} v_{ik}'(s) \quad (24)$$

where $v_{ik}'(s)$ is the velocity of the k th molecule of type i relative to the center of mass. For convenience we define the following molecular velocity correlation functions and their integrals.

$$f_{1\alpha\alpha} \equiv \int_0^{\tau} \langle v_{1\alpha}'(s) v_{1\alpha}'(0) \rangle ds \quad (25)$$

$$f_{1\alpha\beta} \equiv \int_0^{\tau} \langle v_{1\alpha}'(s) v_{1\beta}'(0) \rangle ds \quad (26)$$

and

$$f_{12} \equiv \int_0^{\tau} \langle v_{1\alpha}'(s) v_{2\beta}'(0) \rangle ds \quad (27)$$

where $v_{1\alpha}'$ is the velocity of molecule one of type α , etc.

In terms of these functions the linear coefficients are

$$\Omega_{11} = (1/3kT)(n_1 f_{1\alpha\alpha} + n_1^2 f_{1\alpha\beta}) \quad (28)$$

and

$$\Omega_{12} = (n_1 n_2 f_{12} / 3kT) \quad (29)$$

Using the conservation of momentum we obtain

$$m_1 f_{1\alpha\alpha} + n_1 m_1 f_{1\alpha\beta} + n_2 m_2 f_{12} = 0 \quad (30)$$

and a similar relation for component two. From straightforward algebraic combinations of the above equations we obtain the desired relations

$$D = -(m^2 \bar{v}_2 / 3m_1 m_2 V) (\partial \ln a_1 / \partial \ln n_1) f_{12} \quad (31)$$

$$D_1 = f_{1\alpha\alpha} / 3 \quad (32)$$

$$D_2 = f_{2\alpha\alpha} / 3 \quad (33)$$

The thermodynamic factor $(\partial \ln a_1 / \partial \ln n_1)$ enters simply from the assumption that the fluxes are proportional to the chemical potential gradients.

$$\nabla \mu_1 = (\partial \mu_1 / \partial n_1) \nabla n_1$$

$$\mu_1 = \mu_1^\circ + kT \ln a_1$$

$$(\partial \mu_1 / \partial n_1) = (kT / n_1) (\partial \ln a_1 / \partial \ln n_1) \quad (34)$$

In the self-diffusion experiment the thermodynamic factor is unity.

Owing to the restrictions imposed by the conservation of momentum, only three of the five correlation functions defined above are independent. The three experimental diffusion coefficients are then sufficient to evaluate the integrals of all five correlation functions but one does not obtain a functional relationship among the three diffusion coefficients. Such a general relationship requires information beyond the phenomenological equations. By way of illustration, observe that one may rearrange the foregoing equations to form the identity

$$D - Q(x_2 D_1 + x_1 D_2) = [c_1 c_2 V Q / 3(c_1 + c_2)] \times (f_{1\alpha\beta} + f_{2\alpha\beta} - 2f_{12}) \quad (35)$$

where V is the volume of the system. The right-hand side of this equation is clearly the error made by using the Hartley-Crank relation. In order that the Hartley-Crank relation apply over the entire concentration range, there should be a relation among the cross correlations such that the right-hand side of eq 35 is small compared to D . A related result has been obtained by Tyrrell.²⁸ In dilute solutions the correction is small and eq 35 should apply, but only in a limited sense is it a relationship among the three diffusion coefficients.

This result may be extended somewhat if one observes that the cross correlations in the error term may

(25) J. G. Kirkwood, *Rend. Scuola Intern. Fis. Enrico Fermi*, 10, 200 (1960).

(26) R. W. Zwanzig, *Ann. Rev. Phys. Chem.*, 16, 67 (1965).

(27) S. A. Rice and P. Gray, "Statistical Mechanics of Simple Liquids," Interscience Publishers, Inc., New York, N. Y., 1965.

(28) H. J. V. Tyrrell, *J. Chem. Soc.*, 1599 (1963).

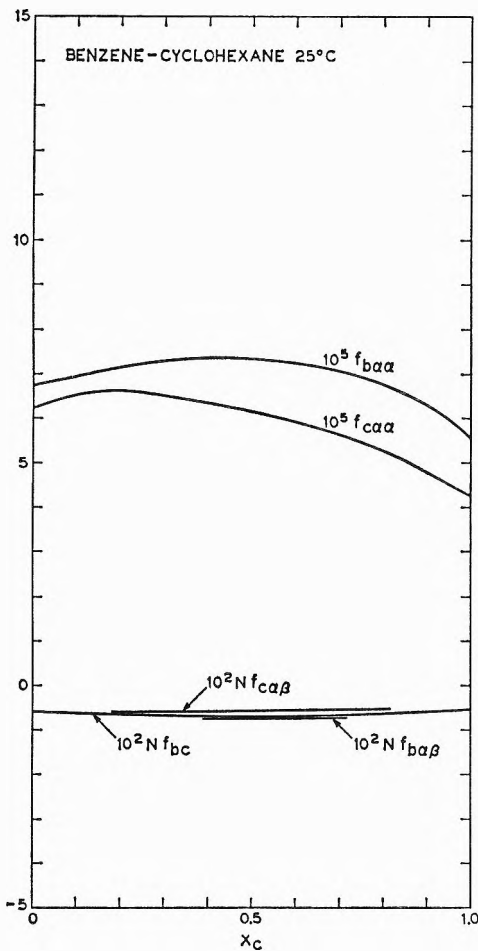


Figure 11. Experimental velocity correlation function integrals for the system benzene-cyclohexane at 25°.

be combined into a single correlation function which has a clear, though esoteric, physical interpretation. Equation 35 becomes

$$D - Q(x_2D_1 + x_1D_2) = (c_1c_2VQ/3(c_1 + c_2)) \int_0^{\infty} \kappa(s) ds \quad (36)$$

where

$$\kappa(s) = \langle [v_{1\alpha}(0) - v_{2\alpha}(0)][v_{1\beta}(s) - v_{2\beta}(s)] \rangle$$

$\kappa(s)$ is the cross-correlation of the relative velocity of one pair of unlike molecules with the relative velocity of a distinct pair of unlike molecules.

The behavior of $\kappa_c(s)$ is unlike that of the other correlation functions. This is readily apparent if one expands the various functions as power series in time.

$$\langle v_{i\alpha}'(0)v_{j\beta}'(s) \rangle = -(kT/m) \{ 1 - (s^2\rho/2m_i m_j) \int g_{ij} \nabla^2 u_{ij} dr_{ij} + \dots \} \quad (37)$$

$$\langle v_{i\alpha}'(0)v_{i\alpha}'(s) \rangle = (kT/m_i) \{ 1 - (s^2/2m_i) c_i \int g_{ii} \nabla^2 u_{ii} dr_{ii} + c_j \int g_{ij} \nabla^2 u_{ij} dr_{ij} + \dots \} \quad (38)$$

and

$$\kappa(s) = (s^2\rho/2m) [(1/m_1^2) \int g_{11} \nabla^2 u_{11} dr_{11} + (1/m_2^2) \int g_{22} \nabla^2 u_{22} dr_{22} - (2/m_1 m_2) \int g_{12} \nabla^2 u_{12} dr_{12}] + \dots \quad (39)$$

With the exception of κ , the correlation functions have a maximum at zero time and subsequently decay. The coefficient of s^2 is the mean-square force on a molecule and is therefore positive in all except the expression for κ . The function κ is zero at zero time and may increase in magnitude before decaying. In many cases, then, the integral contained in κ is smaller than the integrals of the other correlation functions and the Hartley-Crank relation may apply reasonably well over the entire concentration range. The integral of the

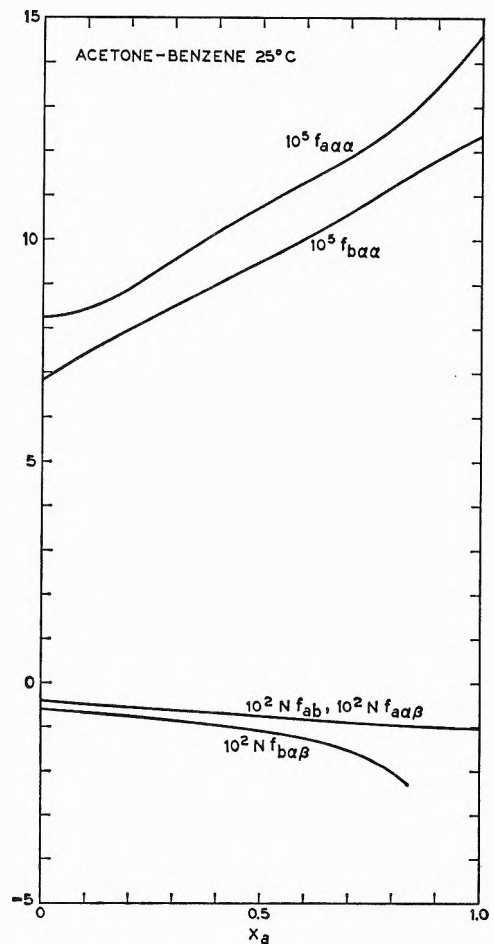


Figure 12. Experimental velocity correlation function integrals for the system acetone-benzene at 25°.

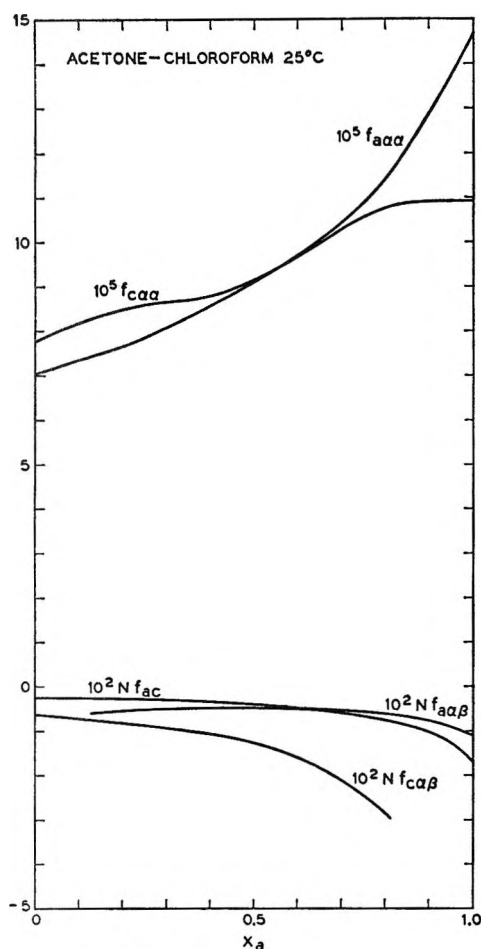


Figure 13. Experimental velocity correlation function integrals for the system acetone-chloroform at 25°.

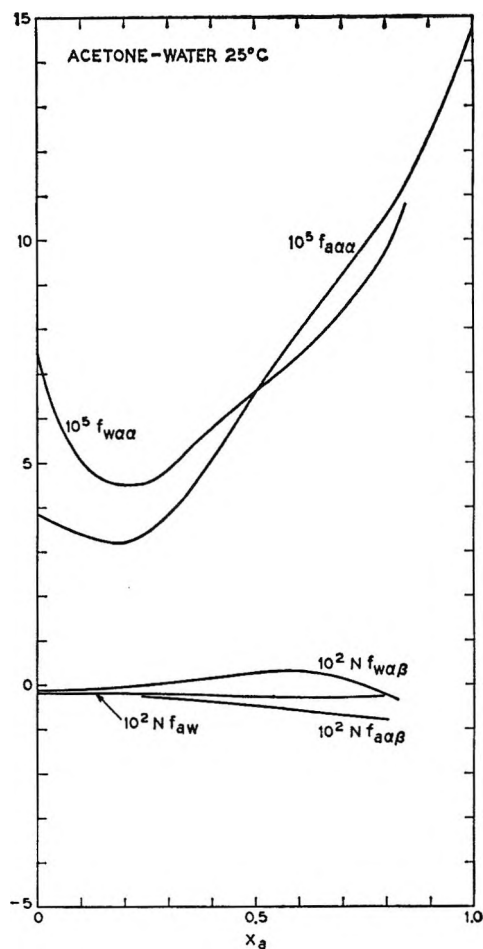


Figure 14. Experimental velocity correlation function integrals for the system acetone-water at 25°.

autocorrelation function of the relative velocities may be obtained directly from the two self-diffusion coefficients.

One might also note that methods employing expansions like eq 37, previously used for the calculation of self-diffusion coefficients, apply with similar assumptions to the calculation of the mutual diffusion. For example, if one assumes that the functional form of the velocity correlation function is gaussian, one finds

$$D = (kT/3(c_1 + c_2))Q[\pi\rho/m_1m_2\int g_{12}\Delta^2u_{12}dr_{12}]^{1/2} \quad (40)$$

As mentioned before, the integrals of the five correlation functions may be obtained from the three diffusion coefficients without recourse to assumptions beyond those inherent in nonequilibrium thermodynamics. These integrals have been determined by use of eq 30 and 36 for the systems studied. These derived quantities are listed in Table VII and plotted in Figures 11-14.

The concentration dependences exhibited by the

f values are not great but the trends in some systems are interesting. Among the cross correlations only $f_{w\alpha\beta}$ in the water-acetone system has a positive excursion. In solutions dilute in acetone $f_{w\alpha\beta}$ is negative. Somewhat loosely speaking this is a consequence of the conservation of momentum. For the pure water system with zero total momentum and with a molecule with specified momentum, p_1 , the remaining molecules must, on the average, have $-p_1/(N - 1)$ as their momentum. This arrangement must persist in such a way that the integrated function is negative. This situation would obtain over the entire concentration range for solutions composed of similar molecules, *e.g.*, the benzene-cyclohexane system. As the concentration of acetone increases, the restriction imposed by the conservation of momentum becomes less dominating since the molecule with specified momentum may distribute its momentum to both water and acetone molecules as dictated by the differing intermolecular forces. The correlation function must be

Table VII

Benzene-cyclohexane						Acetone-benzene					
x_0	$10^5 f_{c\alpha\alpha}$	$10^5 f_{b\alpha\alpha}$	$10^2 N_{f_{b0}}$	$10^2 N_{f_{c\alpha\beta}}$	$10^2 N_{f_{b\alpha\beta}}$	x_0	$10^5 f_{a\alpha\alpha}$	$10^5 f_{b\alpha\alpha}$	$10^2 N_{f_{ab}}$	$10^2 N_{f_{a\alpha\beta}}$	$10^2 N_{f_{b\alpha\beta}}$
0	6.27	6.75	-0.60			0	8.25	6.84	-0.46		-0.61
0.2	6.63	7.14	-0.67	-0.59	-0.65	0.2	8.90	8.00	-0.52	-0.48	-0.78
0.4	6.27	7.32	-0.71	-0.56	-0.68	0.4	10.2	9.03	-0.65	-0.53	-0.99
0.6	5.92	7.24	-0.69	-0.56	-0.72	0.6	11.4	10.1	-0.81	-0.64	-1.26
0.8	5.28	6.79	-0.65	-0.53	-0.71	0.8	12.5	11.2	-0.93	-0.83	-2.02
1.0	4.26	5.64	-0.57			1.0	14.6	12.4	-1.04	-1.07	

Acetone-water						Acetone-chloroform					
x_0	$10^5 f_{a\alpha\alpha}$	$10^5 f_{w\alpha\alpha}$	$10^2 N_{f_{aw}}$	$10^2 N_{f_{a\alpha\beta}}$	$10^2 N_{f_{w\alpha\beta}}$	x_0	$10^5 f_{a\alpha\alpha}$	$10^5 f_{c\alpha\alpha}$	$10^2 N_{f_{ac}}$	$10^2 N_{f_{a\alpha\beta}}$	$10^2 N_{f_{c\alpha\beta}}$
0	3.84	7.36	-0.19		-0.13	0	7.05	7.74	-0.23		-0.63
0.2	3.24	4.54	-0.19	-0.17	-0.03	0.2	7.63	8.50	-0.25	-0.52	-0.82
0.4	5.11	5.74	-0.28	-0.35	+0.11	0.4	8.59	8.7	-0.33	-0.47	-1.06
0.6	7.95	7.33	-0.31	-0.59	+0.29	0.6	9.70	9.6	-0.47	-0.47	-1.58
0.8	10.5	9.70	-0.26	-0.79	-0.24	0.8	11.40	10.8	-0.77	-0.60	-2.83
1.0	14.8					1.0	14.7	10.9	-1.67	-1.08	

zero at zero time but at some later time it must be positive in order that the integral $f_{w\alpha\beta}$ be positive. This implies that a moving water molecule tends to impart its momentum to other water molecules so as to make them move in the same direction in spite of the opposing influence of the conservation of momentum. A corresponding trend may be observed in $f_{a\alpha\beta}$.

One should be careful, however, in drawing detailed conclusions about the reasons for this effect inasmuch

as one may visualize several mechanisms to produce this observation. A deeper insight must come from the details of the correlation functions themselves rather than just their integrals.

Acknowledgment. We are indebted to W. P. Slichter and J. L. Lundberg for helpful comments and suggestions during the preparation of this manuscript. D. R. Falcone and E. W. Anderson assisted in some of the experiments.

Nuclear Magnetic Relaxation in Polytetrafluoroethylene

by D. W. McCall, D. C. Douglass, and D. R. Falcone

Bell Telephone Laboratories, Inc., Murray Hill, New Jersey (Received August 26, 1966)

Pulse methods have been employed in a nuclear magnetic resonance study of polytetrafluoroethylene. T_1 , T_2 , and $T_{1\rho}$ ("rotating frame") data have been obtained as a function of temperature. The results are interpreted in terms of molecular motions and correlated with dielectric and mechanical relaxation results. In a general way the correlation is good. The low-temperature γ transition is identified as an amorphous phenomenon and is detected in T_1 , T_2 , and $T_{1\rho}$. The crystalline transitions near room temperature are observed and evidence is presented for an unusual influence of the crystalline structure on the motions of molecules in amorphous regions. The higher-temperature β transition is identified as a crystalline phenomenon. Molecular motional mechanisms are discussed.

I. Introduction

In this paper we report some fluorine nuclear magnetic relaxation measurements for polytetrafluoroethylene (PTFE) and attempt to interpret these results in terms of molecular motional mechanisms. A large amount of structural and relaxation data have been published and it is well known that PTFE exhibits a very complex pattern of behavior. The substance is partially crystalline and both amorphous and crystalline relaxations occur. There are at least two crystalline transitions (aside from fusion) and at least two amorphous transitions. It is a matter of considerable interest to observe the manner in which the various nmr relaxation times reflect these transitions. As we will show, the nmr relaxation times give important information concerning the molecular nature of the transitions.

Previous nmr results can be summarized as follows. Wilson and Pake¹ suggested the broad-narrow resonance decomposition as a method for measuring the degree of crystallinity. Wilson and Pake² also made a study of the relaxation times T_1 and T_2 by steady-state (*i.e.*, resonance-width and saturation) methods. They identified a sharp narrowing of the broad or crystalline part of the resonance at 293°K and the appearance and continued narrowing of the narrow or amorphous part above about 200°K. A T_{1a} ³ minimum was observed at about 270°K. T_{1c} decreased sharply at 293°K.

A resonance width-temperature study by Smith^{4a}

indicates resonance narrowing near 210°K and some resonance-width effects near room temperature. The full resonance width at low temperatures is about 9 gauss. Slichter,^{4b} in a similar study, did not observe extensive narrowing until the temperature had been raised to about 280°K. Slichter's samples appear to have been unusually highly crystalline. Powles and Kail⁵ carried out resonance-width measurements that confirmed a narrowing near 220°K for a specimen that had been melted and cooled slowly. Powles and Kail also observed that PTFE as polymerized (*i.e.*, not having been melted) did not show narrowing until the temperature had been raised to about 280°K. The latter material was shown to be much more highly crystalline than the former. Thus the superficial discrepancy between Smith's data and Slichter's data was resolved, as Slichter suggested in his paper,

(1) C. W. Wilson, III, and G. E. Pake, *J. Polymer Sci.*, **10**, 503 (1953).

(2) C. W. Wilson, III, and G. E. Pake, *J. Chem. Phys.*, **27**, 115 (1957).

(3) Subscripts a and c are used herein to denote amorphous and crystalline parameters. The distinction between a and c in this paper is based entirely on T_2 , $T_{2a} \geq T_{2c}$. This reflects the fact that an increase in T_2 implies molecular mobility and the generally accepted notion that molecules in the amorphous regions are freer than molecules in crystalline regions. Although the terminology employed carries morphological implications, we emphasize that we know little about the morphology of PTFE and the nmr results do not reveal such features directly.

(4) (a) J. A. S. Smith, *Discussions Faraday Soc.*, **19**, 207 (1955);

(b) W. P. Slichter, *J. Polymer Sci.*, **24**, 173 (1957).

(5) J. G. Powles and J. A. E. Kail, *ibid.*, **31**, 183 (1958).

on the basis of differing sample crystallinity. Eby and Sinnott⁶ have further confirmed this conclusion by measuring resonance widths of PTFE specimens of 48, 71, and 83% crystallinity.

A very neat experiment on PTFE fibers was carried out by Hyndman and Origlio.⁷ They measured resonance width as a function of temperature, for the broad part of the resonance, for various fiber orientations. When the fiber axis was parallel to the magnetic field no abrupt change in width was observed in the room-temperature range. At other orientations the width decreased sharply as the temperature was raised through about 288°K.

Recently, Iwayanagi and Miura⁸ have discussed broadline nmr for PTFE in terms of three resonance widths. An intermediate resonance is discerned above 240°K. This component shows the sharp transition at 293°K, falling from about 3 to 1 gauss in width.

Trappeniers, Gerritsma, and Oosting⁹ employed pulse methods to measure T_1 for PTFE. They observed a minimum in T_{1a} at 295°K, a sharp change in T_{1c} at 298°K, and a shallow minimum in T_{1e} at 441°K. T_{1a} is decreasing as the temperature is raised through the melting point indicating a minimum in T_{1a} at some temperature above 600°K. Reddish, Powles, and Hunt¹⁰ have confirmed these results. Trappeniers, Gerritsma, and Oosting⁹ have also pointed out the influence of oxygen gas on T_1 at low temperatures.

Our measurements are in general agreement with the published work cited. The main emphasis in this paper is on extending the range of nmr experiments and on fitting the nmr results into a general framework with the results of dielectric and mechanical relaxation.

II. Experimental Section

The spectrometer employed is similar to one described previously.¹¹ It has been modified for operation with a single-coil probe and the 90° phase-shift method for aligning the magnetization¹² with the radio-frequency field (for "rotating frame" measurements) was adopted part way through the present study. The spectrometer is operated at 30 MHz, corresponding to an applied field of about 7500 gauss. Specimen temperature is controlled by means of a gas flow thermostat. The data are probably accurate to within 1°K.

The material chosen for study was a commercial PTFE (Allied Chemical Co., Plastics Division, designated Halon, G-80). It is believed to be substantially linear and very pure as indicated by its low dielectric loss. The density is about 2.17 g/cm³, which indicates about 55% crystallinity.⁶ Our nmr results yield 60-

70% crystallinity based on the Wilson-Pake assumption.¹ X-Ray measurements confirm the latter range.

Three types of nmr data are reported here— T_2 , T_1 , and $T_{1\rho}$. T_2 is determined from oscilloscope pictures of the free-induction decay following a 90° pulse. It will be recalled that $T_2 \cong 2/\gamma\delta H$, where γ is the gyromagnetic ratio (for F¹⁹) and δH is the steady-state resonance width. The free-induction decay is a superposition of a short T_2 signal and a long T_2 signal. The former we identify with the crystalline part of the sample and the latter with the amorphous part.¹ Extracting individual T_2 values from the decay curves is not always easy because of both fundamental and practical problems. The free-induction decay tails can be fitted by a sum of a gaussian term, $\exp(-t^2/T_{2c}^2)$, and a lorentzian term, $\exp(-t/T_{2a})$. The coefficients of the two decay functions provide a measure of the number of nuclei and hence the amount of material represented by the individual decay terms. This enables one to use pulse data for determining the degree of crystallinity according to the method of Wilson and Pake.¹ Fitting the free-induction signals is tedious at best. It must be kept in mind that the nuclear signal is not seen for a period t_r after the end of the 90° pulse.¹³ During this recovery period the long and short T_2 components have decayed by different amounts.

T_1 , the spin-lattice relaxation time, is measured by observing the amplitude of the free-induction decay following a 180–90° pulse pair. If the pulse separation is τ_s , a simple resonance will follow

$$V(t) = V^\circ(t)(1 - 2e^{-\tau_s/T_1}) \quad (1)$$

In PTFE the resonance is more complex and can be described by the sum of two such terms

$$V(t) = V_c^\circ(t)(1 - 2e^{-\tau_s/T_{1c}}) + V_a^\circ(t)(1 - 2e^{-\tau_s/T_{1a}}) \quad (2)$$

(6) R. K. Eby and K. M. Sinnott, *J. Appl. Phys.*, **32**, 1765 (1961).

(7) D. Hyndman and G. F. Origlio, *ibid.*, **31**, 1849 (1960).

(8) Cited in N. Saito, K. Okano, S. Iwayanagi, and T. Hideshima, *Solid State Phys.*, **14**, 414 (1963). We are indebted to Drs. Iwayanagi and Miura for providing us with a preprint of an article dealing with their recent nmr results for PTFE. They plan to publish their article in Section C of *J. Polymer Sci.*

(9) N. J. Trappeniers, C. J. Gerritsma, and P. H. Oosting, *Physica*, **30**, 997 (1964).

(10) W. Reddish, J. G. Powles, and B. I. Hunt, *Polymer Letters*, **3**, 671 (1965).

(11) G. P. Jones, D. C. Douglass, and D. W. McClarr, *Rev. Sci. Instr.*, **36**, 1460 (1965).

(12) S. R. Hartmann and E. L. Hahn, *Phys. Rev.*, **128**, 2042 (1962).

(13) This recovery time is a consequence of receiver saturation and "ringing" in the resonant circuit. In our apparatus, which employs a damping pulse, t_r is about 6 μ sec.

$V_c^\circ(t)$ and $V_a^\circ(t)$ correspond to the short and long T_2 components mentioned above. In PTFE, $T_{1c} > T_{1a}$. Detailed fitting of these functions is particularly tedious and we have resorted to making a visual identification¹⁴ of τ_{sa} , defined by $(1 - 2e^{-\tau_{sa}/T_{1a}}) = 0$, and τ_{sc} . Obviously, $T_{1a} = \tau_{sa}/\ln 2$ and $T_{1c} = \tau_{sc}/\ln 2$. Experiments have shown that the T_1 values obtained by this method agree satisfactorily with T_1 values obtained from the appropriate plot, eq 2. There is some ambiguity in identifying τ_{sa} but the uncertainty in T_{1a} should be no larger than about 20%. Relative T_{1a} values are not subject to this difficulty if a consistent procedure is adopted. The temperatures at which T_1 minima occur are not affected.

$T_{1\rho}$, the longitudinal relaxation time in the rotating frame, is measured by observing the amplitude of the free-induction decay that follows the termination of a resonant pulse of radiation, the nuclear magnetization having been aligned with the rotating field, H_1 , at the beginning of the pulse.^{15,16} When the free-induction signal amplitude falls exponentially with pulse length, τ_{rf}

$$V(t) = V^\circ(t) \exp(-\tau_{rf}/T_{1\rho}) \quad (3)$$

defines $T_{1\rho}$. PTFE exhibits more complex behavior that has been analyzed as a sum of three exponential terms. The two long $T_{1\rho}$ terms correspond to T_{2c} . The magnitudes of these two times are probably affected by the presence of oxygen. The short $T_{1\rho}$ corresponds to T_{2a} . Rotating frame measurements were made at two power levels, $H_1 = 3$ gauss and $H_1 = 12$ gauss. The procedure for getting into the rotating frame was different for the two levels but this procedural detail does not influence the interpretation of $T_{1\rho}$.

Steady-state magnetic resonance spectra have been obtained with a Varian DA-60 spectrometer system.^{17a} The resonances were nearly symmetrical supporting a highly linear structure.^{17b} Both modulation and slow-sweep techniques were employed. With the former method derivative spectra are obtained, and with the latter method the absorption is observed directly. We can neither confirm nor deny the existence of three distinct resonance widths on the basis of these observations. At 270°K a superposition of two resonances suffices.

III. Results

Figure 1 shows the temperature dependence of T_2 . The behavior is generally consistent with resonance-width studies, considering $T_2 \cong 2/\gamma\delta H$. In Figure 1 a sharp increase in T_{2c} occurs near 293°K in complete agreement with earlier workers.^{1,6,7} The magnitude of the increase is about a factor of 2 at the transition

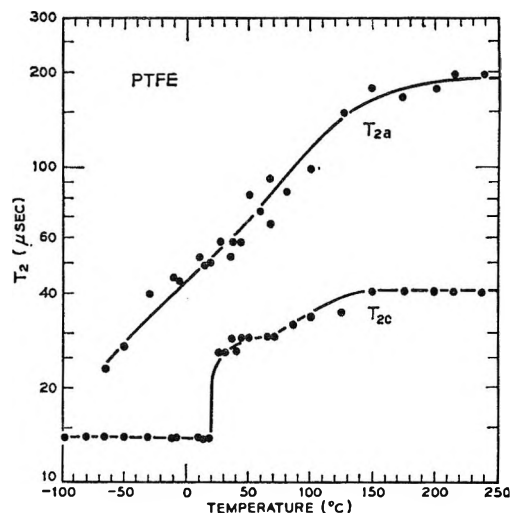


Figure 1. Temperature dependence of the spin-spin relaxation time, T_2 .

followed by a gradual increase to a factor of 3 as the temperature is raised to about 400°K. The scatter of the data simply indicates that it is difficult to separate T_{2a} and T_{2c} quantitatively, particularly when T_{2a} and T_{2c} as well as T_{1a} and T_{1c} are not very different.

T_{2a} is seen to increase gradually over the temperature range studied. T_{2a} has increased by a factor of 2 when the temperature is about 220°K. This agrees with previous reports.^{1,6,7}

Figure 2 shows the temperature dependence of T_1 . T_{1c} shows an abrupt transition at about 293°K. This change was seen by Wilson and Pake² and Trappeniers, Gerritsma, and Oosting.⁹ The latter authors referred to this feature as a T_1 minimum but it seems clear that it is not a T_1 minimum in the usual sense. A fairly sharp increase in T_{1c} occurs near 310°K. The minimum in T_{1c} near 340°K was also observed by Trappeniers, Gerritsma, and Oosting⁹ although they obtained a

(14) This visual estimation of the two T_1 values is convenient and useful. It relies upon the fact that crystalline and amorphous signals have different T_1 and T_2 values. The nuclear signal is examined at a time $\sim 2T_{2a}$ after a 180–90° pulse sequence. The crystalline signal is negligible at this point as $T_{2c} < T_{2a}$. The pulse separation is adjusted until the amorphous signal is zero and τ_{sa} is taken as this pulse separation. In determining T_{1c} , we assumed that the amorphous signal exhibits a smooth, approximately exponential decay. The nuclear signal is examined just after the 90° pulse and the pulse separation is adjusted until the decay is almost flat. This pulse separation is taken to be τ_{sc} , *i.e.*, the interval that nulls the crystalline signal.

(15) (a) D. Ailion and C. P. Slichter, *Phys. Rev. Letters*, **12**, 168 (1964); (b) C. P. Slichter and D. Ailion, *Phys. Rev.*, **135**, A1099 (1964).

(16) (a) D. C. Look and I. J. Lowe, *J. Chem. Phys.*, **44**, 2995 (1966); (b) D. C. Look, I. J. Lowe, and J. A. Northby, *ibid.*, **44**, 3441 (1966).

(17) (a) We are indebted to Mr. E. W. Anderson for recording these spectra; (b) C. W. Wilson, III, *J. Polymer Sci.*, **56**, 516 (1962).

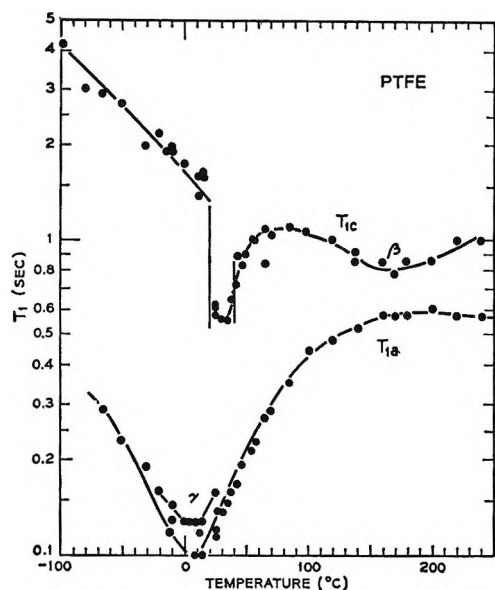


Figure 2. Temperature dependence of the spin-lattice relaxation time, T_1 .

lower minimum T_{1c} — ~ 0.6 sec compared with ~ 0.8 sec in the present study. In either case this is a very shallow minimum.

T_{1a} exhibits a pronounced minimum at about 280°K. Figure 2 shows two curves near this minimum representing two different criteria for separating T_{1a} and T_{1c} . The minimum occurs at $280 \pm 5^\circ\text{K}$. Wilson and Pake² observed this minimum at about 270°K; Trappeniers, Gerritsma, and Oosting⁹ found it at 294°K (although their points do not define the minimum precisely), and Reddish, Powles, and Hunt¹⁰ found it at 295°K. The latter authors did not publish their T_1 vs. temperature curve. These temperature differences are too large to be ascribed to ordinary experimental uncertainty even though the minimum does not appear to be sharp. We find the minimum value for T_{1a} to be $\sim 0.12 \pm 0.02$ sec compared with ~ 0.08 sec published previously.⁹ T_{1a} seems to be falling off at high temperatures suggesting another T_{1a} minimum above the melting point.⁹

$T_{1\rho}$ is plotted as a function of temperature in Figure 3. Below about 290°K, three time constants are observed, the longer two corresponding to T_{2c} and the shorter $T_{1\rho}$ to T_{2a} . Between 290 and 310°K, two $T_{1\rho}$ values suffice. The longer $T_{1\rho}$ in this range corresponds to T_{2c} . Finally, above 310°K a single $T_{1\rho}$ describes the rotating frame decay curves. These general features were apparent for both $H_1 = 3$ gauss and $H_1 = 12$ gauss.

$T_{1\rho a}$, the shortest time constant at temperatures below 310°K, exhibits a well-defined minimum at about

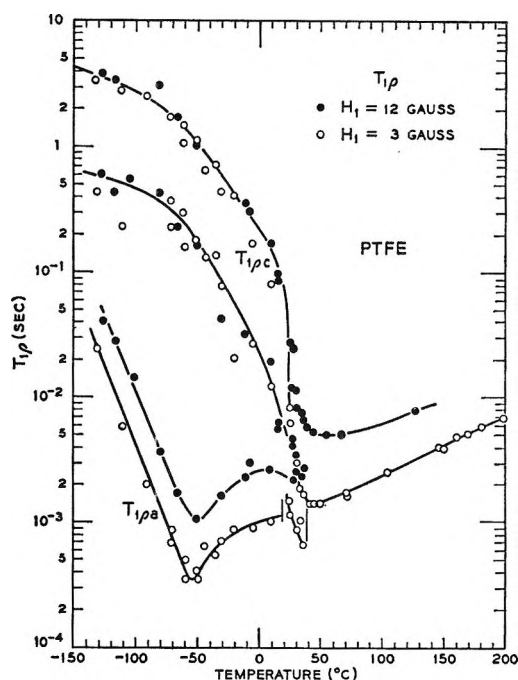


Figure 3. Temperature dependence of the rotating frame relaxation time, $T_{1\rho}$.

218°K for $H_1 = 3$ gauss and 223°K for $H_1 = 12$ gauss. Corresponding minimum values of $T_{1\rho a}$ are 0.3 and 1.0 msec. Abrupt changes in $T_{1\rho a}$ occur near 290 and 310°K.

The two $T_{1\rho c}$ values fall continuously as the temperature is raised and come together at about 290°K. The single $T_{1\rho c}$ merges with $T_{1\rho a}$ at about 310°K. The single $T_{1\rho}$ passes through a shallow minimum near 330°K for $H_1 = 12$ gauss and 320°K for $H_1 = 3$ gauss. The corresponding $T_{1\rho}$ minima are 4.8 and 1.4 msec.

Our steady-state spectra are considerably more symmetrical than those of Iwayanagi and Miura.⁸ We note that they report three T_2 values well above the temperature range for which we detect three or two $T_{1\rho}$ values. Our data do not exhibit three resonance widths in any obvious way.

IV. Discussion

The over-all relaxation behavior of PTFE is indicated on the transition "map" shown in Figure 4. Table I summarizes the observations. The data plotted have been assembled from a number of literature sources, those listed by Eby and Sinnott,⁶ among others. We have attempted to select data obtained for materials that have been sintered or molded and fall into the medium crystallinity range.

Frequencies of maximum loss taken from isotherms or, more often, temperatures of maximum loss at con-

Table I

	α , glass I	β	30°	19°	α , glass II
Transition phase	Amorphous	Probably crystalline	Crystalline	Crystalline	Amorphous
Mechanical activity	Yes	Yes	Yes	Yes	Yes
Dielectric activity	Very weak	No ^a	No	No	Yes
Nmr activity					
δH T_2	No	Yes	No	Yes	Yes
T_1	?	Yes	Yes	Yes	Yes
$T_{1\rho}$	No	?	Yes	Yes	Yes

^a Activity seen only (Krum and Muller²⁸); see text.

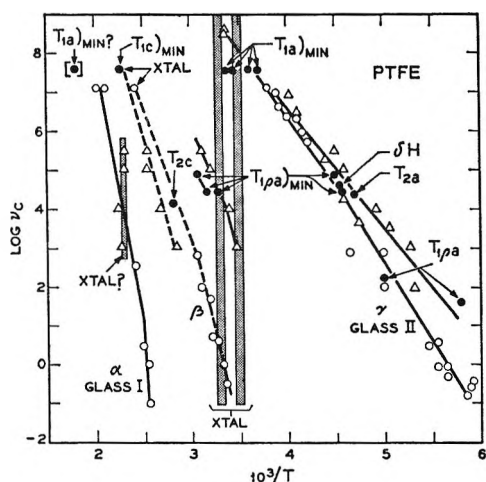


Figure 4. Correlation diagram for various relaxation phenomena in PTFE. Nmr results are indicated by filled circles and were calculated as indicated in the text. The nmr parameters that correspond to the various points are indicated on the graph. Dynamic mechanical relaxation results are indicated by open circles. ν_c was taken as the frequency of measurement at the temperature of maximum loss. Dielectric results are indicated by triangles. ν_c was taken to be the frequency of maximum loss when sufficient data were available (α or glass II process). Higher-temperature dielectric data were analyzed in the same manner used for mechanical-loss data, *i.e.*, ν_c taken as the frequency of measurement at the temperature of maximum loss. A part of the scatter observed in this figure probably arises from these different analyses, *i.e.*, the use of isothermal *vs.* constant-frequency plots.

stant frequency were used for the dielectric and mechanical points. For nmr resonance-width results, the correlation frequency is taken to be $(\gamma\delta H)_{LT}/2\pi$ at the temperature at which the resonance width has fallen to half its low-temperature value, $(\delta H)_{LT}$. T_2 is used similarly. $\nu_c \cong 1/(\pi T_2)_{LT}$, where $(T_2)_{LT}$ is T_2 below the transition range.¹⁸ Temperatures for T_1 minima correspond to $\nu_c \cong \sqrt{2}\nu_0$, where ν_0 is the resonance frequency.¹⁸ At $T_{1\rho}$ minima,¹⁹ $\nu_c \cong 1/2\pi$

$T_{1\rho\beta}(3)$, where $T_{1\rho\beta}(3)$ is the value for $H_1 = 3$ gauss (see eq 6 below).

The following aspects of PTFE relaxation are reasonably well established. (1) A low-temperature (γ or glass II) relaxation is evident in mechanical, dielectric, and nmr data. It is clearly a phenomenon associated with the amorphous regions of the polymer. The activation energy is often quoted as 18 kcal/mole. (2) A first-order crystalline transition occurs just below room temperature ("the 19° transition"). The low-temperature form is triclinic and the room-temperature form is hexagonal.^{20,21} The molecules in the crystalline regions begin to rotate about their long axes at this transition. This is clearly indicated by the results of Hyndman and Origlio⁷ based on nmr resonance widths for PTFE fibers. (3) A first-order crystalline transition occurs just above room temperature ("the 30° transition"). The high-temperature form is pseudo-hexagonal.¹⁹ (4) Relaxation phenomena associated with the two first-order transitions are observed above and below room temperature²² (β -transition region). (5) Rather high-temperature ($> 400^\circ\text{K}$) mechanical relaxations (α or glass I) are observed. Both amorphous and crystalline phenomena are involved. (6) A sharp crystalline melting point is observed at about 600°K. We will now take up the various features individually and interpret the accompanying nmr behavior in detail.

A. *The γ or Glass II Transition.* T_2 increases gradually above 200°K. It has increased by approximately an order of magnitude at 400°K. This indicates fairly extensive molecular motion but by no means liquidlike mobility. The middle of the transi-

(18) N. Bloembergen, E. M. Purcell, and R. V. Pound, *Phys. Rev.*, **73**, 679 (1948).

(19) D. C. Douglass and G. P. Jones, *J. Chem. Phys.*, **45**, 956 (1966).

(20) C. W. Bunn and E. R. Howells, *Nature*, **174**, 549 (1954).

(21) E. S. Clark and L. T. Muus, *Z. Krist.*, **117**, 119 (1962).

(22) K. H. Illers and E. Jenckel, *Kolloid-Z.*, **160**, 97 (1958).

tion can be relied upon to give an indication of that temperature for which $\nu_c = (\gamma\delta H)_{LT}/2\pi$, but attempts to fit the T_2 variation in a detailed way, as Eby and Sinnott did for the resonance width,⁶ are unprofitable. The analysis underlying such a procedure is invalid for systems with distributions of correlation times.

The T_1 minimum as determined by this study and by Wilson and Pake² correlates very well with the assembled data. The other T_1 minima^{9,10} deviate appreciably from the locus of other relaxation data. Reddish, Powles, and Hunt¹⁰ have previously pointed out this discrepancy. A dielectric loss maximum is observed²³ in our PTFE near 300 MHz at 298°K, in agreement with the result of Reddish.¹⁰ This could be interpreted as an indication that the specimens used in this study are similar to those used by Reddish, Powles, and Hunt.

The absolute value of T_1 at the minimum can be estimated as¹⁸

$$(T_1)_{\min} \cong (2\pi\nu_0 T_2)_{LT}^2 / \sqrt{2} = 0.03 \text{ sec} \quad (4)$$

compared with about 0.12 sec observed. This is rather close agreement, as such comparisons go, and can be explained in terms of correlation time distributions^{24,25} or spin diffusion.^{26,27}

The $T_{1\rho a}$ minima at $H_1 = 3$ and 12 gauss fit in very well with the bulk of published relaxation data. The magnitude of $T_{1\rho a}$ at the minimum can be estimated from¹⁹

$$(T_{1\rho a})_{\min} = (4\gamma H_1 T_2)_{LT}^2 \quad (5)$$

which yields 0.6×10^{-4} sec at 3 gauss and 2.4×10^{-4} sec at 12 gauss. These are to be compared with the observed values 3×10^{-4} and 10×10^{-4} sec. Thus the factor of 4 discrepancy between the predicted and measured $(T_1)_{\min}$ carries over to the $(T_{1\rho a})_{\min}$. A distribution of correlation times is the most likely explanation of these results.

At temperatures and radiofrequency fields sufficiently low that $\tau_c \gg T_2$ and $H_1 \cong \delta H$, Slichter and Ailion¹⁵ have shown that

$$\nu_c \cong 1/2\pi T_{1\rho} \quad (6)$$

The two lowest nmr points in Figure 4 were calculated from $T_{1\rho a}$ at $H_1 = 3$ gauss using this relation. Reasonably good correlation is observed but the slope deviates appreciably. The deviation is probably the result of another relaxation mechanism. Rotating frame decay curves indicate the presence of a fourth, very short time constant at the lowest temperatures studied. The dielectric results of Krum and Muller²⁸ provide additional evidence for an additional low-temperature relaxation. It is possible that this relaxation is to

be identified with the low-temperature process observed by Eby and Wilson.²⁹ They suggest that $-\text{CF}_2\text{H}$ groups, in low concentration, give rise to relaxation.

B. The 19° Transition and the 30° Transition. T_{2c} increases sharply by a factor of about 2 while T_{2a} is unaffected by the 19° transition. This confirms the result of Hyndman and Origlio.⁷ An abrupt decrease in T_{1c} is observed but T_{1a} varies smoothly through the transition region. $T_{1\rho a}$ undergoes a sharp change at the 19° transition. This is surprising for two reasons; the transition is a crystalline one, and T_{1a} shows no effect.

In seeking an understanding of these experimental results the following considerations are pertinent. At 19° T_{1a} is dominated by the γ process; the minimum in T_{1a} occurs only 10° below. $T_{1\rho a}$ is not near its γ minimum and is consequently more susceptible to other relaxation phenomena. $T_{1\rho a}$ is shorter than $T_{1\rho c}$ so the molecular motions controlling $T_{1\rho a}$ must be occurring in the amorphous regions. Of course, molecular motions are occurring in the crystalline regions as well. Between the 19° transition and the 30° transition $T_{1\rho a}$ decreases to quite a low value, 0.6×10^{-3} sec. Estimating that the appropriate $(T_{2a})_{LT}$ is about 40×10^{-6} sec, eq 5 yields $(T_{1\rho a})_{\min}$ at about 0.5×10^{-3} sec, $H_1 = 3$ gauss. Thus we suggest that the molecular motions controlling $T_{1\rho a}$ near room temperature must be distinct from the γ mechanism and have correlation frequencies near 2×10^4 Hz at 35°. Krum and Muller²⁸ observed a corresponding dielectric loss peak but none was found in our material.²³ The specimen studied by Krum and Muller may have had polar impurity groups that made this relaxation and others dielectrically active.

Much of what has been said about the 19° transition also applies to the 30° transition. The latter appears to be somewhat less sharp and, in our specimen, occurs nearer to 40 than 30°. The $T_{1\rho a}$ and T_{1c} data give the impression that the motions turned on at the 19° transition are turned off at the 30° transition.

Clark and Muus²¹ propose that the helical molecular conformation changes to a more extended helix at the 19° transition. This results in a hexagonal arrange-

(23) We are indebted to Mr. G. R. Johnson, Bell Telephone Laboratories, for this result.

(24) D. W. McCall, D. C. Douglass, and E. W. Anderson, *J. Chem. Phys.*, **30**, 1272 (1959).

(25) T. M. Connor, *Trans. Faraday Soc.*, **60**, 1574 (1964).

(26) N. Bloembergen, *Physica*, **15**, 386 (1949).

(27) D. W. McCall and D. C. Douglass, *Polymer*, **4**, 433 (1963).

(28) F. Krum and F. H. Muller, *Kolloid-Z.*, **164**, 81 (1959).

(29) R. K. Eby and F. C. Wilson, *J. Appl. Phys.*, **33**, 2951 (1962).

ment and hindered rotation occurs between the preferred orientations. At the 30° transition, further untwisting occurs and the conformation becomes irregular. The rotational hindrances cease to be important. The nmr results indicate a very unusual influence of the room-temperature crystal structure on molecular motions in the amorphous regions.

The nature of the molecular motion in the room-temperature range is not entirely clear. We have found that motions occur in both the crystalline and amorphous regions. The latter motions set in sharply at the 19° transition and must be extensive enough that the local field is modulated by a large fraction of its average value. Inasmuch as the γ transition has already signaled rather general motions in the amorphous regions, considerable activity must be present. Impurity or boundary region motions are not sufficient to explain the data. However, the fact that rotation about the long molecular axes in the crystalline regions triggers the amorphous process might suggest that the amorphous regions have rather small average dimensions, say a few angstroms.

C. The β Transition. The β transition is observed as a minimum in T_{1c} . This minimum is shallow, suggesting that the motion involved does not change the local magnetic fields drastically or, alternatively, that only a small fraction of the nuclei have the motional freedom. The minor change in T_{2c} in the appropriate temperature range, $\sim 375^\circ\text{K}$, would be consistent with the first possibility. The nmr data clearly indicate that the β process occurs in crystalline regions.

T_{1p} exhibits a minimum in the vicinity of 325°K , considerably too low a temperature to be identified with the β mechanism. Krum and Muller²⁸ observed a corresponding dielectric effect although other workers have not.^{27,29,30} We cannot distinguish T_{1pa} from T_{1pc} in this region and T_{1a} and T_{1c} are not too different in the β region, $\sim 440^\circ\text{K}$.

The molecular interpretation of the β process is speculative at best. We propose longitudinal (*i.e.*, parallel to the helical axes) motions of the molecules, which would affect only the intermolecular dipolar fields, as the operative mechanism. The closeness of the crystalline and amorphous T_1 and T_{1p} values could be interpreted as an indication that phase-boundary motions are involved.

D. The α or Glass I Transition. The α or glass I transition is not detected by nmr in any obvious way. T_{1a} is decreasing at the highest temperature studied and it may be presumed that a minimum will be reached, apparently above the melting point.⁹ T_2 and T_{1p} do not give an indication of such a process.

Referring again to the work of Krum and Muller,²⁸ a dielectric loss is observed in the α region which increases in intensity with increasing crystallinity. Its temperature is independent of frequency, suggesting that it may be indicative of another first-order transition. The intensity of this loss increases markedly at low frequencies and it is best interpreted in terms of an ionic conduction mechanism (*i.e.*, a "Maxwell-Wagner" process). This dielectric observation is of interest in the context of the present paper because the minimum in T_{1c} occurs at the same temperatures, $\sim 440^\circ\text{K}$. Thus the T_{1c} minimum that we have associated with the β transition would also be consistent with a diffuse first-order crystalline transition. In any case, there is some evidence²⁸ that crystalline motions also occur in the α region.

Acknowledgment. We are indebted to W. P. Slichter, W. Reddish, and E. S. Clark for valuable comments and discussions.

(30) G. P. Mikhailov, S. P. Kabin, and A. L. Smolianski, *J. Tech. Phys. USSR*, 25, 2179 (1955).

The Effect of Oxygen on the Generation of Radical Ions by Synthetic Zeolites

by F. R. Dollish and W. Keith Hall

Mellon Institute, Pittsburgh, Pennsylvania (Received January 17, 1966)

The concentration of radical ions which can be formed on the decationated zeolites was shown to depend on both the amount of available oxygen and the presence of dehydroxylated sites. The oxygen may be either in the gas phase or tenaciously chemisorbed during pretreatment. In the former case, below a limiting value, a 1:1 relationship apparently exists between the number of perylene radicals which are formed and the number of O₂ molecules added at room temperature; in the latter case, only a portion (10–35%) of the oxygen was effective. Even the maximum concentration of radical ions achieved in the presence of excess oxygen ($\sim 10^{19}$ /g) was much smaller than the density of dehydroxylated sites ($\sim 10^{21}$ /g). When triphenylmethane was the substrate, carbonium ion concentrations of the same magnitude were effected. There was no dependence, however, on chemisorbed or gaseous oxygen. The O₂⁻ ion was formed when the dehydroxylated zeolites were irradiated; hence, the O₂ which cannot be removed by evacuation overnight at 550° must be chemisorbed as some other species.

Introduction

The formation of radical ions from polynuclear aromatic hydrocarbons, arylamines, and phenylalkenes on silica-alumina catalysts has been studied by both optical and epr spectroscopy.^{1–8} It has been found^{3,4,7,8} that treatment of silica-alumina with hydrogen at 500° suppressed radical-ion formation. The literature concerning the effects of the addition of oxygen to the catalyst system are in part contradictory. Several studies^{1,5,9} reported that oxygen decreased the radical-ion concentration. However, it has been shown⁸ that this effect is due to a physical interaction between radical ions and oxygen molecules, with resulting changes in line shape and signal width. Porter and Hall,⁷ by comparing results from epr and optical spectroscopy, confirmed that the radical-ion concentration generated from perylene, anthracene, and thianthrene (when adsorbed on silica-alumina catalysts) was increased on addition of oxygen. Flockhart, Scott, and Pink¹⁰ have shown that alumina dehydrated at 900° can form perylene radical ions only in the presence of molecular oxygen.

The purpose of the present investigation was to study the effects of catalyst pretreatment and of oxygen addition on the formation of radical ions from perylene and triphenylamine adsorbed by synthetic

crystalline zeolites and to correlate these results with what is known concerning the chemistry of the decationation-dehydroxylation process on the NH₄⁺-exchanged zeolites. Also, the formation of triphenylcarbonium ions from triphenylmethane was briefly investigated and these results are compared with those for radical ions.

Turkevich, *et al.*,¹¹ were first to demonstrate the ability of decationated NH₄⁺ Y zeolites to generate radical ions; however, they did not examine the

(1) J. J. Rooney and R. C. Pink, *Proc. Chem. Soc.*, 70 (1961); *Trans. Faraday Soc.*, 58, 1632 (1962).

(2) D. M. Brouwer, *Chem. Ind. (London)*, 177 (1961); *J. Catalysis*, 1, 372 (1962).

(3) J. K. Fogo, *J. Phys. Chem.*, 65, 1919 (1961).

(4) W. K. Hall, *J. Catalysis*, 1, 53 (1962).

(5) H. P. Leftin, M. C. Hobson, and J. S. Leigh, *J. Phys. Chem.*, 66, 1214 (1962).

(6) A. Terenin, *Advan. Catalysis*, 15, 227 (1964).

(7) R. P. Porter and W. K. Hall, *J. Catalysis*, 5, 366 (1966).

(8) F. R. Dollish and W. K. Hall, *J. Phys. Chem.*, 69, 4402 (1965).

(9) H. Imai, Y. Ono, and T. Keii, *ibid.*, 69, 1082 (1965).

(10) B. D. Flockhart, J. A. N. Scott, and R. C. Pink, *Proc. Chem. Soc.*, 139 (1964); *Trans. Faraday Soc.*, 62, 730 (1966).

(11) D. N. Stamires and J. Turkevich, *J. Am. Chem. Soc.*, 86, 749 (1964); J. Turkevich, F. Nozaki, and D. N. Stamires, *Proc. Intern. Congr. Catalysis, 3rd, Amsterdam, 1964*, 1, 586 (1965).

effects of oxygen or catalyst pretreatment and, consequently, were led to suppose that the ionized electrons were held in deep traps associated with the decationated sites of the zeolite. They reported that only about one radical ion was formed per hundred sites or per 20 molecules adsorbed.

Experimental Section

The X- and Y-type zeolites were furnished in the sodium form by the Linde Division of Union Carbide Corp. and the Ca^{2+} and NH_4^+ forms were prepared by conventional cation-exchange procedures using Baker analytical grade $\text{Ca}(\text{NO}_3)_2$ and NH_4Ac . Excess salts were removed from the exchanged zeolites by ten centrifugations with distilled water. The degree of ion exchange was calculated from the residual sodium content as determined by flame photometry.

The equipment and high-vacuum procedures have been described earlier.^{4,7,12} Sealed, greaseless systems were used; no solvent was employed with triphenylmethane, but spectroscopically pure benzene was used to transfer perylene and triphenylamine. It was necessary to seal the tubes (with a torch) under vacuum because small traces of O_2 , inadvertently picked up during an experiment, would invalidate the results.

Four pretreatment procedures were used. When the zeolite was first evacuated at room temperature for several hours before slowly increasing the temperature to 550° where it was evacuated overnight, it was said to have had the *evacuation pretreatment*. The *standard pretreatment* consisted of treating the zeolite in flowing oxygen for 17 hr at 550° before evacuating it for 17 hr at this temperature. A catalyst was *oxygen cooled* if, after the O_2 treatment, it was slowly cooled to room temperature in the presence of oxygen before evacuation overnight. When the O_2 treatment was followed by evacuation for 6 hr, treatment with flowing H_2 for 24 hr, and a final evacuation for 6 hr, all at 550° , the catalyst was said to be *reduced*.

In order to investigate the effect of "added-back" oxygen, samples of NH_4^+ Y zeolite which had been given the evacuation pretreatment were connected to a doser attached to a gas buret and known amounts of oxygen were introduced at room temperature.

The amount of oxygen removed following the standard pretreatment when the Y zeolite was reduced was determined by circulating the H_2 over the catalyst at 547° in an all-glass system. The water evolved was collected in a liquid nitrogen trap and was measured volumetrically (as water vapor) in a gas adsorption system which was connected to the circulation loop through stopcocks.

A weighed amount of reagent (usually about 300 mg

of perylene or triphenylamine) was placed in a reagent reservoir with 10 ml of benzene where it was degassed by the freeze-pump-thaw technique and sealed under vacuum. Transfer of the reagent to the zeolite was effected by rupture of a break-off seal between the catalyst and reagent compartments. The epr measurements were conducted in the presence of benzene. Most samples reached a constant radical-ion concentration after 48-hr contact time. Reproducibility of packing of the zeolite in the probe tube was within 10–20%.

Epr measurements were made with a Varian X-band spectrometer (Model V-4500) with the microwave bridge in the low-power configuration. A 12-in. magnet was employed; the Varian V-4531 multipurpose cavity was used with a modulation frequency of 100 kc/sec. Radical-ion concentrations, expressed as spins per gram of dry zeolite, were determined at room temperature by comparison of the first moment of the overmodulated derivative signals with those of 0.001 *M* 1,1-diphenyl-2-picrylhydrazyl in benzene, whose radical-ion concentration had been determined spectrophotometrically.¹³ Power entering the cavity was measured with a Hewlett-Packard 431B power meter using a 20-db coupler. Power levels of the order of 0.04 mw were ordinarily necessary completely to unsaturate the epr signals.

Optical spectra from triphenylmethane were taken using the apparatus and procedures previously described.^{4,7,12} Optical platelets weighing about 40 mg were made by pressing a mechanical mixture of 10–30% zeolite with 90–70% silica gel or Cab-O-Sil at 50 tons/in². The dilution was necessary in order to give an absorbance less than 2.0. After pretreatment, the entire optical cell assembly was wrapped in aluminum foil to exclude light. Contact of the zeolite with degassed triphenylmethane (40 mg) was effected by rupture of a break-off seal before heating in an oven at 100° for 48 hr. In some experiments, in order to effect contact between zeolite and substrate at room temperature, triphenylmethane was transferred in benzene. The solvent was then removed by vacuum transfer back into the solution vial cooled to -195° . The vial was then removed with a torch. This was not a preferred method because it is doubtful that the solvent (and its trace impurities) could be quantitatively recovered from the zeolite.

Absorption spectra were taken on a Cary Model 14

(12) H. P. Leftin and W. K. Hall, *Actes Congr. Intern. Catalyse*, **2**, Paris, 1960, 1, 1353 (1961).

(13) J. W. Eastman, G. M. Androes, and M. Calvin, *J. Chem. Phys.*, **36**, 1197 (1962).

Table I: Effect of Zeolite Pretreatment on the Generation of Radical Ions

% exchanged Reagent Coverage, molecules/g Catalyst pretreatment at 550°	—NH ₄ ⁺ Y zeolite—			—Ca ²⁺ Y zeolite—		—NH ₄ ⁺ X zeolite ^a —	—Na ⁺ Y zeolite—
	45% Perylene 7 × 10 ²⁰	79% Perylene 7 × 10 ²⁰	79% Triphenylamine 4 × 10 ²⁰	36% Perylene 7 × 10 ²⁰	79% Perylene 7 × 10 ²⁰	48% Perylene 7 × 10 ²⁰	Perylene 7 × 10 ²⁰
Radical-ion concentration, spins/g × 10 ⁻¹⁷							
1. Evacuation	1.3	6.2	1.0	0.3	0.6	0.3	None detected ^b
2. Standard	9.5	32.3	8.1	0.3	9.1	1.0	None detected
3. Cooled in O ₂ , evacuated 25°	36 ^c	58 ^d	20 ^d	0.4 ^c	15 ^c	2.6 ^c	...
4. Reduced	1.0	1.8	0.7	...	0.3

^a Pretreatment of the X zeolite was conducted at 500°, since this material is more unstable than the Y zeolite at high temperatures.

^b When this sample was exposed to dry air for 24 hr, paramagnetism equivalent to 0.9 × 10¹⁷ spins/g of zeolite developed. ^c Little (≤15%) or no change in spin-concentration occurred when exposed to air for 24 hr. ^d When exposed to air for 24 hr, 1.2 × 10¹⁹ spins/g developed.

spectrophotometer. Absorbance values were converted to carbonium ion concentrations by use of the equation

$$C = \frac{ANL \times 10^{-3}}{EW} \quad (1)$$

where C is the concentration of carbonium ions (ions g⁻¹), A the absorbance, N Avogadro's number, L the geometric area of the catalyst platelet (cm²), E the extinction coefficient of the absorbing ion (l. mole⁻¹ cm⁻¹), and W the weight of the platelet (g). A value of 4.0 × 10⁴ l. mole⁻¹ cm⁻¹ was used in the calculations for the extinction coefficient of the triphenylmethyl-carbonium ion.⁷ The measured absorbance was multiplied by a suitable factor (e.g., 10 for platelets containing 10% zeolite, 5 for platelets containing 20% zeolite) in order to obtain the concentration equivalent to a platelet composed entirely of decationated Y zeolite.

X irradiations at room temperature were performed with a Picker unit using an AEG-50-T tube with tungsten target and beryllium window. The sample (2.0 g) of decationated Y zeolite in a sealed Pyrex tube to which an epr quartz probe tube was attached by a graded seal was placed about 5 cm from the target. The voltage and current were set at 45 pkv and 35 ma, respectively. The dose rate was 3 × 10⁶ r hr⁻¹. After irradiation, the zeolite was shaken down into the quartz epr tube and the epr spectra examined at room temperature.

Results

A. Effect of Zeolite Pretreatment on Formation of Radical Ions. The results of experiments defining the effect of the pretreatment on radical-ion concentration are listed in Table I. The parent Na⁺ Y zeolite

did not form detectable amounts of perylene radical ion under the usual experimental conditions, although it had a sodium deficiency equivalent to 6 × 10¹⁹ sites/g, indicating that a small concentration of decationated sites may already have been present. The Y zeolite consistently gave greater radical-ion concentrations than the X form for all catalyst pretreatments. The number of radical ions formed for any given pretreatment depended on the nature of the exchanged ion (NH₄⁺ > Ca²⁺ > Na⁺) and the extent of ion exchange.

The variation of radical-ion concentration with pretreatment of zeolite was consistent with that reported earlier^{3,4,7,8} for silica-alumina. The higher epr spin concentrations following the standard and O₂-cooled pretreatments (than when the zeolite was reduced or given the evacuation pretreatment) indicated that oxygen plays a fundamental role in the reaction.

B. Effect of Oxygen on the Formation of Radical Ions. A quantitative study was made of the increase in the number of perylene radical ions formed on a decationated Y-type zeolite (evacuated at 550°) when a known amount of oxygen was added and also of the decrease caused by the removal of oxygen as water when it was treated with H₂ as it became reduced. These results are summarized in Table II. Both methods yielded values of about one perylene radical ion formed per oxygen molecule.

It was found that the oxygen added at 25° to a sample given the evacuation pretreatment could be quantitatively recovered by pumping at 25°. However, if after the addition of oxygen (10¹⁸ to 10¹⁹ molecules/g) at 25° the zeolite was heated at 550° overnight, no oxygen could be removed, but the increase in radical-ion concentration after contact with perylene was only 10–20% of that produced by the same amount of oxygen added at 25°. When a reduced zeolite was treated

Table II: The Effect of Oxygen on Radical-Ion Formation (Zeolite: NH_4^+ Y Zeolite, 45% Exchanged; Coverage: 7×10^{20} Perylene Molecules/g)

A. Oxygen Sorption by Zeolite Given Evacuation Pretreatment			
No. of O_2 molecules/g added at 25°	Radical-ion concn, spins/ $g \times 10^{-17}$	Increase in radical-ion concn, ^a spins/ $g \times 10^{-17}$	Ratio, increase in spin concn: O_2 molecules added
0	1.3	0	...
57×10^{17}	58	57	1.0
40×10^{17}	35	34	0.84
19×10^{17}	25	23	1.2

B. Relationship between H_2O Removed and Decrease in Radical-Ion Formation			
	—No. per gram of zeolite—		
	Expt 1	Expt 2	
1. Radical-ion concentration after standard pretreatment, spins g^{-1}	9.5×10^{17}	9.5×10^{17}	
2. Radical-ion concentration after reduction pretreatment, spins g^{-1}	0.6×10^{17}	1.4×10^{17}	
3. Decrease in radical-ion concentration due to reduction, spins g^{-1}	8.9×10^{17}	8.1×10^{17}	
4. Amount of H_2O removed during reduction, ^b cc(NTP) g^{-1}	0.079	0.074	
Equivalent O_2 molecules g^{-1}	10.6×10^{17}	10.0×10^{17}	
5. Ratio: $\frac{\Delta(\text{spin concentration})}{\text{O}_2 (2\text{H}_2\text{O}) \text{ removed}}$	0.84 spins/molecule of O_2	0.81 spins/molecule of O_2	

^a Values given in the second column corrected for the ion concentration ($1.3 \times 10^{17}/g$) before addition of specified amount of oxygen. ^b In these experiments, 4.0 g of catalyst was used.

during the first contact with oxygen, presumably by oxidation of residual carbonaceous material on the zeolite. Also, reaction with impurities (mainly iron and titanium) may have occurred, causing a poor mass balance. After the third oxidation-reduction cycle, however, the amount of oxygen adsorbed by the zeolite at 550° ($9.1 \times 10^{17} \text{ O}_2/g$) could be reversibly reduced off as water ($8.0 \times 10^{17} \text{ O}_2/g$) and was equal to that found for the reduction of a zeolite given the standard pretreatment (Table IIB). Therefore, at present it is unclear whether during the initial uptake of oxygen at 550° chemisorption can occur in more than one form; however, it has been established that only that oxygen which can be reversibly chemisorbed and reduced off as water is effective in radical-ion formation.

A sample of the 45% exchanged NH_4^+ Y zeolite, when evacuated at 550° overnight and then X irradiated under vacuum, produced an epr spectrum showing both the six-line hyperfine pattern characteristic of an electron trapped on an aluminum ion¹⁴ and the spectrum of the superoxide, O_2^- , ion.¹⁵ The spin concentration of the former was about 1×10^{16} spins/g and the latter about 4×10^{16} spins/g. Contact of this sample with a solution of perylene in benzene resulted in the disappearance of the two signals and the formation of a perylene epr signal equivalent to 1.3×10^{18} spins/g. An unirradiated sample under similar conditions gave a perylene radical-ion concentration of 1.3×10^{17} spins/g or tenfold less than that obtained after X irradiation. X irradiation of the same material in the presence of $2.2 \times 10^{19} \text{ O}_2$ molecules/g produced only the O_2^- signal with a concentration of 1.0×10^{18} molecules/g, while a sample given the standard pretreatment gave an O_2^- signal equivalent to 1×10^{17} molecules/g.

C. Effect of Temperature of Zeolite Activation on the Formation of Radical Ions. The effect of the temperature of zeolite activation on the generation of perylene radical ions on NH_4^+ Y zeolite is illustrated in Figure 1. Under vacuum (curve A), there was little difference in the radical-ion concentration with zeolites given the evacuation pretreatment at temperatures from 100 to 800°. On addition of oxygen at room temperature to these samples, however, there was a large increase in perylene radical-ion concentration with samples evacuated above 500° as compared with those treated at lower temperatures. Above 700°,

(14) D. N. Stamires and J. Turkevich, *J. Am. Chem. Soc.*, **86**, 757 (1964).

(15) P. H. Kasai, *J. Chem. Phys.*, **43**, 3322 (1965).

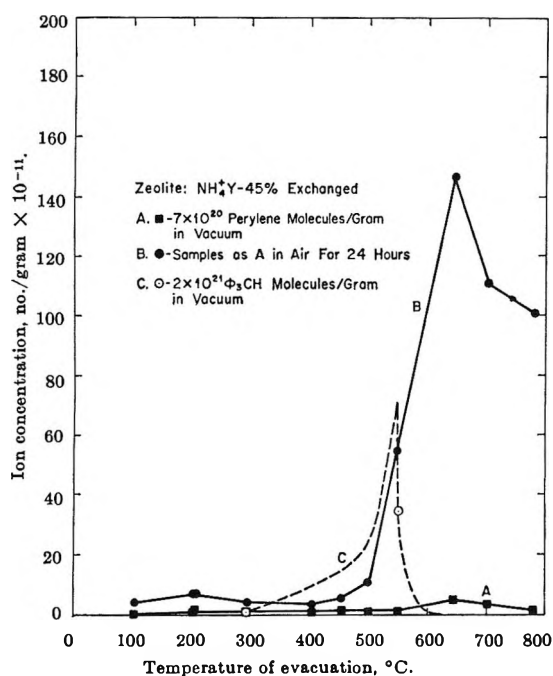


Figure 1. Effect of evacuation temperature on formation of perylene radical ions and triphenylcarbonium ions.

some decomposition of the lattice may have occurred, causing the ion concentration to drop.

Stamires and Turkevich¹¹ published a curve similar to that of Figure 1B for 1,1-diphenylethylene adsorbed on decationated Y-type zeolite. Evidently, oxygen was not rigorously excluded in their experiments, which were prepared in a drybox. Also, the maximum number of triphenylamine cation radicals (1.2 – 1.5×10^{19} spins/g on a 90% decationated Y-type sieve) which they observed could only be duplicated in the present work when excess oxygen was available. Both perylene and triphenylamine adsorbed on decationated Y zeolite (79% exchanged) gave a maximum radical-ion concentration of 1.2×10^{19} spins/g in the presence of air (Table I, footnote *d*). However, very little change in ion concentration occurred with the NH_4^+ Y-type zeolite (45% exchanged) or with the Ca^{2+} zeolite when samples which had been O_2 cooled were exposed to air for 24 hr, indicating that the limiting factor was not lack of sufficient O_2 .

D. Effect of Impurities in Zeolite. The Y zeolite used in most of the experiments contained 479 ppm of iron and 772 ppm of titanium as the major impurities. In order to check whether these had any effect on the formation of radical ions, a Na^+ Y zeolite containing only 1–5 ppm of iron and 1–10 ppm of titanium was tested; it was 81% NH_4^+ exchanged, given a standard pre-treatment, and then contacted with 7×10^{20} perylene molecules/g. A maximum perylene radical-ion con-

centration of 1.0×10^{19} radical ions/g was obtained after exposure to air for 24 hr which was nearly the same as that found for the impure zeolite (1.2×10^{19} radical ions/g) under similar conditions. This shows that the presence of these impurities has no effect on radical-ion formation.

E. Effect of Oxygen on the Formation of Triphenylcarbonium Ions. The formation of triphenylcarbonium ions from triphenylmethane has been observed^{7,16} to occur on silica-alumina catalysts under conditions similar to those for radical-ion formation. Unlike radical-ion formation, however, reduction of the catalyst had little effect. As can be seen in Table III, the zeolites behaved much as silica-alumina. Hydrogen treatment was, within experimental error, ineffective and the addition of air did not affect the absorbance at $430 \text{ m}\mu$ in the absence of light. Also, ultraviolet irradiation with a Hanovia mercury lamp in the absence of O_2 did not alter the carbonium ion concentration. Ion concentration did depend upon the degree of decationation in zeolite (compare Table III-1 and -6) and also upon the temperature of evacuation. In the optical experiments of Table III, it was found that carbonium ions formed, even though the catalyst was maintained mainly in the Brønsted form, once it had been slightly dehydroxylated in the presence of oxygen (Table III-7). The ion concentration was repressed, however, from that obtained from the same material more extensively dehydroxylated (Table III-6) but was still tenfold greater than that from the stoichiometric Brønsted zeolite (Table III-8).

In order to make as exact a comparison as possible with the radical-ion data of Figure 1, a series of samples was prepared in the manner used in the epr experiments and these were contacted with triphenylmethane ($1 \times 10^{21}/\text{g}$) by vacuum transfer at 100° in the dark for 48 hr. The samples were then all examined together and a visual comparison was made; the results of this comparison are indicated by the dashed curve in Figure 1, which is passed through the quantitative data (points) from the optical experiments. The samples which had been evacuated at 250° were white; those evacuated at 300 and 450° were pale yellow (indicating carbonium ion formation), while those treated between 500 and 550° were deep yellow with the maximum intensity occurring at about 540° . Samples evacuated at temperatures between 595 and 640° were again white after contact with substrate. The addition of oxygen to samples evacuated at 300 and 640° did not cause a color change when kept in the dark overnight. Irradiation with ultraviolet light in the pres-

(16) A. E. Hirschler and J. O. Hudson, *J. Catalysis*, 3, 239 (1964).

Table III: Formation of Triphenylcarbonium Ions from Triphenylmethane by Decationated Y Zeolite (Nominal Coverage: 2×10^{21} (C₆H₅)₃CH/g)

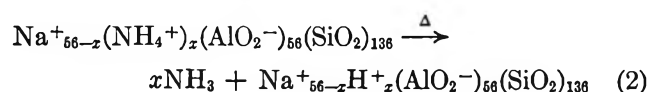
Catalyst platelet	Treatment	Normalized carbonium ion concn $\times 10^{-18}$ ^a
1. 10% NH ₄ ⁺ Y zeolite (79% exchanged) + 90% silica gel	(a) Standard, heated 48 hr at 100°	7.4 ^b
	(1) Irradiated 1 hr with ultraviolet light	7.0
	(2) Exposed to air 1 hr	6.9
	(b) Reduced, heated 48 hr at 100°	5.6
	(1) Irradiated 1 hr with ultraviolet light	4.6
	(2) Exposed to air 1 hr	4.9
2. 10% NH ₄ ⁺ Y zeolite (79% exchanged) + 90% silica gel	(a) Standard, heated 48 hr at 100°	4.4
	(1) Irradiated 1 hr with ultraviolet light	4.3
	(2) Exposed to air 1 hr	5.0
3. 10% NH ₄ ⁺ Y zeolite (79% exchanged) + 90% silica gel	(a) Standard pretreatment at 425°, water added-back and evacuated at 300°, heated 48 hr at 100°	4.7
	(a) Standard, contacted at room temperature for 72 hr	1.3
4. 10% NH ₄ ⁺ Y zeolite (79% exchanged) + 90% silica gel	(1) Irradiated 2 hr with ultraviolet light	2.6
	(2) Heated 16 hr at 100°	4.1
	(a) Evacuated at 300°, contacted at room temperature for 2 hr	0.54
5. 30% Ca ²⁺ Y zeolite (79% exchanged) + 70% Cab-O-Sil	(1) Heated in dark for 24 hr at 100°	1.2
	(a) Standard, heated 48 hr at 100°	1.8
6. 20% NH ₄ ⁺ Y zeolite (45% exchanged) + 80% silica gel	(a) Standard, heated 48 hr at 100°	3.6
	(1) After standing in 150 mm of O ₂ overnight at room temperature	3.2
7. 20% NH ₄ ⁺ Y zeolite (45% exchanged) + 80% silica gel	(a) Standard at 480°, water added-back and evacuated at 300°, heated 48 hr at 100°	1.8
	(1) After standing in 150 mm of O ₂ overnight in the dark at room temperature	1.8
	(a) Evacuated at 300° overnight, contacted with (C ₆ H ₅) ₃ CH by heating 48 hr at 100°	0.16
8. 100% NH ₄ ⁺ Y zeolite (45% exchanged)	(1) After standing in air overnight in the dark at room temperature	0.15
	(2) Irradiated 2 hr with ultraviolet light	0.30

^a All carbonium ion concentrations were normalized to platelet containing 100% Y zeolite and are given as ions/g of zeolite. ^b The same optical platelet was used for parts 1a-c. Between experiments, the platelet was burned free of reagent in O₂ at 550°.

ence of O₂, however, led to the formation of a deep yellow color, characteristic of the carbonium ion.

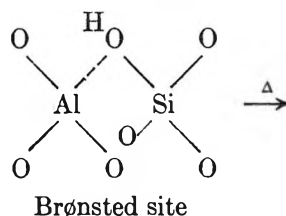
Discussion

A. Decationation of Ammonium Y Zeolites. The unit cell composition of the Na⁺ Y zeolite is Na⁺_{56-}}(AlO₂⁻)₅₆(SiO₂)₁₃₆. On exchange of part of the Na⁺ with NH₄⁺ and heating, NH₃ is evolved, *i.e.*

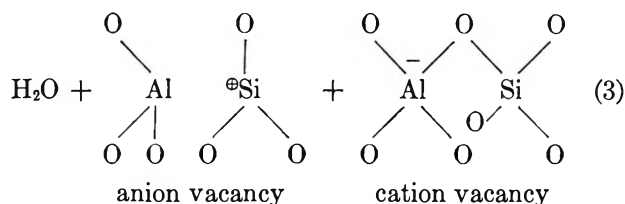


This process has been shown to be complete at about 300° for Y zeolites containing 80% NH₄⁺.¹⁷ On

heating to 550°, the decationated (Brønsted) sites dehydroxylate to give water and anion and cation vacancy pair sites, *i.e.*



(17) J. B. Uytterhoeven, L. G. Christner, and W. K. Hall, *J. Phys. Chem.*, **69**, 2117 (1965).



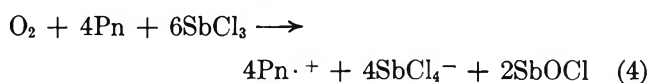
The cation-anion vacancy pairs of the right-hand member of eq 3 are deduced on the basis of stoichiometry. It is not known what (if any) rearrangement occurs beyond this stage. The X-ray patterns of the Y zeolite show slight changes in intensity and position after dehydroxylation but indicate that the gross structure remains intact.¹⁸ On the other hand, eq 3 is not easily reversible. Therefore, the representation used for the anion and cation vacancy pair sites should be regarded as a complex of the system; the indicated formal separation of charge probably does not exist as such because an electronic readjustment would lower the energy of the system. The coulombic energy cost to separate the charge on the sites of eq 3 is about 1.4 eV/pair. Whereas this could be compensated by re-formation of the tetrahedral structure at the cation vacancy, it is unlikely that this would minimize the energy.

In the nomenclature of Rabo,¹⁹ Pickert, *et al.*,²⁰ and Stamires and Turkevich,^{11,21} the sites formed by elimination of water, as in eq 3, are termed "decationized." Uytterhoeven, Christner, and Hall¹⁷ preferred the term "decationated" for sites formed by elimination of NH₃ (eq 2), which resulted in the appearance of OH bands in the infrared at 3570 and 3660 cm⁻¹ and the term "dehydroxylated" for those formed by the subsequent elimination of H₂O. Both terminologies are used in this paper.

B. The Role of Oxygen in Radical-Ion Formation. The decrease in radical-ion concentration, brought about by treatment of silica-alumina with H₂ at elevated temperatures, was first noted by Fogo;³ it was confirmed by Hall,⁴ who also found that an amount of H₂O could be collected during the H₂ treatment which could be equated to the decrease in paramagnetism due to the elimination of one perylene cation radical per oxygen molecule removed. It was pointed out that it was not possible to distinguish whether excess oxygen was present before reduction, or if the catalyst was oxygen deficient after the treatment, *i.e.*, whether chemisorbed oxygen was a reactant in the production of cation radicals or if the decreased effectiveness of the catalyst resulted from a weakening or elimination of Lewis acid sites. The crystalline zeolites offered the possibility of determining the point of stoichiometry by decomposing the NH₄⁺ form under vacuum. The

findings (Table I) that the stoichiometric and reduced zeolites produced nearly equal radical-ion concentrations and that these were much lower than those for the same catalysts after the standard pretreatment indicated that catalysts heated in O₂ contained excess oxygen, even after evacuation at high temperatures. Furthermore, the nearly stoichiometric relationship between the number of cation radicals produced and the amount of this oxygen (Table II) showed that the latter was probably a reactant. This was supported by the fact that the same oxygen could be reacted to H₂O by heating in H₂.

Atkinson, Jones, and Baughan²² found that perylene (Pn) in liquid SbCl₃ was stoichiometrically oxidized to the radical ion on the addition of oxygen according to



The data illustrated in Figure 1 show that the Y zeolite in the Brønsted form did not form radical ions when exposed to oxygen, but that the dehydroxylated zeolite did. Dehydroxylation begins to become significant above 500°.¹⁷

Recently Hirschler²³ suggested that in the conversion of polynuclear aromatic to cation radicals on solid acid catalysts, the electron removed from the aromatic is trapped by acid protons with the oxygen serving as a catalyst rather than as an electron acceptor. The present results are not in accord with this view since there was a nearly 1:1 correspondence between the number of oxygen molecules added or removed from the system and the change in the number of ions formed and since the ion concentration was inversely related to the number of Brønsted sites left on the catalyst. Therefore, the picture which emerged, in agreement with Atkinson, Jones, and Baughan,²² was that radical ions form on electrophilic sites with (adsorbed) molecular oxygen being the oxidizing agent.

The question of the nature of the oxygen chemisorption is intriguing. Since the oxygen sorbed during the standard pretreatment was not removed during overnight evacuation at 550°, it was suggested⁷ that

(18) J. A. Rabo, P. E. Pickert, and J. E. Boyle, U. S. Patent 3,130,006 (1964).

(19) J. A. Rabo, P. E. Pickert, D. N. Stamires, and J. E. Boyle, *Actes Congr. Intern. Catalyse, 2^e, Paris, 1960*, 2, 2055 (1961).

(20) P. E. Pickert, J. A. Rabo, E. Dempsey, and V. Schomaker, *Proc. Intern. Congr. Catalysis, 3rd, Amsterdam, 1964*, 1, 714 (1965).

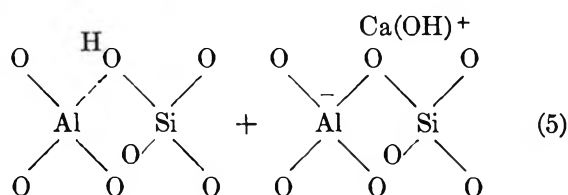
(21) D. N. Stamires and J. Turkevich, *J. Am. Chem. Soc.*, **86**, 749 (1964).

(22) J. R. Atkinson, T. P. Jones, and C. E. Baughan, *J. Chem. Soc.*, 5808 (1964).

(23) A. E. Hirschler, *J. Catalysis*, **5**, 196 (1966).

it is held as O_2^- on anion vacancies, the electrons being furnished by donor sites (presumably cation vacancies) in the solid. This was consistent with current thought²⁴ on oxygen chemisorption on oxides. However, the results of the X irradiation experiments showed that if O_2^- were present before the irradiation, it should have been detected by epr. Since no paramagnetism was found under these circumstances, the chemisorbed oxygen must have been held in some other way. Moreover, this oxygen must be able to react with perylene and triphenylamine to form ion pairs, e.g., $Pn \cdot + O_2^-$. No epr spectrum of O_2^- was found together with that of the cation radical, but this is usual with donor-acceptor systems.^{25,26}

C. Radical-Ion Formation on Calcium Y Zeolites. Very little radical-forming ability was found for the calcium-exchanged Y zeolite containing 36% Ca^{2+} , even in the presence of oxygen (Table I). However, at 79% Ca^{2+} the results were comparable with those of the NH_4^+ Y zeolites. These results are consistent with the data of Rabo, *et al.*,^{19,20} who found that the catalytic activity of Ca^{2+} Y zeolite was very small up to an exchange level of 45%, but increased rapidly above 65% exchange. At low-exchange levels, the Ca^{2+} will first occupy the S_1 site positions.²⁰ These are in the hexagonal prisms which bridge adjacent cub-octahedra and will accommodate Ca^{2+} equivalent to about 50% of the base-exchange capacity. The other type sites are located in or near the planes of the six-membered oxygen rings facing the large cavities. Originally, on the average, there was about one Na^+ for each such ring. Thus, complete exchange with Ca^{2+} would leave about half the rings empty. Under these circumstances, a large separation of charge occurs,²⁰ creating a positive site and a site bearing a partial negative charge (cation vacancy). Conceivably, in the presence of small amounts of water, the calcium Y zeolite can exist as



On heating, CaO may be precipitated out leaving the zeolite decationized. Russell²⁷ has shown that this process occurs with the divalent montmorillonites and saponites. The site on the left of eq 5 is identical with that formed on the NH_4^+ Y zeolite as shown in eq 3. While one cannot be categorical at present, it is at least possible that at high levels of exchange, these sites on the Ca^{2+} Y zeolite can undergo the same

chemistry as described herein for the decationated zeolites.

D. Magnitude of Radical-Ion Concentration. A salient feature of the results was the magnitude of radical-ion concentrations as related to the site concentrations thought to be present. The 79% NH_4^+ Y zeolite contained about 1×10^{21} anion vacancy sites per gram when completely dehydroxylated; this, in agreement with others,^{11,21} is over two orders of magnitude higher than the highest radical-ion concentrations observed. Evidently, there is some limitation to the extent of reaction. Although it is not possible at present to be certain what this factor is, several suggestions based on the zeolite structure may be advanced.

One possible reason is that the substrate molecules may be excluded from the interconnecting channels of the zeolite crystals. These channels have a free diameter in the large cavities of about 13 Å, but the channel openings are only 8–9 Å in diameter (Na^+ form). The molecular size of triphenylmethane and triphenylamine is about 10 Å while perylene is 6.5×9.1 Å. Rabo, Pickert, and Boyle¹⁸ have shown that the maximum number of molecules which can be sorbed by the Y zeolite depends greatly on the level of decationation as well as the critical size of the sorbate molecule. An Na^+ zeolite sorbed 6.2×10^{20} /g molecules of tri-*n*-butylamine (critical dimension = 9.1 Å) at room temperature. When, however, the ammonium ion exchange exceeded about 20%, there was an apparent decrease in pore size after decationating. A 65% NH_4^+ –35% Na^+ Y-type sieve then sorbed only 1.4×10^{20} /g, a decrease of about 80%. By contrast, perfluorotri-*n*-butylamine (critical dimension ≈ 11.5 Å) was sorbed by both the Na^+ and NH_4^+ forms to about the same extent, *i.e.*, about 1.8×10^{19} /g. No change in sorption capacity (13×10^{20} /g) between sodium and decationated Y zeolite was found for molecules of critical dimension 7.5 Å. The dimensions of the perylene and triphenylmethane molecules are sufficiently large to restrict the adsorption and, perhaps, sterically prevent ion formation of those molecules which do manage to pass the shrunken openings of the decationated zeolites and enter the large cavities. Whereas we have no information concerning the distribution throughout the solid of the substrates used in the pres-

(24) H. B. Charman, R. M. Dell, and S. S. Teale, *Trans. Faraday Soc.*, **59**, 453, 470 (1963).

(25) L. S. Singer and J. Kommandeur, *J. Chem. Phys.*, **34**, 133 (1961).

(26) D. N. Stamires and J. Turkevich, *J. Am. Chem. Soc.*, **85**, 2557 (1963).

(27) J. D. Russell, *Trans. Faraday Soc.*, **61**, 2284 (1965)

ent work, Stamires and Turkevich²¹ reported that a maximum of 3.4×10^{20} /g molecules of triphenylamine could be sorbed by a decationized zeolite, indicating that the sorption is restricted, as with tri-*n*-butylamine. This was still more than 20 times the number of radical ions formed.

Ytterhoeven, Christner, and Hall¹⁷ have calculated the number of hydroxyl groups required to terminate the external crystal faces of the zeolite used in this work, *viz.*, 5×10^{19} /g. Since about 40% of these would be expected to be associated with AlO_2^- tetrahedra, there would be $79\% \times 40\% \times 5 \times 10^{19} = 1.6 \times 10^{19}$ /g Lewis acid sites on the external faces, a value near the maximum ion concentration achieved (1.2×10^{19} /g). It should be pointed out that the sites developed on the crystal faces should correspond to the conventional Lewis acid sites of silica-alumina catalysts; anion vacancies may not occur.

There are several reasons for believing that the ion formation was not limited to the crystal faces. Firstly, it was shown that chemisorbed oxygen will effect the reaction. Presumably, O_2 is uniformly distributed throughout the solid after overnight evacuation at 550° , yet at least 30% of this was available for reaction at room temperature. If reaction occurred only at the crystal faces, this tightly bound oxygen would have to migrate with great rapidity throughout the solid. Secondly, the radical and carbonium ion concentrations (per gram) corresponded fairly well with those reported⁷ for silica-alumina catalysts ($\sim 10^{18}$ /g). Here, the surface area was mainly in pores larger than 30 Å, so that the steric restriction should have been much less severe.

Another possibility is that the reaction is thermodynamically restricted, perhaps by an increase in the potential energy of the solid as it takes on electrons. Porter and Hall⁷ noted that radical-ion concentration on silica-alumina did not correlate well with surface area but appeared to depend on mass as well. Also, in the formation of perylene-iodine charge-transfer complexes²⁵ the concentration of neutral perylene molecules is about 30 times greater than the radical-ion concentration.²¹ If ion formation is restricted in this way, then reaction may take place throughout the solid.

The results of the oxygen adsorption study (part B of Results) suggested that radical-ion formation was limited by the maximum amount of oxygen which could be chemisorbed at 550° . This amount (obtained after heating at 545°) was 9×10^{18} O_2 molecules/g of

zeolite which is of the same order of magnitude as the maximum number of radical ions formed on this same zeolite. Higher values were not found when O_2 was present in large excess. Oxygen was ineffective unless the zeolite had been decationized. As found for alumina,¹⁰ ion formation was repressed unless the solid had been dehydroxylated at high temperature. There is a distinct possibility that the sites responsible have not yet been characterized.

E. The Formation of Triphenylcarbonium Ions. The significant difference between carbonium ion and radical-ion formation was in the response to oxygen. The electron acceptor for radical ions probably was O_2 , as in solution,^{28,29} not catalyst hydroxyl groups as suggested by Hirschler.²³ Oxygen was not essential for the reaction of triphenylmethane in the absence of light. The photochemical formation of triphenylmethyl hydroperoxide would understandably increase the carbonium ion concentration when the system is irradiated in the presence of O_2 . Treatment of the zeolite with H_2 removed the oxygen (as H_2O) which effected reaction of perylene and triphenylamine. It is therefore clear that oxygen *does not* participate in carbonium ion formation as it does in radical-ion formation. It is not necessary to oxidize triphenylmethane to triphenylcarbinol (or hydroperoxide) preliminary to carbonium ion formation as claimed.¹⁶ By the same token, however, the true mechanism is still uncertain. Direct hydride ion abstraction by the cation-anion vacancy pair sites⁷ is a possibility, but as with radical-ion formation the maximum concentration of ions developed is many times less than the density of sites available. Again, it is possible that the reaction occurs on defects developed during dehydroxylation, which have not yet been characterized. The loss in ability to form carbonium ions when the zeolite is completely dehydroxylated (Figure 1) is not understood and is under further investigation.

Acknowledgment. This work was sponsored by the Gulf Research and Development Co. as part of the research program of the Multiple Fellowship on Petroleum. Special thanks are due to Dr. P. E. Pickert and to the Linde Co., Division of Union Carbide Corp., for the special sample of ultrapure zeolite.

(28) W. I. Aalbersberg, Thesis, Free University of Amsterdam, The Netherlands, 1960.

(29) W. I. Aalbersberg, G. J. Hoijsink, E. L. Mackor, and W. P. Weijland, *J. Chem. Soc.*, 3049, 3058 (1959).

Tracer Studies of Acid-Catalyzed Reactions. V. Carbon-14 Kinetic

Studies of *n*-Butene Isomerization over Alumina and Silica-Alumina Catalysts

by Joe W. Hightower and W. Keith Hall

Mellon Institute, Pittsburgh, Pennsylvania (Received November 18, 1966)

Carbon-14 tracers have been used in a static reactor to examine the kinetics of *n*-butene isomerization over alumina and silica-alumina. All reactions were first order and all paths interconnecting the various isomers were significant. Relative rate constants were determined for each catalyst at room temperature. The selectivities over both catalysts were temperature dependent, although those of silica-alumina were much less so than those of alumina. The activation energy differences between all paths have been quantitatively determined. Silica-alumina underwent rapid poisoning and this poisoning resulted in apparent selectivity changes when the catalyst-to-charge ratio was large for low-temperature runs. This apparently resulted from the preferential formation of "residue" from 1-butene. Some of the mechanisms which have been advanced in the literature to explain these isomerization reactions were tested in light of the kinetic results. The data presented are consistent with a common intermediate, possibly a classical carbonium ion, for all paths over silica-alumina. Using this model, together with the activation energy profile, it was possible to account quantitatively for the selectivities and reactivities observed for the three *n*-butenes. Over alumina it is probable that the various reactions proceed through different surface complexes, perhaps on different sites.

Introduction

Several investigators¹⁻⁶ who have studied *n*-butene isomerization over oxide catalysts have suggested that the reactions follow first-order kinetics. Haag and Pines have clearly demonstrated that 1-butene isomerization is first order over both sodium dispersed on alumina¹ at room temperature and pure alumina² at 230°. Recently we⁶ have used C¹⁴ tracers in a microcatalytic reactor⁷ to demonstrate the first-order character of *n*-butene reactions over alumina, fluorided alumina, and silica-alumina at temperatures below 100°.

Since there are always some inherent uncertainties about kinetic measurements made using a microcatalytic technique, additional work was undertaken to investigate the kinetics of *n*-butene isomerization over alumina and silica-alumina in a static reactor. C¹⁴ tracers were used in a rather novel way to follow simultaneously the isomerization of both 1-butene and *cis*-2-butene from low conversion to equilibrium. The two sets of results are compared herein.

The effect of temperature on selectivity can supply information about possible common transition states in the formation of any two isomers from the third. Measurements of the selectivities over both catalysts have been made at various temperatures and the activation energy differences between the various paths have been quantitatively determined.

While kinetic studies alone (disregarding isotope effects) can lead only to formal reaction schemes, in some cases they may be used to test the credibility of mechanisms which necessarily imply certain kinetic

- (1) W. O. Haag and H. Pines, *J. Am. Chem. Soc.*, **82**, 387 (1960).
- (2) W. O. Haag and H. Pines, *ibid.*, **82**, 2488 (1960).
- (3) S. Ogasawara and R. J. Cvetanovic, *J. Catalysis*, **2**, 45 (1963).
- (4) D. M. Brouwer, *ibid.*, **1**, 22 (1962).
- (5) J. Wei and C. D. Prater, *Advan. Catalysis*, **13**, 203 (1962).
- (6) J. W. Hightower, H. R. Gerberich, and W. K. Hall, *J. Catalysis*, **7**, 57 (1967).
- (7) R. J. Kokes, H. Tobin, and P. H. Emmett, *J. Am. Chem. Soc.*, **77**, 5860 (1955).

consequences. The relative rate constants developed here have been used to calculate expected molar radioactivities in the products and these are compared with experimentally determined values. In this way it has been possible to exclude several possible mechanisms which have been advanced in the literature.

Experimental Section

Reactor. In all these static experiments the reactor was a 300-cc spherical Pyrex bulb connected through a stopcock and standard taper to a conventional BET-type gas-handling system. The catalyst was placed at the bottom of a 22-mm o.d. well which extended 4 in. below the bulb. An oven which fit around the catalyst well could be maintained within $\pm 1^\circ$ of a given temperature by a Thyatron resistance controller. The gas was stirred by convection. Since the reaction conditions were selected so that measurements could be made over periods of days, this was deemed satisfactory. No attempt was made to protect the catalyst from mercury vapor.

Catalysts and Pretreatment. One alumina and two silica-alumina catalysts were examined in these experiments. The (GA-48) alumina⁸⁻¹⁰ was prepared from the neutral hydrolysis of redistilled aluminum isopropoxide by the MK Research and Development Co., Pittsburgh, Pa. Its total metallic impurity level was less than 50 ppm and its surface area was 158 m²/g. X-Ray measurements, made as the catalyst was dehydrated during the final stages of preparation, revealed that it was probably a mixture of η - and γ -alumina.

The first silica-alumina (DSA-1)¹¹ was a very pure synthetic sample from the same preparation used by Leftin and Hermana¹² in their optical photometric studies. The catalyst contained 88% SiO₂ and 12% Al₂O₃ with less than 50 ppm metallic impurities. Its surface area was 278 m²/g.

The second silica-alumina (M-46) was a commercial Houdry catalyst containing 13% alumina and having a surface area of 270 m²/g. The major metallic impurity was iron which amounted to between 0.1 and 0.3 wt %.

Before use each catalyst was given a standard pretreatment which consisted of the following steps. First, each was outgassed in the reactor at 300° for 2 hr. It was then contacted with 200 mm of O₂ and the temperature was raised to 530° for 1 hr. After a 30-min evacuation at 530°, another 200-mm charge of O₂ was admitted and allowed to stand for 2 hr at the same temperature. This was followed by overnight evacuation at 530° to a sticking vacuum in a McLeod gauge.

The catalysts were then cooled to room temperature; in all cases they were white after this treatment.

Reactants. The 1-butene and *cis*- and *trans*-2-butene (Phillips Research grade) were at least 99.6% pure. Just before use, each was distilled from -78 to -195° and outgassed to a sticking vacuum at -195°. No impurities were detected by glpc analysis.

The 1-butene-1-C¹⁴ (4.2 mcuries/mmole) was purchased from Tracerlab and used without dilution following purification by gas chromatography. *cis*-2-Butene-1-C¹⁴ was prepared from the radioactive 1-butene by isomerization over a small sample of 1.2% fluorided alumina in a microcatalytic apparatus; this catalyst was chosen because of its high selectivity.⁶ The radioactive mixtures were prepared by combining about 0.1% of the radioactive material with the purified gases. Tests using a dilution technique revealed no radioactivity in any of the other isomers.

Procedure. After each catalyst had been pretreated, it was cooled to -195° and a measured amount of the desired reactant was frozen into the reaction vessel which was then rapidly warmed to reaction temperature. In each radioactive experiment 100 cc of the mixture and 30 mg of catalyst were used and 4-cc samples were periodically withdrawn and subjected to glpc and radioactivity analysis. The 30-ft \times 0.25-in. chromatographic column contained a 2:1 ratio of dimethyl sulfolane to hexamethylphosphoramide on firebrick and was thermostated at 0°. The separated products were individually trapped and tested for radioactivity in a vacuum-tight Geiger counter previously described;⁶ all specific activity measurements are given as counts min⁻¹ mm⁻¹ in the counter. These can be converted to counts min⁻¹ mmole⁻¹ by multiplying by 8.5×10^2 mm mmole⁻¹.

In the experiments designed to study effect of temperature on selectivity, 25 cc of each pure compound was used. Samples were taken every 20 min and conditions were adjusted in such a way that less than 5% conversion occurred in 2 hr. Catalyst samples ranged in weight from 1 to 100 mg. Product ratios were plotted as a function of time at a given temperature (see Figure 8). These were extrapolated to obtain initial selectivities. Reproducibility was tested by

(8) W. K. Hall and F. E. Lutinski, *J. Catalysis*, **2**, 518 (1963).

(9) W. K. Hall, F. E. Lutinski, and H. R. Gerberich, *ibid.*, **3**, 512 (1964).

(10) W. K. Hall, H. P. Leftin, F. J. Cheselske, and D. E. O'Reilly, *ibid.*, **2**, 508 (1963).

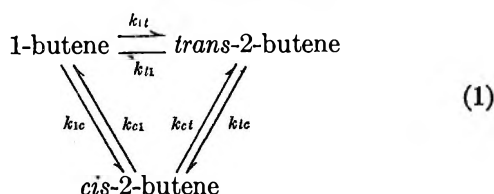
(11) W. K. Hall, D. S. MacIver, and H. P. Weber, *Ind. Eng. Chem.*, **52**, 421 (1960).

(12) H. P. Leftin and E. Hermana, *Proc. Intern. Congr. Catalysis*, **3rd**, Amsterdam, 1963, **2**, 1064 (1964).

evacuating the mixture after several hours reaction and replacing it with a second 25-cc charge of reactant.

The reactions were "clean." Isobutene, *n*-butane, isobutane, or dimers would have appeared on the glpc chromatograms had they been present in appreciable amounts. Since none of these was detected, skeletal isomerization, saturation, or polymerization could not have been important. A carbonaceous (probably polymeric) "residue" did form on the surface of the silica-alumina catalysts, but it was estimated from earlier results⁶ that no more than about 1% of the gas in the present experiments was utilized in this way. This could not be displaced into the gas phase at the temperatures employed.

Treatment of Data from Radioactive Experiments. Haag and Pines¹ have derived the rate equations for parallel, reversible, first-order reactions among members of a three-component mixture of the type



The amount of *trans*-2-butene formed from 1-butene at any time is given by the equation

$$\begin{aligned}
 x = & \frac{a}{\sqrt{m^2 - 4n}} \left[k_{1t} - \frac{p}{2n}(m + \sqrt{m^2 - 4n}) \right] \times \\
 & \exp[-(m - \sqrt{m^2 - 4n})t/2] - \\
 & \frac{a}{\sqrt{m^2 - 4n}} \left[k_{1t} - \frac{p}{2n}(m - \sqrt{m^2 - 4n}) \right] \times \\
 & \exp[-(m + \sqrt{m^2 - 4n})t/2] + \frac{pa}{n} \quad (2)
 \end{aligned}$$

where x = concentration of *trans*-2-butene at time t ; a = starting concentration of 1-butene; $m = k_{1t} + k_{1l} + k_{c1} + k_{1c} + k_{2c} + k_{c2}$; $n = k_{1l}k_{c1} + k_{1t}k_{2c} + k_{1l}k_{c2} + k_{1t}k_{c1} + k_{1l}k_{c1} + k_{1t}k_{c2} + k_{1c}k_{2c} + k_{1c}k_{c1} + k_{1c}k_{c2}$; and $p = k_{1l}k_{c1} + k_{1l}k_{c2} + k_{1c}k_{c1}$. Analogous expressions can be derived for concentrations of other isomers as a function of time.

The rate constants are not all independent, because their product in a clockwise direction must equal the corresponding product in a counterclockwise direction around the three-component mixture, *viz.*

$$k_{1c}k_{c1}k_{1l} = k_{c1}k_{1t}k_{1c} \quad (3)$$

Also, at any temperature the ratio of the rate constants for forward and reverse reactions between any two

isomers must be equal to their respective thermodynamic equilibrium constants, *e.g.*, at 23°¹³

$$\begin{aligned}
 k_{c1}/k_{1c} &= 0.15 \\
 k_{1l}/k_{1t} &= 0.04 \\
 k_{1c}/k_{c1} &= 0.26
 \end{aligned} \quad (4)$$

Application of these equations to our results involved the implicit assumption that the surface reactions are rate controlling; *i.e.*, adsorption and desorption are relatively fast. If this condition is satisfied, the relative rate constants obtained in the homomorphic description of eq 1 reflect the true reaction sequences which occur on the surface. Experiments justifying this assumption are reported elsewhere.⁶

The equations were used as follows. Suppose the starting mixture were 1-butene with a trace of radioactive *cis*-2-butene. Two separate and independent reactions were assumed. The 1-butene reacted as though it were the only species initially present in the system and the product distributions were calculated as a function of time from eq 2 by assuming arbitrary rate constants which satisfied eq 3 and 4. Relative rate constants from our earlier work⁶ provided a first approximation and a "best fit" of the data was obtained by successive approximations (*vide infra*). Similarly, the radioactive *cis*-2-butene also reacted as though it were the only species present and product distributions were again calculated from eq 2 using the same arbitrary time units and rate constants applied to 1-butene isomerization. This yielded amounts of both nonradioactive and radioactive material for each of the three isomers at various times as both reactions proceeded toward equilibrium. The specific activity of any isomer could then be derived from the number of moles originating from the original radioactive gas which is present in each particular isomer and the total number of moles of that gas.

A term, α_a^i ,¹⁴⁻¹⁶ which is a function of time, was defined as

$$\alpha_a^i = \left[\frac{\text{instantaneous specific activity of any isomer (i)}}{\text{instantaneous specific activity of initial radioactive isomer (a)}} \right]_t \quad (5)$$

This parameter can be determined experimentally

(13) D. M. Golden, K. W. Egger, and S. W. Benson, *J. Am. Chem. Soc.*, **86**, 5416 (1964).

(14) W. A. Van Hook and P. H. Emmett, *ibid.*, **84**, 4410 (1962).

(15) J. W. Hightower and P. H. Emmett, *ibid.*, **87**, 939 (1965).

(16) J. W. Hightower and P. H. Emmett, *Proc. Intern. Congr. Catalysis, 3rd, Amsterdam, 1964*, **1**, 688 (1965).

for comparison with values calculated from kinetic models. The α values are very sensitive to changes in relative rate constants and, hence, to mechanism.

Treatment of Data from Selectivity vs. Temperature Experiments. The temperature dependence of the *cis*-to *trans*-2-butene ratio from 1-butene isomerization was obtained from a plot of the log of the initial *cis*/*trans* ratios (assumed proportional to k_{1c}/k_{1t}) vs. $1/T$. The activation energy difference between the two parallel paths ($\Delta E = E_{1c} - E_{1t}$) could then be determined from

$$\log \left[\frac{(k_{1c}/k_{1t})_1}{(k_{1c}/k_{1t})_2} \right] = \frac{\Delta E}{2.303R} \left[\frac{1}{T_2} - \frac{1}{T_1} \right] \quad (6)$$

Analogous plots and calculations were made for selectivities of each of the three *n*-butenes over both alumina and silica-alumina in the temperature region from 0 to 100°.

Results

The six relative rate constants (k_{1c} defined as unity) for the *n*-butene interconversion reactions, together with representative values taken from the literature, are given in Table I. Values from the present work were obtained from plots of α_a^i vs. conversion in which arbitrary rate constants (consistent with eq 3 and 4) were varied until the calculated lines gave good agreement with experimental points. (The k_{1t} derived in this way are refinements of previously determined values; comparison can be made in Table I.) Such plots are shown in Figure 1A for *cis*-2-butene (1-butene- C^{14}) isomerization over DSA-1 and in Figure 2 for 1-butene (*cis*-2-butene- C^{14}) isomerization over GA-48. Similar results were obtained over M-46 silica-alumina. The conversion in each case was based on that of the nonradioactive component and was defined as the sum of the mole fractions of the two nonradioactive product isomers. By this definition it was only possible for the *cis*-2-butene and 1-butene to undergo 80.0 and 96.9% conversion, respectively, at equilibrium.

The corresponding compositional data have been plotted in triangular form for the same two systems in Figures 3 and 4. Over silica-alumina the line and experimental points originating from the *cis*-2-butene corner were based on conversion of the nonradioactive material, while those from the 1-butene corner were based on the radioactive component, the two sets of kinetics being determined simultaneously in the same experiment. The solid lines were calculated with eq 2 using the same parameters which best fit the points in Figures 1 and 2. The satisfactory "fit" of both sets of data demonstrates that both isomers are obeying the

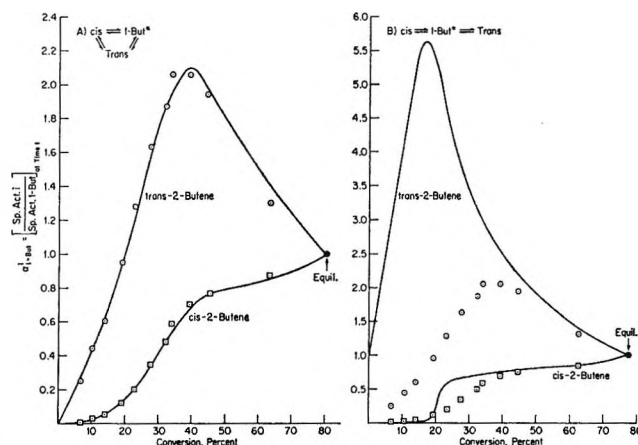


Figure 1. α -Value plot for products of *cis*-2-butene (1-butene- C^{14}) isomerization over synthetic silica-alumina, DSA-1, at 23°. Points are experimental; calculated lines based on two models.

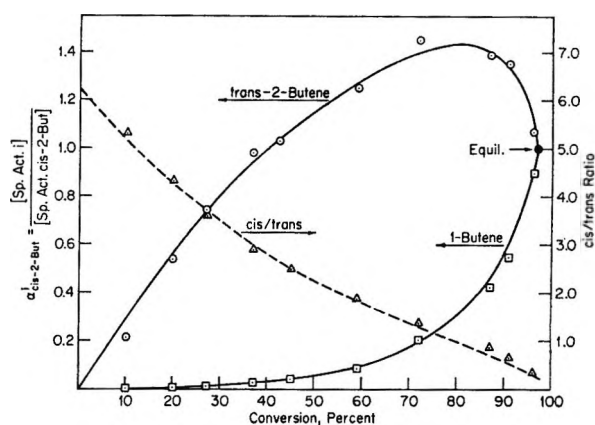


Figure 2. α -Value plot for products of 1-butene (*cis*-2-butene- C^{14}) isomerization over alumina, GA-48, at 23°.

same first-order law, *i.e.*, that the large excess of *cis*-2-butene is not interfering with the reaction of the "trace" amount of butene-1. The radioactive and nonradioactive isomers were reversed in the case of alumina in Figure 4. The dashed lines drawn from the corners representing the two reactants are tangent to the composition curves (solid lines) at low conversion and their intercepts on the opposite sides correspond to the initial selectivities (k_{1c}/k_{1t} and k_{c1}/k_{ct}). The third selectivity (k_{t1}/k_{tc}) was then fixed by a line through the *trans*-2-butene corner and the intercept of the other two tangents, a necessary consequence of the rate constant restrictions given in eq 3 and 4.

It was instructive to plot the data according to a first-order equation which, although based on an incorrect model, delineated poisoning effects and indicated the reactions were generally first order on a time

Table I: Relative Rate Constants for *n*-Butene Isomerization over Alumina and Silica-Alumina

Catalyst	Method ^a	Temp, °C	Ref	Relative rate constants ^c						Selectivities ^b		
				k_{1c}	k_{c1}	k_{1t}	k_{t1}	k_{ct}	k_{tc}	k_{1c}/k_{1t}	k_{ct}/k_{c1}	k_{tc}/k_{t1}
DSA-1	ST	23	b	1.00	0.15	1.10	0.04	0.14	0.04	0.91	0.93	1.00
DSA-1	S	85	12	1.00		0.59		1.70
DSA-1	S	150	12	1.00	0.29	0.78	0.15	1.29
M-46	ST	23	b	1.00	0.15	1.00	0.04	0.16	0.04	1.00	1.07	1.00
M-46	MT	50	6	1.00	0.24	0.95	0.06	0.31	0.09	1.05	1.29	1.50
Ketjen MS3-A	M,F	150	4	1.00	0.29	0.88	0.17	0.29	0.19	1.13	1.00	1.12
Esso SA	Circ	75	21	1.00	0.23	0.94	0.07	0.26	0.09	1.06	1.13	1.28
WRG-SA (11% A)	Circ	35	21	1.00	0.18	0.63	0.03	0.22	0.06	1.59	1.22	2.00
WRG-SA (13% A)	M	24	6	1.00	0.15	1.00	0.05	0.26	0.07	1.00	1.73	1.40
GA-48	ST	23	b	1.00	0.15	0.16	0.01	0.67	0.17	6.25	4.47	17.00
GA-48	MT	50	6	1.00	0.21	0.49	0.03	1.05	0.30	2.04	5.00	10.00
Alcoa	Circ	300	21	1.00	0.63	0.77	0.30	1.30	>200	>200
η -Al ₂ O ₃ pellets	F	230	2	1.00	0.51	0.42	0.11	0.51	0.26	2.38	1.00	2.36
η -Al ₂ O ₃ powder	F	230	2	1.00	0.51	0.23	0.06	0.51	0.26	4.35	1.00	4.34
Na-Al ₂ O ₃	S	30	1	1.00	0.16	0.25	0.01	0.12	0.04	4.00	0.75	4.00
Equil	...	50	13	1.00	0.21	3.35	0.21	3.44	1.02	0.30	16.40	4.86
Equil	...	150	13	1.00	0.36	2.16	0.35	2.24	1.00	0.46	6.22	2.86

^a Methods: ST = static tracer; S = static; MT = microcatalytic tracer; M = microcatalytic; F = flow; Circ = circulation.

^b Results of static tracer experiments reported in this paper. ^c Some rate constants calculated from selectivity observed and K_{eq} (see ref 13).

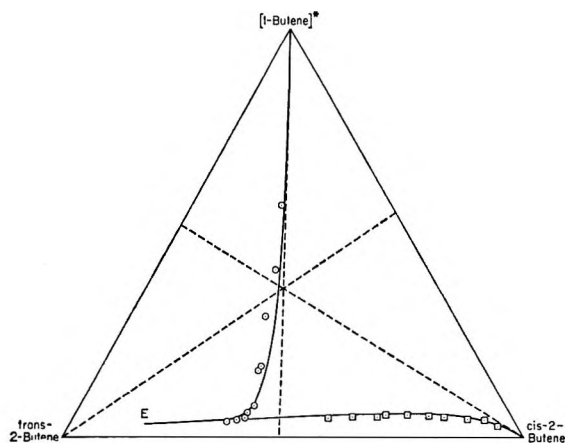


Figure 3. Mole fraction of products of *cis*-2-butene (1-butene-C¹⁴) isomerization over silica-alumina, DSA-1, at 23°. Circles and squares are for the same (successive) times.

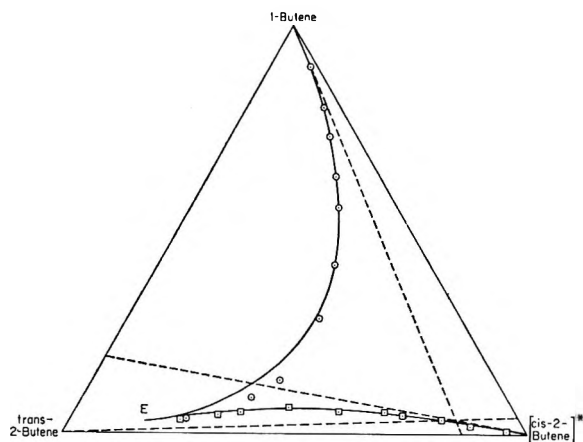


Figure 4. Mole fraction of products of 1-butene (*cis*-2-butene-C¹⁴) isomerization over alumina, GA-48, at 23°. Circles and squares are for the same (successive) times.

as well as on a conversion basis. Figures 5 and 6 contain data for three static experiments. The calculations were based on the nonradioactive component (*cis*-2-butene for silica-alumina and 1-butene for alumina). The data were plotted according to

$$-\ln(X_0 - X) = kt - \ln X_0 \quad (7)$$

where X and X_0 refer to conversions at time t and at equilibrium, respectively. This equation holds rigorously for a reactant going to a single product, the reaction being first order in both directions; it has the ad-

vantage over the exact equations of being linear and therefore useful for data testing. Product distributions calculated using real rate constants in the exact equations were shown to follow this equation through at least 70% conversion. The experimental data for alumina also fitted over the first 70% conversion and the zero-time intercept passed through $\log X_0$, indicating poisoning was not affecting the kinetics during the run.

Both silica-alumina catalysts showed signs of poisoning, but these were manifested in different ways. Over M-46 (Figure 5) the first-order plot was fairly linear

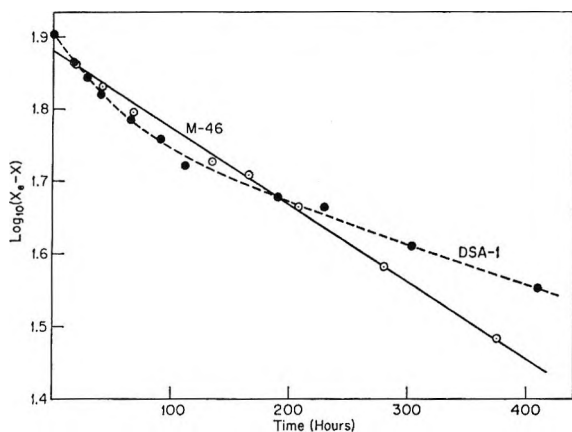


Figure 5. First-order plot for disappearance of *cis*-2-butene over silica-alumina, DSA-1 and M-46, at 23°.

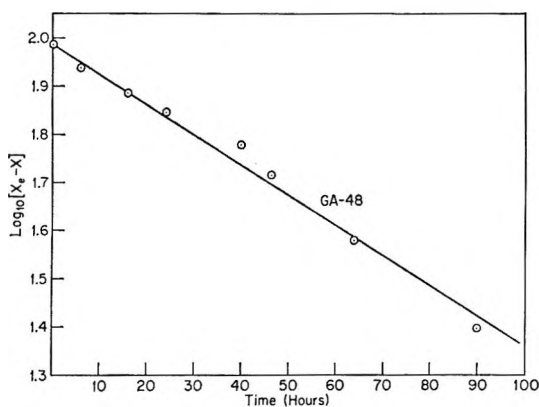


Figure 6. First-order plot for disappearance of 1-butene over alumina, GA-48, at 23°.

through 50% conversion, but its zero-time intercept was significantly below $\log X_e$, indicating a rapid initial poisoning. On the other hand, the first-order plot for DSA-1 passed through $\log X_e$, but its slope decreased continuously for the first 100 hr before becoming linear. This is characteristic of a slow, time-dependent poisoning.

Figure 7 shows the activation energy profiles for the various *n*-butene isomerization reaction paths over alumina and silica-alumina. Each ΔE value was determined from the slope of an Arrhenius plot according to eq 6 and each plot contained from five to two points in the temperature region 0–100°. The product ratios were extrapolations of low-conversion data to zero conversion (*e.g.*, see Figure 8). Duplicate experiments for each isomer showed a maximum ΔE deviation of 0.2 kcal/mole. A significant test of the accuracy of these values lies in the circular agreement obtained for both catalysts. For example, the activation energy profile (Figure 7) can be established from data from

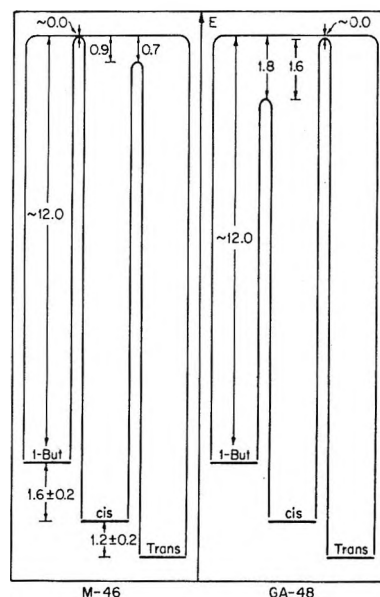


Figure 7. Activation energy profile for *n*-butene interconversion reactions over alumina and silica-alumina. Thermodynamic stabilities¹³ are for 23°.

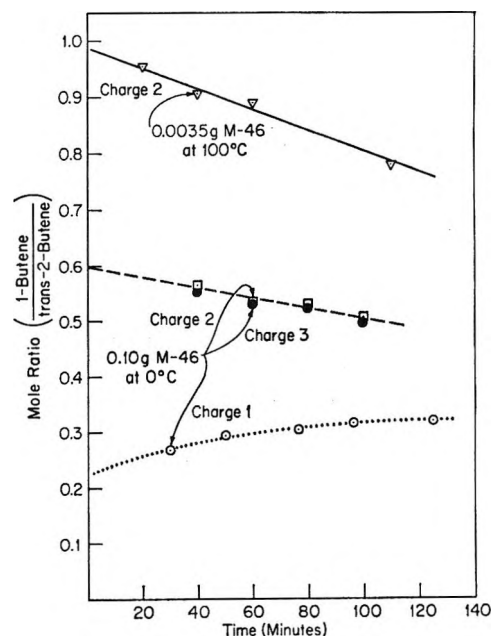


Figure 8. Apparent changes in 1-butene/*trans*-2-butene ratios obtained from *cis*-2-butene isomerization over M-46 silica-alumina in a static reactor as the catalyst is poisoned.

two of the three isomers, *e.g.*, 1-butene and *cis*-2-butene. It can be checked by determining the temperature dependence of the selectivity from the third, *i.e.*, *trans*-2-butene. Comparison of ΔE values always agreed within 0.2 kcal/mole.

The relative stabilities of the three isomers in the figure were taken from values reported by Benson and co-workers.¹³ The absolute activation energy for 1-butene isomerization has been reported^{4,6,12,17} to lie between 8 and 20 kcal/mole over similar catalysts; our results indicated a value of about 12 kcal/mole in both cases.

The *n*-butene selectivities over alumina were much more sensitive to temperature changes than those over silica-alumina. Also, the energy profiles for the two catalysts differed in kind. For example, in *cis* isomerization over silica-alumina the selectivity k_{c_i}/k_{c_t} increased with temperature, whereas it decreased over alumina. The ΔE for 1-butene isomerization over alumina (1.8 kcal/mole) was in the same direction as that reported by Amenomiya and Cvetanovic¹⁸ (2.9 kcal/mole) for a chromia-alumina catalyst. However, the temperature independence of k_{1_c}/k_{1_t} for DSA-1 is in disagreement with the 1.3-kcal/mole activation energy difference reported by Leftin and Hermana.¹² Their experiments were repeated using finely ground particles of the same catalyst preparation. Between 0 and 100°, as was observed with M-46, the 1-butene selectivities showed no temperature dependence. The values obtained by Leftin and Hermana may have been disguised by diffusion due to their larger particle size, higher temperature, and faster reaction rates. Extrapolation of their data to 23° would predict a *cis/trans* ratio of 2.9; the ratio we observed at 23° was 0.91.

No selectivity changes as a result of poisoning were found with alumina. Second and third charges admitted with a 1-min evacuation between each gave selectivities identical with those of the first charge under similar conditions. Over silica-alumina, however, selective poisoning was observed. In these cases when a *2-butene* charge was admitted to a freshly activated catalyst, the initial reaction gave abnormally low 1- to 2-butene ratios, as may be seen in Figure 8. Additional charges gave the expected ratios and these ratios could be reproduced with subsequent charges (Figure 8). The low initial ratio was probably due to the preferential formation of "residue" from 1-butene, as was observed in the microcatalytic C¹⁴ experiments.⁶ Because of this, the initial ratios used in eq 6 to calculate activation energy differences were in all cases those obtained after the catalyst had been "prepoisoned" with one charge of the starting *2-butene*. Such selectivity changes were not observed for 1-butene isomerization.

Discussion

Good agreement between the calculated lines and experimental points in Figures 1-4 justifies the as-

sumption of two independent, first-order sets of reactions—one involving the radioactive component, the other the nonradioactive isomer. Plots such as those in Figures 1 and 2 are extremely sensitive to relative rate constants chosen and even a small change in rate constant ratios during the reaction would make it impossible to fit the data with precision. These α -value plots are significant because they demonstrate the existence of all reaction paths over both catalysts. Had all of the *trans* been formed from the *cis* isomer through intermediate 1-butene over silica-alumina,¹² the experimental α value vs. conversion data of Figure 1 could not have been fitted with a calculated curve. There is insufficient freedom available for adjusting parameters. By definition, $k_{1_c} = 1$ and k_{c_t} is then fixed by eq 4; similarly k_{1_c}/k_{1_t} is derived from the initial *cis/trans* ratio; consequently k_{c_t} is fixed by this condition and by eq 4. Hence, nearly the same rate parameters must be used as in the calculation based on eq 1, except that k_{c_t} and k_{c_c} are assumed to be negligible. Curves calculated on this basis are shown in Figure 1B. The experimental points which are fitted by the curves of Figure 1A are shown for comparison. Note the zero-conversion intercept of unity for this mechanism as compared with the zero intercept for the calculation based on eq 1. This is because if all of the *trans* isomer is formed *via* (the radioactive) 1-butene, the specific radioactivity of the *trans* can never be less than that of the 1-butene. If direct *cis-trans* interconversion is permitted, a zero intercept results because most of the initial *trans* product is formed from the 1000-fold excess of *cis*-2-butene.

Similar reasoning applies to the exclusive formation of *trans* from 1-butene through an intermediate *cis* isomer over alumina (Figure 2). The available data show that all reaction paths interconnecting the three *n*-butenes exist and contribute appreciably to the product ratios.⁶ Thus any mechanism which necessarily implies that rate constants connecting any two isomers are zero^{12,19,20} cannot be solely responsible for the results.

The relative insensitivity of silica-alumina selectivities to degree or nature of poisoning, source of catalyst, silica to alumina ratio, or temperature is consistent with a mechanism which involves one common intermediate for all reactions. The only such complex considered in the literature, which will provide a direct

(17) S. Ogasawara and R. J. Cvetanovic, *J. Catalysis*, **2**, 45 (1963).

(18) Y. Amenomiya and R. J. Cvetanovic, *Can. J. Chem.*, **40**, 2130 (1962).

(19) P. J. Lucchesi, D. L. Baeder, and P. J. Longwell, *J. Am. Chem. Soc.*, **81**, 3235 (1959).

(20) J. Turkevich and R. K. Smith, *J. Chem. Phys.*, **16**, 466 (1948).

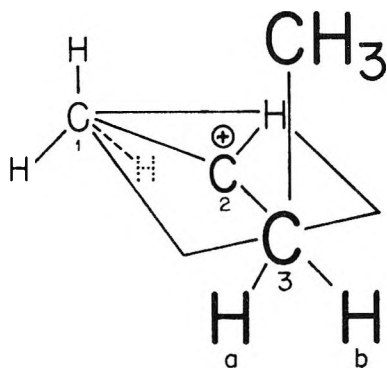


Figure 9. Classical 2-butyl carbonium ion intermediate for *n*-butene isomerization over silica-alumina.

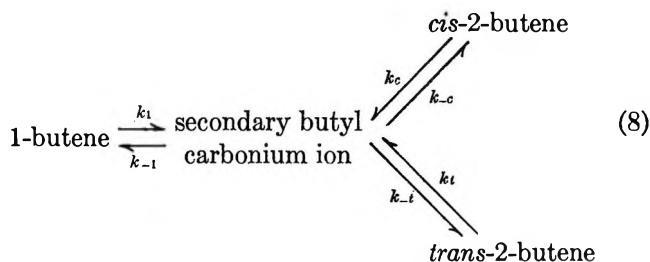
pathway between all of the isomers, is the classical *sec*-butyl carbonium ion.²¹ It was found possible to modify an earlier model²² based on this ion, in view of the new information, so as to predict uniquely the observed selectivities and the relative reactivities of the three isomers as well.

Consider the structure of the carbonium ion shown in Figure 9. The C₁, C₂-H, and C₃ atoms all lie in a plane presumed to be parallel to the surface. Owing to steric interaction, the methyl group extends away from the catalyst and free rotation about the C₂-C₃ bond is greatly inhibited. However, rotation about the C₁-C₂ bond may occur. This ion could be formed from 1-butene by proton addition to C₁ and a 2-butene product would result from loss of either hydrogen atom on C₃. However, these two H atoms (labeled a and b) are geometrically different, for, should the H_a atom be lost, the methyl group would tend to fall into a *cis* configuration, whereas, if H_b were lost, *trans*-2-butene would be the product. Since the two C₃-H bonds are energetically similar, one would expect them to be broken with equal probabilities at all temperatures. As can be seen in Table I, selectivities (k_{1c}/k_{1t}) near unity are generally reported for 1-butene isomerization over silica-alumina and these values were independent of temperature (Figure 7).

On the other hand, the 1- to 2-butene product ratios obtained from isomerization of either 2-butene cannot be satisfactorily explained in this way. The same carbonium ion can be formed from either 2-butene by proton addition to the C₃ position, but statistical product formation would favor 1-butene by odds of 3 to 1 (since there are three hydrogen atoms on C₁). However, the C₁-H primary bonds which must be broken in forming 1-butene may be stronger than the C₃-H secondary bonds whose loss results in a 2-butene. If the 800-cal/mole (Figure 7) higher activation energy barrier to reach the 1-butene reflects this difference in

bond strength, it may be used in the Boltzman equation to calculate the relative probability of barrier crossage in the two directions; this reduces the odds by 1 to 4 at room temperature. A combination of the statistical model (3:1) and energetic argument (1:4) results in a 1- to 2-butene product ratio of 0.75; values ranging from 0.5 to 1.1 are commonly reported (Table I).

If the *sec*-butyl carbonium ion acts as a common intermediate for the isomerization reactions over silica-alumina, the homomorphic eq 1 must be rewritten as



Moreover, the activation energy profile of Figure 7 must be recast as shown in Figure 10. The 2-butyl carbonium ion is a high-energy state; it is unstable with respect to any of the three isomers. It is not, however, identical with the transition states because, were this the case, there would be no temperature dependence of the selectivity for any of the isomers. The transition state therefore corresponds to the top of the energy barrier between a particular isomer and the carbonium ion. The data of Figure 7 show that the barrier for 1-butene is higher by about 0.8 kcal/mole than for either of the other two isomers. In view of the arguments made above concerning the temperature-independent *cis/trans* ratios, it may be supposed that the tops of the barriers between the carbonium ion and *cis*- and *trans*-2-butene, respectively, are of about the same height, ϵ . Present data do not define this height, but it may be that the potential well created by the three barriers is fairly deep. Accordingly, the carbonium ion would be a metastable state. The kinetics may now be formulated. Since all of the reactions are first order, equations for the initial disappearance of each species (neglecting back reactions) become

$$-\frac{d(1\text{-butene})}{dt} = (k_{1c} + k_{1t})P_1 = (A_{1c}e^{-E/RT} + A_{1t}e^{-E/RT})P_1$$

(21) N. F. Foster and R. J. Cvetanovic, *J. Am. Chem. Soc.*, **82**, 4274 (1960).

(22) H. R. Gerberich and W. K. Hall, *J. Catalysis*, **5**, 99 (1966).

$$-\frac{d(cis)}{dt} = (k_{c1} + k_{ci})P_c = [3A_{c1}e^{-(E+\lambda_{1c})/RT} + A_{ci}e^{-(E+\lambda_{1c}-0.8)/RT}]P_c \quad (9)$$

$$-\frac{d(trans)}{dt} = (k_{t1} + k_{ti})P_t = [3A_{t1}e^{-(E+\lambda_{1t})/RT} + A_{ti}e^{-(E+\lambda_{1t}-0.8)/RT}]P_t$$

where the factor 3 represents the statistical weighting factor due to the three equivalent H atoms on the 1-carbon atom which could be lost in formation of 1-butene.

The relative reactivities are the ratios of the initial rates of disappearance of the three isomers under conditions of equal temperature and pressure, *i.e.*, $(k_{1c} + k_{1t}) : (k_{c1} + k_{ci}) : (k_{t1} + k_{ti})$. Experimental values for this ratio may be obtained from Table I and compared with values calculated from the right-hand members of eq 9, if it is assumed that all of the preexponential factors are equal after the statistical weighting factor, 3, has been factored, *e.g.*

$$d(1\text{-butene})/dt : d(trans)/dt \approx 2 : e^{-\lambda_{1t}/RT} [3 + e^{0.8/RT}] = 21.7$$

The resulting comparison of experimental ratios to calculated ratios (for 1-butene and *cis*- and *trans*-2-butene) is

$$1.0:0.15:0.040 = 1.0:0.24 \pm 0.06:0.046 \pm 0.011$$

The uncertainties in the calculated ratios are those quoted by Golden, Egger, and Benson¹³ for their enthalpy differences (λ_{1c} and λ_{1t}). The reasonably good agreement of our experimental data with values calculated from the model suggests that equating all of the A_{ij} is a fair approximation. A corollary is that the same number and kinds of active sites are operative for all reactions.

Selectivity ratios can be calculated in a similar way and the results agree exactly with those derived above, from the consideration of Figure 9, *e.g.*

$$k_{c1}/k_{t1} = 3A_{c1}e^{-(E+\lambda_{1c})/RT} / A_{t1}e^{-(E+\lambda_{1c}-0.8)/RT} \approx 3e^{-0.8/RT} \quad (10)$$

The same expressions may be combined in a different way to yield the thermodynamic equilibrium constants, *e.g.*

$$K_{eq}(1,t) = \frac{k_{t1}}{k_{1t}} = \frac{(3A_{t1}e^{-(E+\lambda_{1t})/RT}) / (A_{1t}e^{-E/RT})}{3e^{-0.8/RT}} \approx 3e^{-\lambda_{1t}/RT} \quad (11)$$

A comparison of values calculated from the model with those taken from the literature is given in Table II.

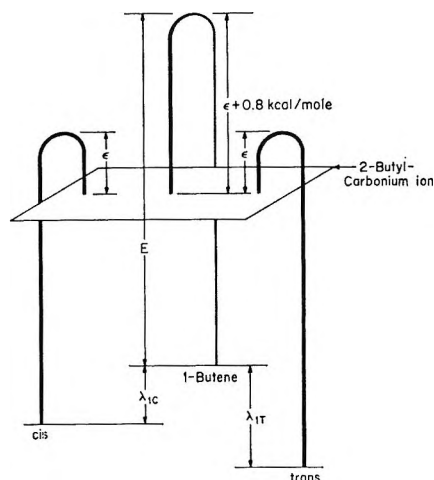


Figure 10. Energy profile showing common intermediate in isomerization of *n*-butenes over silica-alumina values of λ_{1c} and λ_{1t} at 23° are 1.6 and 2.8 kcal/mole, respectively.¹³

Table II: Comparison of True and Calculated Equilibrium Constants Based on a Carbonium Ion Intermediate over Silica-Alumina at 23°

	K_{eq} calcd from model	K_{eq} from lit. ¹³	Entropy factor ^a	
			From ref 13	From model
1-Butene <i>trans</i>	0.03 ± 0.01	0.04	4.7 ± 1.0	3
1-Butene <i>cis</i>	0.21 ± 0.07	0.15 ± 0.01	2.3 ± 0.3	3
<i>cis</i> <i>trans</i>	0.14 ± 0.05	0.26 ± 0.01	1.8 ± 0.2	1

$$^a e^{\Delta S_{ij}/RT} = nA_{ij}/A_{jt} \text{ where } n = 3 \text{ or } 1.$$

The discrepancies may reflect differences in the A_{ij} which were equated to effect the comparison. This cancellation also removed the factors which reduce the entropy differences as the temperature increases. Considering the simplicity of the model, the agreement between the calculated and the thermodynamic values is probably within the approximations made and is deemed satisfactory. This leaves little doubt that the isomerization reactions over silica-alumina proceed by a carbonium ion mechanism.

If a carbonium ion intermediate is involved in these reactions, it is fair to ask the origin of the protons in view of the evidence²³ of their sparsity. This question is dealt with in another paper,²⁴ but suffice it

(23) H. R. Gerberich, J. G. Larson, and W. K. Hall, *J. Catalysis*, **4**, 523 (1965).

(24) J. W. Hightower and W. K. Hall, *J. Am. Chem. Soc.*, **89**, 778 (1967).

to say here that we have evidence which indicates that the required protons are furnished by the adsorbed residue and that the reaction does not involve the catalyst hydroxyls directly.

The situation is more complicated over alumina. Whereas over silica-alumina the selectivities reported by a number of investigators using different catalysts and techniques were all comparable, a cursory examination of the rate constants for alumina in Table I reveals that the reported selectivities vary widely. From this apparently chaotic condition, however, some pertinent conclusions can be drawn. The selectivities are apparently all sensitive functions of the nature of the catalyst surface which, in turn, is dependent on the method of preparation, pretreatment, poisons, and reaction temperature. Using *cis*-2-butene as reactant, *trans*-2-butene/1-butene ratios much greater than unity were frequently found, in spite of the fact that the highest barrier lies between *cis*- and *trans*-2-butene. Hence, it must be concluded that the statistical energetic arguments which were advanced to explain the selectivities observed with silica-alumina cannot be used with alumina. It is

probable that different sites function in the several reaction paths.

Gerberich and Hall²² have demonstrated that in a microcatalytic reactor both the over-all catalytic activity and *cis/trans* ratios increased with evacuation temperature; *i.e.*, the two varied inversely with water content. This suggests that butene isomerization over alumina does not involve catalyst protons. Moreover, the selectivity differences between the microcatalytic (2.04) and static (6.25) experiments were probably due to a larger water content in the former because of poorer outgassing of the larger sample. Again this illustrates the different surface requirements for the different reaction paths and reinforces the belief that they occur on different sites. Amenomiya and Cvetanovic¹⁸ reached a similar conclusion over chromia-alumina.

Acknowledgment. This work was sponsored by the Gulf Research and Development Co. as part of the research program of the Multiple Fellowship on Petroleum. Thanks are due to Mr. F. M. Allen for assistance with some of the experiments and to Drs. H. R. Gerberich and M. Manes for helpful discussions.

Radiation Chemistry of the Aqueous Nitrate System. I.

γ Radiolysis of Dilute Solutions

by Malcolm Daniels and Eric E. Wigg

Radiation Center and Department of Chemistry,
Oregon State University, Corvallis, Oregon (Received May 26, 1966)

The γ radiolysis of the aqueous nitrate system has been investigated as a function of dose, intensity, temperature, concentration, and pH, with oxygen, nitrite, hydrogen, and hydrogen peroxide as scavengers. In neutral solution a simple seven-stage mechanism is deduced which quantitatively accounts for the results. The rate-constant ratios $k(e^- + O_2)/k(e^- + NO_3^-)$ and $k(OH + H_2O_2)/k(OH + NO_2^-)$ are evaluated as 2.5 ± 0.2 and 0.8×10^{-2} , respectively, and only two rate constants of this mechanism remain unknown. Yields of primary products are deduced or measured, and it is shown that stoichiometry is obtained by including $g(O_2) = 0.1$. The mechanism in alkaline solution changes owing to the ionization of OH and the subsequent reactions of the O^- species. It is shown that O^- reacts rapidly with H_2O_2 , $k(O^- + H_2O_2) = 1.3 \times 10^{10} M^{-1} sec^{-1}$. Oxygen is found to compete with H_2O_2 for O^- and also to react with NO_3^{2-} . The complete mechanism in alkaline solution involves six reactions; for these only three rate constants are unknown and the ratio of two of these is determined, $k(NO_3^{2-} + O_2)/k(NO_3^{2-} + H_2O) = 2 \times 10^5$.

Introduction

Despite the considerable volume of work which has been carried out on the radiation chemistry of the aqueous nitrate system,¹ no detailed mechanism in quantitative agreement with experimental observations has yet been proven; indeed the experimental observations reported by different workers are often discordant.² Accordingly, we have undertaken to investigate the radiation-induced decomposition of the nitrate ion in aqueous solution over a wide range of experimental variables including dose, intensity, temperature, concentration, pH, and selected scavengers.

In this paper we discuss in detail the results for dilute solutions, both neutral and alkaline, for which we are able to propose simple self-consistent mechanisms and to substantiate them quantitatively. Reasons are suggested to account for the disagreement found among other workers. Lastly, it is shown that stoichiometry in the neutral solution yields of primary products (from water radiolysis) can only be achieved by including a $G(O_2) = 0.1$, which we derive from the experimental results of Mahlman.³

Experimental Section

The water used throughout this work was triply distilled, water from a Barnstead still being distilled first from basic permanganate solution and then from acid dichromate solution. Baker Analyzed reagent grade sodium nitrate was further purified by the filtration of concentrated solutions followed by recrystallization from triply distilled water. It was found that filtering and recrystallization lowered the $G(NO_2^-)$ in 6 M NaNO₃ by about 0.4, while very little effect could be observed below 1 M NaNO₃. Further recrystallization was not found to be necessary. Reagent grade sodium hydroxide was purified according to the method of d'Ans and Mattner.⁴ The use of unpurified NaOH gave higher NO₂⁻ yields at pH values above 13

(1) See, for example, A. K. Pikaev, *Russ. Chem. Rev.*, **29**, 235 (1960).

(2) M. L. Hyder, *J. Phys. Chem.*, **69**, 1858 (1965).

(3) H. A. Mahlman, *J. Chem. Phys.*, **35**, 936 (1961).

(4) J. d'Ans and J. Mattner, *Angew. Chem.*, **64**, 448 (1952).

compared to identical runs with purified NaOH. Reagent grade sodium nitrite, unstabilized hydrogen peroxide, and nitric acid were used without further purification.

Purification of sweeping gas was accomplished, in the case of hydrogen and helium, by passage through an activated charcoal-filled U tube maintained at liquid nitrogen temperature. Oxygen and air were bubbled, first through concentrated sulfuric acid and then through triply distilled water. Gas saturation was carried out by passing the gas through the solution contained in a cylindrical bubbler of 50-cm length and 3-cm i.d. equipped with a fritted-glass gas dispersion tube. This arrangement gave essentially complete sweeping in 15 min with a gas flow rate of about 50 cc/min. The irradiation cells were constructed from 25-mm Pyrex glass tubing having a volume of about 25 cc. A 3-cm length of 1-mm bore capillary tubing at each end of the cell, one end being equipped with a 5/20 $\overline{\text{F}}$ joint, permitted filling to be done directly from the bubbler, the cell first being filled with the sweeping gas. The cells, when ready for irradiation, contained no gas volume and the capillary tubing served essentially to eliminate exchange of sweeping gas with the atmosphere.

Two Co^{60} sources were employed in this work. Most of the results were obtained using a 2500-curie unit which provided a homogenous field with a maximum dose rate of 4.0×10^{20} ev l.⁻¹ min⁻¹, as determined by the ferrous sulfate dosimeter taking $G(\text{Fe}^{3+}) = 15.5$ ions/100 ev. Repeated dosimetry runs were reproducible to within 1%. A few of the results reported here were obtained through the use of a 2700-curie source whose maximum dose rate was 6.2×10^{20} ev l.⁻¹ min⁻¹. The reproducibility of repeated dosimetry runs in this case was better than 2%.

Nitrite was determined using the method outlined by Shinn⁵ with a slight modification. The sulfanilamide solution was added prior to the addition of HCl. This order of addition was found to eliminate the acid-catalyzed thermal reaction between H_2O_2 and NO_2^- which caused serious errors when the acid was added to the solution first. A value for the molar extinction coefficient of the diazoamino compound was found to be 5.23×10^4 at 540 m μ . Hydrogen peroxide was determined by the iodide method, as modified by Schwartz and Salzman.⁶ The molar extinction coefficient for the I_3^- was determined to be 2.37×10^4 at 352 m μ .

G values were in all cases determined from yield-dose plots having at least three points each and usually more. These points fell on a straight line, in most cases with a precision better than 0.5%. In high-pH solutions, the scatter was somewhat greater. A few

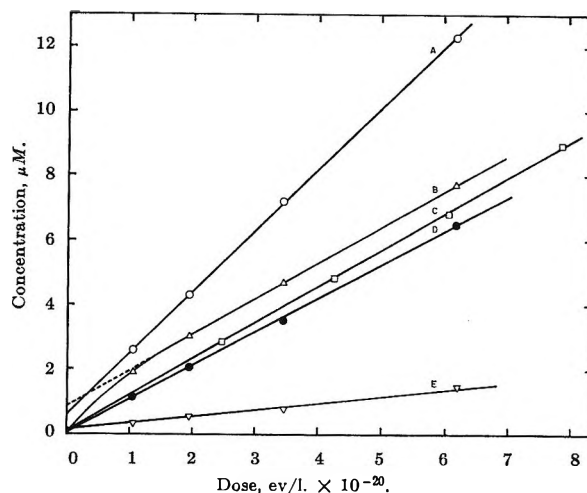


Figure 1. Yield-dose curves for NO_2^- and H_2O_2 formation at an average intensity of 3×10^{20} ev l.⁻¹ min⁻¹: A, NO_2^- formation from 4×10^{-2} M He-swept pH 12 NaNO_3 solution; B, NO_2^- formation from 8×10^{-2} M NO_3^- in neutral, air-equilibrated solution; C, H_2O_2 formation from 1.0×10^{-1} M neutral aerated NaNO_3 solution; D, same as B with $[\text{NO}_2^-]_0 = 4 \mu\text{M}$; E, H_2O_2 formation at pH 12, for He-swept 4×10^{-2} M NO_3^- solution.

representative plots are shown in Figure 1. A repeat of any particular run gave reproducibility within 1%.

$G(\text{H}_2\text{O}_2)$ values, determined at very low conversions, are good to $\pm 3\%$, close to the uncertainty ($\pm 2\%$) reported by Hochanadel and Casey.⁷ The $G(\text{NO}_2^-)$ values we believe good to $\pm 2\%$.

pH measurements were made with a Corning expanded-scale pH meter in conjunction with a Corning triple-purpose glass electrode. Considerable drift at pH values of the unbuffered nitrate solutions between 5 and 9 resulted in an uncertainty of a few tenths of a pH unit in this range.

The G values given in this paper represent yields calculated on the basis of total energy absorbed in the solution. Energy deposition in concentrated solutions was calculated by assuming the absorption of energy to be proportional to electron density, a valid assumption for Co^{60} γ rays and for the low atomic weight elements which were involved.

Results and Discussion

A. *Neutral Solution.* (i) *Yield-Dose Curves.* Although the yield-dose curves for NO_2^- are quite linear, in most cases they extrapolate to a small intercept, usually from 0.5 to 1 μM . The situation is similar to

(5) M. B. Shinn, *Ind. Eng. Chem. Anal. Ed.*, **13**, 33 (1941).

(6) H. A. Schwartz and A. J. Salzman, *Radiation Res.*, **9**, 502 (1958).

(7) C. J. Hochanadel and R. Casey, *ibid.*, **25**, 198 (1965).

Table I: Bimolecular Rate Constants for Reactions of e_{aq}^- , H, and OH with NO_3^- and Radiolytic Products ($M^{-1} \text{ sec}^{-1}$)

	NO_3^-	NO_2^-	H_2O_2	H_2	O_2
e_{aq}^-	$1.1 \times 10^{10}{}^a$ $8.2 \times 10^8{}^b$	$4.6 \times 10^9{}^a$ $3.5 \times 10^8{}^b$	$1.2 \times 10^{10}{}^c$	$<10^7{}^d$	$1.9 \times 10^{10}{}^e$
H	$2.4 \times 10^7{}^f$	$6 \times 10^8{}^g$	9.0×10^7		$2.1 \times 10^{10}{}^h$
OH		$2.5 \times 10^9{}^i$	$4.5 \times 10^7{}^j$ $2.25 \times 10^7{}^k$	$4.5 \times 10^7{}^c$ $3.5 \times 10^7{}^k$	

^a Ref 10a. ^b Ref 11. ^c Ref 13a. ^d J. H. Baxendale, E. M. Fielden, C. Capellos, J. M. Francis, J. V. Davies, M. Ebert, C. W. Gilbert, J. P. Keene, E. J. Land, and A. J. Swallow, *Nature*, **201**, 468 (1964). ^e Ref 10b. ^f A. Appleby, G. Scholes, and M. Simic, *J. Am. Chem. Soc.*, **85**, 3891 (1963). ^g J. Rabani and G. Stein, *J. Chem. Phys.*, **37**, 1865 (1962). ^h S. Gordon, E. J. Hart, and J. K. Thomas, *J. Phys. Chem.*, **68**, 1262 (1964). ⁱ Ref 13b. ^j H. A. Schwarz, *J. Phys. Chem.*, **67**, 2827 (1963). ^k Ref 14.

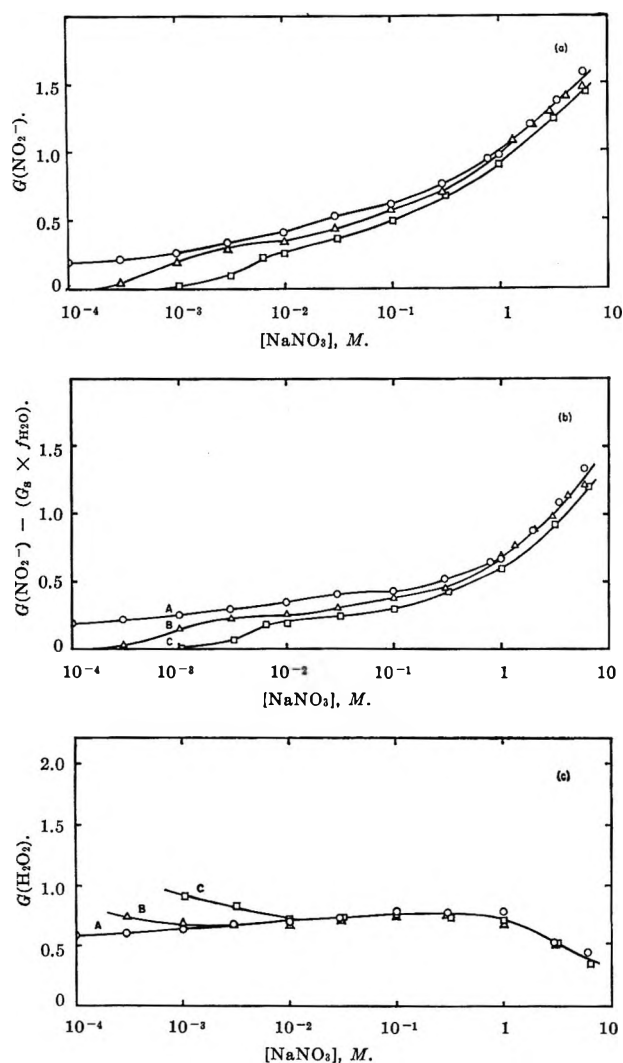


Figure 2. (a) Dependence of $G(NO_2^-)$ on nitrate concentration in neutral solution; intensity, $4 \times 10^{20} \text{ ev l}^{-1} \text{ min}^{-1}$; \circ , He-swept; Δ , aerated; \square , oxygen saturated. (b) Data for Figure 2a corrected for electron and H atom scavenging in the spur by nitrate. (c) Dependence of $G(H_2O_2)$ on nitrate concentration in neutral solution; intensity, $4 \times 10^{20} \text{ ev l}^{-1} \text{ min}^{-1}$.

that found by Allen and Holroyd^{8a} for the hydrogen peroxide formation in aerated water and by Johnson and Weiss^{8b} for Ce(IV) reduction. A true initial yield thus cannot be determined with any confidence for the irradiation of nitrate without added OH scavenger and the G values reported here are "linear" G values obtained as in Figure 1. As such, $G(NO_2^-)$ is then independent of nitrite concentration. We suggest that the higher slope at $(NO_2^-) < 3 \mu M$ is due to incomplete scavenging of OH by NO_2^- and this is supported by the fact that addition of $4 \mu M$ NO_2^- prior to irradiation eliminates the intercept without significantly changing the slope (Figure 1, curve D). Accordingly, the $G(NO_2^-)$ reported here (Figure 2a) must be considered to be determined under conditions of complete OH scavenging by NO_2^- , which is not surprising in view of the high rate constant for this reaction (Table I) and the low reactivity of nitrate to OH.

In previous work^{2,9} an attempt was made to determine "true" initial G values. Such values, higher than those found here, correspond to varying degrees of OH scavenging, depending on the concentration of NO_2^- allowed to build up, and are not susceptible to quantitative interpretation. From the rate constant, gOH , and intensity, it can be shown that concentrations of $\sim 10^{-8} M$ NO_2^- would have to be determined to obtain a good estimate of the initial slope pertaining to conditions of no back reaction. Current techniques do not allow this. In addition, traces of organic impurities will have an unaccountable effect on such initial G values. Accordingly, all G values reported here have been determined with consideration for the presence of radical scavengers, e.g., NO_2^- for OH, O_2 and NO_3^- for e^- and H, and H_2 for OH.

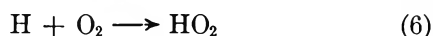
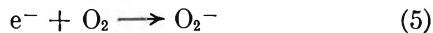
(8) (a) A. O. Allen and R. A. Holroyd, *J. Am. Chem. Soc.*, **77**, 5852 (1955); (b) G. R. A. Johnson and J. Weiss, *Proc. Roy. Soc. (London)*, **A240**, 189 (1957).

(9) A. K. Pikaev, P. Y. Glazunov, and A. A. Yukubovick, *Kinetika i Kataliz*, **4**, 835 (1963).

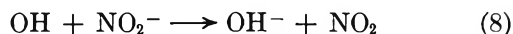
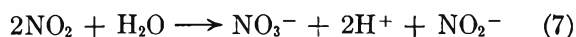
(ii) *Oxygen Scavenging in Neutral Solution. a. Nitrite Formation.* G values of nitrite formation for helium-swept, oxygen-saturated, and air-equilibrated solutions are shown as a function of nitrate concentration in Figure 2a. It can be seen that oxygen has a pronounced effect particularly at lower nitrate concentrations. In view of the known high reactivities of O_2 and NO_3^- toward the solvated electron, it may be anticipated that they will compete on about equal terms for the electron. At this stage an adequate qualitative picture can be presented in which capture of the electron by NO_3^- leads to nitrite formation and capture by the oxygen leads to hydrogen peroxide, the OH being scavenged by NO_2^- . The H atom will act similarly to the electron though with different rate constants and the reduction mechanism can be written as



Competing reactions in the presence of oxygen are known to be



and the sequence is completed by



Clearly such a mechanism, in conjunction with known rate constants, predicts simple competition kinetics between oxygen and nitrate for the solvated electron and this is also suggested by the shapes of the curves of Figure 2a. However, before this can be tested quantitatively, the observed yields must be corrected for scavenging of electrons and hydrogen atoms in the spur by increasing concentrations of nitrate ions. This has been done using the data of Mahlman³ and the adjusted yields are shown in Figure 2b. Scavenging plateaus are now clearly seen at $\sim 10^{-2} M$ in the oxygen-containing solution and at $10^{-1} M$ in the He-swept solution, the difference being ascribed to the higher concentration of nitrate required to scavenge H atoms in the latter case. The data of Figure 2b now follow the competition kinetics of eq A over a certain range of nitrate concentration (Figure 3)

$$\frac{1}{G(NO_2^-)} = \frac{1}{G_0} + \frac{k_A}{G_0} \frac{(O_2)}{(NO_3^-)} \quad (A)$$

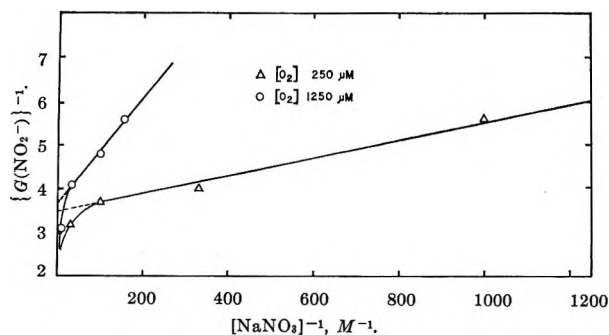


Figure 3. Competition kinetics of O_2 and NO_3^- for the solvated electron; data of Figure 2b.

and k_A is evaluated as 2.5 ± 0.2 . This is, within the limits of experimental error, identical with the ratios of k_5/k_1 in the literature (1.8 ± 0.3^{10a} and $2.3 \pm 0.3^{10b,11}$) and we thus feel the competition can be ascribed to reactions 1 and 5.

The intercepts of Figure 3 give the limiting values of $G(NO_2^-)$ when all electrons are scavenged by nitrate. These values, 0.29 for air-equilibrated solutions and 0.27 for oxygen-saturated solutions, are related to the primary radical yields by eq I

$$G(NO_2^-) = \frac{1}{2}(ge^- - f_1gOH) \quad (I)$$

where $1 - f_1$ is the fraction of OH radicals scavenged by molecular yield H_2O_2 . Experimental evaluation of the extent of this scavenging (see below) leads to the same limiting nitrite yield at both oxygen concentrations.

$$\frac{1}{2}(ge^- - gOH) = 0.20 \pm 0.03 \quad (II)$$

It is apparent from the ratio $k_2/k_1 \sim 10^{-3}$ that scavenging of H will only occur at higher concentrations. The plateau corresponding to this can be seen in the He-swept series of Figure 2b, curve A, at $10^{-1} M$, and from this we estimate

$$\frac{1}{2}(ge^- + gH - gOH) = 0.44 \pm 0.02 \quad (III)$$

b. *Hydrogen Peroxide Formation.* $G(H_2O_2)$ as a function of nitrate concentration is presented in Figure 2c for oxygen-saturated, air-equilibrated, and helium-swept solutions. It can be seen that the magnitude of $G(H_2O_2)$, in general, corresponds to the molecular yield with certain qualifications. Below $10^{-2} M NO_3^-$, significant increases are found in the presence of O_2 , such as would be expected from the competition be-

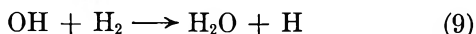
(10) (a) J. K. Thomas, S. Gordon, and E. J. Hart, *J. Phys. Chem.*, **68**, 1262 (1964); (b) M. S. Matheson, *Radiation Res. Suppl.*, **4**, 1 (1964).

(11) J. H. Baxendale, E. M. Fielden, and J. P. Keene, *Proc. Roy. Soc. (London)*, **A286**, 320 (1965).

tween O_2 and NO_3^- for the electron, presented above. In each case, curves B and C meet curve A at the concentration where the corresponding $G(NO_2^-)$ curves of Figure 2b reach their plateau values.

However, it can also be seen that in the absence of oxygen some molecular yield H_2O_2 is consumed, complete protection only being attained at $\sim 10^{-1} M NO_3^-$. A consideration of the various species involved, along with the known rate constants, indicates that the attacking species is most likely the OH radical. The extent of scavenging is dependent on nitrate concentration since $G(NO_2^-)$ increases with increasing nitrate concentration, while gH_2O_2 does not. Such a conclusion does not seriously invalidate the assumption of complete OH radical scavenging by NO_2^- below $10^{-1} M NO_3^-$, since we calculate that only $\sim 2.0\%$ of the OH radicals are scavenged by H_2O_2 and experimentally we measure $\sim 5\%$.

(iii) *Scavenging by Hydrogen.* It is clear from the previous results and discussion that a key role in the mechanism is played by the OH and NO_2^- reaction. To confirm that this does, in fact, account for the OH radicals under present conditions and to determine gOH , a radical scavenger was sought which would compete with NO_2^- for OH and at the same time not introduce new uncertainties into the system. Organic scavengers used in previous work, notably by Allan,¹² have not been free of this fault and gOH could not be determined. Although the reactivity of molecular hydrogen to OH is low, it is possible to adjust conditions to allow scavenging by H_2 and the evaluation of $G(NO_2^-)$ at limiting scavenging conditions. At $6.4 \times 10^{-2} M NO_3^-$ we find $G(NO_2^-) = 3.13$ in H_2 -saturated solution. The dependence of $G(NO_2^-)$ on concentration of hydrogen and nitrite clearly shows competition kinetics (Figure 4). From the above mechanism, with the addition of reaction 9



eq B can be derived, where $G_0(NO_2^-)$ is the limiting value attained when scavenging of OH by H_2 is complete

$$\frac{1}{G_0(NO_2^-) - G(NO_2^-)} = \frac{1}{gOH} + \frac{1}{gOH} k_B \frac{(H_2)}{(NO_2^-)} \quad (B)$$

From the slope we obtain $k_{(OH+H_2)}/k_{(OH+NO_2^-)} = 0.8 \times 10^{-2}$, which can be compared with literature values of 1.8×10^{-2} ^{13a} and 1.4×10^{-2} .^{13b,14} After correcting for scavenging of electrons in the spur by NO_3^- , this mechanism, in which the oxidizing OH

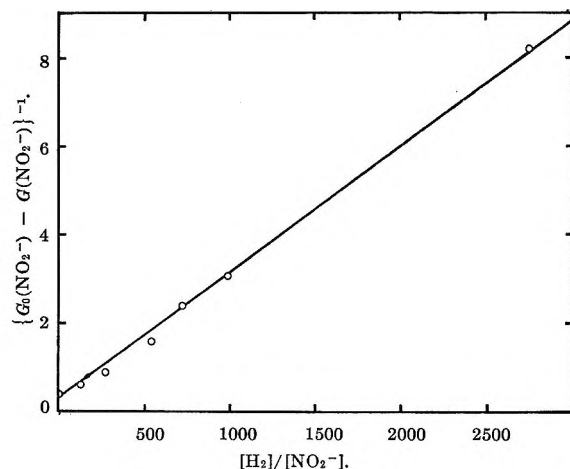


Figure 4. Competition kinetics of H_2 and NO_2^- for OH in $6.4 \times 10^{-2} M NO_3^-$; intensity, $7.5 \times 10^{18} \text{ ev l.}^{-1} \text{ min}^{-1}$.

radicals are converted into the reducing H atoms, allows us to write the reduction yield, $G(NO_2^-)$, as

$$\frac{1}{2}(ge^- + gH + gOH) = 2.97 \pm 0.08 \quad (IV)$$

(iv) *Primary Product Yields and Material Balance.* Expressions II, III, and IV allow the evaluation of the primary radical yields independent of any assumptions of material balance in these primary species and hence allow such an assumption to be tested. Thus from relations III and IV, we obtain gOH and the sum of the reducing species ($ge^- + gH$).

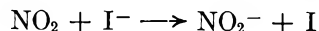
$$gOH = 2.53 \pm 0.10$$

$$g(e^- + H) = 3.41 \pm 0.10$$

Use of relation II then allows the evaluation of ge^- as 2.93 ± 0.16 and by difference we have $gH = 0.48 \pm 0.26$.

In view of the interest attached to these values, it was desirable to obtain other independent relations allowing the determination of the primary yields. This we have done using I^- as a scavenger and analyzing for NO_2^- and $\Sigma I_2 + H_2O_2$ by the methods already described.

It was anticipated that all the OH radicals could easily be scavenged by I^- ($k_{(OH+I^-)} \sim 3 \times 10^9 M^{-1} \text{ sec}^{-1}$). If NO_2 is unreactive toward I^- , $G(NO_2^-)$ would be expected to be ~ 1.8 ; if however it is reduced



(12) J. T. Allan, *J. Phys. Chem.*, **68**, 2697 (1964).

(13) (a) M. S. Matheson and J. Rabani, *ibid.*, **69**, 1324 (1965); (b) H. A. Schwarz and A. O. Allen, *J. Am. Chem. Soc.*, **77**, 1324 (1955).

(14) J. K. Thomas, *Trans. Faraday Soc.*, **61**, 702 (1965).

then $G(\text{NO}_2^-)$ should be ~ 3.6 and the yield of $\Sigma \text{I}_2 + \text{H}_2\text{O}_2$ should be correspondingly higher. Experimentally, the irradiation of oxygen-free nitrate ($6.2 \times 10^{-2} M$) containing $1 \times 10^{-3} M \text{I}^-$ resulted in measured values of $G(\text{NO}_2^-) = 3.76$ and $G(\Sigma \text{I}_2 + \text{H}_2\text{O}_2) = 3.93$. The second mechanism is thus pertinent and we have

$$G(\text{NO}_2^-) = ge^- + g\text{H} + 2[g\text{H}_2 - G(\text{H}_2)] = 3.76$$

and

$$G(\Sigma \text{I}_2 + \text{H}_2\text{O}_2) = \frac{1}{2}(ge^- + g\text{H} + g\text{OH}) + g\text{H}_2\text{O}_2 = 3.93$$

from which we evaluate

$$ge^- + g\text{H} = 3.44$$

and

$$g\text{OH} = 2.58$$

Clearly these results are in excellent agreement with those derived earlier and have the advantage that $(ge^- + g\text{H})$ is almost a direct measurement.

The situation concerning radical yields in neutral solution has been reviewed recently by Schwarz,¹⁵ who concluded that it has "progressed to the point of confusion." Comparison of our results with others in the recent literature is therefore of interest, taking as our starting point the "standard" values quoted by Allen,¹⁶ $g\text{OH} = 2.2$, $ge^- = 2.80$, and $g\text{H} = 0.65$. The $g\text{OH}$ for the nitrate system is significantly larger, though similar to the value of 2.59 reported by Hohanadel for the $\text{CO} + \text{H}_2$ system⁷ and somewhat less than Sutton's value¹⁷ of 2.9 for the NO system. The present ge^- is perhaps larger, but the total yield of reducing species $ge^- + g\text{H} = 3.41$ is close to Allen's value of 3.45 and somewhat lower than $g\text{H}$ for acid solution. Our lower value of $g\text{H}$, if significant, can perhaps be ascribed to scavenging by NO_3^- of the $e^- + \text{H}^+$ reaction.

In addition to the radical yields we also determine $g\text{H}_2\text{O}_2 = 0.75 \pm 0.04$ so that together with $g\text{H}_2 = 0.45$ reported by Mahlman³ all the values necessary for a complete accounting of this system in terms of the commonly considered species are available. When this is done we find $G(-\text{H}_2\text{O}) = \Sigma ge^- + g\text{H} + 2g\text{H}_2 = 4.3$, equal to acid solution, but 4.0 calculated as $\Sigma g\text{OH} + 2g\text{H}_2\text{O}_2$. Thus this system appears to be yet another example of the material balance deficiency discussed by Allen,¹⁶ the deficiency in this case amounting to ~ 0.3 . Uncertainties in the determinations of the separate g values become cumulative¹⁵ when stoichiometry is considered in this way and it is a valid question whether or not a lack of stoichiometry actually exists.

Schwarz, discussing this question recently,¹⁵ concluded that a material balance deficit does exist in neutral solution to the extent of 0.6 ± 0.2 . The uncertainty in our present work may be reduced by considering, not the derived g values, but the experimental G values. When this is done we have, for complete scavenging conditions, $\Sigma G(\text{NO}_2^-) + G(\text{H}_2) = 0.87$ whereas $G(\text{H}_2\text{O}_2) = 0.75$, clearly showing a deficit of ~ 0.25 in oxidized products. It is our opinion then that a deficit exists, although it cannot be determined with precision.

We are further strengthened in our opinion by the existence of another set of experimental data on this system. Mahlman³ has measured oxygen formation from nitrate solutions in the range 1.0–7.0 M . We find his results can be treated quite simply in terms of energy deposition in nitrate and water using

$$G(\text{O}_2) = G(\text{O}_2)_{\text{H}_2\text{O}}f_{\text{H}_2\text{O}} + G(\text{O}_2)_{\text{NO}_3^-}f_{\text{NO}_3^-}$$

where f is the fractional energy deposition and G is the appropriate coefficient. Calculating the f values from the electron densities leads to the results shown in Figure 5. The existence of an intercept clearly indicates that oxygen is formed from water in the radiolysis of dilute nitrate solution with a yield $G(\text{O}_2) \sim 0.1$. This amount is close to that required to give material balance in the primary yields. However, the radical nature of this conclusion requires that other interpretations of this data be considered. Thus there may be a systematic error in the oxygen analysis not found in the hydrogen analysis, but this error must also be linearly related to $f_{\text{NO}_3^-}/f_{\text{H}_2\text{O}}$, which we consider to be somewhat unlikely. Moreover, extrapolation of the linear relation to $\sim 0.1 M$ may not be valid, the relationship changing. However, there is further evidence¹⁸ from the radiolysis of nitrate solutions containing H_2O_2 ¹⁸ that O_2 does originate from the water. The extrapolation of $G(\text{O}_2)$ seems reasonable and the variation of the yield of oxygen from the water with NO_3^- concentration suggests that the oxygen may originate in the atomic form.¹⁹

The sequence of results—(a) the material balance deficit in conventional species, (b) formation of oxygen with a G value filling the deficit, and (c) isotopic evidence that the oxygen does come from the water—seems to be the first experimental evidence supporting

(15) H. A. Schwarz, *Ann. Rev. Phys. Chem.*, **16**, 347 (1965).

(16) A. O. Allen, *Radiation Res. Suppl.*, **4**, 54 (1964).

(17) W. A. Seddon and H. C. Sutton, *Trans. Faraday Soc.*, **59**, 2323 (1963).

(18) H. A. Mahlman, *J. Phys. Chem.*, **67**, 1466 (1963).

(19) M. Daniels and E. E. Wigg, *Science*, **153**, 1533 (1966).

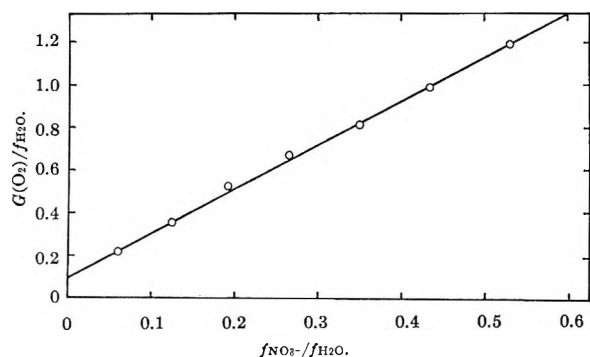


Figure 5. $G(\text{O}_2)/f_{\text{H}_2\text{O}}$ vs. $f_{\text{NO}_2^-}/f_{\text{H}_2\text{O}}$; results of Mahlman.¹⁸

Allen's proposal¹⁶ that O atoms may be formed as a primary radiolysis product. It will be of interest to see if other systems can be investigated in sufficient detail to provide further evidence in this respect.

(v) *Intensity Variation.* No effect of intensity was found for $G(\text{NO}_2^-)$ or $G(\text{H}_2\text{O}_2)$ between 6.2×10^{20} and 8.5×10^{17} $\text{ev l}^{-1} \text{min}^{-1}$. The increase observed in dilute solution by Pikaev, *et al.*,⁹ between 3×10^{20} and 6×10^{27} $\text{ev l}^{-1} \text{min}^{-1}$ indicates that the recombination of OH in the bulk of the solution becomes significant at these very high dose rates. However, his results should probably be reevaluated in the light of the mechanism presented here.

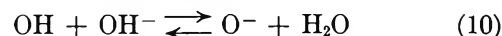
(vi) *Temperature Variation.* An increase in solution temperature from 25 to 60° was found to produce a negligible change in $G(\text{NO}_2^-)$ for 1.6×10^{-3} M NaNO_3 .

(vii) *Comparison with Other Work.* As mentioned earlier, the method of determining $G(\text{NO}_2^-)$ by other workers precludes the possibility of direct comparison with our work. $G(\text{H}_2\text{O}_2)$ could be compared; however the data are scanty and diverse, making comparison pointless. Such behavior would be expected if trace organic impurities were present, as the work of Allan¹² shows. The values obtained by Allan¹² for g_{e^-} and g_{H} of 2.80 and 0.45 in the methanol nitrate system are in reasonable agreement with those presented here, although his mechanism is incomplete and g_{OH} could not be determined.

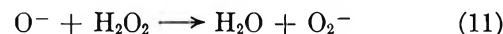
B. Alkaline Solutions. (i) *Effect of pH in Oxygen-Free Solution.* There are many reports in the literature of increased nitrite formation in alkaline solution, but no satisfactory explanation has yet been offered in any of them. Accordingly, we have investigated the formation of nitrite and hydrogen peroxide in oxygen-free solution as a function of pH, with the results shown in Figure 6. The previously reported increase in $G(\text{NO}_2^-)$ is found; however there is a concurrent and equivalent consumption of hydrogen peroxide. Clearly, hydrogen peroxide is involved in the reaction sequence

leading to nitrite formation, whereas in neutral solution, it is essentially unaffected.

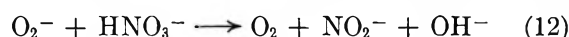
The following modification of the mechanism for neutral solution, involving ionization of OH and H_2O_2 , quantitatively accounts for this behavior. The OH radical is known to ionize in alkaline solution, with a $\text{p}K = 11.9$ ²⁰ to give the O^- species



and we propose that this species can react with H_2O_2 just as does OH, but with greater rate constant, so that H_2O_2 is consumed.



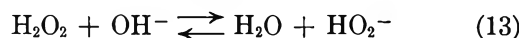
The reaction sequence is completed by O_2^- reducing HNO_3^- (an equivalent ionic form of NO_2) to nitrite.



The evidence for this reaction comes from the scavenging limit (see below). The kinetic expression for the consumption of hydrogen peroxide derived from this mechanism (supposing nitrite to be relatively unreactive to O^-) is given by the equation

$$G(\text{H}_2\text{O}_2) = g_{\text{H}_2\text{O}_2} - \frac{g_{\text{OH}}K_{\text{OH}}k_{11}(\text{OH}^-)(\text{H}_2\text{O}_2)}{K_{\text{OH}}k_{11}(\text{OH}^-)(\text{H}_2\text{O}_2) + k_3\text{NO}_2^-} \quad (\text{C})$$

where K_{OH} is the equilibrium constant of reaction 10. From the experimental results, k_{11} has been calculated using the values $\text{p}K(\text{OH}) = 11.9$ and $k(\text{OH} + \text{NO}_2^-) = 2.5 \times 10^9$ $\text{M}^{-1} \text{sec}^{-1}$ for a range of OH^- concentrations (column 2 of Table II); a definite trend with pH is seen. However, ionization of H_2O_2 , $\text{p}K = 11.75$,²¹ occurs to the same extent as OH



and taking account of this leads to the values in column 3 of Table II, showing now no trend with pH. An average value for k_{11} of 1.3×10^{10} $\text{M}^{-1} \text{sec}^{-1}$ was then used to calculate the curve shown in Figure 6 (broken curve).²²

(20) J. Rabani and M. S. Matheson, *J. Am. Chem. Soc.*, **86**, 3175 (1964).

(21) M. Evans and N. Uri, *Trans. Faraday Soc.*, **45**, 244 (1949).

(22) A referee has pointed out that in view of the closeness of $\text{p}K(\text{OH})$ and $\text{p}K(\text{H}_2\text{O}_2)$, reaction 11 cannot be distinguished from $\text{OH} + \text{HO}_2^-$ if equilibria 10 and 13 are maintained. However, it is doubtful if equilibrium can be regarded as being maintained in the presence of such rapid disturbing reactions as (11), a point emphasized by G. E. Adams, J. W. Boag, and B. D. Michael, *Trans. Faraday Soc.*, **61**, 492 (1965). This is also indicated by Figure 6 in which the curves are clearly not symmetrical about either of the $\text{p}K$ values. However, some ambiguity remains which cannot be resolved by the present type of experiments and must await the results of appropriately designed pulse radiolysis experiments. For the present, we show that a satisfactory interpretation may be given by reaction 11.

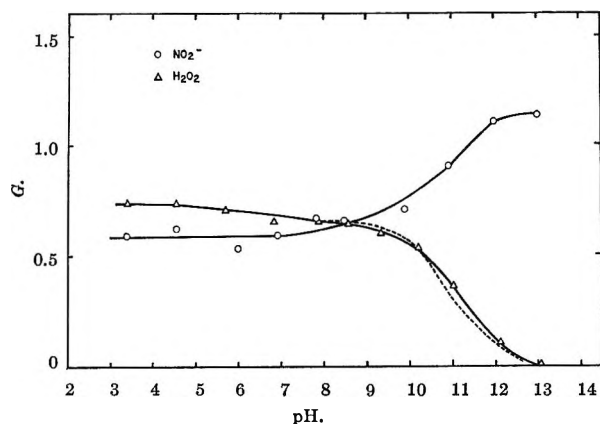
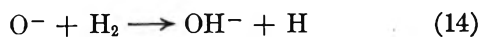


Figure 6. Variation of $G(\text{NO}_2^-)$ and $G(\text{H}_2\text{O}_2)$ with pH in helium-swept, $3 \times 10^{-2} M$ NaNO_3 solutions; intensity, $10^{20} \text{ ev l}^{-1} \text{ min}^{-1}$.

Table II: Calculated Values for $k_{(\text{O}^- + \text{H}_2\text{O}_2)}$ from Expression C

pH	$k_{(\text{O}^- + \text{H}_2\text{O}_2)}$, $M^{-1} \text{ sec}^{-1}$, assuming no effect due to ionization of H_2O_2	$k_{(\text{O}^- + \text{H}_2\text{O}_2)}$, $M^{-1} \text{ sec}^{-1}$, assuming HO_2^- does not react with O^-
10.20	1.1×10^{10}	1.2×10^{10}
11.05	0.69×10^{10}	0.83×10^{10}
12.25	0.49×10^{10}	1.8×10^{10}

Further support for this mechanism comes from two sources. First, addition of hydrogen peroxide prior to irradiation causes a further increase in $G(\text{NO}_2^-)$ as predicted by the mechanism, up to a limit of 2.80 (see Figure 7, curve A). This limit is attained at quite low concentrations of H_2O_2 ($50 \mu\text{M}$), which is not unreasonable in view of the high value of k_{11} , and can be identified with $g\text{OH} + \frac{1}{2}(ge^- - g\text{OH})$. Second, by use of k_{11} determined here, we can account for the results obtained by Hochanadel in the photolysis of hydrogen peroxide in the presence of hydrogen at alkaline pH.²³ The lower rate of consumption of H_2O_2 observed in alkaline solution was ascribed to a "reaction of OH^- with OH to give a species, O^- , which does not react with H_2 ." However, it has recently been shown that^{13a} $k(\text{O}^- + \text{H}_2)/k(\text{OH} + \text{H}_2) \sim 2$, implying that the alternative explanation must hold; i.e., $k(\text{O}^- + \text{H}_2\text{O}_2) > k(\text{OH} + \text{H}_2\text{O}_2)$. Using competing reactions 11 and 14



we have derived eq D for the change in $\phi(-\text{H}_2\text{O}_2)$ in the presence of H_2 .

$$\Delta\phi = 2I_A(\text{H}_2) \left[\frac{k_{(\text{OH} + \text{H}_2)} + k_{(\text{O}^- + \text{H}_2)}K_{\text{OH}}(\text{OH}^-)}{k_{(\text{OH} + \text{H}_2\text{O}_2)} + k_{(\text{O}^- + \text{H}_2\text{O}_2)}K_{\text{OH}}(\text{OH}^-)} \right] \quad (\text{D})$$

The variation of $\Delta\phi$ with (OH^-) calculated from this expression using known rate constants and our value of k_{11} gives excellent agreement with the experimental results as shown in Figure 8.

Accordingly, we feel the mechanism proposed above and the deduced value of k_{11} to be reliable. The high value for k_{11} is rather unexpected, but not im-

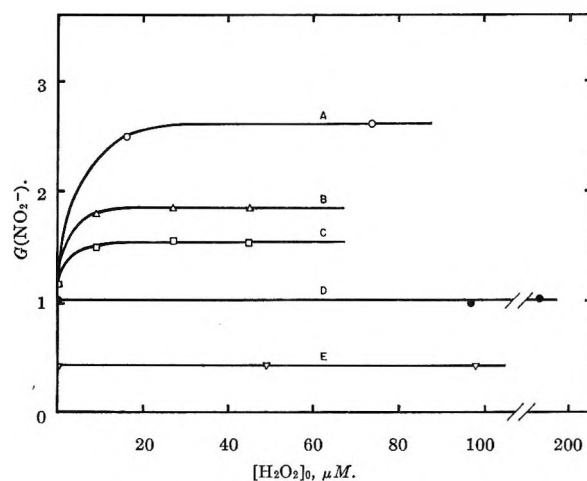


Figure 7. Dependence of $G(\text{NO}_2^-)$ on added H_2O_2 at various oxygen concentrations, $3 \times 10^{-2} M$ NaNO_3 , pH 12. $[\text{O}_2]$: O, zero; Δ , 100 μM ; \square , 150 μM ; \bullet , 250 μM ; ∇ , 1250 μM .

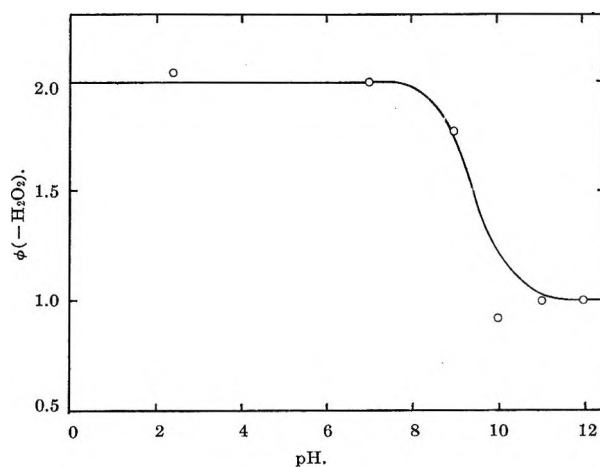


Figure 8. $\phi(-\text{H}_2\text{O}_2)$ vs. pH. Curve calculated using expression D; data from ref 23.

(23) C. J. Hochanadel, *Radiation Res.*, 17, 286 (1962).

possibly high for a diffusion-controlled reaction. Using the approximate Smoluchowski equation for the rate constant of a diffusion-controlled reaction

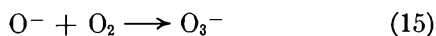
$$k = \frac{4\pi N}{1000}(r_A + r_B)(D_A + D_B)$$

we calculate $k = 2.0 \times 10^{10} M^{-1} \text{ sec}^{-1}$ from the following parameters: $r(\text{O}^-) = 1.76 \text{ \AA}$ (crystal radius)²⁴ and $r(\text{H}_2\text{O}_2) = 1.20 \text{ \AA}$ (estimated from bond lengths), $D(\text{O}^-)$ assumed equal to $D(\text{OH}^-) = 6.5 \times 10^{-5} \text{ cm}^2 \text{ sec}^{-1}$ ^{25a} and $D(\text{H}_2\text{O}_2) = 2.5 \times 10^{-5} \text{ cm}^2 \text{ sec}^{-1}$.^{25b} Adjustment of these values is not justified, although no doubt a closer value could be calculated. Such a calculation does serve to show, however, that the deduced value of k_{11} is not unrealistic.

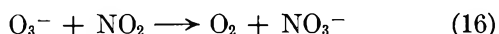
Last, it should be pointed out that the present mechanism eliminates the necessity of postulating reaction of O^- with NO_3^- , suggested by Hyder² to account for the increase of $G(\text{NO}_2^-)$ in alkaline solution.

(ii) *Effect of Oxygen at pH 12.* In the absence of added H_2O_2 very little change is observed with increase in oxygen concentration up to $150 \mu\text{M}$. Higher concentrations, however, decrease $G(\text{NO}_2^-)$ to 0.42 in oxygen-saturated solution, a value essentially identical with that obtained in neutral oxygen-saturated solution at the same nitrate concentration ($3 \times 10^{-2} M$). Superficially this would appear to indicate that radical yields are unchanged from neutral pH; but, as will be shown, the reaction mechanism in the presence of oxygen does not allow this value to be identified immediately with $1/2(g\text{e}^- - g\text{OH})$. At the same time, hydrogen peroxide yields increase with oxygen concentration from 0.12 (at $\text{O}_2 = 0$) to 0.87 in oxygen-saturated solution.

It is clear from these results that oxygen is competing for the species attacking hydrogen peroxide, thus lowering the nitrite yield and protecting the molecular yield H_2O_2 . In view of the previously deduced mechanism this reaction is most probably



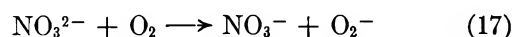
followed by



Czapski and Dorfman²⁶ have reported a transient absorption which they attributed to the O_3^- species and Adams, Boag, and Michael²⁷ have measured the rate constant of reaction 15.

Such a mechanism can easily be verified. By adding H_2O_2 prior to irradiation to solutions containing oxygen, it should be possible to regain the high values found in the absence of oxygen and indeed achieve the

limiting value obtained by adding H_2O_2 to O_2 -free solutions. Experimentally this is not found. Although adding H_2O_2 to O_2 -containing solutions does increase $G(\text{NO}_2^-)$, complete reversal is not observed; rather, in each case, a limiting value is found which depends on the oxygen concentration (Figure 7). Thus the simple competition of reactions 15 and 11 is not adequate and the results indicate that O_2 is also reacting with another precursor of NO_2^- . To account for this effect, we suggest that O_2 can react with NO_3^{2-}



in competition with



Thus for the dependence of $G(\text{NO}_2^-)$ on oxygen concentration in the presence of sufficient H_2O_2 for plateau conditions, we have

$$G(\text{NO}_2^-) = G_0(\text{NO}_2^-) \left[\frac{k_{18}(\text{H}_2\text{O})}{k_{18}(\text{H}_2\text{O}) + k_{17}(\text{O}_2)} \right] \quad (\text{E})$$

where $G_0(\text{NO}_2^-)$ is the value of O_2 -free solution. Figure 9 shows the data to fit this result and we evaluate k_{17}/k_{18} as 2×10^5 . Such behavior will not be observed in neutral solution if $k_3 > k_{17}$.

(iii) *Primary Yields and Material Balance at pH 12.* From the mechanism deduced here, $G(\text{NO}_2^-)$ in oxygen-free solution (Figure 6) can be identified with

$$g\text{H}_2\text{O}_2 - G(\text{H}_2\text{O}_2) + 1/2(g\text{e}^- - g\text{OH}) = 1.15 \quad (\text{V})$$

In the presence of excess O_2 , the hydrogen peroxide and nitrite yields are related by the expression

$$G(\text{H}_2\text{O}_2) - g\text{H}_2\text{O}_2 = 1/2(g\text{e}^- - g\text{OH}) - G(\text{NO}_2^-) \quad (\text{VI})$$

Consistency of interpretation is shown by the fact that these expressions are in close agreement, giving from our best values

$$1/2(g\text{e}^- - g\text{OH}) + g\text{H}_2\text{O}_2 = 1.22 \quad (\text{VII})$$

With excess hydrogen peroxide in oxygen-free solution, we also have $G(\text{NO}_2^-)$ given by

$$1/2(g\text{e}^- + g\text{OH}) = 2.60 \quad (\text{VIII})$$

Clearly if the molecular yield hydrogen peroxide could be measured separately, the primary radical yields

(24) "Handbook of Chemistry and Physics," 44th ed., The Chemical Rubber Publishing Co., Cleveland, Ohio, 1963.

(25) (a) M. Eigen and L. De Maeyer, *Proc. Roy. Soc. (London)*, **A247**, 505 (1958); (b) H. A. Schwarz, *Radiation Res. Suppl.*, **4**, 89 (1964).

(26) G. Czapski and L. M. Dorfman, *J. Phys. Chem.*, **68**, 1169 (1964).

(27) G. E. Adams, J. W. Boag, and B. D. Michael, *Nature*, **205**, 898 (1965).

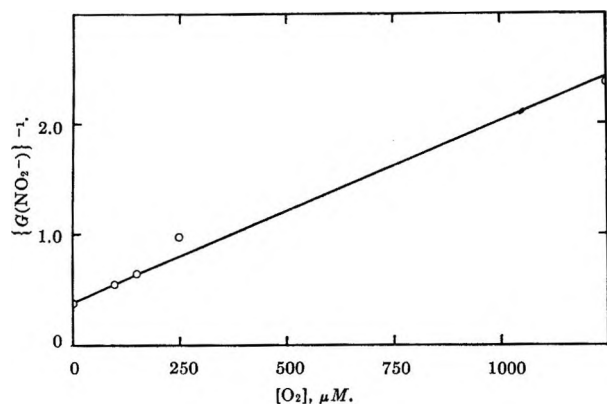


Figure 9. $1/G(\text{NO}_2^-)$ vs. $[\text{O}_2]$ in $3 \times 10^{-2} M$ NaNO_3 , pH 12, at lim $[\text{H}_2\text{O}_2]$.

could be determined. In the presence of excess oxygen, it is easy to see that in our concentration range (2–10 μM H_2O_2) the molecular hydrogen peroxide is protected from attack by O^- , so that the experimental value $G(\text{H}_2\text{O}_2) = 0.87$ represents at least the molecular yield. However, it is not clear to what extent this measurement includes peroxide derived from radical sources. We have attempted to determine $g\text{H}_2\text{O}_2$ in oxygen-free solution using other radical scavengers such as *n*-propyl alcohol and bromide ion. With *n*-propyl alcohol, $G(\text{H}_2\text{O}_2)$ was less than when oxygen was present; however, this was easily shown to be due to a consumption of peroxide rather than an elimination of a contribution from radical processes. Baxendale and Wilson²⁸ have noted a similar effect in the photolysis of H_2O_2 . In the case of Br^- , the $G(\text{H}_2\text{O}_2)$ was quite small and it is concluded that peroxide is not protected by Br^- in alkaline solution; pulse radiolysis studies²⁹ which show that $G(\text{Br}_2^-)$ decreases above pH 9.5 and is quite small at pH 12 lead to the same conclusion.

Accordingly, we can only conclude that $g\text{H}_2\text{O}_2 \leq 0.87$. However, interest in primary yields is such that we have calculated possible values from relations VII and VIII assuming values from 0.87 to 0.60 for $g\text{H}_2\text{O}_2$. Regardless of the exact value of $g\text{H}_2\text{O}_2$, $g\text{OH}$ is always considerably smaller than in neutral solution and similar to the values reported by Cheek and co-workers³⁰ and Draganic and co-workers.^{31,32} Our value for g_{red} is also somewhat lower than in neutral solution but identical with g_{e^-} . Either we are not "seeing" the H

species, although scavenging conditions are very similar to neutral solution, implying $k(\text{O}^- + \text{H}) > k(\text{OH} + \text{H})$, which is hardly likely, or the H species is not formed, or $g(\text{e}^- + \text{H})_{\text{alk}} < g(\text{e}^- + \text{H})_{\text{neutral}}$. Taking $g\text{H}_2 = 0.40$ ³³ material balance can be considered and we can distinguish two likely situations. If $g\text{H}_2\text{O}_2$ is unchanged from neutral solution at 0.75 then we have the same deficit in material balance as in neutral solution, but $g\text{H}_2\text{O}_2$ need only be somewhat higher at 0.80 for material balance to obtain. Further discussion is not warranted until $g\text{H}_2\text{O}_2$ is unambiguously determined.

The difficulty encountered in the present work of unambiguously determining $g\text{H}_2\text{O}_2$ must cause reconsideration of the methods of determination of other reported values, particularly in view of the very rapid reaction of O^- with H_2O_2 . It must be demonstrated experimentally that H_2O_2 is protected against O^- , otherwise apparently low values may be obtained, and it cannot be assumed that O^- behaves as OH , for example $k(\text{O}^- + \text{H}_2\text{O}_2) \gg k(\text{OH} + \text{H}_2\text{O}_2)$ whereas $k(\text{O}^- + \text{Br}^-) \ll k(\text{OH} + \text{Br}^-)$. Similarly, if low values of $G(\text{H}_2)$ are obtained, it is necessary to show that hydrogen is not consumed during the radiolysis before it can be concluded that $G(\text{H}_2) = g\text{H}_2$.

Last, we may note that the use of the nitrate + formate system to determine g values at alkaline pH³³ involves the assumption that the (presumably valid) mechanism obtaining at neutral pH is unchanged at alkaline pH and that only the primary yields change. In view of the considerable change in mechanism which detailed work such as the present shows may occur, such an assumption cannot be regarded as proven.

Acknowledgments. This work was supported in part by PHS Grant AM-10098 and the initial phase was carried out at the Puerto Rico Nuclear Center with the support of the AEC, Division of Biology and Medicine.

(28) J. H. Baxendale and J. A. Wilson, *Trans. Faraday Soc.*, **53**, 344 (1957).

(29) B. Cercek, M. Ebert, C. W. Gilbert, and A. J. Swallow, Symposium on Pulse Radiolysis, University of Manchester, 1965.

(30) C. H. Cheek and V. J. Linnenbom, *J. Phys. Chem.*, **67**, 1856 (1963); C. H. Cheek and J. W. Swinnetton, *ibid.*, **68**, 1429 (1964).

(31) Z. D. Draganic, I. A. Draganic, and M. M. Kosanic, *ibid.*, **68**, 2085 (1964).

(32) Z. D. Draganic, I. A. Draganic, and M. M. Kosanic, *ibid.*, **70**, 1418 (1966).

(33) E. Hayon, *Trans. Faraday Soc.*, **61**, 734 (1965).

The Effect of Ionic Hydration on Equilibria and Rates in Concentrated Electrolyte Solutions. III. The H_- Scale in Concentrated Hydroxide Solutions¹

by G. Yagil

The Radioisotope Training Centre, The Weizmann Institute of Science, and the Israel Atomic Energy Commission, Rehovoth, Israel (Received May 26, 1966)

Derivatives of indole have been found to be suitable compounds for the determination of the indicator acidity of very basic solutions. The H_- acidity scale of concentrated aqueous solutions of KOH, NaOH, and LiOH is determined with these compounds. At low hydroxide concentrations, the values of H_- were found to deviate little from values reported previously,² but at high concentrations the new values are considerably lower than the previous ones, in KOH and in NaOH. Values for H_{2-} in KOH are also reported. The new values confirm the results of calculations based on a model which lead to the conclusion that the OH^- ion is hydrated by three water molecules up to 8 M hydroxide.

Introduction

The indicator acidity of concentrated aqueous potassium hydroxide and sodium hydroxide was first determined by Schwarzenbach and Sulzberger.² The compounds employed as acid-base "indicators" were, however, insoluble in the hydroxide solutions, and the H_- values derived were based on ionization ratios in an immiscible solvent in equilibrium with the aqueous solution. The values obtained thus are valid only if the activity coefficients of acid and base form vary with hydroxide concentration each in the same way in both phases. Schwarzenbach and Sulzberger have been criticized on that account.³ Since then, values based on the ionization ratio of thioacetamide in NaOH up to 5 M have been reported⁴ and largely confirm Schwarzenbach and Sulzberger's values in that range. Values for lithium hydroxide and benzyltrimethylammonium hydroxide in water were also determined.⁵ Kinetic measurements of the rate of lactam hydrolysis yield information on the basicity of alkaline solutions,^{6,7} but the interpretation of rate data in these solutions is not straightforward.^{1b} In addition, a considerable number of measurements on the basicity of nonaqueous solvents and their mixtures with water were done in recent years, and these are well summarized by Stewart

and O'Donnell.⁵ Reliable values of H_- in aqueous KOH and NaOH are not yet available, however.

In the present paper, a new determination of the indicator acidity of KOH, NaOH, and LiOH based on a new class of indicators is reported. This seemed desirable in view of the importance of aqueous hydroxide solutions in many types of studies and also in view of information which can be obtained from indicator acidities on the state of the ions in these solutions, particularly on the hydration of the OH^- ion.^{1a,b} In the following paper, the measurements are extended

(1) (a) Part I, dealing with the hydration of the hydroxide ion, G. Yagil and M. Anbar, *J. Am. Chem. Soc.*, **85**, 2376 (1963). (b) Part II, dealing with reaction rates in concentrated hydroxide solutions, M. Anbar, M. Bobtelsky, D. Samuel, B. Silver, and G. Yagil, *ibid.*, **85**, 2380 (1963). (c) Part IV, dealing with the effect of neutral electrolytes on indicator acidities, G. Yagil, *J. Phys. Chem.*, **71**, 1045 (1967).

(2) G. Schwarzenbach and R. Sulzberger, *Helv. Chim. Acta*, **27**, 348 (1944). The subject was recently reviewed by K. Bowden, *Chem. Rev.*, **66**, 119 (1966).

(3) W. K. Wilmarth and J. M. Fluornoy, *J. Am. Chem. Soc.*, **83**, 2257 (1961).

(4) J. T. Edward and I. C. Wang, *Can. J. Chem.*, **40**, 399 (1962).

(5) R. Stewart and J. P. O'Donnell, *ibid.*, **42**, 1681 (1964).

(6) Y. V. Moiseev and M. I. Vinnik, *Dokl. Akad. Nauk SSSR*, **150**, 845 (1963).

(7) M. I. Vinnik and Y. V. Moiseev, *Tetrahedron*, **19**, 1441 (1963).

to solutions containing neutral electrolytes, to obtain information on the hydration of some additional ions.^{1c} It should be mentioned that work in recent years in acid solutions raised doubts whether the indicator acid concept as developed by Hammett and co-workers, at least in its simple form, is a valid one.⁸⁻¹² This series is based on the more optimistic viewpoint, expounded in more detail in part IV, that indicator acidities do reflect a fundamental property of the solution, and that explanations will ultimately be found for the deviant cases.

In order to perform indicator acidity measurements, a suitable group of weak acids is required, and finding such a group was the main problem in this work. To be suitable as an H_- indicator, a weakly acid compound should have a pK in the range 12-19, and there should be good reason to believe that a proton is dissociated upon ionization. Also, the compound should be sufficiently soluble in hydroxide solutions, should be stable against hydrolysis in alkali, and ionization equilibria should be rapidly established. Finally, either acid or base form should absorb light appreciably above 230 $m\mu$, where OH^- begins to absorb.

The first group of compounds examined was nitro derivatives of benzene such as picric acid and nitroanilines. These compounds have been successfully employed to determine the indicator acidity of several solvent systems containing hydrazine,¹³⁻¹⁵ ethylenediamine,¹⁵ methanol,^{16,17} ethanol,^{18,19} dimethylsulfoxide,⁵ sulfolane,^{5,20} pyridine,⁵ and others. However, the mode of ionization of these compounds is not always clear. In some cases the base is formed by losing a ring proton, while in others an OH^- or RO^- ion is added²¹⁻²⁴ to the ring. It was also observed that the reactions were not always reversible and the base form not stable. We finally abandoned this class of compounds when it was observed that the well-known red color of trinitrobenzene in alkaline media, as well as the similar color of 2,4-dinitroaniline, is not formed in aqueous solutions, unless traces of alcohol are present. This indicates that RO^- is involved in base formation even in water.

A second class of compounds with pK in the desired range is the alcohols. The aliphatic alcohols, however, do not absorb above 230 $m\mu$; phenols reach pK 13-14 only if internally hydrogen bonded, e.g., as salicylate²⁵ or indigo carmine, or if they are substituted with a bulky group in the *ortho* position.²⁶ Next, some single ring heterocyclic compounds were examined, including imidazole and pyrrole, and were found to satisfy most requirements, except of absorbing at a high enough wavelength.

A suitable group was finally found in indole and its derivatives, some of which are soluble enough in concentrated KOH and NaOH. In alkaline solutions, a spectral change occurs which results in a new absorption peak (or shoulder), generally between 310 and 320 $m\mu$. An indicator acidity scale of the H_- type based on these compounds and also a scale of the H_{2-} type are now reported.

Experimental Section and Calculations

Materials and Solutions. Most of the indoles employed were obtained from Fluka A.G. and were of purum or puriss. grade. Where melting point or appearance was unsatisfactory, the compound was recrystallized once or twice, generally from dilute ethanol. The final melting points, as well as the spectral properties, of the indoles employed as indicators are given in Table I. The compounds 4-fluoroindole, 5-fluoroindole, and 6-fluoroindole were the kind gift of Professor E. D. Bergmann of the Hebrew University and Dr. M. Bentov of the Biological Institute in Ness-Ziona.²⁷⁻³⁰ The ready solubility of these derivatives

-
- (8) A. S. Kresge, W. Barry, K. R. Charles, and Y. Chiang, *J. Am. Chem. Soc.*, **84**, 4343 (1962).
- (9) A. R. Katritzky, A. J. Waring, and K. Yates, *Tetrahedron*, **19**, 465 (1963).
- (10) E. M. Arnett, "Progress in Physical Organic Chemistry," Vol. I, Interscience Publishers Inc., New York, N. Y., 1963, p 223.
- (11) R. L. Hinman and J. Lang, *J. Am. Chem. Soc.*, **86**, 3796 (1964).
- (12) Cf. J. F. Bunnett, *ibid.*, **83**, 4956, 4968, 4973, 4978 (1961).
- (13) N. C. Deno, *ibid.*, **74**, 2039 (1952).
- (14) R. Schaal and P. Favier, *Bull. Soc. Chim. France*, 2011 (1959); P. Favier and R. Schaal, *Compt. Rend.*, **249**, 1231 (1959).
- (15) F. Masure and R. Schaal, *Bull. Soc. Chim. France*, 1138, 1143 (1956).
- (16) R. Schaal and G. Lambert, *J. Chim. Phys.*, 1164 (1962); F. Peure and R. Schaal, *Bull. Soc. Chim. France*, 1636 (1963).
- (17) J. H. Ridd, *Chem. Ind. (London)*, 1268 (1957); J. H. Ridd and R. A. M. O'Ferrall, *J. Chem. Soc.*, 5030 (1963).
- (18) R. S. Stearns and G. W. Wheland, *J. Am. Chem. Soc.*, **69**, 2025 (1947).
- (19) K. Bowden and R. Stewart, *Tetrahedron*, **21**, 161 (1965); K. Bowden, *Can. J. Chem.*, **43**, 2624 (1965).
- (20) C. H. Langford and R. L. Burwell, *J. Am. Chem. Soc.*, **82**, 1503 (1960).
- (21) T. Abe, *Bull. Chem. Soc. Japan*, **38**, 1526 (1965).
- (22) V. Gold and C. Rochester, *J. Chem. Soc.*, 1687, 1710, 1717, 1722 (1964).
- (23) M. R. Crampton and V. Gold, *Chem. Commun.*, 256 (1965); *J. Chem. Soc.*, 4293 (1964).
- (24) C. H. Rochester, *Trans. Faraday Soc.*, **59**, 2821, 2826, 2829 (1963).
- (25) L. Ernst, R. J. Irving, and J. Menashi, *ibid.*, **59**, 230 (1962); **60**, 56 (1963).
- (26) C. H. Rochester, *J. Chem. Soc.*, 676 (1965).
- (27) Z. Pelchovitz, A. Kaluszyner, and M. Bentov, *ibid.*, 5418 (1961).
- (28) M. Bentov, A. Kaluszyner, and Z. Pelchovitz, *ibid.*, 2825 (1962).

Table I: Indole Derivatives Employed as Indicators: Melting Points, Absorption Maxima, λ_{max} (with Extinction Coefficients ϵ), Isobestic Wavelength, λ_{is} , and Wavelengths Used for Ionization Calculations, λ_{calcd}

Compound	M.P., ^a °C	BH		B		λ_{calcd} , m μ
		λ_{max} , m μ	(ϵ), ^b mM ⁻¹	λ_{max} , m μ	(ϵ), mM ⁻¹	
3-Formylindole (indole carboxaldehyde)	204-207 (197-199)	244 (13.0); 298 (13.2)	260 (12.2); 323 (19.7)	265 (20.0); 280 (7.8); 252 (8.5); 309 (8.0); 253.7 (3.5)	230 (6.4); 253 (10.9) 307 (11.3) 280 (7.0)	325; 295; 270
3-Acetylindole	196-197 (194)	239 (11.1); 298 (11.2)	255 (11.2); 271 (5.4); 277.3 (5.43)	266 (16.6); 276.5 (7.05); 282.5 (6.02)	252 (8.5); 280 (7.0)	325; 295; 270
Benzimidazole (3-azaindole)	169-171 (170-172)	271 (5.4); 277.3 (5.43)	276 (4.3)	278 (5.6)	252.5 (3.8)	275.5; 282.5; 240
2-Methyl benzimidazole (2-methyl-3-azaindole)	174 (176)	276 (4.3)	276 (4.3)	278 (5.6)	252.5 (3.8)	275.5; 285; 240
Indazole	135 (146)	250 (4.2); 295 (3.1)	285 (3.95); 332 (4.95); ~256	302 (4.1) 401 (6.6); 288 (7.7)	262 (3.65); 275 (2.9) 289.5 (2.56)	310; 305; 250
5-Nitroindole	136 (141-142)	332 (4.95); ~256	~256	401 (6.6); 288 (7.7)	272 (6.2); 310 (3.7) 359 (3.1)	420; 410
5-Cyanoindole	103	275 (4.5)	275 (4.5)	298 (5.25)	284.5 (4.0)	330; 320; 310; 275
5-Bromoindole	87 (91)	~280 (4.95)	~280 (4.95)	297 (4.3); 315 ^f	290 (4.0)	325; 310; 275
5-Fluoroindole	44.5 (46)	270 (5.90)	270 (5.90)	291 (5.25); 315 ^s	286 (4.95)	320; 310; 265
4-Fluoroindole	45.5	268 (6.15)	268 (6.15)	289 (5.8); 315 ^s	~285	320; 310; 265
3-Tryptophan (3-CH ₂ CHNH ₂ ; CH ₂ OH-indole)	72	281 (10.0); 288 (9.0)	288 (9.0)	286 (6.8); 315 (5.2)	292 (5.0)	320; 310
1-Tryptophan	24.0 ^d (289)	280.5 (5.33); 288.5 (4.60)	280.5 (5.33); 288.5 (4.60)	284 (3.5); 293 (3.2); 312 (2.5)	~295	320; 310; 282.5
5-Nitroindole-2-carboxylate	322 (323-328)	322 (12.6)	322 (12.6)	395 (13.6)	359 (9.3)	420; 400; 340
5-Bromoindole-2-carboxylate	274 (279-280)	284 (12.5)	284 (12.5)	319 (11.8)	303 (11.0)	330; 315
Indole-3-carboxylate	225-229 (210-218)	281 (8.1); 287 ^s ^e	281 (8.1); 287 ^s ^e	304 (7.2)	289 (6.3)	310; 305
Indole-5-carboxylate	198-207 (208-209)	272 (4.3)	272 (4.3)	292 (5.25)	283 (4.5)	320; 310
Indole-2-carboxylate	205 (203)	287 (13.1)	287 (13.1)	302 (11.0)	297 (10.0)	330; 320; 280

^a Melting points reported in the literature are given in parentheses. ^b Concentrations are calculated from the weight of the recrystallized compound. ^c s = shoulder.

^d The melting points of this compound and the following ones are of the nonionized acids. ^e More precise λ_{max} and λ_{is} can probably be obtained with a recording instrument.

makes their use as indicators convenient. 5-Nitroindole-2-carboxylate and 5-nitroindole were prepared by Fisher cyclization as described by Parmerter, *et al.*³¹

Lithium hydroxide and sodium hydroxide solutions were prepared by dissolving the analytical grade compounds in water to give a saturated solution; insoluble residues were removed by centrifugation. Potassium hydroxide, with which most of the measurements were performed, was first recrystallized by weighing 800 g of KOH into 700 g of water and leaving at 0° overnight; most of the hydroxide precipitates as KOH·2H₂O. The supernatant was then decanted, the precipitated crystals were dissolved in the necessary amount of water, and the solution was recentrifuged. Even after these steps, considerable absorbance (*vs.* water) remained in the 230–400-m μ range, and this was only in part intrinsic to the solute. The residual absorbance varied not only from batch to batch but even from one diluted sample to the other in the same batch, in the order of 0.005 absorbance unit at 300 m μ . These variations are the prime accuracy limiting factor of the results reported in this paper.

Hydroxide concentrations were determined by titrating weighed amounts with 0.5 *N* H₂SO₄ solution, standardized with TRIS. Spectral measurements were performed on a Beckman DU spectrophotometer. Temperature was kept constant at 25 ± 0.05° by circulating water from a thermostated water bath through double "thermospacer" walls.

Determination of Ionization Ratios. Indicator stock solutions were prepared by weighing the solid compound into water, usually to a concentration of 4 × 10⁻³ *M*. No additional solvent was used. In some cases warming in hot water was necessary to bring about complete dissolution. Turbid solutions were cleared by centrifugation. The final solution was prepared by pipetting the calculated amount of indicator stock solution and of hydroxide (or buffer) into a volumetric flask containing most of the water and filling to the mark. The solution was preheated to 25° and the absorbance relative to water was measured in a cell with 1.000-cm light path. Most compounds were measured at a concentration of 10⁻⁴ *M*. With the following indicators, measurements at more than one concentration of indicator were performed to assure that the observed changes upon ionization are concentration independent: 5-nitroindole, indazole, 3-formylindole, and L-tryptophan. No concentration effects were observed.

Two series of measurements were performed with each indicator. In the first series, the detailed spec-

trum was recorded at a few hydroxide concentrations to find out whether a simple equilibrium occurs and to determine the wavelengths most suitable for ionization ratio determination. A few samples were measured as fast as possible after hydroxide addition to assure that formation of base is complete at observation time; in no case was an observably slow ionization found (*i.e.*, $t_{1/2}$ < 0.5 min). Further, a sample was left in concentrated hydroxide for 15 min and then rediluted so that it reconverted to the acid form. With all the indicators employed, the acid form was rapidly reformed. The stability of both acid form and base form of the indicator was observed for several hours, and indicators showing appreciable decomposition were excluded. Data about those compounds which were not used as indicators for one of the reasons mentioned, with their *pK* values on the *H*₋ scale, are given in a separate publication.³²

A second series was then performed at a large number of hydroxide concentrations, but only at the wavelengths found most suitable for ionization ratio determination. In this series the absorbance of the acid form *A*_{BH} was measured by looking at two or three solutions in phosphate buffer (0.01 *M*) or dilute KOH, pH 9–12. The absorbance of the base form *A*_{B-} was determined by looking at two or more solutions at hydroxide concentrations well above half-ionization.

Calculation of Ionization Ratios. The first step in setting up an indicator acidity scale is the calculation of ionization ratios $r = C_{B-}/C_{BH}$. This is done essentially by the method outlined by Hammett and co-workers.^{33,34} The expression used is $r = (A - A_{BH})/(A_{B-} - A)$; however, two corrections were first applied to the absorbancies recorded in the experiment. First, the reading at a wavelength at which neither form of indole absorbs, *e.g.*, 380 m μ , was subtracted; this corrects for any turbidity still present. The same was done for a "solvent blank" containing hydroxide but not indole. This corrected solvent blank was then subtracted from the corrected reading and the resulting *A* was inserted in the above expression for *r*. In this way fluctuations caused by trace

(29) R. Ikan, E. Hoffmann, E. D. Bergmann, and A. Galun, *Israel J. Chem.*, **2**, 37 (1964).

(30) E. Hoffmann, R. Ikan, and A. B. Galun, *J. Heterocyclic Chem.*, **2**, 298 (1965).

(31) S. G. Parmerter, A. G. Cook, and W. B. Dixon, *J. Am. Chem. Soc.*, **80**, 4621 (1958); *cf.* S. P. Hiremath and S. Siddappa, *J. Indian Chem. Soc.*, **41**, 357 (1964).

(32) G. Yagil, *Tetrahedron*, in press.

(33) L. P. Hammett and A. J. Deyrup, *J. Am. Chem. Soc.*, **54**, 2721 (1932).

(34) L. A. Flexer, L. P. Hammett, and A. Dingwall, *ibid.*, **57**, 2103 (1935); *cf.* ref 10.

turbidities, mainly due to the hydroxide, were minimized.

Reliable A_{BH} values were relatively easy to obtain, using sufficiently low hydroxide concentrations. A_B -values for compounds with a high pK had to be obtained with some extrapolation. The occurrence of solvent shifts was determined by observing absorbance change. Serious medium shifts were found only with the nitro derivatives. For these compounds, A_B -was calculated for each hydroxide concentration by linear extrapolation. After a preliminary H_- scale was established, it was possible to determine the percentage of BH still present at the high hydroxide concentration employed for A_B -determination. In some cases an appreciable amount of BH was still present, leading to a correction in A_B -. The ionization ratios were recalculated with the corrected A_B -, leading to the final H_- scale. The corrections were not large.

The calculation of r was usually performed at more than one wavelength. It was found that the slope of the plot of $\log r$ vs. C_{OH^-} was fairly independent of wavelength, but differences occurred in intercepts which influence the pK values derived. The values reported are the mean of the values at the individual wavelengths. The wavelengths employed for each compound are listed in Table I.

pK of the Most Acid Indicators. In order that the H_- scale be an extension of the conventional pH scale, the pK of the most acid indicators should be determined in a thermodynamically exact way. These lowest lying indicators are 3-formylindole and benzimidazole, $\log r$ of which (and of several additional ones) was plotted against $\log C_{OH^-}$ (Figure 1). The slope of these plots was exactly 1.00. This indicates the activity coefficient ratio $f_{B^-} \cdot f_w / f_{BH} \cdot f_{OH^-}$ is very close to unity, so that correction for this term (e.g., by determining the pK at several constant ionic strengths and extrapolating to zero ionic strength) is not necessary. A considerable variation of the activity coefficient term with ionic strength can hardly be expected, because both the numerator and the denominator of the term contain a single negative charge, so that at least the electrostatic contribution largely cancels.

The pK of 3-formylindole and benzimidazole can thus be determined directly from the plot by reading the value of C_{OH^-} at which $\log r = 0$ (i.e., $C_{B^-} = C_{BH}$) and a pK value equal to $14.00 - \log C_{OH^-}^{-1}$ is assigned to each compound. The values found are $pK = 12.36$ for 3-formylindole and $pK = 12.86$ for benzimidazole (see Table II). These two values serve as base values for the construction of the scale.

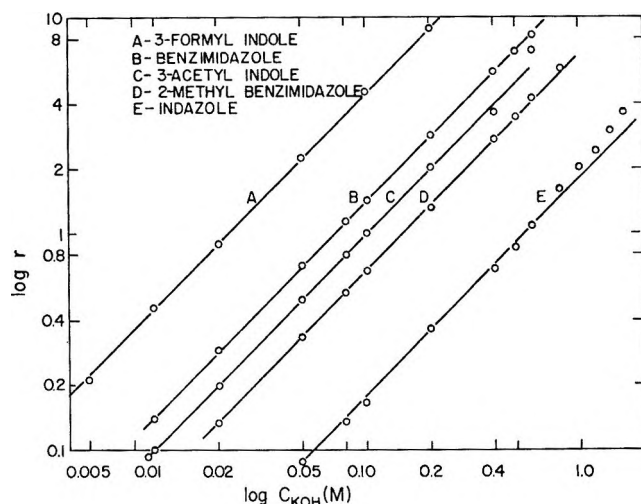


Figure 1. The logarithm of ionization ratio as a function of the logarithm of potassium hydroxide concentration for several indole derivatives.

Construction of the Scale. The next step is to derive the pK of an "overlapping" indicator by the relation $pK_2 = pK_1 + (\log r_2 - \log r_1)$. This relation holds at each value of C_{OH^-} , provided that $(f_{B^-}/f_{BH})_1 = (f_{B^-}/f_{BH})_2$, i.e., provided that the ionization ratio plots (Figures 1-4) run parallel, which is the basic assumption upon which the indicator acidity concept rests. The difference in $\log r$ between 3-acetylindole and 3-formylindole (or benzimidazole), at several overlapping C_{OH^-} concentrations, yields several values of ΔpK between the acids. From the mean of these, a pK of 12.99 for 3-acetylindole was derived (indicating that H_- is still practically identical with $14.00 + \log C_{OH^-}$, but no longer with $\log a_{H^+}$, which is ionic strength dependent). The same was done for 2-methylbenzimidazole. Having these two values, the pK of indazole can be calculated by the same procedure, and so on, until the pK of the most weakly acidic compound, L-tryptophanol, is obtained.

From the known pK values and ionizing ratios, H_- is calculated by the relation which defines the scale: $H_- = pK + \log r$. At each hydroxide concentration, there are several indicators for which $0.1 < r < 10$. Thus, several values of H_- are obtained at each value of C_{OH^-} . After the whole scale was thus established, an iteration with corrected A_B - values was performed as explained under "Calculation of Ionization Ratios" leading to the final values listed in Table III.

In NaOH and LiOH solutions, a somewhat different procedure was adopted. The least basic indicator measured was indazole. The plot of $\log r$ vs. $\log C_{OH^-}$ for this indicator was linear with slope of unity up to 1 M hydroxide (cf. Figure 3 and 4). It could be

Table II: Slopes, Concentrations $C_{1/2}$ at Which $C_{B^-} = C_{BH}$, and pK Values of Indole Derivatives Employed

	KOH			NaOH		
	$\frac{d \log r / d C_{OH^-}}{M^{-1}}$	$C_{1/2}, M$	pK	$\frac{d \log r / d C_{OH^-}}{M^{-1}}$	$C_{1/2}, M$	pK
3-Formylindole	1.00 ^a	0.023	12.36			
3-Acetylindole	1.00 ^a	0.098	12.99			
Benzimidazole (3-azaindole)	1.00 ^a	0.071	12.86 ^b			
2-Methyl benzimidazole (2-methyl-3-azaindole)	1.00 ^a	0.152	13.18 ^c			
Indazole (2-azaindole)	1.00 ^a	0.56	13.80 ^d	1.0 ^a	0.63	13.80
5-Nitroindole	0.30	2.70	14.75	1.0 ^a	3.1	14.69
				0.35		
5-Cyanoindole	0.285	4.50	15.24	0.25	<i>e</i>	15.21
5-Bromoindole	0.29	7.60	16.13	0.28	<i>e</i>	16.32
5-Fluoroindole	0.29	8.00	16.30	0.24	10.6	16.72
4-Fluoroindole	0.32	8.00	16.30		<i>e</i>	
L-Tryptophan	0.29	9.80	16.82	0.21	12.9	16.73
L-Tryptophanol	0.27	10.15	16.91	Solubility $< 10^{-4} M$ above 5 M		
5-Nitroindole-2-carboxylate	0.33	1.95	14.91			
Indole-3-carboxylate	0.36	3.75	15.59			
5-Bromoindole-2-carboxylate	0.39	5.10	16.10			
Indole-5-carboxylate	0.33	7.70	16.92			
Indole-2-carboxylate	0.37	7.80	17.13			

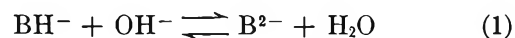
^a Slope of $d \log r / d \log C_{OH^-}$. ^b Several values for the pK of benzimidazole have been reported in the literature. The most thorough measurements, by the potentiometric methods, are reported by H. Walba and I. R. Isensee, *J. Org. Chem.*, **26**, 2789 (1961); *J. Am. Chem. Soc.*, **77**, 5488 (1955), yielding a value of 12.78, close to the present one. Other values by potentiometric titration are 12.3 (M. T. Davies, P. Mamalis, V. Petrow, and B. Sturgeon, *J. Pharm. Pharmacol.*, **3**, 420 (1951)), 12.3 (A. Albert, R. Goldacre, and J. Phillips, *J. Chem. Soc.*, 2240 (1948)), 13.3 (P. J. Brown and R. J. Harrison, *ibid.*, 3332 (1959)), and 12.7 (L. S. Efros and B. A. Porai-Koshitz, *Chem. Abstr.*, **48**, 7603h (1954)). ^c Potentiometric titration gave a value of 11.48 (V. A. Pavlova, *Zh. Nauch i Prikl. Fot. i Kinematogr.*, **3**, 101 (1958); *Chem. Abstr.*, **52**, 21035 (1958)). ^d A value of 14 is mentioned by T. K. Adler and A. Albert, *J. Chem. Soc.*, 1794 (1960). ^e Insoluble at $C_{1/2}$.

assumed, therefore, that the ionization ratios of the less basic indicators are the same as in KOH. It was further assumed that pK values are the same in all three hydroxides, and the reported H_- values are calculated directly from $\log r$ and from the pK in KOH. This procedure seemed more reliable because of the limited solubility of some of the indicators in NaOH. In any case, the difference between the stepwise calculated pK (cf. Table II, column 7) and the pK in KOH did not exceed 0.09 unit even in L-tryptophan. The values arrived at in NaOH are shown in Table IV, and the values for LiOH in Table V.

Accuracy. The value of $\Delta \log r$ between each pair of indicators was constant to 0.03 unit up to 1 M KOH. At higher concentrations, differences reached 0.10 unit. A difference of this order appeared, for instance, whether pK of L-tryptophan was based on 4-fluoroindole or 5-bromoindole. The source of the deviations is either experimental as mentioned above, or might stem from some individuality of the compounds.

Since those errors are cumulative, an accuracy of ± 0.05 – 0.15 (at high KOH concentrations) is attributed to the reported H_- values.

The H_- Scale. This scale represents ionization according to



The determination of the lowest pK is here somewhat more complicated, since the activity coefficient term $\log f_{B^{2-}} \cdot f_w / f_{BH^-} \cdot f_{OH^-}$ cannot be neglected: it contains an electrostatic free energy contribution. The least basic indicator available was 5-nitro-2-carboxylate, the lowest lying point of which was at 0.1 M KOH. In order to determine its pK , $\Delta \log r$ values between this compound and indazole (an H_- indicator) were calculated in the range 0.1–2.5 M KOH as usual. To each difference an electrostatic contribution of $-C^{1/2} / 1 + 2C^{1/2}$ was added,³⁵ assigning thus an ion-size

(35) Cf. R. A. Robinson and R. H. Stokes, "Electrolyte Solutions," Butterworth and Co. Ltd., London, 1959, p 245.

Table III: H_- Values in KOH at 25°

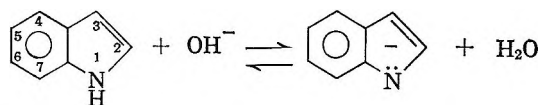
C, M	H_-			H_{2-} , obsd
	Obsd	From ref ^b	Calcd ^a	
0.1	13.00			13.25
0.2	13.32			13.58
0.5	13.75			13.99
0.8	14.00			14.24
1.0	14.11	14.00 ^c	14.10	14.42
1.5	14.33			14.71
2.0	14.51	14.52	14.53	14.95
2.5	14.69			15.12
3.0	14.85	14.83	14.85	15.30
3.5	15.00			15.48
4.0	15.15	15.13	15.13	15.67
4.5	15.28			15.85
5.0	15.44	15.47	15.40	16.03
6.0	15.72	15.80	15.68	16.41
7.0	16.00	16.13	15.97	16.78
8.0	16.33	16.50	16.30	17.09
9.0	16.58	16.85	16.60	17.45
10.0	16.90	17.22	17.08	17.82
11.0	17.14	17.70		18.44
12.0	17.39	18.15		
13.0	17.66	18.60		
14.0	17.95	18.90		
15.0	18.23	19.25		

^a On the molar scale, with $n = 3$. The values are somewhat lower than their values listed in part I^a because of the difference in temperature, which causes a change of 0.166 in pK_w . C_w values listed in Tables I and II of part I are unchanged. ^b From Schwarzenbach and Sulzberger, ref 2, at 20°. ^c Assumed value.

parameter of 6 Å to B^{2-} , BH^- , and the hydroxide ions (somewhat different assignments did not cause considerable change). A mean value of $\Delta pK = 1.11$ results, leading to $pK = 14.91$ for 5-nitroindole-2-carboxylate. With this value, the H_{2-} scale was constructed by the stepwise method outlined above for the H_- scale. The results, in KOH, are given in Table IV. Values in NaOH and LiOH were not determined.

Results

Preliminary experiments indicated that many derivatives of indole have the necessary properties to serve as indicators for determining the acidity, or rather basicity, of concentrated hydroxide solutions. The spectral properties, as well as the melting points, of those derivatives selected for the determination are shown in Table I. As can be seen in the table, the most pronounced change in the ultraviolet spectrum upon ionization is the appearance of a new absorption and with a peak, or a shoulder, between 310 and 320 $m\mu$. The ionization of indole proceeds most probably according to the following reaction.



i.e., the base is formed by proton abstraction from nitrogen, which is the most positive atom in the ring, carrying 0.26 electron charge unit.³⁶ Hydrogen ab-

Table IV: H_- Values in NaOH at 25°

C, M	H_-			
	Obsd	From ref 2 ^b	From ref 4 ^d	Calcd ^a
0.1	12.99			
0.2	13.30			
0.5	13.71			
0.8	13.92			
1.0	14.02	14.00 ^c	13.96	14.10
1.5	14.20			
2.0	14.37	14.36	14.38	14.50
2.5	14.54			
3.0	14.65	14.70	14.63	14.78
3.5	14.81			
4.0	14.95	14.92	14.90	15.03
4.5	15.08			
5.0	15.20	15.18		15.28
6.0	15.40	15.38		15.52
7.0	15.62	15.60		15.76
8.0	15.75	15.80		16.02
9.0	15.97	16.00		
10.0	16.20	16.20		16.63
11.0	16.42	16.50		
12.0	16.58	16.80		
13.0	16.76	17.10		
14.0	16.93	17.40		
15.0	17.10	17.75		
16.0	17.30	18.12		

^a On the molar scale, with $n = 3$. The values are somewhat lower than previous values because of the difference in temperature, which causes a change of 0.166 in pK . ^b From Schwarzenbach and Sulzberger, ref 2, at 20°. ^c Assumed value. ^d From Edward and Wang, ref 4.

Table V: H_- Values LiOH, $T = 25^\circ$

C, M	H_- -obsd
0.5	13.68
1.0	13.96
1.5	14.11
2.0	14.26
2.5	14.36
3.0	14.45
3.5	14.53
4.0	14.58
4.5	14.65

(36) R. A. Coulson and M. Longuet-Higgins, *Proc. Roy. Soc. (London)*, **191**, 39 (1947); **192**, 16 (1947); *cf.* A. Albert, "Heterocyclic Chemistry," The Athlone Press, London, 1959, p 159.

straction from any ring carbon can be ruled out because derivatives with almost every hydrogen atom substituted were measured and no abnormal pK or spectrum of the base form were observed³² (in acid solution conjugate acid is formed by adding a hydrogen to carbon no. 3,³⁷ the atom carrying the highest negative charge, -0.07 unit). OH^- addition to the ring, which occurs to many anilines,²¹⁻²⁴ is also not very likely, because each of the eight possible OH^- adducts can be stabilized by no more than two or three resonantive structures, while eight such structures contribute to the indolate anion shown above. An attempt was made to verify this conclusion by observing the pmr spectrum of some indoles, but none was soluble enough in concentrated hydroxide to make the measurement possible, and measurement in a solvent other than water would not settle the issue.

To determine the acidity scale, the light absorption of each indole derivative was measured at several wavelengths over a range of hydroxide concentrations as described in the Experimental Section. From these data, the ionization ratios, $r = C_B-/C_{BH}$, were calculated and $\log r$ was plotted against the hydroxide concentrations C_{OH^-} . These plots are shown in Figures 2-5 for KOH, NaOH, and LiOH, respectively. In Figure 1, a plot of $\log r$ vs. $\log C_{OH^-}$ is given for compounds which are relatively strong acids, so that the transition from acid to base form takes place below $C_{OH^-} = 0.1 M$. All the plots in Figure 1 have unity slope, so that little deviation from ideality occurs up to $0.2 M$ hydroxide. For these compounds a thermodynamically valid pK was derived as explained, and these serve to anchor the acidity scale to the conventional pH scale in the dilute solution range. 3-Formylindole ($pK = 12.36$) and benzimidazole ($pK = 12.86$) were the starting compounds. From these two compounds, the pK 's of all other compounds were derived by the usual stepwise method (see Experimental Section). The pK value arrived at, as well as $C_{1/2}$, the concentration of hydroxide at which each compound is half-ionized ($r = 1$), are shown in Table II. These pK values, as well as those of a series of additional indoles and related heterocyclic compounds, are discussed separately.³²

Also shown in Table II are the slopes of the plots in Figures 1-3 and 5. All the compounds with $C_{1/2}$ above $C_{OH^-} = 1 M$ gave linear plots over most of the acid to base transition range; there is no apparent reason why this should be so, but it is a convenient fact. Two distinct groups of compounds are evident, one group with slopes around $0.29 M^{-1}$, and another with slopes of around $0.35 M^{-1}$ (4-fluoroindole occupying an intermediate position). To the first class belong all

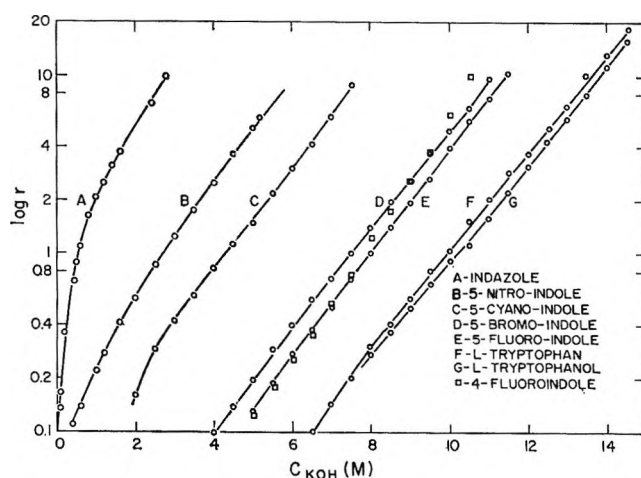


Figure 2. The logarithm of ionization ratio as a function of potassium hydroxide concentration for several indole derivatives.

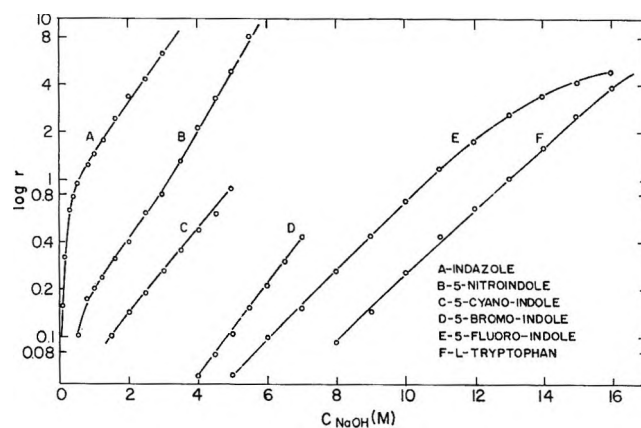
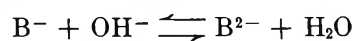
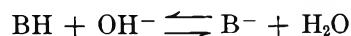


Figure 3. The logarithm of ionization ratio as a function of sodium hydroxide concentration for several indole derivatives.

the uncharged indoles while the second class includes those indoles whose acid form already carries a negative charge. This suggests the ionization behavior of compounds which ionize according to



is different from the behavior of compounds which ionize according to



This means that the indicator acidity scale determined by negative charged acids, which is of the H_{2-} type, is a steeper function of base concentration than the scale derived from neutral acids, H_- . This is expected from electrostatic considerations, which de-

(37) R. L. Hinman and E. B. Whipple, *J. Am. Chem. Soc.*, **84**, 2534 (1962).

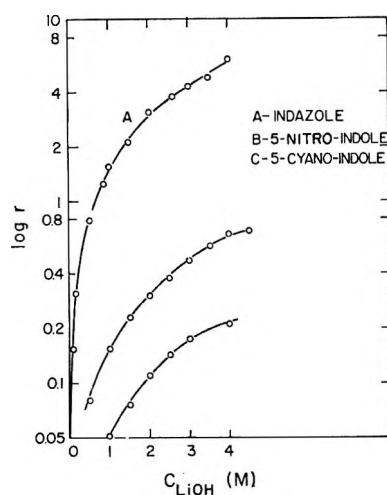


Figure 4. The logarithm of ionization ratio as a function of lithium hydroxide concentration for several indole derivatives. (B is represented by the middle curve and C by the bottom curve.)

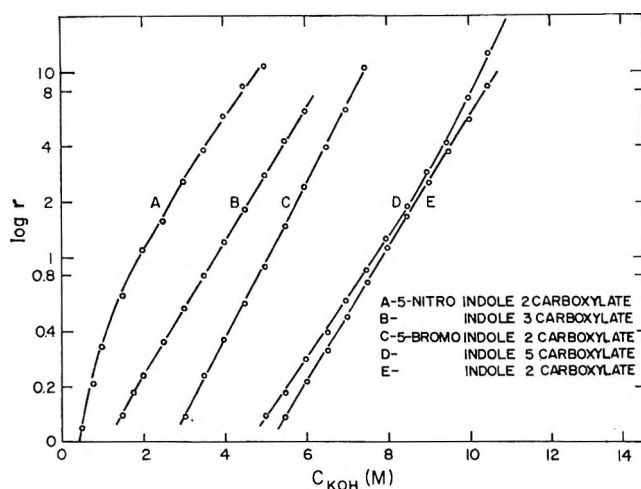


Figure 5. The logarithm of ionization ratio as a function of potassium hydroxide concentration for several negatively charged indole derivatives.

mand that the H_{2-} acidity increases more rapidly with total electrolyte concentration than does the H_- acidity (see Discussion). The constancy of the slopes within each group means that ionization curves are parallel, and demonstrate that the Hammett concept is valid in concentrated hydroxide solutions. An exception seems to be tryptophan, which carries a negative charge, but has a slope of $0.29 M^{-1}$. It should be remembered, however, that this charge is removed up to 5.8 Å from the ring and is not conjugated with it, while the average distance between two anions in a 10 M solution is just 5.5 Å (obtained by dividing 1 l. into $10 \times 6 \times 10^{23}$ cubes). A specific effect of this charge can thus hardly be expected.

Two separate scales were thus constructed. The values for H_{2-} and H_- obtained in KOH, as well as values of H_- in NaOH, are shown in Tables III and IV. The values for LiOH are shown in Table V, and are further discussed in part IV.^{1c} Values obtained by previous workers are also shown in the tables, and it is seen that the present values in KOH and NaOH agree well with the values of Schwarzenbach and Sulzberger,² as well as with the values of Edward and Wang,⁴ up to 6 M NaOH.

It should be noted that the indicator of the latter, $CH_3 \cdot CS \cdot NH_2$, is of very different structure from those used in the present study. Above 6 M the values start to deviate, the present values being lower by a whole unit at 15 M KOH and by somewhat less, 0.65 unit in 16 M NaOH. It cannot be said whether this is a result of a difference in the nature of the compounds employed now, or because the measurements of Schwarzenbach and Sulzberger were not carried out in the aqueous phase. Only measurements on additional classes of weak acid will be able to determine this point (cf. ref 26).

Discussion

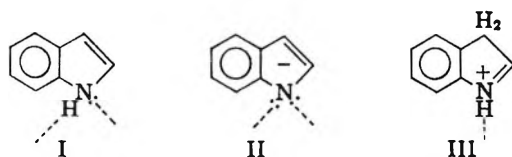
In part I of this series^{1a} a model is proposed to explain the high alkalinity of concentrated hydroxide solutions, which is based on the hydrated proton model of Bascombe and Bell for acid solutions.^{38,39} One aim of the present redetermination of the H_- scale was to substantiate the conclusion arrived at, namely that the hydroxide ion is hydrated by three water molecules in not too concentrated solution. The values of H_- calculated from the model^{1a} are re-shown in column 4 of Table III and column 5 of Table IV. The values calculated with a hydration number $n = 3$, agree with the new experimental value in KOH even better than with the old ones. In NaOH there is a constant difference of 0.10 between the calculated and observed values. This might be due to an inaccuracy in the measurements with the lowest lying indicator, indazole. Except for this difference, agreement between calculated and observed values is good in NaOH too, while calculations with $n = 2$ or $n = 4$ lead to quite different values. The conclusion that the hydroxide ion is trihydrated is thus confirmed. The difference in temperature between the present values (25°) and previous ones (20°) causes changes only in the third decimal figure of the calculated values (due to density changes). This prediction of the hy-

(38) K. N. Bascombe and R. P. Bell, *Discussions Faraday Soc.*, **24**, 158 (1957).

(39) R. P. Bell, "The Proton in Chemistry," Cornell University Press, Ithaca, N. Y., 1959, p 81 ff.

dration model, that indicator acidities change only little with temperature, has also been verified in the case of the steep H_R function in H_2SO_4 ,⁴⁰ where only slight changes were found over a considerable temperature range.

One more requirement of the model is that indole and its conjugate base should be solvated by the same number of solvent molecules. This is likely to be the case as both species are quite large molecules, and the negative charge of the anion is dispersed over the molecule. From the viewpoint of hydrogen bond forming capacity, both forms can bind to an equal number of water molecules: the nitrogen in the neutral molecule can accept one hydrogen and can donate one hydrogen, *i.e.*, coordinate two water molecules (I) while in the anion the nitrogen can accept two hydrogens from the solvent (II)



It should be noted that this is not the situation in acid solution because of C protonation (III): here the nitrogen is left with only one hydrogen bond accepting site, while the methylene group formed is unlikely to participate in hydrogen bonding. It is indeed observed that protonation of indoles is a somewhat steeper function of C_{H^+} than H_0 ,⁴¹ and can be quantitatively accounted for if one assumes that five molecules of water rejoin the solvent upon protonation (one from indole and four from $H_9O_4^+$).

Further work pertinent to the problem of hydration of aqueous hydroxide appeared since the previous report. Agarwal and Diamond bring additional evidence for the three coordination of the OH^- ion from experiments on distribution between solvents.⁴² X-Ray measurements of the structure of solid $NaOH \cdot 4H_2O$ crystals were performed, and lead to the result that each OH^- ion accepts five rather than three hydrogen bonds from water, with a distance of 2.68 to 2.73 Å.⁴³ Even in aqueous solution, X-ray measurements⁴⁴ indicated six oxygens as nearest neighbors to OH^- . This figure is derived from the area of the first peak in the distribution curve. The distance at which this peak occurs goes down from 2.94 Å in pure water to 2.87 Å in 3.4 M KOH. It could not be determined whether decreased O⁻-O distance or K⁺-O distance is the cause of this reduction. Infrared measurements in the interval 1600–1700 cm^{-1} ⁴⁵ reveal considerable differences between water and concentrated KOH, which are explained in terms of the three-hy-

drated model. Measurements at higher frequencies fail, however, to reveal any bands specific for an $HO \cdots HOH$ stretching mode⁴⁶ and such a mode should exist if the $H_7O_4^-$ species has an exceptional stability. It is possible that the considerable width of the bands conceals such a feature, and the problem will probably not be settled until the infrared and Raman spectra of water itself are fully explained. Some theoretical calculations on the stabilization of the hydration of the OH^- by hydration were done,⁴⁷ and showed that the presence of three water molecules in the first hydration shell can well explain the pmr shift of H_2O caused by the OH^- ion. Measurement of the O^{17} shift of water in hydroxide solutions⁴⁸ did not reveal any features relevant to the hydration problem. Finally, it should be mentioned that mass spectrometric measurements in the gas phase elegantly demonstrated^{49,50} the exceptional stability of the species $H_9O_4^+$ which is the acid analog of $H_7O_4^-$. In summary, additional work will be needed to establish finally that state of hydration of OH^- , and indeed of any simple monovalent ion in aqueous solution.

H_{2-} . The ionization ratios of weak acids dissociating according to $BH^- + OH^- \rightleftharpoons B^{2-} + H_2O$ show a steeper increase with hydroxide concentration than the H_- weak acids (Table III). Can the hydration picture explain this behavior? The main difference between the two kinds of indicators is that while in the H_- equilibrium, one singly charged anion (B^-) is formed and one (OH^-) is consumed, in the H_{2-} equilibrium a doubly charged anion is formed out of two singly charged ones (BH^- and OH^-), *cf.* eq 1. Electrostatic energy is needed for the transition of the H_{2-} type and the activity coefficient term cannot be assumed to be negligible in the H_{2-} acidity, as it was in the H_- case. High ionic strength favors the formation of doubly *vs.* singly charged species; the steeper rise of the H_{2-} acidity is therefore in accord

(40) E. M. Arnett and R. D. Bushick, *J. Am. Chem. Soc.*, **86**, 1564 (1964).

(41) R. L. Hinman and J. Lang, *ibid.*, **86**, 3796 (1964).

(42) B. R. Agarwal and R. M. Diamond, *J. Phys. Chem.*, **67**, 2785 (1963).

(43) G. Beurskens and G. A. Jeffrey, *ibid.*, **41**, 924 (1964).

(44) G. W. Brady, *ibid.*, **28**, 464 (1958).

(45) Y. V. Moiseev and M. I. Vinnik, *Zh. Struk. Khim.*, **4**, 336 (1963).

(46) W. Luck, *Ber. Bunsenges. Physik. Chem.*, **67**, 186 (1963).

(47) R. Grahn, *Acta Chem. Scand.*, **19**, 153 (1965); *cf.* A. J. Kresge, *J. Chem. Phys.*, **39**, 1390 (1963).

(48) Z. Luz and G. Yagil, *J. Phys. Chem.*, **70**, 554 (1966).

(49) P. F. Knewstubb and A. W. Tickner, *J. Chem. Phys.*, **38**, 464 (1963).

(50) P. Kebarle and A. M. Hogg, *ibid.*, **42**, 798 (1965).

with this picture. A rough calculation of the difference between H_- and H_{2-} can be made on basis of the finding of Robinson and Stokes³⁵ and Glueckauf⁶¹ that the electrostatic term of the activity coefficient for *hydrated* species dissolved in *free* water is given by $\log f_{el} = -z^2 AC^{1/2}/(1 + BaC^{1/2})$ up to quite high concentrations. The difference $H_- - H_{2-}$ is then simply $-\sum_i z_i AC^{1/2}/(1 + Ba_i C^{1/2})$, where i goes over all ionic species involved. After expansion, the terms of the hydroxide ion cancel, and if one makes the reasonable assumption that all indoles have a similar ion-size parameter a , one remains with $H_{2-} - H_- = 2AC^{1/2}/(1 + BaC^{1/2})$. Values based on this expression with $a = 6 \text{ \AA}$ are shown in column 3 of Table VI, and with $a = 4 \text{ \AA}$ in column 4 of that table. In column 2 are listed the observed values, and it is seen that the calculated values with $a = 6 \text{ \AA}$ comes quite near to the calculated value observed up to 4 M KOH. At higher concentrations, values with $a = 4 \text{ \AA}$ seem to fit better, but it should be remembered that at very high concentrations the ionic atmosphere concept can hardly be expected to hold. The radius of the ionic atmosphere, κ , extends just 1 \AA beyond the ion at 9 M electrolyte, which is less than the distance to the center of many ions if in direct contact. Also, double-charged indolates are not simple bivalent ions, since one charge is on a side group and the other in the ring. The main pur-

pose of the calculation is to point out that comparison of the ionization ratios of compounds differing only in charge type can serve as a method to isolate electrostatic effects from other effects in concentrated solution.

Table VI: The Difference between H_{2-} and H_- Scales in KOH at 25°

C, M	$H_{2-} - H_-$		
	Obsd	$a = 6 \text{ \AA}$	$a = 4 \text{ \AA}$
0.1	0.25 ^a	0.195	0.23
0.5	0.24	0.295	0.36
1	0.31	0.33	0.43
2	0.44	0.37	0.49
3	0.43	0.39	0.51
4	0.52	0.40	0.54
6	0.69	0.415	0.58
8	0.76	0.425	0.595
10	0.92	0.43	0.61

^a The 0.195 of this value were actually calculated as explained under Calculations.

Acknowledgment. The author thanks Mrs. Naomi Aharoni for her competent technical assistance.

(51) E. Glueckauf, *Trans. Faraday Soc.*, **51**, 1235 (1955).

The Effect of Ionic Hydration on Rate and Equilibrium in Concentrated Electrolyte Solutions. IV. The Effect of Neutral Electrolytes on the Indicator Acidity of an Alkaline Solution¹

by G. Yagil

The Radioisotope Training Centre, The Weizmann Institute of Science, and the Israel Atomic Energy Commission, Rehovoth, Israel (Received May 26, 1966)

The change in indicator acidity of aqueous solutions containing a fixed concentration of KOH upon addition of KF, KCl, and KBr was determined. A considerable rise in basicity was observed with KF but not with the other two salts. The results are interpreted in terms of a hydration model for concentrated electrolyte solutions. Calculations based on this model show that the rise in basicity is quantitatively explained if one assumes that 3.5 water molecules are associated with each KF molecule (attributed to the F⁻ ion), while 0.9 molecule is associated with KCl (attributed to Cl⁻) and none with KBr, *i.e.*, with the K⁺ and Br⁻ ions. The same model is applied to LiCl and LiBr in acid solution, and the rise in acidity there is explained by assuming that 5.8 molecules are associated with each of these salts. The basicity of LiOH is explained by the model if the dissociated ions associate with 6–11 water molecules. Several assumptions of the model and implications of the model on the acidity function concept are discussed.

Introduction

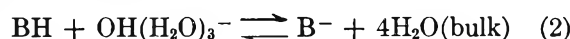
It has been established for some time that the addition of neutral electrolytes changes the indicator acidity of aqueous solutions containing a fixed amount of acid, *e.g.*, 0.1 M HCl.^{2,3} This effect has been extensively surveyed by Paul.^{4,5} Recently, a detailed study of the considerable rise in acidity which occurs upon the addition of LiCl to dilute solutions of HCl in water was carried out by Rosenthal and Dwyer.^{6–8}

The question arises to what extent these effects can be explained in terms of a hydration model of concentrated aqueous solutions. Such a model has been successfully applied by Bascombe and Bell⁹ and by Wyatt¹⁰ to account for the sharp rises of indicator acidity in concentrated mineral acid solutions. The model has been shown to apply equally well to concentrated solution of alkali hydroxides in water.^{1,11} According to the model, the steep rise in acidity is a result of the exceptionally strong coordination of water by the hydroxide and hydronium ion. When a weak acid or weak base ("indicator") molecule dissociates, four water molecules are returned to the bulk.

in acid solution



in alkaline solution



In concentrated solutions, where the concentration of bulk water, *i.e.*, water not firmly bound by proton or hydroxide ion, diminishes appreciably, the equilibria

- (1) Part III, G. Yagil, *J. Phys. Chem.*, **71**, 1034 (1967).
- (2) G. Harbottle, *J. Am. Chem. Soc.*, **73**, 4024 (1951).
- (3) I. V. Moiseev and R. M. Flid, *Zh. Prikl. Khim.*, **27**, 1110 (1954).
- (4) M. A. Paul, *J. Am. Chem. Soc.*, **76**, 3236 (1954).
- (5) M. A. Paul and F. A. Long, *Chem. Rev.*, **57**, 1 (1957).
- (6) D. Rosenthal and J. S. Dwyer, *Can. J. Chem.*, **41**, 80 (1963).
- (7) D. Rosenthal and J. S. Dwyer, *Anal. Chem.*, **35**, 161 (1963).
- (8) D. Rosenthal, I. T. Ojwa, A. D. Saxton, and L. R. Lieto, *J. Phys. Chem.*, **69**, 1588 (1965).
- (9) K. N. Bascombe and R. P. Bell, *Discussions Faraday Soc.*, **24**, 158 (1957); *cf.* R. P. Bell, "The Proton Chemistry," Cornell University Press, Ithaca, N. Y., 1959, p 81.
- (10) P. A. H. Wyatt, *Discussions Faraday Soc.*, **24**, 162 (1957).
- (11) G. Yagil and M. Anbar, *J. Am. Chem. Soc.*, **85**, 2376 (1963).

are shifted to the right to a much larger extent than demanded by concentration of acid or hydroxide ions, thus giving rise to the high acidities encountered.

The addition of electrolyte causes a further depletion of water, first because the salt ions themselves displace some water, and second because some of the cations and anions may also coordinate some water. Among the anions, the fluoride anion is the strongest water coordinating species and can hydrogen bond up to four molecules of water. In the experimental work described below, various amounts of KF were added to potassium hydroxide solutions, and an appreciable rise in basicity was actually observed. Two indole derivatives, which were employed in the preceding paper to determine the basicity of aqueous hydroxide solutions, indazole and indole-3-carboxylate, were utilized. Calculations based on the model show that the observed rise can be quantitatively explained if one assigns a hydration number between 3 and 4 to the F^- ion. The same calculation is carried out for acid solutions containing $LiCl^6$ and $LiBr^{12}$ and show that a hydration number between 5 and 6 does explain the change of acidity caused by these salts as well. These numbers are close to the number of water molecules which each of their ions can coordinate, and give additional confidence in the hydration models of concentrated aqueous solutions.¹³⁻¹⁵

The change in indicator acidity caused by neutral electrolytes in acid solution has been discussed along similar lines, with some differences mentioned in the discussion, by McTigue,¹⁵ Perrin,¹⁶ Ojeda and Wyatt,¹⁷ and Högfeldt and Leifer.¹⁸

Experimental Section

The experimental procedures followed and the calculation of ionization ratios from the experimental data are described in the preceding paper.¹ All of the electrolytes employed were of analytical grade, and stock solutions were cleared by centrifugation. The preparation of potassium fluoride presented serious problems because commercial $KF \cdot 2H_2O$ contained considerable amounts of silicates which neutralized some of the hydroxide which was present at low concentration. For this reason, some data on the effect of electrolyte were obtained at 2.5 M KOH (Table I). The potassium fluoride used was recrystallized twice by dissolving Baker Analyzed $KF \cdot 2H_2O$ in 10% of its weight in water at 50°, centrifuging the residual precipitate, recooling to room temperature, and filtering on a Büchner funnel. The pH of a 1 M solution prepared from these crystals was 6.4, and the addition of 0.05 ml 0.1 M NaOH brought 50 ml to pH 10.1. The addition of further NaOH gave a titration curve with pH

values only slightly below the titration curve of pure water (a quite different behavior was observed with solutions obtained by dissolving the commercial salt). A second batch of potassium fluoride was prepared by adding KOH pellets to 40% HF in water until the pH reached 6.5, and evaporating the solution until $KF \cdot 2H_2O$ separated at 27°; some silicate precipitated in the initial stage of the evaporation and was removed by centrifugation. Fluoride ion concentration in the final solution was determined by titration with thorium nitrate.

Calculations

The amount of water associated with potassium fluoride and other electrolytes was calculated from the ionization ratios, $r = C_B/C_{BH}$, obtained in the experiment in the following manner: the weight of 1 l. of salt containing solution is

$$1000d = (M_h + 3 \times 18)C_h + (M_s + 18n)C_s + 1000C_w \quad (3)$$

where M_h is the molecular weight of the hydroxide (56 for KOH), M_s is the molecular weight of the salt (e.g., 58 for KF), C_h is the concentration of hydroxide in moles/liter, C_s is the concentration of salt in moles/liter, C_w is the concentration of bulk water, i.e., water coordinated neither to hydroxide nor to salt, in kilograms/liter (this unit gives $C_w = 1$ in pure water and is used as previously¹¹ to avoid dragging along a factor of 55.5⁴), d is the density of the solution, and n is the number of water molecules associated with the salt. The equilibrium constant K for an indicator like indazole, which is assumed to ionize according to eq 2,¹ is

$$K = \frac{C_B C_w^4}{C_{BH} C_h} Q = (r C_w^4 / C_h) Q \quad (4)$$

Q denotes the appropriate activity coefficient product of the hydrated species and bulk water. Q is henceforth assumed to be unity in accordance with Glueckauf¹⁴ and others (see Discussion). It should be noted that the equations are not affected if both acid and base form of indicator are hydrated by an equal number of water molecules. Equations 3 and 4 now contain only two quantities not obtainable from the experiment, C_w

(12) D. Kellermann, Thesis, London University, 1962.

(13) R. A. Robinson and R. H. Stokes, "Electrolyte Solutions," 2nd ed, Butterworth and Co. Ltd., London, 1959.

(14) E. Glueckauf, *Trans. Faraday Soc.*, **51**, 1235 (1955).

(15) P. T. McTigue, *ibid.*, **60**, 127 (1964).

(16) C. Perrin, *J. Am. Chem. Soc.*, **86**, 256 (1964).

(17) M. Ojeda and P. A. H. Wyatt, *J. Phys. Chem.*, **68**, 1857 (1964).

(18) E. Högfeldt and L. Leifer, *Acta Chem. Scand.*, **17**, 338 (1963).

and n . Each can thus be calculated from the two equations. However, to minimize errors, mainly due to an uncertainty in the value of K , each ionization ratio is determined relative to the ionization ratio r_0 in a solution containing the same amount of hydroxide but no salt, and the equations are further manipulated as follows: from (4) with $Q = 1$, the free water concentration is

$$C_w = (KC_h)^{1/4}/r^{1/4} \quad (5)$$

When no salt is present ($C_s = 0$), eq 1 becomes

$$1000d_0 = (M_h + 54)C_h + 1000C_w^0 \quad (6)$$

This is combined with (5) at $C_s = 0$

$$1000(KC_h)^{1/4} = r_0^{1/4} \times 1000C_w^0 = r_0^{1/4}[1000d_0 - (M_h + 54)C_h] \quad (7)$$

to give for the bulk water concentration when salt is present

$$1000C_w = (r_0/r)^{1/4}[1000d_0 - (M_h + 54)C_h] \quad (8)$$

Equation 8 is resubstituted in (1) to give the final expression for the hydration number n

$$n = 1/18C_s\{1000d - (M_h + 54)C_h - M_sC_s - \left(\frac{r_0}{r}\right)^{1/4}[1000d_0 - (M_h + 54)C_h]\} \quad (9)$$

For instance, in a 0.4 M KOH solution ($d_0 = 1.020$), the expression for n is

$$n = 1/18C_s\{1000d - 44 - M_sC_s - (1020 - 44)(r_0/r)^{1/4}\} \quad (10)$$

The value of n can thus be calculated if the ionization ratios in a solution containing a certain concentration of salt and in a similar solution without the salt are known. The same expression is good for solutions containing a small constant amount of acid, if one assumes that dissociation proceeds according to eq 1, only that 4×18 substitutes 3×18 in the equation. Further discussion of the assumptions inherent in the calculation are deferred to the Discussion.

Results

The change of the ionization ratio upon the addition of potassium fluoride to a solution containing a constant amount of potassium hydroxide and the following two indicators was determined: indazole in 0.4 M KOH and indole-3-carboxylate in 2.5 M KOH. The higher concentration of KOH was examined to eliminate the possibility that traces of alkaline impurities cause part of the rise in basicity (see Experimental Section). The results are shown in Table I. In addition to the

values of r obtained (columns 2 and 6), values of $\Delta H_- = \log r/r_0$ are shown (columns 3 and 7). It is seen that the addition of KF causes a considerable rise in the basicity of the solution, comparable with the rise in acidity caused by LiCl in acid solutions. Columns 4 and 8 show the free water concentrations calculated from the experimental r values by eq 8. The two final columns give the values of the salt as calculated by eq 9.

It is seen that the value of n decreases somewhat with increasing electrolyte concentration. Extrapolation to zero KF concentration leads to a value of 3.5 in 0.4 M KOH and 3.5–3.8 in 2.5 M KOH. These two values are quite close to the number of four water molecules expected to be withdrawn from the free water pool if one assumes that an F^- ion binds the four water molecules it can potentially coordinate, and that the K^+ ion does not coordinate water appreciably at water concentrations of 30–55 M . The decrease of n with increasing salt concentration may be the consequence of decreasing bulk water concentration, which causes some dissociation of the fully hydrated fluoride ion. The larger decrease observed in 2.5 M KOH supports this. A calculation of an equilibrium constant seems premature, however, since the decrease of n may also be due to some effect of the neglected activity coefficient ratio Q , which in itself reflects some solute–solute or solute–medium effect not included in the model. The use of indole-3-carboxylate is objectionable for one reason, namely that it has been shown to belong to the H_{2-} class of indicators rather than to the H_- class. The behavior of the two functions is similar enough, however, over the electrolyte concentration range employed here to make the conclusion reached valid.¹

It is interesting to compare the effect of potassium fluoride with the effect of an electrolyte the ions of which tend to coordinate water to a lesser extent. Some results obtained with potassium chloride and potassium bromide are shown in Table II. Potassium chloride increases the indicator acidity somewhat, and a hydration number approaching unity was calculated from the observed rise. This should be compared with the figure of 1.7 arrived at by Glueckauf.¹⁴ Potassium bromide does actually cause a slight decrease in the observed basicity, but the decrease is within experimental error. No hydration of the Br^- (and K^+) ions is thus indicated. Some glass electrode measurements have been performed and are shown in the last column of Table II, but cation correction data are not available so that these values have little significance. It is not practicable for that reason to perform glass electrode measurements at the higher hydroxide concentrations employed in the other tables.

Table I: The Effect of Potassium Fluoride on Indicator Acidity of Aqueous KOH Solutions ($T = 25^\circ$)

C_s , M	KOH, 0.4 M (with indazole) ^a				KOH, 2.5 M (with indole-3-carboxylate) ^a			
	τ_{obsd}	ΔH_-	$C_w^{b,d}$ kg/l.	n^c	τ_{obsd}	ΔH_-	$C_w^{b,d}$ kg/l.	n^c
0	0.66	0	0.976	...	0.36	0	0.841	...
0.87	0.86	0.115	0.913	3.35	0.49	0.13	0.764	3.96
1.75	1.14	0.24	0.850	3.35	0.72	0.30	0.708	3.30
2.62	1.58	0.38	0.795	3.20	1.12	0.49	0.630	3.50
3.50	2.02	0.485	0.740	3.15	1.45	0.60	0.588	3.05
4.37	2.31	0.80	0.525	3.00
5.25	3.27	0.695	0.638	2.85
6.12	4.90	1.08	0.446	2.42
7.00	7.00	1.025	0.525	2.70

^a Indicator concentration was $10^{-4} M$. ^b Calculated by eq 8. ^c Calculated by eq 9. ^d The densities of KF solutions, from the "Handbook of Chemistry and Physics," were actually at 15° , but this alters the result very little. Densities of KOH-KF mixtures were obtained by interpolation. Actually, equimolar KF and KOH solutions, as well as equimolar LiCl and HCl solutions, have very close densities, another fact pointing out the similarity between the OH^- and F^- ions as well as between the H^+ and Li^+ ions, in aqueous solution.

Table II: Effect of Potassium Chloride and Potassium Bromide on the Indicator Acidity of Aqueous KOH ($T = 25^\circ$)

C_s , M	KCl, 2.5 M KOH (with indole-3-carboxylate)				KBr, 0.1 M KOH (with indazole)		
	τ_{obsd}	ΔH_-	C_w , kg/l.	n	τ_{obsd}	ΔH_-	pH
0	0.38	0	0.837	...	0.17	0	12.86
1	0.16	-0.010	12.85
2	0.65	0.23	0.734	0.89	0.13	-0.040	12.89
3	0.83	0.33	0.692	0.69	0.105	-0.065	12.91
4	0.165	-0.005	13.00

Table III: The Effect of LiCl and LiBr on the Indicator Acidity of Dilute Aqueous Solutions of HCl

C_s , M	LiCl				LiBr		
	ΔH_-^a	C_w	a_w	n	ΔH_-^b	C_w	n
0	0	1.000	1.000	0	0
1	0.22	0.882	0.963	5.50
2	0.47	0.763	0.917	5.50
3	0.74	0.654	0.859	5.30	0.78	0.648	5.20
4	1.055	0.548	0.789	5.15	1.02	0.566	4.70
5	1.305	0.474	0.708	4.70	1.32	0.457	4.70
6	1.63	0.390	0.619	4.50	1.70	0.376	4.40
7	1.98	0.320	0.525	4.30	2.08	0.302	4.15
8	2.49	0.240	0.434	4.05	2.50	0.237	3.85
9	2.85	0.195	0.350	3.80

^a From Rosenthal and Dwyer, ref 6. ^b From Kellermann, ref 12.

Acid Solutions. It would have been interesting to examine whether fluorides have a similar effect on the acidity of acid solutions. Unfortunately, the fluoride ion associates with the proton (and with HF, to form FHF^-) at a relatively high pH, which is another manifestation of its affinity to hydrogens (the pK of HF is 3.17). The same is true for the lithium ion in alkaline

solutions, as discussed in the next paragraph; Li^+ coordinates well both to H_2O and to OH^- (the combination of the two "hard"¹⁹ ions Li^+ and F^- , lithium fluoride, is relatively insoluble in water). The validity of the approach employed can, however, be further

(19) R. G. Pearson, *J. Am. Chem. Soc.*, **85**, 3533 (1963).

tested from the increase of indicator acidity of dilute acid solutions, caused by lithium salts. The experimental data obtained by Rosenthal and Dwyer⁶ and by Kellermann¹² were utilized, and are shown in columns 2 and 6 of Table III for LiCl and LiBr, respectively. The values of n obtained are shown in columns 4 and 7. The values obtained when extrapolated to zero lithium halide concentration yield 5.8 ± 0.2 for the number of water molecules associated with each lithium halide.

This figure is somewhat higher than the number of coordinating orbitals in the L shell of the Li^+ ion but is close to what has been found by several other methods.^{20,21} The number found by Glueckauf is 4.2.¹⁴ The extrapolation to zero may have led to an exaggerated result, because a detailed examination of the calculation shows that the figures calculated for 1 and 2 M salt are subject to the largest experimental error. In column 4 of Table III the water activities a_w of aqueous LiCl solutions are listed for comparison with bulk water concentration C_w . The differences indicate that the water not bound is more volatile when electrolyte is present than in pure water, a point to be noticed for future refinement.

Lithium Hydroxide. In this case, both cation and anion have already been shown to coordinate water appreciably. It is interesting to examine whether the hydration number arrived at is equal to that estimated from the individual ions or smaller, indicating that a water-bridged ion pair is formed. An examination of the indicator basicity of LiOH solutions (Table V of part III¹) shows that the basicity of LiOH increases much slower than the basicity of KOH and NaOH, and deviates only a little from the hydroxide ion concentration. This is, however, most probably because of the compensation of two effects. Lithium hydroxide is only partly dissociated in water (a reason for this has been mentioned above), while the dissociated molecules cause the usual rise in basicity. In order to make a calculation of hydration number, one has first to determine the fraction of dissociated molecules at each concentration. We shall assume that undissociated LiOH molecules do not interact with bulk water in excess to water-water interactions (LiOH is the most water-like molecule imaginable). To make the calculation, a value for $K_d = (C_{\text{Li}^+} \cdot C_{\text{OH}^-} / C_{\text{LiOH}}) Q_d$ is needed. There is, however, no agreement on the exact value of this constant, and the calculation was performed with two values available. One value, $K_d = 1.5 M$, was calculated by Gimblett and Monk²² from old emf measurements by Harned and co-workers.²³ The other value, $K_d = 0.66 M$, was obtained more recently by Ohtaki²⁴ by emf meas-

urements in 3 M NaClO_4 . The concentration of free hydroxide ions C_h was then calculated by

$$2C_h = (K_d^2 + 4K_d C_t)^{1/2} - K_d \quad (11)$$

C_t is the total concentration of lithium hydroxide. The product $Q_d = f_{\text{Li}^+} f_{\text{OH}^-} / f_{\text{LiOH}}$ was thus neglected (see below). The hydration number n was then calculated by

$$n = \frac{1000d - 23.95C_t - (C_h/b_-)^{1/4}}{18C_h}$$

where b_- is equal to $10^{14}/h_-$, *i.e.*, the nonlogarithmic indicator basicity.²⁵ The values of n obtained for each K_d are shown in columns 4 and 7 of Table IV. In each case a consistent set of values for n is obtained, but the mean value depends strongly on the value for the dissociation constant K_d employed, so that no definite statement is possible. It is clear, however, that both ions are hydrated to a considerable extent, and possibly to the full extent of $5 + 3$ predicted from the Li^+ and OH^- containing salts.

The effect of Q_d could not be determined directly, since most studies on the dissociation of LiOH were carried out at a low LiOH concentration. Values of $\gamma_{\text{Li}^+} \gamma_{\text{OH}^-} = \gamma_{\pm} / \alpha^2$ are available, however (ref 13, Table 9, p 491), and are listed for $\alpha^2 / 1 - \alpha = 0.66 M$ in column 5. It is seen that some error, but not a considerable one, is introduced in the calculation (compensated in part by γ_{LiOH}).

Table IV: Hydration Numbers for Lithium Hydroxide Calculated from the Indicator Acidity of LiOH Solutions ($T = 25^\circ$)

C_{LiOH} M	b_-^a	$K_d = 0.66 M$			$K_d = 1.5 M$	
		C_h, M	n	$\gamma_{\text{Li}^+} \gamma_{\text{OH}^-}$	C_h, M	n
0.5	0.48	0.40	6.0	0.90	0.33	12.0
1	0.93	0.68	5.9	1.13	0.54	12.4
1.5	1.28	0.93	4.5	1.28	0.72	10.4
2	1.81	1.14	5.1	1.52	0.86	10.1
3	2.80	1.50	5.1	1.80	1.09	10.5
4	3.96	1.81	5.25	2.20	1.33	10.9

^a Cf. part III, Table V. Ionization ratios are shown in Figure 4 there.

(20) Cf. Table 3.2 of ref 13, p 63.

(21) B. E. Conway and J. O'M. Bockris in "Modern Aspects of Electrochemistry," Vol. I, Butterworth and Co. Ltd., London, 1954.

(22) F. G. R. Gimblett and C. B. Monk, *Trans. Faraday Soc.*, **50**, 965 (1954).

(23) H. S. Harned and J. G. Donelson, *J. Am. Chem. Soc.*, **59**, 1280 (1937).

(24) H. Ohtaki, *Acta Chem. Scand.*, **18**, 521 (1964).

(25) M. Anbar, M. Bobtelsky, D. Samuel, B. Silver, and G. Yagil, *J. Am. Chem. Soc.*, **85**, 2380 (1963).

Discussion

In recent years, a considerable number of studies concerning the Hammett acidity function, which expresses the indicator acidity of aqueous solutions, were performed.²⁶⁻²⁸ Two main approaches to the problem can be distinguished. The one approach²⁹⁻³³ stresses observations of both rate and equilibrium processes which cannot be explained in terms of the functions formulated by Hammett and subsequent workers.^{34,35} These studies suggest that the acidity function H_0 describes the behavior of just those aniline derivatives employed by Hammett, and, to put it in an extreme way, the ionization of any other compound which follows H_0 does this by coincidence. Indeed, a considerable number of cases hard to explain, such as the diverging behavior of trimethoxybenzene *vs.* triethoxybenzene,^{29,30} can be quoted.

On the other hand, there are numerous examples of compounds of very dissimilar nature which yield a similar change of ionization ratio with acidity. Thus the behavior of the NO^+ ion is quite similar to that of the bulky carbonium $\varphi_3\text{C}^+$ ions though they have not a single atom in common.³⁶ The small inorganic MnO_4^- and CrO_4^- ³⁷ behave in a quite similar way to many bulky aromatic organic species. In part III it is shown that in alkali the ionization of thioacetamide $\text{CH}_3\cdot\text{CS}\cdot\text{NH}_2$ ³⁸ of various indoles,¹ glutacetaldehydes,³⁹ and even of the transition state of the NHCl^- - NH_3 reaction⁴⁰ all show the same dependence upon hydroxide concentration. These facts encourage the other approach which takes the more optimistic viewpoint that the Hammett functions do actually represent some fundamental properties of concentrated acids and other electrolytes, and that the deviant phenomena encountered can and should be explained in terms of special properties of such compounds. The series of papers by Bunnett is the most thorough example of this approach,⁴¹ and the model advanced by Bascombe and Bell⁹ provides a molecular basis to this approach. This last model has been adopted in this series to describe the behavior of weak acids in alkaline solutions. It is realized, however, that much will have to be explained before the issue can be regarded as settled. The policy in this series is to apply the model of Bascombe and Bell to further cases, mainly in alkaline solutions, and to examine how far it is fitting the facts. The ability of the model to explain further cases will ultimately decide to what extent it provides an accurate (and therefore helpful) description of concentrated electrolyte solutions, the structure of which is a problem attacked by many techniques, but for which a satisfactory answer is not yet available.

The calculations presented suggest that the assignment of an solvation number of 4 to the fluoride ion can well explain the change in acidity of aqueous KOH by potassium fluoride. The number 4 is the number of free electron pairs in the outer shell of the F^- ion, and is thus the number of water molecules which can be coordinated to it through hydrogen bonds. The great tendency of the F^- ion to form hydrogen bonds is well known,⁴²⁻⁴⁴ and a hydration number approaching this figure has been assigned to this ion by several methods.^{14,21} As to lithium salts, the data obtained in acid solution suggest that these salts coordinate around five water molecules in dilute solution (Table III). Although this is somewhat higher than 4, the number of free electron pairs which a lithium ion can coordinate in its first vacant shell, the L shell,⁴⁵ it can be regarded a further indication that the Li^+ ion has a coordination number of 4 in solution; the difference might be due to some coordination by the Cl^- ion, as suggested in Table II. The special position of the Li^+ and F^- ions among the simple univalent ions has been often noted;⁴⁶ to mention an example, their limiting conductance is the lowest among cations

-
- (26) H. Zollinger, *Ann. Rev. Phys. Chem.*, **13**, 392 (1961).
 (27) E. M. Arnett in "Progress in Physical Organic Chemistry," Vol. I, Interscience Publishers, Inc., New York, N. Y., 1963, p 223.
 (28) N. C. Deno in "Survey of Progress in Chemistry," Vol. II, Academic Press, New York, N. Y., 1964, p 155.
 (29) W. M. Schubert and R. H. Quacchia, *J. Am. Chem. Soc.*, **84**, 3778 (1962).
 (30) A. J. Kresge, G. W. Barry, K. R. Charles, and Y. Chiang, *ibid.*, **84**, 4343 (1962).
 (31) B. C. Challis and F. A. Long, *ibid.*, **87**, 1196 (1965).
 (32) E. M. Arnett and G. W. Mach, *ibid.*, **86**, 2671 (1964).
 (33) R. L. Hinmann and J. Lang, *ibid.*, **86**, 3796 (1964).
 (34) L. P. Hammett and A. J. Deyrup, *ibid.*, **54**, 2721 (1935).
 (35) Cf. L. P. Hammett, "Physical Organic Chemistry," McGraw-Hill Book Co., Inc., New York, N. Y., 1940, Chapter IX; F. A. Long and M. A. Paul, *Chem. Rev.*, **57**, 925 (1957).
 (36) N. C. Deno, J. J. Jaruzelski, and A. Schreisheim, *J. Am. Chem. Soc.*, **77**, 3044 (1955); N. C. Deno, H. E. Berkheimer, W. L. Evans, and H. J. Peterson, *ibid.*, **81**, 2344 (1959).
 (37) N. Bailey, A. Carrington, K. A. Lott, and M. R. Symons, *J. Chem. Soc.*, 290 (1960); cf. D. G. Lee and R. Stewart, *J. Am. Chem. Soc.*, **86**, 3051 (1964).
 (38) J. T. Edward and I. R. Wang, *Can. J. Chem.*, **40**, 399 (1962).
 (39) G. Schwarzenbach and R. Sulzberger, *Helv. Chim. Acta*, **27**, 348 (1944).
 (40) G. Yagil and M. Anbar, *J. Am. Chem. Soc.*, **84**, 1797 (1962).
 (41) J. F. Bunnett, *ibid.*, **83**, 4956, 4968, 4973, 4978 (1961).
 (42) L. B. Magnusson, *J. Chem. Phys.*, **39**, 1953 (1963).
 (43) B. P. Fabricand, S. S. Goldberg, R. Leifer, and S. G. Ungar, *Mol. Phys.*, **7**, 425 (1964).
 (44) L. Pauling, "The Nature of the Chemical Bond," Cornell University Press, Ithaca, N. Y., 1960, p 460.
 (45) Cf. N. V. Sidgwick, "The Chemical Elements and Their Compounds," Clarendon Press, Oxford, 1950, p 97 ff.
 (46) Cf. P. Mukerjee, *J. Phys. Chem.*, **65**, 740 (1961).

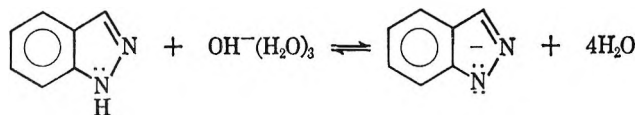
and anions, having thus the largest Stokes radii (which is the classical fact indicating their solvated nature). Also, the heat of dissolution of Li^+ and F^- containing salts is much nearer to that of the analogous H^+ and OH^- electrolytes than to the other alkali or halide salts. Similar trends are apparent with molal entropy and volume.⁴⁷

The slight change in the alkalinity of KOH caused by the addition of KCl and KBr is in line with other evidence that potassium as well as chloride and bromide have little tendency to coordinate water.⁴⁸⁻⁵⁰ It should be noted that in the present model, the absence of an effect on acidity does not mean that there is no interaction between ion and solvent whatsoever, but rather that the free energy of ion-water interaction is of the same magnitude as that of water-water interaction, which in itself is far from negligible. Indeed, large ions such as the tetraalkylammonium halides or *p*-toluenesulfonates, the hydrophobic side chains of which interact little with water, do actually decrease the indicator acidity in water.⁴ Here, structure-breaking effects, which increase the volatility of water, have an important contribution; this effect is being considered negligible with the small ions considered here, and, as mentioned, might be a point where refinement may prove necessary and fruitful. The slight decrease in alkalinity with potassium bromide might already be due to such an effect.

Rosenthal and Dwyer⁶ treat the change in indicator acidity by LiCl in a manner that differs from the present treatment in two respects. First they show that a better fit of the calculated values with the observed ones is obtained if one attributes part of the raise in acidity to a linear change of the activity coefficient ratio with salt concentration $B\mu$. This better fit involves however another adjustable parameter, B ; furthermore, there is no firm theoretical reason to believe that a change in the activity coefficient is a linear function of the ionic strength, so that this type of description offers further insight into the actual structure of the solutions.

The other difference is that the effect of water is introduced here by $\log C_w$, the free water concentration, while $\log a_w$, the water activity, is used by Rosenthal and Dwyer. Since this is the main difference between the treatment in the present series and a number of recent treatments of the subject,^{16,18,38,41,51} a few words seem in place. In each treatment a certain activity coefficient ratio is assumed to be unity. In our treatment, it is assumed that the ratio $f_{\text{BH}^+}f_w^n/f_{\text{B}}f_{\text{H}^+} = 1$, while the other authors assume that $f_{\text{BH}^+}/f_{\text{B}}f_{\text{H}^+} = 1$ (f_p the activity coefficient of the hydrated proton and hydroxide ion). There is no rigorous way at present

to decide which assumption is the better one,⁵² but the following consideration can be brought in favor of the first assumption. Let us consider an example in alkaline solution, *e.g.*, the ionization of indazole employed in this study (an analogous argument can be set up for any equilibrium in acid solution)



when we say that $\log f_{\text{B}}f_w^n/f_{\text{BH}^+}f_{\text{H}^+} = 0$, *i.e.*, $\log f_{\text{B}^-} + n \log f_w = \log f_{\text{BH}^+} + \log f_{\text{H}^+}$, we say that the excess free energy of the left-hand compounds of the equilibrium changes with the medium in the same way as the excess free energy of the right-hand compounds. This is justified for the electrostatic contribution: each side contains a singly charged species, and a hydrated hydroxide ion is probably not much smaller than the indazolate anion (an $\text{O}^- \cdots \text{HO}^{\text{H}}$ hydrogen bond is 2.80 Å long, so that the radius of the hydrated ion is at least 4.2 Å); the electrostatic free energy will thus contribute equally to each side of the equality. Similarly, on each side there is one indole ring the interactions of which with solvent will behave in a like way. Also, the nitrogen on each ring can form two hydrogen bonds with the solvent water, and this interaction requires free energy on both sides of the equilibrium. Such considerations were the classical justification of the activity coefficient assumption of Hammett.⁵ Coming to water, we suggest that the same procedure be adopted because the free water molecules on the right side have their counterparts in the bound molecules and the OH^- ion on the left side. When bound,

(47) Cf. E. A. Moelwyn-Hughes, "Physical Chemistry," 2nd ed, Pergamon Press Ltd., London, 1961, pp 873, 878.

(48) J. C. Hindman, *J. Chem. Phys.*, **36**, 1000 (1962).

(49) G. W. Brady, *ibid.*, **28**, 464 (1958).

(50) E. R. Nightingale, *J. Phys. Chem.*, **65**, 1381 (1959).

(51) R. B. Homer and R. B. Moodie, *J. Chem. Soc.*, 4377 (1963); K. Yates and J. B. Stevens, *Can. J. Chem.*, **43**, 529 (1963).

(52) The most extensive data on activity coefficients of indicator acids and their bases are reported by R. H. Boyd (*J. Am. Chem. Soc.*, **85**, 1555 (1963)). These data show that f_{B} and f_{BH^+} do actually change in a similar way with change in acid concentration. An exact evaluation is not possible, however, because of the following reasons. (a) B and BH^+ do not coexist independently at any single acid concentration. This difficulty may be overcome by conducting measurements in salt, with acid or base as a minor and variable component. (b) To evaluate f_{BH^+} , f_{A^-} has to be known, or at least $f_{\text{BH}^+}f_{\text{A}^-}$, so that the ratio of $f_{\text{BH}^+}/f_{\text{H}^+}$ may be calculated (A^- is the anion of the indicator acid, which in Boyd's systems was different from the anion of the mineral acid). (c) The activity coefficients which are assumed to cancel in the present treatment refer to hydrated species in a solution of "free" water. To calculate these from experimental activity coefficients,¹⁴ one has already to assume a model, so that activity coefficient data can at best demonstrate consistency, but not prove the assumption.

water molecules can still form 10 out of 16 hydrogen bonds which they could form when they were free and these mostly to an enhanced degree, due to their share of the negative charge; they preserve at least part of their dipole. It seems justified, therefore, to cancel $n \log f_w$ against an appropriate component of $\log f_{\text{BH}} + \log f_{\text{h}}$ as done in the present study. When the water activity, a_w , rather than C_w , is chosen to represent water concentration, the activity coefficient of water is treated in a different manner than the other coefficients in the acid-base equilibrium. This may be the reason why plots such as Figure 7 on p 4966 of ref 41 show a marked curvature. A similar plot of $H_0 + \log HX$ vs. $\log C_w$, with $n = 4$, is a straight line over a considerable concentration range.

The same assumption as made here is also present in the treatment of concentrated electrolyte solutions by Robinson and Stokes¹³ and by Glueckauf.¹⁴ These treatments are based on the same model as applied here, namely that concentrated solutions of electrolytes in water are an ideal solution of hydrated ions in free water solution, if one allows for the electrostatic free energy by a simple Debye-Hückel expression. McTigue extended this treatment to solutions containing small amounts of acid in the presence of high concentrations of neutral electrolytes and arrived at conclusions similar to those arrived at here¹⁵ (only that concentrations are expressed on a volume fraction scale).

The main shortcomings of the present model are the following two. First, it is probably an oversimplification to assume that free water molecules are all alike. Water molecules are well known to form a varying number of hydrogen bonds with their neighbors. The

addition of electrolyte dilutes the water and causes some of these bonds to dissociate, increasing the relative number of nonbound water molecules. The growing difference between a_w and C_w shown in Table III reflects such an effect. Recent measurements on the effect of electrolytes on the ¹⁷O chemical shift of water⁵³ indicates, however, that this "structure-breaking" effect may be less important than sometimes suggested, at least for the smaller ions treated in this paper. The second point arises when one proceeds to consider somewhat larger ions such as Na⁺ or NH₄⁺. The number of water molecules bound to these ions can be expected to be dependent on free water concentration, and cannot be regarded as constant. A model taking this effect into account can be set up, using the approach of coordination chemistry, but it involves additional free parameters. This might be a worthwhile undertaking when additional data confirm the simple model for the strongly hydrated ions treated here.

Summing up, it seems that not only can indicator acidities be understood in terms of simple models for electrolytes, but determination of acid-base equilibria can be employed to obtain information on the structure of solutions, under conditions where many nonideality effects are cancelled out due to the equilibrium.

Acknowledgments. The author is indebted to Dr. M. Anbar, during stimulating cooperation with whom the present work was outlined. The author also wishes to thank Dr. E. A. Halevi and Dr. D. Kellerman for interesting talks on the subject.

(53) Z. Luz and G. Yagil, *J. Phys. Chem.*, **70**, 554 (1966).

The Photochemistry of Phosphorus Compounds. V. Far-Ultraviolet Absorption Spectra of Hypophosphite, Phosphite, and Hypophosphate Ions in Aqueous Solution

by Hinga Benderly and M. Halmann

Isotope Department, The Weizmann Institute of Science, Rehovoth, Israel (Received August 15, 1966)

The absorption spectra of solutions of sodium hypophosphite, disodium phosphite, sodium hydrogen phosphite, and disodium dihydrogen hypophosphate were measured in the 300–180-m μ region. All solutions have weak absorptivity above 200 m μ and a steeply increasing absorption edge below 200 m μ . Spectra of sodium hypophosphite solutions at different temperatures form an isosbestic point at 214 m μ with absorptivity increasing with temperature below 214 m μ and decreasing with rising temperature above this wavelength. In D₂O solution the absorption edge of sodium hypophosphite below 200 m μ is shifted toward shorter wavelengths. This absorption edge of hypophosphite, as of other phosphorus oxyanions, is assigned to a charge-transfer-to-solvent (ctts) type of transition. For the dihydrogen hypophosphate anion, application of the theory of such transitions to the temperature and solvent effects enables tentative estimates of the absorption maximum and ionization potential of this ion.

Introduction

The far-ultraviolet absorption spectra of various phosphoric acid oxyanions in aqueous solution has indicated the presence of very weak bands above 200 m μ , as well as the onset of steep absorption edges below 200 m μ , presumably owing to a charge-transfer-to-solvent (ctts) type transition.¹ These studies have now been extended to the reduced oxyacids of phosphorus in order to find out to what extent these ions undergo similar electronic transitions and what photochemical reactions might be expected.

Experimental Section

Materials. Sodium hypophosphite (NaH₂PO₂·H₂O) (Baker Analyzed) and disodium phosphite (Na₂HPO₃·5H₂O) (Fisher Scientific Co.) were used without further purification. The materials were tested by paper chromatography² to contain only hypophosphite and phosphite ions, respectively. Aqueous solutions, prepared by dissolving weighted portions, were assayed for hypophosphite or phosphite, respectively, by iodometric titration.³ The assay agreed within $\pm 5\%$ with that calculated from the weight of the hydrate.

Sodium hydrogen phosphite (NaH₂PO₃) was prepared by mixing under a nitrogen atmosphere equimolar aqueous solutions (concentration determined by titration³) of disodium phosphite (Fisher Scientific Co.) and phosphorous acid (Fluka "puriss"). Fresh solutions (within at least 1 day) were free of orthophosphate, as tested by paper chromatography.

Disodium dihydrogen hypophosphate (Na₂H₂P₂O₆·6H₂O)⁴ was found by paper chromatography to give only one spot. The material was three times recrystallized, once by cooling a hot, saturated, aqueous solution and then twice by adding ethanol (spectroscopic grade) to a saturated aqueous solution at room temperature. The concentration of aqueous solutions

(1) M. Halmann and I. Platzner, *J. Chem. Soc.*, 1440 (1965); *J. Phys. Chem.*, **70**, 2281 (1966).

(2) C. S. Hanes and F. A. Isherwood, *Nature*, **164**, 1107 (1949).

(3) I. M. Kolthoff and V. A. Stenger, "Volumetric Analysis," Vol. III, Interscience Publishers, Inc., New York, N. Y., 1957.

(4) E. Leininger and T. Chulski, *Inorg. Syn.* **4**, 68 (1953). The authors are indebted to Miss Lea Kugel for kindly providing a sample of this material.

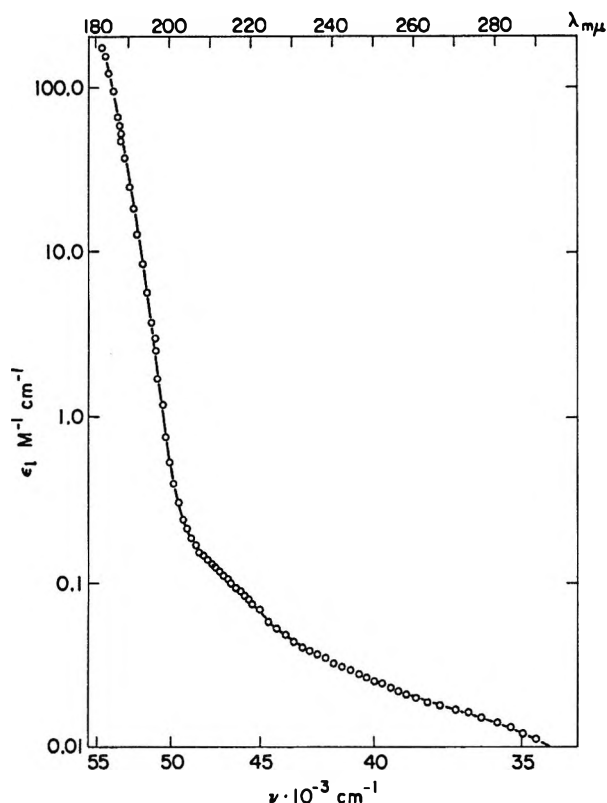


Figure 1. Absorption spectrum of sodium hypophosphite in aqueous solution at room temperature.

of the material was determined by cerimetric titration.⁵

The titrimetric determination of the hypophosphate content of solutions agreed within 5% with that calculated from the weight of the hexahydrate salt used.

Solvents. Distilled water (from the laboratory supply) was redistilled from alkaline permanganate and then from phosphoric acid, atmospheric carbon dioxide being excluded. Deuterium oxide (99.7%, Norsk Hydro Elektrisk Kvaestofaktieselskab), methanol, and ethanol (both British Drug Houses, spectroscopic grade) were used without further purification.

Absorption spectra were measured using a Zeiss PMQ II spectrophotometer, which was especially sealed for work in the far-ultraviolet region and was flushed with nitrogen (purity 99.8%) at a flow rate of 2 l. min⁻¹. Suprasil quartz cells with optical paths of 0.01, 0.1, 0.5, 1.0, 2.0, 5.0, and 20.0 cm were used.

Results

Sodium Hypophosphite. Aqueous solutions of sodium hypophosphite obeyed Beer-Lambert's law. As seen in Figure 1, the absorptivity above 200 mμ is very weak, but increases steeply toward shorter wave-

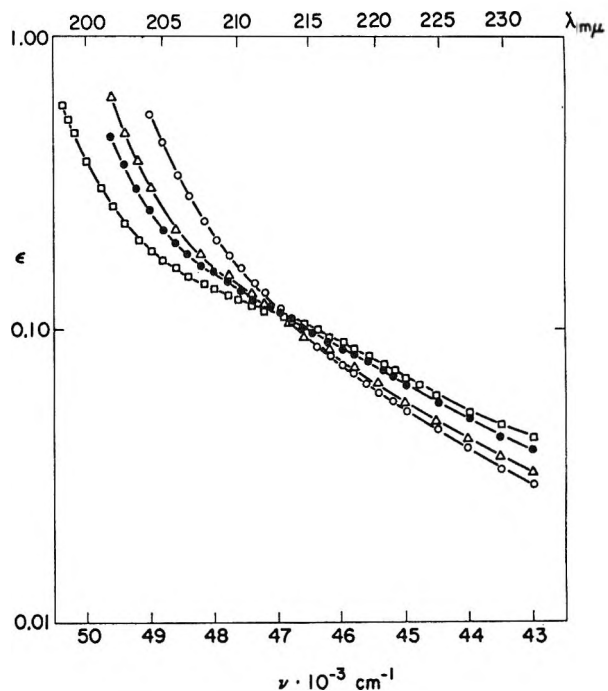


Figure 2. Temperature dependence of the absorption of aqueous sodium hypophosphite at: \square , 4°; \bullet , 25.4°; Δ , 55.7°; and \circ , 83°.

lengths. The temperature dependence of the absorptivity (Figure 2) shows a striking difference between the short- and long-wavelength regions. An isosbestic point is formed at 46,850 cm⁻¹ (214 mμ) with absorptivity increasing with temperature at shorter wavelengths and decreasing with rising temperature at wavelengths above 214 mμ.

The solvent effect on the absorption of sodium hypophosphite in the far-ultraviolet region was measured by comparing the spectra in water and in deuterium oxide solution. As shown in Figure 3, the absorption edge is shifted toward shorter wavelengths in changing from water to deuterium oxide. The magnitude of the shift, $\Delta\nu_{(6.5)} = 320$ cm⁻¹, is similar to that reported for the iodide ion.⁶

Sodium Hydrogen Phosphite. Aqueous solutions of sodium hydrogen phosphite (NaH₂PO₃) do not obey Beer-Lambert's law; with increasing dilution, the absorptivity increases. Since the absorptivity is very weak in the wavelength region accessible in the present work (down to 180 mμ), it was not possible to decrease the concentration sufficiently to obtain solutions in which the absorption follows Beer-Lambert's law.

(5) T. Moeller and G. H. Quinty, *Anal. Chem.*, **24**, 1354 (1952).

(6) (a) I. Burak and A. Treinin, *Trans. Faraday Soc.*, **59**, 1490 (1963); (b) M. Halmann and I. Platzner, *Proc. Chem. Soc.*, 261 (1964).

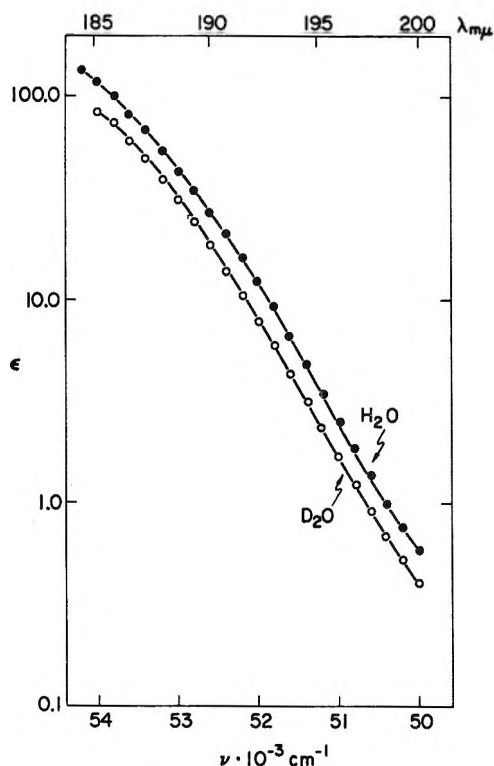


Figure 3. Absorption spectrum of sodium hypophosphite at room temperature in water (●) and deuterium oxide (○).

Therefore, in Figure 4, the observed spectrum of sodium hydrogen phosphite is presented for three different concentrations. The shape of the spectrum reveals similarity with that of the orthophosphate monoanion¹ in showing two weak shoulders above 200 $m\mu$ and a steep absorption edge below this wavelength. These two shoulders show off even more clearly in the temperature effect on the spectrum of aqueous sodium hydrogen phosphite (Figure 5). Only the steep absorption edge is shifted toward shorter wavelengths with decrease in temperature, while the two long-wavelength shoulders are unaffected. This behavior is thus completely analogous to that of the dihydrogen phosphate ion.¹

Disodium Phosphite. Aqueous solutions of disodium phosphite (Na_2HPO_3) also do not obey Beer-Lambert's law. Absorptivity increases with dilution. However, since for this ion the absorptivity at a given wavelength is much larger than for sodium hydrogen phosphite, it was possible by sufficient dilution (to less than 0.02 M solutions) to reach a limiting absorptivity (see Figure 6). The spectrum does not reveal any feature in addition to the steep absorption edge. Also, the temperature effect on the spectrum (measured at dilutions sufficient to ensure adherence to Beer-

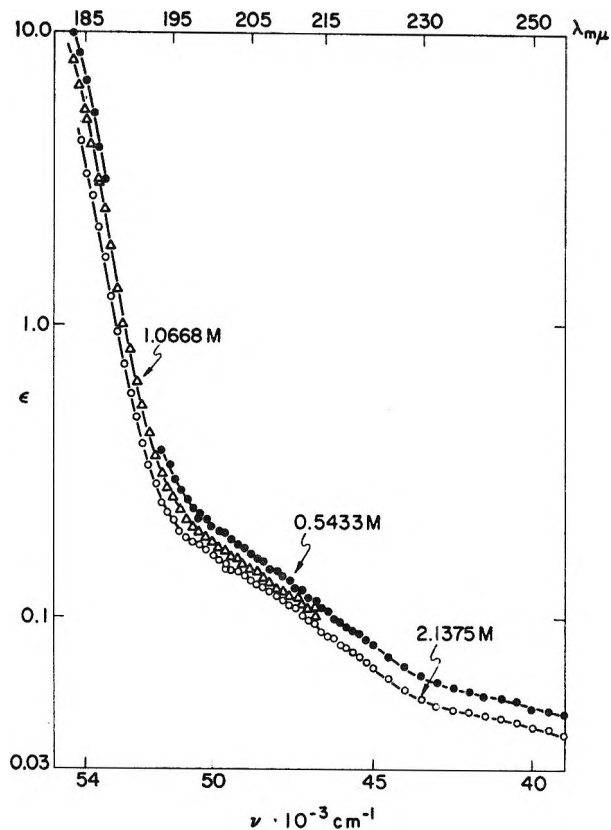


Figure 4. Absorption spectrum of aqueous sodium hydrogen phosphite at room temperature at several concentrations.

Lambert's law) only shows a simple, uniform, red shift of the absorption edge with increasing temperature (Figure 7).

In deuterium oxide solutions, as in water, the absorptivity increases with dilution. The absorption edge in deuterium oxide is blue shifted compared with that in water. In aqueous methanol (40% methanol by volume) the absorption edge is red shifted by comparison with that in water. However, in both deuterium oxide and in alcoholic solutions the limiting dilution necessary to obtain adherence to Beer-Lambert's law could not be reached. Thus, the "true" limiting absorptivity in both cases must be even more shifted toward longer wavelengths.

Disodium Dihydrogen Hypophosphate ($\text{Na}_2\text{H}_2\text{P}_2\text{O}_6$). In aqueous solutions, Beer-Lambert's law is obeyed in a wide range of concentrations and optical paths (0.016–0.041 M and 0.1–20 cm, respectively). As seen in Figure 8, the absorption spectrum contains a distinct shoulder at 260–300 $m\mu$ and a steeply increasing absorption edge below 260 $m\mu$. The absorption coefficients in this region are very much higher than

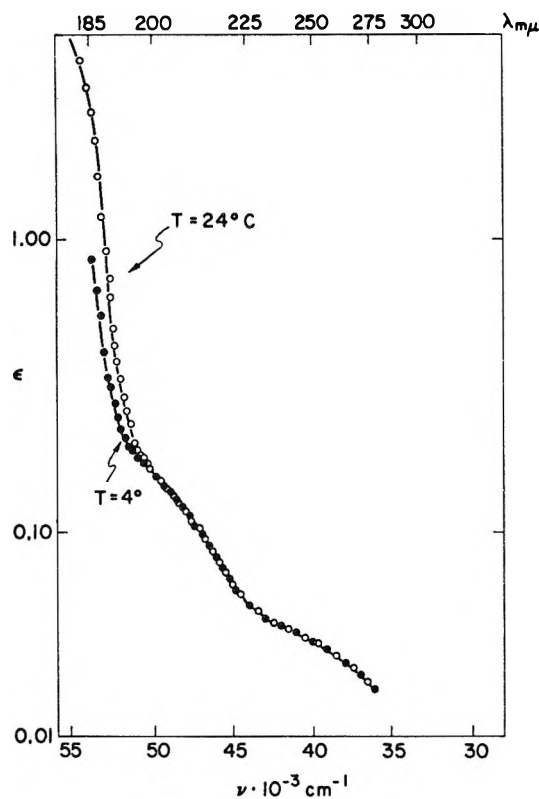


Figure 5. Absorption spectrum of aqueous sodium hydrogen phosphite at: ●, 4°; and ○, 24°.

those of the other phosphorus oxyanions reported above and in the previous paper.¹

The temperature effect of the absorption edge is presented in Figure 9. Increasing temperature results in a red shift of the band, which becomes appreciable above 42,000 cm^{-1} .

The solvent effect could be measured only by comparing the spectrum in water and in deuterium oxide, as shown in Figure 10. Addition of organic solvents (methanol or acetonitrile) drastically decreases the solubility of hypophosphate, which is small even in pure water (2 g/100 ml at room temperature). Above about 44,000 cm^{-1} , the absorption edge in deuterium oxide becomes blue shifted compared with that in water.

Discussion

The far-ultraviolet absorption spectra of anions in solution may be due either to internal electronic excitation or to a charge-transfer-to-solvent type of transition.⁷ Environmental effects (such as temperature or solvent change) on the spectrum may sometimes be used for assignment and interpretation of the excitation process involved.

Among the spectra of aqueous solutions of these

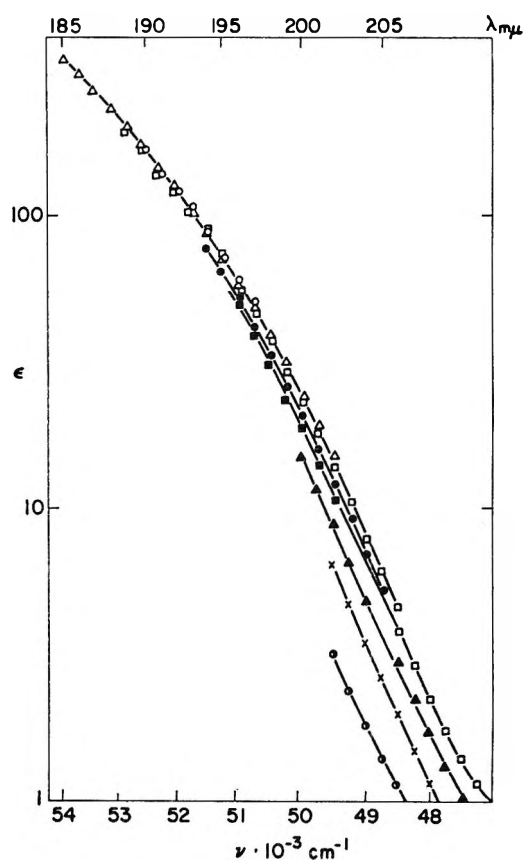
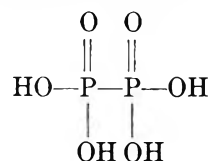


Figure 6. Absorption spectrum of aqueous disodium phosphite at room temperature at several concentrations: ○, 0.00873 *M*; △, 0.02618 *M*; □, 0.0436 *M*; ●, 0.1091 *M*; ■, 0.2182 *M*; ▲, 0.546 *M*; X, 1.091 *M*; ●, 2.182 *M*.

ions, only those of salts of hypophosphorous acid, H_3PO_2 , and of hypophosphoric acid



obey Beer-Lambert's law, thus allowing a semiquantitative study of their spectra.

Sodium Hypophosphite. Owing to the very weak absorptivity of aqueous solutions of sodium hypophosphite, only limited quantitative measurements could be made. The very striking isosbestic point at 214 $\text{m}\mu$ (46,850 cm^{-1}) for the temperature dependence of absorption (Figure 2) may be explained by partial

(7) (a) R. Platzmann and J. Franck in L. Farkas Memorial Volume, Research Council of Israel, Jerusalem, 1952, p 21; (b) G. Stein and A. Treinin, *Trans. Faraday Soc.*, 55, 1086, 1091 (1959); A. Treinin, *J. Phys. Chem.*, 68, 893 (1964); (c) T. R. Griffiths and M. C. R. Symons, *Trans. Faraday Soc.*, 56, 1125 (1960).

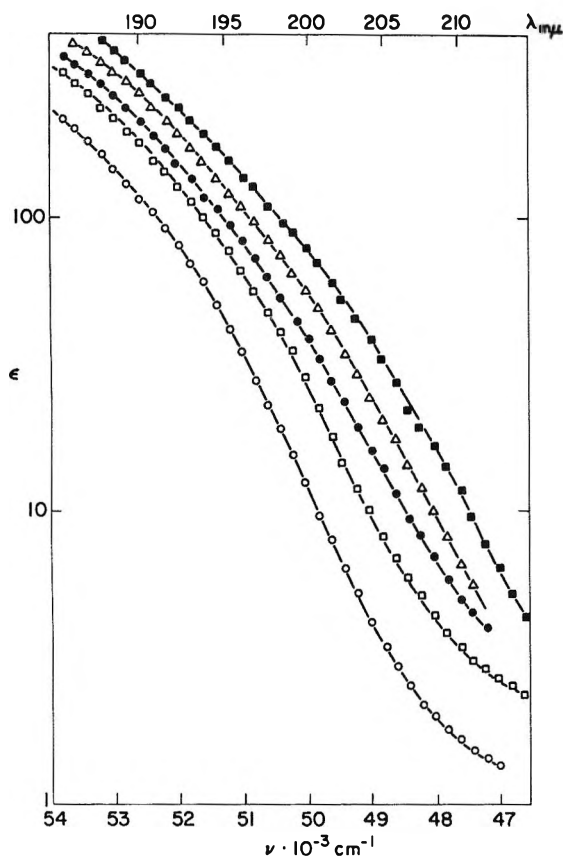
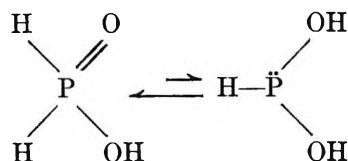


Figure 7. Temperature dependence of the absorption of aqueous disodium phosphite at: O, 4°; □, 25°; ●, 45°; Δ, 65°; and ■, 82°.

overlapping of two band systems. The long-wavelength, very weak band is blue shifted with rise in temperature, while the short-wavelength (below 214 $m\mu$) band is red shifted. The behavior of the red-shifted band is qualitatively similar to that of charge-transfer-to-solvent bands, as those of halides⁷ and of orthophosphates.¹ On the other hand, the blue shift of absorption with increasing temperature seems to be a very rare effect.

Because of the isosbestic point at 214 $m\mu$, it is quite possible that the two bands listed above originate from two different species whose concentrations are dependent on one another. One possible attempt at rationalization is based on the "keto-enolic" tautomerization of hypophosphorous acid



The equilibrium constant of such a tautomerization in

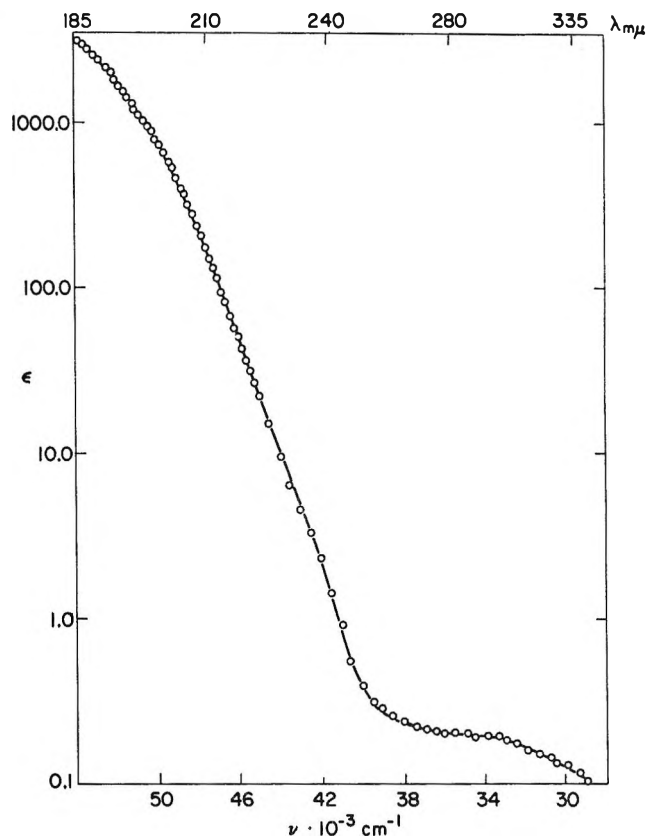


Figure 8. Absorption spectrum of disodium dihydrogen hypophosphate in aqueous solution at room temperature.

aqueous solutions of salts of hypophosphorous acid is very small, as shown by nuclear magnetic resonance spectroscopy.^{8a} However, if the tervalent phosphorus tautomer were to have a much higher absorptivity, then the temperature effect on the above equilibrium constant might result in the observed isosbestic point. As shown by gas-phase spectra in the 200- $m\mu$ region,^{8b} trialkyl phosphites, $(\text{RO})_3\text{P}$, and phosphorus trichloride, PCl_3 , have a much higher absorptivity than dialkyl phosphonates, $(\text{RO})_2\text{PHO}$, and phosphoryl chloride, POCl_3 , respectively.

Sodium Phosphite. The lack of adherence of aqueous solutions of sodium hydrogen phosphite and of disodium phosphite to Beer-Lambert's law suggests some interfering reactions at more concentrated solutions. Increasing concentration converts part of the salt into a form which is less absorbing than the true monomeric phosphite ion. An indication of the possible nature of the species into which phosphite ions are converted at high concentrations (0.05–0.5 M) comes from a specific electric conductivity study. In addition to

(8) (a) H. S. Gutowsky, D. W. McCall, and C. P. Slichter, *J. Chem. Phys.*, 21, 279 (1953); (b) M. Halmann, *J. Chem. Soc.*, 2853 (1963).

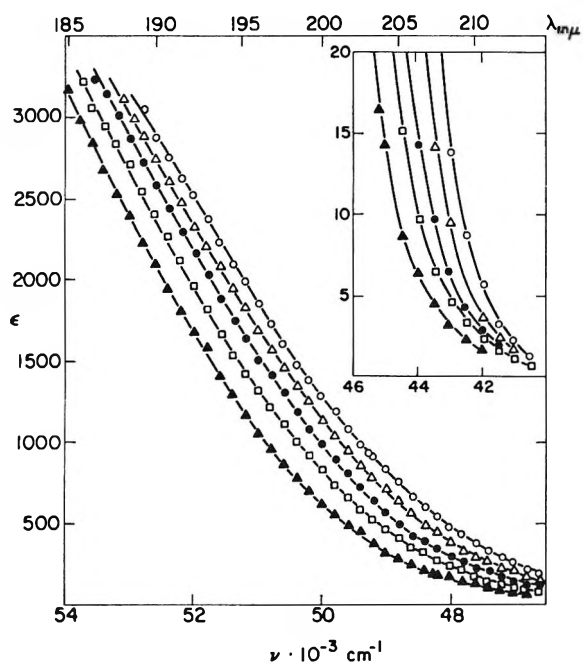


Figure 9. Temperature dependence of the absorption of aqueous disodium dihydrogen hypophosphate at: \blacktriangle , 4° ; \square , 23.6° ; \circ , 40° ; \triangle , 60° ; and \circ , 80° .

KH_2PO_3 , the concentrated solution was found to contain $\text{KH}_5\text{P}_2\text{O}_6$, $\text{K}_2\text{H}_7\text{P}_3\text{O}_9$, and $\text{KH}_8\text{P}_3\text{O}_9$.⁹

Disodium Dihydrogen Hypophosphate. The absorption maximum of this ion is beyond the limit of the instrument used ($180\text{ m}\mu$). Still it is possible to attempt a prediction of the approximate wavelength of this maximum, using the theory of ctt transitions.^{1,6,7b}

From the temperature dependence of the absorption of $\text{Na}_2\text{H}_2\text{P}_2\text{O}_6$ by linear extrapolation of the plot of $-\text{d}\nu/\text{d}T$ against the wavenumber ν (at constant temperature T), an intercept for $\text{d}\nu/\text{d}T = 0$ at ν_0 is obtained. This ν_0 can be related to the ionic radius, R (in angstrom units), the absorption maximum, ν_{max} , and the ionization potential, I_x , of the ion. Such relationships had been proposed both for univalent and for polyvalent ions.^{7b} At first we attempted to use the equations for a divalent anion, according to which

$$\nu_{\text{max}} = \nu_0 - (40,616/R) \quad (1)$$

in cm^{-1} . In this equation, R is the radius of the cavity available to the ion in the crystal.

From a least-squares fit of the data for 23.6° , we get (see Figure 11)

$$\nu_0 = 64,159 \pm 377 \text{ cm}^{-1}$$

The value of R for the hypophosphate ion has not been measured directly. An estimate can, however, be made on the basis of the known P-P single-bond

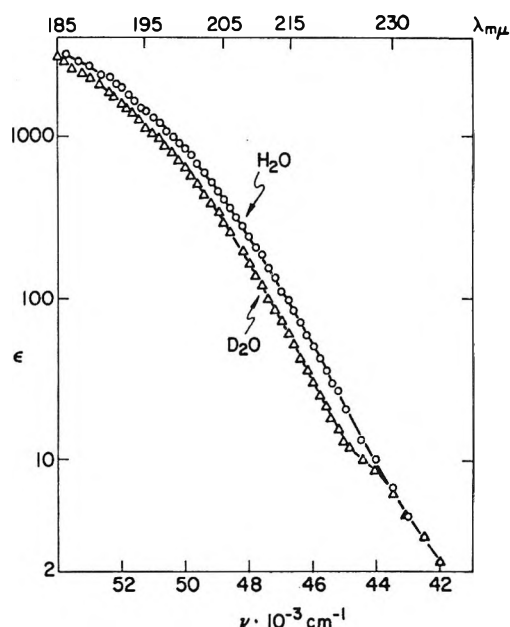


Figure 10. Absorption spectrum of disodium dihydrogen hypophosphate at room temperature in water (\circ) and deuterium oxide (Δ).

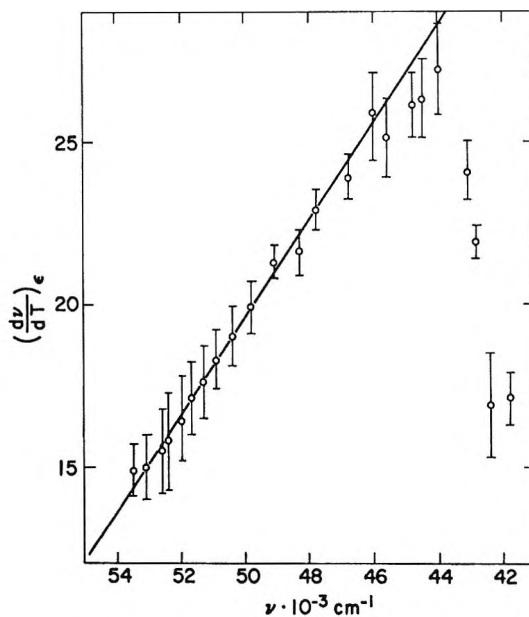


Figure 11. Dependence of $(\text{d}\nu/\text{d}T)_\epsilon$ on $\nu_\epsilon(T)$ at 23.6° .

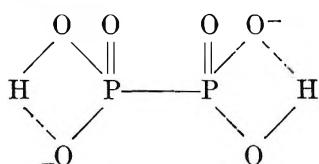
distance (2.21 Å, as in white phosphorus) and of twice the ionic P-O⁻ bond distance (1.54 Å, as in PO_4^{3-}).¹⁰ Assuming $R = [2.21 + (2 \times 1.54)]/2 = 2.64$ Å as a

(9) M. Ebert and J. Ciperá, *Chem. Zvesti*, **19**, 679 (1965); *Chem. Abstr.*, **64**, 2797g (1966).

(10) A. F. Wells, "Structural Inorganic Chemistry," 3rd ed, Clarendon Press, Oxford, 1962, pp 57, 658.

maximal value for the radius of the ionic cavity in the crystal, we would thus get from eq 1, $\nu_{\max} = 48,774 \text{ cm}^{-1}$ or $205 \text{ m}\mu$. As seen in Figure 8, the absorption maximum for the hypophosphate ion must be at a wavelength shorter than $185 \text{ m}\mu$. Equation 1 for a divalent ion leads therefore to an unsatisfactory conclusion.

It is therefore attempted to consider the possibility that, in the light-absorption process, the dihydrogen hypophosphate ion



acts as if it were a monoanion in the sense that the electron localized on the other phosphate group has no influence on the electron released to the solvent. Since the first ionization constant of the hypophosphoric acid is very similar to the second one¹¹

$$K_1 = 6 \times 10^{-3}$$

and

$$K_2 = 1.5 \times 10^{-3}$$

one might assume no interaction between the two electrons which are located on the two phosphate groups of the dihydrogen hypophosphate anion.

For a monoanion, the theory of cttts transitions predicts that^{7b}

$$\nu_{\max} = \nu_0 - (17,845/R) \quad (2)$$

in cm^{-1} and

$$I_x = h\nu_0 + L_x - (255/R) - 35 \quad (3)$$

in kcal mole^{-1} , where L_x is the heat of solvation of the radical ion formed after the ejection of one electron. The value of L_x is usually about 5 kcal mole^{-1} .^{7b}

From eq 2, using again the radius $R = 2.64 \text{ \AA}$, we obtain

$$\nu_{\max} = 57,412 \text{ cm}^{-1}$$

or $174 \text{ m}\mu$ for the absorption maximum, which seems realistic judging from the shape of the absorption curve (Figure 8). From eq 3 we get

$$I_x = 56.6 \text{ kcal mole}^{-1}$$

for the vertical ionization potential of the dihydrogen hypophosphate ion. The "true" (adiabatic) ionization potential should be lower from this one by an unknown amount corresponding to the Franck-Condon strain

Table I: Ionization Potential for the Dihydrogen Hypophosphate Ion Derived from the Deuterium Oxide Solvent Isotope Effect on the Absorption Spectrum

$\epsilon, \text{ l. mole}^{-1} \text{ cm}^{-1}$	$\Delta\nu \text{ (KI), cm}^{-1}$	$\Delta\nu \text{ (H}_2\text{P}_2\text{O}_6^{2-}), \text{ cm}^{-1}$	β_x	$\nu_x, \text{ cm}^{-1}$	$I_x, \text{ kcal mole}^{-1}$
50	400	580	1.45	46,000	34.95
100	410	600	1.46	46,820	36.39
500	400	660	1.65	48,940	25.26
1000	420	660	1.57	50,220	36.04
1500	450	620	1.38	51,140	55.99
2000	410	660	1.61	51,820	37.08
2500	400	600	1.50	52,540	49.11
Av					39.3

which may be released by bringing the excited-state ion to its new equilibrium configuration.

A positive value for the vertical ionization potential of the doubly charged ion, $\text{H}_2\text{P}_2\text{O}_6^{2-}$, seems at first sight surprising. Doubly charged anions are unknown in the gas phase and one might expect the process $\text{H}_2\text{P}_2\text{O}_6^{2-} \rightarrow \text{H}_2\text{P}_2\text{O}_6^- + e^-$ to release energy. However, since the two negative charges on the dihydrogen hypophosphate ion seem to be separated, even removal of one electron from the dianion may require input of energy.

Another estimate of the ionization potential of the dihydrogen hypophosphate ion can be obtained from the solvent isotope effect on the absorption band, as measured in water and in deuterium oxide (see Figure 10). According to the theory of cttts-type transitions, the energy, $h\nu_x$, for absorption by a given ion, x , is given by the equation^{7b}

$$h\nu_x = \beta_x C + I_x - \beta_x I_I + B(\beta_x - 1) \quad (4)$$

or

$$I_x = h\nu_x + \beta_x(I_I - C - B) + B$$

where C is the value of energy for the absorption maximum of the iodide ion in the same solvent at the same temperature; $\beta_x = \Delta\nu_x/\Delta\nu_I$ is the ratio of solvent shifts for the ion x and for the iodide ion; $I_I = 70.8 \text{ kcal mole}^{-1}$ is the ionization potential of iodide ion, and $B = 35 \text{ kcal mole}^{-1}$ is the binding energy of the electron to the polarized medium in the excited state. The absorption maximum for iodide in water is $C = 44,200 \text{ cm}^{-1}$ or $126.5 \text{ kcal mole}^{-1}$. Hence, from eq 4 we get, by insertion of numerical values

(11) J. R. Van Wazer, "Phosphorus and its Compounds," Vol. I, Interscience Publishers, Inc., New York, N. Y., 1958, p 409.

$$I_x = h\nu_x + 35 - 90.7\beta_x$$

in kcal mole⁻¹. Results at various absorption coefficients, ϵ , are presented in Table I. The average ionization potential (40 kcal mole⁻¹) obtained from the solvent effect (which is based only on direct experimental evidence) is in approximate agreement with that obtained from the temperature dependence (57 kcal mole⁻¹) (which requires an assumed value for the radius, R).

The realism of the above calculations of the absorption maximum and ionization potential depends critically on the quantitative validity of the theory of charge-

transfer-to-solvent transitions (which was originally proposed for atomic and spherically symmetric ions) to the relatively large and elongated hypophosphate ion. However, qualitatively the temperature and solvent effects on the absorption of these ions are very similar to those of halide ions which were proven to be due to cttts transitions.

The steep shapes of the absorption edges of hypophosphite, phosphite, and hypophosphate anions seem to indicate that these cttts bands are the Franck-Condon envelopes of transitions to electronic states similar in configuration to the ground states.

Molecular Orbitals for General Polyatomic Molecules. I¹

by Louis Chopin Cusachs and Barbara Breckinridge Cusachs

Richardson Chemistry Laboratories, Tulane University, New Orleans, Louisiana 70118
(Received August 23, 1966)

A procedure for systematically increasing the precision of simple semiempirical molecular orbital calculations by successive refinement at all stages of the same importance is developed. Simplifications necessary to keep the computation manageable on a computer are examined theoretically and numerically, particularly the approximation of off-diagonal matrix elements which are also important in ligand field theory. The significance of atomic parameters and the use of spectral data, the expansion and contraction effects, and the handling of electron repulsion and charge-transfer effects in simple fashion, to be treated in detail in other papers of this series, are placed in the general perspective of obtaining comparable reliability at the several stages of calculation.

Introduction

Just beyond the light molecules now accessible to direct quantum mechanical calculations lie the majority of familiar chemical compounds. Naive procedures, particularly the Hückel methods, characterized by neglect of overlap and consideration of only some of the valence electrons have been notoriously useful in organic chemistry despite these indefensible approximations. Only recently was it discovered that the germ of verisimilitude in such methods is their fidelity to molecular topology² rather than any relation to the self-

consistent field equations. This in turn makes it easier to understand that the Hückel methods should become less and less satisfactory for polar or three-dimensional molecules. Recent extensive calculations, particularly for inorganic molecules and ions, have utilized procedures avoiding the Hückel approximations

(1) Presented in part at the 20th Southwest Regional Meeting of the American Chemical Society, Shreveport, La., Dec 3-5, 1964. Revised version presented at the Symposium on Molecular Structure and Spectroscopy, Columbus, Ohio, Sept 6-10, 1966.

(2) See N. S. Ham and K. Ruedenberg, *J. Chem. Phys.*, **25**, 1 (1956).

as simply as possible. Desire to avoid practical difficulties rather than any particular theory have guided these calculations, for there is no general consensus among theoreticians regarding the limits of reliability of various one-electron methods beyond the Hückel stage. This paper considers the first steps in the theoretical development of a consistent model based on the systematic approximation of major one-electron terms to a comparable degree of precision.

Accumulation in the last few years of accurate calculations for light molecules provides a number of references for development and checking better simplified procedures.^{3a} Progress in the analysis of *ab initio* calculations^{3b} revealing the consequences of various approximations makes it feasible to attempt a systematic development of a one-electron model, useful in itself for some purposes with minimal labor and suitable for refinement. Comparing currently used approximations with the behavior expected of various major terms affords some insight into the successes and failures of one-electron procedures. The result is a synthesis of ideas and observations affording insight into the consequences of various simplifications and providing a more adequate basis for some practices regarded previously as *ad hoc* recipes.

Point of departure from *ab initio* to semiempirical molecular orbital calculation is Ruedenberg's monumental analysis⁴ of chemical binding in terms of an LCAO diffraction theory which reconciles the Hellmann picture of binding with the virial theorem.⁵

Wave Theory of Bonding. Ruedenberg's interference or diffraction picture of chemical binding divides the major one-electron terms involved into overlap region and one-center effects.

In the overlap or bonding region between two nuclei, the charge distribution is described by the product of atomic orbitals. The major contribution to the kinetic and potential energy integrals comes from volumes where both orbitals are appreciable; this results in negative kinetic energy contributions and potential terms small in absolute magnitude. Consistent with the Hellmann picture of binding, this corresponds to valence electrons moving more slowly under the influence of two separate nuclei than when close to either. The interaction between nonorthogonal orbitals, ψ_i and ψ_j , is determined by a term, $H_{ij} - S_{ij}(H_{ii} + H_{jj})/2$. This is made up of a kinetic part, $T_{ij} - S_{ij}(T_{ii} + T_{jj})/2$, and a potential one, $V_{ij} - S_{ij}(V_{ii} + V_{jj})/2$. Since the two-center kinetic integral, $T_{ij} = \langle i|T_{op}|j\rangle$, between valence shell orbitals is smaller in magnitude than $S_{ij}(T_{ii} + T_{jj})/2$, the kinetic term favors binding. The potential term suffers large cancellation between $V_{ij} = \langle i|V|j\rangle$ and $S_{ij}(V_{ii} +$

$V_{jj})/2$, vanishing to the extent that the Mulliken approximation holds.

The effects are quite different around the nuclei for the charge whose distribution is described by the square of individual atomic orbitals. Removal of charge to the bonding region permits a contraction of orbitals involved in bonding molecular orbitals. Antibonding has the opposite effect, expanding the orbitals whence charge migrates from the internuclear region, an effect deduced empirically from ligand field analysis. This expansion or contraction can be approximated by a simple rescaling of atomic orbitals, which immediately predicts a large increase in one-center kinetic energy terms, which are proportional to the square of the scale factors, accompanied by a roughly linear increase in the magnitude of the one-center potential terms upon bonding. The two qualitatively different changes in kinetic energy combine to give the net increase required by the virial theorem, which applies to the molecule as a whole, rather than to the atomic and overlap regions separately. Rescaling of the atomic orbitals has important effects on the magnitude of the overlap charge terms since the two regions are interdependent mathematically.

In the following sections this analysis will be employed in the derivation of a simple model which possesses the virtues of the Mulliken-Wolfsberg-Helmholz approximation without some of its defects.

Procedure

Molecular orbitals, ψ_u , are to be obtained as linear combinations of atomic orbitals, ψ_i

$$\psi_u = \sum_i C_{ui} \psi_i \quad (1)$$

which are assumed normalized and orthogonal to others centered on the same atom

$$\langle i|i\rangle = 1 \quad (2)$$

while there may be overlap between orbitals on different atoms

$$\langle i|j\rangle = S_{ij} \quad (3)$$

The molecular orbitals are to be determined by minimization of the orbital energy

$$E_u = \langle u|H|u\rangle / \langle u|u\rangle \quad (4)$$

(3) (a) J. C. Slater, "Quantum Theory of Molecules and Solids," Vol. I, McGraw-Hill Book Co., Inc., New York, N. Y., 1963; (b) K. Ruedenberg, *J. Chem. Phys.*, **34**, 1861 (1961); see also F. P. Boer, M. D. Newton, and W. N. Lipscomb, *Proc. Natl. Acad. Sci. U. S.*, **52**, 890 (1964).

(4) K. Ruedenberg, *Rev. Mod. Phys.*, **34**, 326 (1962); K. Ruedenberg and C. Edmiston, *J. Phys. Chem.*, **68**, 1628 (1964).

(5) P.-O. Lowdin, *J. Mol. Spectry.*, **3**, 1 (1959).

Substitution of eq 1 in eq 4 and differentiation of E_u with respect to the C_{ui} in succession lead to the standard secular determinant

$$|H_{ij} - ES_{ij}| = 0 \quad (5)$$

The energies, E_u , and the coefficients, C_{ui} , can be determined by routine computation once the H_{ij} and S_{ij} are provided.

The Overlap Matrix. The overlap matrix is determined by a choice of explicit atomic orbitals. The actual computation assumes that the orbitals selected are expressed in a basis set of Slater-type orbitals (STO)

$$\psi(n, l, m, z) = Cr^{n-1} \exp(-zr) Y_l^m(\theta, \phi)$$

where C is a normalization factor, n the principal quantum number, z an assignable parameter, called the orbital exponent or zed, and Y an ordinary spherical harmonic. This form is perfectly general, since any acceptable atomic orbital can be expressed as a sum of terms of this type with constant coefficients.

Of the usual methods for evaluating overlap integrals between STO's on different centers, the direct two-dimensional (gaussian) numerical integration appears to be the most efficient for calculations involving only two-center one-electron integrals. A program for calculating these overlap integrals involving s, p, and d orbitals with a principal quantum number up to 7 was coded for the IBM 1410 computer originally available. Tests using the variable-word-length feature of this machine showed that the numerical integration formula limitations and rounding errors were balanced and small enough to ensure at least six decimal place accuracy in the least favorable case imagined to be chemically interesting. A version of this routine recorded for efficient core utilization on a faster machine occupies appreciably less storage than the A, B, and C function method often employed and at no sacrifice in speed.

Atomic Orbital Choice. Choice of the explicit atomic orbitals to be employed in a semiempirical calculation is a complex and difficult question. While it is true that *ab initio* calculations usually employ functions recognizable as atomic orbitals, they are complicated in accurate calculations and determined as much by molecular as by atomic considerations. *Ab initio* calculations employing only a minimum number of predetermined atomic orbitals almost always produce poorer agreement with experimental properties than a careful semiempirical computation costing a fraction of the effort, while the most accurate calculations are difficult even to interpret in naive chemical terms. In the method suggested here, the explicit atomic

orbitals chosen are used only for the calculation of overlap integrals. The best available atomic orbitals, the many-term SCF functions,⁶ could be used in simplified calculations at the cost of some labor and computer time. Single-term (single-zed) functions require only the specification of a single parameter, usually determined to optimize some atomic property. Slater⁷ has discussed the difference between the effective charges (implying a choice of zeds) suitable for orbital shape and those appropriate for the estimation of energy quantities by screening constant formulas. The single-zed functions of Clementi and Raimondi⁸ were obtained by minimizing the atomic electronic energy for definite spin states. The optimum orbital exponents vary from spin state to spin state, but could be averaged to smooth out variations irrelevant to molecular calculations, or the whole calculations repeated for valence states. An alternative set of zeds proposed by Burns⁹ was chosen to match moments to those computed using more complicated SCF orbitals.

It is also possible to determine a set of zeds that best reproduce overlap integrals calculated using the multi-term SCF atomic functions over the moderate range of chemically interesting interatomic distances. This can even be done in cases, like the 3d orbital of copper, when no single-zed function is a generally adequate approximation to the shape of the accurate SCF orbital.¹⁰ As a specific example, the zed for the 3d orbital of Cu is 4.40,⁸ 3.70,⁹ or 2.62,⁷ depending on which recipe one follows. Overlap matching reveals that the value 2.70 reproduces the overlap calculated with the many-term SCF functions over a useful range. Values for other orbitals and atoms do not generally correspond to those suggested by any one of the recipes considered and the differences in overlap integrals resulting from different choices of zeds may easily be significant. When it is recalled that the one-center kinetic energy calculated for such an orbital is proportional to the square of the orbital exponent, it is evident that energy terms calculated by different prescriptions for orbital exponents may vary by as much as a factor of 2. Tables I, II, III, and IV indicate the magnitude of this effect by exhibiting various one- and two-center quantities calculated using the largest and

(6) E. Clementi, "Tables of Atomic Functions," Supplement to *IBM J. Res. Develop.*, **9**, 2 (1965).

(7) J. C. Slater, "Quantum Theory of Atomic Structure," Vol. I, McGraw-Hill Book Co., Inc., New York, N. Y., 1960, Section 9.7, pp 227-229.

(8) E. Clementi and D. L. Raimondi, *J. Chem. Phys.*, **38**, 2686 (1963).

(9) G. Burns, *ibid.*, **41**, 1521 (1964).

(10) W. C. Nieuwpoort, Dissertation, Amsterdam, 1965; see Figure 5, p 24.

Table I: Copper 3d and Oxygen 2p, Overlap Matched Cu σ

NA = 3 LA = 2.7000 M = 0 NB = 2 LB = 1
 ZB = 1.9750 TAA = 3.6450 VAA = 0.9000
 TBB = 1.95031 VBB = 0.98750^a

R	STT	SSQ	S	SA	SB
1.80	0.2076	0.0047	0.0683	0.1138	0.1830
2.00	0.2087	0.0180	0.1341	0.1471	0.2167
2.20	0.1911	0.0313	0.1769	0.1618	0.2255
2.40	0.1636	0.0397	0.1992	0.1624	0.2169
2.60	0.1327	0.0420	0.2049	0.1534	0.1976
2.80	0.1027	0.0394	0.1984	0.1386	0.1729
3.00	0.0762	0.0338	0.1839	0.1212	0.1466
3.20	0.0541	0.0271	0.1647	0.1031	0.1212
3.40	0.0367	0.0206	0.1435	0.0858	0.0980
3.60	0.0235	0.0149	0.1222	0.0701	0.0780
3.80	0.0139	0.0104	0.1021	0.0564	0.0610
4.00	0.0073	0.0070	0.0839	0.0448	0.0472
4.50	-0.0008	0.0023	0.0484	0.0239	0.0236
5.00	-0.0026	0.0007	0.0261	0.0121	0.0112
7.50	-0.0002	0.0000	0.0007	0.0002	0.0002
10.00	-0.0000	0.0000	0.0000	0.0000	0.0000

^a The abbreviations used in this table and all the following tables are defined in the Appendix.

Table II: Copper 3d and Oxygen 2p, Overlap Matched Cu π

NA = 3 LA = 2 ZA = 2.7000 M = 1 NB = 2 LB = 1
 ZB = 1.9750 TAA = 3.6450 VAA = 0.9000
 TBB = 1.95031 VBB = 0.98750

R	STT	SSQ	S	SA	SB
1.80	0.2110	0.1573	0.3966	0.2793	0.3496
2.00	0.1535	0.1150	0.3391	0.2285	0.2796
2.20	0.1079	0.0804	0.2835	0.1831	0.2191
2.40	0.0732	0.0540	0.2325	0.1443	0.1688
2.60	0.0479	0.0352	0.1875	0.1121	0.1281
2.80	0.0299	0.0222	0.1491	0.0860	0.0960
3.00	0.0176	0.0137	0.1170	0.0653	0.0711
3.20	0.0095	0.0082	0.0908	0.0490	0.0522
3.40	0.0044	0.0049	0.0697	0.0365	0.0380
3.60	0.0013	0.0028	0.0531	0.0270	0.0275
3.80	-0.0005	0.0016	0.0401	0.0199	0.0197
4.00	-0.0014	0.0009	0.0300	0.0145	0.0140
4.50	-0.0017	0.0002	0.0142	0.0065	0.0059
5.00	-0.0012	0.0000	0.0065	0.0028	0.0024
7.50	-0.0000	0.0000	0.0001	0.0000	0.0000
10.00	-0.0000	0.0000	0.0000	0.0000	0.0000

smallest of the zeds described above. It is thus an advantage, rather than a limitation of the method, that one is not faced with an embarrassing choice between atomlike terms and molecular properties. While the overlap-matching orbitals would appear to be very poor for properties depending on the shape of the orbital near the nucleus, they are eminently suitable for semi-

Table III: Copper 3d and Oxygen 2p, C + R Zed for Cu σ

NA = 3 LA = 2 ZA = 4.4000 M = 0 NB = 2 LB = 1
 ZB = 1.9750 TAA = 9.6800 VAA = 1.46667
 TBB = 1.95031 VBB = 0.98750

R	STT	SSQ	S	SA	SB
1.80	0.0844	0.0133	0.1154	0.0830	0.1834
2.00	0.0646	0.0150	0.1226	0.0807	0.1577
2.20	0.0464	0.0139	0.1180	0.0729	0.1281
2.40	0.0314	0.0113	0.1064	0.0627	0.1001
2.60	0.0201	0.0084	0.0917	0.0519	0.0759
2.80	0.0121	0.0058	0.0764	0.0418	0.0563
3.00	0.0068	0.0038	0.0619	0.0330	0.0410
3.20	0.0033	0.0024	0.0491	0.0256	0.0295
3.40	0.0012	0.0015	0.0383	0.0195	0.0210
3.60	0.0001	0.0009	0.0294	0.0147	0.0148
3.80	-0.0005	0.0005	0.0223	0.0110	0.0104
4.00	-0.0008	0.0003	0.0168	0.0082	0.0072
4.50	-0.0007	0.0001	0.0079	0.0037	0.0029
5.00	-0.0005	0.0000	0.0036	0.0017	0.0011
7.50	-0.0000	0.0000	0.0000	0.0000	0.0000
10.00	-0.0000	0.0000	0.0000	0.0000	0.0000

Table IV: Copper 3d and Oxygen 2p, C + R Zed for Cu π

NA = 3 LA = 2 ZA = 4.4000 M = 1 NB = 2 LB = 1
 ZB = 1.9750 TAA = 9.6800 VAA = 1.46667
 TBB = 1.95031 VBB = 0.98750

R	STT	SSQ	S	SA	SB
1.80	0.0425	0.0260	0.1613	0.0934	0.1439
2.00	0.0253	0.0155	0.1243	0.0698	0.0999
2.20	0.0143	0.0088	0.0940	0.0513	0.0683
2.40	0.0075	0.0049	0.0699	0.0372	0.0462
2.60	0.0036	0.0026	0.0513	0.0267	0.0310
2.80	0.0013	0.0014	0.0372	0.0190	0.0206
3.00	0.0002	0.0007	0.0268	0.0134	0.0137
3.20	-0.0004	0.0004	0.0191	0.0094	0.0090
3.40	-0.0006	0.0002	0.0135	0.0066	0.0059
3.60	-0.0006	0.0001	0.0095	0.0046	0.0039
3.80	-0.0005	0.0000	0.0067	0.0032	0.0026
4.00	-0.0004	0.0000	0.0047	0.0022	0.0017
4.50	-0.0002	0.0000	0.0019	0.0009	0.0006
5.00	-0.0001	0.0000	0.0007	0.0003	0.0002
7.50	-0.0000	0.0000	0.0000	0.0000	0.0000
10.00	-0.0000	0.0000	0.0000	0.0000	0.0000

empirical MO calculations when used only to calculate overlap integrals. When the molecular orbitals so obtained are used to calculate derived quantities sensitive to details of shape, the more elaborate expressions for the atomic orbital could then be substituted, up to the limits of validity of the LCAO approximations. The complications attending the use of different atomic orbitals for different terms in the same molecular calculation or accepting questionable results make approxi-

mate methods¹¹ using a minimum atomic orbital set for both overlap and kinetic integral computations unattractive.

The Hamiltonian Matrix: Diagonal Elements. The H_{ii} , or coulomb integrals, contain contributions from the interaction of an electron occupying the orbital and the nuclei and electrons of all other atoms. If these terms cancel, the H_{ii} would reduce to atomic, rather than molecular, parameters. For atomic orbitals similar to those in free atoms or ions, numerical values can be deduced from spectral term values or even from atomic calculations. If rescaling is to be attempted, the kinetic and potential parts of these valence-state ionization potentials (VSIP) must be kept separate, a complication, but possible in principle.

Approximate correction of H_{ii} chosen from VSIP for redistribution of charge in the molecule introduces two types of term at the same order. The first corrects the H_{ii} for changes in the electronic population of that particular orbital as well as the net charge on the atom on which it is located. With certain plausible assumptions, parameters necessary for this first type of correction can be deduced from atomic spectral data.¹² The second class of terms corresponds to the average value of the coulombic interaction between an electron in the orbital and other nuclei and their associated electrons. The one- and two-electron integrals in this class approach asymptotically the Coulomb law expression at sufficiently great distance between nuclei. Incorporation of the limiting form suitable at long distances has been discussed, notably by Jørgensen,¹³ who points out several difficulties arising from complete neglect of the effect. However, the use of the long-distance form of this sort of term in MO calculations at intramolecular distances is theoretically questionable as well as computationally catastrophic when distance is varied. Examination of the qualitative features of the dependence on distance of typical two-center one- and two-electron integrals shows that they approach finite values with finite slope in the united atom limit. Simple approximations satisfying asymptotic requirements at both long- and short-range limits are under study.

Nevertheless, the simple first approximation of adjusting the H_{ii} parameters for the approximate final charge anticipated is quite satisfactory for rough calculations, or for very large molecules where an iterative procedure becomes prohibitively expensive in computer time. Fortunately, many of the useful calculable properties are stable to moderate deviations from charge self-consistency. For example, the magnetic dipole and electric quadrupole transition moment matrix elements for formaldehyde are negligibly dif-

ferent when two *ab initio* sets of molecular orbitals were compared with simple noniterative calculation results using very different orbital exponents.

Off-Diagonal Matrix Elements. The off-diagonal hamiltonian matrix elements, H_{ij} , or resonance integrals, are the principle object of this paper. In an N -orbital problem, there may be as many as $N(N - 1)/2$ of them, so there would be little hope of treating large molecules unless they can be simply and efficiently approximated. Mulliken¹⁴ first suggested taking them proportional to the overlap

$$H_{ij} = KS_{ij} \quad (6)$$

a procedure leading to reasonable results if the H_{ii} are not very different from one another. Much of the dramatic success of Lipscomb, *et al.*,¹⁵ with the polyhedral boron hydrides can be attributed to this requirement being largely satisfied. Wolfsberg and Helmholtz¹⁶ used another form suggested by Mulliken¹⁷

$$H_{ij} = kS_{ij}(H_{ii} + H_{jj}) \quad (7)$$

and determined values of k by working backward from assumed molecular terms, deciding on different values for different types of overlap. It can be shown¹⁸ that $1 < k < 3$ if eq 7 is examined as a formal approximation to integrals over orbitals having reasonable scaling properties. Ballhausen and Gray¹⁹ tried

$$H_{ij} = kS_{ij}(H_{ii}H_{jj})^{1/2} \quad (8)$$

with similar parameter values. Form 8 does not seem to be based on theoretical reasoning, but has the convenient effect of eliminating from consideration atomic orbitals of very different H_{ii} parameters, such as inner shells.

Results of applying these suggestions to the hydrogen molecule are very instructive. Assuming invariant atomic orbitals, a binding energy expression can be obtained by adding up molecular orbital energies and subtracting off atom energies

(11) M. D. Newton, F. P. Boer, and W. N. Lipscomb, *J. Am. Chem. Soc.*, **88**, 2353 (1966), and following papers.

(12) L. C. Cusachs and J. W. Reynolds, *J. Chem. Phys.*, **43**, S160 (1965); L. C. Cusachs, J. W. Reynolds, and D. Barnard, *ibid.*, **44**, 835 (1966).

(13) C. K. Jørgensen, "Orbitals in Atoms and Molecules," Academic Press Inc., London, 1962.

(14) R. S. Mulliken, *J. Phys. Chem.*, **56**, 295 (1952).

(15) R. Hoffmann and W. N. Lipscomb, *J. Chem. Phys.*, **36**, 2179 (1962).

(16) M. Wolfsberg and L. Helmholtz, *ibid.*, **20**, 837 (1952).

(17) R. S. Mulliken, *ibid.*, **46**, 497, 675 (1949).

(18) L. C. Cusachs, Technical Report, Battelle Memorial Institute, Geneva, 1963.

(19) C. J. Ballhausen and H. B. Gray, *Inorg. Chem.*, **1**, 111 (1962).

$$-D_e/2 = (H_{ij} - S_{ij}H_{ii})/(1 + S_{ij}) \quad (9)$$

In eq 6, 7, and 8, the expression is proportional to the quantity $S_{ij}/(1 + S_{ij})$. A minimum in the potential curve occurs only if the overlap as a function of the distance goes through a maximum. In the present case of H_2 , this model predicts collapse to a united atom. An objection can be formulated around the replacement of the SCF-type binding energy expression by the sum of orbital energies. While the adequacy of this approximation does in fact limit the accuracy of calculated equilibrium distances and binding energies, it is not quantitatively sufficient to explain the discrepancy in this case. Slater²⁰ illustrates graphically how, for hydrogen at least, it is the rapid increase of electron kinetic energy, rather than internuclear repulsion or electron repulsion that prevents further contraction past the equilibrium separation. The effect of taking the total energy as a sum of orbital energies instead of the correct function is to exaggerate a large, slowly varying quantity, electron repulsion, and neglect a smaller, but more rapidly varying one, core repulsion.

In a study of the behavior of molecular integrals in aromatic hydrocarbons, Ruedenberg²¹ made the rather startling discovery that the two-center kinetic integral, T_{ij} , is more closely proportional to the square of the overlap than to the first power. The approximations eq 6-8 do not reflect this behavior.

Kinetic and Potential Integral Approximations. The hamiltonian, H , contains a kinetic operator, T , and potential terms, V . If the diagonal matrix elements, H_{ii} , are derived from atomic orbitals in a potential that can be represented by a screened Coulomb field, application of the virial theorem gives

$$H_{ii} = T_{ii} + V_{ii}; \quad T_{ii} = -(1/2)V_{ii}; \\ H_{ii} = (1/2)V_{ii} \quad (10)$$

The off-diagonal hamiltonian matrix elements contain both kinetic and potential terms, but there is no reason to believe that relations of the form of eq 10 would apply in the same way. Assume that the two one-center potential terms V_{ii} and V_{jj} are available for orbitals on different centers. First express the second orbital, ψ_j , in a complete orthogonal set of orbitals centered at i , choosing the first term in the expansion to be ψ_i

$$\varphi_j = S_{ij}\psi_i + (1 - S_{ij}^2)^{1/2}\chi_i \quad (11)$$

where χ_i is an orbital orthogonal to ψ_i .

The second term is then neglected, since it does not reduce further, but it can normally be expected to be unimportant. Since an equivalent result must be ob-

tained by expanding at the other center, half of the sum of the two expansions yields the symmetric form

$$V_{ij} = S_{ij}(V_{ii} + V_{jj})/2 = 2S_{ij}(H_{ii} + H_{jj})/2 \quad (12)$$

This is in at least qualitative agreement with Ruedenberg's results for short-range forces.

The kinetic term requires an entirely different treatment. First transform the kinetic operator to the symmetric form

$$\langle i|T|j\rangle = (-1/2)\langle i|\Delta^2\psi_j\rangle = (1/2)\langle \bar{\Delta}\psi_i|\bar{\Delta}\psi_j\rangle \quad (13)$$

For any bound state, the average value of the momentum must be zero

$$\langle i|\bar{\Delta}\psi_i\rangle = 0 \quad (14)$$

This means that in the last form of eq 13 the first factor is orthogonal to the first orbital and the second to the second orbital. Thus no simple approximation to the kinetic term results from expanding the orbitals about other centers as was done for the potential terms.

Ruedenberg observed that the approximation, the first form of

$$T_{ij} = S_{ij}^2(T_{ii} + T_{jj})/2 \simeq -S_{ij}^2(H_{ii} + H_{jj})/2 \quad (15)$$

was obeyed within 1% or so for the orbitals he examined. Close analysis of the general formulas for kinetic integrals shows this to be proper for the limits of R , the internuclear distance, approaching 0 and ∞ .

Table V: Hydrogen 1s and Oxygen 2p, C + R Zed Oxygen

NA = 1 LA = 0 ZA = 1.0000 M = 0 NB = 2 LP = 1
ZB = 2.2266 TAA = 0.5000 VAA = 1.0000
TBB = 2.47887 VBB = 1.11330

R	STT	SSQ	S	SA	SB
1.80	0.1652	0.1287	0.3588	0.4255	0.2290
2.00	0.1287	0.1108	0.3328	0.3581	0.2051
2.20	0.0977	0.0923	0.3038	0.2975	0.1812
2.40	0.0723	0.0748	0.2735	0.2445	0.1585
2.60	0.0520	0.0592	0.2434	0.1992	0.1373
2.80	0.0362	0.0460	0.2145	0.1612	0.1181
3.00	0.0242	0.0352	0.1875	0.1297	0.1010
3.20	0.0152	0.0265	0.1627	0.1039	0.0859
3.40	0.0086	0.0197	0.1403	0.0830	0.0728
3.60	0.0039	0.0145	0.1204	0.0661	0.0614
3.80	0.0007	0.0106	0.1028	0.0525	0.0516
4.00	-0.0014	0.0076	0.0874	0.0416	0.0433
4.50	-0.0037	0.0033	0.0574	0.0232	0.0276
5.00	-0.0038	0.0014	0.0371	0.0129	0.0174
7.50	-0.0007	0.0000	0.0036	0.0007	0.0016
10.00	-0.0001	0.0000	0.0003	0.0000	0.0001

(20) See ref 3a, pp 36, 56, 57.

(21) K. Ruedenberg, *J. Chem. Phys.*, **34**, 1892 (1961).

Table VI: Hydrogen 1s and Oxygen 2p, Burns Zed Oxygen

NA = 1 LA = 0 ZA = 1.0000 M = 0 NB = 2 LB = 1
 ZB = 1.9750 TAA = 0.5000 VAA = 1.0000
 TBB = 1.95031 VBB = 0.98750

R	STT	SSQ	S	SA	SB
1.80	0.2240	0.1692	0.4114	0.4801	0.2760
2.00	0.1806	0.1503	0.3877	0.4151	0.2506
2.20	0.1421	0.1292	0.3594	0.3538	0.2243
2.40	0.1092	0.1079	0.3285	0.2981	0.1986
2.60	0.0819	0.0880	0.2967	0.2487	0.1741
2.80	0.0598	0.0704	0.2652	0.2059	0.1514
3.00	0.0423	0.0552	0.2350	0.1693	0.1308
3.20	0.0287	0.0427	0.2066	0.1385	0.1123
3.40	0.0184	0.0326	0.1804	0.1127	0.0960
3.60	0.0107	0.0245	0.1566	0.0914	0.0817
3.80	0.0051	0.0183	0.1353	0.0738	0.0692
4.00	0.0011	0.0135	0.1162	0.0595	0.0585
4.50	-0.0039	0.0061	0.0782	0.0343	0.0379
5.00	-0.0050	0.0027	0.0516	0.0196	0.0242
7.50	-0.0013	0.0000	0.0054	0.0012	0.0023
10.00	-0.0001	0.0000	0.0005	0.0001	0.0002

Table VIII: Hydrogen 1s and Sulfur 3s

NA = 1 LA = 0 ZA = 1.0000 M = 0 NB = 1 LB = 0
 ZB = 15.5409 TAA = 0.5000 VAA = 1.0000
 TBB = 0.45042 VBB = 1.70743

R	STT	SSQ	S	SA	SB
1.80	0.3619	0.4292	0.6551	0.4996	0.5948
2.00	0.2935	0.3580	0.5983	0.4386	0.5276
2.20	0.2301	0.2935	0.5417	0.3802	0.4644
2.40	0.1739	0.2367	0.4865	0.3259	0.4059
2.60	0.1258	0.1881	0.4337	0.2766	0.3527
2.80	0.0859	0.1475	0.3841	0.2328	0.3047
3.00	0.0538	0.1142	0.3379	0.1945	0.2620
3.20	0.0287	0.0874	0.2957	0.1614	0.2243
3.40	0.0097	0.0662	0.2573	0.1333	0.1912
3.60	-0.0042	0.0497	0.2229	0.1094	0.1625
3.80	-0.0139	0.0369	0.1922	0.0895	0.1376
4.00	-0.0202	0.0273	0.1651	0.0729	0.1162
4.50	-0.0262	0.0124	0.1112	0.0431	0.0754
5.00	-0.0244	0.0054	0.0735	0.0252	0.0483
7.50	-0.0049	0.0001	0.0078	0.0016	0.0047
10.00	-0.0006	0.0000	0.0007	0.0001	0.0004

Table VII: Hydrogen 1s and Oxygen 2p, Hydrogen Zed = 1.2

NA = 1 LA = 0 ZA = 1.2000 M = 0 NB = 2 LB = 1
 ZB = 2.2266 TAA = 0.7200 VAA = 1.2000
 TBB = 2.47887 VBB = 1.11330

R	STT	SSQ	S	SA	SB
1.80	0.1772	0.1556	0.3944	0.3940	0.2544
2.00	0.1325	0.1282	0.3580	0.3262	0.2218
2.20	0.0959	0.1020	0.3194	0.2662	0.1906
2.40	0.0669	0.0788	0.2807	0.2147	0.1619
2.60	0.0447	0.0594	0.2438	0.1715	0.1363
2.80	0.0281	0.0438	0.2094	0.1359	0.1138
3.00	0.0161	0.0318	0.1783	0.1070	0.0943
3.20	0.0077	0.0227	0.1505	0.0838	0.0777
3.40	0.0020	0.0159	0.1263	0.0653	0.0638
3.60	-0.0017	0.0111	0.1052	0.0507	0.0521
3.80	-0.0039	0.0076	0.0873	0.0393	0.0424
4.00	-0.0051	0.0052	0.0720	0.0303	0.0343
4.50	-0.0055	0.0019	0.0438	0.0157	0.0201
5.00	-0.0044	0.0007	0.0261	0.0081	0.0116
7.50	-0.0005	0.0000	0.0016	0.0003	0.0007
10.00	-0.0000	0.0000	0.0001	0.0000	0.0000

Table IX: Carbon 2p and Oxygen 2p, σ Overlap

NA = 2 LA = 1 ZA = 1.5679 M = 0 NB = 2 LB = 1
 ZB = 2.2266 TAA = 1.22916 VAA = 0.78395
 TBB = 2.47887 VBB = 1.11330

R	STT	SSQ	S	SA	SB
1.80	0.2872	0.0473	0.2175	0.3253	0.2161
2.00	0.2634	0.0719	0.2682	0.3328	0.2326
2.20	0.2290	0.0872	0.2954	0.3204	0.2333
2.40	0.1907	0.0922	0.3636	0.2957	0.2231
2.60	0.1531	0.0886	0.2976	0.2643	0.2061
2.80	0.1187	0.0794	0.2818	0.2304	0.1853
3.00	0.0890	0.0673	0.2595	0.1969	0.1631
3.20	0.0645	0.0547	0.2338	0.1655	0.1410
3.40	0.0448	0.0428	0.2068	0.1372	0.1202
3.60	0.0296	0.0324	0.1801	0.1124	0.1011
3.80	0.0182	0.0240	0.1548	0.0911	0.0842
4.00	0.0099	0.0173	0.1315	0.0732	0.0695
4.50	-0.0012	0.0070	0.0839	0.0410	0.0415
5.00	-0.0044	0.0026	0.0510	0.0222	0.0239
7.50	-0.0008	0.0000	0.0027	0.0007	0.0011
10.00	-0.0000	0.0000	0.0001	0.0000	0.0000

Tables I–XIV of this article provide a fair sample of cases for judging the validity of approximations 12 and 15 and are typical of the much larger number of combinations examined.

Since it is convenient to be able to determine whether a molecular orbital is predominantly bonding, antibonding, or nonbonding by looking at the pattern of signs of the coefficients, the usual practice in diatomic molecule calculations is to choose the sense of the co-

ordinate systems at each nucleus to make as many of the two-center overlap integrals positive as possible. In such a coordinate system about the internuclear axis, eq 15 may be used in its simple form, subject to the reservation that it is a numerical approximation to the behavior of an integral over Slater-type orbitals. More complicated combinations of atomic orbitals, group orbitals, or even hybrids, if one pleases, can be expressed as sums of STO's. The overlap and other

Table X: Carbon 2p and Oxygen 2p, π Overlap

NA = 2 LA = 1 ZA = 1.5679 M = 1 NB = 2 LB = 1
 ZB = 2.2266 TAA = 1.22916 VAA = 0.78395
 TBB = 2.47887 VBB = 1.11330

R	STT	SSQ	S	SA	SB
1.80	0.1456	0.1362	0.3690	0.2943	0.2390
2.00	0.1034	0.0946	0.3076	0.2318	0.1925
2.20	0.0716	0.0645	0.2539	0.1809	0.1537
2.40	0.0481	0.0431	0.2077	0.1401	0.1218
2.60	0.0312	0.0284	0.1685	0.1078	0.0959
2.80	0.0193	0.0184	0.1357	0.0824	0.0751
3.00	0.0111	0.0118	0.1086	0.0627	0.0584
3.20	0.0056	0.0075	0.0864	0.0474	0.0453
3.40	0.0021	0.0047	0.0683	0.0358	0.0350
3.60	-0.0001	0.0029	0.0538	0.0269	0.0269
3.80	-0.0013	0.0018	0.0422	0.0201	0.0206
4.00	-0.0019	0.0011	0.0329	0.0150	0.0157
4.50	-0.0021	0.0003	0.0174	0.0071	0.0079
5.00	-0.0016	0.0001	0.0090	0.0033	0.0039
7.50	-0.0001	0.0000	0.0003	0.0001	0.0001
10.00	-0.0000	0.0000	0.0000	0.0000	0.0000

similar integrals are evaluated in local coordinates. After this is accomplished, the matrix elements can be transformed to an arbitrary system of coordinates in the usual manner. Group theoretical reduction of large secular equations is probably useful in hand calculations, but rather increases the labor of constructing an automatic machine program; a high-speed digital computer can diagonalize the large matrix much more rapidly than it can search for symmetry elements. Classical hybridization theory corresponds to rules for guessing the results of calculations made with unnecessary additional restrictions; from the general molecular orbital viewpoint the choice of hybrid atomic orbitals as a starting basis is merely a complication adding to the labor of the computation. A major attraction of the MO method is the possibility of including all valence shell electrons without initially prejudicing the result by restrictive arbitrary assumptions.

Combining eq 15 with eq 12 produces a general formula²²

$$H_{ij} = S_{ij}(2 - |S_{ij}|)(H_{ii} + H_{jj})/2 \quad (16)$$

This expression is to be used as it stands in a local relative coordinate system, *i.e.*, one where the orbitals all have well-defined m quantum numbers, as well as the usual n and l implied by the choice of H_{ii} . Although it is formally second degree in the overlap, it transforms as a single hamiltonian matrix element under rotations or translations of coordinates. Automatic computer programs can be adapted to compute the

matrix of $S_{ij}(2 - |S_{ij}|)$ at the same time as the overlap matrix. A. T. Armstrong observes that this is easily accomplished by generating this matrix in lower triangular form in the same array in which the overlap appears in upper triangular form.

The restriction of the simple expression eq 16 to use in a local relative coordinate system is important if invariance under rotations of the molecular coordinate system is to be achieved. It means in practice that the quantities $S_{ij}(S - |S_{ij}|)$ must be computed in the local relative coordinate system prior to rotation to the absolute molecular coordinate system. In this and all rotations of coordinates performed subsequently, the entire term must be treated as if it were linear in overlap. Failure to take this precaution results in small but detectable changes in computed properties with different orientations of the molecular coordinate system. The consequences of using eq 16 indiscriminately in absolute molecular coordinates do not, however, appear to be as drastic as those arising in prescriptions¹¹ which fail to assure proper invariance of the diagonal hamiltonian matrix elements under such rotations. Cusachs' original calculations for water²³ did not use the proposed approximation in invariant form, but the calculations of Carroll, Armstrong, and McGlynn²⁴ not only are completely above reproach in this respect, but also agreed more closely with experimental angles and ionization potentials.

Discussion

Returning to the hydrogen molecule example with eq 16 results in a minimum in the energy curve with $S = 0.414$ and a reasonable binding energy. The binding is overestimated with the overlap calculated from free-atom orbitals. Rescaling along the lines indicated by the general theory would have reduced the overlap closer to the optimum and picked up energy terms resulting from the orbital contraction, but at a cost of separating the kinetic and potential terms and determining a scale factor, a nonlinear parameter. The quality of the results in more general cases does not appear to justify this increase in labor. Carroll and McGlynn²⁵ and Carroll, Armstrong, and McGlynn²⁴ have examined the use of eq 16 with a semiempirical adjustment of the H_{ij} for charge redistribution, observing that the molecular orbital coefficients and orbital energies for the

(22) L. C. Cusachs, Sanibel Symposium, 1964; see p 36 of Report No. 50 of the Quantum Theory Project, University of Florida, Gainesville, Fla.

(23) L. C. Cusachs, *J. Chem. Phys.*, **43**, S157 (1965).

(24) D. G. Carroll, A. T. Armstrong, and S. P. McGlynn, *ibid.*, **44**, 1865 (1966).

(25) D. G. Carroll and S. P. McGlynn, *ibid.*, in press.

Table XI: Carbon 2s and Oxygen 2p

NP	N1N2		LA	ZA(1)	ZA(2)	N1	LB	ZB(1)			
16	1	2	0	5.67270	1.60830	2	1	2.22660			
	CA1		CA2			CB1					
	-0.223931		1.024766			1.000000					
TAA	VAA		TBB	VBB	OTAA	OVAA	OTBB	OVBB			
0.43110	0.80415		2.47887	1.11330	1.49243	0.88553	2.47887	1.11330			
R	MQ	OTT	OSQ	STT	SSQ	OS	OA	OB	S	SA	SB
1.80	0	0.1359	0.1214	0.1867	0.1373	0.3484	0.3441	0.2287	0.3705	0.4793	0.2401
2.00	0	0.1189	0.1154	0.1583	0.1253	0.3397	0.3151	0.2175	0.3540	0.4178	0.2235
2.20	0	0.0984	0.1035	0.1284	0.1091	0.3217	0.2798	0.2003	0.3302	0.3573	0.2028
2.40	0	0.0776	0.0884	0.0998	0.0911	0.2973	0.2425	0.1797	0.3018	0.3006	0.1802
2.60	0	0.0584	0.0724	0.0744	0.0734	0.2691	0.2060	0.1579	0.2709	0.2495	0.1573
2.80	0	0.0419	0.0573	0.0528	0.0573	0.2393	0.1722	0.1364	0.2393	0.2045	0.1351
3.00	0	0.0283	0.0439	0.0353	0.0435	0.2095	0.1419	0.1161	0.2085	0.1659	0.1146
3.20	0	0.0177	0.0327	0.0217	0.0322	0.1810	0.1155	0.0976	0.1794	0.1334	0.0961
3.40	0	0.0097	0.0239	0.0115	0.0233	0.1544	0.0931	0.0811	0.1526	0.1063	0.0797
3.60	0	0.0039	0.0170	0.0041	0.0165	0.1304	0.0743	0.0668	0.1286	0.0842	0.0655
3.80	0	-0.0001	0.0119	-0.0009	0.0115	0.1091	0.0589	0.0545	0.1074	0.0662	0.0534
4.00	0	-0.0027	0.0082	-0.0041	0.0079	0.0905	0.0463	0.0442	0.0889	0.0517	0.0433
4.50	0	-0.0051	0.0030	-0.0070	0.0029	0.0549	0.0248	0.0254	0.0538	0.0273	0.0248
5.00	0	-0.0047	0.0010	-0.0064	0.0010	0.0320	0.0128	0.0141	0.0313	0.0141	0.0138
7.50	0	-0.0005	0.0000	-0.0006	0.0000	0.0015	0.0004	0.0006	0.0015	0.0004	0.0005
10.00	0	-0.0000	0.0000	-0.0000	0.0000	0.0000	0.0000	0.0000	0.0000	0.0000	0.0000

Table XII: Carbon 2s and Oxygen 2s

NP	N1N2		LA	ZA(1)	ZA(2)	N1N2	LB	ZB(1)	ZB(2)		
16	1	2	0 0	5.67270	1.60830	1 2 0 0		7.65790	2.24580		
	CA1		CA2			CB2					
	-0.223931		1.024766			1.027724					
TAA	VAA		TBB	VBB	OTAA	OVAA	OTBB	OVBB			
0.43110	0.80415		0.84060	1.12290	1.49243	0.88553	2.99056	1.24536			
R	MQ	OTT	OSQ	STT	SSQ	OS	OA	OB	S	SA	SB
1.80	0	0.0753	0.2784	0.2542	0.2867	0.5277	0.3795	0.3330	0.5354	0.4723	0.4163
2.00	0	0.0575	0.2202	0.1875	0.2228	0.4693	0.3244	0.2900	0.4720	0.3935	0.3570
2.20	0	0.0412	0.1699	0.1302	0.1693	0.4122	0.2730	0.2490	0.4115	0.3241	0.3024
2.40	0	0.0274	0.1281	0.0832	0.1260	0.3579	0.2265	0.2110	0.3549	0.2642	0.2535
2.60	0	0.0162	0.0944	0.0463	0.0919	0.3073	0.1857	0.1768	0.3032	0.2134	0.2105
2.80	0	0.0075	0.0683	0.0184	0.0659	0.2613	0.1506	0.1467	0.2566	0.1709	0.1732
3.00	0	0.0012	0.0485	-0.0015	0.0464	0.2201	0.1210	0.1206	0.2154	0.1359	0.1415
3.20	0	-0.0031	0.0338	-0.0150	0.0322	0.1839	0.0965	0.0984	0.1794	0.1073	0.1147
3.40	0	-0.0059	0.0232	-0.0233	0.0220	0.1524	0.0763	0.0797	0.1483	0.0842	0.0924
3.60	0	-0.0075	0.0157	-0.0278	0.0148	0.1255	0.0599	0.0641	0.1217	0.0657	0.0740
3.80	0	-0.0081	0.0105	-0.0294	0.0099	0.1026	0.0468	0.0513	0.0993	0.0510	0.0590
4.00	0	-0.0082	0.0069	-0.0290	0.0065	0.0833	0.0364	0.0408	0.0806	0.0395	0.0467
4.50	0	-0.0068	0.0023	-0.0238	0.0022	0.0484	0.0189	0.0226	0.0467	0.0204	0.0257
5.00	0	-0.0049	0.0007	-0.0168	0.0007	0.0273	0.0096	0.0122	0.0263	0.0103	0.0138
7.50	0	-0.0004	0.0000	-0.0012	0.0000	0.0012	0.0003	0.0004	0.0011	0.0003	0.0005
10.00	0	-0.0000	0.0000	-0.0000	0.0000	0.0000	0.0000	0.0000	0.0000	0.0000	0.0000

occupied molecular orbitals are close to those for the *ab initio* SCF-MO method. The virtual orbitals, those not occupied in the ground state, are somewhat more realistic than those of the *ab initio* calculation.

This is because this method differs in the effective exchange potential from that of the SCF-MO in the ordinary Hartree-Fock equations, more closely imitating the form of the Hartree-Fock-Slater approxi-

Table XIII: Oxygen 2s and Sulfur 3s

NP	N1N2		LA	ZA(1)		ZA(2)		N1N2		LB	ZB(1)		ZB(2)
16	1	2	0	8.65790		2.24580		2	3	0	5.31440		2.12230
				CA1		CA2					CB1		CB2
				-0.237099		1.027724					-0.329747		1.052964
TAA	VAA		TBB	VBB		OTAA		OVAA		OTBB	OVBB		
0.84060	1.12290		0.45042	0.70743		2.99056		1.24536		1.24564	0.74983		
R	MQ	OTT	OSQ	STT	SSQ	OS	OA	OB	S	SA	SB		
1.80	0	0.0865	0.2662	0.2758	0.2964	0.5159	0.3319	0.3809	0.5444	0.4312	0.5125		
2.00	0	0.0719	0.2178	0.2127	0.2332	0.4666	0.2957	0.3381	0.4829	0.3728	0.4331		
2.20	0	0.0555	0.1725	0.1540	0.1786	0.4153	0.2577	0.2935	0.4226	0.3170	0.3610		
2.40	0	0.0395	0.1324	0.1026	0.1333	0.3639	0.2203	0.2498	0.3651	0.2655	0.2971		
2.60	0	0.0253	0.0988	0.0599	0.0971	0.3142	0.1851	0.2089	0.3115	0.2193	0.2416		
2.80	0	0.0137	0.0717	0.0265	0.0690	0.2677	0.1532	0.1720	0.2627	0.1789	0.1943		
3.00	0	0.0047	0.0507	0.0018	0.0480	0.2252	0.1251	0.1396	0.2192	0.1443	0.1548		
3.20	0	-0.0017	0.0350	-0.0153	0.0327	0.1872	0.1009	0.1119	0.1809	0.1152	0.1221		
3.40	0	-0.0060	0.0237	-0.0261	0.0219	0.1539	0.0805	0.0888	0.1479	0.0911	0.0955		
3.60	0	-0.0086	0.0157	-0.0320	0.0144	0.1253	0.0636	0.0697	0.1198	0.0714	0.0741		
3.80	0	-0.0098	0.0102	-0.0342	0.0093	0.1011	0.0497	0.0542	0.0962	0.0555	0.0571		
4.00	0	-0.0100	0.0065	-0.0338	0.0059	0.0808	0.0386	0.0418	0.0767	0.0428	0.0437		
4.50	0	-0.0084	0.0020	-0.0271	0.0018	0.0447	0.0199	0.0212	0.0421	0.0217	0.0218		
5.00	0	-0.0058	0.0006	-0.0184	0.0005	0.0237	0.0098	0.0103	0.0222	0.0107	0.0105		
7.50	0	-0.0003	0.0000	-0.0009	0.0000	0.0006	0.0002	0.0002	0.0006	0.0002	0.0002		
10.00	0	-0.0000	0.0000	-0.0000	0.0000	0.0000	0.0000	0.0000	0.0000	0.0000	0.0000		

Table XIV: Sulfur 3p and Sulfur 3s

NP	N1N2		LA	ZA(1)		ZA(2)		N1N2		LB	ZB(1)	ZB(2)	ZB(3)	
16	2	3	1	5.98850		1.82730		1	2	3	0	15.54090	5.31440	2.12230
				CA1		CA2						CB1	CB2	CB3
				-0.188792		1.017665						-0.094151	0.358589	1.057224
TAA	VAA		TBB	VBB		OTAA		OVAA		OTBB	OVBB			
0.77911	0.60910		0.45042	0.70743		1.38960		0.62610		2.58190	0.78868			
R	MQ	OTT	OSQ	STT	SSQ	OS	OA	OB	S	SA	SB			
1.80	0	0.1051	0.2255	0.4948	0.3176	0.4749	0.3658	0.3858	0.5636	0.4856	0.6805			
2.00	0	0.1172	0.2445	0.4811	0.3244	0.4945	0.3864	0.3977	0.5696	0.4841	0.6587			
2.20	0	0.1210	0.2527	0.4507	0.3175	0.5027	0.3930	0.3980	0.5635	0.4699	0.6239			
2.40	0	0.1175	0.2496	0.4074	0.2988	0.4996	0.3868	0.3877	0.5466	0.4455	0.5797			
2.60	0	0.1082	0.2365	0.3560	0.2714	0.4863	0.3701	0.3688	0.5210	0.4137	0.5294			
2.80	0	0.0953	0.2156	0.3007	0.2386	0.4643	0.3456	0.3434	0.4885	0.3771	0.4760			
3.00	0	0.0805	0.1897	0.2454	0.2036	0.4356	0.3160	0.3137	0.4512	0.3380	0.4220			
3.20	0	0.0652	0.1617	0.1930	0.1690	0.4022	0.2836	0.2818	0.4111	0.2985	0.3695			
3.40	0	0.0506	0.1339	0.1456	0.1367	0.3659	0.2504	0.2493	0.3698	0.2600	0.3197			
3.60	0	0.0375	0.1078	0.1044	0.1080	0.3284	0.2178	0.2177	0.3287	0.2237	0.2737			
3.80	0	0.0261	0.0848	0.0698	0.0835	0.2912	0.1871	0.1877	0.2890	0.1904	0.2320			
4.00	0	0.0167	0.0651	0.0419	0.0633	0.2552	0.1588	0.1600	0.2515	0.1604	0.1950			
4.50	0	0.0011	0.0309	-0.0026	0.0292	0.1757	0.1009	0.1030	0.1708	0.1004	0.1218			
5.00	0	-0.0056	0.0131	-0.0204	0.0122	0.1146	0.0608	0.0630	0.1103	0.0599	0.0729			
7.50	0	-0.0020	0.0001	-0.0062	0.0001	0.0077	0.0029	0.0032	0.0073	0.0028	0.0036			
10.00	0	-0.0001	0.0000	-0.0004	0.0000	0.0003	0.0001	0.0001	0.0003	0.0001	0.0001			

mation in spirit by using a uniform average exchange potential.²⁶

It should be observed that, except for precautions in the manner of transformation under rotation of coordinates, the use of eq 16 is similar in practice to re-

placing the arbitrary parameter, k , of the Mulliken-Wolfsberg-Helmholz (MWH) formula, eq 7, by (2 -

(26) F. Herman and S. Skillman, "Atomic Structure Calculations," Prentice-Hall, Inc., Englewood Cliffs, N. J., 1963.

$|S\rangle$). Numerical values in most published cases are consistent with this.²⁷ Calculations on water, where the ordinary Wolfsberg-Helmholz treatment fails to predict the correct shape, respond to this improvement.^{23,24,28}

Validity of the Integral Approximations. The development has assumed that the virial theorem in its simplest form can be applied to the H_{ii} in the sense that $T_{ii} = -H_{ii} = -(1/2)V_{ii}$. This is clearly true of the phenomenological valence-state ionization potentials¹² for the simple reason that they are differences between linear combinations of spectroscopic state energies. Each of these individually satisfies the virial theorem, considering all particles. Individual atomic orbitals do not necessarily obey that relation; they must satisfy only the single-particle virial expressions²⁹

$$2T_{ii} = \langle i | \vec{r}_i \vec{\nabla}_i V | i \rangle \quad (17)$$

If V is proportional to $1/r_i$, then $2T_{ii} = -V_{ii}$.

Comparison of the calculated one-center orbital energies and the phenomenological VSIP data shows excellent agreement. However, comparison of calculated one-center kinetic terms and the SCF orbital energies of VSIPs shows that the one-particle potential for a valence shell electron may be far from coulombic. There is a simple second approximation which sheds some light on the discrepancy. At distances outside the core of the atom, the potential is very well approximated by the screened coulombic potential,⁷ but in the inner regions the departure from constant effective atomic number is significant. If the electrons other than the one of interest are replaced by an equivalent uniformly charged spherical shell, the electron repulsion potential is constant within the shell and coulombic outside. Application of eq 17 shows that the constant potential does not affect the kinetic term, but rather that twice the kinetic term should equal the negative of the coulombic part of the total one-particle potential. The energy due to the constant potential is simply the sum of the kinetic energy and the orbital energy or VSIP. For the oxygen 2s and 2p orbitals, this is large, about 0.8 hartree, or greater than 20 ev.

It has been known for a number of years³⁰ that two-center overlap integrals involving an orbital such as the oxygen 2s were insensitive to the difference between the simple nodeless Slater-type 2s function and one properly orthogonalized to the 1s core orbital. This is not true of the calculated kinetic energy terms. Orthogonalization may increase the computed one-center kinetic integral by a factor of from 2 to 5, with a less drastic change in the average value of $1/r$. The orthogonalization primarily affects properties sensitive to the shape of the orbital near the nucleus, while

the nodeless function gives a good account of the bonding regions. This suggests that the simple relation $2T = -V$ may be approximately true in the part of the atom most affected by chemical bonding, though it is certainly not correct locally either near the nucleus nor in the outer regions, where the local kinetic energy is necessarily negative. Tables IV, VII, VIII, IX, and X illustrate the great sensitivity of the two-center kinetic term to orthogonalization to inner orbitals, as well as the insensitivity of the overlap integrals to this.

Including core shells in the calculation achieves at least a measure of consistency in the kinetic energy values. The increase in labor and consequent restriction to smaller molecules is acceptable for hydrocarbons, but would be disastrous for a treatment of a polynuclear tungsten complex with available computers.

Approximation 15 is a clear improvement over the assumption that the kinetic term is proportional to the overlap integral. It is still less rapidly varying with distance than the computed two-center kinetic integrals. Use of eq 16 and the sum of orbital energies as an approximation to the total energy leads to potential curves which are too flat, too shallow, and have minima at internuclear distances which are too long. It is tempting to suppose that using the computed two-center kinetic term, or at least a corrected term proportional to it, would improve results. Mr. B. Trus has constructed a computer program for this purpose and examined the water molecule MO predictions both with the calculated two-center kinetic term as such and with one corrected to give the phenomenological (VSIP) values in the united atom limit. Both of these lead to pathological orbitals, energies, and charges assigned to the atoms as well as grossly unreasonable geometries. The collection of tables in this article is typical of a much larger number examined. While it is very simple to compute two-center kinetic integrals and even the two-center one-electron potential terms, it does not appear that this would constitute an improvement to the semiempirical method.

The classical Mulliken-Wolfsberg-Helmholz expression, with the constant set equal to 1, reduces the two-electron integrals to the Mulliken approximation.³¹ In the expression proposed here, the implied two-electron contribution would be exaggerated in a situation

(27) F. A. Cotton and T. E. Haas, *Inorg. Chem.*, **3**, 1004 (1964), and others cited by ref 24.

(28) R. Hoffmann, *J. Chem. Phys.*, **40**, 2745 (1964).

(29) A. Dalgarno and A. L. Stewart, *Proc. Roy. Soc. (London)*, **A238**, 273 (1956); W. L. Clinton, *J. Chem. Phys.*, **33**, 1603 (1960).

(30) R. S. Mulliken, C. A. Rieke, and D. Orloff, *ibid.*, **17**, 1248 (1949).

(31) F. O. Ellison, *ibid.*, **23**, 2358 (1954).

formally analogous to the relation between the sum of one-electron energies and the total energy of the SCF theory. This is part of the reason for believing that the long distances and small force constants calculated are not resulting from inadequate treatment of electron repulsion in this implicit fashion, but rather of its exaggeration. Kinetic and nuclear attraction terms calculated from SCF orbitals do agree with the individual terms of this approximation more than just qualitatively, yet the agreement between molecular orbital energies and empirical molecular energy levels easily obtained is far better than could be predicted from the individual parts. It is still necessary to select the input data with care.

Hoffmann³² was remarkably successful in predicting the conformation of a variety of molecules using his "extended Hückel" computer program which automated the application of the Mulliken-Wolfsberg-Helmholz (MWH) approximation to all valence shell orbitals. In his calculations, the terms preventing collapse to a united atom came from antibonding orbitals and from the maximum in p - σ overlap. The dubious theoretical repute of the parent approximation combined with the even less well-founded popular prejudice in favor of the dominance of electron repulsion constituted a seductive temptation to dismiss cavalierly a significant achievement. Analysis of the success and limitations of his work reveals that the traditional assumptions neglect major factors in determining the shape of molecules.

Both the approximation recommended here and the MWH approximation, eq 7, lead to "closed-shell repulsions" proportional to $S^2/(1 + S)$. The similarity in form between this and the function obtained by applying the Mulliken approximation to electron repulsion integrals serves as warning that one-electron bonding-antibonding effects cannot be distinguished from electron repulsion on the basis of overlap dependence.

It is to be at least strongly suspected that electron-pair repulsion models are often successful in predicting molecular geometries because the sharp dependence of electron kinetic energy on molecular shape frequently acts in the same sense as the less important changes in electron repulsion energy.

Many-Electron Character of VSIPs. It has been observed that the many-particle virial theorem relation must be satisfied for the energy quantities making up a VSIP. The kinetic and potential terms for an individual orbital do not generally approximate this relation very closely, although the pattern of regularities expected on this basis is very useful in treating experimental data. What the phenomenological quan-

ties include that is missing in the orbital calculations is the adjustment in the kinetic and potential energies of the other electrons as well as those of the one of interest. While these quantities are assigned to one electron, they have many-electron character.¹³ It is then much more reasonable to expect that molecular ionization potentials, ultimately many-electron quantities, should be subject to a parametrization in terms of one-electron quantities in a semiempirical treatment. The content of approximation 16 is that explicit forms for the atomic orbitals, *via* the overlap integrals, are suitable for obtaining the transfer of atomic to molecular VSIP.

This interpretation of the theoretical structure of the one-electron model suggests that it should be semi-quantitatively successful except where degeneracy or near degeneracy of levels of the same symmetry class is predicted. In the same situation, it should be a useful starting point for more precise treatments of two-electron effects on a perturbation basis. This is because correlation effects are long range³³ and may be as easily assimilated into the atomic parameters as truly one-electron ones.³⁴

Atomic Parameters. Transferability of atomic orbital parameters should be good for those valence subshells at least partially occupied in the free atoms. While VSIP data can be generated from spectral term values for virtual orbitals, such as the 3d, 4s, and 4p of the phosphorous-sulfur part of the periodic table, the orbital functions are poorly defined outside the core of the free atom. It remains to be seen how useful these parameters are for molecular calculations. It is encouraging to find that the overlap between this type of orbital and typical ligand orbitals is insensitive to the *z* of the virtual orbital in a range from about 0.8 to 2.0, but some of the difficulties encountered in solid-state LCAO calculations are expected to appear. The result that the 4s orbital of phosphorous is more important than the 3d in PF_5 awaits the test of comparison with *ab initio* calculations of good accuracy expected within the next few years.

It is possible to define VSIP for hybrids and other arbitrary choices of modified atomic orbitals. It does not appear to be easy to incorporate them in any logical fashion into the structure of the molecular orbital theory, nor to provide theoretical basis for the practice of selecting localized atomic or molecular

(32) R. Hoffmann, *J. Chem. Phys.*, **39**, 1397 (1963); **40**, 2474, 2480 (1964).

(33) B. M. Gimarc, W. A. Cooney, and R. G. Parr, *ibid.*, **42**, 21 (1965).

(34) E. Clementi, *IBM J. Res. Develop.*, **9**, 2 (1965); see pp 14, 15.

orbitals to represent an ion or group in a larger molecular aggregate.

Total Energy. The principle of this model is to approximate systematically the one-electron terms identified by Ruedenberg as dominating an optimized LCAO-MO calculation. As a first step eq 16 takes care of terms obtained with the atomic orbitals left fixed as determined by free atoms, ions, or valence states, but replacing the total energy by a sum of one-electron energies. This latter procedure, drastic as it is,²⁵ implies by its success in predicting angles that the two-electron terms vary slowly as compared with electron kinetic energy and that electron repulsion is almost independent of angle in bent molecules such as H₂O, H₂S, etc. For hydrogen, at least, it is safely established that the two-electron terms do satisfy this requirement of varying more gently than electron kinetic energy near the equilibrium distance. Far from the equilibrium distances, no single-configuration MO treatment will behave properly, but in most cases beyond the two-electron problem, the VB model also dissociates incorrectly.

This model, based as it is on atomic energy parameters and overlap integrals, depends on the identification of the molecular ionization potentials with the orbital energies. It should ultimately include some form of rescaling and probably introduction of two-electron terms explicitly to permit calculation of a proper total energy for binding energies. Exchange integral differences can be introduced as a perturbation where necessary to make it possible to treat singlet-triplet differences in spectroscopic applications.

Importance of Overlap. Since overlap occupies such a central place in this method, it is important to point out some of the unhappy consequences of its neglect. Löwdin³⁵ seems to be the first to stress the significance of the fact that terms preventing collapse in crystal cohesive energy calculations require its retention. He further sketched the general procedure generally used in practical calculations, also indicating the usefulness of MO in an orthogonalized basis, or Löwdin orbitals. These permit easy approximate computation of derived quantities, such as transition moments.

Ruedenberg³⁶ observed that neglect of overlap "worked" for aromatic hydrocarbons only because of a fortunate coincidence related to the size of typical carbon p- π overlap integrals and the maximum number of near neighbors per atom. Lipscomb,¹⁵ *et al.*, appear to be the first to encounter a practical case where retention of the overlap matrix was indispensable to the mathematical or computational stability of the problem. Coulson and Schaad³⁷ then showed that neglect of overlap is incompatible with variation of the atomic

orbitals in a molecular calculation. While it may be possible to arrange a method to include explicit electron repulsion terms in a way that tolerates neglect of overlap without collapse of the mathematical structure, it hardly seems logically consistent to do so.

Numerical Consistency Checks. A simple test of the internal consistency of this calculation method is to invert the MO calculation and compare the atomic orbital parameters (H_{ii}) deduced from molecular ionization potentials with those derived from atomic spectra. Nitrogen (N₂) provides an easy test. Using the observed distance and SCF zeds, the π ionization implies an H_{pp} of -14.7 ev. Assuming this to apply to the p- σ orbitals also, the available σ ionization potentials are best fit by $H_{ss} = -22.5$. Valence-state data suggest H_{pp} at about -13.5 and H_{ss} near -25.5 ev. From the π system of ethylene, the carbon H_{pp} should be -9.08, from acetylene, -9.76 *vs.* a spectral value of -10.5, about what would be extrapolated for a closed-shell C₂.

Suitability for Spectra. A quantitatively satisfactory treatment of molecular spectra has been achieved only by exhaustive calculation for very small molecules. Those few cases suggest that valence shell atomic orbitals are insufficient for many easily observed transitions, throwing open the question of determining the conditions necessary for the extra valence shell virtual orbitals to be physically significant. The simple straightforward computation using eq 16 has already been used by Boudreaux³⁸ to give a good account of the reflectance spectra of cupric nitrate.

A procedure for including an augmented set of basis orbitals has been tested on the problem of the relative importance of 3s, 3p, 3d, 4s, and 4p orbitals for phosphorous in PF₅. Real progress in this type of application will require mutually supporting theoretical and experimental study of a few pilot molecules to learn enough about the actual energy levels, preferably including accurate *ab initio* treatments of spectroscopic quality.

Self-Consistency Problems. Nonpolar molecules are reasonably well described by calculations in which the H_{ii} are fixed. Self-consistent methods, such as the technique developed by Carroll, Armstrong, and McGlynn,²⁴ while very good for ionization potentials and showing great potential in understanding molecular energy levels, become very laborious for medium-

(35) P. O. Löwdin, *J. Chem. Phys.*, **18**, 365 (1950).

(36) See ref 3b.

(37) C. A. Coulson and L. J. Schaad, *J. Chem. Phys.*, **35**, 294 (1961).

(38) E. A. Boudreaux, 20th Southwest Regional Meeting of the American Chemical Society, Shreveport, La., Dec 1964, Paper 157.

sized molecules. Suitable Madelung-type terms would certainly speed convergence, but the whole problem of iterative solution needs careful study to determine generally efficient numerical methods for obtaining convergence in at most two or three cycles. Considerable saving in time can be achieved by neglecting changes in the zeds of the atomic orbitals during the iteration.

Conclusion

Reasonable precision in approximating the theoretically important one-electron terms of the LCAO-MO method leads to a useful and theoretical presentable one-electron model. Compatible features and approximations include the following. (1) Ignore inner shells, start with free atom or ion orbitals. (2) Use empirically corrected VSIP for H_{ii} parameters. (3) Do not invest great effort in achieving iterative self-consistency unless Madelung-type terms are included. (4) Approximate H_{ij} by expression 16 with precautions to ensure rotational invariance. (5) Take the sum of orbital energies as approximately proportional to the total energy, aware that distances may be distorted. (6) Use Koopman's theorem to relate orbital energies to molecular ionization potentials.

Questionable practices with uncertain consequences are the following. (1) Mix models by using hybrids or other arbitrary orbitals to represent a ligand such as H_2O or NH_3 . Extensive rearrangement from free-molecule orbitals is expected for such ligands, while the assumption of localized pairs or classical hybridization is treacherous, particularly for spectra. (2) Assume properties calculated at the standard geometry are those which would be predicted at the calculated equilibrium distances. Approximation 5 above is inconsistent with equilibrium distance or force constant prediction, but the distances it suggests vary regularly within families.

Acknowledgment. We have profited from discussions with Professors Klaus Ruedenberg, Roald Hoffmann,

and Sean McGlynn. This work was supported in part by American Cancer Society Grant E-347 and in part by the Tulane Computer Laboratory.

Appendix

Two-Center One-Electron Integrals. Glossary of Abbreviations

NP	Number of distances
N1	Principal quantum number of first basis function
N2	Principal quantum number of second basis function
N3	Principal quantum number of third basis function
ZA(1)	Orbital exponent of first basis function, atom A
ZA(2)	Orbital exponent of second basis function, atom A
ZA(3)	Orbital exponent of third basis function, atom A
LA	Angular momentum quantum number for orbitals, atom A
CA1	Coefficient of first A basis function in orthogonal orbital
CA2	Coefficient of second A basis function in orthogonal orbital
CA3	Coefficient of third A basis function in orthogonal orbital
TAA	One-center kinetic integral for a basis function of highest N
VAA	Average value of $1/R$ for same basis function, one center
OTAA	Kinetic integral, orthogonalized function, one center
OVAA	Average $1/R$, orthogonalized function, one center
R	Interatomic distance in atomic units (bohrs)
MQ	Magnetic quantum number, M
OTT	Ratio of kinetic integral between orthogonal orbitals to average of one-center kinetic terms
OSQ	Square of overlap integral between orthogonalized orbitals
STT	Ratio of two-center to average one-center kinetic terms, functions of highest N
SSQ	Square of overlap integral between outer Slater-type orbitals
OS	Overlap between orthogonalized orbitals
OA	Average of $1/RA$, orthogonalized orbitals, two center
OB	Average of $1/RB$, orthogonalized orbitals, two center
S	Overlap between Slater-type orbitals of highest N
SA	Average of $1/RA$, Slater-type outer orbitals, two center
SB	Average of $1/RB$, Slater-type outer orbitals, two center
	Except when noted otherwise, orbitals of Clementi and Raimondi were used, but with Schmidt orthogonalization.

Spectroscopic Studies of Self-Association Due to Hydrogen Bonding¹

by Surjit Singh and C. N. R. Rao²

Department of Chemistry, Indian Institute of Technology, Kanpur, India (Received August 29, 1966)

Thermodynamics of dimerization of alcohols, phenols, amines, thiophenol, and haloforms have been examined by employing infrared and nmr spectroscopy. The energies of various types of hydrogen bonds have been compared.

The energy of a hydrogen bond $X-H \cdots Y$ depends on the electronegativity of X and Y as well as other environmental factors. In recent years, self-association due to hydrogen bonding has been studied in a number of hydroxylic compounds forming $O-H \cdots O$ bonds employing infrared,³ nmr,⁴ and electronic⁵ spectroscopy. The thermodynamics of self-association of alcohols has been quantitatively investigated in detail,^{6,7} and the results show that the hydrogen-bond energies in aliphatic alcohols are in the order methanol > ethanol > 2-propanol > *t*-butyl alcohol. Although uncertainties of the energy values are rather large, it appears likely that the trend in ΔH° may reflect the steric or electronegativity effects on the strength of the hydrogen bonds. Preliminary studies of trifluoroethanol⁸ indicated that trifluoroethanol was considerably less associated than ethanol. In the light of these observations, it was considered worthwhile to study quantitative aspects of the self-association of fluoro alcohols to examine the effect of acidity of the alcohols on the thermodynamic quantities. In addition, we have also determined the thermodynamics of self-association of substituted phenols of varying acidity.

Earlier studies^{9,10} indicated that sterically hindered alcohols and phenols are considerably less associated. The small magnitude of self-association of sterically hindered hydroxy compounds may be due to either the low enthalpy or the entropy contributions to the free energy. Since no quantitative thermodynamic data are available in the literature on the self-association of hindered hydroxy compounds, we have examined the self-association of a hindered alcohol and a phenol.

There is little information in the literature on the enthalpies of self-association due to hydrogen bonds other than the $O-H \cdots O$. We have now studied the

thermodynamics of self-association of amines, mercaptans, and haloforms in order to obtain energies of $N-H \cdots N$, $S-H \cdots S$, and $C-H \cdots X$ (X for halogen) bonds.

Experimental Section

All of the chemicals employed in the study were of analytical grade and were further purified before use. The self-association of all of the systems with the exception of thiophenol was studied by the variation of the intensity of X-H stretching and the first overtone bands. A Carl Zeiss UR-10 spectrophotometer (LiF prism) and a Cary 14-R spectrophotometer fitted with a variable-temperature cell compartment were employed for recording the infrared spectra in the X-H stretching and the overtone regions, respectively. Association of thiophenol was studied by a Varian A-60 nmr spectrometer.

Optical densities of the first X-H overtone band were determined at the absorption maxima for several concentrations and extinction coefficients calculated

(1) Forms part of the Ph.D. thesis of S. Singh submitted to the Indian Institute of Technology, Kanpur.

(2) To whom all the correspondence should be addressed.

(3) C. N. R. Rao, "Chemical Applications of Infrared Spectroscopy," Academic Press Inc., New York, N. Y., 1963.

(4) J. A. Pople, H. J. Bernstein, and W. G. Schneider, "High Resolution Nuclear Magnetic Resonance," McGraw-Hill Book Co., Inc., New York, N. Y., 1959.

(5) C. N. R. Rao, "Ultraviolet and Visible Spectroscopy," Butterworth and Co. Ltd., London, 1961.

(6) U. Liddel and E. D. Becker, *Spectrochim. Acta*, **10**, 70 (1957).

(7) J. C. Davis, Jr., K. S. Pitzer, and C. N. R. Rao, *J. Phys. Chem.*, **64**, 1714 (1960).

(8) B. D. N. Rao, P. Venkateswarlu, A. S. N. Murthy, and C. N. R. Rao, *Can. J. Chem.*, **40**, 387 (1962).

(9) F. A. Smith and E. C. Creitz, *J. Res. Natl. Bur. Std.*, **46**, 145 (1951).

(10) B. G. Somers and H. S. Gutowsky, *J. Am. Chem. Soc.*, **85**, 3065 (1963).

from Beer's law. The concentration was 0.01–0.30 M in the case of alcohols and phenols, 0.02–0.8 M in the case of haloforms, and 0.05–1.0 M in the case of amines. Equilibrium constants, K , of dimerization were determined employing the method of Liddel and Becker.⁶ The equilibrium constant is related to the slope of the plot of the apparent molar extinction coefficient, ϵ_m , against the concentration, c

$$\left(\frac{d\epsilon_m}{dc}\right)_{c=0} = 2K_c\epsilon_m^0 \quad (1)$$

where ϵ_m^0 is the molar extinction coefficient of the monomer X–H stretching or overtone band extrapolated to infinite dilution ($c = 0$) and K_c is the equilibrium constant of dimerization in liters per mole.

The use of the limiting-slope method in the evaluation of K_c is illustrated in Figure 1. Similar curves are found with both CCl_4 and benzene solvents, although the K_c value in benzene is lower than in CCl_4 . Equation 1 holds good only for cyclic dimers. For open dimers, if one assumes that the absorption coefficient of the open dimer is $r \times \epsilon_m^0$, the equilibrium constant is given by

$$K_{\text{open}} = \frac{2}{2-r} K_{\text{cyclic}} \quad (2)$$

For the particular case where $r = 1$, $K_{\text{open}} = 2K_{\text{cyclic}}$. It can be seen that the K_{open} and K_{cyclic} are proportional to each other. Even if the assumption regarding the structure of the dimer is wrong, the value of the enthalpy of dimerization, ΔH° , will not be affected⁶ since this is obtained from a linear plot of $\log K$ against $1/T$ (Figure 2). The energy per hydrogen bond will, however, be different, depending on whether the dimer is linear or cyclic.

The equilibrium constants were calculated assuming closed dimers in all the cases at several temperatures in the range of 5–50° and the enthalpy of hydrogen bonding was calculated (see Figure 2 for typical plots). The values of equilibrium constants are correct to $\pm 10\%$. Only two values of K are mentioned in Table I as well as in the text for purpose of brevity. The uncertainty in ΔH° is ± 0.5 kcal mole⁻¹ and the uncertainty in $\Delta\nu_{\text{OH}}$ is ± 5 cm⁻¹.

Results and Discussion

Alcohols and Phenols. Thermodynamic data for the dimerization of two fluoro alcohols are compared with the data on the corresponding unfluorinated alcohols in Table I. The enthalpy values are considerably lower for the more acidic fluoro alcohols. However, the ΔH° values for other aliphatic alcohols^{6,7} are not in line with the data for the fluoro alcohols when cor-

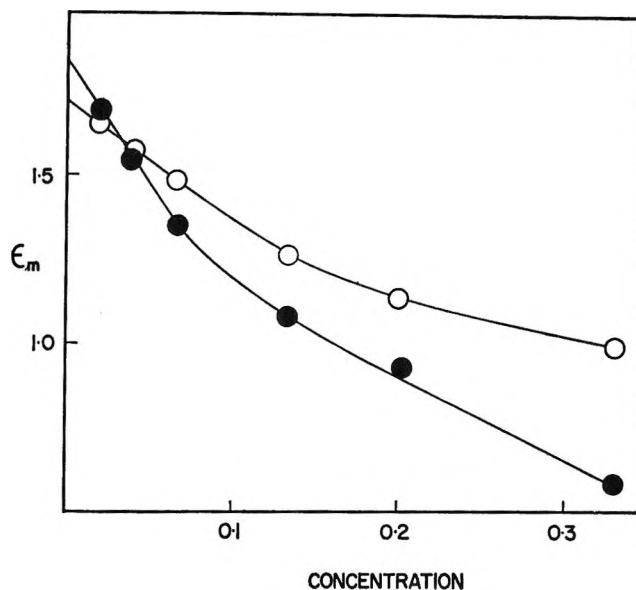


Figure 1. Plot of the extinction coefficient of the monomer O–H stretching first overtone band of 2-propanol vs. concentration (solvent CCl_4) in moles per liter: open circles, 40°; filled circles, 10°.

Table I: Thermodynamics of Dimerization of Alcohols and Phenols (ROH)

ROH	pK_a	K_{25° , l. mole ⁻¹	K_{40° , l. mole ⁻¹	$-\Delta H^\circ$, kcal mole ⁻¹	$\Delta\nu_{\text{OH}}$, cm ⁻¹
C_2H_5^a	16.0	0.39	0.26	5.0	125
CF_3CH_2^a	12.4	0.19	0.14	3.8	230
$n\text{-C}_3\text{H}_7^b$	17.0	1.25	1.00	2.6	125
$\text{CF}_2\text{HCF}_2\text{CH}_2^a$	12.7	0.22	0.20	1.2	195
$\text{C}_6\text{H}_5^{b,c}$	9.95	0.74	0.49	5.1	120
$4\text{-ClC}_6\text{H}_4^b$	9.38	2.20	1.70	3.2	170
$4\text{-CH}_3\text{OC}_6\text{H}_4^b$	10.20	3.00	2.20	3.8	150
$2,6\text{-di-}i\text{-C}_3\text{H}_7\text{C}_6\text{H}_3^b$...	0.53	0.27	8.4	260
$(i\text{-C}_3\text{H}_7)_2\text{-C-C}_2\text{H}_5^b$...	1.00	0.43	10.0	127

^a In benzene solvent; benzene has been used as the solvent owing to the poor solubility of the fluoro alcohols in CCl_4 . The K value as well as the $-\Delta H^\circ$ of ethanol has been found to be lower in benzene solvent than in CCl_4 .⁷ It may not be unreasonable to compare the K and ΔH° values for the self-association of a series of alcohols in benzene solvent although there may be some O–H... π bonding. ^b CCl_4 solvent. ^c M. M. Maguire and R. West, *Spectrochim. Acta*, **17**, 369 (1961).

related with the pK_a values. This is probably because in halogen-substituted alcohols, the halogen atoms may competitively form hydrogen bonds. The same problem would arise in any alcohol where the acidity is changed by substitution with electron-withdrawing groups. It is also possible that there will be no simple relation between the acidity of alcohols

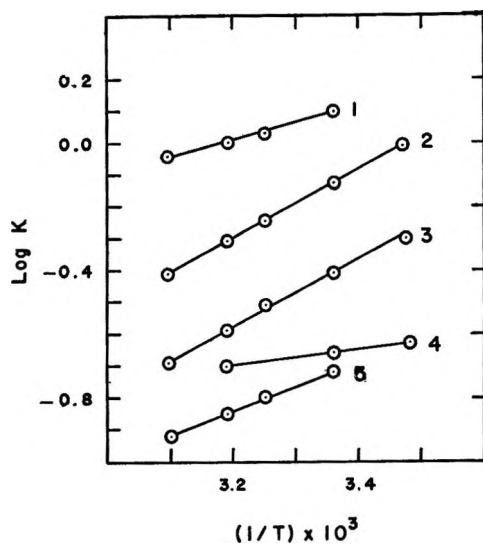


Figure 2. Plots of $\log K$ vs. $1/T$ for various alcohols (ROH): 1, C_3H_7 ; 2, C_6H_5 ; 3, C_2H_5 ; 4, $CF_2HCF_2CH_2$; 5, CF_3CH_2 .

and their self-association equilibria since the same oxygen atom serves as the donor as well as the acceptor site in self-association. The more acidic alcohols, however, form appreciably strong hydrogen bonds with other electron donors.^{11,12}

The $\Delta\nu_{OH}$ values are greater in the fluoro alcohols even though the enthalpy values are lower (Table I). Similar absence of proportionality between $\Delta\nu_{OH}$ and ΔH° has been noticed in the earlier studies of self-association of aliphatic alcohols by Liddel and Becker.⁶ There appears to be no reason why $\Delta\nu_{OH}$ should be linear with respect to ΔH° , particularly when different alcohols are involved. The magnitude of ΔH° is determined by the $O \cdots O$ distance and the linearity between $\Delta\nu_{OH}$ and ΔH° should be expected only in a comparable range of $R_{O \cdots O}$.¹³ Recent studies of hydrogen bonding in various donor-acceptor systems in this laboratory¹¹ have also indicated that the linear $\Delta\nu_{OH}-\Delta H^\circ$ relation is found for the interaction of an acceptor with donors of comparable basicity. The linearity particularly fails in the interaction of sterically hindered hydroxy compounds with donors.¹⁴

Data on the dimerization of a few substituted phenols of varying acidity (Table I) show that the K and ΔH° of hydrogen bonding do not vary systematically with the pK_a values of phenols just as in the case of aliphatic alcohols. The thermodynamics of hydrogen bonding of substituted phenols with other donor molecules have, however, been found to vary linearly with their acidity.¹¹

Sterically Hindered Alcohols and Phenols. The highly hindered 2,6-di-*t*-butylphenol and 2,2,4,4-tetramethyl-3-isopropyl-3-pentanol show no evidence of self-

association and remain monomeric even in the pure state. In these hydroxylic compounds, the δ_{OH} in the nmr and the ν_{OH} in the infrared spectra were found to be concentration independent. The slightly less hindered 2,6-diisopropylphenol and 2,4-dimethyl-3-ethyl-3-pentanol show some dimerization and the thermodynamic data on the self-association values of these two hydroxy compounds are given in Table I. The enthalpy values for the self-association of these hindered hydroxy compounds are comparable to those of simple alcohols and phenols. These results clearly show that the low values of equilibrium constants are mainly due to entropy contributions to the free energy ($\Delta F^\circ = \Delta H^\circ - T\Delta S^\circ$). The $\Delta\nu_{OH}$ value for the association of 2,6-diisopropylphenol is much greater than that found for phenol (120 cm^{-1}) and the $\Delta\nu_{OH}$ for 2,4-dimethyl-3-ethyl-3-pentanol is comparable to that for *t*-butyl alcohol (124 cm^{-1}).

In the evaluation of the equilibrium constants for the dimerization of alcohols and phenols, the cyclic structure for the dimer has been assumed. In the hindered alcohols, however, there is a good possibility that the dimers are linear. If this is true, the enthalpy data from the present study indicate that a linear hydrogen bond in the open dimer is as strong as two bent hydrogen bonds in the cyclic dimer. Further, the enthalpy values for dimerization reported here for the hindered alcohol and phenol are more reliable since higher polymers were totally absent in these cases unlike in simple alcohols.⁷

Amines. The only reliable value of the enthalpy of dimerization for amines is that of aniline ($-1.6\text{ kcal mole}^{-1}$) determined by Lady and Whetsel.¹⁵ From the equilibrium constant data of Lady and Whetsel¹⁶ on *N*-methylaniline, an enthalpy value of $-2.1\text{ kcal mole}^{-1}$ was calculated for its dimerization. The self-association of di-*n*-butylamine has now been examined and the K values at 25 and 40° were found to be 0.13 and 0.12 l. mole⁻¹, respectively, in carbon tetrachloride solution. Triplicate determinations of the equilibrium constants at three temperatures showed that the enthalpy value was of the order of 1.0 kcal mole⁻¹. It is noteworthy that the enthalpy values for the self-association of amines are considerably

(11) S. Singh, A. S. N. Murthy, and C. N. R. Rao, *Trans. Faraday Soc.*, **62**, 1056 (1966).

(12) A. Balasubramanian and C. N. R. Rao, *Spectrochim. Acta*, **18**, 1337 (1962).

(13) E. R. Lippincott and R. Schroeder, *J. Phys. Chem.*, **61**, 921 (1957).

(14) S. Singh and C. N. R. Rao, *J. Am. Chem. Soc.*, **88**, 2142 (1966).

(15) J. H. Lady and K. B. Whetsel, *J. Phys. Chem.*, **68**, 1001 (1964).

(16) J. H. Lady and K. B. Whetsel, *ibid.*, **69**, 1596 (1965).

lower than those for the corresponding hydroxylic compounds.

Thiophenol. Although it has been pointed out that thiophenol undergoes weak dimerization,¹⁷ no thermodynamic data are available for its self-association. The δ_{SH} of thiophenol in the nmr spectra varies linearly with mole fraction in the entire 0–1 mole fraction range and the association shifts are 0.29 and 0.26 ppm, respectively, at 21 and 35° in carbon tetrachloride solution. Making use of these association shifts, the $-\Delta H^\circ$ for the dimerization of thiophenol is estimated to be about 1.2 kcal mole⁻¹. This enthalpy value is close to the value of 1.0 kcal mole⁻¹ estimated for the dimerization of phosphinodithionic acid.¹⁸

Haloforms. Becker¹⁹ pointed out that chloroform forms dimers by self-association. Jumper and co-workers^{20,21} have found the dimerization constant for chloroform by nmr to be ~ 0.01 l. mole⁻¹ in carbon tetrachloride at $\sim 25^\circ$. Calculations based on the infrared data of Becker on the C–H stretching band of chloroform give an equilibrium constant of dimerization of ~ 0.3 l. mole⁻¹ if the method of Liddel and Becker⁶ is employed for the calculations. Since no bonded C–H peak is seen due to the association of chloroform, the equilibrium constant was also evaluated by the method of Spurr and Byers,²² where the contribution from dimers to the intensity of the band is also taken into consideration. The K value thus calculated for the association of chloroform with Becker's data was found to be 0.01 l. mole⁻¹. In the present study, the K values for the dimerization of chloroform and bromoform were determined⁶ by a study of the concentration dependence of the intensity of the first overtone of the C–H stretching band. The data in CCl₄ solvent are given in Table II.

Table II

	K_{250} , l. mole ⁻¹	K_{400} , l. mole ⁻¹	$-\Delta H^\circ$, kcal mole ⁻¹
Chloroform	0.13	0.10	3.2
Bromoform	0.62	0.57	1.0

While the individual values of the equilibrium constants may vary with the method of evaluation, the enthalpy values for the dimerization will remain nearly the same. The ΔH° of dimerization found for chloroform is considerably greater than for bromoform, although the equilibrium constant is higher in the latter case. The nmr association shift of bromoform (0.95

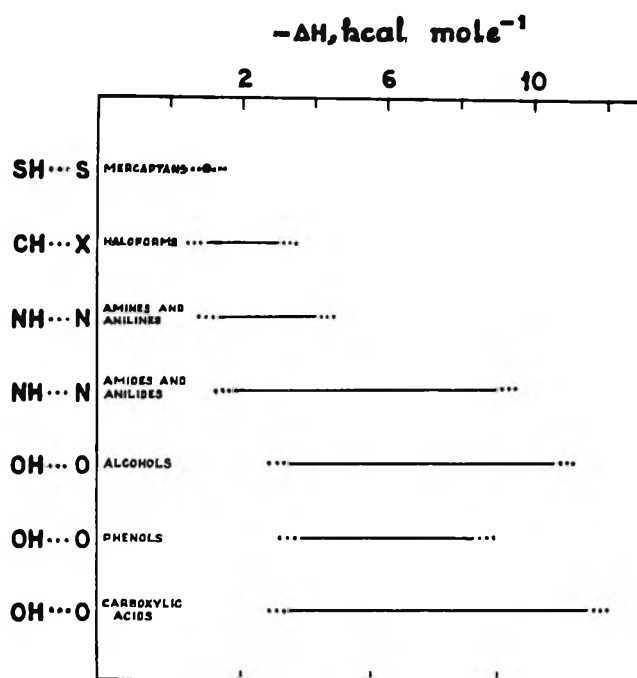


Figure 3. Energy ranges for various types of hydrogen bonds formed by self-association.

ppm) is also greater than that of chloroform (0.28 ppm) in cyclohexane solvent.

Concluding Remarks

The energy ranges for various types of hydrogen bonds caused by self-association, after taking into consideration all the data available in the literature,²³ are shown in Figure 3. Even though there is no simple trend in the energy ranges, a comparison of the hydrogen-bond energies found in systems of related structures shows (Figure 3) the energy order of O–H...O > N–H...N > S–H...S, a trend which has been found by Singh, Murthy, and Rao¹¹ in donor-acceptor hydrogen bonding. This trend is similar to what one would expect from electronegativity considerations.²³ The energies found for the CH...X bonds in the self-association of haloforms do not fall in line.

(17) B. D. N. Rao, P. Venkateswarlu, A. S. N. Murthy, and C. N. R. Rao, *Can. J. Chem.*, **40**, 963 (1962).

(18) J. Allen and R. O. Colclough, *J. Chem. Soc.*, 3912 (1957).

(19) E. D. Becker, *Spectrochim. Acta*, **743** (1959).

(20) B. B. Howard, C. F. Jumper, and M. T. Emerson, *J. Mol. Spectry.*, **10**, 117 (1963).

(21) C. F. Jumper, M. T. Emerson, and B. B. Howard, *J. Chem. Phys.*, **35**, 1911 (1961).

(22) R. A. Spurr and H. F. Byers, *J. Phys. Chem.*, **62**, 425 (1952).

(23) G. C. Pimentel and A. L. McClellan, "The Hydrogen Bond," W. H. Freeman and Co., San Francisco, Calif., 1960.

It is quite likely that the carbon atom in haloforms is much more electronegative owing to the presence of the highly electron-withdrawing CX_3 groups.

Acknowledgments. The authors' thanks are due to the Council of Scientific and Industrial Research, India, for a research grant.

Hydrothermal Aging of Silica-Alumina Cracking Catalysts

by Arpad Elo, Jr., and Porter Clements

Catalyst Division, Nalco Chemical Company, Chicago, Illinois 60629 (Received September 6, 1966)

A logical consequence of the steam deactivation mechanism proposed by Schlaffer, Morgan, and Wilson is that stability to steam should be inversely related to virgin surface area. When several catalysts were steamed for times between 0.18 and 199 hr at temperatures between 568 and 746° and pressures between 1.0 and 7.7 atm, the expected inverse relationship was found. At the most severe steaming conditions, an unexpected dramatic reduction was found in the pore volume as measured with carbon tetrachloride; however, the pore volume as measured with water remained high, and skeletal density measurements show that the phenomenon reflects the formation of trapped voids rather than catastrophic structural collapse.

Introduction

The physical structure of silica-alumina catalysts is generally thought to consist of loose, irregular aggregates of spheroidal ultimate particles. To account for the BET surface areas of fresh catalysts, the ultimate particles would need to have diameters of about 50 Å, and particles of this size have been observed with the electron microscope.^{1,2} The pore volume of the catalyst must then consist of the interstices in the primary aggregates of these ultimate particles. If lower orders of aggregation exist within the 50-Å particles, the interstices are of dimensions too small to admit the hydrocarbon molecules whose reaction is to be catalyzed or the adsorbate molecules used for measuring the surface properties. In this sense, it is useful to regard the 50-Å particles as the ultimate particles.

Numerous investigators have studied the hydrothermal aging of silica-alumina catalysts. Inasmuch as it is generally acknowledged that, for any given conventional silica-alumina composition, catalytic activity is directly proportional to surface area, the term

"deactivation" has frequently been used as synonymous with loss of surface area. Ries³ showed that in steam deactivation large decreases in surface area are not accompanied by correspondingly large decreases in pore volume, whereas in thermal deactivation in the absence of steam the pore radius (strictly, the ratio of pore volume to surface area) remains relatively constant. Ashley and Innes,² and later Adams and Voge,¹ presented electron micrographs to support the view that the loss of surface area results from the coalescence of numbers of ultimate particles to form larger spheroidal bodies. Schlaffer, Morgan, and Wilson⁴ studied the kinetics of thermal and steam deactivation, reaching the conclusion that the mechanism is the same for both processes, the presence of steam serving merely to hasten the process of thermal deactivation. They

- (1) C. R. Adams and H. H. Voge, *J. Phys. Chem.*, **61**, 722 (1957).
- (2) K. D. Ashley and W. B. Innes, *Ind. Eng. Chem.*, **44**, 2857 (1952).
- (3) H. E. Ries, Jr., *Advan. Catalysis*, **4**, 87 (1952).
- (4) W. G. Schlaffer, C. Z. Morgan, and J. N. Wilson, *J. Phys. Chem.*, **61**, 714 (1957).

postulated that deactivation proceeds at first by the growth of fillets between adjacent particles, and in more advanced stages by the formation of larger ultimate particles at the expense of smaller ones. Inasmuch as the rate of material transport in such a process is inversely related to particle diameter, a consequence of this hypothesis is that steam stability should be inversely related to virgin surface area. The present study was undertaken to test this point. As the work progressed, there emerged a new picture of the processes of steam and thermal deactivation, differing in several important respects from that envisioned by previous workers. Evidence and arguments supporting the new model are presented below.

Experimental Section

Six commercial synthetic fluid cracking catalysts were selected for study. This group represented compositions in which the alumina content ranged from 13 to 40%, virgin surface areas from 400 to 550 m²/g, and pore volume from 0.7 to 0.96 ml/g. Chemical properties of the catalysts are shown in Table I.

Table I: Chemical Properties of Virgin Catalysts^a

	Catalyst					
	I	II	III	IV	V	VI
Al ₂ O ₃	25.6	27.0	27.3	14.2	13.4	41.7
Na ₂ O	0.022	0.028	0.031	0.025	0.050	0.041
SO ₄ ²⁻	0.38	0.44	0.36	0.55	<0.2	0.48
Fe	0.016	0.026	0.032	0.017	0.025	0.024

^a Volatile-free basis, based on ignition at 980°.

Steaming was conducted under pressure in a 2-in. diameter stainless steel tube mounted vertically in an electrically heated furnace (see Figure 1). Deionized water was introduced at the bottom of the tube and vaporized in the hot zone below the catalyst support grid. Water flow rates were chosen to give an upward flow of steam at approximately 20 times the calculated minimum fluidization velocity at system temperature and pressure.

The upper section of the tube contained an internal disengager assembly which permitted separation of steam from the catalyst before condensation could occur. Uniform control of steaming pressure was achieved by means of a back-pressure regulator connected to the outlet of the effluent steam condensing coil. Furnace temperature was automatically controlled, and catalyst bed temperature was monitored continuously by means of a thermocouple installed in a thermowell extending axially through the steaming tube.

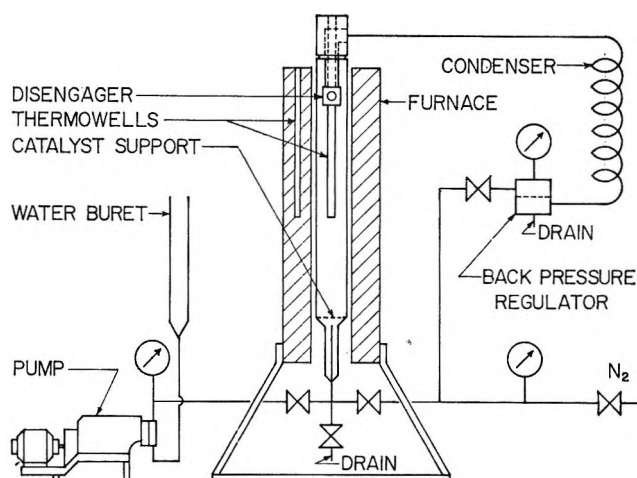


Figure 1. Apparatus for steam deactivation.

Catalyst samples were dried for about 16 hr at 204° before steaming; this treatment was intended to minimize "self-steaming" during the period when the catalyst was being heated to the steam deactivation run temperature. The steaming tube was charged with approximately 1 l. of catalyst and mounted in the furnace while the latter was at or near room temperature. Dry nitrogen was passed over the catalyst while the furnace was brought to operating temperature. The back-pressure regulator was then set to maintain the desired pressure, and the system was brought to this pressure with nitrogen. The water pump was started, and the steaming period was considered to have begun when the first drop of condensate appeared at the system outlet. At the end of the steaming period, the system pressure was reduced to 1 atm, and the catalyst was purged with nitrogen while cooling to room temperature.

Surface areas were determined by a single-point modification of the BET method.⁵ Pore volumes were determined both by carbon tetrachloride adsorption⁶ and by titration with water.⁷ The virgin surface properties were taken to be those measured after 2 hr calcination in air at 565°. Electron micrographs were made with an RCA Model EMU-2D instrument operated at maximum magnification. Samples were ground to less than 1 μ before examination; nevertheless, useful observations could be made only at the edges of the particles. In order to avoid damage to the catalyst under observation, it was necessary to

(5) Catalyst Division, Nalco Chemical Co., "Methods for the Analysis and Testing of Catalysts," Chicago, Ill., 1964.

(6) H. A. Benesi, R. V. Bonnar, and C. F. Lee, *Anal. Chem.*, **27**, 1963 (1955).

(7) W. B. Innes, *ibid.*, **28**, 332 (1956).

operate at a low beam intensity and to keep exposure times short.¹

In order to minimize the number of runs required, the steaming experiments were arranged in a factorial design,⁸ as shown in Table II. The tests on each of the six catalysts comprised a half-replicate of this design, each of the two available blocks being assigned to three of the catalysts. Center points were run for all but one of the catalysts. The range of variables was extended for two of the catalysts by the addition of "star" points at $\alpha = 1.68$. The model assumed in analyzing the results of the factorial design was

$$y = y_0(1 - k\theta^m P^n e^{B/T}) \quad (1)$$

where y is a property of the steamed catalyst, y_0 is the same property of the virgin catalyst, θ is the steaming time in hours, P is the pressure in atmospheres, T is the temperature in °K, e is the base of natural logarithms, and k , m , n , and B are constants.

Table II: Factorial Design

Treatment combination	Factor		
	A Time, hr	B Temp., °C	C Pressure, atm
(1)	0.75	600	1.5
a	48	600	1.5
b	0.75	704	1.5
ab	48	704	1.5
c	0.75	600	5.1
ac	48	600	5.1
bc	0.75	704	5.1
abc	48	704	5.1
cp	6	649	2.8
$\alpha 1 -$	0.18	649	2.8
$\alpha 1 +$	199	649	2.8
$\alpha 2 -$	6	568	2.8
$\alpha 2 +$	6	746	2.8
$\alpha 3 -$	6	649	1.0
$\alpha 3 +$	6	649	7.7

Model: $\ln(1 - y/y_0) = b_0 + b_1x_1 + b_2x_2 + b_3x_3 + \text{interactions}$;
 $x_1 = \ln(\theta/6)/2.08$; $x_2 = (1.0846 - 10^3/T)/0.061$; $x_3 = \ln(P/2.8)/0.60$;
 $\theta = \text{time, hr}$; $T = \text{temp, } ^\circ\text{K}$; $P = \text{pressure, atm}$.

In order to obtain some data on thermal deactivation for direct comparison with steam deactivation data, a few thermal deactivation runs were made on catalyst IV. For these, the material which had been calcined at 565° was further treated for 6 hr in air at 816, 871, and 927°. Recent work⁹ has shown that although thermal aging in air yields lower surface areas than does vacuum sintering at the same temperature, the ratio

of pore volume to surface area is the same for both treatments.

Results and Discussion

The surface areas determined on the deactivated catalysts are shown in Table III. The pore volumes measured with carbon tetrachloride and with water are shown in Tables IV and V, respectively. In each of these tables, the data on the first line represent the properties of the virgin catalysts.

Table III: Surface Areas of Deactivated Catalysts^a

Steaming conditions			Catalyst					
Time, hr	Temp., °C	Pres- sure, atm	I	II	III	IV	V	VI
Virgin			410	425	455	492	550	490
0.75	600	1.5	350		355			355
48	600	1.5		245		250	245	
0.75	704	1.5		300		300	280	
48	704	1.5	180		190			202
0.75	600	5.1		260		290	325	
48	600	5.1	180		170			195
0.75	704	5.1	240		215			245
48	704	5.1		45		66	75	
						80		
6	649	2.8	230	230	215	225	220	
						235		
						220		
0.18	649	2.8				415		
199	649	2.8				132		
6	568	2.8	275					
6	746	2.8	195					
6	649	1.0				275		
6	649	7.7				115		
48	600	7.7				55		
Thermal deactivation								
6	816	Dry				264		
6	871	Dry				81		
6	827	Dry				15		

^a Surface areas expressed in square meters per gram.

After attempting to fit eq 1 to the data for the individual catalysts, it was decided that the number and precision of the data points for the individual catalysts were insufficient to warrant such treatment. Since over-all response to changes in experimental variables was quite similar for all of the catalysts, the data were

(8) O. L. Davies, "Design and Analysis of Industrial Experiments," Hafner, New York, N. Y., 1956.

(9) R. M. Dobres, L. Rheume, and F. G. Ciapetta, *Ind. Eng. Chem.*, 5, 174 (1966).

Table IV: Pore Volume^a

Steaming conditions			Catalyst					
Time, hr	Temp, °C	Pressure, atm	I	II	III	IV	V	VI
Virgin			0.87	0.79	0.75	0.70	0.76	0.92
0.75	600	1.5	0.87		0.72			0.84
48	600	1.5		0.67		0.62	0.63	
0.75	704	1.5		0.64		0.61	0.60	
48	704	1.5	0.69		0.66			0.81
0.75	600	5.1		0.69		0.66	0.67	
48	600	5.1	0.82		0.68			0.82
0.75	704	5.1	0.81		0.63			0.85
48	704	5.1		0.17		0.30	0.36	
						0.41		
6	649	2.8	0.82	0.63	0.65	0.61	0.58	
			0.76			0.60		
						0.60		
0.18	649	2.8				0.67		
199	649	2.8				0.57		
6	568	2.8	0.78					
6	746	2.8	0.69					
6	649	1.0				0.61		
6	649	7.7				0.59		
48	600	7.7				0.28		
Thermal deactivation								
6	816	Dry				0.38		
6	871	Dry				0.14		
6	827	Dry				0.06		

^a In milliliters per gram, by CCl₄ adsorption.

 Table V: Pore Volume^a

Steaming conditions			Catalyst					
Time, hr	Temp, °C	Pressure, atm	I	II	III	IV	V	VI
Virgin			0.87	0.80	0.76	0.73	0.80	0.96
0.75	600	1.5	0.80		0.81			0.96
48	600	1.5		0.67		0.63	0.65	
0.75	704	1.5		0.66		0.62	0.58	
48	704	1.5	0.69		0.67			0.88
0.75	600	5.1		0.69		0.66	0.68	
48	600	5.1	0.75		0.68			0.91
0.75	704	5.1	0.75		0.64			0.90
48	704	5.1		0.49		0.54	0.57	
						0.58		
6	649	2.8	0.77	0.65	0.65	0.63	0.63	
			0.75			0.62		
						0.61		
0.18	649	2.8				0.69		
199	649	2.8				0.59		
6	568	2.8	0.78					
6	746	2.8	0.70					
6	649	1.0				0.61		
6	649	7.7				0.61		
48	600	7.7				0.51		
Thermal deactivation								
6	816	Dry				0.44		
6	871	Dry				0.15		
6	827	Dry				0.06		

^a In milliliters per gram, by water titration.

pooled, leading to the following equations for surface area (S) and carbon tetrachloride pore volume (V)

$$S = S_0(1 - 5.23\theta^{0.13}P^{0.30}e^{-2700/T}) \quad (2)$$

$$V = V_0(1 - 151\theta^{0.16}P^{0.26}e^{-7000/T}) \quad (3)$$

The interaction terms were negligible, except for the three-factor interaction in the expression for pore volume. This interaction was about as large as the main effects, and is related to the sharp break in the surface area-pore volume plots discussed below. When an attempt was made to derive a similar expression for the pore volume as measured by titration with water, all of the interaction terms were found to be of the same order as the main effects, presumably because the differences between the various pore volumes measured on a given catalyst are not much larger than the inherent error in the water titration procedure.

The above equations are to be regarded as concise summaries of the results of the experiments rather than as serious attempts to describe the kinetics of steam deactivation. The small exponents on time and pressure are in at least qualitative agreement with the

findings of others^{4,10} that the course of steam deactivation may be represented by kinetic equations for reactions having apparent orders between about 4 and 7, and that the effect of changes in steam partial pressure is small. The most striking feature of eq 2 and 3 is that the effect of temperature in reducing pore volume is much more pronounced than is its effect in reducing surface area.

Equations 2 and 3 apply to the six catalysts as a group. In order to test the hypothesis that steam stability is inversely related to virgin surface area, it is necessary to consider the responses of the individual catalysts to steaming. A convenient index of steam stability is the fraction of the virgin surface area which remains after steaming under prescribed conditions. In the present work all but one of the catalysts were tested under the "cp" steaming conditions; the corresponding value for the remaining catalyst may be calculated by interpolation. In Table VI, both meas-

(10) J. Hoogschagen and P. Zwietering, *J. Chem. Phys.*, **21**, 2224 (1953).

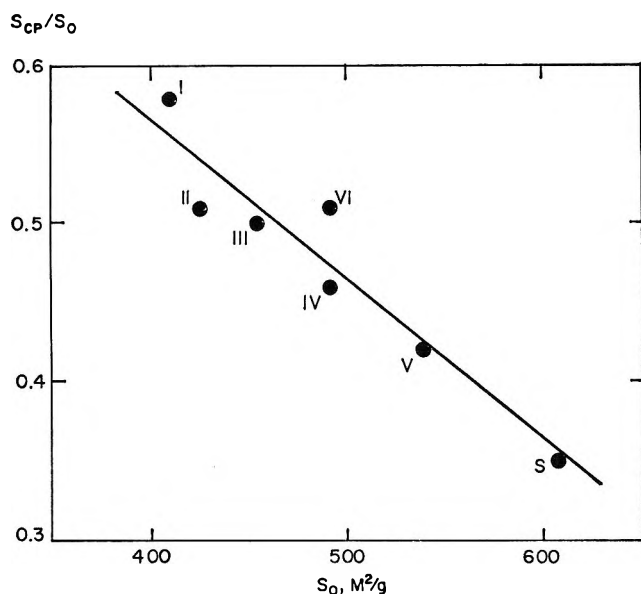


Figure 2. Inverse relationship between virgin surface area, S_0 , and steam stability, S_{cp}/S_0 . Roman numerals refer to catalysts studied in present work. Point marked S interpolated from data of Schlaffer, *et al.* (see ref 4).

ured and interpolated values of S_{cp} are given for the five catalysts on which S_{cp} was measured; the agreement between the interpolated and observed values validates the interpolation procedure. In addition to the interpolated value for the sixth catalyst, Table VI gives a value interpolated from the data of Schlaffer, *et al.*, for a catalyst with a virgin surface area higher than any of those included in the present work. The data of Table VI are plotted in Figure 2; it is evident that the expected inverse relationship between virgin surface and steam stability was found.

In Figure 3, the pore volume as measured with water is plotted against the surface area for the thermal and

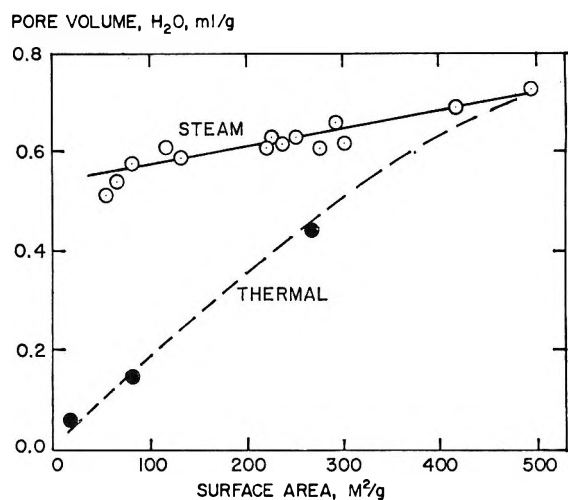


Figure 3. Relationship between surface area and pore volume as measured by water titration for catalyst IV.

hydrothermal deactivation of catalyst IV of the present study. The behavior of the other catalysts is similar; in accord with the findings of previous workers, in steam deactivation only a slight reduction in pore volume accompanies a sevenfold decrease in surface area, whereas in thermal deactivation the loss in pore volume is commensurate with the loss in surface area.

Figure 4 is a similar plot for the pore volumes as measured with carbon tetrachloride. The dramatic decrease in pore volume at surface areas below 100 m^2/g has not previously been reported for the steam deactivation of silica-alumina catalyst, although Schlaffer, Adams, and Wilson¹¹ found a similar effect in their study of the hydrothermal aging of silica gel. They attributed the effect to a major structural collapse, but that interpretation is inapplicable here, because the pore volume as measured with water is maintained at very low surface areas. An alternative explanation is offered below for the phenomena observed in the present work.

Although the packing of the ultimate particles of catalyst material is probably irregular, it can be described in terms of an average coordination number, n , the average number of particles touching each other particle. As pointed out by Kruyer,¹² for regular packings of spheres, a quasi-functional relationship exists between the coordination number and the fraction void, f . This relationship is well represented by the empirical equation

$$\log f = 0.28 - 0.80 \log n \quad (4)$$

(11) W. G. Schlaffer, C. R. Adams, and J. N. Wilson, *J. Phys. Chem.*, **69**, 1530 (1965).

(12) S. Kruyer, *Trans. Faraday Soc.*, **54**, 1758 (1958).

Table VI: Calculated and Observed Surface Areas for Centerpoint Steaming Runs

Catalyst	Surface area after "cp" steaming ^a	
	Obsd	Inter- polated
I	230	238
II	230	212
III	215	232
IV	227	228
V	220	231
VI	...	249
b	...	210

^a In square meters per gram. ^b Low alumina catalyst, virgin surface area 608 m^2/g . See ref 4.

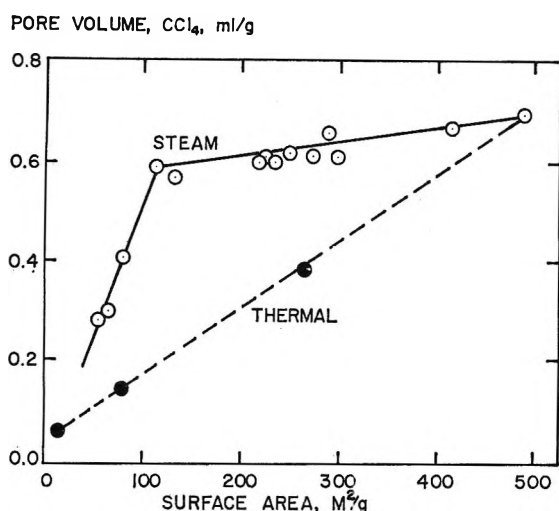


Figure 4. Relationship between surface area and pore volume as measured by carbon tetrachloride adsorption for catalyst IV.

The fraction void is related to the pore volume by

$$V = \frac{f}{\rho(1-f)} \quad (5)$$

where V is pore volume in milliliters per gram and ρ is skeletal density in grams per milliliter. Combining eq 4 and 5, the pore volume is related to the average coordination number by the empirical equation

$$\log \left(1 + \frac{1}{\rho V} \right) = 0.80 \log n - 0.28 \quad (6)$$

Figure 5 shows this relationship for a skeletal density of 2.5, a typical value for silica-alumina catalysts.

The virgin pore volumes of the catalysts used in the present study range from 0.70 to 0.96 ml/g, corresponding to average coordination numbers between 4.0 and 3.5. This result is in agreement with the finding of Wade¹³ that coordination numbers for silica gels and alumina gels fall between 3 and 5. Because the packing of the ultimate particles in virgin silica-alumina catalysts is, on the average, approximately 4-coordinated, it will be useful to consider the behavior of regular 4-coordinated packings in regard to the proposed mechanisms of steam and thermal deactivation.

The earlier stages of deactivation probably involve the growth of fillets of catalyst material between adjacent ultimate particles. Kingery and Berg¹⁴ distinguish between two classes of mechanism for fillet growth: (A) those mechanisms, exemplified by surface or vapor phase diffusion, wherein the centers of gravity of the particles remain at fixed distance while the diameter of each particle decreases; and (B) those mechanisms, exemplified by grain boundary diffusion, wherein

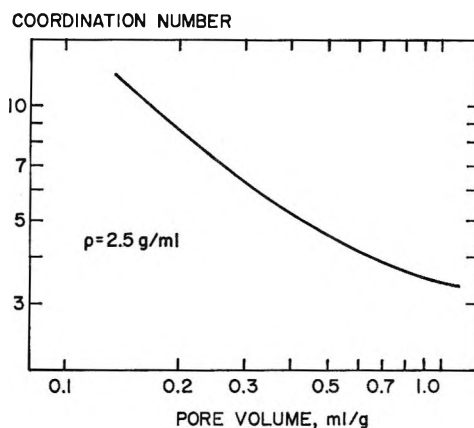


Figure 5. Relationship between pore volume and coordination number for skeletal density of 2.5 g/ml.

the diameters of the particles remain unchanged while the centers of gravity approach each other. As pointed out by Schlaffer, Morgan, and Wilson,⁴ mechanisms of class A result in the loss of surface area at constant pore volume, whereas mechanisms of class B result in the loss of pore volume along with surface area.

In steam deactivation, the reactive constancy of the pore volume at the higher surface areas constitutes an argument for a mechanism of class A, in agreement with the findings of Adams and Vogge. In thermal deactivation, the commensurate decline in surface area and pore volume constitutes an argument for a mechanism of class B.

There is no reason to suppose that either mechanism operates to the exclusion of the other. The slight positive slopes in the steam deactivation plots of Figures 3 and 4 suggest that, although a class A mechanism predominates, there is a simultaneous minor contribution from a mechanism of class B. In support of this view, it has been observed⁵ that calcination of microspheroidal cracking catalysts at 565° causes a reduction of about 6% in the average diameter of the microspheres. Further, it is well known that silica-alumina catalysts retain water at quite high temperatures, so that no matter how carefully the catalyst is predried, self-steaming cannot be ruled out in thermal deactivation. It is probably more realistic to say that both mechanisms operate at all times, and that increasing temperatures enhance the contribution of the class B mechanism while the presence of steam enhances the contribution of the class A mechanism.

It has been pointed out⁴ that fillet formation is insufficient to account for the reductions in surface area

(13) W. H. Wade, *J. Phys. Chem.*, **68**, 1029 (1964).

(14) W. D. Kingery and M. Berg, *J. Appl. Phys.*, **26**, 1205 (1955).

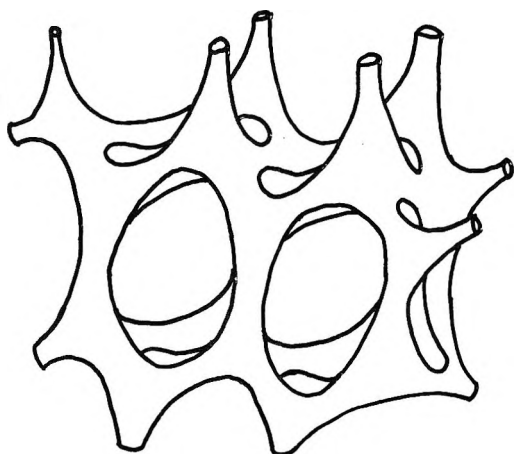


Figure 6. Toroidal stage in steam deactivation, drawn for the diamond lattice.

which have been attained experimentally. For example, the operation of either mechanism A or mechanism B on a regular 4-coordinated structure, that of the diamond, would produce eventually a toroidal form resembling that shown in Figure 6. At this stage of deactivation, the loss of surface per fillet amounts to about 8% for mechanism A or 17% for mechanism B. For a material with a virgin surface area of 500 m²/g, additional material transport would be required to attain surface areas below 350 m²/g for mechanism A or 170 m²/g for mechanism B. Previous workers have postulated that further reduction in surface area results from the complete coalescence of groups of ultimate particles. Under this interpretation, the reduction of surface area from 500 to 100 m²/g would require the coalescence of groups of about 125 particles. In view of the rather low density of the initial packing, it seems unlikely that such a process could occur without a profound effect on the pore structure of the catalyst.

If a configuration resembling that shown in Figure 6 is attained at some stage in steam deactivation, further material transport must be in the direction of the regions of lowest potential (*i.e.*, greatest concavity), the mouths of the pores. Such a process would tend to trap spherical voids by closing the mouths of the pores. Evidently, in the operation of such a process, a stage would be reached where the mouth of the pore is too small to admit a molecule of carbon tetrachloride, but still large enough to admit the smaller water or nitrogen molecules. The pore volume measurements in the present work suggest that this stage is reached in steam deactivation at a surface area somewhat below 100 m²/g.

The concept of trapped voids is not new. Wilson, *et al.*,^{15a} have observed that trapped voids occur in

catalysts which have been deactivated by commercial use, and Drake^{15b} has noted the similarity of the pore structure of steam deactivated catalysts to that of commercially deactivated catalysts. Schlaffer, Adams, and Wilson¹¹ found that for hydrothermally aged silica gel surface areas estimated from electron micrographs were significantly lower than the BET areas, suggesting that these materials, too, may have contained trapped voids.

As a further test of the hypothesis that trapped voids are formed, the skeletal densities of selected steam-deactivated samples of catalyst IV were determined by isopropyl alcohol displacement. The apparent skeletal density declined with increasing severity of steaming from 2.40 g/ml for the sample steamed for 0.18 hr at 649°, 2.8 atm, to 2.31 g/ml for the sample steamed to a surface area of 66 m²/g. Although this decline is smaller than would be expected on the basis of the difference between the pore volumes measured with water and with carbon tetrachloride on the latter sample, it should be noted that the isopropyl alcohol molecule is slightly smaller than the carbon tetrachloride molecule, and presumably could therefore penetrate a larger fraction of the partially trapped voids.

Against the proposed model stands the evidence of published electron micrographs which appear to show particle growth on steaming to diameters of sufficient magnitude to account for the reduction in BET areas observed. It is here suggested that the operation of a process such as that proposed above might produce domains of sufficient opacity to electrons to be interpreted as solid masses. The boundaries of the apparently large particles are then to be regarded rather as the boundaries of domains in which extensive fillet growth has occurred, but in which appreciable porosity remains. In Figure 7 are shown electron micrographs of catalyst IV in the virgin state and after steaming to a surface area of 115 m²/g. The corresponding particle diameters calculated from the BET areas are 52 and 222 Å, respectively. While the micrograph of the steam-deactivated catalyst shows some particles or clusters a few hundred angstroms in diameter, numerous toroidal aggregates of much smaller particles appear, and a careful examination of the original photographic negative suggests that many of the apparently large particles may in fact be such aggregates.

The proposed model is consistent with the behavior of the nitrogen adsorption isotherms determined on virgin, thermally deactivated, and hydrothermally

(15) (a) W. B. Wilson, G. M. Good, T. J. Deahl, C. P. Brewer, and W. G. Appleby, *Ind. Eng. Chem.*, **48**, 1982 (1956); (b) L. C. Drake, *ibid.*, **41**, 780 (1949).

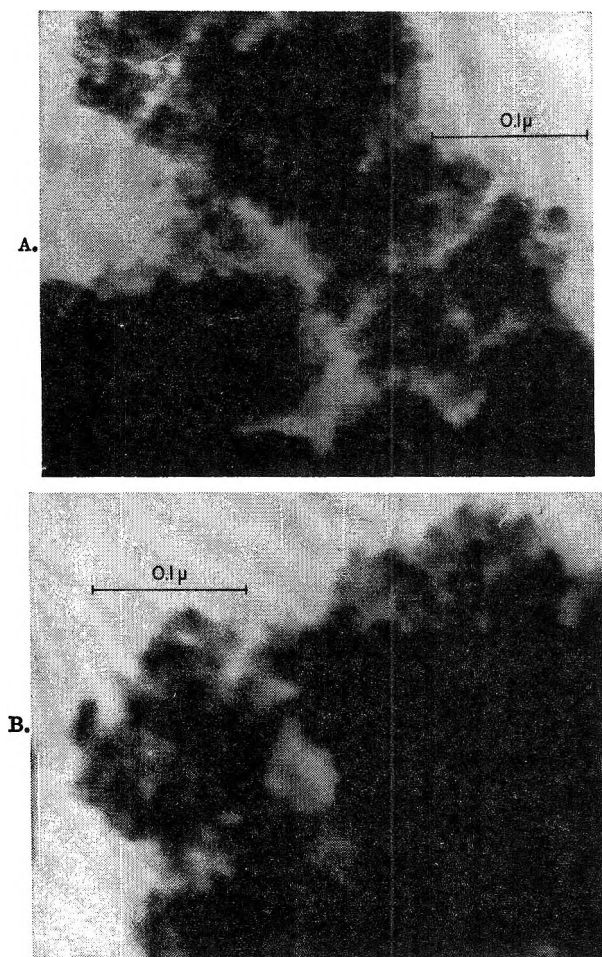


Figure 7. Photomicrographs of virgin catalyst IV (A) and catalyst IV after steaming to $115 \text{ m}^2/\text{g}$ (B).

deactivated catalysts. The interstices in any reasonably compact array of spheroids clearly constitute "ink bottle" pores.¹⁶ Kruyer¹² has shown that when 0.4-mm nonporous spheres are packed to a coordination number of about 8, the arrays exhibit hysteresis

with respect to mercury intrusion. The operation of a class A mechanism at first tends to enlarge the mouth of the pore, while the diameter of the pore interior remains nearly unchanged. Thus, on steam deactivation, the hysteresis loop should be narrowed in the direction of the higher values of P/P_0 . The operation of a class B mechanism tends to decrease the diameter of the pore mouth more rapidly than that of the pore interior. The simultaneous operation of a class A mechanism, *e.g.*, self-steaming, would oppose this tendency, maintaining a more nearly constant pore diameter. Thus, on thermal deactivation, the shape of the hysteresis loop should remain unchanged. Figure 14 of the article by Ries³ shows that these conditions are fulfilled.

Summary

The existence of the expected inverse relationship between steam stability and virgin surface area of silica-alumina cracking catalysts has been established experimentally. Steam and thermal deactivation are believed to occur by means of separate mechanisms, differing primarily in the mode of mass transport. In the presence of steam, a surface diffusion or vapor phase transport process predominates, whereas in the absence of steam a bulk diffusion process predominates. It is suggested that the trapping of voids within catalysts steamed to low surface areas may be considerably more extensive than has previously been visualized.

Acknowledgment. The authors thank S. Sokolowski for his assistance in carrying out the steam treatments, J. Shwatal for making the surface area and pore volume measurements, L. Lutwitz for making the electron micrographs, and R. C. Davidson, J. R. Polky, and B. Gaddis for their invaluable contributions to the theoretical development.

(16) J. W. McBain, *J. Am. Chem. Soc.*, **57**, 699 (1935).

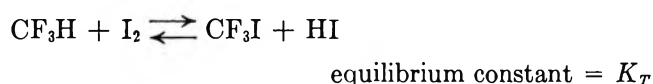
Kinetics and Thermodynamics of the Reaction between Iodine and Fluoroform and the Heat of Formation of Trifluoromethyl Iodide

by C. A. Goy, Allan Lord, and H. O. Pritchard

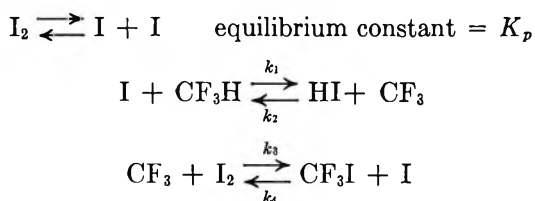
Centre for Research in Experimental Space Science, York University, Toronto, Canada
(Received September 28, 1966)

The equilibrium $\text{CF}_3\text{H} + \text{I}_2 \rightleftharpoons \text{CF}_3\text{I} + \text{HI}$ has been studied in the gas phase over the temperature range 653–802°K. The heat of this reaction is calculated to be $\Delta H_{298}^\circ = 17.10 \pm 0.17$ kcal/mole. Assuming $\Delta H_f^\circ(298)(\text{CF}_3\text{H, gas}) = -165.1$ kcal/mole, this gives $\Delta H_f^\circ(298)(\text{CF}_3\text{I, gas}) = -139.4$ kcal/mole. The equilibrium is established *via* the reaction $\text{I} + \text{CF}_3\text{H} \rightarrow \text{HI} + \text{CF}_3$, which has a rate constant $k = 10^{13.6} \exp[(-36.3 \pm 3)10^3/RT]$ cc mole⁻¹ sec⁻¹ over the temperature range 589–672°K.

In this paper we report measurements on the iodination of fluoroform which follow very closely our previous experiments on the iodination of methane.¹ An over-all equilibrium



is set up *via* the reaction sequence



Since k_3 has zero activation energy,² the over-all activation energy for the formation of CF_3I will be $\frac{1}{2}D(\text{I}_2) + E_1$. This work was complicated by the fact that commercial fluoroform contains about 0.2% CF_3Cl , which catalyzes the formation of CF_3I through the formation of Cl atoms. Thus, using the impure fluoroform, the over-all activation energy was about 40 kcal and rose to a value around 55 kcal as the CF_3Cl content was successively reduced.

Experimental Section

The experimental procedure used was identical with that used previously in the methane experiments (with the exception that in the kinetic runs a 1200-ml Pyrex vessel was used to increase the product yield somewhat).

Known amounts of CF_3H (5–10 cm pressure) and I_2 (0.25–1.0 g) were sealed in the reaction vessel and heated for the required period of time (3–350 hr for equilibrium runs, 3–135 hr for kinetic runs). The reaction was terminated by pumping the contents of the vessel into a trap containing ICN and converting the HI to HCN. The products were analyzed gas chromatographically.

Fluoroform was obtained from Matheson of Canada Ltd., and after removal of water and CO_2 , mass spectrometer analysis showed it to contain 0.2% CF_3Cl . This was removed by passing the gas repeatedly over sodium heated to 350° and after about 60 purifications the CF_3Cl content became unobservable, *i.e.*, less than 5 ppm.

Iodine was Baker's Analyzed reagent grade and was purified by sublimation *in vacuo*. No chlorine could be detected in the product by mass spectrometer analysis.

Equilibrium Measurements. In our previous experiments on methane, the equilibrium constant was calculated from the ratio $[\text{CH}_3\text{I}]^2/[\text{CH}_4][\text{I}_2]$. In the fluoroform experiments, however, the yields of products were much smaller and it was found that the CF_3I and HI (*i.e.*, HCN) were never equivalent. There appears to be a mechanism whereby the surface causes a small but variable loss of HI. Consequently, the equilibrium constants, K_T , were evaluated as the ratio

- (1) C. A. Goy and H. O. Pritchard, *J. Phys. Chem.*, **69**, 3040 (1965).
- (2) J. C. Amphlett and E. Whittle, *Trans. Faraday Soc.*, **62**, 1662 (1966).

$[\text{CF}_3\text{I}][\text{HCN}]/[\text{CF}_3\text{H}][\text{I}_2]$. Since the analysis of HI as HCN is not as reliable as the analysis for CF_3I and because of the much smaller quantities of products obtained, the results presented in Table I have a scatter about ten times larger than the corresponding methane results. The van't Hoff plot of these equilibrium constants leads to a value of ΔH°_{298} of 17.01 kcal/mole, which is in fortuitously good agreement with the more reliable value derived in Table I by third-law methods. It is known³ that CF_3 radicals attack glass and quartz to give SiF_4 , but in the present system, owing to the large concentration of I_2 present, this did not present

Table I:^a The Equilibrium $\text{CF}_3\text{H} + \text{I}_2 \rightleftharpoons \text{CF}_3\text{I} + \text{HI}$

T , °K	Log K_T	$\Delta[-(F^\circ_T - H^\circ_{298})/T]$, cal mole ⁻¹ deg ⁻¹	ΔH°_{298} , cal mole ⁻¹
802	-4.7688	-0.530	17,082
787	-4.9371	-0.560	17,346
787	-4.9928	-0.570	17,396
765	-4.8934	-0.595	16,668
762	-4.9150	-0.600	16,692
751	-5.1458	-0.618	17,231
737	-5.1645	-0.645	16,953
726	-5.2647	-0.665	17,015
714	-5.4513	-0.695	17,309
708	-5.5002	-0.710	17,316
698	-5.6479	-0.730	17,525
688	-5.5950	-0.750	17,098
684	-5.6438	-0.760	17,140
672	-5.5997	-0.780	16,702
655	-5.9060	-0.820	17,172
653	-5.8659	-0.825	16,997
		Av	17,103
		Std dev	±168

^a Free-energy functions for CF_3H , I_2 , and HI taken from ref 4; for CF_3I from P. R. McGee, F. F. Cleveland, A. G. Meister, and C. E. Decker, *J. Chem. Phys.*, **21**, 242 (1953). Further details of experimental conditions, etc., can be found in A. Lord, Ph.D. Thesis, York University, Toronto, 1967.

any serious difficulty. The production of SiF_4 was only noticed above 770°K, resulting in the progressive loss of CF_3I with time (about 1%/hr at 800°K); however, when the experiments were continued for just long enough to establish equilibrium (3 hr at 802°K), constants consistent with those found at lower temperatures were obtained.

The heat of formation of fluoroform given in the "JANAF Tables"⁴ is $\Delta H_f^\circ_{298} = -165.1$ kcal/mole. Our measurements show that there is a substantially larger difference in heat of formation between CF_3H and CF_3I than between CH_4 and CH_3I and we find $\Delta H_f^\circ_{298}(\text{CF}_3\text{I, gas}) = -139.4$ kcal/mole, subject to the same

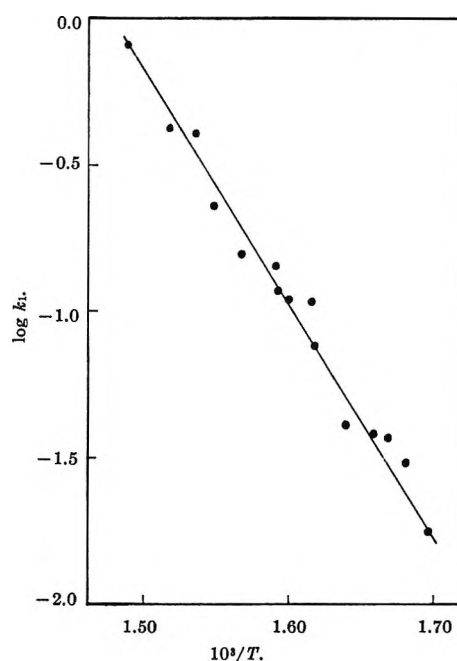


Figure 1. Arrhenius plot for the reaction $\text{I} + \text{CF}_3\text{H} \rightarrow \text{HI} + \text{CF}_3$.

uncertainties as $\Delta H_f^\circ_{298}(\text{CF}_3\text{H, gas})$ with respect to the heat of formation of HF.^{4,5}

Kinetic Measurements. The results of 15 kinetic experiments carried out in the temperature range 589–672°K give an Arrhenius plot for the rate of formation of CF_3I having an over-all activation energy of 54.5 ± 3 kcal/mole. Removing the temperature dependence of the I atom concentration⁴ from the equations through K_p (assuming perfect-gas behavior) gives $k_1 = 10^{13.6} \exp[(-36.3 \pm 3)10^3/RT]$ cc mole⁻¹ sec⁻¹; the results are shown graphically in Figure 1. A rather high frequency factor of $10^{14.95}$ was obtained for the $\text{I} + \text{CH}_4$ reaction and after allowing for a factor of 4 in the number of available hydrogens and a factor of 2 in the ratio of the collision frequencies, one might expect to get a value of A for $\text{I} + \text{CF}_3\text{H}$ of around 10^{14} cc mole⁻¹ sec⁻¹ if the same factors are operative.

The activation energy, E_2 , of the reverse reaction⁶ is 0.5 kcal/mole in the temperature range 333–523°K. Assuming E_2 is independent of temperature, we have $D(\text{CF}_3 - \text{H}) = 35.8 + D(\text{H} - \text{I}) = 106.8$ at about 625°K, or about 105.6 kcal/mole at 298°K. This is

(3) G. O. Pritchard, H. O. Pritchard, H. I. Schiff, and A. F. Trotman-Dickenson, *Trans. Faraday Soc.*, **52**, 849 (1956).

(4) "JANAF Interim Thermochemical Tables," Dow Chemical Co., Midland, Mich.

(5) J. D. Cox and D. Harrop, *Trans. Faraday Soc.*, **61**, 1328 (1965).

(6) E. Whittle, personal communication.

Table II: Dissociation on Energies Calculated from Pairs of Opposed Reactions

Reaction	E_{forward} , kcal/mole	E_{reverse} , kcal/mole	Dissociation energy (calcd), kcal/mole at 298°K
(a) $\text{CH}_3 + \text{H}_2 \rightleftharpoons \text{CH}_4 + \text{H}$	10.0 ^h	7.4 ⁱ	~102
(b) $\text{CH}_3 + \text{HCl} \rightleftharpoons \text{CH}_4 + \text{Cl}$	~2.1 ^j	3.8 ^k	~105
(c) $\text{CH}_3 + \text{HBr} \rightleftharpoons \text{CH}_4 + \text{Br}$	1.4 ^l	17.8 ^{m,n}	103.5
(d) $\text{CH}_3 + \text{HI} \rightleftharpoons \text{CH}_4 + \text{I}$	1.3 ^o	35.0 ^b	103.2
(e) $\text{CH}_3 + \text{I}_2 \rightleftharpoons \text{CH}_3\text{I} + \text{I}$	0 ^p	19.8 ^{o,q}	54.3
(f) $\text{CF}_3 + \text{I}_2 \rightleftharpoons \text{CF}_3\text{I} + \text{I}$	0 ^{c,r}	17.6 ^o	53.5
(g) $\text{CF}_3 + \text{HCl} \rightleftharpoons \text{CF}_3\text{H} + \text{Cl}$	5.1 ^c	8.4 ^f	106.3
(h) $\text{CF}_3 + \text{HBr} \rightleftharpoons \text{CF}_3\text{H} + \text{Br}$	2.9 ^c	21.1 ^r	106.0
(i) $\text{CF}_3 + \text{HI} \rightleftharpoons \text{CF}_3\text{H} + \text{I}$	0.5 ^d	36.3 ^a	105.6
(j) $\text{CF}_3 + \text{CH}_4 \rightleftharpoons \text{CF}_3\text{H} + \text{CH}_3$	10.6 ^{d,s,t,u}	10.0 ^{d,v}	102.5
(k) $\text{CF}_3 + \text{CH}_3\text{Br} \rightleftharpoons \text{CF}_3\text{Br} + \text{CH}_3$	8.3 ^u	12.5 ^w	~72
(l) $\text{CF}_3 + \text{CH}_3\text{I} \rightleftharpoons \text{CF}_3\text{I} + \text{CH}_3$	3.3 ^u	7.4 ^w	~59

^a This work. ^b Ref 1. ^c Ref 2. ^d Ref 3. ^e Ref 6. ^f Ref 7. ^g Ref 9. ^h E. Whittle and E. W. R. Steacie, *J. Chem. Phys.*, **21**, 993 (1953). ⁱ J. W. S. Jamieson and G. R. Brown, *Can. J. Chem.*, **42**, 1638 (1964). ^j R. J. Cvetanovic, F. Raal, and E. W. R. Steacie, *ibid.*, **31**, 171 (1953). ^k H. O. Pritchard, J. B. Pyke, and A. F. Trotman-Dickenson, *J. Am. Chem. Soc.*, **77**, 2629 (1955). ^l G. C. Fettis and A. F. Trotman-Dickenson, *J. Chem. Soc.*, 3037 (1961). ^m G. C. Fettis, J. H. Knox, and A. F. Trotman-Dickenson, *ibid.*, 4177 (1960). ⁿ P. Corbett, A. M. Tarr, and E. Whittle, *Trans. Faraday Soc.*, **59**, 1609 (1963). ^o E. O'Neal and S. W. Benson, *J. Chem. Phys.*, **36**, 2196 (1962). ^p M. I. Christie, *Proc. Roy. Soc. (London)*, **A244**, 411 (1958). ^q M. C. Flowers and S. W. Benson, *J. Chem. Phys.*, **38**, 882 (1963). ^r A. M. Tarr, J. W. Coomber, and E. Whittle, *Trans. Faraday Soc.*, **61**, 1182 (1965). ^s R. E. Dodd and J. W. Smith, *J. Chem. Soc.*, 1465 (1957). ^t P. B. Ayscough, J. C. Polanyi, and E. W. R. Steacie, *Can. J. Chem.*, **33**, 743 (1955). ^u W. G. Alcock and E. Whittle, *Trans. Faraday Soc.*, **61**, 244 (1965). ^v G. O. Pritchard and R. L. Thommarson, *J. Phys. Chem.*, **68**, 568 (1964). ^w D. M. Tomkinson and H. O. Pritchard, *ibid.*, **70**, 1579 (1966).

in excellent agreement with the values obtained⁷ from the bromination (106.0 kcal) and chlorination (106.3 kcal) of fluoroform, but the limits of error on our determination are unfortunately large. It seems therefore that a value of $D(\text{CF}_3 - \text{H})$ of 106.0 kcal/mole can now be accepted with some confidence. Our equilibrium measurements give the heat of formation of CF_3I relative to that of CF_3H and also the heat of formation of C_2F_6 has recently been quoted⁸ relative to CF_3H . Hence we may calculate $D(\text{CF}_3 - \text{I}) = 53.7$ kcal/mole and $D(\text{F}_3\text{C} - \text{CF}_3) = 97$ kcal/mole, both independent of any uncertainty in the heat of formation of HF ; the former value is very close to that obtained^{9,10} from a study of the pyrolysis of CF_3I (53.5 kcal) and the latter is consistent with recent shock-tube studies¹¹ on the dissociation of C_2F_6 (93 ± 4 kcal).

Discussion

There has been considerable confusion over the value of $D(\text{CF}_3 - \text{H})$ in recent years, with values ranging from 102 to 109 kcal being calculated from the difference in activation energy of pairs of opposed reactions. The present situation in respect to pairs of opposed reactions is summarized in Table II. The table seems to divide into two parts those reactions where one species involved is an atom and those in which radicals

are involved on both sides of the equation. Reaction pairs a-d give reasonably consistent values for $D(\text{CH}_3 - \text{H})$, e and f give acceptable values for $D(\text{CH}_3 - \text{I})$ and $D(\text{CF}_3 - \text{I})$, respectively, and pairs g-i, as we have already noted, give remarkably consistent values for $D(\text{CF}_3 - \text{H})$. However, reactions j, k, and l give unacceptable values for $D(\text{CF}_3 - \text{H})$, $D(\text{CF}_3 - \text{Br})$, and $D(\text{CF}_3 - \text{I})$, respectively, the error in each case being about 4 kcal, which is considerable in comparison with the individual activation energies involved. In each case, however, the reverse reaction in each pair has a frequency factor which may be regarded as "abnormal," and we feel that there may be some as yet undetermined experimental effect which causes

(7) J. C. Amphlett, J. W. Coomber, and E. Whittle, *J. Phys. Chem.*, **70**, 593 (1966).

(8) G. C. Sinke, *ibid.*, **70**, 1326 (1966).

(9) R. K. Boyd, G. W. Downs, J. S. Gow, and C. Horrex, *ibid.*, **67**, 719 (1963).

(10) The referee has pointed out that our measurement of the quantity $[\Delta H_f^{\circ 298}(\text{CF}_3\text{H}) - \Delta H_f^{\circ 298}(\text{CF}_3\text{I})] = -25.7 \pm 0.2$ kcal, taken together with the value of $D(\text{CF}_3 - \text{I}) = 53.5 \pm (?)$ kcal from ref 9 (cf. also ref 2), constitutes a determination of $D(\text{CF}_3 - \text{H}) = 105.8 \pm (?)$ kcal. We prefer to interpret it as establishing the mutual consistency of the kinetic studies on CF_3H and CF_3I ; certainly it inspires considerable confidence in them.

(11) E. T. Roux, *J. Chem. Phys.*, **43**, 2251 (1965).

the Arrhenius parameters of these reactions to be distorted from their true values. It would not appear, however, to be simply "experimental error," since in

all three cases the experiments were carefully done and, in the case of reaction j, there is agreement between independent determinations.

The Radiation Chemistry of Liquid Methane¹

by Hugh A. Gillis

Radiation Research Laboratories, Mellon Institute, Pittsburgh, Pennsylvania,
and Department of Chemistry, Western Reserve University, Cleveland, Ohio² (Received October 4, 1966)

Liquid methane at 112°K has been irradiated by Co⁶⁰ γ rays in the pure state and with small amounts of added ethylene or propylene. The effects of these olefins on products up to C₆ can be interpreted by a simple hydrogen atom scavenging mechanism. The ratios $k_{\text{dis}}/k_{\text{comb}}$ were estimated to be 1.0 for ethyl plus ethyl, 3.6 for isopropyl plus isopropyl, and 0.9 for methyl plus isopropyl. These are all much higher than gas-phase results. The isotope effect in the disproportionation reaction was found to be small ($k_{\text{H}}/k_{\text{D}} \simeq 1.1$). In experiments with CH₄-CD₄ solutions, the isotopic composition of the product ethane showed that the methylene radical is an important intermediate. In an experiment with a CD₄-C₃H₈ solution, a product of the ion-molecule reaction between CD₅⁺ and C₃H₈, for the occurrence of which there is good evidence in the gas phase, was looked for and not found.

Introduction

The radiation chemistry of gaseous methane has been investigated in a number of studies.³ Good evidence that ion-molecule reactions are important above 0.01% conversion was obtained,^{3d-f} and the important role played by product ethylene and acetylene in determining over-all product formation was stressed.^{3a-c} In studies of the radiation chemistry of solid methane, ionic reactions have been invoked to explain the production of polymer with a $G(-\text{CH}_4)$ of 0.3,⁴ and a major role was assigned to methylene radicals in the formation of ethane.⁵

This study was undertaken to determine the significance of ion-molecule reactions in the irradiated liquid and to see if a correlation could be found with results obtained in esr studies.⁶ In the course of the investigation, evidence was found which bears on the interesting question of possible temperature and phase

effects on the ratios of disproportionation to combination of alkyl radicals.

Experimental Section

Purification. The starting material was Phillips

- (1) Supported in part by the U. S. Atomic Energy Commission.
- (2) Where correspondence should be addressed. The experimental work was performed at the first address.
- (3) For example: (a) L. W. Sieck and R. H. Johnson, *J. Phys. Chem.*, **67**, 2281 (1963); (b) R. W. Hummell, *Discussions Faraday Soc.*, **36**, 75 (1963); (c) J. F. Riley and T. C. Hung, Chemistry Division Annual Progress Report, Oak Ridge National Laboratory, ORNL-3679, June 20, 1964, pp 39-41; (d) P. J. Ausloos and S. G. Lias, *J. Chem. Phys.*, **38**, 2207 (1963); (e) P. Ausloos, S. G. Lias, and R. Gorden, Jr., *ibid.*, **39**, 3341 (1963); (f) P. Ausloos, R. Gorden, Jr., and S. G. Lias, *ibid.*, **40**, 1854 (1964).
- (4) (a) D. R. Davis and W. F. Libby, *Science*, **144**, 991 (1962); (b) D. R. Davis, W. F. Libby, and W. G. Meinschein, *J. Chem. Phys.*, **45**, 4481 (1966). The author is grateful to one of the referees for making available a preprint of this work.
- (5) P. Ausloos, R. E. Rebbert, and S. G. Lias, *ibid.*, **42**, 540 (1965).
- (6) R. W. Fessenden and R. H. Schuler, *ibid.*, **39**, 2147 (1963).

research grade methane, which was found to contain ethane (0.014%) as the principal organic impurity. It was subjected to the following vacuum-line manipulations, designed to eliminate ethane, higher boiling hydrocarbons, and traces of oxygen. It was passed through a trap containing thoroughly degassed silica gel at -120° . The last 20%, presumably containing high-boiling impurities, was left behind. Then oxygen-free helium was bubbled through the liquid methane at liquid oxygen temperature for a few minutes. The tank helium had been rendered oxygen-free by passing it through a degassed molecular sieve 5A column at 77°K . This methane was kept in a storage bulb, then before each run a sample was exposed for at least 4 hr to a film of misch metal which had been evaporated under high vacuum onto the surface of a 2-l. bulb. A fresh surface of metal was deposited at least every three runs. This procedure had been previously found to be very effective in the removal of traces of oxygen,⁷ but a test was performed under the conditions used here. A mixture of methane and 0.1% oxygen (27% O^{17} , 73% O^{18}) was prepared and exposed to a misch metal film. It was then analyzed on a mass spectrometer at high pressure and high electron current. A CEC 21-103 instrument was used throughout this work. From the observation that peaks at masses 35 and 36 were zero within experimental error, the maximum oxygen content was calculated to be 4 ppm. The use of ordinary oxygen would not have permitted as sensitive an analysis because of the much higher background in the mass spectrometer at mass 32. The mass spectrum also indicated a maximum of 0.02% argon and 0.14% nitrogen. Other impurities found in a blank analyzed by the procedures used throughout this work and described below were H_2 , 0.6 ppm; C_2H_6 , 0.4 ppm; C_3H_8 , 0.2 ppm. Samples were sealed off the line with the cell at 77°K in the blank and all other runs; the low level of impurities in the blank indicates that there is no measurable pyrolysis of methane vapor in this operation.

Methane- d_4 , obtained from Volk Radiochemical Co. was purified in the same way. Phillips research grade propylene and Volk ethylene- d_4 were used as received except for degassing.

Irradiation Conditions. Samples weighing 0.43 g were irradiated in glass cells by Co^{60} γ rays. Less than 0.4% of the sample was in the gas phase. Irradiation temperature was 112°K , provided by liquid methane as a refrigerant. The dose rate was about 8×10^{17} $\text{ev g}^{-1} \text{min}^{-1}$, and was accurately determined by the Fricke dosimeter with appropriate corrections for electron density of the sample and for decay of the source.

Product Analyses. Hydrogen was separated from the irradiated methane in two stages. Gas was removed with a Töpler pump with the cell at 77°K . This gas, very rich in methane, was then passed through a solid nitrogen trap at 55°K and the *PVT* of the resultant sample was measured. It was analyzed mass spectrometrically for hydrogen, usually consisting of roughly equal parts of hydrogen and methane. In one run, a check was made of the efficiency of the hydrogen analysis by going through the regular procedure, then liquefying the methane, cooling it down again, and removing a second gas sample for analysis. It was found to contain only 0.5% of the hydrogen in the first sample.

Hydrocarbons were analyzed by gas chromatography. The total sample was swept by the carrier gas from the rapidly warmed irradiation cell into a short silica gel column at -78° . Most of the methane was removed in this operation. The remainder plus products were then removed from this column by heating it quickly, and passed through another temperature programmed silica gel column and silicone grease column. The separated components passed through a thermal conductivity detector and a hydrogen flame detector. Components were sometimes trapped for mass spectrometric analysis after passing through just the thermal conductivity detector.

Isotopic Analyses. Isotopic analyses of the various deuterated products were made mass spectrometrically. For the ethylenes, the fragmentation patterns of C_2HD_3 and $\text{C}_2\text{H}_3\text{D}$ were taken from API tables. The best fit left no appreciable residues at any mass. The analysis of the ethanes was not as clean. Patterns for C_2H_6 , CH_3CD_3 , and C_2D_6 were obtained by using authentic samples. The pattern for C_2HD_5 was calculated from our spectrum of C_2D_6 in the manner indicated by Quinn and Mohler.⁸ The patterns used for $\text{C}_2\text{H}_2\text{D}_4$ -1,1,1,2, $\text{C}_2\text{H}_4\text{D}_2$ -1,1, and $\text{C}_2\text{H}_5\text{D}$ were taken from Bell and Kistiakowsky,⁹ whose spectra for C_2H_6 , CH_3CD_3 and C_2D_6 agree with ours.

For the isotopic analysis of the propanes, the spectra for C_3D_8 and $\text{C}_3\text{H}_7\text{D}$ -1 were calculated by multiplying the ratios of intensities of ions in the deuterated species to the intensities of the corresponding ions in C_3H_8 , as reported in the literature,^{10,11} by our intensities for C_3H_8 .

(7) H. S. Sandhu, J. Lees, and M. Bloom, *Can. J. Chem.*, **38**, 493 (1960).

(8) E. I. Quinn and F. L. Mohler, *J. Res. Natl. Bur. Std.*, **65A**, 93 (1961).

(9) J. A. Bell and G. B. Kistiakowsky, *J. Am. Chem. Soc.*, **84**, 3417 (1962).

(10) F. E. Condon, *ibid.*, **73**, 4675 (1951).

(11) D. P. Stevenson and C. D. Wagner, *J. Chem. Phys.*, **19**, 11 (1951).

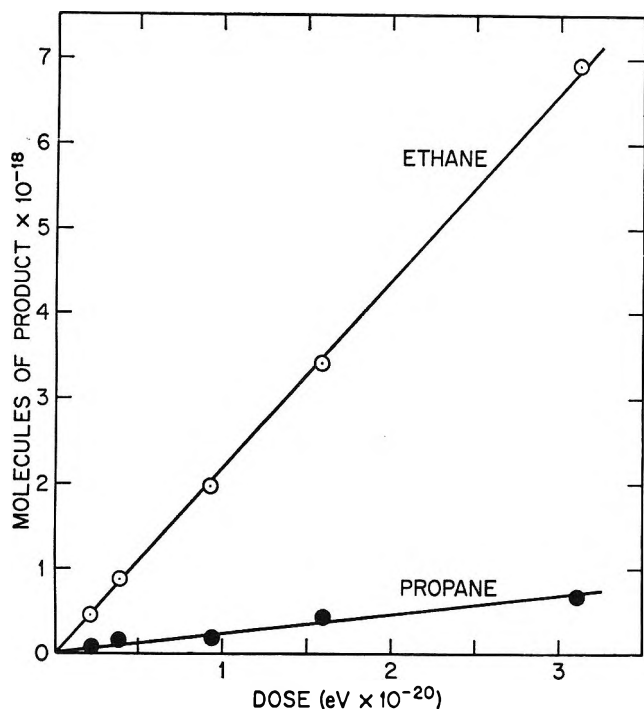


Figure 1. Ethane and propane yields as a function of dose in the radiolysis of pure liquid CH_4 at 112°K . Sample weight, 0.43 g.

The pattern for $\text{C}_3\text{H}_6\text{D}_2$ -1,2 was estimated from those for $\text{C}_3\text{H}_7\text{D}$ -1 and $\text{C}_3\text{H}_7\text{D}$ -2.¹¹ The isotopic analyses reported in Table IV are based on ratios of intensities of parent peaks. As a check, estimates of the ratios of $\text{C}_3\text{H}_6\text{D}_2$ -1,2 to $\text{C}_3\text{H}_7\text{D}$ -1 based on the ratios of 31 to 30 peaks were also made, on the assumption of no isotopic scrambling. This method is expected to be less accurate, but gave ratios only 15–20% higher.

Results and Discussion

The yields of the main products in the radiolysis of pure liquid methane are shown in Table I. The hydrogen yield is estimated from only one run, and the pentanes and hexanes from two runs. Yields of ethane and propane as a function of dose are shown in Figure 1. Based on $G(-\text{CH}_4) = 6$, the per cent decomposition for the points shown ranges from 0.008 to 0.12. The yields of *n*-butane and isobutane show an equally good linear dependence, and the G values for the individual pentanes and hexanes were constant within 20% for the two runs at doses of 1.0 and 3.3×10^{20} ev. These results suggest that absorption of higher hydrocarbons by a possible polymeric product, found to occur under the somewhat different analytical conditions of Davis, Libby, and Meinschein,^{4b} is not important in this study since otherwise the percentages of the various products absorbed would probably vary

with dose. The linearity with dose also suggests that any type of energy, charge, or proton transfer to products either does not occur even at 0.12% conversion or, less plausibly, is completely efficient even at 0.008% conversion. Evidence that proton transfer does not occur under these conditions is presented below.

Table I: Products of the Radiolysis of Pure CH_4

Product	G
H_2	3.15
C_2H_6	2.21
C_3H_8	0.23
<i>n</i> - C_4H_{10}	0.016
<i>i</i> - C_4H_{10}	0.021
<i>n</i> - C_5H_{12}	0.0027
<i>i</i> - C_5H_{12}	0.0036
<i>neo</i> - C_5H_{12}	0.0024
3-Methylpentane	0.0005
2,2-Dimethylbutane	0.0012
Diisopropyl	0.0015

The H:C ratio of the products reported is 4.14. This compares with 4.77 for the gaseous products in the radiolysis of gaseous CH_4 ,^{3a} in which an appreciable yield of polymer was also found. No polymer was found in this work, but it was not looked for carefully. The excess hydrogen in the material balance corresponds to a deficiency in CH_2 groups with a G of only 0.3, so that an appreciable polymer yield is unlikely.

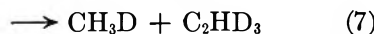
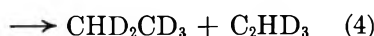
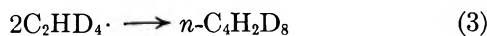
Effect of Ethylene. Results of experiments in which dilute solutions of C_2D_4 were irradiated are given in Table II. The ethylene yields have been corrected

Table II: Yields from Solutions of C_2D_4 in CH_4

	Average mole % C_2D_4	
	0.0182	0.0555
	G values of products	
$-\text{C}_2\text{D}_4$	4.64	6.30
C_2H_4	...	0.23
C_2HD_3	...	0.25
$\text{C}_2\text{H}_3\text{D}$...	0.05
Total ethane	2.29	2.27
C_2H_6	...	1.89
C_2HD_6	...	0.23
$\text{C}_2\text{H}_2\text{D}_4$...	0.14
C_2D_6	...	0.015
Propylene	0.005	...
Propane	1.22	1.30
<i>n</i> -Butane	0.44	0.38
Isobutane	0.005	...

^a ... indicates analysis was not performed.

to account for a small amount of consumption of product ethylenes during the run. The results may be interpreted in terms of the reactions



For one of the runs, the propane product was analyzed mass spectrometrically. Standards were not available, so quantitative analysis was not possible, but the following conclusions were reached: (a) propane- d_4 is certainly the main component; (b) from the ratio of peaks at masses 49 and 48, propane- d_5 was 3% of propane- d_4 ; (c) if all of the mass 27 peak were due to propane- d_0 , then propane- d_0 would be 30% of propane- d_4 . However, propane- d_4 must contribute significantly to this peak, so this upper limit is probably considerably above the actual value.

The isotope effect in the disproportionation of $\text{C}_2\text{HD}_4\cdot$ radicals may be estimated from the ethane yields as

$$\frac{G(\text{CHD}_2\text{CHD}_2)}{G(\text{CHD}_2\text{CD}_3)} = \frac{0.14}{0.23} = \frac{k_{\text{H}}}{2k_{\text{D}}}$$

$$k_{\text{H}}/k_{\text{D}} = 1.2$$

Watkins and Moser¹² calculated a tritium isotope effect in the disproportionation of ethyl radicals in the solid phase at 63°K by two methods and found $k_{\text{H}}/k_{\text{T}} = 1.7 \pm 0.7$ and 2.3 ± 0.5 .

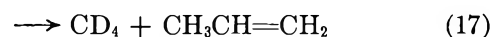
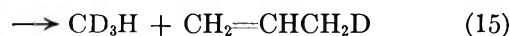
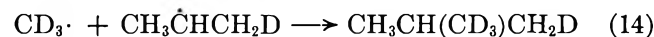
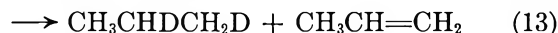
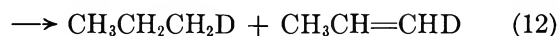
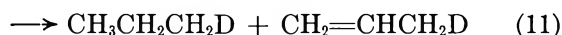
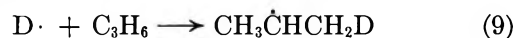
The above seems to establish reasonably that the C_2HD_5 and $\text{C}_2\text{H}_2\text{D}_4$ are produced by disproportionation of $\text{C}_2\text{HD}_4\cdot$ radicals. It is seen that the ratio of yields of these products to that of butane is quite high. The ratio of disproportionation to combination of ethyl radicals, $(k_4 + k_5)/k_3$, should be given by $[G(\text{C}_2\text{HD}_5) + G(\text{C}_2\text{H}_2\text{D}_4)]/G(n\text{-C}_4\text{H}_2\text{D}_8)$. The observed value of 1.0 contrasts to that of 0.14 found in the gas phase between 25 and 200°.¹³ From studies of the photolysis of azoethane in liquid methane, a ratio of 0.35 for ethyl radicals at 89°K was reported,¹⁴ but no account was taken of the possibility of intramolecular formation of butane which might be very important under these conditions where quantum yields are very

low.¹⁵ The possibility that intramolecular formation of ethane might be significant in the photolysis of azomethane in the liquid phase has been pointed out.¹⁶ Watkins and Moser¹² reported $k_{\text{dis}}/k_{\text{comb}} = 0.8$ for ethyl radicals in the solid phase at 63°K, but their interpretation of the experiments in which alkyl radicals are produced by the reaction of thermally generated hydrogen atoms with olefin films has been questioned.¹⁷

A lower limit for the yield of thermal, nonspur hydrogen atoms, $G(\text{H}\cdot)$, should be $2G(\text{butane}) + 2G(\text{C}_2\text{HD}_5) + 2G(\text{C}_2\text{H}_2\text{D}_4) + G(\text{propane}) = 2.76$. This neglects reactions 7 and 8.¹⁸ In order to estimate $G(\text{CH}_3\cdot)$, the yield of ethane resulting from a combination of methyl radicals must be estimated. In the gas phase it is well established that for random reactions between radicals A and B, $k_{\text{AB}}/(k_{\text{AA}}k_{\text{BB}})^{1/2} = 2$.¹⁹ On the assumption that this relationship holds here, a lower limit of $G(\text{C}_2\text{H}_6)$ from freely diffusing methyl radicals is 0.54, and G of C_2H_6 formed by other processes is 1.35. A lower limit to $G(\text{CH}_3\cdot) = 2(0.54) + G(\text{propane}) = 2.34$.

Effect of Propylene. Product yields of the irradiation of solutions containing propylene are shown in Tables III and IV. The dose increased as the propylene concentration increased, and ranged from 0.66 to 2.36×10^{20} ev. The constancy of product yields again indicates that products were recovered efficiently.

The results may be interpreted in terms of reactions analogous to those proposed for ethylene solutions. When methane- d_4 is the solvent, these are



(12) K. W. Watkins and H. C. Moser, *J. Phys. Chem.*, **69**, 1040 (1965).

(13) D. G. L. James and E. W. R. Steacie, *Proc. Roy. Soc. (London)*, **A244**, 289 (1958).

(14) P. S. Dixon, A. P. Stefani, and M. Szwarc, *J. Am. Chem. Soc.*, **85**, 2551 (1963).

(15) S. Kodama, S. Fukita, J. Takeiski, and O. Tayama, *Bull. Chem. Soc. Japan*, **39**, 1009 (1966).

Table III: Yields from Solutions of C₃H₆ in Methane

	Solvent					
	CH ₄	CD ₄	1:1 CH ₄ -CD ₄		CH ₄	CD ₄
	0.037	0.051	Average mole % C ₃ H ₆		0.116 ^a	0.146
	G values of products					
-C ₃ H ₆	8.3	6.5	5.5	4.6	6.1	5.5
D ₂	2.09	0.007	1.98
HD	0.07	0.034	0.08
H ₂	0.03	2.31	0.09
Ethylene	0.18	0.17	0.22	0.19	...	0.21
Ethane	1.93	1.62	1.78	1.79	...	1.77
Propane	0.70	0.60	0.69	0.63	...	0.55
n-Butane	0.010	...	0.010
Isobutane	0.78	0.61	0.65	0.65	...	0.65
Isopentane	0.023	0.040	0.030	0.044	...	0.062
Diisopropyl	0.153	0.153	0.169	0.155	0.169	0.160
Propane-diiso-propyl	4.6	3.9	4.1	4.1	...	3.4

^a Solute is C₃D₆.Table IV: Isotopic Analysis of Propanes from Solutions of C₃H₆ in CD₄

Av mole % C ₃ H ₆	G							G(C ₃ H ₇ D)/G(C ₃ H ₆ D ₃) ^a
	C ₃ D ₈	C ₃ D ₇ H	C ₃ H ₆	C ₃ H ₅ D ₂	C ₃ H ₇ D	C ₃ H ₆ D ₂		
0.051	0.059	0.004	0.045	0.004	0.40	0.090	5.6	
0.057	0.067	0.006	0.036	0.011	0.39	0.118	5.1	
0.146	0.050	0.004	0.049	0.005	0.36	0.079	6.0	

^a Corrected; see text.

The product isobutane was analyzed mass spectrometrically for two of the runs with almost identical results. About 5% of it was isobutane-*d*₅, but most of it seemed to have the structure indicated by eq 14 as seen by the following comparison. Based on the assumptions that (a) the ions of masses 43, 42, and 41 from *i*-C₄H₁₀ have the structures CH₃CHCH₃⁺, CH₃-CH=CH₂⁺, and CH₂CH=CH₂⁺, respectively, (b) there is no isotope effect in the fragmentations to form these ions, and (c) there is no scrambling of hydrogens in the fragmentation, then the relative intensities of masses 47, 46, 45, 44, and 43 were calculated to be 100, 110, 36, 144, and 83 for CH₃CH(CD₃)CH₂D. The average ratios of intensities found were: 100, 116, 49, 123, and 60. In view of the nature of the assumptions, the agreement is probably good.

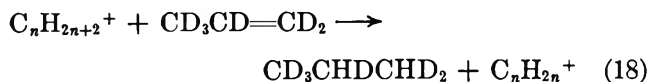
From the ratio of *n*-butane to isobutane, a maximum of 1-2% of the hydrogen atoms add to propylene to give *n*-propyl radicals rather than isopropyl radicals. Holroyd and Klein²⁰ concluded that thermal hydrogen atom reaction with propylene in the liquid phase at 25° gives 87% isopropyl, 9% *n*-propyl, and 4% allyl

radicals. Other estimates of nonterminal addition are 2% in the solid at 90°K,²¹ 5% in the solid at 77°K,²² and 6% in the gas phase at 298°K.²³

Very recently, Ausloos, Scala, and Lias²⁴ have ir-

(16) R. E. Rebbert and P. Ausloos, *J. Phys. Chem.*, **66**, 2253 (1962).(17) A. N. Hughes and J. H. Purnell, *Trans. Faraday Soc.*, **61**, 2710 (1962).(18) According to the mechanism proposed, the yield of C₂HD₃ should be greater than that of C₂H₂D₃ by an amount equal to $G(\text{CH}_3\text{-CD}_2\text{CHD}_2) \times (k_7/k_8)$. This difference should be appreciable even though $k_{\text{dis}}/k_{\text{comb}}$ for methyl plus ethyl is probably considerably less than the ratio for the ethyl plus ethyl reaction (0.06¹⁹ vs. 0.14 in the gas phase). In fact, the difference is only $\Delta G = 0.02$, but the experimental uncertainty is quite large.(19) J. A. Kerr and A. F. Trotman-Dickenson, *Progr. Reaction Kinetics*, **1**, 111 (1961).(20) R. A. Holroyd and G. W. Klein, *J. Appl. Radiation Isotopes*, **13**, 493 (1962).(21) R. D. Kelley, R. Klein, and M. D. Scheer, *J. Phys. Chem.*, **69**, 905 (1965).(22) A. N. Hughes and J. H. Purnell, *Trans. Faraday Soc.*, **62**, 156 (1966).(23) W. E. Falconer, B. S. Rabinovitch, and R. J. Cvetanovic, *J. Chem. Phys.*, **39**, 40 (1963).(24) P. Ausloos, A. A. Scala, and S. G. Lias, *J. Am. Chem. Soc.*, **88**, 1583 (1966).

radiated solutions of pentanes and hexanes containing propylene- d_6 , and found $\text{CD}_3\text{CHDCHD}_2$ as a major product. They attributed it to the reaction



Similarly, they found $\text{CD}_2\text{HCD}_2\text{H}$ is produced with a G of 2 when a $\text{C}_5\text{H}_{12}-\text{CCl}_4$ (1:0.03) solution containing C_2D_4 is irradiated. Reactions analogous to this must be considered as possible sources of propane- d_2 in the $\text{CD}_4-\text{C}_3\text{H}_8$ solutions, and of ethane- d_4 in the $\text{CH}_4-\text{C}_2\text{D}_4$ solutions. However, from gas-phase thermochemical^{25,26} data it is found that this reaction is endothermic when the solvent is methane, by 18 kcal for propylene as solute and by 15 kcal for ethylene as solute. It is very unlikely that differences in solvation energies would be sufficient to make these reactions exothermic in the liquid state. Further, reactions analogous to (18) cannot explain the large yields of propane- d_1 found in the $\text{CD}_4-\text{C}_3\text{H}_8$ solutions, and of ethane- d_6 found in $\text{CH}_4-\text{C}_2\text{D}_4$ solutions.

According to the mechanism, propylene- d_1 should be produced in yields somewhat larger than those of propane- d_1 since it is a product of reactions 15 and 16 as well as 11 and 12. In fact, the propylene- d_1 yields measured were less than 0.2 for the experiments with $\text{CD}_4-\text{C}_3\text{H}_8$ solutions described in Table IV. The explanation is that considerable exchange occurred between protons of the silica gel used in the gas chromatographic analysis and the deuterium atoms of the propylene. This was demonstrated by a blank experiment in which propylene- d_6 was converted apparently quantitatively into propylene- d_1 (probably $\text{CH}_3\text{CD}=\text{CH}_2$) by passage through the gas chromatograph under similar conditions.

In a further experiment, a solution of 0.116 mole % (average) propylene- d_6 in CH_4 was irradiated. The analytical system was modified so that it contained only a small amount of silica gel and this was kept at a low temperature (around 50°). Although only propylene and diisopropyl could be determined under these conditions, the exchange induced was small; a blank showed the propylene- d_6 content of otherwise pure propylene- d_6 increased only from 3.11 to 4.23% on passage through the system. For this experiment, $G(\text{propylene-}d_6) = 0.92$ after corrections for the blank and consumption of propylene during irradiation were made.

For the experiments of Table IV, $G(\text{propylene-}d_1)$ should also be 0.92. The calculated average concentrations of propylene- d_1 are appreciable (4–8% of the C_3H_8), and some of the propane- d_2 must result from the

addition of D atoms to propylene- d_1 , followed by abstraction of H by the isopropyl- d_2 radicals in reactions similar to (11) and (12). Corrections were applied on this basis to obtain the ratios of G values of propane- d_1 to propane- d_2 given in Table IV, and these should represent the ratios of rate constants $(k_{11} + k_{12})/k_{13}$. The very small amounts of propane- d_3 must be produced by the abstraction of D by the isopropyl- d_2 radicals in a reaction similar to (13). Yields calculated on this assumption agree satisfactorily with experimental values (G values of 0.003, 0.007, and 0.004 compared to 0.004, 0.011, and 0.005, respectively). The isobutane- d_5 noted above is satisfactorily accounted for by the reaction between isopropyl- d_2 and methyl- d_3 radicals.

From the average corrected ratio $G(\text{C}_3\text{H}_7\text{D})/G(\text{C}_3\text{H}_8\text{D}_2)$ in Table IV, it is concluded that $(k_{11} + k_{12})/k_{13} = 5.6$. On a purely statistical basis, this ratio should be 5, so the isotope effect, $k_{\text{H}}/k_{\text{D}}$, is 1.1. Yun and Moser²⁷ reported $k_{\text{H}}/k_{\text{T}} = 1.7 \pm 0.2$ for the disproportionation of two tritium-labeled isopropyl radicals.

The ratio $k_{\text{dis}}/k_{\text{comb}}$ for isopropyl radicals should be equal to the average value of $G(\text{propane})/G(\text{diisopropyl})$ of 4.0 less 10% to correct for C_3D_8 for a net of 3.6. Again, this value is much higher than that of 0.65 found in gas-phase studies.²⁸ Ratios of 9,²⁹ 5.5,²⁷ and 3,³⁰ have been reported in studies in which the radicals have been generated by hydrogen atom addition to propylene at 77°K , and a value of 2³¹ was found from the photolysis of azoisopropane at 77°K . The interpretations of these experiments of other investigators are, of course, subject to the same difficulties indicated above for the analogous studies on ethyl radical reactions.

The ratio $k_{\text{dis}}/k_{\text{comb}}$ for the reaction between methyl and isopropyl radicals may also be calculated. The average G of the combination product, isobutane, is 0.67. The yields of reactions 15–17 may be estimated from $G(\text{propylene-}d_1)$ for the $\text{CD}_4-\text{C}_3\text{H}_8$ experiments. After the contributions from reactions 11 and 12, as

(25) F. H. Field and J. L. Franklin, "Electron Impact Phenomena," Academic Press, New York, N. Y., 1957.

(26) F. D. Rossini, *et al.*, Selected Values of Chemical Thermodynamic Properties of the National Bureau of Standards, American Petroleum Institute, Project 44, Carnegie Institute of Technology, Pittsburgh, Pa.

(27) H. B. Yun and H. C. Moser, *J. Phys. Chem.*, **69**, 1059 (1965).

(28) J. C. J. Thynne, *Trans. Faraday Soc.*, **58**, 1394 (1962).

(29) R. Klein, M. D. Scheer, and J. G. Waller, *J. Phys. Chem.*, **64**, 1247 (1960).

(30) C. G. Hill, Jr., R. C. Reid, and M. W. P. Strandberg, *J. Chem. Phys.*, **42**, 4170 (1965).

(31) R. Klein, M. D. Scheer, and R. Kelley, *J. Phys. Chem.*, **68**, 598 (1964).

measured by the propane- d_1 yields, have been subtracted out, $G(\text{propylene-}d_1)$ from reactions 15 and 16 is found to be 0.51. The yield of reaction 17 may be taken to be 0.10 on a purely statistical basis. Then $k_{\text{dis}}/k_{\text{comb}}$ is $0.61/0.67 = 0.9$. The gas-phase value is 0.20.²⁸

It is noteworthy that $k_{\text{dis}}/k_{\text{comb}}$ ratios are consistently much higher under the conditions of this study than the values measured in the gas phase at higher temperatures. They are higher by factors of 5 for methyl plus isopropyl, 7 for ethyl plus ethyl, and 6 for isopropyl plus isopropyl.

In both ethylene and propylene solutions, a large fraction of the products result from reactions of radicals A and B, where A and B are methyl and ethyl in the case of ethylene solutions. Changing the solute to propylene changes the identity of B to isopropyl, but does not change the number of B. It has been assumed above that radical-radical reactions take place on a simple statistical basis in ethylene solutions; this should be equally true for propylene solutions. Therefore, the yield of A + A, A + B, and B + B reactions should be the same in the two types of solutions. The yield of C_2H_6 in Table II is approximately equal to the ethane yields in Table III.³² The B + B reactions are reactions 3-5 for ethylene solutions, with a total G of 0.75, and reactions 10-13 for propylene solutions, with a total yield of 0.69. The A + B reactions are reactions 6-8 for ethylene solutions, with an estimated yield, expected to be slightly low, equal to $G(\text{propane})$, 1.20. This should be compared to the sum of the yields of reactions 14-17, which is 1.28. Thus within experimental error these radical reactions are obeying simple statistical considerations in propylene solutions.

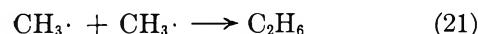
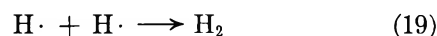
The C_3D_8 and $\text{C}_3\text{D}_7\text{H}$ produced in $\text{CD}_4\text{-C}_3\text{H}_6$ solutions must arise from some process not involving propylene. The ratio of these products corresponds approximately to the CD_3H impurity (2.3% in this lot). The C_3H_8 is probably not formed *via* H atoms from the C_3H_6 since it does not increase significantly as the C_3H_6 concentration increases. It could arise from the formation of H atoms from the CD_3H , probably favored by a large isotope effect,^{33,34} which subsequently add to propylene, and this is followed by the disproportionation of the $i\text{-C}_3\text{H}_7\cdot$ radicals.

As the concentration of propylene increases, $G(\text{isopentane})$ increases. This product could arise from the addition of methyl radicals to propylene followed by the reaction of the resulting *sec*-butyl radicals with methyl radicals. A calculation indicates this addition reaction could be occurring for $A = 10^8$ mole⁻¹ l. sec⁻¹ and an activation energy of 4.5 kcal.³⁵ This is 1-2 kcal lower than gas-phase values.¹⁹

For both ethylene and propylene solutions, the G values for consumption of olefin, though imprecise, are consistently higher than $G(\text{H}\cdot)$. This additional olefin must be converted to products higher than C_6 , but no explanation is offered. Similar observations were made by Riley and Hung.^{3c}

Reactions in Pure Methane. From both ethylene and propylene experiments, it is seen that ethylene is produced with an initial $G = 0.20$. In the absence of a protective agent this ethylene reacts with hydrogen atoms to give ethyl radicals. This conclusion from product yields is supported by the esr studies which indicated that the signal due to the $\text{C}_2\text{H}_5\cdot$ radical disappeared on the addition of C_2D_4 to CH_4 before irradiation.⁶ Most of the ethyl radicals must react with methyl radicals to give propane, and the rest react with hydrogen atoms. The experiments with propylene solutions indicate that propane is produced with $G = 0.06$ by some other mechanisms. From this study the steady-state ratio $[\text{C}_2\text{H}_5\cdot]/[\text{CH}_3\cdot] = 0.20/2.34 = 0.09$. By contrast, esr measurements on methane during radiolysis indicated $[\text{C}_2\text{H}_5\cdot]/[\text{CH}_3\cdot] \simeq 0.2$.⁶

Both methyl radicals and hydrogen atoms which are in excess of ethylene must be consumed by the reactions



If abstraction by hydrogen atoms were occurring, then $G(\text{H}_2)$ in pure methane would be larger than in olefin solutions by about 2.6, and $G(\text{C}_2\text{H}_6)$ would be larger by 1.9. Also, it has been suggested that abstraction does not contribute significantly to formation of hydrogen in the radiation chemistry of gaseous methane at 25 and 100°.³⁶

However, since ethane yields are somewhat larger in pure methane than in olefin solutions, it must be concluded that the ratio $k_{20}/(k_{19}k_{21})^{1/2}$ does not equal 2. The value of this ratio was determined as follows. By comparing the G values for total hydrogen and ethane from pure methane, as given in Table I, with the G

(32) The ethane was analyzed for one of the runs in Table III in which CD_4 was the solvent. It consisted of 94.5% C_2D_6 , 5.2% C_2HD_6 , and 0.3% $\text{C}_2\text{H}_2\text{D}_4$.

(33) For example, Yang and Marcus³⁴ found that cyclohexane- d_{12} containing 0.6 atom % H gave hydrogen with an isotopic composition of 1.6% H_2 , 11.0% HD, and 87.4% D_2 .

(34) J. Y. Yang and I. Marcus, *J. Chem. Phys.*, **43**, 1585 (1965).

(35) The methyl radical concentration is calculated by taking k for the combination of methyls to be equal to k for the combination of ethyls at 98°K, 3.0×10^8 l. mole⁻¹ sec⁻¹.⁶

(36) L. I. Bone and R. F. Firestone, *J. Phys. Chem.*, **69**, 3652 (1965).

values for nonradical hydrogen and ethane, as estimated from the G values for olefin solutions, the G values for reactions 19 and 21 were estimated to be 0.80 and 0.84, respectively, for pure methane. By using the further information that $G(\text{H}\cdot) = 2.76$ and $G(\text{CH}_3\cdot) = 2.34$, and correcting for the hydrogen atoms consumed in reactions with ethylene and ethyl radicals, and the methyl radicals which react with ethyl radicals, G for reaction 20 was calculated to be 0.67. These yields give $k_{20}/(k_{19}k_{21})^{1/2} = 0.8 \pm 0.2$. This ratio is expected to be 2 if the rate constants are equal except for a statistical factor which doubles the rate of the cross-combination reaction 20. However, the rate constant for a diffusion-controlled reaction between A and B is given by the Smoluchowski relation³⁷

$$k_{AB} = 4\pi r_{AB}D_{AB}$$

where r_{AB} is the encounter distance and D_{AB} is the sum of the binary diffusion coefficients of A and B with respect to the solvent. The diffusion coefficients of alkyl radicals are probably comparable, but it has been observed that H_2 , D_2 , He, and HT have abnormally large diffusion coefficients in liquids at 298 and 75°K because of quantum effects,³⁸ so that the diffusion coefficient of a hydrogen atom may be expected to be very much larger than that of a methyl radical under the conditions of this study. Because of the statistical factor, k_{20} should be larger than k_{19} and both should be larger than k_{21} . These considerations indicate that $k_{20}/(k_{19}k_{21})^{1/2}$ should be greater than 2, and the experimental result remains unexplained.

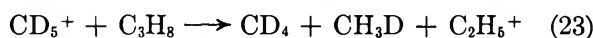
Solutions of $\text{CH}_4 + \text{CD}_4$. The results of isotopic analysis of product ethane from equimolar mixtures of CH_4 and CD_4 are shown in Table V. The appreciable yields of ethane- d_2 and ethane- d_4 suggest that some ethane is produced by methylene radicals inserting into methane. Ausloos and Lias^{3d} made a similar observation and conclusion for a single experiment with an equimolar solution without additives. Ausloos, Rebbert, and Lias⁵ also found strong evidence that methylene radical reactions are important in the direct and inert gas sensitized photolysis and radiolysis of solid $\text{CH}_4\text{-CD}_4$ mixtures. Quantitative analysis of the results is very difficult because of a lack of knowledge of the reactions of singlet and triplet methylenes, especially at low temperatures. It has sometimes been assumed that singlet methylene reacts with hydrocarbons by insertion into carbon-hydrogen bonds and that triplet methylene reacts by abstraction of hydrogen atoms,³⁹ but this view has been challenged.⁴⁰ The observation that all ethanes are reduced by propylene indicates that $\text{CH}_2\text{D}\cdot$ and $\text{CHD}_2\cdot$ radicals are produced in the system. Added HI and O_2 are expected

to react with all freely diffusing methyl radicals,⁴¹ so that the increased percentages of ethane- d_2 and ethane- d_4 with these solutes strengthens the conclusion that methylene radicals are inserting under these conditions. The remaining CH_3CD_3 and some of the C_2H_6 and C_2D_6 could result from spur reactions of $\text{CH}_3\cdot$ and $\text{CD}_3\cdot$.

Table V: Ethanes from $\text{CH}_4\text{-CD}_4$ Solutions

	Mole % CD_4		
	50.7	49.9	44.8
	Solute		
	None	0.08 mole % C_3H_8	0.03 mole % HI + 0.08 mole % O_2
Total ethane	2.32	1.78	0.94
C_2D_6	0.31	0.24	0.12
C_2HD_5	0.09	0.06	0.02
CH_2DCD_3	0.26	0.19	0.15
CH_3CD_3	0.62	0.50	0.16
CH_3CHD_2	0.38	0.24	0.18
$\text{C}_2\text{H}_5\text{D}$	0.12	0.06	0.02
C_2H_6	0.56	0.48	0.29

Solution of C_3H_8 in CD_4 . In both mass spectrometric studies⁴² and the gas phase radiolysis,^{3d-f} the following ion-molecule reactions have been observed in mixtures ($\approx 0.01\%$) of C_3H_8 in CD_4



Thus, C_2H_6 and $\text{C}_2\text{D}_5\text{H}$ were major products of the gas phase work. However, with increase in pressure, $G(\text{C}_2\text{D}_5\text{H})$ decreased steadily from the lowest pressure used (1.4 cm), whereas $G(\text{C}_2\text{H}_6)$ went through a maximum around 14 atm.^{3f} Therefore, if these ion-mole-

(37) A. M. North, "The Collision Theory of Chemical Reactions in Liquids," John Wiley and Sons, Inc., New York, N. Y., 1964, p 68.

(38) K. Nakanishi, E. M. Voigt, and J. H. Hildebrand, *J. Chem. Phys.*, **42**, 1860 (1965).

(39) R. W. Carr, Jr., *J. Phys. Chem.*, **70**, 1970 (1966).

(40) W. B. DeMore and S. W. Benson, *Advan. Photochem.*, **2**, 235 (1964).

(41) HI probably reacts with electrons also under these conditions, as indicated by the fact that a solution of 0.03 M DI in CH_4 gave an appreciable yield of D_2 ($G = 0.89$).

(42) M. S. B. Munson and F. H. Field, *J. Am. Chem. Soc.*, **87**, 3294 (1965).

cule reactions occur at all in the liquid, the sequence of reactions 22, 23, and 24 would be more likely than reactions 25 and 26. In this study, a solution of 0.43 mole % C_3H_8 in the liquid methane- d_4 was irradiated, and the product ethane was analyzed. The results were: $G(C_2D_6) = 1.47$; $G(C_2D_5H) = 0.154$; $G(C_2H_2D_4) = 0.015$; $G(CH_3CD_3) = 0.018$; $G(C_2H_5D) = 0.037$; $G(C_2H_6) = 0.017$. A statistical production of CD_2H from the small CD_3H impurity in the CD_4 would lead to $G(C_2D_5H) = 0.084$, if all the ethane comes from methyl radicals. It can be concluded that the ion-

molecule reactions 24 and 26 make at most a minor contribution in the liquid phase. Of course, nothing can be concluded from the data about the occurrence of reactions 22, 23, and 25.

In this experiment, there were appreciable yields of isobutane and 2,3-dimethylbutane, indicating that some of the hydrogen atoms had abstracted from propane. A calculation shows that this is in accord with $\log A = 13.0 - 6300/2.3RT$,⁴³ with A in $cc\ mol^{-1}\ sec^{-1}$.

(43) K. Yang, *J. Am. Chem. Soc.*, **84**, 719 (1962).

Proton Mobility in Solids. I. Hydrogenic Vibration Modes and

Proton Delocalization in Boehmite

by J. J. Fripiat,^{1a} H. Bosmans, and P. G. Rouxhet^{1b}

Laboratoire de Physico-Chimie Minérale, Institut Agronomique, University of Louvain, Heverlee-Louvain, Belgium (Received November 7, 1966)

When boehmite is heated progressively to elevated temperatures, a continuous decrease in the intensity of the fundamental OH vibration bands is observed. The effect is more pronounced for the deformation and torsion modes than for the stretching modes, but it is perfectly reversible on cooling when the temperature has not exceeded 400°. To explain these observations, a proton delocalization process was postulated. In terms of this process, the observations may be explained by the disappearance of discrete vibrational energy levels above a specified level where the probability of the proton tunneling through the potential energy barrier is close to the absorption frequency. This interpretation is in agreement with the large band widths and with their increase upon heating. The frequency shifts accompanying the loss of intensity are due to the thermal expansion of the crystal unit cell. A complete assignment of the hydrogenic modes has been attempted in relation to the hydrogenic structure proposed by Wickersheim and Korpi.

I. Introduction

Upon heating minerals which contain constitutional hydroxyls, such as micas, a progressive loss in intensity of the OH stretching infrared bands has been observed and has been assigned to a proton delocalization process.² The decrease in intensity was fully reversible below the dehydroxylation temperature. The

delocalization process was considered as a translation of protons in the mica framework but their compli-

(1) (a) University of Louvain and M.R.A.C. (Tervuren); (b) Aspirant au F.N.R.S.

(2) (a) J. J. Fripiat, P. Rouxhet, and H. Jacobs, *Am. Mineralogist*, **50**, 1937 (1965); (b) J. J. Fripiat, H. Jacobs, and P. Rouxhet, *Silicates Ind.*, **31**, 469 (1966).

cated structure did not favor a thorough analysis of the phenomenon.

Aluminum monohydrate boehmite offers an interesting opportunity to extend these investigations to a well-known and rather simple structure³⁻⁵ (Figure 1). The natural as well as the synthetic forms of this mineral are polycrystalline. The random orientation of the particles averages the beam polarization by the lattice and avoids any pleochroism in the absorption.

An interesting solution to the problem of hydrogenic structure in boehmite has recently been developed through application of infrared spectroscopy. According to Wickersheim and Korpi,⁶ an infinite OH-OH zigzag chain seems to be responsible for the hydrogenic modes of vibration. The presence of an OH chain and of relatively strong hydrogen bonds between two adjacent oxygen atoms would favor proton tunneling and would enhance greatly an eventual proton delocalization process. Indeed, a rapid decrease in the intensity of the two stretching modes and of the three deformation modes has been observed for boehmite AlOOH, as well as for AlOOD: the change was completely reversible below 400°. A rather complete treatment to explain these observations has been attempted on the basis of the computation of the probability of the proton tunneling through the potential barriers between lattice points.

The infrared absorption has been experimentally characterized by the measurement of the integrated band intensity. For sufficiently thin layers, the absorbance of a fundamental infrared band of frequency ν_{nm} is

$$A(\nu_{nm}) = \frac{h\nu_{nm}N_0}{c} \sum_w N_w B_{nm}(1 - N_{w'}) \quad (1)$$

where B_{nm} is the Einstein coefficient of absorption and N_w and $N_{w'}$ are the fraction of the N_0 OH oscillators in the initial and in the final energy levels, respectively. N_w represents the relative population of the initial level w (quantum number n) while $(1 - N_{w'})$ accounts for the lack of occupancy of the final level w' (quantum number m). The vibrational quantum numbers m and n of the considered normal mode ν_{nm} are related by the selectivity rule $m = n + 1$. The summation included in relationship 1 is theoretically extended to all the possible energy levels of the oscillator. No anharmonicity effect will be considered since, according to Pimentel and McClellan,⁷ there is no evidence that these effects are stronger in hydrogen-bonded systems than in other systems.

The transition probability between the w and w' levels, represented by B_{nm} , is proportional to the square of the transition moment, defined as

$$\langle M^{n,m} \rangle = \int \psi_n M \psi_m^* d\tau \quad (2)$$

If the dipole moment M is split into its three components along x , y , and z , for sufficiently small displacement, one obtains

$$\langle M_x^{n,m} \rangle = M_{0x} \int \psi_n \psi_m^* d\tau + \sum_i \left(\frac{\delta M_x}{\delta \xi_i} \right)_0 \int \psi_n \xi_i \psi_m^* d\tau \quad (3)$$

ξ_i is the normal coordinate corresponding to the fundamental mode of frequency ν_{nm} and $\psi_n \psi_m^*$ is set for the complete series of $\psi_n(\xi_i)$ and $\psi_m^*(\xi_i)$. The subscript zero indicates the equilibrium position. Because of the orthogonality of the eigenfunctions, relationship 3 reduces to eq 4 and 5.

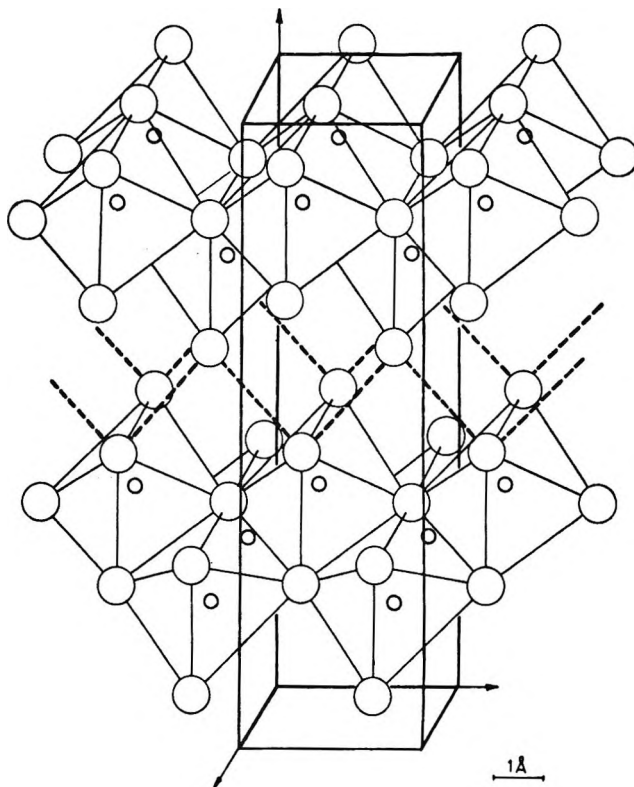


Figure 1. Structure of boehmite:⁶ small circle, aluminum; large circle, oxygen or hydroxyl; dashed line, hydrogen bonds.

(3) W. V. Milligan and J. L. McAtee, *J. Phys. Chem.*, **60**, 273 (1956).

(4) H. Bosmans and P. Michel, *Compt. Rend.*, **249**, 1532 (1959).

(5) H. Bosmans, to be published.

(6) K. A. Wickersheim and G. K. Korpi, *J. Chem. Phys.*, **42**, 579 (1965).

(7) G. C. Pimentel and A. McClellan, "The Hydrogen Bond," W. H. Freeman and Co., San Francisco, Calif., 1960.

$$\langle M_z^{n,m} \rangle = \sum_i \left(\frac{\delta M_z}{\delta \xi_i} \right)_0 \langle \xi_i^{n,m} \rangle \quad (4)$$

and

$$B_{nm} = \frac{8\pi^3}{3h^2} \langle (M_z^{n,m})^2 \rangle \quad (5)$$

It will be shown that the decrease in intensity of the fundamental modes of vibration observed on heating is accounted for by a tunnel effect and by an increase in the populations of the higher vibrational energy levels.

II. Infrared Spectra at Room Temperature

1. *Band Assignment.* The infrared spectra obtained for boehmite and partially deuterated boehmite diluted in KBr pellets are shown in Figure 2, as recorded with a Beckman IR-12 spectrometer. It is observed that the 3297- and 3090-cm⁻¹ OH stretching bands are replaced in a 95% deuterated sample by one single band at $\frac{1}{2}(3090 + 3297)$ cm⁻¹ = 3193 cm⁻¹. Accordingly, the two OD stretching bands are replaced by one band at 2400 cm⁻¹ in a 10% deuterated sample. This suggests that these bands are coupled stretching modes and from these observations, Wickersheim and Korpi⁶ have explained the hydrogenic modes of vibration on the basis of an infinite OH...OH...OH zigzag chain similar to structures proposed by Hornig and Osberg⁸ and Hornig and Hiebert⁹ for crystalline hydrogen halides or HX-DX mixed crystals.

Extending these investigations into the lower frequency region, we found three other hydrogenic modes for AlOOH at 1160, 1080, and 736 cm⁻¹. Partial deuteration causes the 1160- and 1080-cm⁻¹ bands to collapse into one component as shown in Figure 1. Therefore, these bands may probably be assigned to coupled bending bands.

Neglecting interactions between the chain and the rest of the structure, Wickersheim and Korpi⁶ anticipated the six optically active hydrogenic modes, shown in Figure 3. The "unit cell" contains two coplanar OH groups, and the bisectors of the angle formed by two adjacent OH bonds are parallel or perpendicular to the chain direction. The factor group of the chain is then isomorphous with the point group C_{2v}. Wickersheim and Korpi⁶ assigned the high-frequency stretching mode S₃ to the 3297-cm⁻¹ band and the low-frequency stretching mode S₁ to the 3090-cm⁻¹ band. Accordingly, we assign the S₄ bending mode to the 1160-cm⁻¹ band and the S₂ bending mode to the 1080-cm⁻¹ band although the former has only one-third of the integrated intensity of the latter. This is supported by the following considerations.

According to eq 4 and 5, the absorption coefficient B_{nm} is proportional to the square of the partial derivative of the dipole moment components x, y, and z, with respect to the normal coordinates. Mixing the symmetry coordinates to produce the actual normal modes is slight because of the appreciable frequency separation between the various motions belonging to different symmetry coordinates within each irreducible representation. The partial derivatives with respect to the symmetry coordinates may thus be used to approximate the intensity factor. Let S₁ and S₃ be parallel to the O-O links and the angle 2α between two adjacent links be slightly different from 90°. S₂ and S₄ are normal to S₁ and S₃. Assume that δ is the angle between the direction of the OH bond and the O-O link. For the two stretching modes, it is easily seen that

$$\left(\frac{\delta M}{\delta S_1} \right)^2 = \mu_x^2 + \mu_y^2 = 4\mu^2 \sin^2 \alpha \quad (6)$$

$$\left(\frac{\delta M}{\delta S_3} \right)^2 = \mu'_x{}^2 + \mu'_y{}^2 = 4\mu^2 \cos^2 \alpha$$

where μ is the absolute value of the change of the dipole. Accordingly, but with other values for μ_x, μ_y, and μ_z, one obtains for the bending modes

$$\left(\frac{\delta M}{\delta S_2} \right)^2 = \mu_x^2 + \mu_y^2 = 4\mu^2 \cos^2 (\alpha + \delta) \quad (7)$$

$$\left(\frac{\delta M}{\delta S_4} \right)^2 = \mu'_x{}^2 + \mu'_y{}^2 = 4\mu^2 \sin^2 (\alpha + \delta)$$

From (6) and (7), the intensity ratios for the two stretching modes and the two bending modes are S₃/S₁ = cotg² α and S₄/S₂ = tg² (α + δ), respectively. From the X-ray structure data,⁵ 2α = 85°22'; S₃/S₁ should then be equal to 1.17. This is in perfect agreement with the experimental ratio of 1.17 ± 0.05 found for the integrated intensities of the two OH stretching bands. Using α = 42°41', the ratio S₄/S₂ may be computed for various values of δ. For δ equal to -5, -10, and -15°, the following values are obtained for S₄/S₂: 0.594, 0.41, and 0.274. This shows that for an approximate deviation of 12° outward from the O-O link, the difference observed in the intensity ratio of the S₄ and S₂ bands is of the right order of magnitude. Such a strong deviation has also been found in diaspore by neutron diffraction.¹⁰ The intensity

(8) D. F. Hornig and W. E. Osberg, *J. Chem. Phys.*, **23**, 662 (1955).

(9) D. F. Hornig and G. L. Hiebert, *ibid.*, **27**, 752 (1957).

(10) W. R. Busing and E. A. Levy, *Acta Cryst.*, **11**, 798 (1958).

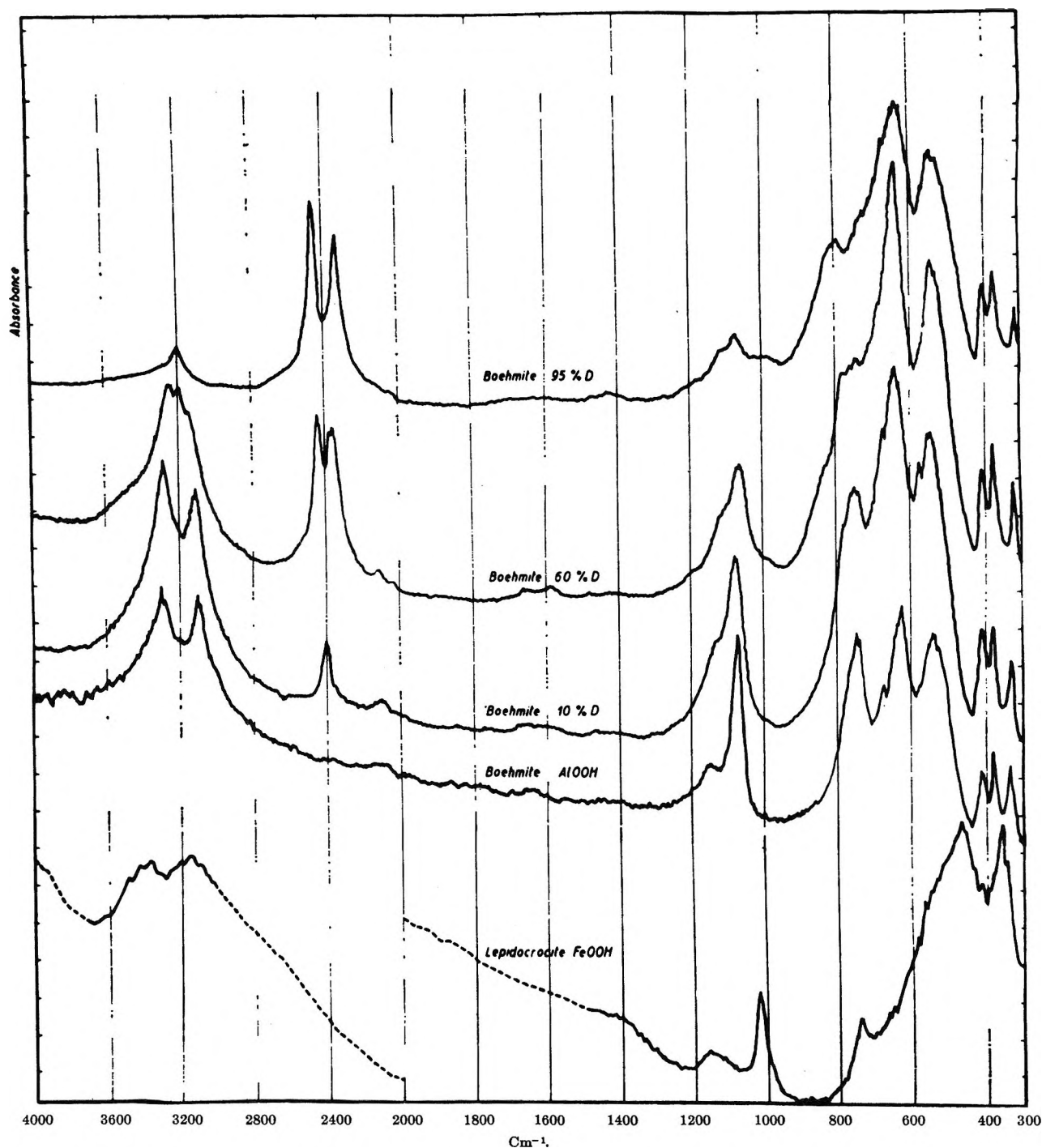


Figure 2. Infrared spectra of boehmite samples in KBr (dilution: 0.75%). One division of the ordinate axis = 10% absorbance. Deuterated samples were obtained by synthesizing boehmite from bayerite at 150° under pressure in presence of a mixture of H₂O-D₂O. Below: FeOOH, lepidocrocite.

ratio S_4/S_2 as well as the tendency for these two bands to collapse into one band on partial deuteration supports the assignment of S_4 and S_2 to the two bending modes in the x - y plane.

The remaining hydrogenic mode at 755 cm⁻¹ will be assigned to S_6 and it will be assumed that it occurs

at the same frequency as the infrared-inactive mode S_6 . The bands at 618 and at 522 cm⁻¹ present in both AlOOH and AlOOD are probably the ν_3 and ν_4 modes, respectively, of an AlO₆ octahedron. They are also present in aluminum trihydrates: gibbsite, bayerite, and nordstrandite.⁵ Weaker spectral components at

410 and 372 cm^{-1} are assigned to skeletal modes as similar bands were found in trihydrates. The bands observed at 326 cm^{-1} in AlOOH and at 305 cm^{-1} in AlOOD , which have an isotopic ratio lower than 1.35, might be $\text{Al}-(\text{OH})$ or $\text{Al}-(\text{OD})$ mode.

Table I summarizes these assignments; they are supported also by the infrared spectrum of lepidocrocite (FeOOH). In particular, the five active hydrogenic modes are found at approximately the same positions with comparable intensities while the ν_3 and ν_4 of FeO_6 octahedron are shifted toward lower frequencies, at 480 and 360 cm^{-1} , respectively.

2. *The Potential Energy Function.* Consider the symmetry coordinates of species A_1 , B_1 , A_2 , and B_2 shown in Figure 3, the only ones for which genuine normal vibrations occur for the symmetry point groups C_{2v} of the zigzag chain. The orientation of the cartesian axes has been chosen such that the y axis

corresponds to the $\text{O}-\text{O}$ axis. The $\widehat{\text{O}-\text{O}-\text{O}}$ angle in the zigzag chain will be considered as exactly equal to 90° and the $\text{O}-\text{H}$ bond will be assumed to coincide with the $\text{O}-\text{O}$ axis. These assumptions bring a considerable simplification since the normal and the cartesian coordinates are mutually orthogonal.

The potential and the kinetic energies expressed in terms of symmetry coordinates are then, according to the above

$$2V = c_{11}S_1^2 + 2c_{12}S_1S_2 + c_{22}S_2^2 + c_{33}S_3^2 + 2c_{34}S_3S_4 + c_{44}S_4^2 + c_{55}S_5^2 + c_{66}S_6^2$$

$$2T = d_{11}\dot{S}_1^2 + 2d_{12}\dot{S}_1\dot{S}_2 + d_{22}\dot{S}_2^2 + d_{33}\dot{S}_3^2 + 2d_{34}\dot{S}_3\dot{S}_4 + d_{44}\dot{S}_4^2 + d_{55}\dot{S}_5^2 + d_{66}\dot{S}_6^2 \quad (8)$$

where $\dot{S}_i = dS_i/dt$. The secular determinant is then

$$\begin{vmatrix} c_{11} - d_{11}\lambda & c_{12} - d_{12}\lambda & 0 & 0 & 0 & 0 \\ c_{21} - d_{21}\lambda & c_{22} - d_{22}\lambda & 0 & 0 & 0 & 0 \\ 0 & 0 & c_{33} - d_{33}\lambda & c_{34} - d_{34}\lambda & 0 & 0 \\ 0 & 0 & c_{43} - d_{43}\lambda & c_{44} - d_{44}\lambda & 0 & 0 \\ 0 & 0 & 0 & 0 & c_{55} - d_{55}\lambda & 0 \\ 0 & 0 & 0 & 0 & 0 & c_{66} - d_{66}\lambda \end{vmatrix} = 0 \quad (9)$$

It can be immediately factored into six equations where $\lambda_i = 4\pi^2\nu_i^2$

$$\left. \begin{aligned} \lambda_5 &= \frac{c_{55}}{d_{55}} & \lambda_6 &= \frac{c_{66}}{d_{66}} \\ \lambda_1 + \lambda_2 &= \frac{c_{22}d_{11} + c_{11}d_{22} - 2c_{12}d_{12}}{d_{11}d_{22} - d_{12}^2}; & \lambda_1\lambda_2 &= \frac{c_{11}c_{22} - c_{12}^2}{d_{11}d_{22} - d_{12}^2} \\ \lambda_3 + \lambda_4 &= \frac{c_{44}d_{33} + c_{33}d_{44} - 2c_{34}d_{34}}{d_{33}d_{44} - d_{34}^2}; & \lambda_3\lambda_4 &= \frac{c_{33}c_{44} - c_{34}^2}{d_{33}d_{44} - d_{34}^2} \end{aligned} \right\} \quad (10)$$

Table I: Assignments of the Infrared Bands (cm^{-1})

AlOOH	AlOOD	Assignments
3297	2470	Hydrogenic mode S_3
3090	2350	Hydrogenic mode S_1
1160	?	Hydrogenic mode S_4
1080	790	Hydrogenic mode S_2
755	540 ^a	Hydrogenic mode S_6
618	625	ν_3 of AlO_6 octahedron
522	530 ^a	ν_4 of AlO_6 octahedron
410	394	Skeletal mode of $\text{Al}-\text{O}$ layers
372	366	Skeletal mode of $\text{Al}-\text{O}$ layers
326	305	$\text{Al}-(\text{OH})$ or $\text{Al}-(\text{OD})$ mode

^a Broadened bands.

In order to express the c_{ij} and d_{ij} coefficients in terms of more familiar quantities, the potential and kinetic energies have to be translated into other systems of coordinates. As shown in Figure 3, the hydrogen atom displacements are in cartesian coordinates

$$\begin{aligned} x_1 &= S_2 + S_4 & x_2 &= S_1 - S_3 \\ y_1 &= S_1 + S_3 & y_2 &= S_2 - S_4 \\ z_1 &= S_6 - S_5 & z_2 &= S_5 + S_6 \end{aligned}$$

since the most general displacement is simply a superposition of the symmetry coordinates. For the kinetic energy, it follows that

$$2T = 2m_{\text{H}}(\dot{S}_2^2 + \dot{S}_4^2 + \dot{S}_1^2 + \dot{S}_3^2 + \dot{S}_5^2 + \dot{S}_6^2) \quad (11)$$

From (11) and (8), $d_{11} = d_{22} = d_{33} = d_{44} = d_{55} = d_{66} = 2m_{\text{H}}$ and $d_{12} = d_{34} = 0$. The potential energy will be expressed in terms of valence force coordinates, *i.e.*, as a function of the change of the internuclear distances $\text{O}-\text{H}$ and of the angles $\widehat{\text{HOO}}$. Let Q_1 and Q_3 be

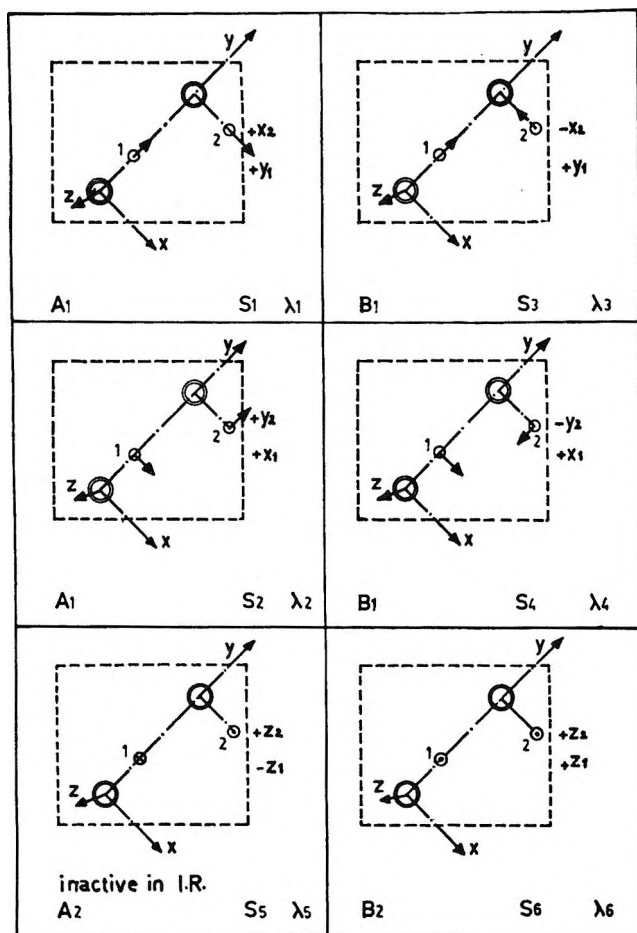


Figure 3. Hydrogenic modes in boehmite according to Wickersheim and Korpi.⁶ The symmetry coordinates $S_1 \dots S_6$, the roots of the secular equation $\lambda_1 \dots \lambda_6$, and the cartesian displacement coordinates are indicated with respect to the symmetry species $A_1, B_1, A_2,$ and B_2 .

the displacement of the H atoms, 1 and 2, along the O-O axes

$$Q_1 = S_1 + S_3; \quad Q_3 = S_1 - S_3$$

The deformation coordinates are

$$Q_2 = r_{OH}\delta_1 = S_2 + S_4; \quad Q_4 = r_{OH}\delta_2 = S_2 - S_4$$

$$Q_5 = r_{OH}\gamma_1 = S_5 - S_6; \quad Q_6 = r_{OH}\gamma_2 = S_5 + S_6$$

where r_{OH} is the internuclear distance O-H and where δ_1 and δ_2 are the deformation angles of O-H₁ and O-H₂ in the x - y plane of the zigzag chain and γ_1 and γ_2 are the deformation angles of O-H₁ and O-H₂ along the z axis.

Three additional coefficients will be considered in order to take into account (1) the coupling of the valence vibrations (k_{13}), (2) the coupling of the bending vibrations (k_{24}), and (3) the coupling of the stretching

and of the bending vibrations ($k_{14} = k_{32}$). If k_1 is the restoring force in the line of OH bond, and if k_2 and k_5 are the restoring forces opposing the deformation of the OH bonds in the plane ("bending") or out of plane ("torsion"), respectively, the potential energy function becomes

$$2V = k_1(Q_1^2 + Q_3^2) + 2k_{13}Q_1Q_3 + 2k_{14}(Q_1Q_4 + Q_3Q_2) + k_2(Q_2^2 + Q_4^2) + 2k_{24}Q_2Q_4 + k_5(Q_5^2 + Q_6^2) \quad (12)$$

or, in terms of symmetry coordinates

$$2V = 2(k_1 + k_{13})S_1^2 + 2(k_2 + k_{24})S_2^2 + 4k_{14}S_1S_2 - 4k_{14}S_3S_4 + 2(k_1 - k_{13})S_3^2 + 2(k_2 - k_{24})S_4^2 + 2k_5S_5^2 + 2k_5S_6^2 \quad (13)$$

From (13) and (8), it follows that $c_{11} = 2(k_1 + k_{13})$; $c_{12} = 4k_{14}$; $c_{22} = 2(k_2 + k_{24})$; $c_{33} = 2(k_1 - k_{13})$; $c_{34} = -4k_{14}$; $c_{44} = 2(k_2 - k_{24})$; $c_{55} = c_{66} = k_5$.

Using the c_{ij} and d_{ij} coefficients, (10) is solved in terms of the restoring forces. The system of simultaneous equations has been treated as follows. First k_{24} has been put equal to zero; k_{13} is then found equal to -0.41 . Secondly, k_{14} has been neglected; k_{13} was then equal to -0.36 ; k_{13} was thus essentially unaffected by this change in assumptions. An average value of -0.385 was then taken and (10) was solved for the other coefficients. Table II contains the results. The calculated frequencies are within a few per cent of the experimental data. If, instead of m_H , the reduced mass is used, all the restoring forces should be multiplied by 0.942.

Table II: Restoring Forces Obtained for AlOOH

Restoring forces ($\times 10^6$ dynes cm^{-1})	Frequencies	
	Calcd	Obsd
Stretching k_1	5.714	$\nu_1 = 3100 \text{ cm}^{-1}$
Bending k_2	1.036	$\nu_2 = 1075 \text{ cm}^{-1}$
Torsion k_5	0.318	$\nu_3 = 3290 \text{ cm}^{-1}$
Coupling stretch- ing-stretching, k_{13}	-0.385	$\nu_4 = 1150 \text{ cm}^{-1}$
Coupling stretch- ing-bending, k_{14}	± 0.630	$\nu_5 = 740 \text{ cm}^{-1}$
Coupling bend- ing-bending, k_{24}	-0.025	$\nu_6 = 755 \text{ cm}^{-1}$

The negative sign of k_{13} is rather surprising at first sight. It may be understood as follows. Suppose that Q_1 and Q_3 are both positive. Coupling term $2k_{13}Q_1Q_3$

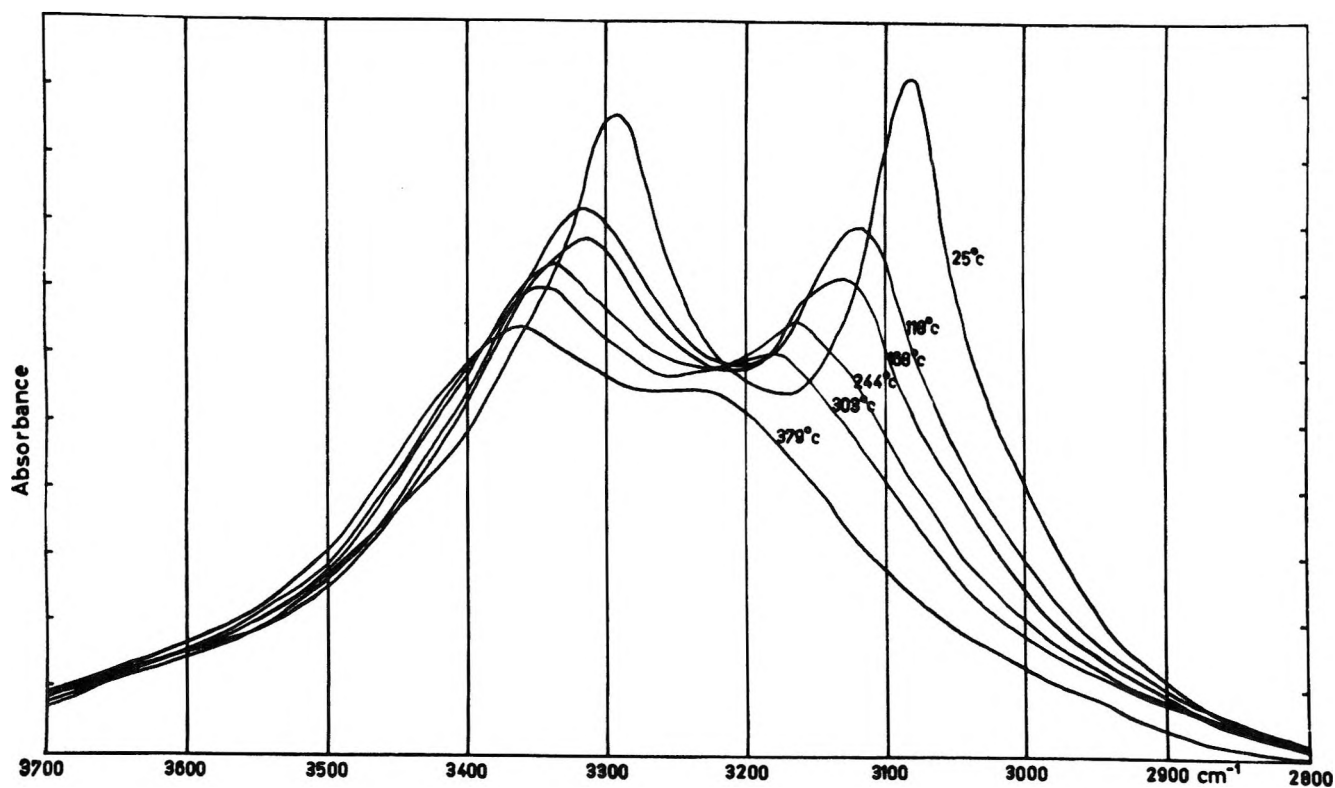


Figure 4. Stretching modes S_3 and S_1 at increasing temperatures. One division of the ordinate scale = 10% absorbance.

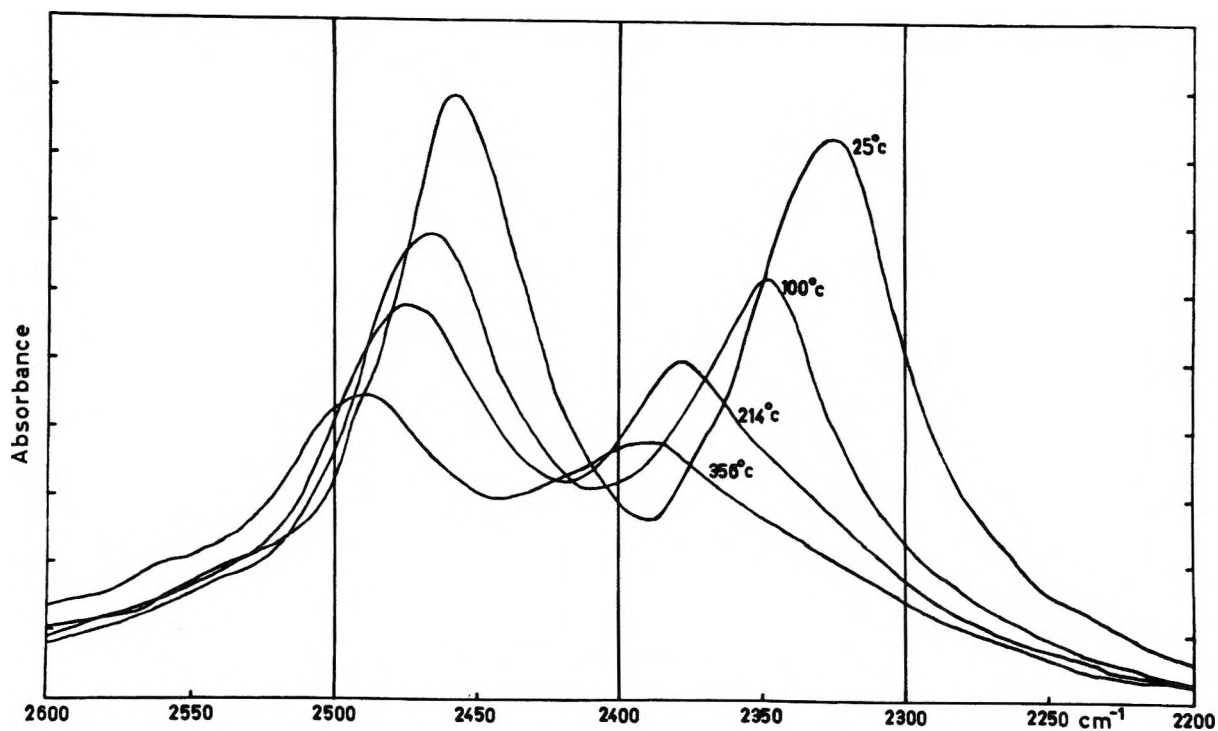


Figure 5. Stretching modes S_3 and S_1 for the 95% deuterated sample at increasing temperatures. One division of the ordinate scale = 10% absorbance.

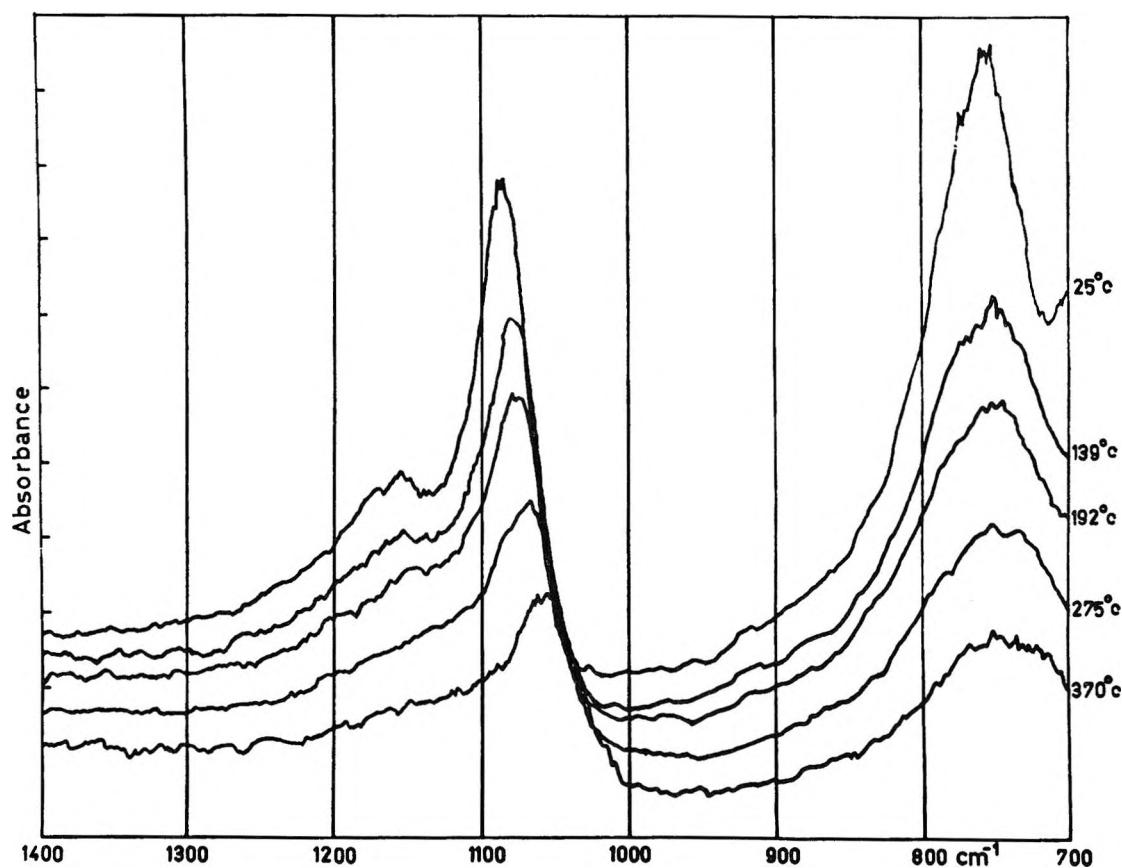


Figure 6. Bending modes S_4 and S_2 and torsion mode S_6 at increasing temperatures. One division of the ordinate scale = 10% absorbance.

forces hydrogen atom 1 to approach the oxygen atom to which hydrogen atom 2 is attached, while the latter approaches the opposite oxygen atom. This reinforces hydrogen bonds and decreases the potential energy. Therefore, $(k_1(Q_1^2 + Q_3^2) + 2k_{13}Q_1Q_3) < k_1(Q_1^2 + Q_3^2)$. It follows that $2k_{13}Q_1Q_3 < 0$ and that $k_{13} < 0$ if $Q_1Q_3 > 0$. A negative interaction force constant has been obtained for other H-bonded systems, such as $B(OH)_3$ ¹¹ and ice.¹² The coupling of the stretching and of the bending vibrations is also characterized by a high restoring force k_{14} . It has been

shown⁵ that \widehat{AlOO} angles are close to the tetrahedral value $109^\circ 28'$ while the \widehat{OOO} angle in the chain is noticeably smaller ($2\alpha = 85^\circ 30'$). When hydrogen atom 1 approaches the opposite oxygen atom, the positive electrical field arising from Al^{3+} and acting on hydrogen atom 2 is somewhat attenuated. Therefore, the force opposing the bending of OH toward the Al-O bond must be decreased to some extent.

III. Infrared Spectra at Increasing Temperatures

Samples of boehmite diluted in thin KBr pellets

(0.75%) were heated and the spectra were recorded at increasing temperatures, using the double-beam IR-12 Beckman spectrometer. Figures 4, 5, and 6 show some examples of the changes observed for the stretching, bending, and torsion modes.

Three main features are observed at increasing temperatures: a shift of the two stretching modes toward higher frequencies and of the bending modes toward lower frequencies, a progressive broadening, and a marked decrease in intensity for all the hydrogenic modes. Whatever the changes, all the observed phenomena are reversible on cooling the samples to room temperature, provided the limit of 400° has not been exceeded. Below this temperature, dehydroxylation of boehmite does not occur.

1. *Frequency Shifts.* From Table III, it may be observed that the S_3 and S_1 frequencies for AlOOH and AlOOD become progressively closer to each other as the temperature is increased. According to equations in (10), the coupling force constant k_{13} decreases

(11) D. F. Hornig and R. C. Plumb, *J. Chem. Phys.*, **26**, 637 (1956).

(12) C. Haas and D. F. Hornig, *ibid.*, **32**, 1763 (1960).

Table III: Frequency Shifts with Respect to the Temperature

—AIOOH—			—AIOOH—				—AIOOD—		
Temp, °K	S_1 , cm ⁻¹	S_3 , cm ⁻¹	Temp, °K	S_4 , cm ⁻¹	S_2 , cm ⁻¹	S_6 , cm ⁻¹	Temp, °K	S_1 , cm ⁻¹	S_3 , cm ⁻¹
300	3089	3297	300	1162	1080	755	300	2347	2475
391	3112	3320	372	1158	1080	755	373	2350	2469
439	3123	3330	412	1160	1080	755	436	2375	2475
541	3155	3345	465	1150	1073	755	487	2375	2475
576	3170	3355	502	1150	1070	755	569	2375	2490
652	3215	3375	548	(1145)	1070	(750)	629	2390	2493
			600	(1140)	1060	750			
			643	(1145)	1058	(750)			

accordingly. The weakening of the hydrogen bond is probably at the origin of this, since both the S_3 and S_1 bands shift simultaneously toward higher frequencies. As expected, the effect of temperature on the frequencies of the bending modes S_2 and S_4 is less pronounced and the shift is in the opposite direction.⁷ The frequency of the S_6 "torsion" mode is apparently not temperature sensitive. This is to be expected since parallel OH chains are not hydrogen bonded.

Coggeshall¹³ has attempted to calculate the frequency shift and the intensity of absorption of a hydroxyl group which is hydrogen bonded to a neighboring oxygen atom on the basis of an electrostatic interaction. If the change of the potential energy of the OH group due to the polarization is introduced into the Schrödinger equation with a Morse potential energy function, the energy levels are shifted by a term

$$\frac{ah(D_e - qE_p/a)(v + 1/2)}{\pi(2\mu)^{1/2}(D_e - qE_p/2a)^{1/2}}$$

where $a = 1/2\sqrt{2k_1/D_e}$ is the constant of the Morse function given by

$$U = D_e(1 - e^{-a(y - r_{OH})})^2 \quad (14)$$

and D_e is the dissociation energy of the O-H bond. q is the charge unbalance for the OH group and E_p is the electric field component parallel to the direction of the valence bond. Therefore, for a $0 \rightarrow 1$ transition, the frequency (ν_s) of the stretching band of the perturbed OH oscillator is shifted with respect to that for the unperturbed oscillator (ν_0) as

$$\frac{qE_p}{D_e a} = 1 - \frac{1}{4}\left(\frac{\nu_s}{\nu_0}\right)^2 - \left(\frac{\nu_s}{\nu_0}\right)\sqrt{\frac{1}{4} + \frac{1}{16}\left(\frac{\nu_s}{\nu_0}\right)^2} \quad (15)$$

Between 300 and 660°K, the shift of the mean stretching vibration $\nu_s = 1/2(\nu_1 + \nu_3)$ is of the order of magnitude of 100 cm⁻¹. Assuming the "free" OH stretching frequency ν_0 to be 3750 cm⁻¹ and D_e to be 110.2 kcal,¹⁴ a shift of 100 cm⁻¹ corresponds to a decrease of

the polarization force qE_p from 0.324×10^{-3} to 0.265×10^{-3} esu.

According to Bosmans,⁵ the coefficient of thermal expansion along the direction normal to the OH-O chain and parallel to the zigzag plane is 2.81×10^{-5} . As the width of the chain is about 2 Å, an increase in temperature of the order of magnitude of 300°K lengthens the O-O distance by about 0.02 Å. Such a change corresponds to a reasonable decrease of the potential energy, amounting to 0.85 kcal mole⁻¹.

The lengthening of the O-O distance is also in agreement with the frequency shift predicted by the one-dimensional model for hydrogen bonding proposed by Lippincott and Schroeder.¹⁵ An average stretching frequency of 3193 cm⁻¹ (at 300°K) corresponds to an O-O bond length of 2.72 Å, while the value observed at 650°K, *i.e.*, 3295 cm⁻¹, is in agreement with a bond length of 2.74 Å. The X-ray structural data⁵ at 300°K indicate an O-O distance of 2.73 Å. It may be therefore concluded that the frequency shift observed at increasing temperature accounts for the thermal dilatation of the crystal unit cell.

2. *Broadening of the Absorption Bands.* Table IV shows the half band widths observed for the S_1 , S_3 , S_2 , and S_6 modes at two temperatures. According to the Heisenberg uncertainty principle, the half band width $\Delta\nu$ is approximately equal to the sum of the half-widths of the upper and lower states, or, for a transition from the energy level w to w'

$$\Delta\nu = \frac{1}{4\pi}\left(\frac{1}{\tau_w} + \frac{1}{\tau_{w'}}\right) = \frac{1}{2\pi}\left(\frac{P_w + P_{w'}}{2}\right) = \frac{1}{2\pi}\bar{P}_w \quad (16)$$

where τ_w is the lifetime of the proton at the energy level w . P_w is then the probability of the proton

(13) N. Coggeshall, *J. Chem. Phys.*, **18**, 978 (1950)

(14) L. Pauling, "The Nature of the Chemical Bond," 3rd ed, Cornell University Press, Ithaca, N. Y., 1960.

(15) E. R. Lippincott and R. Schroeder, *J. Phys. Chem.*, **61**, 921 (1957).

leaving the state w per unit time. Table IV shows that \bar{P}_w is always slightly lower than the vibration frequency ν but that it is much greater than the Einstein transition coefficients. It may then be assumed that P_w represents a probability of the proton leaking out of the potential well at the energy level w .

Table IV: Observed Half Band Widths and "Leaking Out" Probability Values at 300°K and at Approximately 600°K for AIOOH

	Temp. °K	Vibrational modes			
		S_1	S_3	S_2	S_4
Half band width, cm ⁻¹	300	180	120	42	0.82
\bar{P}_w/ν	300	0.37	0.23	0.24	0.68
Half band width, cm ⁻¹	600	210	210	61	133
\bar{P}_w/ν	600	0.41	0.41	0.36	~1

For the OD stretching modes, S_1 and S_3 , \bar{P}_w/ν deduced from the observed band widths is only 0.175 at 300°K as compared to 0.37 and 0.23 for the corresponding bands in AIOOH. The results shown in Table IV are only approximate because of the overlapping of the S_1 and S_3 and of the S_2 and S_4 modes. It must be emphasized that the actual broadening is probably higher than that reported in Table IV because of the deformation of the high-frequency side of the bands. This is more apparent for the low-frequency modes S_2 , S_4 , and S_6 than for the stretching modes as shown in Figures 4, 5, and 6.

If the leak through the potential barrier is attributed to a tunnel effect of protons, the increase of \bar{P}_w with temperature may be due to an increase in the populations of vibrational levels closer to the top of the energy barrier.

3. Loss in Intensity of Hydrogenic Modes. At low dilution in KBr, it is assumed that the integrated band intensity represents adequately the characteristic absorbance. The relative absorbance A_r is then defined as the ratio of the integrated intensity at the temperature T to the integrated intensity at the temperature $T_0 = 300^\circ\text{K}$; k_ν being the absorption coefficient, it follows that

$$A_r = \frac{\int_{\nu_1}^{\nu_2} k_\nu(T) d\nu}{\int_{\nu_1}^{\nu_2} k_\nu(T_0) d\nu} \quad (17)$$

In order to express the loss of intensity shown in Table V, the two S_3 and S_1 stretching bands were integrated together because the delineation between them is more hazardous at high temperature. The ratios

Table V: Change of Relative Absorbances with Respect to the Temperature

AIOOH		AIOOD	
Temp. °K	Stretch. bands, $S_1 + S_3$	Temp. °K	Stretch. bands, $S_1 + S_3$
300	1.00	300	1.00
391	0.91	373	0.85
439	0.865	436	0.76
541	0.79	487	0.72
576	0.755	569	0.59
652	0.65	629	0.56

of the integrated intensities S_3/S_1 were calculated between 300 and 500°K for AIOOH and AIOOD. They do not change by more than $\pm 4\%$. In agreement with eq 6 one may conclude that the angle 2α between two adjacent O-O links is not noticeably modified. The radiant energy emitted by the hot sample has to be considered. In the instrument used in this work, the infrared beam is chopped first between the Nernst glover and the sample, and secondly, between the sample and the detector. The energy emitted by the hot sample is thus added to the radiant energy transmitted through the sample and therefore it contributes to decrease the over-all absorbance. On the contrary, when the 2^d chopper is stopped, the additional energy is not detected as it is not modulated.

By recording the hydrogenic fundamental bands at increasing temperatures under this condition and by comparing with those obtained with the instrument in "normal" operation, *no significant difference was observed below 650°K for the stretching modes.* However, for the lower frequency bending and torsion modes, at the same temperature, the contribution of the radiant energy emission decreases the relative absorbances by about 0.15. Actually, the relative absorbances of the AIOOH bending and torsion bands are equal, within the experimental error (± 0.05), to those shown in Table V for the AIOOH stretching bands.

When $\log(1 - A_r)$ is plotted against the inverse of the temperature, the activation energies of the process responsible for the intensity losses are close to 2 kcal, whatever the vibrational modes.

Before going further, it seems necessary to examine a possible explanation for the intensity loss observed upon heating. It is well known that hydrogen bonding provokes an enhancement of the intensity of the OH stretching bands.⁷ On the contrary, as the thermal dilatation reduces the strength of the OH...O bond, it might be assumed that this effect contributes to de-

Table VI

Level	Energy, kcal	Multi- plicity	Temp, °K				
			300	400	500	600	700
A. Population of the Energy Levels ($\times 10^4$) in ALOOH							
Fundamental	0	1	9330.6	8320.7	7117.0	5949.5	4879.5
$\nu_5 = \nu_6$	2.11	2	546.7	1175.7	1708.5	2026.7	2155.9
ν_2	3.08	1	53.5	173.5	323.8	450.8	535.3
ν_4	3.30	1	37.7	133.8	262.4	380.3	460.7
$2\nu_6$	4.22	3	24.0	124.6	307.6	517.8	714.4
$\nu_5 + \nu_2$	5.19	2	3.1	24.5	77.7	153.6	236.5
$\nu_5 + \nu_4$	5.41	2	2.2	18.9	63.0	129.6	203.5
$2\nu_2$	6.16	1	0.3	3.62	14.7	34.1	58.7
$3\nu_5$	6.33	4	0.9	11.7	49.2	117.6	210.4
$\nu_2 + \nu_4$	6.38	1	0.2	2.79	11.9	28.8	50.5
$2\nu_4$	6.60	1	0.1	2.15	9.68	24.3	43.5
$2\nu_5 + \nu_2$	7.30	3	0.1	2.59	13.99	39.2	78.4
$2\nu_5 + \nu_4$	7.52	3	0.1	1.98	11.4	32.7	66.9
$2\nu_2 + \nu_5$	8.27	2		0.52	3.50	13.2	26.0
$4\nu_6$	8.44	5		1.05	7.5	25.5	58.0
$\nu_6 + \nu_2 + \nu_4$	8.49	2		0.4	2.86	9.81	22.33
$\nu_6 + 2\nu_4$	8.71	2		0.3	2.3	8.2	19.0
ν_1	8.89	1		0.12	0.95	3.5	8.4
$3\nu_2$	9.24	1		0.08	0.67	2.6	6.6
$3\nu_6 + \nu_2$	9.41	4		0.24	2.24	8.91	23.08
ν_3	9.43	1			0.56	2.2	5.70
B. Population of Energy Levels ($\times 10^4$) in ALOD							
Fundamental	0	1	8219.8	6574.2	5067.8	3845.6	2925.2
$\nu_5 = \nu_6$	1.55	2	1233.3	1889.4	2151.1	2117.1	1928.0
ν_2	2.26	1	185.7	384.0	523.5	580.9	578.9
ν_4	2.42	1	140.3	311.3	441.7	505.0	513.4
$2\nu_5$	3.10	3	138.8	407.3	684.8	874.2	953.1
$\nu_5 + \nu_2$	3.81	2	27.6	108.0	216.0	316.0	380.0
$\nu_6 + \nu_4$	3.97	2	21.0	89.5	187.5	278.0	338.4
$2\nu_2$	4.52	1	4.1	21.7	52.5	87.0	113.0
$3\nu_6$	4.65	4	13.2	74.0	186.0	312.0	412.0
$\nu_2 + \nu_4$	4.68	1	3.1	17.8	45.0	76.0	102.0
$2\nu_4$	4.84	1	2.39	14.7	38.5	66.3	90.1
$2\nu_5 + \nu_2$	5.36	3	3.0	23.4	69.0	129.0	186.0
$2\nu_6 + \nu_4$	5.52	3	2.3	19.2	58.5	112.5	165.0
$\nu_6 + 2\nu_2$	6.07	2	0.62	6.4	22.96	48.3	75.5
$4\nu_6$	6.20	5	0.75	14.0	50.0	106.0	170.0
$\nu_6 + \nu_2 + \nu_4$	6.23	2	0.50	5.4	19.6	41.4	66.0
$\nu_6 + 2\nu_4$	6.39	2	0.40	3.8	16.8	36.0	59.0
ν_1	6.59	1	0.10	1.4	6.8	15.3	26.0
$3\nu_2$	6.78	1	0.10	1.3	5.6	13.0	22.5
ν_3	6.90	1		1.1	5.0	11.8	20.5

crease the absorption coefficients. In this case, the matrix element $\langle M^{0,1} \rangle$ of the dipole moment for the transition between the ground and first excited states calculates to be¹³

$$\langle M^{0,1} \rangle = (b_0 - 2)^{1/2}/a(b_0 - 1) \quad (18)$$

For an unperturbed Morse function, b_0 is given by $b_0 = 4\pi(2\mu D_e)^{1/2}/(ah - 1)$, while b_0 for the Morse function perturbed by the electrical polarization qE_p is

$$b_0 = \frac{4\pi(2\mu)^{1/2}(D_e - qE_p/a)}{ah(D_e - qE_p/2a)^{1/2}} - 1$$

According to eq 5, the ratio of the absorption coefficients is equal to

$$\langle \langle M^{0,1} \rangle_{\text{pert}} / \langle M^{0,1} \rangle_{\text{unpert}} \rangle^2 \quad (19)$$

Using the same ν_s , ν_0 , D_e , and a values as in eq 15, this ratio decreases from 1.166 at 300°K to 1.137 at

650°K. This effect is much smaller than that shown in Table V and the proposed explanation does not hold.

In order to interpret the loss in intensity of the OH fundamentals at increasing temperatures, we will assume that energy levels above a limiting value do not contribute to the discrete absorption of radiant energy. It may be considered that a transition will not contribute to the absorption band when it takes place toward a level w' for which $P_{w'} = P_w/\nu_i \simeq 1$, $P_{w'}$, being the tunneling probability per period ν_i^{-1} of the i th vibration mode. The physical meaning of this hypothesis will be given later. The phenomenon should become more noticeable with increasing populations of vibrational states characterized by higher P_w values. This hypothesis is in agreement with the reported broadening of the absorption bands.

Therefore, the summation of eq 1 cannot be extended beyond the energy level w' for which the tunneling probability per vibration period is close to 1. For a transition from w toward $w' = w + h\nu_i$

$$A = \frac{h\nu_i N_0}{c} \sum_{w(P_{w'} < 1)} N_w B(1 - N_{w'}) \quad (20)$$

The relative absorbance defined previously by eq 17 becomes

$$A_r = \frac{\left(\sum_{w(P_{w'} < 1)} N_w (1 - N_{w'}) \sqrt{v+1} \right)_{T^\circ(K)}}{\left(\sum_{w(P_{w'} < 1)} N_w (1 - N_{w'}) \sqrt{v+1} \right)_{300^\circ K}} \quad (21)$$

where v is the vibrational quantum number at the energy level w . The square root of $(v+1)$ is introduced to take into account the change of the B absorption coefficient above the fundamental level.

The relative population of a vibrational state w , as defined in eq 1, is given by the relationship

$$N_w = gQ^{-1}e^{-w/kT} \quad (22)$$

where $w = \sum_i \nu_i h\nu_i$, ν_i being the vibrational quantum numbers and ν_i the corresponding frequencies. The statistical weight g is introduced to take into account the assumed mechanical degeneracy of the S_6 and S_6 modes: $g = v_6 + 1$ with $v_6 = v_6$. From the vibrational characteristic temperatures θ_i , N_w may be easily computed as shown in Table VI, the partition function being

$$Q^{-1} = \prod_i (1 - e^{-\theta_i/T}) \quad (23)$$

The activation energies determined above for the process involved in the loss of intensity of the OH fundamentals are of the order of magnitude of the first energy levels. This is an indication that a notice-

able population shift toward slightly higher vibrational states affects the intensity of the absorption bands.

In order to emphasize this point, let us proceed empirically as follows. The average temperature coefficient obtained by plotting $\log(1 - A_r)$ against T^{-1} being about 2 kcal for the stretching, bending, and torsion modes, it may be assumed that for AlOOH the vibrational levels above the fundamental (Table VIA) do not contribute to the discrete absorption of radiant energy. This means that the energy levels for which $P_{w'} \rightarrow 1$ are approximately equal to 11, 5, and 4 kcal for the stretching, bending, and torsion OH modes, respectively. Under these conditions, eq 21 gives the relative absorbances (computed) shown in Table VII. They are compared with the values deduced from the best-fitting curves plotted with the experimental values (obsd) of Table V. The differences are approximately within the experimental errors.

Table VII: Computed and Observed Relative Absorbances

Temp. °K	AlOOH				AlOOD	
	Obsd	$S_1 + S_3$ comp	$S_2 + S_4$ comp	S_6 comp	Obsd	$S_1 + S_7$ Comp
300	1	1	1	1	1	1
400	0.91	0.89	0.88	0.83	0.83	0.85
500	0.82	0.76	0.74	0.67	0.70	0.72
600	0.71	0.64	0.61	0.54	0.57	0.60

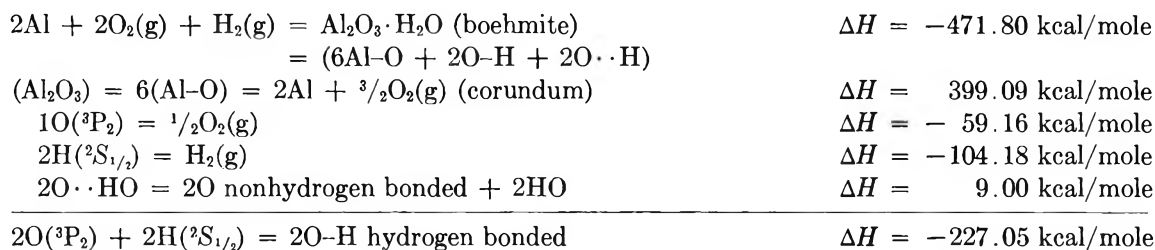
For the OD stretching modes, the computed data of Table VII were obtained using the relative populations of the two first vibrational levels (Table VIB). The limiting energy level is then located at about 9 kcal.

IV. Discussion on the Tunnel Effect

It is now necessary to verify whether the assumed leak of proton out of the potential well may be accounted for by an acceptable potential barrier.

An evaluation of the dissociation energy is necessary to obtain the Morse function of the OH bond. The Al-O bond energies in analogous crystalline substances (corundum and boehmite) were selected in order to allow for the electrostatic long range forces. The energy of the hydrogen bonds in boehmite has been estimated to 4.5 kcal mole⁻¹ according to Lippincott and Schroeder.¹⁵ The calculation is made as shown hereafter using the enthalpy data proposed by Latimer.¹⁶

(16) W. Latimer, "Oxidation Potentials," 2nd ed, Prentice-Hall Inc., New York, N. Y., 1952.



Thus ΔH for O-H = -113.5 kcal/mole. A similar calculation gives 115.3 kcal/mole for the O-H bond in gibbsite, $\text{Al}(\text{OH})_3$, and 120.3 kcal/mole for brucite, $\text{Mg}(\text{OH})_2$. It must be understood that ΔH represents the difference between the energies of the free H and O atoms and that of a OH group in the solid. The dissociation energy D_0 of OH is therefore referred to the lowest energy W and $D_0 = 113.5$ kcal.

The potential function along the O-O axis has been constructed using the Morse function given by eq 14. The height of the potential barrier may be computed if the positions of the minima are determined with respect to the energy scale. If, as usual, the fundamental level is considered as the zero level, the minimum of $U(y)$ is lowered below this level by 4.6 kcal, *i.e.*, the average energy of $1/2 h\nu_1$ and $1/2 h\nu_3$ and $D_e = D_0 + 4.6$ kcal. For the deuterated system, the corresponding energies were introduced into the calculation.

The distance between two adjacent $U(y)$ minima, $2l_0 = 0.698$ Å, was obtained by subtracting from the O-O distance (2.73 Å in boehmite⁵), twice the length r_{OH} of the OH bond (1.016 Å). In the decomposition of the hydrogenic motions, oxygen atoms were supposed to be immobile; this assumption holds so far as the O-O and OH frequency domains are very different. For the calculation of the tunneling probability P_w , a distribution function of the O-O distances should be considered and the average quantum mechanical value $\langle P_w \rangle$ should be computed. An alternative less sophisticated treatment may be proposed in order to correct the width ($2l_0$) and consequently the height of the energy barrier E^* for the O-O vibration.

Let R be the distance between two oxygen atoms and R_0 the equilibrium value ($R_0 = 2.73$ Å). The mean quadratic value of $(R - R_0)$ is easily obtained from

$$\langle (R - R_0)^2 \rangle = \int_{-\infty}^{+\infty} \psi_v(R - R_0) \times (R - R_0)^2 \psi_v^*(R - R_0) dR = \left(v + \frac{1}{2} \right) \frac{1}{\alpha} \quad (24)$$

and

$$\psi_v(R - R_0) = \left(\left(\frac{\alpha}{\pi} \right)^{1/2} \frac{1}{2^v v!} \right)^{1/2} e^{-\alpha/2(R-R_0)^2} H_v(R - R_0)$$

where H_v is the Hermite orthogonal function and $\alpha = 4\pi^2 m\nu_0/h$, ν_0 being the fundamental O-O frequency. Averaging $\langle (R - R_0)^2 \rangle$ over all the energy levels produces

$$\langle (R - R_0)^2 \rangle = \sum_v \langle (R - R_0)^2 \rangle \frac{N_v}{N_0} = (\alpha Q)^{-1} \sum_{v=0}^{\infty} (v + 1/2) e^{-v h\nu_0/kT}$$

If $kT/h\nu_0$ is small enough, allowing for a continuous sequence of energy levels

$$\langle (R - R_0)^2 \rangle = (\alpha Q)^{-1} \int_0^{\infty} v e^{-v h\nu_0/kT} dv + (2\alpha)^{-1} = (2\alpha)^{-1} + (\alpha Q)^{-1} \left(\frac{kT}{h\nu_0} \right)^2$$

Under the same conditions, the partition function Q is equal to $kT/h\nu_0$. Therefore

$$\langle (R - R_0)^2 \rangle = \frac{1}{\alpha} \left(\frac{kT}{h\nu_0} + \frac{1}{2} \right) \quad (25)$$

Assuming $\nu_0 = 200$ cm^{-1} , in agreement with the frequency proposed by Haas and Hornig¹² for the O-O vibration in ice, the square root of $\langle (R - R_0)^2 \rangle$ changes with respect to the temperature as shown in Table VIII. The correction due to the oxygen vibration is thus quite appreciable. The height E^* of the potential barrier is obtained graphically for each l_0 value. At the equilibrium position $R = R_0$, $2l_0 = 0.698$ Å and

Table VIII: Square Roots of the Mean Quadratic Values of the O-O Stretching Amplitude. Maximum and Minimum Widths ($2l_0$) of the Potential Barrier along the O-O Axis and Corresponding Barrier Heights (E^*)

T , °K	$\sqrt{\langle (R - R_0)^2 \rangle}$, Å	$2l_{0\text{max}}$, Å	E^*_{max} , kcal	$2l_{0\text{min}}$, Å	E^*_{min} , kcal
300	0.181	0.879	35.3	0.517	16.6
400	0.200	0.898	36.4	0.498	15.6
500	0.217	0.915	37.4	0.481	14.7
600	0.233	0.931	38.1	0.465	14.0
700	0.248	0.946	39.1	0.450	13.0

$E^* = 26$ kcal above the minimum of the potential energy curve.

Eckart¹⁷ has given an exact solution of the Schrödinger equation for a particle of mass m and of total energy w^* approaching a single energy barrier of height E^* and of decreasing thickness. $w^* = w + h\nu_s/2$ and E^* are measured with respect to the minimum of the potential curve. Hence the probability of tunneling per stretching period is

$$P_w^s = \frac{\cosh 4\pi\beta - 1}{\cosh 4\pi\beta + \cosh 2\pi\delta} \quad (26)$$

where

$$\beta = \frac{l_0}{h}(2mw^*)^{1/2}, \quad \delta = \frac{1}{2}\left(\frac{32E^*ml_0^2}{h^2} - 1\right)^{1/2}$$

From (26), it follows

$$P_w^s = \left[1 + \left(\frac{e^{\pi\delta} + e^{-\pi\delta}}{e^{2\pi\beta} - e^{-2\pi\beta}}\right)^2\right]^{-1} \quad (27)$$

From eq 27, it is found that the barrier height has to be equal to 21.2 kcal for P_w^s , the tunneling probability along the O–O axis, being very close to 1 at the energy level $w = 11$ kcal. Under these conditions, eq 21 gives the computed relative absorbance shown in Table VII for the OH stretching modes. A barrier height of 21.2 kcal is still in the range predicted by Table VIII, taking into account the vibration of the oxygen atoms. The tunneling probabilities P_w^s for ALOOH and ALOOD are reproduced in Figure 7. For the latter, P_w^s approximates 0.94 at the limiting energy level of 9 kcal used for computing the corresponding data of Table VII.

It follows that the estimated variation of the tunneling probability along the O–O axis with respect to the energy levels allows one to account for the loss in intensity of the stretching modes at increasing temperatures.

It might be suggested that the barrier permeability defined as the tunneling probability per unit time, $P_w^s\nu_s = P_w$, is representative of the leaking process out of the specified potential well. If this assumption is accepted, P_w^b and P_w^t the tunneling probabilities per period of the bending or of the torsion vibration, may be derived from the relationship

$$P_w^b\nu_b = P_w^t\nu_t = P_w^s\nu_s \quad (28)$$

where ν_s , ν_b , and ν_t are the fundamental stretching, bending, and torsion frequencies, respectively (Table I). The summation involved in eq 21 breaks down, consequently, at the energy levels corresponding to $P_w^b \simeq 1$ or $P_w^s \simeq 0.352$ for the bending absorption bands ($S_2 + S_4$) and to $P_w^t \simeq 1$ or $P_w^s \simeq 0.237$ for

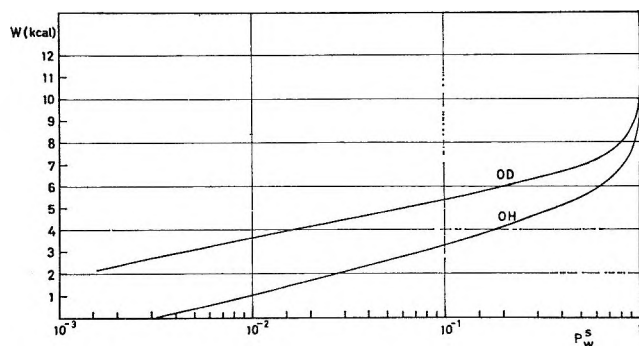


Figure 7. Tunneling probability P_w^s through the potential barrier along the O–O link. w = energy level above the fundamental. Barrier height: $E^* = 21.2$ kcal.

the torsion absorption band (S_6). One may easily check on Figure 7 that P_w^s reaches 0.237 at 4.3 kcal and 0.352 at 5 kcal. This is in excellent agreement with the empirical limiting energy levels used for computing the relative absorbances in Table VII.

In summary, the loss in intensity observed upon heating may be explained as follows: (1) there is a domain of energy levels, below the top of the potential energy barrier, where the tunneling probability is close to unity; (2) any optical transition leading to this domain does not contribute to the absorption band; (3) the shift of the population toward vibrational levels, from which such an optical transition is possible, accounts quantitatively for the observed variations of the relative absorbances. The physical meaning of point 2 will be discussed now.

V. Delocalization Processes

In a static model of a perfect crystal, every proton has a well-defined position and all the protons are oriented in a regular fashion, as shown for instance in Figure 3. The wave function of the whole protonic system is then defined by the product of individual proton wave functions in their different vibrational states. For such an independent particle model, the total transition probability between energy levels results from transitions of individual protons within their own potential well.

For an imperfect crystal, at increasing temperatures, it may be assumed that the movement of each proton is independent of the movement of the other protons and that each proton has a given probability to move to neighboring but less stable positions. Such a movement may be performed either along the directions of a stretching, bending, or torsion vibration. The individual wave function will no longer correspond to

(17) C. Eckart, *Phys. Rev.*, **35**, 1303 (1930).

that of a simple harmonic oscillator. Assuming that the general form of the potential well is that represented in Figure 8A, it can be easily deduced that the spacing between energy levels will vary rather abruptly as soon as the proton displacement becomes very probable. One may assume that optical absorption at the fundamental frequency is obtained only for transitions between levels, below some critical energy value. When the temperature is raised, one would thus expect a decrease of the fundamental absorption while secondary absorptions should appear at different frequencies. These absorptions may be weak enough to be masked in the background.

Another possibility exists that a proton stays in the neighborhood of one given oxygen but that it produces two configurations by "flipping" between two equilibrium positions as shown in Figure 8B. The passage from one configuration to another may result from displacements along the directions of the stretching or the bending vibrations, but all the displacements have to be coherent. This means a breakdown of the independent particle model. As far as the radiant energy absorption is concerned, this model would produce consequences similar to those discussed above. The mechanisms represented by these two first models cannot be described as true delocalization processes since the proton movement is restricted to a narrow domain.

One might also consider a third model that is fundamentally different from the previous ones. Instead of considering a proton that moves around in the vicinity of some specified oxygen ion, it might be assumed that all the protons belong collectively to all oxygen ions as schematically represented in Figure 8C. The proton would thus be considered in a way similar to electrons in a metal. In order to construct such a wave function, it would be necessary to consider the protonic movements as independent of the movements of electrons and heavy ions in the lattice. The energy bands that arise from the vibrational levels in independent potential wells should be narrow at the bottom since protons have only a small tunneling probability. They become quite large when the proton may pass easily through or over the potential barriers between neighboring crystallographic positions. At increasing temperatures, the absorption bands would be flattened out so much on the high-

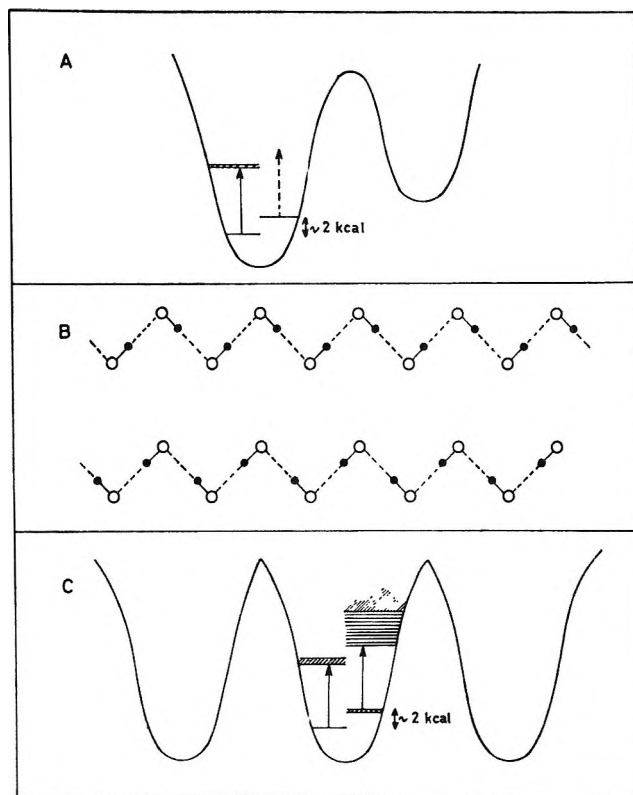


Figure 8. Schematic models proposed to explain the delocalization processes (see text).

frequency side that they are partially lost in the background. This last model should correspond to what may be considered as a true delocalization process.

The deductions exposed above support the concept that tunneling of protons through potential barriers causes the decrease in intensity of the OH fundamental obtained upon heating. The simultaneous deformation of the high-frequency side of the bands might be in favor of the third model. However, it would be too hazardous to conclude whether the proton movement is restricted to a narrow domain or is extended through the whole crystal.

Acknowledgments. We wish to acknowledge the part taken by Professor A. Meessen of the University of Louvain in the preparation of this manuscript and especially in the discussion of the various models proposed for the delocalization processes.

Radical Reactions in Liquid Cyclohexane. II. The Mercury-Photosensitized Decomposition of Cyclohexane

by W. A. Cramer

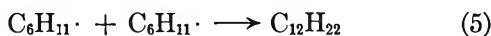
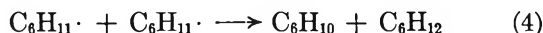
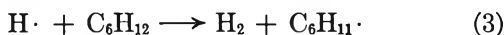
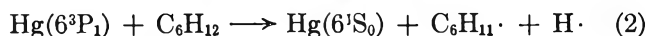
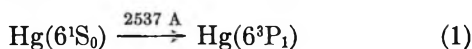
Reactor Institute, Delft, The Netherlands (Received November 23, 1966)

Accepted and Transmitted by The Faraday Society (September 5, 1966)

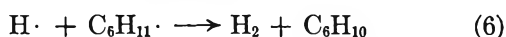
The mercury-photosensitized decomposition of liquid cyclohexane has been investigated in the presence and absence of oxygen. Dicyclohexyl and part of the cyclohexene are produced in reactions between cyclohexyl radicals. An appreciable fraction of the cyclohexyl radicals reacts with their sibling hydrogen atoms within the liquid cage, giving rise to unscavengeable cyclohexene formation. At higher conversions cyclohexyl radicals and hydrogen atoms react with cyclohexene. This results in the formation of cyclohexylcyclohexene and products with more than 12 carbon atoms.

Introduction

The mercury-photosensitized decomposition of hydrocarbons has recently been investigated to study radical reactions in the liquid phase.¹⁻⁴ In the case of cyclohexane, the following reaction mechanism has generally been assumed to occur,^{1,2,3,5} and experimental results have been interpreted accordingly.



However, it has recently been suggested that cyclohexene is not only formed in reaction 4 but also in reaction 6 between a cyclohexyl radical and its sibling hydrogen atom immediately after their formation within the cage of surrounding molecules.⁴



This reaction may be favored by the formation of the intermediate HgH in reaction 2, as was suggested by Kuntz and Mains.¹ An isotope effect, observed in the quenching of excited mercury atoms by saturated hydrocarbons and their deuterated analogs, has been interpreted as to indicate that HgH and HgD are

formed in the primary process.^{4,6,7} Evidence for reaction 6 was obtained by Hentz, *et al.*,⁴ who studied the mercury-photosensitized decomposition of mixtures of C₆H₁₂ and C₆D₁₂.

In the present work, we have tried to confirm the occurrence of reaction 6 in the mercury-photosensitized decomposition of cyclohexane. Furthermore, some experiments were carried out at high conversions to investigate reactions of cyclohexyl radicals with the product cyclohexene. Controversy still exists about these reactions. Addition of cyclohexyl radicals to cyclohexene has been proposed to account for polymer formation in the γ radiolysis of cyclohexane.⁸ On the other hand, it has also been suggested that cyclohexyl radicals do not react with cyclohexene, even in pure cyclohexene.⁹

(1) R. R. Kuntz and G. J. Mains, *J. Am. Chem. Soc.*, **85**, 2219 (1963).

(2) C. E. Klots and R. H. Johnson, *Can. J. Chem.*, **41**, 2702 (1963).

(3) J. W. Falconer and M. Burton, *J. Phys. Chem.*, **67**, 1743 (1963).

(4) R. R. Hentz, J. Y. Chang, and M. Burton, *ibid.*, **69**, 2027 (1965).

(5) P. W. Beck, D. V. Kniebes, and H. E. Gunning, *J. Chem. Phys.*, **22**, 672 (1954).

(6) E. G. Spittler, P. Jordan, L. M. Dorfman, and M. C. Sauer, *J. Phys. Chem.*, **67**, 2235 (1963).

(7) M. G. Bellas, Y. Rousseau, O. P. Strausz, and H. E. Gunning, *J. Chem. Phys.*, **41**, 768 (1964).

(8) R. Barker and M. R. H. Hill, *Nature*, **194**, 277 (1962).

(9) B. R. Wakeford and G. R. Freeman, *J. Phys. Chem.*, **68**, 2635 (1964).

Experimental Section

The preparation and purification of cyclohexane used in our experiments have been described elsewhere.¹⁰

Irradiations with light of 2537 Å from a low-pressure mercury lamp were carried out at 23° in Vycor cells. Prior to irradiation, the liquid, containing a drop of mercury, was degassed by the conventional freeze-thaw technique. Solutions containing oxygen were prepared by passing a stream of oxygen gas through the liquid during 2 min prior to irradiation. During the irradiations, which lasted from 1 min to 26 hr, the vapor phase above the liquid was masked.

Hydrogen, the only product volatile at -196°, was collected at this temperature and measured volumetrically. Other products were separated by gas-liquid partition chromatography and measured with a flame-ionization detector. Column materials and temperatures used in the analysis of cyclohexene, dicyclohexyl, cyclohexanol, and cyclohexanone, the latter two products being formed in the presence of oxygen, have been given in a previous publication.¹⁰

In addition to dicyclohexyl, two other C₁₂ products were formed at high conversions in the absence of oxygen. They were separated at 150° on a 4-m column containing 20% polyglycol 4000 (E. Merck Ltd) on 70-100 mesh Embacel. Both products could be converted to dicyclohexyl by catalytic hydrogenation at room temperature and were identified by their mass spectra. For this purpose, an appreciable amount of the cyclohexane from an irradiated sample was evaporated. Part of the resulting concentrated solution was injected in a gas chromatograph. The two unsaturated C₁₂ products were collected separately, using a stream splitter and introduced into a mass spectrometer. Both products showed parent peaks with a mass of 164. Since only C-H bond rupture occurs in the reaction between excited mercury atoms and saturated hydrocarbons, these parent peaks with a mass of 164 indicate that the C₁₂ products are two isomers of cyclohexylcyclohexene. Another part of the concentrated solution was introduced directly into a mass spectrometer. It was observed that, in addition to products with 12 carbon atoms, product molecules with 18, 24, and 30 carbon atoms were also present. Products containing 18 carbon atoms were also detected gas chromatographically, using a 2-m column containing 20% silicon oil on 70-100 mesh Embacel. Since no standard solutions were available for the quantitative measurement of the unsaturated C₁₂ and the C₁₈ products, the detector response for these products was assumed to be equal to the response for dicyclohexyl and *n*-octadecane, respectively.

Ultraviolet irradiation of oxygen containing solu-

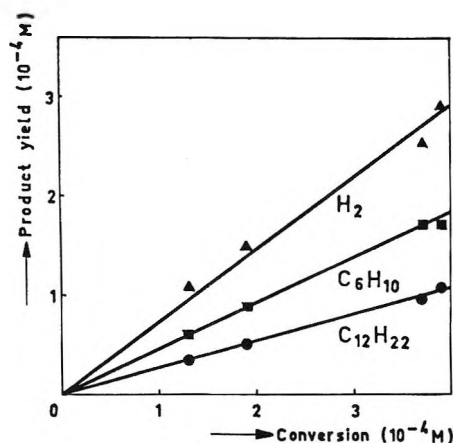


Figure 1. Product yields at low conversions.

tions resulted in the formation of three new products, cyclohexanol, cyclohexanone, and a product with a retention volume slightly higher than that of dicyclohexyl on columns containing silicon oil or polyglycol. The polyglycol column was used for the separation of this unknown product. In one experiment, it was isolated gas chromatographically from a concentrated solution and injected into a mass spectrometer. A parent peak with a mass of 182 was observed, suggesting that the product can be represented by the formula C₁₂H₂₂O. The detector response for this product in the gas chromatographic analysis was again assumed to be equal to the response for dicyclohexyl. A product with similar retention volumes on both the silicon oil and the polyglycol columns could be prepared by catalytic hydrogenation of diphenyl ether at 150°, using platinum oxide as a catalyst. This synthesis strongly suggests that it consists of dicyclohexyl ether.

Results

Experimental results, obtained with deaerated cyclohexane, are given in Table I and Figures 1 and 2. It was observed that the rate of decomposition of cyclohexane was not very reproducible and varied by as much as a factor of 2.¹¹ The average rate for hydrogen formation was about 56×10^{-4} mole of H₂ (l. of cyclohexane)⁻¹ hr⁻¹. Product formation in Figures 1 and 2 is therefore not represented as a function of exposure time but as a function of cyclohexane conversion, -C₆H₁₂. This conversion was approximated by the relation



(10) W. A. Cramer, part I of this series, to be published.

(11) This may be due to the differences in transparency of the Vycor cells used in these experiments. Moreover, not only was the vapor phase above the liquid masked during the irradiations, but part of the liquid was also.

Table I: Product Yields (in 10^{-4} mole/l.) in the Mercury-Photosensitized Decomposition of Cyclohexane

H ₂	C ₆ H ₁₀	C ₁₂ H ₂₂	C ₁₂ H ₂₀ (A) ^a	C ₁₂ H ₂₀ (B) ^a	C ₁₈	A/B	(A + B)/C ₁₈	Conversion
1.11	0.61	0.34	N.d. ^b	N.d.	N.d.			1.3
1.50	0.88	0.50	N.d.	N.d.	N.d.			1.9
2.54	1.72	0.97	N.d.	N.d.	N.d.			3.7
2.94	1.72	1.09	N.d.	N.d.	Trace			3.9
32.6	20.4	13.0	0.39	Trace	Trace			47.2
50.8	33.6	24.2	0.85	Trace	0.70			85.8
69.5	41.8	28.8	1.8	0.38	2.2	4.7	1.0	110
97.4	54.8	38.5	2.7	0.61	2.7	4.4	1.2	147
103	54.7	39.7	2.5	0.51	2.6	4.9	1.2	148
150	74.2	57.8	4.1	1.0	4.8	4.1	1.1	214
261	103	104	8.7	2.3	13	3.8	0.85	372
323	110	139	13	4.1	N.m. ^c	3.2		
491	136	218	19	7.3	30	2.6	0.88	715
1193	145	608	34	28	123	1.2	0.50	1854
1587	159	531	32	25	N.m. ^d	1.3		

^a A and B correspond with two isomers of cyclohexylcyclohexene. ^b Not detectable. ^c Not measured. ^d C₁₈, C₂₄, and C₃₀ compounds were present.

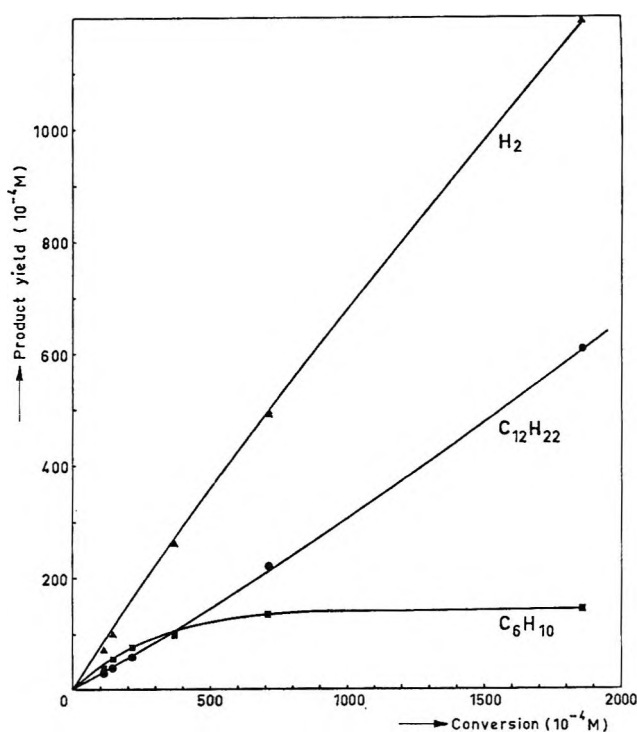


Figure 2. Yields of hydrogen, cyclohexene, and dicyclohexyl at high conversions.

Initial products consist of hydrogen, cyclohexene, and dicyclohexyl. From Figure 1 it can be seen that, at low conversions, the yields of these products increase linearly with increasing conversion. Figure 2 shows that at higher conversions a considerable decrease is observed in the yield of cyclohexene, relative to the yields of the other products. This is accompanied

by the formation of two cyclohexylcyclohexene isomers and products with 18 carbon atoms. Formation of products with 24 and 30 carbon atoms was also observed at the highest conversions. The material balance is reasonably good at all conversions.

Results of experiments carried out in the presence of oxygen are listed in Table II. No attempt was made to measure the formation of hydrogen gas in these experiments.

Discussion

Experiments at Low Conversions. From the experimental results at low conversions, shown in Table I and Figure 1, a value of 1.73 ± 0.09 is obtained for the ratio of the yields of cyclohexene and dicyclohexyl. The cause of the discrepancies between this value and the reported values of 1.31 ± 0.04^2 and 1.47^3 is not clear. It has been discussed previously that this ratio is not equal to k_4/k_5 if reaction 6 contributes.¹⁰ The experiments carried out in the presence of oxygen served to obtain more information about the occurrence of this reaction. Even at relatively low concentrations, this radical scavenger can interfere with reactions between randomly distributed radicals. However, only at much higher concentrations can this additive interfere with reactions between a cyclohexyl radical and its sibling hydrogen atom immediately after their formation. Hence, interference with reactions 4 and 5 may be expected at moderate oxygen concentrations, but not with reaction 6. The yield of dicyclohexyl may thus be reduced to zero, but if reaction 6 also contributes to product formation, the yield of cyclohexene will not be completely suppressed. The

Table II: Yields of Liquid Products (in 10^{-4} mole/l.) in the Mercury-Photosensitized Decomposition of Cyclohexane in the Presence of Oxygen

C_6H_{10}	$C_{12}H_{22}$	$C_6H_{11}OH$	$C_6H_{10}O$	$C_{12}H_{22}O$	ΣC_6H_{11}	C_6H_{10} reaction 6
2.9	Trace	5.3	8.9	0.8	18.7	2.9
3.7	Trace	8.7	17.3	1.3	32.3	3.7
3.9	0.1	11.1	17.7	1.3	35.6	3.8
3.6	0.2	10.4	19.7	1.8	37.9	3.4
4.2	0.3	11.9	22.5	1.7	42.9	3.9
4.7	0.2	14.0	22.6	1.8	45.5	4.5
8.6	0.3	24.0	42.1	3.4	82.4	8.3
15.4	0.7	42.6	86.7	6.7	160.3	14.6

experimental results, listed in Table II, are in accordance with these expectations. However, the residual cyclohexene formation could also be due to reaction 7, which was proposed by Ho and Freeman¹²

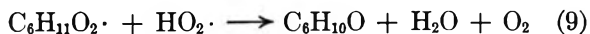


It has been shown recently that this reaction does not occur at room temperature.¹⁰

In order to make a more quantitative estimate of the contribution of reaction 6, the number of cyclohexyl radicals formed in the presence of oxygen must be known. This number can be deduced from the products which are formed in these solutions. It can be seen in Table II that cyclohexanol, cyclohexanone, and dicyclohexyl ether are important new products.¹³ The formation of cyclohexanol and cyclohexanone has been assumed to occur according to the over-all reaction¹⁴



The cyclohexylperoxy radicals will be produced in reactions between cyclohexyl radicals and oxygen. Equal yields of the two products are to be expected if only reaction 8 occurs. This has been observed in the photolysis of solutions of diphenylmercury in cyclohexane¹⁰ and in the radiolysis of cyclohexane,¹⁴ both in the presence of oxygen. The results listed in Table II show that in the present case cyclohexanone is formed in excess. We have no explanation for this observation, although a reaction similar to (8) but involving hydrogen peroxy radicals might contribute.



Hydrogen peroxy radicals may be formed in reactions between hydrogen atoms and oxygen. Excess formation of cyclohexanone may also be partly due to a sensitized reaction of cyclohexanol. It was found that irradiation of a dilute solution (10^{-1} M) of cyclohexanol, with light of 2537 Å and in the presence of oxygen and

mercury, results in a sensitized decomposition of cyclohexanol. Cyclohexanone and dicyclohexyl ether were observed as the main products. This process may also be involved in the formation of dicyclohexyl ether.

In calculating the total amount of cyclohexyl radicals produced, it was assumed that one cyclohexyl radical is involved in the formation of each cyclohexanol and cyclohexanone molecule, as follows from the proposed mechanism, but that two cyclohexyl radicals are required for the formation of dicyclohexyl ether. To estimate the contribution of reaction 6, the amounts of residual cyclohexene, listed in the first column of Table II, should be corrected for any contribution of reaction 4. This correction can be deduced from the figures in the second column of Table II by using an acceptable value for k_4/k_5 , for which we have taken the value 1.1.¹⁰ It will be clear that all these reactions must also be taken into account when calculating the amount of cyclohexyl radicals produced. The results of these calculations are given in the last two columns of Table II. It can be seen from these figures that about 10% of all the cyclohexyl radicals react within the liquid cage with sibling hydrogen atoms to give rise to unscavengeable hydrogen formation.

The fraction of cyclohexyl radicals formed in reaction 2 that react according to reaction 6 is of interest. If it is assumed that in the presence of oxygen all cyclohexyl radicals are formed in reaction 2, this fraction is equal to ca. 10% as was shown before. However, not all the cyclohexyl radicals are necessarily formed in reaction 2 only. In the absence of oxygen, for ex-

(12) S. K. Ho and G. R. Freeman, *J. Phys. Chem.*, **68**, 2189 (1964).

(13) Some reaction products may not have been observed by our analytical methods. The formation of peroxides and hydroperoxides, for example, has been reported in similar systems, although the observed yields were lower than the yields of alcohols and ketones.¹⁴

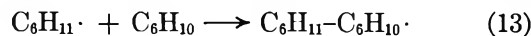
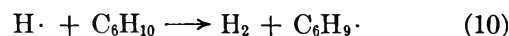
(14) R. Blackburn and A. Charlesby, *Trans. Faraday Soc.*, **62**, 1159 (1966).

ample, a considerable part of these radicals is produced according to reaction 3. In the presence of oxygen this reaction will be less important because hydrogen atoms may be scavenged. The rate of reactions between hydrogen atoms and oxygen is about 5×10^8 times the rate of abstraction reaction 3.¹⁵ However, whereas phenyl radicals react with oxygen about 10^8 times as readily as with cyclohexane,¹⁶ they were still found to react with cyclohexane in the presence of oxygen at concentrations similar to those in the experiments under discussion.¹⁰ This suggests that reaction 3 may contribute, even in the presence of oxygen. Assuming that all hydrogen atoms not reacting according to reaction 6 also form cyclohexyl radicals ultimately, even in the presence of oxygen, a maximum value of 19% is obtained for the fraction of cyclohexyl radicals formed in reaction 2 that react according to reaction 6.

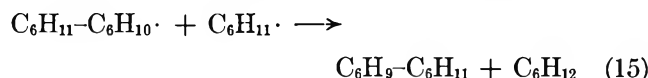
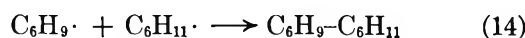
Similar calculations can also be made based on the results listed in Table I, which were obtained at low conversions, by making use of the measured value of 1.1 for k_4/k_5 .¹⁰ Since dicyclohexyl is produced only according to reaction 5, the corresponding yield of cyclohexene formed in reaction 4 can be calculated. According to the proposed mechanism, the additional cyclohexene yield may be attributed to reaction 6. This calculation, taking into account reactions 1–6, shows that about 13% of all cyclohexyl radicals and 23% of the cyclohexyl radicals formed in reaction 2 react according to reaction 6 under the experimental conditions employed. The possibility that reaction 6 also occurs outside the liquid cage cannot be excluded in the absence of oxygen. In that case, the calculated values of 13 and 23% represent the total contributions of reaction 6, occurring both within the liquid cage between a sibling radical pair as well as in the bulk of the solution.

Experiments at High Conversions. At higher conversions, a considerable decrease in the yield of cyclohexene is observed relative to the yields of the other major products, as is shown in Figure 2. The results suggest that prolonged irradiation results in a "steady-state" concentration of cyclohexene. A similar situation occurs when cyclohexane is irradiated with ionizing radiation.^{17,18} This has been attributed to energy transfer from excited or ionized cyclohexane molecules to cyclohexene followed by a sensitized decomposition of cyclohexene, in addition to reactions of cyclohexyl radicals and hydrogen atoms with cyclohexene.^{7,18–21} In the mercury-photosensitized decomposition of cyclohexane, excited or ionized cyclohexane molecules are not produced. Therefore, energy transfer from cyclohexane to cyclohexene cannot occur and

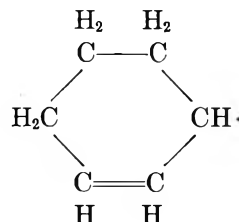
only reactions of hydrogen atoms and cyclohexyl radicals with cyclohexene will be considered.^{22,23}



The radicals formed in reactions 10–13 may again react with cyclohexene or with other radicals present in the solution, most of them being cyclohexyl radicals. It has indeed been observed that new products are formed at higher conversions, notably two cyclohexylcyclohexene isomers and products with 18, 24, and 30 carbon atoms. The C_{24} and C_{30} compounds were present in trace amounts at the highest conversions. Cyclohexylcyclohexene may be produced according to the reactions



Most of the cyclohexenyl radicals formed in reactions 10 and 12 will have the configuration



which is stabilized by resonance.²⁴ As a consequence, reaction 14 will result in the formation of 3-cyclohexyl-1-cyclohexene, with the structure

(15) M. Anbar and P. Neta, *Intern. J. Appl. Radiation Isotopes*, **16**, 227 (1965).

(16) G. A. Russell and R. F. Bridger, *J. Am. Chem. Soc.*, **85**, 3765 (1963).

(17) H. A. Dewhurst, *J. Phys. Chem.*, **63**, 813 (1959).

(18) P. J. Dyne and J. W. Fletcher, *Can. J. Chem.*, **38**, 851 (1960).

(19) M. Burton and J. Y. Chang, Abstracts, 137th National Meeting of the American Chemical Society, Cleveland, Ohio, 1960, p R109.

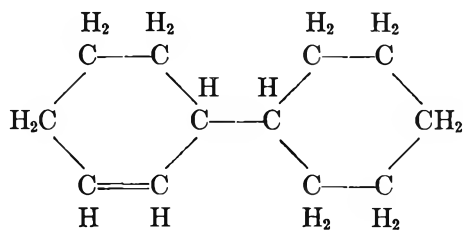
(20) S. Z. Toma and W. H. Hamill, *J. Am. Chem. Soc.*, **86**, 1478 (1964).

(21) S. Z. Toma and W. H. Hamill, *ibid.*, **86**, 4676 (1964).

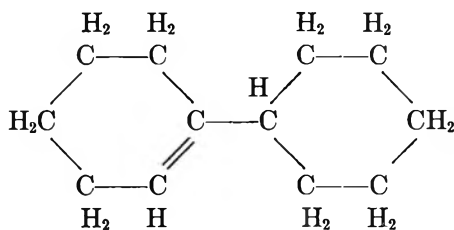
(22) Direct quenching of excited mercury atoms by cyclohexene may be neglected at the prevailing cyclohexene concentrations, as follows from a consideration of the respective quenching cross sections of saturated and olefinic hydrocarbons.²³

(23) R. J. Cvetanović, *Progr. Reaction Kinetics*, **2**, 39 (1964).

(24) R. F. Bridger and G. A. Russell, *J. Am. Chem. Soc.*, **85**, 3754 (1963).

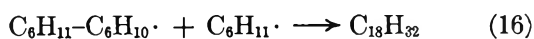


Cyclohexylcyclohexene, formed in reaction 15, may have a similar structure, but may also consist of 2-cyclohexyl-1-cyclohexene

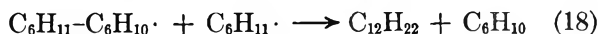
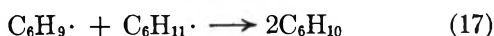


It was observed, when comparing the mass spectra of the two $C_{12}H_{20}$ isomers, that the contribution of the major fragment peak with mass 82 differed considerably. The central C-C bond between the two rings is expected to be stronger in 2-cyclohexyl-1-cyclohexene. Hence, it is suggested that the $C_{12}H_{20}$ isomer with the highest contribution at mass 82 consists of 3-cyclohexyl-1-cyclohexene.

Reaction 15 will be accompanied by the corresponding combination reaction 16, resulting in the formation of products with 18 carbon atoms.



In addition to the reactions mentioned so far, reactions 17 and 18 may also contribute to product formation



With this reaction mechanism and using the steady-state approximation, the following relations can be derived

$$\frac{d(A+B)/dt}{dC_{18}/dt} = \frac{k_{15}}{k_{16}} + \frac{k_{12}k_{14}(k_{15} + k_{16} + k_{18})}{k_{13}k_{16}(k_{14} + k_{17})} + \frac{k_{10}k_{14}(k_{15} + k_{16} + k_{18})}{k_{13}k_{16}(k_{14} + k_{17})} \frac{[H]}{[C_6H_{11}]} \quad (I)$$

$$\frac{dA/dt}{dB/dt} = \frac{k_{15}^A}{k_{15}^B} + \frac{k_{12}k_{14}(k_{15} + k_{16} + k_{18})}{k_{13}k_{15}^B(k_{14} + k_{17})} + \frac{k_{10}k_{14}(k_{15} + k_{16} + k_{18})}{k_{13}k_{15}^B(k_{14} + k_{17})} \frac{[H]}{[C_6H_{11}]} \quad (II)$$

where A and B stand for 3-cyclohexyl-1-cyclohexene and 2-cyclohexyl-1-cyclohexene, respectively, and k_{15}^A and k_{15}^B are the rate constants for the formation of A and B according to reaction 15. From these relations, it follows that

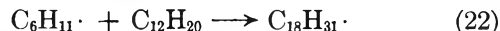
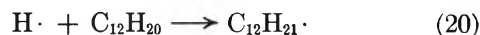
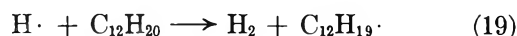
$$\frac{d(A+B)/dt}{dC_{18}/dt} = \frac{k_{15}^B}{k_{16}} \frac{dA/dt}{dB/dt} + \frac{k_{15}^B}{k_{16}} \quad (III)$$

It can be seen from the results listed in Table I that approximately constant ratios are found for $[d(A+B)/dt]/[dC_{18}/dt]$ and $(dA/dt)/(dB/dt)$ up to conversions of 200 to 300, with values of *ca.* 1.1 and 4.5, respectively. Substitution into eq III leads to a value of 0.2 for the ratio k_{15}^B/k_{16} . Considering that in all probability $k_{15}^A > k_{15}^B$ and allowing for a contribution of reaction 14 to cyclohexylcyclohexene formation, it may be concluded from the values of k_{15}^B/k_{16} and $[d(A+B)/dt]/[dC_{18}/dt]$, that $0.4 < k_{15}/k_{16} < 1.1$ or $0.2 < k_{15}^A/k_{16} < 0.9$.

At still higher conversions, the ratios $[d(A+B)/dt]/[dC_{18}/dt]$ and $(dA/dt)/(dB/dt)$ are found to decrease. If this were the result of a change in the ratio $[H]/[C_6H_{11}]$, it follows from eq I and II that the experimental results would show the relationship

$$\Delta\left(\frac{d(A+B)/dt}{dC_{18}/dt}\right) = \Delta\left(\frac{dA/dt}{dB/dt}\right) \frac{k_{15}^B}{k_{16}} = 0.2\Delta\left(\frac{dA/dt}{dB/dt}\right)$$

The results listed in Table I clearly show that this is not the case. The changes are observed when unsaturated C_{12} compounds are present in considerable concentrations and reactions of these molecules with cyclohexyl radicals and hydrogen atoms can no longer be neglected.



These reactions can account for the observed decrease in the ratio $[d(A+B)/dt]/[dC_{18}/dt]$. The change in the ratio $(dA/dt)/(dB/dt)$ may be due to a steric effect in addition reaction 22. It is to be expected that the addition of cyclohexyl radicals to 3-cyclohexyl-1-cyclohexene is favored relative to addition to 2-cyclohexyl-1-cyclohexene.

Acknowledgment. The author wishes to thank Miss L. E. W. van den Dool for her assistance in performing the experimental work.

Primary Processes in the Formation of Hydrogen Atoms in the Radiolysis of Water Vapor

by G. R. A. Johnson and M. Simic

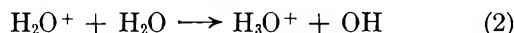
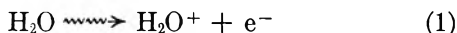
Laboratory of Radiation Chemistry, School of Chemistry, The University, Newcastle upon Tyne, England (Received November 23, 1966)

Accepted and Transmitted by The Faraday Society (June 27, 1966)

In the radiolysis of $D_2O + C_3H_8$ mixtures, the energy absorbed by each component contributes to the formation of D atoms. The yield due to the energy absorbed by C_3H_8 ($G(D)_p^0 = 4.6 \pm 0.3$) is explained in terms of proton transfer from propane positive ions to D_2O and subsequent formation of D atoms by neutralization of the hydronium ion produced. In the presence of N_2O or of SF_6 , which act as electron scavengers, $G(D)_p^0 = 0$ showing that D atoms are not formed when hydronium ions are neutralized by the negative ions from N_2O and SF_6 . The yield due to the energy absorbed by D_2O was $G(D)_w^0 = 7.6 \pm 0.4$ in the absence and $G(D)_w^0 = 4.9 \pm 0.4$ in the presence of electron scavengers. It is concluded that neutralization of hydronium ions by electrons gives D atoms with a yield corresponding to $G = 2.7 \pm 0.8$, and that D atoms are also formed ($G = 4.9 \pm 0.4$) by reactions which do not involve hydronium ion neutralization.

Introduction

Several studies have been made of the radiation-induced decomposition of water vapor.¹⁻⁶ It is generally assumed that hydrogen atoms are formed by two main processes: neutralization of hydronium ions and dissociation of excited molecules.^{7,8} Hydronium ions are formed by the reactions



and, at the pressures used in radiolysis, will be present mainly as clustered ions, $H_3O^+(H_2O)_n$, where $n \geq 7$.^{9,10} In the absence of any component capable of capturing electrons, neutralization of the clustered hydronium ions will occur mainly by reaction with electrons. Dissociation, following electronic excitation, to give hydrogen atoms



is well established in the photolysis of water vapor,^{11,12} but the extent to which this process occurs in the radiolysis has not previously been established. The main aim of the present work was to determine the relative

yields of hydrogen atoms formed by hydronium ion neutralization and by other processes in irradiated water vapor.

Experimental Section

H_2O and D_2O (Norsk Hydro-Elektrisk 99.83%) were distilled from alkaline $KMnO_4$ and then redistilled.

- (1) R. F. Firestone, *J. Am. Chem. Soc.*, **79**, 5593 (1957).
- (2) J. H. Baxendale and G. P. Gilbert, *Discussions Faraday Soc.*, **36**, 186 (1963).
- (3) J. H. Baxendale and G. P. Gilbert, *J. Am. Chem. Soc.*, **86**, 576 (1964).
- (4) A. R. Anderson, B. Knight, and J. A. Winter, *Nature*, **201**, 1026 (1964).
- (5) A. R. Anderson, B. Knight, and J. A. Winter, *Trans. Faraday Soc.*, **62**, 359 (1966).
- (6) A. R. Anderson, B. Knight, and J. A. Winter, *Nature*, **209**, 199 (1966).
- (7) E. J. Hart and R. L. Platzman, *Mech. Radiobiol.*, **1**, 176 (1961).
- (8) F. Fiquet-Fayard, *J. Chim. Phys.*, **57**, 453 (1960).
- (9) P. F. Knewstubb and A. W. Tickner, *J. Chem. Phys.*, **38**, 464 (1963).
- (10) P. Kebarle and A. M. Hogg, *ibid.*, **42**, 798 (1965).
- (11) G. Black and G. Porter, *Proc. Roy. Soc. (London)*, **A266**, 185 (1962).
- (12) J. R. McNesby, I. Tanaka, and H. Okabe, *J. Chem. Phys.*, **36**, 605 (1962).

Propane and propene (Phillips research grade), SF₆ (I.C.I., 99.95%), and N₂O (British Oxygen Gases, medical grade) were condensed at 77°K and distilled still several time before use.

Irradiations were carried out in Pyrex vessels (~400 ml) fitted with break-seals. Before filling, the vessels were baked in air at 500° for at least 6 hr and pumped to <10⁻⁵ torr. The weighed water sample, after deaerating by freezing and pumping at 77°K, was distilled into the irradiation vessel while this was at 77°K. Required amounts of additives were introduced by condensing from a gas sample vessel (known PVT). The vessels were sealed before warming to room temperature.

Two different ⁶⁰Co γ-ray sources, of about 400 and 1000 curies, were used. During irradiation, the vessels were heated in an oven with the temperature controlled to ±2°.

The dose rate was measured by the N₂O dosimeter assuming $G(N_2) = 12.0$.¹³ The energy absorbed in the water vapor (E_w) was calculated from that in N₂O (E_n) assuming the energy absorbed in each gas to be directly proportional to its electron density. The energy absorbed in the propane (E_p) was calculated from E_n using the ratio of stopping powers per molecule obtained by Meisels.¹⁴

The total energy absorbed in a mixture (E_t) is the sum of the energies absorbed in the components. The dose rates used were 6×10^{16} to 2×10^{17} ev mole⁻¹ sec⁻¹ in D₂O.

Gases present after irradiation, which were noncondensable at 77°K, were transferred to a gas buret by means of a one-stage diffusion pump and a Toepler pump. After PVT measurement, the gas composition was determined mass spectrometrically.

Results

$G(X)_t$, $G(X)_w$, and $G(X)_p$ are the number of molecules of product X formed per 100 ev absorbed by the gas mixture, by the water fraction, and by the propane fraction, respectively. The energy fractions are $f_w = E_w/E_t$ and $f_p = E_p/E_t$. The yields obtained by extrapolation to $f_p = 0$ and $f_w = 0$ are written $G(X)_w^0$ and $G(X)_p^0$, respectively.

D₂O + C₃H₈ Mixtures. The hydrogen yields from D₂O + C₃H₈ mixtures were independent of the temperature of radiolysis between 100 and 185° and were linear with dose to the highest dose used (~3 × 10¹⁹ ev mole⁻¹). Erroneously low yields were obtained if the radiolysis temperature was near the boiling point of water at the water vapor pressure used. The quantity of water in each experiment therefore was selected so that the boiling point, at the pressure used, was at

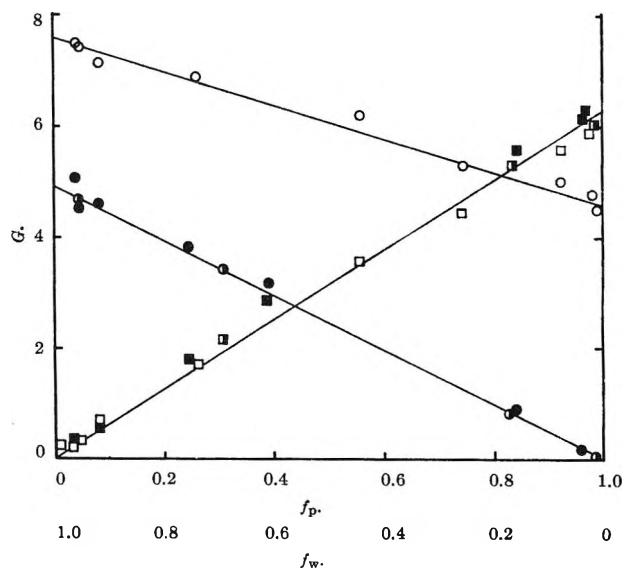


Figure 1. Radiolysis of D₂O + C₃H₈ mixtures (140°, density 0.8–2.7 g l.⁻¹). Dependence of $G(HD)_t$ and $G(H_2)_t$ on the fraction of dose absorbed by C₃H₈ ($f_p = E_p/E_t$) and by D₂O ($f_w = E_w/E_t$). HD yields: ○, from D₂O + C₃H₈; ●, with N₂O (~3 mole %); ●, with SF₆ (~0.3 mole %). H₂ yields: □, from D₂O + C₃H₈; ■, with N₂O (~3 mole %); ■, with SF₆ (~0.3 mole %).

least 20° below the irradiation temperature. The D₂O vapor concentrations used were from 1.3×10^{-2} to 6.2×10^{-2} mole l.⁻¹.

In Figure 1, $G(HD)_t$ and $G(H_2)_t$ from D₂O + C₃H₈ are plotted against f_p and f_w . The yields obtained by extrapolation to $f_p = 0$ and $f_w = 0$ are $G(HD)_w^0 = 7.6 \pm 0.4$ and $G(HD)_p^0 = 4.6 \pm 0.3$, respectively. Also, over the concentration range studied, $G(H_2)_t = f_p G(H_2)_p^0$, where $G(H_2)_p^0 = 6.3 \pm 0.3$.

D₂O + C₃H₈ + N₂O (or SF₆) Mixtures. In the presence of N₂O (3 mole %) or of SF₆ (0.3 mole %), $G(HD)_t = f_w G(HD)_w^0$ where $G(HD)_w^0 = 4.9 \pm 0.4$ (Figure 1). To obtain this value from the measured HD yield, it was necessary to determine the extent to which the energy absorbed by the N₂O or SF₆ in these mixtures contributed to the formation of HD. For this purpose, a study was made of the radiolysis of D₂O + N₂O and D₂O + SF₆ mixtures, with small amounts of C₃H₈ (1.5 mole %) present. In Figure 2, $G(HD)_t$, from these mixtures, is plotted against the fraction of energy absorbed by N₂O or by SF₆.

In the case of D₂O + N₂O, over the whole concentration range studied, $G(HD)_t = f_w G(HD)_w^0$, where $G(HD)_w^0 = 4.7 \pm 0.4$. This shows that the energy absorbed by N₂O does not contribute to the yield of

(13) G. R. A. Johnson, *J. Inorg. Nucl. Chem.*, **24**, 461 (1962).

(14) G. G. Meisels, *J. Chem. Phys.*, **41**, 51 (1964).

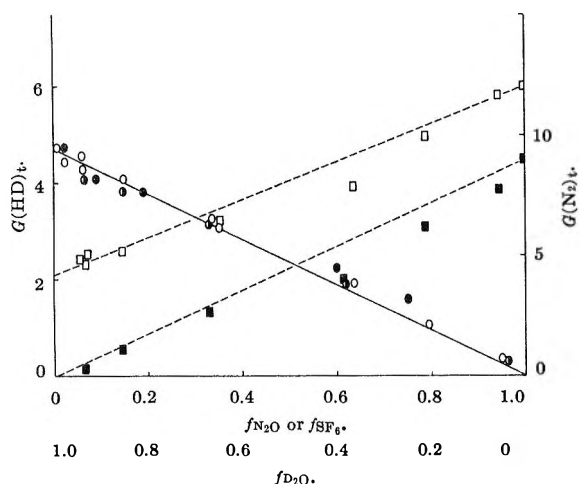


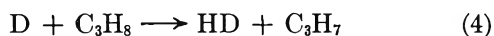
Figure 2. Radiolysis of $\text{D}_2\text{O} + \text{N}_2\text{O}$ and $\text{D}_2\text{O} + \text{SF}_6$ mixtures (140° , density $0.8\text{--}2.7 \text{ g l}^{-1}$) with C_3H_8 (~ 1.5 mole %). Dependence of $G(\text{HD})_t$ and $G(\text{N}_2)_t$ on the fraction of dose absorbed by D_2O ($f_w = E_w/E_t$). HD yields: ○, $\text{D}_2\text{O} + \text{N}_2\text{O}$; ●, $\text{D}_2\text{O} + \text{N}_2\text{O}$ with SF_6 (~ 0.3 mole %); ●, $\text{D}_2\text{O} + \text{SF}_6$. N_2 yields: □, $\text{D}_2\text{O} + \text{N}_2\text{O}$; ■, $\text{D}_2\text{O} + \text{N}_2\text{O}$ with SF_6 (~ 0.3 mole %).

HD. In the case of $\text{D}_2\text{O} + \text{SF}_6$, there appears to be a small contribution, at high SF_6 concentrations, from the energy absorbed by SF_6 . However, it may be concluded that the contribution of the energy absorbed by SF_6 to the HD yield is negligible in the experiments where SF_6 was present at a concentration of 0.3 mole %. The N_2 yields from $\text{D}_2\text{O} + \text{N}_2\text{O}$ with C_3H_8 (1.5 mole %), in the presence and absence of SF_6 (0.3 mole %), are also given in Figure 2. The extrapolated value $G(\text{N}_2)_w^0 = 4.2 \pm 0.4$ in the absence and zero in the presence of SF_6 .

Molecular Hydrogen. The yield of D_2 from the various systems is plotted against f_w in Figure 3. $G(\text{D}_2)_w$ decreased with decreasing f_w for $\text{D}_2\text{O} + \text{C}_3\text{H}_8$ mixtures and increased with decreasing f_w for $\text{D}_2\text{O} + \text{N}_2\text{O}$ or $\text{D}_2\text{O} + \text{SF}_6$ mixtures.

Discussion

Formation of HD and H_2 from $\text{D}_2\text{O} + \text{C}_3\text{H}_8$ Mixtures. The system $\text{D}_2\text{O} + \text{C}_3\text{H}_8$ was selected for investigation since the reaction



($k_4 \sim 2 \times 10^6 \text{ M}^{-1} \text{ sec}^{-1}$ ^{15,16}) results in efficient scavenging of D atoms, and the product of this reaction can be distinguished both from the H_2 produced by the reaction of H atoms formed from C_3H_8 , and from the D_2 formed as a molecular product from D_2O . Furthermore, both charge transfer and proton transfer

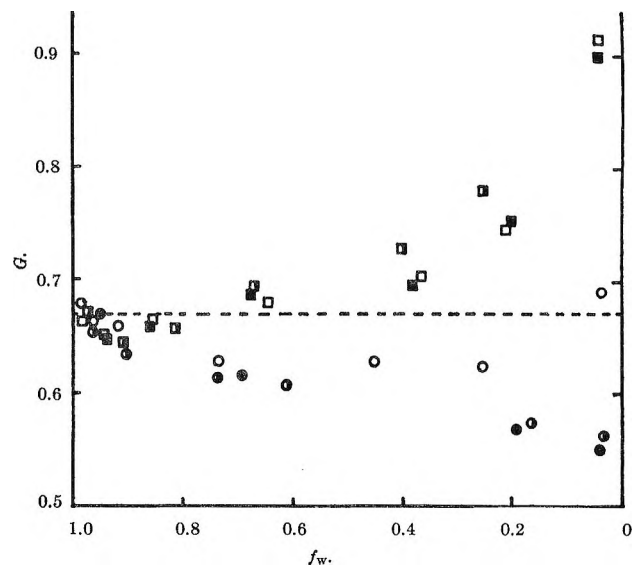
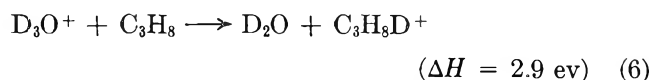
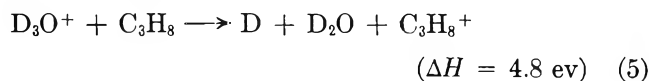


Figure 3. Formation of D_2 from D_2O vapor (140°) in the presence of various additives. Dependence of $G(\text{D}_2)_w$ on the fraction of dose absorbed by water ($f_w = E_w/E_t$): ○, $\text{D}_2\text{O} + \text{C}_3\text{H}_8$; ●, $\text{D}_2\text{O} + \text{C}_3\text{H}_8$ with N_2O (2.5 mole %); ○, $\text{D}_2\text{O} + \text{C}_3\text{H}_8$ with SF_6 (0.3 mole %); □, $\text{D}_2\text{O} + \text{N}_2\text{O}$ with C_3H_8 (1.5 mole %); ■, $\text{D}_2\text{O} + \text{N}_2\text{O}$ with C_3H_8 (1.5 mole %), and SF_6 (0.3 mole %); □, $\text{D}_2\text{O} + \text{SF}_6$ with C_3H_8 (1.5 mole %).

from hydronium ions to C_3H_8 can be excluded on energetic grounds



(ΔH was calculated assuming proton affinities $P(\text{C}_3\text{H}_8) = 4.3 \text{ ev}$, $P(\text{D}_2\text{O}) = 7.2 \text{ ev}$ ¹⁷ and ionization potentials $I(\text{C}_3\text{H}_8) = 11.2 \text{ ev}$, $I(\text{D}) = 13.6 \text{ ev}$. It is also assumed that the proton affinity of D_2O is the same as that of H_2O and that the hydration energies of the ions can be neglected.)

From the results (Figure 1), it may be concluded that the energy absorbed by both D_2O and C_3H_8 contributes to the D atom yield. Thus the linear dependence of $G(\text{HD})_t$ on the fraction of energy absorbed by each component is most reasonably explained by the assumption that $G(\text{HD})_t = f_w G(\text{HD})_w^0 + f_p G(\text{HD})_p^0$, where $G(\text{HD})_w^0 = 7.6 \pm 0.4$ and $G(\text{HD})_p^0 = 4.6 \pm 0.3$ are the values of $G(\text{HD})_t$ at $f_p = 0$ and $f_w =$

(15) H. A. Kazmi, R. J. Diefendorf, and D. J. Le Roy, *Can. J. Chem.*, **41**, 690 (1963).

(16) H. I. Schiff and E. W. R. Steacie, *ibid.*, **29**, 1 (1951).

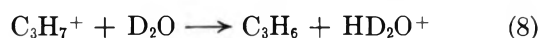
(17) F. W. Lampe and F. H. Field, *Tetrahedron*, **7**, 189 (1958).

0, respectively. The value of $G(\text{HD})_{\text{w}}^0 = 7.6 \pm 0.4$ is in agreement with previously reported values for hydrogen atom yield from water vapor measured using organic scavengers.²

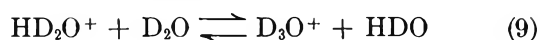
Radiolysis of C_3H_8 can give a number of different positive ions. It may be assumed that C_3H_8^+ and C_3H_7^+ will be the main positive ions¹⁸ reacting with D_2O . The proton-transfer reaction



($k_7 = 1.2 \times 10^{12} \text{ M}^{-1} \text{ sec}^{-1}$) has been observed in a mass spectrometer.¹⁹ Evidence for proton transfer from C_3H_7^+ to H_2O , *i.e.*, the reaction analogous to



has been obtained from mass spectrometric studies of ions in $\text{CH}_4 + \text{H}_2\text{O}$ mixtures.²⁰ Proton-transfer reactions of this type, *i.e.*, from a carbonium ion to a molecule of sufficiently high proton affinity, have also been postulated in the radiolysis of liquid hydrocarbons.²¹ HD_2O^+ ions formed by reactions 7 and 8 will enter into the equilibrium



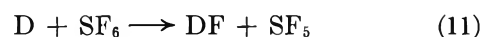
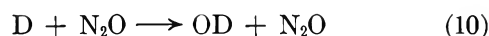
By comparison with similar proton-transfer reactions in the gas phase,²¹ it may be assumed that equilibrium will be rapidly established. Since D_2O is always in considerable excess over any HDO formed by reaction 9, D_3O^+ will be the only positive ion involved in the neutralization reaction. The observed $G(\text{HD})_{\text{p}} = 4.6$ is close to the yield of positive ions in propane, $G(\text{RH}^+) = 4.3$, calculated from the value of $W(\text{C}_3\text{H}_8) = 23.4$.¹⁴ This suggests that all of the positive ions from propane are capable of undergoing proton transfer (reactions 7 and 8) and that neutralization of the resulting D_3O^+ ion gives one D atom per neutralization.

N_2O and SF_6 can capture electrons to form negative ions.²² In the presence of these scavengers, therefore, neutralization of the hydronium ions by negative ions will occur rather than neutralization by electrons. Since, when N_2O or SF_6 are present, $G(\text{HD})_{\text{p}}^0 = 0$, it appears that neutralization of D_3O^+ , by the negative ions from these scavengers does not result in D atom formation.

The yield of H_2 , $G(\text{H}_2)_{\text{p}} = 6.3 \pm 0.3$, supports the assumption that all the positive ions from propane react with D_2O by reactions 7 or 8. This conclusion may be drawn from a comparison of the present results with those obtained in a study of hydrogen formation in the radiolysis of propane.²² In the radiolysis of pure C_3H_8 , hydrogen is formed by two processes: *via* H atoms produced by positive ion + electron recombination and by decomposition of excited propane molecules. The

formation of H atoms from positive ions can be prevented by the addition of electron scavengers (N_2O , SF_6 , CCl_4) and the yield with these present is $G(\text{H}_2) = 5$ at 20° . Recent work²³ has shown that the yield of H_2 from $\text{C}_3\text{H}_8 + \text{N}_2\text{O}$ is slightly dependent upon the temperature of radiolysis and that, at 140° , the temperature of the $\text{D}_2\text{O} + \text{C}_3\text{H}_8$ experiments, $G(\text{H}_2) = 6.2 \pm 0.2$. This value is close to $G(\text{H}_2)_{\text{p}}^0$ from $\text{D}_2\text{O} + \text{C}_3\text{H}_8$ mixtures, in agreement with the view that in both cases the formation of H atoms from propane positive ions is eliminated. Furthermore, $G(\text{H}_2)_{\text{p}}^0$ is not depressed by the addition of electron scavengers (Figure 1) confirming that, in the presence of D_2O , the H_2 yield from propane results from processes other than positive ion neutralization. The above conclusion, that the D_3O^+ ions formed *via* reactions 7, 8, and 9 give one D atom per ion when neutralized by electrons and no D atoms when neutralized by the negative ions from N_2O or SF_6 , holds over the whole concentration range studied, since $G(\text{HD})_{\text{p}}^0$ is independent of f_{p} (Figure 1). It is, therefore, reasonable to assume the same behavior on neutralization for the D_3O^+ ions formed as a result of energy absorption by D_2O . On this basis, it is possible to explain the depression of the HD yield from $G(\text{HD})_{\text{w}}^0 = 7.6 \pm 0.4$ to $G(\text{HD})_{\text{w}}^0 = 4.9 \pm 0.4$ by N_2O and SF_6 (Figure 1). The residual yield in the presence of these scavengers must be due to a process or processes not involving D_3O^+ neutralization. (In the following discussion these processes are referred to as the "residual process.") It follows that the yield of D atoms due to D_3O^+ neutralization corresponds to the depression of the HD yield, $\Delta G(\text{HD})_{\text{w}}^0 = 2.7 \pm 0.8$. This is slightly less than value for the yield of hydronium ions, $G(\text{D}_3\text{O}^+)_{\text{w}} = 3.1\text{--}3.6$, calculated from reported values of $W(\text{H}_2\text{O})$.⁸

Any possibility that the observed effect of N_2O and SF_6 in D_2O radiolysis is due to D atom scavenging, *e.g.*, by the reactions



may be excluded since $G(\text{HD})_{\text{w}}$ is independent of the concentration of N_2O and of SF_6 up to molar ratios $\text{N}_2\text{O}/\text{C}_3\text{H}_8 = 80$ and $\text{SF}_6/\text{C}_3\text{H}_8 = 30$ (Figure 2). Since

(18) P. Ausloos and R. Gorden, *J. Chem. Phys.*, **41**, 1278 (1964).

(19) F. W. Lampe, F. H. Field, and J. L. Franklin, *J. Am. Chem. Soc.*, **79**, 6132 (1957).

(20) M. S. B. Munson and F. H. Field, *ibid.*, **87**, 4242 (1965).

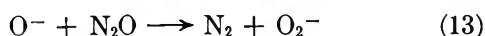
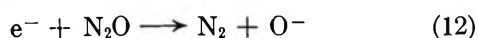
(21) W. R. Busler, D. H. Martin, and F. Williams, *Discussions Faraday Soc.*, **36**, 102 (1963).

(22) G. R. A. Johnson and J. M. Warman, *Trans. Faraday Soc.*, **61**, 1709 (1965).

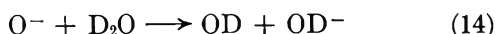
(23) G. R. A. Johnson, M. Simic, and L. Redpath, unpublished results.

a change of 10% in the measured $G(\text{HD})_w$ would have been detected, it follows that the rate constant ratios are $k_4/k_{10} \geq 800$ and $k_4/k_{11} \geq 300$. The former ratio may be compared with the value $k_{\text{H}+\text{C}_3\text{H}_8}/k_{\text{H}+\text{N}_2\text{O}} \sim 400$ calculated from reported values for these constants.^{15,24} The inability of N_2O and SF_6 to depress the HD yield below $G(\text{HD})_w = 4.9$ may be contrasted with the effect of propene, which is an efficient hydrogen atom scavenger. With propene present ($\text{C}_3\text{H}_6/\text{C}_3\text{H}_8 = 1.0$), the yield from $\text{D}_2\text{O} + \text{C}_3\text{H}_8$ mixtures is depressed to $G(\text{HD})_w < 0.1$. This is in accord with the rate constant ratio $k_{\text{H}+\text{C}_3\text{H}_6}/k_{\text{H}+\text{C}_3\text{H}_8} \sim 40$ calculated from reported rate constants.²⁵

Reactions in the Presence of N_2O and of SF_6 . Assuming that the mixture law holds for $\text{D}_2\text{O} + \text{N}_2\text{O}$ mixtures, the total N_2 yield should correspond to $G(\text{N}_2)_t = f_w G(\text{N}_2)_w^0 + f_{\text{N}_2\text{O}} G(\text{N}_2)_{\text{N}_2\text{O}}^0$. The results (Figure 2) indicate that there is some deviation from the mixture law. This deviation and the values of $G(\text{N}_2)_{\text{N}_2\text{O}}^0$ in the absence and presence of SF_6 will be discussed elsewhere. $G(\text{N}_2)_w^0 = 4.2 \pm 0.4$ lies between $G(e^-)_w$ and $2G(e^-)_w$ (where $G(e^-)_w \sim 3$ is the electron yield). A value corresponding to $2G(e^-)_w$ would be expected if N_2 is formed by



It is possible that the reaction



can compete with reaction 13. If it is assumed that reaction 14 does occur, it must compete to the exclusion of reaction 13 at all N_2O concentrations used, since $G(\text{N}_2)_w^0$ does not increase with increasing $f_{\text{N}_2\text{O}}$ (Figure 2). In this case, N_2 must be formed by some process other than reactions 12 and 13, with $G(\text{N}_2) = 1 \pm 0.5$. Baxendale and Gilbert²⁶ have suggested that in the system $\text{H}_2\text{O} + \text{methanol}$, the part of the N_2 yields in excess of $G(e^-)$ may be due to the reaction of free radicals with N_2O . Similarly, free radicals from C_3H_8 may react to give N_2 , *e.g.*



However, this seems improbable since SF_6 decreased $G(\text{N}_2)_w^0$ to zero (Figure 2) and, to explain the effect of SF_6 in terms of a competition between SF_6 and N_2O for the free radicals, it would be necessary to make the unreasonable assumption that the specific rate for reaction with SF_6 is at least 1000 times that for reaction with N_2O .

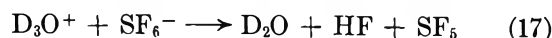
If it is assumed that all of the O^- ions react according

to reaction 14, when N_2O is present neutralization of hydronium ions will involve reaction 16.

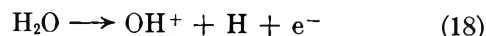


This is in keeping with the finding that D atoms are not formed by hydronium ion neutralization under these conditions.

With SF_6 present, the predominant negative ion will be SF_6^- . Since neutralization of D_3O^+ by this ion does not give D atoms, it follows that neutralization does not simply involve electron transfer but that rearrangement occurs, *e.g.*



Hydrogen Atom Formation by Processes Other Than Hydronium Ion Neutralization. Under mass spectrometric conditions, approximately 18% of the positive ions are formed by the process⁸



In the radiolysis, this could result in $G(\text{H}) \sim 0.7$, but the actual extent of this process cannot be determined from evidence available at present. Reaction 18 would probably not alter the yield of hydronium ions since the charge-transfer reaction



may be expected to occur⁸ and would be followed by reaction 2. The majority of hydrogen atoms which contribute to the "residual" yield presumably result from electronic excitation (reaction 3). From the value of the "residual" yield, assuming a contribution of $G = 0.7$ from reaction 18, it appears that the yield due to reaction 3 corresponds to $G \sim 4.2$. This is quite close to the value $G \sim 3.3$ calculated for this process by Fiquet-Fayard.⁸

It is of interest to compare the yield of hydrogen atoms from excitation in the vapor phase with that in liquid water. It has been suggested that the formation of hydrogen atoms ($G \sim 0.6$) in neutral aqueous solutions is due to excitation.²⁷ This has not been definitely established and other possible modes of hydrogen atom formation have been discussed.²⁸ However, the yield of atoms from excitation in liquid water is clearly less than in the vapor phase. In the liquid it is possible that the observed yield is decreased by either (a) deactivation of excited states before dissociation and/or

(24) M. Schiavello and G. G. Volpi, *J. Chem. Phys.*, **37**, 1510 (1962).

(25) B. A. Thrush, *Progr. Reaction Kinetics*, **3**, 65 (1965).

(26) J. H. Baxendale and G. R. Gilbert, *Science*, **147**, 1571 (1965).

(27) J. T. Allan and G. Scholes, *Nature*, **187**, 218 (1960).

(28) C. Lifshitz and G. Stein, *Israel J. Chem.*, **2**, 337 (1964).

(b) rapid recombination, within the solvent cage, of the free radicals produced by dissociation. However, since the quantum yield in the photolysis of liquid water (1470 Å) is close to unity,²⁹ processes (a) and (b) do not appear to be important, at least for water excited photochemically. This suggests either that the excited states produced by photolysis of liquid water differ markedly from those produced radiolytically or that the radiolytic excitation process responsible for decomposition in the vapor phase does not occur in the liquid phase.

Molecular Yield of Hydrogen. The value of $G(D_2)_w = 0.64 \pm 0.06$ obtained in D_2O -rich mixtures (Figure 3) agrees with values for the molecular yield of hydrogen reported previously.^{3,4} $G(D_2)_w$ from $D_2O +$

C_3H_8 decreased with increasing C_3H_8 concentration, suggesting that C_3H_8 may react with some precursor of D_2 . In the systems $D_2O + N_2O$ and $D_2O + SF_6$, on the other hand, $G(D_2)_w$ increased as the concentration of N_2O or SF_6 increased. This indicates that the energy absorbed by N_2O and by SF_6 can, to some extent, contribute to the formation of D_2 . Further investigation of these effects would be of interest.

Acknowledgments. We thank Professor J. J. Weiss for his interest and Dr. G. Scholes for helpful discussions. The work was supported financially by the Atomic Energy Research Establishment, Harwell, England.

(29) U. Sokolov and G. Stein, *J. Chem. Phys.*, **44**, 2189 (1966).

Diffusion Coefficients for Gases in Liquids from the Rates of Solution of Small Gas Bubbles

by Irvin M. Krieger, George W. Mulholland, and Charles S. Dickey

Department of Chemistry, Case Institute of Technology, Cleveland, Ohio (Received August 31, 1966)

A new technique is described for suspending a small gas bubble in a liquid and measuring its size as a function of time while it dissolves. From these data and the gas solubility, diffusion coefficients for the gas in the liquid can be calculated. The experimental technique involves catching a bubble on a fine horizontal fiber and photographing its projected image. To analyze the data, Fick's law is integrated for unsteady, spherically symmetrical conditions; the resultant equation is fitted to the data by an iterative least-squares technique. Results are presented for O_2 , N_2 , and He in H_2O and in organic liquids.

Introduction

The study of the liquid state encompasses both equilibrium and nonequilibrium phenomena. Diffusion, which is the transport of matter under the influence of a concentration gradient, is an important nonequilibrium process for which an adequate general theory is not yet available. Diffusion in dilute gases has been treated successfully by the kinetic theory, as has the diffusion of colloidal particles in a continuous

medium. The diffusion of ordinary molecules in a dense gas or a liquid has shown itself to be much less tractable, however.

To stimulate and guide the development of theory, it would be desirable to have on hand a large body of accurate diffusion coefficient measurements on many diversified systems. Unfortunately, the data available are meager and, judging from the discrepancies among different techniques and observers, they are

frequently inaccurate. Part of this lack is due to difficulty in making accurate measurements.

Of the various experiments suitable for quantitative study of diffusion of gases in liquids, the dissolution of a stationary bubble into an essentially infinite liquid is particularly simple, since the spherical symmetry and the absence of troublesome boundaries greatly facilitate the theoretical analysis. The rate of solution of a stationary gas bubble in a liquid is governed by both the solubility and the diffusion coefficient of the gas in the liquid. The liquid at the bubble surface maintains a gas concentration equal to the saturated solution concentration at the local pressure. If the surrounding fluid has a lower concentration, then the gas molecules diffuse outward, thereby depleting the solution at the bubble surface and permitting more gas to dissolve. By considering the diffusion to occur radially outward into an essentially infinite solution and by applying Fick's law with a concentration-independent diffusion coefficient, an equation can be obtained giving the bubble radius as a function of time. The parameters of this equation are the solubility and the diffusion coefficient; if the solubility is known, then the diffusion coefficient may be determined by fitting the equation to experimental radius *vs.* time data.

The theoretical analysis of the bubble solution rate problem was developed by Epstein and Plesset¹ in 1950. Because the analysis is restricted to a stationary bubble, it could only be applied to experiments in very viscous fluids, where the upward motion of the bubble due to buoyancy could be neglected. In 1957, Lieberman² developed the technique of catching the bubble under a microscope slide and measuring the radius *a* as a function of the time *t*. He assumed steady-state behavior and introduced a correction factor for the plane boundary calculated from the analogous electrostatic problem. Because of the steady-state assumption, a linear graph of *a*² *vs.* *t* was predicted.

Lieberman used his technique to study the rate of solution of air in water and found a slight upward curvature in the *a*² *vs.* *t* graph, which he attributed to the formation of a film of organic impurities at the bubble surface. Manley³ obtained similar results. Houghton⁴ and co-workers performed extensive studies and concluded that the initial linear portion of the *a*² *vs.* *t* curve could be used with Lieberman's analysis to give diffusion coefficients which agreed with literature values to within ±10%.

The present study differs from those described above in both the experimental method and the data analysis. An experimental technique was developed in which the bubble was caught and held on a fine horizontal

fiber, thereby approximating closely the assumed condition of a spherical bubble in an infinite solution. In the analysis of the data, the steady-state assumption was discarded, permitting the use of radius *vs.* time data extending all the way to complete disappearance of the bubble. The curvature in the *a*² *vs.* *t* graph appears as a natural result of the departure from a steady-state concentration gradient.

Theory

Consider a gas bubble of radius *a* at the center of a large volume of solution whose initial gas concentration is *C*₀ g/cm³. If the liquid at the bubble's surface is saturated, then the gas concentration *C* in the solution should vary with the radial coordinate *r* from *C*_s, the saturated solution concentration at *r* = *a*, to *C*₀ at *r* = ∞. Assuming a constant diffusion coefficient *D*, Fick's second law for this spherically symmetrical geometry is

$$\frac{1}{D} \frac{\partial C}{\partial t} = \nabla^2 C = \frac{1}{r} \frac{\partial^2}{\partial r^2} (rC) \quad (1)$$

The solution of eq 1 subject to the boundary conditions at *r* = *a* and *r* = ∞ is expressible as an error integral

$$C - C_0 = \frac{a}{r} (C_s - C_0) \left[1 - 2\pi^{-1/2} \int_0^{\frac{r-a}{\sqrt{2(Dt)^{1/2}}}} e^{-y^2} dy \right] \quad (2)$$

The rate at which the mass *m* of the bubble decreases is determined by the outward flux *J*_a of gas at the bubble surface

$$\frac{dm}{dt} = -4\pi a^2 J_a \quad (3)$$

Now if *ρ* is the density of the gas bubble, then *m* = $\frac{4}{3}\pi a^3 \rho$ and

$$\frac{dm}{dt} = 4\pi a^2 \rho \frac{da}{dt} \quad (4)$$

Thus the rate of decrease of the bubble radius is

$$\frac{da}{dt} = -\frac{J_a}{\rho} \quad (5)$$

We may obtain *J*_a from Fick's first law

$$J = -D\nabla C = -D \frac{\partial C}{\partial r} \quad (6)$$

(1) P. S. Epstein and M. S. Plesset, *J. Chem. Phys.*, **18**, 1507 (1950).

(2) L. Lieberman, *J. Appl. Phys.*, **28**, 207 (1957).

(3) M. Manley, *Bril. J. Appl. Phys.*, **11**, 41 (1960).

(4) G. Houghton, P. D. Ritchie, and J. A. Thomson, *Chem. Eng. Sci.*, **17**, 224 (1962).

The concentration gradient at $r = a$ is available from eq 2

$$\frac{\partial C}{\partial r}\Big|_{r=a} = -\frac{C_s - C_0}{a} \left[1 + \frac{a}{(\pi Dt)^{1/2}} \right] \quad (7)$$

We thus obtain Epstein and Plesset's differential equation for the bubble radius

$$\frac{da}{dt} = -\frac{D(C_s - C_0)}{\rho a} \left(1 + \frac{a}{(\pi Dt)^{1/2}} \right) \quad (8)$$

At sufficiently long times, $a/\sqrt{\pi Dt} \ll 1$; neglect of the term $a(\pi Dt)^{-1/2}$ leads to the same "steady-state" solution as would have been obtained by setting $\partial C/\partial t = 0$ in eq 1

$$a^2 = a_0^2 - \frac{2D}{\rho}(C_s - C_0)t \quad (9)$$

Here a_0 is the bubble radius at $t = 0$. This equation was used by Lieberman with an additional factor of $(\ln 2)^{-1}$ in the second term on the left to take into account the planar upper boundary condition.

To solve eq 8 for the general case, it is convenient to let $u^2 = a^2(\pi Dt)^{-1}$ and $\beta = 2(C_s - C_0)(\pi\rho)^{-1}$. Equation 8 then becomes

$$\frac{d}{dt}(u^2t) = -\beta(1 + u) \quad (10)$$

Equation 10 may be integrated by separation of variables

$$\ln(u^2 + \beta u + \beta) - \frac{2\beta}{(4\beta - \beta^2)^{1/2}} \tan^{-1} \frac{\beta + 2u}{(4\beta - \beta^2)^{1/2}} = -\ln t + \text{constant} \quad (11)$$

The constant of integration can be expressed in terms of the boundary condition at $t = 0$, to give

$$\ln \frac{\pi Dt}{a_0^2}(u^2 + \beta u + \beta) - \frac{2\beta}{(4\beta - \beta^2)^{1/2}} \tan^{-1} \frac{(4\beta - \beta^2)^{1/2}}{\beta + 2u} = 0 \quad (12)$$

Alternatively, it may be more convenient to use as the limiting condition the time t_t when the bubble vanishes; in this case eq 11 becomes

$$\ln \frac{t}{\beta t_t}(u^2 + \beta u + \beta) - \frac{2\beta}{(4\beta - \beta^2)^{1/2}} \tan^{-1} \frac{u(4\beta - \beta^2)^{1/2}}{\beta(2 + u)} = 0 \quad (13)$$

Expressed in terms of a and t , eq 12 can be written

$$\ln \frac{a^2}{a_0^2} \left(1 + \frac{\beta(\pi Dt)^{1/2}}{a} + \frac{\beta\pi Dt}{a} \right) - \frac{2\beta}{(4\beta - \beta^2)^{1/2}} \tan^{-1} \frac{(4\beta - \beta^2)^{1/2}}{\beta + \frac{2a}{(\pi Dt)^{1/2}}} = 0 \quad (14)$$

This is a highly nonlinear equation; methods for recovering D from eq 14 are discussed in the section on analysis of data.

Experimental Section

The brief description which follows will be divided into five sections: the fiber, the optical cell, catching the bubble, the optical system, and measurement of concentrations. Further details of the experimental techniques are given in the theses referred to below.^{5,6}

The Fiber. Quartz fibers of thicknesses of the order of a few microns were prepared by a standard technique.⁷ This consisted of first drawing a coarse fiber in the oxygen gas blowtorch and then allowing the coarse fiber to be blown into a fine one by a "brush" flame from the same torch. The fine fibers were stored in a large desiccator; fibers stored in the open air were found to lose the surface properties needed for adherence of a bubble. A holder was constructed of 1-mm Pyrex rod in the shape of a fork whose two tines were separated by ca. 3 cm; the quartz fibers were fused to the ends of the tines. Nylon or dacron fibers were made by heat-drawing monofilament fiber (commercial nylon fishing line, for example); these fibers were glued to the holder with polystyrene cement.

The Optical Cell. A drawing of the optical cell is shown in Figure 1. The two end windows were optical flats; the large spherical ground-glass joint served as the opening through which the fiber holder, attached to a male joint, was inserted; the other port served for admission of the liquid. The cell was suspended in a thermostatic water bath whose sides were of plate glass.

Catching the Bubble. Gas from the cylinder passed through a pressure-reducing valve and two needle valves before entering the cell. The delivery tube terminated in a very fine needle (Hamilton Co., Whittier, Calif., No. N73731, 3 in.) of the type used in medicine for injections into the exposed surface capillaries of the eyeball. A screw-driven manipulator was used to position the syringe tip accurately beneath the

(5) G. Mulholland, B.S. Thesis, Case Institute of Technology, 1965.

(6) C. Dickey, B.S. Thesis, Case Institute of Technology, 1966.

(7) J. Strong, "Procedures in Experimental Physics," Prentice-Hall, Inc., New York, N. Y., 1938, pp 188-217.

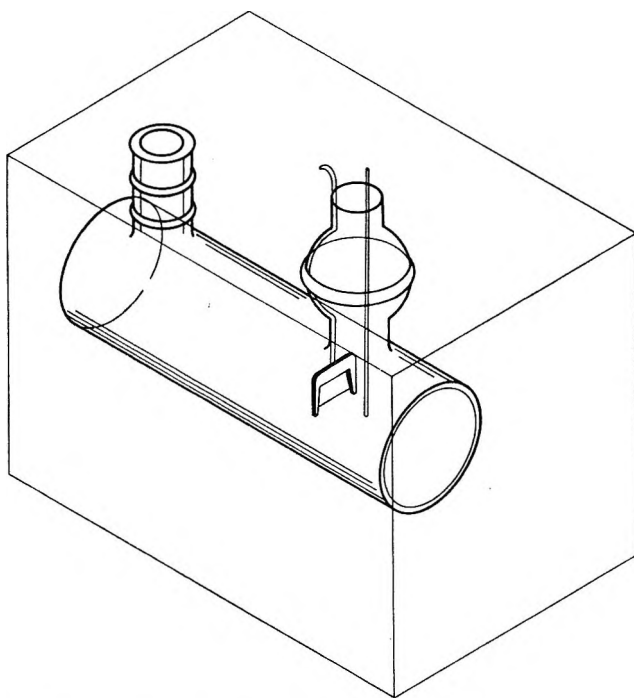


Figure 1. The diffusion cell, with the fiber holder in place.

fiber. A slow, fine bubble stream was ejected through the syringe needle until a single bubble was caught.

In organic liquids, the bubble would adhere to nylon or dacron fibers, but not to quartz. Difficulty in catching a bubble on a single strand was encountered in viscous solutions; in these cases closely spaced parallel fibers were attached to the holder and the bubble was caught between them. In very viscous solutions even this technique proved very difficult, but fortunately in these cases the bubbles rose so slowly that they remained effectively suspended without any fiber at all!

The Optical System. To permit magnification of the bubble without disturbing the cell, the projection system of Figure 2 was used. A standard microscope lamp, located outside the bath, served as light source and condensing lens. Two $f/4.5$ lenses spaced by *ca.* 5 cm and placed *ca.* 10 cm beyond the object were used to project an image on a plane 50 cm away, with *ca.* five-fold magnification. For initial alignment and manipulation while catching the bubble a cardboard screen was used, but for actual measurement the screen was removed and a horizontal microscope with a $2.8\times$ objective and a $10\times$ eyepiece was focused on the virtual image. Over-all magnification was $140\times$. An Exakta single-lens reflex 35-mm camera with microscope adapter was attached to the microscope to photograph the image. Using a green filter on the light

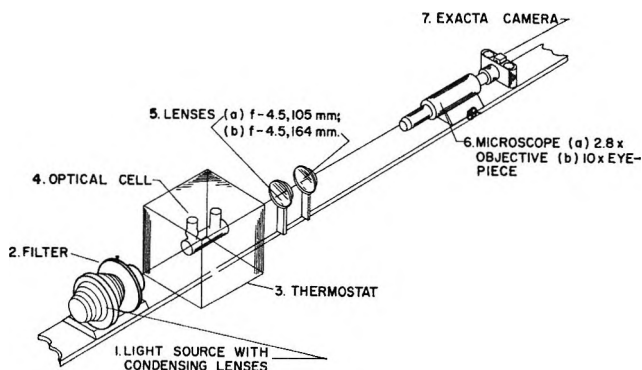


Figure 2. The optical system: (1) microscope lamp with condensing lens; (2) filter; (3) thermostat; (4) diffusion cell; (5) projection lenses; (6) microscope; (7) camera.

source, Kodak Tri-X film at $1/25$ sec, and Diafine developer, the system gave a resolution of 160 lines/mm.

Measurement of Concentration. The system selected for study during the development phase of this investigation was oxygen in water, because of the existence of an accurate chemical analysis for dissolved oxygen.⁸ This consisted of addition of manganous sulfate and alkaline iodide solutions to precipitate hydrous MnO_2 , re-solution with H_2SO_4 , liberating iodine, and titration of the iodine with standard thiosulfate solution to the starch end point. Accuracy to better than 0.5% was achieved.

Later measurements of dissolved gas were made with a Van Slyke blood gas analyzer,⁹ modified to take a Teflon stopcock for use with organic liquids. This apparatus outgasses the sample by agitation under reduced pressure and measures the volume of gas liberated.

To prepare a solution having a desired gas content C_0 , a volume of liquid $V = V_c C_0 / C_s$ was placed in the cell whose volume is V_c . With the cell in the water bath and a reflux condenser in place, gas was bubbled through the liquid for 30 min. The cell was then filled with previously thermostated liquid which had been degassed by refluxing under partial vacuum for 30 min. Determination of dissolved gas content after completion of the bubble solution measurement verified the value of C_0 .

Measurement of Bubble Solution Rate. As soon as the bubble was caught, a stop watch was started and the first frame exposed. Subsequent exposures were made at suitable timed intervals until the bubble either dissolved completely or broke away from the

(8) "Standard Methods for the Examination of Water, Sewage and Industrial Wastes," American Public Health Association, New York, N. Y., 1955, pp 250-259.

(9) F. S. Orcutt and M. H. Seevers, *J. Biol. Chem.*, **117**, 501 (1937).

fibers. (When it was possible to use a single fiber, the bubble always remained in place until it dissolved.) The time of solution ranged from a very few minutes to 1 hr, depending mainly upon the solubility. In some instances a second bubble was caught and measured in the same solution. A standard wire of known diameter, inserted in the cell at the position of the bubble, was photographed in order to determine the magnification factor. After development of the film, the image diameters of the bubble and the standard wire were measured on the film using a traveling microscope. Figure 3 shows a representative film strip of an oxygen bubble dissolving in water; at all stages of the dissolution process, the bubble remains spherical.

Analysis of Data. To obtain values for diffusion coefficients, eq 14 was fitted to the radius *vs.* time data by an iterative least-squares procedure. This equation is of the form $f(a, t, a_0, D) = 0$. For each datum point (a_i, t_i) , let $f_i(a_0, D) = f(a_i, t_i, a_0, D)$. Then a discrepancy function $\Delta(a_0, D)$ can be defined

$$\Delta(a_0, D) = \sum_i f_i^2 \quad (15)$$

The discrepancy function is to be minimized with respect to variation of the parameters a_0 and D , by setting $\partial\Delta/\partial a_0$ and $\partial\Delta/\partial D$ equal to zero. Two simultaneous equations are thereby obtained, which may be solved for a_0 and D by an iterative procedure. The initial trial value of a_0 is the experimental value, and the trial value of D may be obtained in either of two ways. The initial slope of the a^2 *vs.* t graph may be used in conjunction with eq 9, or we may set $u = 0$ and $t = t_i$ in eq 12 to give

$$D = \frac{a_0^2}{\pi t_i \beta} \exp \left[\frac{2\beta}{(4\beta - \beta^2)^{1/2}} \tan^{-1} \frac{(4\beta - \beta^2)^{1/2}}{\beta^2} \right] \quad (16)$$

A digital computer was programmed to find the "best values" of D and a_0 , to calculate values a_i^* for the radius at each value of t_i , and to compute a standard deviation σ

$$\sigma = \left[\frac{1}{n} \sum_{i=1}^n (a_i^* - a_i)^2 \right]^{1/2} \quad (17)$$

Results

In Figure 4 the square of the bubble radius is graphed as a function of time for oxygen dissolving in water which is 4.5% saturated at 29.6°. The points are experimental, the dotted lines are limiting straight lines at short and long times, and the curve is calculated from eq 14 using an initial bubble radius $a_0 = 3.82 \times 10^{-2}$ cm and a diffusion coefficient $D = 3.53 \times 10^{-5}$ cm²/sec. The closest temperature at which litera-

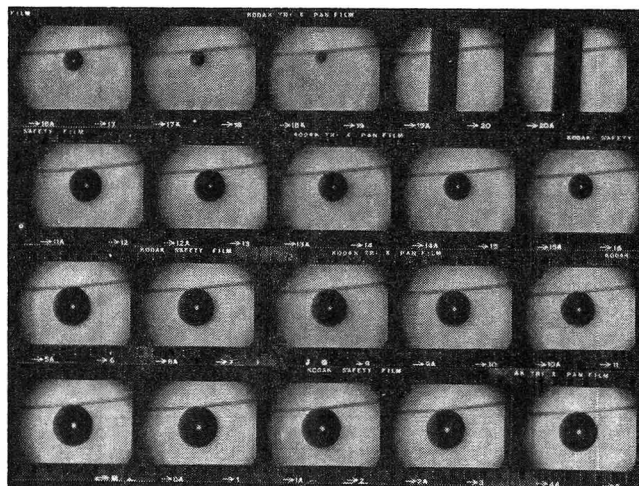


Figure 3. Representative film strip showing decrease of bubble size with time and photograph of standard wire.

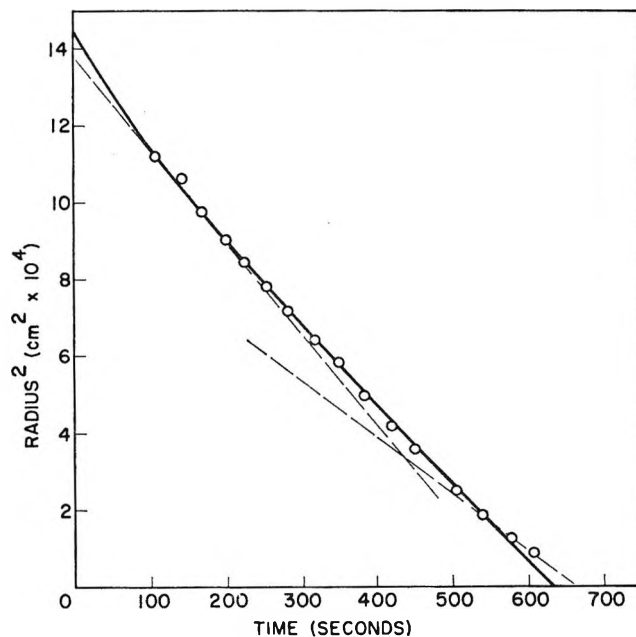


Figure 4. Radius squared *vs.* time for O₂ dissolving into H₂O which is 4.5% saturated at 29.6°. Points are experimental; line is least-squares fit of eq 14; dotted lines are limiting tangents to the experimental points.

ture values have been measured is 25.0°, where diffusion coefficients ranging from 1.9×10^{-5} to 2.6×10^{-5} cm²/sec have been reported.¹⁰ Table I summarizes the results of nine separate determinations of the diffusion coefficient for oxygen in water at 30° into solutions having dissolved oxygen content ranging between zero and 90% of saturation. The disappear-

(10) D. M. Himmelblau, *Chem. Rev.*, **64**, 544 (1964).

ance times varied from 10 min at low concentrations to 75 min at high concentrations. Table II groups these data according to the initial dissolved oxygen content and shows clearly that within experimental error (average deviation from the mean) the diffusion coefficient is concentration independent. Diffusion coefficients calculated from the initial slopes using eq 9 were concentration independent and ran about 15% high; diffusion coefficients calculated from the final slopes were 20 to 50% low, depending on the initial oxygen concentration.

Table I: Determinations of Diffusion Coefficients for O₂ in H₂O at 29.6 ± 0.2°

Bubble	Initial diameter, cm × 10 ²	Concn, g/cm ³ × 10 ⁵	Diffusion coefficient, cm ² /sec × 10 ⁵	Std dev, cm × 10 ²
1	3.11	3.21	3.38	0.032
2	3.30	3.13	3.38	0.021
3	3.13	3.10	3.76	0.030
4	3.35	0.11	4.08	0.034
5	2.86	0.08	3.18	0.040
6	2.82	0.16	3.53	0.054
7	2.39	1.79	3.10	0.026
8	3.00	1.74	3.33	0.033
9	2.91	1.78	3.67	0.014

Table II: Effect of Concentration on Diffusion Coefficient of O₂ in H₂O

Concn, g/cm ³ × 10 ⁵	Diffusion coefficient, cm ² /sec × 10 ⁵
3.13-3.21	3.51 ± 0.17
0.08-0.16	3.60 ± 0.32
1.74-1.79	3.37 ± 0.20

For the nine determinations of the diffusion coefficient of oxygen in water, a mean of 3.49×10^{-5} cm²/sec was obtained, with an average deviation of 0.24×10^{-5} cm²/sec. A series of eight determinations of the diffusion coefficient for nitrogen in gas-free water at 29.6° gave a mean of 3.47×10^{-5} cm²/sec, with an average deviation of 0.22×10^{-5} cm²/sec. These values are consistent with literature values reported at 25°; the errors are comparable to those of other methods. Table III summarizes the results of measurements made on these and other gas-liquid systems; in each case the error is expressed as the average deviation. In addition, oxygen in aqueous solutions of several polymers (hydroxyethylcellulose, Carbowax)

was also studied in order to test the applicability of the method to measurements in viscous liquids. The results obtained were of the same order of precision as those in pure liquids.

Table III: Diffusion Coefficients of Gases in Liquids at 29.6°

Gas	Liquid	Solubility, g/cm ³ × 10 ⁵	No. of determinations	Diffusion coefficient, cm ² /sec × 10 ⁵
O ₂	H ₂ O	3.60	9	3.49 ± 0.24
N ₂	H ₂ O	1.62	8	3.47 ± 0.22
He	H ₂ O	0.198	4	5.42 ± 0.33
O ₂	Ethanol	27.0	4	2.64 ± 0.14
He	Ethanol	0.161	5	14.3 ± 1.2
O ₂	Benzene	26.0	4	2.89 ± 0.31
O ₂	Cyclohexane	31.7	2	5.31 ± 0.17

Conclusions and Discussion

The method of bubble solution offers a convenient means to determine diffusion coefficients of gases in transparent liquids. The accuracy achieved in this first study is comparable to that of most other techniques, being exceeded only by the liquid jet method. It should be preferred over the jet method for use with non-Newtonian liquids such as polymer solutions and for studies with rare gases, since the amount of gas required is miniscule.

The errors of this method can be reduced by refinement of the measurement techniques and the analysis of the data. A significant source of experimental error lies in the optical system; the magnification factor is not completely uniform over the film plane, and the measured diameters are sensitive to the placement of the object. These errors, which can be as large as 2%, can be minimized in future work by the use of aplanatic lenses and an optical alignment system for placement of the object. Another possible source of error is vibration, which would lead to an increased rate of solution; convective effects due to the density difference between the gas-containing solution and the pure liquid would operate in the same way.

The role of the vapor of the host liquid has been neglected, for the following reasons. (1) Its partial pressure would reduce the amount of diffusing gas in the bubble, but through Henry's law it would have an exactly compensating effect on the solubility. (2) It is reasonable to assume that the concentrations of gas and vapor are uniform throughout the bubble because of the high diffusion coefficients in the gas phase and the small dimensions of the bubble. (3) Although

the heats of solution of the gas and the vapor might cause some local temperature inhomogeneities, especially in rapidly dissolving bubbles, the agreement among the O₂-in-H₂O results, where the time of the experiment varied over a tenfold range, indicates that this is not a serious source of error.

The stationary bubble assumption made in the analysis introduces an error whose magnitude should be estimated. The surface of the bubble moves inward and its center moves downward during the experiment, causing small liquid flows in the radial and vertical

directions. These effects may be the principal source of the small but systematic discrepancies between the calculated and observed radii and for the deviations in the diffusion coefficients.

Acknowledgments. The authors are indebted to Mr. Henry Gurr, who instructed them in the art of catching a bubble on a fiber, and to Mr. Harry Atkinson for developing the computer program used in the data analysis. This research was performed in part under a National Science Foundation Undergraduate Research Participation program.

NOTES

The Crystal Structure of

1,3-Dichloro-2,4,6-trinitrobenzene

by James R. Holden and Charles Dickinson

U. S. Naval Ordnance Laboratory, White Oak, Silver Spring, Maryland (Received August 22, 1966)

As part of a study of substituted polynitroaromatic compounds at this laboratory, the crystal and molecular structure of 1,3-dichloro-2,4,6-trinitrobenzene was determined. Of primary interest was the steric effect of the chlorine atom and the comparison of this effect with that observed in similar compounds.¹⁻³

Crystals of the material were grown by slow cooling of a chloroform solution. Weissenberg and precession photographs indicated the orthorhombic space group, P_bcn, with cell dimensions: $a = 5.93$ Å, $b = 14.98$ Å, and $c = 10.91$ Å. These cell dimensions give a calculated density of 1.93 g/cc with four molecules per cell. The density, measured by flotation, is 1.86 g/cc. Weissenberg photographs with the crystal rotating about the a axis were taken for levels 0-4 kl using a multiple-film technique. Intensities were visually estimated using a gray scale prepared from graduated exposures of a typical reflection. Of the 767 reflections in the region considered, 430 had detectable intensity.

The intensities were scaled together and 1/ Lp corrections were applied using the crystallographic computing system X-Ray 63.⁴ No corrections for absorption were made. Since four asymmetric units can be accommodated in this space group only if they each

possess a twofold axis or a center of symmetry, this molecule must contain a twofold axis. This information was employed with a Patterson map to determine coordinates for the nonoxygen atoms. A structure factor calculation using these positions for carbon, nitrogen, hydrogen, and chlorine gave an R value of 0.45. A difference Fourier clearly indicated oxygen positions, and a structure factor calculation over all atoms (including oxygen atoms) gave an R value of 0.34. These positions served as the starting point of the refinement.

Fourier and full-matrix least-squares refinement lowered the R value to 0.084 using individual anisotropic temperature factors for Cl₁, O₂, O₄, and O₄' and individual isotropic temperature factors for the remaining atoms. The temperature factor for H was assumed to be 4.0 and not refined. This gives a final overdetermination ratio (number of observed reflections/number of independent parameters) of 430/60 = 7.2. This we feel is large enough to be sound. The final atomic parameters and the errors in the least significant places are given in Table I. The final scale factors were calculated on a level basis from the ratio of the sums of calculated and observed structure factors. The final agreement factors based on the results of the last least-squares cycle are given in

(1) J. R. Holden, *Acta Cryst.*, in press.

(2) H. Cady and A. C. Larson, *Acta Cryst.*, 18, 485 (1965).

(3) C. Dickinson, J. M. Stewart, and J. R. Holden, *ibid.*, 21, 663 (1966).

(4) J. M. Stewart, *et al.*, Technical Report TR-64-6, NsG-398, Computer Science Center of the University of Maryland, 1964.

Table I: Final Atomic Parameters (Errors)

Atom	<i>x</i>	<i>y</i>	<i>z</i>	<i>B</i> or <i>B</i> ₁₁ ^o	<i>B</i> ₂₂	<i>B</i> ₃₃	<i>B</i> ₁₂	<i>B</i> ₁₃	<i>B</i> ₂₃
Cl ₃	0.3374 (5)	0.0904 (1)	0.0906 (2)	4.71 (15)	2.93 (7)	4.79 (10)	0.54 (9)	1.82 (11)	-0.18 (9)
C ₂	0.0000	0.1070 (8)	0.2500	3.57 (26)					
C ₃	0.1601 (16)	0.1520 (5)	0.1776 (7)	3.07 (16)					
C ₄	0.1546 (15)	0.2435 (5)	0.1798 (7)	2.77 (15)					
C ₅	0.0000	0.2894 (8)	0.2500	3.05 (23)					
N ₂	0.0000	0.0104 (7)	0.2500	3.52 (21)					
N ₄	0.3189 (15)	0.2970 (5)	0.1111 (6)	3.20 (13)					
O ₂	0.1480 (13)	-0.0265 (4)	0.3064 (6)	6.13 (44)	3.76 (28)	4.30 (29)	0.32 (31)	0.93 (32)	0.37 (25)
O ₄	0.5119 (12)	0.2686 (4)	0.1028 (6)	3.46 (38)	4.01 (27)	5.35 (33)	-0.12 (28)	1.15 (27)	-0.03 (29)
O ₄ '	0.2520 (11)	0.3665 (4)	0.0662 (6)	4.12 (37)	2.99 (25)	5.43 (31)	-0.85 (24)	-1.60 (29)	1.87 (25)
H	0.0000	0.3601 (10)	0.2500	4.00					

^a Temperature factor = $\exp[-1/4(h^2a^2B_{11} + k^2b^2B_{22} + l^2c^2B_{33} + 2hka^*b^*B_{12} + 2hla^*c^*B_{13} + 2klb^*c^*B_{23})]$ or $\exp(-B \sin^2 \theta / \lambda^2)$.

Table II: Final Agreement Factors^a

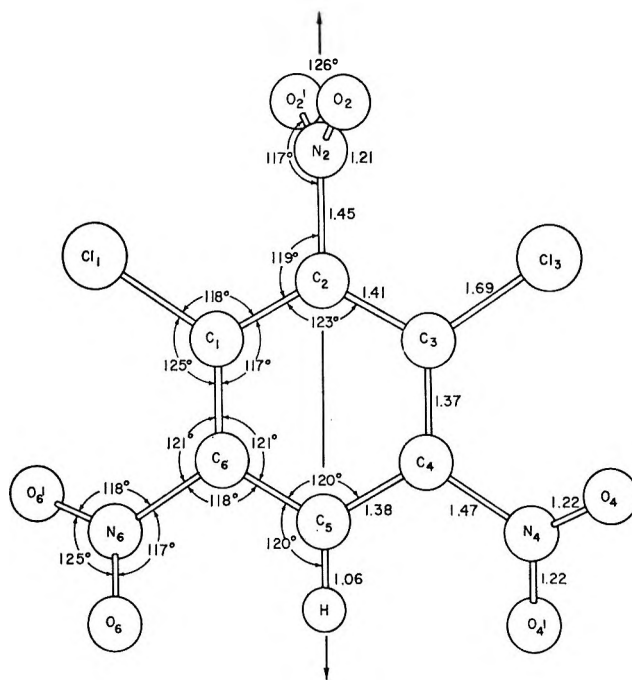
$\Sigma w(F_o - F_c)^2$	2418
<i>R</i>	0.084
<i>R</i> with reflection multiplicity	0.088
<i>R</i> with weighting	0.102

^a 21 of 337 unobserved calculated greater than *F*_{min}.

Table II. A list of observed and calculated structure factors is available from the authors on request.

The least-squares refinement was based on minimizing $\Sigma w(F_o - F_c)^2$. For unobserved reflections, $(F_o - F_{\min})^2$ was included in the sum when the calculated structure factor, *F*_c, was greater than *F*_{min}, the structure factor calculated from the minimum observable intensity. No contribution was included for unobserved reflections when *F*_c was smaller than *F*_{min}. The values of *F*_{min} ranged from 0.9 to 3.0. The weight, *w*, was taken as 1.0 for reflections with *F*_{rel} < 8.0 and $8.0/(0.5F_{\text{rel}} + 4.0)$ for reflections with *F*_{rel} greater than 8.0. The maximum *F*_{rel} was 45.5 and this reflection (102) had a weight of 0.30 with this scheme.

Unobserved reflections were included in the least-squares refinement because they contribute useful information; *i.e.*, it is known that their structure factors are smaller than their *F*_{min} values, although their precise values are unknown. However, the question then arises as to whether to include unobserved reflections which did not contribute to the least-squares refinement as "observations" when calculating the estimated errors in the atomic parameters. When the relative number of unobserved reflections is small, the difference is not significant; however, in this structure determination 44% of the reflections were too weak for observation. The errors listed in Table I

**Figure 1.** Bond distances and angles.

were calculated with all reflections included as "observations." If the unobserved reflections not contributing to the last refinement cycle are not included, these errors are multiplied by a factor of 1.34.

The bond lengths and angles calculated from the final atomic parameters are shown in Figure 1. On the basis of the errors listed in Table I, the largest error in bond length for nonhydrogen atom bonds is 0.016 Å for C₂-N₂ and the average error is 0.011 Å. The corresponding errors in bond angles are 0.83° for C₂-C₃-C₄ and 0.70°. If the unobserved reflections not contributing to the last cycle are not included as "observations," the average errors are 0.015 Å and 0.93°.

and the maximum errors are 0.021 Å and 1.11°. We believe that the smaller number is more representative in each case and that the larger number might be regarded as an upper limit.

The only intermolecular separation less than the sum of Pauling's van der Waals radii⁵ is a separation of 3.06 Å between O₄' and Cl₃ of the molecule at $1/2 + x$, $1/2 - y$, $2 - z$.

Within experimental error, the carbon atoms, H, and N₁ lie in the same plane. Atoms N₄, O₂, and O₄ lie on one side of this plane and atoms Cl₃ and O₄' on the other. The nitro group in the 2 position is rotated 75° from the plane of the ring and the nitro group in the 4 position by 37°. An examination of the bond angles indicates a displacement of the Cl atom toward the nitro group in the 2 position, probably allowed because the closest approach between the Cl atom and this nitro group is to the nitrogen atom, rather than to oxygen. This displacement would appear definitely significant. Also the endocyclic angles at C₂ and C₄ appear to be definitely greater than 120° and the endocyclic angle at C₃ less than 120°.

Chemically equivalent bonds within the molecule appear, at least to a first approximation, to be of the same length. Thus the three N–O bonds are the same and also the two C–N bonds, within experimental error. The similarity is not so great among the C–C bonds. Certainly C₃–C₄ and C₄–C₅ are the same. However, the difference between these bonds and C₂–C₃ is in the range 2–3σ. Also it should be noted that such a deviation has been reported in similar compounds.^{1–3}

Acknowledgment. The authors gratefully acknowledge the Foundational Research Fund, Task FR-44, of the Naval Ordnance Laboratory, White Oak, Md., which supported this work.

(5) L. Pauling, "The Nature of the Chemical Bond," 3rd ed, Cornell University Press, Ithaca, N. Y., 1960.

The Association of MnSO₄ in Methanol–Water Mixtures of High Methanol Content

by H. Tsubota and G. Atkinson

Department of Chemistry, University of Maryland, College Park, Maryland 20740 (Received August 29, 1966)

In a series of papers^{1–3} we have examined the association of MnSO₄ and MnBDS in various water–organic solvent mixtures. These particular salts were chosen

as good examples of 2–2 electrolytes with MnSO₄ being associated in water ($K_A = 133$) and MnBDS essentially unassociated ($K_A < 5$). Marked deviations from the predictions of simple electrolyte theories were found as higher organic content solvent mixtures were used. In the typical case of MnBDS in methanol–water mixtures, above a methanol mole fraction of 0.25 the log K_A vs. $1/D$ plot changes slope, the Walden product decreases drastically, and a_r (mean distance of closest approach) increases drastically.¹

The demonstration that association in 2–2 salts such as MnSO₄ takes place in a stepwise fashion^{4,5} has opened a new phase in the investigation of such systems. The occurrence of stepwise association is caused by strong and selective solvent coordination by one or both of the ions involved in the association. It has also been demonstrated that the strong solvent specificity noted in the classical measurements is qualitatively explicable⁶ in terms of different solvent effects on different steps in the association process. It is then our belief⁷ that the following factors must all be considered before a quantitative explanation of association in a system such as MnSO₄–CH₃OH–H₂O can be offered: (1) selective solvation of one or both ions, (2) changing availability of a given solvent component due to strong solvent–solvent H-bonding interactions, and (3) coupling of factors 1 and 2.

In the previous work¹ MnSO₄ was not examined in high CH₃OH content CH₃OH–H₂O mixtures because of the very limited solubility. Therefore, as an extension of this work and an attempt to compare MnSO₄ and MnBDS over a wide range of solvent compositions, we have measured the conductance of MnSO₄ in four high CH₃OH content mixtures.

Experimental Section

The purification and analysis of solvents and salt have been described previously.¹ The experimental technique has been described⁸ and conforms to high-precision conductance practice.

Results

The experimental results are given in Table I. The

- (1) C. J. Hallada and G. Atkinson, *J. Am. Chem. Soc.*, **83**, 3759 (1961).
- (2) G. Atkinson and C. J. Hallada, *ibid.*, **84**, 721 (1962).
- (3) G. Atkinson and S. Petrucci, *ibid.*, **86**, 7 (1964).
- (4) M. Eigen, G. Kurtze, and K. Tamm, *Z. Elektrochem.*, **57**, 103 (1963).
- (5) M. Eigen and K. Tamm, *ibid.*, **66**, 107 (1962).
- (6) G. Atkinson and S. K. Kor, *J. Phys. Chem.*, **69**, 128 (1965).
- (7) "Molecular Relaxation Processes," Chemical Society Special Publication No. 20, Academic Press Inc., New York, N. Y., 1966, p 243.
- (8) G. Atkinson and S. Petrucci, *J. Phys. Chem.*, **67**, 337 (1963).

data were analyzed using the Fuoss-Onsager equation for an associated symmetrical electrolyte

$$\Lambda = \Lambda^0 - S(C\gamma)^{1/2} +$$

$$E(C\gamma) \log(C\gamma) + J(C\gamma) - K_A \Lambda f_{\pm}^2(C\gamma)$$

where the terms have been defined.⁹

Table I: Conductances of MnSO₄ in Methanol-Water^a

$C \times 10^4$	Λ	$C \times 10^4$	Λ
—49.98% methanol—		—60.16% methanol—	
0.77230	53.431	0.84325	44.548
2.2002	43.852	1.8756	36.065
3.4968	39.266	3.0128	31.265
4.8004	36.038	4.0452	28.393
		5.2942	25.923
		6.7176	23.867
		8.2927	22.144
		10.450	20.276
—69.94% methanol—		—80.06% methanol—	
1.1656	30.312	0.39364	27.347
3.1130	21.260	0.92415	20.025
4.6855	18.158	1.5408	16.293
6.3944	16.074	2.2097	13.891
8.6496	14.264	3.2009	11.957
10.462	13.224	4.3331	10.548
		5.2391	9.7526

^a C is in moles per liter and Λ in $\text{ohm}^{-1} \text{cm}^2 \text{equiv}^{-1}$. Results are reported to one more significant figure than the precision justifies so that rounding-off errors are not propagated in recalculation.

The data were analyzed using an IBM 7090/7094 computer to yield the "best" Λ_0 , K_A , and a_J parameters. These are given in Table II together with the values obtained in the previous work. The Walden product ($\Lambda^0\eta$) exhibits the decrease noted before for MnBDS in CH₃OH-H₂O mixtures. At the same time the a_J values show a very marked increase. With the present uncertainties in the conductance theory it does not seem fruitful to speculate on the actual size of the a_J values.

Figure 1 compares the K_A values as a function of dielectric constant on the traditional $\log K_A$ vs. $1/D$ plot. Although the MnSO₄ plot does not exhibit as pronounced a change of slope as the MnBDS plot, there is still a marked change. The dotted line represents the extrapolation of the low CH₃OH content mixture points. It is clear that the extrapolated K_A at the highest CH₃OH content (80%) is markedly higher than the actual value.

It has then been shown that MnBDS and MnSO₄ exhibit similar behavior in high organic content, H-

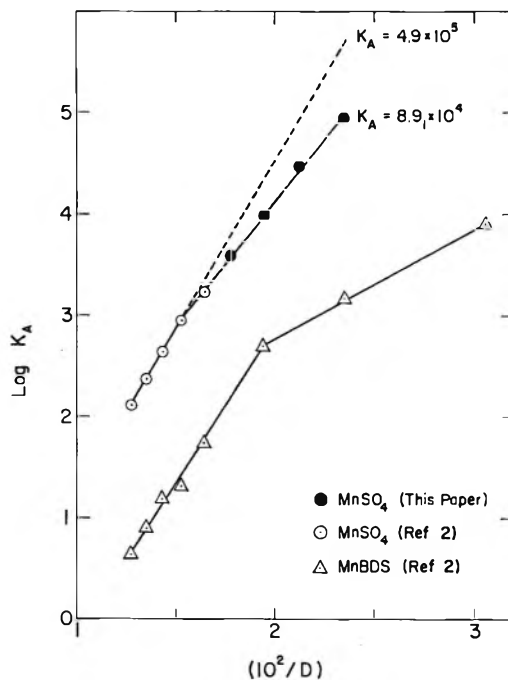


Figure 1.

Table II: Conductance Parameters—MnSO₄ in CH₃OH-H₂O Mixtures

% CH ₃ OH (w/w)	D	Λ^0	$\Lambda^0\eta$	$K_A \times 10^{-2}$	a_J, A
0 ^a	78.48	133.2	1.19	1.33	5.0
10.00 ^a	74.21	104.9	1.21	2.37	5.2
20.00 ^a	70.01	85.8	1.20	4.39	5.8
30.00 ^a	65.55	74.7	1.14	8.81	8.0
40.00 ^a	60.92	68.9	1.10	17.1	8.2
49.98 ^b	56.30	67.1	1.06	38.7	11.1
60.16 ^b	51.63	67.6	0.946	96.1	10.5
69.94 ^b	47.18	70.2	0.847	295.	19.2
80.08 ^b	42.57	64.9	0.652	891.	20.7

^a Reference 1. ^b This work.

bonding solvent mixtures. Although the details of the deviations from simple predictions are not identical, the pattern is similar. The authors believe that the three factors described above must be examined in detail before a quantitative explanation of such systems can be advanced.

Acknowledgment. The authors wish to express their appreciation to the U. S. Atomic Energy Commission for their support of this research under Contract AT-

(9) R. M. Fuoss and F. Accascina, "Electrolytic Conductance," Interscience Publishers, Inc., New York, N. Y., 1959.

(40-1)-2983. They also wish to express their appreciation for the support of the University of Maryland Computer Science Center and to Mr. David W. Ebdon.

Dielectric Study of the Hydration of Acetone in 1,2-Dichloroethane¹

by T. F. Lin, S. D. Christian, and H. E. Affsprung

Department of Chemistry, The University of Oklahoma, Norman, Oklahoma 73069 (Received September 26, 1966)

In a previous communication from this laboratory,² it was reported that acetone interacts with water to form hydrated species in 1,2-dichloroethane. Partition, water solubility, and nmr data were analyzed to show that the acetone monomer monohydrate is the major associated species in the acetone-water-1,2-dichloroethane system. In order to obtain additional information about the geometric structure of the acetone monomer monohydrate, the dielectric constants of solutions of acetone and water in 1,2-dichloroethane were measured.

Experimental Section

Dielectric constants were determined with the Kahl Dipolmeter DMO1 which operates on the superposition (beat) method. An MFL2 cell (range from $\epsilon = 7$ to 21) with a capacity of 45 ml was used for all the measurements. Constant-temperature water was circulated through the water jacket of the cell; the circulated water temperature was maintained at $25.00 \pm 0.03^\circ$. Once a series of measurements was started, the cell was not removed or turned in its connector in order to avoid the possibility of error due to slight change in the electric contact. After the dielectric constant of each sample solution was measured, the cell was drained and rinsed with the new solution to be measured and the new solution was introduced without moving the cell. The estimated error in the dielectric constant measurements was about 0.06%.

Results and Discussion

Dielectric data of water in 1,2-dichloroethane and acetone in 1,2-dichloroethane are given in Tables I and II, respectively. These data appear to obey Onsager's equation³ which is suitable for the interpretation of data for solutions of polar solutes in a slightly polar solvent

$\epsilon = \text{constant} +$

$$\frac{2\pi(n_s^2 + 2)^2\mu_s^2}{9kT} f_s + \frac{2\pi(n_A^2 + 2)^2\mu_A^2}{9kT} f_A$$

Note that changes in dielectric constant are linearly related to the concentration of polar solute, f_A , and solvent, f_s , where n_A and n_s are the refractive indices of the solute and solvent, respectively, if the dipole moment of solvent term is approximately constant. If ϵ is plotted against f_A , a straight line is obtained with the slope $2\pi(n^2 + 2)^2\mu_A^2/9kT$. Plots of ϵ vs. f_A for water in 1,2-dichloroethane and acetone in 1,2-dichloroethane

Table I: Dielectric Constants of the System Water-1,2-Dichloroethane at 25°

	f_w, M	ϵ	ϵ_{calcd}
Run 1	0.0000	10.303	10.303
	0.0250	10.322	10.325
	0.0375	10.336	10.336
	0.0555	10.348	10.351
	0.0580	10.354	10.353
	0.0903	10.380	10.381
	0.1110	10.397	10.398
	0.1160	10.402	10.402
Run 2	0.0000	10.282	10.282
	0.0333	10.310	10.311
	0.0555	10.334	10.330
	0.0777	10.348	10.349
	0.0888	10.362	10.359
	0.1110	10.378	10.378
	0.1180	10.387	10.384

Table II: Dielectric Constants and Refractive Indices for the System Acetone-1,2-Dichloroethane at 25°

f_A, M	ϵ	ϵ_{calcd}
0.0000	10.323	10.325
0.0000	10.330	10.325
0.0217	10.347	10.350
0.0217	10.354	10.350
0.0869	10.425	10.422
0.1086	10.445	10.447
0.1086	10.449	10.447
0.1521	10.495	10.496
0.1956	10.537	10.546
0.2173	10.573	10.570

(1) Abstracted in part from the Ph.D. dissertation of T. F. Lin, University of Oklahoma, Norman, Okla., 1966.

(2) T. F. Lin, S. D. Christian, and H. E. Affsprung, *J. Phys. Chem.*, **69**, 2980 (1965).

(3) L. Onsager, *J. Am. Chem. Soc.*, **58**, 1486 (1936).

have slopes of 0.86 and $1.13 M^{-1}$, respectively. From these values we obtain the calculated dipole moments of water (2.43 D.) and of acetone (2.74 D.).

For the ternary system acetone–water–1,2-dichloroethane, the dielectric constants (in Table III) can be expressed according to Onsager's equation as

$$\epsilon = \epsilon_0 + \alpha_W(f_W - K_{11}C_A C_W) + \alpha_{AW}K_{11}C_A C_W + \alpha_A C_A \quad (1)$$

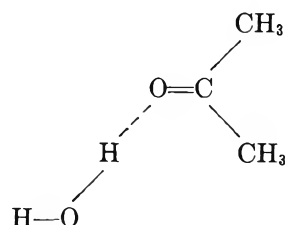
where ϵ_0 is the dielectric constant for pure 1,2-dichloroethane; C_A is the concentration of acetone monomer; C_W is the concentration of water monomer; α_W , α_A , and α_{AW} are proportionality constants, and f_W is the formal concentration of water. If $f_W = 0$

$$\epsilon_{f_W=0} = \epsilon_0 + \alpha_A f_A \quad (2)$$

where f_A is the formal concentration of acetone. Since each set of measurements requires a slightly

$K_{11}C_A C_W$, using the known constants $K_{11} = 0.85$, $\alpha_W = 0.86$, and $\alpha_A = 1.13 M^{-1}$. The values of C_W were obtained by solving the equation, $f_W = C_W + 3K_3 C_W^3$, using the values $K_3 = 4.6 M^{-2}$ from ref 2. A linear plot was obtained having the least-squares slope $\alpha_{AW} = 1.7 \pm 0.2$ D. Using these derived values of the parameters α_W , α_A , and α_{AW} , values of the dielectric constant were calculated corresponding to each set of measurements in Table III. The calculated results are in excellent agreement with experimentally determined dielectric constant values.

The oxygen of the carbonyl group has two lone pairs of electrons which are capable of hydrogen bonding. A plausible structure of acetone monomer monohydrate can be constructed as follows



The angle between the carbonyl group and O---H—O is 120° and the water molecule in this structure is assumed capable of rotation about the —H---O hydrogen bond. If this model and the dipole moment of water (1.85 D.) and that of acetone (2.8 D.) are used, the dipole moment of the complex species can be calculated by averaging the vector for the dipole of water about the axis of the O—H---O bond and adding to the vector of acetone. The result, 3.5 D., is in good agreement with the experimental value, 3.4 D. Fritzsche⁴ has also proposed this type of structure for the ketone–phenol complex.

Using Onsager's equation, the dipole moment of monomeric water was found to be 2.43 D., which is considerably higher than the vapor-phase value of 1.85 D., but the calculated value for acetone is 2.74 D. which is in good agreement with the vapor value (2.8 D.). The higher value of calculated water dipole moment may result from the large solvent effect or the inadequacy of Onsager's equations or both. However, the linear dependence of dielectric constants on the concentration of solute or complex species seems to be established for this system. Although the mutual inductive effect⁵ of the component molecules complicates interpretation of the data in terms of the geometric structure of the complex species, the hydrogen bond in the acetone monomer monohydrate is relatively

Table III: Dielectric Constants of the System Acetone–Water–1,2-Dichloroethane at 25°

	f_W, M	ϵ	$\Delta\epsilon$	$\Delta\epsilon_{\text{calcd}}$
$f_A = 0.108 M$	0.0000	10.433	0.000	0.000
	0.0226	10.450	0.017	0.019
	0.0454	10.468	0.035	0.035
	0.0680	10.485	0.052	0.057
	0.0906	10.502	0.069	0.076
	0.1022	10.513	0.080	0.086
	0.1133	10.525	0.091	0.096
$f_A = 0.216 M$	0.0000	10.570	0.000	0.000
	0.0234	10.588	0.018	0.019
	0.0468	10.608	0.038	0.039
	0.0702	10.622	0.052	0.058
	0.0935	10.640	0.070	0.077
	0.1052	10.655	0.085	0.087
	0.1170	10.665	0.095	0.097
$f_A = 0.407 M$	0.000	10.758	0.000	0.000
	0.0271	10.778	0.020	0.022
	0.0542	10.802	0.044	0.044
	0.0678	10.816	0.058	0.055
	0.0813	10.824	0.066	0.066
	0.1083	10.848	0.090	0.088
	0.1220	10.863	0.105	0.099

different apparent initial value of ϵ_0 to obtain an unbiased result, we subtracted eq 2 from eq 1 to eliminate ϵ_0

$$\epsilon - \epsilon_{f_W=0} + \alpha_A f_A - \alpha_W(f_W - K_{11}C_A C_W) - \alpha_{AW}K_{11}C_A C_W = \alpha_A C_A$$

The dielectric constant data were analyzed by plotting $\epsilon - \epsilon_{f_W=0} + \alpha_A f_A - \alpha_W(f_W - K_{11}C_A C_W) - \alpha_{AW}K_{11}C_A C_W$ vs.

(4) H. Fritzsche, *Acta Chim. Acad. Sci. Hung.*, **40**, 37 (1964).

(5) C. F. Jumper and B. B. Howard, *J. Phys. Chem.*, **70**, 588 (1966).

weak and should not involve a large mutual inductive effect owing to ionic bond character.

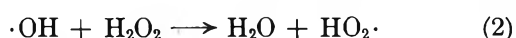
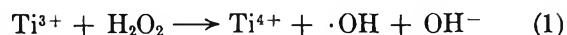
Acknowledgment. This research was supported by the United States Department of the Interior, Office of Saline Water, Washington, D. C.

An Electron Spin Resonance Study of Intermediates Induced in Carbohydrates by Titanium Trichloride-Hydrogen Peroxide

by Peter J. Baugh,¹ Oscar Hinojosa, and Jett C. Arthur, Jr.

Southern Regional Research Laboratory,² New Orleans, Louisiana (Received June 6, 1966)

Dixon and Norman³ have successfully used the $Ti^{3+}-H_2O_2$ system as a means of generating $\cdot OH$ and $HO_2\cdot$ radicals in studying intermediates formed during the oxidation of alcohols. The reactions likely to produce $\cdot OH$ and $HO_2\cdot$ radicals are



When $TiCl_3$ and H_2O_2 are mixed in the cavity with no alcohol present, Dixon and Norman observed only a narrow singlet spectrum, line width 1 gauss, which they attributed to the $\cdot OH$ radical. In the presence of an alcohol, this spectrum was replaced by the more complex spectrum of the alcohol radical. Livingston and Zeldes⁴ have shown that the same alcohol radical as Dixon and Norman observed can be produced if an alcohol solution containing 1% H_2O_2 is photolyzed as it flows through the microwave cavity of the spectrometer. The $HO_2\cdot$ radical, according to Saito and Bielski,⁵ was observed when H_2O_2 was oxidized by ceric ion and exhibited a broad singlet spectrum, line width 27 gauss. We repeated the $Ti^{3+}-H_2O_2$ experiment and under various experimental conditions also observed a narrow singlet spectrum, line width 1 gauss.

When carbohydrates are added to the $Ti^{3+}-H_2O_2$ system, we have found that more than one radical species contributes to the esr spectra; usually one species is more strongly defined than the others. The straight-chain hexitols, such as sorbitol and mannitol, show identical spectra. The aldohexoses show very similar spectra but are quite different from those of the ketohexoses. An attempt has been made to analyze

the spectra observed to account for at least one of the radical species contributing to the hyperfine structure.

Experimental Section

The esr spectra were observed at 22° in the cavity of a Varian 4502-15 epr spectrometer system⁶ operating at 100-kc field modulation and using an aqueous flow cell. The flow rate was varied between 1 and 6 ml sec^{-1} by pressurizing the reactant reservoirs with nitrogen (0.5 atm) and adjusting a clip on the exit line. One reservoir was charged with $TiCl_3$ (15 ml of a 20% solution) and concentrated H_2SO_4 (15 ml) in water (2 l.) and the other reservoir was charged with H_2O_2 (6 ml of 30% solution) and concentrated H_2SO_4 (15 ml) in water (2 l.). For observations of the radicals the solutions in the reservoirs were made 0.05 or 0.1 M with respect to the carbohydrate. The flow rate of mixing of the reactants in the aqueous cell in the resonant cavity and the concentration of carbohydrate indicated were not critical in the observation of the esr spectra. Reagent grade chemicals were used.

Results and Discussion

The esr spectrum observed for glycerol (see Figure 1A) appeared to be one of seven lines of which all do not appear to be associated with the same radical species. The three inner less intense lines (18.7 gauss apart) split into triplets (1:2:1, $\Delta H = 2$ gauss) at lower modulation and power level (see Figure 1A'). There is some interference from the two more intense lines. The center triplet is almost twice as intense as the outer two. The second-order splitting could only occur in the radical $CH_2OHCHOH\dot{C}HOH$ due to the two C_3 protons. Normally if $a_{C_1-H} \neq a_{C_2-H}$, this radical would appear as a quartet with possible second-order splitting of each line into a triplet by further interaction with the two C_3 protons. A triplet of triplets would only be observed if $a_{C_1-H} = a_{C_2-H} = 18.7$ gauss. Dixon and Norman³ proposed the formation of the radicals $CH_2\dot{C}HCH_2$ and $\cdot CH_2CHCH_2$ from allyl alcohol by addition of OH to the double bond. To explain the observed sextet and quartet, the coupling constants of the five protons in the first radical and the

(1) Resident Postdoctoral Research Associate.

(2) One of the laboratories of the Southern Utilization Research and Development Division, Agricultural Research Service, U. S. Department of Agriculture.

(3) W. T. Dixon and R. O. C. Norman, *J. Chem. Soc.*, 3119 (1963).

(4) R. Livingston and H. Zeldes, *J. Chem. Phys.*, **44**, 1245 (1966).

(5) E. Saito and B. H. J. Bielski, *J. Am. Chem. Soc.*, **83**, 4467 (1961).

(6) Trade names are given as part of the exact experimental conditions and not as an endorsement of the products over those of other manufacturers.

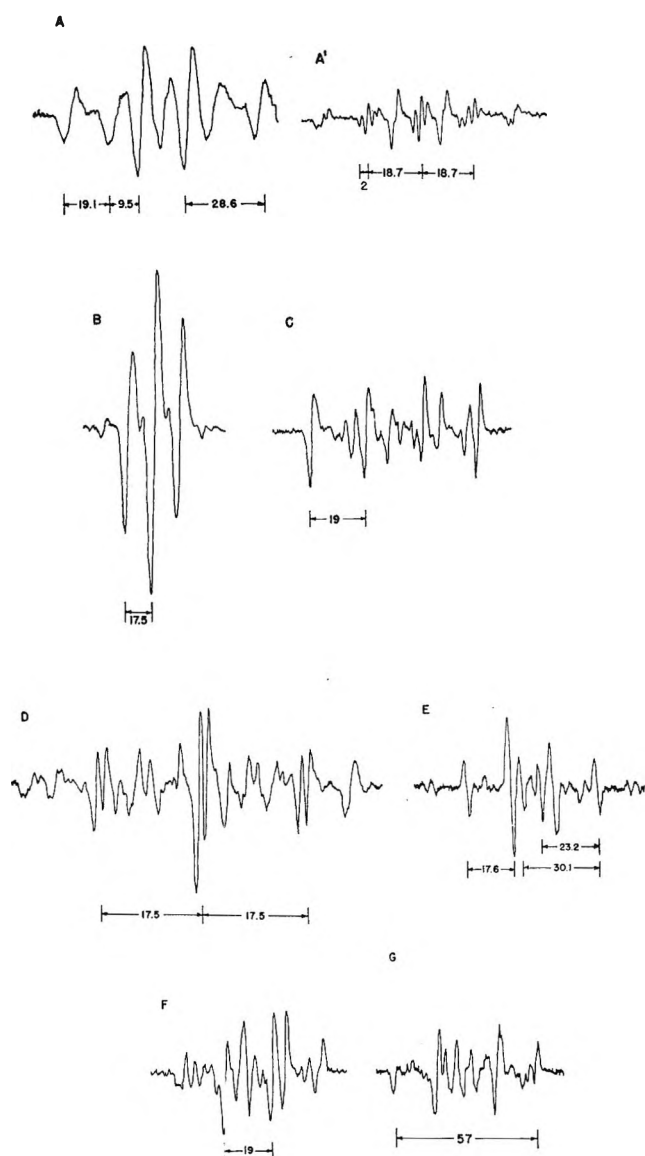
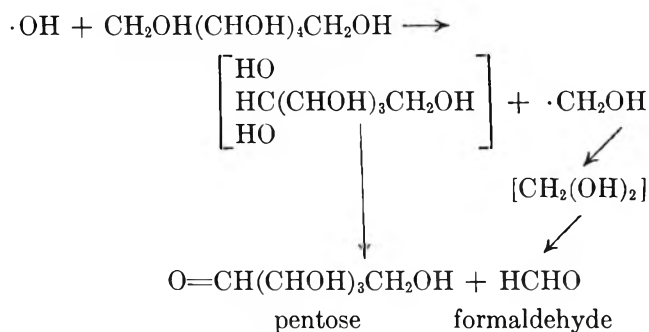


Figure 1. ESR spectra of carbohydrates generated by the $Ti^{3+}-H_2O_2$ system: A, glycerol; A', glycerol at lower modulation; B, sorbitol or mannitol; C, D-glucose or D-galactose; D, α -methyl glucose; E, fructose; F, maltose; and G, cellobiose. Magnetic field increasing left to right.

three protons in the second radical were assumed to be the same. Similarly this could explain our observation of a spectrum of a triplet of triplets.

The spectrum observed for sorbitol and mannitol (see Figure 1B) appeared to be a triplet (1:2:1, $\Delta H = 17.5$ gauss). This may be attributed to the $\cdot CH_2OH$ radical which has been observed in methanol and α, β -diols.^{3,4} At lower power and modulation there was some interference due to overlapping lines from other radical species. One process taking place in the hexitols appears to be scission of the C_1-C_2 or C_5-C_6 bonds



The ring sugars, such as D-glucose and D-galactose, give spectra distinctly different from those for the hexitols as shown in Figure 1C. The ESR spectra obtained were identical. Two quartets (1:1:1:1) can be observed, one being half the intensity of the other. The more intense quartet was equally spaced ($\Delta H = 19.7$ gauss for D-galactose and $\Delta H = 19.4$ gauss for D-glucose) while the less intense quartet was not equally spaced. The radical formed by abstraction of a proton from C_6 , *i.e.*, $R\dot{C}HOH$, would give a quartet (1:1:1:1)

formed by the unpaired electron further splitting with the proton on C_5 , taking the C_6-H splitting constant to be half the splitting constant of C_5-H or *vice versa*. The splitting constants are 19.7 and 39.4 gauss and 19.4 and 38.8 gauss for D-galactose and D-glucose, respectively. It appears likely that the smaller value is associated with C_6-H . The oxygen of the hydroxyl would reduce the spin density of C_6 below the hydrogen-coupling value in alkyl radicals. The C_5-H splitting constant is above this value.

α -Methyl glucose gave a complex spectrum, but a triplet (1:2:1, $\Delta H = 17.5$ gauss) was clearly discernible (see Figure 1D). Each line is further split ($\Delta H = 1.4$ gauss). A radical, such as $ROCH_2\cdot$, formed by the abstraction of a proton from the methyl group on C_1 , would give a triplet spectrum which might be split by further interaction of the unpaired electron with the proton on C_1 . Abstraction of the proton on C_5 would also result in the formation of a triplet by interaction of the unpaired electron with the protons on C_6 . This is less likely in view of the results obtained with D-glucose.

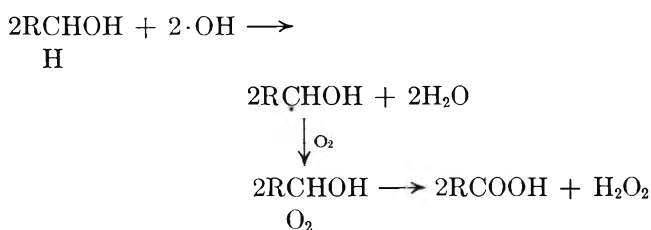
Fructose gave a spectrum of six approximately equally spaced lines (see Figure 1E) of relative intensity 1:5:14:8:5:1. Two lines appear at the center of the spectrum having the same intensity as two of the six lines (5:5) and 6.9 gauss apart. If these four equally intense lines form a quartet, then the splitting constants for the two carbon atoms concerned would be 23.2 and 30.1 gauss. In the fructopyranose ring C_6 is the only carbon atom which has no hydroxyl group attached. Abstraction of a proton from this

carbon would give a_{C-H} near to the accepted value for hydrocarbons ($a_{C-H} = 22$ gauss). The assignment is therefore $a_{C-H} = 23.2$ gauss and $a_{C-H} = 30.1$ gauss. The two main lines could be associated with abstraction of a proton from the primary alcohol group at C_1 to form a doublet ($a_{C-H} = 17.6$ gauss), although intensities are not equal. No further large splitting would occur, since C_2 has no protons.

Maltose and cellobiose (see Figure 1F and 1G, respectively) gave different spectra. Maltose gave a spectrum which could be mainly two doublets ($\Delta H = 19$ and 18.5 gauss). The spectrum for cellobiose was poorly defined.

It can be concluded that the mode of formation of radicals induced in a carbohydrate by the $Ti^{3+}-H_2O_2$ system depends on the structure of the carbohydrate concerned. The esr spectra of the straight-chain hexitols examined were identical; however, these were distinctly different from those observed for the hexoses. Comparison of the aldo- and ketohexoses indicated that the glucopyranose and fructopyranose rings behave quite differently. The splitting constants observed (a_{C-H}) are generally in the range reported for radicals formed from alcohols due to proton abstraction by OH radicals,^{3,4} although in one case a splitting constant of 39 gauss was indicated.

The radical intermediates produced during γ radiolysis of aqueous solutions of carbohydrates have not been observed by esr spectroscopy but their structure has been proposed by the nature of the decomposition products which are formed.⁷ $H\cdot$, $OH\cdot$, and $HO_2\cdot$ radicals formed during the γ radiolysis of the water present in these systems play a role in the production of the postulated species. Using the $TiCl_3-H_2O_2$ system to generate one of these primary radicals, *i.e.*, $\cdot OH$, we have observed radicals formed by $\cdot OH$ attack on certain carbohydrates. There is the possibility that the same carbohydrate radicals are produced in both this process and γ radiolysis. For example, during γ radiolysis of aqueous solutions of D-glucose, the radical species, $R\dot{C}HOH$, has been proposed as a primary radical due to the formation of the corresponding uronic acid as a primary product. The mechanism for the formation of this uronic acid is



This proposed radical appears to be the dominant one

in the spectra observed for the aldohexoses in this paper. On the other hand, during γ radiolysis of the straight-chain hexitols, the production of formaldehyde which leads to the proposal of the intermediate species, $\cdot CH_2OH$, is a secondary process. Therefore this radical is not one of the primary species. In this paper the spectra observed in the case of these hexitols indicate this proposed intermediate to be the dominant one. The dominant radical, observed during proton abstraction from carbohydrates by $\cdot OH$ radicals generated by the $TiCl_3-H_2O_2$ system, may not necessarily be making a major contribution to the actual mechanism.

(7) G. O. Phillips, *Advan. Carbohydrate Chem.*, **16**, 13 (1961).

Thermodynamics of Aqueous Solutions of Noble Gases. IV. Effect of Tetraalkylammonium Salts

by A. Ben-Naim¹

Department of Physical Chemistry, Hebrew University, Jerusalem, Israel (Received June 24, 1966)

In an extension of a previous work² we report here some solubility data of argon in aqueous solutions of tetraalkylammonium salts. The solubility measurements were performed according to a method described elsewhere.³ The mean values of the Ostwald absorption coefficients obtained from three to four measurements at each temperature are recorded in Table I. The reproducibility of the present results was not as good as for pure water or for aqueous solutions of the simpler electrolytes. The maximum deviation found between successive measurements was about 1%. This is apparently due to the higher viscosity of the solutions which put some limitations on the performance of the dissolution method.³

However, the accuracy of these results is sufficient to draw conclusions on the direction of the change of the thermodynamic quantities which accompanies the transfer of argon from pure water into the corresponding solution of R_4N^+ salts. These were calculated from the slopes of the curves in Figure 1 and are given in Table II. The pertinent relations are¹

(1) To whom all correspondence should be addressed at Bell Telephone Laboratories, Murray Hill, N. J.

(2) (a) A. Ben-Naim, *J. Phys. Chem.*, **69**, 3240, 3245 (1965); (b) A. Ben-Naim and M. Egel-Thel, *ibid.*, **69**, 3250 (1965).

(3) A. Ben-Naim and S. Baer, *Trans. Faraday Soc.*, **59**, 2735 (1963).

Table I: Ostwald Absorption Coefficient ($\gamma \times 10^3$) for Argon in Aqueous Solutions of Tetraalkylammonium Salts at Different Temperatures

	5°	10°	15°	20°	25°
(CH ₃) ₄ NCl, 0.5 m	44.07	40.03	37.02	34.29	32.14
(CH ₃ CH ₂) ₄ NI, 0.5 m	44.88	40.73	37.59	34.96	33.00
(CH ₃ CH ₂ CH ₂) ₄ NI, 0.5 m	43.45	39.50	36.40	34.04	32.20

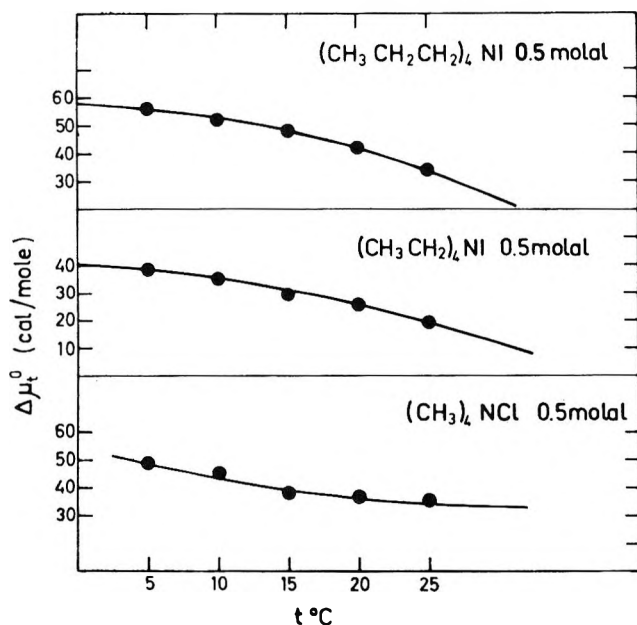
Table II: Values of $\Delta\mu_t^\circ$ (cal/mole), $\Delta\bar{S}_t^\circ$ (cal/mole deg), and $\Delta\bar{H}_t^\circ$ (cal/mole) for the Transfer of Argon from Pure Water into the Various Solutions of Tetraalkylammonium Salts

		5°	10°	15°	20°	25°
(CH ₃) ₄ NCl, 0.5 m	$\Delta\mu_t^\circ$	48.4	45.1	38.2	37.4	35.2
	$\Delta\bar{S}_t^\circ$	1.1	0.9	0.7	0.5	0.3
	$\Delta\bar{H}_t^\circ$	354	300	254	184	125
(CH ₃ CH ₂) ₄ NI, 0.5 m	$\Delta\mu_t^\circ$	38.3	34.8	29.5	26.0	19.6
	$\Delta\bar{S}_t^\circ$	0.5	0.7	0.8	1.2	1.4
	$\Delta\bar{H}_t^\circ$	177	247	274	378	437
(CH ₃ CH ₂ CH ₂) ₄ NI, 0.5 m	$\Delta\mu_t^\circ$	56.2	52.2	47.8	41.5	33.8
	$\Delta\bar{S}_t^\circ$	0.5	0.8	1.1	1.4	1.8
	$\Delta\bar{H}_t^\circ$	195	279	365	466	570

$$\Delta\mu_t^\circ = -RT \ln (\gamma/\gamma_0)$$

$$\Delta\bar{H}_t^\circ = \Delta\mu_t^\circ + T\Delta\bar{S}_t^\circ$$

$$\Delta\bar{S}_t^\circ = R \frac{\partial}{\partial T} T \ln (\gamma/\gamma_0) - RT \frac{\partial}{\partial T} \ln (\rho/\rho_0)$$

**Figure 1.** Values of $\Delta\mu_t^\circ$ (cal/mole) as a function of temperature for the transfer of argon from pure water into an aqueous solution of tetraalkylammonium salt.

where γ_0 and γ are the Ostwald coefficients of argon in pure water and in the electrolytic solution, respectively; ρ_0 and ρ are the corresponding densities of the solvents.

The calculated thermodynamic functions correspond to the following process: argon (in pure water) \rightarrow argon (in water + electrolyte) at equal molar concentration of argon in the two solvents.

From Table II and Figure 1 one sees that the signs of both $\Delta\bar{H}_t^\circ$ and $\Delta\bar{S}_t^\circ$ for the transfer of argon from pure water into these solutions are the same as that found for the other electrolytes.² However, two of the curves in Figure 1 have different curvature to the corresponding curves for all other electrolytes. This feature corresponds to a positive change of the partial molar heat capacity of argon for the above-mentioned process.

Presumably, this peculiar feature of the tetraalkylammonium salts is due to a different structural effect of these salts on the structure of water. However, an analysis of the various contributions to the partial molar heat capacity of a gas in aqueous solutions shows that, even in terms of a simple model for water, it is impossible to draw from these results any definite conclusion regarding the kind of structural changes produced by these ions.

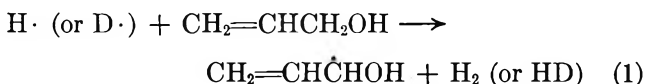
Reaction of Hydrogen Atoms with Allyl Alcohol at 77°K¹

by R. H. Johnsen, A. K. E. Hagopian,
and H. B. Yun

Department of Chemistry, Florida State University,
Tallahassee, Florida 32306 (Received July 11, 1966)

This investigation is concerned with the reactions of thermal hydrogen atoms generated in the gas phase with solid substances at low temperatures. The system investigated was allyl alcohol and a series of composite systems composed of allyl alcohol and saturated hydrocarbons including cyclohexane, isopentane, *n*-hexane, isooctane, and 3-methylpentane. These composite systems were either homogeneous glasses or two distinct layers.

The reactions of allyl alcohol with hydrogen atoms have been investigated previously by Chachaty and Schmidt,² who reported that when hydrogen atoms produced by a microwave discharge were allowed to impinge on a cold finger covered with allyl alcohol at 77°K, the resulting radicals were unsaturated. The radicals were detected by esr and the authors claimed that hydrogen abstraction from the α -carbon atom was indicated. Although these spectra were too poorly resolved to measure line intensities, their conclusion was supported by the fact that the same quartet was observed independent of whether hydrogen or deuterium atoms were used.



In our investigation, the method employed was very similar to that used by Klein and Scheer³ in which H atoms produced by hydrogen pyrolysis on a tungsten filament (2000°K) were allowed to react with a film of frozen alcohol of approximately 10⁻³ cm thickness. The geometry of the reaction vessel and the pressure of the hydrogen employed were such that the hydrogen atoms were thermalized before reaching the organic layer except at the very end of those runs in which the hydrogen pressure was brought essentially to zero. The chemical results from these runs, however, did not differ appreciably from those in which the hydrogen was only partially depleted. The rate of hydrogen uptake was followed by means of either a calibrated Pirani gauge or a calibrated thermocouple gauge operated in the region of linear response. When large amounts of hydrogen were required in the high-conversion experi-

ments, successive aliquots of gas were used. Initially, an attempt was made to relate the kinetics of the reaction to the observed rate of hydrogen uptake. However, numerous runs have shown that this rate and the apparent rate law are functions of sample size, thickness, amount of surface area exposed, and in general of the nature of the preparation. This has also been the observation of Hughes and Purnell in their study of propene by this method.⁴

In every experiment the hydrogen pressure fell rapidly at first and then, as the reaction continued, at a slower rate. Sometimes the initial part seemed to follow a first-order rate law and sometimes a zero-order law. In general, the thinner films seemed to follow the first-order law more often. In any event, hydrogen was absorbed, which would not be the case if abstraction were the principal reaction.

That hydrogen atom addition is the initial step is also attested to by the nature of the products of the reaction. These were analyzed using a 20% Carbowax-600 on Chromosorb-W column and flame ionization detection. The only products observed were propanol and propionaldehyde. Dimeric products were sought but could not be found. The ratio of alcohol to aldehyde varied with the degree of conversion, being approximately 2:1 at the lowest conversion (0.07%) to 20:1 at the highest conversion (1.4%). In this experiment at high conversion, the yield of propanol was found to correspond to within 5% to the total observed change in hydrogen pressure. This latter observation essentially rules out both abstraction by hydrogen atoms and dimerization of radicals as significant reactions in this system.

It thus seems likely that the results of Chachaty and Schmidt were due either to direct photolysis of the allyl alcohol by the recombination radiation in the radiofrequency discharge (a phenomenon they noted in the case of ethanol) or possibly to poor temperature control. In the latter context, it has been noted⁵ that in the photolysis of allyl alcohol the five-line spectrum obtained by C-C bond cleavage at 77°K changes to a quartet around 177°K and this has been attributed to hydrogen abstraction by OH radicals occurring at this temperature.

Klein and Scheer⁶ have proposed that reactions of hy-

(1) Supported in part by U. S. Atomic Energy Commission under Contract AT-(40-1)-2001. Paper ORO-2001-2.

(2) C. Chachaty and M. C. Schmidt, *J. Chim. Phys.*, **62**, 529 (1965).

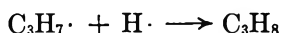
(3) R. Kein and M. D. Scheer, *J. Chem. Phys.*, **65**, 324 (1961).

(4) A. N. Hughes and J. H. Purnell, *Trans. Faraday Soc.*, **61**, 2710 (1965).

(5) K. A. Mass and D. H. Volman, *ibid.*, **60**, 1 (1964).

(6) R. Klein and M. D. Scheer, *J. Chem. Phys.*, **66**, 2677 (1962).

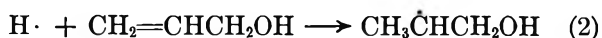
drogen atoms with solid alkenes at 77°K can be explained on the basis of surface reaction wherein the surface is replenished by diffusion of fresh olefin from the interior of the layer. For hexene-1, where $77/T_m = 0.6$ (where T_m is the melting point),⁷ the rate of diffusion is too low to sustain reaction, and this they claim explains the inertness of this olefin to H atom bombardment. Likewise, when propene, which reacts very rapidly was embedded in a rigid matrix, the over-all rate of reaction was decreased while the proportion of the reaction



was increased. For allyl alcohol, $77/T_m = 0.53$ and the matrix will be even more rigid than for hexene-1. Nevertheless, appreciable hydrogen uptake was observed in the present experiments.

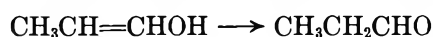
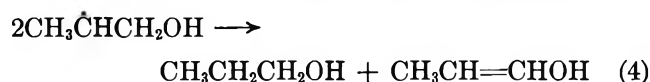
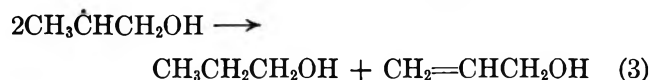
The results suggest that initially there is a rapid reaction at the surface which is later replaced by much slower reaction within the matrix itself. Thus the contention of Klein and Scheer that the reaction takes place at the surface seems to be borne out at least partially, but in a rigid matrix it does not cease completely when the surface is depleted but continues at a lower rate by means of hydrogen atom diffusion. This is in agreement with the work of Hughes and Purnell,⁴ who concluded that hydrogen atom diffusion occurs as well as olefin replenishment by diffusion to the surface. Radical diffusion is ruled out by the observation using esr spectrometry, that most alkyl radicals are quite stable in rigid matrices at these temperatures. It is further borne out by earlier studies in this laboratory on the reaction of H atoms with trapped alcohol radicals,⁸ and by a series of experiments in which thick layers (10^{-2} cm) of hydrocarbons, such as isopentane or cyclohexane, were formed on top of the allyl alcohol. The rate of hydrogen uptake was only slightly lower and the ratio of alcohol to aldehyde was essentially the same as that for the corresponding degree of conversion in pure allyl alcohol. Similar results were obtained when a glassy mixture of allyl alcohol and the hydrocarbon was used.

The following reaction scheme is postulated. Initial H atom addition occurs on the terminal carbon atom as in the case of unsymmetric alkyl-substituted ethylenes.⁹



The resulting propanol radical cannot diffuse in the solid and thus generally does not undergo reaction until the matrix temperature is raised. If, however, the reaction is carried to high conversions, these

radicals will react with a second hydrogen atom, presumably by addition, leading to the observed propanol. At low conversion, the trapped radicals react upon matrix softening by disproportionation to yield propanol and propionaldehyde by the reactions.



On statistical grounds alone, a ratio of *n*-propyl alcohol to propionaldehyde of 2.5:1 is predicted. The observed ratio at low conversion is 2:1.

(7) A. M. Bass and H. P. Broida, "Formation and Trapping of Free Radicals," Academic Press Inc., New York, N. Y., 1960, Chapter 4.

(8) R. H. Johnson, A. K. E. Hagopian, and H. B. Yun, *J. Phys. Chem.*, **70**, 2420 (1966).

(9) R. D. Kelley, R. Klein, and M. D. Scheer, *ibid.*, **69**, 905 (1965).

Complexes of PMDA with Aromatic Hydrocarbons in Solution

by Ivor Ilmet and Paul M. Rashba

Department of Chemistry, University of Connecticut, Storrs, Connecticut 06268 (Received August 25, 1966)

Original predictions of a red shift of the charge-transfer absorption with increasing solvent polarity have not been substantiated by experiment where more often a reverse relationship is observed. The various proposals to account for the observed variations in the spectra in different solvents have been reviewed recently.¹ In an attempt to evaluate further the effect of the solvent on molecular complexes, we have determined the absorption maxima and the formation constants for the complexes of pyromellitic dianhydride (PMDA), an acceptor of recent interest,²⁻⁶ with twelve

(1) H. W. Offen and M. S. F. A. Abidi, *J. Chem. Phys.*, **44**, 4642 (1966).

(2) L. L. Ferstandig, W. G. Toland, and C. D. Heaton, *J. Am. Chem. Soc.*, **83**, 1151 (1961).

(3) J. C. A. Boeyens and F. H. Herbststein, *J. Phys. Chem.*, **69**, 2153 (1965).

(4) J. C. A. Boeyens and F. H. Herbststein, *ibid.*, **69**, 2160 (1965).

Table I: The Charge-Transfer Maxima of PMDA-Aromatic Hydrocarbon Complexes in Various Solvents

Donors	Wavelength of the charge-transfer maxima, m μ					
	Chloroform n^{20}_D 1.44643 D^{20} 4.806	Methylene chloride n^{20}_D 1.42456 D^{20} 9.08	Acetic anhydride n^{20}_D 1.3906 D^{19} 20.7	2-Butanone n^{20}_D 1.3795 D^{20} 18.5	Acetone n^{20}_D 1.3591 D^{25} 20.7	Benzene n^{20}_D 1.50110 D^{25} 2.284
Phenanthrene	407	402	382 ^a	sh	sh	...
Durene	...	410	372	375	368	...
Naphthalene	413	409	382	382	381	...
Triphenylene	414	409	397	392	391	409
Fluoranthene	420 ^a	412 ^a	sh	sh	sh	409 ^a
Fluorene	433	423	402	398	394	...
Hexamethyl- benzene	437	435	409	404	396	...
Chrysene	439	434	...	sh	sh	...
Tetraphene	497 ^a	494 ^a	459 ^a	450 ^a	443 ^a	...
Pyrene	500	497	472	465	461	495
Anthracene	517	513	482	471	467	510
Perylene	592	576	578

^a These maxima were determined with an equivalent concentration of the donor in the reference cell.

Table II: Formation Constants (in l. mole⁻¹) and Molar Absorptivities of PMDA-Aromatic Hydrocarbon Complexes in Various Solvents

Donor	Chloroform		Methylene chloride		Acetic anhydride		Benzene	
	<i>K</i>	ϵ	<i>K</i>	ϵ	<i>K</i>	ϵ	<i>K</i>	ϵ
Phenanthrene	7.0	1410	2.6	1610	0.5	<i>a</i>
Durene	1.3	704	0.9	714
Naphthalene	2.8	1033	1.3	1104	0.7	752
Triphenylene	16.4	1471	4.4	1923	1.3	2353	8.7	1587
Fluoranthene	23.8	<i>a</i>	7.9	<i>a</i>	1.5	<i>a</i>	9.8	<i>a</i>
Fluorene	2.3	893	1.4	820	0.2	2222
Hexamethyl- benzene	2.2	1887	1.6	2110	1.3	1621
Chrysene	23.3	676	14.1	556
Tetraphene	10.7	<i>a</i>	6.2	<i>a</i>	0.6	<i>a</i>
Pyrene	18.3	1040	9.0	1029	2.4	1064	10.6	1061
Anthracene	5.5	1416	3.7	1179	1.1	1064	3.9	1176
Perylene	57.8	769	19.4	840	39.0	652

^a These values were obtained from measurements on the long-wavelength side of the absorption bands to eliminate overlap from other absorption bands.

aromatic hydrocarbons in a number of solvents of varying properties.

Experimental Section

The donors were reagent grade chemicals from either Eastman or Aldrich and were used without further purification except for tetraphene which was recrystallized from acetic acid. PMDA from Aldrich was used without further purification for reasons noted below. Fisher reagent grade methylene chloride, benzene, and 2-butanone were dried over calcium sulfate and distilled. Fisher reagent grade chloroform was passed through a column of Woelm I basic alumina just

prior to use. Fisher reagent grade acetic anhydride and Matheson Spectrograde absolute acetone were used without further purification. Solid complexes were prepared by precipitation from hot acetic anhydride. The solid complexes and excess donor were then weighed into NBS calibrated volumetric flasks just prior to measurement. This method of preparing complexes in solution appears preferable to any other method as any hydrolysis products of PMDA

(5) Y. Nakayama, Y. Itchikawa, and T. Matsuo, *Bull. Chem. Soc. Japan*, **38**, 1674 (1965).

(6) T. Matsuo, *ibid.*, **38**, 2110 (1965).

are reconverted in the hot acetic anhydride. The solid complexes appear quite resistant to hydrolysis so that no special precautions during handling are necessary. All spectra were determined on a Cary 14 spectrophotometer, maintained at $25 \pm 1^\circ$, using cells of 1-cm or 10-cm path lengths. Absorption maxima for a few cases, as indicated in Table I, were determined with an equivalent concentration of donor in the reference cell to compensate for partial overlap from neighboring absorption bands. The formation constants and molar absorptivities were calculated by means of the Benesi-Hildebrand equation. Where there was interference from neighboring bands, as indicated in Table II, calculations were carried out on data obtained from the long-wavelength sides of the absorption bands.⁷

Results and Discussion

The maxima of the charge-transfer spectra for the PMDA-aromatic hydrocarbon complexes in six solvents are listed in Table I. Despite an apparent general trend, benzene solutions excepted, of the charge-transfer maxima toward shorter wavelengths with decreasing refractive index of the solvent, no unambiguous correlation with this solvent property is possible owing to a distinct and discontinuous change in the shift of the charge-transfer maxima in going from the group of low dielectric constant solvents to the group with high dielectric constant. Variation in the dielectric constant of the solvent cannot solely account for the present results either as then the observed blue shift from acetic anhydride to 2-butanone should be reversed. In view of the limited successes of any general interpretations of solvent effects on molecular complexes, we would prefer to forego any assessment of the significance of the present observations except to point out that both the dielectric constant and refractive index of the solvent appear to be significant factors in determining the charge-transfer spectra, at least for the complexes of this study.

Benzene clearly seems to form an exception to the general trends observed in other solvents. Competitive equilibria between complex-forming solvents and acceptors have been considered for other complexes⁸ but appear to be a negligible factor in the present case as we have found no evidence in the form of benzene-PMDA charge transfer, which should be detectable considering the large concentration of benzene present. Investigation in the region of the expected benzene-PMDA charge transfer is complicated by the overlapping absorption of the donors and acceptor, as well as benzene itself, so presence of a competitive equilibrium cannot be ruled out absolutely. However, the observation that the formation constants in benzene are

comparable to those in methylene chloride and chloroform, as shown in Table II, lends further support to the idea of a negligible competitive equilibrium. The relative blue shift in the charge-transfer maxima in benzene with respect to methylene chloride and chloroform, despite a higher refractive index, is best accounted for by assuming a specific interaction of the type donor-acceptor-benzene.

Finally, it may be of interest to note that in the present case a rough parallelism exists between the shifts of the charge-transfer maxima and the variation of formation constants in the four solvents in which the constants have been measured. Owing to the many additional factors that may affect an equilibrium, it is doubtful whether a similar trend may be expected in other systems.

Acknowledgments. This work was supported in part by a grant from the University of Connecticut Research Foundation. P. R. wishes to thank the United Aircraft Corp., East Hartford, Conn., for the use of some of their facilities.

(7) W. B. Person, *J. Am. Chem. Soc.*, **87**, 167 (1965).

(8) R. E. Merrifield and W. D. Phillips, *ibid.*, **80**, 2778 (1958).

Nitrogen-14 Chemical Shifts in Nitro Compounds

by C. F. Poranski, Jr., and W. B. Moniz

Naval Research Laboratory, Washington, D. C. 20390
(Received September 6, 1966)

In spite of the N^{14} quadrupole moment, the use of high field strengths and internal reference standards provides a capability for accurately measuring relatively small variations in the N^{14} chemical shift of nitro compounds. Witanowski, Urbanski, and Stefaniak,¹ working at 4.3 MHz ($\sim 14,000$ gauss), were able to characterize the nitro groups in nitramines and primary, secondary, and tertiary nitroalkanes by their N^{14} chemical shifts. Additionally, they observed in the series R_3CNO_2 that if an R group has a negative inductive effect, *i.e.*, withdraws electrons, the N^{14} chemical shift moves to higher fields. For nitro compounds this appears to be a secondary effect superimposed on the primary factor influencing nitrogen (N^{14} or N^{15}) chemi-

(1) M. Witanowski, T. Urbanski, and L. Stefaniak, *J. Am. Chem. Soc.*, **86**, 2569 (1964).

cal shifts. The primary factor is currently believed^{2,3} to be the paramagnetic term of Saika and Slichter⁴ and its effect can be stated as follows: as the electronegativity of the atom *directly* bonded to the nitrogen increases, the nitrogen resonance moves to lower field. The secondary effect is evident in the data from the present work presented in Table I and in Figure 1, which is a plot of the available N^{14} chemical shifts *vs.* the Taft polar substituent constant,⁵ σ^* , for the R group in RNO_2 .

Table I: N^{14} Chemical Shifts and Line Widths of Aliphatic Nitro Compounds

Compound	δ , ^a ppm	Line width, Hz	
		b	c
$CH_3CH_2NO_2$	-10.8 ± 0.1	30 ± 1.5	20
$CH_3CH_2CH_2NO_2$	-9.5 ± 0.3	...	30
$HOCH_2CH_2NO_2$	-5.5 ± 1.4	...	
$CH_3CH_2CHClNO_2$	-2.6 ± 1.5	...	
CH_3NO_2	0	18 ± 1.0	14
$CH_3C(NO_2)_3$	26.2 ± 0.2	11 ± 1.0	
$HOCH_2C(NO_2)_3$	29.9 ± 0.3	10 ± 1.0	
$CH_3CH_2ONO_2$	37.5 ± 0.1	12 ± 1.0	7

^a A positive chemical shift indicates resonance at higher field than CH_3NO_2 . The error is the standard deviation. ^b This work. ^c Calculated from ref 6.

Besides showing the upfield shift which occurs upon substituting polar groups for H or CH_3 , the data also suggest that the N^{14} chemical shifts fall on lines whose slopes and displacements depend on the types of substituents in R. For example, the points for the mono-nitroalkanes (and nitrocyclohexane) fall on a straight line. Additional data for other classes of R groups might allow the separation of anisotropic, inductive, and hybridization effects.

The line width of nitromethane in a 1:1 mixture with ethyl nitrate was 17.6 Hz. This is close to the value of 14.3 Hz obtained from T_1 data.⁶ With nitromethane as solvent for 2,2,2-trinitroethanol, line widths of both compounds were dependent on concentration. As the concentration of the alcohol was decreased from 3.7 to 1.0 M the nitromethane and alcohol line widths changed from 37 to 23 Hz and from 12.5 to 10.2 Hz, respectively. No change in the chemical shift of the alcohol was observed. Addition of ethyl nitrate to one of the solutions caused no change in line widths. The cause of the broadening has not been established, but possible explanations are hydrogen bonding or viscosity changes. It may be significant that the chemical shift of ethyl nitrate was 0.6 ppm to higher field in the ternary solution than in the $CH_3NO_2-C_2H_5ONO_2$ system, for this

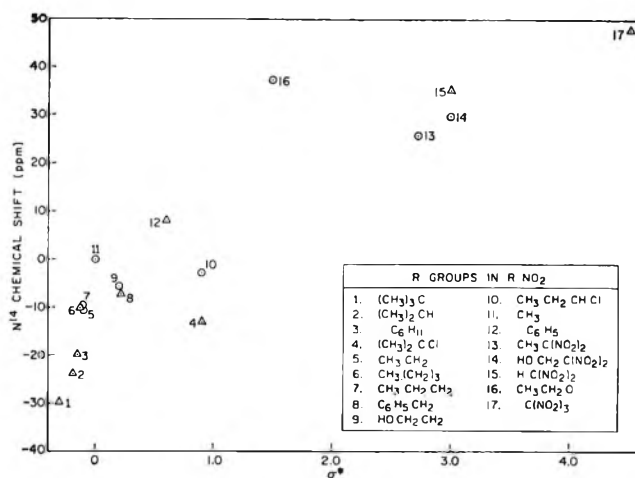


Figure 1. Plot of N^{14} chemical shift *vs.* Taft polar substituent constant, σ^* , for R in RNO_2 : \circ , this work; Δ , ref 1.

could be interpreted as a downfield shift of the nitromethane resonance. However, the shift of 2,2,2-trinitroethanol remained constant, relative to nitromethane, at all concentrations measured.

Experimental Section

1,1,1-Trinitroethane and 2,2,2-trinitroethanol were supplied by Dr. T. N. Hall of the Naval Ordnance Laboratory, Silver Spring, Md. The other compounds were used as received from commercial sources. Measurements were made at 6.1 MHz in the HR side-band mode of a Varian HA-100 spectrometer system at 24°. Calibrations were made using the audio side band method. All shifts were measured from an internal reference of CH_3NO_2 or $CH_3CH_2ONO_2$ and related to $\delta_{CH_3NO_2} = 0$. Samples were prepared in standard 5-mm o.d. nmr tubes. The larger line widths obtained in this work compared to those calculated from T_1 data⁶ are believed to be due to the sweep rates and filtering employed, since resolution was found to be ~ 6 Hz from measurements on the quintet of an acidified NH_4NO_3 solution. Sample spinning improved S/N . For sharp signals, N^{14} magnetic resonance can be fairly sensitive. Johnson⁷ has recorded the 7.22-MHz spectrum of 1.0 M NH_4NO_3 (acidified) in which the S/N of the center peak of the NH_4^+ quintet was 5:1.

(2) D. Herbison-Evans and R. E. Richards, *Mol. Phys.*, **8**, 19 (1964).

(3) D. T. Clark and J. D. Roberts, *J. Am. Chem. Soc.*, **88**, 745 (1966), and references cited therein.

(4) A. Saika and C. P. Slichter, *J. Chem. Phys.*, **22**, 26 (1954).

(5) R. W. Taft, Jr., "Steric Effects in Organic Chemistry," M. S. Newman, Ed., John Wiley and Sons, Inc., New York, N. Y., 1956, p 619.

(6) W. B. Moniz and H. S. Gutowsky, *J. Chem. Phys.*, **38**, 1155 (1963).

(7) L. Johnson, private communications.

Sodium Bifluoride: Decomposition Pressure by the Knudsen Effusion Method¹

by Alan R. Miller

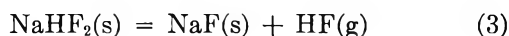
Aerajet-General Nucleonics, San Ramon, California 94583
(Received October 17, 1966)

In the course of work with tritiated sodium bifluoride we found it necessary to determine the decomposition pressure of natural sodium bifluoride at room temperature. The system has been studied at higher temperatures by Fischer,² who made direct pressure measurements, and by Froning, *et al.*,³ who used a transpiration method. Their results can be expressed, respectively, as

$$\log P_{\text{HF}}(\text{atm}) = 6.594 - 3521/T^{\circ}\text{K} \quad (430-542^{\circ}) \quad (1)$$

$$\log P_{\text{HF}}(\text{atm}) = 5.821 - 3196/T^{\circ}\text{K} \quad (473-548^{\circ}) \quad (2)$$

for the reaction



Extrapolation to 273°K gives, respectively, 5.0×10^{-7} and 1.3×10^{-6} atm—values that are readily measurable by the Knudsen effusion technique.⁴ However, a room-temperature effusion experiment gave an immeasurable (less than 0.05 mg) weight loss, indicating that the apparent pressure was less than $1/_{100}$ the extrapolated value. Thirty-five additional effusion experiments were performed at temperatures from 310 to 371°K in an effort to obtain a more meaningful value.

Samples for NaHF₂ were produced by reaction of NaF and HF in a Teflon vessel at room temperature. Anhydrous HF was prepared at room temperature by reaction of H₂ and F₂ which had been separately passed through liquid nitrogen-cooled traps to remove water and other impurities. The resulting white sample gave a well-resolved X-ray diffraction pattern identical with that reported for NaHF₂.⁵

Heating in a Pt crucible to constant weight produced a 32.3% weight loss and a material exhibiting only the NaF X-ray diffraction pattern,⁶ indicating that the sample had been originally NaHF₂.

Knudsen effusion experiments were performed in a Pt cell with one of three cylindrical orifice sizes: 0.675, 1.03, or 1.88-mm diameter. The cylindrical cell was $1/2$ in. high by $3/8$ in. in diameter (inside dimensions). Loss of sample between the lid and crucible was accounted for by experiments in which a lid with no orifice was used. This loss amounted to 13, 7, and 4.5%

for the 0.675, 1.03, and 1.88-mm diameter orifices respectively. The temperature dependence of the weight-loss rate was the same as the value found for effusion through the three orifices. Container reaction was negligible inasmuch as the crucible lost less than 0.1 mg (5×10^{-7} g-atom of Pt) while a total of 1.0 g of HF (0.05 mole) was sublimed during the experimental program.

The Pt cell was placed into a brass cup and attached to a vacuum system; the connection was sealed with a rubber O-ring lubricated with silicone grease. The system was equipped with a liquid nitrogen trap, a silicone oil diffusion pump, and a mechanical pump. Residual pressures were read with a Veeco ionization gauge positioned on the opposite side of the manifold from the effusion cell.

When residual pressure became less than 10^{-5} torr, an isothermal bath was raised around the sample chamber. Residual pressure during heating was usually less than 10^{-5} torr and never larger than 5×10^{-5} torr. Temperatures were measured with a chromel-alumel thermocouple fastened to the outside of the brass cup containing the Knudsen cell.

Heating times of 106–5568 min were chosen to give 5–17-mg weight losses. The effusion data were obtained with three chargings of the cell; in each case, the initial composition was *ca.* 1 mole % NaF in NaHF₂. The composition shifted 3–6% during each effusion run. When the composition reached *ca.* 85–90% NaF in NaHF₂, the sample was discarded and the cell recharged. Orifice sizes and temperatures were chosen randomly.

The diameters of the cylindrical effusion orifices were determined by comparison with a calibrated slide under a microscope. Orifice lengths were measured with a vernier micrometer. Clausing factors calculated by DeMarcus⁷ were used to correct for the finite length of the orifice.

The experimental results are summarized in Figure 1. The three solid lines in Figure 1 are linear least-square fits (with $1/T$ the dependent variable) for the three orifices; the root-mean squares of the $1/T$ deviations about the fitted curves are 0.01, 0.02, and

(1) Supported by the Advanced Research Projects Agency through a contract with the Office of Naval Research.

(2) J. Fischer, *J. Am. Chem. Soc.*, **79**, 6363 (1957).

(3) J. F. Froning, M. K. Richards, T. W. Stricklin, and S. G. Turnbull, *Ind. Eng. Chem.*, **39**, 275 (1947).

(4) M. Knudsen, *Ann. Physik*, **28**, 999 (1909).

(5) ASTM X-Ray Card 6-0479.

(6) ASTM X-Ray Card 4-0793.

(7) W. C. DeMarcus, Union Carbide Nuclear Co., Oak Ridge Gaseous Diffusion Plant, Report K-1302, Part III (1957), AD 124 579.

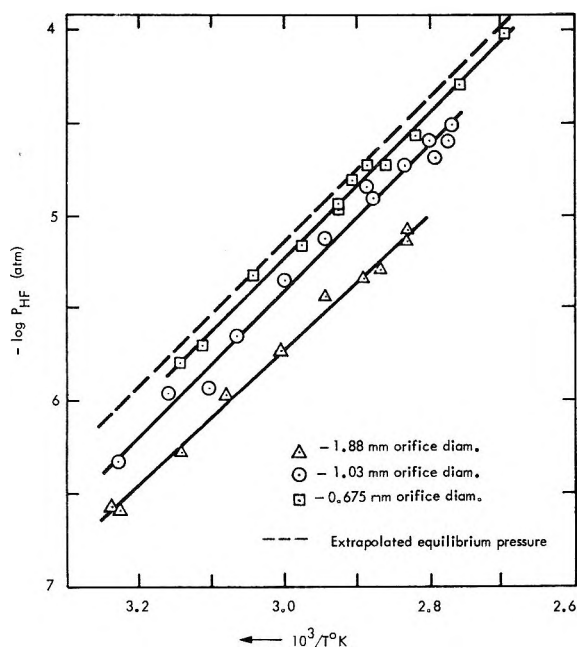


Figure 1. The HF partial pressure as a function of temperature over the NaHF_2 - NaF two-phase region.

0.01 for the large, medium, and small orifice, respectively, (equivalent to *ca.* 1°K). The dashed line in Figure 1 was obtained by extrapolation to zero orifice size according to a method suggested by Motzfeldt;⁸ the equation of this line

$$\log P_{\text{HF}}(\text{atm}) = 6.677 - 3940/T^\circ\text{K} \quad (4)$$

leads to a second-law heat for reaction 1 of 18.0 ± 0.5 kcal. The sublimation coefficient is calculated to be 0.006.⁸

Third-law heats (for reaction 3) were obtained by combining corrected apparent pressures with free-energy functions for reaction 3. The individual apparent pressures were multiplied by the ratio of the equilibrium pressures to the least-squares-fit pressure (corresponding to the proper orifice) at 333.3°K . These factors are 3.85, 1.83, and 1.22 for the large, medium, and small orifices, respectively. The free-energy functions for NaHF_2 given by Westrum and Burney⁹ were extrapolated from 300 to 400°K and combined with those for NaF and HF given in the "JANAF Tables"¹⁰ to yield

$$\frac{-\Delta(F^\circ_T - H^\circ_{298})}{T} = 8 \times 10^{-4}T^\circ\text{K} - 32.28 \quad (5)$$

in cal/deg for reaction 3. A third-law heat of 18.5 ± 0.3 was obtained.

Higgins and Westrum¹¹ obtained a heat of formation of -218.1 kcal/mole for NaHF_2 and assigned an en-

thalpy of 17.88 kcal to reaction 3; values in NBS Circular 500¹² lead to an enthalpy of 20.06 kcal.

Although the decomposition pressures reported in ref 2 and 3 are not directly comparable with the present data because of a temperature gap of 60 – 100° , second-law heats were obtained by extrapolating eq 1 and 2 to 298°K and the NaHF_2 free-energy functions to 500°K . These second- and third-law heats are 16.1 and 17.0 for ref 2 and 14.6 and 17.2 for ref 3.

(8) K. Motzfeldt, *J. Phys. Chem.*, **59**, 139 (1955).

(9) E. F. Westrum, Jr., and G. A. Burney, *ibid.*, **65**, 344 (1961).

(10) D. R. Stull, "JANAF Thermochemical Tables," Dow Chemical Co., Midland, Mich.

(11) T. L. Higgins and E. F. Westrum, Jr., *J. Phys. Chem.*, **65**, 830 (1961).

(12) F. D. Rossini, D. D. Wagman, W. H. Evans, S. Levine, and I. Jaffe, "Selected Values of Chemical Thermodynamic Properties," National Bureau of Standards Circular 500, U. S. Government Printing Office, Washington, D. C., 1952.

Attractive Potentials between Fluorochemicals and Aliphatic Hydrocarbons

by J. H. Dymond and J. H. Hildebrand

Department of Chemistry, University of California, Berkeley, California (Received November 1, 1966)

We reported in a recent paper¹ that the solubility of iodine in cyclopentane, cyclohexane, and two decalins agrees well with the equation

$$RT \ln (a_2/x_2) = v_2^0 \varphi_1^2 (\delta_2 - \delta_1)^2 \quad (1)$$

with which a total 13 solutions of iodine conform, but that methyl- and ethylcyclohexanes are better solvents for iodine as calculated from eq 1 to the extent of ~ 300 cal/mole, dimethylcyclohexane excels to the extent of 400 cal/mole, and furthermore that solvents such as triptane, 2,2,3-trimethylbutane, with one methylene hydrogen atom and 15 methyl hydrogen atoms per molecule, show an enhancement of solvent power for iodine amounting to ~ 800 cal/mole.

In eq 1, a_2 is the activity of the solute referred to its pure liquid, x_2 its mole fraction, v_2^0 its liquid volume, φ_1 is the volume fraction of the solvent; the δ 's are the two solubility parameters, evaluated from the square roots of their energies of vaporization per cubic centimeter.

(1) J. H. Hildebrand and J. H. Dymond, *Proc. Natl. Acad. Sci. U. S.*, **54**, 1001 (1965). See also J. H. Hildebrand, *Science*, **150**, 441 (1965).

The work herein described was undertaken in order to learn whether similar differences between effects of methyl- and methylene hydrogen are to be found in the mixtures of the above substances with perfluorochemicals. It has been known² for some time that alkanes and fluorochemicals are considerably less soluble in one another than they would be if they obeyed eq 1.

Experimental Section

The hydrocarbons used were cyclohexane, methylcyclohexane, ethylcyclohexane, and *trans*-1,2-dimethylcyclohexane; the fluorocarbons were perfluorotributylamine (molar volume 356 cm³ at 25°) and perfluorodimethylcyclohexane (molar volume 218 cm³ at 25°). The hydrocarbons were of the highest purity obtainable from commercial sources. All were fractionally distilled shortly before use. The perfluorotributylamine, obtained from the Minnesota Mining and Manufacturing Co., was refluxed with alkaline potassium permanganate, repeatedly washed with water, separated, dried, and distilled. The fraction with bp 177.1–177.4° and density 1.8838 g cm⁻³ at 25° was used for all measurements. The perfluorodimethylcyclohexane was refluxed for 24 hr with saturated acid potassium permanganate and then neutralized, washed with water, dried, and distilled. It had bp 100.2–100.5° and a density of 1.8376 g cm⁻³ at 25°.

We determined liquid-liquid solubilities at 25° by the method employed by Fujishiro and Hildebrand,³ who compared the densities of the saturated phases with densities of unsaturated solutions of known composition, a procedure that is simple and especially accurate for hydrocarbon + fluorocarbon mixtures. The results are given in Table I.

Table I: Mole Fractions in Phases A and B at Equilibrium at 25°. The Fluorochemical Is Component 2. The Mole Fraction of the Other Component in Each Phase is Given by $x_{1A} + x_{2A} = 1$; $x_{1B} + x_{2B} = 1$

	$\text{---}(\text{C}_4\text{H}_9)_3\text{N}\text{---}$		$\text{---C}_6\text{F}_{10}(\text{CF}_2)_2\text{---}$	
	A 100 x_2	B x_1	A 100 x_2	B x_1
<i>c</i> -C ₆ H ₁₂	0.255	0.198	3.90	0.243
<i>c</i> -C ₆ H ₁₁ CH ₃	0.495	0.168	5.98	0.231
<i>c</i> -C ₆ H ₁₀ C ₂ H ₅	0.290	0.097	4.25	0.139
<i>trans</i> -1,2, <i>c</i> -C ₆ H ₁₀ (CH ₃) ₂	0.595	0.142	6.37	0.198

Interpretation

The term $(\delta_1 - \delta_2)^2$ in eq 1 is, by definition of the δ 's, $\Delta E_1^v/v_1 + \Delta E_2^v/v_2 - 2 [(\Delta E_1^v/v_1)(\Delta E_2^v/v_2)]^{1/2}$. It contains the assumption that the interaction between

the molecules of species 1 and 2 is the geometric mean of the interactions between molecules of the same species. In the case of a mixture for which the value of $(\delta_1 - \delta_2)^2$ calculated from experimental solubilities is greater than the square of the difference between the δ 's derived from $\Delta E^v/v$, the interaction between the unlike species is correspondingly less than as given by the geometric mean.

In order to calculate $(\delta_1 - \delta_2)^2$ from solubility data, we write four equations in the form of eq 1, one for each component in each of the two phases, A and B, and combine them in pairs since the activity of each component is the same in both phases, *i.e.*, $a_{1A} = a_{1B}$ and $a_{2A} = a_{2B}$. We thus obtain the equations

$$RT \ln \frac{x_{1A}}{x_{1B}} = v_1(\varphi_{2B}^2 - \varphi_{2A}^2)(\delta_1 - \delta_2)^2 \quad (2a)$$

$$RT \ln \frac{x_{2B}}{x_{2A}} = v_2(\varphi_{1A}^2 - \varphi_{1B}^2)(\delta_1 - \delta_2)^2 \quad (2b)$$

If the experimental x 's are more accurate for one component than for the other, the more appropriate of these two equations may serve for calculating $(\delta_1 - \delta_2)^2$, but if all four x 's are equally accurate, then the two equations can be combined to give the equation given in ref 3.

$$\frac{RT}{2} \left(\frac{1}{v_1} \ln \frac{x_{1A}}{x_{1B}} + \frac{1}{v_2} \ln \frac{x_{2B}}{x_{2A}} \right) = (\varphi_{1A} - \varphi_{1B})(\delta_1 - \delta_2)^2 \quad (3)$$

The right-hand member has been simplified by the aid of the relations $\varphi_{1A} + \varphi_{2A} = 1$ and $\varphi_{1B} + \varphi_{2B} = 1$. This equation gives for $\delta_1 - \delta_2$ the mean of values that might be obtained from eq 2a and 2b.

Table II gives the excess of $(\delta_1 - \delta_2)^2$ as calculated from the compositions of the two phases by eq 3 over the squares of the difference between the solubility parameters of the pure components. We see that all four cyclic hydrocarbons are much less miscible with both (C₄F₉)₃N and C₆F₁₀(CF₂)₂ than would be expected from their solubility parameters, and that the deviations increase with the number of methyl groups in virtually the same order. We see also that the order is the reverse of that found for these hydrocarbons as solvents for iodine,⁴ but that the increases from C₆H₁₂ to C₆H₁₀(CH₂)₂ are much less in the two fluorochemicals

(2) J. H. Hildebrand, *J. Chem. Phys.*, **18**, 1337 (1950). See also G. J. Rotariu, R. J. Hanrahan, and R. E. Fruin, *J. Am. Chem. Soc.*, **76**, 3752 (1954); R. L. Scott, *J. Phys. Chem.*, **62**, 136 (1958); D. E. L. Dyke, J. S. Rowlinson, and R. Thacker, *Trans. Faraday Soc.*, **55**, 903 (1959).

(3) R. Fujishiro and J. H. Hildebrand, *J. Phys. Chem.*, **66**, 573, (1962).

(4) J. H. Hildebrand and J. H. Dymond, *Proc. Natl. Acad. Sci. U. S.*, **54**, 1001 (1965); also, J. H. Hildebrand, *Science*, **150**, 441 (1965).

than with iodine. This may be the result of the much smaller size of the iodine molecule, enabling it to orient more selectively toward the methyl groups. It is noteworthy that whereas C_6H_{12} virtually conforms to the geometric mean relation in its interaction with iodine, it deviates strongly in its interaction with both fluorochemicals. This is a peculiarity of hydrocarbons; it exists only to a minor extent in mixtures of C_6H_{12} with CCl_4 and with CS_2 , as revealed in a study by Shinoda and Hildebrand.⁵ The discrepancies are only 1.6 and 2.8, respectively.

Table II: The Excess of $(\delta_1 - \delta_2)^2$ Calculated by Eq 3 over Its Value from Regular Solution Parameters (cal/cc)

	v , cc/mole	δ	Component 2		
			C_6F_{10} -		
			$(C_4F_9)_2N$	$(CF_3)_2$	I_2
			v , cc/mole		
			356	218	58.5
			δ		
			5.9	6.1	14.1
C_6H_{12}	109	8.20	4.7	5.5	-1.0
$C_6H_{11}CH_3$	128	7.83	5.4	6.0	-4.8
$C_6H_{11}C_2H_5$	143	7.97	5.8	6.1	-4.9
$C_6H_{10}(CH_3)_2$	145	7.68	5.6	6.2	-7.6

These results reemphasize the fact that further progress in the theory of regular solutions requires, more than anything else, a far more sophisticated treatment than we now possess of the forces between molecules of different species.

Acknowledgment. This work was supported by the National Science Foundation.

(5) K. Shinoda and J. H. Hildebrand, *J. Phys. Chem.*, **68**, 3904 (1964).

The Effect of Electrolyte Addition on the Viscosity of Water under Pressure

by R. A. Horne and D. S. Johnson

Arthur D. Little, Inc., Cambridge, Massachusetts
(Received November 8, 1966)

Unlike other liquids, the pressure dependence of the viscosity of water relative to its value at 1 atm exhibits a minimum.¹ The destruction by the application of hydrostatic pressure of the regions of bound water in liquid water is responsible for this phenomenon.

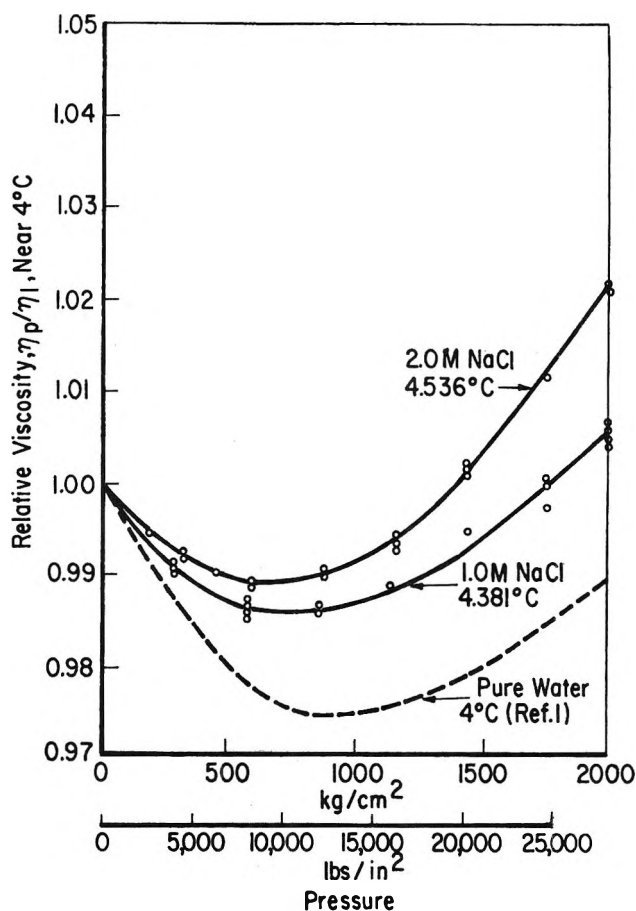


Figure 1. Pressure dependence of the relative viscosity of aqueous NaCl solutions near 4°.

If the water structure is previously altered by increasing the temperature or by adding electrolyte, this anomaly tends to disappear. However, our measurements on the viscosity of sea water under pressure² indicated that the effect of electrolyte addition on the viscosity of water under pressure is considerably less than one would expect on the basis of Cohen's measurements of the viscosity of aqueous NaCl solutions under pressure.³

The high-pressure, rolling-ball type viscometer and its operation has been described elsewhere.¹ Viscosities of pure water and sea water measured at 1 atm with this equipment gave results in agreement with the literature.⁴

(1) See R. A. Horne and D. S. Johnson, *J. Phys. Chem.*, **70**, 2182 (1966).

(2) R. A. Horne and D. S. Johnson, *J. Geophys. Res.*, **71**, 5275 (1966).

(3) R. Cohen, *Ann. Phys.*, **45**, 666 (1892).

(4) R. A. Horne, A. Courant, D. S. Johnson, and F. F. Margosian, *J. Phys. Chem.*, **69**, 3988 (1966).

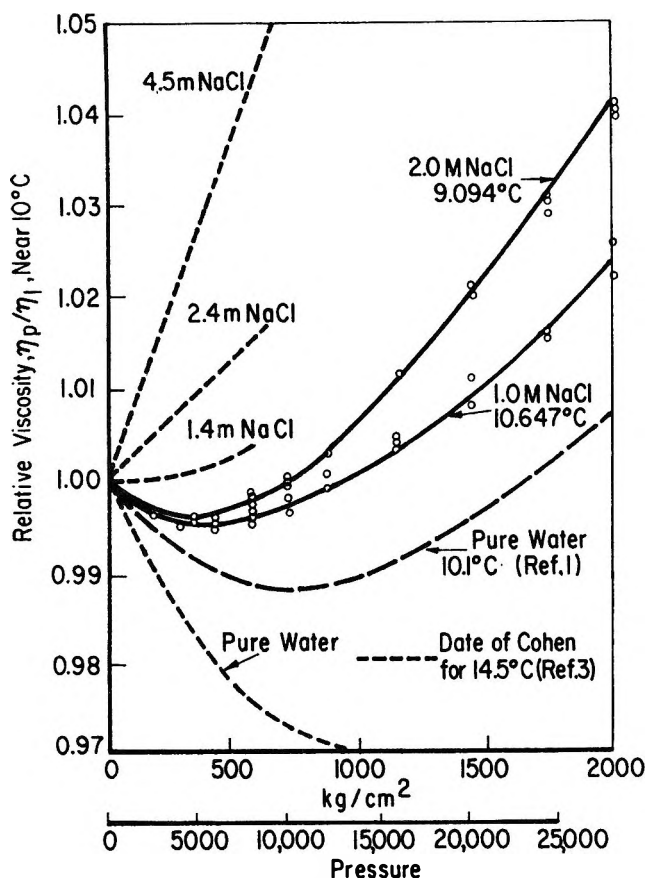


Figure 2. Pressure dependence of the relative viscosity of aqueous NaCl solutions near 10°.

The present results (Figures 1 and 2) are qualitatively in agreement with the earlier work of Cohen.³ The addition of an electrolyte such as NaCl does appear to smear out the minimum in the pressure dependence of the relative viscosity. However, Figure 2 shows that the effect is considerably less pronounced than suggested by the earlier work.³ In Figures 3 and 4, isobars are plotted in order to show the dependence of the relative viscosity on electrolyte concentration at a given pressure. Measurements were made only at three electrolyte concentrations (0.0, 1.0, and 2.0 M); nevertheless the curves near 4° appear to be definitely convex while those near 10° are concave. In both cases it is clear that the addition of the electrolyte increases the relative viscosity at a given pressure.

Arrhenius activation energies of viscous flow calculated from the expression

$$E_a = \left[\log \left(\frac{1}{\eta_p} \right)_{T_2} - \log \left(\frac{1}{\eta_p} \right)_{T_1} \right] 4.576 T_2 T_1 / \Delta T \quad (1)$$

where $\eta_p = (\eta_p/\eta_1)\eta_1$ are listed in Table I. "International Critical Tables" values of η_1 were used for the 1.0

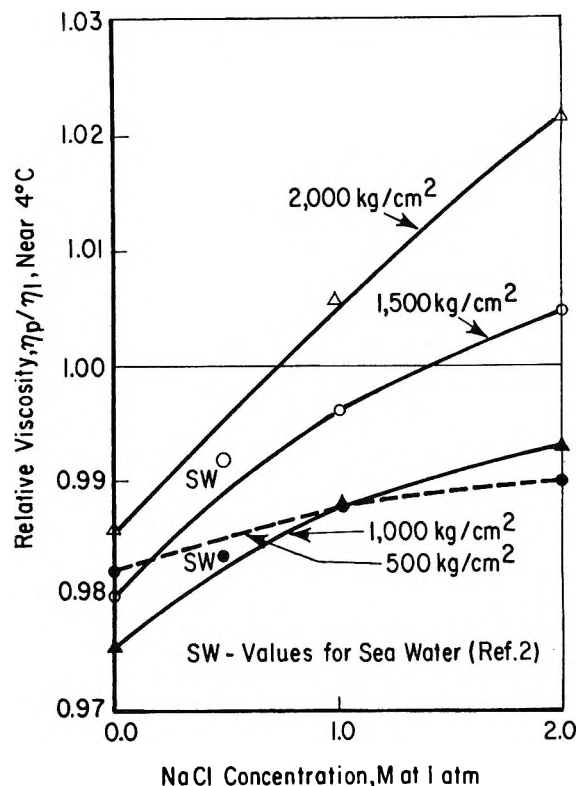


Figure 3. Isobaric concentration dependence of the relative viscosity of aqueous NaCl solutions near 4°.

and 2.0 M NaCl solutions. E_a decreased with increasing pressure at all electrolyte concentrations studied and with electrolyte concentration at all pressures studied. E_a of electrical conductivity behaves similarly.⁵ Inasmuch as a decrease in E_a can be interpreted to signify a disruption of the solvent structure, pressure or the addition of NaCl are structure-breaking influences. These conclusions are comparable to those drawn earlier on the basis of the Arrhenius activation energy of electrical conduction,⁶ but in contrast the

Table I: Pressure and Electrolyte Concentration Dependence of the Arrhenius Activation Energy of Viscous Flow

NaCl concn, M	Activation energy, E_a (av over 4–10°) at				
	1 atm	500 kg/cm ²	1000 kg/cm ²	1500 kg/cm ²	2000 kg/cm ²
0.0	4.58 (4.8) ^a	4.64	4.54	4.48	4.38
1.0	4.53 (4.4) ^a	4.28	4.16	4.12	4.07
2.0	4.52 (4.4) ^a	4.27	4.11	4.05	4.05

^a The 1-atm values in parentheses are those calculated for 5° by W. Good, *Electrochim. Acta*, 9, 203 (1964).

(5) R. A. Horne, R. A. Courant, and D. S. Johnson, *Electrochim. Acta*, 11, 987 (1966).

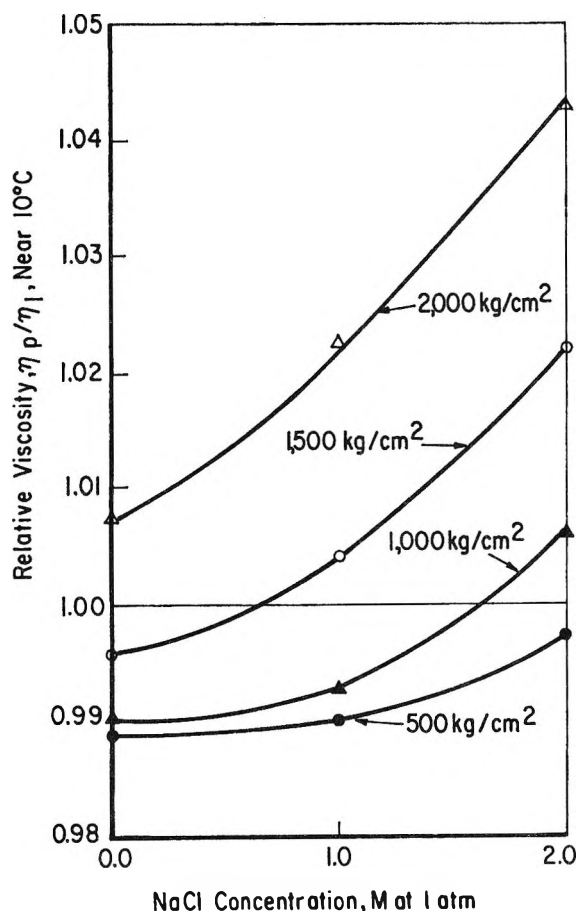


Figure 4. Isobaric concentration dependence of the relative viscosity of NaCl solutions near 10°.

addition of NaCl increases the viscosity of water so that this electrolyte is usually classed as a "structure maker."⁷

Acknowledgment. This work was supported in part by the Office of Naval Research.

(6) R. A. Horne and R. A. Courant, *J. Geophys. Res.*, **69**, 1152 (1964).

(7) R. W. Gurney, "Ionic Processes in Solution," McGraw-Hill Book Co., Inc., New York, N. Y., 1953, Chapter 9.

Diffusional and Electrical Mobilities of Tracer Alkali Ions in Alkali Nitrates

by J. A. A. Ketelaar and J. C. Th. Kwak

Laboratory of Electrochemistry, University of Amsterdam, Amsterdam, The Netherlands (Received November 2, 1966)

The determination of diffusional and electrical mobilities of tracer ions by means of a paper electro-

phorus technique has been used in our laboratory for the investigation of transport properties of ions in molten alkali nitrates.¹⁻³ As was already reported,³ some of the data have been influenced by the exchange or absorption of cations on the glass paper and glass plate support. This effect was found to be important when the ions, present in tracer quantities, are smaller or have a greater charge than the solvent ions, but in the CsNO₃-NaNO₃ system the values of u and especially D of Na²² ions were appreciably lowered even in mixtures containing up to 25% NaNO₃.

We have repeated the measurements of ref 1 and 2 for the cases mentioned above using a similar technique but with a paper of quartz fibers and an alumina plate as support. In all the experiments done with these materials, no activity could be detected in the alumina support. In pure CsNO₃ at 450°, 10 ± 5% of the Na²² tracer quantity was found in the quartz fiber paper; upon addition of inactive NaNO₃, this value decreased to 2 ± 2%. Therefore, we always added 1 or 2% inactive salt of the tracer ion to the melt. In the migration experiments reported, autoradiographic records of the activity distribution did not show a "tail," as was found in experiments with glass paper and glass plate support. Agreement with the data of Honig and Ketelaar¹⁻³ for pure salts was excellent.

We will now report the deviating results in the cases that the solute ions are smaller than the solvent ions. The values for the diffusion coefficients at 450° are: Na⁺ in KNO₃, 3.19 ± 0.09; Na⁺ in RbNO₃, 2.85 ± 0.15; K⁺ in RbNO₃, 2.52 ± 0.10; Rb in RbNO₃, 2.51 ± 0.08; Na⁺ in CsNO₃, 2.41 ± 0.10; K⁺ in CsNO₃, 2.44 ± 0.15; Rb in CsNO₃, 2.32 ± 0.08.

The values for the ionic mobilities are: Na⁺ in RbNO₃, 2.36 ± 0.03; Na⁺ in CsNO₃, 1.70 ± 0.03. In

Table I: Nernst-Einstein Parameters RTu/FD for Tracer Ions in Four Alkali Nitrates

Solvent	$(RTu/FD)^{Na^{22}}$	$(RTu/FD)^{K^{42}}$	$(RTu/FD)^{Rb^{86}}$	$(RTu/FD)^{Ca^{47}}$	$(RTu/FD)^{NO_3^-}$
NaNO ₃	0.68 ^a	0.89 ^a	0.82 ^a	0.85 ^a	0.66 ^b
KNO ₃	0.56	0.57 ^a	0.65 ^a	0.68 ^a	0.65 ^b
RbNO ₃	0.49	0.55	0.58	0.62 ^a	
CsNO ₃	0.44	0.47	0.52	0.55 ^a	0.65 ^b

^a See ref 2. ^b Calculated from ref 4 and 5.

(1) J. A. A. Ketelaar and E. P. Honig, *J. Phys. Chem.*, **68**, 1596 (1964).

(2) E. P. Honig, Thesis, University of Amsterdam, 1964.

(3) E. P. Honig and J. A. A. Ketelaar, *Trans. Faraday Soc.*, **62**, 190 (1966).

Table II: Friction Coefficients r_{ij} (joules $\text{cm}^{-2} \text{sec}^{-1}$) in Four Alkali Nitrates at 450°

Solvent	NaNO_3	KNO_3	RbNO_3	CsNO_3
$\text{Na}^+-\text{NO}_3^-$	2.58 ± 0.03	3.60 ± 0.15	4.07 ± 0.10	4.73 ± 0.15
K^+-NO_3^-	2.64 ± 0.10	3.48 ± 0.04	4.18 ± 0.08	4.55 ± 0.18
$\text{Rb}^+-\text{NO}_3^-$	2.91 ± 0.12	3.58 ± 0.12	4.11 ± 0.04	4.48 ± 0.10
$\text{Cs}^+-\text{NO}_3^-$	3.05 ± 0.13	3.62 ± 0.13	4.20 ± 0.08	4.39 ± 0.08
Na^+-Na^+	0.03 ± 0.30			
K^+-K^+		0.28 ± 0.29		
Rb^+-Rb^+			0.68 ± 0.28	
Cs^+-Cs^+				0.91 ± 0.30
Na^+-K^+	0.90 ± 0.45	0.18 ± 0.23		
Na^+-Rb^+	0.69 ± 0.20		0.15 ± 0.38	
Na^+-Cs^+	0.92 ± 0.24			0.25 ± 0.36
K^+-Rb^+		0.66 ± 0.33	0.73 ± 0.30	
K^+-Cs^+		0.92 ± 0.31		0.29 ± 0.33
Rb^+-Cs^+			1.30 ± 0.26	0.69 ± 0.34
$\text{NO}_3^--\text{NO}_3^-^a$	2.03	1.28		0.99

^a See ref 5.

the other cases, no deviation between the two methods was found.

The values of the Nernst-Einstein parameter are given in Table I. The ionic mobilities of the nitrate ions were calculated from conductivity data of De Nooyer.⁴ The diffusion coefficients of the nitrate ions are those given by Dworkin, Escue, and van Artsdalen.⁵ It follows that D , u , and RTu/FD for a given tracer cation all decrease with increasing radius of the solvent cation. In a given solvent for tracer cations larger than the solvent cations, u and D decrease with increasing radius of the tracer ion. This was also found by Bockris, *et al.*,⁶ for diffusion of alkali ions in molten NaCl and by Berlin, *et al.*,⁷ for the ionic mobilities in the NaNO_3 - KNO_3 eutectic.⁸

We feel that in ionic liquids the relative rather than the absolute value of the Nernst-Einstein parameter can be important for the study of ionic interactions. So will, for instance, the decrease of RTu/FD for Na^{22} in the four alkali nitrates be due to a stronger $\text{Na}^+-\text{NO}_3^-$ interaction as the NO_3^- mobility remains constant. This is a similar effect to the decrease of RTu/FD for both Li^+ and K^+ in the LiNO_3 - KNO_3 system found by Lantelme and Chemla,⁹ and for both Na^+ and K^+ in the NaNO_3 - KNO_3 system.²

On the other hand, there is an increase of RTu/FD for increasing tracer cation radius in the same solvent. This means that in, for instance, CsNO_3 , the $\text{Na}^+-\text{NO}_3^-$ interaction is stronger than the $\text{Cs}^+-\text{NO}_3^-$ interaction.

The constancy of u , D , and RTu/FD for the nitrate ions in the four alkali nitrates is remarkable. This can perhaps be compared with the comparatively small differences observed in the viscosities.

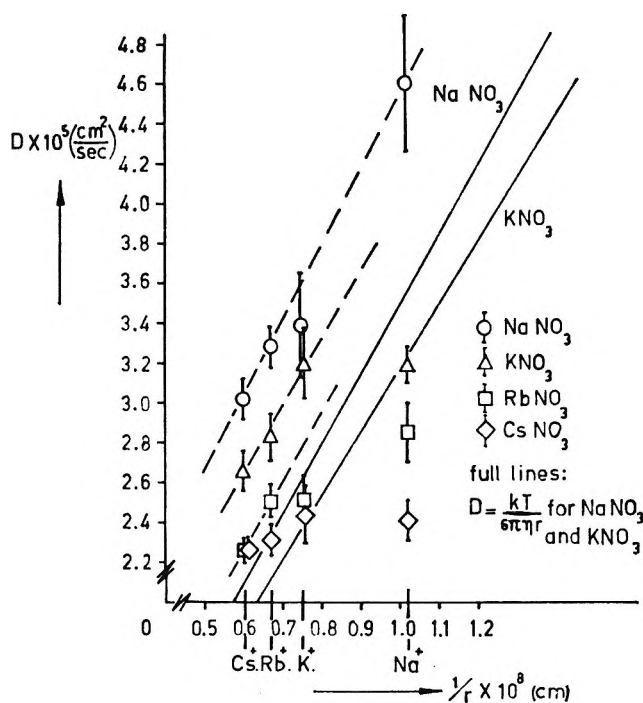


Figure 1. Diffusion coefficients of Na^+ , K^+ , Rb^+ , and Cs^+ in NaNO_3 , KNO_3 , RbNO_3 , and CsNO_3 vs. $1/r$.

- (4) B. De Nooyer, Thesis, University of Amsterdam, 1965.
- (5) A. D. Dworkin, R. B. Escue, and E. R. van Artsdalen, *J. Phys. Chem.*, **64**, 1872 (1960).
- (6) J. O'M. Bockris, S. Yoshikawa, and S. R. Richards, *ibid.*, **68**, 1838 (1964).
- (7) A. Berlin, F. Menés, S. Forcheri, and C. Monfrini, *ibid.*, **67**, 2505 (1963).
- (8) Both authors found a mobility for the Li^+ ion greater than that of the solvent ions. There are reasons to believe that the transport mechanism for Li^+ is different from the other alkali metals.⁴
- (9) F. Lantelme and M. Chemla, *Electrochim. Acta*, **10**, 663 (1965).

The friction coefficients r_{+-} , $r_{+'-}$, r_{++} , and $r_{++'}$, where + means the solvent cation, +' is the tracer cation, and - is the anion, have been calculated in Table II, following the formalism of Laity.¹⁰ At this moment no theory provides a calculation of these basically macroscopic coefficients starting from microscopic concepts.^{11,12}

For ions equal to or larger than the solvent ions, the experimental data for the self-diffusion coefficients are represented rather well by the Stokes-Einstein equation

$$D_i = \frac{kT}{6\pi\eta r_i}$$

Figure 1 shows that the slopes of the D_i-1/r_i curves in NaNO_3 and KNO_3 agree remarkably well with the expected values. Ionic radii are those given by Ketelaar.¹³ For tracer cations smaller than the solvent cations, the diffusion coefficients are, within experimental accuracy, found to be equal to those of the solvent cations. This is in agreement with a suggestion of Cohen and Turnbull, based on the free volume theory of diffusion.¹⁴

Acknowledgment. The present investigations have been carried out under the auspices of the Netherlands Foundation for Chemical Research (S.O.N.) and with financial aid from the Netherlands Organization for the Advancement of Pure Research (Z.W.O.).

- (10) R. W. Laity, *J. Chem. Phys.*, **30**, 682 (1959).
 (11) R. J. Bearman, *J. Phys. Chem.*, **65**, 1961 (1961).
 (12) B. Berne and S. A. Rice, *J. Chem. Phys.*, **40**, 1347 (1964).
 (13) J. A. A. Ketelaar, *Chemical Constitution*, Amsterdam, 1957.
 (14) M. H. Cohen and D. Turnbull, *J. Chem. Phys.*, **31**, 1164 (1959).

Stepped Isotherms on Carbons

by E. Greenhalgh and E. Redman¹

Morganite Research and Development Ltd., London
 (Received November 7, 1966)

Smith and Ford^{2a} in their paper, "Adsorption Studies On Heterogeneous Titania . . .," show a typical stepped isotherm for argon on Sterling MTG carbon black. This is stated to be typical of the behavior found with other gases (O_2 , N_2 , and CO), emphasizing the extraordinary uniformity of the surface. They further state that the extent of surface homogeneity may be associated with the area of exposed graphite

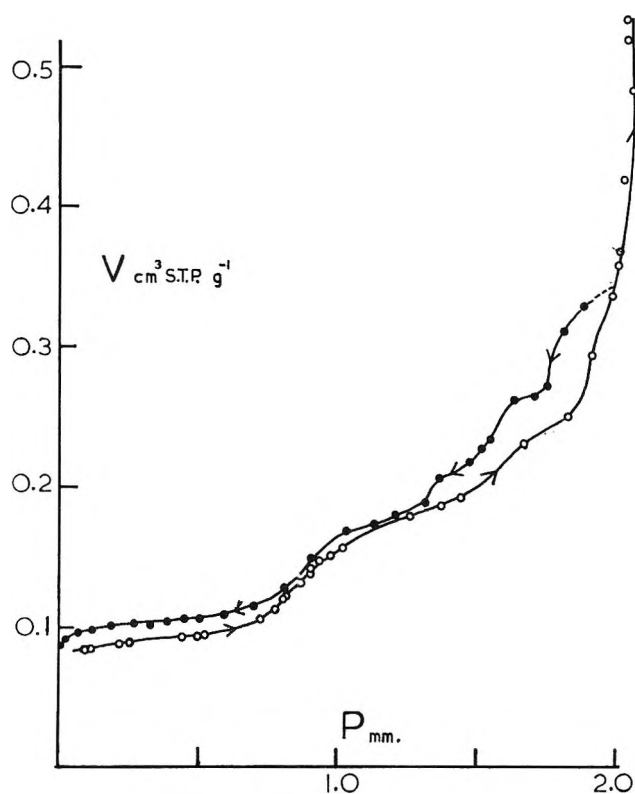


Figure 1. Krypton isotherm (-195°) for PVDC carbon (2500°).

planes on the surface of the black and that for MTG and FTG, the boundary of the planes represents only a small fraction of the exposed surface, and the heterogeneity introduced cannot be detected on the isotherms.

This may be true for readily graphitizable carbon blacks, but we present evidence to show that stepped isotherms on carbon are not always due to the presence of extensive graphite basal planes. Figure 1 shows the 77.95°K isotherm for krypton on the carbon obtained from polyvinylidene chloride after heat treatment to 2500° . The isotherm exhibits pronounced steps, but the carbon is far from graphitic ($L_a = 60 \text{ \AA}$, $L_c = 20 \text{ \AA}$, $d = 3.42\text{--}3.48 \text{ \AA}$).

The adsorbate used was krypton, while that used by Smith and Ford was argon. It could therefore be argued that the comparison is invalid. However, Crowell and Young^{2b} show isotherms for both adsorbates on graphitized P33 carbon black. The only difference appears to be that krypton gives more pro-

(1) To whom all correspondence should be addressed at Department of Chemistry, State University of New York at Buffalo, Buffalo, N. Y.

(2) (a) W. R. Smith and D. G. Ford, *J. Phys. Chem.*, **69**, 3587 (1965); (b) A. D. Crowell and D. M. Young, "Physical Adsorption of Gases," Butterworth and Co. Ltd., London, 1962, p 174.

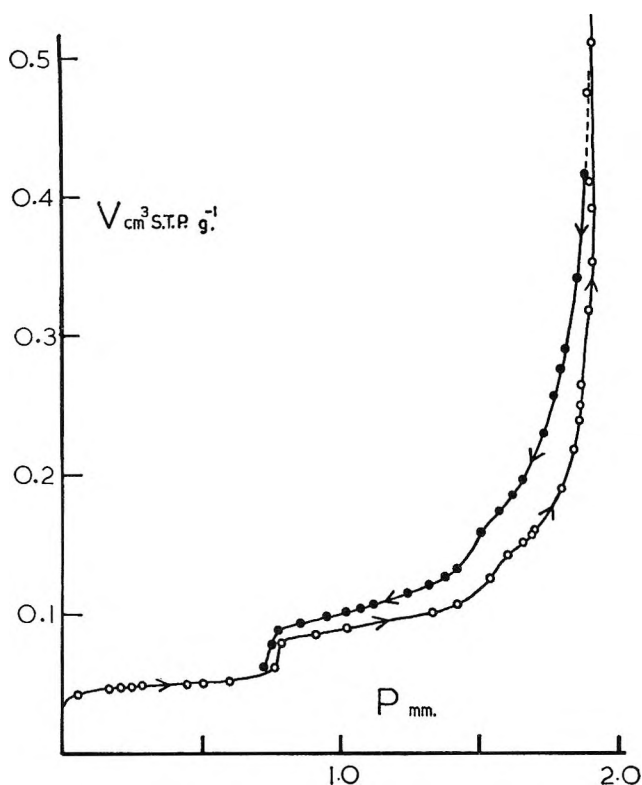


Figure 2. Krypton isotherm (-195°) for PVC carbon (2500°).

nounced steps than argon, possibly reflecting the higher heat of sorption.³

Figure 2 shows the 77.9°K isotherm obtained with krypton and the carbon prepared at 2500° from polyvinyl chloride. This carbon is more graphitic ($L_a = 570 \text{ \AA}$, $L_c = 690 \text{ \AA}$, $d = 3.37 \text{ \AA}$), but the steps are not much more pronounced than those in Figure 1.

Both isotherms exhibit hysteresis and this would normally be taken to imply that the samples were porous. Further, if this were so, it might possibly invalidate the interpretation of the isotherms in terms of whether the steps which we have observed correspond to those obtained on materials which are normally considered to be nonporous. However, the observed hysteresis cannot arise from capillary condensation in pores since the equivalence of the mercury and helium displacement densities⁴ indicates that both samples were nonporous. At atmospheric pressure, mercury will penetrate all pores with an entry diameter above approximately $15 \mu\text{m}$. These pores are outside the range of capillary condensation as detected by hysteresis in adsorption-desorption cycles. The hysteresis must therefore result from condensation in the interparticulate voids of the powdered sample.

Similar effects must be present for sorption on carbon blacks⁵ but few workers appear to have studied the

complete sorption cycle. Polley, Schaeffer, and Smith⁶ have observed hysteresis at $p/p_0 > 0.75$ and they attributed this to either interparticulate condensation or slow pressure equilibration. Joyner and Emmett⁷ claim that the adsorption and desorption curves were superimposable for nitrogen on Graphon, but they did not carry out a complete sorption cycle nor did they reach saturation.

Bonnetain, Duval, and Letort⁸ have reported stepped isotherms for methane on natural graphite and other nonporous solids, which exhibit hysteresis almost identical with that shown here.

Finally, we feel that even if capillary condensation is a complicating factor on the adsorption half-cycle, it would be unlikely to produce regular well-defined steps of the type shown.

The structure of polyvinylidene chloride (2500°) carbon is not certain, but provided that one accepts that an energetically homogeneous surface is required for stepped isotherms, then whatever the heterogeneities in the surface are, they must be either (a) so small that they cannot be detected by the krypton atom, or (b) so numerous that they form the homogeneous surface. The disappearance of the pore structure of this material on heat treatment,⁴ resulting in the equivalence of the mercury and helium displacement densities, would tend to support model (a) above.

Acknowledgment. The authors thank the Directors of Morganite Research and Development Ltd. for permission to publish this note.

- (3) R. M. Barrer, *Nature*, **181**, 176 (1958).
- (4) E. Greenhalgh, B. M. Miles, E. Redman, and S. A. Sharman, Second Industrial Carbon and Graphite Conference, Society of Chemical Industry, London, 1965.
- (5) C. Pierce, J. Mooi, and R. E. Harris, *J. Phys. Chem.*, **62**, 655 (1958).
- (6) M. H. Polley, W. D. Schaeffer, and W. R. Smith, *ibid.*, **57**, 469 (1953).
- (7) L. G. Joyner and P. H. Emmett, *J. Am. Chem. Soc.*, **70**, 2353 (1948).
- (8) L. Bonnetain, X. Duval, and M. Letort, *Compt. Rend.*, **234**, 1363 (1952).

Surface Tension of Binary Liquid Mixtures

by Raymond L. Schmidt

Department of Chemistry, Emory University, Atlanta, Georgia 30322
(Received September 26, 1966)

Current interest in the surface tension of binary liquid mixtures has resulted in new equations which

relate the mixture surface tension to properties of the pure components. By comparing these new equations with older treatments, several interesting results can be shown.

Nearly 60 years ago, Szyszkowski¹ proposed an empirical equation for binary mixture surface tension to fit his experimental data on aqueous solutions of organic acids. Belton and Evans² later derived an equation relating the mixture surface tension to pure component properties and properties of the bulk and surface phase of the mixture

$$\sigma = \sigma_1 + \frac{RT}{\Sigma_1} \ln \frac{a_{1s}}{a_1} = \sigma_2 + \frac{RT}{\Sigma_2} \ln \frac{a_{2s}}{a_2} \quad (1a)$$

where σ is the mixture surface tension, σ_1 and σ_2 are the pure component surface tensions, Σ_1 and Σ_2 are the pure component molal surface areas, and a_{1s} and a_i are the activities of component i in the surface phase and the bulk phase, respectively. The combined ratio of the surface- and bulk-phase activities can be expressed in terms of pure component parameters as

$$\left(\frac{a_{1s}}{a_1}\right) / \left(\frac{a_{2s}}{a_2}\right)^{\Sigma_1/\Sigma_2} = \exp\left[-\frac{(\sigma_1 - \sigma_2)\Sigma_1}{RT}\right] \quad (1b)$$

By assuming (a) equal surface areas, $\Sigma_1 = \Sigma_2 = \Sigma$, and (b) the ratio of the activity coefficients equal to unity, $(\gamma_{1s}/\gamma_1)/(\gamma_{2s}/\gamma_2) = 1$, where $a = \gamma X$ and γ is the activity coefficient of the component in the respective phase, eq 1b can be solved for X_{1s} in terms of X_1 and X_2 . Substitution of the resulting expression for X_{1s} into eq 1a gives the mixture surface tension as

$$\sigma = \sigma_1 - \frac{RT}{\Sigma} \ln (X_1 + X_2C) \quad (2)$$

where $C = \exp\{[(\sigma_1 - \sigma_2)/RT]\Sigma\}$, an empirical parameter in Szyszkowski's equation. Guggenheim³ has derived an expression for the mixture surface tension which he writes in a more symmetrical form but can be rearranged to give eq 2. The above equation is also derived by Hildebrand and Scott.⁴

Eberhart⁵ proposed that the mixture surface tension is a linear function of the surface layer mole fraction, $\sigma = X_{1s}\sigma_1 + X_{2s}\sigma_2$. By use of distribution constants, $K_i = a_{is}/a_i$, a separation factor, S , is defined for the enrichment of the surface layer in the component of lower surface tension

$$\left(\frac{a_{1s}}{a_1}\right) / \left(\frac{a_{2s}}{a_2}\right) = \frac{1}{S} \quad (3)$$

By assuming $(\gamma_{1s}/\gamma_1)/(\gamma_{2s}/\gamma_2) = 1$, the mixture surface tension can be written as a linear function in surface mole fraction

$$\sigma = X_{1s}\sigma_1 + X_{2s}\sigma_2 = \frac{X_1\sigma_1}{X_1 + SX_2} + \frac{SX_2\sigma_2}{X_1 + SX_2} \quad (4)$$

Equations of this form have been proposed empirically for a variety of binary mixture properties⁶ and used to fit the surface tension data of the silver-tin molten metal system⁷ for tin mole fraction between 0.35 and 1 and for fused salt systems.⁸

Equation 2 can be shown to predict the mixture surface tension to be a linear function of the surface mole fraction as far as first-order terms are concerned. Expand $\ln (X_1 + X_2C)$ by the relation $\ln Z = (Z - 1)/Z + \dots$ and rearrange to

$$\ln (X_1 + X_2C) = \frac{CX_2(1 - 1/C)}{X_1 + X_2C}$$

Now $1/C = \exp\{-[(\sigma_1 - \sigma_2)/RT]\Sigma\}$ can be expanded thru first order by $e^{-Z} = 1 - Z + \dots$. Thus $1/C = 1 - [(\sigma_1 - \sigma_2)/RT]\Sigma$. By substituting the above expressions into eq 2 and letting $C = S$ as required by eq 1b and 3, the surface tension relation given by eq 4 is obtained. Thus Eberhart's result is a first-order approximation⁹ to the result of Belton and Evans.

Considering the liquid-vapor interface as the adsorbent and the layer adsorbed at this interface as a layer in a force field, Erdős and Šišková^{10,11} derive a general equation which relates the activities in the bulk phase with activities and adsorption potentials, ϕ , at a given point in the adsorbed layer

$$\left(\frac{a_{1s}}{a_1}\right) / \left(\frac{a_{2s}}{a_2}\right)^B = \exp\left[-\frac{(\phi_1 - B\phi_2)}{RT}\right] \quad (5)$$

where $B = V_1/V_2$, the ratio of the molar volume of the pure components. By applying ideal solution assumptions, $a = X$ and $B = 1$, and considering the ad-

(1) B. V. Szyszkowski, *Z. Physik. Chem.* (Frankfurt), **64**, 385 (1908).

(2) J. W. Belton and M. G. Evans, *Trans. Faraday Soc.*, **41**, 1 (1945).

(3) E. A. Guggenheim, "Mixtures," Oxford University Press, London, 1952, Chapter 9; *Trans. Faraday Soc.*, **41**, 150 (1945).

(4) J. H. Hildebrand and R. L. Scott, "Solubility of Nonelectrolytes," 3rd ed, Reinhold Publishing Corp., New York, N. Y., 1950; also Dover Publications, 1964, pp 406-408.

(5) J. G. Eberhart, *J. Phys. Chem.*, **70**, 1183 (1966).

(6) M. A. Reshetnikov, *Dokl. Akad. Nauk SSSR*, **68**, 709 (1949); **69**, 45 (1949).

(7) I. Lauer mann, G. Metzger, and F. Sauerwald, *Z. Physik. Chem.* (Leipzig), **216**, 42 (1961).

(8) I. D. Sokolova and N. K. Voskresenskaya, *Russ. J. Phys. Chem.*, **36** (5), 502 (1962).

(9) The first-order nature of Eberhart's equation can also be shown by truncating eq 28b of ref 4 after the first two terms.

(10) E. Erdős and M. Šišková, *Collection Czech. Chem. Commun.*, **31**, 415 (1966).

(11) E. Erdős, *ibid.*, **20**, 111 (1955); **25**, 1729 (1960).

Table I: Parameters for Ideal Surface Tension Equations

System	Temp. °K	Eq 4		Eq 6			$\exp\left[\frac{\sigma_1 - \sigma_2}{RT}\Sigma_2\right]$	$(\phi_1 - \phi_2)$, cal/mole
		S	Av dev, dyne/cm	f	e'	Av dev, dyne/cm		
Ar-N ₂ ¹²	83.82	1.56	0.11	0.96	2.62	0.3	...	161
CH ₄ -N ₂ ¹²	90.67	2.59	1.10	2.41	11.15	0.12	...	435
CH ₄ -Ar ¹²	90.67	2.16	0.09	1.48	4.41	0.05	...	268
CH ₄ -CO ¹²	90.67	2.35	0.13	2.03	7.60	0.10	...	365
CO-N ₂ ¹²	83.82	2.10	0.04	1.24	3.47	0.02	...	224
C ₆ H ₆ -C ₆ H ₁₄ ^{13c}	298.16	2.43	0.53	2.05	7.75	0.08	2.46	1210
	303.16	2.69	0.06	1.98	7.25	0.14	2.40	1190
	308.16	2.50	0.19	1.91	6.78	0.01	2.34	1170
	313.16	2.40	0.10	1.79	6.00	0.08	2.29	1120
C ₆ H ₆ -C ₁₂ H ₂₆ ^{13c}	298.16	1.26	0.20	7.74	2300	0.13	1.55	4590
	303.16	1.21	0.06	5.64	281	0.16	1.49	3400
	308.16	1.00	0.19	5.28	194	0.21	1.44	3230
	313.16	1.66	0.09	6.03	415	0.16	1.40	3750
C ₆ H ₁₂ -C ₆ H ₁₄ ^{13a}	298.16	1.49	0.21	0.95	2.59	0.03	1.74	564
	303.16	1.50	0.12	0.86	2.36	0.05	1.74	517
	308.16	1.33	0.25	0.71	2.08	0.06	1.70	437
C ₁₂ H ₂₆ -C ₆ H ₁₄ ^{13d}	298.16	0.76	0.10	-0.56	0.572	0.06	1.81	-331
	303.16	0.74	0.11	-0.55	0.574	0.07	1.82	-334
	308.16	0.77	0.06	-0.49	0.610	0.00	1.82	-302
	313.16	0.77	0.11	-0.49	0.610	0.06	1.82	-307
C ₆ H ₆ -C ₈ H ₁₈ ^{13b}	303.16	3.01	0.15	2.37	10.65	0.11	2.66	1430
C ₆ H ₁₂ -C ₈ H ₁₈ ^{13b}	303.16	2.09	0.11	1.58	4.85	0.02	1.82	952
C ₁₂ H ₂₆ -C ₈ H ₁₈ ^{13b}	303.16	0.93	0.09	-0.42	0.680	0.04	1.95	-252

sorption potentials to be independent of composition and position in the adsorbed phase, the following expression is derived

$$\sigma = \sigma_1 - \frac{(\sigma_1 - \sigma_2)}{f} \ln(X_1 + X_2 e^f) \quad (6)$$

where $f = [(\phi_1 - \phi_2)/RT]$. This expression is identical in form with eq 2.

Since the left-hand sides of eq 1b, 3, and 5 are identical, if $\Sigma_1 = \Sigma_2 = \Sigma$ and $B = 1$, the following must be true

$$S = \exp\left[\frac{\sigma_1 - \sigma_2}{RT}\Sigma\right] = \exp\left[\frac{\phi_1 - \phi_2}{RT}\right] = e^f = C \quad (7a)$$

Thus the surface tension of a third system can be predicted from knowledge of the surface tension of two systems with a common component.

$$S(1, 2)/S(2, 3) = S(1, 3)$$

$$(\sigma_1 - \sigma_2)\Sigma + (\sigma_2 - \sigma_3)\Sigma = (\sigma_1 - \sigma_3)\Sigma \quad (7b)$$

$$(\phi_1 - \phi_2) + (\phi_2 - \phi_3) = (\phi_1 - \phi_3)$$

Equation 7a shows how these equations for the surface tension of binary liquid mixtures are related.

Results and Discussion

The parameters obtained by fitting eq 4 and 6 to

experimental surface tension data of simple cryogenic¹² and hydrocarbon mixtures¹³ are given in Table I, with the average deviation between the experimental and the calculated surface tension over the entire composition range. The S parameter of eq 4 was determined using a stepwise linear regression computer program. Equation 6 was fit to the experimental data using a nonlinear least-squares computer program which employs the Marquardt algorithm to estimate the parameters.¹⁴ For systems where temperature-dependent data are available, the f parameter approaches zero with increasing temperature, as predicted by eq 6. By comparing the average deviation of the fit by eq 6 to that by eq 4, one can easily see that eq 6 represents the data better in most cases.

The effect of the various approximations on the parameters of the mixture surface tension equations are shown by the comparisons in Table I. The f parameter is the most meaningful since no assumption or approximation has been made in its determination

(12) F. B. Sprow and J. M. Prausnitz, *Trans. Faraday Soc.*, **62**, 1105 (1966).

(13) (a) H. L. Clever and W. E. Chase, *J. Chem. Eng. Data*, **8**, 291 (1963); (b) H. B. Evans, Jr., and H. L. Clever, *J. Phys. Chem.*, **68**, 3433 (1964); (c) R. L. Schmidt, J. C. Randall, and H. L. Clever, *ibid.*, **70**, 3912 (1966); (d) R. L. Schmidt and H. L. Clever, unpublished results.

(14) D. W. Marquardt, *J. Soc. Ind. Appl. Math.*, **11**, 431 (1963).

from the experimental data. The Eberhart S parameter is a first-order approximation to the more precise parameters as shown by the derivation of eq 4 from eq 2. Comparison of S to $\exp f$ illustrates this first-order nature of S . The C parameter used in eq 2 has been estimated and is shown in column 8 of Table I. The surface area, Σ , was calculated assuming a spherical molecule from the $2/3$ power of the liquid molar volume for the component with the lower surface tension. Comparison of $\exp\{[(\sigma_1 - \sigma_2)/RT]\Sigma\}$ to the S parameter indicates that this surface area calculation amounts to about a first-order approximation for hydrocarbon systems.

From the f parameter, one can calculate the difference in the adsorption potentials of the two components at the liquid-vapor interface. This difference is given in the last column of the table. The ability to calculate the adsorption potential difference of a third system from measurements on two related systems by eq 7 is fair in most cases and is limited by the uncertainties in the adsorption potential differences.

Acknowledgments. The author wishes to thank Dr. H. L. Clever for his helpful discussions in preparing this note, the Emory Biomedical Data Processing and Analysis Center for use of the computer, and Dr. Louis Homer for discussions concerning the nonlinear least-squares program. This work was supported by National Science Foundation Grant GP-5937.

Solubilities of Alkylammonium Iodides in Water and Aqueous Urea

by F. Franks¹ and D. L. Clarke

*Department of Chemical Technology, University of Bradford,
Bradford 7, England (Received November 11, 1966)*

Attention has recently been drawn to the effect produced by urea on the solubilities of hydrocarbons,² micelle formation by surfactants,³ and the behavior of amino acids⁴ in aqueous solution. The view is held that urea lowers the tendency of nonpolar groups to form hydrophobic bonds by some modification of the structural properties of water. Aqueous solutions of hydrocarbons no doubt provide the simplest systems in which these effects can be studied, but as the size of the solute molecule is increased, the solubility soon becomes so low that its temperature dependence must be subject to a considerable experimental uncertainty.

One method of introducing reasonable concentrations of alkyl groups into aqueous solution consists of the employment of tetraalkylammonium halides. These compounds possess several properties which distinguish them from normal univalent electrolytes and in some respects they behave almost like hydrocarbons, *e.g.*, they form interstitial clathrate hydrates.⁵ The hydrocarbon-like behavior becomes more pronounced as the size of the alkyl groups is increased and it was therefore believed that useful information regarding the influence of urea on hydrocarbon-water interactions might be obtained from a study of the solubilities of tetra-*n*-butyl- and tetra-*n*-amylammonium iodides.

Experimental Section

Solubility determinations in water and 7 *M* urea were carried out over a temperature range 2–40°, care being taken to avoid supersaturation of the solutions. Samples were taken in duplicate, weighed, and the iodide was titrated against silver nitrate with an automatic potentiometric method which enabled the rate of addition of silver nitrate to be varied according to the total amount of iodide in the sample.

The alkylammonium iodides were recrystallized from ethanol-chloroform mixtures containing small amounts of water. Analysis showed them to be >99% pure. Since urea slowly decomposes on standing,⁶ all freshly made solutions were purified by ion exchange on a mixed column of Amberlite CG-400 and Amberlite IR-120(H).

Results and Discussion

The mole fraction solubilities of (*n*-Bu)₄NI and (*n*-Am)₄NI in water and 7 *M* urea are shown in Table I. The $\log x$ (T^{-1}) plots can be fitted satisfactorily by parabolic functions, showing that at low temperatures solution occurs exothermally. For the aqueous solutions, the enthalpy of solution, ΔH_s , passes through zero at 12 and 16° for (*n*-Bu)₄NI and (*n*-Am)₄NI, respectively. For the solutions in 7 *M* urea, the minima in the $\log x$ (T^{-1}) curves are displaced to much lower temperatures. The results indicate that for (*n*-Am)₄NI this temperature is near 0°. The temperature de-

(1) To whom all correspondence should be addressed at Unilever Research Laboratory, Colworth House, Sharnbrook, Bedford, England.

(2) D. B. Wetlaufer, S. K. Malik, L. Stoller, and R. L. Coffin, *J. Am. Chem. Soc.*, **86**, 508 (1964).

(3) M. J. Schick, *J. Phys. Chem.*, **68**, 3585 (1964).

(4) G. C. Kresheck and L. Benjamin, *ibid.*, **68**, 2476 (1964).

(5) *E.g.*, R. McMullan and G. A. Jeffrey, *J. Chem. Phys.*, **31**, 1231 (1959).

(6) H. B. Bull, K. Breese, and G. L. Ferguson, *Arch. Biochem. Biophys.*, **104**, 297 (1964).

pendence of ΔH_s shows that solution is associated with large, positive changes in the heat capacities of the systems, but the degree of accuracy of the solubility determinations makes a quantitative evaluation of ΔC_p values meaningless.

Table I: Mole Fraction Solubilities of Tetra-*n*-butylammonium Iodide and Tetra-*n*-amylammonium Iodide in Water (x_w) and 7 *M* Aqueous Urea (x_u)

Temp, °C	(n-Bu) ₄ NI		(n-Am) ₄ NI	
	10 ³ x_w	10 ³ x_u	10 ⁵ x_w	10 ⁶ x_u
2.0	1.06, 1.02	2.01, 2.01	4.79, 4.81	8.12, 7.98
4.0	1.01, 1.02	2.09, 2.11	4.57, 4.50	8.08, 8.04
9.0	0.99, 0.98	2.25, 2.25	4.37, 4.40	8.51, 8.46
15.0	0.97, 0.99	2.43, 2.50	4.17, 4.14	8.81, 8.90
21.0	1.07, 1.04	2.75, 2.69	4.32, 4.39	9.29, 9.18
26.0	1.14, 1.10	3.00, 2.97	4.52, 4.48	10.4, 10.2
31.0	1.26, 1.26	3.35, 3.40	4.76, 4.80	11.8, 11.7
36.0	1.41, 1.39	3.98, 4.02	5.62, 5.40	13.2, 13.7
43.0	1.60, 1.62	..., ...	6.46, 6.38	16.3, 16.0

The thermodynamic functions associated with the transfer at 25° of 1 mole of solute from an aqueous medium to a 7 *M* urea solution are set out in Table II. They reveal a type of behavior which has been reported for the hydrocarbons,² *i.e.*, that the transfer of solute from water to aqueous urea is spontaneous ($\Delta G_t^\circ < 0$) but endothermic ($\Delta H_t^\circ > 0$), indicating that the process is entropy directed and might be interpreted in terms of solvent structure. In contrast to the behavior shown by the hydrocarbons, ΔG_t° decreases in magnitude with an increase in the number of carbon atoms and is not as large as might be expected from a rough extrapolation of the ΔG_t° values quoted for the lower paraffins. On the other hand, ΔH_t° and ΔS_t° are of the same order of magnitude as the corresponding hydrocarbon values quoted by Wetlaufer, *et al.*² Unfortunately, there is at present not enough information regarding the alkylammonium halides to assess the magnitude of the ionic contributions to the transfer functions.

Qualitatively, the positive ΔH_t° and ΔS_t° results are in accord with the concept that urea reduces the structuredness of the aqueous medium and hence the tendency of the alkyl chains to participate in the formation of hydrophobic bonds.⁷ It is of course arguable

Table II: Free Energy (ΔG_t°), Enthalpy (ΔH_t°), and Entropy (ΔS_t°) of Transfer of Alkylammonium Iodides from Water to 7 *M* Aqueous Urea at 25° (cal mole⁻¹)

	ΔG_t°	ΔH_t°	ΔS_t°
(<i>n</i> -Bu) ₄ NI	-570	860	4.8
(<i>n</i> -Am) ₄ NI	-492	1240	5.8

whether hydrophobic bonds can significantly affect the behavior of systems in which the mole ratio of solute to solvent is of the order 1–10⁵. Partial molar volume studies on dilute solutions of (*n*-Bu)₄NBr have indicated that this substance behaves as a normal univalent electrolyte at concentrations up to about 10⁻² *M* (mole ratio 1:6 × 10³)⁸ and that the volume anomalies first observed by Wen and Saito⁹ only occur at higher concentrations.

There is, however, a more fundamental reason why the results cannot be interpreted solely in terms of a shift of the structural equilibrium in water, produced by the addition of urea, at least not on the basis of the currently available water structure models.^{10,11} For any shift in an equilibrium, the associated enthalpy and entropy changes must cancel in the free energy and hence such a process cannot affect the solute chemical potential, which alone is a measure of the solubility. By an extension of the mixture model^{10,11} for water to aqueous solutions, it has been found possible to derive expressions for μ_2 , \bar{H}_2 , and \bar{S}_2 of hydrocarbons in aqueous and 7 *M* urea solutions in terms of experimentally accessible quantities¹² and it has been found that the experimentally determined ΔG_t° values of Wetlaufer, *et al.*,² can be accounted for. It is intended to apply the treatment to the tetra-alkylammonium halides after isopiestic and calorimetric measurements, now in progress on the lower members of the series, have been completed.

(7) Although the view has recently been advanced [M. Abu-Hamdiyah, *J. Phys. Chem.*, **69**, 2720 (1965)] that urea *increases* the degree of hydrogen bonding in water, in the authors' opinion this is incompatible with the physical properties of water-urea mixtures and with the effects here described.

(8) F. Franks and H. T. Smith, Collected Abstracts: 16th CITCE Meeting, Budapest, Hungary, 1965, to be published.

(9) W. Y. Wen and S. Saito, *J. Phys. Chem.*, **68**, 2639 (1964).

(10) H. S. Frank and A. S. Quist, *J. Chem. Phys.*, **34**, 604 (1961).

(11) G. Némethy and H. A. Scheraga, *ibid.*, **36**, 3382 (1962).

(12) H. S. Frank and F. Franks, presented at the London Chemical Society Anniversary Meeting, Nottingham, England, April 1964.

Heats of Adsorption of Carbon Dioxide on Doped Zinc Oxide

by O. Levy and M. Steinberg

Department of Inorganic and Analytical Chemistry,
The Hebrew University, Jerusalem, Israel
(Received November 23, 1966)

Doping of zinc oxide results in change in the heat of chemisorption of carbon dioxide on its surface.¹ It

is of great practical importance that data on the activity of catalysts be obtained not only through methods based on measurements of adsorption properties under vacuum.²

Flow methods where conditions of adsorption resemble those dominating industrial processes are desirable. The transient response technique (TRT)³ probably holds the best promise for the fulfillment of some of the above requirements, since it provides means of measuring heats of adsorption in flow systems, and was used in the present study for the measurement of heat of adsorption of carbon dioxide on zinc oxide preparations of varying semiconducting character. Doped zinc oxides both of n and p type were used here. The TRT was normally applied to physical adsorption. To the best of the authors' knowledge, it has not hitherto been used to determine heats of adsorption where the interaction is primarily chemical.

Experimental Section

The pulse injection technique and measurement of the corrected retention times were as described previously.^{4,5}

Calibration of the desorption peak areas were carried out as follows. Various volumes of carbon dioxide corrected to STP were injected into a column packed with silica gel. The pulses were injected at temperatures matching those of the chemisorption runs (Table I). Linear relationships were obtained between the carbon dioxide injected and the peak areas. From the calibration curve it was found that the desorptions of carbon dioxide from all the zinc oxide preparations used at the working temperatures were quantitative. The columns in all the runs were flushed with the carrier gas, helium (Air Reduction Co., stated purity 99.99%) for 16 hr at 370°. This treatment was found to give reproducible results. Zinc oxide was prepared by the oxalate method.¹ The 1 mole % lithiated zinc oxide was prepared by the method described by Cimino, Molinari, and Cramarossa.⁶ The doped oxide so obtained was yellow even when left in air at room temperature, and its apparent density was 6.5 g/cm³. The 1 mole % galliated zinc oxide was prepared by the method described by Hart and Sebba.¹ The color of this preparation was white.

Results and Discussion

The logarithms of the corrected retention times were plotted against the reciprocals of the absolute temperature.⁴ The retention times were independent of the flow rates. In this study, flow rates of 7–10 ml sec⁻¹ were taken. These rates were found optimal for reasonable elution times. The elution curves for

Table I: Heats of Adsorption of Carbon Dioxide on Various Zinc Oxide Preparations

Absorbent	Pulse volume, ml	Temp, °C	ΔH , kcal mole ⁻¹
ZnO	0.5	280–310	30.8
	1.0	315–380	28.5
	1.5	320–365	26.5
ZnO + 1 mole % Li	0.1	340–360	25.3
	0.15	320–360	21.6
	0.25	320–360	19.5
ZnO + 1 mole % Ga	1.0	337–360	35.8
	2.0	332–360	32.5
	3.0	337–360	28.7

the same flow rate in the doped and undoped zinc oxide were similar, thus indicating the same type of sorption isotherm. The relationships obtained were linear and the calculated heats of adsorption are presented in Table I. It is clearly seen that the heats of adsorption (ΔH) of carbon dioxide on lithiated zinc oxide are lower than those obtained for undoped and galliated zinc oxide. The highest ΔH values obtained were for the galliated zinc oxide. The same trend was observed by Hart and Sebba,¹ using a different method of measurement. The results obtained in this work are in correspondence with the semiconducting character of the oxides under study here. Carbon dioxide, being an electron acceptor, is adsorbed more strongly on n type than on p type surfaces of semiconducting oxides. The heat of chemisorption on the p type lithiated zinc oxide is the lowest of the zinc oxide preparations in this study. The n type galliated zinc oxide and the undoped zinc oxide will tend to absorb carbon more strongly than the p type, and hence the higher values for the heats. It is also observed here that the ΔH values decrease with the increase in the gas pulse volumes.¹ Preliminary experiments on the adsorption of carbon monoxide on the surface of the above preparations at the same temperatures (Table I) were discontinued. The adsorptions in our flow method were irreversible. The TRT is not suitable for the ΔH

(1) P. N. G. Hart and F. Sebba, *Trans. Faraday Soc.*, **56**, 551 (1960).

(2) S. J. Gregg, "The Surface Chemistry of Solids," Reinhold Publishing Corp., New York, N. Y., 1961, pp 122–131.

(3) J. J. Carberry, *Nature*, **189**, 391 (1961).

(4) S. A. Greene and H. Pust, *J. Phys. Chem.*, **62**, 55 (1958).

(5) R. S. Hansen, J. A. Murphy, and T. C. McGee, *Trans. Faraday Soc.*, **60**, 597 (1964).

(6) A. Cimino, E. Molinari, and F. Cramarossa, *J. Catalysis*, **2**, 315 (1963).

calculations for this system at the temperature region 280–360°.

The fairly good agreement between the results obtained in our study and those from adsorption isosters¹ shows that the application of the transient response technique to reversible chemisorptions is worth studying, being a quick technique and pertinent to practical uses.

Acknowledgment. The authors thank Dr. F. S. Stone of the Department of Physical Chemistry, The University of Bristol, for his interest in this work.

Density, Viscosity, and Dielectric Constant of Tetrahydrofuran between –78 and 30°¹

by Donald J. Metz and Althea Glines

Brookhaven National Laboratory, Upton, New York 11973
(Received November 1, 1966)

Recently, Szwarc, *et al.*,² published data on the density, viscosity, and dielectric constant of tetrahydrofuran between –70 and 25°. In an independent and simultaneous study, we determined these properties between –78 and 30°. We would like to report that our data substantiate and confirm those previously published by both Szwarc² and others.^{3–5}

We determined our densities pycnometrically, using dried and purified ethyl bromide as standard.⁵ Viscosity was measured in a modified Ubbelohde viscometer *vs.* both ethyl bromide⁵ and diethyl ether.⁵ Dielectric constants were determined, *vs.* ethyl bromide,⁶

over the frequency range 60 kc–10 Mc using a Boonton Radio Q-Meter (Type 260-A) and a General Radio Schering-type capacitance bridge (Type 716C).

The comparison of both sets of data is shown in Table I.

Table I

	This work	Szwarc ²
Density, ρ_{25°	0.883	0.880 ^a
$d \ln v/dT^b$	0.00133	0.001085 ^a
Viscosity $\log \eta$	$-3.670 + 395/T$	$-3.655 + 393/T^a$
Dielectric constant, ϵ	$-1.50 + 2650/T$	$-1.495 + 2659/T^a$
$d \ln \epsilon/d \ln T$	-1.19	-1.16 ^a

^a Determined from –70 to 25°. ^b v = molar volume.

With the exception of the temperature dependence of density, the agreement between both sets of data is excellent. When the data of Kuss³ on the variation of density in the region of room temperature are included, there is a suggestion that the larger coefficient of expansion may be more nearly correct.

(1) This work was performed under the auspices of the U. S. Atomic Energy Commission.

(2) C. Carvajal, K. J. Tölle, J. Smid, and M. Szwarc, *J. Am. Chem. Soc.*, **87**, 5548 (1965).

(3) E. Kuss, *Z. Angew. Phys.*, **7**, 376 (1955).

(4) F. E. Critchfield, J. A. Gibson, Jr., and J. L. Hall, *J. Am. Chem. Soc.*, **75**, 6044 (1953).

(5) "International Critical Tables."

(6) A. A. Maryott and E. R. Smith, National Bureau of Standards Circular 514, U. S. Government Printing Office, Washington, D. C., 1951.

COMMUNICATIONS TO THE EDITOR

Volume Change Accompanying the

Helix-Coil Transition in

Poly- γ -benzyl-L-glutamate

Sir: Considerable progress has been made recently in measuring enthalpy changes related to the helix-coil transition in polypeptides, particularly poly- γ -benzyl-L-glutamate¹ (PBG), and rationalizing these results in light of prevailing theories. Rather surprisingly, less is known concerning the corresponding volume changes, ΔV° . Noguchi and Yang² have studied ΔV° for aqueous poly-L-glutamic acid dilatometrically, and have found that the volume of the coil (the high-temperature conformation) exceeded that of the helix (low-temperature form) by 1.0 ml (mole residues)⁻¹. For the system PBG-dichloroacetic acid (DCA)-1,2-dichloroethane (DCE), in which the helix is stable above the transition temperature, two estimates for ΔV° have been made, and they stand in gross disagreement. Bradbury, Fenn, and Gosney³ have determined ΔV° dilatometrically by measuring the apparent specific volume of PBG in 75:25 v/v DCA-DCE as a function of temperature and arrive at a value of $V_{\text{helix}} - V_{\text{coil}} (\equiv \Delta V^\circ)$ of -0.077 ml (mole residues)⁻¹. Gill and Glogovsky⁴ have measured the effect of pressure on the course of the transition and use the equation

$$\left(\frac{\partial f}{\partial P}\right)_{T, f=1/2} = -\frac{\Delta V^\circ}{4RT_c\sigma^{1/2}} \quad (1)$$

where f is the fraction of helix present in the polypeptide at the midpoint of the transition and σ is the Zimm-Bragg parameter related to the cooperativeness of the transition.⁵ Using known values for this parameter, Gill and Glogovsky calculate $\Delta V^\circ = 0.6$ ml mole⁻¹, averaged over their pressure range, 1 to 1020 atm. It may be noted also that the partial specific volume of PBG in pure DCA and in DCE at 25° is 0.780 and 0.786 ml g⁻¹, respectively.³ PBG is known to adopt a random coil conformation in DCA and a helical conformation in DCE.

Recently, we have formulated a general treatment in which the transition enthalpy, ΔH° , for polypeptide-mixed organic solvent systems was obtained from the dependence of the transition temperature, T_c , upon the solvent composition.⁶ The values calculated for PBG were in reasonable agreement with those found calorimetrically. In this treatment, the DCE was viewed as a nonbinding diluent which lowered the

chemical potential of the DCA in the solvent mixture. It is one of the purposes of this note to show that essentially the same principle can be used to calculate ΔV° , except now we are concerned with the effect of pressure, rather than temperature, upon the chemical potential of the DCA. In this respect, the approach is precisely analogous to the treatment of the effect of diluent on the equilibrium melting pressure of any chemical species at constant temperature, and leads to the equation

$$\left(\frac{\partial \ln N}{\partial P}\right)_{T_c} = -\frac{\Delta V^\circ}{RT_c} \quad (2)$$

in which (for the case being considered here) N is the mole fraction of DCA in the DCA-DCE mixture. The assumptions inherent in this approach and in particular the arguments leading to the identification of ΔV° in eq 2 with the quantity ΔV° referred to in the first paragraph are discussed elsewhere.⁶ Equation 2 can be utilized by noting that

$$\left(\frac{\partial \ln N}{\partial P}\right)_{T_c} = -\left(\frac{\partial \ln N}{\partial T_c}\right)_P \left(\frac{\partial T_c}{\partial P}\right)_N \quad (3)$$

The value of $(\partial \ln N / \partial T_c)_P$ taken from ref 1d (at 23°) is $(0.007^\circ)^{-1}$; from the results of Gill and Glogovsky,⁴ we calculate $(\partial T_c / \partial P)_N$ averages 0.0056° atm⁻¹ at $N = 0.73$. Consequently, using (2) and (3), $\Delta V^\circ = 0.96$ ml mole⁻¹. Our result actually refers to the change of volume at 1 atm and since Gill and Glogovsky find ΔV° to be very pressure dependent, it is necessary to recalculate their results to make a valid comparison. Their value, therefore, at 1 atm and 23° is 0.9 ml mole⁻¹.

Considering the limitations in both the theory and experimental data, this agreement is surprisingly good. We should emphasize that the agreement does not follow automatically from the use of Gill's value of $(\partial T_c / \partial P)_N$; it is confirmation, rather, of the assumptions contained in the solvent composition theory, and

(1) (a) F. E. Karasz, J. M. O'Reilly, and H. E. Bair, *Nature*, **202**, 693 (1964); (b) T. Ackermann and H. Rüterjans, *Z. Physik. Chem.*, **41**, 116 (1964); (c) F. E. Karasz, J. M. O'Reilly, and H. E. Bair, *Biopolymers*, **3**, 241 (1965); (d) F. E. Karasz and J. M. O'Reilly, *Advances in Chemistry Series*, American Chemical Society, Washington, D.C., in press.

(2) H. Noguchi and J. T. Yang, *Biopolymers*, **1**, 359 (1963).

(3) J. H. Bradbury, M. D. Fenn, and I. Gosney, *J. Mol. Biol.*, **11**, 137 (1965).

(4) S. J. Gill and R. L. Glogovsky, *J. Phys. Chem.*, **69**, 1515 (1965).

(5) B. H. Zimm and J. K. Bragg, *J. Chem. Phys.*, **31**, 526 (1959); J. Applequist, *ibid.*, **38**, 934 (1963).

(6) F. E. Karasz and J. M. O'Reilly, *Biopolymers*, **5**, 27 (1967).

of our value for $(\partial \ln N/\partial T_c)_P$. We note further that our calculated value is of the same sign and agrees moderately well in magnitude with the difference in the partial specific volumes of PBG at 25° in pure DCA and DCE. The interesting question of why the direct dilatometric measurement is so anomalous is thus raised. (The possibility of the anomaly arising solely from the somewhat different PBG concentrations used in the various experiments seems to us remote.) Barring any irreversible behavior, it is required that the change in volume (and in enthalpy) on passing through the conformational transition would be totally independent of the path. In particular, we would expect ΔV° obtained by varying T (N and P constant) to equal ΔV° obtained by varying N (T and P constant). The analogous paths have actually been followed in the case of the heat of transition, ΔH° —the former in heat capacity measurements,¹ and the latter in a heat of mixing experiment.⁷ Unfortunately, the latter results were qualitative only, but the signs of ΔH° were in agreement in the two cases. It should therefore be of considerable interest to determine the partial molal or specific volume of PBG, at 25° and at atmospheric pressure, as a function of solvent composition, over the entire composition range, in an attempt to resolve the apparent anomaly.

(7) H. Block and J. B. Jackson, *Proc. Chem. Soc.*, 381 (1963).

GENERAL ELECTRIC RESEARCH AND
DEVELOPMENT CENTER
SCHENECTADY, NEW YORK

F. E. KARASZ
J. M. O'REILLY

RECEIVED SEPTEMBER 27, 1966

Remarks on the Structure and Properties of Some Organocobalt Compounds,

$RCoX(L)_2$ and $R_2Co(L)_2$

Sir: By the reaction of $CoBr_2(P(Et)_2Ph)_2$ with Grignard reagents, Chatt¹ obtained yellow compounds, $R_2Co(P(Et)_2Ph)_2$ (R , mesityl-, pentachlorophenyl-, etc.), and their structures were determined to be *trans* square planar.^{1,2} On the other hand, green compounds obtained by the reactions of equimolar amounts of $CoBr_2(P(Et)_2Ph)_2$ and Grignard reagents were considered to be $RCoBr(P(Et)_2Ph)_2$,¹ but their structures remain unsettled.

Recently, we observed that the visible spectra of the green solution obtained by $CoCl_2(P(Et)_2Ph)_2-C_6Cl_5-MgCl$ was quite similar to that of $CoCl_2(P(Et)_2Ph)_2$ (tetrahedral), the bands at 600–800 $m\mu$ shifting as a

whole to longer wavelengths, *i.e.*, from 725, 625, and 580 $m\mu$ to 740, 650, and 620 $m\mu$, respectively.

On the contrary, with the system $CoI_2(P(Et)_2Ph)_2-C_6Cl_5MgCl$, the bands shifted to shorter wavelengths; *i.e.*, the bands at 775, 710, and 680 $m\mu$ of $CoI_2(P(Et)_2Ph)_2$ shifted to 765, 705, and 675 $m\mu$, respectively.

Similarly, with the system $CoCl_2(P(Et)_2Ph)_2-Me-MgBr$, absorptions were observed at 760, 670, and 630 $m\mu$. On the other hand, yellow solutions obtained by the reaction of $CoX_2(P(Et)_2Ph)_2$ with excess Grignard reagents showed no absorptions in the region 600–800 $m\mu$.

Hence we can consider that the green compounds, $RCoX(P(Et)_2Ph)_2$ (R , C_6Cl_5 or Me), are tetrahedral and that, according to the rule of average environment,³ the ligand field strength of these anions is fairly weak and is represented by $Cl^- > C_6Cl_5^- > Me^- > I^-$ in the spectrochemical series.

The esr study supports the above conclusions; *i.e.*, the green solutions as well as $CoCl_2(P(Et)_2Ph)_2$ showed symmetrical signals with g factor close to 2, whereas the yellow solutions showed broad unsymmetrical signals with fine structures (at -196°), which might be ascribed to g anisotropy. In contrast to tetrahedral complexes of Co^{2+} ion, the *trans* square planar complexes would have an anisotropic g factor.⁴ In glassy state at low temperature, anisotropy is observed as separate absorptions and, at the same time, signals become broad owing to the lack of Brownian motion.⁵

Anhydrous $CoCl_2$ dissolved into 10% toluene solution of various pyridine derivatives showed visible spectra with three fine structures in the region 600–800 $m\mu$ which were quite similar to that of tetrahedral $CoCl_2(pyridine)_2$,⁶ the wavelengths of these absorptions being nearly the same for all complexes.

By the reaction of $CoCl_2(pyridine\ derivatives)_2$ with $MeMgBr$ at -30° , violet-red solutions were obtained, which were quite unstable at room temperature. By analogy with the results of $R_2Co(P(Et)_2Ph)_2$, we can consider that square planar compounds, $Me_2Co(pyridine\ derivatives)_2$, were formed.

Figure 1 shows the esr spectra of these solutions at -130° . The g factor decreases as the basicity of coordinating base increases. The contribution to the g factor

(1) J. Chatt and B. L. Shaw, *J. Chem. Soc.*, 286 (1961).

(2) P. C. Owston and J. M. Rowe, *ibid.*, 3411 (1963).

(3) C. K. Jørgensen, "Absorption Spectra and Chemical Bonding in Complexes," Pergamon Press, Ltd., London, 1964, p 109.

(4) W. Low, "Paramagnetic Resonance in Solids," Solid State Physics, Supplement 2, Academic Press, New York, N. Y., 1959, p 39.

(5) F. K. Kneubuhl, *J. Chem. Phys.*, **33**, 1074 (1960).

(6) J. Ferguson, *ibid.*, **32**, 528 (1960).

of the orbital magnetic moment is reduced when unpaired electrons spread out to ligands through covalent metal-ligand bonds.⁷ Hence, for the present systems, we can consider that the unpaired electron of cobalt ion is increasingly back-donated to ligand molecules as the coordinating base becomes more basic.

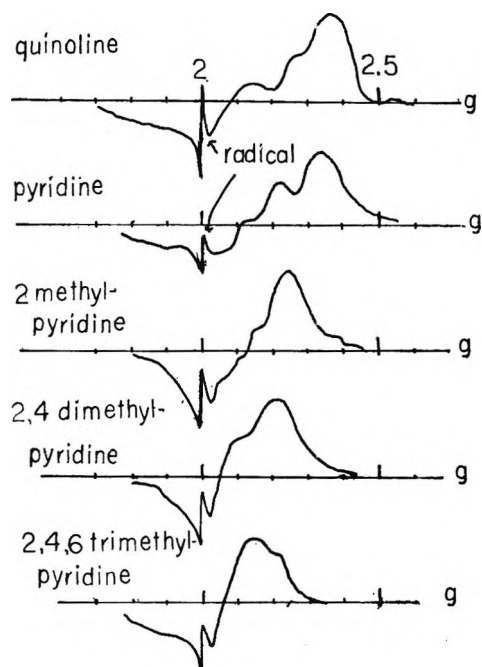


Figure 1. The esr spectra of reaction products between CoCl_2 (pyridine derivatives)₂ and MeMgBr (observed at -130°).

In the present work, most compounds were fairly unstable and, therefore, the esr study was carried out mostly at low temperature. Kneubühl⁸ showed that in the glassy state the esr signals become broad and the anisotropy becomes observable separately owing to the lack of Brownian motion.

Above -60° the esr signal of yellow solution from $\text{CoCl}_2(\text{P}(\text{Et})_2\text{Ph})_2/\text{C}_6\text{Cl}_5\text{MgCl}$ became fairly sharp and symmetrical, showing that ferromagnetic impurities were not responsible for the line width.

Details of results and discussions will be presented in the near future.

(7) Reference 4, p 96.

DEPARTMENT OF INDUSTRIAL CHEMISTRY
FACULTY OF ENGINEERING
UNIVERSITY OF TOKYO
HONGO, TOKYO, JAPAN

KEI MATSUZAKI
TAMIO YASUKAWA

RECEIVED NOVEMBER 1, 1966

Comments on the Paper, "A Chemical Kinetics Computer Program for Homogeneous and Free-Radical Systems of Reactions," by R. H. Snow

Sir: A recent article by Snow¹ dealt with the numerical computation of a homogeneous reaction system with emphasis on the use of the steady-state assumption. I should like to comment on three aspects of this article.

The article states that "...so far as we know such calculations have been reported only for oxidation of hydrogen in addition to ethane pyrolysis." There are, however, numerous published papers and reports dealing with the numerical calculation of reacting gases. References 2 through 6 constitute a very brief list of such work. Each of these references gives the equations used in the respective computer program plus detailed results for various chemical systems. These programs generally allow for an arbitrary system of reacting species whose composition is determined by an arbitrary system of reactions. A constant temperature is not assumed, as it is in ref 1. Instead, the programs are for more complicated physical processes such as shock tube or nozzle flow. Of course, most of them are adaptable to a constant-temperature calculation.

The problem of numerical instability that frequently plagues this type of calculation has also been investigated.⁷⁻⁹ These studies encompass Runge-Kutta, predictor-corrector, and other numerical methods. Reference 9, for example, derives a simple criterion for maintaining stability when the Runge-Kutta method is used.

Finally, Libby¹⁰ has previously discussed the partial

(1) R. H. Snow, *J. Phys. Chem.*, **70**, 2780 (1966).

(2) A. Q. Eschenroeder, D. W. Boyer, and J. G. Hall, *Phys. Fluids*, **5**, 615 (1962).

(3) A. A. Westenberg and S. Favin, "Complex Chemical Kinetics in Supersonic Nozzle Flow," Ninth Symposium (International) on Combustion, Academic Press, New York, N. Y., 1963, pp 785-798.

(4) G. Emanuel and W. G. Vincenti, "Method for Calculation of the One-Dimensional Nonequilibrium Flow of a General Gas Mixture Through a Hypersonic Nozzle," Report AEDC-TDR-62-131 for Arnold Engineering Development Center, June 1962.

(5) R. E. Duff and N. Davidson, *J. Chem. Phys.*, **31**, 1018 (1959).

(6) G. Moretti, *AIAA J.*, **3**, 223 (1965).

(7) J. Certaine, "The Solution of Ordinary Differential Equations with Large Time Constants," Mathematical Methods for Digital Computers, John Wiley and Sons, Inc., New York, N. Y., 1960 pp 128-132.

(8) C. F. Curtiss and J. O. Hirschfelder, *Proc. Natl. Acad. Sci. U. S.*, **38**, 235 (1952).

(9) G. Emanuel, "Numerical Analysis of Stiff Equations," Report No. TDR-269(4230-20)-3, Aerospace Corp., Jan 1964.

(10) P. A. Libby, *ARS J.*, **32**, 1090 (1962).

equilibrium approximation, which in some cases is the same as the steady-state approximation. For example, the two are the same in the illustrative example given in ref 1. Libby has shown that the use of this approximation requires some care due to the appearance of indeterminate quantities in the retained rate equations. The neglect of these quantities in no way hinders the numerical calculation, which may produce answers that appear reasonable. Nevertheless, these answers are generally incorrect.

AEROPHYSICS DEPARTMENT
AEROSPACE CORPORATION
LOS ANGELES, CALIFORNIA 90045

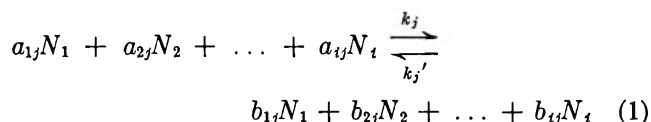
GEORGE EMANUEL

RECEIVED NOVEMBER 4, 1966

Computer Program for Chemical Kinetics

Sir: Snow¹ reported a computer program capable of handling the product distribution of any homogeneous reaction mechanism. This program involves a direct integration of the pertinent equation (2) below as well as an integration based on the assumption of steady state and a switch-over-mechanism going from one type of integration to the other. Besides the validity of the steady-state assumption being questionable for many reactions, the complexity incorporated seems to make the reported method¹ inferior to other methods^{2,3} which are based on an alteration of the direct integration. In the following, the basic ideas of the latter methods are described.

The pertinent reaction scheme can be represented by a set of elementary reactions of the type



where a_{ij} is the stoichiometric coefficient of the i th component being a reactant for the j th reaction; b_{ij} is the stoichiometric coefficient of the i th component being a product for the j th reaction; k_j is the forward rate constant of the j th reaction; k_j' is the backward rate constant of the j th reaction; and N_i is the name of i th component.

The rate of production of the i th component is given by

$$\frac{dC_i}{dt} = \sum_j \left\{ (b_{ij} - a_{ij}) \left[k_j \prod_i C_i^{a_{ij}} - k_j' \prod_i C_i^{b_{ij}} \right] \right\} \quad (2)$$

where C_i is the concentration of i th component, and t is the reaction time.

The integration of these equations by standard methods such as Runge-Kutta fails because of the following numerical difficulty. In the square brackets at the right side of eq 2, there are two large terms subtracted from each other. Near chemical equilibrium, these two terms approach each other. This numerical difficulty can easily be overcome by introducing the following set of new variables

$$\lambda_j = \frac{k_j}{k_j'} \prod_i C_i^{(a_{ij} - b_{ij})} - 1 \quad (3)$$

Equation 3 combined with eq 2 results in

$$\frac{dC_i}{dt} = \sum_j \left[(b_{ij} - a_{ij}) k_j' \lambda_j \prod_i C_i^{b_{ij}} \right] \quad (4)$$

Equation 4 does not cause any numerical difficulty in respect to its integration by such standard methods as Runge-Kutta. Methods of the type presented do not need any further assumptions like the sometimes questionable assumption of steady state. Due to their simplicity, these methods appear to require much less computer time than the method by Snow.

(1) R. H. Snow, *J. Phys. Chem.*, **70**, 2780 (1966).

(2) T. F. Zupnik, E. N. Nilson, and V. J. Sarli, NASA-Report CR-54042 (1964).

(3) J. P. Gurney, *AIAA J.*, **3**, 3, 538 (1965).

PRATT AND WHITNEY AIRCRAFT
DIVISION OF UNITED AIRCRAFT
EAST HARTFORD, CONNECTICUT

REINER KOLLRACK

RECEIVED DECEMBER 1, 1966

Reply to Comments on the Paper, "A Chemical Kinetics Computer Program for Homogeneous and Free-Radical Systems of Reactions"

Sir: The main question raised by Emanuel and also by Kollrack is whether it is really necessary to use the special technique given in my paper for avoiding numerical difficulties in solving the differential equations of chemical kinetics. Certainly, for some reactions under limited conditions a satisfactory solution can be obtained by standard numerical methods. Emanuel's ref 2-6 give further examples of this. However, the methods which they give do not solve the peculiar difficulties encountered in chemical kinetics, and so they are not truly general.

Some reaction systems with free-radical chains may

be solved by standard integration methods, if the radical concentrations are not too low, as Duff did for the H_2-O_2 system (quoted in Emanuel's ref 5). Nevertheless, this calculation was said to require 5000 iterations. Under conditions such that the free-radical concentrations are lower, the number of iterations will increase rapidly.

Emanuel's ref 6-9 concern mathematical techniques for speeding numerical solution of differential equations. Techniques such as forward difference schemes, instability analysis, etc., can speed such calculations by a factor of perhaps 10 or 100, while there are practical problems in chemical kinetics where the calculation speed of standard methods is too slow by a factor of 10^6 , even with the fastest computers. In these cases, the steady-state hypothesis is the answer. My main contribution was to demonstrate a method of applying it in general for any reacting system where it is needed, and to analyze the situations where it is useful.

Emanuel's remark that my paper gives only the constant-temperature case is irrelevant, since methods of generalizing are known.

Emanuel's final comments concern the validity of the steady-state hypothesis. His ref 10 by Libby concerns possible errors in assuming "a partial equilibrium or steady-state treatment of those reactions with specific rate constants considerably higher than the others involved in the series." The comment by Kollrack gives essentially the same information as Libby's publication. Libby essentially says that conservation of matter is satisfied as long as one calculates the extent of each reaction in a mechanism according to the standard rate equations. However, if one abandons some of the rate equations and calculates some components by means of equilibrium expressions, then changes are made in the amounts of certain components without regard to the stoichiometry of the reactions that produce them. He then formulates equations to take into account both equilibria and stoichiometry.

This argument is answered in my paper: the steady-state assumption is valid only when the components that are to be determined from other-than-stoichiometric equations (the free radicals) are present in such small quantities that neglect of the principle of conservation of matter applied to them will introduce negligible error in the amounts of other components present. Libby's warning is not important under the conditions for which the steady-state assumption is valid.

Incidentally, the standard rate expressions can lead to error in numerical integration. An example is the pyrolysis of ethane, where the forward and reverse chain-propagating steps approach equilibrium, and the

difference is beyond the number of significant digits carried by the computer. Libby's method should be of use in this problem.

The work of Giddings and Shin on the hydrogen-bromine system¹ should have been mentioned in my paper.

(1) J. C. Giddings and H. K. Shin, *J. Phys. Chem.*, **65**, 1164 (1961); *J. Chem. Phys.*, **36**, 640 (1962); *Trans. Faraday Soc.*, **57**, 468 (1961); *J. Chem. Phys.*, **39**, 2937 (1963).

IIT RESEARCH INSTITUTE
TECHNOLOGY CENTER
CHICAGO, ILLINOIS 60616

RICHARD H. SNOW

RECEIVED JANUARY 16, 1967

On The Heat Precipitation of Poly-L-proline¹

Sir: In a recent paper,² a study of the change in certain physical-chemical properties that occur during the well-known heat precipitation^{3,4} of a dilute aqueous solution of poly-L-proline (form II)^{3,5,6} was reported. The thermodynamic, dimensional, and frictional properties prior to precipitation were interpreted in terms of conventional polymer solution theory appropriate to chains in random-coiled, nonordered conformations.⁷ The experimental evidence⁸ which favors a rigid rod-like structure in dilute solution was ignored. It was concluded in this work² that the precipitation was a consequence of a liquid-crystal transition rather than a liquid-liquid phase separation. These are the two obvious possibilities to choose from when observing precipitation phenomena from a dilute solution of random-coiled polymer.⁷ However, the liquid-crystal transition involving randomly coiled polymers is

(1) This work was supported by a contract with the Division of Biology and Medicine, U. S. Atomic Energy Commission.

(2) A. Ciferri and T. A. Orofino, *J. Phys. Chem.*, **70**, 3277 (1966).

(3) J. Kurtz, A. Berger, and E. Katchalski in "Recent Advances in Gelatin and Glue Research," G. Stainsby, Ed., Pergamon Press, New York, N. Y., 1958, p 31.

(4) W. F. Harrington and M. Sela, *Biochem. Biophys. Acta.*, **27**, 24 (1958).

(5) E. R. Blout and G. D. Fasman, "Recent Advances in Gelatin and Glue Research," G. Stainsby, Ed., Pergamon Press, New York, N. Y., 1958, p 122.

(6) A. Yaron and A. Berger, *Bull. Res. Council Israel*, **A10**, 46 (1961).

(7) P. J. Flory, "Principles of Polymer Chemistry," Cornell University Press, Ithaca, N. Y., 1953.

(8) I. Z. Steinberg, W. F. Harrington, A. Berger, M. Sela, and E. Katchalski, *J. Am. Chem. Soc.*, **82**, 5263 (1960).

invariably accompanied by a major conformational change.⁹

The theoretical approach that was used in the analysis and the conclusion reached² have led to a serious misconception in regard to the actual molecular phenomena that are involved during the heat precipitation of poly-L-proline. We wish to review^{10,11} and introduce new evidence that demonstrates that although this phenomenon is a phase transition there is no accompanying conformational change in the macromolecular component. This process is of the type discussed theoretically by Onsager¹² and by Flory¹³ and results from the geometric asymmetry of the solute molecules with the phase separation being aided by slightly positive interaction free energies between these species.¹³ A dense fibrillar, crystalline phase has been theoretically predicted to occur from a dilute solution of such molecules.¹³ The conclusion that no conformational change is involved during the heat precipitation of poly-L-proline is supported by two main lines of experimental evidence.

It has been reported^{4,14} that the specific optical rotation of form II, $[\alpha]_D = -500^\circ$, remains virtually invariant from room temperature to 60° . Above this temperature, precipitation of the solute prevents any further optical rotation measurements that can be given a molecular interpretation. This large negative specific rotation is characteristic of the ordered helical conformation^{3-6,8} with imide groups in a *trans* orientation. We have also recently observed that the optical rotatory dispersion (ORD), from 600 to 400 $m\mu$, is invariant with temperature up to 63° . However, after standing for 1 min at 63° , the ORD measurements become spurious as a consequence of precipitation. The utilization of optical rotation measurements as a sensitive method of describing conformations and conformational changes for polypeptides has been extensively demonstrated and documented.^{15,16} We can, therefore, conclude from the above results that until the point of precipitation, there is no conformational change in poly-L-proline.

The foregoing conclusion is substantiated by studies of the wide-angle X-ray patterns. In the first column of Table I, there are listed the major d spacings characteristic of poly-L-proline in form II. Detailed crystallographic studies^{17,18} have demonstrated that these spacings are consistent with an ordered helical, *trans* structure. Prior to dissolution at room temperature, freeze-dried poly-L-proline possesses the same major spacings as is indicated in the second column of Table I. After precipitation at 51° , the data in the last column demonstrate that all of these spacings are still present. These results thus confirm

Table I: Spacings (in angstroms) for Poly-L-proline II^a

Ref ^b	Before dissolution	After precipitation
5.80 (s)	5.85 (s)	5.83 (s)
4.92 (s)	4.98 (s)	4.94 (s)
	4.36 (vw)	4.42 (w)
3.61 (s)	3.70 (m)	3.66 (m)
2.74 (m)	2.74 (mw)	2.74 (m)
2.45 (m)		2.47 (mw)
2.28 (m)		2.28 (mw)
2.15 (m)		2.18 (mw)
1.90 (m)		1.98 (w)

^a w = weak; s = strong; m = moderate; vw = very weak; mw = moderately weak. ^b F. Gornick, L. Mandelkern, A. F. Diorio, and D. E. Roberts, *J. Am. Chem. Soc.*, **82**, 5263 (1960).

the conclusions drawn from optical rotation studies in regard to the maintenance of conformation during precipitation.

Quantitative studies that we have made of the precipitation kinetics indicate that the process is one in which nucleation acts play a predominant and rate-determining role. For example, for a 0.16% solution the half-time for precipitation at 51° is 37,500 min. However, at 60° the half-time has been reduced to 1550 min. Similar results are obtained for higher polymer concentrations. This extraordinary variation of rate with temperature can only be attributed to nucleation control, through the dependence of precipitation rate on the supersaturation or undercooling. Theoretically, a first-order phase transition is predicted for this process.¹³ Therefore, nucleation control, from a kinetic viewpoint, is consistent with this equilibrium stipulation. Similar quantitative rate studies, with essentially the same conclusions, have already been published for the heat precipitation of soluble collagen (tropocollagen) in an ordered conformation.^{19,20}

The collagen and poly-L-proline systems that have

(9) L. Mandelkern, "Crystallization of Polymers," McGraw-Hill Book Co., Inc., New York, N. Y., 1964, p 38 ff.

(10) Reference 9, p 66 ff.

(11) L. Mandelkern, *J. Polymer Sci.*, **49**, 125 (1961).

(12) L. Onsager, *Ann. N. Y. Acad. Sci.*, **51**, 627 (1949).

(13) P. J. Flory, *Proc. Roy. Soc. (London)* **A234**, 60 (1956).

(14) J. Engel, J. Kurtz, E. Katchalski, and A. Berger, *J. Mol. Biol.*, **17**, 255 (1966).

(15) P. Urnes and P. Doty, *Advan. Protein Chem.*, **16**, 402 (1961).

(16) J. A. Schellman and C. Schellman, *Proteins*, **2**, 1 (1964).

(17) P. M. Cowan and S. McGavin, *Nature*, **176**, 501 (1955).

(18) V. Sasisekharan, *Acta. Cryst.*, **12**, 897 (1959).

(19) G. C. Wood and M. K. Keech, *Biochem. J.*, **75**, 588, 598 (1960).

(20) J. M. Cassel, L. Mandelkern, and D. E. Roberts, *J. Am. Leather Chemists' Assoc.*, **42**, 556 (1962).

been described represent a unique situation that is not encountered with random-coiled polymers. A phase transition occurs, wherein a concentrated ordered phase is formed from a dilute solution, without the macromolecular species undergoing any conformational change. The theoretical basis for this phenomenon has already been set forth.^{12,13}

DEPARTMENT OF CHEMISTRY AND
INSTITUTE OF MOLECULAR BIOPHYSICS
THE FLORIDA STATE UNIVERSITY
TALLAHASSEE, FLORIDA

L. MANDELKERN
M. H. LIBERMAN

RECEIVED NOVEMBER 28, 1966

**Comments on the Note, "On the Heat
Precipitation of Poly-L-proline," by L.
Mandelkern and M. H. Liberman**

Sir: In the preceding letter, Mandelkern and Liberman¹ suggest that no conformational change is involved in the heat precipitation of form II poly-L-proline from aqueous solutions. Essentially, they contend that (i) the model of a rigid rod in solution is more appropriate, and (ii) a liquid-liquid separation resulting in formation of fibrous aggregates, as described by Flory,² is the only reasonable representation of the transition.

In our paper,³ we have also repeatedly called attention to the relatively rigid conformation of this polymer in solution and have invoked, for purposes of qualitative examination, an accordingly appropriate conformational model⁴ based upon the existence of a single minimum in the potential for internal rotation. Nonetheless, it is constructive to recognize that even so-called rigid molecules in dilute solution possess some degree of flexibility.^{4,5} In the case of poly-L-proline, the recent optical rotatory dispersion experiments of Engel, *et al.*,⁶ reveal a decrease in the parameter $[\alpha]_D$ with temperature and with salt concentration (LiBr) which is not at all negligible. Moreover, Blout and Fasman⁷ reported that the value of $[\alpha]$ changes markedly with the solvent medium; *i.e.*, $[\alpha]_{646}^{25} = -768$, -694 , and -406 , respectively, in 8 *M* urea, water, and 2 *M* KSCN. Our data³ also indicate that the intrinsic viscosity is strongly affected by salt concentration.

Thus, although a helix \rightarrow coil transformation is not observed, it appears that both temperature and solvents are able to affect considerably the conformation of poly-L-proline II in solution. Clearly, optical rotation and optical rotatory dispersion might well be observed also in a solution of molecules that consist of helical sequences connected by flexible joints for which the

thermodynamic, dimensional, and frictional properties would be normally ascribed to stiff coils. In short, there is certainly no unassailable evidence to support the rod-like model, and consequently, there is no definite evidence that the liquid-liquid separation considered by Flory³ is the controlling factor for the precipitation of poly-L-proline. Indeed, even for completely rigid particles, one must allow for the possibility of phase separation as a direct liquid-crystal transformation, rather than the aggregation resulting from liquid-liquid separation involving an anisotropic phase.

The primary object of the work reported by us³ was to provide reasonable evidence for identification of the observed phase change characteristic of poly-L-proline with a direct liquid-crystal transition. For purposes of analysis, we chose to adopt the familiar Flory-Huggins⁸ form for the chemical potential of the dispersed species. On this basis, two sufficient criteria for elimination of liquid-liquid separation as either the ultimate or transient phase separation process are: (i) verification of the ordered nature of the precipitate in the presence of the supernatant liquid (possible complications arising from *subsequent* crystallization of a concentrated liquid phase upon removal of solvent can thus be avoided); and (ii) verification of a positive value for the second virial coefficient just prior to the separation of the solution into two phases. Obviously, our conclusions must be viewed in light of the model invoked to reach them.

The interesting model and the process suggested by Mandelkern and Liberman are, possibly, a better approximation to the case of tropocollagen, although this remains to be seen. In our work,³ the comparison between poly-L-proline and tropocollagen is to be viewed principally in the direction in which the temperature change affects the precipitation.

(1) L. Mandelkern and M. H. Liberman, *J. Phys. Chem.*, **71**, 1163 (1967).

(2) P. J. Flory, *Proc. Roy. Soc.*, (London), **A234**, 73 (1956).

(3) A. Ciferri and T. A. Orofino, *J. Phys. Chem.*, **70**, 3277 (1966).

(4) M. L. Volkenstein, "Conformational Statistics of Chain Molecules," Interscience Publishers, Inc., New York, N. Y., 1961, p 189.

(5) G. Cohen and H. Eisenberg, *Biopolymers*, **4**, 429 (1966).

(6) J. Engel, J. Kurtz, E. Katchalski, and A. Berger, *J. Mol. Biol.* **17**, 255 (1966).

(7) E. R. Blout and G. D. Fasman, "Recent Advances in Gelatin and Glue Research," G. Stainsby, Ed., Pergamon Press, London, 1958, p 158.

(8) P. J. Flory, "Principles of Polymer Chemistry," Cornell University Press, Ithaca, N. Y., 1953.

CHEMSTRAND RESEARCH CENTER, INC.
DURHAM, NORTH CAROLINA 27702

A. CIFERRI
T. A. OROFINO

RECEIVED JANUARY 1, 1967

Constant-Volume Parameters of Activation for the Hydrolysis of Benzyl Chloride in Ethanol-Water Mixtures

Sir: Recent measurements of the volume of activation ΔV^\ddagger for the spontaneous solvolysis of benzyl chloride in ethanol-water mixtures,¹ when combined with earlier measurements² of the enthalpy ΔH_p^\ddagger and entropy ΔS_p^\ddagger of activation at constant pressure, allow a calculation of the internal energy ΔU_v^\ddagger and entropy ΔS_v^\ddagger of activation at constant volume according to the formula

$$\Delta H_p^\ddagger - \Delta U_v^\ddagger = T\Delta S_p^\ddagger - T\Delta S_v^\ddagger = T\alpha\Delta V^\ddagger/\kappa$$

where T is the temperature, and α and κ are the thermal expansivity and compressibility of the reaction mixture. The values of α and κ for the pure solvent can be used without causing significant error. The thermal expansivities were obtained from published data.³ The compressibilities were Moesveld's⁴ values at 25°; the compressibilities of mixtures of water and organic solvents are little dependent on temperature between 25 and 60°, and this approximation should be unimportant. The values of α , κ , ΔV^\ddagger , and $T\alpha\Delta V^\ddagger/\kappa$ are listed in Table I.

Table I: Thermal Expansivity and Compressibility of Ethanol-Water Mixtures, and Volumes of Activation for the Hydrolysis of Benzyl Chloride in These Mixtures

% v/v of ethanol	$10^6\alpha/\text{deg}^{-1}$ (Temp 51.0°)	$10^6\kappa/\text{bar}^{-1}$ (Temp 25°)	$\Delta V^\ddagger/\text{cm}^3 \text{ mole}^{-1}$ (Temp 50.25°)	$(T\alpha\Delta V^\ddagger/\kappa)$ cal mole ⁻¹
0	465	44.2	-8.5	-692
26.5	813	40.4	-16.4	-2551
44.8	917	46.2	-20.4	-3129
58.2	976	54.0	-22.8	-3185

The parameters of activation relative to the values in pure water are plotted in Figure 1. There is no minimum in ΔU_v^\ddagger , and only a small minimum (~ 0.7 kcal mole⁻¹) in $T\Delta S_v^\ddagger$, in contrast to minima of 1.8 and 2.8 kcal mole⁻¹ in ΔH_p^\ddagger and $T\Delta S_p^\ddagger$. It was reported earlier⁵ that the minima in the constant-pressure parameters for the acid-catalyzed hydrolysis of methyl acetate at 35° that occur at about 35% v/v of acetone in water are not present in the constant-volume parameters. The constant-volume parameters are undoubtedly simpler functions of the solvent composition in both systems. In addition, the entropy-energy compensation is a good deal smaller in the constant-volume parameters for both systems, and also for the

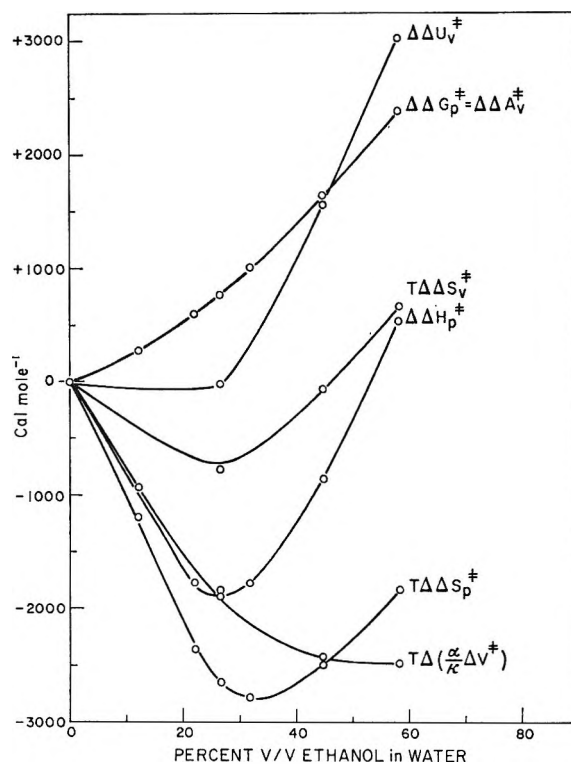


Figure 1. Changes with solvent of the parameters of activation for the hydrolysis of benzyl chloride.

acid-catalyzed enolization of acetone and of acetophenone in ethanol-water mixtures.⁶

Although there are no compelling reasons for preferring one set of parameters over the other, it was suggested⁶ that the relative simplicity in the variation of the constant-volume parameters was reflected in a relative simplicity of fundamental processes. Specifically, it was suggested that a large part of the minima was due to the use of water as one component, which causes a large variation of the thermal expansivity α with composition (see Table I), and so causes $\Delta H_p^\ddagger - \Delta U_v^\ddagger (= T\alpha\Delta V^\ddagger/\kappa)$, to be strongly solvent dependent. It seems likely that for the hydrolysis of benzyl chloride in ethanol-water mixtures, the constant-volume parameters are the simpler, and the minima in the constant-pressure parameters can be ascribed to the high effect of solvent composition on both the thermal

(1) J. B. Hyne, H. S. Golinkin, and W. G. Laidlaw, *J. Am. Chem. Soc.*, **88**, 2104 (1966).

(2) J. B. Hyne, R. Wills, and R. E. Wonkka, *ibid.*, **84**, 2914 (1962).

(3) N. S. Osborne, E. C. McKelvy, and H. W. Bearce, *Bull. Natl. Bur. Std.*, **9**, 327 (1913).

(4) A. L. Th. Moesveld, *Z. Physik. Chem.*, **105**, 450 (1923).

(5) B. T. Baliga, R. J. Withey, D. Poulton, and E. Whalley, *Trans. Faraday Soc.*, **61**, 517 (1965).

(6) B. T. Baliga and E. Whalley, *Can. J. Chem.*, **42**, 1835 (1964).

expansivity and the volume of activation. The effect of solvent on the compressibility is of little importance.

If this view is accepted, the solvent variation of ΔU_v^\ddagger and $T\Delta S_v^\ddagger$ can be simply interpreted. When ethanol is added, some of the benzyl chloride has some of its neighboring water molecules replaced by ethanol. Because ethanol is a poorer solvent than water for a polar transition state, such molecules hydrolyze comparatively slowly. Consequently, the rate decreases, but because the reaction is carried essentially by benzyl chloride wholly solvated by water, ΔU_v^\ddagger changes little, and ΔS_v^\ddagger decreases. At higher concentrations more of the reaction is carried by benzyl chloride partly solvated by ethanol, and then ΔU_v^\ddagger increases. Presumably, ΔS_v^\ddagger for benzyl chloride partly solvated by ethanol is less negative than when it is solvated by water only, so that $\Delta\Delta S_v^\ddagger$ increases at the higher concentrations, and there is a minimum value. The minimum in ΔH_p^\ddagger is caused by the superposition of this "concave" variation of ΔU_v^\ddagger and a nearly linear variation of $T\alpha\Delta V^\ddagger/\kappa$ (see Figure 1), and the minimum in $T\Delta S_p^\ddagger$ is caused in a similar way.

Are the minima in ΔH_p^\ddagger and $T\Delta S_p^\ddagger$ closely related to mechanism? There is undoubtedly a relation, but it appears that the concave variation in ΔU_v^\ddagger and the small minimum in $T\Delta S_v^\ddagger$ are more directly related, and should be considered as more fundamental.

DIVISION OF APPLIED CHEMISTRY
NATIONAL RESEARCH COUNCIL
OTTAWA, CANADA

B. T. BALIGA
E. WHALLEY

RECEIVED DECEMBER 15, 1966




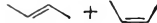
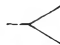


Benzene Photosensitization of 4-Pentalenal

Sir: The studies of gas-phase photochemical decomposition of 4-pentalenal have been reported only briefly in connection with the photolysis of cyclopentanone,^{1,2} since 4-pentalenal is a photochemical rearrangement product of excited cyclopentanone.³ We wish to report a novel gas-phase decomposition of excited 4-pentalenal produced by the benzene photosensitization technique⁴ at 2537 Å. The major decomposition product with benzene photosensitization is methylcyclopropane, whereas the major product of direct photolysis at 3130 Å is 1-butene.²

The samples were handled in a vacuum line free of mercury and grease, and photolyses were carried out in a cylindrical quartz cell with a mercury resonance lamp at room temperature. Products were separated by a conventional gas chromatograph, and mass anal-

ysis was recorded with a thermistor detector. The relative yields of hydrocarbon products as a function of benzene pressure between 0 and 4 mm are shown in Figure 1. The comparison of decomposition product yields among various modes of excitation is shown in Table I.

Table I: Comparison of Radical, Direct Photochemical, and Benzene-Photosensitized Decompositions

Method	—Klemm, <i>et al.</i> —		—This work—	
	Toluene carrier	3130 Å	2537 Å	2537 Å
Temp, °C	575	100	23	23
Gas, } 4-Pentalenal	?	1-30	0.5	0.4
mm (Benzene	None	None	None	0.5
	—Hydrocarbon product yields, mole %—			
	Most	2	25	<10
	Most	2	40	16
	Some	90	35	17
	Some	2
	57
	Some
	...	2

It is clear that methylcyclopropane is the most important photodecomposition product in the benzene photosensitization of 4-pentalenal. The study of benzene fluorescence quenching by 4-pentalenal and of competitive chemical quenching of triplet benzene by *cis*-2-butene and 4-pentalenal in our laboratory⁵ indicates that triplet benzene is responsible for the production of methylcyclopropane. For example, 50% of the benzene fluorescence is quenched at 4 mm of 4-pentalenal, and the yield of methylcyclopropane does not vary between 0.4 and 1.6 mm of 4-pentalenal, while the yields of olefins increase with increasing 4-pentalenal pressure. Furthermore, this study⁵ shows that 4-pentalenal is a more efficient quencher of triplet benzene than *cis*-2-butene by a factor of 4. This observation and the fact that unsaturated aldehyde (3-butenal) is an order of a magnitude better quencher of acetone phosphores-

(1) J. N. Butler, A. T. Drake, J. C. Mitchell, and P. Singh, *Can. J. Chem.*, **41**, 2704 (1963).

(2) R. F. Klemm, D. N. Morrison, P. Gilderson, and A. T. Blades, *ibid.*, **43**, 1934 (1965).

(3) R. Srinivasan, *J. Am. Chem. Soc.*, **81**, 1546 (1959).

(4) (a) H. Ishikawa and W. A. Noyes, Jr., *J. Chem. Phys.*, **37**, 583 (1962); (b) see for a recent review W. A. Noyes, Jr., and I. Unger, *Advan. Photochem.*, **4**, 49 (1966).

(5) G. A. Haninger, Jr., and E. K. C. Lee, unpublished work.

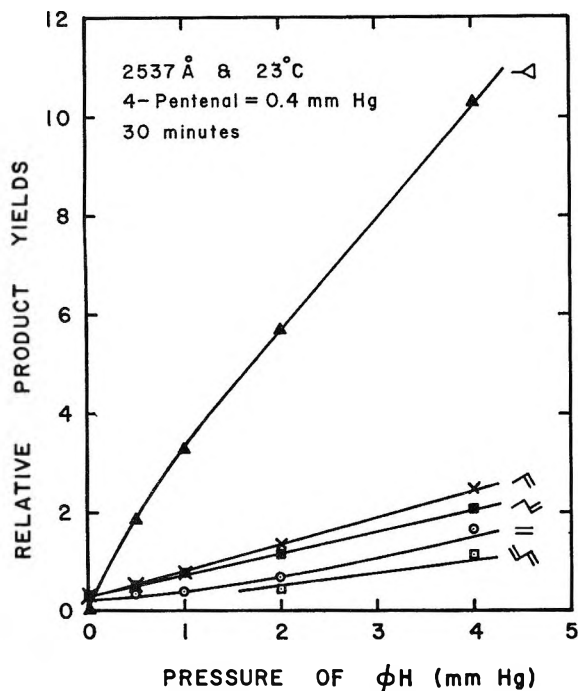


Figure 1.

cence than saturated aldehydes (C_2 , C_3 , and C_4)⁶ strongly suggest that the triplet energy transfer takes place primarily through the olefinic part of the molecule. It is therefore proposed that triplet benzene sensitization of $CH_2=CH-CH_2-CH_2-CH=O$ gives a 4,5-diradical, $\dot{C}H_2-\dot{C}H-CH_2-CH_2-CH=O$, and 1,5-H migration gives a 1,4-diradical, $CH_3-\dot{C}H-CH_2-CH_2-\dot{C}H=O$. The subsequent elimination of CO and cyclization, or the reverse, can yield methylcyclopropane. The C—H bond strength in formaldehyde is known to be 87 kcal/mole,⁷ and by analogy the aldehydic C—H bond strength in 4-pentenal is probably comparable to 87 kcal/mole and is much weaker than any other C—H bond in 4-pentenal. Therefore, intramolecular abstraction of the aldehydic hydrogen atom is probably the lowest threshold reaction mode and consequently 1,5-H migration is favored over other possible migration modes.

Triplet benzene is responsible for *cis-trans* isomerization of 2-butenes,⁸ while triplet mercury photosensitization of 1-butene yields methylcyclopropane *via* H migration in vibrationally excited triplet 1-butene.⁹ Similarly, triplet mercury photosensitization of 1-pentene gives methylcyclobutane¹⁰ and 1,2-dimethylcyclopropane.¹¹ In view of these illustrative examples, the above proposed mechanism is certainly reasonable and it reveals very interesting intermolecular energy transfer and intramolecular rearrangement in benzene photosensitization of an unsaturated nonconjugated aldehyde.

It can be seen from Table I that ethylene and propylene appear to be radical products since they are predominant in the toluene carrier study.² Furthermore, these yields are higher for direct photolysis at 2537 than at 3130 Å and they have intermediate values for the benzene photosensitization. This indicates that more fragmentation occurs at higher excitation energy, as expected, and that while less excitation occurs in benzene photosensitization than in 2537-Å direct photolysis, more excitation occurs than in 3130-Å direct photolysis. Furthermore, the olefinic products arise primarily through singlet benzene sensitization at the carbonyl position of 4-pentenal. The details of the experiment will more appropriately be discussed elsewhere.

Acknowledgment. Helpful discussion with Professor F. S. Rowland and Dr. Charles McKnight is appreciated.

(6) R. E. Rebert and P. Ausloos, *J. Am. Chem. Soc.*, **86**, 4803 (1964).

(7) R. Walsh and S. W. Benson, paper presented at the Physical Chemistry Division, 152nd National Meeting of the American Chemical Society, New York, N. Y., Sept 4, 1966.

(8) R. B. Cundall, F. J. Fletcher, and D. G. Milne, *Trans. Faraday Soc.*, **60**, 1146 (1964).

(9) R. J. Cvetanovic and L. C. Doyle, *J. Chem. Phys.*, **37**, 543 (1962).

(10) R. J. Majer, J. F. T. Pinkard, and J. C. Robb, *Trans. Faraday Soc.*, **60**, 1247 (1964).

(11) D. W. Placzek and B. S. Rabinovitch, *Can. J. Chem.*, **43**, 820 (1965).

DEPARTMENT OF CHEMISTRY
UNIVERSITY OF CALIFORNIA AT IRVINE
IRVINE, CALIFORNIA 92664

EDWARD K. C. LEE
NORMAN W. LEE

RECEIVED JANUARY 3, 1967

Amended Kohlrausch Ratio for

Transport Numbers

Sir: In our paper,¹ "Transport Numbers of Concentrated Sodium Chloride Solutions at 25°," we derived an expression for the ratio of Hittorf transport numbers of leading and following solutions in a moving boundary experiment (eq 8 in ref 1)

$$t_{Na}^h/t_K^h = m'_{Na}/m_K$$

in which t_{Na}^h and t_K^h are the Hittorf transport numbers of sodium and of potassium, respectively, and m'_{Na}

(1) L. J. M. Smits and E. M. Duyvis, *J. Phys. Chem.*, **70**, 2747 (1966).

and m_K are the adjusted concentration of the sodium ions and the concentration of the potassium ions, respectively, in moles per kilogram of H_2O .

Through a recently published review by Kaimakov and Varshavskaya,² we have now become aware that Hartley,³ when introducing the adjusted indicator method in 1934, had already derived this equation. This fact seems to have been overlooked in the literature that has appeared since then.

(2) E. A. Kaimakov and N. L. Varshavskaya, *Russ. Chem. Rev.*, **35**, 89 (1966).

(3) G. S. Hartley, *Trans. Faraday Soc.*, **30**, 648 (1934).

KONINKLIJKE/SHELL EXPLORATIE EN
PRODUKTIE LABORATORIUM
RIJSWIJK, THE NETHERLANDS

L. J. M. SMITS
E. M. DUYVIS

RECEIVED JANUARY 12, 1966

ACCEPTED AND TRANSMITTED BY THE FARADAY SOCIETY

DECEMBER 6, 1966

Comments on the Paper, "Gibbs Equation for the Adsorption of Organic Ions in Presence and Absence of Neutral Salts," by D. K. Chattoraj

Sir: It is now well established that in the interpretation of surface and interfacial tensions at air-water and oil-water interfaces the Gibbs equation should be used in the "one kT " form if neutral salts are present in excess to the surface active electrolyte, and in the "two kT " form if neutral salts are absent.¹

In a recent paper in this journal, Chattoraj² investigated how the kT coefficient varies between 1 and 2 in the intermediate salt concentration range. His basic equation (eq 8), in a slightly different notation, reads

$$-d\gamma = \Gamma_{R-} \frac{dc_{R-}}{c_{R-}} kT \left[1 + \frac{1}{1 - \frac{\Gamma_{Cl-} c + c_{R-}}{\Gamma_{Na+}}} \right] \quad (1)$$

γ is the interfacial tension; Γ_{R-} , Γ_{Na+} , and Γ_{Cl-} are the surface excesses of surface-active anions, sodium ions, and chloride ions, respectively. It is assumed that the Na^+ ion is common to both anions present; c_{R-} is the concentration of the surface-active anion and c is the $NaCl$ concentration, so that $c_{Na+} = c + c_{R-}$. k is the Boltzmann constant and T is the absolute temperature.

Chattoraj states that the ratio of the surface excesses, $\Gamma_{Cl-}/\Gamma_{Na+}$, can be replaced by the ratio of the surface concentrations c_{Cl-}^s/c_{Na+}^s with

$$c_{Na+}^s = (c + c_{R-})e^{-e\psi/kT} \quad (2)$$

$$c_{Cl-}^s = ce^{e\psi/kT} \quad (3)$$

where e is the elementary charge and ψ is the surface potential inclusive of (negative) sign. Ultimately this leads to

$$-d\gamma = \Gamma_{R-} \frac{dc_{R-}}{c_{R-}} kT m' \quad (4)$$

with

$$m' = 1 + \frac{1}{1 + x(1 - e^{2e\psi/kT})} \quad (5)$$

and $x = c/c_{R-}$.

However, Chattoraj's statement is incorrect. In a diffuse double layer, surface excesses of ionic species cannot be obtained by application of the Boltzmann equation in one plane of adsorption but should be calculated *via* integration over the whole double layer. According to the Gouy theory, the ratio of the surface excesses is given by

$$\frac{\Gamma_{Cl-}}{\Gamma_{Na+}} = \frac{c}{c + c_{R-}} \frac{\int_0^\infty (1 - e^{\psi z/kT}) dx}{\int_0^\infty (e^{-e\psi z/kT} - 1) dx} \quad (6)$$

After solving the integrals, eq 6 reads³

$$\frac{\Gamma_{Cl-}}{\Gamma_{Na+}} = \frac{c}{c + c_{R-}} \frac{1 - e^{\psi_\delta/2kT}}{e^{-e\psi_\delta/2kT} - 1} \quad (7)$$

ψ_δ is the potential of the outer Stern plane, which also should replace ψ in eq 5. Substituting eq 7 into eq 1 gives

$$-d\gamma = \Gamma_{R-} \frac{dc_{R-}}{c_{R-}} kT m'' \quad (8)$$

with

$$m'' = 1 + \frac{1}{1 + x \left[1 - \frac{1 - e^{\psi_\delta/2kT}}{e^{-e\psi_\delta/2kT} - 1} \right]} \quad (9)$$

In Figure 1, m' and m'' at 20° are compared for two values of ψ_δ . Although it is realized that $\psi_\delta = -5$ mv is an unrealistically low potential, the correspond-

(1) See, e.g., J. T. Davies and E. K. Rideal, "Interfacial Phenomena," Academic Press Inc., New York, N. Y., 1961, p 198.

(2) D. K. Chattoraj, *J. Phys. Chem.*, **70**, 2687 (1966).

(3) D. C. Grahame, *Chem. Rev.*, **41**, 481 (1947).

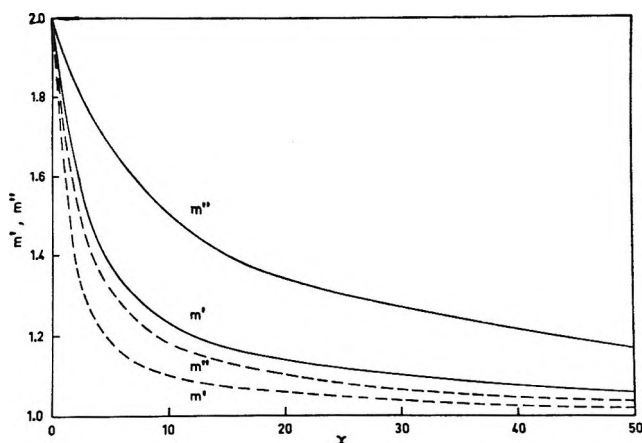


Figure 1. m' and m'' as a function of salt ratio x : full lines, $\psi_\delta = -5$ mv; broken lines, $\psi_\delta = -30$ mv.

ing values are given by way of illustration. $\psi_\delta = -30$ mv also is a rather low potential but it may be encountered under certain conditions, and therefore it is worthwhile to note that even then m'' is substantially

higher than m' . At potentials more negative than $\psi_\delta = -30$ mv, m' and m'' both approach the parameter m as given in eq 5 of Chatteraj's paper

$$m = 1 + \frac{1}{1 + x} \quad (10)$$

and line I of Chatteraj's Figure 1 applies.

When specific adsorption of Na^+ ions in the Stern layer occurs, the factor $1 - (\Gamma_{\text{Cl}^-}/\Gamma_{\text{Na}^+})$ in eq 1 approaches unity at lower x values than in the pure diffuse case. Under these circumstances the kT coefficient will be between m'' and m .

In conclusion, we can say that the kT coefficient in the Gibbs equation approaches unity only at high values of x , the deviation from unity growing progressively more than 1% when $x < 100$.

LABORATORY FOR PHYSICAL AND
COLLOID CHEMISTRY
AGRICULTURAL UNIVERSITY
WAGENINGEN, THE NETHERLANDS

B. H. BIJSTERBOSCH
H. J. VAN DEN HUL

RECEIVED JANUARY 30, 1967